Experimental analysis of aerosol dispersion and containment solutions in aircraft cabins

by

Seif Mahmoud

B.S., Qatar University, 2013
M.S., Hamad Bin Khalifa University, 2017

AN ABSTRACT OF A DISSERTATION

submitted in partial fulfillment of the requirements for the degree

DOCTOR OF PHILOSOPHY

Alan Levin Department of Mechanical & Nuclear Engineering
Carl R. Ice College of Engineering

KANSAS STATE UNIVERSITY
Manhattan, Kansas

2021

Abstract

This dissertation is focused on the dispersion and containment solutions of possibly infectious aerosols in aircraft cabins. In this study, a Boeing 767 mockup cabin, a Boeing 737 section, and a modified cabin were utilized. The Boeing 767 and the modified cabins have eleven rows with each row consisting of seven seats in a 3-2-3 configuration. The Boeing 737 section has five rows of seats with six seats in each row in a 3-3 configuration. Seats were occupied by inflatable manikins that generate approximately 100 W of sensible heat per manikin, representing heat load from a sedentary human being and cabin equipment. An aerosols containment solution called “ISOPass” was tested in the different aircraft cabins.

A total of 183 tests were performed using: two tracer gas source types, different source seat locations, different ISOPass conditions in the three different aircraft cabins. The source types were a continuous injection source and a coughing manikin. The source locations were two seats at each cabin side, a front seat, a middle seat, and a rear seat. The ISOPass conditions were ISOPass deployed and ISOPass undeployed.

Four injection source locations were selected. A 25.4 mm (1 inch) inner diameter copper tube was used as the continuous injection source. A mix of 5 L/min (0.176 ft^3/min) of carbon dioxide and 3.07 L/min (0.108 ft^3/min) of helium was injected at the average of seated passenger breathing level of 1.25 m (4.1 ft) above the cabin floor. A total of 42 tests were conducted in matching pairs. It was noticed that the contaminant transport pattern is dominated by the cabin airflow pattern in the near field and by distance in the far field. Also, the contaminant concentration was not necessarily the same at similar radial distances in different directions from the source, especially in the near field. Furthermore, tracer gas concentrations at some seats were higher than the source seat due to the airflow pattern inside the cabin.

Using a coughing manikin of a 4.2 L (0.148 ft^3) cough volume, 93 tests were conducted in matching triplets. Five coughing manikin locations were selected in different locations inside the cabin. Tracer gas samples were collected up to 3.35 m (11 ft) from the manikin in different orientations. Without the ISOPass and due to the cough momentum, the tracer gas concentration at further distances from the coughing manikin were sometimes higher than in the vicinity of the manikin. Also, tracer gas concentration at the rear of the cabin was negligibly affected by the coughing manikin compared to the longitudinal or diagonal directions.

The ISOPass, when deployed in different aircraft cabins and using either source types, was proven an effective tool to contain aerosols from spreading to other passengers and crew.

Smoke visualization was performed at five different locations to qualitatively analyze the dispersion of the tracer gas in the aircraft cabin. The smoke visualization results provided an explanation for some of the phenomena that were recorded using the tracer gas measurements such as the increase in the tracer gas concentration in some seats over the source seat.

Experimental analysis of aerosol dispersion and containment solutions in aircrafts cabins

by

Seif Mahmoud

B.S., Qatar University, 2013
M.S., Hamad Bin Khalifa University, 2017

A DISSERTATION

submitted in partial fulfillment of the requirements for the degree

DOCTOR OF PHILOSOPHY

Alan Levin Department of Mechanical & Nuclear Engineering
Carl R. Ice College of Engineering

KANSAS STATE UNIVERSITY
Manhattan, Kansas

2021

Approved by

Co-Major Professor
M.H. Hosni

Approved by

Co-Major Professor
B. W. Jones

Copyright

© Seif Mahmoud 2021.

Abstract

This dissertation is focused on the dispersion and containment solutions of possibly infectious aerosols in aircraft cabins. In this study, a Boeing 767 mockup cabin, a Boeing 737 section, and a modified cabin were utilized. The Boeing 767 and the modified cabins have eleven rows with each row consisting of seven seats in a 3-2-3 configuration. The Boeing 737 section has five rows of seats with six seats in each row in a 3-3 configuration. Seats were occupied by inflatable manikins that generate approximately 100 W of sensible heat per manikin, representing heat load from a sedentary human being and cabin equipment. An aerosols containment solution called “ISOPass” was tested in the different aircraft cabins.

A total of 183 tests were performed using: two tracer gas source types, different source seat locations, different ISOPass conditions in the three different aircraft cabins. The source types were a continuous injection source and a coughing manikin. The source locations were two seats at each cabin side, a front seat, a middle seat, and a rear seat. The ISOPass conditions were ISOPass deployed and ISOPass undeployed.

Four injection source locations were selected. A 25.4 mm (1 inch) inner diameter copper tube was used as the continuous injection source. A mix of 5 L/min (0.176 ft^3/min) of carbon dioxide and 3.07 L/min (0.108 ft^3/min) of helium was injected at the average of seated passenger breathing level of 1.25 m (4.1 ft) above the cabin floor. A total of 42 tests were conducted in matching pairs. It was noticed that the contaminant transport pattern is dominated by the cabin airflow pattern in the near field and by distance in the far field. Also, the contaminant concentration was not necessarily the same at similar radial distances in different directions from the source, especially in the near field. Furthermore, tracer gas concentrations at some seats were higher than the source seat due to the airflow pattern inside the cabin.

Using a coughing manikin of a 4.2 L (0.148 ft^3) cough volume, 93 tests were conducted in matching triplets. Five coughing manikin locations were selected in different locations inside the cabin. Tracer gas samples were collected up to 3.35 m (11 ft) from the manikin in different orientations. Without the ISOPass and due to the cough momentum, the tracer gas concentration at further distances from the coughing manikin were sometimes higher than in the vicinity of the manikin. Also, tracer gas concentration at the rear of the cabin was negligibly affected by the coughing manikin compared to the longitudinal or diagonal directions.

The ISOPass, when deployed in different aircraft cabins and using either source types, was proven an effective tool to contain aerosols from spreading to other passengers and crew.

Smoke visualization was performed at five different locations to qualitatively analyze the dispersion of the tracer gas in the aircraft cabin. The smoke visualization results provided an explanation for some of the phenomena that were recorded using the tracer gas measurements such as the increase in the tracer gas concentration in some seats over the source seat.

Table of Contents

List of Figures xii
List of Tables lxxi
Acknowledgements lxxii
Dedication lxxiii
Chapter 1 - Introduction 1
Chapter 2 - Literature Review 4
2.1 Aircraft Cabin Air Quality Standards 5
2.1.1 Cabin Air Temperature and Humidity 6
2.1.2 Cabin Air Pressure 7
2.1.3 Cabin Air Ventilation 8
2.2. Contamination Exposure in Aircraft Cabins 10
2.2.1 Contamination Sources in Aircraft Cabins 10
2.2.2 Common Infectious Diseases Transmitted in Aircraft Cabins 12
2.2.2.1 Influenza 13
2.2.2.2 Measles 15
2.2.2.3 Tuberculosis (TB) 16
2.2.2.4 Meningococcal Disease 17
2.2.2.5 Middle Eastern Respiratory Syndrome Coronavirus (MERS-CoV) 18
2.2.2.6 Ebola 21
2.2.2.7 Severe Acute Respiratory Syndrome (SARS) 22
2.2.2.8 Severe Acute Respiratory Syndrome Coronavirus 2 (SARS-CoV-2) 24
2.3 Aerosols Contaminants Transmission in Aircraft Cabins 30
2.4 Isolation and Control of Exposure to Biological Agents in Aircraft Cabins 36
Chapter 3 - Experimental Setup 43
3.1 Experimental Facility Description 44
3.1.1 Boeing 767 Mockup Cabin Description 44
3.1.1.1 Modified Cabin Description 53
3.1.2 Boeing 737 Section Cabin Description 57
3.1.3 Air Supply System Description 62

3.1.3.2.1 Boeing 767 Cabin 67
3.1.3.2.2 Modified Cabin 74
3.1.3.2.3 Boeing 737 Cabin 76
3.1.4 Tracer Gas Experimental Setup Description 78
3.1.4.1 Tracer Gas Injection System 78
3.1.4.1.1 Tracer Gas Injection System Description 78
3.1.4.1.2 CO2 and He Equilibrium 79
3.1.4.1.3 Mass Flow Controllers 81
3.1.4.1.4 Tracer Gas Control System 82
3.1.4.2 Tracer Gas Sampling System 83
3.1.4.2.1 CO2 Tracer Gas Analyzers 83
3.1.4.2.2 CO2 Tracer Gas Sampling Tree 90
3.2 Thermal Manikins 92
3.3 Coughing Manikin 93
Chapter 4 - Testing Procedures and Results 94
4.1 Aerosols Dispersion Tests 96
4.1.1 Continuous Injection Source Tests 96
4.1.1.1 Boeing 767 Cabin Mockup 96
4.1.1.2 Modified Cabin 101
4.1.1.3 Boeing 737 Cabin Section 102
4.1.2 Coughing Manikin Tests 104
4.1.2.1 Boeing 767 Cabin Mockup Coughing Manikin Tests 104
4.2 Aerosols Containment Tests 106
4.2.2 ISOPass Tests 109
4.2.2.1 Boeing 767 Cabin ISOPass Tests 109
4.2.2.1.1 ISOPass Deployed Coughing Tests 109
4.2.2.1.2 ISOPass Deployed Continuous Injection Source Tests 109
4.2.2.2 Boeing 737 Cabin ISOPass Tests 110
4.2.2.2.1 ISOPass Deployed Continuous Injection tests 110
4.3 Cabin Air Smoke Visualization 111
4.3.1 Equipment and Procedures 111

4.3.2 Smoke Visualization of Various Source Locations 115
4.4. Uncertainty Analysis 118
4.4.1 Uncertainty Analysis Approach: Root Sum Square (RSS) Method 118
4.4.2 Supply Air Uncertainty 121
4.4.3 Tracer Gas Injection Uncertainty 126
4.4.3 Tracer Gas Sampling Uncertainty 128
4.4.4 Overall Uncertainty 132
Chapter 5 - Analysis and Discussions 136
5.1 ISOPass Undeployed Tests Analysis 138
5.1.1 Continuous Tracer Gas Injection Tests 138
5.1.1.1 Boeing 767 Cabin Mockup 138
5.1.1.2 Modified Cabin 143
5.1.1.3 Boeing 737 Cabin Section 147
5.1.2 Coughing Manikin Tests 148
5.1.2.1 Boeing 767 Cabin Mockup 148
5.2 ISOPass deployed tests 153
5.2.1 Boeing 767 Cabin 153
5.2.2 Boeing 737 Cabin 154
Chapter 6 - Summary and Conclusions 156
References 160
Appendix A - T-Sections and Diffusers Locations on the PVC Ducts 171
Appendix B - Modified Cabin Design 181
Appendix B.1 Modified Cabin Diffusers Air Velocity Calculation 181
Appendix B.2 Modified Cabin Diffusers Air Velocity Measurements 182
Appendix C - Boeing 767 ISOPass Undeployed Continuous Injection Results 188
Appendix D - Boeing 767 ISOPass Deployed Continuous Injection Results 329
Appendix E - Modified Cabin ISOPass Undeployed Continuous Injection Results 336
Appendix F - Boeing 737 ISOPass Undeployed Continuous Injection Results 474
Appendix G - Boeing 737 ISOPass Deployed Continuous Injection Results 481
Appendix H - Boeing 767 ISOPass Undeployed Coughing Manikin Results 490
Appendix I - Boeing 767 ISOPass Deployed Coughing Manikin Results 681

Appendix J - Seat A6 Smoke Visualization Snapshots 803
J.1 Cross-sectional View 804
J.2 Frontal View 818
Appendix K - Seat D1 Smoke Visualization Snapshots 832
K.1 Cross-sectional View 833
K.2 Frontal View 847
Appendix L - Seat D6 Smoke Visualization Snapshots 860
L.1 Cross-sectional View 861
L.2 Frontal View 875
Appendix M - Seat D11 Smoke Visualization Snapshots 890
M.1 Cross-sectional View 891
M.2 Frontal View 905
Appendix N - Seat G6 Smoke Visualization Snapshots 919
N.1 Cross-sectional View 920
N.2 Frontal View 934
Appendix O - Analytical comparisons 948
Appendix P - List of Publications 952

List of Figures

Figure 1.1. Annual passengers on all United States scheduled airline flights (domestic & international) and foreign airline flights to and from the United States between 2003-2019 (Bureau of Transportation Statistics, 2020). 1
Figure 2.1. Passenger isolation system Darrah (2018). 39
Figure 2.2. Containerized bio-containment system inside a Boeing 747-400 aircraft (Cornelius et al., 2020). 40
Figure 2.3. Plastic sheeting installed at the back of a B747-400 aircraft (Cornelius et al., 2020). 41
Figure 3.1. An inside view of the ACER lab showing the Boeing 737 section and the Boeing 767 mockup enclosure. 43
Figure 3.2. Boeing 767 mockup cabin section layout and dimensinos. 45
Figure 3.3. Boeing 767 cabin cross section. 46
Figure 3.4. Hallways and crawl space below the Boeing 767 mockup cabin. 47
Figure 3.5. Boeing 767 mockup cabin interior. 48
Figure 3.6. Single seat dimensions in the Boeing 767 mockup cabin. 49
Figure 3.7. Two-seat section dimensions. 50
Figure 3.8. Three-seat section dimensions. 51
Figure 3.9. Inside view of the exhaust gaps in the Boeing 767 mockup. 52
Figure 3.10. Outside (hallway) view of the exhaust gaps in the Boeing 767 mockup. 52
Figure 3.11. Different supply air configurations in aircraft cabins. 53
Figure 3.12. A320 supply air configuration (Central American Corporation for Air Navigation Services, 2020). 54
Figure 3.13. A340 cabin cross-section with dimensions. 55
Figure 3.14. An inside view of the modified cabin. 56
Figure 3.15. Newly installed supply air diffusers inside the modified cabin. 56
Figure 3.16. Boeing 737 cabin section at the ACER lab. 57
Figure 3.17. Boeing 737 cross-section with dimensions in inch. 58
Figure 3.18. Boeing 737 cabin section layout and dimensinos. 59
Figure 3.19. Boeing 737 cabin section single seat dimensions. 60

Figure 3.20. Three-seat section dimensions in the Boeing 737 cabin. 61
Figure 3.21. Schematic flow diagram of the air conditioning system (Madden, 2015). 62
Figure 3.22. Air conditoning system setup at the ACER lab. 64
Figure 3.23. Gaspers blower and PVC ductwork. 65
Figure 3.24. Utilized LabVIEW software to control supply air. 66
Figure 3.25. Main supply air duct in the Boeing 767 mockup cabin and the 17 pairs connecting the supply duct to the linear diffusers. 68
Figure 3.26. A section of the actual salvaged Boeing 767 main supply air duct. 68
Figure 3.27. Dimensions of the main supply air duct of the Boeing 767 mockup in inch. 69
Figure 3.28. Supply hoses from the main supply duct located at the top to the linear diffusers at the bottom. 69
Figure 3.29. Top connections between the clear plastic hoses and the main supply duct. 70
Figure 3.30. Bottom connections between the clear plastic hoses and the main supply duct. 70
Figure 3.31. Inside view of the main supply duct. 71
Figure 3.32. Main air supply duct orffices. 71
Figure 3.33. Linear diffuser assembly for the Boeing 767 cabin mockup. 72
Figure 3.34. Inside view of the Boeing 767 cabin mockup showing the linear diffusers. 73
Figure 3.35. Modified cabin supply air configuration. 74
Figure 3.36. Supply air hoses connecting the main supply air duct to the newly installed top PVC ducts. 75
Figure 3.37. Supply air hoses connecting the main supply air duct to the newly installed bottom PVC ducts. 75
Figure 3.38. Linear diffusers and connectors on the Boeing 737 ceiling. 77
Figure 3.39. Ventilation grills at the Boeing 737 sidewalls. 78
Figure 3.40. Tracer gas injection system schematic. 79
Figure 3.41. Tracer gas injection tube. 80
Figure 3.42. Mass flow controllers with flow meters. 82
Figure 3.43. 2-channel power supply unit (Top) and Agilent 34970A DAQ (Bottom). 82
Figure 3.44. LabVIEW interface used to control different equipment. 83
Figure 3.45. WMA-4 gas analyzer. 84
Figure 3.46. WMA-5 gas analyzer. 84

Figure 3.47. Custom-made Edinburg Gascard gas analyzer. 85
Figure 3.48. Balancing system for the WMA-4 and custom-made Edinburg Gascard gas analyzers. 86
Figure 3.49. Calibration curve of gas analyzer A1. 87
Figure 3.50. Calibration curve of gas analyzer A2. 87
Figure 3.51. Calibration curve of gas analyzer A3. 88
Figure 3.52. Calibration curve of gas analyzer A4. 88
Figure 3.53. Calibration curve of gas analyzer A5. 89
Figure 3.54. Calibration curve of gas analyzer A6. 89
Figure 3.55. Tracer gas sampling tree with 4 sampling ports. 90
Figure 3.56. Thermal manikins inside the Boeing 767 mockup cabin. 92
Figure 3.57. Automated coughing manikin. 93
Figure 4.1. Sample of the figures showing the tracer gas source location and the sampling tree orientation in appendix C. 98
Figure 4.2. Sample of the figures showing the instantaneous tracer gas concentration at each sampling location versus experimental time in the figures in in appendix C. 99
Figure 4.3. Sample of the figures showing the tracer gas concentration at each sampling tree port versus experimental time in the figures in in appendix C. 100
Figure 4.4. Boeing 737 cabin section layout and dimsneions. 102
Figure 4.5. Exterior view of the ISOPass deployed in the Boeing 737 cabin section. 106
Figure 4.6. Interior view of the ISOPass deployed in the Boeing 737 cabin section. 107
Figure 4.7. Exterior view of the ISOPass deployed in the Boeing 767 cabin mockup. 107
Figure 4.8. ISOPass exhaust fan connected to the cabin wall in the Boeing 737 cabin section. 108
Figure 4.9. Grey 1.25-inch inner diameter hose connected to the smoke generation machine. 112
Figure 4.10. Tested 2-inch inner diameter unobstructed duct. 112
Figure 4.11. Tested 2-inch inner diameter duct obstructed with a sponge. 113
Figure 4.12. Tested 2-inch inner diameter duct obstructed with a honeycomb mesh. 113
Figure 4.13. Tested 8.5-inch inner diameter unobstructed bucket. 114
Figure 4.14. Selected design of the 8.5-inch inner diameter bucket covered with a sponge from the top. 114
Figure 4.15. Smoke visualization cross-sectional view 116

Figure 4.16. Smoke visualization frontal view 116
Figure 4.17. Smoke visualization cross-sectional view snapshot 117
Figure 4.18. Smoke visualization frontal view snapshot 117
Figure 4.19. Tracer gas sampling system..... 129
Figure 4.20. Uncertainty percentage of the tracer gas concentration increase above supply air concentration for each sampling location. 135
Figure 5.1. Breakdown of all the tests performed within this study. 136
Figure 5.2. Percentage increase in tracer gas concentration in different sampling locations above supply air concentration in the Boeing 767 cabin mockup. 142
Figure 5.3. Percentage increase in tracer gas concentration in different sampling locations above supply air concentration in the modified cabin. 145
Figure 5.4. Percentage increase in tracer gas concentration in different sampling locations above supply air concentration with the ISOPass undeployed in the Boeing 767 mockup cabin. 150
Figure 5.5. Percentage increase in tracer gas concentration in different sampling locations above supply air concentration with the ISOPass deployed in the Boeing 767 mockup cabin..... 154
Figure A.1 PVC ducts locations in the Boeing 767 cabin mockup 172
Figure A.2 T-sections locations (in inch) on the top right PVC duct. 173
Figure A.3 T-sections locations (in inch) on the top left PVC duct. 174
Figure A. 4 T-sections locations (in inch) on the bottom left PVC duct. 175
Figure A. 5 T-sections locations (in inch) on the bottom right PVC duct. 176
Figure A.6 Diffusers locations (in inch) on the top right PVC duct pipe. 177
Figure A.7 Diffusers locations (in inch) on the top left PVC duct pipe. 178
Figure A.8 Diffusers locations (in inch) on the bottom right PVC duct pipe. 179
Figure A. 9 Diffusers locations (in inch) on the bottom left PVC duct pipe. 180
Figure B.2. 1 Measured diffusers air velocity in the top right PVC duct. 183
Figure B.2. 2 Measured diffusers air velocity in the bottom right PVC duct. 184
Figure B.2. 3 Measured diffusers air velocity in the top left PVC duct. 185
Figure B.2. 4 Measured diffusers air velocity in the bottom left PVC duct. 186
Figure B.2.5 Main duct supply Air flowrate versus time. 187

Figure C.1 Seat D6 ISOPass undeployed continuous injection tracer gas test numbers and sampling tree orientations in the Boeing 767 cabin mockup. 189
Figure C.2 Seat G6 ISOPass undeployed continuous injection tracer gas test numbers and sampling tree orientations in the Boeing 767 cabin mockup. 190
Figure C.3 Seat D1 ISOPass undeployed continuous injection tracer gas test numbers and sampling tree orientations in the Boeing 767 cabin mockup. 191
Figure C.4 Seat D11 ISOPass undeployed continuous injection tracer gas test numbers and sampling tree orientations in the Boeing 767 cabin mockup. 192
Figure C.5 Test 3 (B-I) ISOPass undeployed source location and sampling tree orientation. ... 193
Figure C.6 Ininstantaneous CO_2 concentration at each sampling location for Test 3 (B-I) ISOPass undeployed. 194
Figure C.7 Average CO_2 concentration at each sampling location for Test 3 (B-I) ISOPass undeployed. 195
Figure C.8 Test 14 (B-I) ISOPass undeployed source location and sampling tree orientation. . 196
Figure C.9 Ininstantaneous CO_2 concentration at each sampling location for Test 14 (B-I) ISOPass undeployed. 197
Figure C.10 Average CO_2 concentration at each sampling location for Test 14 (B-I) ISOPass undeployed. 198
Figure C.11 Test 4 (B-I) ISOPass undeployed source location and sampling tree orientation. . 199
Figure C.12 Ininstantaneous CO_2 concentration at each sampling location for Test 4 (B-I) ISOPass undeployed. 200
Figure C.13 Average CO_2 concentration at each sampling location for Test 4 (B-I) ISOPass undeployed. 201
Figure C.14 Test 10 (B-I) ISOPass undeployed source location and sampling tree orientation. 202
Figure C.15 Ininstantaneous CO_2 concentration at each sampling location for Test 10 (B-I) ISOPass undeployed. 203
Figure C.16 Average CO_2 concentration at each sampling location for Test 10 (B-I) ISOPass undeployed. 204
Figure C.17 Test 5 (B-I) ISOPass undeployed source location and sampling tree orientation. . 205
Figure C.18 Ininstantaneous CO_2 concentration at each sampling location for Test 5 (B-I) ISOPass undeployed. 206

Figure C.19 Average CO_2 concentration at each sampling location for Test 5 (B-I) ISOPass undeployed. 207
Figure C.20 Test 12 (B-I) ISOPass undeployed source location and sampling tree orientation. 208
Figure C.21 Ininstantaneous CO_2 concentration at each sampling location for Test 12 (B-I) ISOPass undeployed. 209
Figure C.22 Average CO_2 concentration at each sampling location for Test 12 (B-I) ISOPass undeployed. 210
Figure C.23 Test 25 (B-I) ISOPass undeployed source location and sampling tree orientation. 211
Figure C.24 Ininstantaneous CO_2 concentration at each sampling location for Test 25 (B-I) ISOPass undeployed. 212
Figure C.25 Average CO_2 concentration at each sampling location for Test 25 (B-I) ISOPass undeployed. 213
Figure C.26 Test 16 (B-I) ISOPass undeployed source location and sampling tree orientation. 214
Figure C.27 Ininstantaneous CO_2 concentration at each sampling location for Test 16 (B-I) ISOPass undeployed. 215
Figure C.28 Average CO_2 concentration at each sampling location for Test 16 (B-I) ISOPass undeployed. 216
Figure C.29 Test 7 (B-I) ISOPass undeployed source location and sampling tree orientation. . 217
Figure C.30 Ininstantaneous CO_2 concentration at each sampling location for Test 7 (B-I) ISOPass undeployed. 218
Figure C.31 Average CO_2 concentration at each sampling location for Test 7 (B-I) ISOPass undeployed. 219
Figure C.32 Test 13 (B-I) ISOPass undeployed source location and sampling tree orientation. 220
Figure C.33 Ininstantaneous CO_2 concentration at each sampling location for Test 13 (B-I) ISOPass undeployed. 221
Figure C.34 Average CO_2 concentration at each sampling location for Test 13 (B-I) ISOPass undeployed. 222
Figure C.35 Test 17 (B-I) ISOPass undeployed source location and sampling tree orientation. 223
Figure C.36 Ininstantaneous CO_2 concentration at each sampling location for Test 17 (B-I) ISOPass undeployed. 224

Figure C.37 Average CO_2 concentration at each sampling location for Test 17 (B-I) ISOPass undeployed. 225
Figure C.38 Test 22 (B-I) ISOPass undeployed source location and sampling tree orientation. 226
Figure C.39 Ininstantaneous CO_2 concentration at each sampling location for Test 22 (B-I) ISOPass undeployed. 227
Figure C.40 Average CO_2 concentration at each sampling location for Test 22 (B-I) ISOPass undeployed. 228
Figure C.41 Test 18 (B-I) ISOPass undeployed source location and sampling tree orientation. 229
Figure C.42 Ininstantaneous CO_2 concentration at each sampling location for Test 18 (B-I) ISOPass undeployed. 230
Figure C.43 Average CO_2 concentration at each sampling location for Test 18 (B-I) ISOPass undeployed. 231
Figure C.44 Test 21 (B-I) ISOPass undeployed source location and sampling tree orientation. 232
Figure C.45 Ininstantaneous CO_2 concentration at each sampling location for Test 21 (B-I) ISOPass undeployed. 233
Figure C.46 Average CO_2 concentration at each sampling location for Test 21 (B-I) ISOPass undeployed. 234
Figure C.47 Test 19 (B-I) ISOPass undeployed source location and sampling tree orientation. 235
Figure C.48 Ininstantaneous CO_2 concentration at each sampling location for Test 19 (B-I) ISOPass undeployed. 236
Figure C.49 Average CO_2 concentration at each sampling location for Test 19 (B-I) ISOPass undeployed. 237
Figure C.50 Test 20 (B-I) ISOPass undeployed source location and sampling tree orientation. 238
Figure C.51 Ininstantaneous CO_2 concentration at each sampling location for Test 20 (B-I) ISOPass undeployed. 239
Figure C.52 Average CO_2 concentration at each sampling location for Test 20 (B-I) ISOPass undeployed. 240
Figure C.53 Test 23 (B-I) ISOPass undeployed source location and sampling tree orientation. 241
Figure C.54 Ininstantaneous CO_2 concentration at each sampling location for Test 23 (B-I) ISOPass undeployed. 242

Figure C.55 Average CO_2 concentration at each sampling location for Test 23 (B-I) ISOPass undeployed. 243
Figure C.56 Test 24 (B-I) ISOPass undeployed source location and sampling tree orientation. 244
Figure C.57 Ininstantaneous CO_2 concentration at each sampling location for Test 24 (B-I) ISOPass undeployed. 245
Figure C.58 Average CO_2 concentration at each sampling location for Test 24 (B-I) ISOPass undeployed. 246
Figure C.59 Test 26 (B-I) ISOPass undeployed source location and sampling tree orientation. 247
Figure C.60 Ininstantaneous CO_2 concentration at each sampling location for Test 26 (B-I) ISOPass undeployed. 248
Figure C.61 Average CO_2 concentration at each sampling location for Test 26 (B-I) ISOPass undeployed. 249
Figure C.62 Test 27 (B-I) ISOPass undeployed source location and sampling tree orientation. 250
Figure C.63 Ininstantaneous CO_2 concentration at each sampling location for Test 27 (B-I) ISOPass undeployed. 251
Figure C.64 Average CO_2 concentration at each sampling location for Test 27 (B-I) ISOPass undeployed. 252
Figure C.65 Test 28 (B-I) ISOPass undeployed source location and sampling tree orientation. 253
Figure C.66 Ininstantaneous CO_2 concentration at each sampling location for Test 28 (B-I) ISOPass undeployed. 254
Figure C.67 Average CO_2 concentration at each sampling location for Test 28 (B-I) ISOPass undeployed. 255
Figure C.68 Test 29 (B-I) ISOPass undeployed source location and sampling tree orientation. 256
Figure C.69 Ininstantaneous CO_2 concentration at each sampling location for Test 29 (B-I) ISOPass undeployed. 257
Figure C.70 Average CO_2 concentration at each sampling location for Test 29 (B-I) ISOPass undeployed. 258
Figure C.71 Test 30 (B-I) ISOPass undeployed source location and sampling tree orientation. 259
Figure C.72 Ininstantaneous CO_2 concentration at each sampling location for Test 30 (B-I) ISOPass undeployed. 260

Figure C.73 Average CO_2 concentration at each sampling location for Test 30 (B-I) ISOPass undeployed. 261
Figure C.74 Test 31 (B-I) ISOPass undeployed source location and sampling tree orientation. 262
Figure C.75 Ininstantaneous CO_2 concentration at each sampling location for Test 31 (B-I) ISOPass undeployed. 263
Figure C.76 Average CO_2 concentration at each sampling location for Test 31 (B-I) ISOPass undeployed. 264
Figure C.77 Test 32 (B-I) ISOPass undeployed source location and sampling tree orientation. 265
Figure C.78 Ininstantaneous CO_2 concentration at each sampling location for Test 32 (B-I) ISOPass undeployed. 266
Figure C.79 Average CO_2 concentration at each sampling location for Test 32 (B-I) ISOPass undeployed. 267
Figure C.80 Test 33 (B-I) ISOPass undeployed source location and sampling tree orientation. 268
Figure C.81 Ininstantaneous CO_2 concentration at each sampling location for Test 33 (B-I) ISOPass undeployed. 269
Figure C.82 Average CO_2 concentration at each sampling location for Test 33 (B-I) ISOPass undeployed. 270
Figure C.83 Test 34 (B-I) ISOPass undeployed source location and sampling tree orientation. 271
Figure C.84 Ininstantaneous CO_2 concentration at each sampling location for Test 34 (B-I) ISOPass undeployed. 272
Figure C.85 Average CO_2 concentration at each sampling location for Test 34 (B-I) ISOPass undeployed. 273
Figure C.86 Test 35 (B-I) ISOPass undeployed source location and sampling tree orientation. 274
Figure C.87 Ininstantaneous CO_2 concentration at each sampling location for Test 35 (B-I) ISOPass undeployed. 275
Figure C.88 Average CO_2 concentration at each sampling location for Test 35 (B-I) ISOPass undeployed. 276
Figure C.89 Test 36 (B-I) ISOPass undeployed source location and sampling tree orientation. 277
Figure C.90 Ininstantaneous CO_2 concentration at each sampling location for Test 36 (B-I) ISOPass undeployed. 278

Figure C.91 Average CO_2 concentration at each sampling location for Test 36 (B-I) ISOPass undeployed. 279
Figure C.92 Test 37 (B-I) ISOPass undeployed source location and sampling tree orientation. 280
Figure C.93 Ininstantaneous CO_2 concentration at each sampling location for Test 37 (B-I) ISOPass undeployed. 281
Figure C.94 Average CO_2 concentration at each sampling location for Test 37 (B-I) ISOPass undeployed. 282
Figure C.95 Test 38 (B-I) ISOPass undeployed source location and sampling tree orientation. 283
Figure C.96 Ininstantaneous CO_2 concentration at each sampling location for Test 38 (B-I) ISOPass undeployed. 284
Figure C.97 Average CO_2 concentration at each sampling location for Test 38 (B-I) ISOPass undeployed. 285
Figure C.98 Test 42 (B-I) ISOPass undeployed source location and sampling tree orientation. 286
Figure C.99 Ininstantaneous CO_2 concentration at each sampling location for Test 42 (B-I) ISOPass undeployed. 287
Figure C.100 Average CO_2 concentration at each sampling location for Test 42 (B-I) ISOPass undeployed. 288
Figure C.101 Test 45 (B-I) ISOPass undeployed source location and sampling tree orientation. 289
Figure C.102 Ininstantaneous CO_2 concentration at each sampling location for Test 45 (B-I) ISOPass undeployed. 290
Figure C.103 Average CO_2 concentration at each sampling location for Test 45 (B-I) ISOPass undeployed. 291
Figure C.104 Test 46 (B-I) ISOPass undeployed source location and sampling tree orientation. 292
Figure C.105 Ininstantaneous CO_2 concentration at each sampling location for Test 46 (B-I) ISOPass undeployed. 293
Figure C.106 Average CO_2 concentration at each sampling location for Test 46 (B-I) ISOPass undeployed. 294
Figure C.107 Test 47 (B-I) ISOPass undeployed source location and sampling tree orientation. 295

Figure C.108 Ininstantaneous CO_2 concentration at each sampling location for Test 47 (B-I) ISOPass undeployed. 296
Figure C.109 Average CO_2 concentration at each sampling location for Test 47 (B-I) ISOPass undeployed. 297
Figure C.110 Test 48 (B-I) ISOPass undeployed source location and sampling tree orientation. 298
Figure C.111 Ininstantaneous CO_2 concentration at each sampling location for Test 48 (B-I) ISOPass undeployed. 299
Figure C.112 Average CO_2 concentration at each sampling location for Test 48 (B-I) ISOPass undeployed. 300
Figure C.113 Test 51 (B-I) ISOPass undeployed source location and sampling tree orientation. 301
Figure C.114 Ininstantaneous CO_2 concentration at each sampling location for Test 51 (B-I) ISOPass undeployed. 302
Figure C.115 Average CO_2 concentration at each sampling location for Test 51 (B-I) ISOPass undeployed. 303
Figure C.116 Test 52 (B-I) ISOPass undeployed source location and sampling tree orientation. 304
Figure C.117 Ininstantaneous CO_2 concentration at each sampling location for Test 52 (B-I) ISOPass undeployed. 305
Figure C.118 Average CO_2 concentration at each sampling location for Test 52 (B-I) ISOPass undeployed. 306
Figure C.119 Test 53 (B-I) ISOPass undeployed source location and sampling tree orientation. 307
Figure C.120 Ininstantaneous CO_2 concentration at each sampling location for Test 53 (B-I) ISOPass undeployed. 308
Figure C.121 Average CO_2 concentration at each sampling location for Test 53 (B-I) ISOPass undeployed. 309
Figure C.122 Test 54 (B-I) ISOPass undeployed source location and sampling tree orientation. 310

Figure C.123 Ininstantaneous CO_2 concentration at each sampling location for Test 54 (B-I) ISOPass undeployed. 311
Figure C.124 Average CO_2 concentration at each sampling location for Test 54 (B-I) ISOPass undeployed. 312
Figure C.125 Test 55 (B-I) ISOPass undeployed source location and sampling tree orientation. 313
Figure C.126 Ininstantaneous CO_2 concentration at each sampling location for Test 55 (B-I) ISOPass undeployed. 314
Figure C.127 Average CO_2 concentration at each sampling location for Test 55 (B-I) ISOPass undeployed. 315
Figure C.128 Seat D6 continuous injection source tests in the Boeing 767 cabin mockup with the ISOPass undeployed. 316
Figure C.129 Seat G6 continuous injection source tests in the Boeing 767 cabin mockup with the ISOPass undeployed. 317
Figure C.130 Seat D1 continuous injection source tests in the Boeing 767 cabin mockup with the ISOPass undeployed. 318
Figure C.131 Seat D11 continuous injection source tests in the Boeing 767 cabin mockup with the ISOPass undeployed. 319
Figure C.132 Diagonal front left sampling tree orientation tests in the Boeing 767 cabin mockup with the ISOPass undeployed. 320
Figure C.133 Longitudinal front sampling tree orientation tests in the Boeing 767 cabin mockup with the ISOPass undeployed. 321
Figure C.134 Longitudinal rear sampling tree orientation tests in the Boeing 767 cabin mockup with the ISOPass undeployed. 322
Figure C.135 Diagonal front right sampling tree orientation tests in the Boeing 767 cabin mockup with the ISOPass undeployed. 323
Figure C.136 Lateral sampling tree orientation tests in the Boeing 767 cabin mockup with the ISOPass undeployed. 324
Figure C.137 Diagonal rear left sampling tree orientation tests in the Boeing 767 cabin mockup with the ISOPass undeployed. 325

Figure C.138 Diagonal rear right sampling tree orientation tests in the Boeing 767 cabin mockup with the ISOPass undeployed. 326
Figure C.139 Boeing 767 mockup cabin continuous injection source tests with the ISOPass undeployed. 327
Figure C.140 Boeing 767 mockup cabin continuous injection source tests with the ISOPass undeployed, Absolute distances from the source. 328
Figure D.1 Test 1 (B-I) ISOPass deployed source location and sampling tree orientation. 330
Figure D.2 Ininstantaneous CO_2 concentration at each sampling location for Test 1 (B-I) ISOPass deployed. 331
Figure D.3 Test 2 (B-I) ISOPass deployed source location and sampling tree orientation. 332
Figure D.4 Ininstantaneous CO_2 concentration at each sampling location for Test 2 (B-I) ISOPass deployed. 333
Figure D.5 Test 3 (B-I) ISOPass deployed source location and sampling tree orientation. 334
Figure D.6 Ininstantaneous CO_2 concentration at each sampling location for Test 3 (B-I) ISOPass deployed. 335
Figure E.1 Seat D6 ISOPass undeployed continuous injection tracer gas test numbers and sampling tree orientations in the modified cabin mockup. 337
Figure E.2 Seat G6 ISOPass undeployed continuous injection tracer gas test numbers and sampling tree orientations in the modified cabin mockup. 338
Figure E.3 Seat D1 ISOPass undeployed continuous injection tracer gas test numbers and sampling tree orientations in the modified cabin mockup. 339
Figure E.4 Seat D11 ISOPass undeployed continuous injection tracer gas test numbers and sampling tree orientations in the modified cabin mockup. 340
Figure E.5 Test 5 (A-I) ISOPass undeployed source location and sampling tree orientation. ... 341
Figure E.6 Ininstantaneous CO_2 concentration at each sampling location for Test 5 (A-I) ISOPass undeployed. 342
Figure E.7 Average CO_2 concentration at each sampling location for Test 5 (A-I) ISOPass undeployed. 343
Figure E.8 Test 6 (A-I) ISOPass undeployed source location and sampling tree orientation. ... 344

Figure E.9 Ininstantaneous CO_2 concentration at each sampling location for Test 6 (A-I) ISOPass undeployed. 345
Figure E.10 Average CO_2 concentration at each sampling location for Test 6 (A-I) ISOPass undeployed. 346
Figure E.11 Test 7 (A-I) ISOPass undeployed source location and sampling tree orientation. . 347
Figure E.12 Ininstantaneous CO_2 concentration at each sampling location for Test 7 (A-I) ISOPass undeployed. 348
Figure E.13 Average CO_2 concentration at each sampling location for Test 7 (A-I) ISOPass undeployed. 349
Figure E.14 Test 8 (A-I) ISOPass undeployed source location and sampling tree orientation. . 350
Figure E.15 Ininstantaneous CO_2 concentration at each sampling location for Test 8 (A-I) ISOPass undeployed. 351
Figure E.16 Average CO_2 concentration at each sampling location for Test 8 (A-I) ISOPass undeployed. 352
Figure E.17 Test 9 (A-I) ISOPass undeployed source location and sampling tree orientation. . 353
Figure E.18 Ininstantaneous CO_2 concentration at each sampling location for Test 9 (A-I) ISOPass undeployed. 354
Figure E.19 Average CO_2 concentration at each sampling location for Test 9 (A-I) ISOPass undeployed. 355
Figure E.20 Test 10 (A-I) ISOPass undeployed source location and sampling tree orientation. 356
Figure E.21 Ininstantaneous CO_2 concentration at each sampling location for Test 10 (A-I) ISOPass undeployed. 357
Figure E.22 Average CO_2 concentration at each sampling location for Test 10 (A-I) ISOPass undeployed. 358
Figure E.23 Test 21 (A-I) ISOPass undeployed source location and sampling tree orientation. 359
Figure E.24 Ininstantaneous CO_2 concentration at each sampling location for Test 21 (A-I) ISOPass undeployed. 360
Figure E.25 Average CO_2 concentration at each sampling location for Test 21 (A-I) ISOPass undeployed. 361
Figure E.26 Test 22 (A-I) ISOPass undeployed source location and sampling tree orientation. 362

Figure E.27 Ininstantaneous CO_2 concentration at each sampling location for Test 22 (A-I) ISOPass undeployed. 363
Figure E.28 Average CO_2 concentration at each sampling location for Test 22 (A-I) ISOPass undeployed. 364
Figure E.29 Test 27 (A-I) ISOPass undeployed source location and sampling tree orientation. 365
Figure E.30 Ininstantaneous CO_2 concentration at each sampling location for Test 27 (A-I) ISOPass undeployed. 366
Figure E.31 Average CO_2 concentration at each sampling location for Test 27 (A-I) ISOPass undeployed. 367
Figure E.32 Test 28 (A-I) ISOPass undeployed source location and sampling tree orientation. 368
Figure E.33 Ininstantaneous CO_2 concentration at each sampling location for Test 28 (A-I) ISOPass undeployed. 369
Figure E.34 Average CO_2 concentration at each sampling location for Test 28 (A-I) ISOPass undeployed. 370
Figure E.35 Test 29 (A-I) ISOPass undeployed source location and sampling tree orientation. 371
Figure E.36 Ininstantaneous CO_2 concentration at each sampling location for Test 29 (A-I) ISOPass undeployed. 372
Figure E.37 Average CO_2 concentration at each sampling location for Test 29 (A-I) ISOPass undeployed. 373
Figure E.38 Test 30 (A-I) ISOPass undeployed source location and sampling tree orientation. 374
Figure E.39 Ininstantaneous CO_2 concentration at each sampling location for Test 30 (A-I) ISOPass undeployed. 375
Figure E.40 Average CO_2 concentration at each sampling location for Test 30 (A-I) ISOPass undeployed. 376
Figure E.41 Test 31 (A-I) ISOPass undeployed source location and sampling tree orientation. 377
Figure E.42 Ininstantaneous CO_2 concentration at each sampling location for Test 31 (A-I) ISOPass undeployed. 378
Figure E.43 Average CO_2 concentration at each sampling location for Test 31 (A-I) ISOPass undeployed. 379
Figure E.44 Test 32 (A-I) ISOPass undeployed source location and sampling tree orientation. 380

Figure E.45 Ininstantaneous CO_2 concentration at each sampling location for Test 32 (A-I) ISOPass undeployed. 381
Figure E.46 Average CO_2 concentration at each sampling location for Test 32 (A-I) ISOPass undeployed. 382
Figure E.47 Test 1 (A-I) ISOPass undeployed source location and sampling tree orientation. . 383
Figure E.48 Ininstantaneous CO_2 concentration at each sampling location for Test 1 (A-I) ISOPass undeployed. 384
Figure E.49 Average CO_2 concentration at each sampling location for Test 1 (A-I) ISOPass undeployed. 385
Figure E.50 Test 2 (A-I) ISOPass undeployed source location and sampling tree orientation. . 386
Figure E.51 Ininstantaneous CO_2 concentration at each sampling location for Test 2 (A-I) ISOPass undeployed. 387
Figure E.52 Average CO_2 concentration at each sampling location for Test 2 (A-I) ISOPass undeployed. 388
Figure E.53 Test 3 (A-I) ISOPass undeployed source location and sampling tree orientation. . 389
Figure E.54 Ininstantaneous CO_2 concentration at each sampling location for Test 3 (A-I) ISOPass undeployed. 390
Figure E.55 Average CO_2 concentration at each sampling location for Test 3 (A-I) ISOPass undeployed. 391
Figure E.56 Test 4 (A-I) ISOPass undeployed source location and sampling tree orientation. . 392
Figure E.57 Ininstantaneous CO_2 concentration at each sampling location for Test 4 (A-I) ISOPass undeployed. 393
Figure E.58 Average CO_2 concentration at each sampling location for Test 4 (A-I) ISOPass undeployed. 394
Figure E.59 Test 19 (A-I) ISOPass undeployed source location and sampling tree orientation. 395
Figure E.60 Ininstantaneous CO_2 concentration at each sampling location for Test 19 (A-I) ISOPass undeployed. 396
Figure E.61 Average CO_2 concentration at each sampling location for Test 19 (A-I) ISOPass undeployed. 397
Figure E.62 Test 19 (A-I) ISOPass undeployed source location and sampling tree orientation. 398

Figure E.63 Ininstantaneous CO_2 concentration at each sampling location for Test 19 (A-I) ISOPass undeployed. 399
Figure E.64 Average CO_2 concentration at each sampling location for Test 19 (A-I) ISOPass undeployed. 400
Figure E.65 Test 23 (A-I) ISOPass undeployed source location and sampling tree orientation. 401
Figure E.66 Ininstantaneous CO_2 concentration at each sampling location for Test 23 (A-I) ISOPass undeployed. 402
Figure E.67 Average CO_2 concentration at each sampling location for Test 23 (A-I) ISOPass undeployed. 403
Figure E.68 Test 24 (A-I) ISOPass undeployed source location and sampling tree orientation. 404
Figure E.69 Ininstantaneous CO_2 concentration at each sampling location for Test 24 (A-I) ISOPass undeployed. 405
Figure E.70 Average CO_2 concentration at each sampling location for Test 24 (A-I) ISOPass undeployed. 406
Figure E.71 Test 25 (A-I) ISOPass undeployed source location and sampling tree orientation. 407
Figure E.72 Ininstantaneous CO_2 concentration at each sampling location for Test 25 (A-I) ISOPass undeployed. 408
Figure E.73 Average CO_2 concentration at each sampling location for Test 25 (A-I) ISOPass undeployed. 409
Figure E.74 Test 26 (A-I) ISOPass undeployed source location and sampling tree orientation. 410
Figure E.75 Ininstantaneous CO_2 concentration at each sampling location for Test 26 (A-I) ISOPass undeployed. 411
Figure E.76 Average CO_2 concentration at each sampling location for Test 26 (A-I) ISOPass undeployed. 412
Figure E.77 Test 11 (A-I) ISOPass undeployed source location and sampling tree orientation. 413
Figure E.78 Ininstantaneous CO_2 concentration at each sampling location for Test 11 (A-I) ISOPass undeployed. 414
Figure E.79 Average CO_2 concentration at each sampling location for Test 11 (A-I) ISOPass undeployed. 415
Figure E. 80 Test 12 (A-I) ISOPass undeployed source location and sampling tree orientation. 416

Figure E.81 Ininstantaneous CO_2 concentration at each sampling location for Test 12 (A-I) ISOPass undeployed. 417
Figure E.82 Average CO_2 concentration at each sampling location for Test 12 (A-I) ISOPass undeployed. 418
Figure E.83 Test 13 (A-I) ISOPass undeployed source location and sampling tree orientation. 419
Figure E.84 Ininstantaneous CO_2 concentration at each sampling location for Test 13 (A-I) ISOPass undeployed. 420
Figure E.85 Average CO_2 concentration at each sampling location for Test 13 (A-I) ISOPass undeployed. 421
Figure E.86 Test 14 (A-I) ISOPass undeployed source location and sampling tree orientation. 422
Figure E.87 Ininstantaneous CO_2 concentration at each sampling location for Test 14 (A-I) ISOPass undeployed. 423
Figure E.88 Average CO_2 concentration at each sampling location for Test 14 (A-I) ISOPass undeployed. 424
Figure E.89 Test 15 (A-I) ISOPass undeployed source location and sampling tree orientation. 425
Figure E.90 Ininstantaneous CO_2 concentration at each sampling location for Test 15 (A-I) ISOPass undeployed. 426
Figure E.91 Average CO_2 concentration at each sampling location for Test 15 (A-I) ISOPass undeployed. 427
Figure E.92 Test 16 (A-I) ISOPass undeployed source location and sampling tree orientation. 428
Figure E.93 Ininstantaneous CO_2 concentration at each sampling location for Test 16 (A-I) ISOPass undeployed. 429
Figure E.94 Average CO_2 concentration at each sampling location for Test 16 (A-I) ISOPass undeployed. 430
Figure E.95 Test 17 (A-I) ISOPass undeployed source location and sampling tree orientation. 431
Figure E.96 Ininstantaneous CO_2 concentration at each sampling location for Test 17 (A-I) ISOPass undeployed. 432
Figure E.97 Average CO_2 concentration at each sampling location for Test 17 (A-I) ISOPass undeployed. 433
Figure E.98 Test 18 (A-I) ISOPass undeployed source location and sampling tree orientation. 434

Figure E.99 Ininstantaneous CO_2 concentration at each sampling location for Test 18 (A-I) ISOPass undeployed. 435
Figure E.100 Average CO_2 concentration at each sampling location for Test 18 (A-I) ISOPass undeployed. 436
Figure E.101 Test 33 (A-I) ISOPass undeployed source location and sampling tree orientation. 437
Figure E.102 Ininstantaneous CO_2 concentration at each sampling location for Test 33 (A-I) ISOPass undeployed. 438
Figure E.103 Average CO_2 concentration at each sampling location for Test 33 (A-I) ISOPass undeployed. 439
Figure E.104 Test 34 (A-I) ISOPass undeployed source location and sampling tree orientation. 440
Figure E.105 Ininstantaneous CO_2 concentration at each sampling location for Test 34 (A-I) ISOPass undeployed. 441
Figure E.106 Average CO_2 concentration at each sampling location for Test 34 (A-I) ISOPass undeployed. 442
Figure E.107 Test 35 (A-I) ISOPass undeployed source location and sampling tree orientation. 443
Figure E.108 Ininstantaneous CO_2 concentration at each sampling location for Test 35 (A-I) ISOPass undeployed. 444
Figure E.109 Average CO_2 concentration at each sampling location for Test 35 (A-I) ISOPass undeployed. 445
Figure E.110 Test 36 (A-I) ISOPass undeployed source location and sampling tree orientation. 446
Figure E.111 Ininstantaneous CO_2 concentration at each sampling location for Test 36 (A-I) ISOPass undeployed. 447
Figure E.112 Average CO_2 concentration at each sampling location for Test 36 (A-I) ISOPass undeployed. 448
Figure E.113 Test 37 (A-I) ISOPass undeployed source location and sampling tree orientation. 449

Figure E.114 Ininstantaneous CO_2 concentration at each sampling location for Test 37 (A-I) ISOPass undeployed. 450
Figure E.115 Average CO_2 concentration at each sampling location for Test 37 (A-I) ISOPass undeployed. 451
Figure E.116 Test 38 (A-I) ISOPass undeployed source location and sampling tree orientation. 452
Figure E.117 Ininstantaneous CO_2 concentration at each sampling location for Test 38 (A-I) ISOPass undeployed. 453
Figure E.118 Average CO_2 concentration at each sampling location for Test 38 (A-I) ISOPass undeployed. 454
Figure E.119 Test 39 (A-I) ISOPass undeployed source location and sampling tree orientation. 455
Figure E.120 Ininstantaneous CO_2 concentration at each sampling location for Test 39 (A-I) ISOPass undeployed. 456
Figure E.121 Average CO_2 concentration at each sampling location for Test 39 (A-I) ISOPass undeployed. 457
Figure E.122 Test 40 (A-I) ISOPass undeployed source location and sampling tree orientation. 458
Figure E.123 Ininstantaneous CO_2 concentration at each sampling location for Test 40 (A-I) ISOPass undeployed. 459
Figure E.124 Average CO_2 concentration at each sampling location for Test 40 (A-I) ISOPass undeployed. 460
Figure E.125 Seat D6 continuous injection source tests in the modified cabin with the ISOPass undeployed. 461
Figure E.126 Seat G6 continuous injection source tests in the modified cabin with the ISOPass undeployed. 462
Figure E.127 Seat D1 continuous injection source tests in the modified cabin with the ISOPass undeployed. 463
Figure E.128 Seat D11 continuous injection source tests in the modified cabin with the ISOPass undeployed. 464

Figure E.129 Diagonal front left sampling tree orientation tests in the modified cabin with the ISOPass undeployed. 465
Figure E.130 Longitudinal front sampling tree orientation tests in the modified cabin with the ISOPass undeployed. 466
Figure E.131 Longitudinal rear sampling tree orientation tests in the modified cabin with the ISOPass undeployed. 467
Figure E.132 Diagonal front right sampling tree orientation tests in the modified cabin with the ISOPass undeployed. 468
Figure E.133 Lateral sampling tree orientation tests in the modified cabin with the ISOPass undeployed. 469
Figure E.134 Diagonal rear left sampling tree orientation tests in the modified cabin with the ISOPass undeployed. 470
Figure E.135 Diagonal rear right sampling tree orientation tests in the modified cabin with the ISOPass undeployed. 471
Figure E.136 Modified cabin continuous injection source tests with the ISOPass undeployed. 472
Figure E.137 Modified cabin continuous injection source tests with the ISOPass undeployed, Absolute distances from the source. 473
Figure F.1 Seat B4 ISOPass undeployed Test 1 (C-I) continuous injection tracer gas source and gas analyzers locations in the Boeing 737 cabin section. 475
Figure F.2 Ininstantaneous CO_2 concentration at each sampling location for Test 1 (C-I) ISOPass undeployed. 476
Figure F.3 Seat B4 ISOPass undeployed Test 2 (C-I) continuous injection tracer gas source and gas analyzers locations in the Boeing 737 cabin section. 477
Figure F.4 Ininstantaneous CO_2 concentration at each sampling location for Test 2 (C-I) ISOPass undeployed. 478
Figure F.5 Seat B4 ISOPass undeployed Test 3 (C-I) continuous injection tracer gas source and gas analyzers locations in the Boeing 737 cabin section. 479
Figure F.6 Ininstantaneous CO_2 concentration at each sampling location for Test 3 (C-I) ISOPass undeployed. 480

Figure G.1 Seat B4 ISOPass deployed Test 4 (C-I) continuous injection tracer gas source and gas analyzers locations in the Boeing 737 cabin section. 482
Figure G.2 Ininstantaneous CO_2 concentration at each sampling location for Test 4 (C-I) ISOPass deployed. 483
Figure G.3 Seat B4 ISOPass deployed Test 5 (C-I) continuous injection tracer gas source and gas analyzers locations in the Boeing 737 cabin section. 484
Figure G.4 Ininstantaneous CO_2 concentration at each sampling location for Test 5 (C-I) ISOPass deployed. 485
Figure G.5 Seat B4 ISOPass deployed Test 6 (C-I) continuous injection tracer gas source and gas analyzers locations in the Boeing 737 cabin section. 486
Figure G.6 Ininstantaneous CO_2 concentration at each sampling location for Test 6 (C-I) ISOPass deployed. 487
Figure G.7 Seat B4 ISOPass deployed Test 7 (C-I) continuous injection tracer gas source and gas analyzers locations in the Boeing 737 cabin section. 488
Figure G.8 Ininstantaneous CO_2 concentration at each sampling location for Test 7 (C-I) ISOPass deployed. 489
Figure H.1 Seat G6 ISOPass undeployed coughing manikin tracer gas test numbers and sampling tree orientations in the Boeing 767 cabin mockup. 491
Figure H.2 Seat F6 ISOPass undeployed coughing manikin tracer gas test numbers and sampling tree orientations in the Boeing 767 cabin mockup. 492
Figure H.3 Seat D6 ISOPass undeployed coughing manikin tracer gas test numbers and sampling tree orientations in the Boeing 767 cabin mockup. 493
Figure H.4 Seat A6 ISOPass undeployed coughing manikin tracer gas test numbers and sampling tree orientations in the Boeing 767 cabin mockup. 494
Figure H.5 Seat B6 ISOPass undeployed coughing manikin tracer gas test numbers and sampling tree orientations in the Boeing 767 cabin mockup. 495
Figure H.6 Test 1 (B-M) ISOPass undeployed source location and sampling tree orientation.. 496
Figure H.7 Ininstantaneous CO_2 concentration at each sampling location for Test 1 (B-M) ISOPass undeployed. 497

Figure H.8 Average CO_2 concentration at each sampling location for Test 1 (B-M) ISOPass undeployed. 498
Figure H.9 Test 2 (B-M) ISOPass undeployed source location and sampling tree orientation.. 499
Figure H.10 Ininstantaneous CO_2 concentration at each sampling location for Test 2 (B-M) ISOPass undeployed. 500
Figure H.11 Average CO_2 concentration at each sampling location for Test 2 (B-M) ISOPass undeployed. 501
Figure H.12 Test 3 (B-M) ISOPass undeployed source location and sampling tree orientation.502
Figure H.13 Ininstantaneous CO_2 concentration at each sampling location for Test 3 (B-M) ISOPass undeployed. 503
Figure H.14 Average CO_2 concentration at each sampling location for Test 3 (B-M) ISOPass undeployed. 504
Figure H.15 Test 4 (B-M) ISOPass undeployed source location and sampling tree orientation.505
Figure H.16 Ininstantaneous CO_2 concentration at each sampling location for Test 4 (B-M) ISOPass undeployed. 506
Figure H.17 Average CO_2 concentration at each sampling location for Test 4 (B-M) ISOPass undeployed. 507
Figure H.18 Test 5 (B-M) ISOPass undeployed source location and sampling tree orientation.508
Figure H.19 Ininstantaneous CO_2 concentration at each sampling location for Test 5 (B-M) ISOPass undeployed. 509
Figure H.20 Average CO_2 concentration at each sampling location for Test 5 (B-M) ISOPass undeployed. 510
Figure H.21 Test 6 (B-M) ISOPass undeployed source location and sampling tree orientation.511
Figure H.22 Ininstantaneous CO_2 concentration at each sampling location for Test 6 (B-M) ISOPass undeployed. 512
Figure H.23 Average CO_2 concentration at each sampling location for Test 6 (B-M) ISOPass undeployed. 513
Figure H.24 Test 7 (B-M) ISOPass undeployed source location and sampling tree orientation.514
Figure H.25 Ininstantaneous CO_2 concentration at each sampling location for Test 7 (B-M) ISOPass undeployed. 515

Figure H.26 Average CO_2 concentration at each sampling location for Test 7 (B-M) ISOPass undeployed. 516
Figure H.27 Test 8 (B-M) ISOPass undeployed source location and sampling tree orientation.517
Figure H.28 Ininstantaneous CO_2 concentration at each sampling location for Test 8 (B-M) ISOPass undeployed. 518
Figure H.29 Average CO_2 concentration at each sampling location for Test 8 (B-M) ISOPass undeployed. 519
Figure H.30 Test 9 (B-M) ISOPass undeployed source location and sampling tree orientation.520
Figure H.31 Ininstantaneous CO_2 concentration at each sampling location for Test 9 (B-M) ISOPass undeployed. 521
Figure H.32 Average CO_2 concentration at each sampling location for Test 9 (B-M) ISOPass undeployed. 522
Figure H.33 Test 10 (B-M) ISOPass undeployed source location and sampling tree orientation. 523
Figure H.34 Ininstantaneous CO_2 concentration at each sampling location for Test 10 (B-M) ISOPass undeployed. 524
Figure H.35 Average CO_2 concentration at each sampling location for Test 10 (B-M) ISOPass undeployed. 525
Figure H.36 Test 11 (B-M) ISOPass undeployed source location and sampling tree orientation. 526
Figure H.37 Ininstantaneous CO_2 concentration at each sampling location for Test 11 (B-M) ISOPass undeployed. 527
Figure H.38 Average CO_2 concentration at each sampling location for Test 11 (B-M) ISOPass undeployed. 528
Figure H.39 Test 12 (B-M) ISOPass undeployed source location and sampling tree orientation. 529
Figure H.40 Ininstantaneous CO_2 concentration at each sampling location for Test 12 (B-M) ISOPass undeployed. 530
Figure H.41 Average CO_2 concentration at each sampling location for Test 12 (B-M) ISOPass undeployed. 531

Figure H.42 Test 31 (B-M) ISOPass undeployed source location and sampling tree orientation. 532
Figure H.43 Ininstantaneous CO_2 concentration at each sampling location for Test 31 (B-M) ISOPass undeployed. 533
Figure H.44 Average CO_2 concentration at each sampling location for Test 31 (B-M) ISOPass undeployed. 534
Figure H.45 Test 32 (B-M) ISOPass undeployed source location and sampling tree orientation. 535
Figure H.46 Ininstantaneous CO_2 concentration at each sampling location for Test 32 (B-M) ISOPass undeployed. 536
Figure H.47 Average CO_2 concentration at each sampling location for Test 32 (B-M) ISOPass undeployed. 537
Figure H.48 Test 33 (B-M) ISOPass undeployed source location and sampling tree orientation. 538
Figure H.49 Ininstantaneous CO_2 concentration at each sampling location for Test 33 (B-M) ISOPass undeployed. 539
Figure H.50 Average CO_2 concentration at each sampling location for Test 33 (B-M) ISOPass undeployed. 540
Figure H.51 Test 34 (B-M) ISOPass undeployed source location and sampling tree orientation. 541
Figure H.52 Ininstantaneous CO_2 concentration at each sampling location for Test 34 (B-M) ISOPass undeployed. 542
Figure H.53 Average CO_2 concentration at each sampling location for Test 34 (B-M) ISOPass undeployed. 543
Figure H.54 Test 35 (B-M) ISOPass undeployed source location and sampling tree orientation. 544
Figure H.55 Ininstantaneous CO_2 concentration at each sampling location for Test 35 (B-M) ISOPass undeployed. 545
Figure H.56 Average CO_2 concentration at each sampling location for Test 35 (B-M) ISOPass undeployed. 546

Figure H.57 Test 36 (B-M) ISOPass undeployed source location and sampling tree orientation. 547
Figure H.58 Ininstantaneous CO_2 concentration at each sampling location for Test 36 (B-M) ISOPass undeployed. 548
Figure H.59 Average CO_2 concentration at each sampling location for Test 36 (B-M) ISOPass undeployed. 549
Figure H.60 Test 37 (B-M) ISOPass undeployed source location and sampling tree orientation. 550
Figure H.61 Ininstantaneous CO_2 concentration at each sampling location for Test 37 (B-M) ISOPass undeployed. 551
Figure H.62 Average CO_2 concentration at each sampling location for Test 37 (B-M) ISOPass undeployed. 552
Figure H.63 Test 38 (B-M) ISOPass undeployed source location and sampling tree orientation. 553
Figure H.64 Ininstantaneous CO_2 concentration at each sampling location for Test 38 (B-M) ISOPass undeployed. 554
Figure H.65 Average CO_2 concentration at each sampling location for Test 38 (B-M) ISOPass undeployed. 555
Figure H.66 Test 39 (B-M) ISOPass undeployed source location and sampling tree orientation. 556
Figure H.67 Ininstantaneous CO_2 concentration at each sampling location for Test 39 (B-M) ISOPass undeployed. 557
Figure H.68 Average CO_2 concentration at each sampling location for Test 39 (B-M) ISOPass undeployed. 558
Figure H.69 Test 40 (B-M) ISOPass undeployed source location and sampling tree orientation. 559
Figure H.70 Ininstantaneous CO_2 concentration at each sampling location for Test 40 (B-M) ISOPass undeployed. 560
Figure H.71 Average CO_2 concentration at each sampling location for Test 40 (B-M) ISOPass undeployed. 561

Figure H.72 Test 41 (B-M) ISOPass undeployed source location and sampling tree orientation. 562
Figure H.73 Ininstantaneous CO_2 concentration at each sampling location for Test 41 (B-M) ISOPass undeployed. 563
Figure H.74 Average CO_2 concentration at each sampling location for Test 41 (B-M) ISOPass undeployed. 564
Figure H.75 Test 42 (B-M) ISOPass undeployed source location and sampling tree orientation. 565
Figure H.76 Ininstantaneous CO_2 concentration at each sampling location for Test 42 (B-M) ISOPass undeployed. 566
Figure H.77 Average CO_2 concentration at each sampling location for Test 42 (B-M) ISOPass undeployed. 567
Figure H.78 Test 43 (B-M) ISOPass undeployed source location and sampling tree orientation. 568
Figure H.79 Ininstantaneous CO_2 concentration at each sampling location for Test 43 (B-M) ISOPass undeployed. 569
Figure H.80 Average CO_2 concentration at each sampling location for Test 43 (B-M) ISOPass undeployed. 570
Figure H.81 Test 44 (B-M) ISOPass undeployed source location and sampling tree orientation. 571
Figure H.82 Ininstantaneous CO_2 concentration at each sampling location for Test 44 (B-M) ISOPass undeployed. 572
Figure H.83 Average CO_2 concentration at each sampling location for Test 44 (B-M) ISOPass undeployed. 573
Figure H.84 Test 45 (B-M) ISOPass undeployed source location and sampling tree orientation. 574
Figure H.85 Ininstantaneous CO_2 concentration at each sampling location for Test 45 (B-M) ISOPass undeployed. 575
Figure H.86 Average CO_2 concentration at each sampling location for Test 45 (B-M) ISOPass undeployed. 576

Figure H.87 Test 46 (B-M) ISOPass undeployed source location and sampling tree orientation. 577
Figure H.88 Ininstantaneous CO_2 concentration at each sampling location for Test 46 (B-M) ISOPass undeployed. 578
Figure H.89 Average CO_2 concentration at each sampling location for Test 46 (B-M) ISOPass undeployed. 579
Figure H.90 Test 47 (B-M) ISOPass undeployed source location and sampling tree orientation. 580
Figure H.91 Ininstantaneous CO_2 concentration at each sampling location for Test 47 (B-M) ISOPass undeployed. 581
Figure H.92 Average CO_2 concentration at each sampling location for Test 47 (B-M) ISOPass undeployed. 582
Figure H.93 Test 48 (B-M) ISOPass undeployed source location and sampling tree orientation. 583
Figure H.94 Ininstantaneous CO_2 concentration at each sampling location for Test 48 (B-M) ISOPass undeployed. 584
Figure H.95 Average CO_2 concentration at each sampling location for Test 48 (B-M) ISOPass undeployed. 585
Figure H.96 Test 67 (B-M) ISOPass undeployed source location and sampling tree orientation. 586
Figure H.97 Ininstantaneous CO_2 concentration at each sampling location for Test 67 (B-M) ISOPass undeployed. 587
Figure H.98 Average CO_2 concentration at each sampling location for Test 67 (B-M) ISOPass undeployed. 588
Figure H.99 Test 68 (B-M) ISOPass undeployed source location and sampling tree orientation. 589
Figure H.100 Ininstantaneous CO_2 concentration at each sampling location for Test 68 (B-M) ISOPass undeployed. 590
Figure H.101 Average CO_2 concentration at each sampling location for Test 68 (B-M) ISOPass undeployed. 591

Figure H.102 Test 69 (B-M) ISOPass undeployed source location and sampling tree orientation. 592
Figure H.103 Ininstantaneous CO_2 concentration at each sampling location for Test 69 (B-M) ISOPass undeployed. 593
Figure H.104 Average CO_2 concentration at each sampling location for Test 69 (B-M) ISOPass undeployed. 594
Figure H.105 Test 70 (B-M) ISOPass undeployed source location and sampling tree orientation. 595
Figure H.106 Ininstantaneous CO_2 concentration at each sampling location for Test 70 (B-M) ISOPass undeployed. 596
Figure H.107 Average CO_2 concentration at each sampling location for Test 70 (B-M) ISOPass undeployed. 597
Figure H.108 Test 71 (B-M) ISOPass undeployed source location and sampling tree orientation. 598
Figure H.109 Ininstantaneous CO_2 concentration at each sampling location for Test 71 (B-M) ISOPass undeployed. 599
Figure H.110 Average CO_2 concentration at each sampling location for Test 71 (B-M) ISOPass undeployed. 600
Figure H.111 Test 72 (B-M) ISOPass undeployed source location and sampling tree orientation. 601
Figure H.112 Ininstantaneous CO_2 concentration at each sampling location for Test 72 (B-M) ISOPass undeployed. 602
Figure H.113 Average CO_2 concentration at each sampling location for Test 72 (B-M) ISOPass undeployed. 603
Figure H.114 Test 73 (B-M) ISOPass undeployed source location and sampling tree orientation. 604
Figure H.115 Ininstantaneous CO_2 concentration at each sampling location for Test 73 (B-M) ISOPass undeployed. 605
Figure H.116 Average CO_2 concentration at each sampling location for Test 73 (B-M) ISOPass undeployed. 606

Figure H.117 Test 74 (B-M) ISOPass undeployed source location and sampling tree orientation. 607
Figure H.118 Ininstantaneous CO_2 concentration at each sampling location for Test 74 (B-M) ISOPass undeployed. 608
Figure H.119 Average CO_2 concentration at each sampling location for Test 74 (B-M) ISOPass undeployed. 609
Figure H.120 Test 75 (B-M) ISOPass undeployed source location and sampling tree orientation. 610
Figure H.121 Ininstantaneous CO_2 concentration at each sampling location for Test 75 (B-M) ISOPass undeployed. 611
Figure H.122 Average CO_2 concentration at each sampling location for Test 75 (B-M) ISOPass undeployed. 612
Figure H.123 Test 76 (B-M) ISOPass undeployed source location and sampling tree orientation. 613
Figure H.124 Ininstantaneous CO_2 concentration at each sampling location for Test 76 (B-M) ISOPass undeployed. 614
Figure H.125 Average CO_2 concentration at each sampling location for Test 76 (B-M) ISOPass undeployed. 615
Figure H.126 Test 77 (B-M) ISOPass undeployed source location and sampling tree orientation. 616
Figure H.127 Ininstantaneous CO_2 concentration at each sampling location for Test 77 (B-M) ISOPass undeployed. 617
Figure H.128 Average CO_2 concentration at each sampling location for Test 77 (B-M) ISOPass undeployed. 618
Figure H.129 Test 78 (B-M) ISOPass undeployed source location and sampling tree orientation. 619
Figure H.130 Ininstantaneous CO_2 concentration at each sampling location for Test 78 (B-M) ISOPass undeployed. 620
Figure H.131 Average CO_2 concentration at each sampling location for Test 78 (B-M) ISOPass undeployed. 621

Figure H.132 Test 79 (B-M) ISOPass undeployed source location and sampling tree orientation. 622
Figure H.133 Ininstantaneous CO_2 concentration at each sampling location for Test 79 (B-M) ISOPass undeployed. 623
Figure H.134 Average CO_2 concentration at each sampling location for Test 79 (B-M) ISOPass undeployed. 624
Figure H.135 Test 80 (B-M) ISOPass undeployed source location and sampling tree orientation. 625
Figure H.136 Ininstantaneous CO_2 concentration at each sampling location for Test 80 (B-M) ISOPass undeployed. 626
Figure H.137 Average CO_2 concentration at each sampling location for Test 80 (B-M) ISOPass undeployed. 627
Figure H.138 Test 81 (B-M) ISOPass undeployed source location and sampling tree orientation. 628
Figure H.139 Ininstantaneous CO_2 concentration at each sampling location for Test 81 (B-M) ISOPass undeployed. 629
Figure H.140 Average CO_2 concentration at each sampling location for Test 81 (B-M) ISOPass undeployed. 630
Figure H.141 Test 82 (B-M) ISOPass undeployed source location and sampling tree orientation. 631
Figure H.142 Ininstantaneous CO_2 concentration at each sampling location for Test 82 (B-M) ISOPass undeployed. 632
Figure H.143 Average CO_2 concentration at each sampling location for Test 82 (B-M) ISOPass undeployed. 633
Figure H.144 Test 83 (B-M) ISOPass undeployed source location and sampling tree orientation. 634
Figure H.145 Ininstantaneous CO_2 concentration at each sampling location for Test 83 (B-M) ISOPass undeployed. 635
Figure H.146 Average CO_2 concentration at each sampling location for Test 83 (B-M) ISOPass undeployed. 636

Figure H.147 Test 84 (B-M) ISOPass undeployed source location and sampling tree orientation. 637
Figure H.148 Ininstantaneous CO_2 concentration at each sampling location for Test 84 (B-M) ISOPass undeployed. 638
Figure H.149 Average CO_2 concentration at each sampling location for Test 84 (B-M) ISOPass undeployed. 639
Figure H.150 Test 85 (B-M) ISOPass undeployed source location and sampling tree orientation. 640
Figure H.151 Ininstantaneous CO_2 concentration at each sampling location for Test 85 (B-M) ISOPass undeployed. 641
Figure H.152 Average CO_2 concentration at each sampling location for Test 85 (B-M) ISOPass undeployed. 642
Figure H.153 Test 86 (B-M) ISOPass undeployed source location and sampling tree orientation. 643
Figure H.154 Ininstantaneous CO_2 concentration at each sampling location for Test 86 (B-M) ISOPass undeployed. 644
Figure H.155 Average CO_2 concentration at each sampling location for Test 86 (B-M) ISOPass undeployed. 645
Figure H.156 Test 87 (B-M) ISOPass undeployed source location and sampling tree orientation. 646
Figure H.157 Ininstantaneous CO_2 concentration at each sampling location for Test 87 (B-M) ISOPass undeployed. 647
Figure H.158 Average CO_2 concentration at each sampling location for Test 87 (B-M) ISOPass undeployed. 648
Figure H.159 Test 88 (B-M) ISOPass undeployed source location and sampling tree orientation. 649
Figure H.160 Ininstantaneous CO_2 concentration at each sampling location for Test 88 (B-M) ISOPass undeployed. 650
Figure H.161 Average CO_2 concentration at each sampling location for Test 88 (B-M) ISOPass undeployed. 651

Figure H.162 Test 89 (B-M) ISOPass undeployed source location and sampling tree orientation. 652
Figure H.163 Ininstantaneous CO_2 concentration at each sampling location for Test 89 (B-M) ISOPass undeployed. 653
Figure H.164 Average CO_2 concentration at each sampling location for Test 89 (B-M) ISOPass undeployed. 654
Figure H.165 Test 90 (B-M) ISOPass undeployed source location and sampling tree orientation. 655
Figure H.166 Ininstantaneous CO_2 concentration at each sampling location for Test 90 (B-M) ISOPass undeployed. 656
Figure H.167 Average CO_2 concentration at each sampling location for Test 90 (B-M) ISOPass undeployed. 657
Figure H.168 Test 91 (B-M) ISOPass undeployed source location and sampling tree orientation. 658
Figure H.169 Ininstantaneous CO_2 concentration at each sampling location for Test 91 (B-M) ISOPass undeployed. 659
Figure H.170 Average CO_2 concentration at each sampling location for Test 91 (B-M) ISOPass undeployed. 660
Figure H.171 Test 92 (B-M) ISOPass undeployed source location and sampling tree orientation. 661
Figure H.172 Ininstantaneous CO_2 concentration at each sampling location for Test 92 (B-M) ISOPass undeployed. 662
Figure H.173 Average CO_2 concentration at each sampling location for Test 92 (B-M) ISOPass undeployed. 663
Figure H.174 Test 93 (B-M) ISOPass undeployed source location and sampling tree orientation. 664
Figure H.175 Ininstantaneous CO_2 concentration at each sampling location for Test 93 (B-M) ISOPass undeployed. 665
Figure H.176 Average CO_2 concentration at each sampling location for Test 93 (B-M) ISOPass undeployed. 666

Figure H.177 Seat D6 coughing manikin source tests in the Boeing 767 cabin mockup with the ISOPass undeployed. 667
Figure H.178 Seat G6 coughing manikin source tests in the Boeing 767 cabin mockup with the ISOPass undeployed. 668
Figure H.179 Seat F6 coughing manikin source tests in the Boeing 767 cabin mockup with the ISOPass undeployed. 669
H. 180 Seat A6 coughing manikin source tests in the Boeing 767 cabin mockup with the ISOPass undeployed. 670
Figure H.181 Seat B6 coughing manikin source tests in the Boeing 767 cabin mockup with the ISOPass undeployed. 671
Figure H.182 Diagonal front left sampling tree orientation coughing manikin source tests in the Boeing 767 cabin mockup with the ISOPass undeployed. 672
Figure H.183 Longitudinal rear sampling tree orientation coughing manikin source tests in the Boeing 767 cabin mockup with the ISOPass undeployed. 673
Figure H.184 Longitudinal front sampling tree orientation coughing manikin source tests in the Boeing 767 cabin mockup with the ISOPass undeployed. 674
Figure H.185 Diagonal front right sampling tree orientation coughing manikin source tests in the Boeing 767 cabin mockup with the ISOPass undeployed. 675
Figure H.186 Lateral sampling tree orientation coughing manikin source tests in the Boeing 767 cabin mockup with the ISOPass undeployed. 676
Figure H.187 Diagonal rear left sampling tree orientation coughing manikin source tests in the Boeing 767 cabin mockup with the ISOPass undeployed. 677
Figure H.188 Diagonal rear right sampling tree orientation coughing manikin source tests in the Boeing 767 cabin mockup with the ISOPass undeployed. 678
Figure H.189 Boeing 767 cabin mockup coughing manikin source tests with the ISOPass undeployed. 679
Figure H.190 Boeing 767 cabin mockup coughing manikin source tests with the ISOPass undeployed, Absolute distances from the source. 680
Figure I.1 Seat G6 ISOPass deployed coughing manikin tracer gas test numbers and sampling tree orientations in the Boeing 767 cabin mockup. 682

Figure I.2 Seat F6 ISOPass deployed coughing manikin tracer gas test numbers and sampling tree orientations in the Boeing 767 cabin mockup. 683
Figure I.3 Seat A6 ISOPass deployed coughing manikin tracer gas test numbers and sampling tree orientations in the Boeing 767 cabin mockup. 684
Figure I.4 Seat B6 ISOPass deployed coughing manikin tracer gas test numbers and sampling tree orientations in the Boeing 767 cabin mockup. 685
Figure I.5 Test 16 (B-M) ISOPass deployed source location and sampling tree orientation. 686
Figure I.6 Ininstantaneous CO_2 concentration at each sampling location for Test 16 (B-M) ISOPass deployed. 687
Figure I.7 Average CO_2 concentration at each sampling location for Test 16 (B-M) ISOPass deployed. 688
Figure I.8 Test 17 (B-M) ISOPass deployed source location and sampling tree orientation. 689
Figure I.9 Ininstantaneous CO_2 concentration at each sampling location for Test 17 (B-M) ISOPass deployed. 690
Figure I.10 Average CO_2 concentration at each sampling location for Test 17 (B-M) ISOPass deployed. 691
Figure I.11 Test 18 (B-M) ISOPass deployed source location and sampling tree orientation. 692
Figure I.12 Ininstantaneous CO_2 concentration at each sampling location for Test 18 (B-M) ISOPass deployed. 693
Figure I.13 Average CO_2 concentration at each sampling location for Test 18 (B-M) ISOPass deployed. 694
Figure I.14 Test 19 (B-M) ISOPass deployed source location and sampling tree orientation. 695
Figure I.15 Ininstantaneous CO_2 concentration at each sampling location for Test 19 (B-M) ISOPass deployed. 696
Figure I.16 Average CO_2 concentration at each sampling location for Test 19 (B-M) ISOPass deployed. 697
Figure I.17 Test 20 (B-M) ISOPass deployed source location and sampling tree orientation. 698
Figure I.18 Ininstantaneous CO_2 concentration at each sampling location for Test 20 (B-M) ISOPass deployed. 699
Figure I.19 Average CO_2 concentration at each sampling location for Test 20 (B-M) ISOPass deployed. 700

Figure I.20 Test 21 (B-M) ISOPass deployed source location and sampling tree orientation. .. 701
Figure I.21 Ininstantaneous CO_2 concentration at each sampling location for Test 21 (B-M) ISOPass deployed. 702
Figure I.22 Average CO_2 concentration at each sampling location for Test 21 (B-M) ISOPass deployed. 703
Figure I.23 Test 28 (B-M) ISOPass deployed source location and sampling tree orientation. .. 704
Figure I.24 Ininstantaneous CO_2 concentration at each sampling location for Test 28 (B-M) ISOPass deployed. 705
Figure I.25 Average CO_2 concentration at each sampling location for Test 28 (B-M) ISOPass deployed. 706
Figure I.26 Test 29 (B-M) ISOPass deployed source location and sampling tree orientation. .. 707
Figure I.27 Ininstantaneous CO_2 concentration at each sampling location for Test 29 (B-M) ISOPass deployed. 708
Figure I.28 Average CO_2 concentration at each sampling location for Test 29 (B-M) ISOPass deployed. 709
Figure I.29 Test 30 (B-M) ISOPass deployed source location and sampling tree orientation. .. 710
Figure I.30 Ininstantaneous CO_2 concentration at each sampling location for Test 30 (B-M) ISOPass deployed. 711
Figure I.31 Average CO_2 concentration at each sampling location for Test 30 (B-M) ISOPass deployed. 712
Figure I.32 Test 13 (B-M) ISOPass deployed source location and sampling tree orientation. .. 713
Figure I.33 Ininstantaneous CO_2 concentration at each sampling location for Test 13 (B-M) ISOPass deployed. 714
Figure I.34 Average CO_2 concentration at each sampling location for Test 13 (B-M) ISOPass deployed. 715
Figure I.35 Test 14 (B-M) ISOPass deployed source location and sampling tree orientation. .. 716
Figure I.36 Ininstantaneous CO_2 concentration at each sampling location for Test 14 (B-M) ISOPass deployed. 717
Figure I.37 Average CO_2 concentration at each sampling location for Test 14 (B-M) ISOPass deployed. 718
Figure I.38 Test 15 (B-M) ISOPass deployed source location and sampling tree orientation. .. 719

Figure I.39 Ininstantaneous CO_2 concentration at each sampling location for Test 15 (B-M) ISOPass deployed. 720
Figure I.40 Average CO_2 concentration at each sampling location for Test 15 (B-M) ISOPass deployed. 721
Figure I.41 Test 22 (B-M) ISOPass deployed source location and sampling tree orientation. .. 722
Figure I.42 Ininstantaneous CO_2 concentration at each sampling location for Test 22 (B-M) ISOPass deployed. 723
Figure I.43 Average CO_2 concentration at each sampling location for Test 22 (B-M) ISOPass deployed. 724
Figure I.44 Test 23 (B-M) ISOPass deployed source location and sampling tree orientation. .. 725
Figure I.45 Ininstantaneous CO_2 concentration at each sampling location for Test 23 (B-M) ISOPass deployed. 726
Figure I.46 Average CO_2 concentration at each sampling location for Test 23 (B-M) ISOPass deployed. 727
Figure I.47 Test 24 (B-M) ISOPass deployed source location and sampling tree orientation. .. 728
Figure I.48 Ininstantaneous CO_2 concentration at each sampling location for Test 24 (B-M) ISOPass deployed. 729
Figure I.49 Average CO_2 concentration at each sampling location for Test 24 (B-M) ISOPass deployed. 730
Figure I.50 Test 25 (B-M) ISOPass deployed source location and sampling tree orientation. .. 731
Figure I.51 Ininstantaneous CO_2 concentration at each sampling location for Test 25 (B-M) ISOPass deployed. 732
Figure I.52 Average CO_2 concentration at each sampling location for Test 25 (B-M) ISOPass deployed. 733
Figure I.53 Test 26 (B-M) ISOPass deployed source location and sampling tree orientation. .. 734
Figure I.54 Ininstantaneous CO_2 concentration at each sampling location for Test 26 (B-M) ISOPass deployed. 735
Figure I.55 Average CO_2 concentration at each sampling location for Test 26 (B-M) ISOPass deployed. 736
Figure I.56 Test 27 (B-M) ISOPass deployed source location and sampling tree orientation. .. 737

Figure I.57 Ininstantaneous CO_2 concentration at each sampling location for Test 27 (B-M) ISOPass deployed. 738
Figure I.58 Average CO_2 concentration at each sampling location for Test 27 (B-M) ISOPass deployed. 739
Figure I.59 Test 49 (B-M) ISOPass deployed source location and sampling tree orientation. .. 740
Figure I.60 Ininstantaneous CO_2 concentration at each sampling location for Test 49 (B-M) ISOPass deployed. 741
Figure I.61 Average CO_2 concentration at each sampling location for Test 49 (B-M) ISOPass deployed. 742
Figure I.62 Test 50 (B-M) ISOPass deployed source location and sampling tree orientation. .. 743
Figure I.63 Ininstantaneous CO_2 concentration at each sampling location for Test 50 (B-M) ISOPass deployed. 744
Figure I.64 Average CO_2 concentration at each sampling location for Test 50 (B-M) ISOPass deployed. 745
Figure I.65 Test 51 (B-M) ISOPass deployed source location and sampling tree orientation. .. 746
Figure I.66 Ininstantaneous CO_2 concentration at each sampling location for Test 51 (B-M) ISOPass deployed. 747
Figure I.67 Average CO_2 concentration at each sampling location for Test 51 (B-M) ISOPass deployed. 748
Figure I.68 Test 52 (B-M) ISOPass deployed source location and sampling tree orientation. .. 749
Figure I.69 Ininstantaneous CO_2 concentration at each sampling location for Test 52 (B-M) ISOPass deployed. 750
Figure I.70 Average CO_2 concentration at each sampling location for Test 52 (B-M) ISOPass deployed. 751
Figure I.71 Test 53 (B-M) ISOPass deployed source location and sampling tree orientation. .. 752
Figure I.72 Ininstantaneous CO_2 concentration at each sampling location for Test 53 (B-M) ISOPass deployed. 753
Figure I.73 Average CO_2 concentration at each sampling location for Test 53 (B-M) ISOPass deployed. 754
Figure I.74 Test 54 (B-M) ISOPass deployed source location and sampling tree orientation. .. 755

Figure I.75 Ininstantaneous CO_2 concentration at each sampling location for Test 54 (B-M) ISOPass deployed. 756
Figure I.76 Average CO_2 concentration at each sampling location for Test 54 (B-M) ISOPass deployed. 757
Figure I.77 Test 64 (B-M) ISOPass deployed source location and sampling tree orientation. .. 758
Figure I.78 Ininstantaneous CO_2 concentration at each sampling location for Test 64 (B-M) ISOPass deployed. 759
Figure I.79 Average CO_2 concentration at each sampling location for Test 64 (B-M) ISOPass deployed. 760
Figure I.80 Test 65 (B-M) ISOPass deployed source location and sampling tree orientation. .. 761
Figure I.81 Ininstantaneous CO_2 concentration at each sampling location for Test 65 (B-M) ISOPass deployed. 762
Figure I.82 Average CO_2 concentration at each sampling location for Test 65 (B-M) ISOPass deployed. 763
Figure I.83 Test 66 (B-M) ISOPass deployed source location and sampling tree orientation. .. 764
Figure I.84 Ininstantaneous CO_2 concentration at each sampling location for Test 66 (B-M) ISOPass deployed. 765
Figure I.85 Average CO_2 concentration at each sampling location for Test 66 (B-M) ISOPass deployed. 766
Figure I.86 Test 55 (B-M) ISOPass deployed source location and sampling tree orientation. .. 767
Figure I.87 Ininstantaneous CO_2 concentration at each sampling location for Test 55 (B-M) ISOPass deployed. 768
Figure I.88 Average CO_2 concentration at each sampling location for Test 55 (B-M) ISOPass deployed. 769
Figure I.89 Test 56 (B-M) ISOPass deployed source location and sampling tree orientation. .. 770
Figure I.90 Ininstantaneous CO_2 concentration at each sampling location for Test 56 (B-M) ISOPass deployed. 771
Figure I.91 Average CO_2 concentration at each sampling location for Test 56 (B-M) ISOPass deployed. 772
Figure I.92 Test 57 (B-M) ISOPass deployed source location and sampling tree orientation. .. 773

Figure I.93 Ininstantaneous CO_2 concentration at each sampling location for Test 57 (B-M) ISOPass deployed. 774
Figure I.94 Average CO_2 concentration at each sampling location for Test 57 (B-M) ISOPass deployed. 775
Figure I.95 Test 58 (B-M) ISOPass deployed source location and sampling tree orientation. .. 776
Figure I.96 Ininstantaneous CO_2 concentration at each sampling location for Test 58 (B-M) ISOPass deployed. 777
Figure I.97 Average CO_2 concentration at each sampling location for Test 58 (B-M) ISOPass deployed. 778
Figure I.98 Test 59 (B-M) ISOPass deployed source location and sampling tree orientation. .. 779
Figure I.99 Ininstantaneous CO_2 concentration at each sampling location for Test 59 (B-M) ISOPass deployed. 780
Figure I.100 Average CO_2 concentration at each sampling location for Test 59 (B-M) ISOPass deployed. 781
Figure I.101 Test 60 (B-M) ISOPass deployed source location and sampling tree orientation. 782
Figure I.102 Ininstantaneous CO_2 concentration at each sampling location for Test 60 (B-M) ISOPass deployed. 783
Figure I.103 Average CO_2 concentration at each sampling location for Test 60 (B-M) ISOPass deployed. 784
Figure I.104 Test 61 (B-M) ISOPass deployed source location and sampling tree orientation. 785
Figure I.105 Ininstantaneous CO_2 concentration at each sampling location for Test 61 (B-M) ISOPass deployed. 786
Figure I.106 Average CO_2 concentration at each sampling location for Test 61 (B-M) ISOPass deployed. 787
Figure I.107 Test 62 (B-M) ISOPass deployed source location and sampling tree orientation. 788
Figure I.108 Ininstantaneous CO_2 concentration at each sampling location for Test 62 (B-M) ISOPass deployed. 789
Figure I.109 Average CO_2 concentration at each sampling location for Test 62 (B-M) ISOPass deployed. 790
Figure I.110 Test 63 (B-M) ISOPass deployed source location and sampling tree orientation. 791

Figure I.111 Ininstantaneous CO_2 concentration at each sampling location for Test 63 (B-M) ISOPass deployed. 792
Figure I.112 Average CO_2 concentration at each sampling location for Test 63 (B-M) ISOPass deployed. 793
Figure I.113 Seat G6 coughing manikin source tests in the Boeing 767 cabin mockup with the ISOPass deployed. 794
Figure I.114 Seat F6 coughing manikin source tests in the Boeing 767 cabin mockup with the ISOPass deployed. 795
I. 115 Seat A6 coughing manikin source tests in the Boeing 767 cabin mockup with the ISOPass deployed. 796
Figure I.116 Seat B6 coughing manikin source tests in the Boeing 767 cabin mockup with the ISOPass deployed. 797
Figure I.117 Diagonal front left sampling tree orientation coughing manikin source tests in the Boeing 767 cabin mockup with the ISOPass deployed. 798
Figure I.118 Longitudinal front sampling tree orientation coughing manikin source tests in the Boeing 767 cabin mockup with the ISOPass deployed. 799
Figure I.119 Diagonal front right sampling tree orientation coughing manikin source tests in the Boeing 767 cabin mockup with the ISOPass deployed. 800
Figure I.120 Lateral sampling tree orientation coughing manikin source tests in the Boeing 767 cabin mockup with the ISOPass deployed. 801
Figure I.121 Boeing 767 cabin mockup coughing manikin source tests with the ISOPass deployed. 802
Figure J.1.1 A schematic showing the cross-sectional laser sheet direction and the camera location relative to the seat where the smoke generation source is located on seat A6. 804
Figure J.1.2 Seat A6 cross-sectional view snapshot 01 805
Figure J.1.3 Seat A6 cross-sectional view snapshot 02 805
Figure J.1.4 Seat A6 cross-sectional view snapshot 03 805
Figure J.1.5 Seat A6 cross-sectional view snapshot 04 805
Figure J.1.6 Seat A6 cross-sectional view snapshot 05. 806
Figure J.1.7 Seat A6 cross-sectional view snapshot 06. 806

Figure J.1.8 Seat A6 cross-sectional view snapshot 07. 806
Figure J.1.9 Seat A6 cross-sectional view snapshot 08. 806
Figure J.1.10 Seat A6 cross-sectional view snapshot 09. 807
Figure J.1.11 Seat A6 cross-sectional view snapshot 10. 807
Figure J.1.12 Seat A6 cross-sectional view snapshot 11. 807
Figure J.1.13 Seat A6 cross-sectional view snapshot 12. 807
Figure J.1.14 Seat A6 cross-sectional view snapshot 13. 808
Figure J.1.15 Seat A6 cross-sectional view snapshot 14. 808
Figure J.1.16 Seat A6 cross-sectional view snapshot 15. 808
Figure J.1.17 Seat A6 cross-sectional view snapshot 16. 808
Figure J.1.18 Seat A6 cross-sectional view snapshot 17. 809
Figure J.1.19 Seat A6 cross-sectional view snapshot 18. 809
Figure J.1.20 Seat A6 cross-sectional view snapshot 19. 809
Figure J.1.21 Seat A6 cross-sectional view snapshot 20. 809
Figure J.1.22 Seat A6 cross-sectional view snapshot 21. 810
Figure J.1.23 Seat A6 cross-sectional view snapshot 22. 810
Figure J.1.24 Seat A6 cross-sectional view snapshot 23. 810
Figure J.1.25 Seat A6 cross-sectional view snapshot 24. 810
Figure J.1.26 Seat A6 cross-sectional view snapshot 25. 811
Figure J.1.27 Seat A6 cross-sectional view snapshot 26. 811
Figure J.1.28 Seat A6 cross-sectional view snapshot 27. 811
Figure J.1.29 Seat A6 cross-sectional view snapshot 28. 811
Figure J.1.30 Seat A6 cross-sectional view snapshot 29. 812
Figure J.1.31 Seat A6 cross-sectional view snapshot 30. 812
Figure J.1.32 Seat A6 cross-sectional view snapshot 31. 812
Figure J.1.33 Seat A6 cross-sectional view snapshot 32. 812
Figure J.1.34 Seat A6 cross-sectional view snapshot 33. 813
Figure J.1.35 Seat A6 cross-sectional view snapshot 34. 813
Figure J.1.36 Seat A6 cross-sectional view snapshot 35. 813
Figure J.1.37 Seat A6 cross-sectional view snapshot 36. 813
Figure J.1.38 Seat A6 cross-sectional view snapshot 37. 814

Figure J.1.39 Seat A6 cross-sectional view snapshot 38. 814
Figure J.1.40 Seat A6 cross-sectional view snapshot 39. 814
Figure J.1.41 Seat A6 cross-sectional view snapshot 40. 814
Figure J.1.42 Seat A6 cross-sectional view snapshot 41. 815
Figure J.1.43 Seat A6 cross-sectional view snapshot 42. 815
Figure J.1.44 Seat A6 cross-sectional view snapshot 43. 815
Figure J.1.45 Seat A6 cross-sectional view snapshot 44. 815
Figure J.1.46 Seat A6 cross-sectional view snapshot 45. 816
Figure J.1.47 Seat A6 cross-sectional view snapshot 46. 816
Figure J.1.48 Seat A6 cross-sectional view snapshot 47. 816
Figure J.1.49 Seat A6 cross-sectional view snapshot 48. 816
Figure J.1.50 Seat A6 cross-sectional view snapshot 49. 817
Figure J.1.51 Seat A6 cross-sectional view snapshot 50. 817
Figure J.2.1 A schematic showing the frontal laser sheet direction and the camera location relative to the seat where the smoke generation source is located on seat A6. 818
Figure J.2.2 Seat A6 frontal view snapshot 01. 819
Figure J.2.3 Seat A6 frontal view snapshot 02. 819
Figure J.2.4 Seat A6 frontal view snapshot 03. 819
Figure J.2.5 Seat A6 frontal view snapshot 04. 819
Figure J.2.6 Seat A6 frontal view snapshot 05. 820
Figure J.2.7 Seat A6 frontal view snapshot 06. 820
Figure J.2.8 Seat A6 frontal view snapshot 07. 820
Figure J.2.9 Seat A6 frontal view snapshot 08. 820
Figure J.2.10 Seat A6 frontal view snapshot 09. 821
Figure J.2.11 Seat A6 frontal view snapshot 10. 821
Figure J.2.12 Seat A6 frontal view snapshot 11. 821
Figure J.2.13 Seat A6 frontal view snapshot 12. 821
Figure J.2.14 Seat A6 frontal view snapshot 13. 822
Figure J.2.15 Seat A6 frontal view snapshot 14. 822
Figure J.2.16 Seat A6 frontal view snapshot 15. 822

Figure J.2.17 Seat A6 frontal view snapshot 16. 822
Figure J.2.18 Seat A6 frontal view snapshot 17. 823
Figure J.2.19 Seat A6 frontal view snapshot 18. 823
Figure J.2.20 Seat A6 frontal view snapshot 19. 823
Figure J.2.21 Seat A6 frontal view snapshot 20. 823
Figure J.2.22 Seat A6 frontal view snapshot 21. 824
Figure J.2.23 Seat A6 frontal view snapshot 22. 824
Figure J.2.24 Seat A6 frontal view snapshot 23. 824
Figure J.2.25 Seat A6 frontal view snapshot 24. 824
Figure J.2.26 Seat A6 frontal view snapshot 25. 825
Figure J.2.27 Seat A6 frontal view snapshot 26. 825
Figure J.2.28 Seat A6 frontal view snapshot 27. 825
Figure J.2.29 Seat A6 frontal view snapshot 28. 825
Figure J.2.30 Seat A6 frontal view snapshot 29. 826
Figure J.2.31 Seat A6 frontal view snapshot 30. 826
Figure J.2.32 Seat A6 frontal view snapshot 31. 826
Figure J.2.33 Seat A6 frontal view snapshot 32. 826
Figure J.2.34 Seat A6 frontal view snapshot 33. 827
Figure J.2.35 Seat A6 frontal view snapshot 34. 827
Figure J.2.36 Seat A6 frontal view snapshot 35. 827
Figure J.2.37 Seat A6 frontal view snapshot 36. 827
Figure J.2.38 Seat A6 frontal view snapshot 37. 828
Figure J.2.39 Seat A6 frontal view snapshot 38. 828
Figure J.2.40 Seat A6 frontal view snapshot 39. 828
Figure J.2.41 Seat A6 frontal view snapshot 40. 828
Figure J.2.42 Seat A6 frontal view snapshot 41. 829
Figure J.2.43 Seat A6 frontal view snapshot 42. 829
Figure J.2.44 Seat A6 frontal view snapshot 43. 829
Figure J.2.45 Seat A6 frontal view snapshot 44. 829
Figure J.2.46 Seat A6 frontal view snapshot 45. 830
Figure J.2.47 Seat A6 frontal view snapshot 46. 830

Figure J.2.48 Seat A6 frontal view snapshot 47. 830
Figure J.2.49 Seat A6 frontal view snapshot 48. 830
Figure J.2.50 Seat A6 frontal view snapshot 49. 831
Figure J.2.51 Seat A6 frontal view snapshot 50. 831
Figure K.1.1 A schematic showing the cross-sectional laser sheet direction and the camera location relative to the seat where the smoke generation source is located on seat D1. 833
Figure K.1.2 Seat D1 cross-sectional view snapshot 01. 834
Figure K.1.3 Seat D1 cross-sectional view snapshot 02. 834
Figure K.1.4 Seat D1 cross-sectional view snapshot 03. 834
Figure K.1.5 Seat D1 cross-sectional view snapshot 04. 834
Figure K.1.6 Seat D1 cross-sectional view snapshot 05. 835
Figure K.1.7 Seat D1 cross-sectional view snapshot 06. 835
Figure K.1.8 Seat D1 cross-sectional view snapshot 07. 835
Figure K.1.9 Seat D1 cross-sectional view snapshot 08. 835
Figure K.1.10 Seat D1 cross-sectional view snapshot 09. 836
Figure K.1.11 Seat D1 cross-sectional view snapshot 10. 836
Figure K.1.12 Seat D1 cross-sectional view snapshot 11. 836
Figure K.1.13 Seat D1 cross-sectional view snapshot 12. 836
Figure K.1.14 Seat D1 cross-sectional view snapshot 13. 837
Figure K.1.15 Seat D1 cross-sectional view snapshot 14. 837
Figure K.1.16 Seat D1 cross-sectional view snapshot 15. 837
Figure K.1.17 Seat D1 cross-sectional view snapshot 16. 837
Figure K.1.18 Seat D1 cross-sectional view snapshot 17. 838
Figure K.1.19 Seat D1 cross-sectional view snapshot 18. 838
Figure K.1.20 Seat D1 cross-sectional view snapshot 19. 838
Figure K.1.21 Seat D1 cross-sectional view snapshot 20. 838
Figure K.1.22 Seat D1 cross-sectional view snapshot 21. 839
Figure K.1.23 Seat D1 cross-sectional view snapshot 22. 839
Figure K.1.24 Seat D1 cross-sectional view snapshot 23. 839
Figure K.1.25 Seat D1 cross-sectional view snapshot 24. 839

Figure K.1.26 Seat D1 cross-sectional view snapshot 25. 840
Figure K.1.27 Seat D1 cross-sectional view snapshot 26. 840
Figure K.1.28 Seat D1 cross-sectional view snapshot 27. 840
Figure K.1.29 Seat D1 cross-sectional view snapshot 28. 840
Figure K.1.30 Seat D1 cross-sectional view snapshot 29. 841
Figure K.1.31 Seat D1 cross-sectional view snapshot 30. 841
Figure K.1.32 Seat D1 cross-sectional view snapshot 31. 841
Figure K.1.33 Seat D1 cross-sectional view snapshot 32. 841
Figure K.1.34 Seat D1 cross-sectional view snapshot 33. 842
Figure K.1.35 Seat D1 cross-sectional view snapshot 34. 842
Figure K.1.36 Seat D1 cross-sectional view snapshot 35. 842
Figure K.1.37 Seat D1 cross-sectional view snapshot 36. 842
Figure K.1.38 Seat D1 cross-sectional view snapshot 37. 843
Figure K.1.39 Seat D1 cross-sectional view snapshot 38. 843
Figure K.1.40 Seat D1 cross-sectional view snapshot 39. 843
Figure K.1.41 Seat D1 cross-sectional view snapshot 40. 843
Figure K.1.42 Seat D1 cross-sectional view snapshot 41. 844
Figure K.1.43 Seat D1 cross-sectional view snapshot 42. 844
Figure K.1.44 Seat D1 cross-sectional view snapshot 43. 844
Figure K.1.45 Seat D1 cross-sectional view snapshot 44. 844
Figure K.1.46 Seat D1 cross-sectional view snapshot 45. 845
Figure K.1.47 Seat D1 cross-sectional view snapshot 46. 845
Figure K.1.48 Seat D1 cross-sectional view snapshot 47. 845
Figure K.1.49 Seat D1 cross-sectional view snapshot 48. 845
Figure K.1.50 Seat D1 cross-sectional view snapshot 49. 846
Figure K.1.51 Seat D1 cross-sectional view snapshot 50. 846
Figure K.2.1 A schematic showing the frontal laser sheet direction and the camera location relative to the seat where the smoke generation source is located on seat D1. 847
Figure K.2.2 Seat D1 frontal view snapshot 01. 848
Figure K.2.3 Seat D1 frontal view snapshot 02. 848

Figure K.2.4 Seat D1 frontal view snapshot 03. 848
Figure K.2.5 Seat D1 frontal view snapshot 04. 848
Figure K.2.6 Seat D1 frontal view snapshot 05. 849
Figure K.2.7 Seat D1 frontal view snapshot 06. 849
Figure K.2.8 Seat D1 frontal view snapshot 07. 849
Figure K.2.9 Seat D1 frontal view snapshot 08. 849
Figure K.2.10 Seat D1 frontal view snapshot 09. 850
Figure K.2.11 Seat D1 frontal view snapshot 10. 850
Figure K.2.12 Seat D1 frontal view snapshot 11. 850
Figure K.2.13 Seat D1 frontal view snapshot 12. 850
Figure K.2.14 Seat D1 frontal view snapshot 13. 851
Figure K.2.15 Seat D1 frontal view snapshot 14. 851
Figure K.2.16 Seat D1 frontal view snapshot 15. 851
Figure K.2.17 Seat D1 frontal view snapshot 16. 851
Figure K.2.18 Seat D1 frontal view snapshot 17. 852
Figure K.2.19 Seat D1 frontal view snapshot 18. 852
Figure K.2.20 Seat D1 frontal view snapshot 19. 852
Figure K.2.21 Seat D1 frontal view snapshot 20. 852
Figure K.2.22 Seat D1 frontal view snapshot 21. 853
Figure K.2.23 Seat D1 frontal view snapshot 22. 853
Figure K.2.24 Seat D1 frontal view snapshot 23. 853
Figure K.2.25 Seat D1 frontal view snapshot 24. 853
Figure K.2.26 Seat D1 frontal view snapshot 25. 854
Figure K.2.27 Seat D1 frontal view snapshot 26. 854
Figure K.2.28 Seat D1 frontal view snapshot 27. 854
Figure K.2.29 Seat D1 frontal view snapshot 28. 854
Figure K.2.30 Seat D1 frontal view snapshot 29. 855
Figure K.2.31 Seat D1 frontal view snapshot 30. 855
Figure K.2.32 Seat D1 frontal view snapshot 31. 855
Figure K.2.33 Seat D1 frontal view snapshot 32. 855
Figure K.2.34 Seat D1 frontal view snapshot 33. 856

Figure K.2.35 Seat D1 frontal view snapshot 34. 856
Figure K.2.36 Seat D1 frontal view snapshot 35. 856
Figure K.2.37 Seat D1 frontal view snapshot 36. 856
Figure K.2.38 Seat D1 frontal view snapshot 37. 857
Figure K.2.39 Seat D1 frontal view snapshot 38. 857
Figure K.2.40 Seat D1 frontal view snapshot 39. 857
Figure K.2.41 Seat D1 frontal view snapshot 40. 857
Figure K.2.42 Seat D1 frontal view snapshot 41. 858
Figure K.2.43 Seat D1 frontal view snapshot 42. 858
Figure K.2.44 Seat D1 frontal view snapshot 43. 858
Figure K.2.45 Seat D1 frontal view snapshot 44. 858
Figure K.2.46 Seat D1 frontal view snapshot 45. 859
Figure K.2.47 Seat D1 frontal view snapshot 46. 859
Figure K.2.48 Seat D1 frontal view snapshot 47. 859
Figure K.2.49 Seat D1 frontal view snapshot 48. 859
Figure K.2.50 Seat D1 frontal view snapshot 49. 860
Figure K.2.51 Seat D1 frontal view snapshot 50. 860
Figure L.1.1 A schematic showing the cross-sectional laser sheet direction and the camera location relative to the seat where the smoke generation source is located on seat D6. 862
Figure L.1.2 Seat D6 cross-sectional view snapshot 01. 863
Figure L.1.3 Seat D6 cross-sectional view snapshot 02. 863
Figure L.1.4 Seat D6 cross-sectional view snapshot 03. 863
Figure L.1.5 Seat D6 cross-sectional view snapshot 04. 863
Figure L.1.6 Seat D6 cross-sectional view snapshot 05. 864
Figure L.1.7 Seat D6 cross-sectional view snapshot 06. 864
Figure L.1.8 Seat D6 cross-sectional view snapshot 07. 864
Figure L.1.9 Seat D6 cross-sectional view snapshot 08. 864
Figure L.1.10 Seat D6 cross-sectional view snapshot 09. 865
Figure L.1.11 Seat D6 cross-sectional view snapshot 10. 865
Figure L.1.12 Seat D6 cross-sectional view snapshot 11. 865

Figure L.1.13 Seat D6 cross-sectional view snapshot 12. 865
Figure L.1.14 Seat D6 cross-sectional view snapshot 13. 866
Figure L.1.15 Seat D6 cross-sectional view snapshot 14. 866
Figure L.1.16 Seat D6 cross-sectional view snapshot 15. 866
Figure L.1.17 Seat D6 cross-sectional view snapshot 16. 866
Figure L.1.18 Seat D6 cross-sectional view snapshot 17. 867
Figure L.1.19 Seat D6 cross-sectional view snapshot 18. 867
Figure L.1.20 Seat D6 cross-sectional view snapshot 19. 867
Figure L.1.21 Seat D6 cross-sectional view snapshot 20. 867
Figure L.1.22 Seat D6 cross-sectional view snapshot 21. 868
Figure L.1.23 Seat D6 cross-sectional view snapshot 22. 868
Figure L.1.24 Seat D6 cross-sectional view snapshot 23. 868
Figure L.1.25 Seat D6 cross-sectional view snapshot 24. 868
Figure L.1.26 Seat D6 cross-sectional view snapshot 25. 869
Figure L.1.27 Seat D6 cross-sectional view snapshot 26. 869
Figure L.1.28 Seat D6 cross-sectional view snapshot 27. 869
Figure L.1.29 Seat D6 cross-sectional view snapshot 28. 869
Figure L.1.30 Seat D6 cross-sectional view snapshot 29. 870
Figure L.1.31 Seat D6 cross-sectional view snapshot 30. 870
Figure L.1.32 Seat D6 cross-sectional view snapshot 31. 870
Figure L.1.33 Seat D6 cross-sectional view snapshot 32. 870
Figure L.1.34 Seat D6 cross-sectional view snapshot 33. 871
Figure L.1.35 Seat D6 cross-sectional view snapshot 34. 871
Figure L.1.36 Seat D6 cross-sectional view snapshot 35. 871
Figure L.1.37 Seat D6 cross-sectional view snapshot 36. 871
Figure L.1.38 Seat D6 cross-sectional view snapshot 37. 872
Figure L.1.39 Seat D6 cross-sectional view snapshot 38. 872
Figure L.1.40 Seat D6 cross-sectional view snapshot 39. 872
Figure L.1.41 Seat D6 cross-sectional view snapshot 40. 872
Figure L.1.42 Seat D6 cross-sectional view snapshot 41. 873
Figure L.1.43 Seat D6 cross-sectional view snapshot 42. 873

Figure L.1.44 Seat D6 cross-sectional view snapshot 43. 873
Figure L.1.45 Seat D6 cross-sectional view snapshot 44. 873
Figure L.1.46 Seat D6 cross-sectional view snapshot 45. 874
Figure L.1.47 Seat D6 cross-sectional view snapshot 46. 874
Figure L.1.48 Seat D6 cross-sectional view snapshot 47. 874
Figure L.1.49 Seat D6 cross-sectional view snapshot 48. 874
Figure L.1.50 Seat D6 cross-sectional view snapshot 49. 875
Figure L.1.51 Seat D6 cross-sectional view snapshot 50. 875
Figure L.2.1 A schematic showing the frontal laser sheet direction and the camera location relative to the seat where the smoke generation source is located on seat D6. 876
Figure L.2.2 Seat D6 frontal view snapshot 01. 877
Figure L.2.3 Seat D6 frontal view snapshot 02. 877
Figure L.2.4 Seat D6 frontal view snapshot 03. 877
Figure L.2.5 Seat D6 frontal view snapshot 04. 877
Figure L.2.6 Seat D6 frontal view snapshot 05. 878
Figure L.2.7 Seat D6 frontal view snapshot 06. 878
Figure L.2.8 Seat D6 frontal view snapshot 07. 878
Figure L.2.9 Seat D6 frontal view snapshot 08. 878
Figure L.2.10 Seat D6 frontal view snapshot 09. 879
Figure L.2.11 Seat D6 frontal view snapshot 10. 879
Figure L.2.12 Seat D6 frontal view snapshot 11. 879
Figure L.2.13 Seat D6 frontal view snapshot 12. 879
Figure L.2.14 Seat D6 frontal view snapshot 13. 880
Figure L.2.15 Seat D6 frontal view snapshot 14. 880
Figure L.2.16 Seat D6 frontal view snapshot 15. 880
Figure L.2.17 Seat D6 frontal view snapshot 16. 880
Figure L.2.18 Seat D6 frontal view snapshot 17. 881
Figure L.2.19 Seat D6 frontal view snapshot 18. 881
Figure L.2.20 Seat D6 frontal view snapshot 19. 881
Figure L.2.21 Seat D6 frontal view snapshot 20. 881

Figure L.2.22 Seat D6 frontal view snapshot 21. 882
Figure L.2.23 Seat D6 frontal view snapshot 22. 882
Figure L.2.24 Seat D6 frontal view snapshot 23. 882
Figure L.2.25 Seat D6 frontal view snapshot 24. 882
Figure L.2.26 Seat D6 frontal view snapshot 25. 883
Figure L.2.27 Seat D6 frontal view snapshot 26. 883
Figure L.2.28 Seat D6 frontal view snapshot 27. 883
Figure L.2.29 Seat D6 frontal view snapshot 28. 883
Figure L.2.30 Seat D6 frontal view snapshot 29. 884
Figure L.2.31 Seat D6 frontal view snapshot 30. 884
Figure L.2.32 Seat D6 frontal view snapshot 31. 884
Figure L.2.33 Seat D6 frontal view snapshot 32. 884
Figure L.2.34 Seat D6 frontal view snapshot 33. 885
Figure L.2.35 Seat D6 frontal view snapshot 34. 885
Figure L.2.36 Seat D6 frontal view snapshot 35. 885
Figure L.2.37 Seat D6 frontal view snapshot 36. 885
Figure L.2.38 Seat D6 frontal view snapshot 37. 886
Figure L.2.39 Seat D6 frontal view snapshot 38. 886
Figure L.2.40 Seat D6 frontal view snapshot 39. 886
Figure L.2.41 Seat D6 frontal view snapshot 40. 886
Figure L.2.42 Seat D6 frontal view snapshot 41. 887
Figure L.2.43 Seat D6 frontal view snapshot 42. 887
Figure L.2.44 Seat D6 frontal view snapshot 43. 887
Figure L.2.45 Seat D6 frontal view snapshot 44. 887
Figure L.2.46 Seat D6 frontal view snapshot 45. 888
Figure L.2.47 Seat D6 frontal view snapshot 46. 888
Figure L.2.48 Seat D6 frontal view snapshot 47. 888
Figure L.2.49 Seat D6 frontal view snapshot 48. 888
Figure L.2.50 Seat D6 frontal view snapshot 49. 889
Figure L.2.51 Seat D6 frontal view snapshot 50. 889

Figure M.1.1 A schematic showing the cross-sectional laser sheet direction and the camera location relative to the seat where the smoke generation source is located on seat D11.... 891
Figure M.1.2 Seat D11 cross-sectional view snapshot 01. 892
Figure M.1.3 Seat D11 cross-sectional view snapshot 02. 892
Figure M.1.4 Seat D11 cross-sectional view snapshot 03. 892
Figure M.1.5 Seat D11 cross-sectional view snapshot 04. 893
Figure M.1.6 Seat D11 cross-sectional view snapshot 05. 893
Figure M.1.7 Seat D11 cross-sectional view snapshot 06. 893
Figure M.1.8 Seat D11 cross-sectional view snapshot 07. 893
Figure M.1.9 Seat D11 cross-sectional view snapshot 08. 894
Figure M.1.10 Seat D11 cross-sectional view snapshot 09. 894
Figure M.1.11 Seat D11 cross-sectional view snapshot 10. 894
Figure M.1.12 Seat D11 cross-sectional view snapshot 11. 894
Figure M.1.13 Seat D11 cross-sectional view snapshot 12. 895
Figure M.1.14 Seat D11 cross-sectional view snapshot 13. 895
Figure M.1.15 Seat D11 cross-sectional view snapshot 14. 895
Figure M.1.16 Seat D11 cross-sectional view snapshot 15. 895
Figure M.1.17 Seat D11 cross-sectional view snapshot 16. 896
Figure M.1.18 Seat D11 cross-sectional view snapshot 17. 896
Figure M.1.19 Seat D11 cross-sectional view snapshot 18. 896
Figure M.1.20 Seat D11 cross-sectional view snapshot 19. 896
Figure M.1.21 Seat D11 cross-sectional view snapshot 20. 897
Figure M.1.22 Seat D11 cross-sectional view snapshot 21. 897
Figure M.1.23 Seat D11 cross-sectional view snapshot 22. 897
Figure M.1.24 Seat D11 cross-sectional view snapshot 23. 897
Figure M.1.25 Seat D11 cross-sectional view snapshot 24. 898
Figure M.1.26 Seat D11 cross-sectional view snapshot 25. 898
Figure M.1.27 Seat D11 cross-sectional view snapshot 26. 898
Figure M.1.28 Seat D11 cross-sectional view snapshot 27. 898
Figure M.1.29 Seat D11 cross-sectional view snapshot 28. 899
Figure M.1.30 Seat D11 cross-sectional view snapshot 29. 899

Figure M.1.31 Seat D11 cross-sectional view snapshot 30. 899
Figure M.1.32 Seat D11 cross-sectional view snapshot 31. 899
Figure M.1.33 Seat D11 cross-sectional view snapshot 32. 900
Figure M.1.34 Seat D11 cross-sectional view snapshot 33. 900
Figure M.1.35 Seat D11 cross-sectional view snapshot 34. 900
Figure M.1.36 Seat D11 cross-sectional view snapshot 35. 900
Figure M.1.37 Seat D11 cross-sectional view snapshot 36. 901
Figure M.1.38 Seat D11 cross-sectional view snapshot 37. 901
Figure M.1.39 Seat D11 cross-sectional view snapshot 38. 901
Figure M.1.40 Seat D11 cross-sectional view snapshot 39. 901
Figure M.1.41 Seat D11 cross-sectional view snapshot 40. 902
Figure M.1.42 Seat D11 cross-sectional view snapshot 41. 902
Figure M.1.43 Seat D11 cross-sectional view snapshot 42. 902
Figure M.1.44 Seat D11 cross-sectional view snapshot 43. 902
Figure M.1.45 Seat D11 cross-sectional view snapshot 44. 903
Figure M.1.46 Seat D11 cross-sectional view snapshot 45. 903
Figure M.1.47 Seat D11 cross-sectional view snapshot 46. 903
Figure M.1.48 Seat D11 cross-sectional view snapshot 47. 903
Figure M.1.49 Seat D11 cross-sectional view snapshot 48. 904
Figure M.1.50 Seat D11 cross-sectional view snapshot 49. 904
Figure M.1.51 Seat D11 cross-sectional view snapshot 50. 904
Figure M.2.1 A schematic showing the frontal laser sheet direction and the camera location relative to the seat where the smoke generation source is located on seat D11. 905
Figure M.2.2 Seat D11 frontal view snapshot 01. 906
Figure M.2.3 Seat D11 frontal view snapshot 02. 906
Figure M.2.4 Seat D11 frontal view snapshot 03. 906
Figure M.2.5 Seat D11 frontal view snapshot 04. 906
Figure M.2.6 Seat D11 frontal view snapshot 05. 907
Figure M.2.7 Seat D11 frontal view snapshot 06. 907
Figure M.2.8 Seat D11 frontal view snapshot 07. 907

Figure M.2.9 Seat D11 frontal view snapshot 08. 907
Figure M.2.10 Seat D11 frontal view snapshot 09. 908
Figure M.2.11 Seat D11 frontal view snapshot 10. 908
Figure M.2.12 Seat D11 frontal view snapshot 11. 908
Figure M.2.13 Seat D11 frontal view snapshot 12. 908
Figure M.2.14 Seat D11 frontal view snapshot 13. 909
Figure M.2.15 Seat D11 frontal view snapshot 14. 909
Figure M.2.16 Seat D11 frontal view snapshot 15. 909
Figure M.2.17 Seat D11 frontal view snapshot 16. 909
Figure M.2.18 Seat D11 frontal view snapshot 17. 910
Figure M.2.19 Seat D11 frontal view snapshot 18. 910
Figure M.2.20 Seat D11 frontal view snapshot 19. 910
Figure M.2.21 Seat D11 frontal view snapshot 20. 910
Figure M.2.22 Seat D11 frontal view snapshot 21. 911
Figure M.2.23 Seat D11 frontal view snapshot 22. 911
Figure M.2.24 Seat D11 frontal view snapshot 23. 911
Figure M.2.25 Seat D11 frontal view snapshot 24. 911
Figure M.2.26 Seat D11 frontal view snapshot 25. 912
Figure M.2.27 Seat D11 frontal view snapshot 26. 912
Figure M.2.28 Seat D11 frontal view snapshot 27. 912
Figure M.2.29 Seat D11 frontal view snapshot 28. 912
Figure M.2.30 Seat D11 frontal view snapshot 29. 913
Figure M.2.31 Seat D11 frontal view snapshot 30. 913
Figure M.2.32 Seat D11 frontal view snapshot 31. 913
Figure M.2.33 Seat D11 frontal view snapshot 32. 913
Figure M.2.34 Seat D11 frontal view snapshot 33. 914
Figure M.2.35 Seat D11 frontal view snapshot 34. 914
Figure M.2.36 Seat D11 frontal view snapshot 35. 914
Figure M.2.37 Seat D11 frontal view snapshot 36. 914
Figure M.2.38 Seat D11 frontal view snapshot 37. 915
Figure M.2.39 Seat D11 frontal view snapshot 38. 915

Figure M.2.40 Seat D11 frontal view snapshot 39. 915
Figure M.2.41 Seat D11 frontal view snapshot 40. 915
Figure M.2.42 Seat D11 frontal view snapshot 41. 916
Figure M.2.43 Seat D11 frontal view snapshot 42. 916
Figure M.2.44 Seat D11 frontal view snapshot 43. 916
Figure M.2.45 Seat D11 frontal view snapshot 44. 916
Figure M.2.46 Seat D11 frontal view snapshot 45. 917
Figure M.2.47 Seat D11 frontal view snapshot 46. 917
Figure M.2.48 Seat D11 frontal view snapshot 47. 917
Figure M.2.49 Seat D11 frontal view snapshot 48. 917
Figure M.2.50 Seat D11 frontal view snapshot 49. 918
Figure M.2.51 Seat D11 frontal view snapshot 50. 918
Figure N.1.1 A schematic showing the cross-sectional laser sheet direction and the camera location relative to the seat where the smoke generation source is located on seat G6. 920
Figure N.1.2 Seat G6 cross-sectional view snapshot 01. 921
Figure N.1.3 Seat G6 cross-sectional view snapshot 02. 921
Figure N.1.4 Seat G6 cross-sectional view snapshot 03. 921
Figure N.1.5 Seat G6 cross-sectional view snapshot 04. 921
Figure N.1.6 Seat G6 cross-sectional view snapshot 05. 922
Figure N.1.7 Seat G6 cross-sectional view snapshot 06. 922
Figure N.1.8 Seat G6 cross-sectional view snapshot 07. 922
Figure N.1.9 Seat G6 cross-sectional view snapshot 08. 922
Figure N.1.10 Seat G6 cross-sectional view snapshot 09. 923
Figure N.1.11 Seat G6 cross-sectional view snapshot 10. 923
Figure N.1.12 Seat G6 cross-sectional view snapshot 11. 923
Figure N.1.13 Seat G6 cross-sectional view snapshot 12. 923
Figure N.1.14 Seat G6 cross-sectional view snapshot 13. 924
Figure N.1.15 Seat G6 cross-sectional view snapshot 14. 924
Figure N.1.16 Seat G6 cross-sectional view snapshot 15. 924
Figure N.1.17 Seat G6 cross-sectional view snapshot 16. 924

Figure N.1.18 Seat G6 cross-sectional view snapshot 17. 925
Figure N.1.19 Seat G6 cross-sectional view snapshot 18. 925
Figure N.1.20 Seat G6 cross-sectional view snapshot 19. 925
Figure N.1.21 Seat G6 cross-sectional view snapshot 20. 925
Figure N.1.22 Seat G6 cross-sectional view snapshot 21. 926
Figure N.1.23 Seat G6 cross-sectional view snapshot 22. 926
Figure N.1.24 Seat G6 cross-sectional view snapshot 23. 926
Figure N.1.25 Seat G6 cross-sectional view snapshot 24. 926
Figure N.1.26 Seat G6 cross-sectional view snapshot 25. 927
Figure N.1.27 Seat G6 cross-sectional view snapshot 26. 927
Figure N.1.28 Seat G6 cross-sectional view snapshot 27. 927
Figure N.1.29 Seat G6 cross-sectional view snapshot 28. 927
Figure N.1.30 Seat G6 cross-sectional view snapshot 29. 928
Figure N.1.31 Seat G6 cross-sectional view snapshot 30. 928
Figure N.1.32 Seat G6 cross-sectional view snapshot 31. 928
Figure N.1.33 Seat G6 cross-sectional view snapshot 32. 928
Figure N.1.34 Seat G6 cross-sectional view snapshot 33. 929
Figure N.1.35 Seat G6 cross-sectional view snapshot 34. 929
Figure N.1.36 Seat G6 cross-sectional view snapshot 35. 929
Figure N.1.37 Seat G6 cross-sectional view snapshot 36. 929
Figure N.1.38 Seat G6 cross-sectional view snapshot 37. 930
Figure N.1.39 Seat G6 cross-sectional view snapshot 38. 930
Figure N.1.40 Seat G6 cross-sectional view snapshot 39. 930
Figure N.1.41 Seat G6 cross-sectional view snapshot 40. 930
Figure N.1.42 Seat G6 cross-sectional view snapshot 41. 931
Figure N.1.43 Seat G6 cross-sectional view snapshot 42. 931
Figure N.1.44 Seat G6 cross-sectional view snapshot 43. 931
Figure N.1.45 Seat G6 cross-sectional view snapshot 44. 931
Figure N.1.46 Seat G6 cross-sectional view snapshot 45. 932
Figure N.1.47 Seat G6 cross-sectional view snapshot 46. 932
Figure N.1.48 Seat G6 cross-sectional view snapshot 47. 932

Figure N.1.49 Seat G6 cross-sectional view snapshot 48. 932
Figure N.1.50 Seat G6 cross-sectional view snapshot 49. 933
Figure N.1.51 Seat G6 cross-sectional view snapshot 50. 933
Figure N.2.1 A schematic showing the frontal laser sheet direction and the camera location relative to the seat where the smoke generation source is located on seat G6. 934
Figure N.2.2 Seat G6 frontal view snapshot 01. 935
Figure N.2.3 Seat G6 frontal view snapshot 02. 935
Figure N.2.4 Seat G6 frontal view snapshot 03. 935
Figure N.2.5 Seat G6 frontal view snapshot 04. 935
Figure N.2.6 Seat G6 frontal view snapshot 05. 936
Figure N.2.7 Seat G6 frontal view snapshot 06. 936
Figure N.2.8 Seat G6 frontal view snapshot 07. 936
Figure N.2.9 Seat G6 frontal view snapshot 08. 936
Figure N.2.10 Seat G6 frontal view snapshot 09. 937
Figure N.2.11 Seat G6 frontal view snapshot 10. 937
Figure N.2.12 Seat G6 frontal view snapshot 11. 937
Figure N.2.13 Seat G6 frontal view snapshot 12. 937
Figure N.2.14 Seat G6 frontal view snapshot 13. 938
Figure N.2.15 Seat G6 frontal view snapshot 14. 938
Figure N.2.16 Seat G6 frontal view snapshot 15. 938
Figure N.2.17 Seat G6 frontal view snapshot 16. 938
Figure N.2.18 Seat G6 frontal view snapshot 17. 939
Figure N.2.19 Seat G6 frontal view snapshot 18. 939
Figure N.2.20 Seat G6 frontal view snapshot 19. 939
Figure N.2.21 Seat G6 frontal view snapshot 20. 939
Figure N.2.22 Seat G6 frontal view snapshot 21. 940
Figure N.2.23 Seat G6 frontal view snapshot 22. 940
Figure N.2.24 Seat G6 frontal view snapshot 23. 940
Figure N.2.25 Seat G6 frontal view snapshot 24. 940
Figure N.2.26 Seat G6 frontal view snapshot 25. 941

Figure N.2.27 Seat G6 frontal view snapshot 26. 941
Figure N.2.28 Seat G6 frontal view snapshot 27. 941
Figure N.2.29 Seat G6 frontal view snapshot 28. 941
Figure N.2.30 Seat G6 frontal view snapshot 29. 942
Figure N.2.31 Seat G6 frontal view snapshot 30. 942
Figure N.2.32 Seat G6 frontal view snapshot 31. 942
Figure N.2.33 Seat G6 frontal view snapshot 32. 942
Figure N.2.34 Seat G6 frontal view snapshot 33. 943
Figure N.2.35 Seat G6 frontal view snapshot 34. 943
Figure N.2.36 Seat G6 frontal view snapshot 35. 943
Figure N.2.37 Seat G6 frontal view snapshot 36. 943
Figure N.2.38 Seat G6 frontal view snapshot 37. 944
Figure N.2.39 Seat G6 frontal view snapshot 38. 944
Figure N.2.40 Seat G6 frontal view snapshot 39. 944
Figure N.2.41 Seat G6 frontal view snapshot 40. 944
Figure N.2.42 Seat G6 frontal view snapshot 41. 945
Figure N.2.43 Seat G6 frontal view snapshot 42. 945
Figure N.2.44 Seat G6 frontal view snapshot 43. 945
Figure N.2.45 Seat G6 frontal view snapshot 44. 945
Figure N.2.46 Seat G6 frontal view snapshot 45. 946
Figure N.2.47 Seat G6 frontal view snapshot 46. 946
Figure N.2.48 Seat G6 frontal view snapshot 47. 946
Figure N.2.49 Seat G6 frontal view snapshot 48. 946
Figure N.2.50 Seat G6 frontal view snapshot 49. 947
Figure N.2.51 Seat G6 frontal view snapshot 50. 947
O.1 A comparison between all tests performed with a continuous injection source (Blue) vs. a coughing manikin (Red) in the Boeing 767 cabin mockup. 949
O.2 A comparison between common tests performed with continuous injection source (Blue) vs. coughing manikin (Red) in the Boeing 767 cabin mockup. 950

O.3 A comparison between all tests performed with a continuous injection source in the Boeing 767 cabin mockup (Blue) and the modified cabin (Red). 951

List of Tables

Table 1.1. List of Main Contaminants that are of Concern in Aircraft Cabins..... 3
Table 3.1. Air conditioning system equipment list and specifications. 63
Table 3.2. Air conditioning system sensors locations and details. 66
Table 3.3. Average supply air velocity at each newly installed PVC duct in the modified cabin. 76
Table 4.1. Tests notations and interpretation. 95
Table 4.2. Experimental procedures sequence for the tests performed in the Boeing 767 cabin mockup and the modified cabin. 97
Table 4.3. Experimental procedures sequence for the tests performed in the Boeing 737 cabin section. 103
Table 4.4. Experimental procedures sequence for the tests performed using the coughing manikin. 105
Table 4.5. Subsystems and associated uncertainty elements. 120
Table 4.6. Supply air instruments uncertainty and range. 121
Table 4.7. Purity and uncertainty of each tracer gas components. 127
Table 4.8. Mass flow controllers' uncertainty and rated flowrate. 128
Table 4.9. CO_2 sampling system uncertainty and range. 130
Table 4.10. Repeatability analysis results for the four main CO_2 gas analyzers. 131
Table 4.11. CO_2 gas analyzers calibration results. 131
Table 4.12. CO_2 gas analyzers uncertainty results. 132
Table 5.1. Number of tests for each test category listed in Figure 5.1. 137
Table 5.2. Average percentage increase in tracer gas concentration over supply air concentration for the Boeing 767 cabin mockup and the modified cabin. 146

Acknowledgements

I would like to express my sincere gratitude to Dr. Mo. Hosni and Dr. Byron Jones for their guidance and support throughout my Ph.D. journey. I would like to thank Dr. Hosni for his enormous support and advice on the academic and personal sides. Dr. Hosni has always been encouraging and made sure that I get the best out of my Ph.D. degree, not only academically but professionally. Special thanks to Dr. Jones, as well, for his extraordinary advice and fruitful feedbacks on my work. I have learnt so much beyond academia from my discussions with him.

I would like to thank Dr. Mingjun Wei, and Dr. Donald L. Fenton for being members on my supervisory committee and for providing suggestions and corrections to my dissertation. I would like to give special thanks to Dr. James Bennett for being the sponsor`s project officer and an external committee member. His support and feedback were vital for my Ph.D. degree accomplishment. In addition, I would like to thank Dr. Christopher Sorenson for serving as an outside chairperson on my committee. Finally, I would like to thank my family, friends, and colleagues for their encouragement, help, and support.

This research was funded by the Centers for Disease Control (CDC) of the National Institute for Occupational Health (NIOSH). The findings and conclusions in this dissertation are those of the author and do not necessarily represent the views of NIOSH.

Dedication

This dissertation is dedicated to everyone who believed in me one day.

Chapter 1 - Introduction

The Bureau of Transportation Statistics (BTS) indicated that U.S. airlines and foreign airlines serving just the U.S. carried an all-time high of 1.1 billion domestic and international scheduled service passengers in 2019. This number is 3.9% more than the previous annual record high of 1.0 billion reached in 2018 (Bureau of Transportation Statistics, 2020). The load factor is a terminology used to measure the capacity utilization of public transport services including aircrafts. In 2019, the load factor increased by 0.8 points from 83% to 83.8% compared to the previous year. This means that more passengers were filling the same size aircrafts as compared to the previous year. Figure 1.1 shows the number of annual passengers on all U.S. scheduled airline flights (domestic & international) and foreign airline flights to and from the United States between 2003-2019.

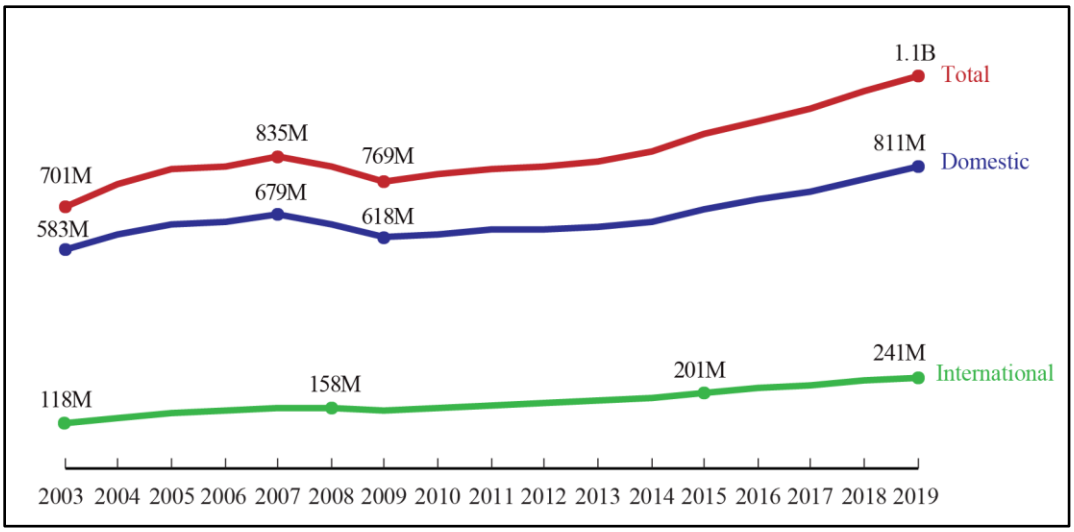

Figure 1.1. Annual passengers on all United States scheduled airline flights (domestic & international) and foreign airline flights to and from the United States between 2003-2019 (Bureau of Transportation Statistics, 2020).

Travelling on-board aircrafts can present a high infection risk especially in highly occupied flights. While apparently not frequent, events related to cabin air quality do occur on aircraft. For this discussion, these events are divided into two broad categories: 1) chemical events that result for chemical contaminants in the cabin air, and 2) biological events related to onboard disease transmission. Table 1.1 classifies the contaminants that are of concern in aircraft cabins. With the recent outbreak of disease spread during several flights, researchers directed more attention to cabin air distribution and infectious disease control in aircraft cabins. Chemical incidents that were reported can be related to smoke and fumes detected inside passengers' aircraft cabins. The smoke and fumes are thought to be a result of oil that may leak into the propulsion engine compressor and be thermally degraded under high temperature and pressure inside the compressor. This contamination would then be present in the bleed air extracted from the compressor which supplies the ventilation for the cabin and can be of a potential toxicity. On the other hand, several cases of biological incidents were documented for actual on-board infectious diseases transmission. These include cases such as cholera (R. Baron et al., 2002), influenza (Baker et al., 2010; Foxwell et al., 2011; Lim Ooi et al., 2010), measles (Hoad et al., 2013), norovirus (Kirking et al., 2010), severe acute respiratory syndrome (SARS) (T.-J. Chen et al., 2003; Desenclos et al., 2004), shigellosis, and tuberculosis (Kenyon et al., 1996).

Table 1.1. List of Main Contaminants that are of Concern in Aircraft Cabins.

Chemical	Carbon Monoxide CO
	Carbon Dioxide CO_2
	Ozone O_3
	Volatile Organic Compounds (VOC)
	Semi-volatile Organic Compounds (SVOC)
	Insecticides
Biological	Bacteria
	Fungi
	Viruses
Physical	Particulate matters

This dissertation is focused on the dispersion of aerosols that can cause infections by biological agents. The dissertation is divided into several chapters breaking down the main topic into first understanding the literature background of the subject, then detailing the experimental setup that was used in the development of this work. Later on, the testing procedures and results for analyzing the transport and containment of the possibly infectious aerosols in different aircraft cabins are discussed. Also, a smoke visualization work is reported to highlight the main cabin airflow patterns and qualitatively inspect the dispersion of the aerosols in the cabin. Finally, an analysis and conclusion of the results is provided.

Chapter 2 - Literature Review

The enormous number of travelers that utilize air travel everyday has led to an increased awareness about exposure to airborne contaminants in aircraft cabins and raised concerns over the safety and wellbeing of the travelers on-board the aircraft. The aircraft cabin is similar to the rest of indoor environments, such as, homes and workplaces, in that individuals are presented to a blend of outside and recirculated air. In contrast, the cabin environment is distinctive in numerous regards—for instance, the high number of occupants, the inability of occupants to leave willingly, and the requirement for pressurization. In flight, passengers and crew experience a combination of physical factors that includes low humidity, and low air pressure. At times, they could also be introduced to air contaminants, such as, ozone (O_3), carbon monoxide (CO), different natural synthetic compounds, and biological agents. Although the recirculated air on most aircraft passes through high efficiency particulate air (HEPA) filters, travelers and cabin crew have raised concerns and complaints about the air quality in aircraft cabins (National Research Council, 1986). These complains include weakness, dizziness, headaches, sinus and ear problems, dry eyes, sore throat, and incidentally more serious illnesses, for example, nervous system disorders and incapacitation. Subsequently, to guarantee the thermal comfort of travelers and cabin crew, various organizations have set guidelines and standards related to aircraft cabins. These include cabin air pressure, thermal comfort and temperature within the cabin, ventilation rate, and carbon dioxide (CO_2), CO, and O_3 allowable concentrations. While humidity may influence traveler comfort and wellbeing, the FAA does not regulate allowable humidity levels in aircraft cabins.

Regardless of the apparent guidelines and recommendations, there has been a few transmission incidents of infectious diseases in aircraft cabins. The transmission of Ebola, MERS, influenza, SARS, etc. were recorded on actual flights. Nevertheless, the airlines stay uncertain about strategies to mitigate disease spread in aircraft cabins. This is largely due to the enormous number of travelers and the unknown nature of some infectious diseases and their asymptomatic behavior.

2.1 Aircraft Cabin Air Quality Standards

Many guidelines and standards which were established by different organizations for air quality in indoor and outdoor environments may be applicable to aircraft cabins. At the same time, there are specific regulations established for aircraft cabins by a limited number of organizations and authorities. Among those organizations are: Federal Aviation Administration (FAA), the Environmental Protection Agency (EPA), Occupational Safety and Health Administration (OSHA), the American Conference of Governmental Industrial Hygienists (ACGIH), and the American Society of Heating, Refrigerating and Air-Conditioning Engineers (ASHRAE). FAA is the only organization with administrative authority to establish standards for the aircraft cabin environment. EPA publishes national ambient air-quality standards (NAAQSs) for outdoor air. OSHA establishes permissible occupational exposure limits (PELs), and ACGIH recommends threshold limit values (TLVs) to protect workers health. ASHRAE is a professional society that has committees that provide guidelines on exposure in indoor environments, including those of aircraft. Because the limits established by OSHA and ACGIH are intended for application in workplaces populated by healthy adults of working age, they are not expected to apply in

environments where infants, children, the elderly, or those with medical conditions might be exposed.

Commercial aircrafts are designed to operate in harsh external environments. The external environments of the aircraft during taxiing, takeoff, cruise, and descent could vary largely. Outside ambient temperature can range from -55°C (-65°F) to 50°C (122°F), ambient pressure from about 10.1 kPa (1.5 psi) to 101 kPa (14.7 psi), and water content from virtually dry to greater than saturation (National Research Council, 2002). For an aircraft to transport passengers in those extremes of external environment, they are equipped with an environmental control system (ECS) that provides a suitable indoor environment. During flight, the aircraft cabin is a ventilated and enclosed environment whose occupants are totally dependent on the conditioned air provided by the ECS. The ECS is designed and operated to provide a healthy and comfortable environment for the aircraft occupants from boarding to arrival times. The ECS must pressurize the aircraft cabin and maintain its temperature within the standard limits. While the other functions of the ECS are important, they are subordinate to those requirements especially at cruise altitudes.

2.1.1 Cabin Air Temperature and Humidity

While the FAA does not specify the acceptable temperature or humidity ranges for aircraft cabins, it requires reasonable passenger comfort to be provided (Federal Aviation Administration, 2010). The national aeronautics and space administration (NASA) sets the reasonable temperature range for comfortable working and living as 18 to 27 °C (65 to 80 °F), and the relative humidity (RH) from 25 to 70% (National Aeronautics and Space Administration, 1994). ASHRAE develops standards for commercial aircraft air quality

through its relevant committees. The target temperature range for both in-flight and ground operation according to ASHRAE is 18.3°C to 23.9°C (65°F to 75°F). The maximum operative temperature for ground operations is 26.7°C (80°F) if in-flight entertainment systems are not present or not operating and 29.4°C (85°F) if all such systems are in operation (ASHRAE, 2018). ASHRAE also requires that the horizontal and vertical temperature variation across a temperature control zone be within 4.4°C and 2.8°C (8°F and 5°F), respectively (ASHRAE, 2018). Cabin sections temperature must be within 2.8°C (5°F) of each other as required by the FAA. ASHRAE does not specify a range for RH because minimum RH limit may negatively affect the safe operation of the aircraft and may conflict with the fresh air ventilation requirements (ASHRAE, 2018). Similarly, ASHRAE does not impose any restrictions on the maximum limit of the RH range (ASHRAE, 2018). This is because the maximum allowable RH for safety considerations is actually lower than the upper limits of RH for occupant comfort. Furthermore, slight increases in RH in the aircraft cabin air may have a positive impact on occupant health and comfort (ASHRAE, 2016).

2.1.2 Cabin Air Pressure

The Federal Aviation Regulation (FAR) requires the pressurization system to provide a cabin pressure altitude of not more than 2,440 m (8000 ft) under normal operating conditions. This limit corresponds to a cabin pressure of 75 kPa (10.9 psi). Thus, the cabin pressure can range from a maximum of 101 kPa (14.7 psi) on the ground at sea level to a minimum of 75 kPa (10.9 psi) in flight regardless of the altitude at which the aircraft is operating at (National Research Council, 2002).

2.1.3 Cabin Air Ventilation

Four major factors are considered when determining flowrate requirements for the ECS. Those are: outside air flowrate required to remove contaminants from the cabin, conditioned air flowrate required to remove heat from the cabin, total air flowrate required to provide adequate circulation in the cabin, and the outside air flowrate required to pressurize the aircraft. In older aircrafts, all the air supplied to the cabin was provided from outside air. Hence, the outside air flowrate had to be large enough to meet the maximums of all four requirements even though it usually resulted in outside air flowrates larger than the minimum required. This practice was shown to be cost ineffective in supplying compressed air to the cabin during flight. Therefore, using air recirculation has been common in the design of ECSs for both buildings and aircrafts for many years. In contrast with aircraft, in which the total air flow to the cabin varies from 0% to 55% of recirculated air, building ECS are commonly designed and operated with up to 90% recirculated air (National Research Council, 2002).

In addition to supplying outside air to the cabin, the ventilation system distributes and circulates air in the aircraft cabin. Typically, air is supplied and exhausted along the whole length of the cabin. Although the air mixes locally in the cabin, the air supply and exhaust flowrates are matched along the length of the cabin. This practice is carried out to minimize net flows along the length of the aircraft. A number of diffusers are used to distribute the air in the aircraft cabin. They are usually located along the ceiling and above center of the aisles, above the windows, or along the overhead luggage compartments. In general, air is supplied to the cabin from one or more linear diffusers that extend along the length of the cabin. Wide-body aircrafts usually use multiple diffusers. The velocities and circulation patterns in the

cabin are determined by the location, configuration, and flowrates of the inlet diffusers. The supply air is balanced with the exhaust air of an equal amount. The exhausted air is generally removed from the cabin at floor level and at the side walls and sometimes through the ceiling. Some of the exhausted air is recirculated to the cabin after passing through HEPA filters. The remaining exhausted air from the cabin is usually passed around or through the cargo compartment before being dumped overboard through an outflow valve. Air from the lavatories and galley areas are exhausted directly to the outflow valves to avoid contaminating air in other parts of the cabin with odors or other contaminants.

The FAA requires that commercial aircraft provide at least 0.25 kg/min (0.55 lb./min) of fresh air per occupant. At a cabin altitude of 2440 m (8000 ft), this is equivalent to 0.283 m^3/min (10 ft^3/min). ASHRAE standard 161 requires a minimum of 0.425 m^3/min (15 ft^3/min) of fresh air per person and recommends a minimum of 0.566 m^3/min (20 ft^3/min) per person (ASHRAE, 2007). The 0.425 m^3/min (15 ft^3/min) minimum requirement may be met with either 100% outside air or a mixture of outside and recirculated air but at least .2125 m^3/min (7.5 ft^3/min) per person must be outside air, assuming a ventilation effectiveness of at least one (ASHRAE, 2018). Most aircraft nowadays provide extra ventilation with recirculated air in addition to the minimum required fresh air per occupant. To reduce the spread of contaminants through the cabin, the recirculated air goes through the HEPA filters before returning to the cabin. While not mandated by the FAA, HEPA filters are used almost universally for aircraft recirculation air for the health and safety of the occupants. This is due to their capability of removing most of the airborne contaminants in the recirculation air before it is mixed with the outside air and supplied back into the cabin.

2.2. Contamination Exposure in Aircraft Cabins

In the aircraft cabin, occupants may be exposed to various air contaminants, including CO from engine exhaust, O_3 that enters with outside air, organic compounds generated by emissions from materials in the cabin and the human body, and infectious agents, allergens, irritants, and other contaminants of biological origin.

2.2.1 Contamination Sources in Aircraft Cabins

Contaminants can originate in the aircraft cabin itself or in sources outside the cabin and then migrate to the cabin. The concentrations of contaminants in the cabin can change as a result of fluctuations in the source emission, ventilation rates, or contaminants reactions with other chemicals in the cabin. Outdoor air up to an altitude of about 1500 m (4900 ft) contains abundant biological materials (Lacey & Venette, 1995; Lighthart & Mohr, 1994) especially fungal spores, pollen grains, airborne bacteria and fragments of insects, plants, and soil depending on where the plane is located and the ambient conditions. At flight altitude, the air outside an aircraft may also contain many of the same bioaerosols found at ground level, but at much lower concentrations (Lighthart & Mohr, 1994). There are several factors that greatly reduce the severity or harmfulness of infectious agents that may be in the outside air at flight altitude. Those include: exposure to solar radiation, the presence of ambient air pollutants, and low air temperature and relative humidity (Kim, 1994; Mohr, 1997). Furthermore, the high compression temperatures of about 250°C (482°F) and pressure of about 3000 kPa (435 psi) of the bleed air used for ventilation are likely to change allergenic proteins and inactivate microorganisms (Withers & Christopher, 2000). Therefore, the likelihood of allergic reactions from components of outside air during flight is low and in-

flight biological agents in aircraft cabins arise mainly from sources that exist in the cabin itself.

Contaminants inside the cabin can be from different sources including the passengers and crew members. Those sources can take the form of bio effluents, viruses, bacteria, allergens, and spores and are shed from clothing, skin, or expelled from oral, nasal, or rectal orifices. Those microorganisms are normally found on the human body and rarely cause infections. They can also be found on other surfaces in the aircraft cabin such as passengers' luggage and personal items, food, and sanitation fluids. For example, settled dust is one of the most important reservoirs of indoor allergens and other biological agents, and the allergen content of dust is a primary indicator of exposure to many allergens (Platts-Mills & Carter, 1997; Trudeau & Fernández-Caldas, 1994). Although some of those microorganisms have inflammatory properties, very few are infectious, or they cause infection only in severely immunosuppressed persons. Hence, the main route for infectious agents inside the aircraft cabin remains via human to human interaction and people are the primary source of airborne bacteria and are the main reservoirs of infectious agents (Bagshaw & Illig, 2019). The infectious agents' sources and dispersion mechanism are not specific to the aircraft cabin environment. However, aircraft cabins are denser in passenger's occupancy and smaller in area. The several known human to human transmission modes for infectious agents are airborne and droplet particles, fomite, and physical contact.

2.2.2 Common Infectious Diseases Transmitted in Aircraft Cabins

On aircraft, people are confined in a small space for long periods and then disembark to many destinations (Wilson, 1995). Thus, the risk of exposure to infectious agents is higher for travelers than other persons, especially on long-haul international flights. In addition to direct infection, their exposure to infectious agents may extend to all others with whom they later have contact with even after their arrival. Air travel is rapid, and people can complete a journey in the preclinical stage of an infectious disease (Clayton et al., 1976; Dupont et al., 2001). Passengers now can complete longer nonstop flights which increase both the time that travelers spend together in an aircraft and the opportunities for exposure to infectious agents. In the earlier days of transportation, infectious disease commonly had time to develop to its recognized clinical form before travelers reached their destinations (Grainger et al., 1995). Those factors give considerable public-health significance to the connection between infectious diseases and air travel (British Research Establishment, 2005; Brown et al., 2001; Sato et al., 2000).

In the aircraft cabin, infectious agents transmitted by person-to-person droplet contact and airborne transmission of droplet nuclei are the main concern (National Research Council, 2002). Droplet nuclei can remain suspended in cabin air and be distributed throughout an aircraft. Many authors studied the spread of different infectious substances in aircraft cabins. Several cases were documented for actual on-board infection transmission. These include cases of cholera (R. Baron et al., 2002), influenza (Baker et al., 2010; Foxwell et al., 2011; Lim Ooi et al., 2010), measles (Hoad et al., 2013), norovirus (Kirking et al., 2010), SARS (T.-J. Chen et al., 2003; Desenclos et al., 2004), shigellosis, and tuberculosis (Kenyon et al., 1996).

Of the communicable diseases discussed in the literature, tuberculosis, meningococcal meningitis, and plague are among the diseases for which there are special requirements related to travelers and the operation of conveyances and for which travelers can be detained to prevent the introduction, transmission, or spread of the disease in the United States (National Research Council, 2002). As of 2020, the list includes cholera, diphtheria, tuberculosis, plague, smallpox, yellow fever, viral hemorrhagic fevers (Lassa, Marburg, Ebola, Crimean-Congo, South American, and others not yet isolated or named), severe acute respiratory syndromes (e.g., SARS, MERS), and influenza caused by novel or reemergent influenza viruses that are causing, or have the potential to cause, a pandemic (Centers for Disease Control and Prevention, 2020a).

2.2.2.1 Influenza

Influenza is a highly contagious, viral respiratory illness. Influenza A and influenza B are the major types of influenza viruses that cause disease in persons of all ages (Centers for Disease Control and Prevention, 2001b). Influenza virus spreads from person to person primarily via the airborne route when the sick infectious person coughs or sneezes (Murphy & Webster, 1996). The incubation period for influenza is 1–4 days (Centers for Disease Control and Prevention, 2017) and the infectious period can start the day before symptoms begin until about 5 days after illness onset with the children having the ability to remain infectious for longer periods. In 1977, an outbreak of influenza among passengers and crew exposed to an acutely ill passenger on-board a 56-seat commercial jet had occurred as reported by (Moser et al., 1979). Out of the 56 passengers and the cabin crew, 38 (72% of persons on-board) got infected with the influenza virus and four passengers required

hospitalization. The flight had a greater than 3 hours ground delay before taking off. While on the ground, the ventilation system was not operating, and the doors were kept closed for about 2 hours. The authors concluded that proper operation of the air circulation equipment and isolation of the ill passenger might have prevented this outbreak and that the high attack rate was attributed to the failure of the ventilation system. In another incident, suspected transmission of influenza associated with air travel also has been reported by (Klontz et al., 1989). In this case, in contrast to the one reported by (Moser et al., 1979), the ventilation system was operating and no ground delay took place. Ninety team members traveled on a roundtrip flight on-board a DC-9 from Puerto Rico to Florida. Twenty-three of 77 previously well passengers on these 2.5 hours flights developed severe influenza-like respiratory illness within 72 hours of their return. Eleven of the case patients reported actively coughing during the return flight. When comparing the two incidents, a significant difference in risk of acquiring influenza is observed and was related to the number of symptomatic persons on-board. Secondary transmission of influenza to family member and roommates was also identified.

Immunization is the primary method used to prevent influenza infection and its complications (Centers for Disease Control and Prevention, 2001b). Annual influenza immunization is recommended for tourism industry workers (Centers for Disease Control and Prevention, 1999). Public-health authorities do not recommend general use of antiviral medications for all travelers to prevent influenza because the drugs can have side effects and must be prescribed by a physician. However, antiviral medications might be appropriate during an influenza outbreak for unvaccinated travelers and persons who are at increased risk for influenza-related complications (Centers for Disease Control and Prevention, 2009).

2.2.2.2 Measles

Measles is an acute, highly communicable viral disease with an average incubation period of 10–12 days (Centers for Disease Control and Prevention, 2015b). Similar to influenza, measles spreads through the air when an infected person coughs or sneezes. It is so contagious that if one person has it, up to 9 out of 10 people around them can get infected (Centers for Disease Control and Prevention, 2019b). Before widespread immunization, measles was common in childhood; 90% of people were infected by the age of 20. Between 1993 and 2002, fewer than 1,000 measles cases have been reported each year in the United States (Centers for Disease Control and Prevention, 2001b), many of which are imported from outside the United States. Between 2010 and 2020, about 3429 cases were recorded in the United States (Centers for Disease Control and Prevention, 2020b).

Measles is still a widespread disease in several countries, including some developed countries in Europe and Asia. Hence, air travel exposure is still considered a possibility. Suspected transmission of measles at an airport and between passengers who shared a domestic flight has been reported (Centers for Disease Control and Prevention, 1983), and transmission also may have occurred during international air travel (Mangili & Gendreau, 2005). Amler et al. (1982) reported a case where three children who traveled from Venezuela to the United and were tested positive for measles after arriving. During the flight, one of the three children had early symptoms and the onset of rash in the other two children was noticed 12 days after the flight. In addition, secondary transmission to other children was also identified. In 2005, eight cases of measles were associated with a New York-Tel Aviv commercial flight (Mangili & Gendreau, 2005). Although the source passenger was not identified, the authors believed that the transmission could have occurred during a 2-hour

ground delay during which the aircraft's air-conditioning system was not operating or during the 10-hour flight.

2.2.2.3 Tuberculosis (TB)

Tuberculosis is caused by Mycobacterium tuberculosis, a bacterium that can attack any part of the body but most frequently is associated with pulmonary infection. TB is mainly spread when the patient is coughing and has numerous organisms in secretions from the lungs (Heymann, 2004). People can become infected when spending a long period of time in a closed environment where the air is contaminated by a patient with untreated tuberculosis. The typical time from exposure to a detectable infection is 4–12 weeks (Heymann, 2004). About 25% of the world`s population is estimated to be infected with tuberculosis (World Health organization (WHO), 2020), however, about 90% of otherwise healthy adults who acquire tuberculosis infection never develop active disease and therefore do not experience symptoms and are not infectious to others.

TB is the most thoroughly studied communicable disease possibly associated with transmission during commercial air travel (World Health organization (WHO), 2013b). It is also a disease with several formal guidelines for recognition and prevention (British Research Establishment, 2005). Yet, no case of confirmed active tuberculosis has been identified as a result of exposure on a commercial aircraft, but the number of potentially exposed people who have been successfully screened in these investigations remains very small (Kotila et al., 2016).

2.2.2.4 Meningococcal Disease

Meningococcal disease is an acute bacterial infection characterized by sudden onset with fever, intense headache, nausea, and stiff neck. The incubation period typically is 3 to 4 days but may range from 2 to 10 days (Heymann, 2004). Case-fatality rates of meningococcal disease used to exceed 50%, but even with early diagnosis, modern therapy, antibiotic, and supportive measures, they are still between 10–15% (Centers for Disease Control and Prevention, 2015c).

Several persons with meningococcal disease flew on commercial aircrafts, and passengers seated next to an infected person may be at higher risk than other passengers for developing meningococcal disease (Centers for Disease Control and Prevention, 2001a). Most recorded cases of meningococcal disease between air passengers are not detected until after the flight has landed and the passengers have dispersed (Centers for Disease Control and Prevention, 2001a). However, studies such as by (Kenyon et al., 1996) emphasized on the possibility of in-flight meningococcal disease infection. The authors analyzed an actual transmission case and regarded the high infection rate to several reasons. Those are: the highly infectious passenger, the long flight duration, and the close proximity of contacts to the index patient.

2.2.2.5 Middle Eastern Respiratory Syndrome Coronavirus (MERS-CoV)

The Middle East respiratory syndrome coronavirus (MERS-CoV) was first discovered in 2012 in a patient who died from a severe respiratory disease. Since then, and as of January 2020, around 2521 cases have been reported worldwide, including 919 deaths with a crude case fatality rate of 36% (European Centre For Disease Prevention And Control, 2020). MERS-CoV, is believed to spread from an infected person's respiratory secretions, such as by coughing. However, the precise ways the virus spreads are not currently well-understood. MERS-CoV has spread from ill people to others through close contact, such as caring for or living with an infected person. Infected people have spread MERS-CoV to others in healthcare settings, such as hospitals (Centers for Disease Control and Prevention, 2015a). The typical symptoms include fever, cough, dyspnea, and gastrointestinal symptoms. Renal or pulmonary failure have also been reported in fatal cases. Travel-associated MERS-CoV cases have been reported in at least 17 countries and all of them were related to travelers incubating MERS-CoV during their travel. No transmission on aircrafts has been documented to date (Baharoon & Memish, 2019).

In a report prepared by (European Centre For Disease Prevention And Control, 2020), 728 articles that discussed MERS transmission cases during the symptomatic phase of the disease were reviewed. During the screening process, 21 cases of MERS-CoV who had travelled by aircraft were identified to be included. Those 21 cases boarded a total of 31 flights with flights durations between 1 hour and 20 minutes to 9 hours and 30 minutes. During the screening process, 16 records were found describing eight cases of MERS-CoV infection who had travelled by aircraft before symptom onset. For two of these cases, contact tracing of passengers on the flights was conducted. No secondary cases related to any of the

eight confirmed cases of MERS who undertook flights have been reported. The report suggested that the absence of any detected on-board transmission event suggested a low probability of transmission. However, this does not preclude that the impact of one exported case could possibly be high.

The 2015 MERS-CoV outbreak in South Korea began from a single imported case. The index patient was a 68-year-old male with a recent travel history to several Middle Eastern countries. Among the countries the patient had travelled to, were countries which had reported human cases of MERS-CoV during the same period of time. Those countries were Bahrain, the United Arab Emirates, Saudi Arabia, and Qatar. The patient required medical assistance at several clinics before being admitted to a hospital, where he was confirmed to be infected with MERS-CoV (World Health organization (WHO), 2015). The index patient was called a super-spreader because twenty-nine secondary infections resulted indirectly from him. Furthermore, two of the infected secondary cases were also called super-spreaders and were responsible for causing 106 subsequent infections, out of 166 known cases at the time (Cowling & Yu, 2015). Although this MERS-CoV outbreak is the second largest on record and the largest outside of the Middle East, it appears to be under control nowadays, with no other infections reported in South Korea since July 4, 2015.

Two cases with confirmed MERS-CoV have been documented in the UK. Of these two cases, the first was transported to the UK via private air ambulance and the second travelled on a commercial flight. Both were symptomatic during their flights. No transmissions were identified among the contacts on either of these flights. However, two family contacts of the second case were later reported as confirmed cases after a transmission that occurred in the household and hospital settings in the UK (Parry-Ford et al., 2015).

178 passengers took a flight on 24 April 2014, including a passenger infected with MERS-CoV. Of the 49 passengers who were seated around the infected passenger, eleven were seated within two seats all around the case and the remaining were seated elsewhere. Authorities successfully contacted 36 of those passengers. None of the eleven passengers seated within two rows reported any symptoms in the 14 days after taking the flight. However, three of the remaining passengers reported mild respiratory symptoms during this period and were still symptomatic (Parry-Ford et al., 2015). For such unpredicted transmission cases, some researchers adopted mathematical models to predict the potential for within flight transmission of MERS-CoV (Coburn & Blower, 2014). Using this statistical analysis model, the authors calculated the number of new infections that could be caused by one person with MERS-CoV taking a long-distance flight. The model was parameterized to simulate the conditions in a Boeing 747. The MERS-CoV infectivity was as the number of infectious quanta per hour and the authors used 10,000 different infectivity scenarios. The mathematical modelling showed that the transmission will be confined to the cabin where the infectious passenger is seated. For an example, on a 5 hour flight, roughly one and three infection(s) could occur if the infectious passenger is seated in first or economy class, respectively. On a 13 hour flight, the number of infections would double and if the infectious passenger is a super-spreader, this can cause roughly four infections in first class or 15 infections in economy.

2.2.2.6 Ebola

Ebola virus disease (EVD), commonly referred to as "Ebola", is transmitted by direct contact of infected fluids such as blood, urine, saliva, feces, and vomit with small skin lesions or with mucous membranes. The virus can also survive in breast milk and semen even after recovery from the disease, and there are reports of disease transmission to partners or children from individuals who have recovered from the disease (Madariaga, 2015). Ebola symptoms can appear between from 2 to 21 days after coming in contact with the virus, with an average period of 8 to 10 days. The symptoms of Ebola progresses from fever, aches and pains, and fatigue, to diarrhea and vomiting as the person becomes sicker (Centers for Disease Control and Prevention, 2019a). Ebola has a long incubation period of typically 8-10 days, but up to 21 days.

The first identified Ebola case in the United States was a traveler from Liberia who resulted in 2 secondary cases in health care personnel who cared for the index case (Fischer et al., 2015). In October 2014, an American health care worker who had traveled domestically on two commercial flights, was confirmed to have Ebola. Since the time of onset of symptoms was uncertain, the airline conducted an Ebola contact investigation. Follow-up was conducted for 268 contacts in nine states. Out of those 268 contacts, 247 were passengers from both flights that infected person took. In addition, 12 flight crew members, 8 cleaning crew members, and one airport staff were also contacted. All 268 contacts were required to complete 21 days of an incubation period. The contact investigation resulted with no secondary cases of Ebola, suggesting that transmission of Ebola during commercial air travel did not occur (Regan et al., 2015).

Ebola is highly infectious, but the use of personal protective equipment, contact follow-up, and infection control measures can contain the disease spread. There are no vaccines or specific treatment for Ebola, however, supportive treatment is extremely important (Madariaga, 2015).

2.2.2.7 Severe Acute Respiratory Syndrome (SARS)

Severe acute respiratory syndrome (SARS) is a respiratory disease caused by a virus called SARS-associated coronavirus (SARS-CoV). SARS was identified as a global threat in March 2003, after discovered for the first time in Southern China in November 2002. In March 2003, the World Health Organization (WHO) issued two travel advisories to SARS-affected countries. Yet, some already infected patients traveled by air internationally causing the illness to spread to more than twenty-four countries in North America, South America, Europe, and Asia in just few months before the outbreak was controlled.

SARS is transmitted primarily by close person-to-person contact through the respiratory droplets which are produced when an infected person coughs or sneezes (Centers for Disease Control and Prevention, 2004). Infection with SARS happens when the infectious droplets from the cough or sneeze of an infected person get deposited on the mucous membranes of the mouth, nose, or eyes of well-being persons in the nearby. SARS can also be transmitted when a person touches a surface or object contaminated with infectious droplets and then touches his or her mouth, nose, or eye(s). The main symptoms of SARS disease are fever, cough, myalgia, shortness of breath, or difficulty breathing and approximately 14% of case-patients require mechanical ventilation (Breugelmans et al., 2004).

A study by (Li et al., 2018) rated the in-flight SARS transmission routes according to the likelihood. According to the study, the airborne, close contact, and fomite routes contribute 21% (95% CI: 19%-23%), 29% (95% CI: 27%-31%), and 50% (95% CI: 48%-53%), to SARS transmission, respectively. A study was conducted by the Robert Koch Institute in Berlin, Germany, to document SARS transmission during international flights. On April 11, 2003, the Institute was notified that a probable SARS-infected person had flown from Hong Kong to Frankfurt, Germany, on March 30 to 31, 2003, and then traveled extensively in Europe after onset of symptoms. In 5 days, the traveler flew on seven flights throughout Europe. On March 31, the traveler developed symptoms of SARS, including fever and general malaise. Upon returning to Hong Kong, he was admitted to a hospital and mechanical ventilation was initiated. He was reported to WHO as a suspected SARS patient on April 9 before being diagnosed with SARS on April 10. A contact investigation study was conducted with a total of 250 passenger. The study was concluded with no SARS transmission among passengers seated in close proximity to the infected passenger. This result suggested that in-flight transmission of SARS did not occur. It is worth to mention that the infectious patient was in his first week of illness and the infectivity of SARS is greatest in the second week. Therefore, the likelihood of SARS transmission on the indicated flights was already not high. These results are further supported by the fact that all contacts were asymptomatic 13 days after their last contact with the SARS patient. Although the authors did not observe any SARS transmission, they could not rule out the possibility that it may have occurred.

On March 15, 2003, a 3 hour flight from Hong Kong to Beijing carried 120 passengers and crew including a SARS symptomatic person. After the flight, laboratory-

confirmed SARS developed in 16 persons, 2 others were given diagnoses of probable SARS, and 4 were reported to have SARS but could not be interviewed (Olsen et al., 2003). The 22 persons with illness had an average of four days after flight to the onset of symptoms. In addition, the passengers and crew did not recall any recognized exposures to patients with SARS before or after the flight. The illness was reported in 8 of the 23 persons who were seated within three rows in front of the index patient and 10 of the 88 persons who were seated elsewhere. It was also estimated that more than 300 people might have been infected indirectly by the passengers who took this flight.

2.2.2.8 Severe Acute Respiratory Syndrome Coronavirus 2 (SARS-CoV-2)

Severe acute respiratory syndrome coronavirus 2 (SARS-CoV-2) is also known as COVID-19 with the number 19 indicating that the first case identified in Wuhan, China, the epicenter of the outbreak, was in December 2019. The virus quickly spread across China and the globe, until the World Health Organization declared COVID-19 a pandemic on March 11, 2020. SARS-CoV-2 is highly infectious and pathogenic, especially in crowded environments such as public transportation (Shen et al., 2020). It is believed to be transmitted from human to another by different ways such as by droplets, aerosols, and fomites (Jayaweera et al., 2020). Recent studies have shown that SARS-CoV-2 can survive for up to 3 hours in aerosols, 4 hours on the copper surface, 24 hours on the cardboard surface, and up to 2-3 days on plastic or stainless steel surfaces under laboratory conditions with a relative humidity of 40%-65% and a temperature of 21 ^{o}C-23^{o}C (69.8 ^{o}F-73.4 ^{o}F) (Van Doremalen et al., 2020). Respiratory infecting agents can spread via inhalation of droplets during talking, coughing, and sneezing (Xie et al., 2009; Zhu et al., 2006). When a large amount of aerosols

is generated, they can remain suspended in air for a long time and spread over a long distance with air circulation (S. C. Chen et al., 2009; Gralton et al., 2011; Kwon et al., 2012; Zhu et al., 2006). The risk of contamination and spread of the SARS-CoV-2 disease is greatly minimized when a social distance of 1-2 m (3.3-6.6 ft) is maintained (Silva, 2020).

The research on COVID-19 infection in aircraft cabins is still premature. Since aircraft cabins are densely packed environments, the cough-jet released by a hypothetical SARS-Cov-2 infected person is expected to break the local airflow, particularly the jet zone, and travel both forward and backward directions in the proximity of the point of infected person`s mouth. Since the velocity of the coughed air is around 10 m/s, the droplets may travel four to five seats ahead, and the aerosol-cloud go even further away (Jayaweera et al., 2020). However, (Jayaweera et al., 2020) believe that only the immediate passenger on either side of the infected passenger could be in high probability to get infected. In contrast to the forward movement, there is a backward movement of droplets typically by one seat, but the aerosol movement may be more (Jayaweera et al., 2020). This phenomenon suggested by (Jayaweera et al., 2020) estimates that one infected passenger could infect from five to ten people onboard. Oztig & Askin (2020) suggested a positive relationship between higher volume of airline passenger traffic carried in a country and higher numbers of patients with COVID-19. Furthermore, (Shen et al., 2020) believe that public transport and stations can be vectors of the virus during the pandemic of COVID-19, resulting in a “super-spreading” occurrence.

Eldin et al., (2020) reported a probable aircraft transmission of Covid-19 in-flight from the Central African Republic to France. The authors believe that the patient likely got infected in the plane, while traveling with a patient who was diagnosed eleven days later with

COVID-19, in Cameroun. This report illustrated how easily SARS-CoV-2 may travel together with their human carriers and spread the virus on-board. To the authors, travel restrictions is essential not only to limit the spread of the disease to unaffected areas but also to prevent travelers from getting infected on-board. Qian et al. (2020) investigated 91 confirmed COVID-19 cases out of which, 9 were diagnosed as severe pneumonia, 31 were discharged, 60 remained hospitalized and no patient died. Using contact tracing, the authors concluded that 31 (34.07%) patients had been to Wuhan/Hubei, while 48 (52.75%) patients had not been Wuhan/Hubei, and 11 (12.09%) cases are thought to be confirmed aircraft transmissions.

J. Chen et al., (2020) analyzed another possible transmission incident on-board a Boeing 787-9 in a flight from Singapore to China on 24th of January 2020. On January 24, 2020, a flight from Singapore to China was strictly controlled upon landing since about 100 passengers on-board the flight had recently been to Wuhan. During the airport inspection, several passengers had already developed fever or upper respiratory infection symptoms. Some passengers were confirmed to have COVID-19 infections early following day. The total seat occupancy on the flight was 89% (335/375) in addition to 11 crew members. The aircraft was equipped with air handling systems and all cases wore facemasks most of time. The study confirmed that none of the symptomatic cases visited a hospital or had contact with suspected or confirmed COVID-19 case during their travel. The passengers were divided to Group A including those who departed from Wuhan to Singapore on January 19th, 2020 and Group B including those who did not depart from Wuhan and did not have a history of travel to Wuhan. Among all flight passengers, the study identified a total of 16 COVID-19 infected passengers with a confirmed diagnosis with an overall attack rate of 4.8%. A

passenger on-board the same flight was seated near four infected passengers from Wuhan for approximately an hour and did not wear his facemask correctly during the flight. As a result, the passenger was infected with COVID-19 despite not having any exposure to the virus before boarding. Although the authors concluded that COVID-19 transmission may have occurred during the flight, they also believe that the majority of the transmission cases could not be directly attributed to transmission on the flight. The authors believe that the remaining infections happened in Wuhan or among already infected members in a single tour group that was on-board the same flight. While the study by (J. Chen et al., 2020) showed that wearing facemasks could still possess a risk of COVID 19 transmission in aircraft cabins, another study by (Nir-paz et al., 2020) showed that facemasks were effective in preventing COVID-19 spread on-board of an even smaller aircraft cabin. On February 20th, 2020 11 passengers were repatriated from the Diamond Princesses cruise ship on-board of a charter Bombardier Galaxy 6000 commercial aircraft. Upon arrival, 11 passengers were retested, and two were found to be positive for COVID-19. During the 13.5 hours flight, the passengers were allowed to take off their facemasks for eating and drinking for a period of 15 minutes. The passengers were also allowed to move and use the restrooms on the back of the aircraft. Upon their arrival, all passengers were put into compulsory isolation for 14 days. During the isolation period, all the passengers who tested negative upon arrival were found to be negative on six consecutive tests, even after being in close proximity to those who tested positive for COVID-19 upon arrival. Hoehl et al. (2020) reported another transmission case on-board a Boeing 737-900 aircraft that landed in Frankfurt, Germany on March 9th, 2020. Among 102 passengers were 24 members of a tourist group. The group had an earlier contact with a hotel manager who tested positive for COVID-19. Before travelling,

none of the tourist group members had a positive test for COVID-19 and they were not wearing facemasks during the 4 hours 40 minutes flight. Upon arrival, 7 tested positive for COVID-19 in a throat swab sample. Four of the 7 were symptomatic during the flight, 2 were presymptomatic, and 1 remained asymptomatic. A total of 71 of the other 78 passengers who had been exposed to the group on the flight completed the interview. Only 13 of those 71 passengers were tested 6 to 9 weeks after the flight. Only one passenger tested positive for COVID-19 in a test conducted 4 days after the flight. This passenger did not recall any symptoms and no contact with patients with COVID-19 before or after the flight. Eighteen other passengers reported having symptoms suggestive of COVID-19 within 14 days after the flight with few tests coming back with a borderline result.

Due to the COVID-19 pandemic, United States Transportation Command (USTRANSCOM), The Defense Advanced Research Project Agency (DARPA), and Air Mobility Command gathered their focus to investigate infectious aerosols dispersion in commercial aircraft cabins (Silcott et al., 2020). One of the main objectives of this study was to collect aerosol data sets for COVID-19 risk analysis. This data can mainly be used to determine the optimal capacity of commercial aircrafts and the relative exposure risk for different aircraft seating configurations. It will also help optimizing the boarding and deboarding processes and determine the procedures for contact tracing if a passenger tests positive after landing. The study applied two different techniques to achieve the objective of the study. The first, was using fluorescent aerosol tracers between 1-3 μm (3.9e-5 and 11.8e-5 inch) and real time optical sensors. The second technique was using DNA-tagged tracers. Using those two aerosol tracing techniques the study conducted more than 300 aerosol release tests including both inflight and ground tests on Boeing 777-200 and 767-300

aircrafts. The study used around 40 instantaneous biological analyzer and collector (IBAC) sensors to measure the concentration of the simulated virus particles. The researchers also built an “Infectious Model” that can generalize the testing results to different flight durations, infectious passenger location, etc. The authors found that the dilution and mixing of the aerosols with the cabin airflow was achieved in all tested seat sections of both the Boeing 767 and Boeing 777 aircrafts. As a result, the maximum recorded exposure in a nearby seat was just 0.3% of the released aerosolized source of contamination such as the virus causing COVID-19. The reduction was 99.99% in the further seats from the source. Using the developed transmission model, the study showed that even at a 100% seating capacity in a Boeing 767 or 777 aircraft, if an infectious passenger is shedding 4000 viruses/hour with an infectious dose of 1000 viruses, a 12-hour flight will have no inflight aerosol transmission. Due to the nonuniform airflow pattern inside the cabin, the collected tracer particles concentration data showed a nonuniform dispersion at different locations inside the aircraft cabins. This means that at some cabin locations, the tracer particles concentration at further seats were higher than those closer to the source.

2.3 Aerosols Contaminants Transmission in Aircraft Cabins

Airborne transmission may be described as the transmission of microorganisms from a source to an individual by aerosols, resulting in infection and illness. Airborne disease transmission is often divided into droplet transmission and aerosol transmission. Droplet transmission is defined as disease transmission through ejected droplets that settle rapidly because of their larger size. Aerosol transmission is characterized as disease transmission through ejected particles that are smaller in size; typically less than 5 μm (19.7e-5 inch) (P. Baron, 2010). Such aerosols can be transmitted over short and long distances. Long range transmission occurs between distant areas and is mainly governed by the airflow from the ventilation systems and the movement of people (Kwon et al., 2012). The size of either droplets or particles impacts their circulation in ventilated spaces. For example, relatively larger particles are subject to gravity effects which affect their transmission and distribution patterns.

The airflow in an aircraft cabin is non-uniform (W. Yan et al., 2009). Therefore, the expiratory droplet distribution and the risk of infection in an aircraft cabin are not homogeneous and are temporal (Gupta et al., 2012). Hence, the prediction of contaminants dispersion pattern in an aircraft cabin is a challenging task. In their attempts to study this topic, researchers have conducted tests on actual flights, mockup cabins, simulated cabins using Computational Fluid Dynamics (CFD), or probabilistic studies. Gupta et al. (2012) used CFD and probabilistic studies to evaluate the spatial and temporal distributions of the risks from airborne infectious diseases. Experiments and CFD simulations are the two most effective approaches used to investigate indoor air pollutant transportation within aircraft cabins. Experiments are usually conducted on either a full scale or a mockup section of an

aircraft cabin (W. Yan et al., 2009). CFD simulations of temporal distributions of expiratory aerosols allow for easier analysis but can be impractical or unfeasible to perform for a full-length cabin. CFD simulations are also of high cost if performed for an entire flight time. Bennett et al. (2013) formed a meta database incorporating data from multiple experimental studies to develop a model to describe the potential for airborne disease spread in aircraft cabins.

To perform the experimental work aimed to investigate aerosols transportation, tracer gas has been widely used in different research fields. It is mainly used to study ventilation effectiveness, airflow circulations, airflow velocities, and other parameters. It has been an effective tool used in aircraft cabins, enclosed environments and structures, buildings, hospitals, and many other applications. Some of the properties of the tracer gases to result in good simulation are reactivity and sensibility. The utilized tracer gas should not react chemically or physically with any part of the system under study. The tracer gas should also be insensible so that it does not affect the processes under study. It should also not affect airflow or air density of the system. In addition to that, the tracer gas should have a measurable criterion in order to be quantified. The tracer gas should also be safe and should be non-flammable, non-toxic, and non-allergenic. Some of the gases that have been used are carbon mono oxide, carbon dioxide, nitrous mono oxide, hydrogen, sulfur hexafluoride, ethane, methane, and argon (Laussmann & Helm, 2011). Tracer gases may have different accuracies and certain applications may require selecting one with a relatively high accuracy.

Several studies noted that the risk of disease transmission is limited to two seats away from the infectious passenger. Other authors found that the contaminant concentration was still high 4 rows away from the source. Moreover, in several actual cases, passengers became

infected despite sitting several rows away from the infected passenger (Jayaweera et al., 2020; Shankar et al., 2014). Hertzberg & Weiss, (2016) claimed that the risk of becoming infected beyond the two seats is one-third less than being within two seats from the infected passenger. Others believe that the risk, if any, of in-flight transmission remains unknown (T.-J. Chen et al., 2003).

In order to limit airborne disease transmission, a better understanding of the flow dynamics of human respiratory processes is required (Gupta et al., 2009). It is important to investigate the characteristics of human exhalation flow and dispersal of exhaled air to reduce the risk of disease transmission (Feng et al., 2015). There are currently several methods used to simulate human coughing and breathing processes. Those include CFD (Hwang et al., 2011; Zhu et al., 2006), coughing manikins (Lindsley et al., 2014, 2013), continuous injection sources (Mahmoud et al., 2019), and mechanical lung simulators (Vanyi et al., 2012). It is essential to carefully model aerosols and droplets transmission in aircraft cabin since small changes of the local airflow would cause very different transport trajectories of the particles and droplets (Y. Yan et al., 2019). An experimental study performed by (Jiang et al., 2017) focused on the flow behavior of breathing activity produced by a thermal manikin. The authors showed that the breathing flow at different phases presented different flow behaviors during breathing process. It has long been recognized that the droplets and aerosols expelled through coughing and sneezing can spread infectious disease like measles, influenza, bronchitis, chicken pox, tuberculosis, pneumonic plague, etc. Sun & Ji (2007). Since the aerosols and droplets expelled by a cough have high initial momentum, transport of contaminants produced by coughing can vary from transport of contaminants produced by stationary injection sources (Sun & Ji, 2007). The high-velocity cough airflow can induce

instability at the mucous air interface. The droplets generated due to the instability mechanism can be carried a long distance by airflow after being expelled from the human respiratory system (Wei & Li, 2015). A cough typically has a high velocity and a large quantity of droplets and aerosol. Kwon et al. (2012) has shown that the average initial coughing velocity was 15.3 m/s (50.2 ft/s) for males and 10.6 m/s (34.8 ft/s) for females, while the average initial speaking velocity was 4.07 m/s (13.4 ft/s) and 2.31 m/s (7.6 ft/s) respectively. The number of droplets during a single cough can be as high as 3000 (Wei & Li, 2015). The reported volume of aerosols produced by a cough varies considerably in published literature. The total cough volume measured by (Zhu et al., 2006) had a range of 0.8–2.2 liters (0.03-0.078 ft^3) with an average of 1.4 liters (0.05 ft^3) which actually was the low end as compared with that from (Mahajan et al., 1994), who observed a range of up to 5 liters (0.176 ft^3) with an average of about 3 liters (0.106 ft^3). Another study by (Noti et al., 2012), used a digital coughing simulator that had a 4.2 liters (0.148 ft^3) cough volume. Acikgoz et al. (2011) simulated a coughing passenger in an aircraft cabin using CFD. The simulated infected passenger coughed for 0.5 seconds with 22 m/s (72.18 ft/s) coughing velocity and expels 150 mg (0.0053 ounces) liquid water droplets of various sizes. The study simulated both horizontal and oblique coughing directions. The authors concluded that the exposure of the host passenger to airborne pathogens was strongly dependent on seat position relative to the infected passenger and cough direction. Yang et al. (2018) investigated the effect of cough-jet on local airflow and contaminant transport in a typical cabin environment using CFD (Yang et al., 2018). The infectious contaminants were simulated using a coughing passenger seated in different seats inside the cabin. The authors found that the jet caused by the cough had significant effects on airflow in front of the coughing passenger for a short

period of time. Also, it was found that, in order to have the results precisely represent the transport and distribution of cough-generated airborne contaminant, the cough-jet model has to be applied. Between 0–0.5 s after the cough and at a distance of less than 0.45 m (1.48 ft) from the mouth, the cough-jet dominates the airflow. Beyond this distance, the effects of the jet produced by the cough, gradually decrease until the airflow goes back to the steady state. The "dispersion and deposition characteristics of polydispersed expiratory aerosols" were investigated in an aircraft cabin mockup to study the transmission of infectious diseases by (Sze To et al., 2009). Results showed that a significant amount of aerosol reached the row of seats in front of the cougher and the aerosols were then dispersed by the airflow movements in the lateral direction. It took between 20–30 s for the aerosols expelled by the cough to travel up to two rows away from the cougher. Increasing the ventilation rate was shown to increase the dilution and reduce the aerosol exposure to passengers seated in the vicinity of the source. Doing so also increased the aerosol dispersion which in return increased the exposure to passengers seated further away from the coughing passenger. The authors noted that 60–70% of the mass of expiratory aerosols were deposited, on surfaces close to the source, suggesting that disease transmission risk via indirect contact in addition to airborne risk is possible. In a related research, (Lindsley et al. 2013) constructed a cough aerosol simulator to produce a humanlike cough in a controlled environment. The simulator was used with live pathogens, including influenza virus, which allows isolation precautions used in the healthcare field to be tested without risk of exposure for workers (Lindsley et al., 2014). Bennett et al. (2013) produced a general aircraft cabin air-contaminant transport effect model that was applied to datasets from different sources. They showed that if the source passenger

was assumed to breathe, cough, or sneeze in the forward direction, a one-row offset can be applied so that the row in front of the index row became the effective source location.

2.4 Isolation and Control of Exposure to Biological Agents in Aircraft Cabins

The design, maintenance, and operation of the ventilation systems on commercial aircraft are not a proven source of biological agents exposure (National Research Council, 2002). The up-to-date research did not conclude a confirmed significant risk when the ventilation system functions normally. Even in aircraft with air recirculation, the biological air quality remains acceptable. As in any other public transport or public places, the proximity to an infectious person can be a factor in transmission. However, the aircraft ventilation system has not been implicated as a confirmed factor in disease transmission. The airflow pattern inside the aircraft cabin is still a debatable question among researchers. Some authors (Withers & Christopher, 2000) believe that the air flow is mainly laminar, from top to bottom and from front to back. Others (Hoad et al., 2013; Mangili & Gendreau, 2005; Sze To et al., 2009), believe that the longitudinal airflow is minimal. Therefore, in a suspected case of disease transmission on an aircraft, the public health authorities do not necessarily have to contact all the passengers, as only those in the immediate vicinity may be at risk.

Crew members and passengers on commercial aircraft can protect themselves and others from infectious diseases by adhering to current recommendations for immunization, personal hygiene, and avoid travelling when unwell. The CDC publishes a regular publication with guidelines to prevent diseases spread in aircraft cabins for both passengers and crew members (Centers for Disease Control and Prevention, 2019c). Persons with communicable diseases that do not pose a direct threat to the health or safety of others cannot be denied access to air travel (14 CFR 382, Nondiscrimination on the Basis of Disability in Air Travel). Yet, airlines can impose restrictions such as the wearing of a facemask. Ill and

well passengers have worn respiratory protection during air travel to avoid transmission of infectious agents. Jones et al. (2009) performed a study that examined a passenger with tuberculosis on an aircraft. The authors found that the median risk of infection to the other 169 passengers on the aircraft was between 1 in 10,000 to 1 in a million if the infectious passenger is not wearing a facemask. In contrast, wearing a facemask reduced the infection probability by another 10-fold.

Immunization is the best way to protect travelers against diseases that could be prevented by taking a vaccine (Dupont et al., 2001). Immunizations for travelers should be based on the requirements of the local health authorities at the travel destination and individual travelers' risk of infection. Potential exposures to infectious agents during the time spent on an aircraft to reach a destination generally are not considered in these decisions. This is due to the short exposure time during flight when compared to other travel-related exposures. Furthermore, some contagious and infectious diseases, such as COVID-19, did not have a vaccine even until about a year of its first discovery.

Passengers and crew members occasionally become ill in flight (National Research Council, 2002). In commercial flights, cabin crew are trained to recognize passengers with air sickness or even excessive alcohol consumption. Passengers are considered to be infectious if they started showing symptoms such as diarrhea, vomiting or fever (Grainger et al., 1995). A WHO guideline (World Health organization (WHO), 2013b) outlines basic actions that flight attendants should take when a person reports or is suspected of having tuberculosis during a flight. The CDC recommends frequent handwashing, minimizing contact with possibly contaminated surfaces, and avoiding contact with bodily fluids; along with wearing gloves and facemasks when possible. Additionally, the CDC recommends

moving the sick passenger to keep them at least 1.8 m (6 ft) away from other passengers (Centers for Disease Control and Prevention, 2019c). This is not always a possibility, especially on smaller aircraft. Likewise, the World Health Organization recommends relocating the infected passenger to a seat located further away from other passengers and to use facemasks when possible, by both the sick passenger and the flight attendant who is assigned to help them (World Health organization (WHO), 2013b). The International Civil Aviation Organization (ICAO) have the same recommendations in addition to disinfecting the affected areas around the infected passenger and safely disposing of any contaminated supplies or equipment (International Civil Aviation organization, 2005). Many of the recommendations also would apply to other communicable diseases. For example, a symptomatic person should be isolated from other passengers, made comfortable, provided with tissues and waste containers, advised to move around the cabin as little as possible, and instructed to cover the nose and mouth when coughing. Yet, the established procedures to reduce on-board spread of the contagion beyond basic hygiene and disinfectant procedures are limited (Centers for Disease Control and Prevention, 2019c).

The concept of personalized isolation rooms to control the spread of contagious airborne diseases is not new. Isolation rooms are equipped with a blower to create negative pressure in the room, and a filtration system to purify the air before dumping it to the outside. Mobile isolation systems exist as well. These range in design from a portable isolation room with an aluminum frame and clear vinyl walls to isolation systems designed to fit over a hospital stretcher. Each of these systems utilize HEPA filters and generate a negative pressure inside the chamber to provide appropriate airflow direction. However, each of these isolation solutions is large and impractical for use in an aircraft cabin. Darrah (2018) studied

the utilization of a passenger isolation system on a Boeing 767 mockup as shown in Figure 2.1. The study showed that the passenger isolation system is effective at containing a tracer gas released through a gas distribution tube and preventing its spread in the cabin.

Figure 2.1. Passenger isolation system Darrah (2018).

Another study performed by the University of Denmark utilized a system which directs air from the seat back in front of the passenger and collects it through a suction system integrated into the seat back at the sides of the passenger's head. The air is then exhausted before being recirculated back to the cabin. This personal ventilation system was found to reduce the average background concentration of the tracer gas by up to 42% in the cabin mockup, with a flowrate of 10 L/s (0.35 ft^3/s) (Melikov & Dzhartov, 2013). An airborne biological containment system was developed in a cooperative effort between the US government and WHO in Phoenix (Cornelius et al., 2020). A single-patient, negative-pressure isolation unit was designed for use on the Gulfstream III aircraft. During the 2014 Ebola outbreak, this system was used to transport 41 patients to medical facilities in the United States and Europe. The Containerized Bio-Containment System is able to transport 4 infectious patients in an intensive care unit environment. It was used on overseas repatriation

missions inside a Boeing 747-400 aircraft, which was reconfigured for mixed passenger/cargo work as shown in Figure 2.2. In order to avoid potential fecal exposure during transport, a plastic sheeting was installed as shown in Figure 2.3 to isolate an area to segregate and treat patients who developed symptoms while airborne. This was primarily at the rear of the plane to allow a separate egress to avoid additional exposure to the non-symptomatic patients. An additional area was sometimes created in the forward section of the aircraft to allow crew to remove PPE for hydration and lavatory use.

Figure 2.2. Containerized bio-containment system inside a Boeing 747-400 aircraft. Reproduced with permission (Cornelius et al., 2020).

Figure 2.3. Plastic sheeting installed at the back of a B747-400 aircraft. Reproduced with permission (Cornelius et al., 2020).

Aircrafts disinsection has been a controversial procedure to limit diseases spread with some countries banning one or more disinsection procedure(s). Several publications (Ellis, 1996; World Health organization (WHO), 2012, 2013a) form the basis of current disinsection practices that are used, or required, by various countries. For passenger cabins, five disinsection procedures are used including "blocks away" spraying, "top-of-descent" spraying, "on-arrival" spraying, residual treatment, and pre-embarkation spraying (World Health organization (WHO), 2013a). All procedures with the exception of pre-embarkation spraying have been approved by the World Health Organization (WHO) (World Health organization (WHO), 2013a).

Another procedure followed by airlines to reduce the concentration of microorganisms suspended in cabin air is to use maximum airflow within the aircraft cabin. The concentration of microorganisms can increase if there is little air movement or the exhaust rate is very low (Moser et al., 1979). It has been recommended by (National Research

Council, 1986) “that maximal airflow be used with full passenger complements to decrease the potential for microbial exposure and that recirculated air be filtered (to remove particles larger than 2–3 μm (7.9e-5 and 11.8e-5 inch) to reduce microbial aerosol concentrations”. The FAA does not require airlines to use maximal airflow or HEPA filters on the recirculated air, but it has been a common practice to do so. Control of exposure to biological agents, except for bio effluents is not a primary function of cabin ventilation. Increasing the aircraft cabin ventilation rates or changing the air mixing patterns are not a guaranteed procedure to prevent infectious disease transmission in aircraft cabins. Nevertheless, aircraft cabins should be provided with the minimal recommended outside air supply whenever passengers are on-board. If this minimum ventilation requirement cannot be provided, passengers should be deplaned and moved to a better-ventilated location, such as an airport terminal (National Research Council, 1986).

Chapter 3 - Experimental Setup

The test facility houses a mockup cabin that mimics a twin-aisle Boeing 767 passenger cabin and an actual section of the smaller single-aisle Boeing 737 as shown in Figure 3.1. The Boeing 767 mockup cabin was later modified to mimic a different supply air configuration similar to the one used in some Airbus aircraft models. The aircraft equipment and fixtures that were used to build the Boeing 767 mockup were extracted from a salvaged Boeing 767. This chapter provides the details about the experimental setup and methodologies used to achieve the objectives of the study. It also outlines the instruments setup inside each cabin with details about connections, and configuration.

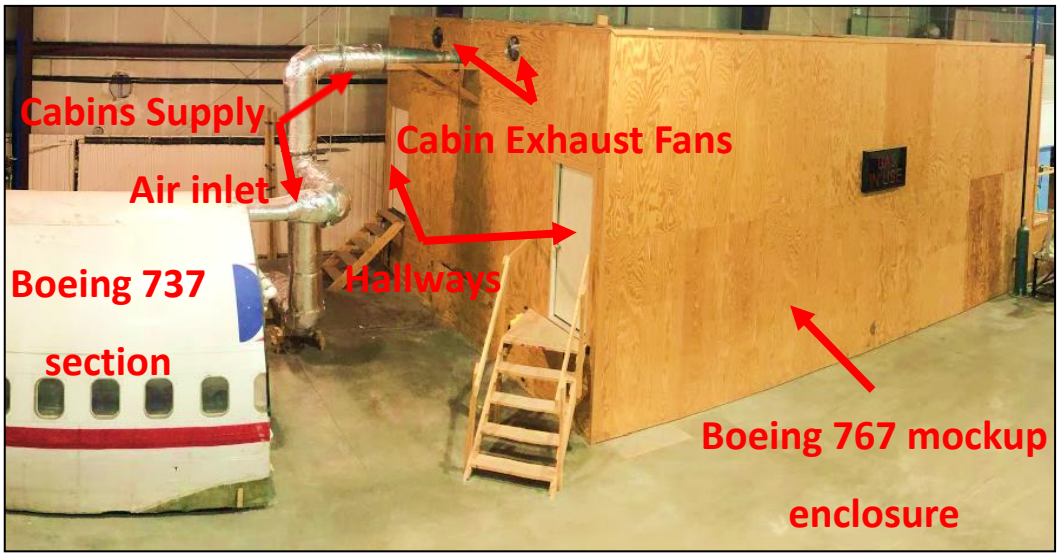

Figure 3.1. An inside view of the ACER lab showing the Boeing 737 section and the Boeing 767 mockup enclosure.

3.1 Experimental Facility Description

3.1.1 Boeing 767 Mockup Cabin Description

To understand the airflow behavior inside aircraft cabins in a realistic way that is close to actual conditions, a Boeing 767 aircraft mockup cabin housed within the Airliner Cabin Environment Research (ACER) laboratory at Kansas State University was utilized. The mockup cabin seats, the air supply ducts, and the diffusers are parts from an actual salvaged Boeing 767 aircraft. The mockup cabin was enclosed within a wooden enclosure as shown in Figure 3.1. The Boeing 767 cabin mockup has a total inside length of 9.41 m (30.84 ft) and width of 4.72 m (15.48 ft). The overall dimensions of the cabin with two hallways located to the east and west sides of the mockup cabin are shown in Figure 3.2. All equipment used for testing purposes were located in the east and west hallways. The cabin has 11 rows of seats distributed longitudinally with 7 seats in each row. The seats are in a 2-3-2 configuration, separated by two aisles similar to a wide-body aircraft mockup cabin. The rows are numbered from the front of the cabin at the southern wall to the back of the cabin at the northern wall. The 7 seats columns are labeled A thorough G from left to right.

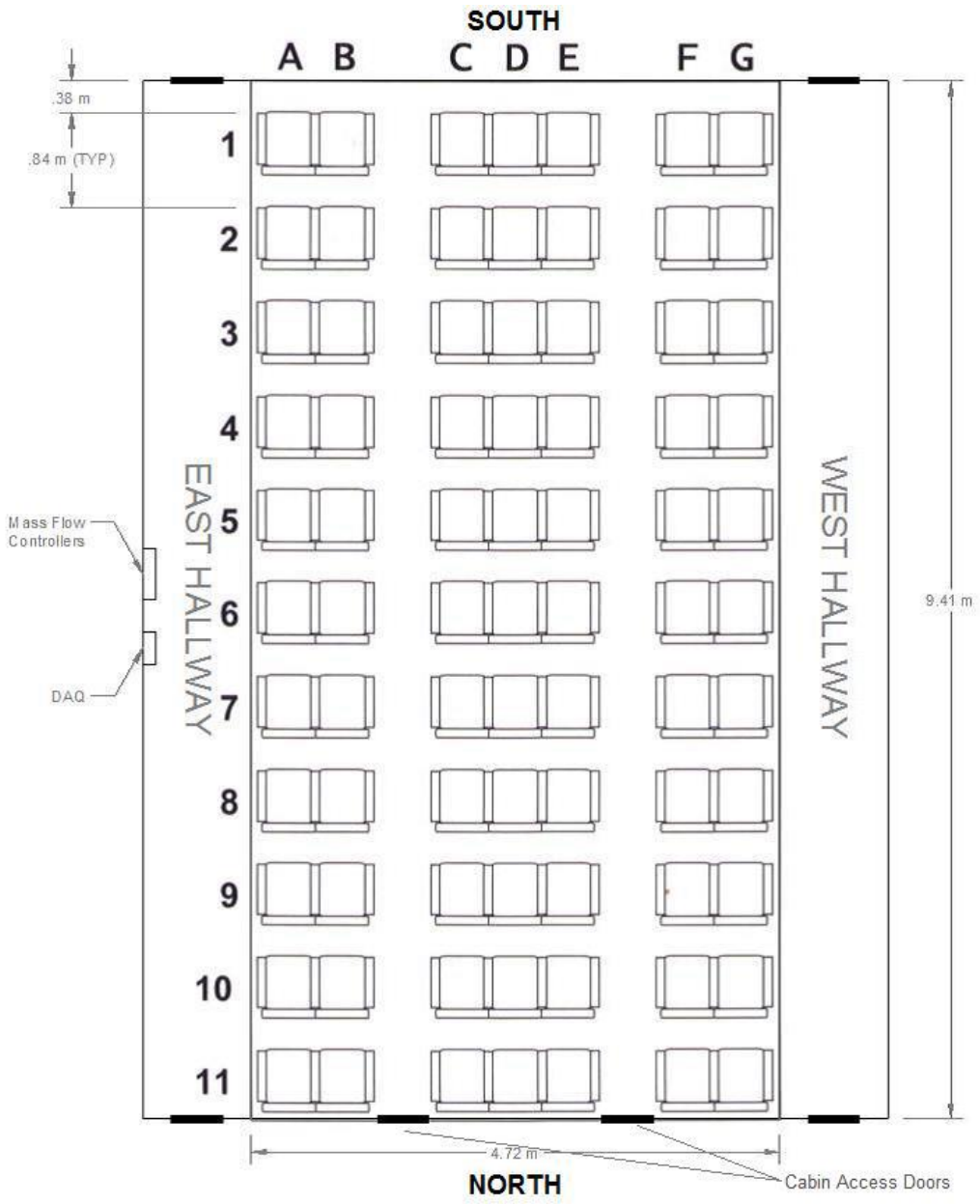

Figure 3.2. Boeing 767 mockup cabin section layout and dimensinos.

A cross-sectional diagram of the Boeing 767 mockup section is shown in Figure 3.3. There are two outboard and two centered stowage bins installed along the length of the cabin. Two center linear air diffusers are located between the two centered stowage bins.

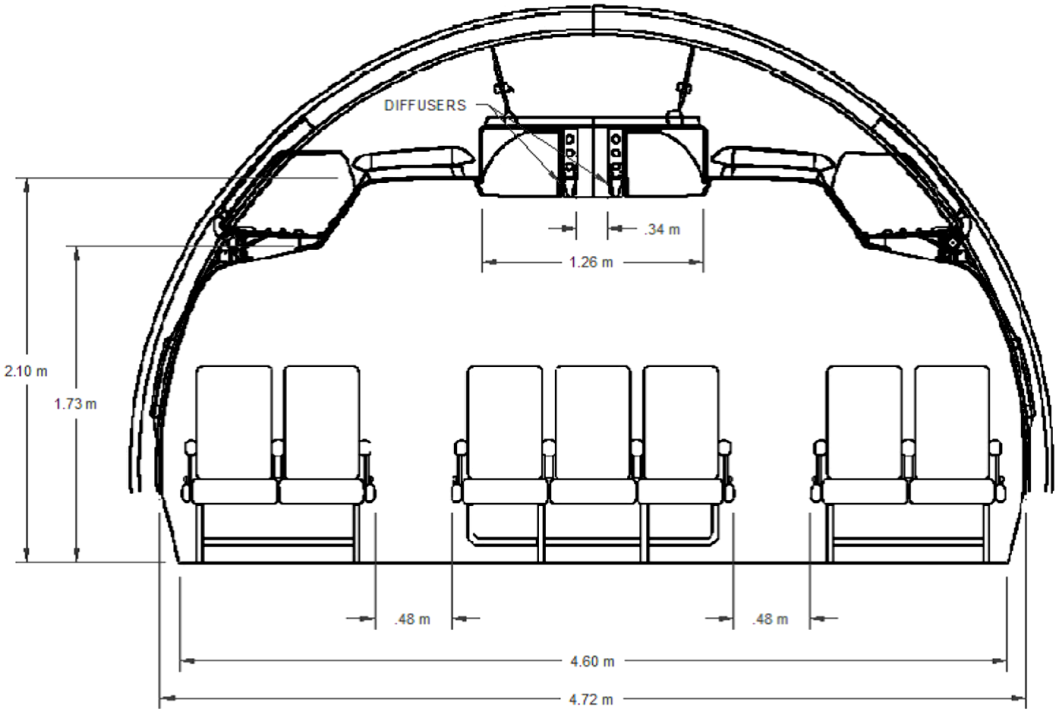

Figure 3.3. Boeing 767 cabin cross section (Boeing Commercial Airplanes, 2005).

There are two hallways to the east and west sides of the cabin. Below the cabin there is a crawl space used to pass the equipment cables and wires between the two hallways. The hallways and the crawl space are both shown in Figure 3.4.

Figure 3.4. Hallways and crawl space below the Boeing 767 mockup cabin.

The actual interior of the mockup cabin is shown in Figure 3.5. The cabin seats are occupied by inflatable manikins which are equipped with 10 m (32.8 ft) wire heater elements to generate approximately 100 W each, equivalent to the average heat load from a resting adult in addition to the cabin entertainment equipment (ASHRAE, 2013).

Figure 3.5. Boeing 767 mockup cabin interior.

The Boeing 767 mockup cabin has a total of 77 identical seats with 44 seats in the 2-seat section and 33 seats in the 3-seat section. The dimensions of a single seat are shown in Figure 3.6 and the dimensions for both the 3-seat and 2-seat sections are shown in Figure 3.7 and Figure 3.8, respectively.

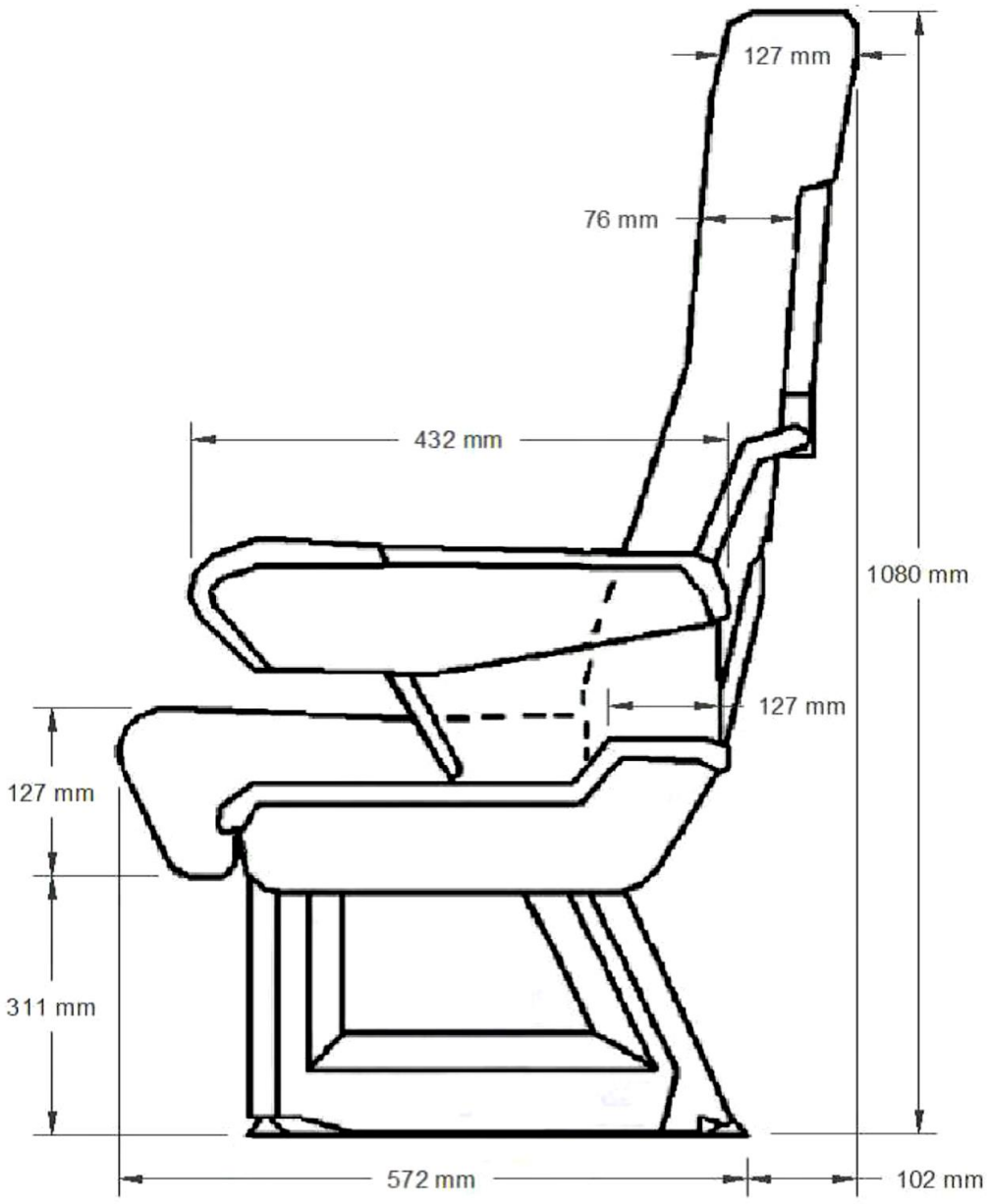

Figure 3.6. Single seat dimensions in the Boeing 767 mockup cabin.

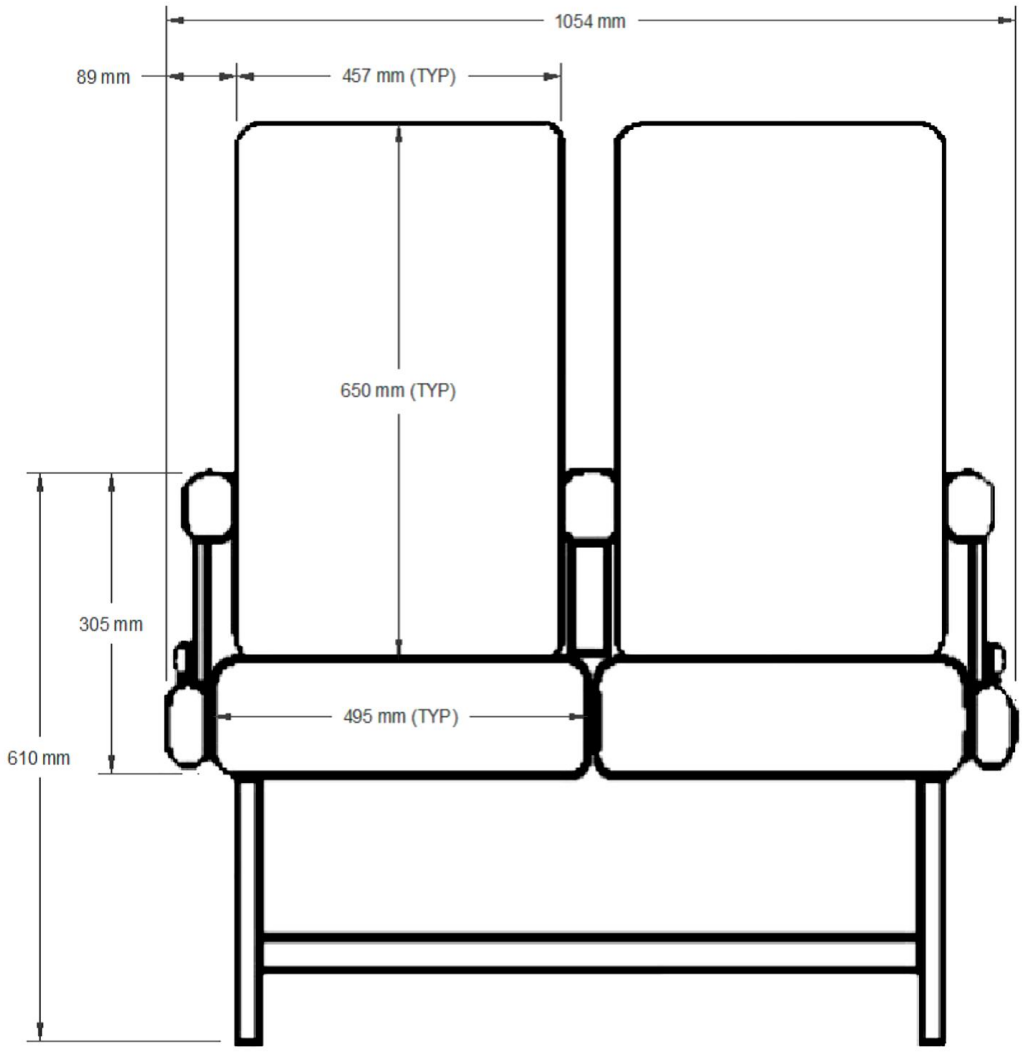

Figure 3.7. Two-seat section dimensions.

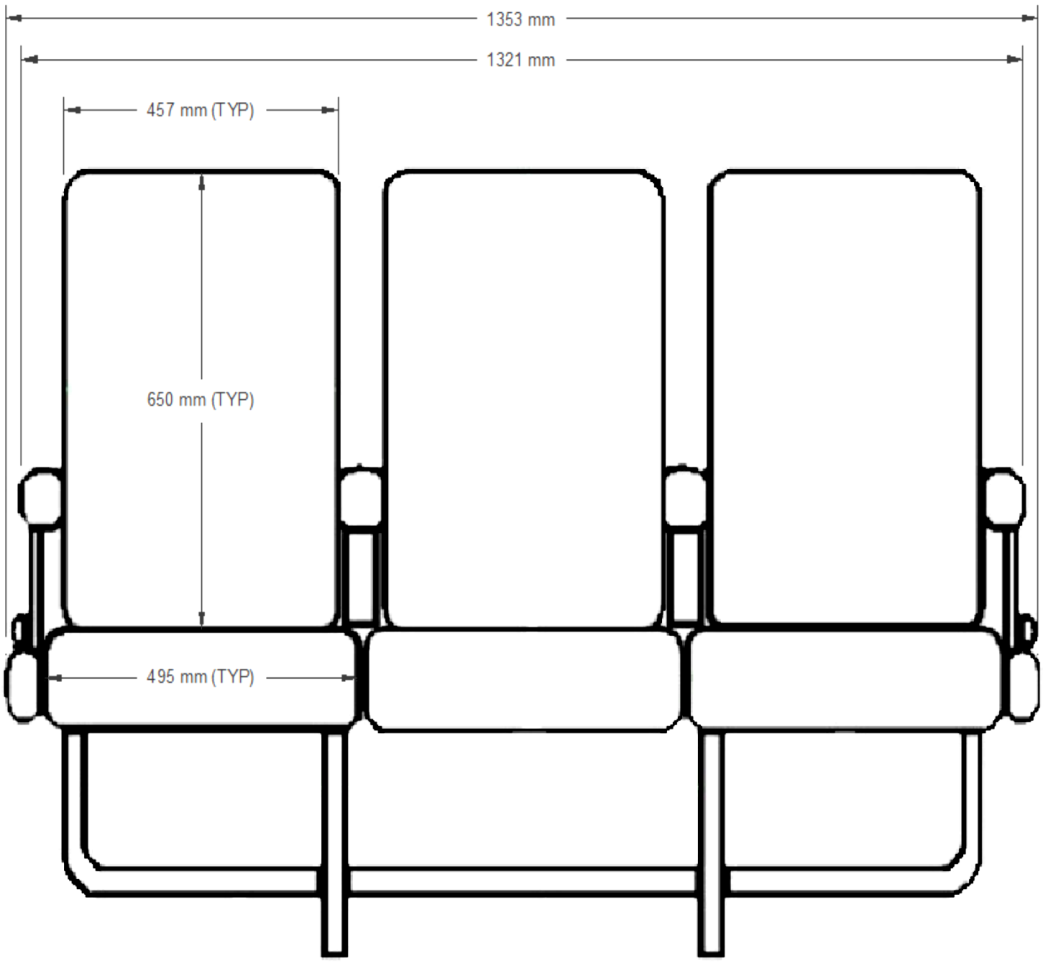

Figure 3.8. Three-seat section dimensions.

To exhaust the air from the cabin, the air is ventilated through evenly spaced gaps at the base of the cabin sidewalls. The air is ventilated into the hallway and is eventually drawn out by the exhaust fans shown in Figure 3.1. The ventilation gaps of 60 x 18 cm (23.5 x 7 inch) (width x height) for the Boeing 767 mockup are shown in Figure 3.9 and 3.10 from the inside and outside the cabin, respectively.

Figure 3.9. Inside view of the exhaust gaps in the Boeing 767 mockup.

Figure 3.10. Outside (hallway) view of the exhaust gaps in the Boeing 767 mockup.

3.1.1.1 Modified Cabin Description

There are several types of supply air configurations in aircraft cabin other than the linear diffusers used in the Boeing 767 cabin. The schematic in Figure 3.11 shows different techniques to supply air to aircraft cabins. Configuration b is the most common for wide body aircrafts in order to provide thermal comfort to all the passengers on-board. This configuration is used in some common airliners such as the Airbus A310, A340, A350, and A320 as shown in Figure 3.12.

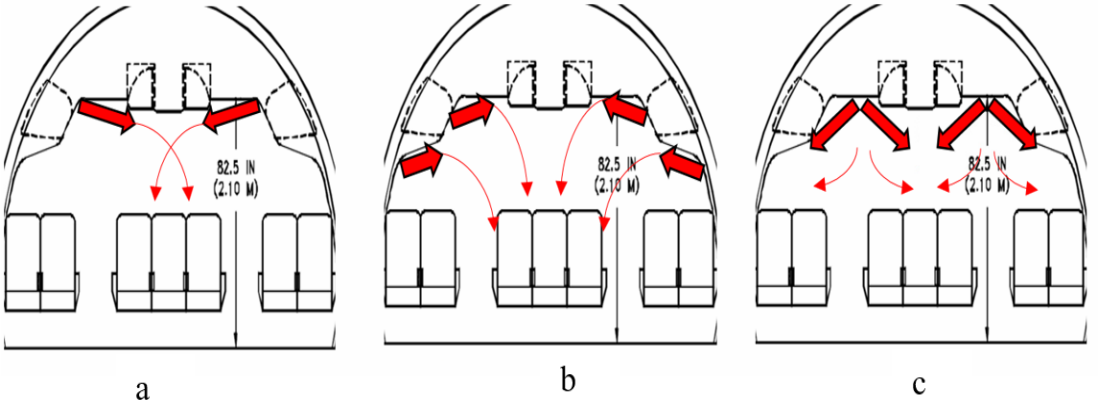

Figure 3.11. Different supply air configurations in aircraft cabins.

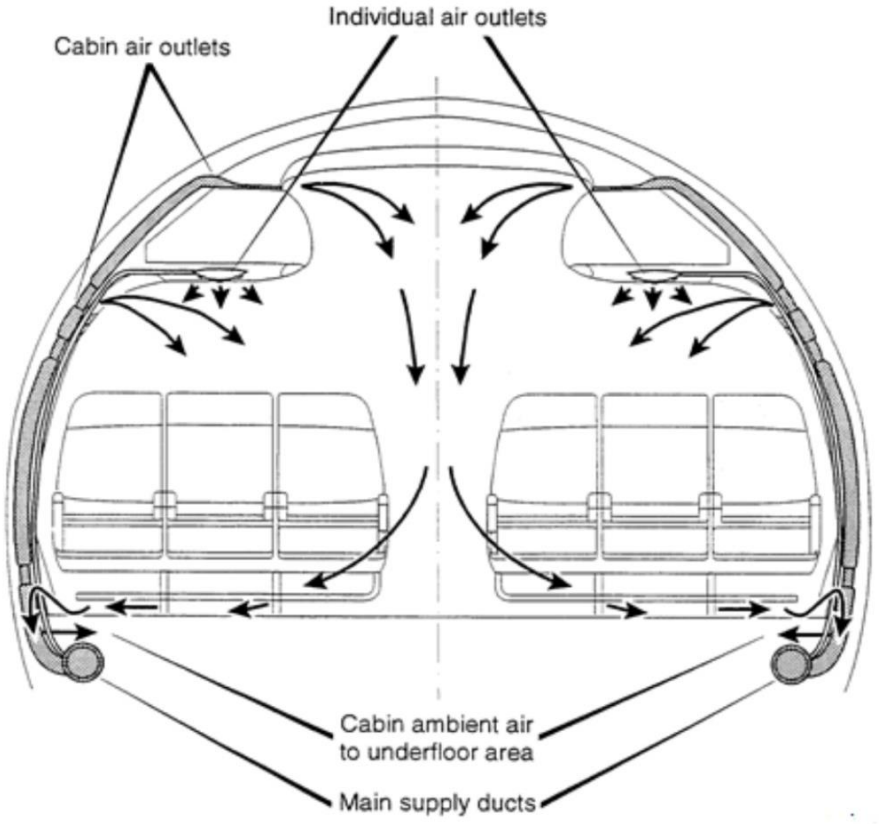

Figure 3.12. A320 supply air configuration (Central American Corporation for Air Navigation Services, 2020).

Since the Airbus A340 model has a similar cabin width to the existing Boeing 767 cabin mockup at the ACER lab, as shown in Figure 3.13, it was decided to select this model for the modified cabin study.

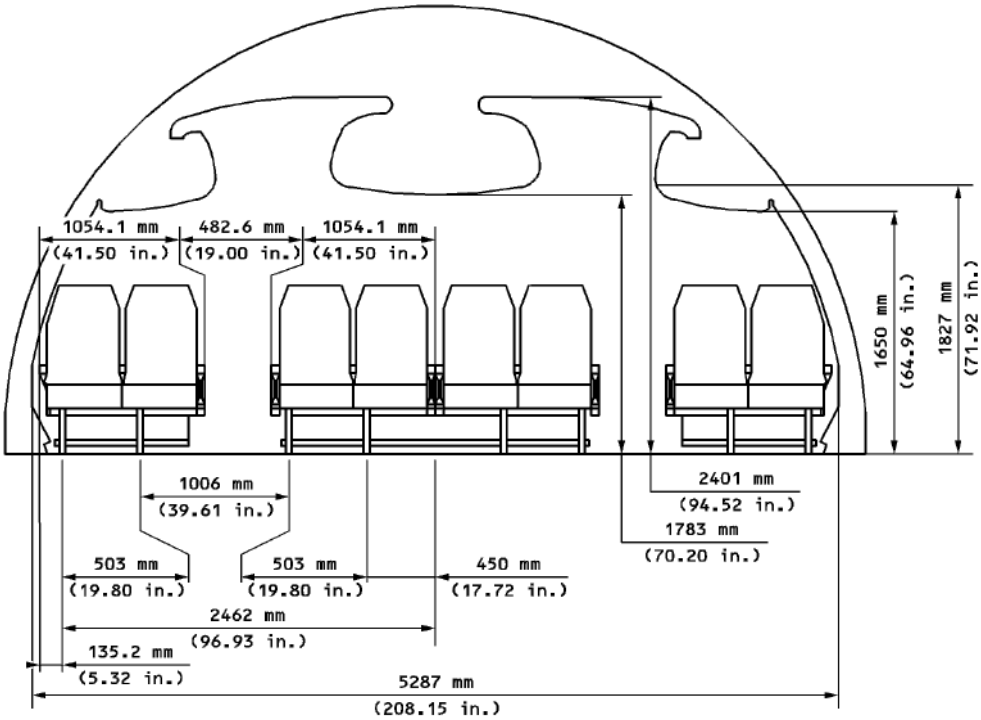

Figure 3.13. A340 cabin cross-section with dimensions (Airbus, 2020).

Figure 3.14 shows an inside view of the modified cabin and Figure 3.15 shows a close view of the newly installed supply air ducts. The detailed conversion process from the Boeing 767 cabin to the modified cabin is discussed in chapter 3.1.3.2.2 of this dissertation.

Figure 3.14. An inside view of the modified cabin.

Figure 3.15. Newly installed supply air diffusers inside the modified cabin.

3.1.2 Boeing 737 Section Cabin Description

The actual Boeing 737 aircraft section at the ACER lab includes the original structure, seats, fixtures, ventilation and exhaust systems, and gaspers. Unlike the Boeing 767 mockup, the Boeing 737 cabin section has a gasper for each seat. The cabin section shown in Figure 3.16 has 5 rows of seats with 6 seats per row in a 3-3 seat configuration with a single aisle in the middle. The dimensions of the cabin section are 5.6 m (18.3 ft) long x 3.6 m (11.8 ft) wide x 2.8 m (9.2 ft) tall. The Boeing 737 cabin is not enclosed by a structure like the Boeing 767. Hence, the supply air is exhausted out into the lab environment. The front and back ends of the cabin are sealed using plywood sheets and insulated from the inside using insulation boards. The back of the cabin has a door for access to the cabin space as depicted in Figure 3.16. Since there are no hallways on the side of the Boeing 737 section, the equipment required to the run the tests were kept at the east hallway of the Boeing 767 mockup.

Figure 3.16. Boeing 737 cabin section at the ACER lab.

The Boeing 737 section has an interior length of about 4.83 m (15.85 ft) and width of 2.84 m (9.33 ft). A cross-sectional diagram of the Boeing 737 cabin section with more detailed dimensions is shown in Figure 3.17.

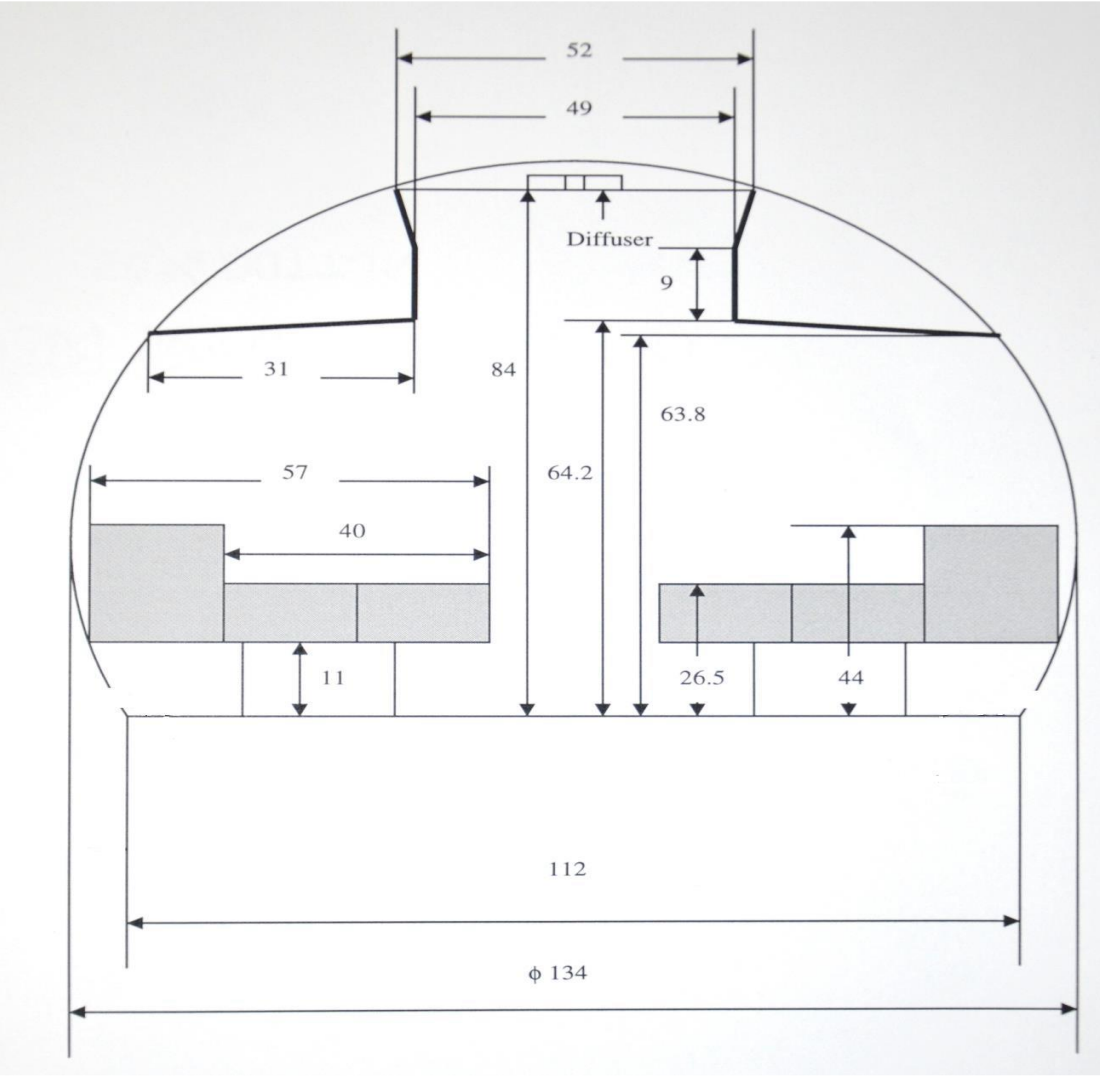

Figure 3.17. Boeing 737 cross-section with dimensions in inch.

As previously mentioned, the Boeing 737 cabin section has 5 rows of seats in a 3-3 configuration, separated by a single aisle. The rows are numbered from the front of the cabin at the northern wall to the back of the cabin at the southern wall. The seats columns are

labeled A thorough F from left to right. The cabin layout and dimensions are shown in Figure 3.18.

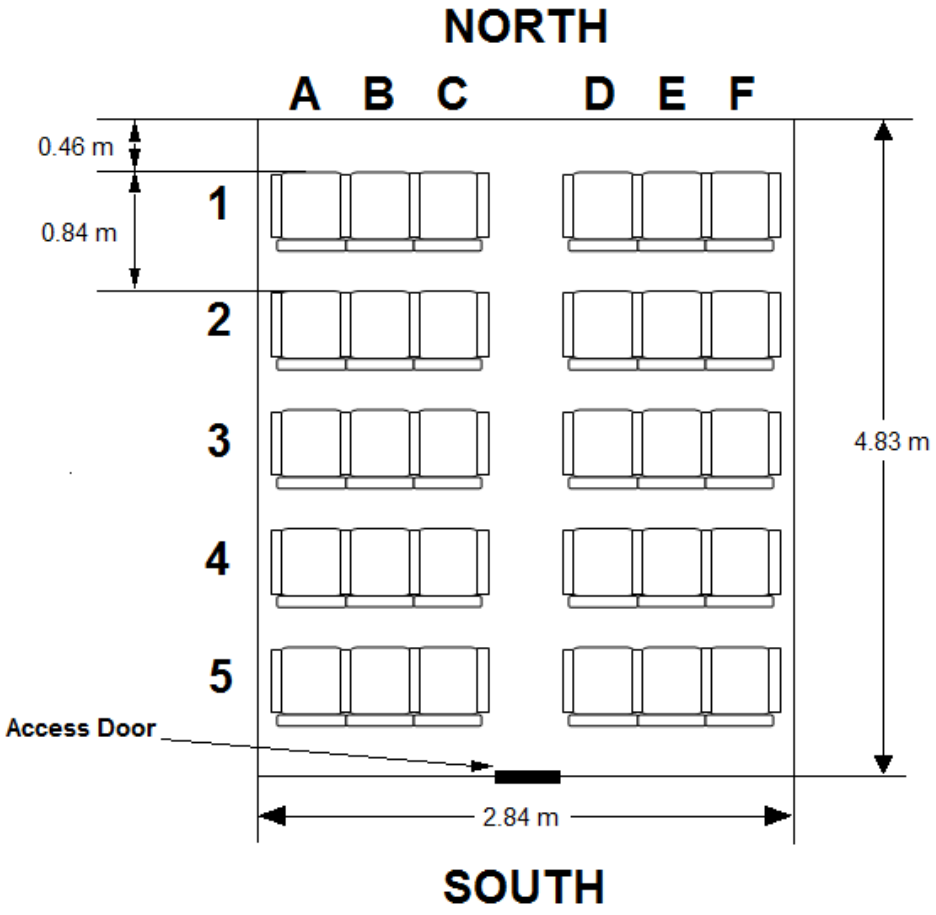

Figure 3.18. Boeing 737 cabin section layout and dimensinos.

Similar to the Boeing 767 mockup, the Boeing 737 cabin section has seats from an actual Boeing 737 aircraft. The Boeing 737 cabin section has a total of 30 seats in 5 rows arranged in two 3-seat sections. Figure 3.19 shows the side-view dimensions of a single seat inside the Boeing 737 cabin section while the dimensions of the 3-seat section are shown in Figure 3.20.

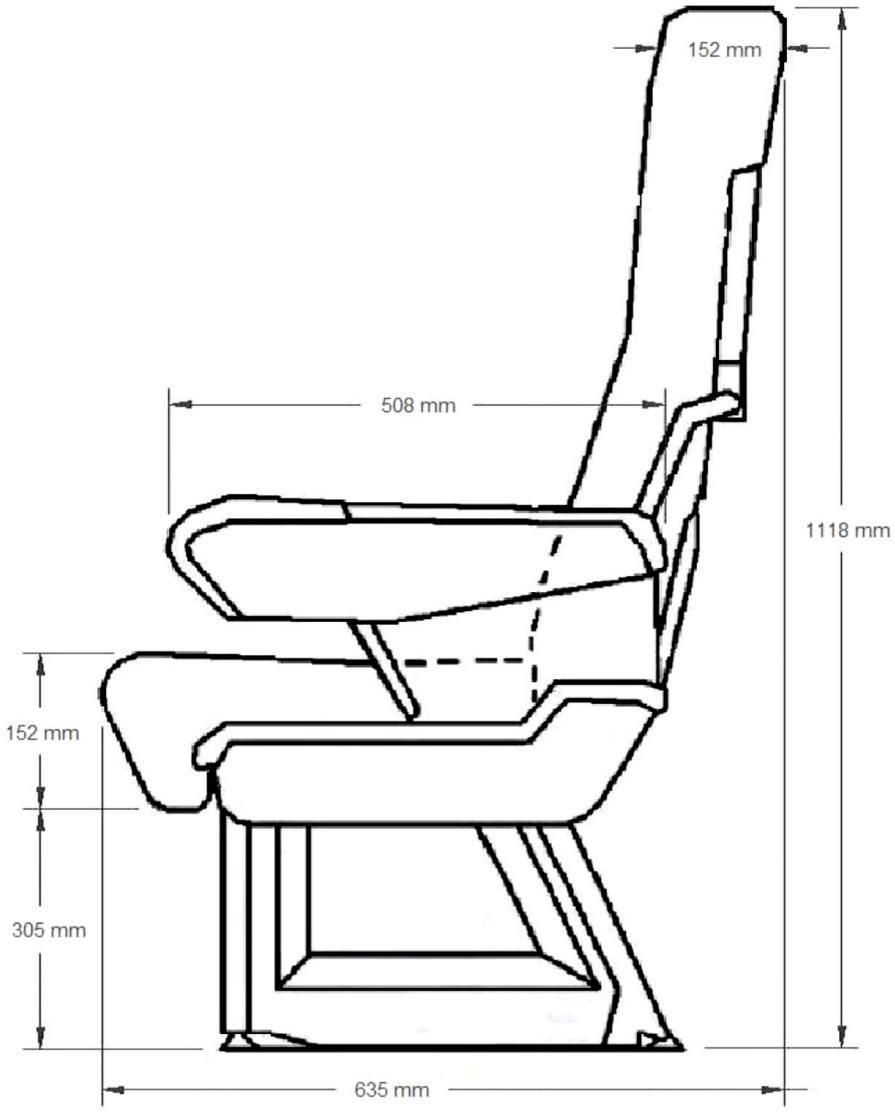

Figure 3.19. Boeing 737 cabin section single seat dimensions.

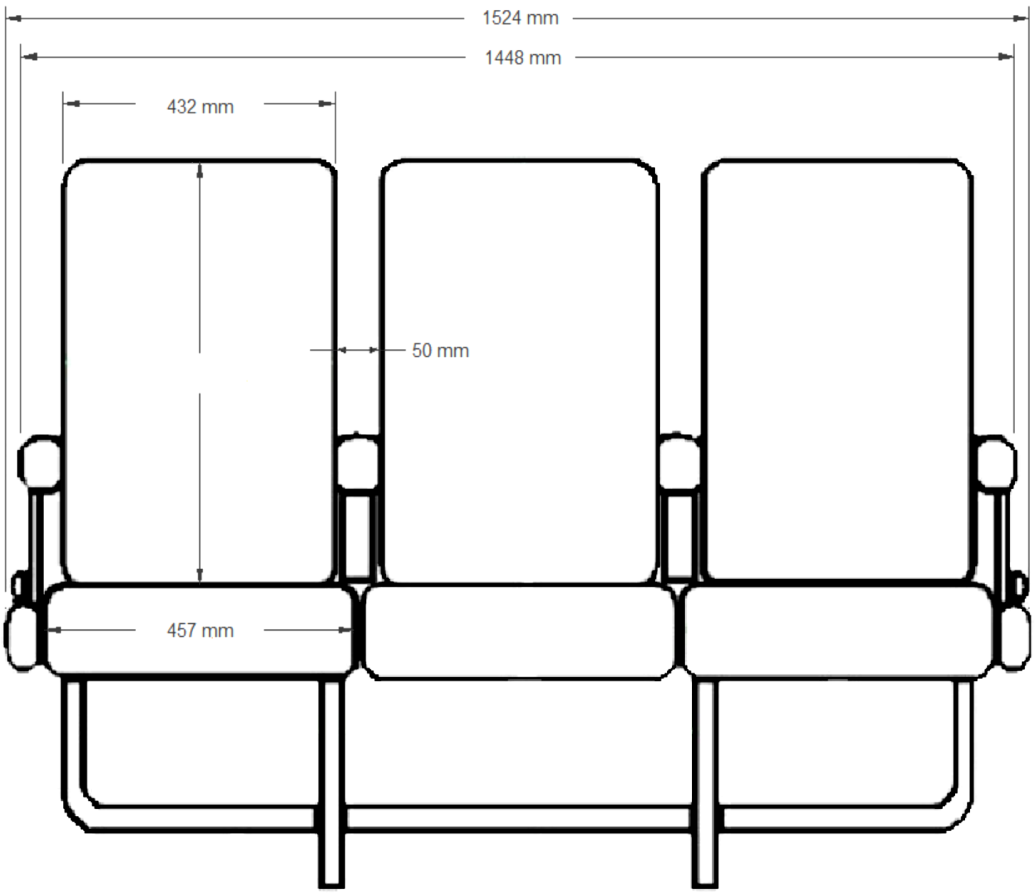

Figure 3.20. Three-seat section dimensions in the Boeing 737 cabin.

3.1.3 Air Supply System Description

3.1.3.1 Heating, cooling, and dehumidifying cycles

The air supply system consisted of 3 main cycles including the cooling loop, the heating loop, and the primary loop as shown in Figure 3.21. Before getting in the cycles, the outside air is passed through filters before being blown to the desiccant dehumidification wheels. The cooling loop brings the temperature of the air down to about 10°C (50°F) using an industrial water chiller. Likewise, the heating loop brings the temperature of the air up to 10°C (50°F) using a natural gas water heater and is only used when the temperature of the processed air is below 10°C (50°F). In the primary loop, the temperature of the air is fine-tuned to 15.6°C (60°F) and held steady in preparation to supply.

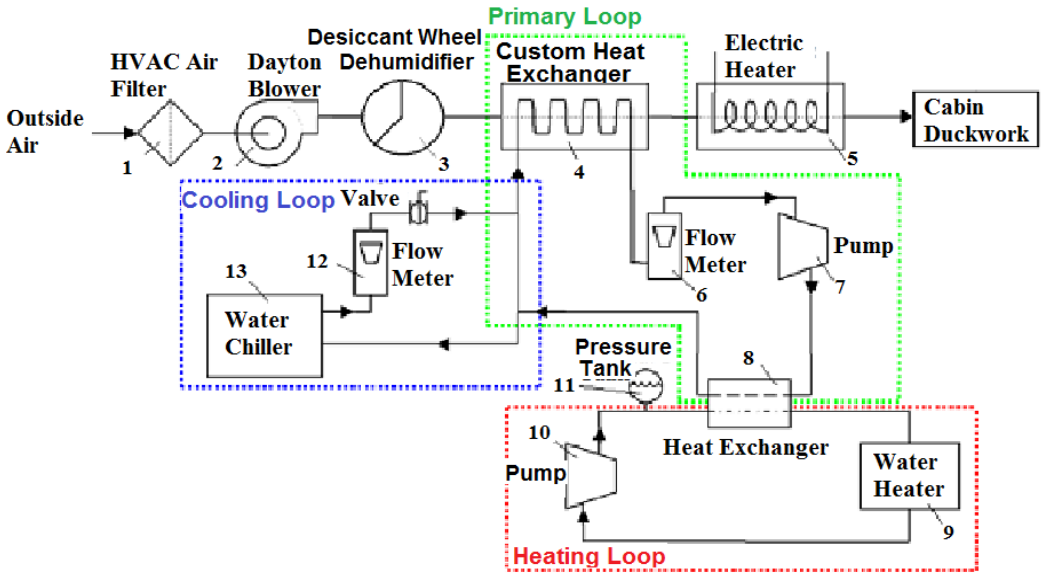

Figure 3.21. Schematic flow diagram of the air conditioning system (Madden, 2015).

Table 3.1 lists the specifications of the equipment that form the air conditioning system.

Table 3.1. Air conditioning system equipment list and specifications.

Serial #	Equipment	Specifications
1	Air Filters	Glass Floss Z-line series
		2 parallel filters 24 × 24 inch
2	Blower/Supply Fan	Model # Yaskawa GPD315/V7 VFD
		12 ¼ inch Dayton Blower at 3 hp
3	Dehumidifier	Model # Munters ICA-0750-020
		Desiccant dehumidifier type
		Maximum Flow Rate: 42475 L/min (1500 ft^3/min)
4	Heat Exchanger	Custom made: 24 × 24 inch
5	Electric Heater	Model # AccuTherm DLG-9-3
		220 V, 3 phase
6	Flow Meter	Model # Omega FL7204
		Water Range: 40 GPH
7	Pump	Model # Marathon CQM 56C34D212OF P
8	Heat Exchanger	Custom made: 24 × 24 inch
9	Heat Exchanger	Model # Alfa Laval CB27-18H T06
10	Water Heater	Model # Rheem GT-199PVN-1
		Temperature Range: 100° to 180° F
		Gas Input Range: 19,000 to 199,900 Btu/hr.
		120 V, 60 Hz

11	Pump	Model # FHP C4T34DC35A26
12	Pressure Tank	Model # Dayton 4MY57
		Capacity: 24.6 liter (6.5 gallons)
		Pre-charge pressure: 206.8 kPa (30 psi)
		Model # King 7205023133W
		Flow range: 1 to 200 GPM
13	Commercial Water Chiller	Model # AccuChiller LQ2R15 PV-B311 Condensing coils

Figure 3.22 shows the actual air conditioning system built around the Boeing 737 cabin section. The figure also shows the supply air ductwork of both Boeing 737 and Boeing 767 cabins.

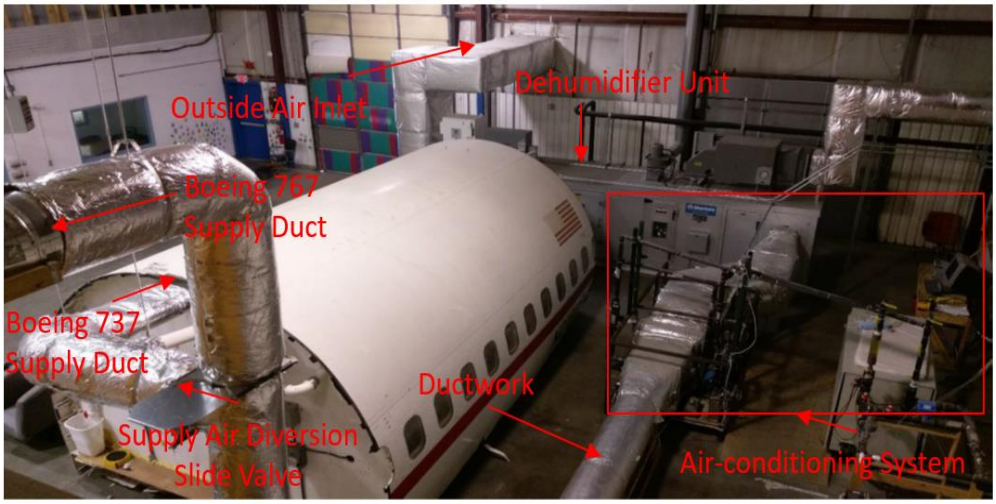

Figure 3.22. Air conditoning system setup at the ACER lab.

To supply air to the gaspers inside the aircraft cabin, a blower pulls conditioned air from the supply duct and delivers it to the gaspers via a separate PVC duct. The gaspers were

maintained at 5 cm (2 inch) water pressure to meet the actual aircraft cabin design specifications. The gaspers blower and connections are shown in Figure 3.23.

Figure 3.23. Gaspers` blower and PVC ductwork.

The entire air supply system is controlled by a computer using National Instruments LabVIEW software. A screenshot of the LabVIEW program interface is shown in Figure 3.24. The supply air system components are connected to an Agilent 34970A and a National Instruments FP-1000 Data Acquisition (DAQ) units. Various other measurements are also collected and recorded by the LabVIEW software. Table 3.2 shows the location and the function of each temperature sensor.

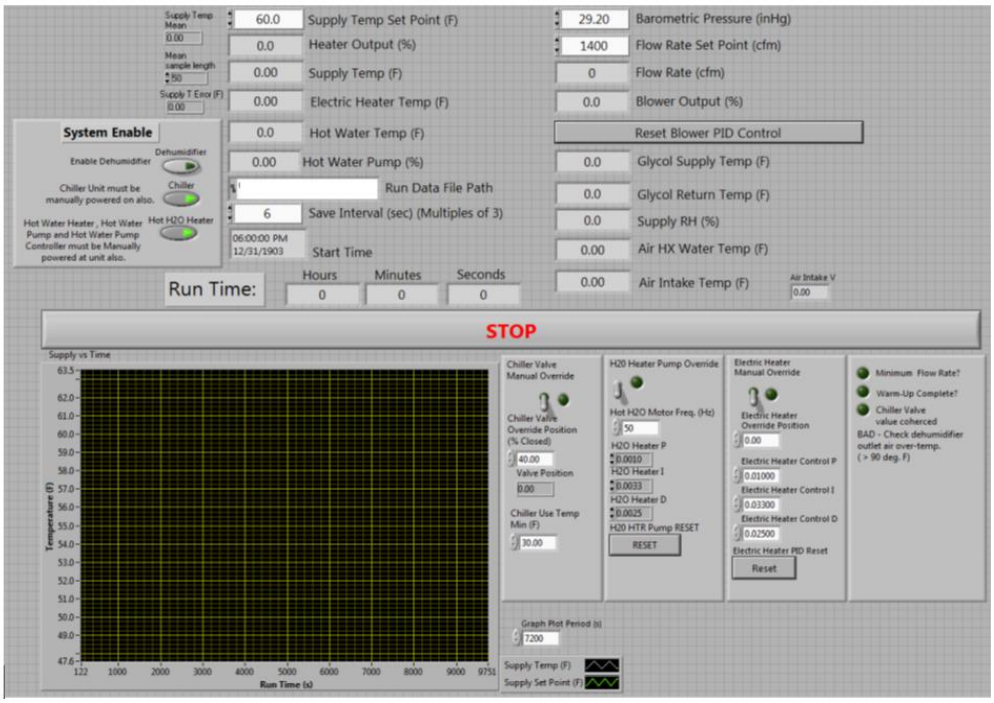

Figure 3.24. Utilized LabVIEW software to control supply air.

Table 3.2. Air conditioning system sensors` locations and details.

Sensor Location	Feedback	Control
Cabin Inlet Duct	Supply Air Temperature	Heater Temperatures
Thermistor in Heater	Electric Heater Water Temperature	Heating Loop Pump VFD
Water Heater Exit	Hot Water Temperature	Mixing Valves
Cabin Inlet Duct	Supply Flow Rate	Blower VFD
Chiller Exit Line	Glycol Supply Temperature	Duct Heater
Chiller Inlet Line	Glycol Return Temperature	Duct Heater
Cabin Inlet Duct	Supply Air Relative Humidity	None
Primary Water Loop	Heat Exchanger Water Temperature	None
Dehumidifier Inlet	Air Intake Temperature	None

The air supply system supplies the cabins with conditioned air to simulate actual aircraft environment and meeting FAA ventilation requirements. The Boeing 767 mockup cabin, with 77 seats, was supplied with 40 m^3/min (1400 ft^3/min) of conditioned air as shown in Figure B.2 5 in Appendix B while the Boeing 737 section, with 30 seats, was supplied with (600 ft^3/min). Fresh air is drawn-in from outside and passed through the dehumidifier unit and into the air conditioning system, which maintains the air at 15.6°C (60°F). For the work reported in this dissertation, the dehumidifier was not operated. Additionally, only fresh air was used for these tests; no recirculated air was used. Since HEPA filters are normally used on recirculation air, it is believed to be pathogen free. However, tracer gas would not be removed by these filters if recirculation was employed in the mockup. Therefore, using 100% outside air is the appropriate option if the tracer gas is to accurately reflect airborne pathogen dispersion.

3.1.3.2 Air distribution system

3.1.3.2.1 Boeing 767 Cabin

Figure 3.1 shows the external enclosure of the Boeing 767 mockup cabin with the supply air inlet and exhaust fans indicated. A schematic of the main supply duct is shown in Figure 3.25 and the actual salvaged duct is shown in Figure 3.26. The cross-section of the main supply duct decreases along the length of the mockup cabin to maintain the supply air flowrate. Figure 3.27 shows the different sections of the main supply duct. There are 17 pairs of clear and smooth-wall plastic hoses attached to the main supply duct as shown in Figure 3.25 and Figure 3.28, to supply air to the center linear diffusers.

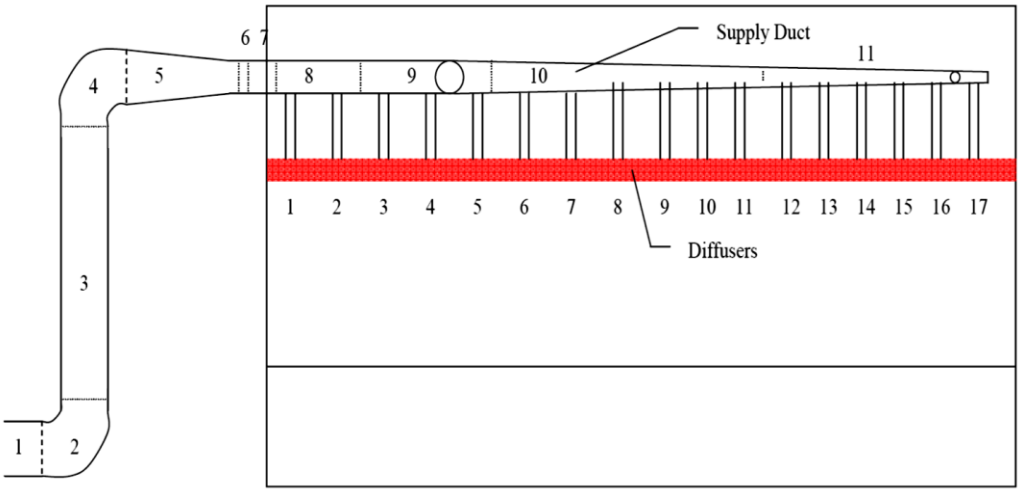

Figure 3.25. Main supply air duct in the Boeing 767 mockup cabin and the 17 pairs connecting the supply duct to the linear diffusers.

Figure 3.26. A section of the actual salvaged Boeing 767 main supply air duct.

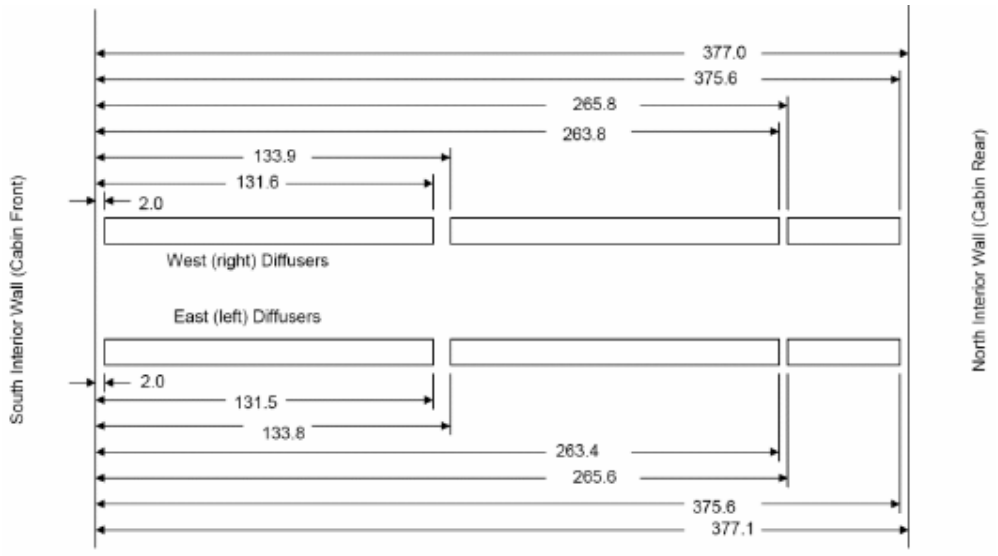

Figure 3.27. Dimensions of the main supply air duct of the Boeing 767 mockup in inch.

Figure 3.28. Supply hoses connecting the main supply duct, at the top, to the linear diffusers, at the bottom.

The clear plastic hoses are connected from the top to the main supply duct and from the bottom to the central diffusers using connectors which extend approximately 38 mm (1.5

inch) from the supply duct. The connectors to the top and bottom are shown in Figure 3.29 and Figure 3.30, respectively. Inside the duct, the connectors are flush with the supply duct wall as shown in Figure 3.31.

Figure 3.29. Top connections between the clear plastic hoses and the main supply duct.

Figure 3.30. Bottom connections between the clear plastic hoses and the main supply duct.

Figure 3.31. Inside view of the main supply duct.

Each hose connector is fitted with a round and thin orifice as shown in Figure 3.32. The orifices are used to balance the airflow along the length of the cabin.

Figure 3.32. Main air supply duct orffices.

A linear diffuser is used in the Boeing 767 cabin to distribute the supply air from the main supply duct into the cabin. Figure 3.33 shows the linear diffusers assembly. The linear diffuser is built of 3.35 m (11 ft) sections as shown in Figure 3.33 A. The diffuser section mounts to the back side of the centered overhead bin assembly. Air enters through the clear

plastic hoses shown in Figure 3.30 to the top of the diffuser assembly shown in Figure 3.33 B. From there, the air joins a plenum that extends the full length of the diffuser section. The diffuser is sealed to the back of the overhead bin assembly at the top. Air passes from the plenum through a narrow gap of about 3.2 mm (0.125 inch) width near the top of the assembly as shown Figure 3.33 C. The use of this narrow gap is to provide uniform flow over the entire length of the linear diffuser. End caps were used to cap both ends of the diffuser assembly as shown in Figure 3.33 D.

Figure 3.33. Linear diffuser assembly for the Boeing 767 cabin mockup.

The inside of the Boeing 767 mockup cabin is shown in Figure 3.34. When mounted in the cabin, the linear diffusers form a single continuous unit from the front to the back of the cabin. Nevertheless, airflow is disrupted between the diffuser sections (shown in Figure

3.27) due to the blockage created by the end caps. The two back-to-back end caps take up approximately 50.8 mm (2 inch) of space. Thus, there are approximately 50.8 mm (2 inch) at each joint between the sections where there was no airflow.

Figure 3.34. Inside view of the Boeing 767 cabin mockup showing the linear diffusers.

To test the homogeneity and uniformity of the mixed air temperature inside the cabin, (Shehadi, 2015) conducted measurements within the same cabin at different vertical distances away from the diffusers along the cabin. The average supply air temperature inside the cabin ranged between 18.7 ^{o}C (65.7^{o}F) at the tip of the diffuser and 24.2 ^{o}C (75.6^{o}F) in regions close to the floor. Furthermore, the difference in the maximum recorded temperature between the east and west aisles ranged from as low as 0.05^{o}C to 0.45^{o}C (32.1^{o}F to 32.8^{o}F).

3.1.3.2.2 Modified Cabin

To convert the cabin from the existing Boeing 767 air supply configuration to the modified configuration, the clear supply hoses shown in Figure 3.28 connecting the main supply duct to the central diffusers were disconnected from the center diffuser and connected to newly installed PVC ducts on each side of the cabin. The connections were done through T-sections installed on the cabin ceiling and connected to the new supply air PVC ducts. Figure 3.35 shows the new design of the supply air diffusers. The 34 clear hoses shown in Figure 3.28 were connected to the new supply ducts inside the cabin alternatingly between the top and bottom supply air PVC ducts. Nine pairs of clear hoses were connected to the top duct (Figure 3.36) and 8 pairs to the bottom duct (Figure 3.37) in each side of the cabin. Appendix A shows the location of the T-sections and supply air diffusers inside the cabin for each of the top and bottom PVC ducts.

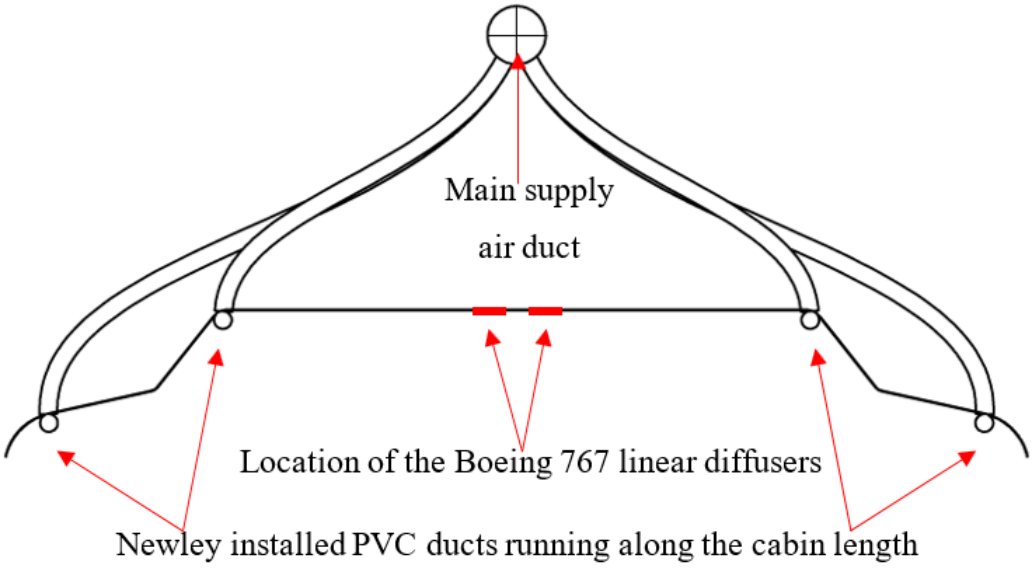

Figure 3.35. Modified cabin supply air configuration.

The 17 clear plastic hose pairs were connected to the four newly installed PVC ducts in an alternating manner. For example, the first pair was connected to the top PVC ducts as shown in Figure 3.36, the next pair was connected to the bottom PVC ducts as shown in Figure 3.37, and so on.

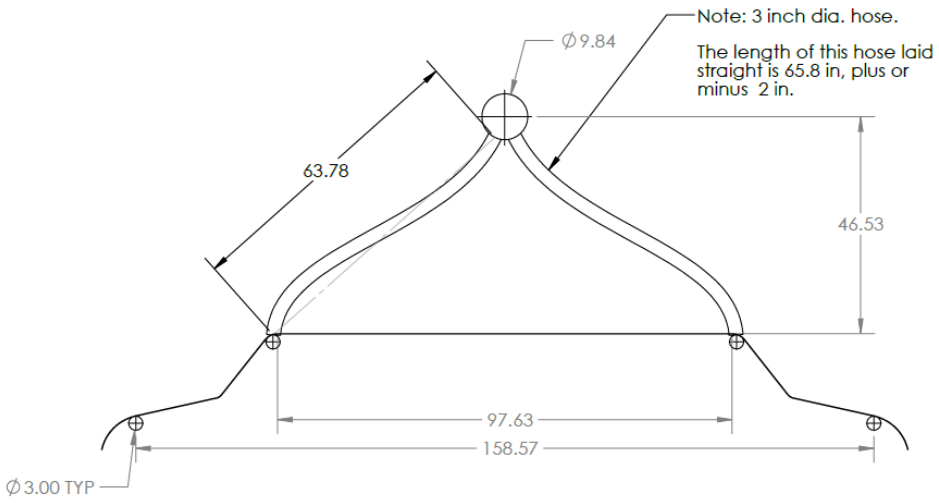

Figure 3.36. Supply air hoses connecting the main supply air duct to the newly installed top PVC ducts.

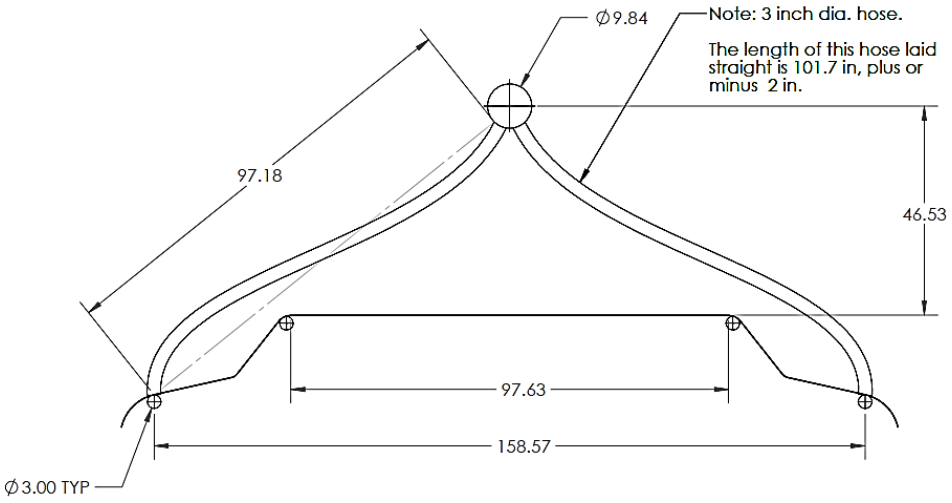

Figure 3.37. Supply air hoses connecting the main supply air duct to the newly installed bottom PVC ducts.

In order to have the same diffusers supply air velocity in the new cabin configuration, a mass balance calculation was carried out. The complete calculations are shown in Appendix B.1. Using PVC ducts of 76.2 mm (3 inch) diameter along the cabin, the diffusers hole diameter and spacing were calculated to be 40 mm (1.58 inch) and 203.2 mm (8 inch), respectively. Velocity measurements were taken for each single hole on each PVC duct (47 holes/duct) and recorded in Appendix B.2. The average air velocity from each newly installed PVC ducts are listed in Table 3.3. A diagram showing the location of each of those PVC ducts is shown in Figure A.1 in Appendix A.

Table 3.3. Average supply air velocity at each newly installed PVC duct in the modified cabin.

PVC Duct Location	Average air velocity	Standard deviation
Top Right	2.1m/s (6.9 ft/s)	0.4 m/s (1.3 ft/s)
Bottom Right	2.5 m/s (8.2 ft/s)	0.4 m/s (1.3 ft/s)
Top Left	2.2 m/s (7.2 ft/s)	0.4 m/s (1.3 ft/s)
Bottom Left	2.6 m/s (8.5 ft/s)	0.4 m/s (1.3 ft/s)

3.1.3.2.3 Boeing 737 Cabin

Similar to the Boeing 767, air enters the Boeing 737 cabin section through a center linear diffuser as shown in Figure 3.38. The diffuser covers 4.02 m (13.2 ft) of the cabin length with a gap of 0.41 m (1.33 ft) from both end walls of the cabin. The linear diffuser is made up of sections linked using connectors which break the supply air flow along the length of the cabin to establish a uniform airflow inside the cabin.

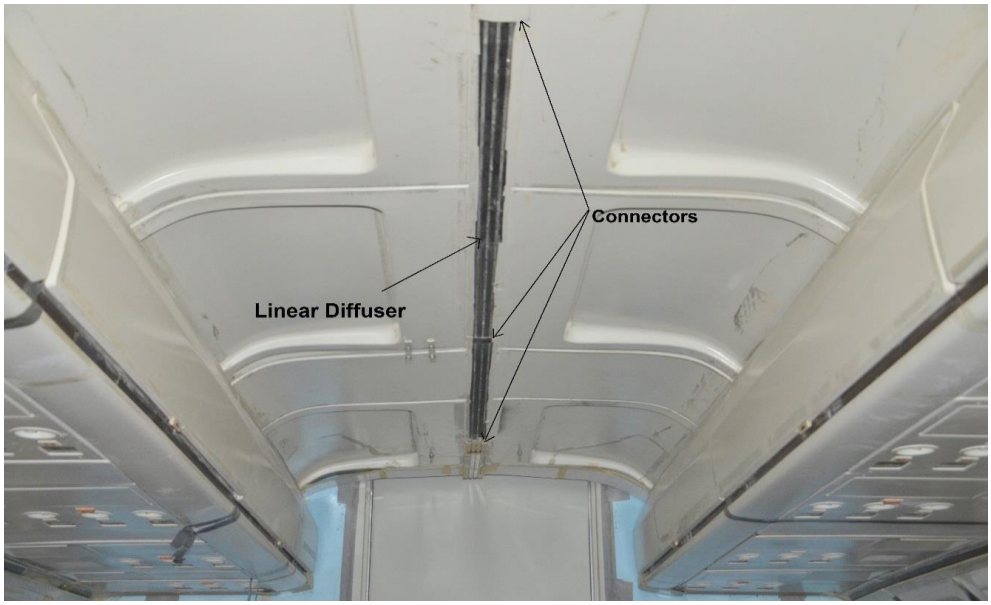

Figure 3.38. Linear diffusers and connectors on the Boeing 737 ceiling.

After entering the cabin through the central linear diffuser, the air is ventilated through exhaust grills of 40.64 cm x 6.35 cm (16 x 2.5 inch) (width x height) at the base of the cabin sidewalls as shown in Figure 3.39. The air is ventilated out directly into the environment of the lab.

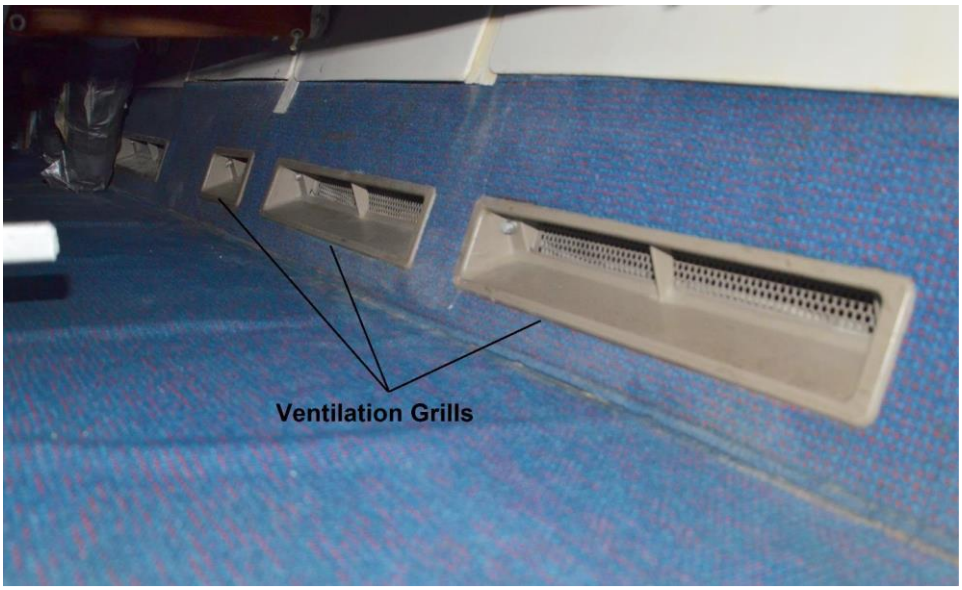

Figure 3.39. Ventilation grills at the Boeing 737 sidewalls.

3.1.4 Tracer Gas Experimental Setup Description

Tracer gas has been widely used in experimental studies to study ventilation effectiveness, airflow circulations, airflow velocities, and other characteristics and parameters inside aircraft cabins, enclosed environments, buildings, hospitals, and many other applications. In this work, the tracer gas was composed of carbon dioxide that was mixed in the continuous injection tests with helium to model the buoyancy of air. Carbon dioxide was used by itself as the tracer gas in the coughing manikin tests. Carbon dioxide was sampled at different locations in the cabin using carbon dioxide gas analyzers.

3.1.4.1 Tracer Gas Injection System

3.1.4.1.1 Tracer Gas Injection System Description

A tracer gas injection system was used to inject the tracer gas into the different aircraft cabins. The tracer gas was composed of CO_2 and He and was mixed and injected into the

cabin through a vinyl tube. Both CO_2 and He were supplied at 200 kPa (29 psi) using the pressure gauge fitted on the gas tanks. The mass flow controllers were controlled through a DAQ system and a 2-channel power supply unit. Figure 3.40 shows a schematic of the tracer gas injection system.

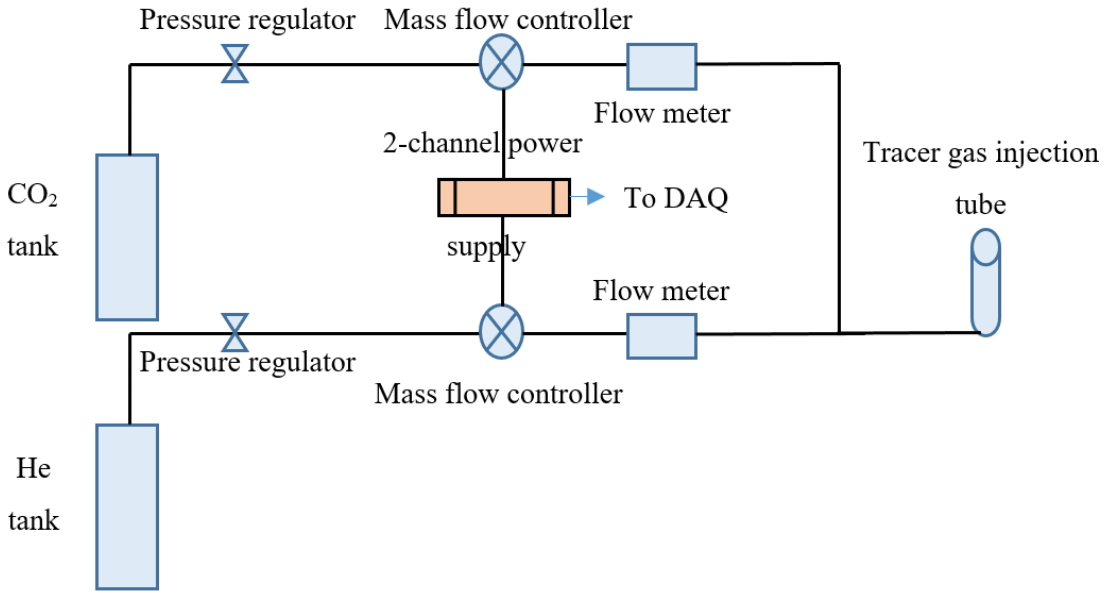

Figure 3.40. Tracer gas injection system schematic.

3.1.4.1.2 CO_2 and He Equilibrium

He was injected and mixed with the CO_2 in order to maintain the buoyancy between the injected tracer gas and the air inside the cabin. Using the fact that CO_2 is 1.5 denser than atmospheric air and based on ideal gas principles it was found that the injected tracer gas should consist of 62.4% CO_2 and 37.6% He as shown mathematically in equations (3.1)-(3.4). A total of 5 L/min (0.176 ft^3/min) of CO_2 and 3.07 L/min (0.108 ft^3/min) of He were injected at the average of seated passenger breathing level of 1.25 m (4.92 ft) above the cabin floor. For the tracer gas injection tests, a 25.4 mm inner diameter copper tube was used as shown in Figure 3.41.

Figure 3.41. Tracer gas injection tube.

The flowrate of each gas was calculated based on the buoyancy of air as shown below. The ideal gas law is given in equation (3.1):

$$P.V = m.R.T \tag{3.1}$$

Where:

P is the pressure, V is the volume, m is the mass, R is the gas constant, and T is the temperature. Assuming that the pressure, volume, and temperature do not change, then the only variables are m and R, where:

$$R = \bar{R}\, M \tag{3.2}$$

where $\bar{R}$ is the universal gas constant, and M is the molar mass. To maintain buoyancy between air and the tracer gas consisting of CO_2 and He, equation (3.3) has to be satisfied:

$$mair = x.mCO_2 + y.mHe \tag{3.3}$$

where x & y are percent fraction of CO_2 and He, respectively. Using the ideal gas law, as in equation (3.1), and substituting the values of R from equation (3.2) into equation (3.3):

$$Mair = x.MCO_2 + y.MHe \quad (3.4)$$

Where: Mair = 28.96 g/mol ; MCO_2 = 44.01 g/mol ; MHe = 4.003 g/mol.

To meet the conditions of equation (3.4), it was found that x=0.624 and y=0.376. Therefore, the injected mixture consisted of 62.4% CO_2 and 37.6% of He. With 5 L/min (0.176 ft^3/min) of CO_2 and 3.07 L/min (0.108 ft^3/min) of He was required to maintain this balance and to maintain the buoyancy of the tracer gas in the cabin air.

3.1.4.1.3 Mass Flow Controllers

The injection of CO_2 and He was controlled using two mass flow controllers. CO_2 flowrate was controlled by an MKS GE250A025105SBV0020 electric mass flow controller, and the He flowrate was controlled by an MKS 2179A00114CS pneumatic mass flow controller. Two flow meters were connected downstream of the flow controllers as shown in Figure 3.42 to verify the mass flow rates going into the injection port inside the cabin. The mass flow controllers were connected to a 2-channel power supply which in turn was connected to the main DAQ as shown in Figure 3.43. This allowed automatic input of the required flowrate of CO_2 and He.

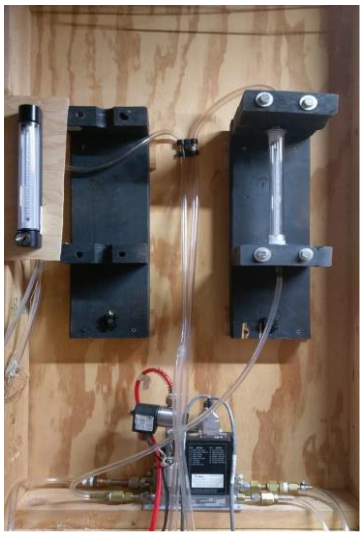

Figure 3.42. Mass flow controllers with flow meters.

Figure 3.43. 2-channel power supply unit (Top) and Agilent 34970A DAQ (Bottom).

3.1.4.1.4 Tracer Gas Control System

To measure tracer gas dispersion throughout different seat locations in the cabin, a measurement from each of the CO_2 analyzers was recorded every five seconds during experiments with the continuous injection source and every three seconds for coughing manikin experiments. All measurement equipment were controlled by commercial LabVIEW package. The data acquisition system was an Agilent 34970A DAQ. A separate LabVIEW program was used to control the cabin supply air through the Agilent DAQ. Using the LabVIEW program, the tracer gas injection rate, duration, and timing were also set. A

snapshot of the LabVIEW program interface is shown in Figure 3.44. The program was also used to control the sampling interval and ports for the tests at which the sampling tree was utilized.

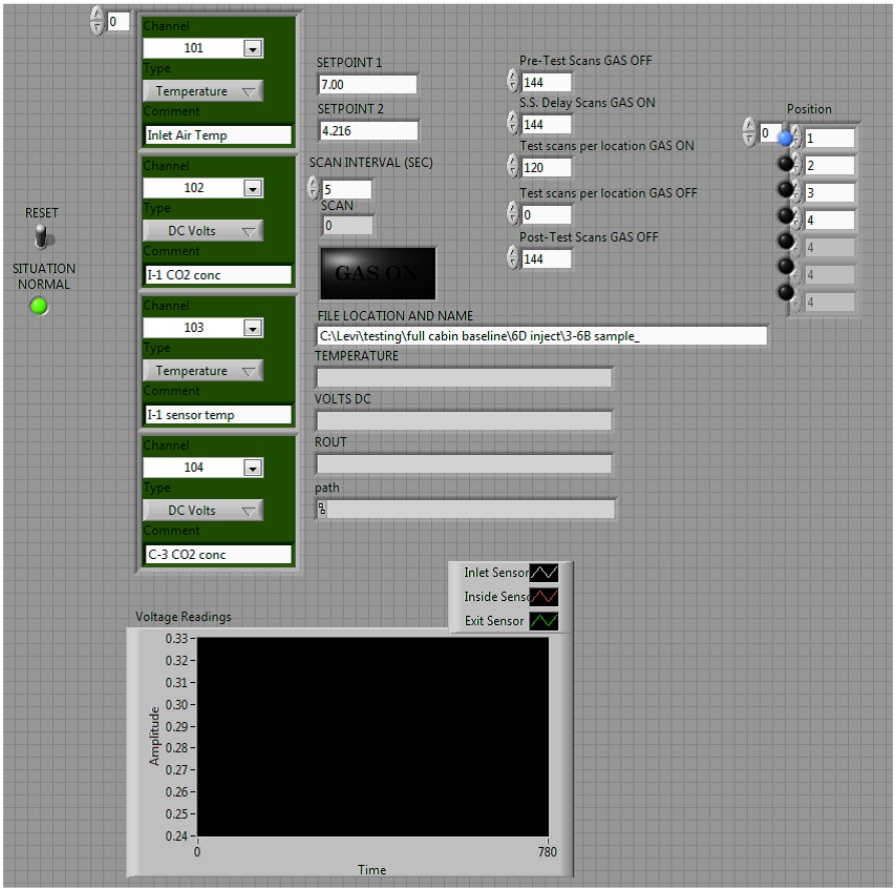

Figure 3.44. LabVIEW interface used to control different equipment.

3.1.4.2 Tracer Gas Sampling System

3.1.4.2.1 CO_2 Tracer Gas Analyzers

The utilized CO_2 analyzers were of an NDIR (Non-dispersive Infrared) type that are linearly related to the concentration of carbon-dioxide. The absorption of CO_2 by NDIR is governed by Lambert-Beer law which states that the absorption of a gas is directly proportional to its concentration (International Union of Pure and Applied Chemistry, 2014).

Three types of CO_2 analyzers were used. The first is a PP Systems WMA-4 analyzer, shown in Figure 3.45. The second is a PP Systems WMA-5 analyzer, shown in Figure 3.46. The third is a custom-made Edinburg Gascard analyzer, shown in Figure 3.47. The basic principle for all three analyzers is the same.

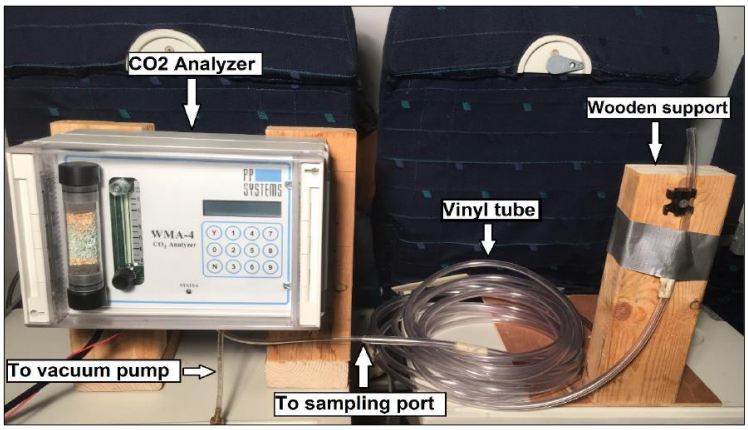

Figure 3.45. WMA-4 gas analyzer.

Figure 3.46. WMA-5 gas analyzer.

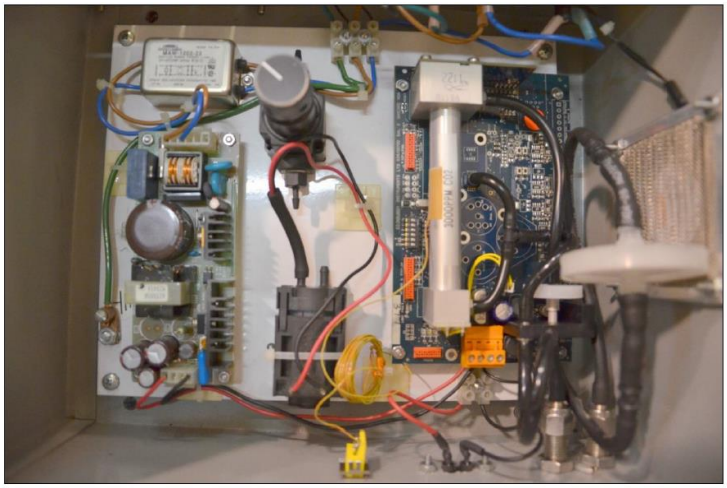

Figure 3.47. Custom-made Edinburg Gascard gas analyzer.

For the older model gas analyzers such as the WMA-4 and the Edinburg Gascard, a vacuum pump was required in order to withdraw the gas sample from the sampling location. For the newer models such as the WMA-5, the analyzer has a built-in pump. The CO_2 analyzers utilize the external vacuum pump to withdraw the samples at a rate of 1 L/min (0.035 ft^3/min). Since there is a difference in pressure drop between each analyzer based on the length of the tubes connecting the pump and the analyzers, a balancing system, shown in Figure 3.48, was used to ensure that each analyzer draws in the same flowrate. While both WMA-4 analyzers and the custom-made Edinburg Gascard analyzers require this system, the new WMA-5 analyzer has a different design which requires a lower flowrate and has a built-in pump that is strong enough to draw a sample at the correct flowrate without the need for an external pump.

Figure 3.48. Balancing system for the WMA-4 and custom-made Edinburg Gascard gas analyzers.

The analyzers output the concentration to the DAQ as a voltage. The voltage received at the DAQ unit is then recorded by the LabVIEW program and is output to a Microsoft Excel spreadsheet. The WMA-4 and the custom-made Edinburg Gascard analyzers are calibrated for a range of 0 –2000 parts per million (ppm), while the WMA-5 analyzer is calibrated for a range of 0 – 3000 ppm. To calibrate the gas analyzers, calibration gasses with known concentrations of 500 ppm and 2000 ppm of CO_2 were used. To avoid damaging the analyzers, a pressure regulator was attached to the cylinders. Each analyzer directly sampled each calibration gas individually for 6 minutes. The average voltage was taken over the last 5 minutes to ensure that the analyzers had reached a stable concentration. The average voltages were then plotted on a graph versus the recorded gas concentration and the corresponding linear equation developed by Microsoft Excel was used to relate the voltage to the concentration in ppm. The calibration curve for each analyzer is shown in Figures 3.49-3.54. Analyzers A1, A5, and A6 are the older WMA-4 analyzers which had a range of

0-2000 ppm while A2 and A3 are the newer WMA-5 analyzers with a 0-3000 ppm range and A4 is the custom-made Edinburg Gascard analyzer with a 0-2000 ppm range.

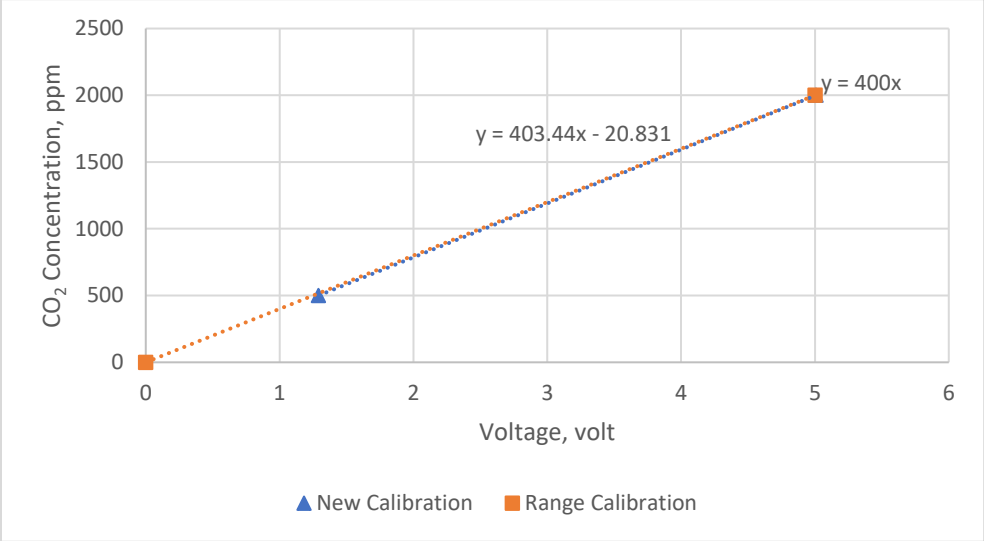

Figure 3.49. Calibration curve of gas analyzer A1.

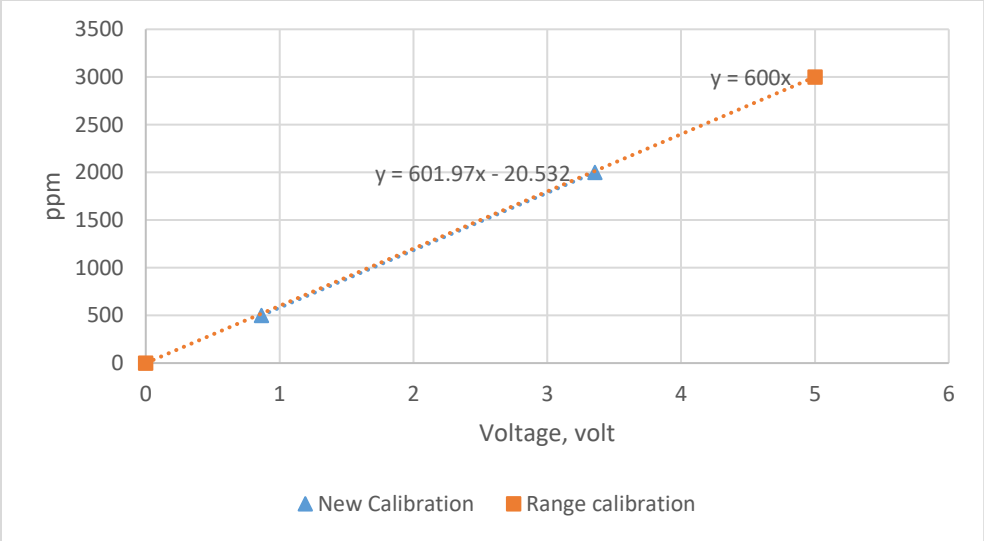

Figure 3.50. Calibration curve of gas analyzer A2.

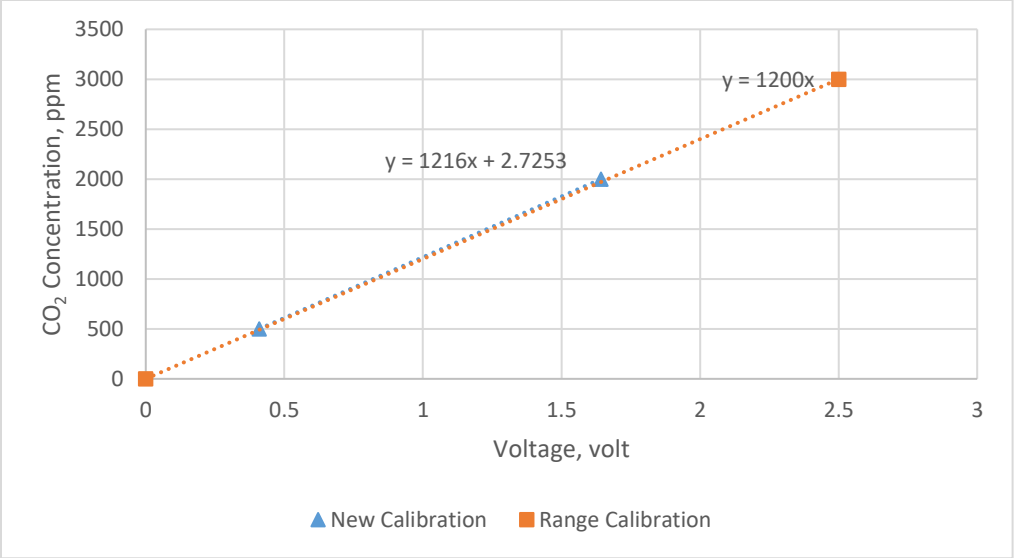

Figure 3.51. Calibration curve of gas analyzer A3.

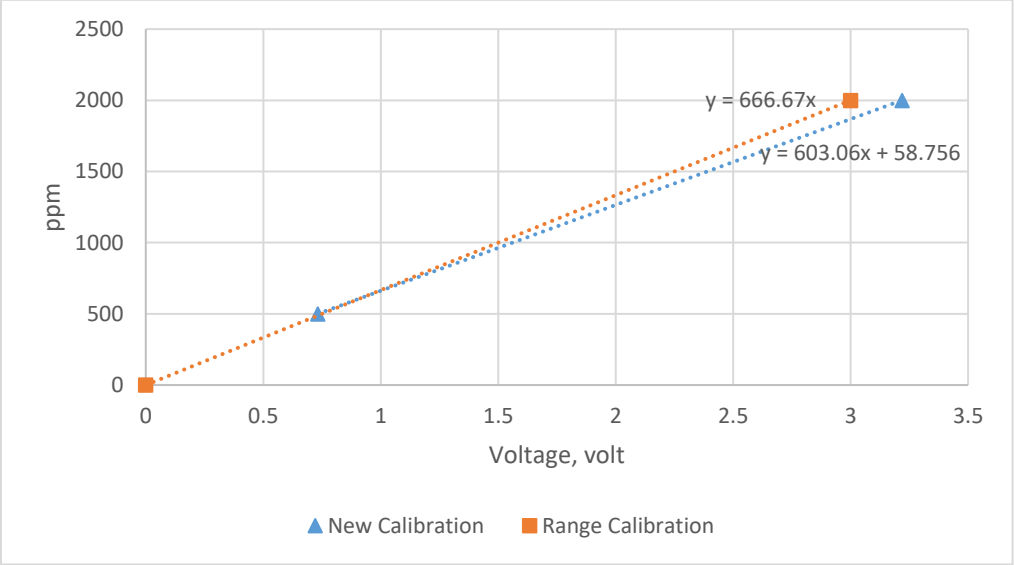

Figure 3.52. Calibration curve of gas analyzer A4.

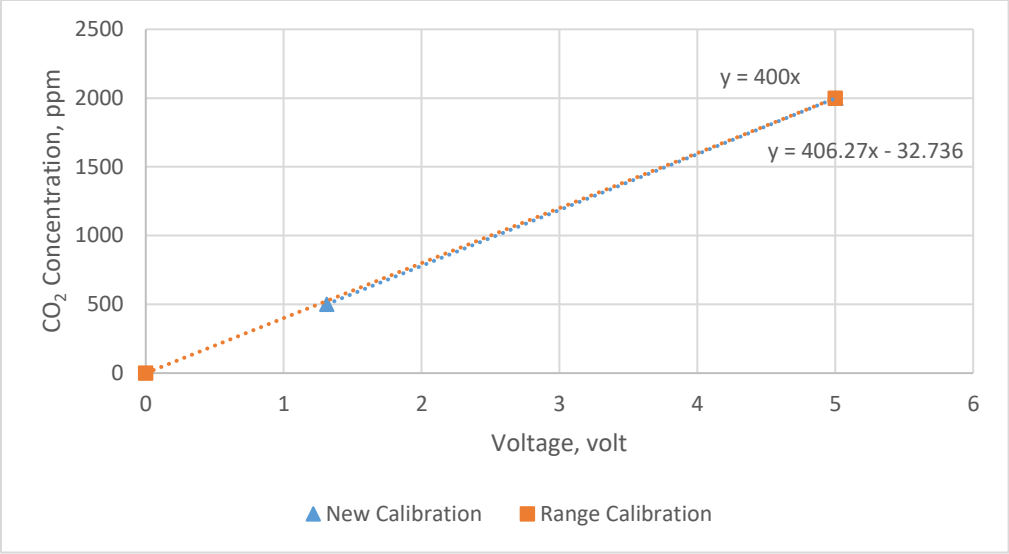

Figure 3.53. Calibration curve of gas analyzer A5.

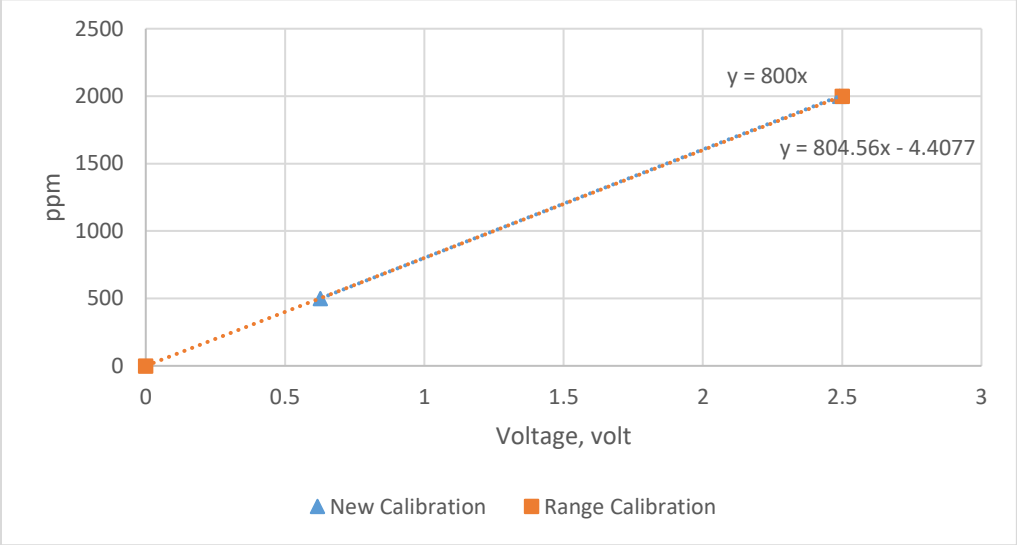

Figure 3.54. Calibration curve of gas analyzer A6.

3.1.4.2.2 CO_2 Tracer Gas Sampling Tree

A sampling tree was used to decrease the number of required gas analyzers needed to sample the trace gas at different locations inside the cabin. The sampling tree is a 3.1 m (10.17 ft) metal rod composed of 4 equidistant sampling ports as shown in Figure 3.55 and is used to collect samples at 4 different locations sequentially. Each port was controlled with a normally closed (NC) SMC Pneumatics NVKF334V-3G 2-way solenoid valve connecting each of the 4-sampling ports to a common outlet port that was connected to the inlet of a single CO_2 analyzer. Thus, the ports were opened sequentially, one at a time, allowing for isolated sampling in each location. Each sampling line was made of 304 stainless steel welded tubing with an inside diameter of 5 mm (0.2 inch). A fifth normally open solenoid valve was mounted to the manifold in reverse orientation. This allows the tube connected to the common rail of the manifold on one side and to the CO_2 analyzer on the other side to constantly be pulling a sample through to the CO_2 analyzer.

Figure 3.55. Tracer gas sampling tree with 4 sampling ports.

When a test was conducted, the normally opened (NO) reversed valve would close and the valve corresponding to the port being used for sampling would open. This would ensure that the air that was leaving the manifold and being analyzed by the CO_2 analyzer is the air being sampled through that single corresponding opened port.

3.2 Thermal Manikins

The average heat generation by a comfortable, sedentary person, excluding heat loss due to evaporation of moisture, is about 70 W (ASHRAE, 2013). The thermal output of the occupants has a significant effect on the airflow patterns inside the aircraft cabin. To simulate a partially filled cabin, heated manikins were installed as shown in Figure 3.56. Each manikin was uniformly wrapped with heater wire on the arms, legs, chest, and head. Each manikin was plugged in to a 115 V outlet and generated about 100 W (341 BTU/hr.) of heat. This accounted for the average sensible thermal output of a resting adult, 70 W (238 BTU/hr.), plus additional heat from in-flight entertainment systems, avionics, and personal electronics such as laptops. As a safety precaution, a thermostat was installed inside the cabin to shut off the power to the manikins in case the temperature inside the cabin exceeds the set temperature.

Figure 3.56. Thermal manikins inside the Boeing 767 mockup cabin.

3.3 Coughing Manikin

An automated coughing manikin was used to simulate a coughing passenger as shown in Figure 3.57. The cough airflow was produced by a metal bellows driven by a computer controlled linear motor. It was based on coughs recorded from influenza patients and had a volume of 4.2 L (0.148 ft^3) and a peak flowrate of 11.4 L/s (0.403 ft^3/s) with the entire cough lasting approximately 1 second. The coughing frequency for this study was one cough every 75 seconds. Due to the high velocity of the cough generated by the manikin, momentum effects dominate, and minimal buoyancy effects were present. Hence, pure CO_2 gas was used during coughing manikin tests. To ensure sufficient CO_2 supply, each test was run for 30 coughs which allowed measurements at all sampling tree locations before refilling the Tedlar bags. The CO_2 gas was supplied to the coughing manikin through two 100-liter Tedlar bags. The bags are filled with pure CO_2 before each test. When a cough is activated, the manikin mouth valve closes, and the manikin bellows get filled with the CO_2 gas using the Tedlar bags. Once the bellows are filled with the CO_2, the manikin mouth opens, and the bellows rapidly compress causing the cough to be released.

Figure 3.57. Automated coughing manikin.

Chapter 4 - Testing Procedures and Results

The objective of this study is to understand both dispersion and containment of infectious aerosols in aircraft cabins. This was accomplished by injecting a tracer gas into the cabin mockup from a point source or via a coughing manikin and measuring the concentration at various locations in the mockup cabin. Two different source types were used. Namely, a continuous injection point source and a coughing manikin source. The tests were carried out in different aircraft cabins using both source types. A passenger isolation system called ISOPass was also tested in different aircraft cabins.

Although selected test results are presented in this chapter, the majority of the tests results and replications are presented in the appendices of this dissertation. Results from tests performed in the modified cabin are designated by the letter A after the test number. Those performed in the Boeing 767 cabin are designated by the letter B after the test number. Tests performed in the Boeing 737 cabin are designated by the letter C after the test number. Furthermore, tests performed with the continuous injection source include the letter I and those performed with the coughing manikin include the letter M. For example, a test named "Test 3 (B-I)" is the test number 3 performed in the Boeing 767 cabin using a continuous injection source. The term "deployed" is used for tests with the ISOPass installed on the source seat, and similarly, the term "undeployed" is used to refer to tests with the ISOPass removed from the source seat. Table 4.1 shows the notations used in naming the tests within this dissertation.

Table 4.1. Tests notations and interpretation.

Notation	Interpretation
A	Test performed in the modified cabin mockup
B	Test performed in the Boeing 767 cabin mockup
C	Test performed in the Boeing 737 cabin section
I	Test performed using a continuous injection source
M	Test performed using a coughing manikin
ISOPass deployed	ISOPass installed on the source seat
ISOPass undeployed	ISOPass uninstalled on the source seat

The tracer gas measurements were collected using the CO_2 gas analyzers and the sampling tree. The CO_2 concentration data was then plotted against the corresponding measurement location from the source (at location 0) to provide a reference for the measurement locations. All of the measurements were then plotted as a function of distance relative to the reference point. To avoid confusion between measurements taken at the same distance but in the opposite directions, such as to the front and back of the source in a longitudinal direction using the sampling tree, the positive direction is the one pointing from the source to the sampling tree solenoid valves block in the tests conducted with a longitudinal or a diagonal sampling tree direction. The positive direction was taken as the right direction from the source in the tests performed with a lateral sampling tree direction similar to a typical coordinate system. The solenoid valves block is marked by a dashed line crossing the sampling tree in the figures in the appendices and as shown below in Figure 4.1.

4.1 Aerosols Dispersion Tests

4.1.1 Continuous Injection Source Tests

4.1.1.1 Boeing 767 Cabin Mockup

Four tracer gas injection locations were tested separately and are marked by a star symbol in Figures C.1-4 in Appendix C. Each test in this experimental set was repeated twice to confirm tests repeatability. For each tracer gas injection location, the sampling tree was positioned in several orientations to capture the tracer gas concentration at different radial distances in different directions. Appendix C shows the location of the tracer gas injection source indicated by the star shape along with the sampling tree orientation in each test. The sampling tree is indicated by the long solid line while the shorter solid bars crossing the sampling tree perpendicularly indicate the location of each of the four measurement ports. The dashed line at the end of the sampling tree indicates the location of the solenoid valves block. As mentioned earlier, the gas injection flowrates used in this study were 5.0 L/min (0.176 ft^3/min) for CO_2 and 3.07 L/min (0.108 ft^3/min) for He. A typical test in this experimental set was conducted in the sequence as listed in Table 4.2.

Table 4.2. Experimental procedures sequence for the tests performed in the Boeing 767 cabin mockup and the modified cabin.

Sequence	Period	Gas injection status	Sampling status	Duration
1	Steady-state	Off	Off	Until thermal steady state conditions were achieved
2	Pre-test	Off	On	20 minutes
3	Steady-state	On	On	15 minutes
4	Test	On	On	30 minutes/ sampling port
5	Post-test	Off	On	20 minutes

The data collected from each test included the CO_2 concentration at the cabin supply air, each of the four sampling tree ports, and near the tracer gas injection source. Furthermore, the cabin temperatures at different locations were also collected. For the objectives of this study, only the tracer gas concentrations were analyzed. Figures C.5-127 in Appendix C show the sampling tree orientation and the CO_2 tracer gas concentration at different locations during each test. Each test in Appendix C has three consecutive figures as shown in the sample figures, Figure 4.1-3. The first figure shows the source and the sampling tree locations. The second figure shows the instantaneous CO_2 tracer gas concentration for each sampling location versus time. Finally, the third figure shows the CO_2 tracer gas concentration for the sampling tree ports averaged across the testing period in addition to the instantaneous supply air concentration.

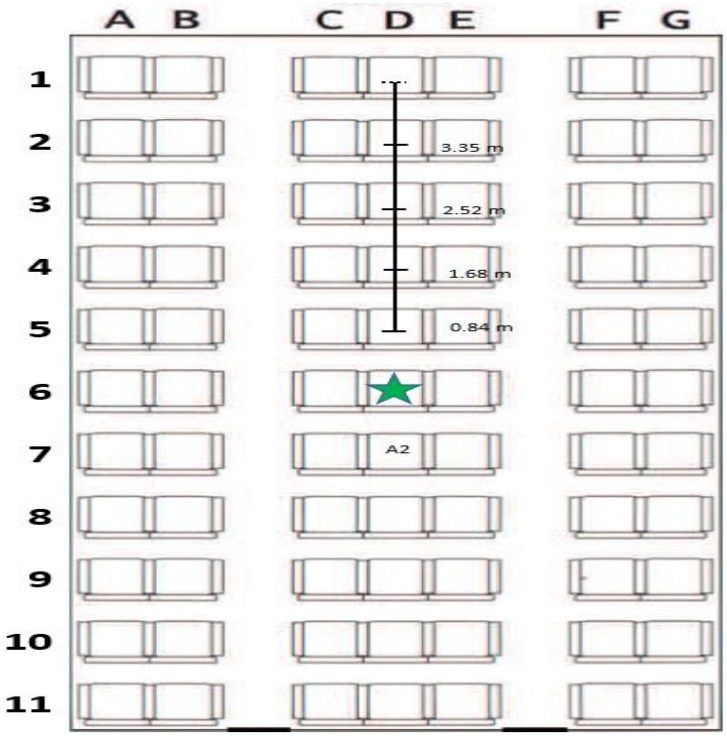

Figure 4.1. Sample of the figures showing the tracer gas source location and the sampling tree orientation in appendix C.

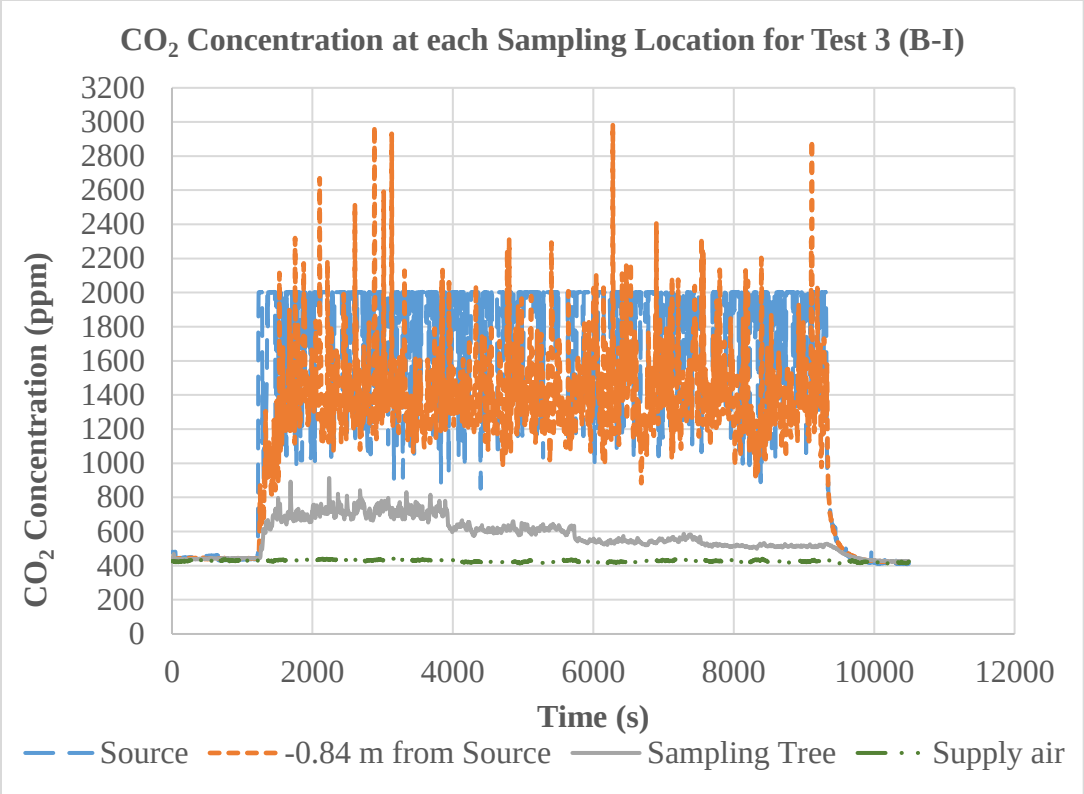

Figure 4.2. Sample of the figures showing the instantaneous tracer gas concentration at each sampling location versus experimental time in the figures in in appendix C.

In Figure 4.2, the x axis shows the time in seconds and the y axis shows the CO_2 tracer gas concentration in parts per million (ppm) at each measurement location.

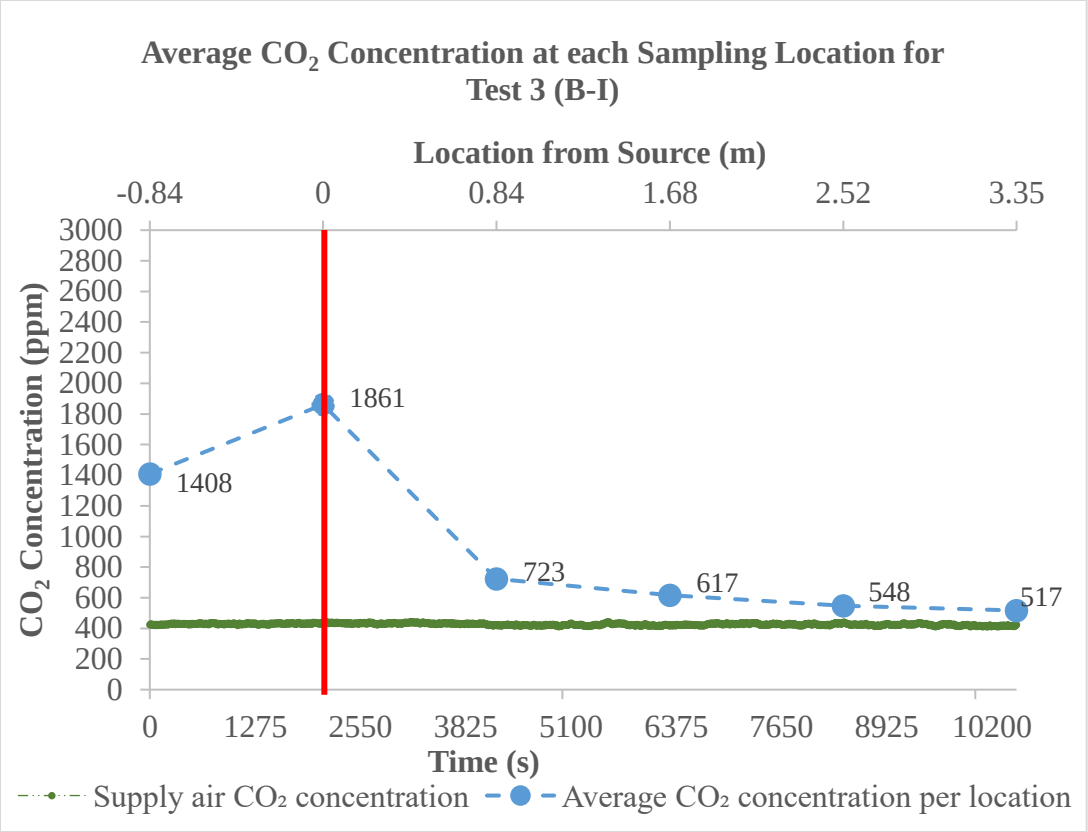

Figure 4.3. Sample of the figures showing the tracer gas concentration at each sampling tree port versus experimental time in the figures in in appendix C.

In Figure 4.3, the primary (bottom) x-axis shows the time in seconds used to plot the instantaneous tracer gas concentration in the supply air. The secondary (top) x-axis shows the measurement location from the source in meters. The y-axis shows the CO_2 tracer gas concentration at each measurement location in ppm. On the secondary (top) x-axis, measurement locations are listed with reference to the tracer gas injection location located at point 0. The measurement point behind the tracer gas injection location was at -0.84 m. Sampling tree ports (1 to 4) were located at 0.84, 1.68, 2.52, and 3.35 m away from the tracer gas source location, respectively. The supply air CO_2 analyzer tube was placed in the supply air diffuser at the front end or back end of the cabin opposite to the tracer gas source location.

The measured supply air concentrations are shown as the green line in the Figures in the appendices. The CO_2 analyzer tube assigned to the tracer gas injection source was taped to the source at breathing level to measure the tracer gas concentration at the source seat.

4.1.1.2 Modified Cabin

As mentioned earlier in section 3.1.1.1 of this dissertation, the Boeing 767 cabin mockup was modified to represent a different cabin supply air configuration. Similar to the tests carried out in the Boeing 767 cabin mockup, the gas injection flowrates were 5 L/min (0.176 ft^3/min) for CO_2 and 3.07 L/min (0.108 ft^3/min) for He. A typical test was also conducted in the same sequence as shown in Table 4.2. Appendix E shows the results of the tests conducted in the modified cabin. Each test in this experimental set was repeated twice to confirm tests repeatability. Figures E.1–E.4 in Appendix E show the four continuous injection tracer gas source locations inside the modified cabin indicated by the star shape. The figures also show the test numbers and the sampling tree orientation for each test. Both the tracer gas source locations and the sampling tree orientations were matched with those in the continuous injection source tests in the Boeing 767 mockup cabin, shown in Appendix C, for comparison purposes. Figures E.5-124 in Appendix E show the sampling tree orientation and the CO_2 tracer gas concentration at different locations during each test. Each test in Appendix E has three consecutive figures. The first figure shows the source and the sampling tree locations. The second figure shows the instantaneous CO_2 tracer gas concentration for each sampling location versus the time. Finally, the third figure shows the CO_2 tracer gas concentration for the sampling tree ports averaged across the testing period in addition to the instantaneous supply air concentration.

4.1.1.3 Boeing 737 Cabin Section

Three identical continuous injection source tests were conducted in the Boeing 737 cabin by (Darrah, 2018) using the same tracer gas injection and sampling systems. The tracer gas injection source was located on seat B4 as indicated by the star shape in Figure 4.4. In addition, three gas analyzer tubes were positioned individually on different seats as indicated by the solid dot to record the tracer gas concentrations at different locations.

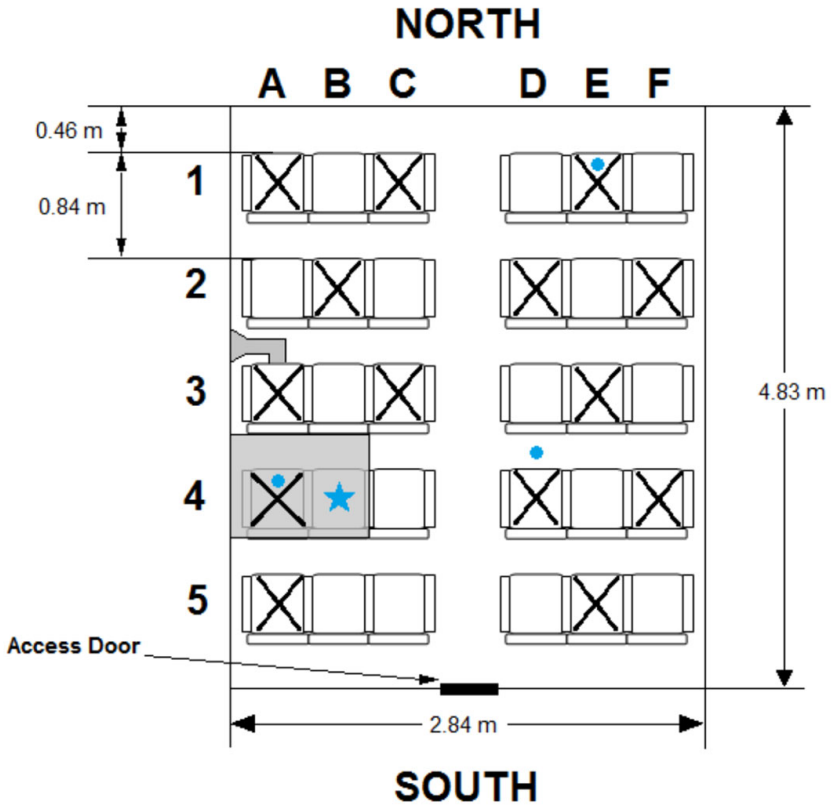

Figure 4.4. Boeing 737 cabin section layout and dimsneions.

Similar to the tests carried out in both the Boeing 767 cabin mockup and the modified cabin, the gas injection flowrates were 5 L/min (0.176 ft^3/min) for CO_2 and 3.07 L/min (0.108 ft^3/min) for He. A typical test in this experimental set was also conducted in the same

sequence, but for shorter durations since the sampling tree was not utilized. The test sequence was as shown below in Table 4.3.

Table 4.3. Experimental procedures sequence for the tests performed in the Boeing 737 cabin section.

Sequence	Period	Gas injection status	Sampling status	Duration
1	Steady-state	Off	Off	Until thermal steady state conditions were achieved
2	Pre-test	Off	On	10 minutes
3	Test	On	On	30 minutes
4	Post-test	Off	On	20 minutes

The study carried out by (Darrah, 2018) used the exact same tracer gas injection conditions for all the continuous injection source tests in this study including supply air conditions. Since the tracer gas source concentration was known to be saturating the tracer gas analyzers and due to the limited number of gas analyzers available to the researcher at that time, the tracer gas concentration near the source location was not recorded. Figures F.1-6 in Appendix F show the tracer gas source location and concentration at different locations for each identical test. Since the sampling tree was not used in the tests performed in the Boeing 737, each test in Appendix F has only two consecutive figures. The first figure shows the source and the tracer gas analyzer tubes locations. The second figure shows the instantaneous CO_2 tracer gas concentration for each sampling location versus the time.

4.1.2 Coughing Manikin Tests

4.1.2.1 Boeing 767 Cabin Mockup Coughing Manikin Tests

Five coughing manikin locations were tested separately and marked with a manikin head symbol (in black) in Figures H.1-5 in Appendix H. For each coughing manikin location, the sampling tree was positioned in several orientations to capture the tracer gas concentration at different radial distances in different orientations. Each of the 93 tests was formed by choosing a source location accompanied by a sampling tree orientation. Each test in this experimental set was repeated thrice to confirm tests repeatability. Figures H.6-176 show the source location, sampling tree orientation, and the recorded tracer gas concentration for each of the 93 tests. The sampling tree is depicted by the long solid line where the dashed line at the end of the sampling tree denotes the location of the solenoid valves block which controls the opening and closing of the valves to the ports where the sampling is happening. Each test in Appendix E has three consecutive figures. The first figure shows the source and the sampling tree locations. The second figure shows the instantaneous CO_2 tracer gas concentration for each sampling location versus the time. Finally, the third figure shows the CO_2 tracer gas concentration for the sampling tree ports averaged across the testing period in addition to the instantaneous supply air concentration. A typical test in this experimental set was conducted as shown in Table 4.4. The cough airflow was produced by a metal bellows driven by a computer controlled linear motor. It was based on coughs recorded from influenza patients and had a volume of 4.2 L (0.148 ft^3) and a peak flowrate of 11.4 L/s (0.403 ft^3/s) with the entire cough lasting approximately 1 second. The coughing frequency for this study was one cough every 75 seconds.

Table 4.4. Experimental procedures sequence for the tests performed using the coughing manikin.

Sequence	Period	Coughing status	Sampling status	Duration
1	Steady-state	Off	Off	Until thermal steady state conditions were achieved
2	Pre-test	Off	On	10 minutes
3	Test	On	On	6 minutes/ sampling port
4	Post-test	Off	On	10 minutes

4.2 Aerosols Containment Tests

The passenger isolation system (ISOPass) is a compact, lightweight, and rapidly deployable intervention that in-flight airline cabin personnel can use to protect passengers and crew from exposure to infectious passengers. The ISOPass is designed to be installed over two adjacent, same-row seats by a flight attendant during the flight. The ISOPass is shown in Figure 4.5 and Figure 4.6 in the Boeing 737 cabin section and in Figure 4.7 in the Boeing 767 mockup cabin. Figure 4.5 shows an exterior view of ISOPass as viewed from inside of the Boeing 737 cabin while Figure 4.6 shows an inside view in the same cabin. Figure 4.7 shows an exterior view of the ISOPass in the Boeing 767 mockup cabin.

Figure 4.5. Exterior view of the ISOPass deployed in the Boeing 737 cabin section.

Figure 4.6. Interior view of the ISOPass deployed in the Boeing 737 cabin section.

Figure 4.7. Exterior view of the ISOPass deployed in the Boeing 767 cabin mockup.

The ISOPass has a battery powered exhaust fan located in the feet area which provided a 4530.7 L/min (160 ft^3/min) airflow. Its discharge is ducted to the cabin exhaust port as shown in Figure 4.8. In an actual aircraft, the contaminated air from the ISOPass would either exit the aircraft through the outflow valve or pass through the recirculation filters if returned to the cabin. The ISOPass exhaust generates a negative pressure inside the enclosure, and ventilation air enters through gaps around the edges of the ISOPass as well as the supply air gaspers.

Figure 4.8. ISOPass exhaust fan connected to the cabin wall in the Boeing 737 cabin section.

4.2.2 ISOPass Tests

4.2.2.1 Boeing 767 Cabin ISOPass Tests

4.2.2.1.1 ISOPass Deployed Coughing Tests

Figures I.1-4 in Appendix I show the coughing manikin locations for the tests performed with the coughing manikin and the ISOPass deployed in the Boeing 767 cabin. Those locations match those with the ISOPass undeployed for comparison purposes except for tests performed with the coughing manikin on seat D6. This is because the ISOPass is only deployable on the sides of the cabin in order to duct the exhaust air out. Figures I.5-112 in Appendix I show the coughing manikin location, the sampling tree orientation, and the tracer gas concentration at different locations for each test. Each test in Appendix I has three consecutive figures. The first figure shows the source and the sampling tree locations. The second figure shows the instantaneous CO_2 tracer gas concentration for each sampling location versus the time. Finally, the third figure shows the CO_2 tracer gas concentration for the sampling tree ports averaged across the testing period in addition to the instantaneous supply air concentration.

4.2.2.1.2 ISOPass Deployed Continuous Injection Source Tests

Figures D.1-6 in Appendix D show the tracer gas source location, sampling locations, and tracer gas concentration at different locations for each identical test performed with the continuous injection source and the ISOPass deployed. Each test in Appendix D has two consecutive figures. The first figure shows the source and the tracer gas analyzer tubes locations. The second figure shows the instantaneous CO_2 tracer gas concentration for each sampling location versus the time. The tests were conducted by (Darrah, 2018) using the

same tracer gas injection and sampling systems as in the ISOPass undeployed tests. To test the containment effectiveness of the ISOPass prototype within the 767 cabin, tracer gas was injected through a point source at approximate breathing level mounted to a seat within the ISOPass. Matched pairs were used to confirm statistical repeatability. For each test, the exhaust fan was set to 60%, with a fresh battery. This setting corresponds to approximately 4530.7 L/min (160 ft^3/min) at the start of the test.

4.2.2.2 Boeing 737 Cabin ISOPass Tests

4.2.2.2.1 ISOPass Deployed Continuous Injection tests

The ISOPass was installed in the Boeing 737 cabin to test its effectivity in a different aircraft. The ISOPass design for the Boeing 737 cabin is identical to the design for the Boeing 767 cabin. In the Boeing 737 cabin, the ISOPass fits over two of the three seats in the 3-seats section keeping one unoccupied seat for the person taking care of the hypothetical sick passenger. Figures G.1-8 in Appendix G show the tracer gas source location, sampling locations, and tracer gas concentration at different locations for each one of the identical tests performed in the Boeing 737 cabin. Each test in Appendix G has two consecutive figures. The first figure shows the source and the tracer gas analyzer tubes locations. The second figure shows the instantaneous CO_2 tracer gas concentration for each sampling location versus the time.

4.3 Cabin Air Smoke Visualization

4.3.1 Equipment and Procedures

Qualitative smoke visualization studies were conducted using theatrical smoke to visualize the airflow inside the modified mockup cabin. A portable Aries 125 mW green laser was used as a light source. The laser was fixed on a tripod and moved around the cabin to conduct smoke visualization tests at different locations. A custom-made cylindrical lens which converted the laser beam to a laser sheet was fitted on the laser outlet. An ADJ VF400 smoke generation machine was used to generate the smoke to visualize the cabin airflow pattern. All lights inside the cabin were turned off and a laser sheet was created using the laser source. A Sony HDR CX230 camera was used to capture videos and snapshots of the detected smoke.

The outlet type for the smoke visualization machine was varied to provide a good visualization of the cabin airflow patterns. In order to accurately visualize the airflow of the cabin air, the smoke must be injected with low momentum in order to not disturb the cabin airflow. However, adequate flow to provide good visualization was also required. Six different outlets were tested to reach to the best representation. The first outlet was a hose of 31.75 mm (1.25 inch) inner diameter as shown in Figure 4.9.

Figure 4.9. Grey 1.25-inch inner diameter hose connected to the smoke generation machine.

The second outlet type was a larger 50.8 mm (2 inch) inner diameter unobstructed duct as shown in Figure 4.10.

Figure 4.10. Tested 2-inch inner diameter unobstructed duct.

The third type was the same duct used in type 2 obstructed by a sponge as shown in Figure 4.11.

Figure 4.11. Tested 2-inch inner diameter duct obstructed with a sponge.

The fourth type was the same duct used in type 2 and 3 obstructed by a honeycomb mesh as shown in Figure 4.12.

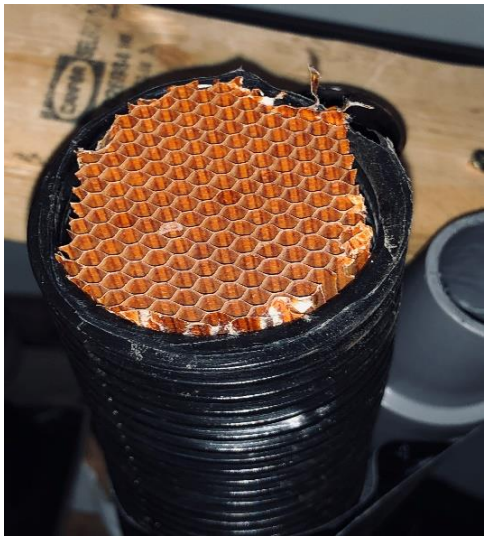

Figure 4.12. Tested 2-inch inner diameter duct obstructed with a honeycomb mesh.

The fifth type was a bucket with a 216 mm (8.5 inch) inner diameter as shown in Figure 4.13.

Figure 4.13. Tested 8.5-inch inner diameter unobstructed bucket.

All of the previous 5 outlet types resulted in a large smoke momentum that disturbed the cabin air flow. The final and the selected type was the bucket with a sponge cover on top as shown in Figure 4.14. This design was selected since it presented the least disturbance to the cabin airflow pattern.

Figure 4.14. Selected design of the 8.5-inch inner diameter bucket covered with a sponge from the top.

4.3.2 Smoke Visualization of Various Source Locations

Appendices J-N show the snapshots taken from the smoke visualization videos with the injection source in different locations inside the modified cabin. Since the cabin was already modified from the original Boeing 767 cabin, the qualitative smoke visualization study was conducted only on the modified cabin. The selected seats for the smoke visualization were the same seats which were selected earlier for the tracer gas studies performed on both the Boeing 767 and the modified cabins. Each of the appendices is divided to two parts. The first part is a cross-sectional view of the laser sheet and the second part is a frontal view of the laser sheet. A cross-sectional view is a view with the laser sheet along the width of the cabin while the frontal view is a view with the laser sheet along the length of the cabin. The first figure in each of Appendices J-N shows a schematic for each test configuration. A sample figure for the cross-sectional view and the frontal view is shown in Figure 4.15 and Figure 4.16, respectively. A smoke visualization snapshot for each view is shown in Figure 4.17 for the cross-sectional view and in Figure 4.18 for the frontal view. In total, 50 snapshots were taken from each smoke visualization video for each seat and each laser view. The snapshots are numbered from 1-50 in each appendix for each seat. All the smoke visualization tests were performed with the exact same conditions used to perform the tests within this study. This includes supply air conditions, thermal manikins' installation, and gaspers in-operation.

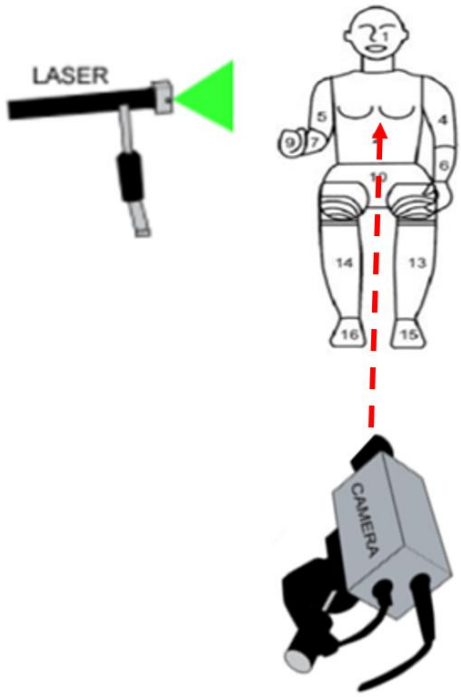

Figure 4.15. Smoke visualization cross-sectional view

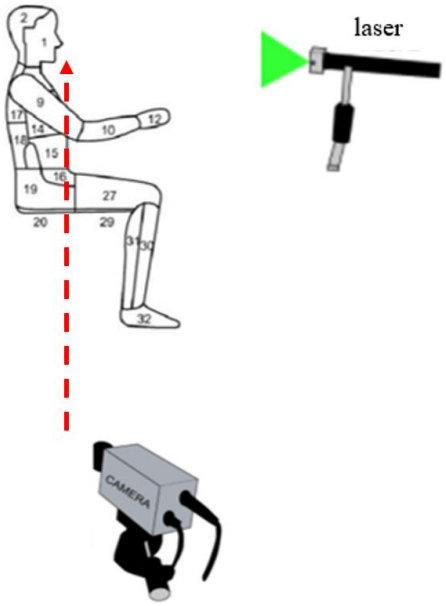

Figure 4.16. Smoke visualization frontal view

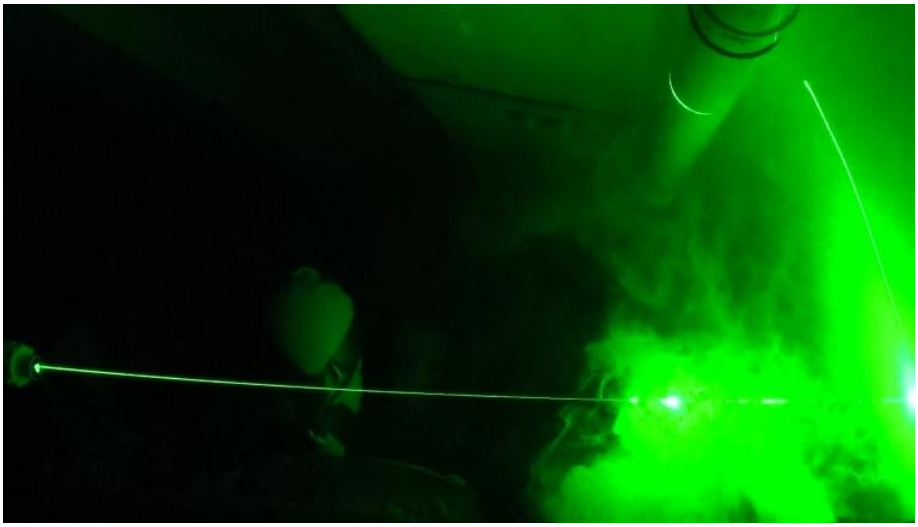

Figure 4.17. Smoke visualization cross-sectional view snapshot

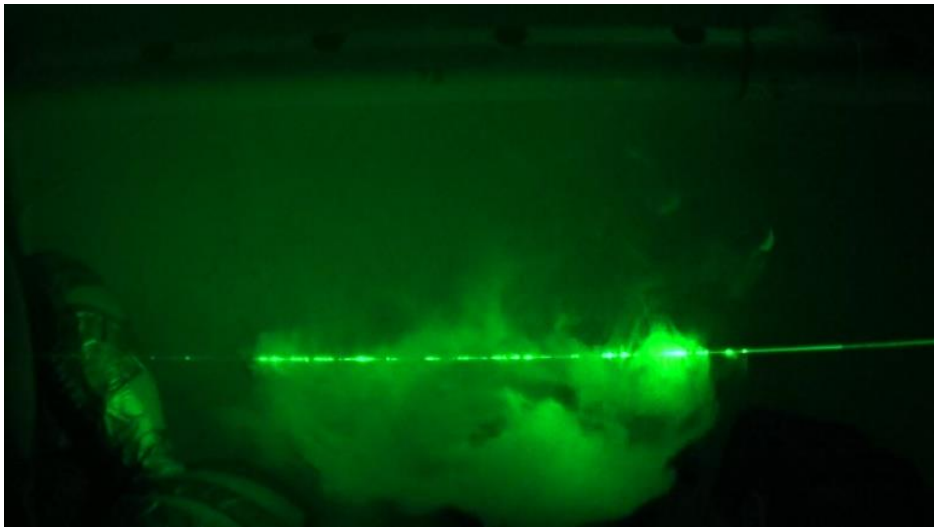

Figure 4.18. Smoke visualization frontal view snapshot

4.4. Uncertainty Analysis

4.4.1 Uncertainty Analysis Approach: Root Sum Square (RSS) Method

The uncertainty in a measured value x is a measure of the extent that values of x are spread around the expectation value ⟨x⟩ (Castrup, 2004). The more spread out the distribution around ⟨x⟩, the larger the uncertainty (u_x). The deviations of x from ⟨x⟩ are just the measurement errors (ε_x), given by equation (4.1) as:

$$\varepsilon_x = x - \langle x \rangle \tag{4.1}$$

Hence, the uncertainty is related to the measurement errors (ε_x). If we take the uncertainty as the average value for ε_x. So,

$$u_x \sim average\ (x - \langle x \rangle) = (x - \langle x \rangle) \tag{4.2}$$

This quantity is always zero as shown by equation (4.3):

$$\langle x - \langle x \rangle \rangle = \langle x \rangle - \langle x \rangle \tag{4.3}$$

So, we need an unsigned quantity. One option is the square of the deviations as shown by equation (4.4):

$$u_x \sim average\ [(x - \langle x \rangle)^2] = \langle (x - \langle x \rangle)^2 \rangle \tag{4.4}$$

This quantity is the average or mean value of the error squared. Accordingly, it is called the mean square error. The only problem is that the mean square error is not in the same units as the measured values. For instance, if we are measuring volts, the mean square error is expressed in volts squared. Hence, comes the use of the square root of the mean square error. This quantity has the desired properties and is also expressed in the same units as the measured values. Hence, we can write :

$$u_x = \sqrt{(x - \langle x \rangle)^2} \tag{4.5}$$

By definition, we can notice that the square root of the mean square error is just the standard deviation. So, the uncertainty in the measurement of ⟨x⟩ is equal to the standard deviation of the distribution of measurements of ⟨x⟩. Substituting Equation (4.1) into Equation (4.5) gives:

$$u_x = \sqrt{\varepsilon_x{}^2} \tag{4.6}$$

If the error in x is composed of errors from two sources such as the measurement parameter bias (ε_{xb}) and the measurement process random (repeatability) error (ε_{xr}), we then have equation (4.7):

$$x = \langle x \rangle + \varepsilon_{xb} + \varepsilon_{xr} \tag{4.7}$$

where ε_{xb} is the error due to parameter bias and ε_{xr} is the random error. Given the earlier definition of measurement uncertainty we have:

$$u_x^2 = \left(\varepsilon_{x_b} + \varepsilon_{xr}\right)^2 \tag{4.8}$$

Or by expansion:

$$u_x^2 = \varepsilon_{xb}^2 + \varepsilon_{xr}^2 + 2\varepsilon_{xb}\varepsilon_{xr} \tag{4.9}$$

By substituting equation (4.6) into equation (4.9), we get:

$$U_x^2 = u_{xb}^2 + u_{xr}^2 + 2\langle \varepsilon_{xb}\varepsilon_{xr} \rangle \tag{4.10}$$

The additional term $\langle \varepsilon_{xb}\varepsilon_{xr} \rangle$ is called the covariance of ε_{xb} and ε_{xr}. For most measurements, the bias of the measuring parameter and the error due to random variations are completely independent of one another. If so, it can be shown that:

$$\langle \varepsilon_{xb}\varepsilon_{xr} \rangle = 0 \tag{4.11}$$

In this case, we have:

$$u_x = \sqrt{u_{xb}^2 + u_{xr}^2} \tag{4.12}$$

Equation (4.12) indicates that the total uncertainty in the measurement of x is the square root of the sum of the constituent uncertainties. This is called the Root Sum Square (RSS) of the constituent uncertainties. In general, we can make the following assertion: The total uncertainty in the sum of independent errors is an RSS combination of their uncertainties.

It is important to carry out a general uncertainty analysis of each instrument to determine the uncertainty of the results found from the conducted experiments. The various instruments used to conduct all experiments are categorized into three subsystems as shown in Table 4.5. These are: air supply system, the tracer gas injection, and the tracer gas sampling.

Table 4.5. Subsystems and associated uncertainty elements.

Instrument	Associated uncertainty element
Air supply system	Supply air temperature
	Supply air pressure
Tracer gas injection system	CO_2 purity
	He purity
	CO_2 mass flowrate controller
	He mass flowrate controller
Tracer gas sampling system	Tracer gas analyzers
	Data acquisition system (DAQ)

The uncertainties related to each of these subsystems (components) is calculated separately and combined to represent the overall uncertainty of the results for various studies. The detailed uncertainty analysis of each of the above-mentioned subsystems is carried out in the following sub-sections. The uncertainty analysis is shown in detail below for the tests

performed using the continuous injection source in the Boeing 767 and modified cabins since the majority of the tests were conducted in them. A similar uncertainty analysis was conducted using the coughing manikin and the results are plotted in Figure 4.20.

4.4.2 Supply Air Uncertainty

The air supply system provides the Boeing 767 and the modified cabin with 39643.6 L/min (1400 ft^3/min) of conditioned air. The flowrate, temperature, and pressure of the conditioned air is controlled by an Agilent DAQ using temperature sensors, pressure transducer, and flowmeter. The range and uncertainty of each instrument is in Table 4.6.

Table 4.6. Supply air instruments uncertainty and range.

Instrument	Use	Uncertainty	Range
Agilent 34970A DAQ	Data acquisition for the RTD wires	0.06°C (0.11°F)	49Ω – 2.1kΩ
NI FieldPoint AI-110	16-Bit Analog input modules	0.07% of reading +0.007% of range	0 – 5 V
PCI FE-1500	Insertion type airflow sensing element	2%	100-10000 ft/min
Omega PX 653	Low pressure laboratory transducer	±0.25% full scale	±1” Water Column
		0.05% full scale Repeatability	1– 5 Vdc
Omega 3-wire RTD	Thermocouple wires	±(0.3 + 0.005*T) °C	-50 – 250 °C, Class B

In order to calculate the uncertainty for the flowrate of the supply air, the uncertainty of the two variables related to the air flowrate, temperature, and pressure, must be calculated. The uncertainty of the supply air temperature is calculated using RSS method as shown in equation (4.13) below where 'U' denotes uncertainty. Since the temperature measurements are collected using only the Omega 3-wire RTD wires and the Agilent 34970A DAQ, its uncertainty depends only on them.

$$\begin{aligned} U_T &= \sqrt{U_{Omega\ 3-wire\ RTD}{}^2 + U_{Agilent\ 34970A\ DAQ}{}^2} \\ &= \sqrt{(0.3 + (0.005 * 15.6))^2\ °C\ + 0.06^2\ °C} \\ &= 0.38°C = 0.38\ K = 0.69°F \end{aligned} \tag{4.13}$$

The temperature uncertainty is:

$$U_{Temp} = \frac{U_T}{T_{Supply}} = \frac{0.38\ K}{288.8\ K} = 0.13 \tag{4.14}$$

Likewise, the uncertainty for the supply air pressure was calculated based on the instruments involved in the pressure measurements. For the uncertainty in the pressure measurement, the uncertainties of the PCI FE-1500 flowmeter, the Omega PX 653 differential pressure transducer, and the NI FieldPoint AI-110 modules were considered. Equations (4.15)-(4.21) show the uncertainty value calculation for the Omega PX 653 differential pressure transducer. Equation (4.22) shows the uncertainty equation for the PCI FE-1500 flowmeter. Finally, equations (4.23)-(4.25) show the uncertainty value calculation for the NI FieldPoint AI-110 modules. The overall pressure measurement uncertainty was then combined and calculated as shown in equation (4.26).

For the Omega PX 653 differential pressure transducer:

$$U_{\text{Omega PX 653}} = 0.05\% \text{ full scale} \tag{4.15}$$

$$U_{\text{Omega PX 653}} = 0.05\% * \frac{\text{full range}}{\text{actual velocity pressure}} \tag{4.16}$$

$$U_{\text{Omega PX 653}} = 0.05\% * \frac{1\ inch\ of\ water}{0.0622 \text{ inch of water}} \tag{4.17}$$

$$U_{\text{Omega PX 653}} = 0.05\% * 16.077 = 0.80\% \tag{4.18}$$

The actual velocity pressure in inches of water was obtained as shown below. The air velocity in the duct is:

$$V_{supply\ air} = \frac{1400 \text{ CFM}}{\left(\pi * \frac{1.336^2}{4}\right)} = 999 \frac{ft}{min} \tag{4.19}$$

To get the velocity pressure in inches of water we use the following equation:

$$Air\ velocity\ (foot\ per\ minuite) = 4005 * \sqrt{Velocity\ pressure\ (inches\ of\ water)} \tag{4.20}$$

Plugging the air velocity and solving for the velocity pressure:

$$\left(\frac{999}{4005}\right)^2 = Velocity\ pressure\ (inches\ of\ water) \tag{4.21}$$

So, 999 ft/min produces 0.0622-inch water column.

For the PCI FE-1500 flowmeter:

$$U_{\text{PCI FE}-1500} = 2\%\ of\ reading \tag{4.22}$$

For the NI FieldPoint AI-110 modules:

$$U_{\text{NI FieldPoint AI}-110} = 0.07\% \text{ reading} + 0.007\% \text{ full scale} \tag{4.23}$$

$$U_{\text{NI FieldPoint AI}-110} = 0.07\% + 0.007\ \% * \frac{\text{full range}}{\text{actual voltage}} \tag{4.24}$$

As calculated earlier, the velocity of the supply air is 999 ft/min or 5.075 m/s. This corresponds to a generated differential pressure translated to an excitation voltage reading of around 3.5 V. Hence,

$$U_{\text{NI FieldPoint AI}-110} = 0.07\% + 0.007\% * \frac{5 \text{ volts}}{3.5 \text{ volts}} = 0.08\ \% \tag{4.25}$$

The overall pressure measurement uncertainty is then:

$$U_{Press} = \sqrt{{U_{PCI\ FE-1500}}^2 + {U_{Omega\ PX\ 653}}^2 + {U_{NI\ FieldPoint\ AI-110}}^2} = \sqrt{2^2 + 0.80^2 + 0.08^2} = 2.16\ \% \tag{4.26}$$

The overall supply air uncertainty can now be calculated using the same RSS method. Bur first, we need to obtain a relation between the uncertainty of the supply air flowrate and both the pressure and temperature uncertainties in order to be able to calculate the relative uncertainty of each property. First, the flow rate is related to the velocity as shown in equation (4.27):

$$Q = \mathrm{v}.A = \mathrm{v}(\pi.r^2) \tag{4.27}$$

Where: v is the air velocity, A is the duct cross sectional area, and r is the duct radius. From Bernoulli's Equation, the pressure is related to the square of the velocity as shown in equation (4.28).

$$\mathrm{v} = (2\frac{\Delta P}{\rho})^{\frac{1}{2}} \tag{4.28}$$

Using the general uncertainty analysis procedure, the uncertainty of the velocity in the Bernoulli`s equation can be written as:

$$\left(\frac{\mathrm{U_v}}{\mathrm{v}}\right)^2 = \frac{1}{4}\left(\frac{\mathrm{U}_{\Delta P}}{\Delta P}\right)^2 + \frac{1}{4}\left(\frac{\mathrm{U}_{\rho}}{\rho}\right)^2 \tag{4.29}$$

Since the pressure differential term (ΔP) is measured, and the pressure measurement uncertainty was calculated earlier, we need to obtain the uncertainty for the density term (U_ρ). The ideal gas equation can be written as:

$$\rho = \frac{P}{RT} \tag{4.30}$$

The uncertainty in the density in the ideal gas law can be written as:

$$\left(\frac{\mathrm{U}_\rho}{\rho}\right)^2 = \left(\frac{\mathrm{U}_P}{P}\right)^2 + \left(\frac{\mathrm{U}_T}{T}\right)^2 \tag{4.31}$$

By plugging equation (4.31) in equation (4.29), we obtain:

$$\left(\frac{\mathrm{U_v}}{\mathrm{v}}\right)^2 = \frac{1}{4}\left(\frac{\mathrm{U}_{\Delta P}}{\Delta P}\right)^2 + \frac{1}{4}\left(\left(\frac{\mathrm{U}_P}{P}\right)^2 + \left(\frac{\mathrm{U}_T}{T}\right)^2\right) \tag{4.32}$$

Since the same pressure transducer was used, $\mathrm{U}_{\Delta P} = \mathrm{U}_P$. So,

$$\left(\frac{\mathrm{U_v}}{\mathrm{v}}\right)^2 = \frac{1}{4}\left(\left(\frac{\mathrm{U}_{\Delta P}}{\Delta P}\right)^2 + \left(\frac{\mathrm{U}_P}{P}\right)^2\right) + \frac{1}{4}\left(\frac{\mathrm{U}_T}{T}\right)^2 \tag{4.33}$$

Or by simplifying:

$$\left(\frac{\mathrm{U_v}}{\mathrm{v}}\right)^2 = \frac{1}{4}\left(2\left(\frac{\mathrm{U}_P}{P}\right)^2\right) + \frac{1}{4}\left(\frac{\mathrm{U}_T}{T}\right)^2 \tag{4.34}$$

Based on equation (4.27), the flowrate uncertainty is:

$$\left(\frac{\mathrm{U_Q}}{\mathrm{Q}}\right)^2 = \frac{1}{4}\left(2\left(\frac{\mathrm{U}_P}{P}\right)^2\right) + \frac{1}{4}\left(\frac{\mathrm{U}_T}{T}\right)^2 + 4\left(\frac{\mathrm{U}_r}{r}\right)^2 \tag{4.35}$$

Assuming a measurement uncertainty of 0.05 inch for an approximately 10 inch circular duct, the relative uncertainty for the duct radius is considered negligible as show in equation 4.36.

$$\left(\frac{\mathrm{U}_r}{r}\right)^2 = \left(\frac{0.05}{10}\right)^2 = 2.5x10^{-5} \tag{4.36}$$

Hence, equation (4.35) becomes:

$$\frac{\mathrm{U_Q}}{\mathrm{Q}} = \left[\frac{1}{2}\left(\frac{\mathrm{U}_P}{P}\right)^2 + \frac{1}{4}\left(\frac{\mathrm{U}_T}{T}\right)^2\right]^{\frac{1}{2}} \tag{4.37}$$

The temperature and the pressure measurements uncertainty can then be plugged from equation (4.14) and (4.26); respectively, into equation (4.37) to calculate the supply air uncertainty as shown in equation (4.38).

$$U_{Supply\ air} = \frac{U_Q}{Q} = \sqrt{\frac{1}{4}\left(U_{Temp}\right)^2 + \frac{1}{2}(U_{Press})^2}$$
$$= \sqrt{\frac{1}{4}(0.13)^2 + \frac{1}{2}(2.16)^2} = 1.5\ \% \tag{4.38}$$

It should be noted that since the uncertainties in the two pressure measurements are correlated, this supply air uncertainty is considered a conservative (overestimated) uncertainty.

4.4.3 Tracer Gas Injection Uncertainty

The tracer gas injection subsystem involves the purity of the gases used for calibrating the CO_2 gas analyzers and the purity of the CO_2 and He used in the tracer gas, along with the mass flow controllers used to control the flowrate of the He and CO_2 gases used in the tracer gas. The purity and uncertainty of each gas is given in Table 4.7 below.

Table 4.7. Purity and uncertainty of each tracer gas components.

Gas	Uncertainty/Purity
CO_2	0.5% / 99.5% pure
He	0.003% / 99.997% pure
500 ppm CO_2 – Air Mixture	2%
1000 ppm CO_2 – Air mixture	1%
2000 ppm CO_2 – Air Mixture	1%

The calibration gas uncertainty was taken as 2% since it is highest value among the three calibration gases uncertainty. This is considered as the worst case or the conservative value for the calibration gas uncertainty. In addition to the calibration and tracer gas uncertainties, the tracer gas injection system also includes the CO_2 and He mass flow controllers and the PR 4000 power supply that controls them. The PR 4000 has 16-bit uncertainty and is considered to be negligible for this study. The uncertainties of the mass flow controllers are given in Table 4.8.

Table 4.8. Mass flow controllers' uncertainty and rated flowrate.

Instrument	Uncertainty	Rated flow
CO_2 mass flow controller	1.0% full scale (accuracy)	100 SLM
	0.2% of full scale (repeatability)	
	0.1% full scale (resolution)	
	10 to 50 °C (operation)	
He mass flow controller	1.0% full scale (accuracy)	10,000 SCCM (10 LMP)
	0.2% full scale (repeatability)	
	0.1% full scale (resolution)	
	0 to 50 °C (operation)	

The gas injection flowrates used in this study are 5 L/min (0.176 ft^3/min) for CO_2 and 3.07 L/min (0.108 ft^3/min) for He. The CO_2 and the He injection uncertainty were calculated as shown in equation (4.39) and equation (4.40), respectively.

$$U_{CO_2\ tracer\ gas} = \sqrt{{U_{CO_2\ rep}}^2 + {U_{CO_2\ purity}}^2} = \sqrt{\left(\frac{0.2 * 100\ L/min}{5\ L/min}\right)^2 + (1)^2} = 4\% \quad (4.39)$$

$$U_{He\ tracer\ gas} = \sqrt{{U_{He\ rep}}^2 + {U_{He\ purity}}^2} = \sqrt{\left(\frac{0.2 * 10\ L/min}{3.07\ L/min}\right)^2 + (0.01)^2} = 0.65\% \quad (4.40)$$

4.4.3 Tracer Gas Sampling Uncertainty

Four different types of CO_2 gas analyzers were used throughout the cabin during testing. These measure the concentration of the CO_2 in the air at each location and output the concentration in volts to an Agilent 34970 DAQ unit. One of the four analyzers is connected to the sampling tree to measure the concentration of the tracer gas at a radial distance from

the injection source as shown in Figure 4.15. The range and uncertainty of each component in the sampling system are given in Table 4.9. Since the secondary DAQ, shown in Figure 4.19, is only used as a moderator between the LabVIEW software and the solenoid block, it is not involved in sampling the tracer gas. Similarly, the solenoid valves block is only used to control opening and closing the sampling tree valves and hence is not involved in tracer gas sampling.

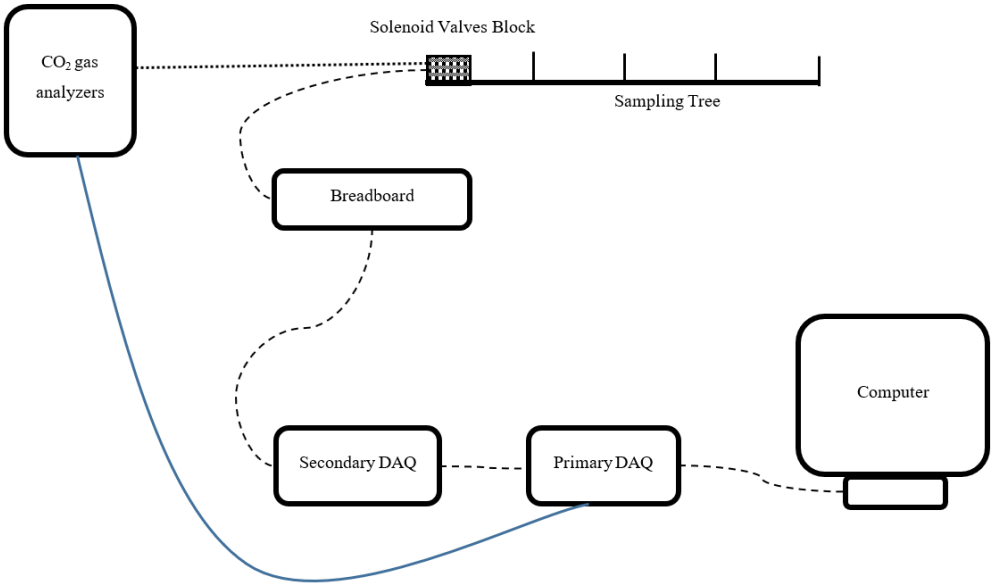

Figure 4.19. Tracer gas sampling system.

Table 4.9. CO_2 sampling system uncertainty and range.

Model/Instrument	Uncertainty	Range
Edinburgh gas card NG	2% of range (accuracy)	0 – 3000 ppm
	0.3 at zero, 1.5% at span (repeatability)	
PP Systems WMA-4	<1% at span (repeatability)	0 – 2000 ppm
	20 ppm (accuracy)	
PP Systems WMA-5	<1% at span (repeatability)	0 – 3000 ppm
	30 ppm (accuracy)	
Agilent 34970A DAQ	0.0035% of reading + 0.0005% of range	10V

The samples statistics for the gas analyzers of the same test are listed in Table 4.10 below. Using the standard deviation of the mean as a measure of repeatability, the repeatability of each gas analyzer was calculated. Using another 3 tests which were done with the exact conditions back to back, Table 4.10 below shows the repeatability analysis. A total of 4861 data points during the gas injection period were used in obtaining the results of Table 4.10.

Table 4.10. Repeatability analysis results for the four main CO_2 gas analyzers.

	Gas analyzer A-1	**Gas analyzer A-2**	**Gas analyzer A-3**	**Gas analyzer A-4**
Average voltage (volt)	1.25	2.30	0.45	0.65
Standard deviation (volt)	0.03	0.93	0.05	0.01
Mean of standard deviation (volt)	0.0005	0.0133	0.0007	0.0002
Average reading (ppm)	483	1362	550	451

Table 4.11 shows the calibration equations of the four CO_2 gas analyzers. It can be shown from Table 4.11 that the linearity uncertainty is very close to zero that can be neglected from the analyzer uncertainty equation (equation (4.42)).

Table 4.11. CO_2 gas analyzers calibration results.

CO_2 gas analyzer	**Range calibration equation**	**Actual calibration equation**	**R-squared value**
A-1	y = 400x	y = 393.02x + 29.678	$R^2 = 1$
A-2	y = 600x	y = 601.97x - 20.532	$R^2 = 1$
A-3	y= 1200x	y = 1216x + 2.7253	$R^2 = 1$
A-4	y = 666.67x	y = 603.06x + 58.756	$R^2 = 1$

The uncertainty of the data acquisition system depends on the reading that is being collected. To calculate U_{DAQ}, equation (4.41) was used, and the results are tabulated in Table 4.12. To calculate the overall analyzers uncertainty, equation (4.42) was used, and the results were also tabulated in Table 4.12.

$$U_{DAQ} = 0.0035\% \, of \, reading + 0.0005\% \, of \, range \quad (4.41)$$

$$U_{analyzer} = \sqrt{U_{CO_2 \, Repeatability}{}^2 + U_{Calibration}{}^2 + U_{Linearity}{}^2 + U_{DAQ}{}^2} \quad (4.42)$$

Table 4.12. CO_2 gas analyzers uncertainty results.

CO_2 gas analyzer	**$U_{Repeatability}$ (%)**	**$U_{calibration}$ (%)**	**U_{DAQ} (%)**	**$U_{Analyzer}$ (%)**
A-1	0.05	2	0.02	2.45
A-2	1.33		0.05	2.79
A-3	0.07		0.02	2.45
A-4	0.02		0.02	2.45

4.4.4 Overall Uncertainty

After the uncertainties of all the subsystems were calculated, the uncertainties were combined to calculate the overall uncertainty of the results found. The overall uncertainty was calculated using the general equation (4.43), where 'U' stands for uncertainty, 'X' stands for a variable and 'r' stands for the desired result (Hugh W. Coleman, W. Glenn Steele, Jr., 1999).

$$U_r^2 = \left(\frac{\partial r}{\partial X_1} * U_{X_1}\right)^2 + \left(\frac{\partial r}{\partial X_2} * U_{X_2}\right)^2 + \left(\frac{\partial r}{\partial X_j} * U_{X_j}\right)^2 \quad (4.43)$$

The partial differentials of the equation above are separately solved using equations (4.45)-(4.49) below, where N is the normalized concentration calculated using equation (4.44):

$$N = \frac{C_{sample} - C_{supply\ air}}{\left(\frac{\dot{V}_{CO_2}}{\dot{V}_{supply\ air}}\right)} \tag{4.44}$$

$$U_N^2 = \left(\frac{\partial N}{\partial C_{sample}} * U_{Sample}\right)^2 + \left(\frac{\partial N}{\partial C_{supply\ air}} * U_{supply\ air}\right)^2 + \left(\frac{\partial N}{\partial \dot{V}_{CO_2}} * U_{inject,CO_2}\right)^2 + \left(\frac{\partial N}{\partial \dot{V}_{supply\ air}} * U_{Supply\ air}\right)^2 \tag{4.45}$$

$$\frac{\partial N}{\partial C_{sample}} = \frac{\dot{V}_{supply\ air}}{\dot{V}_{CO_2}} \tag{4.46}$$

$$\frac{\partial N}{\partial C_{supply\ air}} = -\frac{\dot{V}_{Supply\ air}}{\dot{V}_{CO_2}} \tag{4.47}$$

$$\frac{\partial N}{\partial \dot{V}_{CO_2}} = \frac{\dot{V}_{supply\ air}}{\dot{V}_{CO_2}^{\ 2}} * \left(C_{supply\ air} - C_{sample}\right) \tag{4.48}$$

$$\frac{\partial N}{\partial \dot{V}_{supply\ air}} = \frac{C_{sample} - C_{supply\ air}}{\dot{V}_{CO_2}} \tag{4.49}$$

Equations (4.46)-(4.49) were then plugged back in equation (4.45) and divided by N^2 to obtain equation (4.50). The uncertainties related to supply air and injection of CO_2 are already in terms of percentages i.e., the air supply rate and injection rate have already been utilized. Thus, the two flowrates should be removed from equation (4.50). Doing this gives the reduced equation (4.51).

$$\left(\frac{U_N}{N}\right)^2 = \left(\frac{U_{Sample}}{C_{sample-}\ C_{supply\ air}}\right)^2 + \left(\frac{U_{supply\ air}}{C_{sample-}\ C_{supply\ air}}\right)^2 + \left(\frac{U_{inject,CO_2}}{\dot{V}_{CO_2}}\right)^2 + \left(\frac{U_{\ Supply\ air}}{\dot{V}_{Supply\ air}}\right)^2 \quad (4.50)$$

$$\left(\frac{U_N}{N}\right)^2 = \left(\frac{U_{Sample}}{C_{sample-}\ C_{supply\ air}}\right)^2 + \left(\frac{U_{supply\ air}}{C_{sample-}\ C_{supply\ air}}\right)^2 + \left(U_{inject,CO_2}\right)^2 + \left(U_{supply\ air}\right)^2 \quad (4.51)$$

By plugging the measured and calculated data into equation (4.51) and solving for $U_N\ /N$, the uncertainty result was plotted in Figure 4.20 for both the tracer gas injection source and the coughing manikin source. Figure 4.20 can be used in order to obtain the uncertainty percentage for any normalized tracer gas concentration for measurements collected in different directions around the source. Figure 4.20 shows that the uncertainty in the tracer gas measurement increses with the decrease of the normalized gas ceoncentration, or as the distance increases further away from the source. This is due to the tracer gas concentration

at the sampling location C_{sample} getting closer to the concentration of the tracer gas in the cabin supply air $C_{supply\ air}$ in equation 4.51.

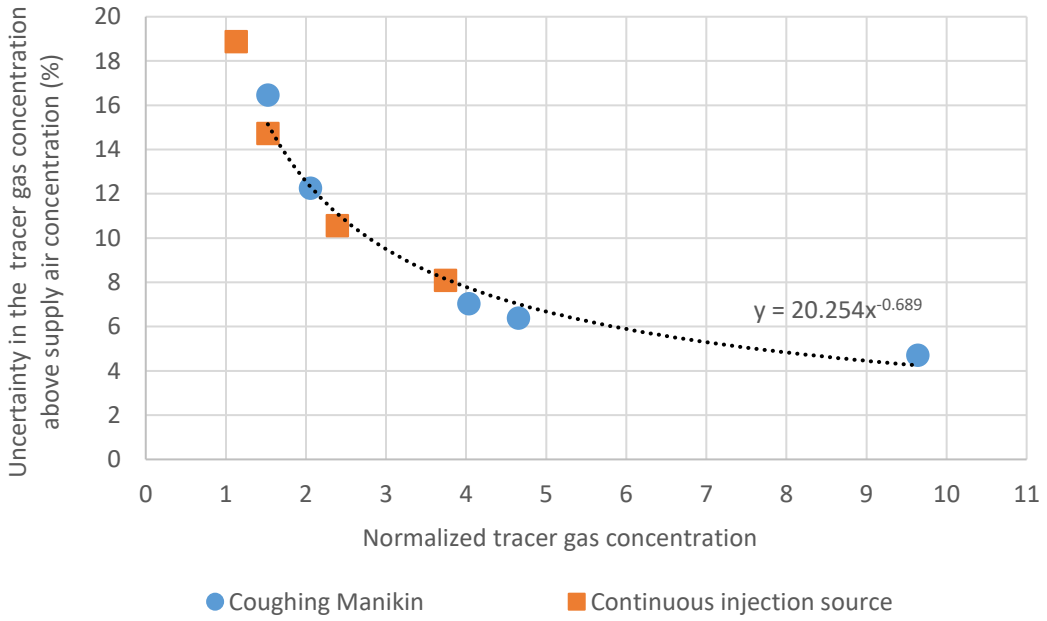

Figure 4.20. Uncertainty percentage of the tracer gas concentration increase above supply air concentration versus the normalized tracer gas concentration for both the coughing manikin and the continuous injection sources.

Chapter 5 - Analysis and Discussions

The diagram in Figure 5.1 shows a breakdown of the tests which were performed in this study. The following sections provide an analysis and discussion for each category. Since the effectiveness of the ISOPass in containing the source tracer gas was intensively studied using a continuous injection source in the study conducted by (Darrah, 2018), and using a coughing manikin demonstrated within this study, the utilization of the ISOPass in the modified cabin was not required. Furthermore, since the results of the coughing tests performed in the Boeing 767 cabin showed that the effect of the cough is mainly in the front longitudinal direction, the utilization of the coughing manikin was limited to certain sampling tree orientations in the Boeing 767 mockup cabin.

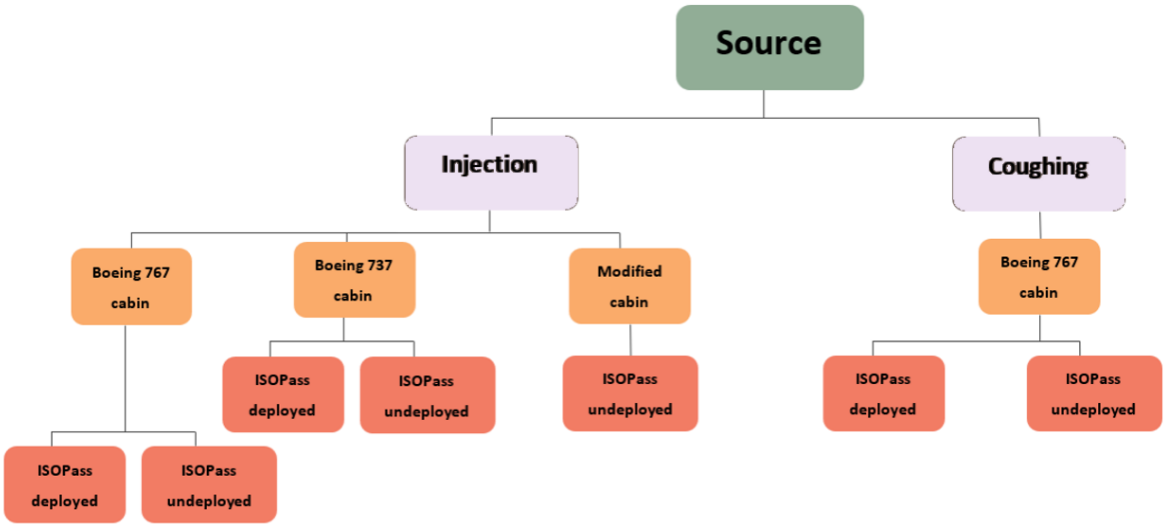

Figure 5.1. Breakdown of all the tests performed within this study.

The number of tests in each category is shown in Table 5.1 below:

Table 5.1. Number of tests for each test category listed in Figure 5.1.

	Source Type			
	Continuous injection		**Coughing manikin**	
	ISOPass Deployed	**ISOPass Undeployed**	**ISOPass Deployed**	**ISOPass Undeployed**
Boeing 767 cabin	3	40	36	57
	(Appendix D)	(Appendix C)	(Appendix I)	(Appendix H)
Boeing 737 cabin	4	3	N/A	
	(Appendix G)	(Appendix F)		
Modified cabin	N/A	40		
		(Appendix E)		

Each test has 3 individual consecutive figures included in appendices C-I. For example, Test 3 (B-I) in appendix C has Figures C.5-C.7. In the first figure (C.5), the source location and the sampling tree orientation are shown in the cabin layout. In the second figure (C.6), the instantaneous tracer gas concentration at each sampling location is plotted versus the time. In the third figure (C.7), the average recorded tracer gas concentration at the gas injection period is plotted for each sampling location. This figure arrangement is used for all tests.

5.1 ISOPass Undeployed Tests Analysis

5.1.1 Continuous Tracer Gas Injection Tests

Continuous tracer gas injection tests were conducted in all three cabins. To provide a reasonable comparison, the source locations and the sampling tree orientations were matched between the Boeing 767 cabin mockup and the modified cabin tests without using the ISOPass or in the "ISOPass undeployed" category listed in Table 5.1.

5.1.1.1 Boeing 767 Cabin Mockup

In the Boeing 767 cabin mockup, a total of 40 test combinations were conducted by varying the tracer gas injection source location and/or the sampling tree orientation without the ISOPass present as shown in Appendix C. Figures C.5-127 show the source location and the sampling tree orientation for each test. A comparison is constructed in Figures C.128-131 in Appendix C between all sampling tree directions for a fixed source seat location. Another comparison is made in Figures C.132-138 in Appendix C between all source locations for a fixed sampling tree orientation.

The results showed that the CO_2 tracer gas concentration is not necessarily the same at the same radial distance from the source but varies for different orientations around the tracer gas injection location. For example, Figure C.13 and Figure C.31 show the CO_2 concentration plotted at each radial location for tests 4 (B-I) and 7 (B-I), respectively. Figure C.13 shows that the average CO_2 concentration at 0.84 m from the tracer gas injection location is about 550 ppm. At the same distance but on the opposites side of the tracer gas injection location, Figure C.31 shows that the average concentration is about 1095 ppm. This unequal concentration of the sampled tracer gas is due to the non-uniform rotational airflow

inside the aircraft cabin as was noticed in several previous studies. This phenomenon, if not considered, could lead to underestimation of the contaminating aerosols concentration at the seats downstream of the infectious passenger.

Figure C.94 shows the CO_2 concentration plotted at each radial distance from the source for test 37 (B-I). In this test, the tracer gas injection source was positioned at the first row of the cabin on seat D1 close to the front wall of the mockup. In actual aircrafts, the separation wall is placed between different cabin classes and may be formed of a combination of static wall and curtains. Figure C.124 shows the CO_2 concentration plotted at each radial distance for test 54 (B-I). In this test, the tracer gas injection source was positioned at the last row of the cabin on seat D11 in front of the rear wall of the mockup facing the rest of the seats of the cabin. Figure C.94 shows that the concentration of the tracer gas on seat E1, to the right of the tracer gas injection source, is higher than the concentration on the tracer gas injection source seat D1. This is due to the nature of the airflow direction in the mockup that tends to take a clockwise direction. This airflow circulation is inherent to the cabin ventilation system and is not an anomaly of the mockup (Keshavarz et al., 2015). This phenomenon was also captured by the smoke visualization performed on the same seat. The snapshots in Figures K.1. 35-40 in Appendix K.1 clearly show the smoke directed from the source seat D1 to seat E1 which can explain the increased tracer gas concentration on seat E1. This phenomenon was not only captured in seat D1. Figures C.128-130,134, and 136-138 show that, in other tests, the sampling tree port at 0.84 m away from the tracer gas injection location recorded a tracer gas concentration higher than the tracer gas injection source location. Specifically, tests 16 (B-I), 23-25 (B-I), 28-29 (B-I), and 37-38 (B-I). With the exception of tests 37-38 (B-I), the sampling tree port at 0.84 was located behind the tracer

gas injection location towards the back of the cabin. The clockwise airflow direction in the cabin helps push the tracer gas towards the backside of the cabin which is captured by the sampling tree port closest to the tracer gas injection location at 0.84 m. This phenomenon was captured in each of these test pairs indicating that it was a repeatable behavior. Similar phenomenon was not noticed when the tracer gas injection source was placed at seat D11 at the rear of the cabin in test 54 (B-I) as shown in Figure C.124 which demonstrates the complexity and unpredictability of air circulation patterns in aircraft cabins.

Figures C.139 and C.140 show the combined results of the 40 tests in Appendix C. The difference between Figure C.139 and C.140 is that in Figure C.140 the sampling distances from the source are in the absolute value of the distance. Both figures show three important pieces of information. First, the variation in the tracer gas concentration between different tests at the same sampling distance from the source. Second, the variation in the tracer gas concentration at different distances from the source located at point 0. Third, the concentration variation of the sampled tracer gas at the same distance but at different orientations around the source. The variation in the tracer gas concentration decreases as the distance increases away from the injection source. If the cabin was imagined to be very long, the CO_2 concentration in the cabin air at the furthest sampling point will be equal to the concentration in the supply air. Furthermore, the tracer gas concentration between all tests decreases as the distances increases away from the tracer gas injection location due to the dilution caused by the ventilation air. The variation in the tracer gas concentration at the same sampling distance from the source varies from one location to another but, it tends to decrease with distance from the source. This is due to the reduction in the concentration of the injected

tracer gas in the cabin air as distance increases away from the source caused by the dispersion and mixing with the cabin supply air.

Figure 5.2 shows the percentage increase in tracer gas concentration at each sampling location over the supply air concentration for all the tests performed using the continuous tracer gas injection source in the Boeing 767 cabin mockup. The percentage is calculated using equation (4.1):

$$\begin{gathered} Increase\ in\ tracer\ gas\ concentration\ at\ the\ sampling\ location \\ over\ the\ supply\ air\ concentration\ (\%) = \\ \frac{(Tracer\ gas\ conc.\ at\ the\ sampling\ location - Tracer\ gas\ conc.\ in\ the\ supply\ air) * 100}{Tracer\ gas\ concentration\ in\ the\ supply\ air} \end{gathered} \tag{4.1}$$

The figure shows the average percentage increase for all source locations and sampling tree orientations. As depicted in the figure, the difference between tracer gas concentration in the sampling location and in the supply air, gets smaller with distance from the injection source due to the dilution created by the cabin supply air. The average increase in tracer gas concentration decreased by almost a half in each of the 3 consecutive sampling locations from the source at 0 to 2.52 m (0 to 8.27 ft) from the source. It then decreased further by about 30% at the furthest sampling location at 3.35 m (11 ft) from the source.

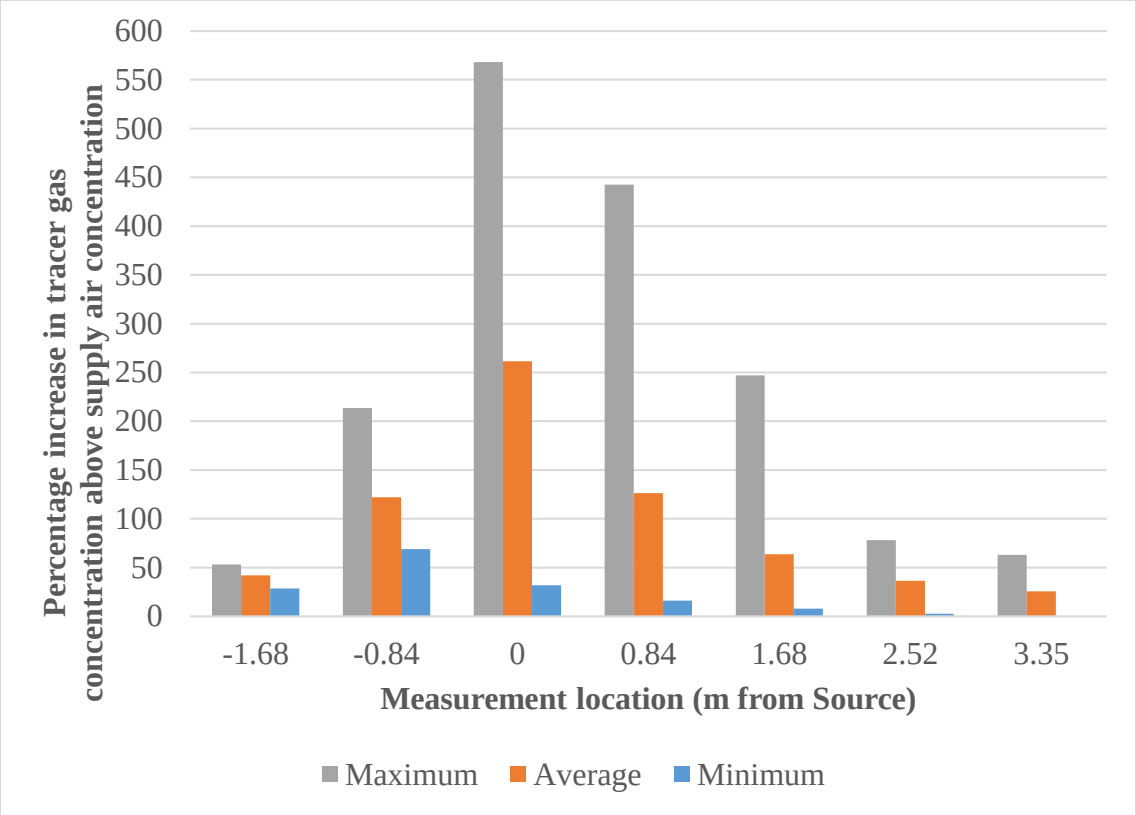

Figure 5.2. Percentage increase in tracer gas concentration in different sampling locations above supply air concentration in tests perofrmed using continuous injection source in the Boeing 767 cabin mockup.

Since the tracer gas concentration was measured by different gas analyzers in different locations, as highlighted in the uncertainty section, the percentage differences are not exact. This is because the uncertainty in the readings of each analyzer is different. Also, because different analyzers are not of the same model or have the same calibration, their readings are not exactly the same even if placed at the same location. This also impacts the percentage difference at the further locations from the source by not showing them as zero because the tracer gas concentration at the sampling location and the supply air were not measured by the same gas analyzer.

5.1.1.2 Modified Cabin

In the modified cabin mockup, a total of 40 test combinations were conducted by varying the tracer gas injection location and/or the sampling tree orientation with the ISOPass undeployed as shown in Appendix E. Figures E.5-124 show the source location and the sampling tree orientation for each test. A comparison is constructed in Figures E.125-128 in Appendix E between all sampling tree directions for a fixed source location. The figures show that the concentration of the tracer gas is not necessarily the same for the same tracer gas source location in different directions around the source. Figures E.129-135 show a comparison between all tracer gas continuous injection source locations for a fixed sampling tree orientation. The figures show that the tracer gas concentration could be different along the same sampling direction but for a different source location inside the cabin.

Compared to the Boeing 767 supply air configuration, there was no noticeable increase in tracer gas concentration over the source concentration at any sampling location. Nonetheless, due to the change of airflow pattern from the central linear diffusers in the Boeing 767 cabin to the modified cabin, there were sampling locations which recorded a higher tracer gas concentration than the locations closer to the source. This can also be affected by the location of the air diffusers located on the PVC duct relative to the tracer gas sampling probe. It was mainly observed in the tests performed in the middle of the cabin with the source located on seat D6 as can be seen in Tests 5-6 (A-I), Test 9-10 (A-I) and 31-32 (A-I). A similar phenomenon was recorded when the source was located near the cabin walls on seat G6. Specifically, when the sampling tree was placed in the longitudinal back direction as seen in Tests 23-24 (A-I).

Figures E.136 and E.137 show a summary of the tracer gas concentrations of the 40 tests performed in the modified cabin. The difference between Figure E.136 and E.137 is that in Figure C.137 the sampling distances from the source are taken in absolute. The figures show three important pieces of information. First, the variation in the tracer gas concentration between different tests at the same measurement location. Second, the variation in the tracer gas concentration at different sampling distances from the source located at point 0. Third, the concentration variation of the sampled tracer gas at the same distance but at different orientations around the source. With the exception of some points highlighted in the previous paragraph, the variation in the tracer gas concentration decreases as the distance increases away from the injection source. If the cabin was imagined to be very long, the CO_2 concentration in the cabin air at the furthest sampling point will be equal to the concentration in the supply air. Furthermore, the tracer gas concentration between all tests decreases as the distances increases away from the tracer gas injection location due to the dilution by ventilation air.

Figure 5.3 shows the percentage increase in tracer gas concentration at each sampling location over the supply air concentration for all the tests performed using the continuous tracer gas injection source in the modified cabin. The figure shows the average percentage increase for all source locations and sampling tree orientations. By looking at the average percentage increase in the tracer gas concentration over the supply air concentration, the difference gets smaller away from the injection source due to the dilution created by the cabin supply air. The reason behind some of the high percentages between the sampling locations, especially at location behind the source, is the small number of sampled tracer gas data that included those specific distances from the source. On the other hand, the distances covered

in most of the tests, such as at different sampling tree ports, got averaged along a high number of sampled data points with different high and low values causing the percentage difference to be somehow lower as compared to distances with just few data points recorded.

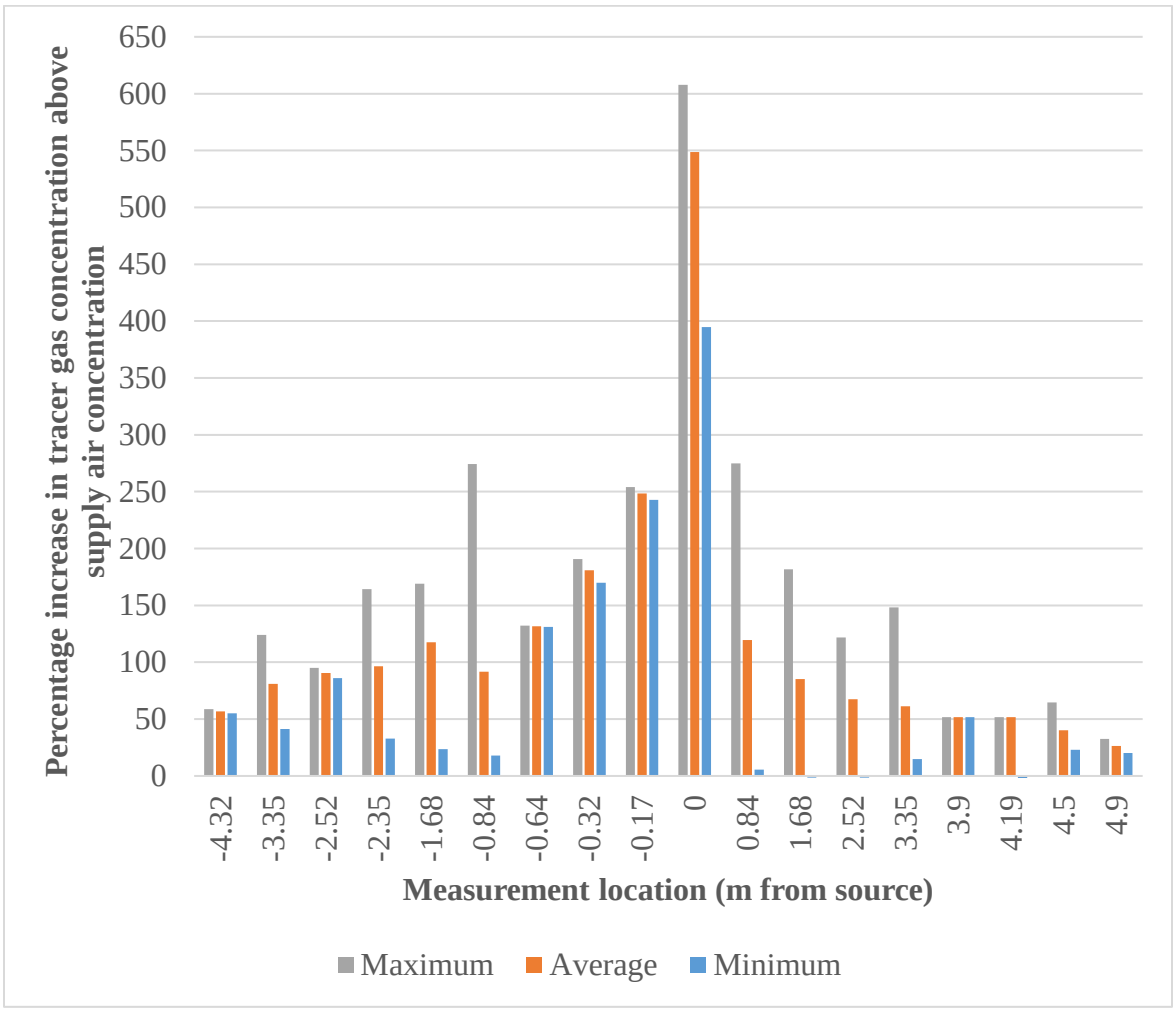

Figure 5.3. Percentage increase in tracer gas concentration in different sampling locations above supply air concentration in tests perofrmed using continuous injection source in the modified cabin.

The average increase in tracer gas concentration in the source seat was more than 2x the one in the Boeing 767 mockup cabin. Compared to 262% increase in tracer gas concentration in the source seat in the Boeing 767 mockup cabin, the increase was about 549% in the modified cabin. Table 5.2 shows a comparison for the rest of the shared sampling locations between the Boeing 767 mockup cabin and the modified cabin. Although both cabins had different tracer gas concentration reduction trends, the overall reduction in the tracer gas concentration at 3.35 m (11 ft) from the source is not very much different. At 3.35 m from the source, the tracer gas concentration was reduced by an average of about 89% and 90% from the source concentration for the Boeing 767 cabin mockup and the modified cabin, respectively.

Table 5.2. Average percentage increase in tracer gas concentration over supply air concentration for the Boeing 767 cabin mockup and the modified cabin.

Sampling location (m away from source)	**Average percentage increase in tracer gas concentration over supply air concentration (%)**	
	Boeing 767 mockup cabin	**Modified cabin**
-1.68	42	118
-0.84	122	92
0	262	549
0.84	126	120
1.68	64	85
2.52	37	68
3.35	26	61

Figure O.3 in Appendix O shows a comparison of the tracer gas concentration at each sampling location for all the tests performed in the Boeing 767 cabin mockup and the modified cabin using the continuous tracer gas injection source. As noted earlier in Table 5.2, the tracer gas concertation average for the tests performed in the modified cabin is always higher except at the sampling locations located closest to the source at +/- 0.84 m (2.75 ft) from the source. Both Table 5.2 and Figure O.3 show that the tracer gas concentrations remain higher at further distances from the source in the modified cabin despite using the same tracer gas flowrate and concentration. For example, at 3.35 m (11 ft) from the source, the average tracer gas concentration for all tests in the modified cabin was 61% above the supply air concentration during the gas injection period. On the other hand, in the Boeing 767 cabin mockup the percentage increase at the same location was 26% above the supply air concentration. Since the modified cabin is the same Boeing 767 cabin mockup with the only change in the cabin supply air configuration, this change in tracer gas concentration could be due to the change in the airflow pattern inside the cabin. The central linear diffusers in the Boeing 767 cabin mockup help dispersing the tracer gas in the cabin and induce mixing with the cabin supply air which dilutes its concentration.

5.1.1.3 Boeing 737 Cabin Section

Three identical continuous injection tracer gas tests were performed by (Darrah, 2018) in the Boeing 737 cabin section with the ISOPass undeployed. The tracer gas concentrations were collected from seats A4, D4, and E1 with the source being on seat B4.The recorded tracer gas concentrations was shown to decrease gradually away from the source. As expected, the seat closest to the source, seat A4, had the largest increase in tracer gas concentration by about 359% followed by seat D4 (~40%), and seat E1 (~28%).

5.1.2 Coughing Manikin Tests

5.1.2.1 Boeing 767 Cabin Mockup

Appendix H shows the results of 57 tests performed using the coughing manikin with the ISOPass undeployed in the Boeing 767 cabin mockup. Figures H.6-176 show the coughing manikin location and sampling tree orientation for each test. A comparison is constructed in Figures H.177-181 in Appendix H between all sampling tree orientations for a fixed coughing manikin location. Another comparison is made in Figures H.182-188 in Appendix H between all coughing manikin locations for a fixed sampling tree orientation.

For all the tests, the average CO_2 concentration was the highest on the coughing manikin seat and decreased to near supply air levels at the furthest sampling point. However, the dispersion pattern varied substantially depending on the location and the direction from the coughing manikin. Generally, in most of the tests performed with the sampling tree in the longitudinal front orientation, as shown in Figure H.184, the tracer gas concentration decreased gradually away from the coughing manikin. Nonetheless, similar to the tests performed in the modified cabin, there were some sampling locations which recorded a higher tracer gas concentration than the locations closer to the source such as Tests 37-42 (B-M), and Tests 68-72 (B-M). This could be due to the cough momentum which tends to push the coughed tracer gas to further distances bypassing the closest sampling port. If the cabin airflow pattern happens to be in the same cough direction, this can even push the coughed tracer gas to further distances or change its direction.

In contrast to the front direction, the tracer gas concentration to the back of the coughing manikin remained almost unchanged as can be shown in Figure H.183. This is due to the cough momentum that causes the tracer gas to increase in the front direction rather

than the rear. On the other hand, in continuous injection source tests, for example Test 17 (B-I) and 22 (B-I), the tracer gas concentration increased noticeably to the back of the source due to dispersion and the effect of the cabin airflow. Similar to the longitudinal rear sampling tree orientation, a very slight increase was recorded in the tracer gas concentrations in tests performed with the diagonal and the lateral sampling tree directions.

Figure 5.4 shows the percentage increase in tracer gas concentration at each sampling location over the supply air concentration for all the tests performed using the coughing manikin source in the Boeing 767 mockup cabin with the ISOPass undeployed. The figure shows the average percentage increase for all source locations and sampling tree orientations. As depicted in the figure, the difference between tracer gas concentration in the sampling location and in the supply air gets smaller away from the coughing manikin source due to the dilution created by the cabin supply air and the decrease in the cough momentum. The average reduction in the tracer gas concentration from the coughing manikin seat to the first sampling location was about 85%. At the furthest sampling point from the source, at 3.35 m, the total reduction from the source was about 92%. Hence, a minor reduction in the tracer gas concentration occurred between those two ends.

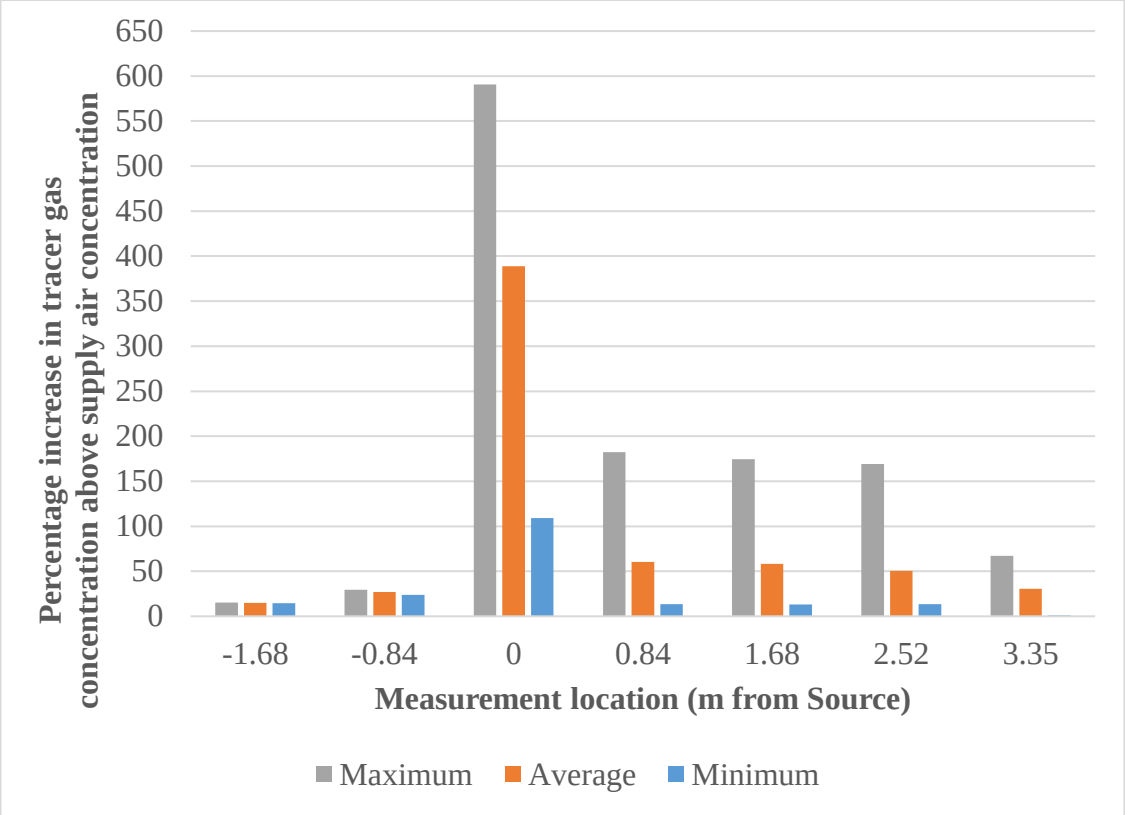

Figure 5.4. Percentage increase in tracer gas concentration in different sampling locations above supply air concentration with the ISOPass undeployed in tests perofrmed using coughing manikin source in the Boeing 767 mockup cabin.

Figure O.1 in Appendix O shows a comparison of the tracer gas concentration at each sampling location for all the tests performed using both the continuous injection source and the coughing manikin in the Boeing 767 mockup cabin. The general observation from this figure is that the recorded tracer gas concentration range at each sampling location is somehow similar between both source types except at 0.84 m (2.75 inch) and 2.52 m (8.26 inch) from the source. At 0.84 m (2.75 inch) from the source, the tests performed with the continuous injection tracer gas had a higher concentration range between about 500 ppm and 2300 ppm compared to about 500 ppm-1100 ppm for the coughing manikin tests. At 2.52 m (8.26 inch) from the source, tests performed with the coughing manikin had a higher tracer

gas concentration range between about 500 ppm-1050 ppm compared to about 450 ppm-800 ppm. While the higher tracer gas concentration is expected at the further distances from the source for tests performed with the coughing manikin, due to the cough momentum, this was not noticed at 0.84 m (2.75 inch) from the source. Hence, a comparison between only the common tests setups was constructed in Figure O.2 in Appendix O. In this figure, the results of the tests performed with the same source location and sampling tree orientation were plotted. By looking at Figure O.2, the tracer gas concentration range at the source seat is almost twice as large in the tests performed with the coughing manikin when compared to tests performed with the continuous injection source. This is a realistic observation since the injected tracer gas plume tends to disperse in all directions when it comes out from the continuous injection point source as compared to coughed tracer gas that can go in a better-defined jet direction. Also, the location of probe that analyzes the concentration of the tracer gas at the source seat has a determining factor. In the continuous injection tracer gas tests, the analyzer probe is taped to the injection tube. Any movement in the injected tracer gas plume, caused mainly by the supply air from the central diffusers of the Boeing 767 cabin mockup, would change the reading of the tracer gas analyzer. On the other hand, the analyzer probe is taped to the manikin mouth in the tests performed with the coughing manikin. Hence, it records the concentration of the tracer gas on the source seat as soon as the manikin coughs with less disturbance from the central diffusers supply air. The range of the tracer gas concentration at the rest of the sampling locations seems to be higher for the tests performed with the coughing manikin due to the cough momentum that tends to push the coughed tracer gas to the front. It should be noted that both Figure O.1 and Figure O.2 show the sampling locations at absolute distanced from the source. This means for example, that measurement

taken at a certain distance behind the source are plotted with those at the same distance to the front. While this provides means to understand the dispersion trend, it might be misinterpreted if the tracer gas concentration range is considered. In Figure O.2, the tracer gas concentration range at 0.84 m (2.75 inch) from the source is expected to be higher in the tests performed with the coughing manikin similar to the rest of the sampling locations due to the cough momentum. Since the cough momentum causes all the coughed tracer gas to go to the front of the manikin rather than the back, the tracer gas concentration at -0.84 m (-2.75 inch) from the manikin is usually very low. When those concentration collected at the back of the manikin are plotted with those to the front, the concentration range decreases. Furthermore, the increase in the tracer gas caused by the coughing was noticed in some tests until the second sampling location away from the source. This is due to a combination of both the cough momentum and the airflow pattern inside the cabin that can change the cough jet direction.

5.2 ISOPass deployed tests

5.2.1 Boeing 767 Cabin

The effectiveness of the ISOPass in containing both the injected and the coughed tracer gas aerosols is demonstrated in Appendix D and Appendix I, respectively. Using a continuous tracer gas injection source in 3 identical tests as shown in Appendix D, the concentration of the tracer gas on the seat across from the source and 3 rows away, both remained unchanged. The percentage-difference for each sampling location were -1% (Seat E4 and Seat E7), and +368% (Seat F7) inside the ISOPass as reported in (Darrah et al., 2019). Using 36 different tests with several coughing manikin locations and sampling tree orientations, the ISOPass was also proven effective. As shown in Figures I.113- I.116, the concentration of the tracer gas outside the ISOPass remained at the supply air level for different coughing manikin locations.

Figure 5.5 shows the percentage increase in tracer gas concentration at each sampling location over the supply air concentration for all the tests performed using the coughing manikin source in the Boeing 767 mockup cabin with the ISOPass deployed. The figure shows the average percentage increase for all source locations and sampling tree orientations. As depicted in the figure, the difference between tracer gas concentration in the sampling location and in the supply air, at its maximum inside the ISOPass and remained almost unchanged outside of it. The small percentage difference in the concentration outside the ISOPass is a result of the gas analyzers different uncertainty as explained previously. Within the accuracy of the measurements of the CO_2, there was no evidence of any leakage of the tracer gas from the ISOPass.

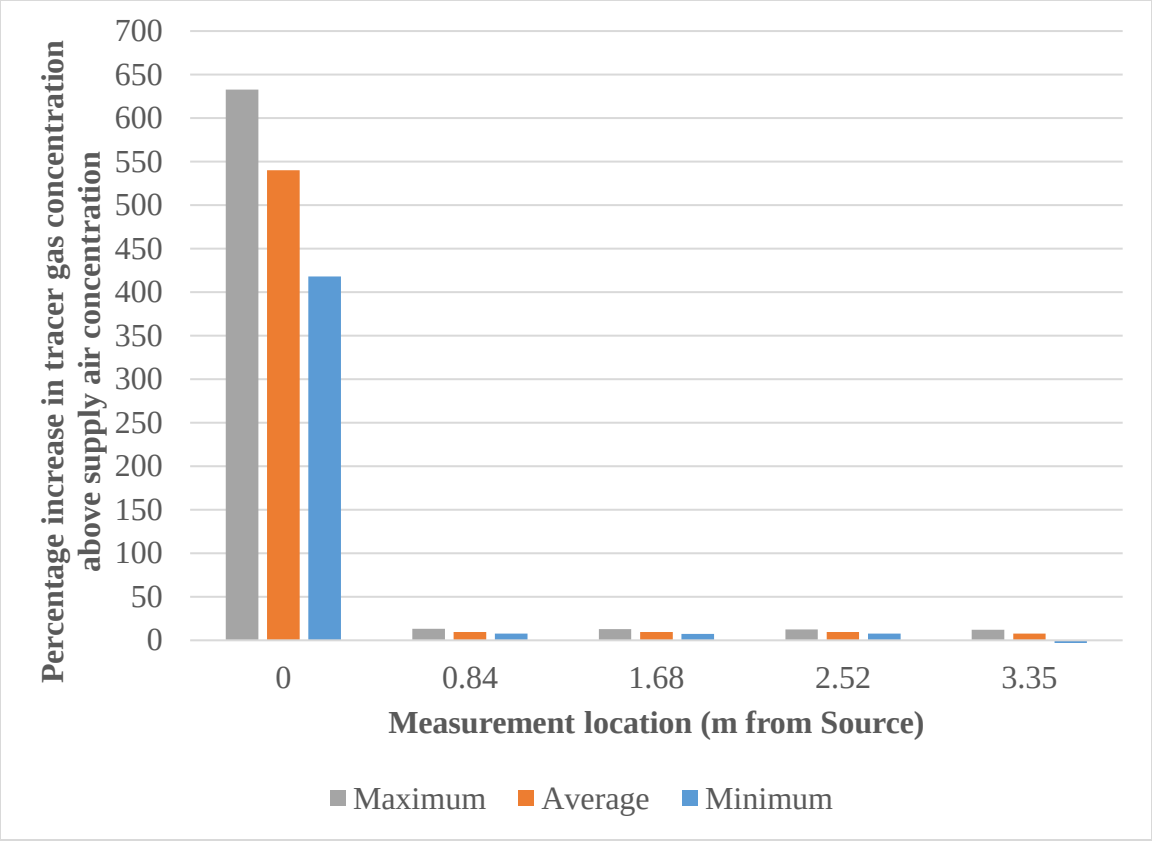

Figure 5.5. Percentage increase in tracer gas concentration in different sampling locations above supply air concentration with the ISOPass deployed in tests perofrmed using coughing manikin source the Boeing 767 mockup cabin.

5.2.2 Boeing 737 Cabin

The ISOPass was tested in 4 identical tests in the Boeing 737 cabin section. Three gas analyzers were used to measure the tracer gas concentration at 3 different locations as shown in Appendix G. The concentrations outside the ISOPass remained unchanged proving the effectiveness of the ISOPass in containing the injected tracer gas. The parentage-difference for seat D4 and seat E1 was 4% and 2%, respectively, and 345% for seat A4 located inside the ISOPass as reported by (Darrah, 2018). It was noticed that the CO_2 concentrations outside of the ISOPASS increased very slightly during the tracer gas injection.

This was attributed to the fluctuations in CO_2 concentration in the atmosphere in addition to the uncertainty difference of the tracer gas analyzers.

Chapter 6 - Summary and Conclusions

A total of 183 tests were performed in this work using two tracer gas source types, different tracer gas source locations, sampling locations, and different passenger isolation system (ISOPass) conditions in three different aircraft cabin configurations. The tracer gas source types were a continuous injection source and a coughing manikin. The source locations were two seats at both cabin sides (seats A6, B6, F6, and G6), a front seat (D1), a middle seat (D6), and a rear seat (D11). The ISOPass conditions were ISOPass deployed and ISOPass undeployed. The different aircraft cabin configurations were a Boeing 767 cabin mockup, a Boeing 737 cabin section, and a modified airflow cabin mockup. The modified cabin mockup was a modification of the Boeing 767 mockup`s air distribution configuration.

Using the continuous injection source, four injection source locations were selected. To represent the continuous injection source, a copper tube of 25.4 mm (1 inch) inner diameter was used. A mixture of 5 L/min (0.176 ft^3/min) of CO_2 and 3.07 L/min (0.108 ft^3/min) of He were injected at the average seated passenger breathing level of 1.25 m above the cabin floor. Prior to conducting the tests, the testing chamber was operated until thermal steady state conditions were achieved followed by a pre-test period of 20 minutes without tracer gas injection, with tracer gas sampling. A steady state period of 15 minutes with tracer gas injection, without tracer gas sampling was then conducted. This was followed by the actual testing period of 30 minutes of tracer gas injection for each sampling tree port, with tracer gas sampling. Finally, a post-test period of 20 minutes without tracer gas injection, with sampling was conducted before completing the test. A total of 42 tests were conducted in matching pairs. It was noticed that the contaminant transport pattern is dominated by the cabin airflow pattern in the near field and by distance in the far field. Another key finding is

that the contaminant concentration is not necessarily the same for similar radial distances in different directions from the source, especially in the near field. Furthermore, tracer gas concentrations at some seats were higher than the source seat due to the airflow pattern inside the cabin which can direct the tracer gas to one direction causing a significant increase at certain locations. This effect was noticed mainly in seats D1 and G6 of the Boeing 767 cabin mockup.

Using the coughing manikin, 93 tests were conducted in matching triplets. The cough airflow volume of 4.2 L (0.148 ft^3) was produced by metal bellows driven by a computer controlled linear motor. It was based on coughs recorded from influenza patients and had a peak flowrate of 11.4 L/s (0.403 ft^3/s) with the entire cough lasting approximately 1 second. The coughing frequency for this study was one cough every 75 seconds. To ensure sufficient CO_2 supply, each test was run for 30 coughs which allowed measurements at all sampling tree locations before refilling the Tedlar bags. Five coughing manikin locations were selected in different locations inside the cabin and both ISOPass conditions were tested. Tracer gas samples were collected up to 3.35 m (11 ft) from the manikin in different directions. Without the ISOPass and due to the cough momentum, the tracer gas concentration at further distances from the coughing manikin were sometimes higher than in the vicinity of the manikin. Also, tracer gas concentration at the rear of the cabin was negligibly affected by the coughing manikin compared to the longitudinal or diagonal directions.

When comparing the results of the continuous injection source and the coughing manikin tests, the tracer gas dispersion patterns were similar for both source types in the far field. Nonetheless, due to the cough momentum, the tracer gas concentration in the near field was higher in the front direction in the coughing manikin tests as compared to the continuous

injection source tests. Without the ISOPass, the cough generated by the manikin had a minimal effect in the lateral direction as compared to the longitudinal and diagonal directions.

The ISOPass, when deployed in different aircraft cabins and using either source types, was proven an effective tool to contain aerosols from spreading to passengers and crew. The tracer gas concentration outside the ISOPass remained unchanged as the tracer gas was introduced inside the ISOPass. Using a continuous tracer gas injection source in three identical tests as shown in Appendix D, the concentration of the tracer gas on the seat across from the source and three rows away, both remained unchanged. The percentage-difference in tracer gas concentration over the supply air concentration for each sampling location were -1% (Seat E4 and Seat E7), and +368% (Seat F7) inside the ISOPass. In the Boeing 737 cabin, the parentage-difference for seat D4 and seat E1 was 4% and 2%, respectively, and 345% for seat A4 located inside the ISOPass. The changes measured outside the ISOPass were well within the accuracy of the measurements.

Smoke visualization was performed at five different locations to qualitatively analyze the dispersion of the tracer gas in the aircraft cabin. The smoke visualization results provided an explanation for some of the phenomenon that were recorded using the tracer gas measurements such as the increase in the tracer gas concentration in some seats over the source seat. Another phenomenon was the increase in tracer gas concentration in seats located at further distances from the source than the ones closer to the source due to the cabin airflow pattern and the cabin structures.

This work will provide information to help understand infectious aerosol spread from an infectious passenger in an aircraft cabin. It will also provide information to assist in

identifying potential exposures in the case of confirmed/suspected infectious passengers. Ultimately, the work presented in this dissertation will provide the CDC with valuable data towards their efforts in tracing and containing infectious diseases in aircraft cabins.

As future work, the utilization of models to predict optimal seating arrangements for pandemic response can be analyzed. Also, other economically viable and practical transmission mitigation strategies could be developed. A detailed study of aerosols in the context of aircraft cabin exposure pathway matrix is also necessary. Finally, an objective evaluation of relative exposure risk for air travel is needed to give recommendations to different airlines and related organizations.

References

Acikgoz, M. B., Akay, B., Miguel, A. F., & Aydın, M. (2011). Airborne pathogens transport in an aircraft cabin. *Defect and Diffusion Forum*, *312–315*(April), 865–870. https://doi.org/10.4028/www.scientific.net/DDF.312-315.865

Airbus. (2020). A 340-500/-600 Characteristics, Airport and Maintenance Planning. In *Airbus S.A.S.* https://www.airbus.com/content/dam/corporate-topics/publications/backgrounders/techdata/aircraft_characteristics/Airbus-Aircraft-AC-A380.pdf

Amler, R. ., Bloch, A. ., Orenstein, W. ., Bart, K. ., Turner, P. ., & Hinman, A. . (1982). Imported measles in the United States. *JAMA*, *248*(17), 2219–2133.

ASHRAE. (2007). *ASHRAE Handbook – Heating, Ventilating and Air-Conditioning Applications*.

ASHRAE. (2013). ASHRAE Fundamentals Handbook. In *ASHRAE Fundamentals Handbook*. ASHRAE.

ASHRAE. (2016). *Air quality in commercial aircraft. ASHRAE guideline 28-2016*.

ASHRAE. (2018). *Air quality within commercial aircraft. ANSI/ASHRAE standard 161-2018*.

Bagshaw, M., & Illig, P. (2019). The aircraft cabin environment. *Travel Medicine*, *3*, 429–436. https://doi.org/10.1016/B978-0-323-54696-6.00047-1

Baharoon, S., & Memish, Z. A. (2019). MERS-CoV as an emerging respiratory illness: A review of prevention methods. *Travel Medicine and Infectious Disease*, *32*. https://doi.org/10.1016/j.tmaid.2019.101520

Baker, M. G., Thornley, C. N., Mills, C., Roberts, S., Perera, S., Peters, J., Kelso, A., Barr, I., & Wilson, N. (2010). Transmission of pandemic A/H1N1 2009 influenza on passenger aircraft: retrospective cohort study. *BMJ*, *340*(may21 1), c2424–c2424. https://doi.org/10.1136/bmj.c2424

Baron, P. (2010). Generation and behavior of airborne particles (aerosols). In *The National Institute for Occupational Safety and Health (NIOSH)*.

Baron, R., Wells, J., Mascola, L., Besser, R. E., Griffin, P. M., Feikin, D., Rutherford, G. W., Tormey, M. P., Araneta, M. R., Eberhart-Phillips, J., & Kilman, L. (2002). An outbreak of cholera from food served on an international aircraft. *Epidemiology and Infection*, *118*(1), 79–79. https://doi.org/10.1017/s095026889600948x

Bennett, J. S., Jones, B. W., Hosni, M. H., Zhang, Y., Topmiller, J. L., & Dietrich, W. L. (2013). Airborne exposure patterns from a passenger source in aircraft cabins.

HVAC&R Research, *19*(8), 962–973. https://doi.org/10.1080/10789669.2013.838990

Boeing Commercial Airplanes. (2005). 767 Airplane Characteristics for Airport Planning. In *Comerical airplanes - Overview* (Issue September).

Breugelmans, G., Zucas, P., Porten, K., Broll, S., Niedrig, M., Ammon, A., & Krause, G. (2004). SARS transmission and commercial aircraft. *Emerging Infectious Diseases*, *10*(8), 1502–1503.

British Research Establishment. (2005). *Study of possible effects on health of aircraft cabin environments-stage 2*. https://www.semanticscholar.org/paper/Study-of-possible-effects-on-health-of-aircraft-2/418fb1940b58b0a23755e9ec2c5cca33da9ed27e

Brown, T. P., Shuker, L. K., Rushton, L., Warren, F., & Stevens, J. (2001). The possible effects on health, comfort and safety of aircraft cabin environments. *Journal of The Royal Society for the Promotion of Health*, *121*(3), 177–184. https://doi.org/10.1177/146642400112100315

Bureau of Transportation Statistics. (2020). *2019 Traffic data for U.S. airlines and foreign airlines*. https://www.bts.dot.gov/newsroom/final-full-year-2019-traffic-data-us-airlines-and-foreign-airlines-us-flights

Castrup, H. (2004). Estimating and combining uncertainties. In *8th Annual ITEA Instrumentation Workshop, Lancaster*.

Centers for Disease Control and Prevention. (1983). *Interstate importation of measles following transmission in an airport--California, Washington*. *32*(16), 215–216. – California,Washington

Centers for Disease Control and Prevention. (1999). *Preliminary guidelines for the prevention and control of influenza-like illness among passengers and crew members on cruise ships*.

Centers for Disease Control and Prevention. (2001a). Exposure to patients with meningococcal disease on aircraft--United States, 1999-2001. In *Morbidity and Mortality Weekly Report (MMWR)* (Vol. 50, Issue 23). https://doi.org/10.1067/mem.2001.119344

Centers for Disease Control and Prevention. (2001b). Health information for international travel. In *School Library Journal* (Vol. 54, Issue 5).

Centers for Disease Control and Prevention. (2004). *Guidance about SARS for airline flight crews, cargo and cleaning personnel, and personnel interacting with arriving passengers*.

Centers for Disease Control and Prevention. (2009). Influenza. In *Manual for the Surveillance of Vaccine-Preventable Diseases* (Issue April, pp. 1–16).

Centers for Disease Control and Prevention. (2015a). *Information about Middle East Respiratory Syndrome (MERS)*. https://www.cdc.gov/coronavirus/mers/

Centers for Disease Control and Prevention. (2015b). Measles. In *Epidemiology and Prevention of Vaccine-Preventable Diseases* (Vol. 80, Issue 2, pp. 162–168). https://doi.org/10.5222/jopp.2013.105

Centers for Disease Control and Prevention. (2015c). Meningitis. In *Epidemiology and Prevention of Vaccine-Preventable Diseases* (13th ed., pp. 231–246). Public Health Foundation.

Centers for Disease Control and Prevention. (2017). Influenza. In *Vaccine-Preventable Diseasess Surveillance Manual* (Issue October, pp. 1–16). Centers for Disease Control and Prevention. www.cdc.gov/vaccines/pubs/surv-manual/chpt06-influenza.html

Centers for Disease Control and Prevention. (2019a). *Ebola (ebola virus disease)*. https://www.cdc.gov/vhf/ebola/symptoms/index.html

Centers for Disease Control and Prevention. (2019b). *Measles outbreak*.

Centers for Disease Control and Prevention. (2019c). *Preventing Spread of Disease on Commercial Aircraft: Guidance for Cabin Crew*. https://www.cdc.gov/quarantine/air/managing-sick-travelers/commercial-aircraft/infection-control-cabin-crew.html

Centers for Disease Control and Prevention. (2020a). *Legal authorities for isolation and quarantine*. https://www.cdc.gov/quarantine/aboutlawsregulationsquarantineisolation.html

Centers for Disease Control and Prevention. (2020b). *Measles cases and outbreaks*. https://www.cdc.gov/measles/cases-outbreaks.html

Central American Corporation for Air Navigation Services. (2020). *Cabin air quality air filtration systems and other technologies*. https://acsa.cocesna.org

Chen, J., He, H., Cheng, W., Liu, Y., Sun, Z., Chai, C., Kong, Q., Sun, W., Zhang, J., Guo, S., Shi, X., Wang, J., Chen, E., & Chen, Z. (2020). Potential transmission of SARS-CoV-2 on a flight from Singapore to Hangzhou, China: An epidemiological investigation. *Travel Medicine and Infectious Disease*, *36*(July-August). https://doi.org/10.1016/j.tmaid.2020.101816

Chen, S. C., Chio, C. P., Jou, L. J., & Liao, C. M. (2009). Viral kinetics and exhaled droplet size affect indoor transmission dynamics of influenza infection. *Indoor Air*, *19*(5), 401–413. https://doi.org/10.1111/j.1600-0668.2009.00603.x

Chen, T.-J., Olsen, S. J., Dowell, S. F., Chang, H.-L., Lando, J., Tang, A. F.-Y., Hsu, K.-H., Kuo, H.-W., Cheung, T. Y.-Y., Jiang, D. D.-S., Ooi, S. P.-L., Fisk, T. L., & Chen, K.-T. (2003). Transmission of the Severe Acute Respiratory Syndrome on Aircraft. *New*

England Journal of Medicine, *349*(25), 2416–2422. https://doi.org/10.1056/nejmoa031349

Clayton, A. J., O'Connell, D. C., Gaunt, R. A., & Clarke, R. E. (1976). Study of the microbiological environment within long- and medium-range Canadian forces aircraft. *Space Environmental Medicine*, *47*(5), 471–482.

Coburn, B. J., & Blower, S. (2014). Predicting the potential for within-flight transmission and global dissemination of MERS. In *The Lancet Infectious Diseases* (Vol. 14, Issue 2). Elsevier Ltd. https://doi.org/10.1016/S1473-3099(13)70358-X

Cornelius, B., Cornelius, A., Crisa, L., Collins, C., Mccarthy, S., Foster, C., Shannon, H., Bennett, R., Brown, S., Rodriguez, K., & Bachini, S. (2020). Mass air medical repatriation of coronavirus disease 2019 patients. *Air Medical Journal*, *39*, 251–256. https://doi.org/10.1016/j.amj.2020.04.005

Cowling, B. J., & Yu, H. (2015). Ebola: Worldwide dissemination risk and response priorities. *The Lancet*, *385*(9962), 7–9. https://doi.org/10.1016/S0140-6736(14)61895-X

Darrah, I. (2018). *Experimental analysis of infectious passenger isolation system for aircraft*. Kansas State University.

Darrah, I., Bennett, J. S., & Jones, B. W. (2019). Infectious passenger isolation system for aircraft. *ASHRAE Transactions*, *125*(2), 288–296.

Desenclos, J. C., Van Der Werf, S., Bonmarin, I., Levy-Bruhl, D., Yazdanpanah, Y., Hoen, B., Emmanuelli, J., Lesens, O., Dupon, M., Natali, F., Michelet, C., Reynes, J., Guery, B., Larsen, C., Semaille, C., Mouton, Y., Christmann, D., André, M., Escriou, N., … Scheidegger, S. (2004). Introduction of SARS in France, March-April, 2003. *Emerging Infectious Diseases*, *10*(2), 195–200. https://doi.org/10.3201/eid1002.030351

Dupont, H. L., Wilder-Smith, A., & Steffen, R. (2001). Investigation and management of infectious diseases on international conveyances (airplanes and cruise ships). In *Textbook of Travel Medicine and Health* (2nd ed., pp. 519–530). PMPH USA, Ltd.

Eldin, C., Lagier, J. C., Mailhe, M., & Gautret, P. (2020). Probable aircraft transmission of Covid-19 in-flight from the Central African Republic to France. *Travel Medicine and Infectious Disease*, *35*(April). https://doi.org/10.1016/j.tmaid.2020.101643

Ellis, R. . (1996). *Aircraft disinsection: A guide for military & civilian air carriers* (Issue April).

European Centre For Disease Prevention And Control. (2020). *Risk assessment guidelines for infectious diseases transmitted on aircraft (RAGIDA) - Influenza* (Issue January).

Federal Aviation Administration. (2010). *Environmental control and life support systems for flight crew and space flight participants in suborbital space flight: Vol. 1.0* (Issue

April).

Feng, L., Yao, S., Sun, H., Jiang, N., & Liu, J. (2015). TR-PIV measurement of exhaled flow using a breathing thermal manikin. *Building and Environment*, *94*, 683–693. https://doi.org/10.1016/j.buildenv.2015.11.001

Fischer, W. A., Uyeki, T. M., & Tauxe, R. V. (2015). Ebola virus disease : What clinicians in the United States need to know. *American Journal of Infection Control*, *43*(8), 788–793. https://doi.org/10.1016/j.ajic.2015.05.005

Foxwell, R., Roberts, L., Lokuge, K., & Kelly, P. M. (2011). Transmission of influenza on international flights, may 2009. *Emerging Infectious Diseases*, *17*(7), 1188–1194. https://doi.org/10.3201/eid1707.101135

Grainger, C., Young, M. J. F., & John, H. (1995). A code of practice on dealing with infectious diseases on aircraft. *Journal of the Royal Society of Health*, *115*(3), 175–177. https://doi.org/10.1177/146642409511500310

Gralton, J., Tovey, E., McLaws, M.-L., & Rawlinson, W. D. (2011). The role of particle size in aerosolised pathogen transmission: A review. *Journal of Infection*, *62*(1), 1–13. https://doi.org/10.1016/j.jinf.2010.11.010

Gupta, J. K., Lin, C., & Chen, Q. (2009). Flow dynamics and characterization of a cough. *Indoor Air*, 517–525.

Gupta, J. K., Lin, C. H., & Chen, Q. (2012). Risk assessment of airborne infectious diseases in aircraft cabins. *Indoor Air*, *22*(5), 388–395. https://doi.org/10.1111/j.1600-0668.2012.00773.x

Hertzberg, V. S., & Weiss, H. (2016). On the 2-row rule for infectious disease transmission on aircraft. *Annals of Global Health*, *82*(5), 819–823. https://doi.org/10.1016/j.aogh.2016.06.003

Heymann, D. L. (2004). Control of Communicable Diseases Manual. In *Journal of the American Medical Association* (Issue 18th). American Public Health Association. https://doi.org/10.1001/jama.1921.02630340012005

Hoad, V. C., O'Connor, B. A., Langley, A. J., & Dowse, G. K. (2013). Risk of measles transmission on aeroplanes: Australian experience 2007-2011. *Medical Journal of Australia*, *198*(6), 320–323. https://doi.org/10.5694/mja12.11752

Hoehl, S., Karaca, O., Kohmer, N., Westhaus, S., Graf, J., Goetsch, U., & Ciesek, S. (2020). Assessment of SARS-CoV-2 transmission on an international flight and among a tourist group. *JAMA Network Open*, *3*(8). https://doi.org/10.1001/jamanetworkopen.2020.18044

Hugh W. Coleman, W. Glenn Steele, Jr., W. G. S. (1999). *Experimentation and uncertainty analysis for engineers* (2nd ed.). John Wiley & Sons.

Hwang, G. M., DiCarlo, A. A., & Lin, G. C. (2011). An analysis on the detection of biological contaminants aboard aircraft. *PLoS ONE*, *6*(1). https://doi.org/10.1371/journal.pone.0014520

International Civil Aviation organization. (2005). *Guidelines for states concerning the management of communicable disease posing a serious public helath risk*. http://www.icao.int/safety/aviation-medicine/guidelines/AvInfluenza_guidelines.pdf

International Union of Pure and Applied Chemistry. (2014). Compendium of chemical terminology. In *Synthesis of Solid Catalysts* (2nd ed.). https://doi.org/10.1002/9783527626854.ch7

Jayaweera, M., Perera, H., Gunawardana, B., & Manatunge, J. (2020). Transmission of COVID-19 virus by droplets and aerosols: A critical review on the unresolved dichotomy. *Environmental Research*, *188*(May). https://doi.org/10.1016/j.envres.2020.109819

Jiang, N., Yao, S., Feng, L., Sun, H., & Liu, J. (2017). Experimental study on flow behavior of breathing activity produced by a thermal manikin. *Building and Environment*, *123*, 200–210. https://doi.org/10.1016/j.buildenv.2017.07.004

Jones, R. M., Masago, Y., Bartrand, T., Haas, C. N., Nicas, M., & Rose, J. B. (2009). Characterizing the risk of infection from mycobacterium tuberculosis in commercial passenger aircraft using quantitative microbial risk assessment. *Risk Analysis*, *29*(3), 355–365. https://doi.org/10.1111/j.1539-6924.2008.01161.x

Kenyon, T. A., Valway, S., Ihle, W. W., Onorato, I. M., & Castro, K. G. (1996). Transmission of multidrug-resistant mycobacterium tuberculosis during a long airplane flight. *The New England Journal of Medicine*, *334*(15).

Keshavarz, A., Jones, B. W., Hosni, M. H., & Beneke, J. M. (2015). Experimental measurements for gaseous transport within an aircraft cabin. *Building and Environment*, *89*, 327–335. https://doi.org/10.1016/j.buildenv.2015.03.011

Kim, J. (1994). Atmospheric environment of bioaerosols. In *Atmospheric Microbial Aerosols* (pp. 28–67). Springer US. https://doi.org/10.1007/978-1-4684-6438-2_3

Kirking, H. L., Cortes, J., Hall, A. J., Burrer, S., Fishbein, D. B., Lipman, H., Cohen, N. J., Daly, E. R., & Kim, C. (2010). Likely transmission of norovirus on an airplane. *Clinical Infectious Diseases*, *50*(9), 1216–1221. https://doi.org/10.1086/651597

Klontz, K. C., Hynes, N. A., Gunn, R. A., Wilder, M. H., Harmon, M. W., & Kendal, A. P. (1989). An outbreak of influenza a/Taiwan/1/86 (H1N1) infections at a naval base and its association with airplane travel. *American Journal of Epidemiology*, *129*(2), 341–348. https://doi.org/10.1093/oxfordjournals.aje.a115137

Kotila, S. M., Payne Hallström, L., Jansen, N., Helbling, P., & Abubakar, I. (2016). Systematic review on tuberculosis transmission on aircraft and update of the European

centre for disease prevention and control risk assessment guidelines for tuberculosis transmitted on aircraft (RAGIDA-TB). *Euro Surveillance*, *21*(4), 1–12. https://doi.org/10.2807/1560-7917.ES.2016.21.4.30114

Kwon, S.-B., Park, J., Jang, J., Cho, Y., Park, D.-S., Kim, C., Bae, G.-N., & Jang, A. (2012). Study on the initial velocity distribution of exhaled air from coughing and speaking. *Chemosphere*, *87*(11), 1260–1264. https://doi.org/10.1016/j.chemosphere.2012.01.032

Lacey, J., & Venette, J. (1995). Outdoor air sampling techniques. In *Bioaerosols handbook* (pp. 407–471). C.S.Cox, and C.M.Wathes.

Laussmann, D., & Helm, D. (2011). Air change measurements using tracer gases. In *Chemistry, Emission Control, Radioactive Pollution and Indoor Air Quality*. InTech. https://doi.org/10.5772/18600

Li, H. L. Y., Lin, S. X. C., Wei, S. L. N. D., & Ji, Z. H. S. (2018). *Routes of transmission of influenza A H1N1 , SARS CoV , and norovirus in air cabin : Comparative analyses*. *December 2017*, 394–403. https://doi.org/10.1111/ina.12445

Lighthart, B., & Mohr, A. J. (1994). *Atmospheric microbial aerosols: theory and applications*. Chapman & Hall. https://doi.org/10.1007/978-1-4684-6438-2

Lim Ooi, P., Yuk Lin Lai, F., Ling Low, C., Lin, R., Wong, C., Hibberd, M., & Anath Tambyah, P. (2010). Clinical and molecular evidence for transmission of novel influenza A(H1N1/2009) on a commercial airplane. *Arch Intern Med.*, *170*(10), 913–915. https://doi.org/10.1001/archinternmed.2010.127

Lindsley, W. G., Noti, J. D., Blachere, F. M., Szalajda, J. V., & Beezhold, D. H. (2014). Efficacy of face shields against cough aerosol droplets from a cough simulator. *Journal of Occupational Environmental Hygiene*, *11*(8), 509–518. https://doi.org/10.1080/15459624.2013.877591

Lindsley, W. G., Reynolds, J. S., Szalajda, J. V, Noti, J. D., Beezhold, D. H., Effects, H., Virginia, W., Personal, N., & Technology, P. (2013). A cough aerosol simulator for the study of disease transmission by human cough-generated aerosols. *Aerosol Sci Technol.*, *47*(8), 937–944. https://doi.org/10.1080/02786826.2013.803019.A

Madariaga, M. G. (2015). Ebola Virus Disease : A Perspective for the United States. *The American Journal of Medicine*, *128*(7), 682–691. https://doi.org/10.1016/j.amjmed.2015.01.035

Madden, M. L. (2015). *The effects of passenger loading and ventilation air on airflow patterns within an aircraft cabin*. Kansas State University.

Mahajan, R. ., Singh, P., Murty, G. ., & Aitkenhead, A. . (1994). Relationship between expired lung volume, peak flow rate and peak velocity time during a voluntary cough manoeuvre. *British Journal of Anaesthesia*, *72*(3), 298–301. https://doi.org/10.1093/bja/72.3.298

Mahmoud, S., Hosni, M. H., Jones, B., & Bennett, J. (2019). Mapping The Potential For Infectious Disease Transmission In A Wide-Body Aircraft Cabin. *International Mechanical Engineering Congress and Exposition*, 1–10.

Mangili, A., & Gendreau, M. A. (2005). Transmission of infectious diseases during commercial air travel. *The Lancet*, *365*(9463), 989–996. https://doi.org/10.1016/S0140-6736(05)71089-8

Melikov, A. K., & Dzhartov, V. (2013). Advanced air distribution for minimizing airborne cross-infection in aircraft cabins. *HVAC&R Research*, *19*(8), 926–933. https://doi.org/10.1080/10789669.2013.818468

Mohr, A. J. (1997). Fate and transport of microorganisms in air. In *Manual of environmental microbiology* (pp. 641–650). ASM Press.

Moser, M. R., Bender, T. R., Margolis, H. S., Noble, G. R., Kendal, A. P., & Ritter, D. G. (1979). An outbreak of influenza aboard a commercial airliner. *American Journal of Epidemiology*, *110*(1), 1–6. https://doi.org/10.1093/oxfordjournals.aje.a112781

Murphy, B. ., & Webster, R. . (1996). Orthomyxoviruses. In *Fields Virology* (3rd ed., pp. 1397–1445). Lippincott-Raven Publishers.

National Aeronautics and Space Administration. (1994). *Design for human presence in space: an introduction to environmental control and life support systems*.

National Research Council. (1986). *The Airliner Cabin Environment: Air Quality and Safety*. https://doi.org/10.17226/913

National Research Council. (2002). *The airliner cabin environment and the health of passengers and crew*. National Academies Press. https://doi.org/10.17226/10238

Nir-paz, R., Grotto, I., Strolov, I., Salmon, A., Mandelboim, M., Mendelson, E., & Regev-yochay, G. (2020). Absence of in-flight transmission of SARS-CoV-2 likely due to use of face masks on board. *Journal of Travel Medicine*, 1–3. https://doi.org/10.1093/jtm/taaa117

Noti, J. D., Lindsley, W. G., Blachere, F. M., Cao, G., Michael, L., Thewlis, R. E., Mcmillen, C. M., King, W. P., & Jonathan, V. (2012). Detection of infectious influenza virus in cough aerosols generated in a simulated patient examination room. *Clin Infect Dis*, *54*(11), 1569–1577. https://doi.org/10.1093/cid/cis237.Detection

Olsen, S. J., Chang, H.-L., Cheung, T. Y.-Y., Tang, A. F.-Y., Fisk, T. L., Ooi, S. P.-L., Kuo, H.-W., Jiang, D. D.-S., Chen, K.-T., Lando, J., Hsu, K.-H., Chen, T.-J., & Dowell, S. F. (2003). Transmission of the severe acute respiratory syndrome on aircraft. *New England Journal of Medicine*, *349*(25), 2416–2422. https://doi.org/10.1056/NEJMoa031349

Oztig, L. I., & Askin, O. E. (2020). Human mobility and coronavirus disease 2019 (COVID-19): A negative binomial regression analysis. *Public Health*, *185*, 364–367.

https://doi.org/10.1016/j.puhe.2020.07.002

Parry-Ford, F., Boddington, N., Pebody, R., Phin, N., & On behalf of the Incident Management Team. (2015). Public health response to two incidents of confirmed MERS-CoV cases travelling on flights through London Heathrow Airport in 2014 – lessons learnt. *Euro Surveillance*, *20*(18), 1–7.

Platts-Mills, T. A. E., & Carter, M. C. (1997). Asthma and indoor exposure to allergens. *The New England Journal of Medicine*, *336*(19), 1382–1384. https://doi.org/10.1056/NEJM199705083361909

Qian, G. Q., Yang, N. B., Ding, F., Ma, A. H. Y., Wang, Z. Y., Shen, Y.-F., Shi, C. W., Lian, X., Chu, J. G., Chen, L., Wang, Z. Y., Ren, D. W., Li, G. X., Chen, X.-Q., Shen, H. J., & Chen, X. M. (2020). Epidemiologic and clinical characteristics of 91 hospitalized patients with COVID-19 in Zhejiang, China: a retrospective, multi-centre case series. *QJM: An International Journal of Medicine*, *113*(7), 474–481. https://doi.org/10.1093/qjmed/hcaa089

Regan, J. J., Jungerman, R., Montiel, S. H., Newsome, K., Objio, T., Washburn, F., Roland, E., Petersen, E., Twentyman, E., Olaiya, O., Naughton, M., & Alvarado-ramy, F. (2015). *Public health response to commercial airline travel of a person with ebola virus infection — United States , 2014* (Vol. 64, Issue 3).

Sato, K., Morishita, T., Nobusawa, E., Suzuki, Y., Miyazaki, Y., Fukui, Y., Suzuki, S., & Nakajima, K. (2000). Surveillance of influenza viruses isolated from travellers at Nayoga international airport. *Epidemiol. Infec.*, *124*, 507–514.

Shankar, A. G., Janmohamed, K., Olowokure, B., Smith, G. E., Hogan, A. H., De Souza, V., Wallensten, A., Oliver, I., Blatchford, O., Cleary, P., & Ibbotson, S. (2014). Contact tracing for influenza A(H1N1) pdm09 virus-infected passenger on international flight. *Emerging Infectious Diseases*, *20*(1), 118–120. https://doi.org/10.3201/eid2001.120101

Shehadi, M. (2015). *Airflow distribution and turbulence analysis in the longitudinal direction of a Boeing 767 mockup cabin*. Kansas State University.

Shen, J., Duan, H., Zhang, B., Wang, J., Ji, J. S., Wang, J., Pan, L., Wang, X., Zhao, K., Ying, B., Tang, S., Zhang, J., Liang, C., Sun, H., Lv, Y., Li, Y., Li, T., Li, L., Liu, H., … Shi, X. (2020). Prevention and control of COVID-19 in public transportation: Experience from China. *Environmental Pollution*, *266*. https://doi.org/10.1016/j.envpol.2020.115291

Silcott, D., Kinahan, S., Santarpia, J., Silcott, B., Silcott, R., Silcott, P., Silcott, B., Distelhorst, S., Herrera, V., Rivera, D., Crown, K., Lucero, G., Bryden, W., McLoughlin, M., Cetta, M., & Accardi, R. (2020). TRANSCOM/AMC commercial aircraft cabin aerosol dispersion tests. In *United States Transportation Command (USTRANSCOM) & Air Mobility Command (AMC)*.

Silva, M. G. Da. (2020). An analysis of the transmission modes of COVID-19 in light of the

concepts of Indoor Air Quality. *The REHVA European HVAC Journal*, *57*(3), 46–54. https://doi.org/10.13140/RG.2.2.28663.78240

Sun, W., & Ji, J. (2007). Transport of droplets expelled by coughing in ventilated rooms. *Indoor and Built Inviroment*, 493–504. https://doi.org/10.1177/1420326X07084290

Sze To, G. N., Wan, M. P., Chao, C. Y. H., Fang, L., & Melikov, A. (2009). Experimental study of dispersion and deposition of expiratory aerosols in aircraft cabins and impact on infectious disease transmission. *Aerosol Science and Technology*, *43*(5), 466–485. https://doi.org/10.1080/02786820902736658

Trudeau, W. L., & Fernández-Caldas, E. (1994). Identifying and measuring indoor biologic agents. *The Journal of Allergy and Clinical Immunology*, *94*(2), 393–400. https://doi.org/10.1053/ai.1994.v94.a56022

Van Doremalen, N., Bushmaker, T., Morris, D. H., Holbrook, M. G., Gamble, A., Williamson, B. N., Tamin, A., Harcourt, J. L., Thornburg, N. J., Gerber, S. I., Lloyd-Smith, J. O., De Wit, E., & Munster, V. J. (2020). Aerosol and surface stability of SARS-CoV-2 as compared with SARS-CoV-1. *New England Journal of Medicine*, *382*(16), 1564–1567. https://doi.org/10.1056/NEJMc2004973

Vanyi, G., Gut, N., Kretschmer, J., & Moeller, K. (2012). Concept study of a nonlinear mechanical lung simulator. *IFAC Proceedings Volumes*, *45*(18), 149–153. https://doi.org/10.3182/20120829-3-HU-2029.00089

Wei, J., & Li, Y. (2015). Enhanced spread of expiratory droplets by turbulence in a cough jet. *Building and Environment*, *93*, 86–96. https://doi.org/10.1016/j.buildenv.2015.06.018

Wilson, M. E. (1995). Travel and the emergence of infectious diseases. *Emerging Infectious Diseases*, *1*(2), 39–46. https://doi.org/10.1300/J096v09n02_10

Withers, M. R., & Christopher, G. W. (2000). Aeromedical evacuation of biological warfare casualties: A treatise on infectious diseases on aircraft. *Military Medicine*, *165*(suppl. 3:001), 1–21. https://doi.org/10.1093/milmed/165.suppl_3.1

World Health organization (WHO). (2012). Guidelines for testing the efficacy of insecticide products used in aircraft. In *Control of Neglected Tropical Diseases*. https://doi.org/978 92 4 150323 5

World Health organization (WHO). (2013a). *Aircraft disinsection insecticides*. www.who.int/

World Health organization (WHO). (2013b). *Tuberculosis and air travel. Guidelines for prevention and control*.

World Health organization (WHO). (2015). *Middle East respiratory syndrome coronavirus (MERS-CoV) – Republic of Korea*. https://www.who.int/csr/don/24-may-2015-mers-

korea/en/

World Health organization (WHO). (2020). *Tuberculosis*. https://www.who.int/health-topics/tuberculosis#tab=tab_1

Yan, W., Ã, Y. Z., Sun, Y., & Li, D. (2009). Experimental and CFD study of unsteady airborne pollutant transport within an aircraft cabin mock-up. *Building and Environment*, *44*, 34–43. https://doi.org/10.1016/j.buildenv.2008.01.010

Yan, Y., Li, X., & Tu, J. (2019). Thermal effect of human body on cough droplets evaporation and dispersion in an enclosed space. *Building and Environment*, *148*, 96–106. https://doi.org/10.1016/j.buildenv.2018.10.039

Yang, L., Li, X., Yan, Y., & Tu, J. (2018). Effects of cough-jet on airflow and contaminant transport in an airliner cabin section. *Computational Multiphase Flows*, *10*(2), 72–82. https://doi.org/10.1177/1757482X17746920

Zhu, S., Kato, S., & Yang, J. (2006). Study on transport characteristics of saliva droplets produced by coughing in a calm indoor environment. *Building and Environment*, *41*, 1691–1702. https://doi.org/10.1016/j.buildenv.2005.06.024

Appendix A - T-Sections and Diffusers Locations on the PVC Ducts

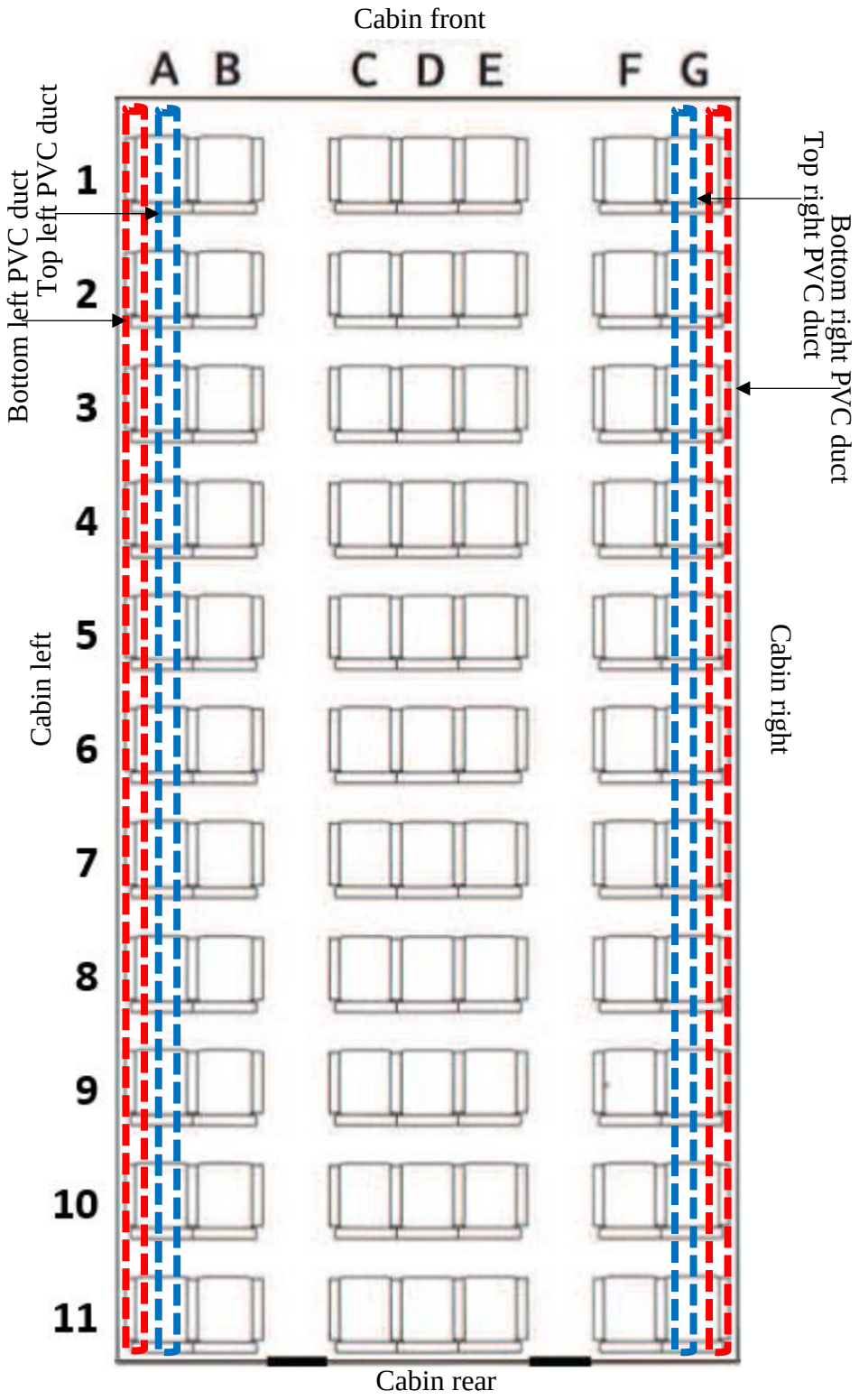

Figure A.1 PVC ducts locations in the Boeing 767 cabin mockup

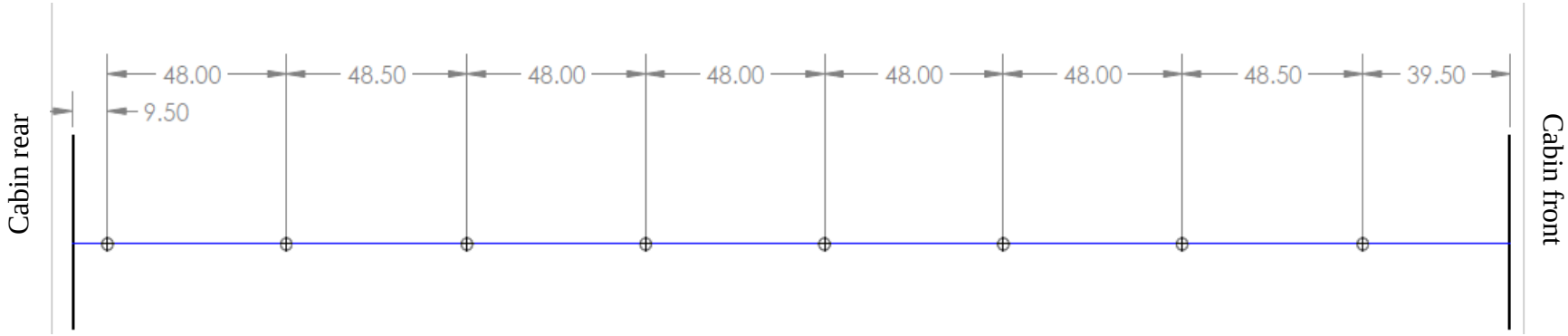

Figure A.2 T-sections locations (in inch) on the top right PVC duct.

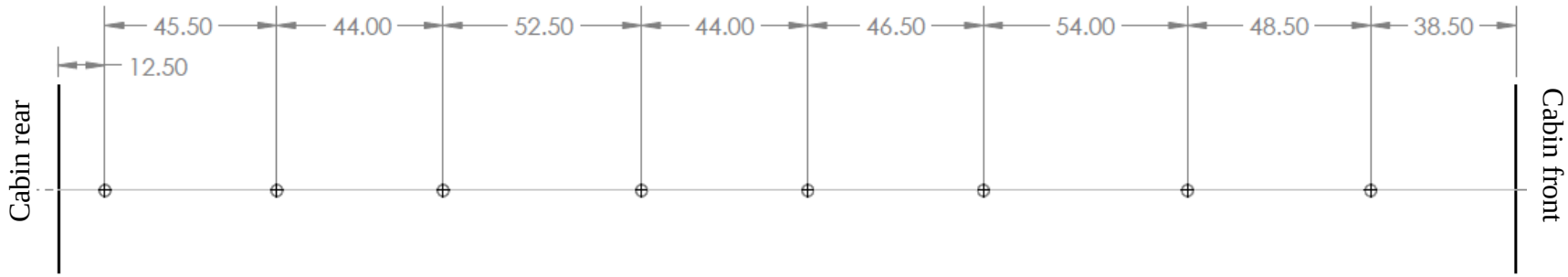

Figure A.3 T-sections locations (in inch) on the top left PVC duct.

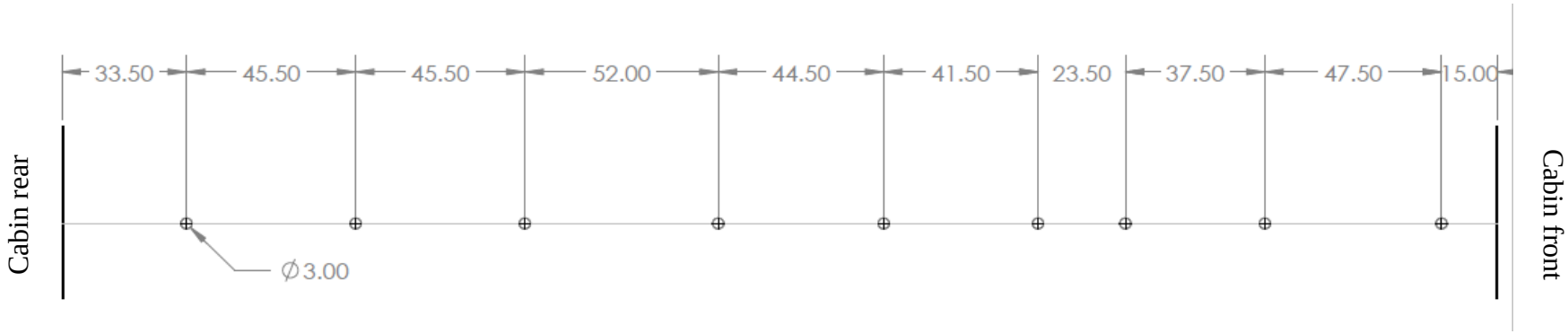

Figure A. 4 T-sections locations (in inch) on the bottom left PVC duct.

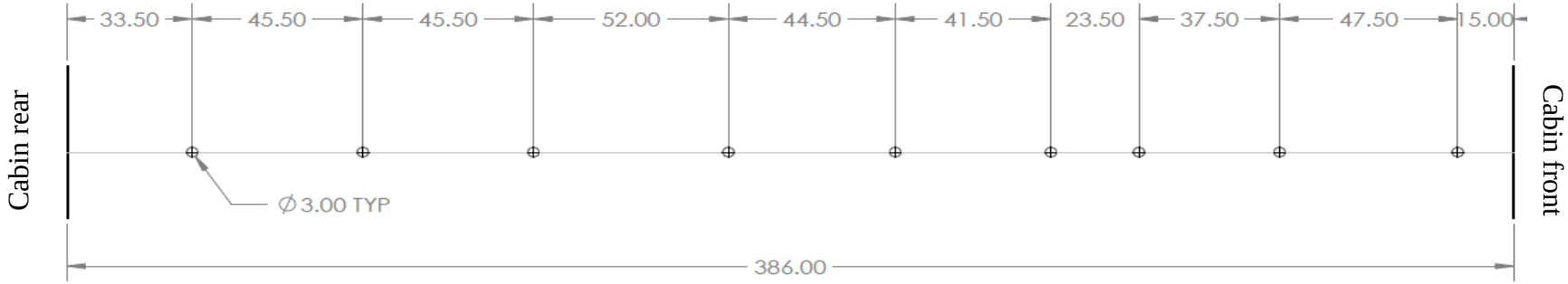

Figure A. 5 T-sections locations (in inch) on the bottom right PVC duct.

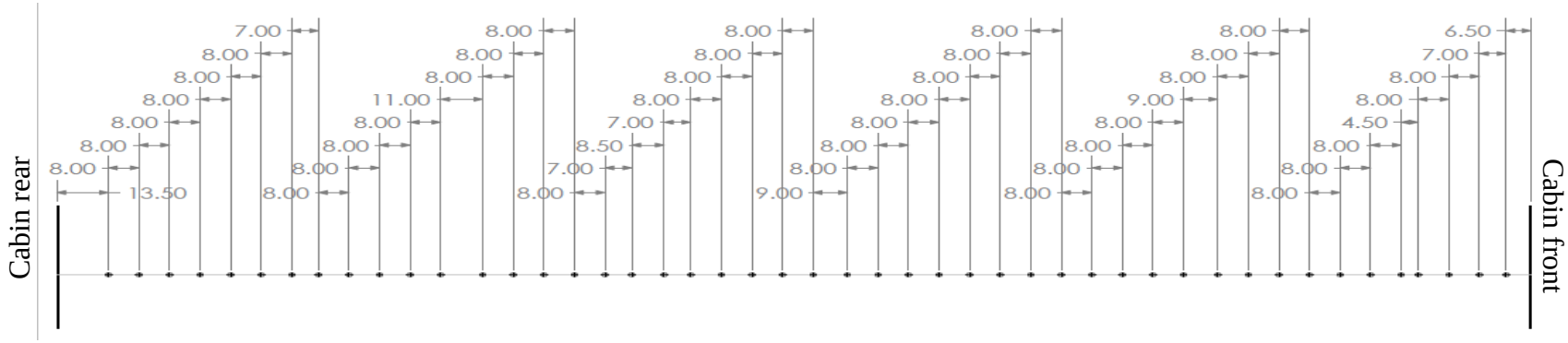
Cabin rear
Cabin front
8.00
8.00
8.00
8.00
8.00
8.00
7.00
13.50
8.00
8.00
8.00
8.00
8.00
8.00
11.00
8.00
8.00
8.00
8.00
8.00
8.00
8.00
7.00
8.50
7.00
8.00
8.00
8.00
8.00
8.00
8.00
8

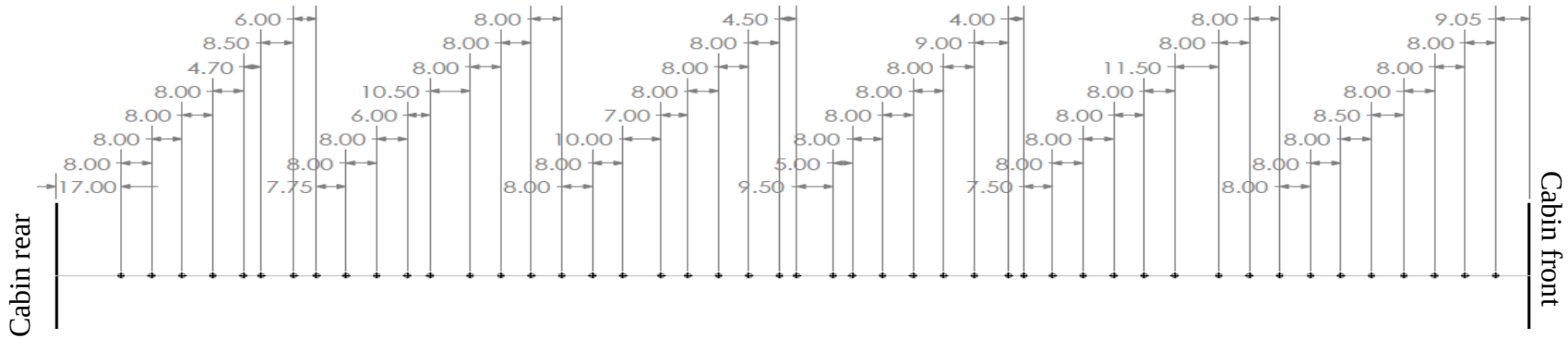

Figure A.7 Diffusers locations (in inch) on the top left PVC duct pipe.

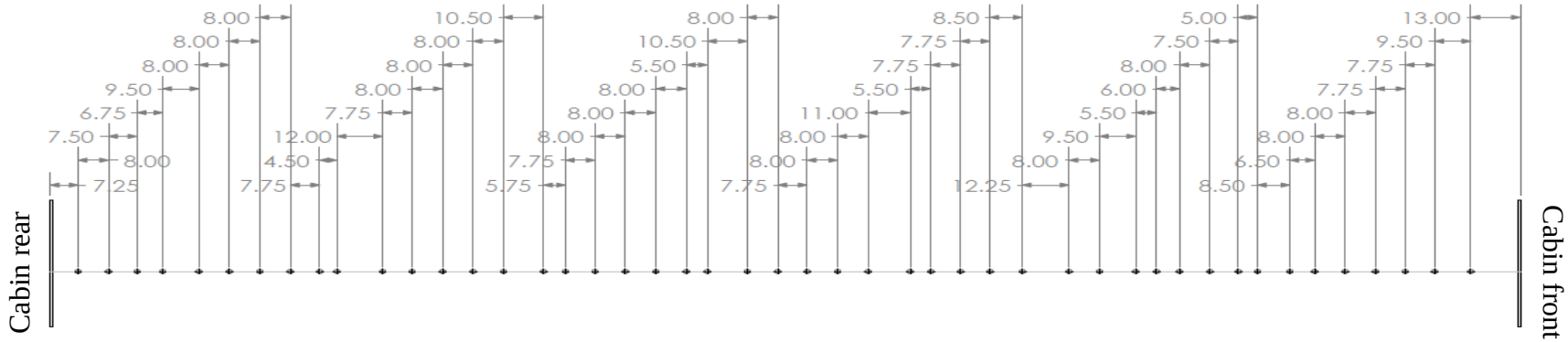

Figure A.8 Diffusers locations (in inch) on the bottom right PVC duct pipe.

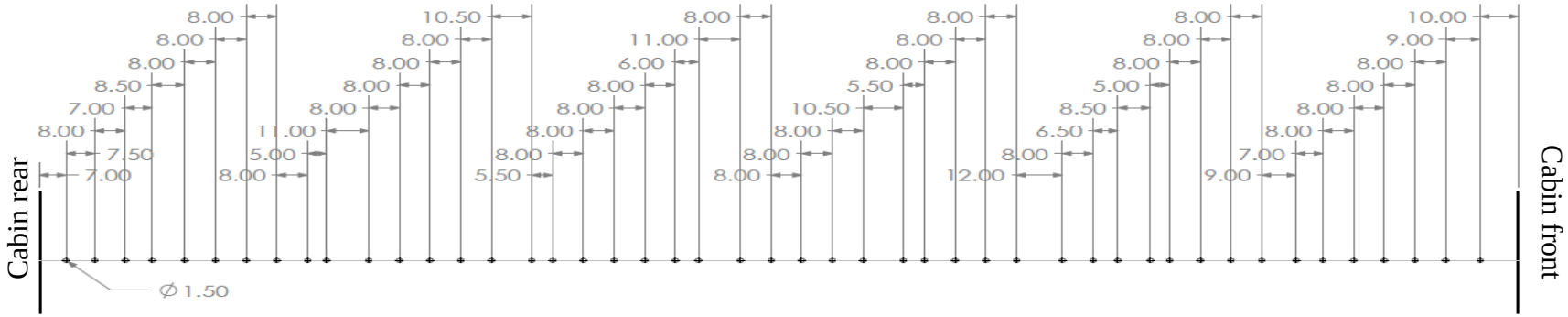

Figure A. 9 Diffusers locations (in inch) on the bottom left PVC duct pipe.

Appendix B - Modified Cabin Design

Appendix B.1 Modified Cabin Diffusers Air Velocity Calculation

From the existing design of the Boeing 767 mockup cabin supply air system:

The linear diffuser width is 0.0127 m and the length is 9.38 m. So,

$$\text{Linear diffuser square area} = \text{Linear diffuser width x Linear diffuser length} = 0.0127 \text{ x } 9.38 = 0.12 \text{ m}^2 \quad (B.1)$$

Also, the air flowrate per linear diffuser is 700 ft^3/min. Hence,

$$\text{Linear diffusers air velocity} = \frac{\text{Air flowrate per diffuser}}{\text{Linear diffuser square area}} = 2.80 \frac{\text{m}}{\text{s}} \quad (B.2)$$

For the modified design:

The PVC duct diameter and length are 0.0762 m and 9.38 m, respectively. In order to have the same velocity in the new diffuser holes, 47 diffuser holes of 0.04 m. diameter each are needed. As shown in equation (B.3), the air coming out of the newly installed diffusers should have a velocity of 2.8 m/s.

$$\text{Total holes area per one PVC duct} = 3.14 \text{ x} \left(\frac{\text{Hole diameter}}{2}\right)^2 \text{ x Number of holes} = 0.06 \text{ m}^2 \quad (B.3)$$

The air flowrate per PVC duct is ¼ the total air flowrate to the cabin since it will be divided equally to 4 PVC ducts. Hence, the air flowrate at each PVC duct is 350 ft^3/min.

$$\text{Air velocity in each hole} = \frac{\text{Air flowrate per PVC duct}}{\text{Total holes area per PVC duct}} = 2.80 \frac{\text{m}}{\text{s}} \quad (B.3)$$

Appendix B.2 Modified Cabin Diffusers Air Velocity Measurements

It is expected that the actual velocity in the diffusers of the modified cabin to be different than the designed value. This is due to the pressure drop through the PVC duct in addition to the existence of the T-sections between the PVC duct sections. Hence, a complete velocity measurement for every single diffuser hole was conducted in order to adjust the velocities as much as possible by controlling the air flowrate through the connections to the diffusers. For the figures in this section of the appendix, the following notations are used:

Table B.2.1 Notations used in the figures of Appendix B. 2

Notation	Interpretation
Vertical green lines	Location of T-sections on the PVC duct
Red line	Mean value of the readings
Inclined blue dotted line	Curve-fit of the readings

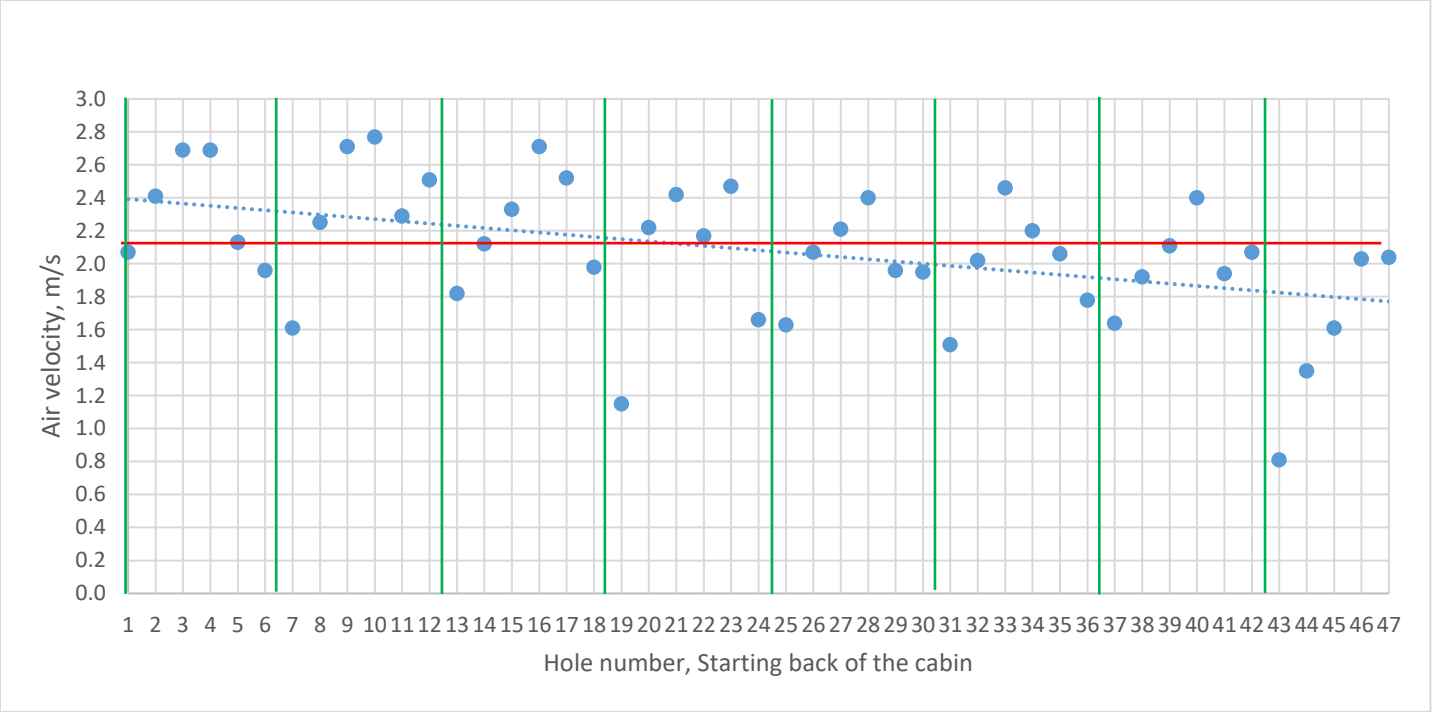

Figure B.2. 1 Measured diffusers air velocity in the top right PVC duct.

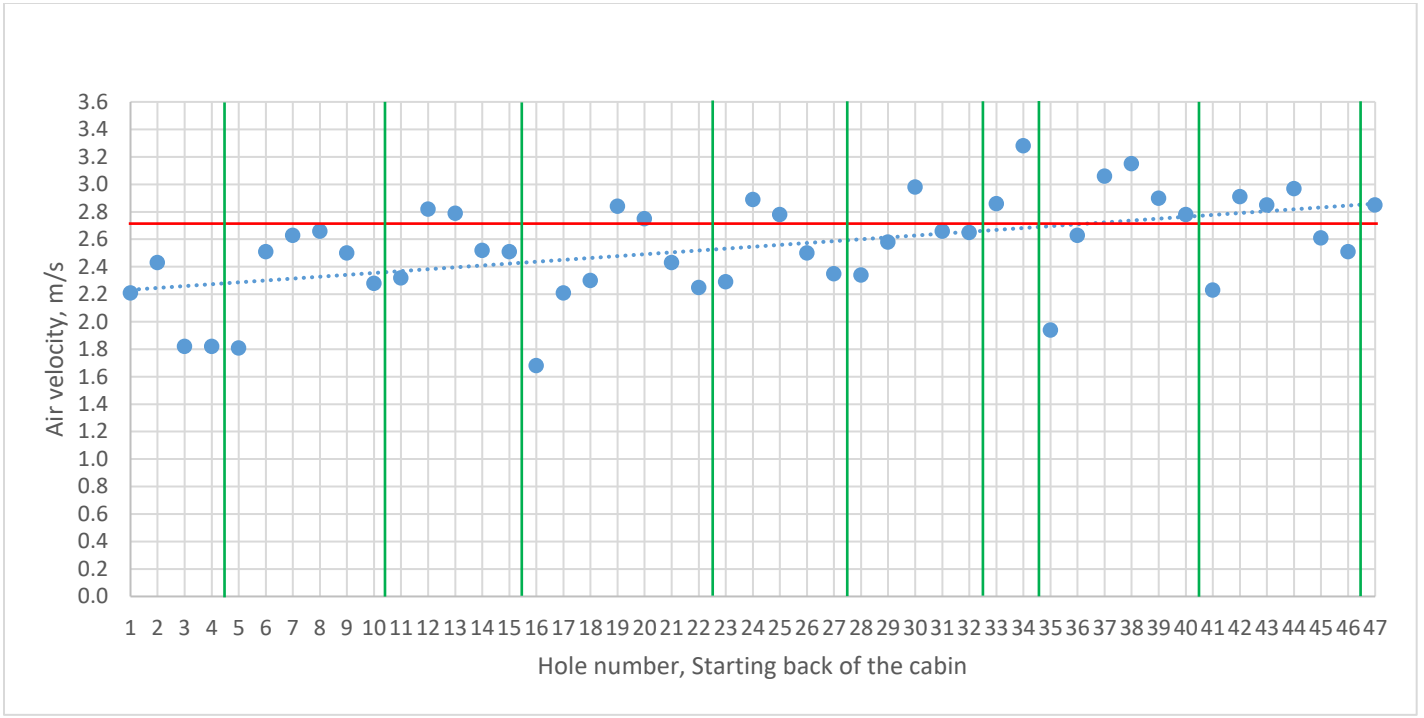

Figure B.2. 2 Measured diffusers air velocity in the bottom right PVC duct.

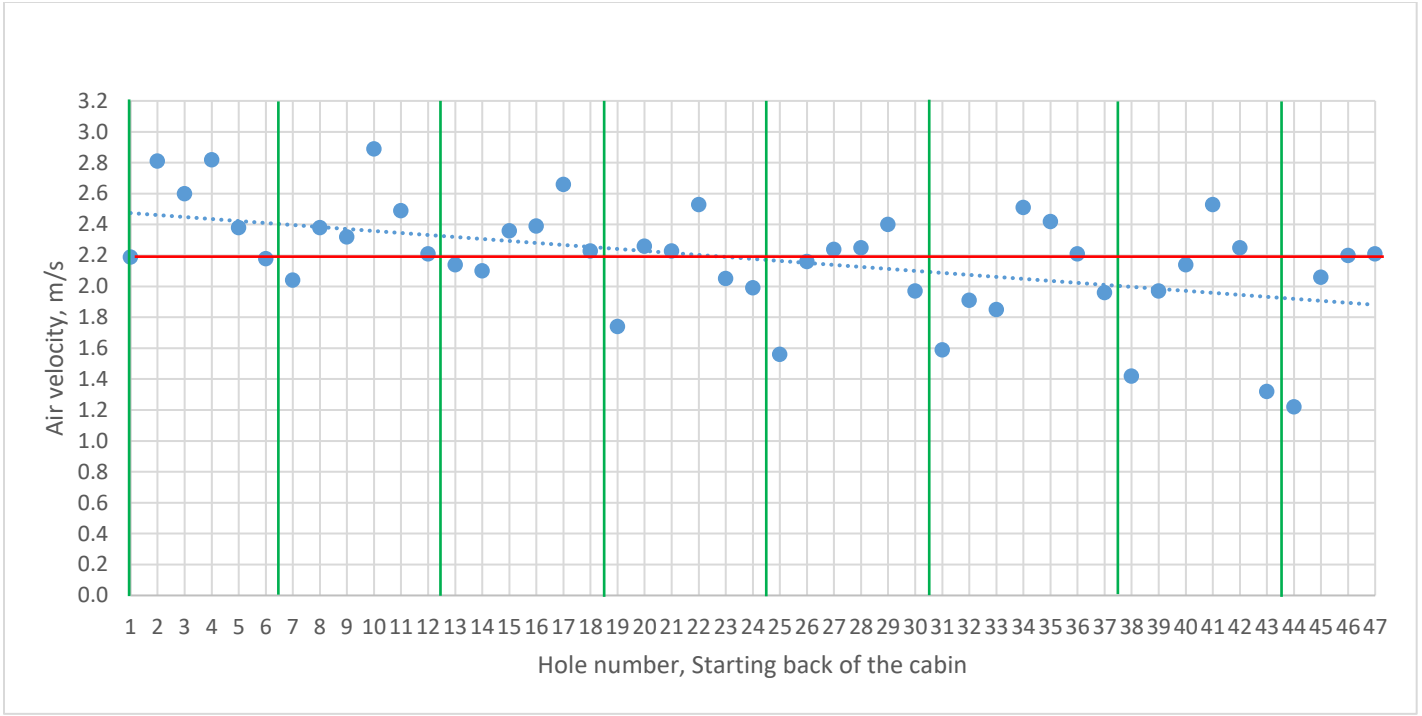

Figure B.2. 3 Measured diffusers air velocity in the top left PVC duct.

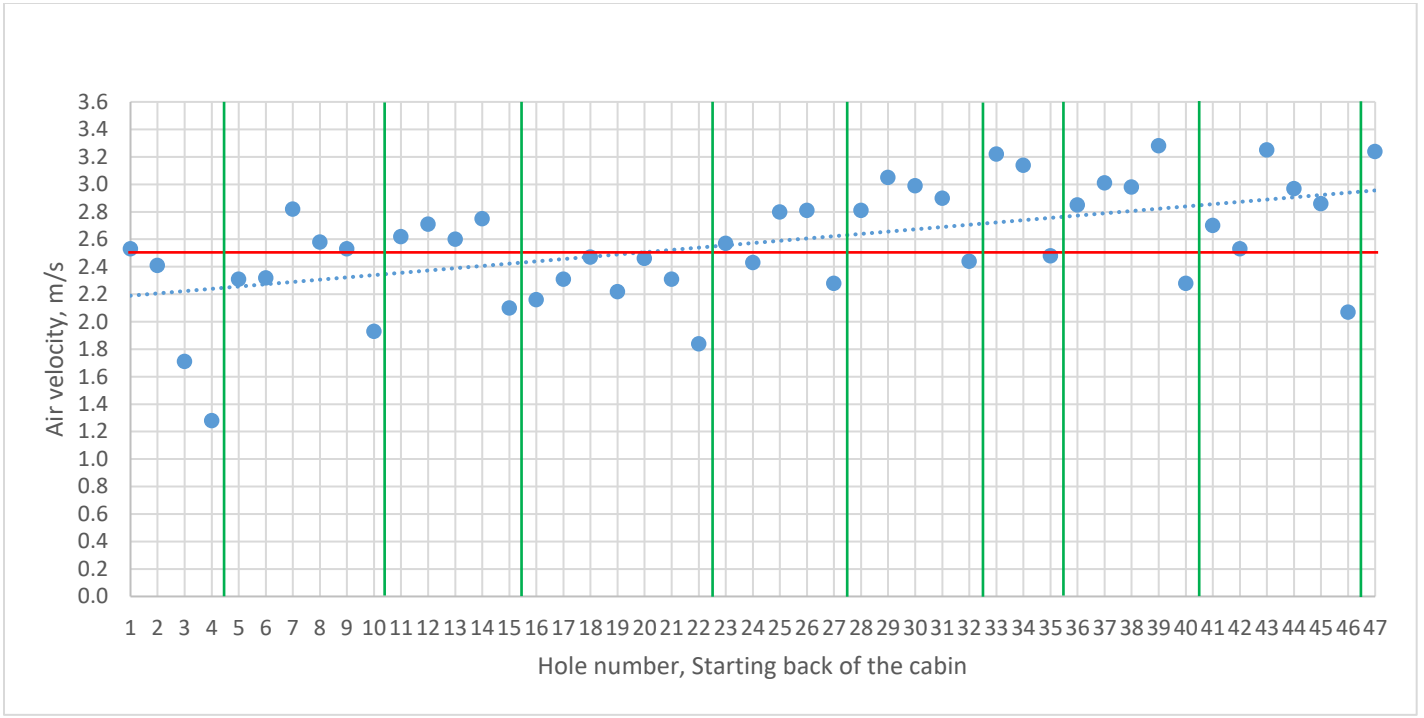

Figure B.2. 4 Measured diffusers air velocity in the bottom left PVC duct.

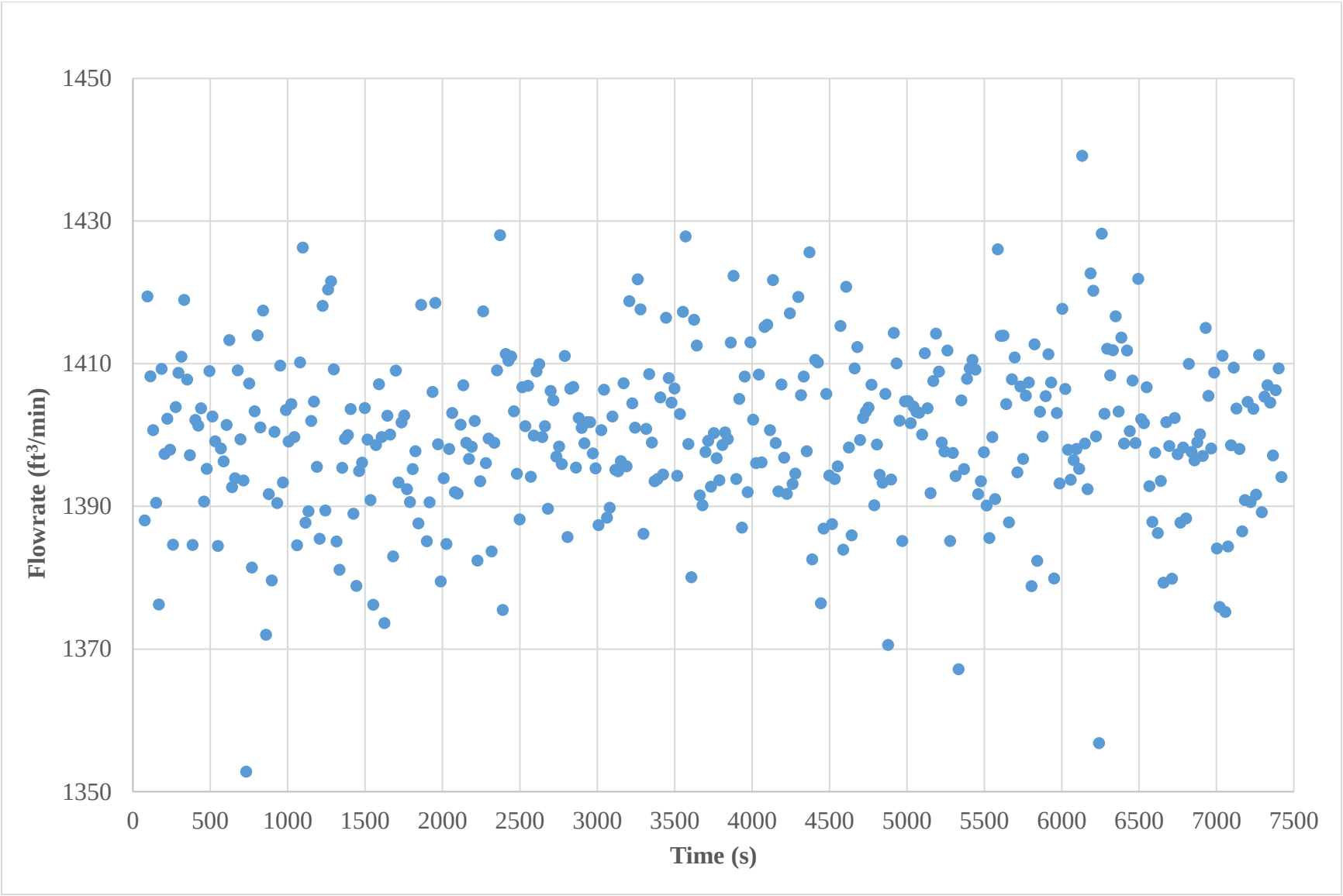

Figure B.2.5 Main duct supply air flowrate versus time in the Boeing 767 and modified cabins.

Appendix C - Boeing 767 ISOPass Undeployed Continuous Injection Results

Notes about this appendix:

- The positive direction is the one pointing from the source to the sampling tree solenoid valves block in the tests conducted with a longitudinal or a diagonal sampling tree directions.
- The positive direction was taken as the right direction from the source in the tests performed with a lateral sampling tree direction similar to a typical coordinate system.
- The letter "B" after the test number indicates that the test was done in the Boeing 767 mockup cabin and the letter "I" indicates that it was done using a continuous injection source.
- The sampling tree is a metal rod that has 4 ports controlled by solenoid valves. The measurements are collected sequentially from each of the ports. The tree is connected to a single gas analyzer to measure the concentration of the tracer gas from the opened port.
- The solenoid valves block is marked by a dashed line crossing the sampling tree.
- In addition to the sampling tree, additional tracer gas analyzers are placed in the cabin to collect measurements at the cabin supply air, injection source seat, and other locations of interest.
- The tracer gas analyzers are not of the same model or calibration and hence, the accuracy of the readings is not identical. For the tracer gas measurements accuracy, refer to chapter 4.4. Uncertainty Analysis of this dissertation.

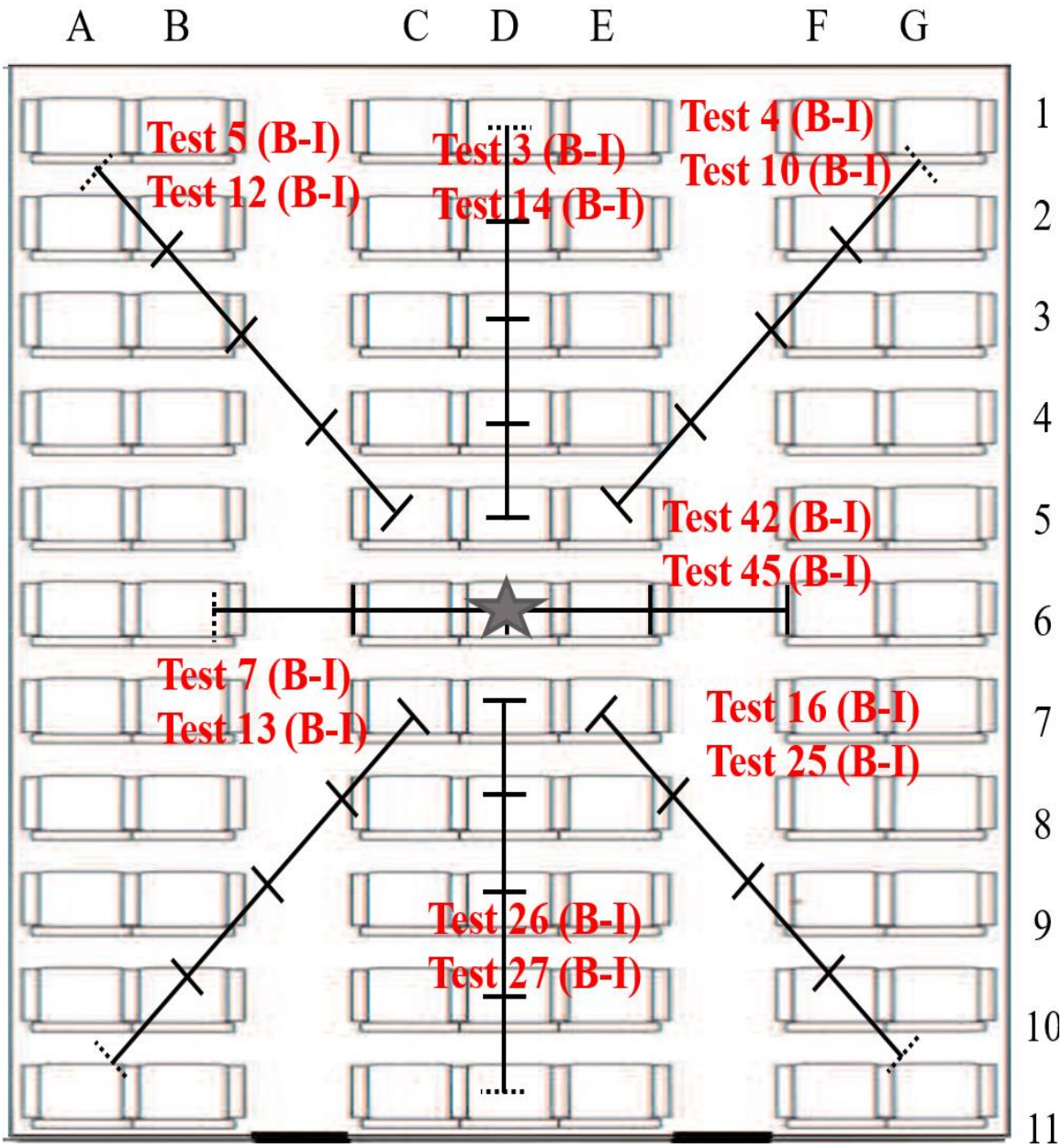

Figure C.1 Seat D6 ISOPass undeployed continuous injection tracer gas test numbers and sampling tree orientations in the Boeing 767 cabin mockup.

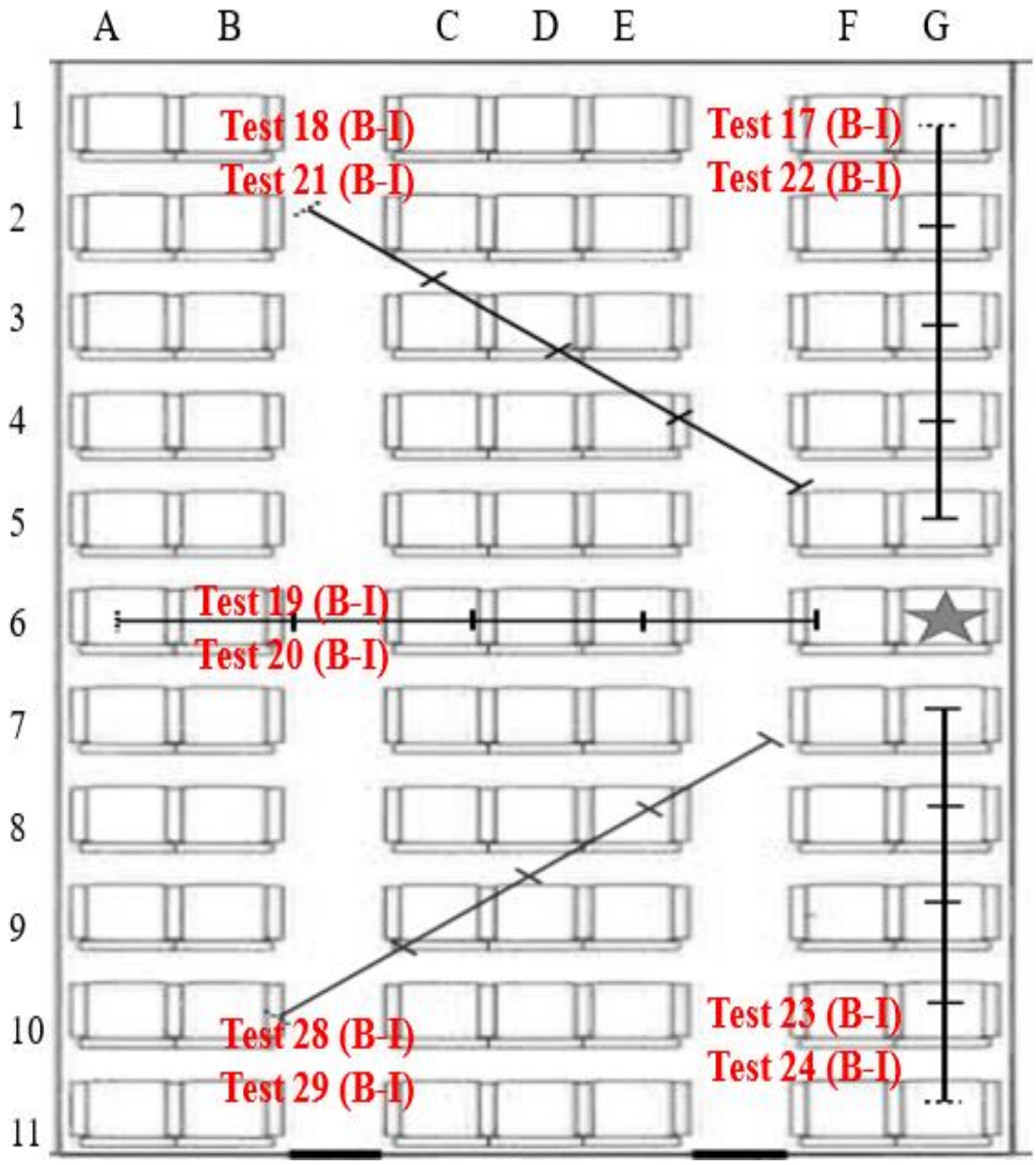

Figure C.2 Seat G6 ISOPass undeployed continuous injection tracer gas test numbers and sampling tree orientations in the Boeing 767 cabin mockup.

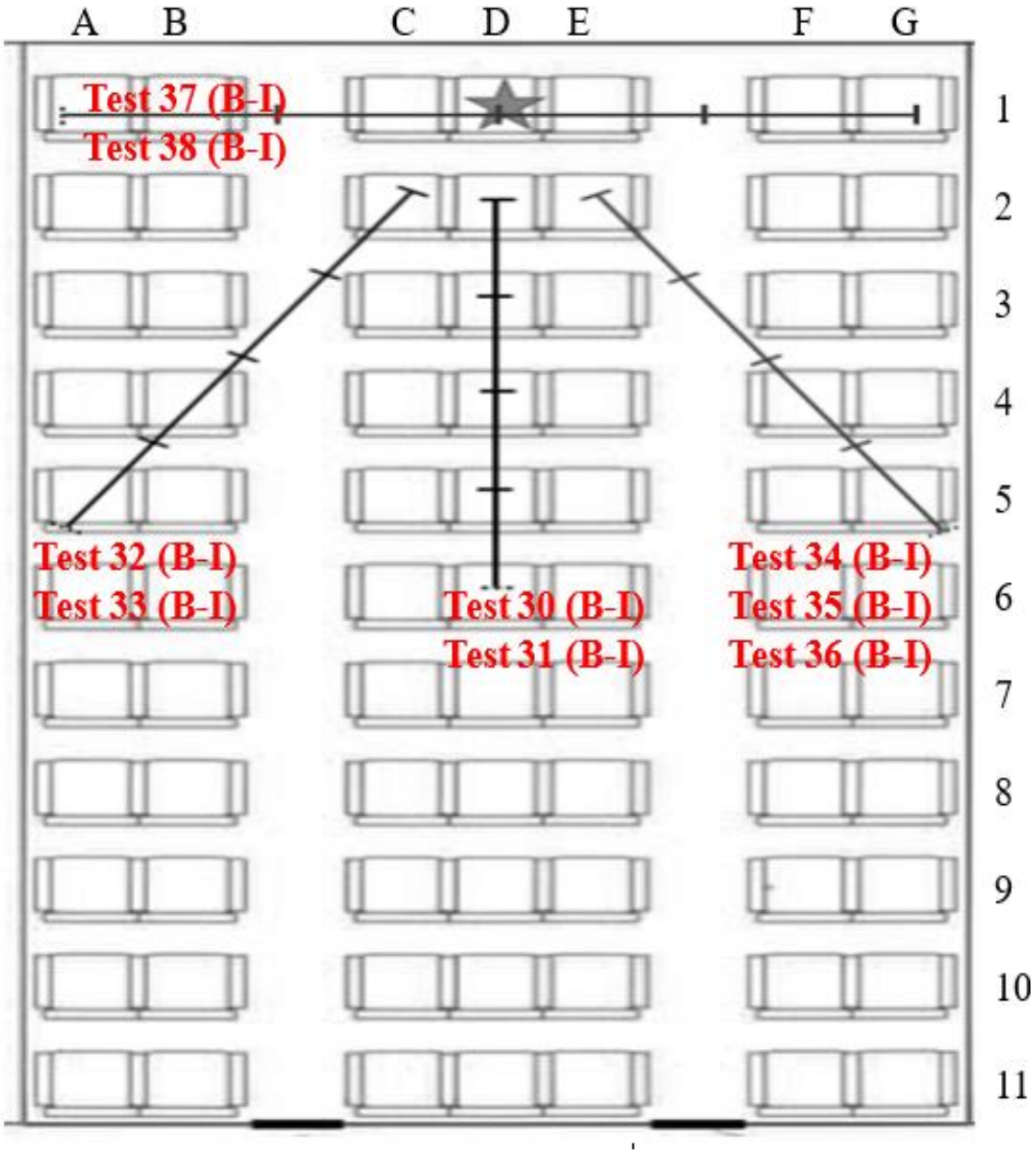

Figure C.3 Seat D1 ISOPass undeployed continuous injection tracer gas test numbers and sampling tree orientations in the Boeing 767 cabin mockup.

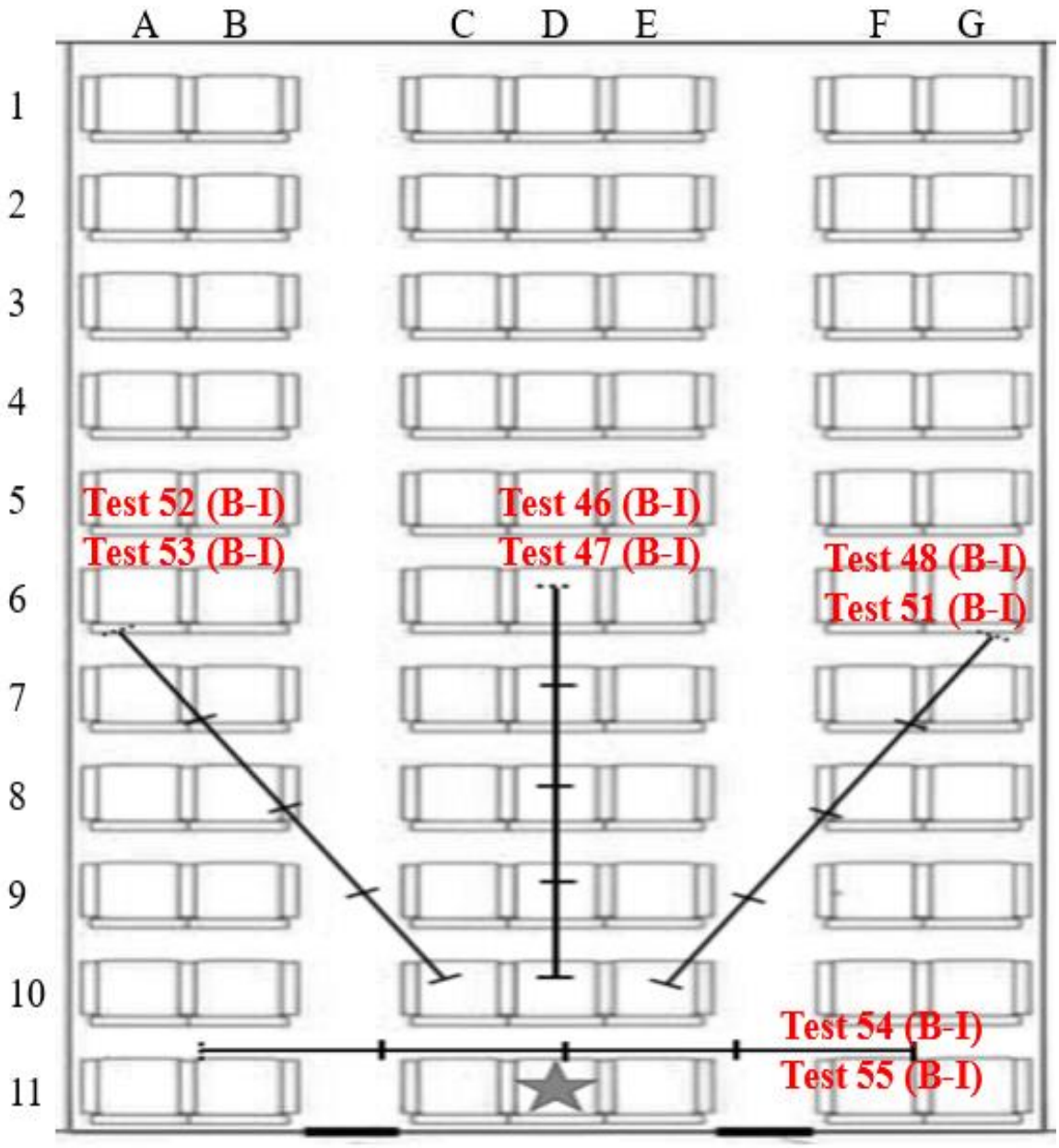

Figure C.4 Seat D11 ISOPass undeployed continuous injection tracer gas test numbers and sampling tree orientations in the Boeing 767 cabin mockup.

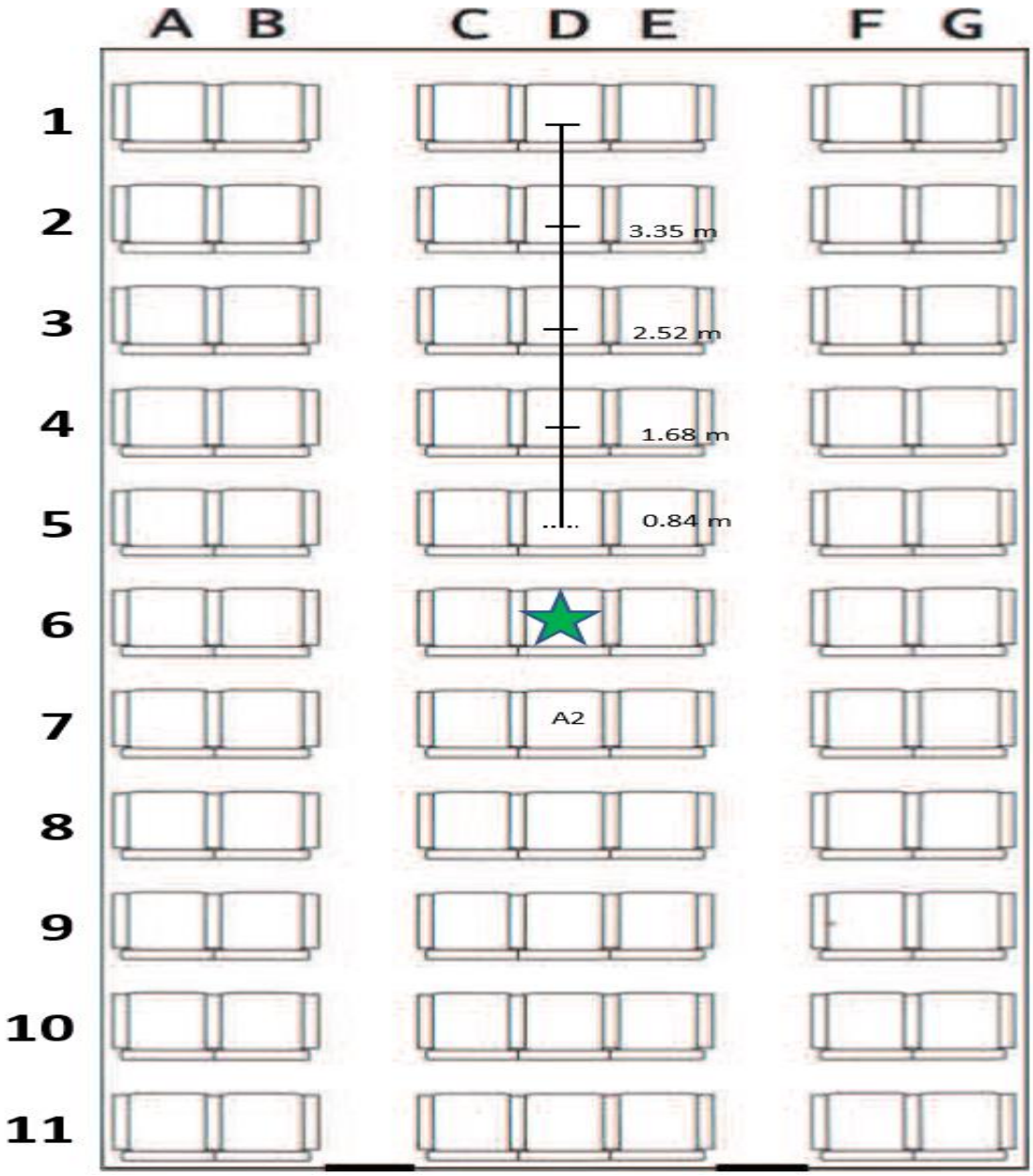

Figure C.5 Test 3 (B-I) ISOPass undeployed source location and sampling tree orientation.

Note: In this test, the solenoid block on the sampling tree was located next to the source as indicated by the dashed line. This was done in order to check if the block would have an effect on the dispersed tracer gas. Hence, in Figure C.6, the concentration of the tracer gas on the sampling tree decreases away from the source. Also, the positive direction is still considered to be from the source to the solenoid block.

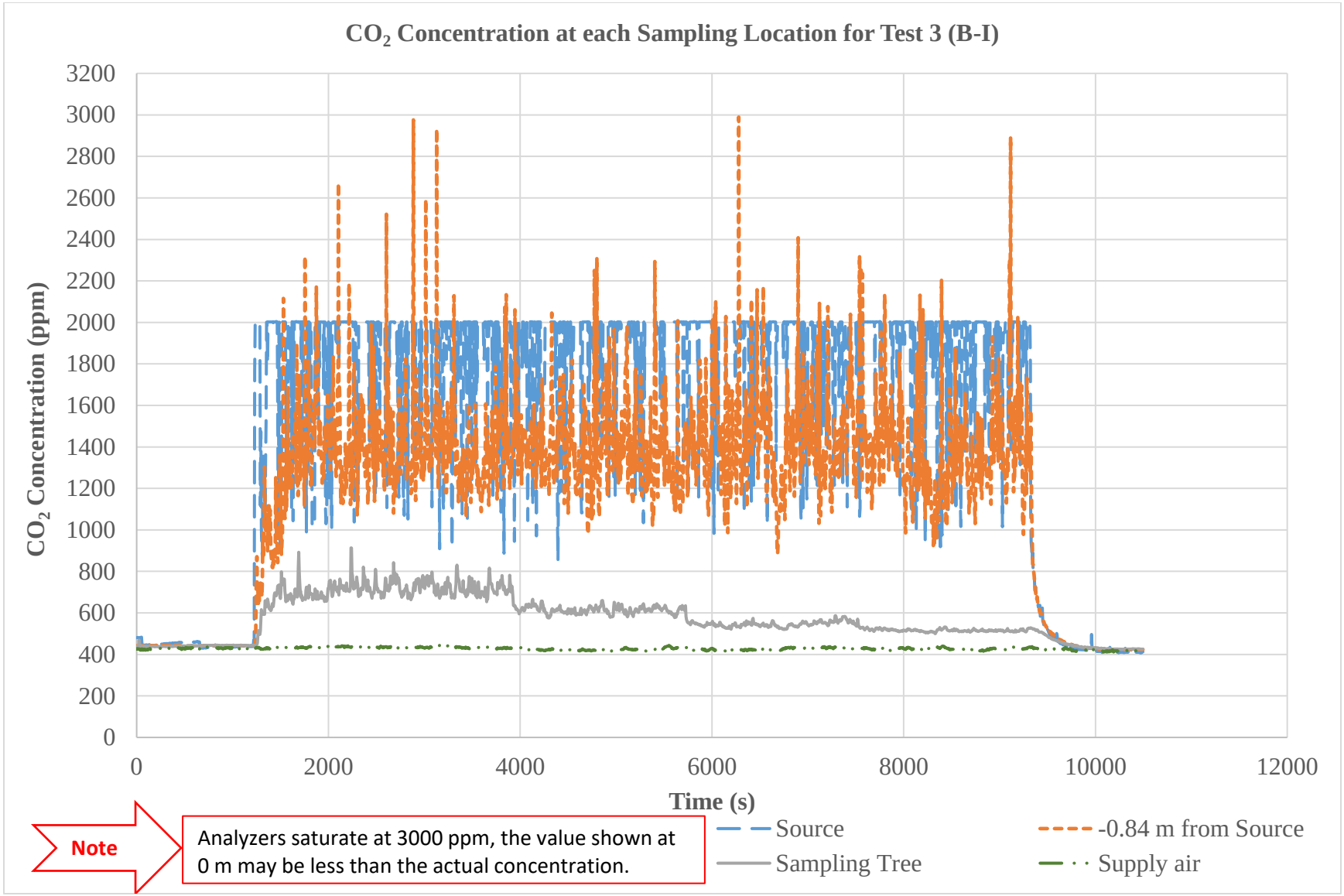

Figure C.6 Ininstantaneous CO_2 concentration at each sampling location for Test 3 (B-I) ISOPass undeployed.

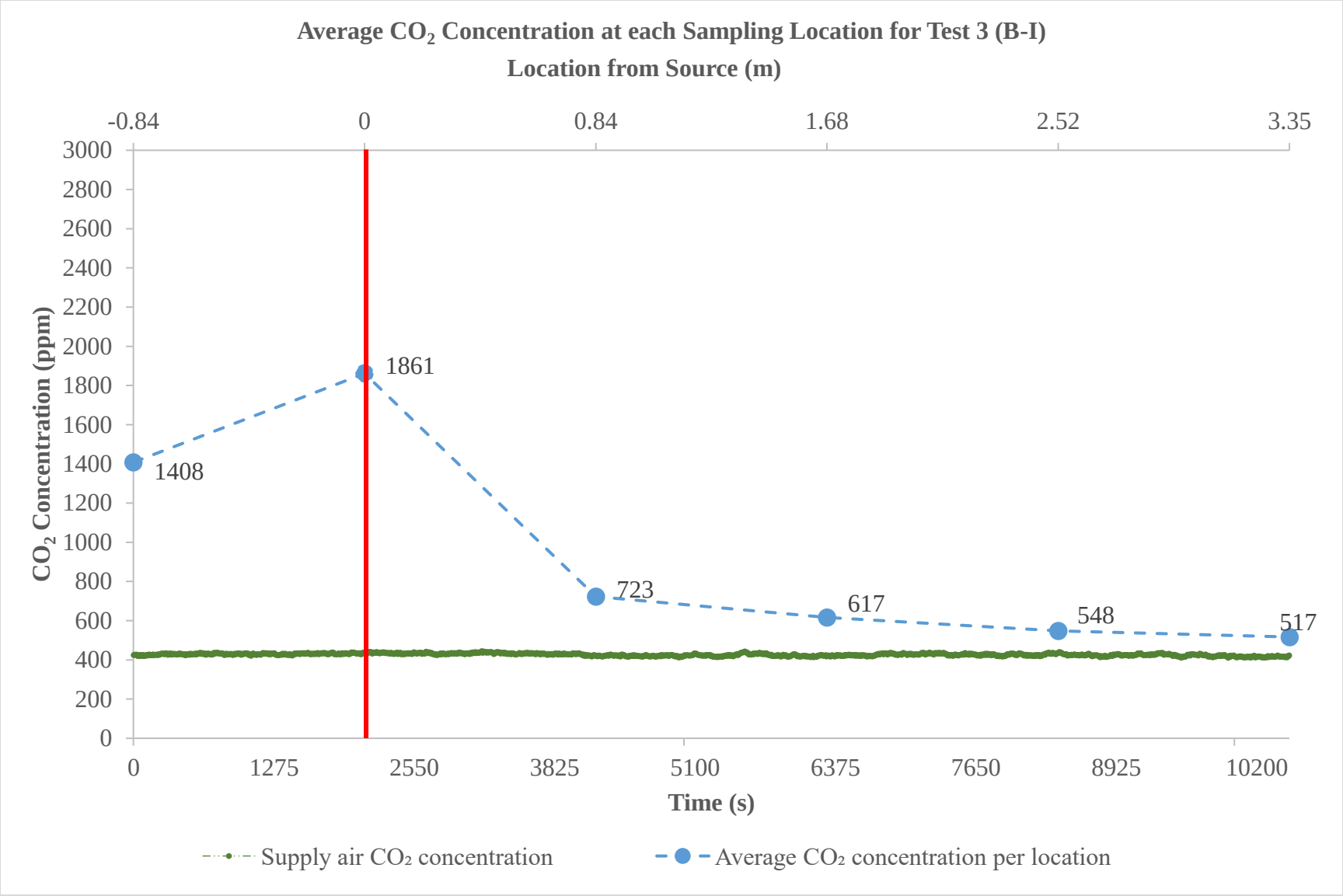

Figure C.7 Average CO_2 concentration at each sampling location for Test 3 (B-I) ISOPass undeployed.

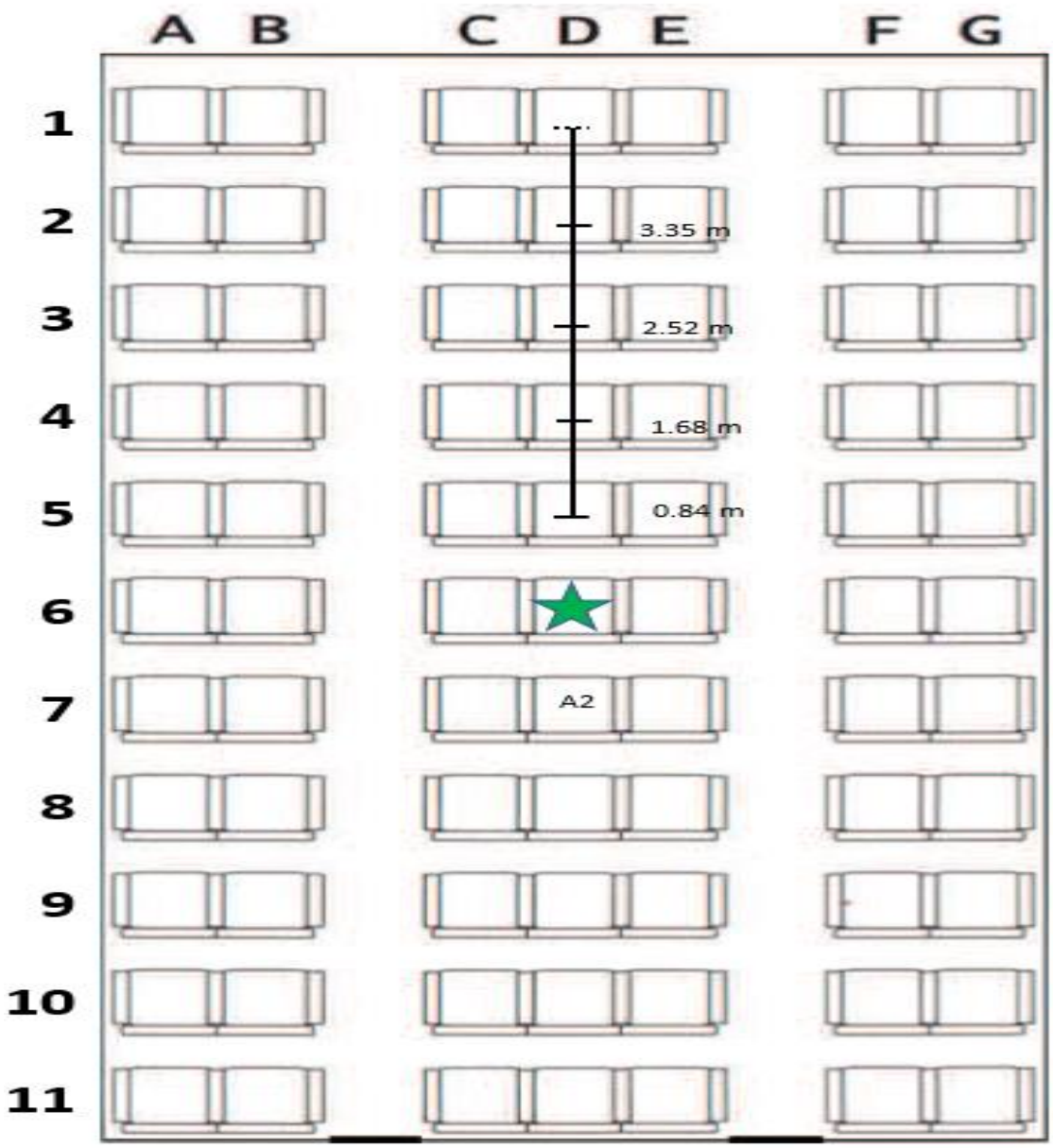

Figure C.8 Test 14 (B-I) ISOPass undeployed source location and sampling tree orientation.

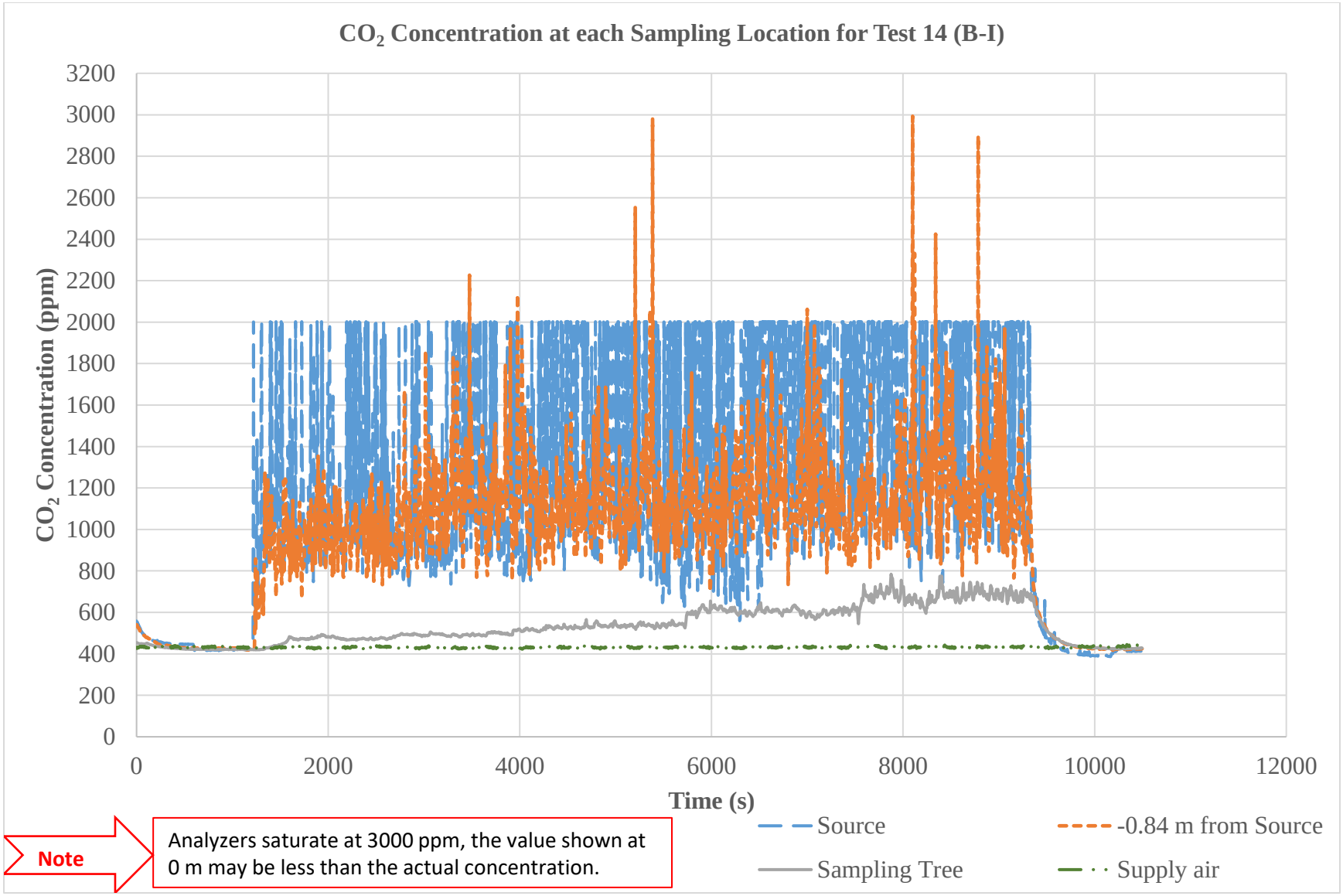

Figure C.9 Ininstantaneous CO_2 concentration at each sampling location for Test 14 (B-I) ISOPass undeployed.

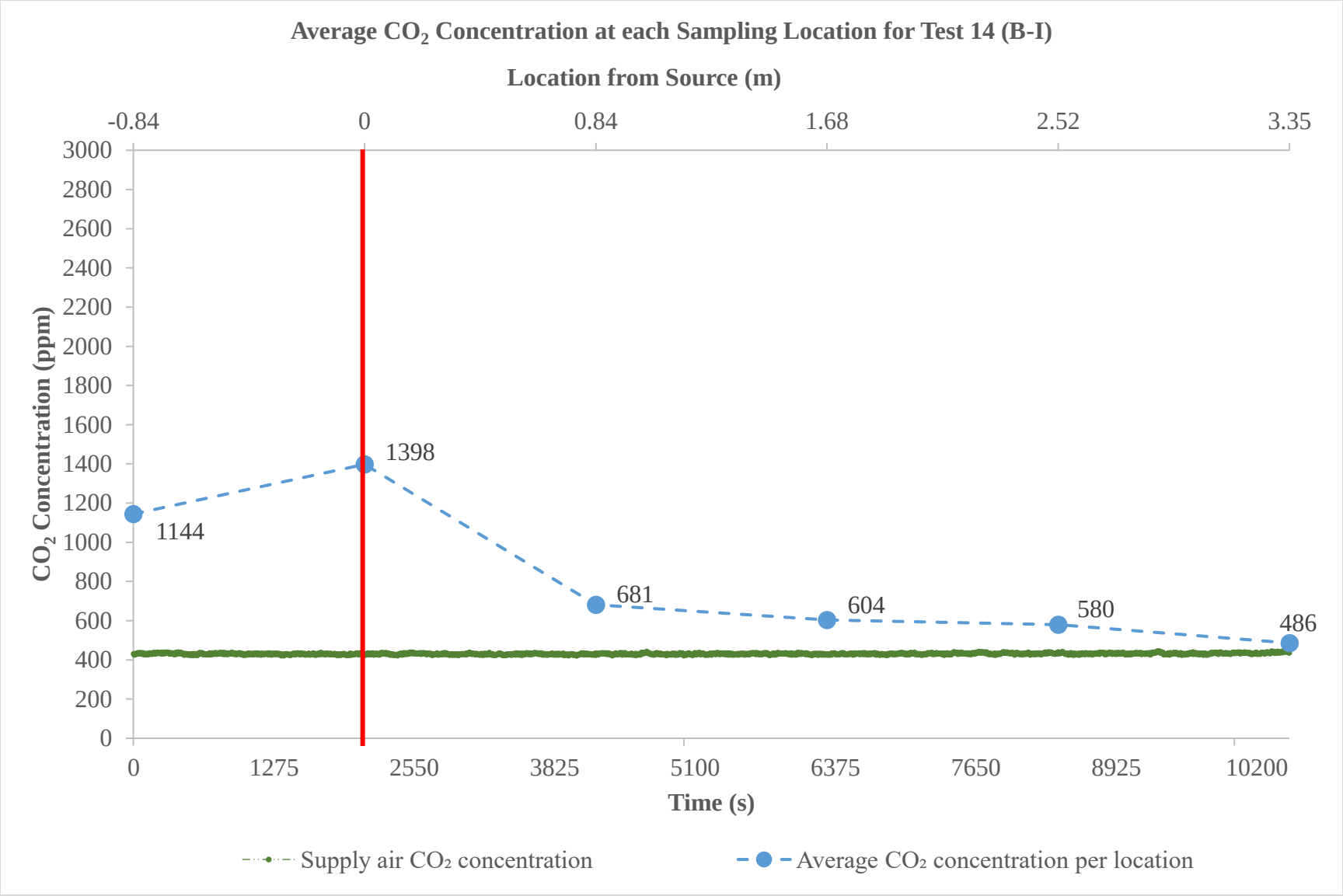

Figure C.10 Average CO_2 concentration at each sampling location for Test 14 (B-I) ISOPass undeployed.

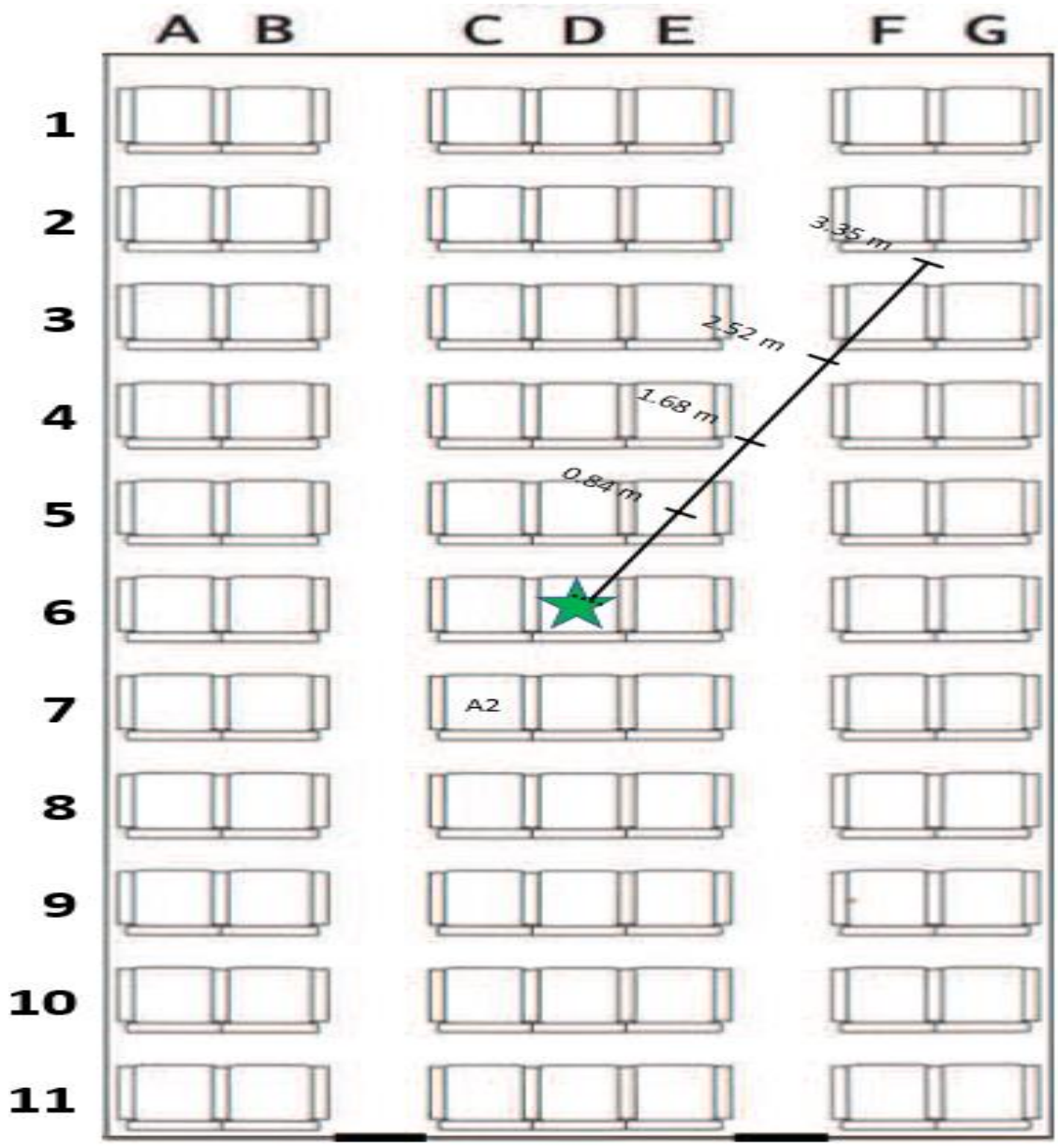

Figure C.11 Test 4 (B-I) ISOPass undeployed source location and sampling tree orientation.

Note: In this test, the solenoid block on the sampling tree was located next to the source as indicated by the dashed line. This was done in order to check if the block would have an effect on the dispersed tracer gas. Hence, in Figure C.6, the concentration of the tracer gas on the sampling tree decreases away from the source. Also, the positive direction is still considered to be from the source to the solenoid block.

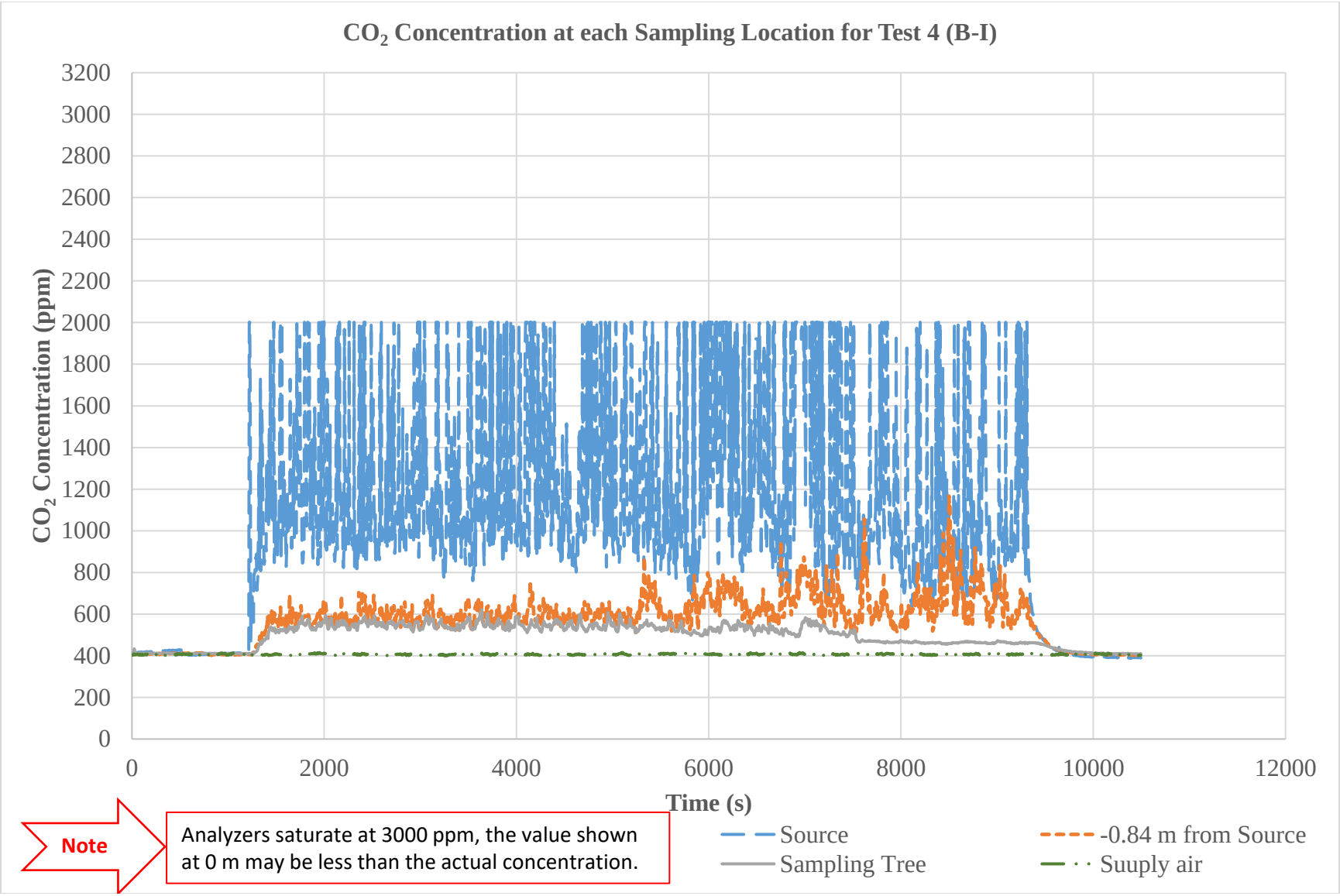

Figure C.12 Ininstantaneous CO_2 concentration at each sampling location for Test 4 (B-I) ISOPass undeployed.

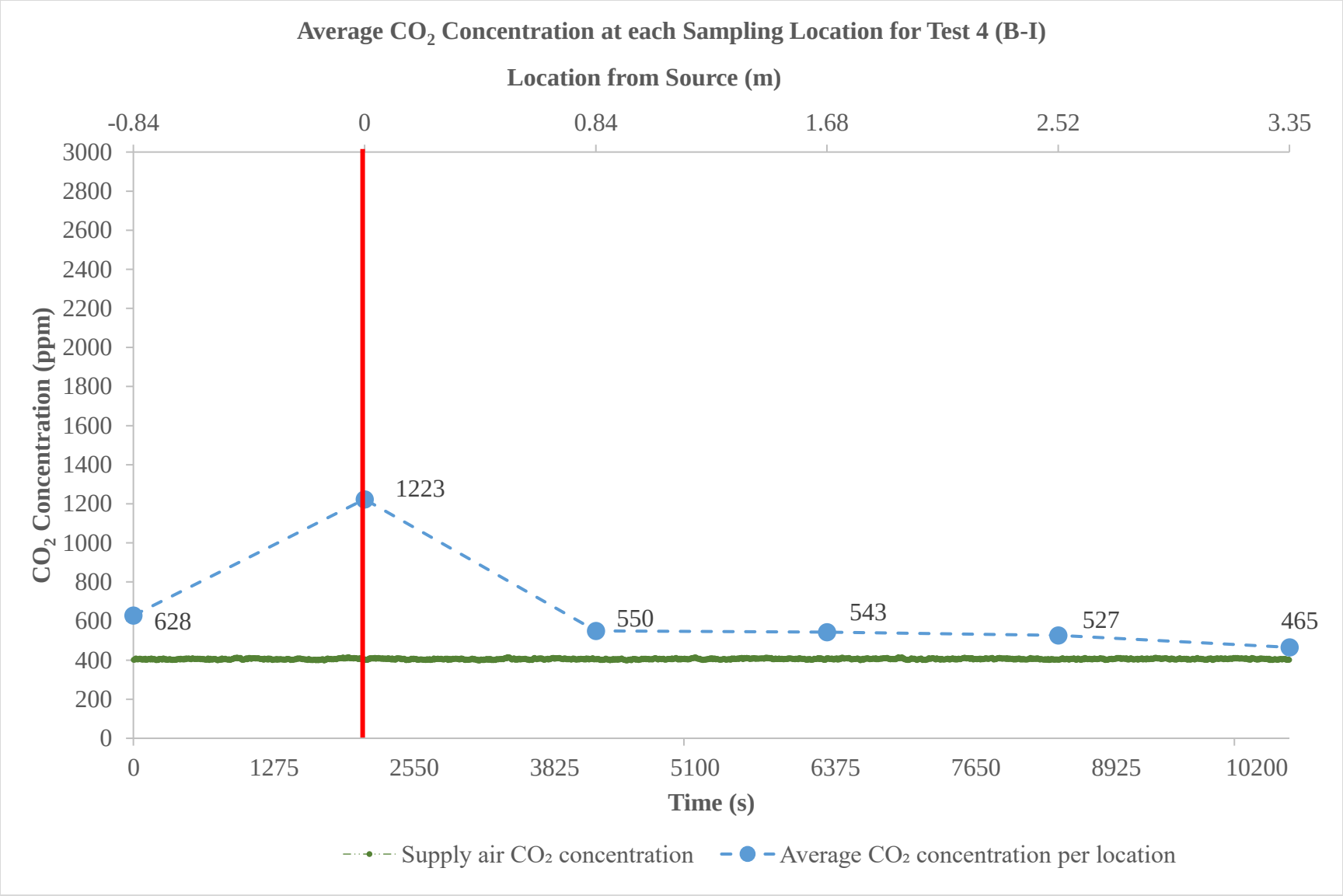

Figure C.13 Average CO_2 concentration at each sampling location for Test 4 (B-I) ISOPass undeployed.

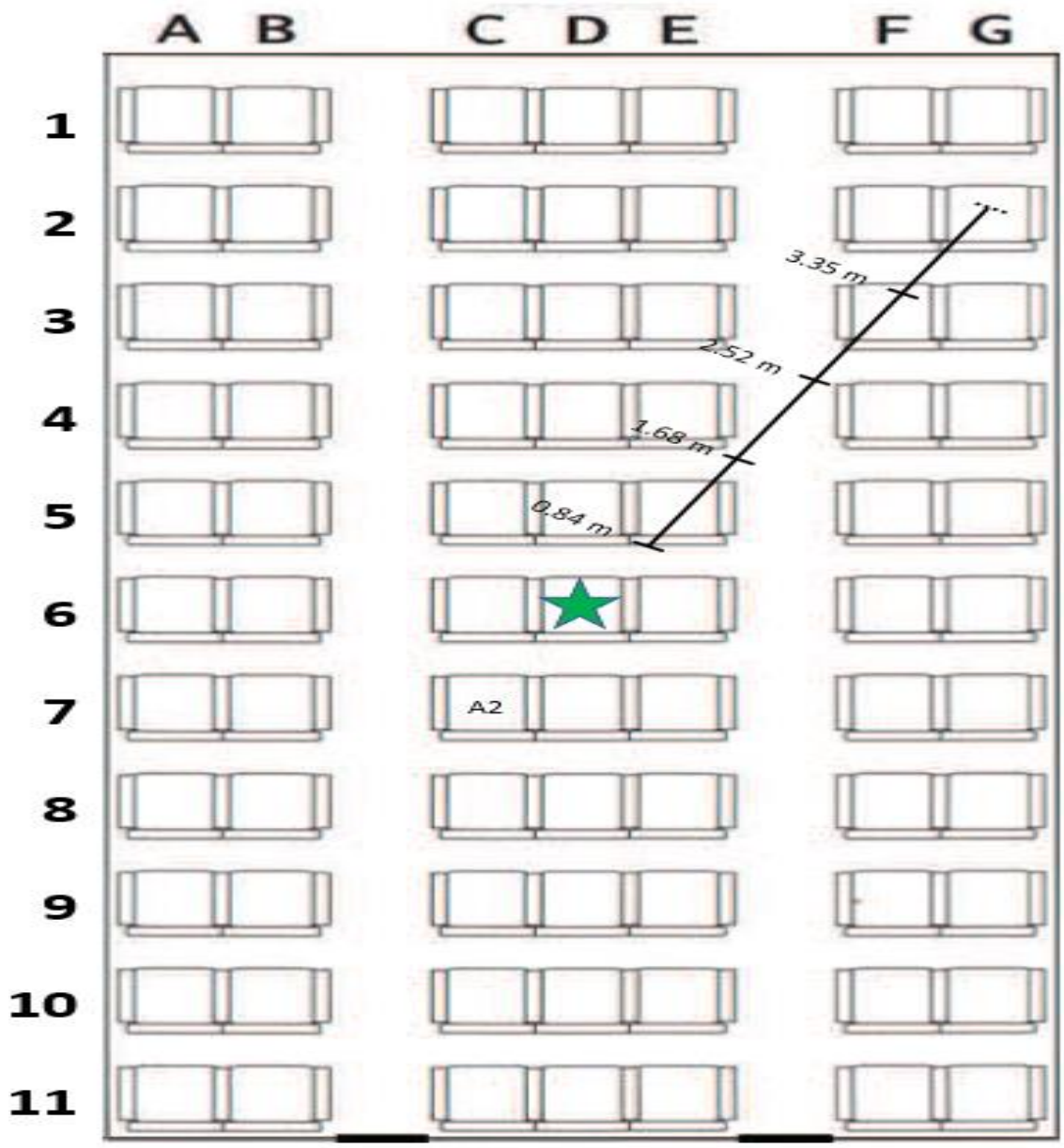

Figure C.14 Test 10 (B-I) ISOPass undeployed source location and sampling tree orientation.

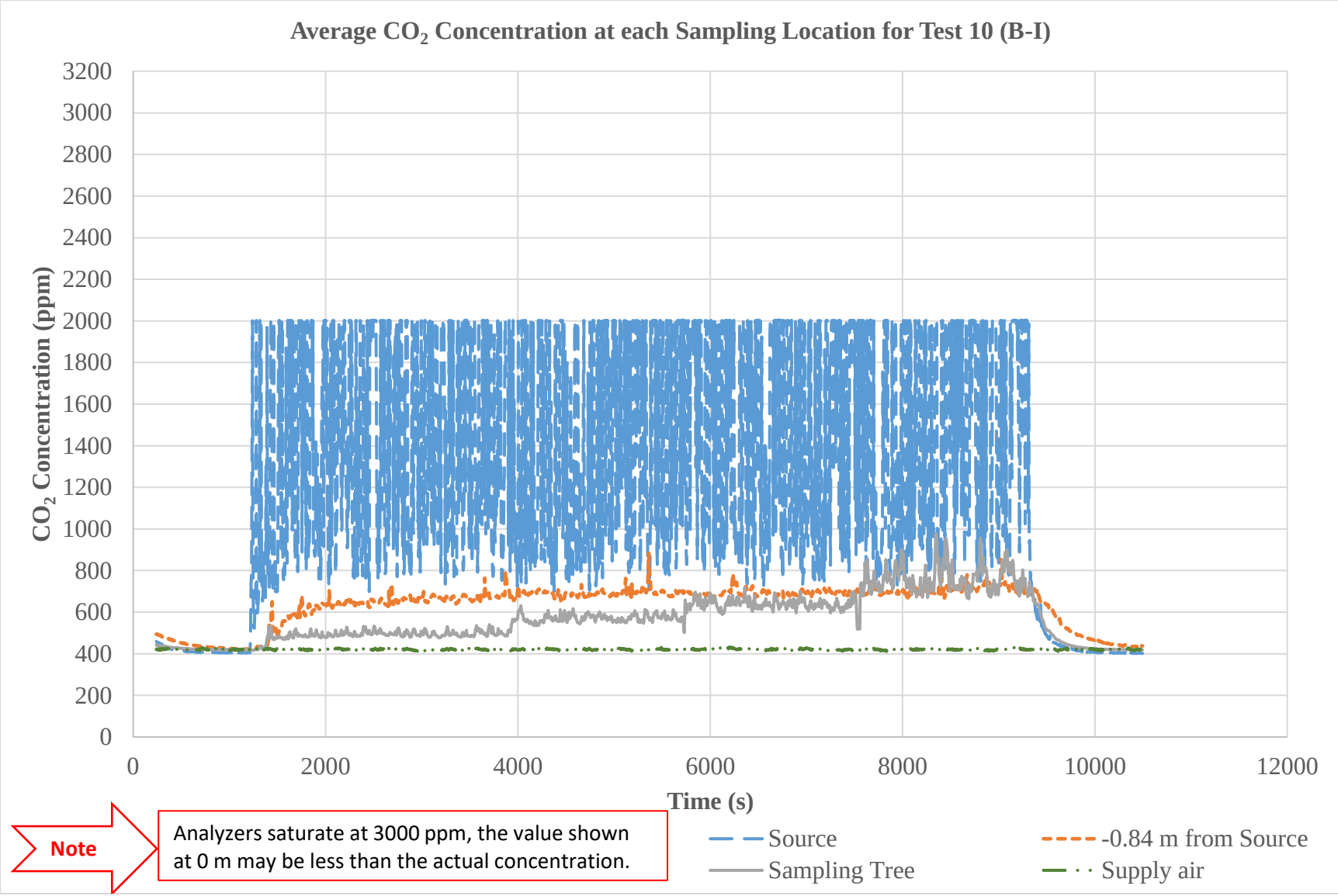

Figure C.15 Ininstantaneous CO_2 concentration at each sampling location for Test 10 (B-I) ISOPass undeployed.

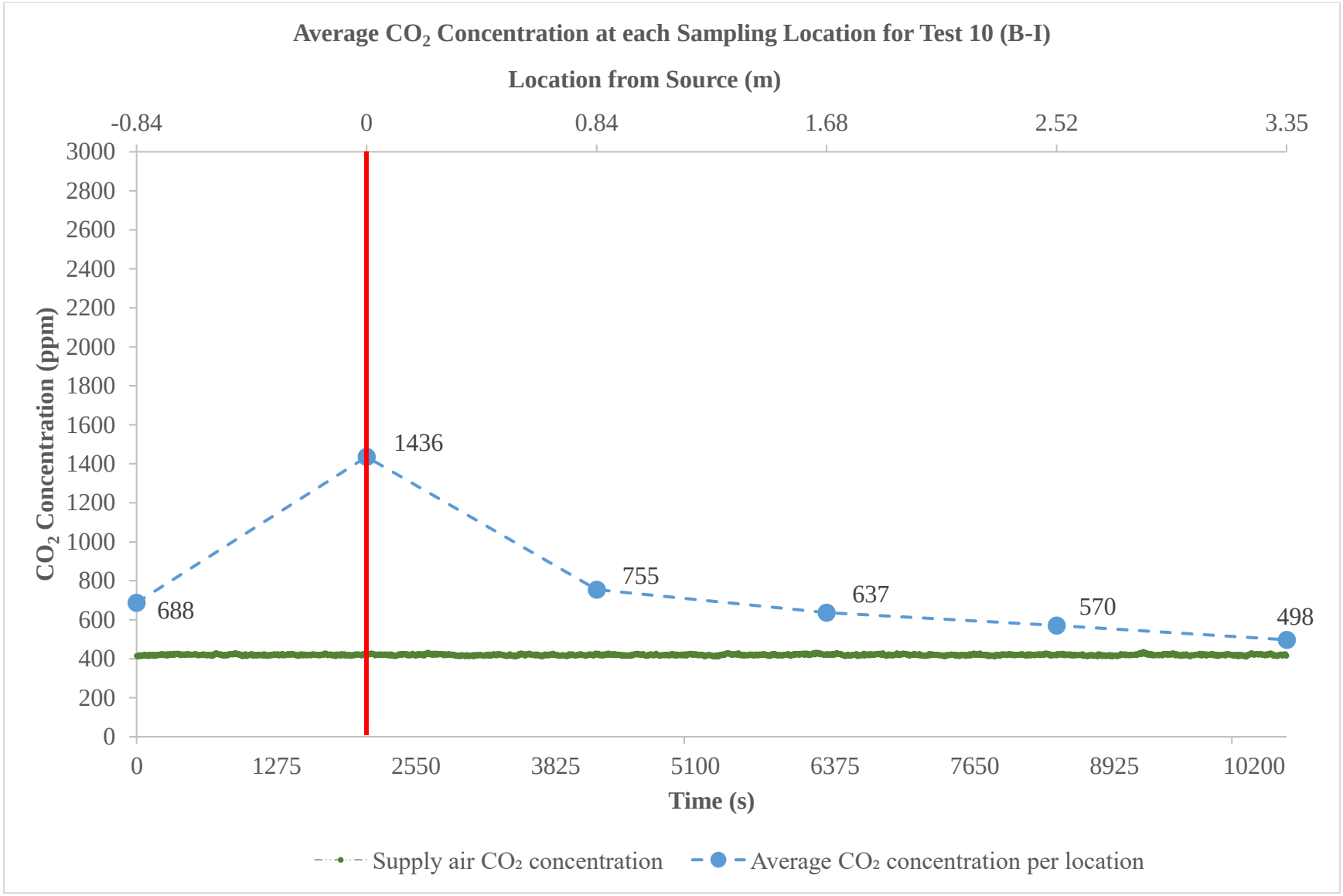

Figure C.16 Average CO_2 concentration at each sampling location for Test 10 (B-I) ISOPass undeployed.

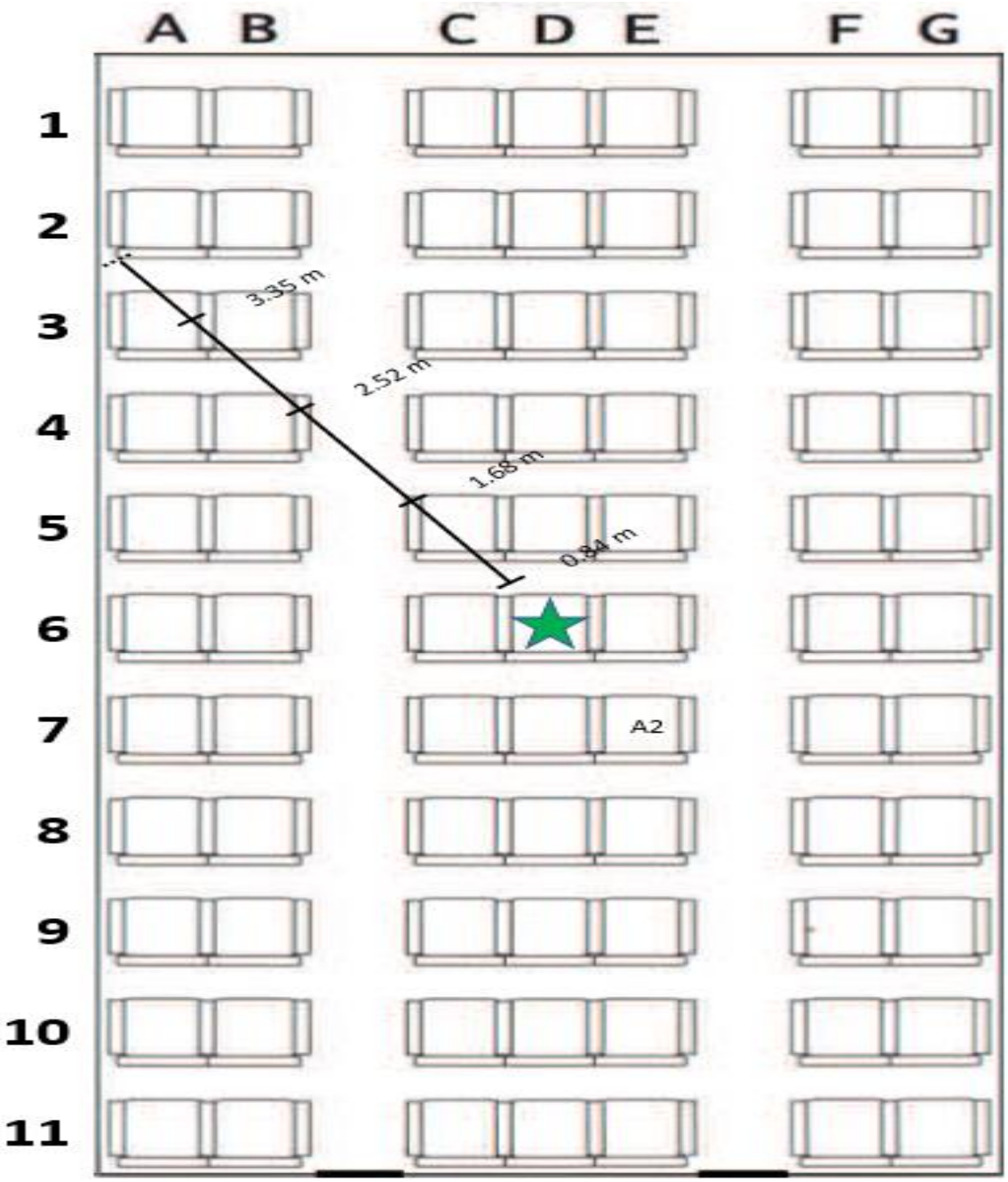

Figure C.17 Test 5 (B-I) ISOPass undeployed source location and sampling tree orientation.

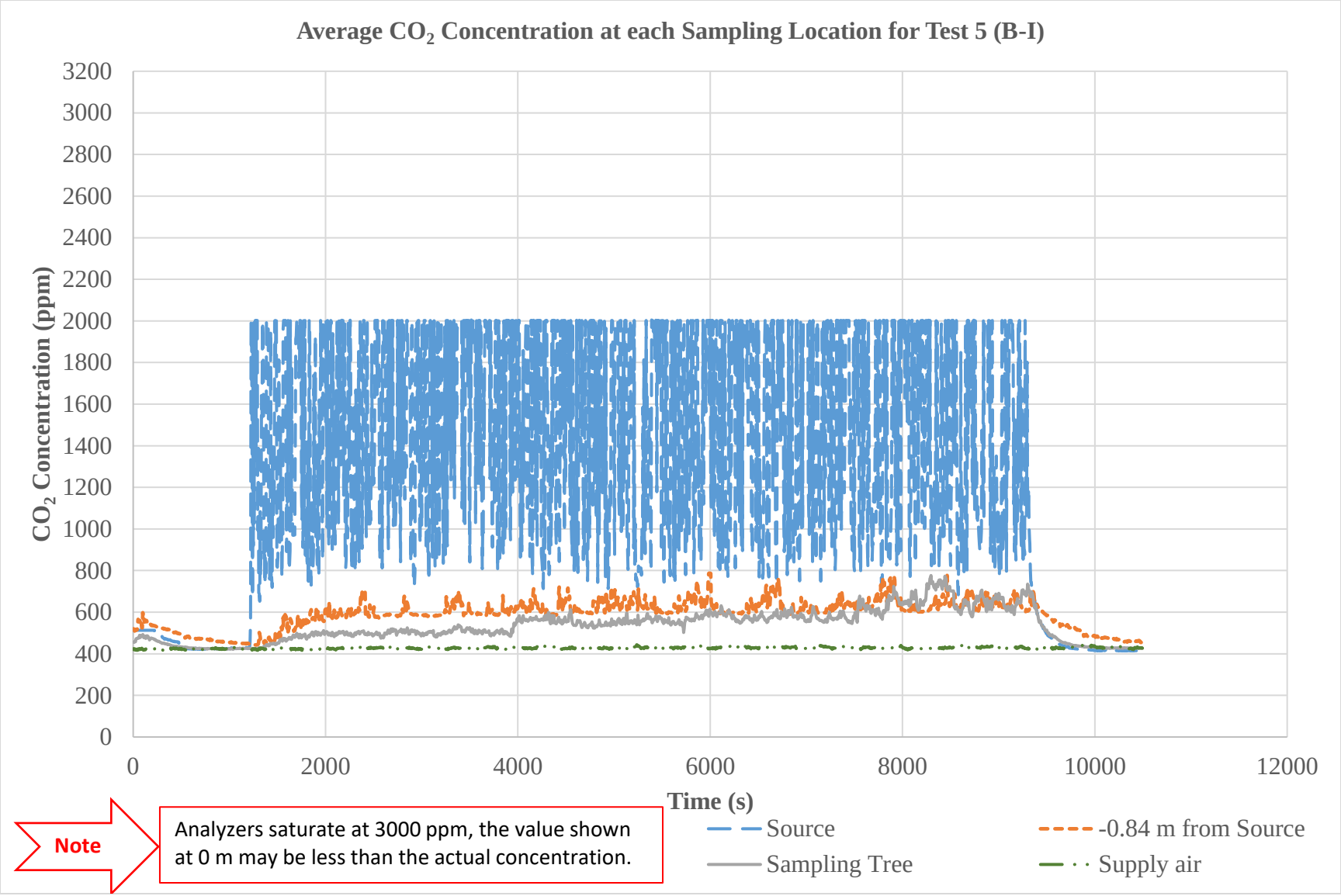

Figure C.18 Ininstantaneous CO_2 concentration at each sampling location for Test 5 (B-I) ISOPass undeployed.

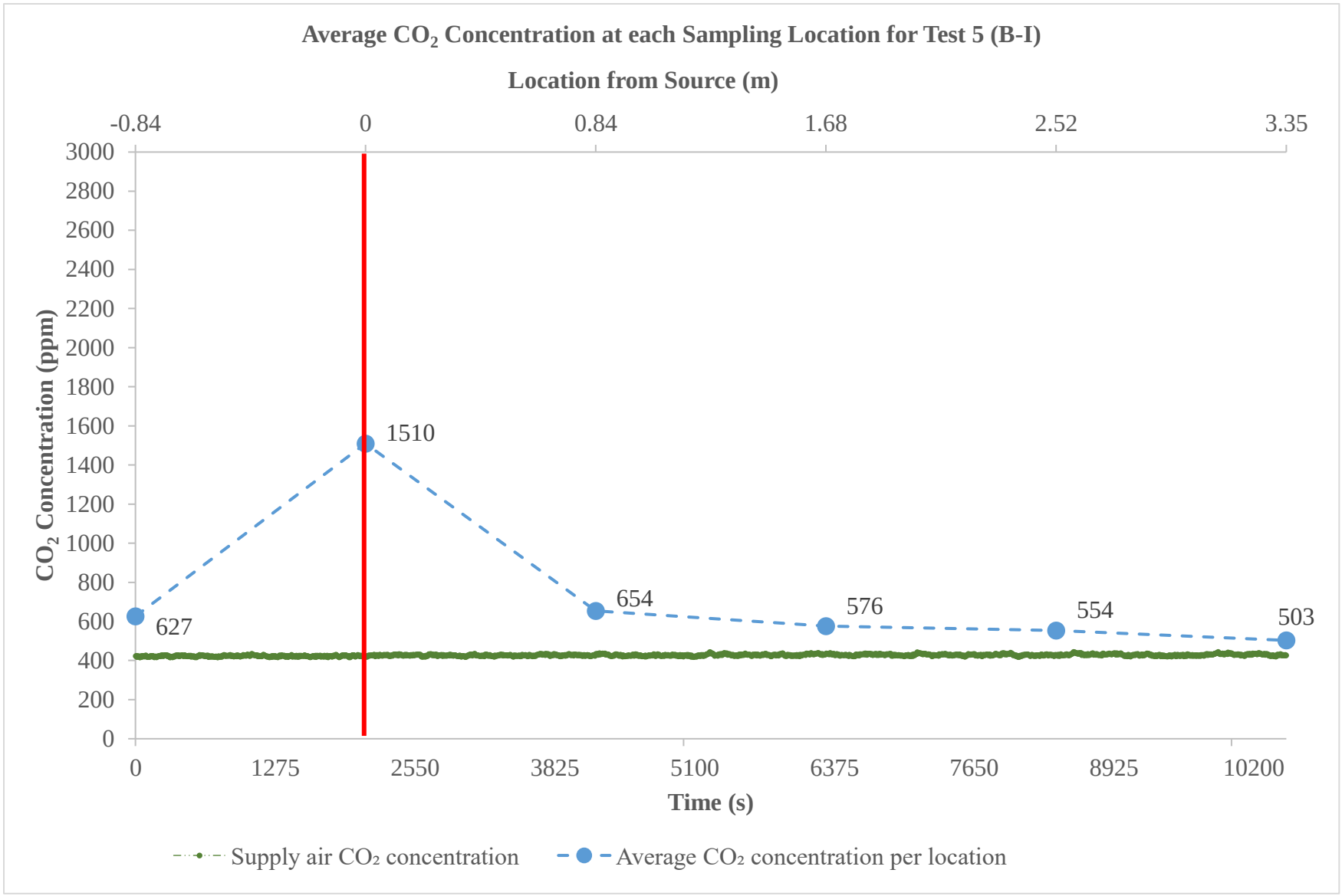

Figure C.19 Average CO_2 concentration at each sampling location for Test 5 (B-I) ISOPass undeployed.

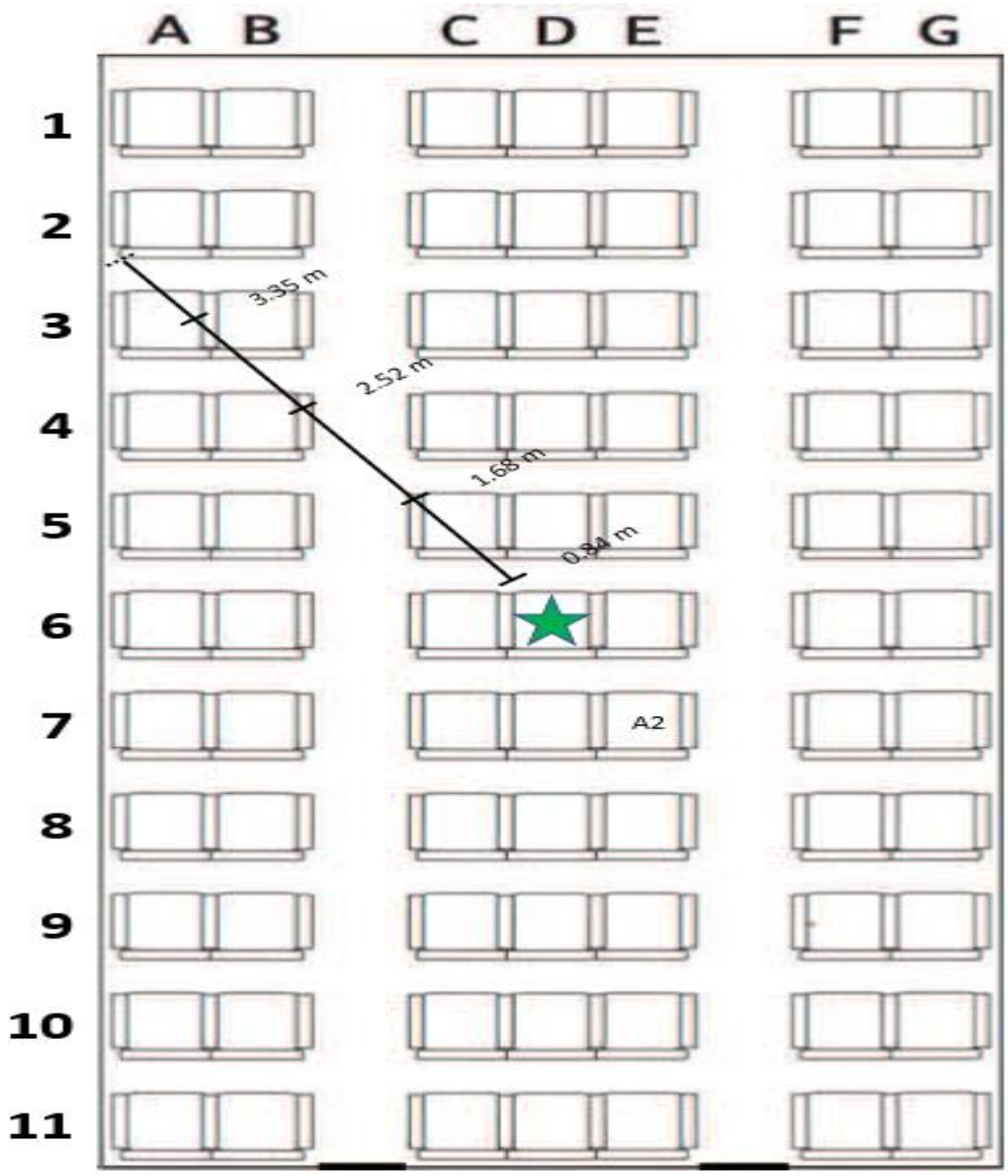

Figure C.20 Test 12 (B-I) ISOPass undeployed source location and sampling tree orientation.

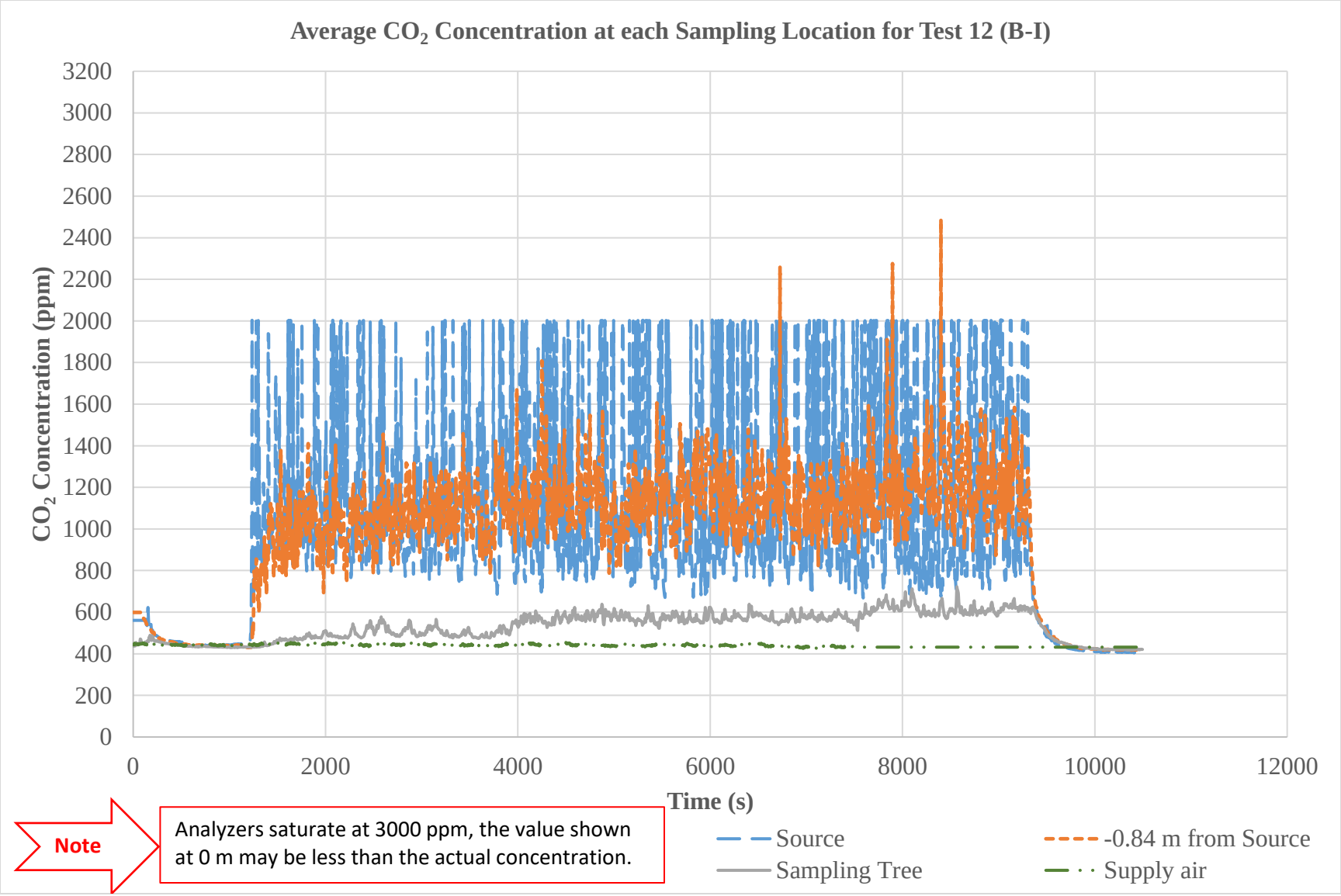

Figure C.21 Ininstantaneous CO_2 concentration at each sampling location for Test 12 (B-I) ISOPass undeployed.

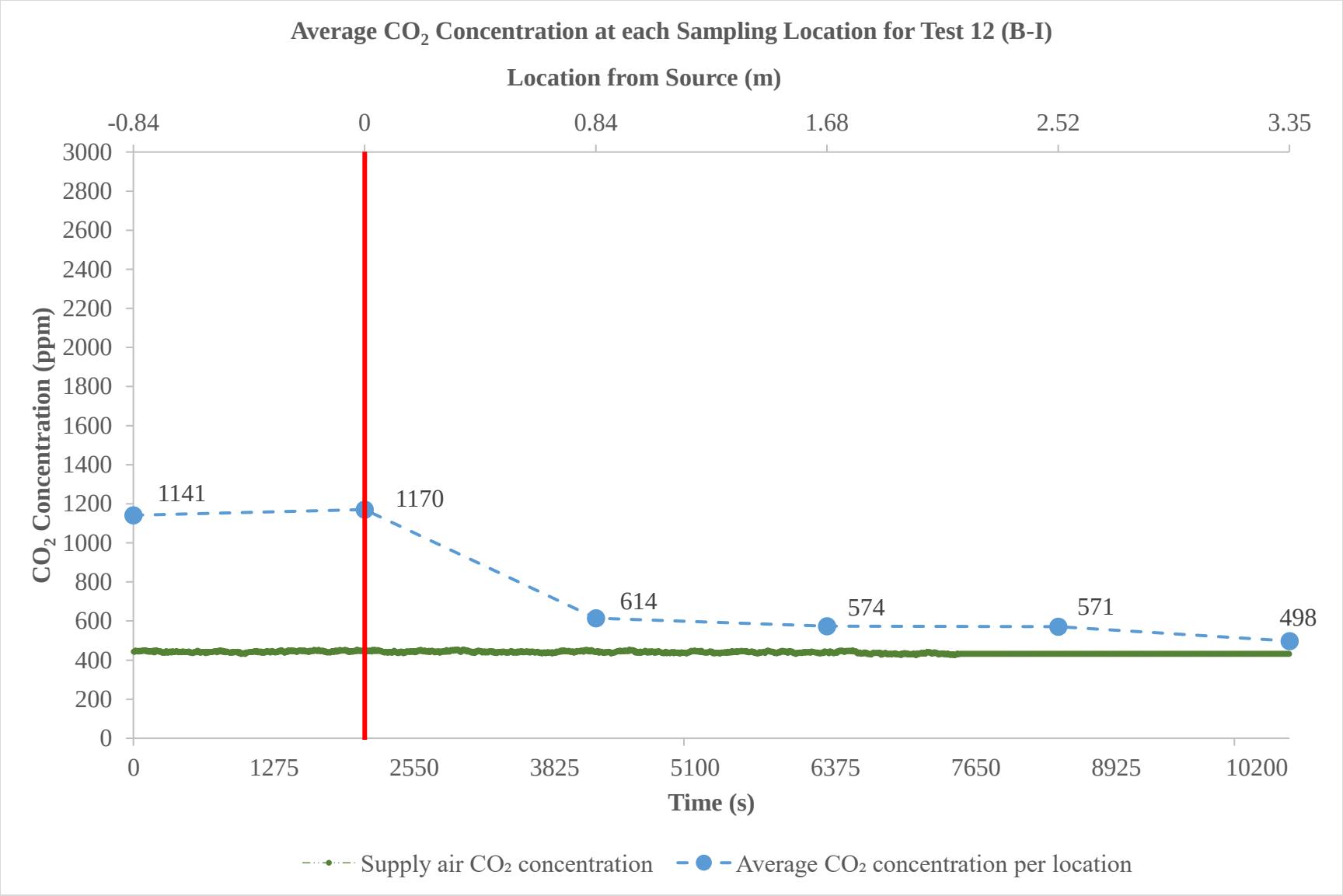

Figure C.22 Average CO_2 concentration at each sampling location for Test 12 (B-I) ISOPass undeployed.

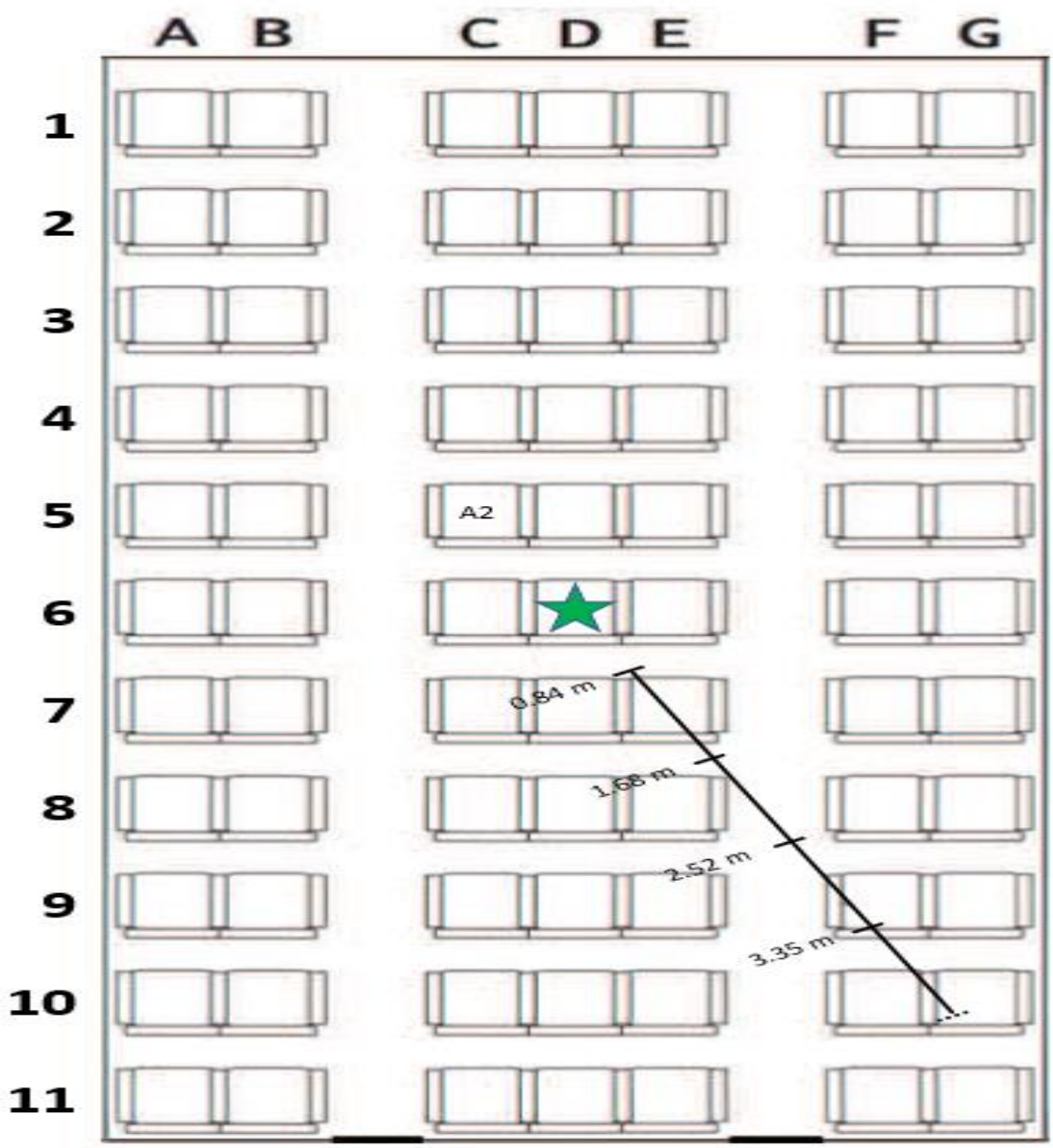

Figure C.23 Test 25 (B-I) ISOPass undeployed source location and sampling tree orientation.

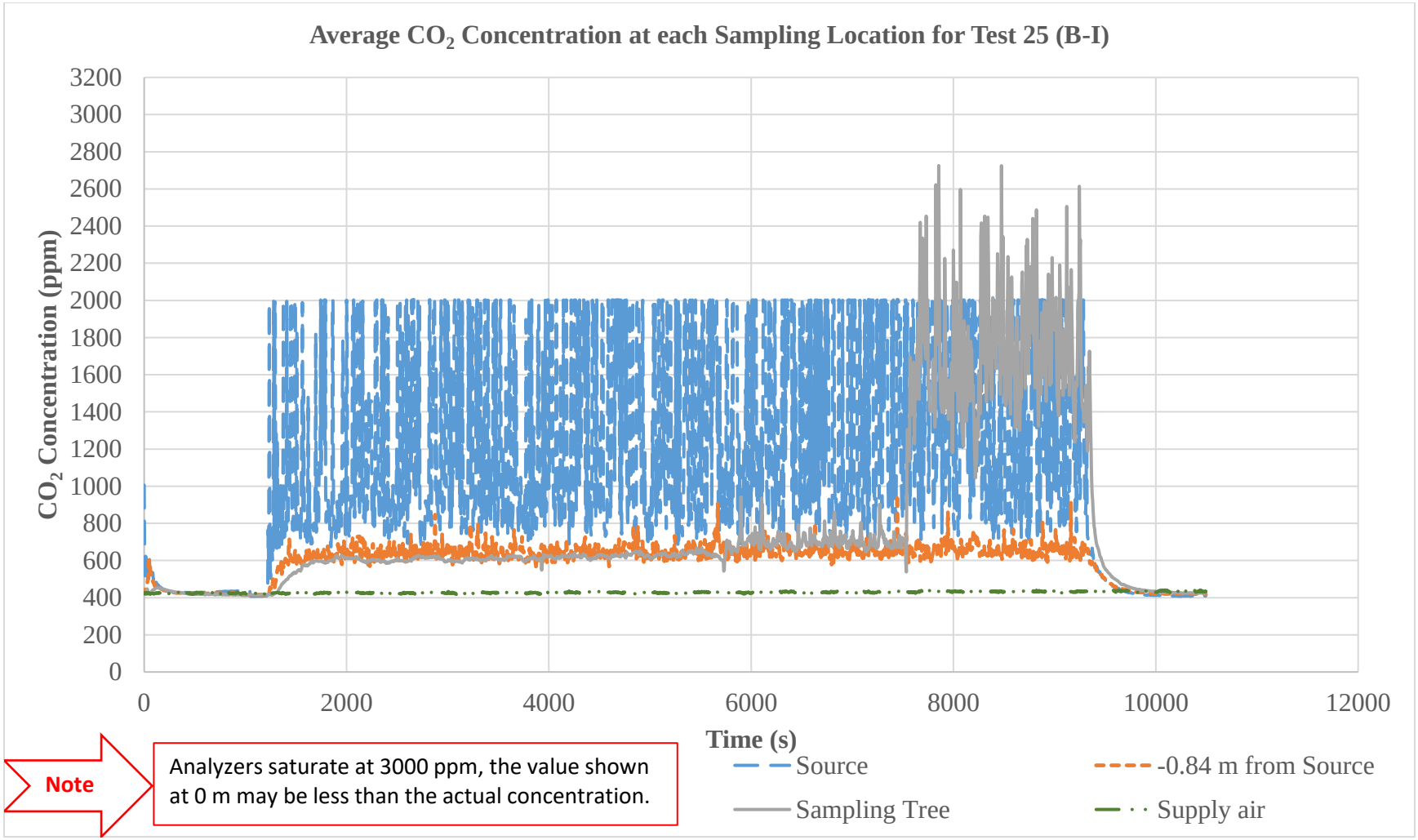

Figure C.24 Ininstantaneous CO_2 concentration at each sampling location for Test 25 (B-I) ISOPass undeployed.

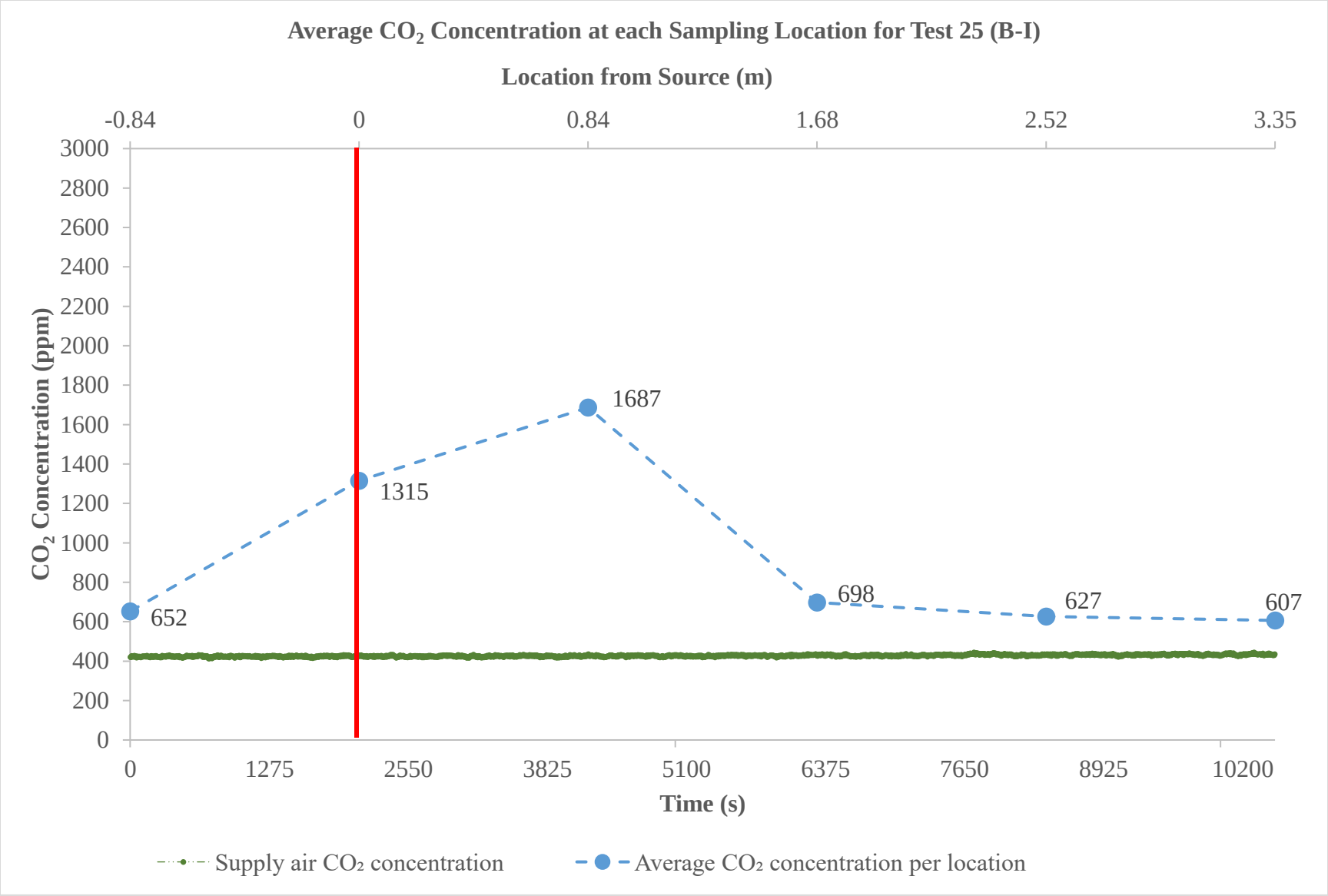

Figure C.25 Average CO_2 concentration at each sampling location for Test 25 (B-I) ISOPass undeployed.

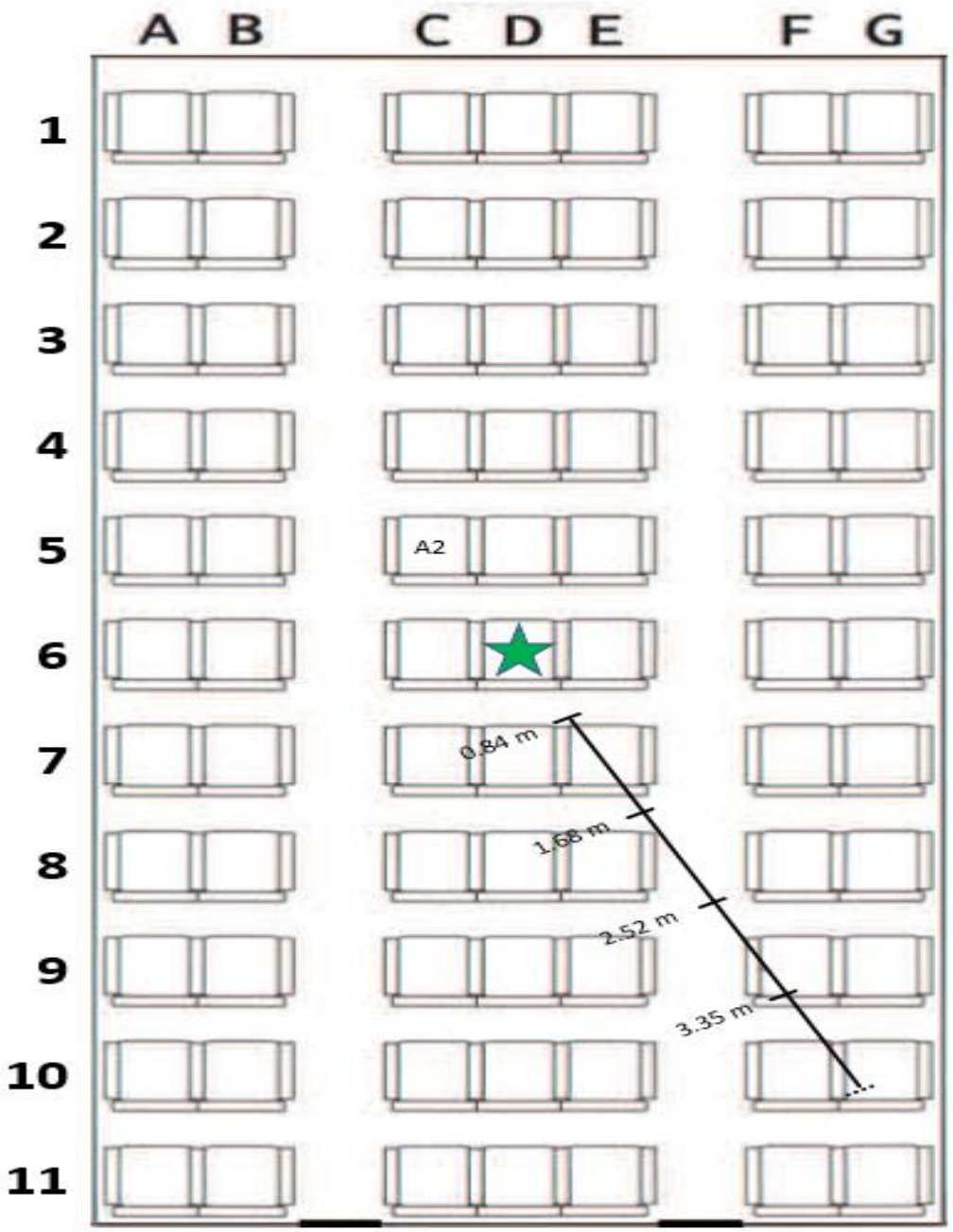

Figure C.26 Test 16 (B-I) ISOPass undeployed source location and sampling tree orientation.

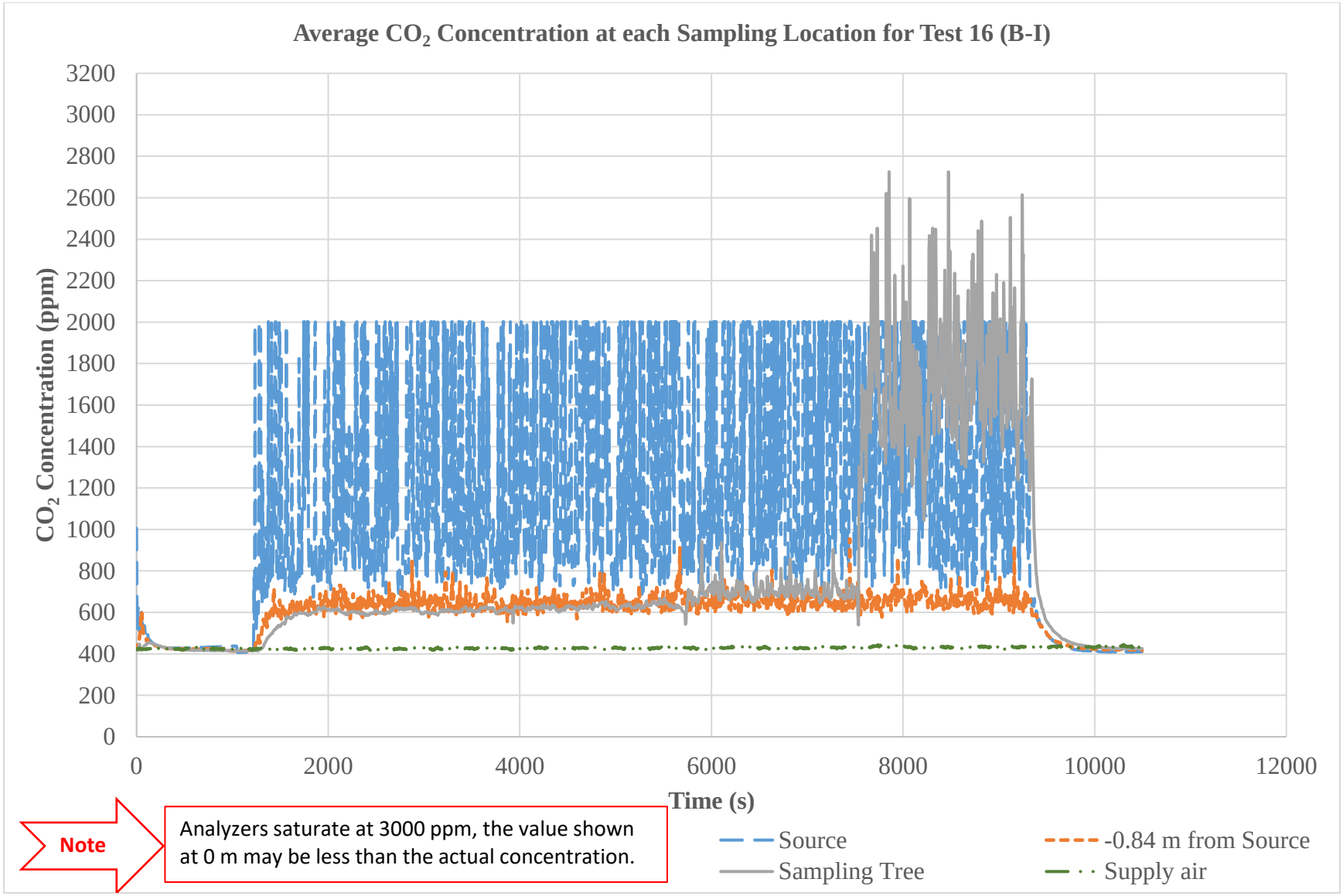

Figure C.27 Ininstantaneous CO_2 concentration at each sampling location for Test 16 (B-I) ISOPass undeployed.

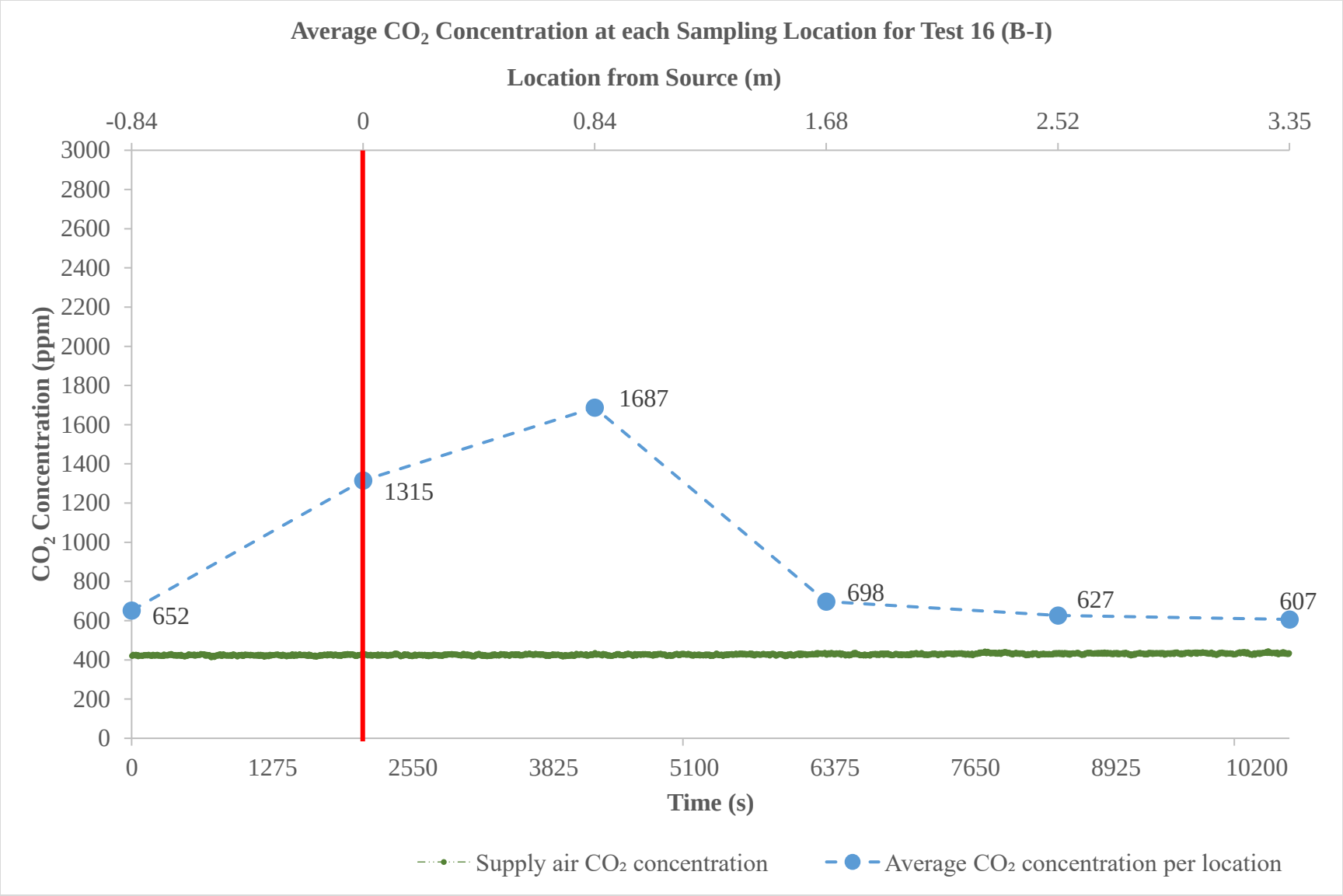

Figure C.28 Average CO_2 concentration at each sampling location for Test 16 (B-I) ISOPass undeployed.

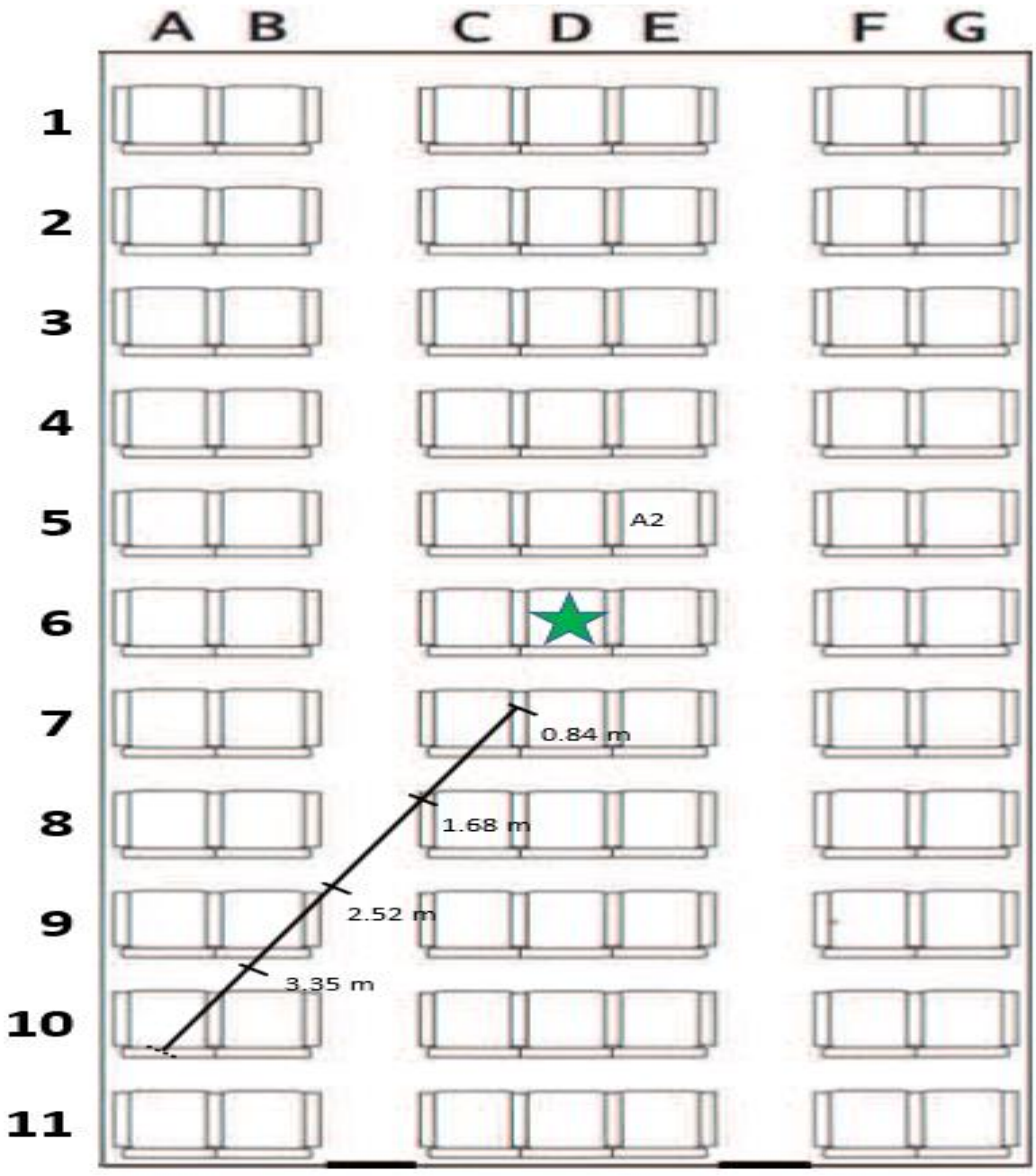

Figure C.29 Test 7 (B-I) ISOPass undeployed source location and sampling tree orientation.

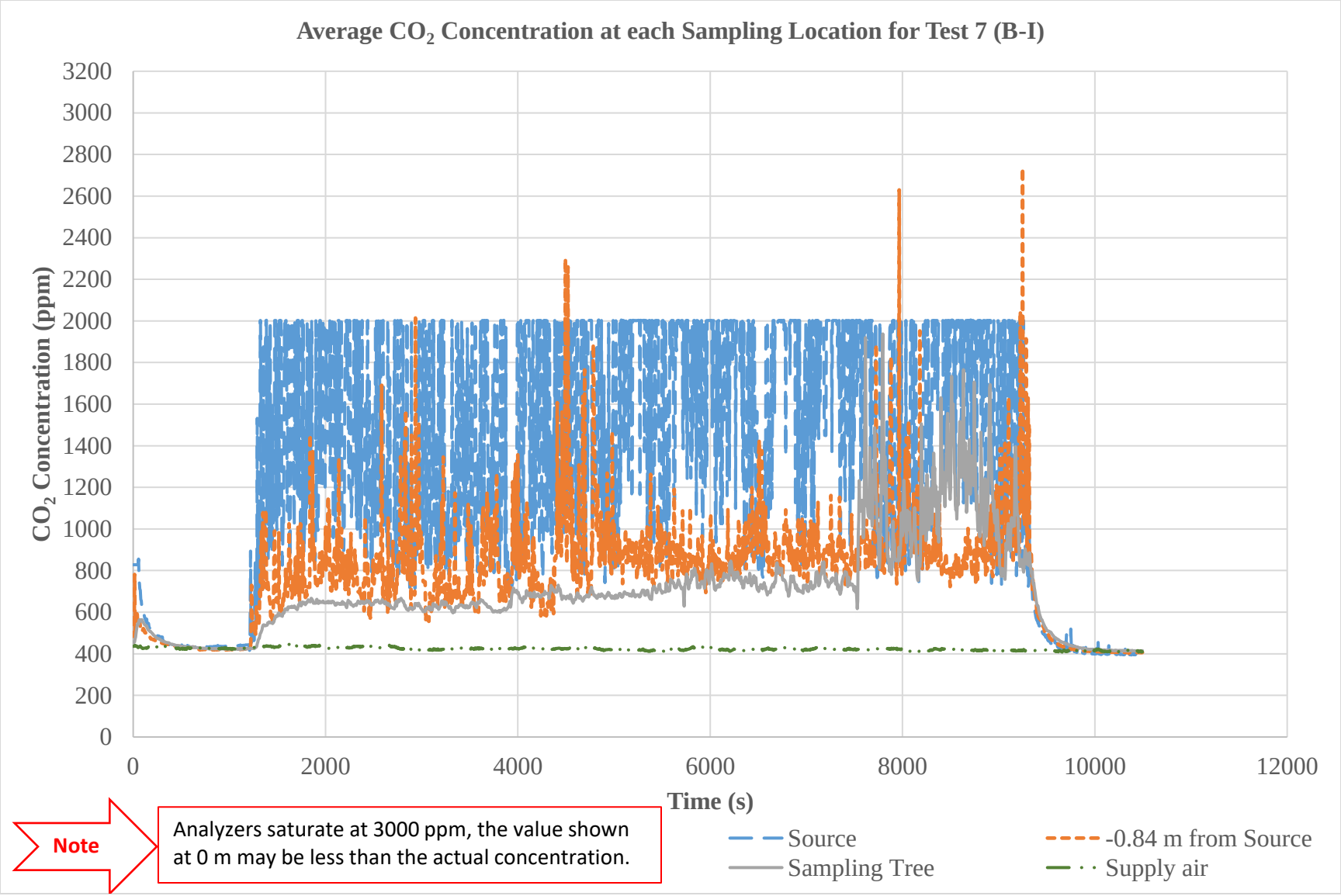

Figure C.30 Ininstantaneous CO_2 concentration at each sampling location for Test 7 (B-I) ISOPass undeployed.

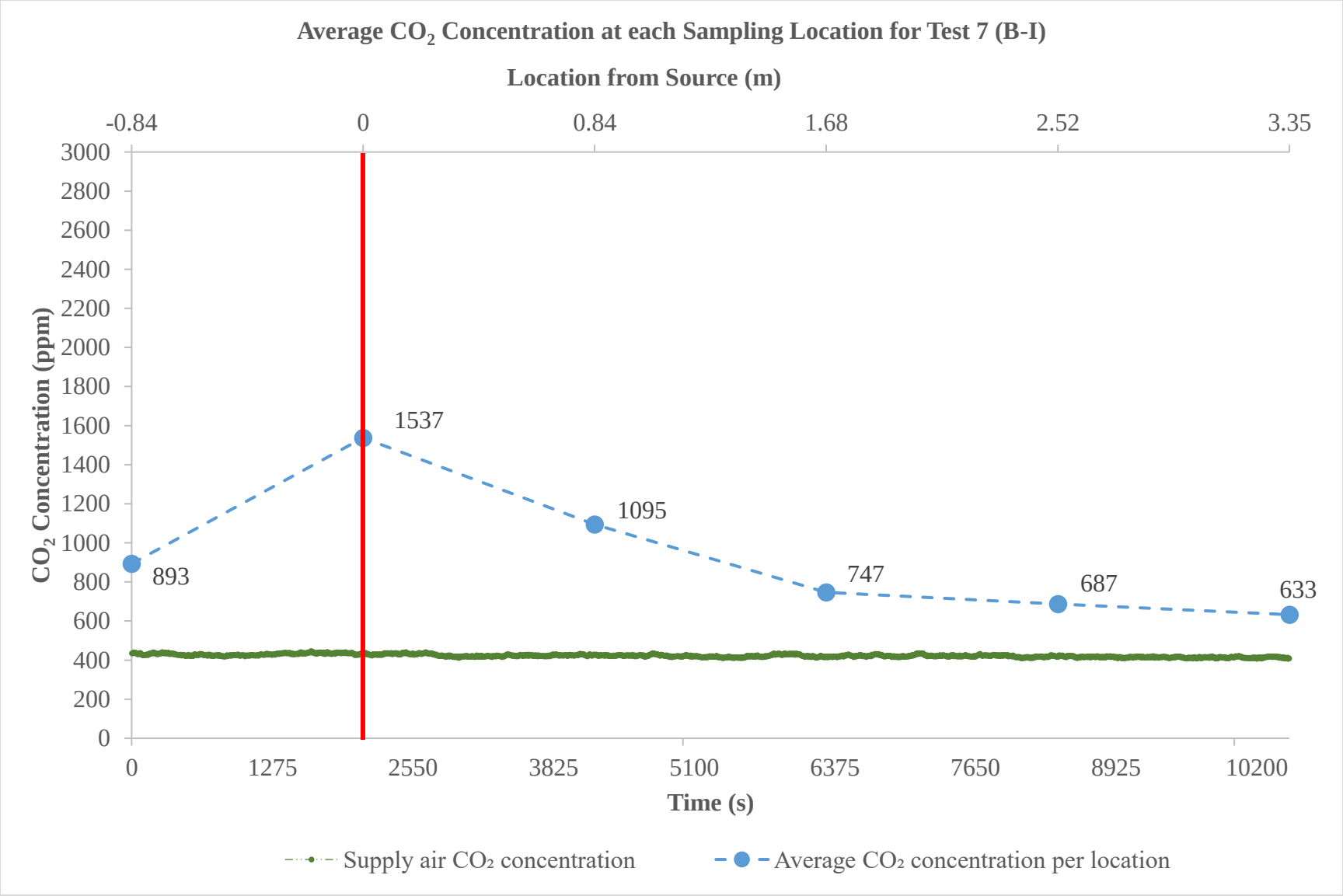

Figure C.31 Average CO_2 concentration at each sampling location for Test 7 (B-I) ISOPass undeployed.

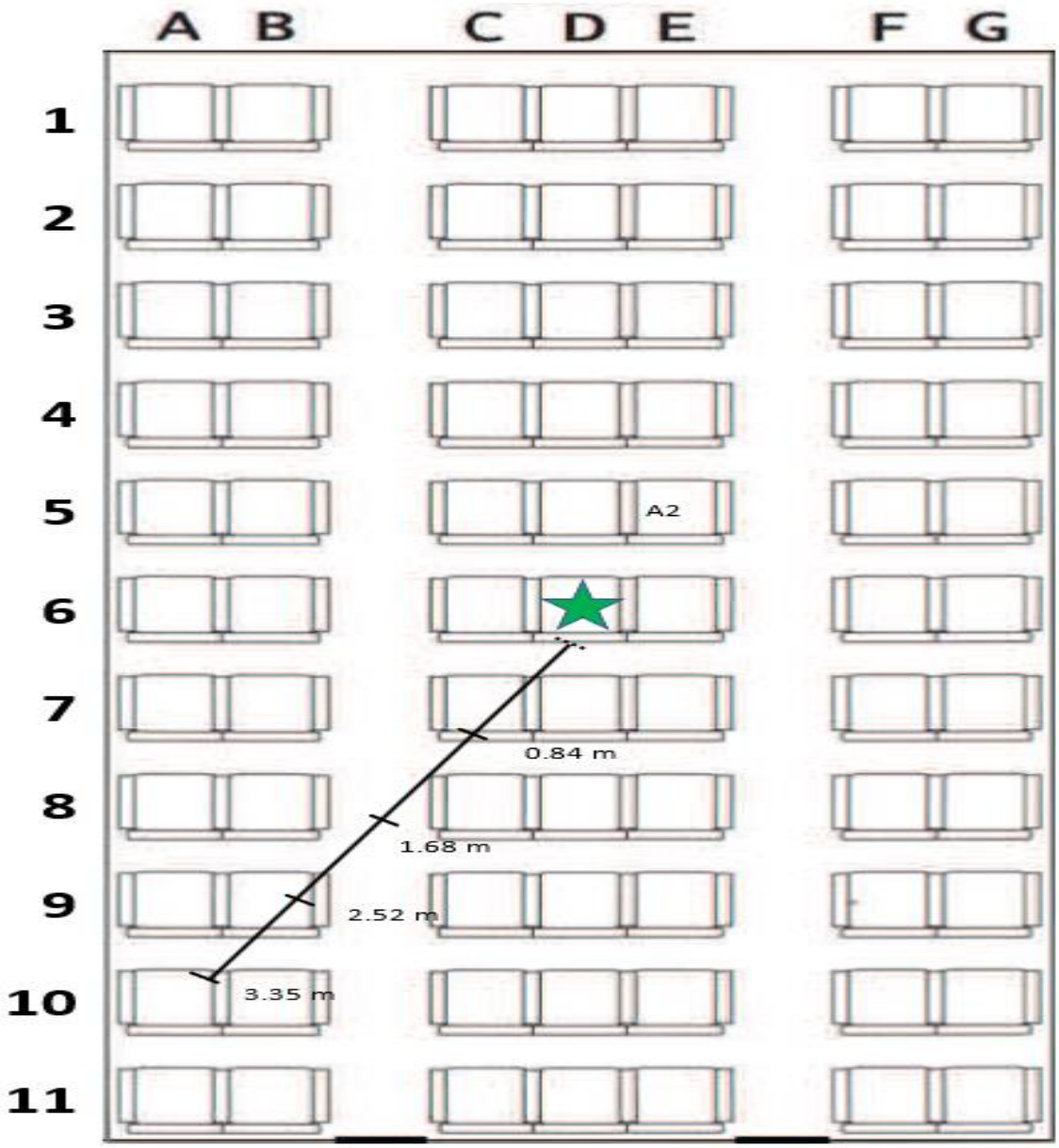

Figure C.32 Test 13 (B-I) ISOPass undeployed source location and sampling tree orientation.

Note: In this test, the solenoid block on the sampling tree was located next to the source as indicated by the dashed line. This was done in order to check if the block would have an effect on the dispersed tracer gas. Hence, in Figure C.33, the concentration of the tracer gas on the sampling tree decreases away from the source. Also, the positive direction is still considered to be from the source to the solenoid block.

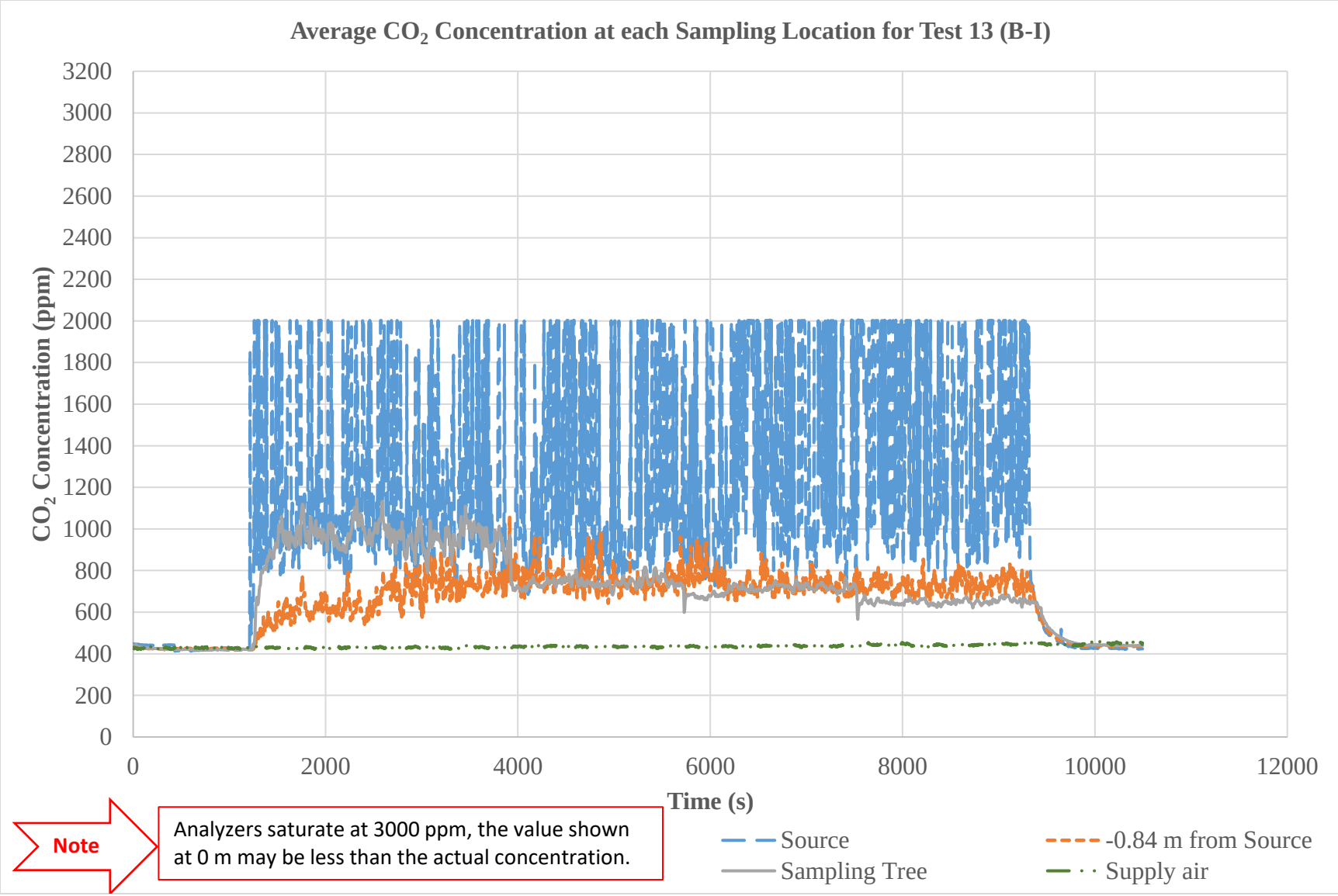

Figure C.33 Ininstantaneous CO_2 concentration at each sampling location for Test 13 (B-I) ISOPass undeployed.

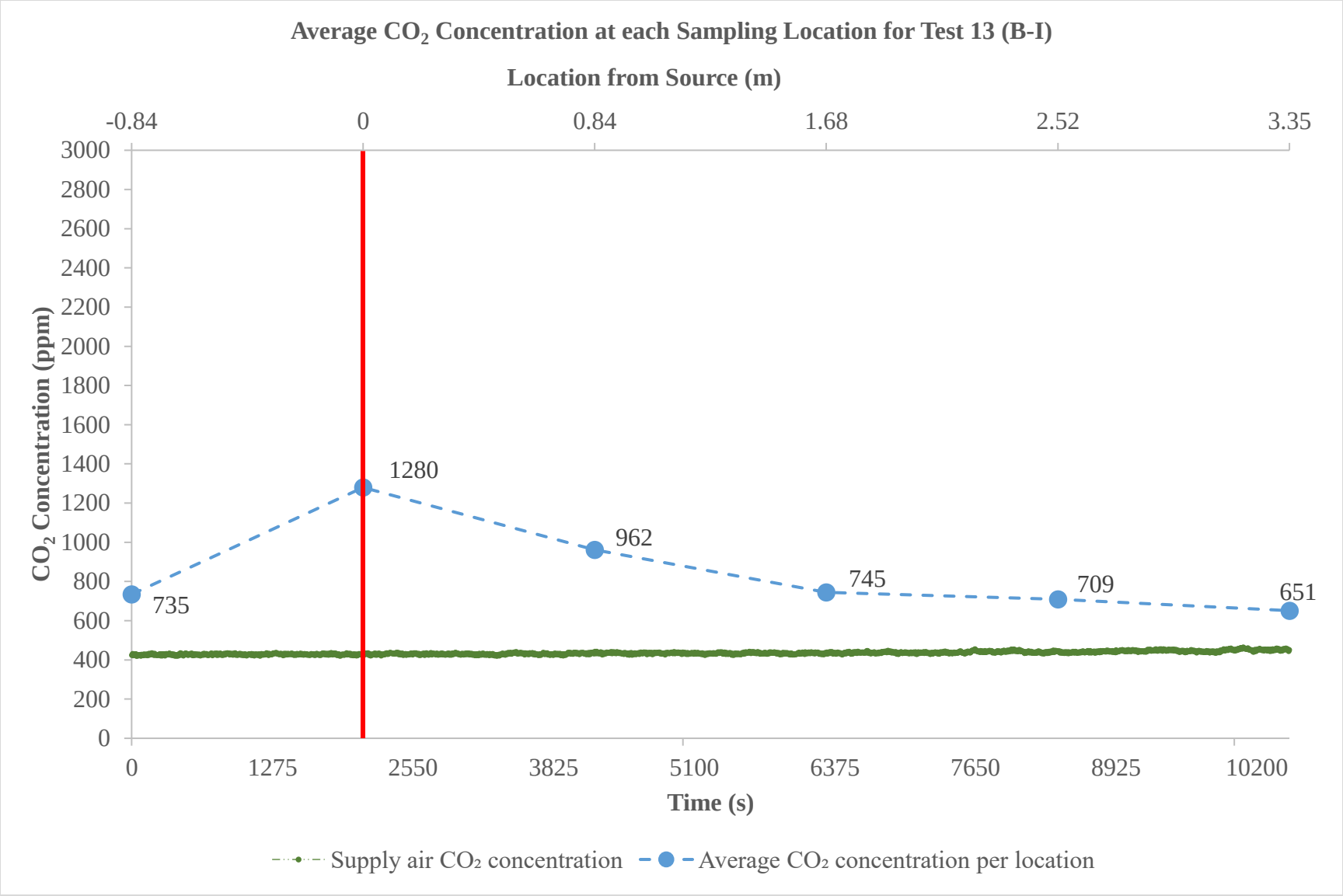

Figure C.34 Average CO_2 concentration at each sampling location for Test 13 (B-I) ISOPass undeployed.

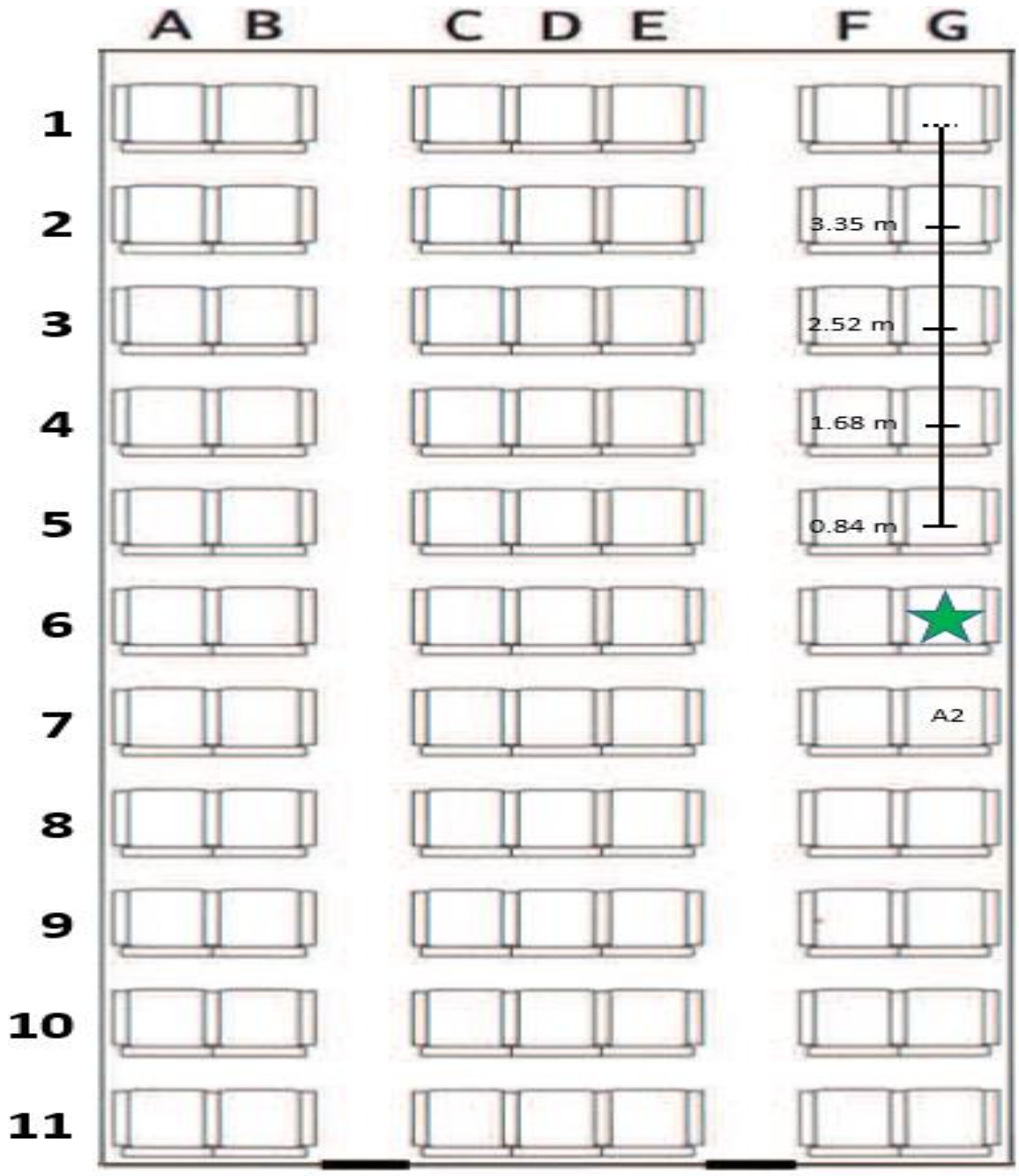

Figure C.35 Test 17 (B-I) ISOPass undeployed source location and sampling tree orientation.

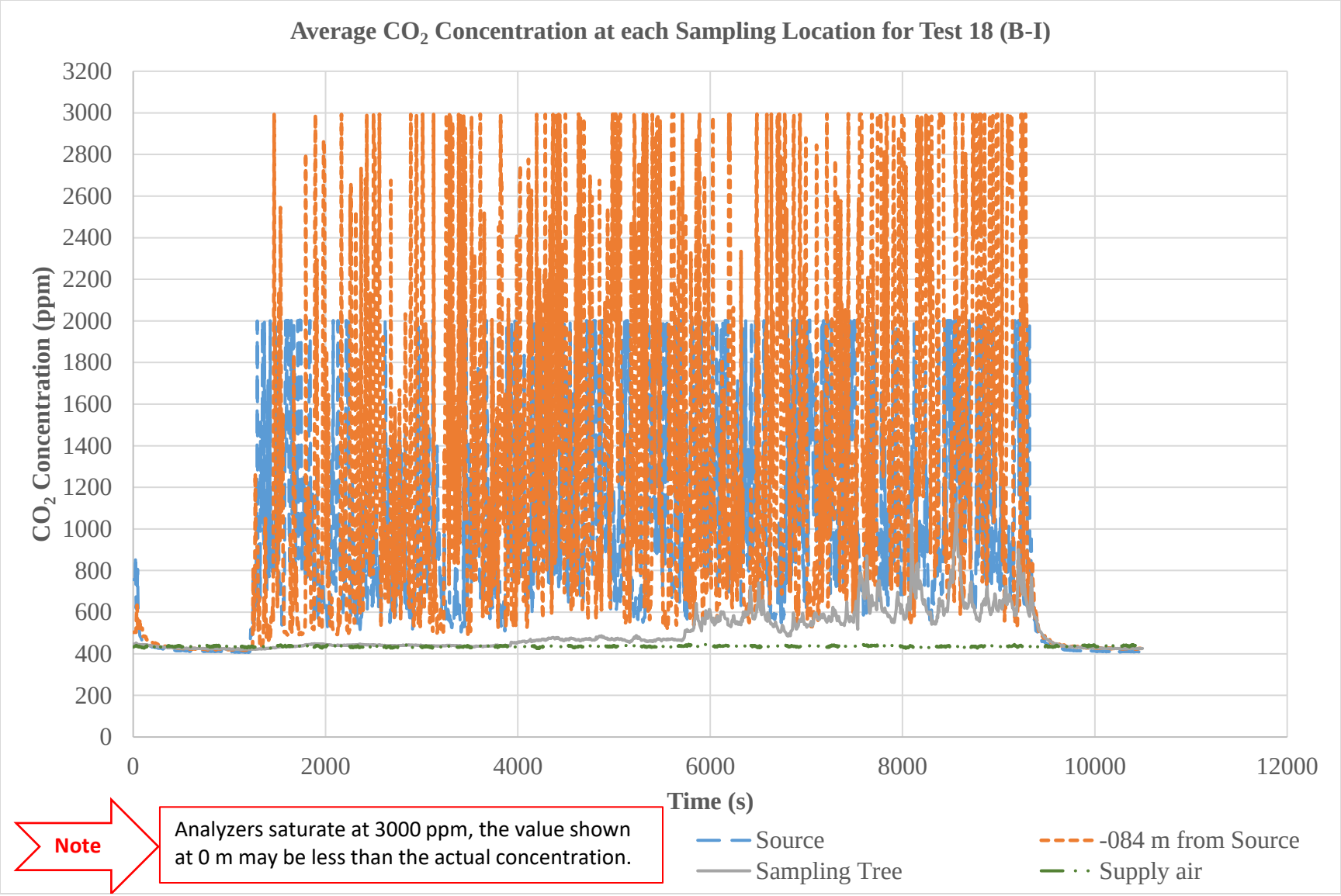

Figure C.36 Ininstantaneous CO_2 concentration at each sampling location for Test 17 (B-I) ISOPass undeployed.

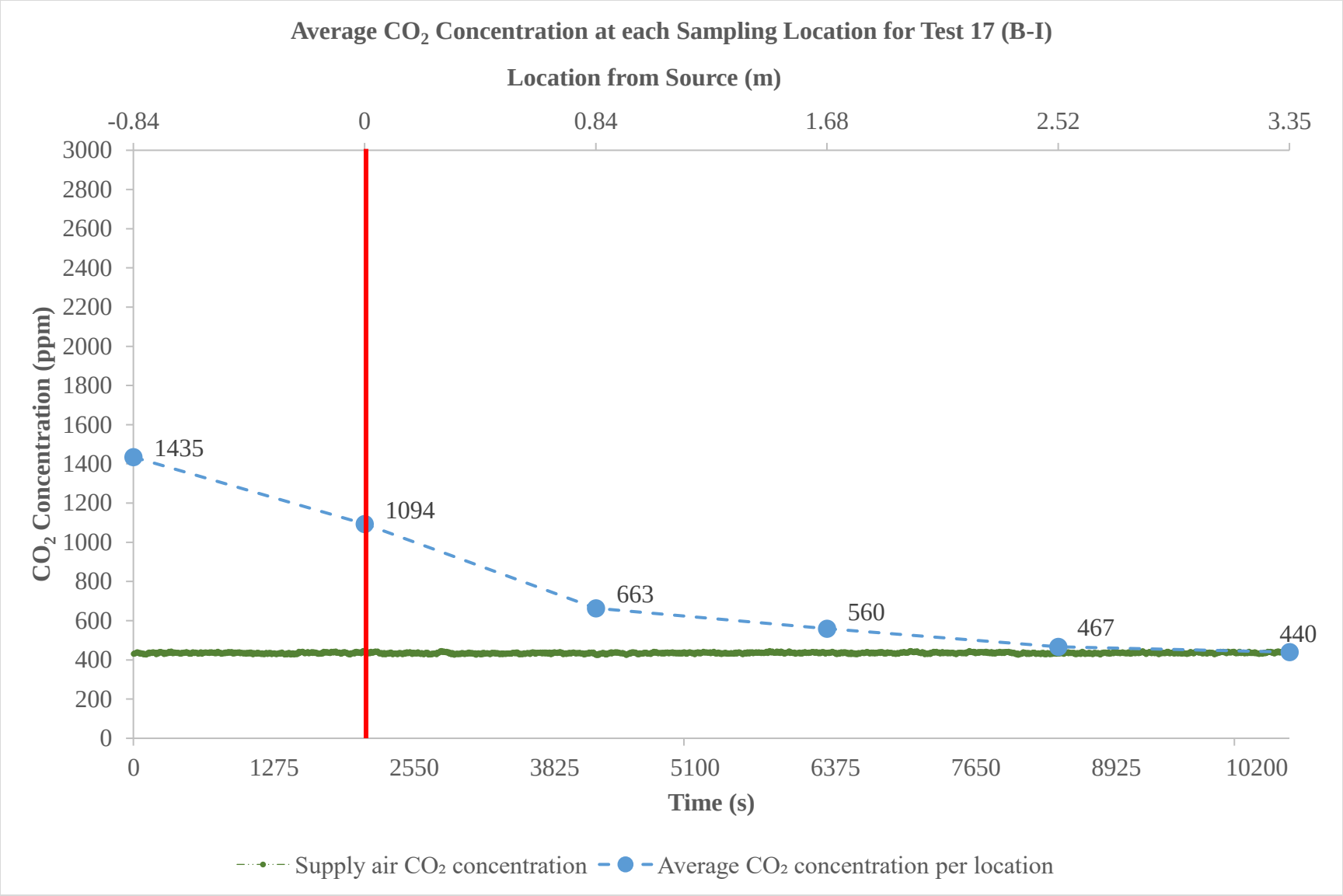

Figure C.37 Average CO_2 concentration at each sampling location for Test 17 (B-I) ISOPass undeployed.

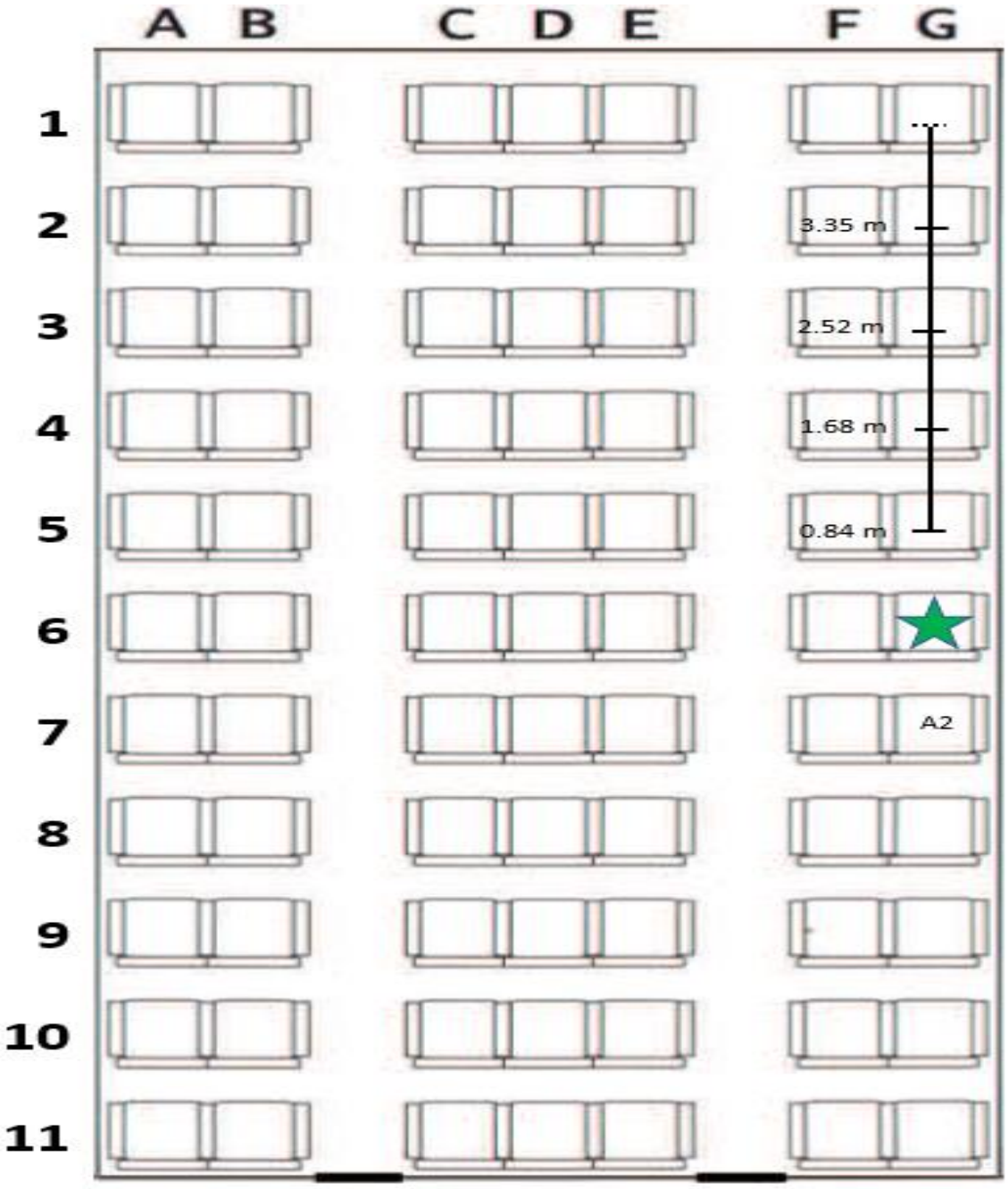

Figure C.38 Test 22 (B-I) ISOPass undeployed source location and sampling tree orientation.

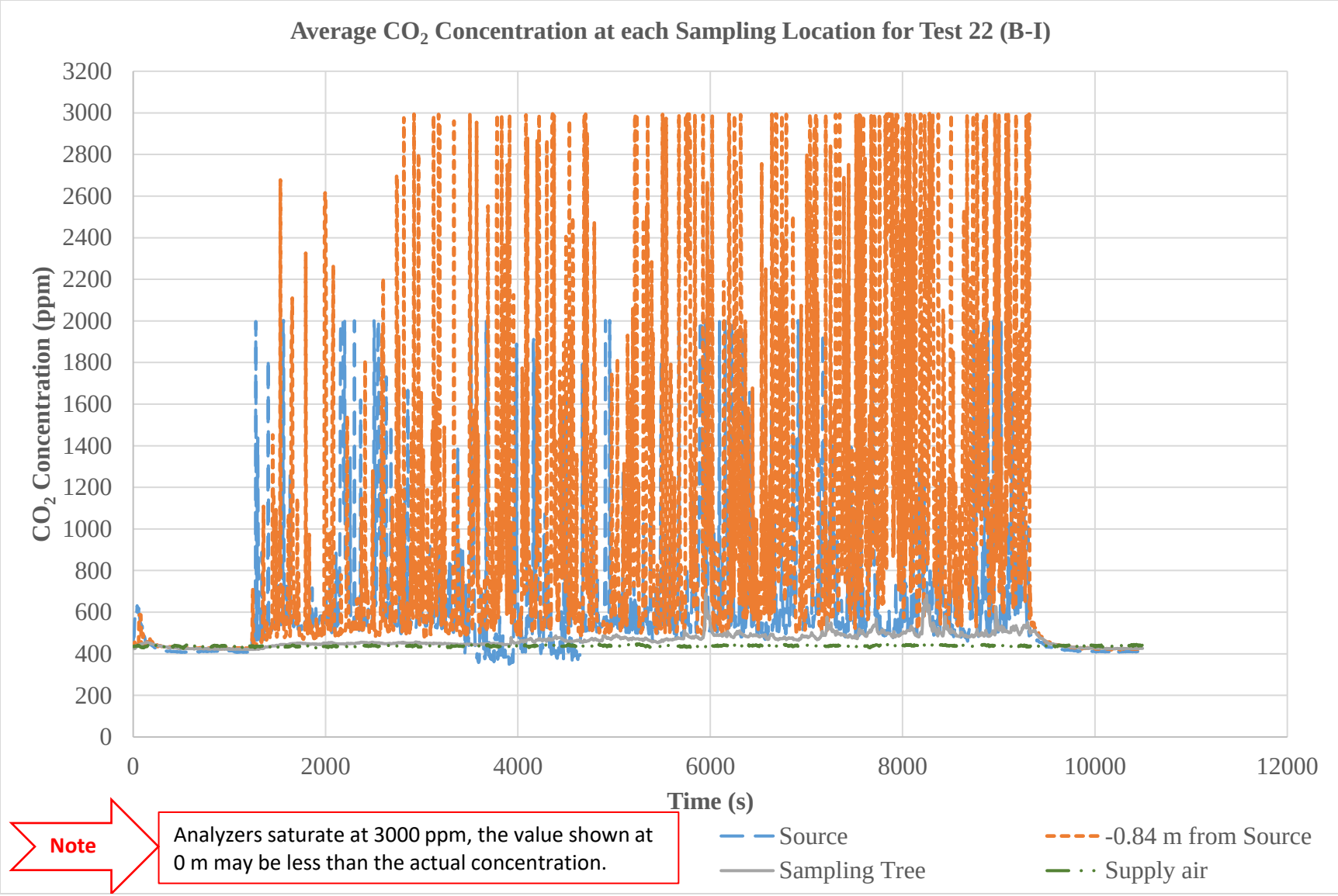

Figure C.39 Ininstantaneous CO_2 concentration at each sampling location for Test 22 (B-I) ISOPass undeployed.

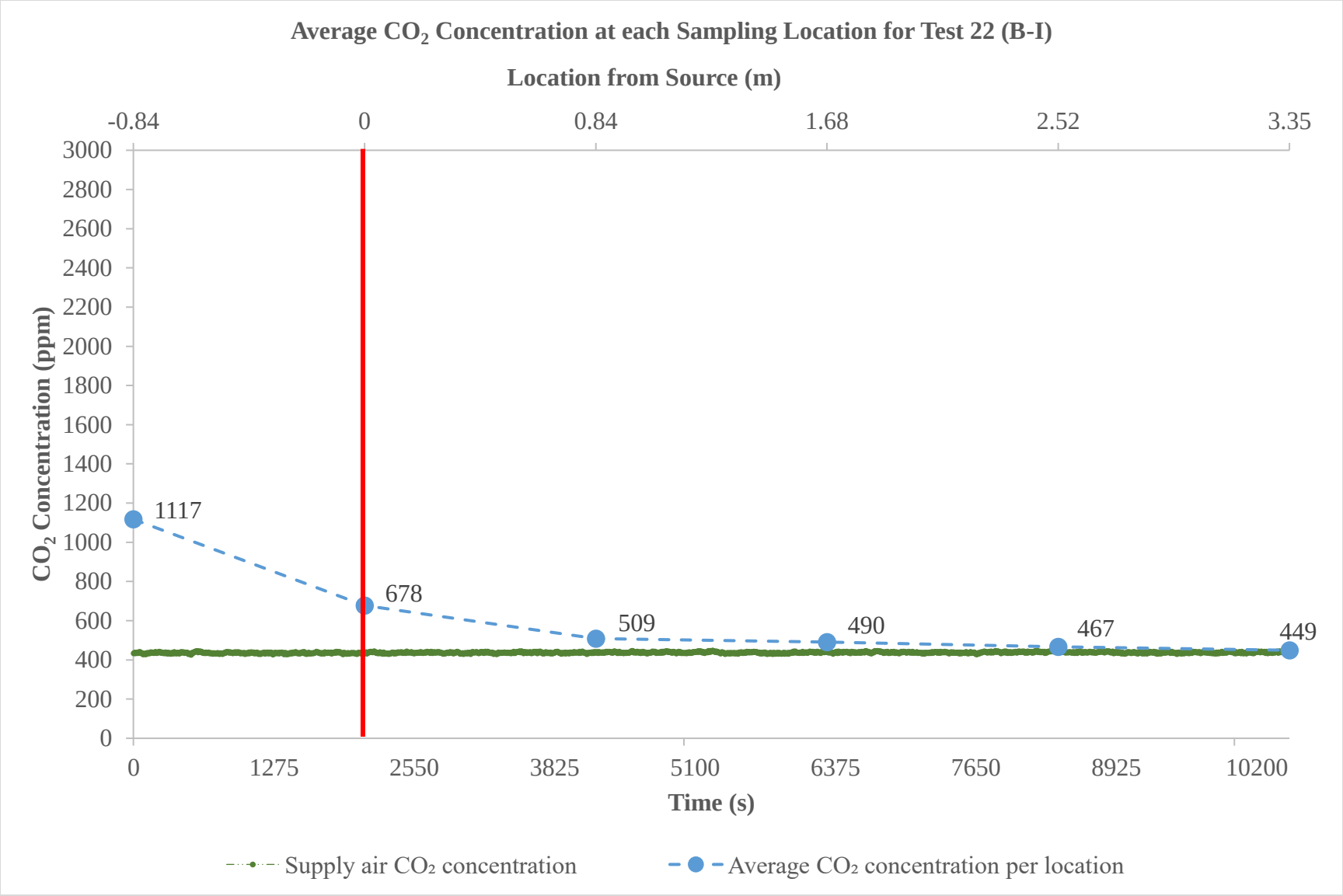

Figure C.40 Average CO_2 concentration at each sampling location for Test 22 (B-I) ISOPass undeployed.

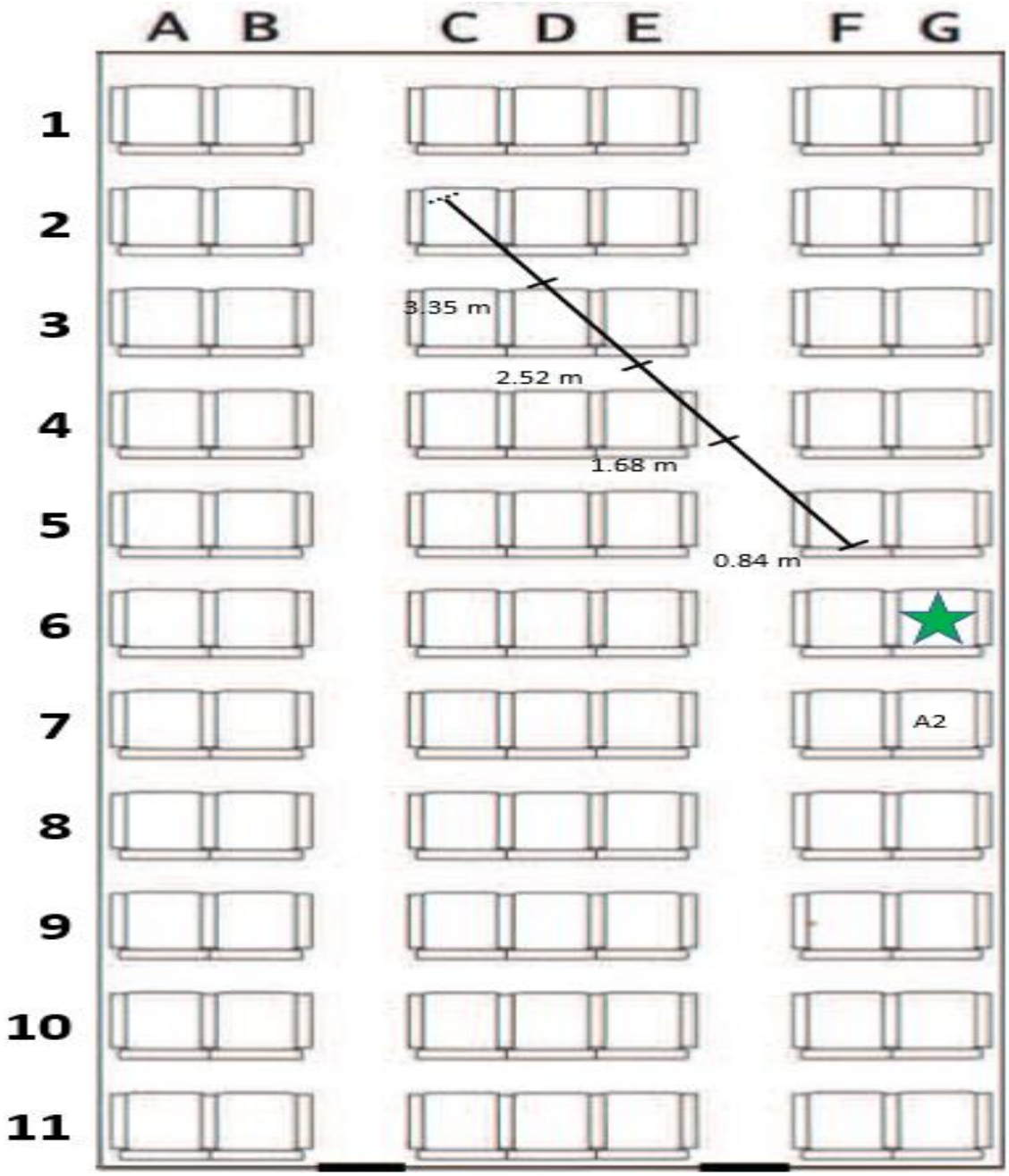

Figure C.41 Test 18 (B-I) ISOPass undeployed source location and sampling tree orientation.

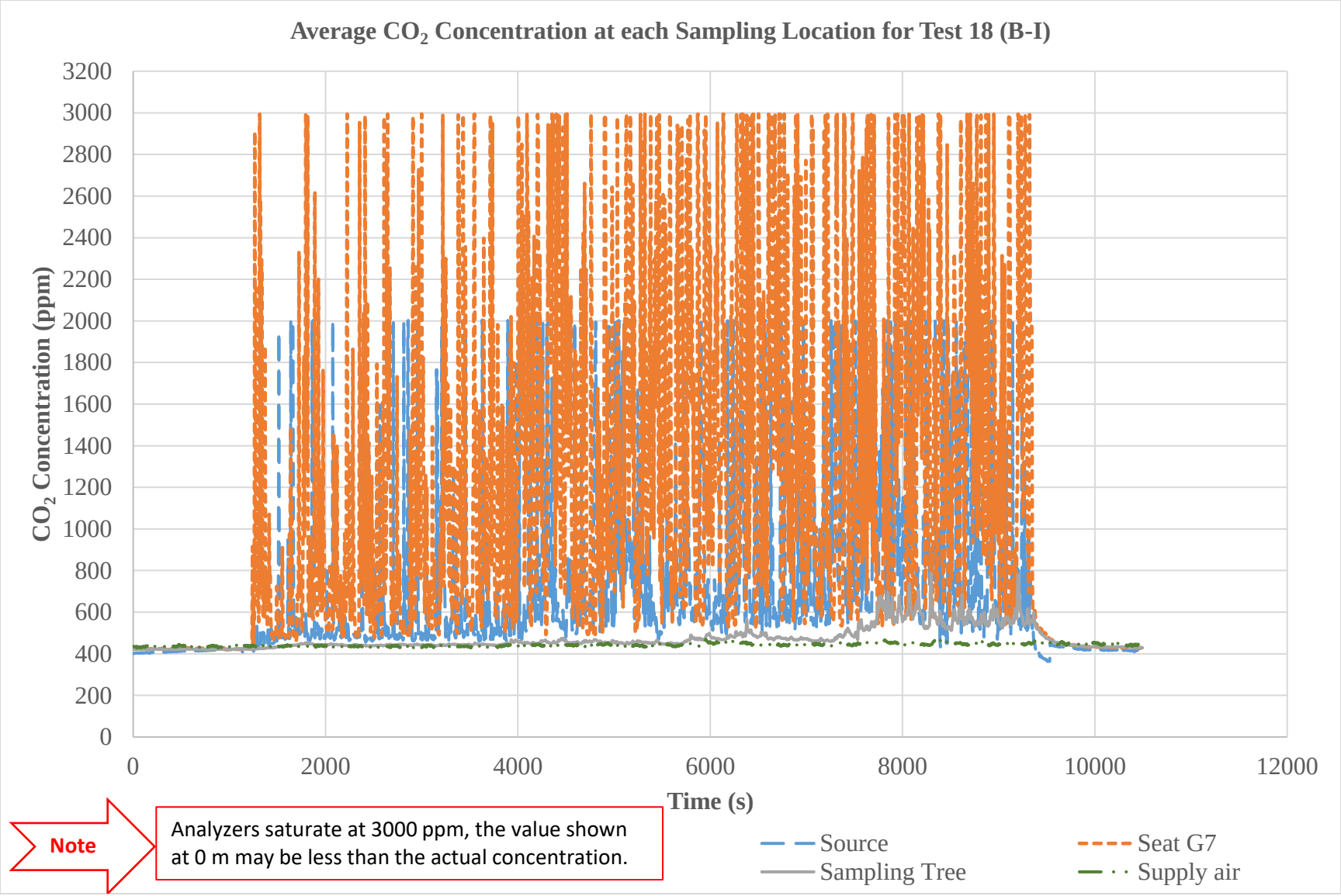

Figure C.42 Ininstantaneous CO_2 concentration at each sampling location for Test 18 (B-I) ISOPass undeployed.

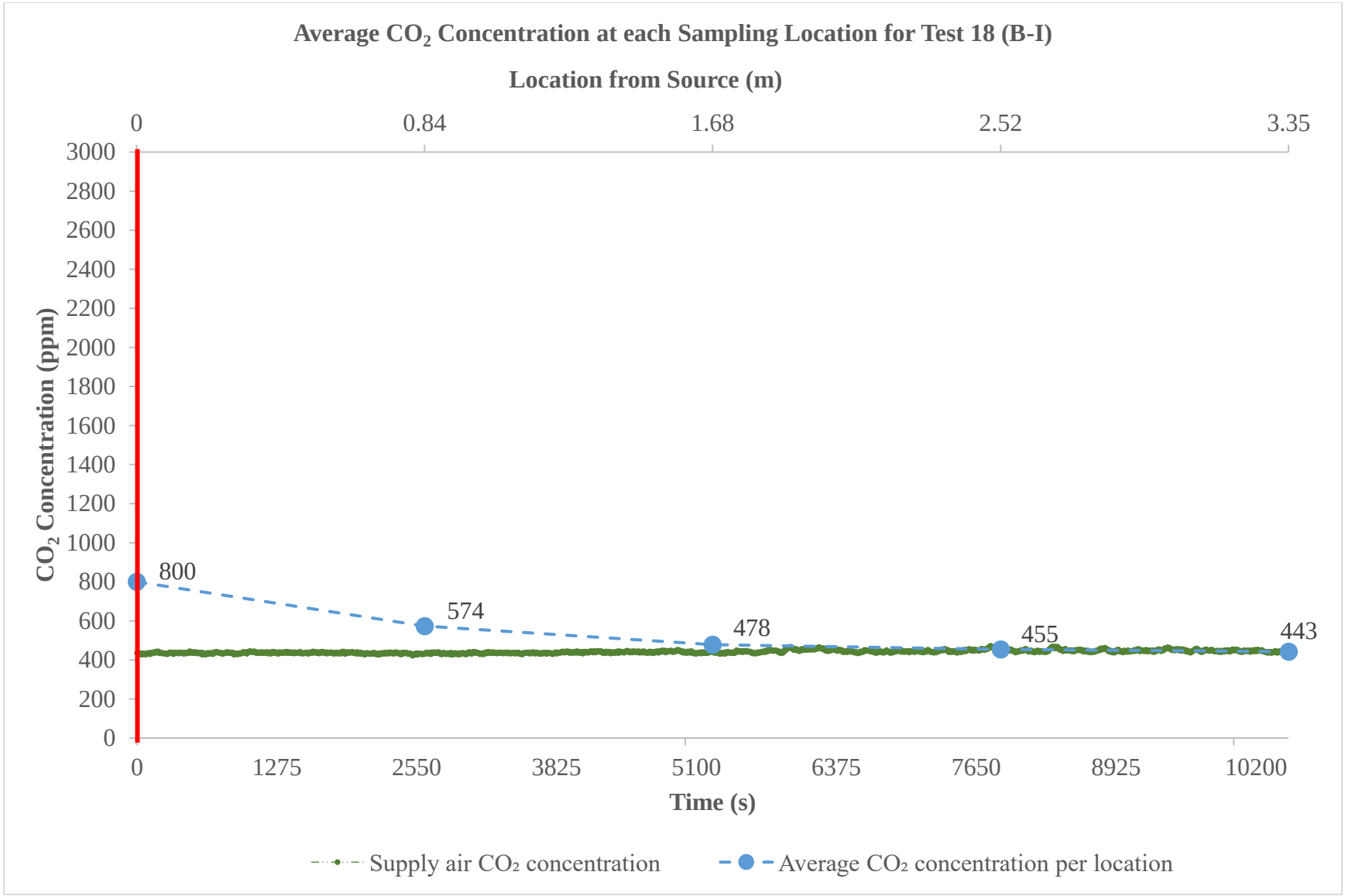

Figure C.43 Average CO_2 concentration at each sampling location for Test 18 (B-I) ISOPass undeployed.

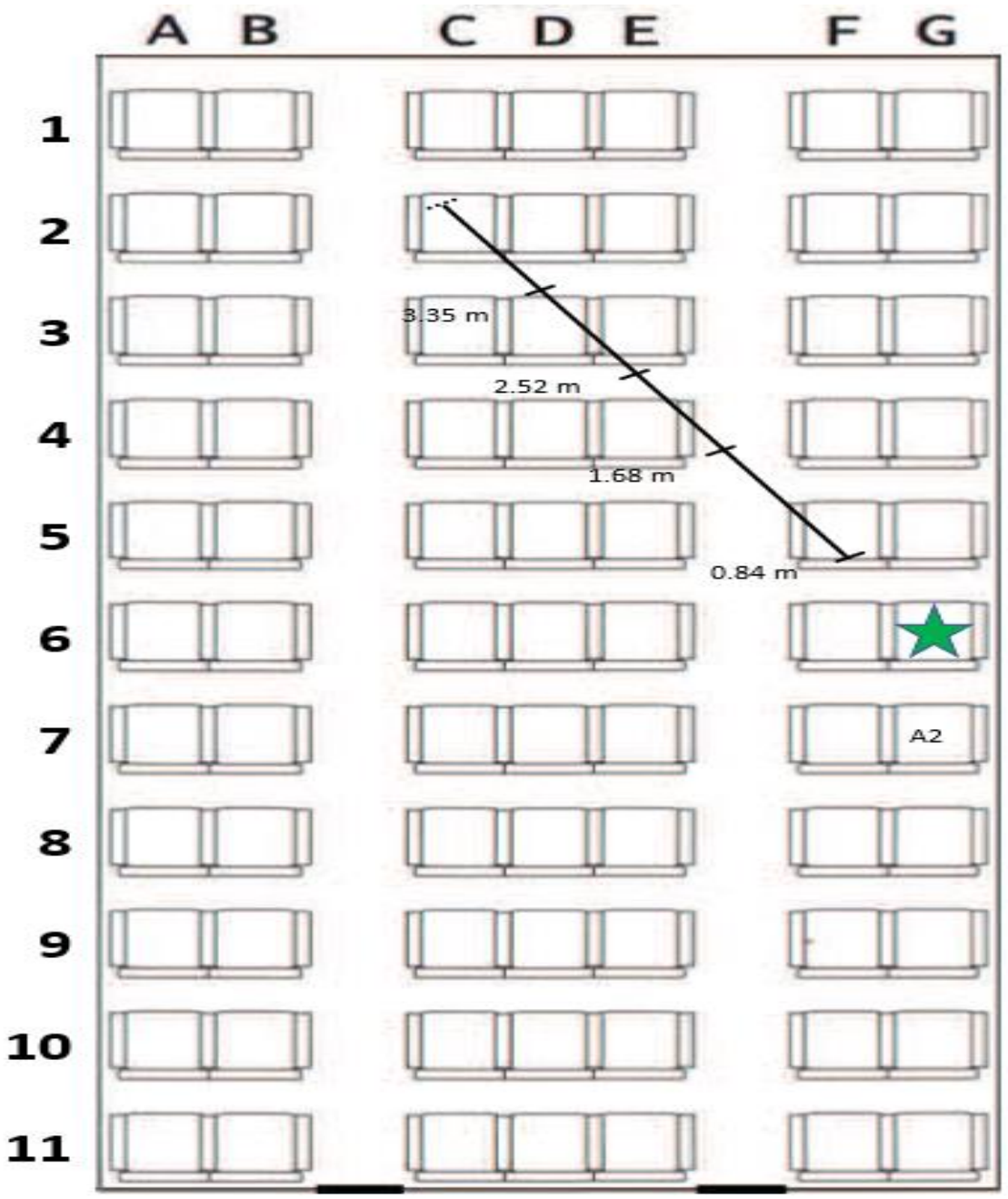

Figure C.44 Test 21 (B-I) ISOPass undeployed source location and sampling tree orientation.

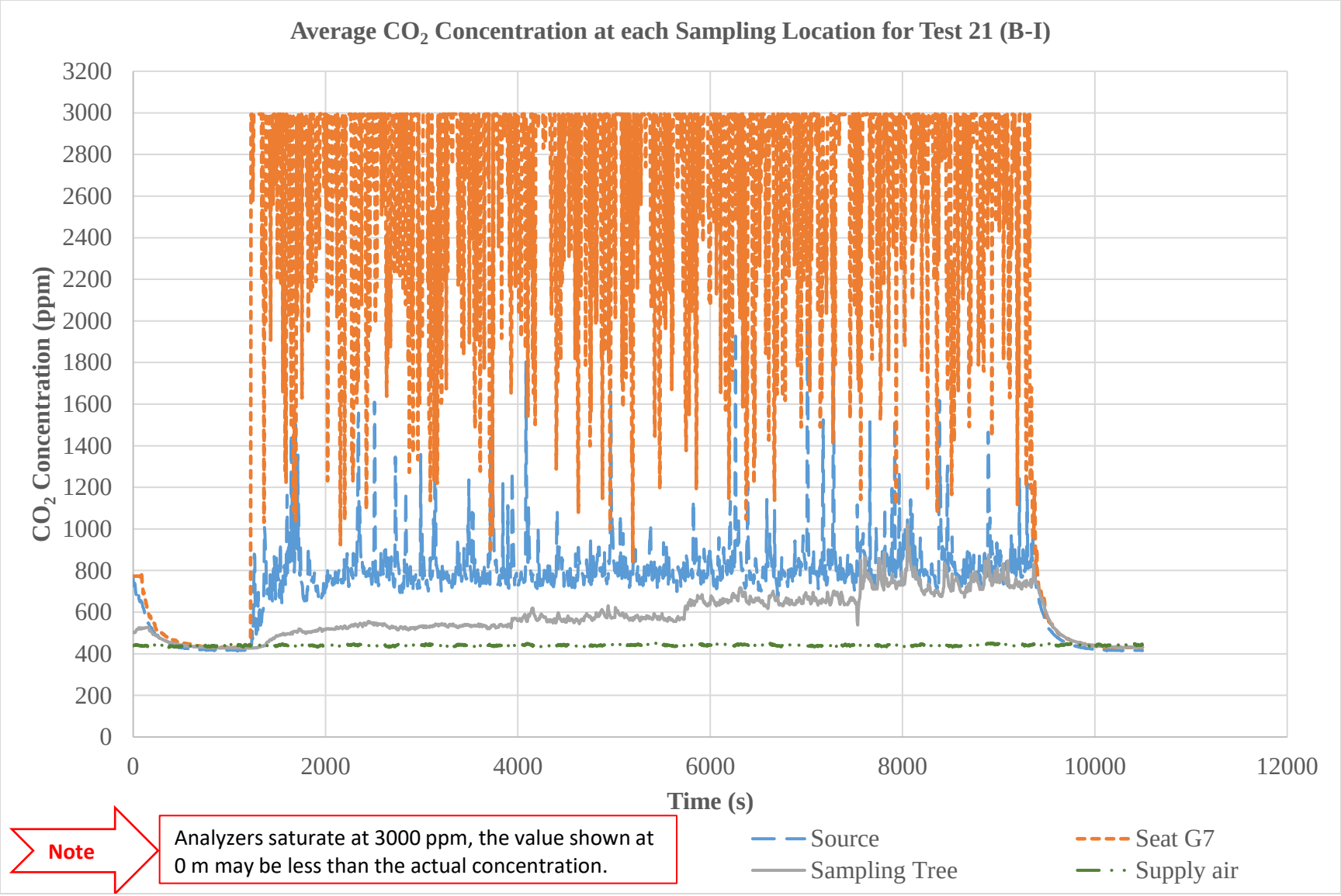

Figure C.45 Ininstantaneous CO_2 concentration at each sampling location for Test 21 (B-I) ISOPass undeployed.

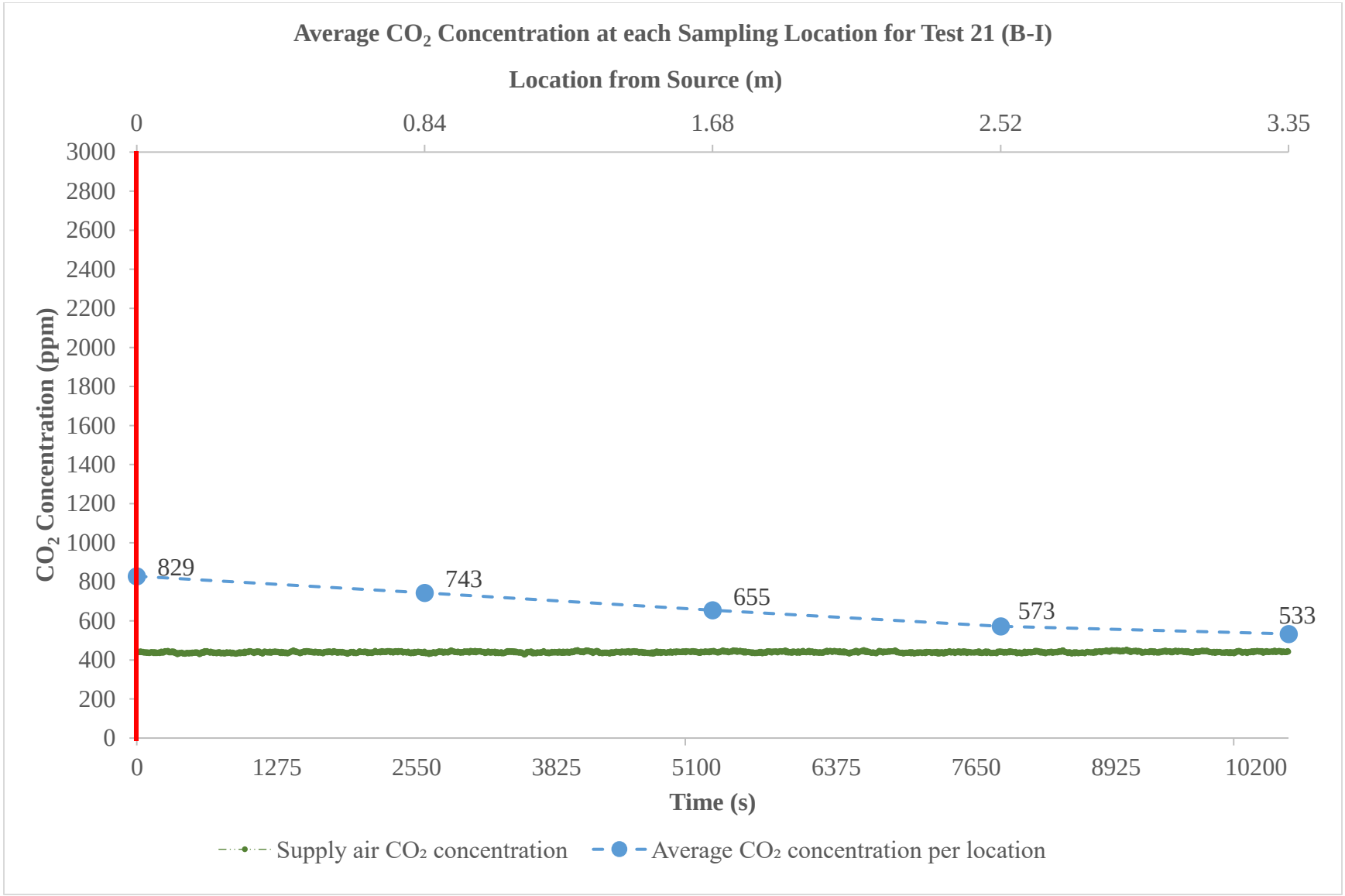

Figure C.46 Average CO_2 concentration at each sampling location for Test 21 (B-I) ISOPass undeployed.

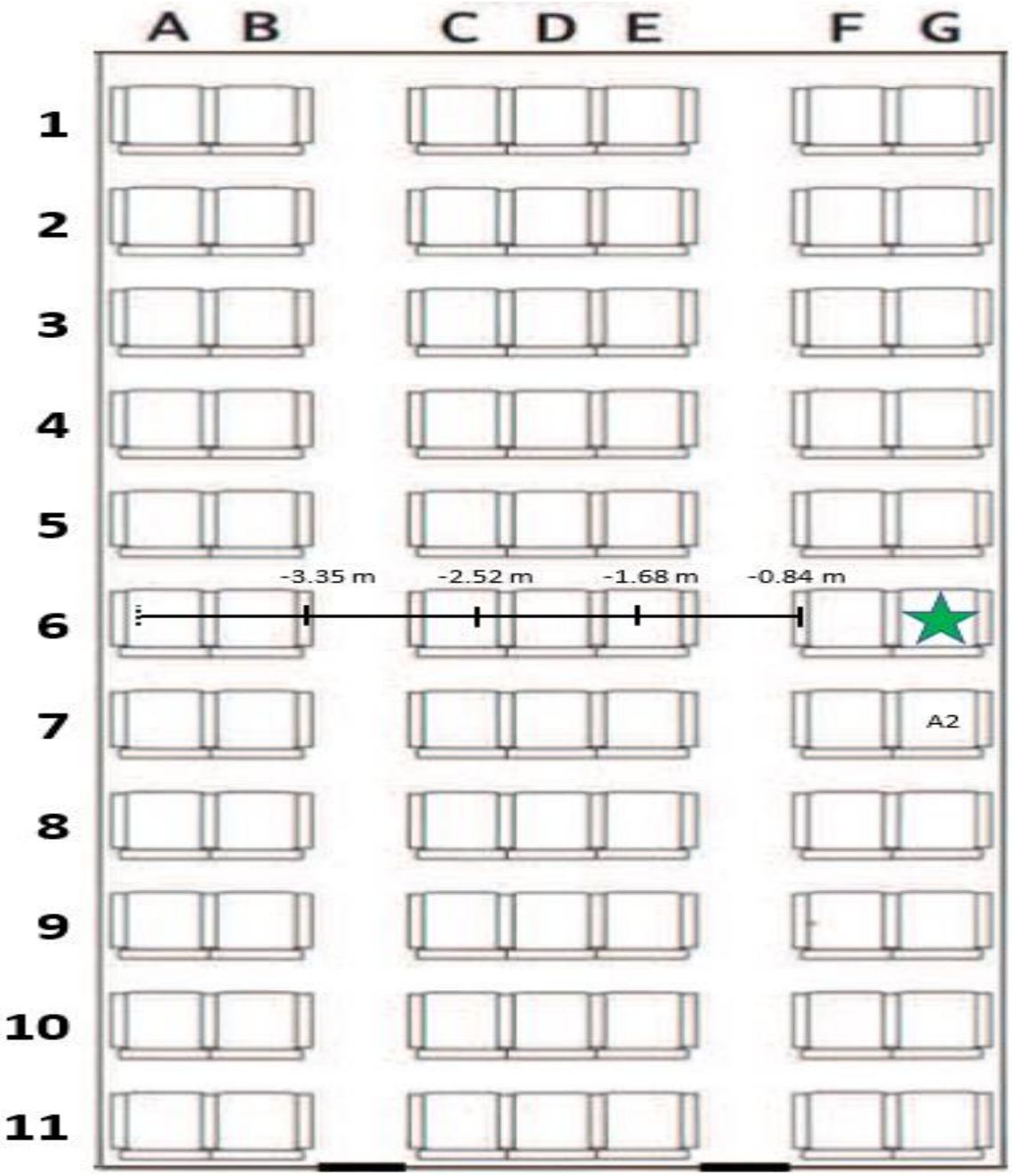

Figure C.47 Test 19 (B-I) ISOPass undeployed source location and sampling tree orientation.

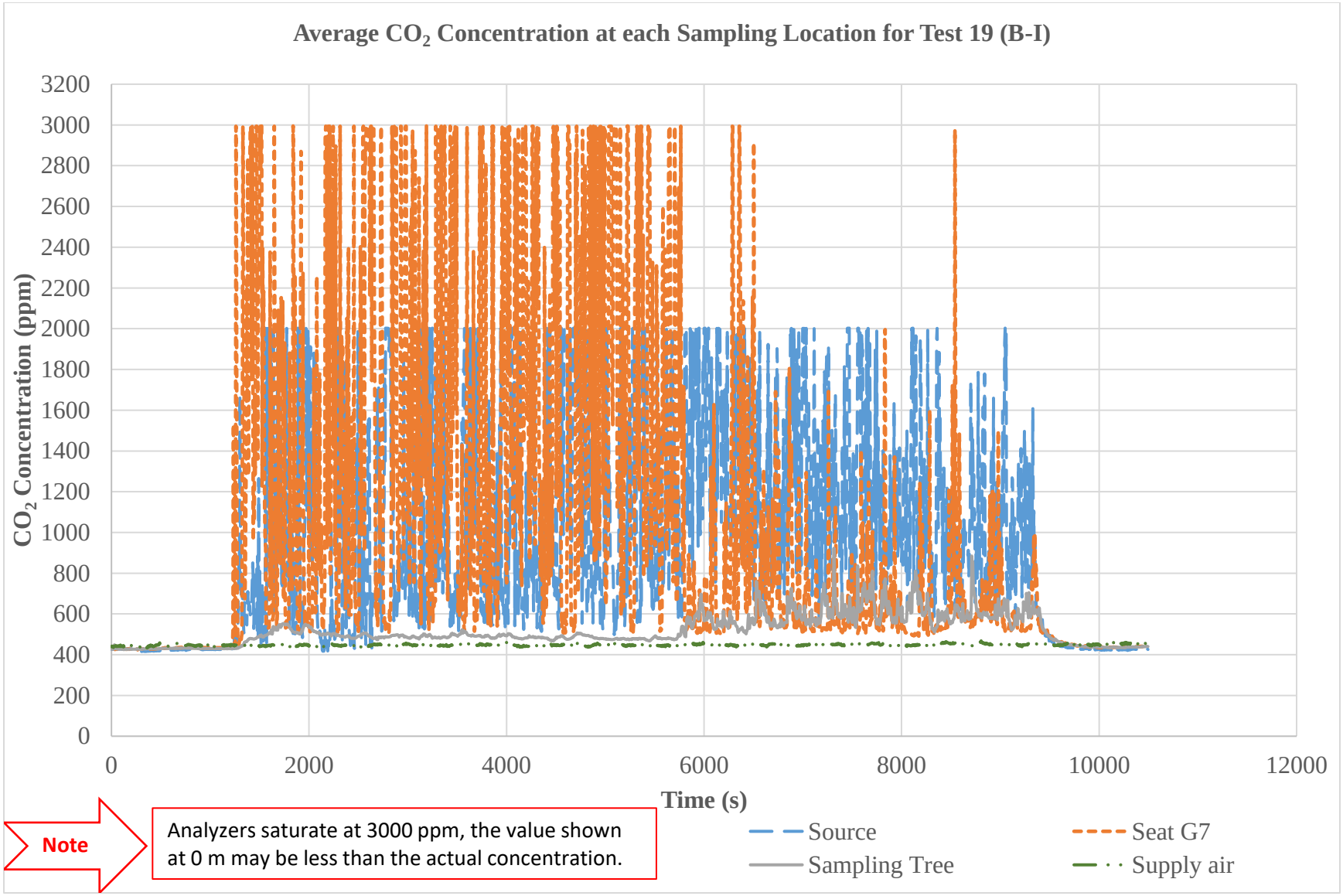

Figure C.48 Ininstantaneous CO_2 concentration at each sampling location for Test 19 (B-I) ISOPass undeployed.

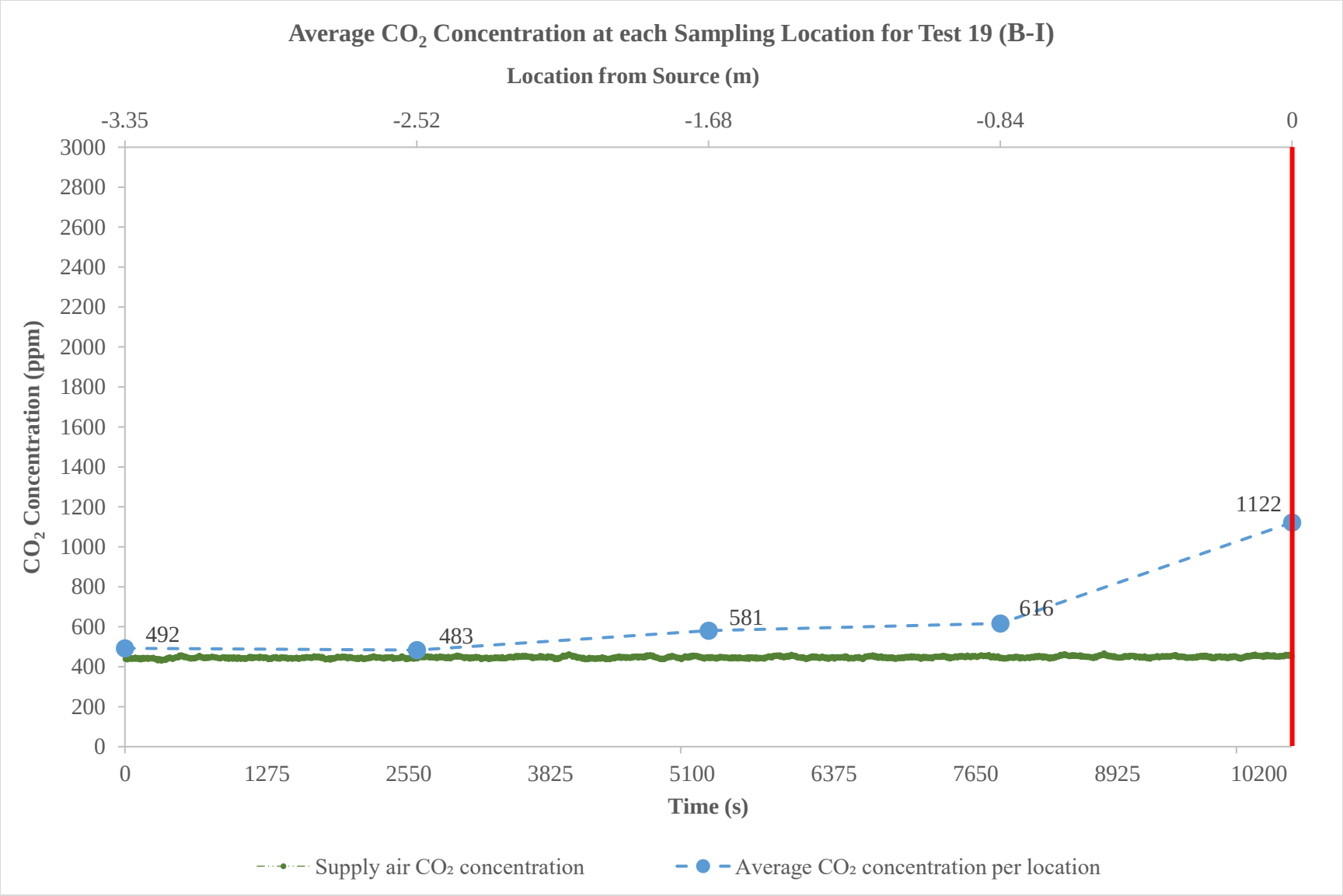

Figure C.49 Average CO_2 concentration at each sampling location for Test 19 (B-I) ISOPass undeployed.

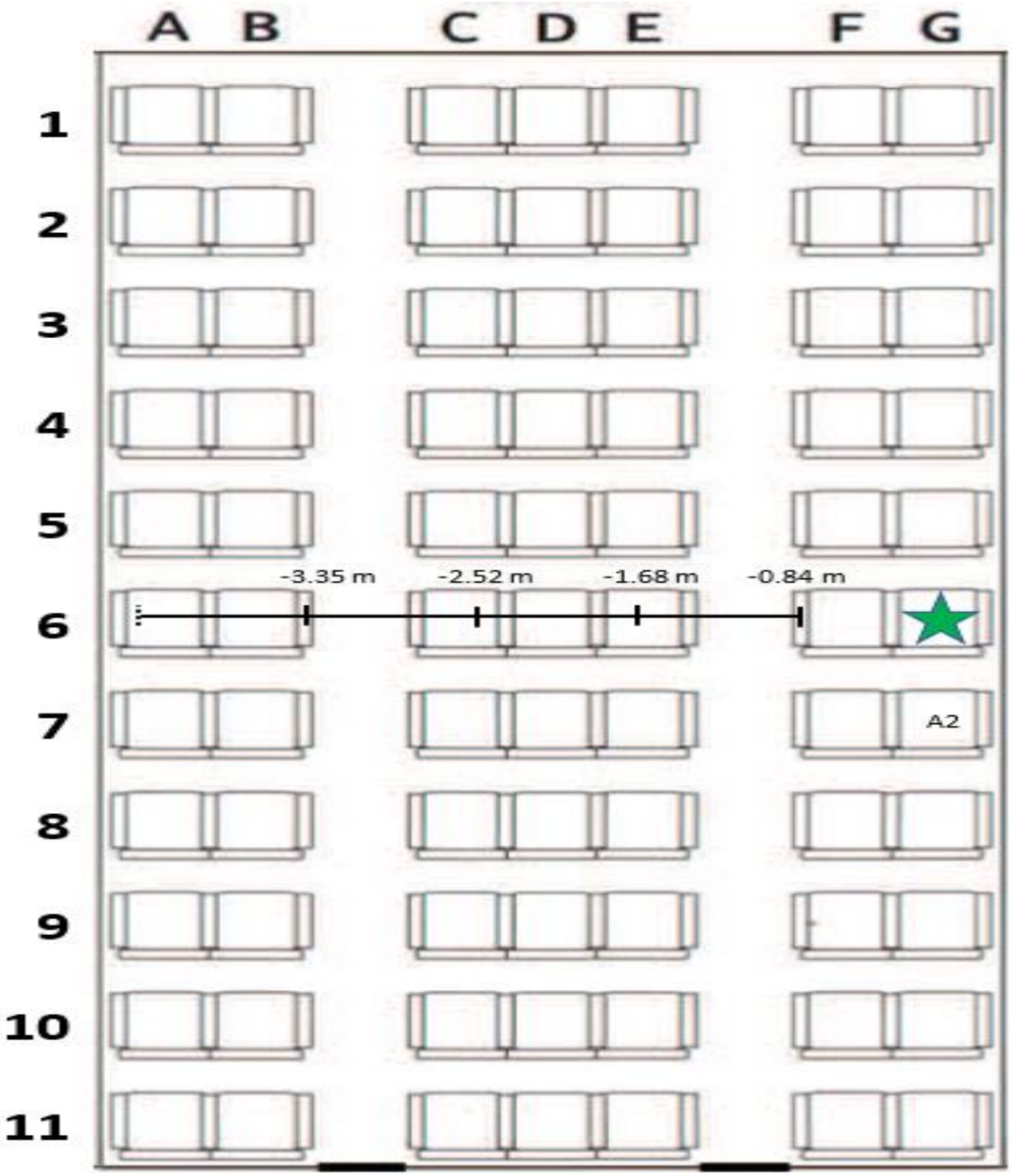

Figure C.50 Test 20 (B-I) ISOPass undeployed source location and sampling tree orientation.

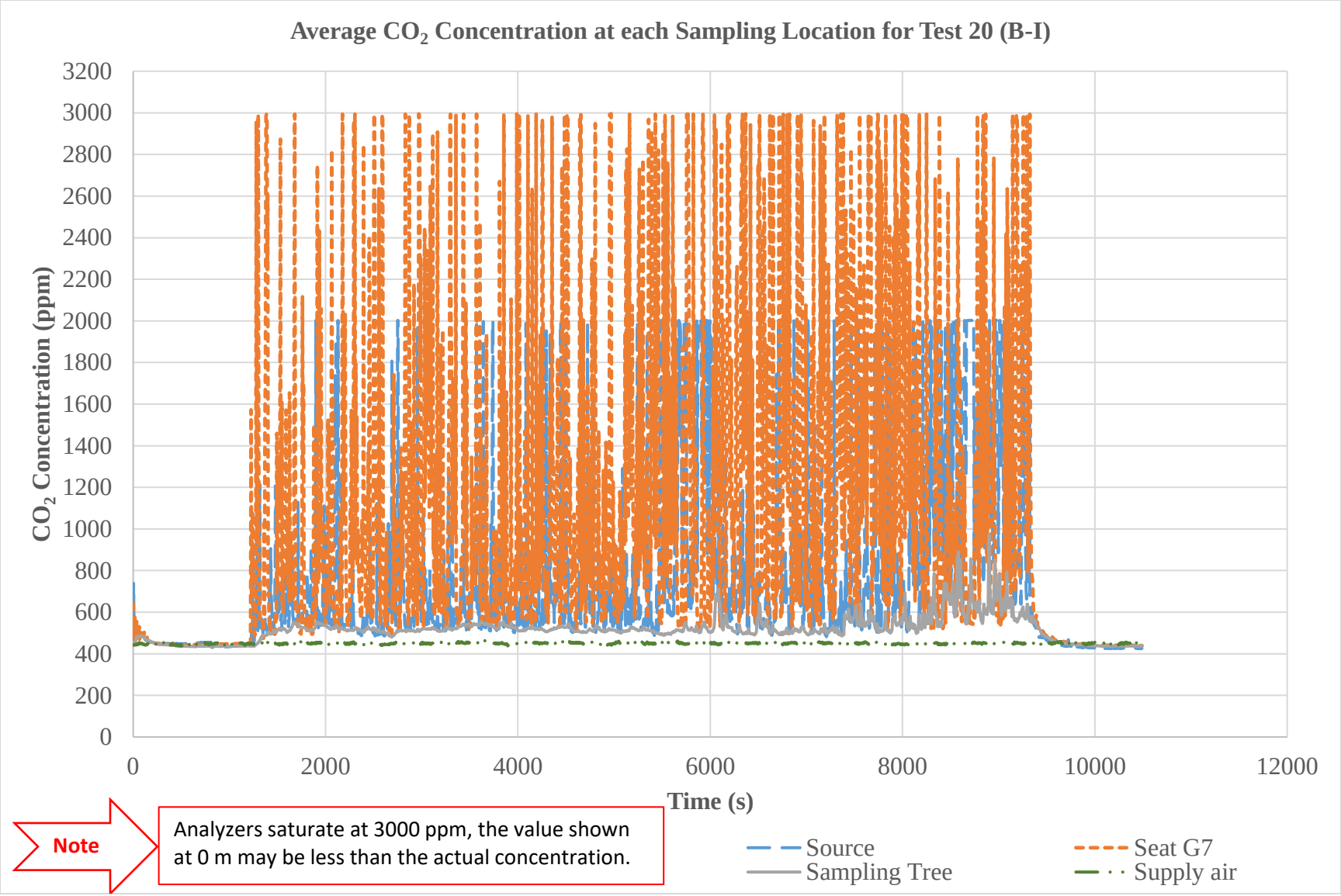

Figure C.51 Ininstantaneous CO_2 concentration at each sampling location for Test 20 (B-I) ISOPass undeployed.

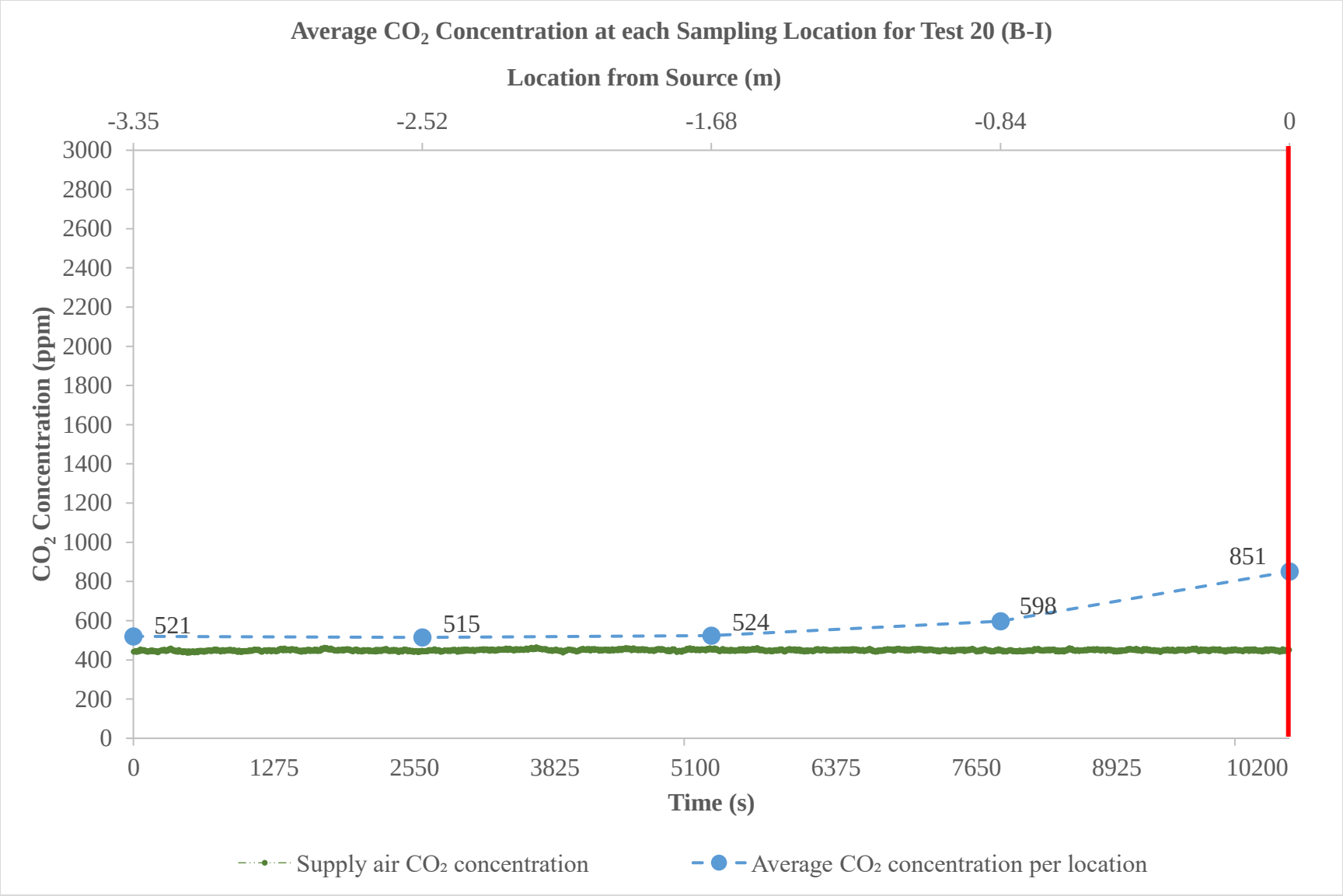

Figure C.52 Average CO_2 concentration at each sampling location for Test 20 (B-I) ISOPass undeployed.

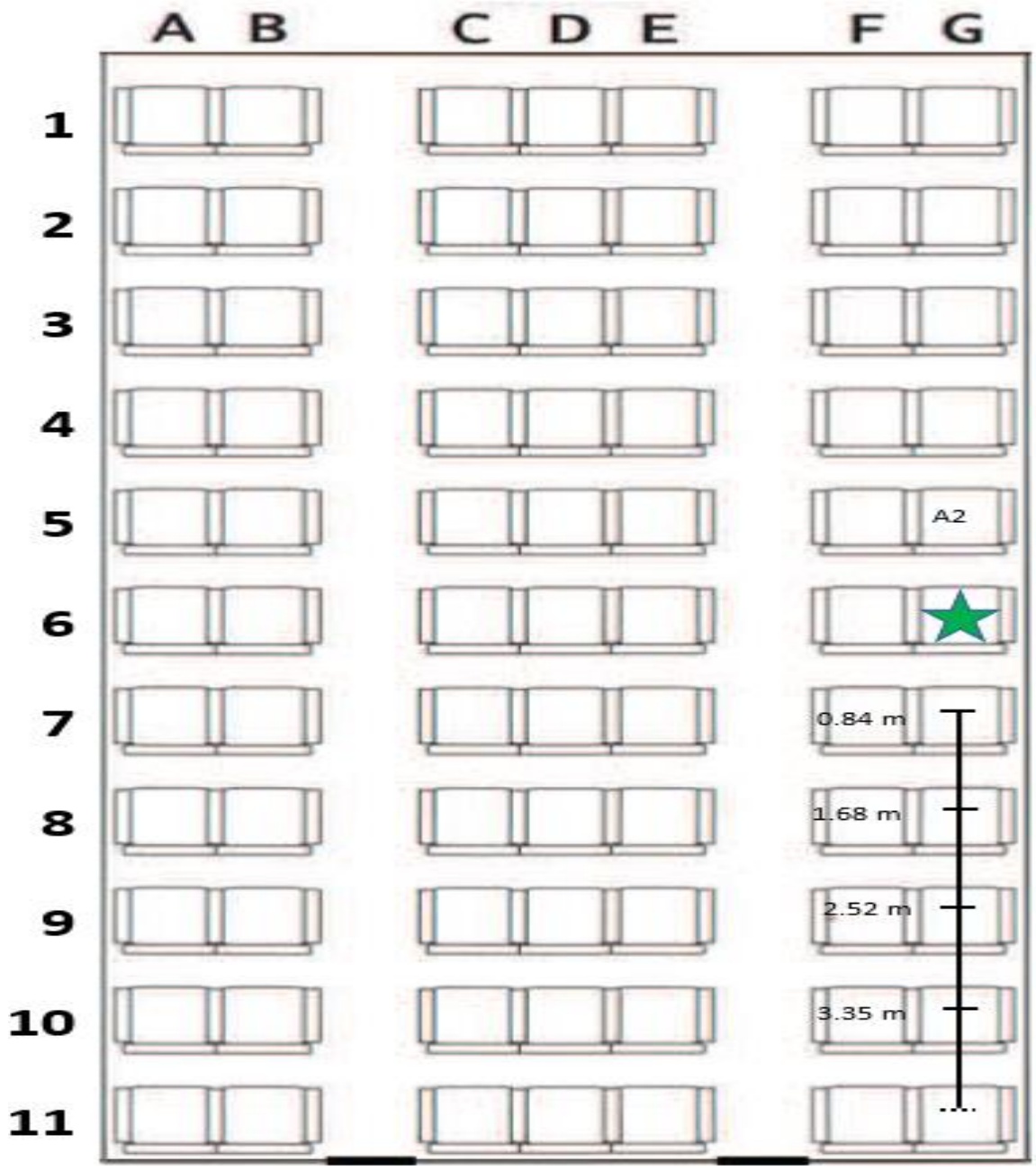

Figure C.53 Test 23 (B-I) ISOPass undeployed source location and sampling tree orientation.

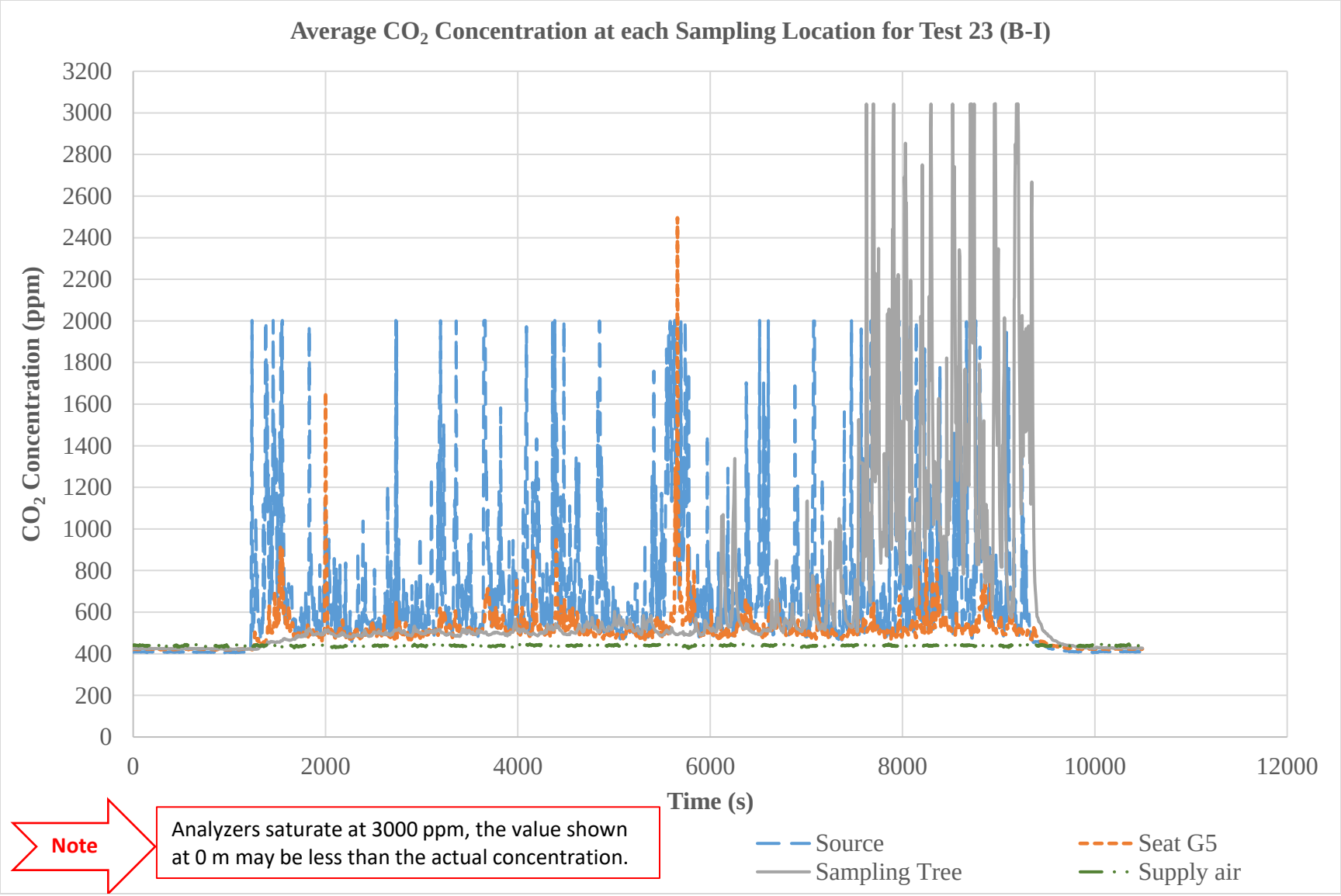

Figure C.54 Ininstantaneous CO_2 concentration at each sampling location for Test 23 (B-I) ISOPass undeployed.

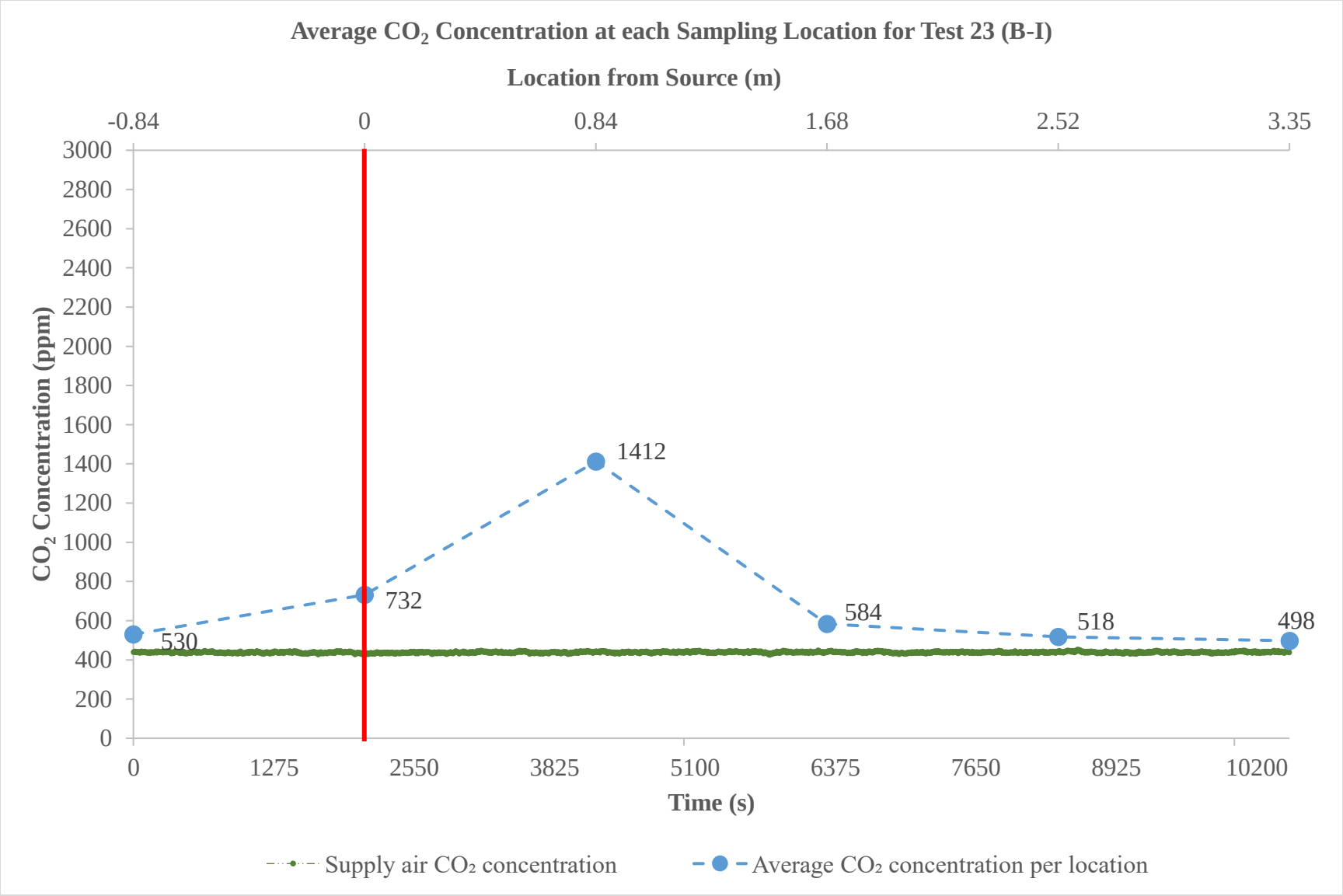

Figure C.55 Average CO_2 concentration at each sampling location for Test 23 (B-I) ISOPass undeployed.

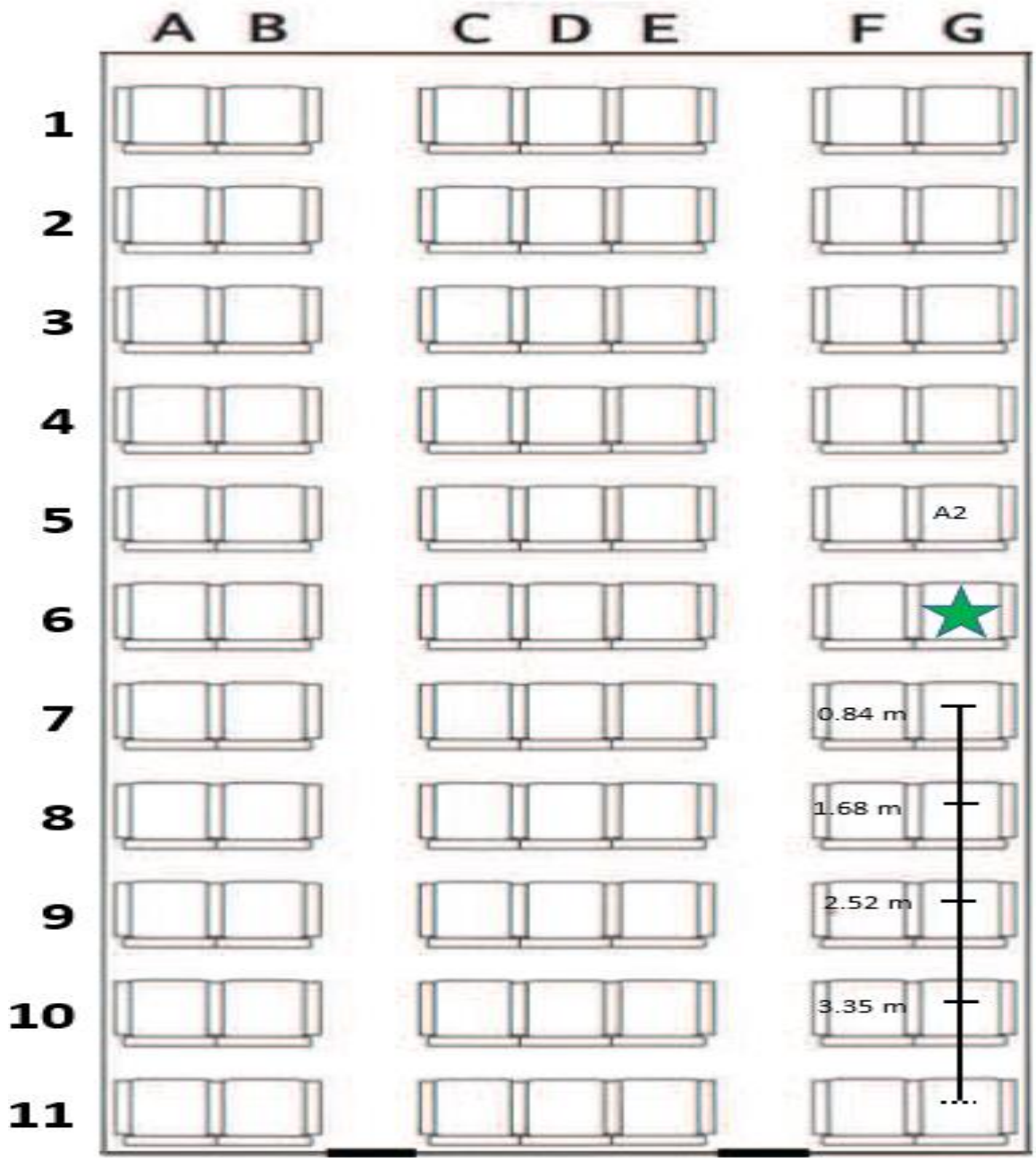

Figure C.56 Test 24 (B-I) ISOPass undeployed source location and sampling tree orientation.

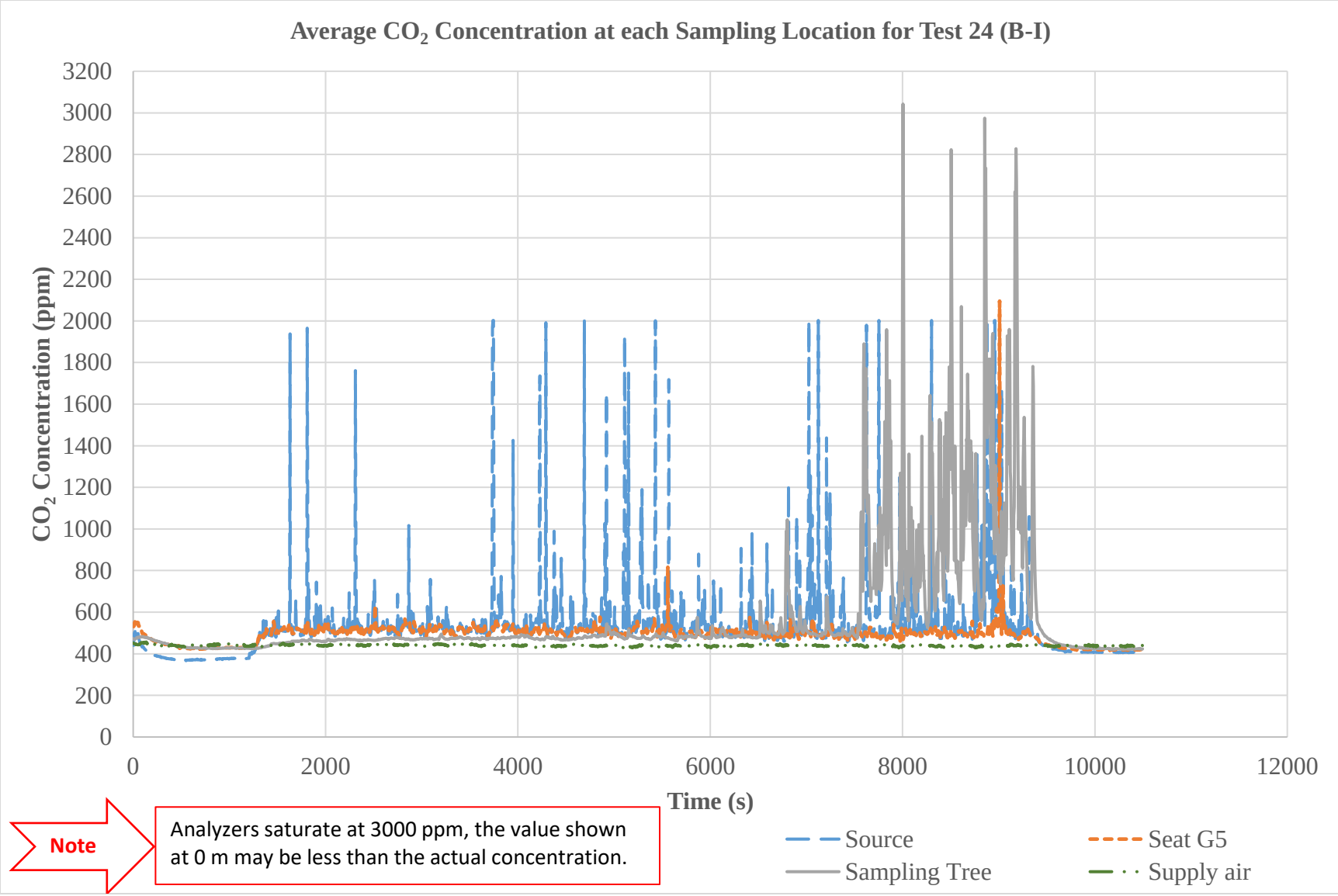

Figure C.57 Ininstantaneous CO_2 concentration at each sampling location for Test 24 (B-I) ISOPass undeployed.

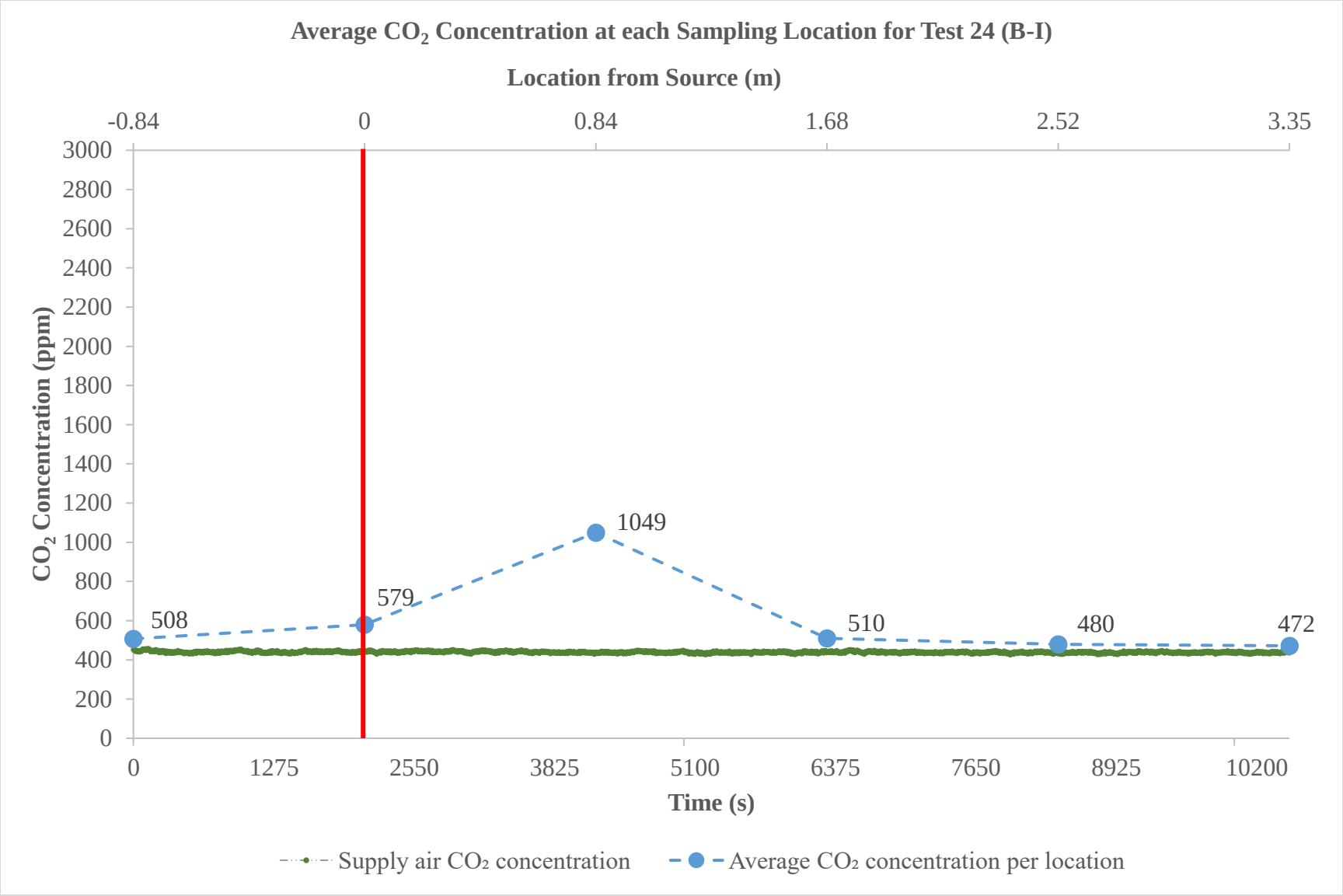

Figure C.58 Average CO_2 concentration at each sampling location for Test 24 (B-I) ISOPass undeployed.

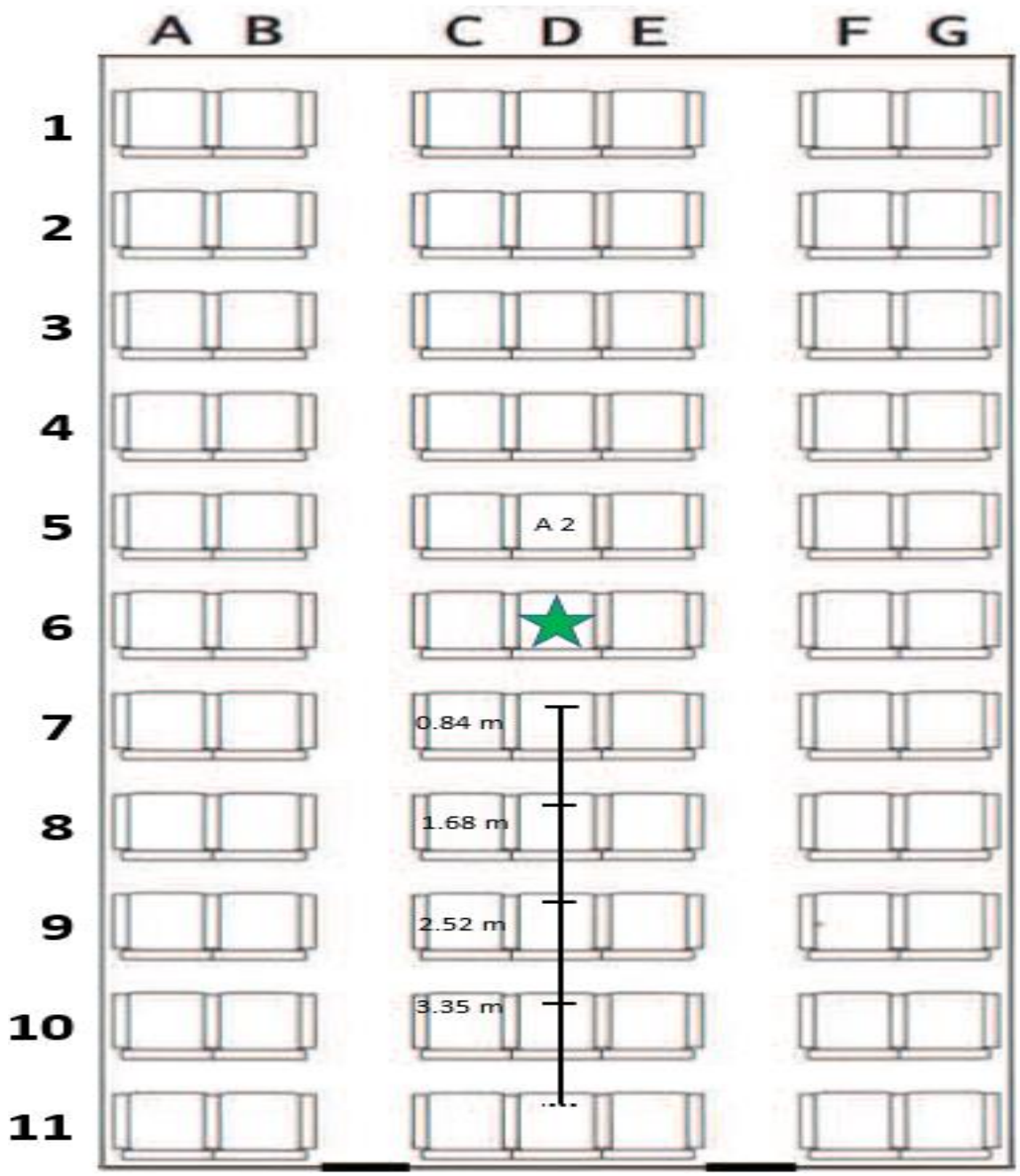

Figure C.59 Test 26 (B-I) ISOPass undeployed source location and sampling tree orientation.

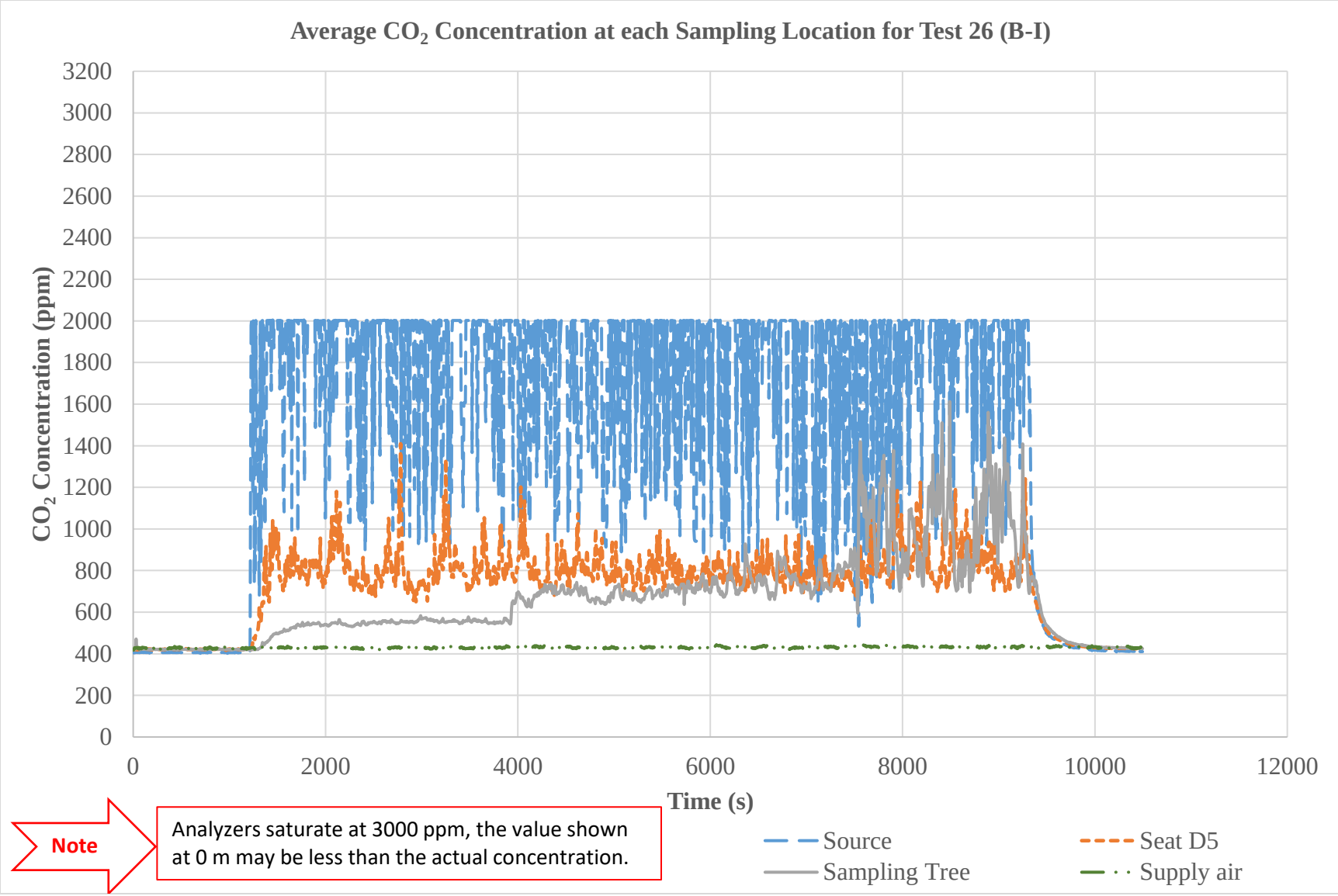

Figure C.60 Ininstantaneous CO_2 concentration at each sampling location for Test 26 (B-I) ISOPass undeployed.

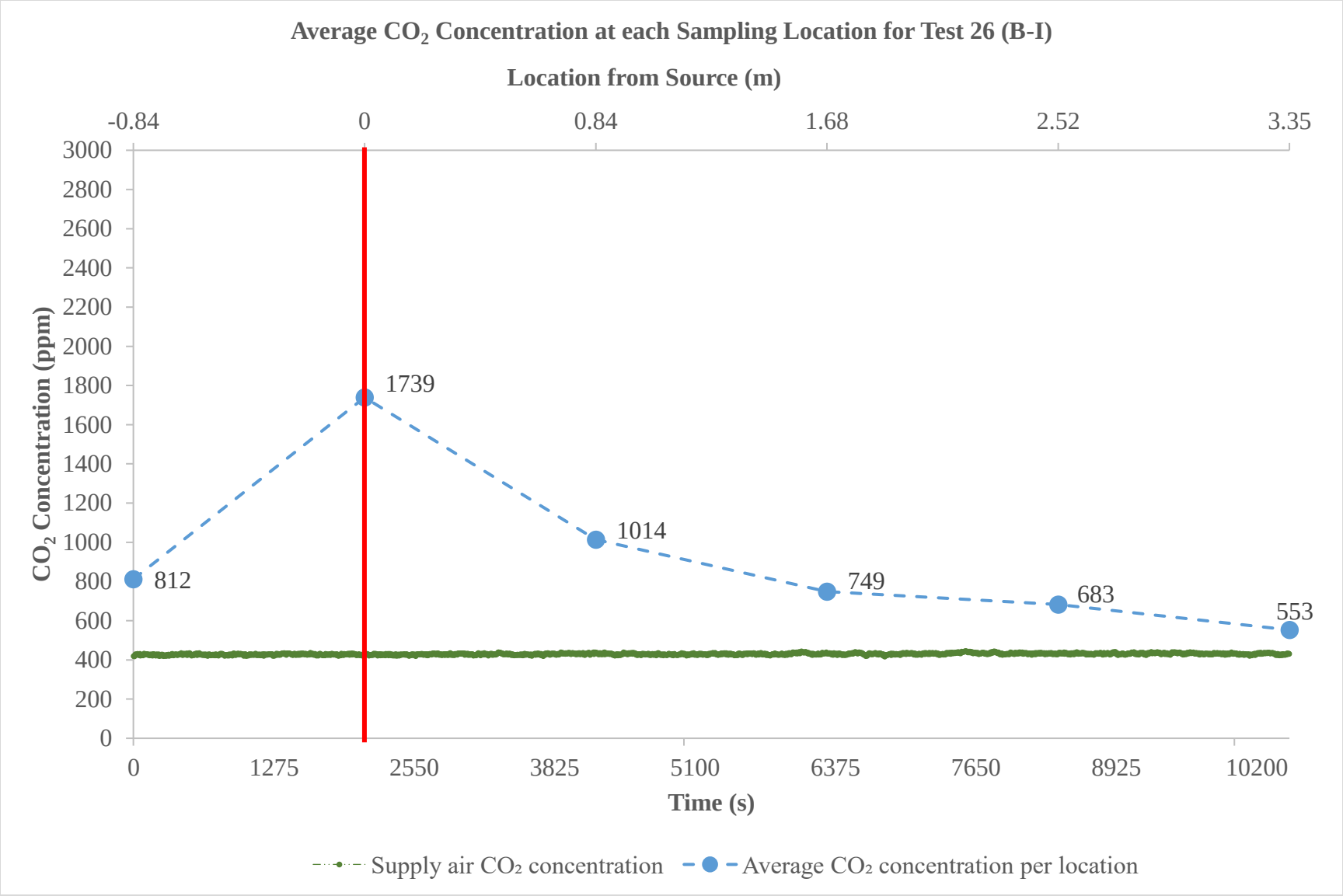

Figure C.61 Average CO_2 concentration at each sampling location for Test 26 (B-I) ISOPass undeployed.

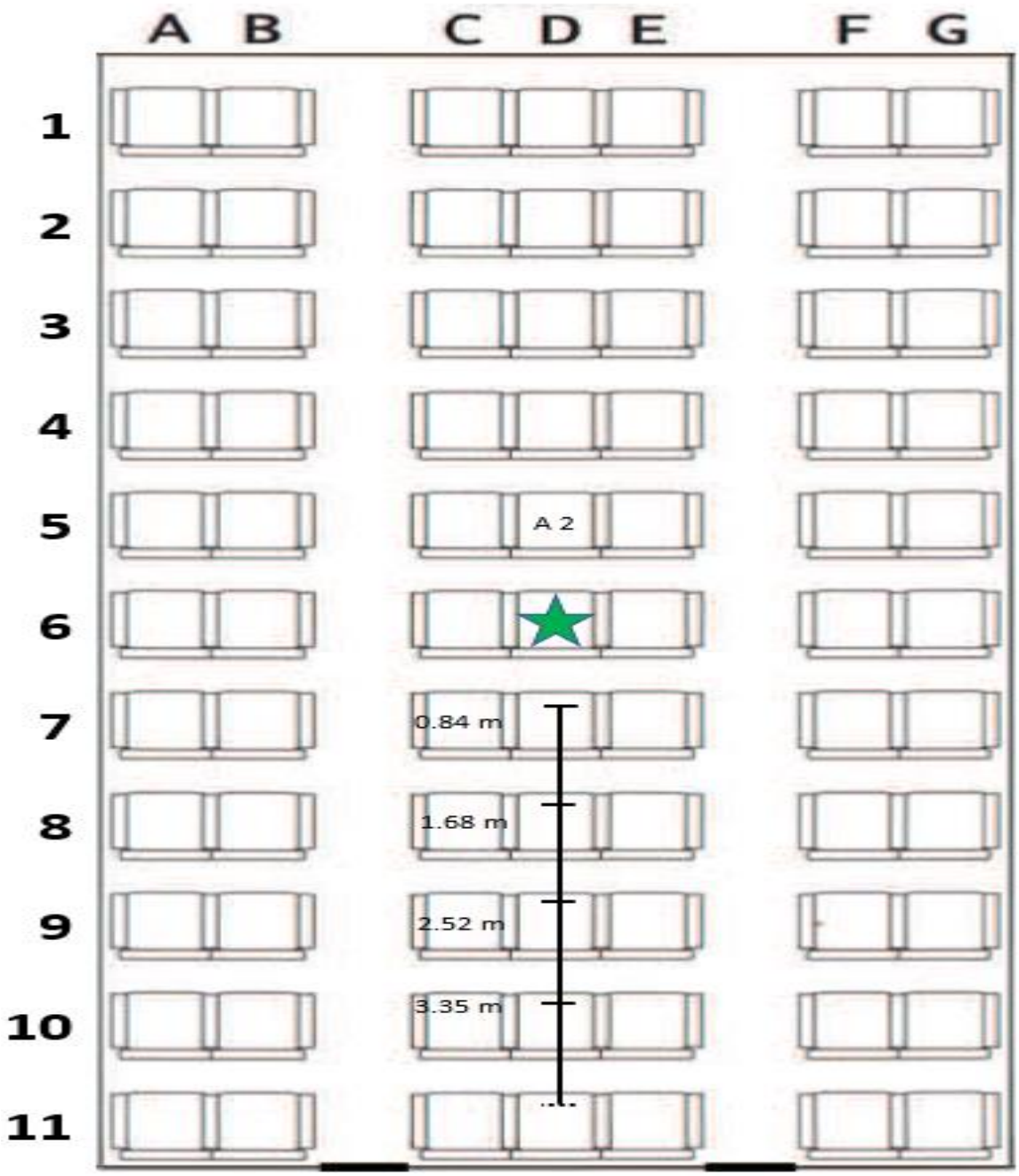

Figure C.62 Test 27 (B-I) ISOPass undeployed source location and sampling tree orientation.

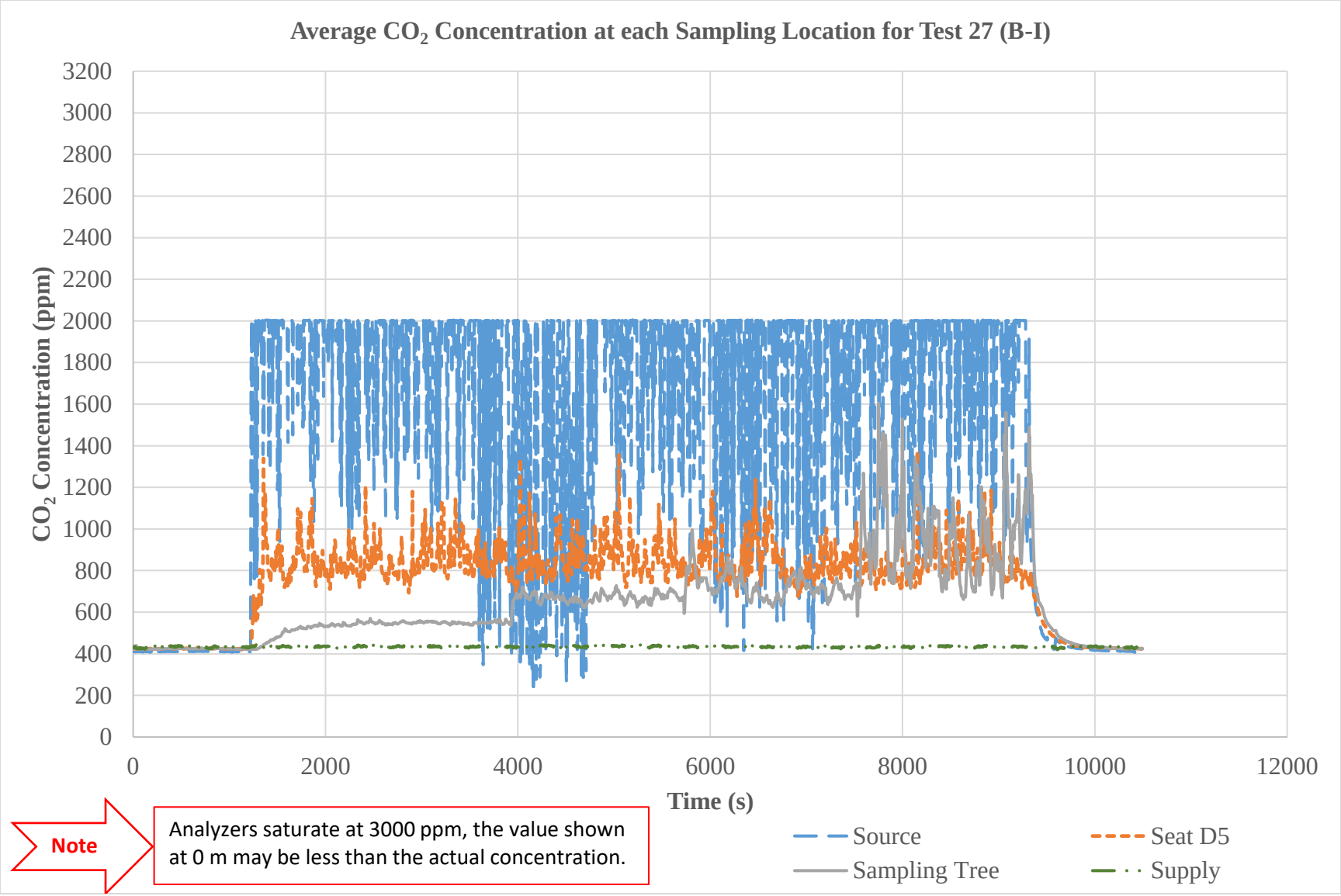

Figure C.63 Ininstantaneous CO_2 concentration at each sampling location for Test 27 (B-I) ISOPass undeployed.

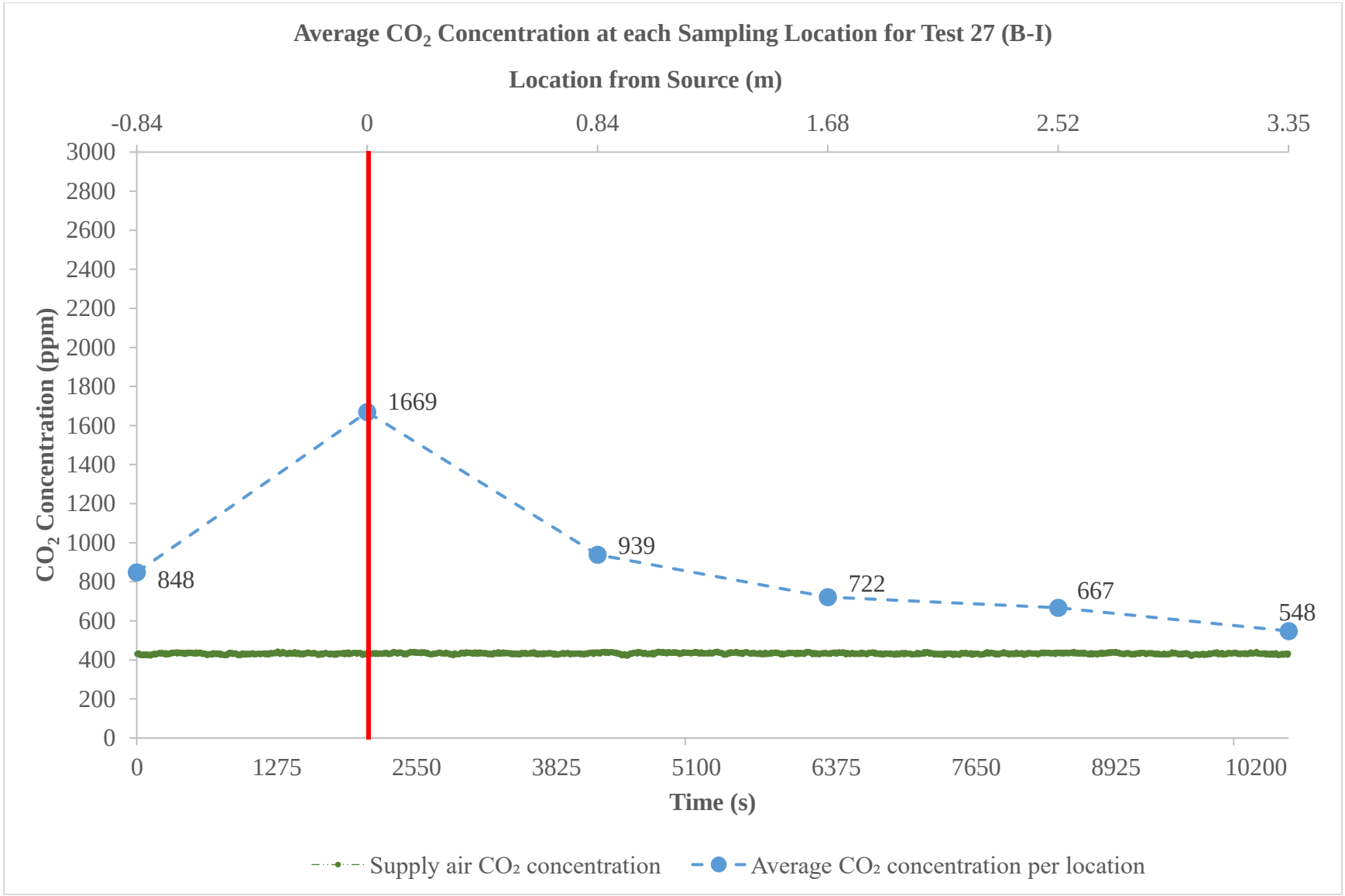

Figure C.64 Average CO_2 concentration at each sampling location for Test 27 (B-I) ISOPass undeployed.

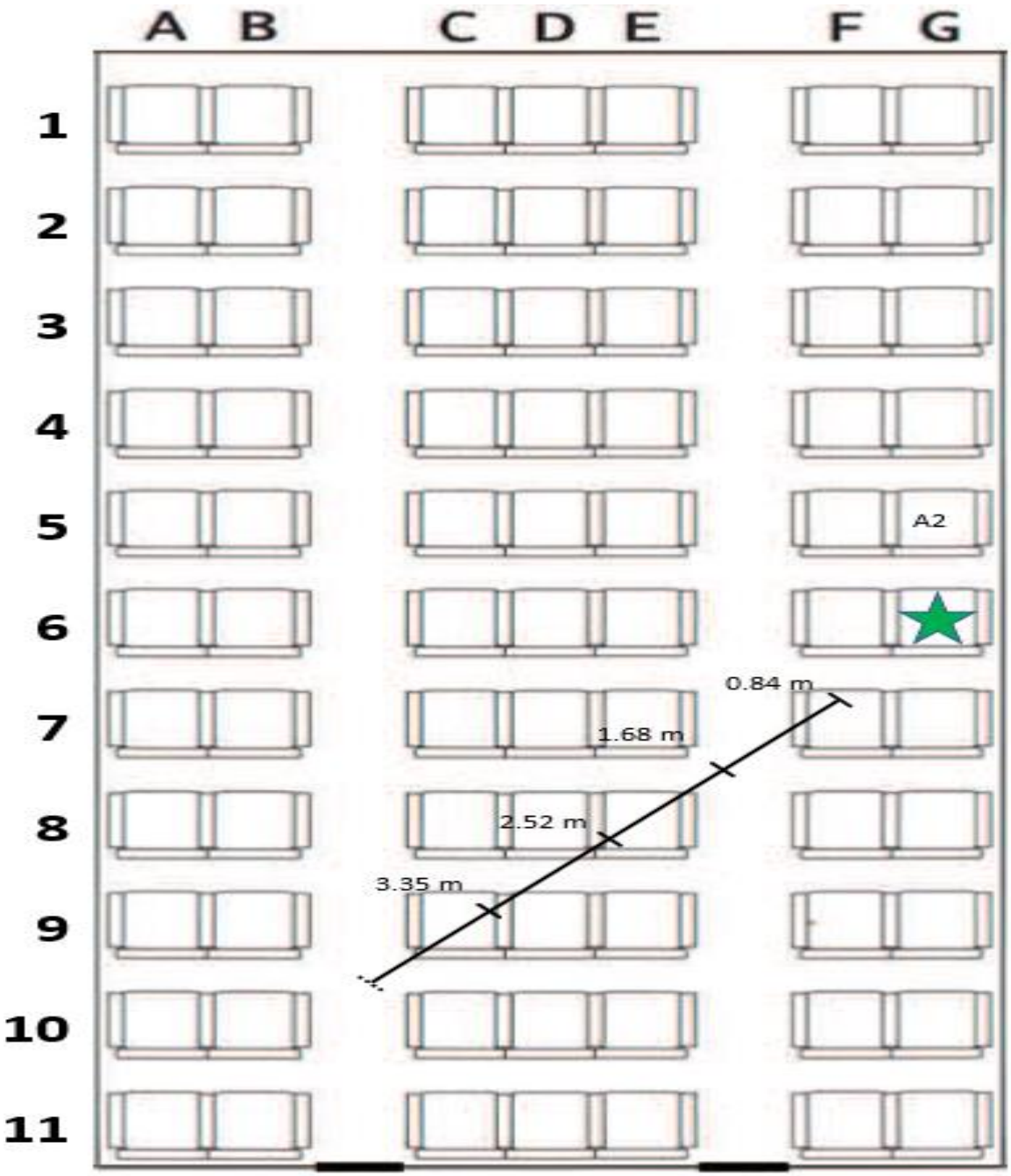

Figure C.65 Test 28 (B-I) ISOPass undeployed source location and sampling tree orientation.

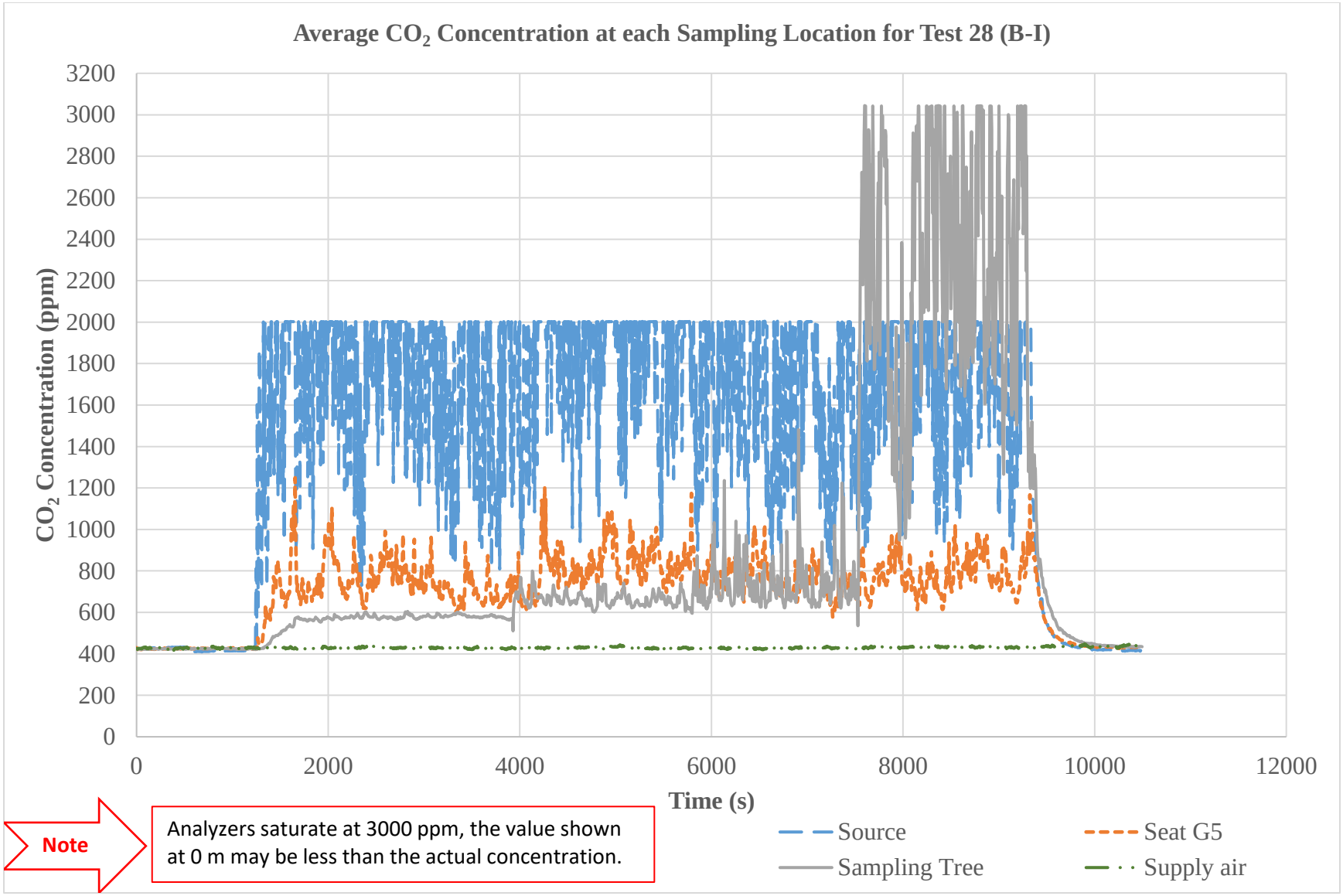

Figure C.66 Ininstantaneous CO_2 concentration at each sampling location for Test 28 (B-I) ISOPass undeployed.

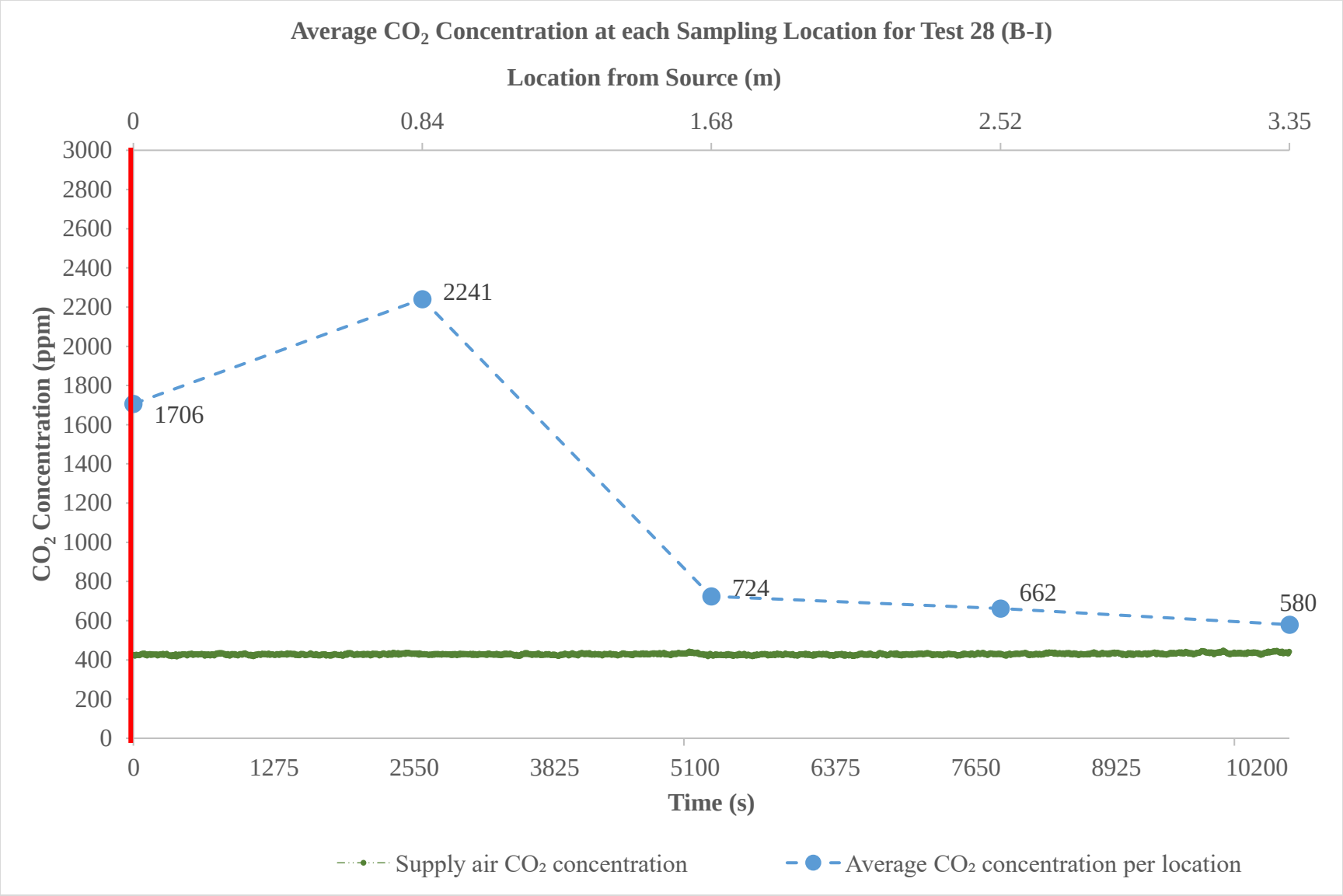

Figure C.67 Average CO_2 concentration at each sampling location for Test 28 (B-I) ISOPass undeployed.

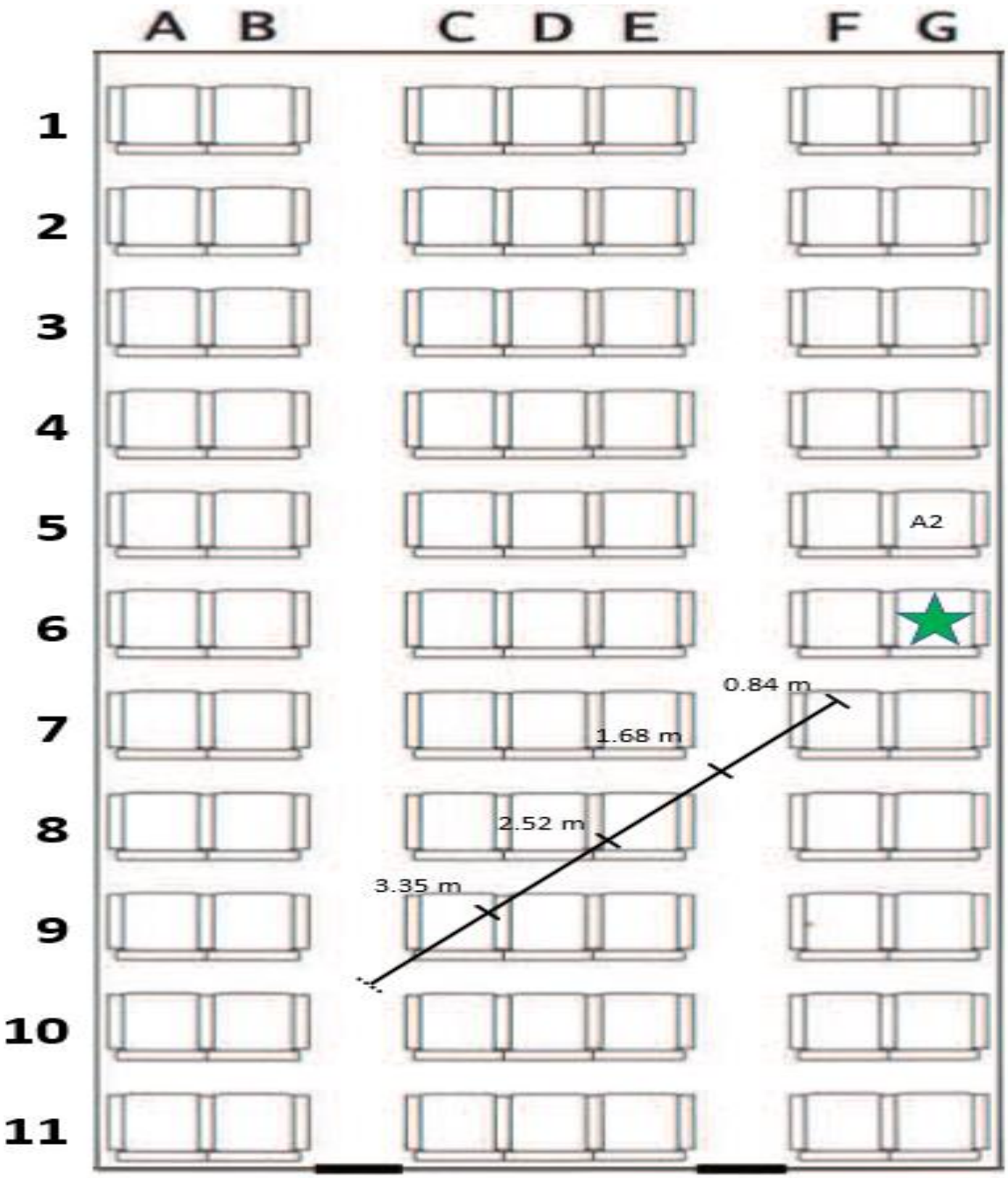

Figure C.68 Test 29 (B-I) ISOPass undeployed source location and sampling tree orientation.

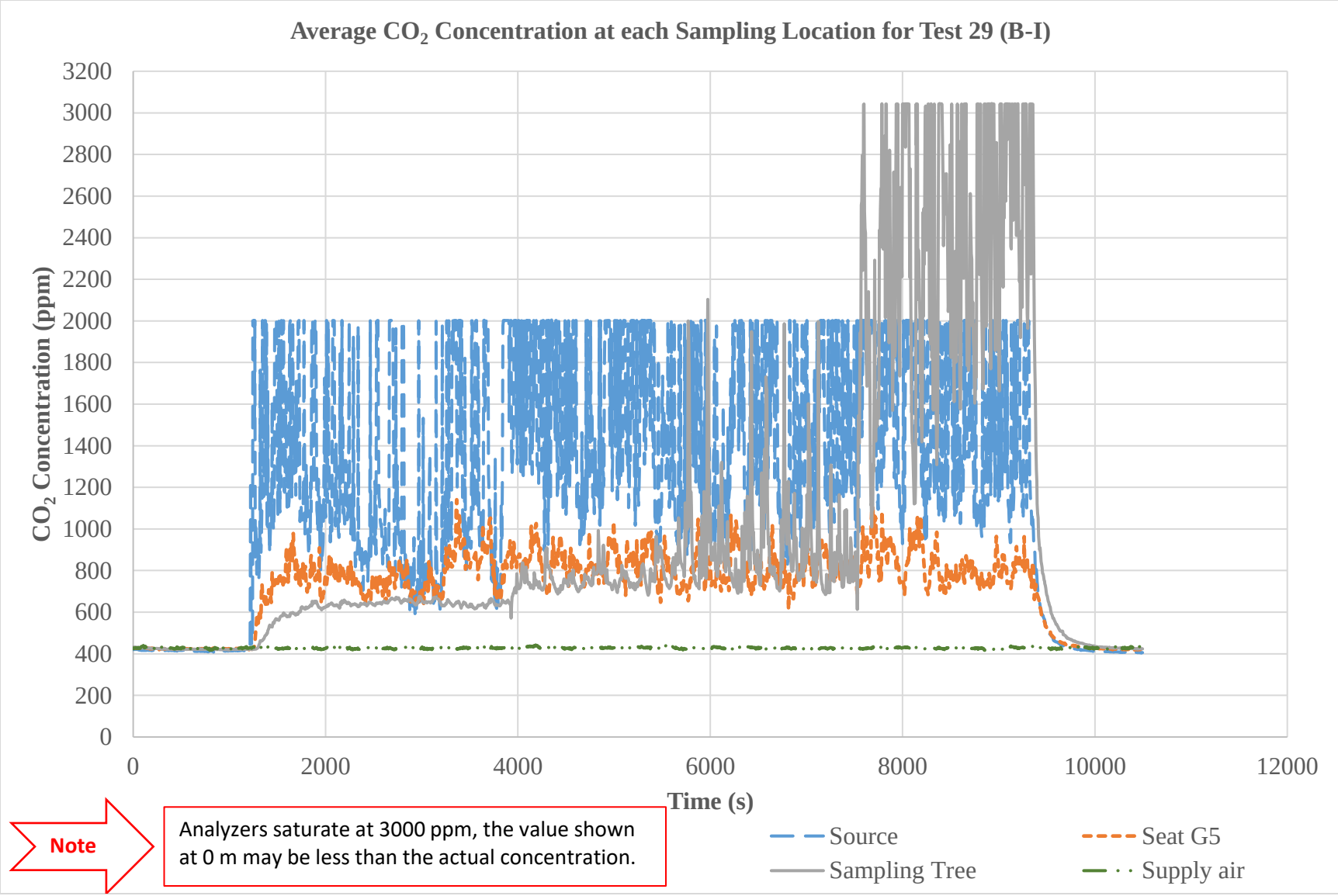

Figure C.69 Ininstantaneous CO_2 concentration at each sampling location for Test 29 (B-I) ISOPass undeployed.

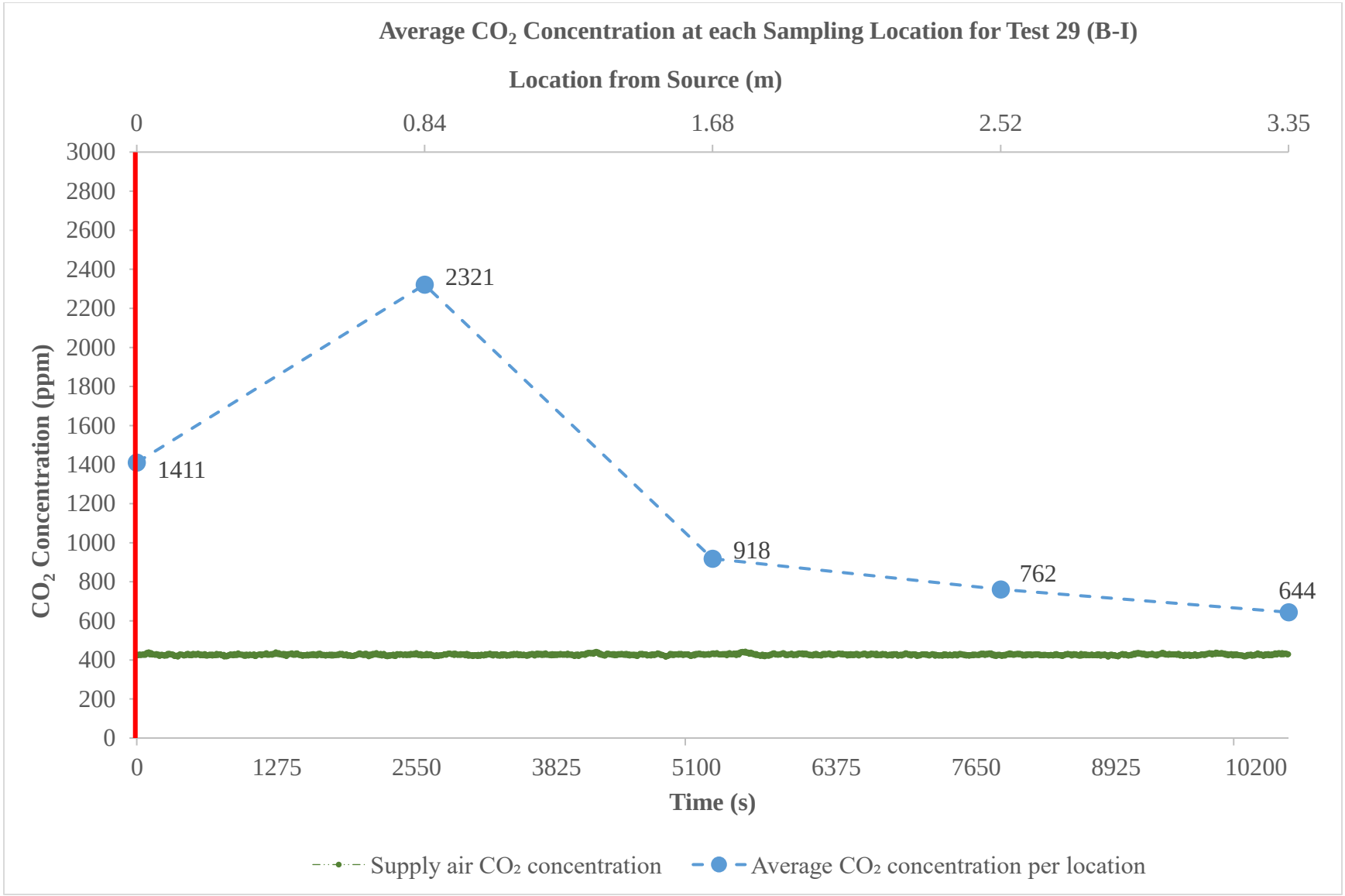

Figure C.70 Average CO_2 concentration at each sampling location for Test 29 (B-I) ISOPass undeployed.

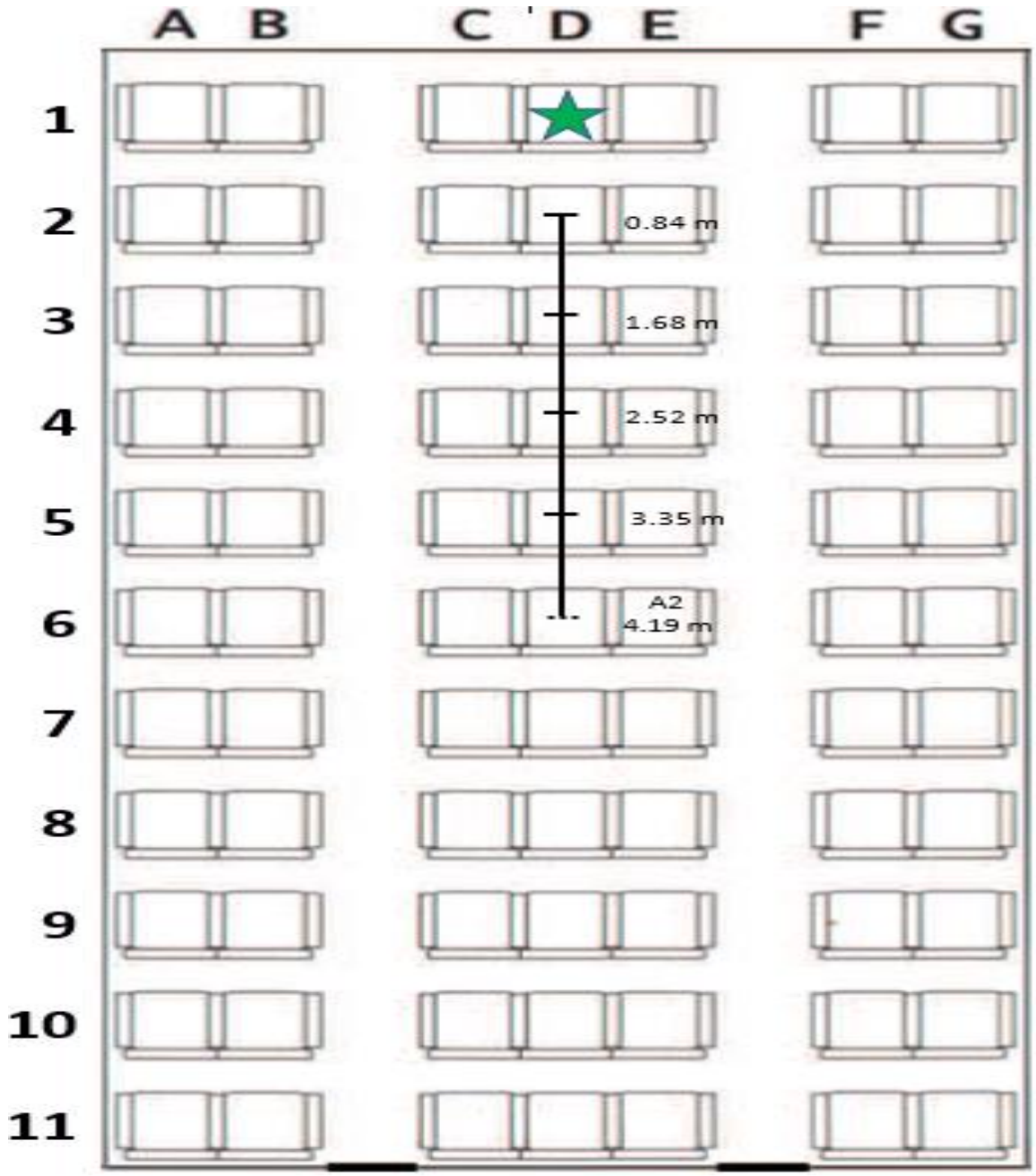

Figure C.71 Test 30 (B-I) ISOPass undeployed source location and sampling tree orientation.

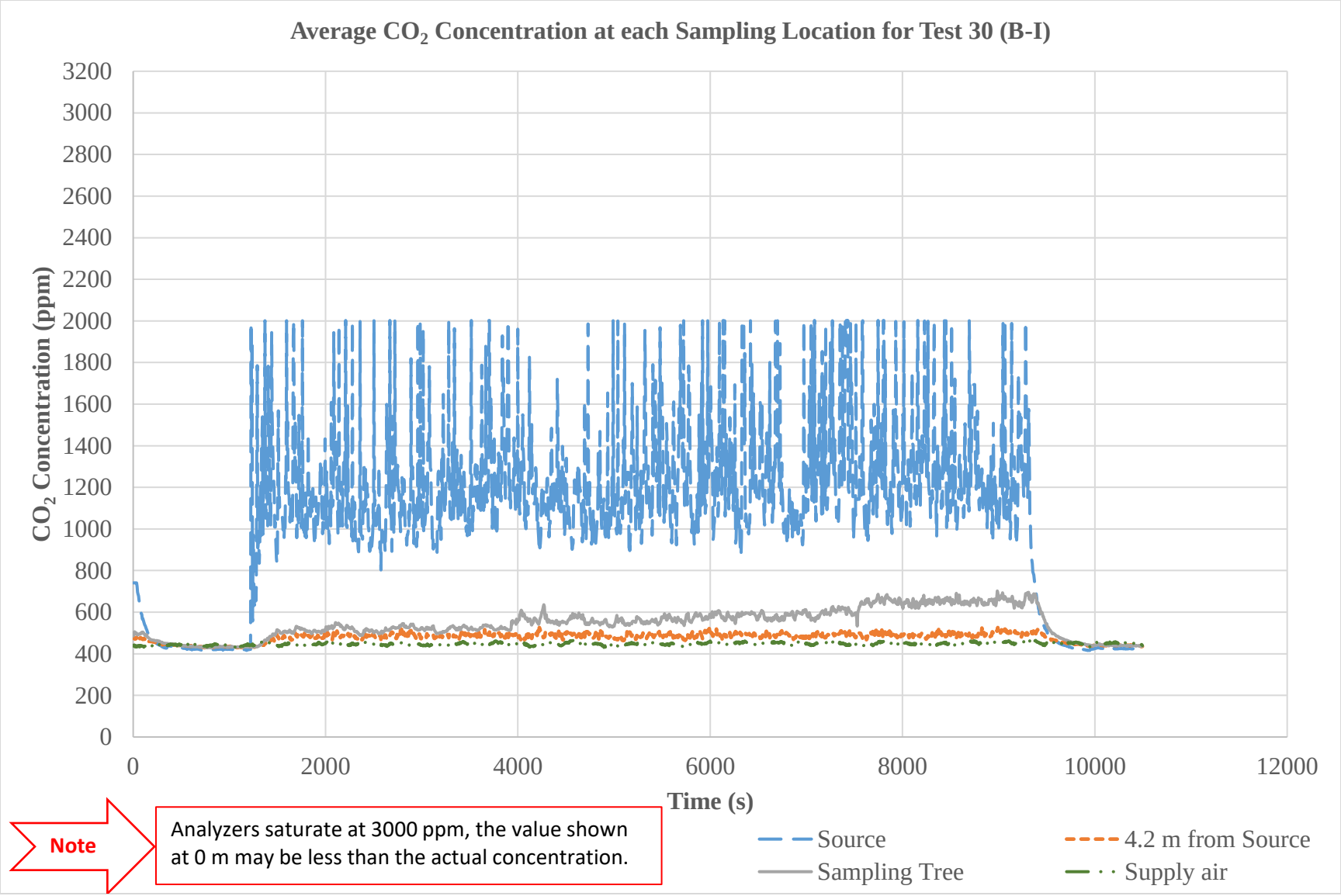

Figure C.72 Ininstantaneous CO_2 concentration at each sampling location for Test 30 (B-I) ISOPass undeployed.

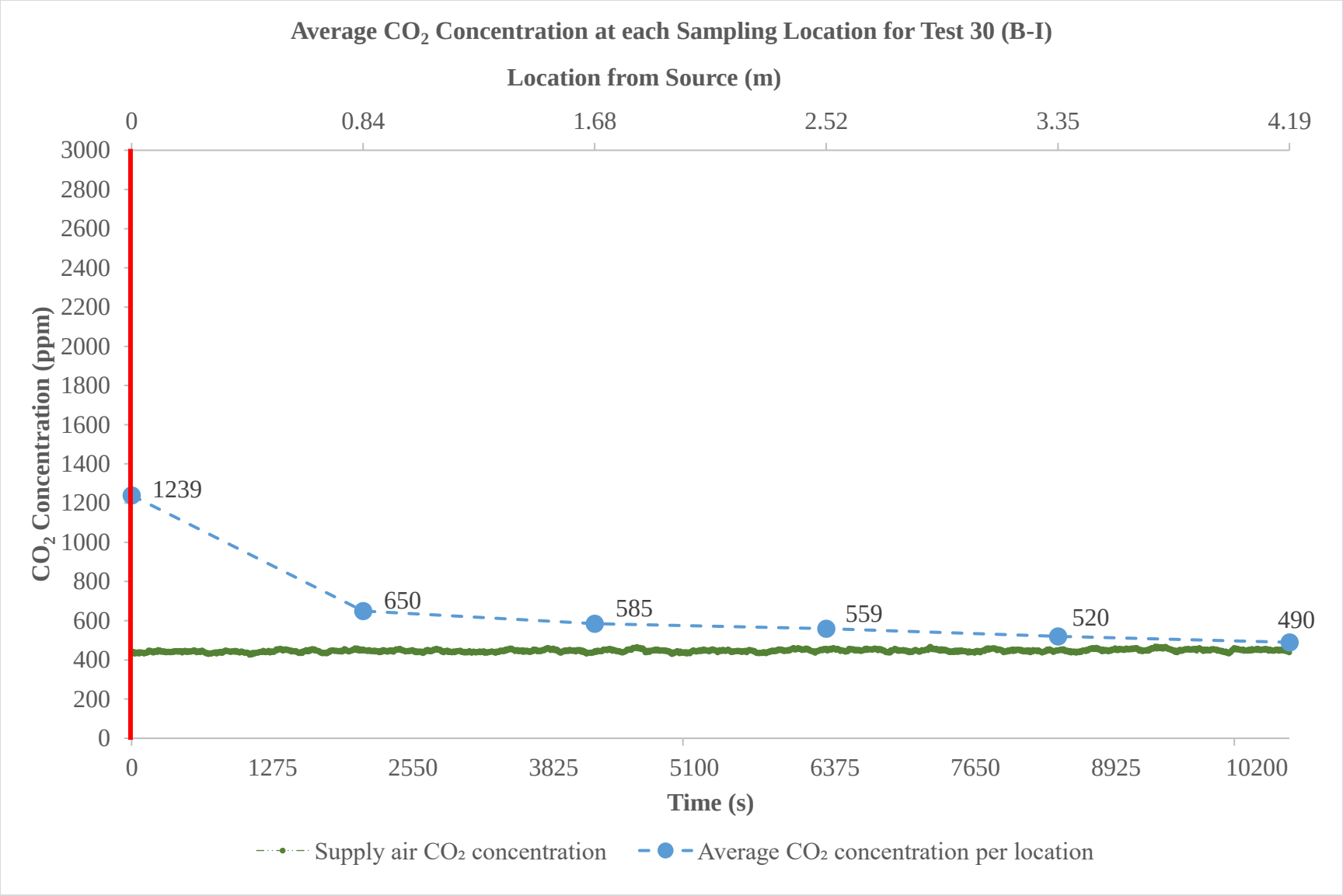

Figure C.73 Average CO_2 concentration at each sampling location for Test 30 (B-I) ISOPass undeployed.

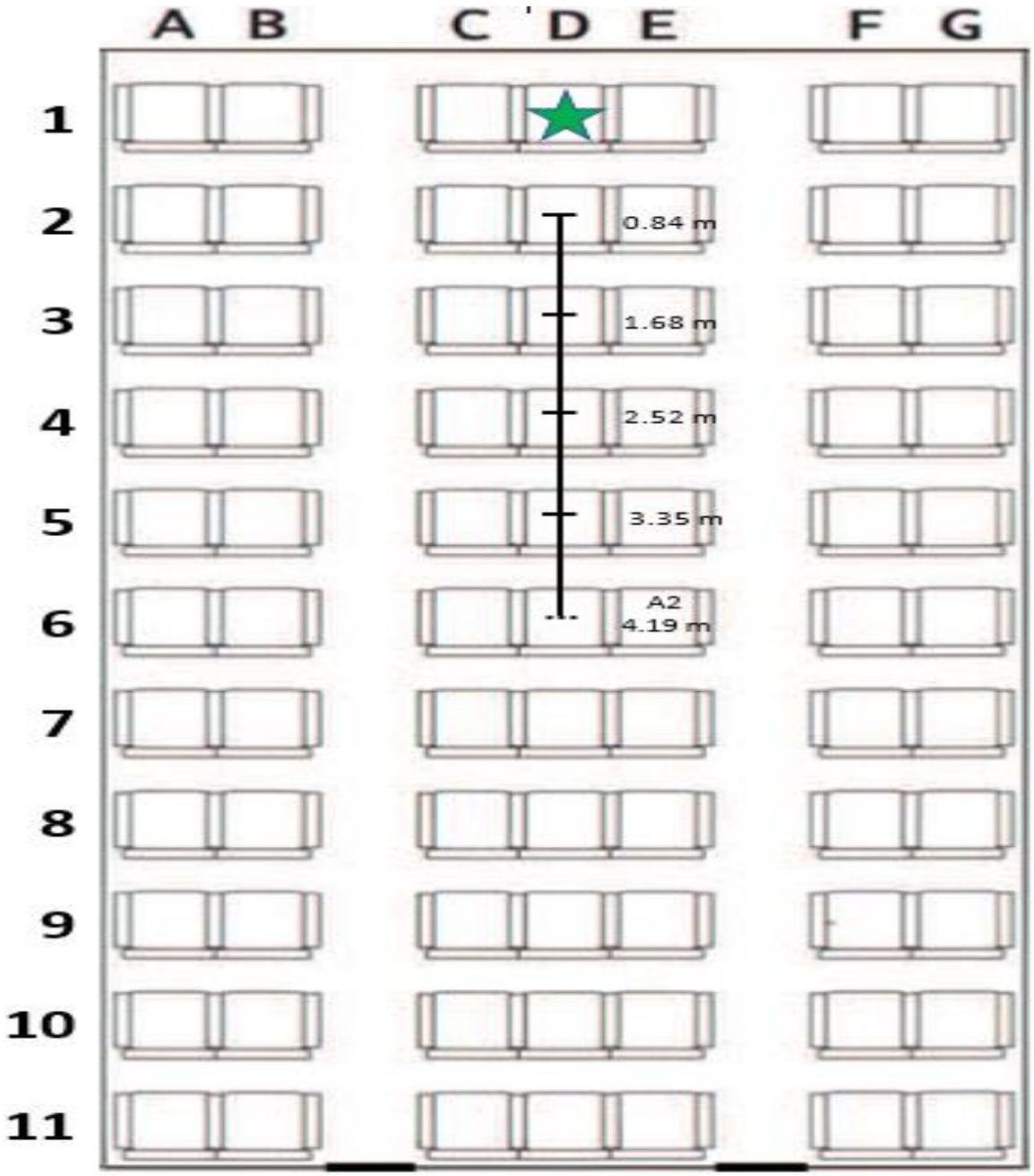

Figure C.74 Test 31 (B-I) ISOPass undeployed source location and sampling tree orientation.

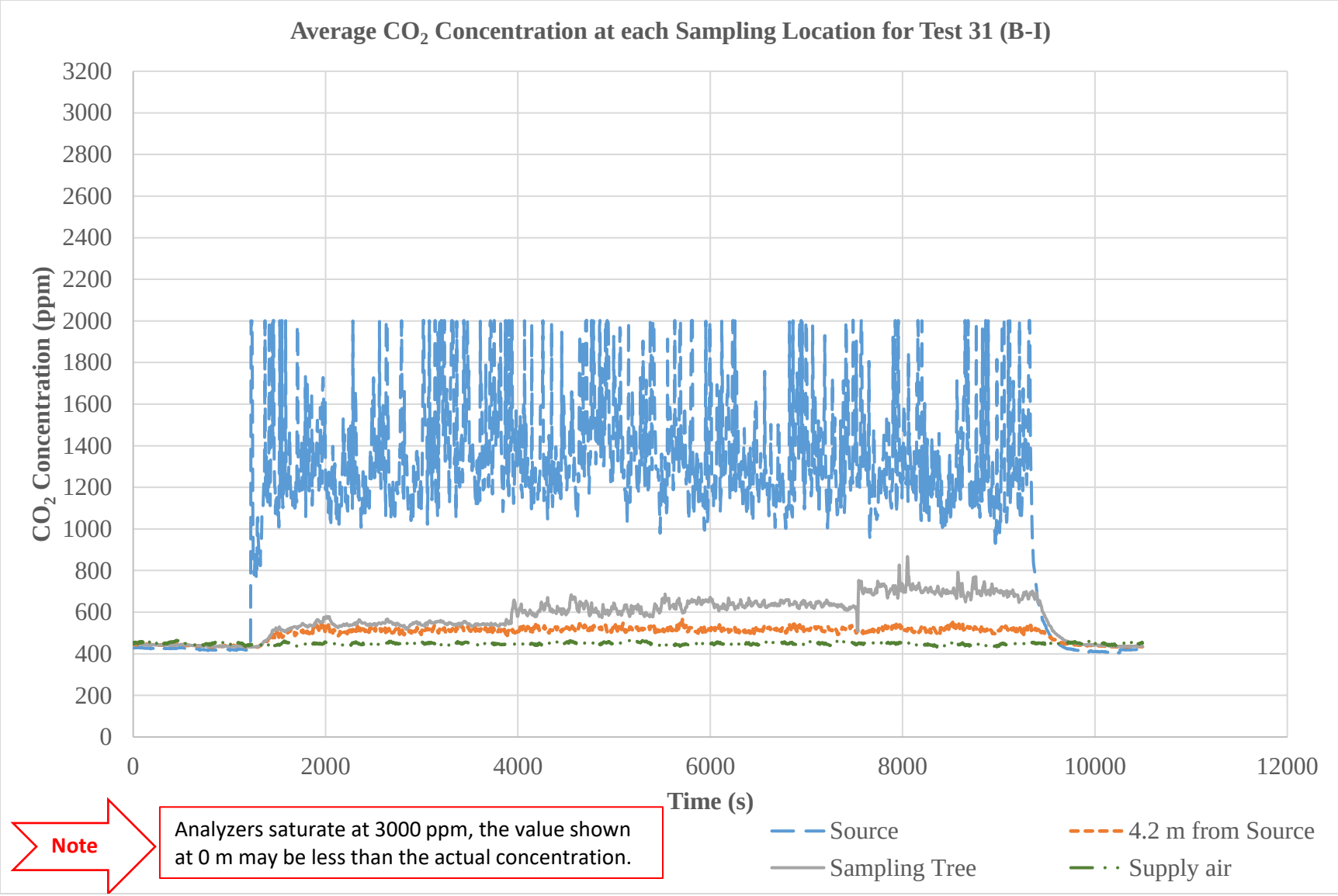

Figure C.75 Ininstantaneous CO_2 concentration at each sampling location for Test 31 (B-I) ISOPass undeployed.

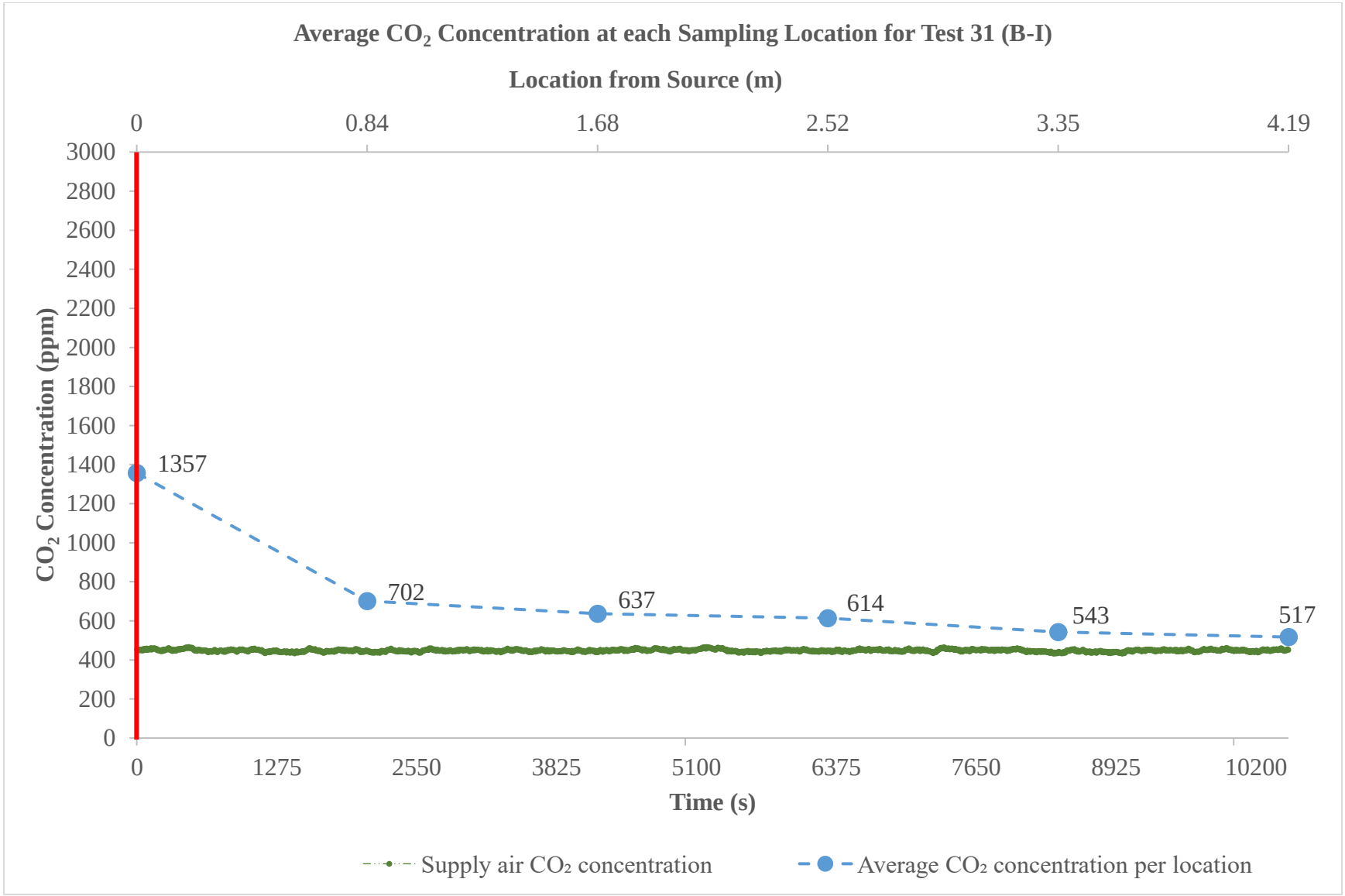

Figure C.76 Average CO_2 concentration at each sampling location for Test 31 (B-I) ISOPass undeployed.

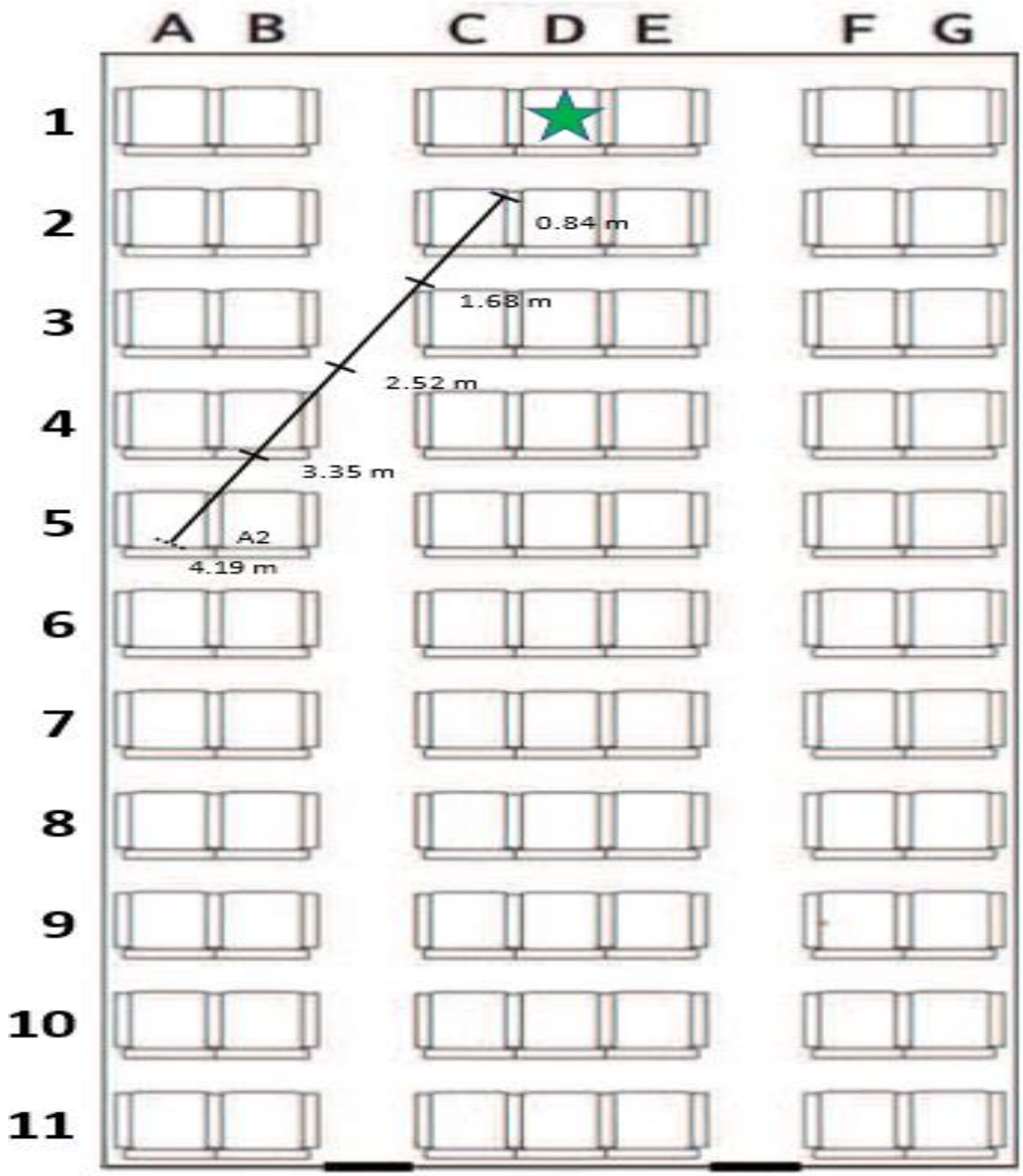

Figure C.77 Test 32 (B-I) ISOPass undeployed source location and sampling tree orientation.

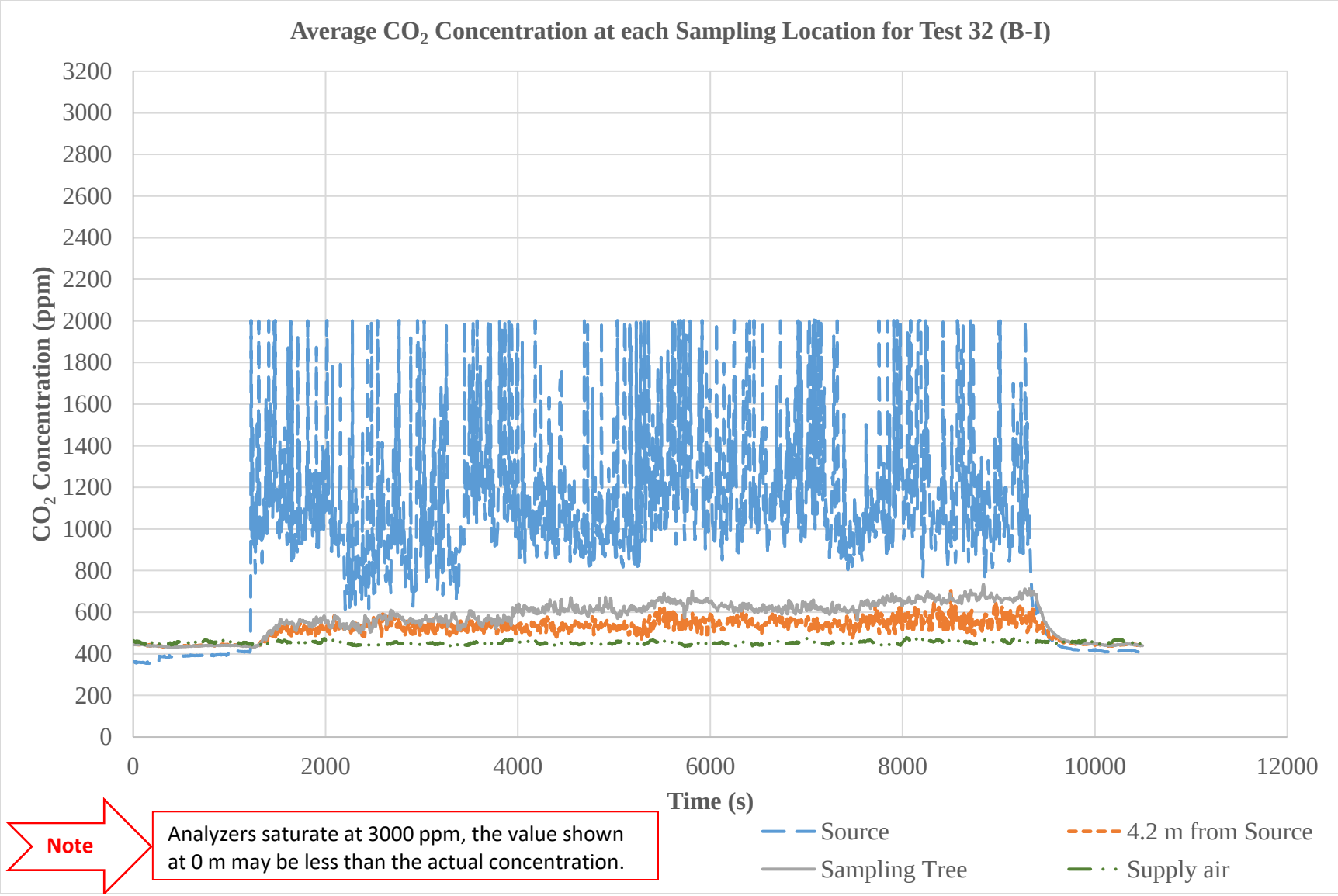

Figure C.78 Ininstantaneous CO_2 concentration at each sampling location for Test 32 (B-I) ISOPass undeployed.

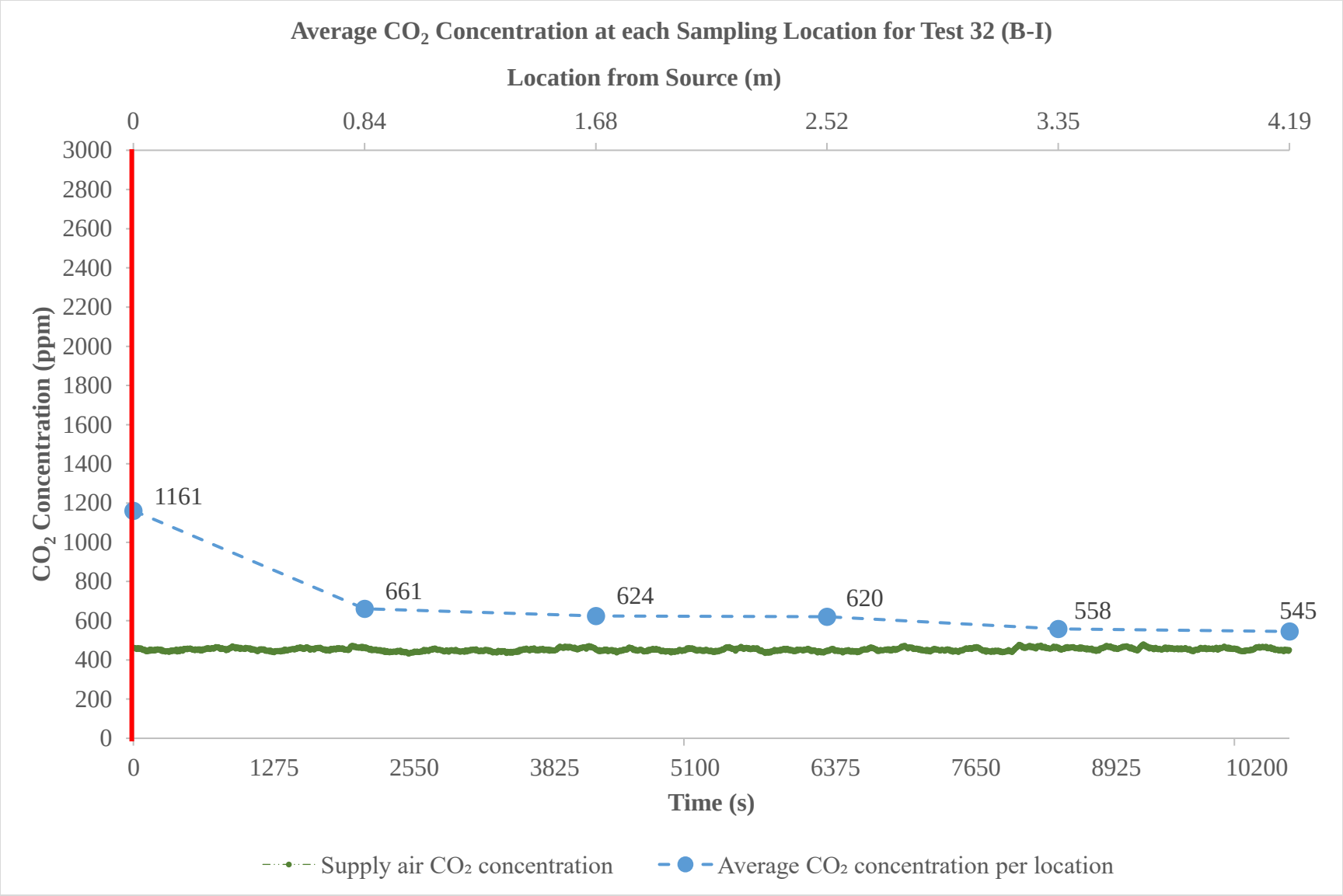

Figure C.79 Average CO_2 concentration at each sampling location for Test 32 (B-I) ISOPass undeployed.

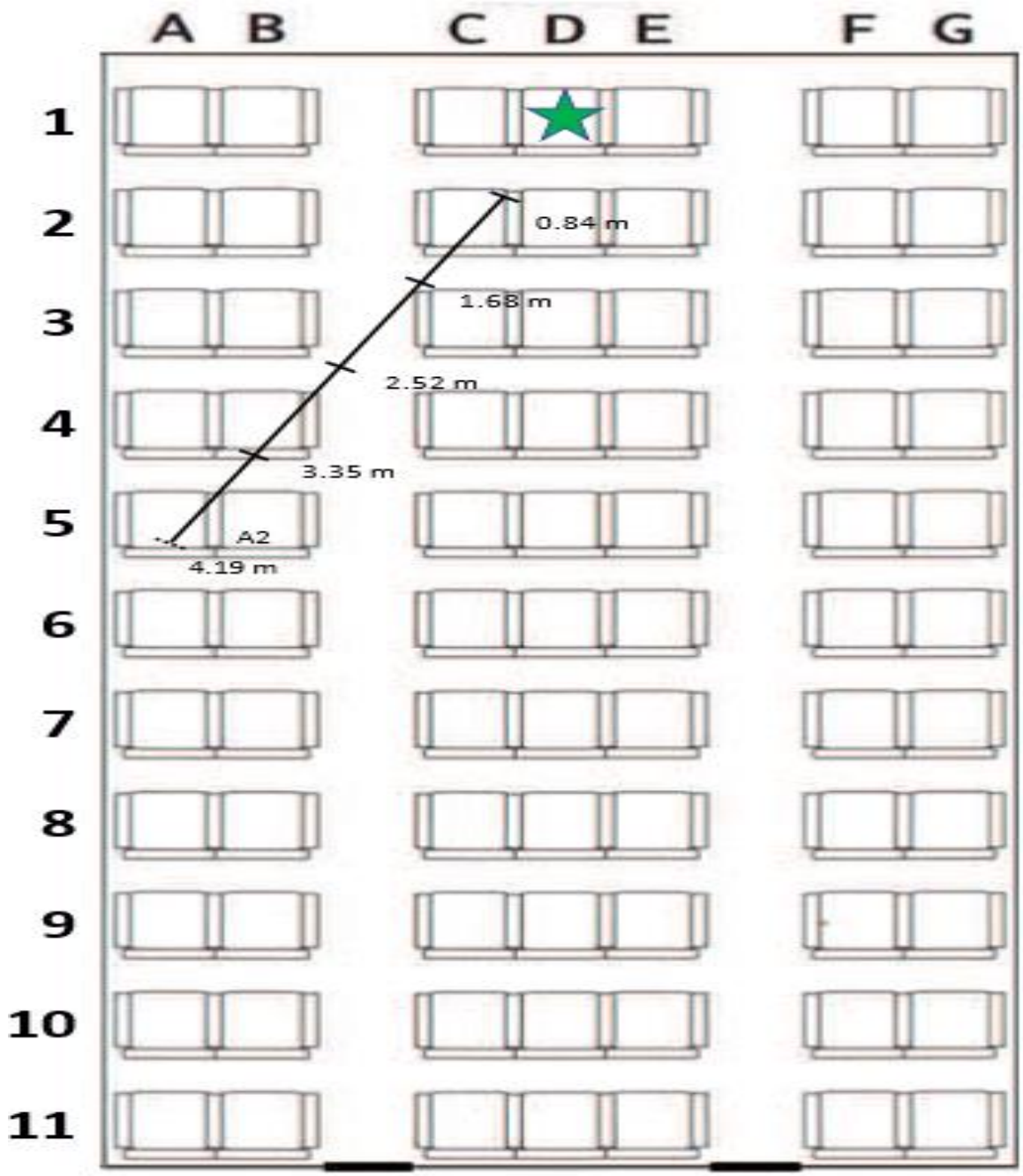

Figure C.80 Test 33 (B-I) ISOPass undeployed source location and sampling tree orientation.

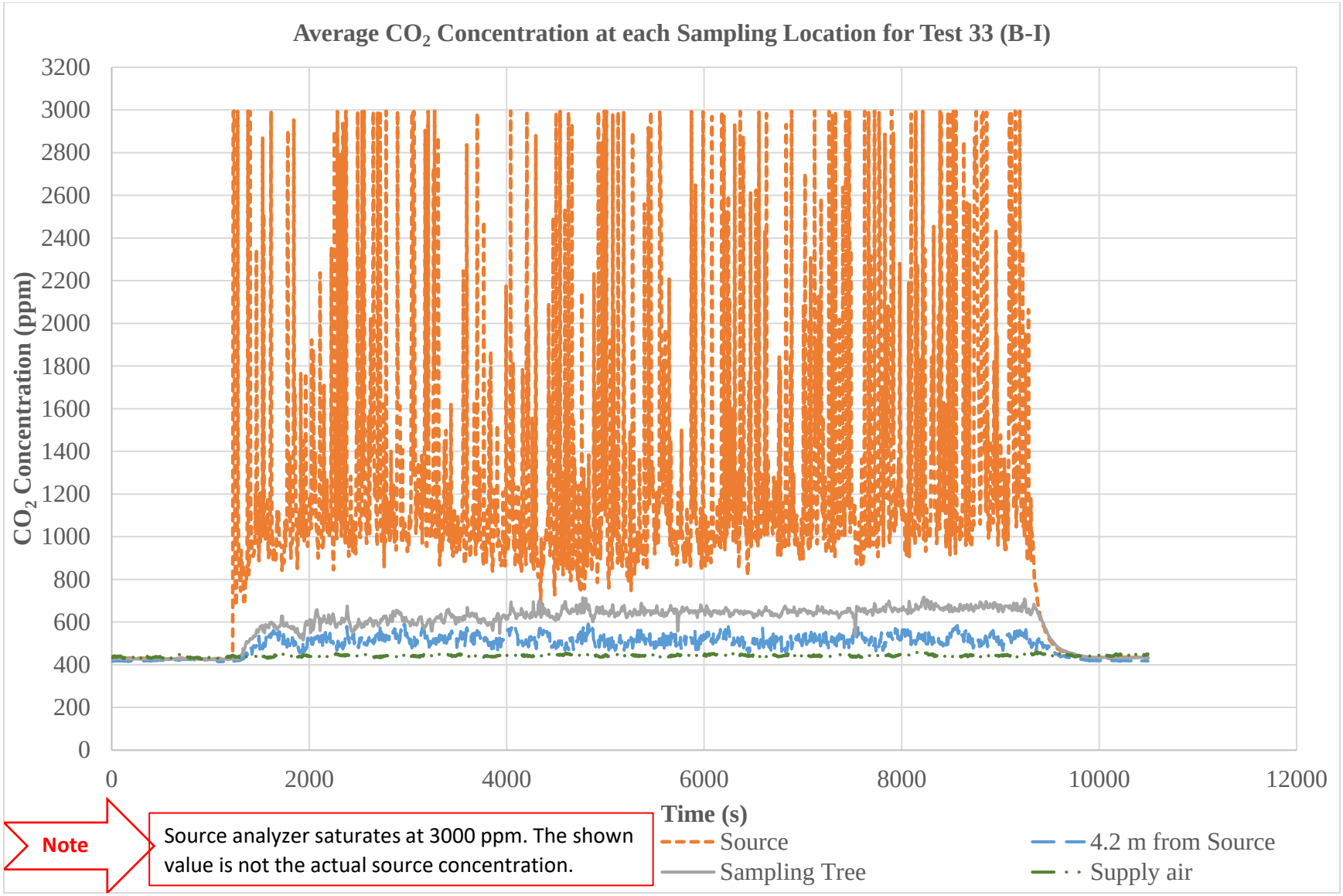

Figure C.81 Ininstantaneous CO_2 concentration at each sampling location for Test 33 (B-I) ISOPass undeployed.

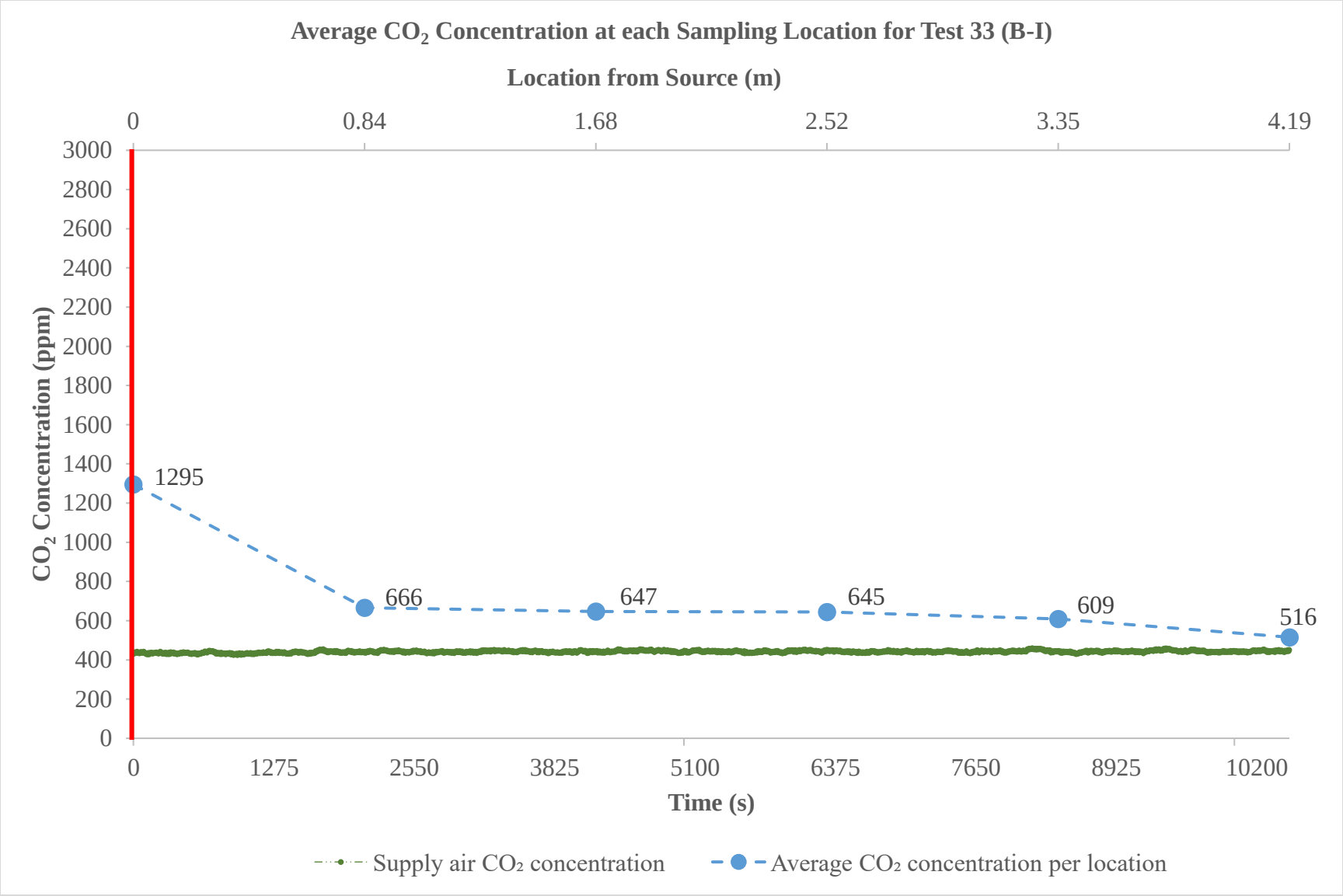

Figure C.82 Average CO_2 concentration at each sampling location for Test 33 (B-I) ISOPass undeployed.

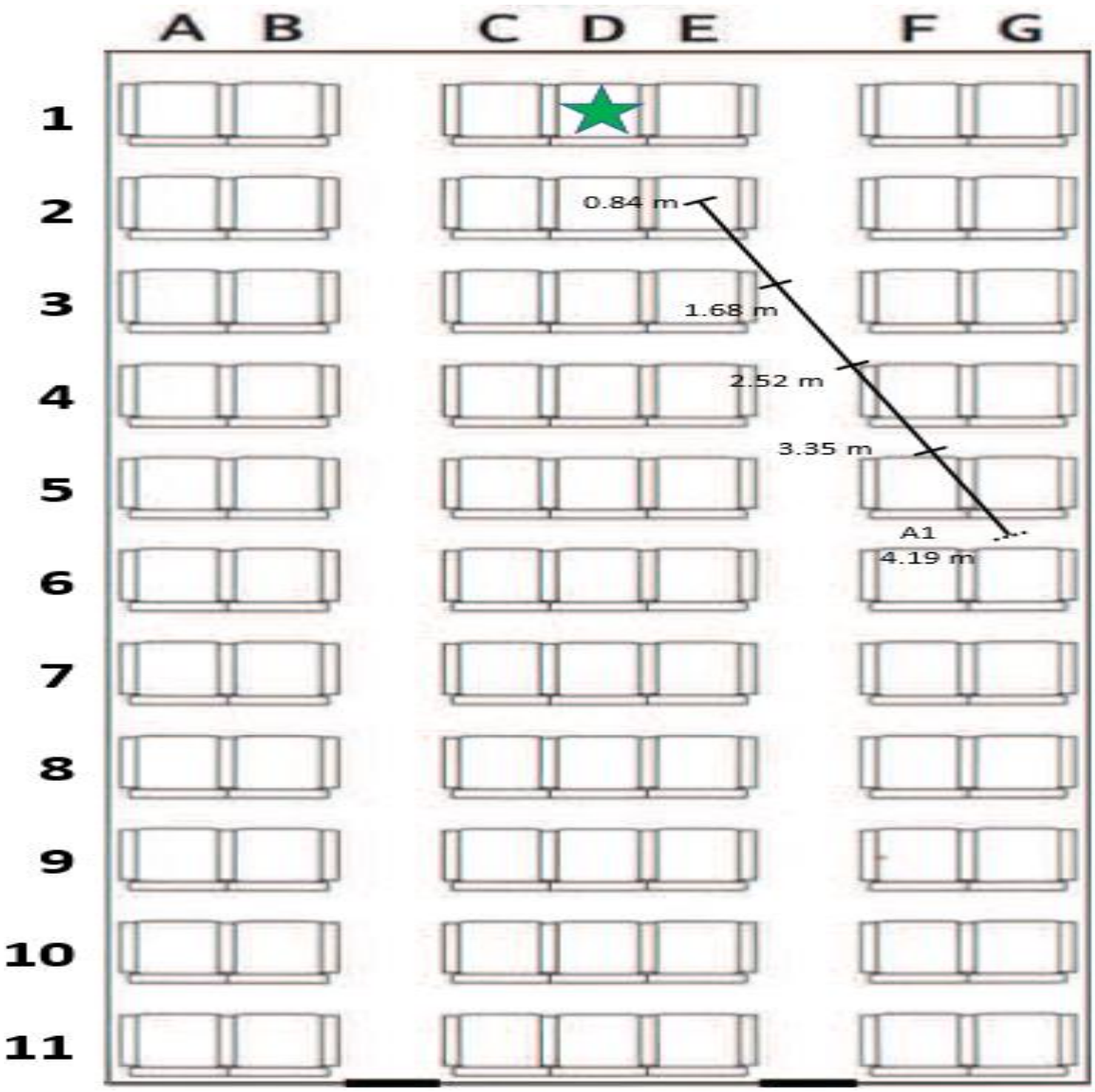

Figure C.83 Test 34 (B-I) ISOPass undeployed source location and sampling tree orientation.

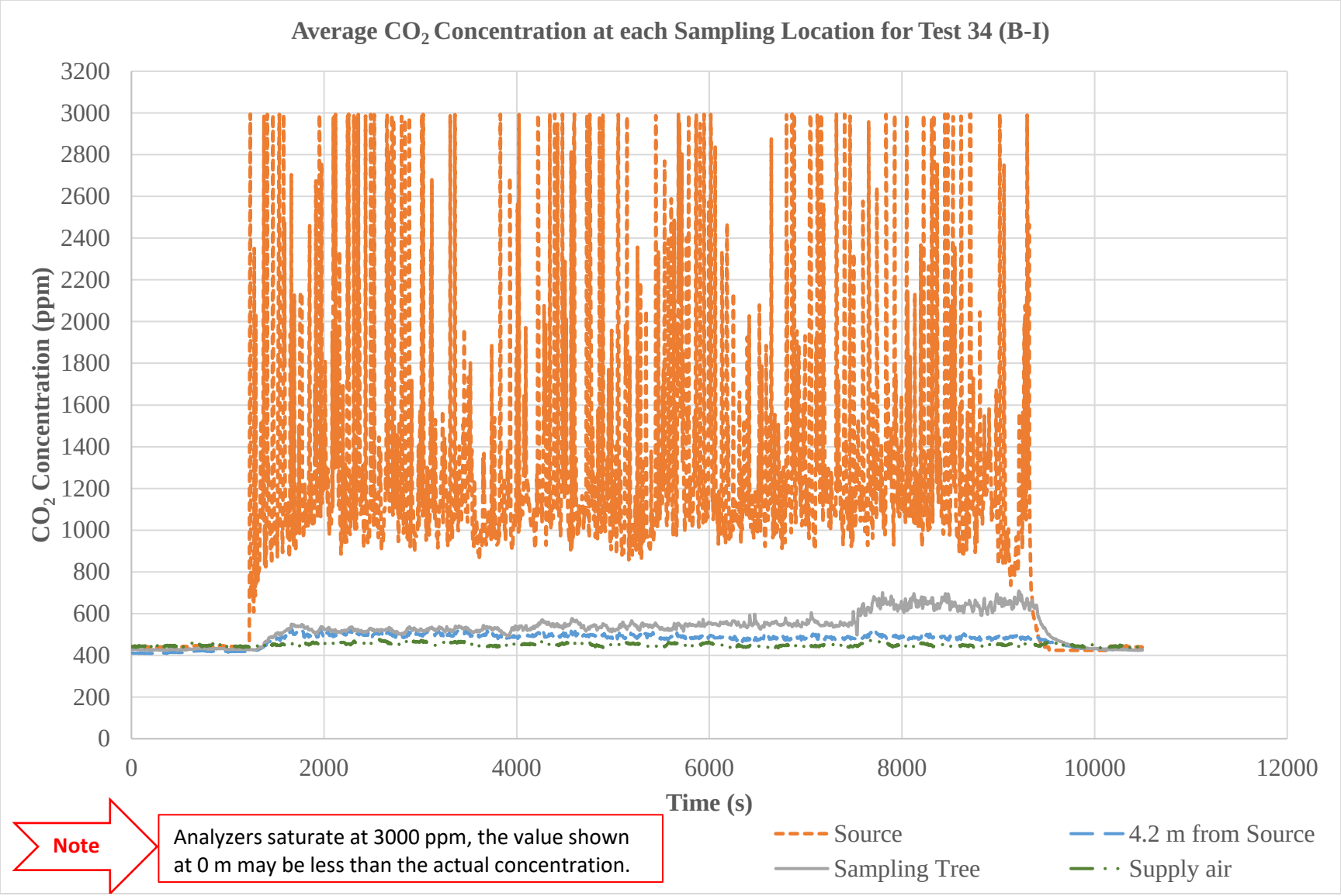

Figure C.84 Ininstantaneous CO_2 concentration at each sampling location for Test 34 (B-I) ISOPass undeployed.

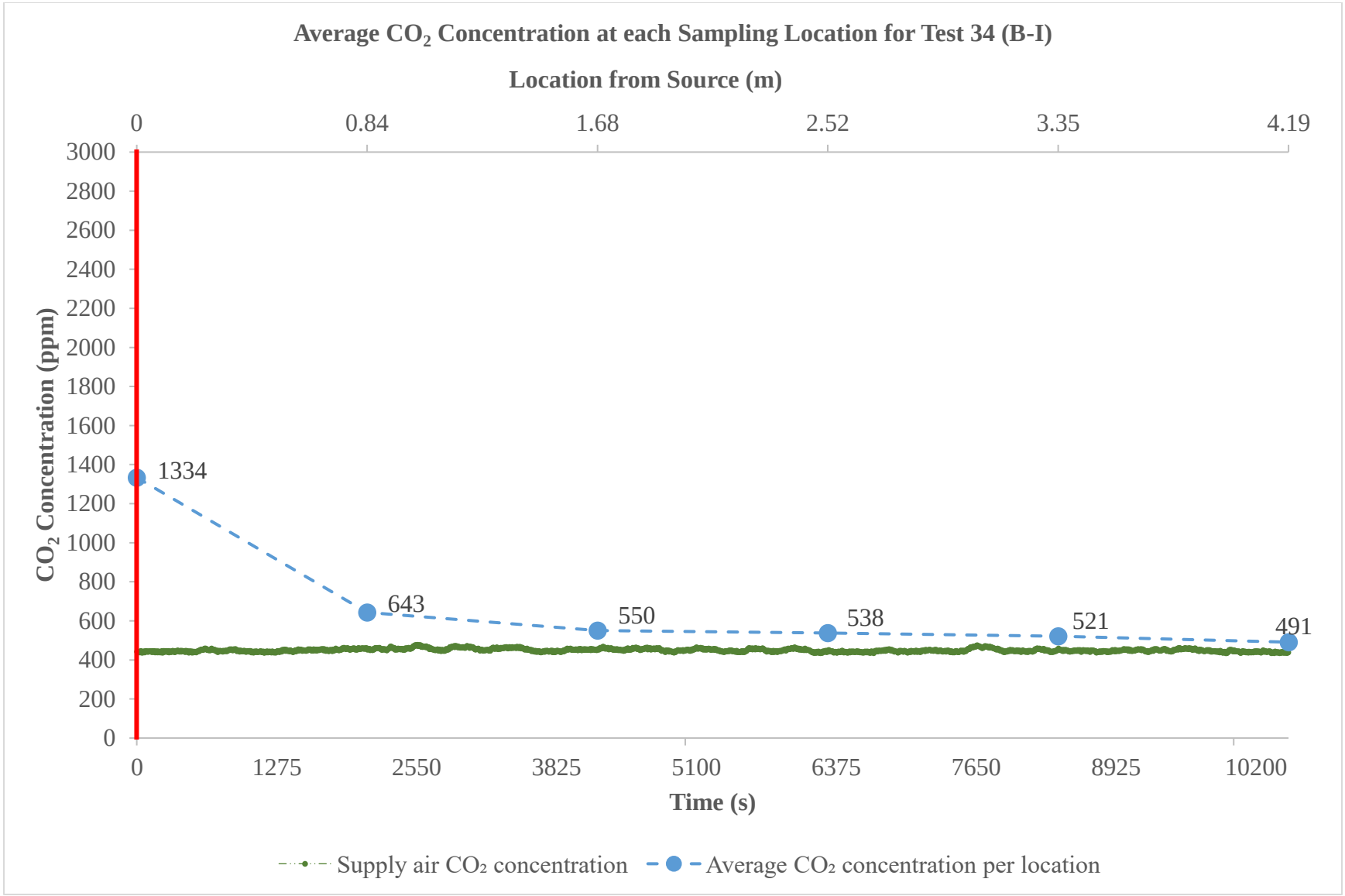

Figure C.85 Average CO_2 concentration at each sampling location for Test 34 (B-I) ISOPass undeployed.

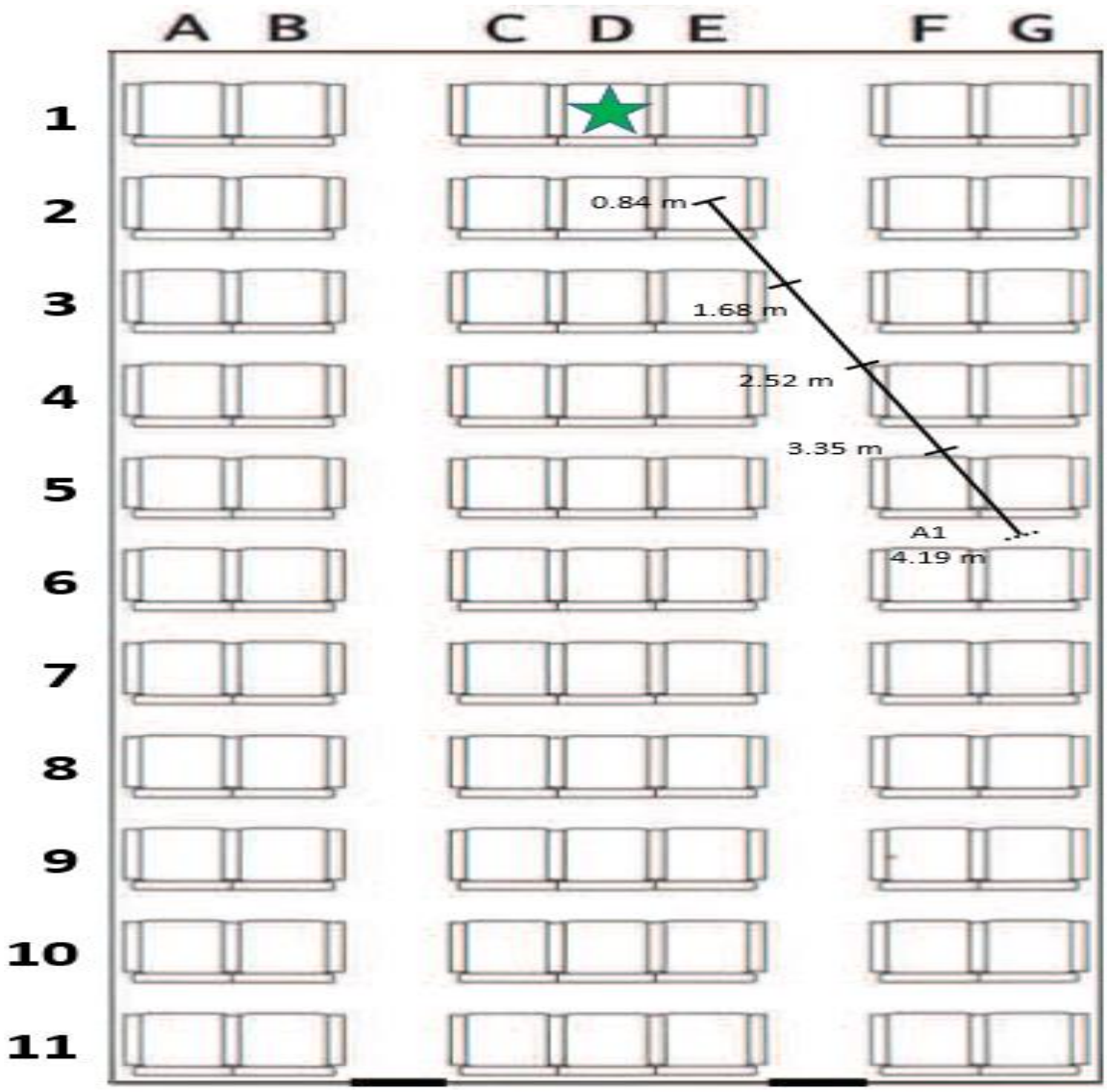

Figure C.86 Test 35 (B-I) ISOPass undeployed source location and sampling tree orientation.

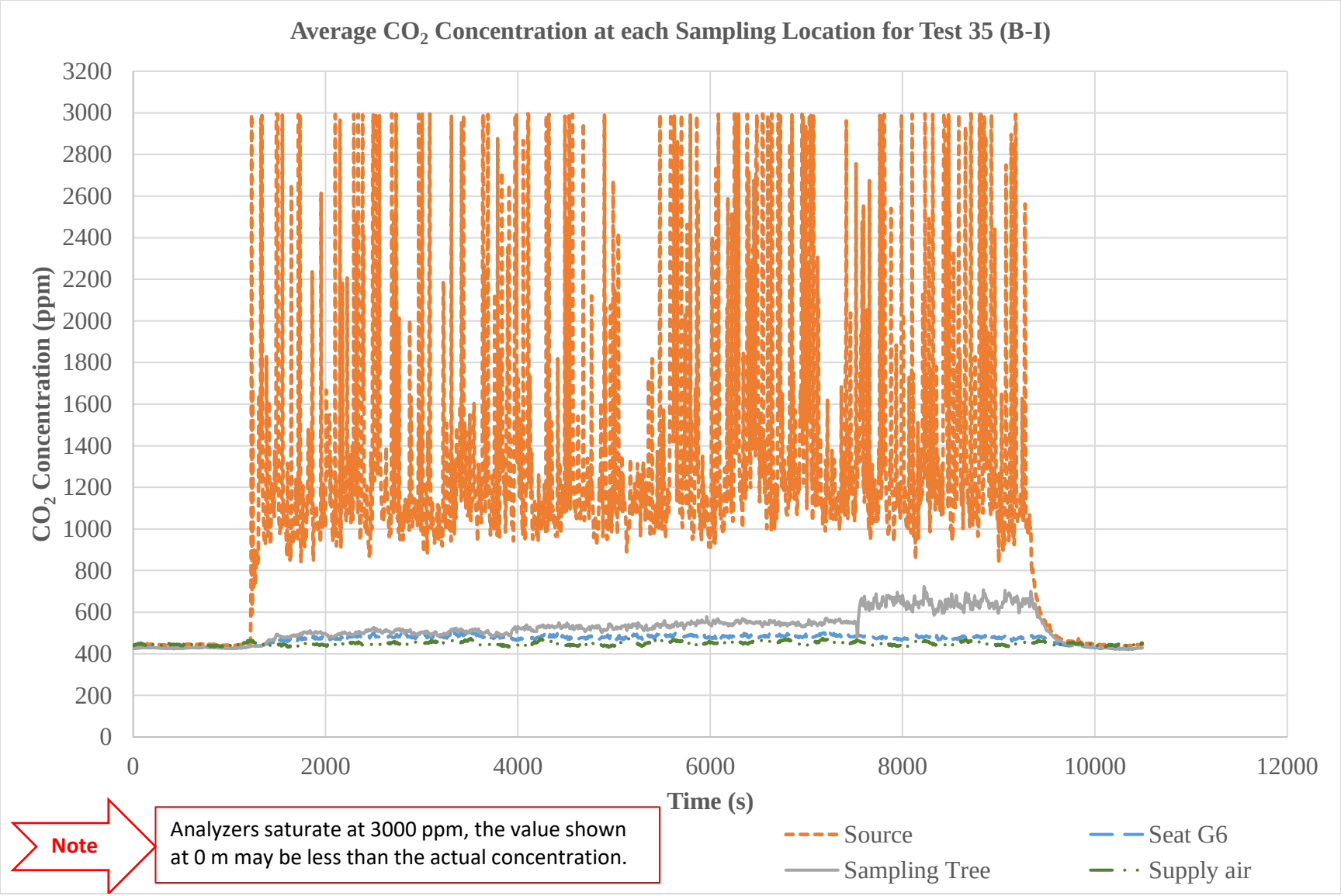

Figure C.87 Ininstantaneous CO_2 concentration at each sampling location for Test 35 (B-I) ISOPass undeployed.

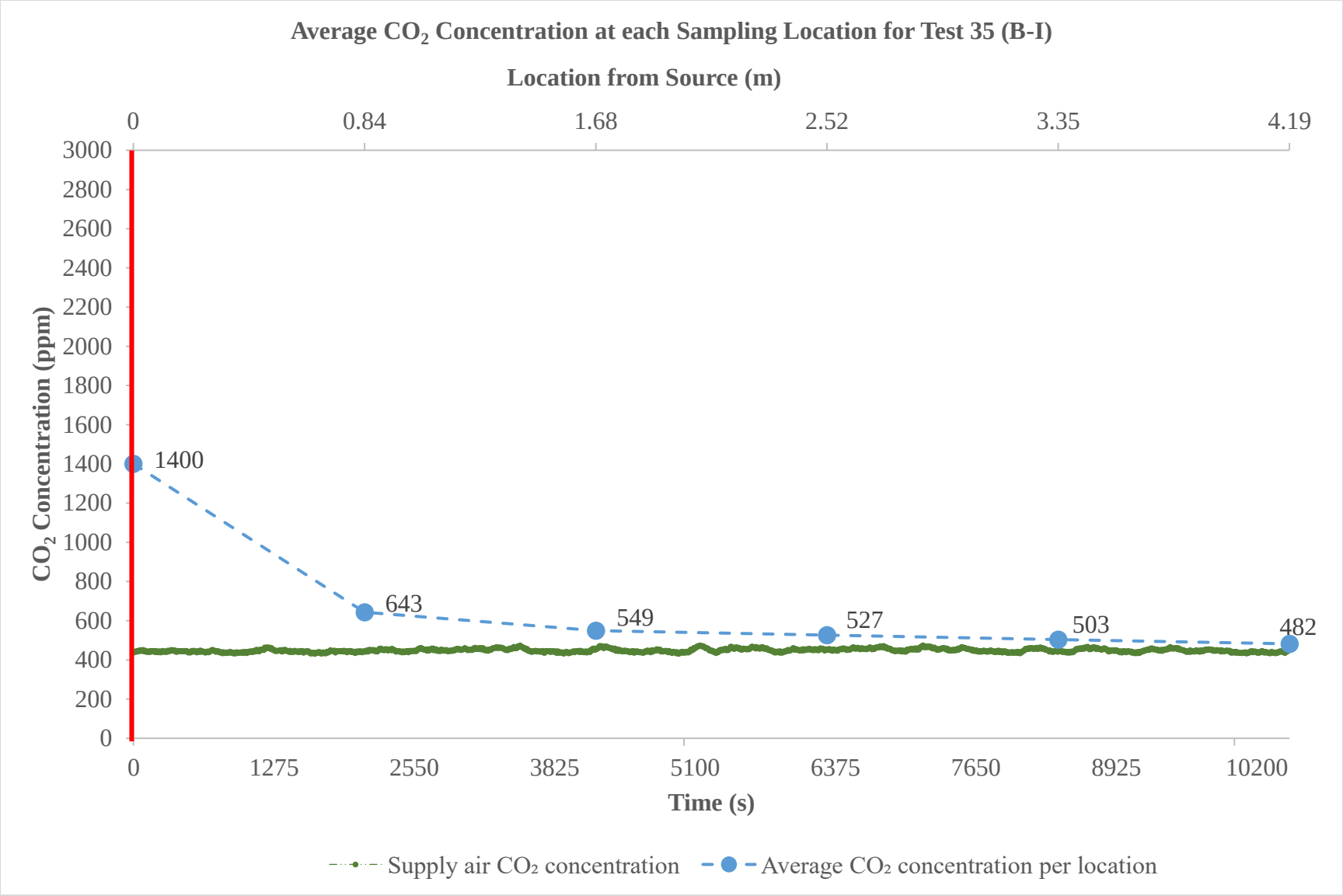

Figure C.88 Average CO_2 concentration at each sampling location for Test 35 (B-I) ISOPass undeployed.

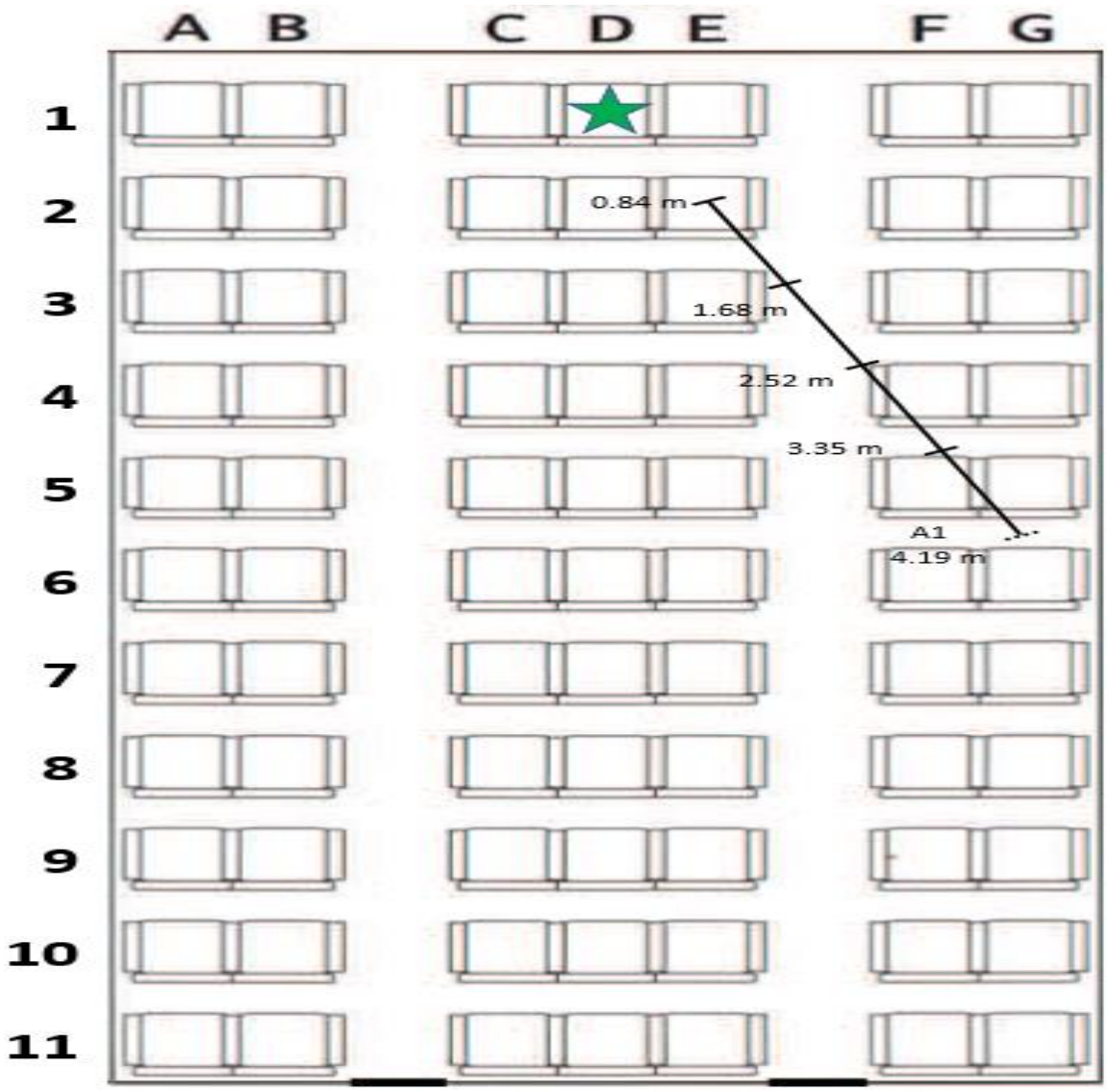

Figure C.89 Test 36 (B-I) ISOPass undeployed source location and sampling tree orientation.

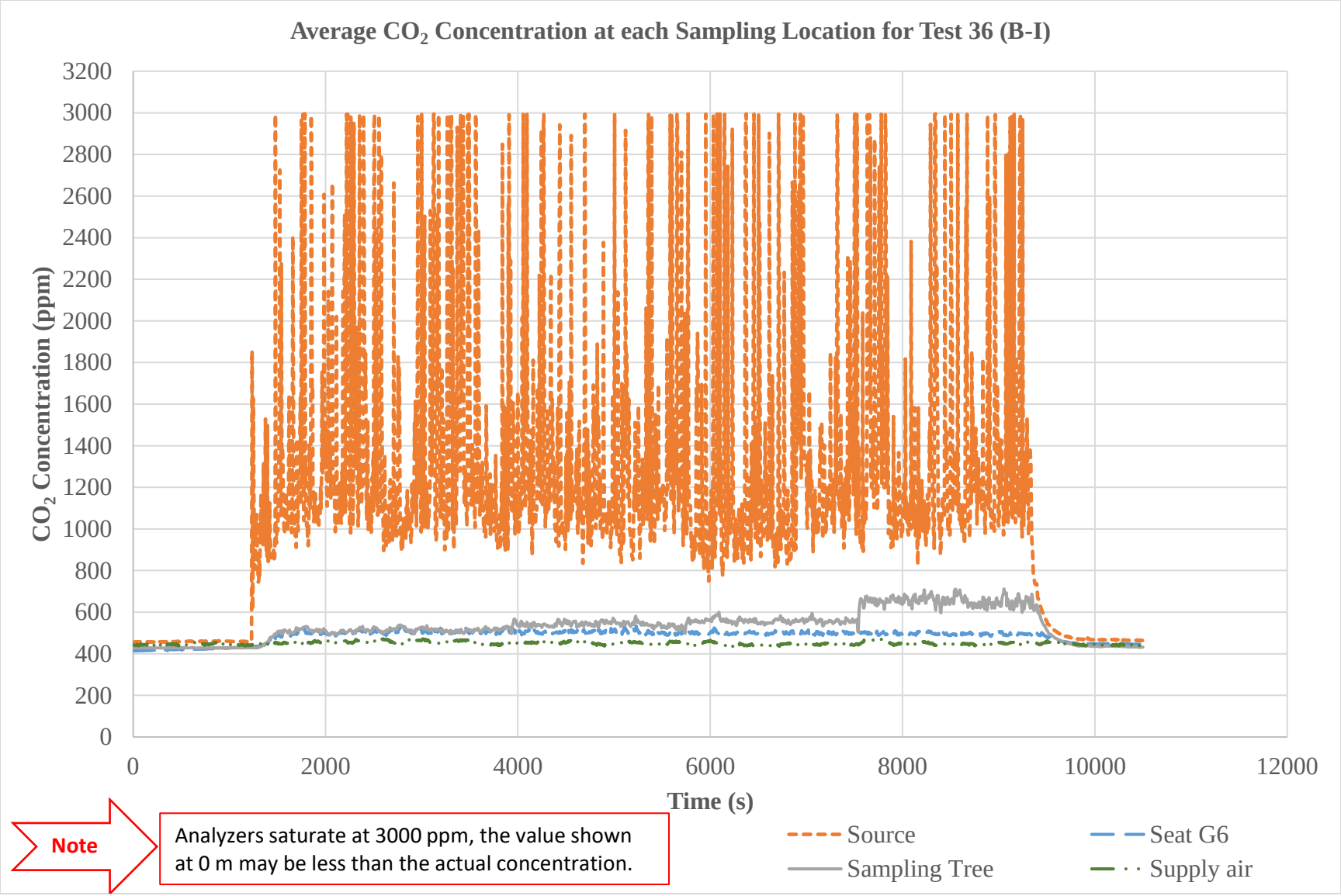

Figure C.90 Ininstantaneous CO_2 concentration at each sampling location for Test 36 (B-I) ISOPass undeployed.

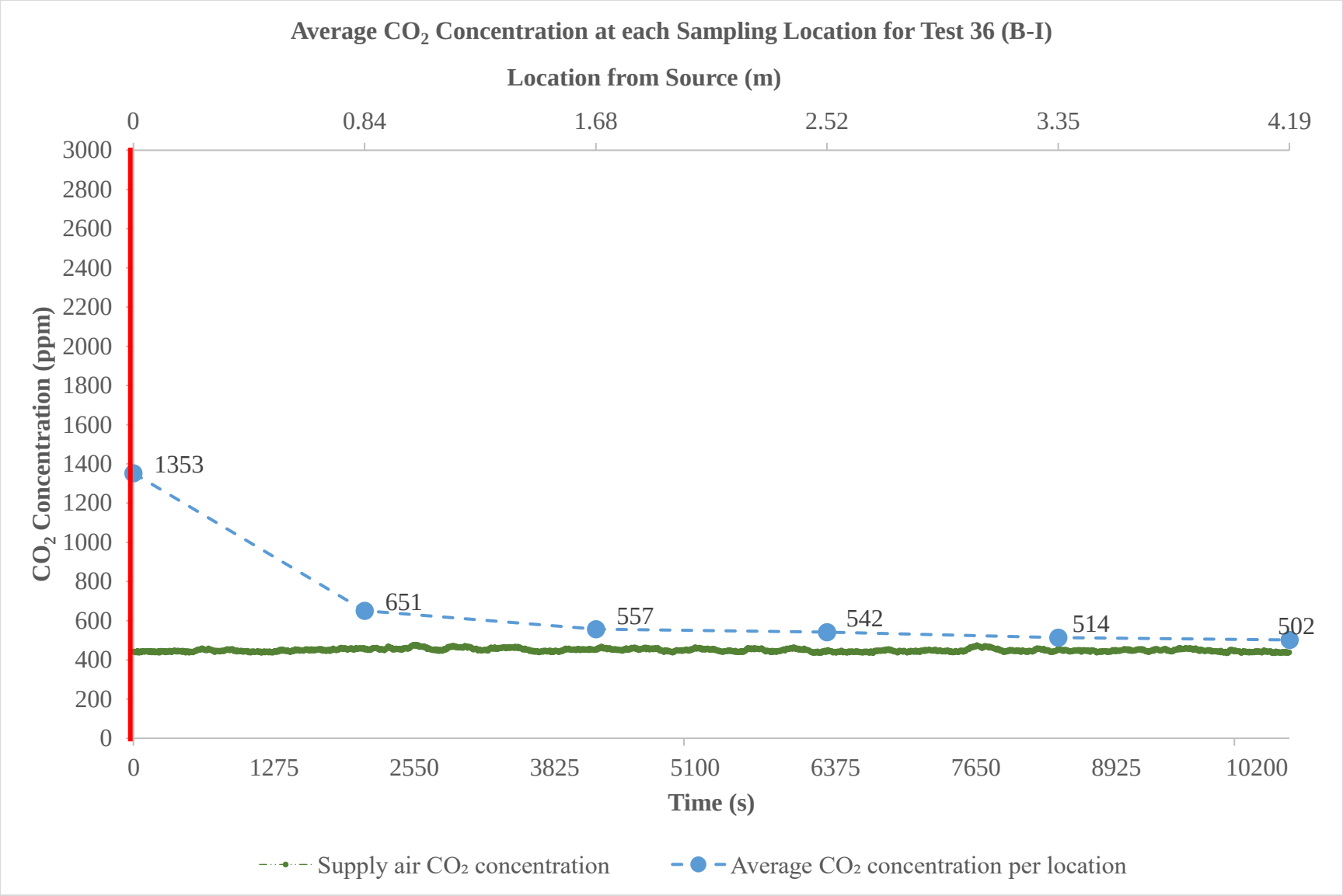

Figure C.91 Average CO_2 concentration at each sampling location for Test 36 (B-I) ISOPass undeployed.

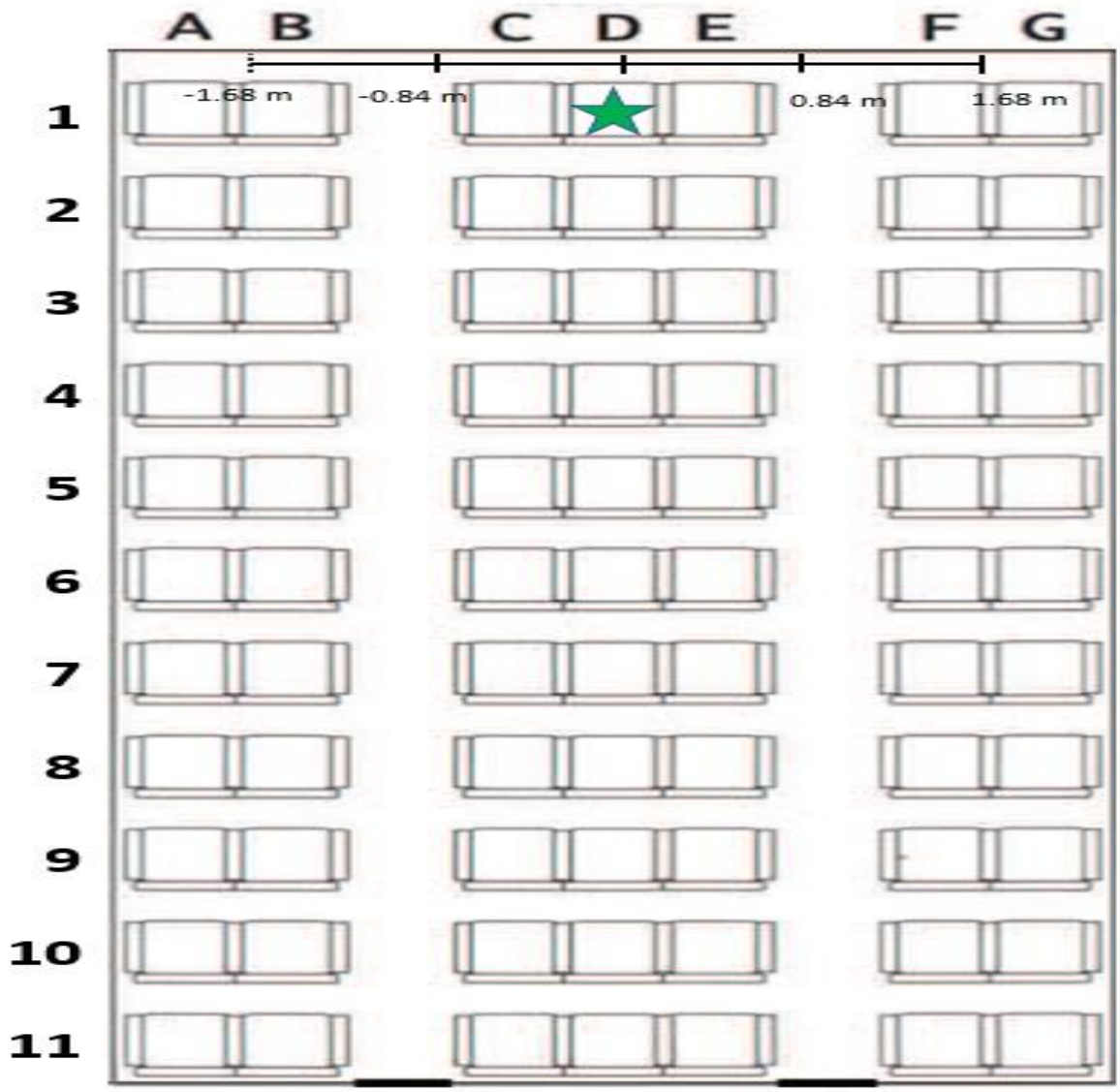

Figure C.92 Test 37 (B-I) ISOPass undeployed source location and sampling tree orientation.

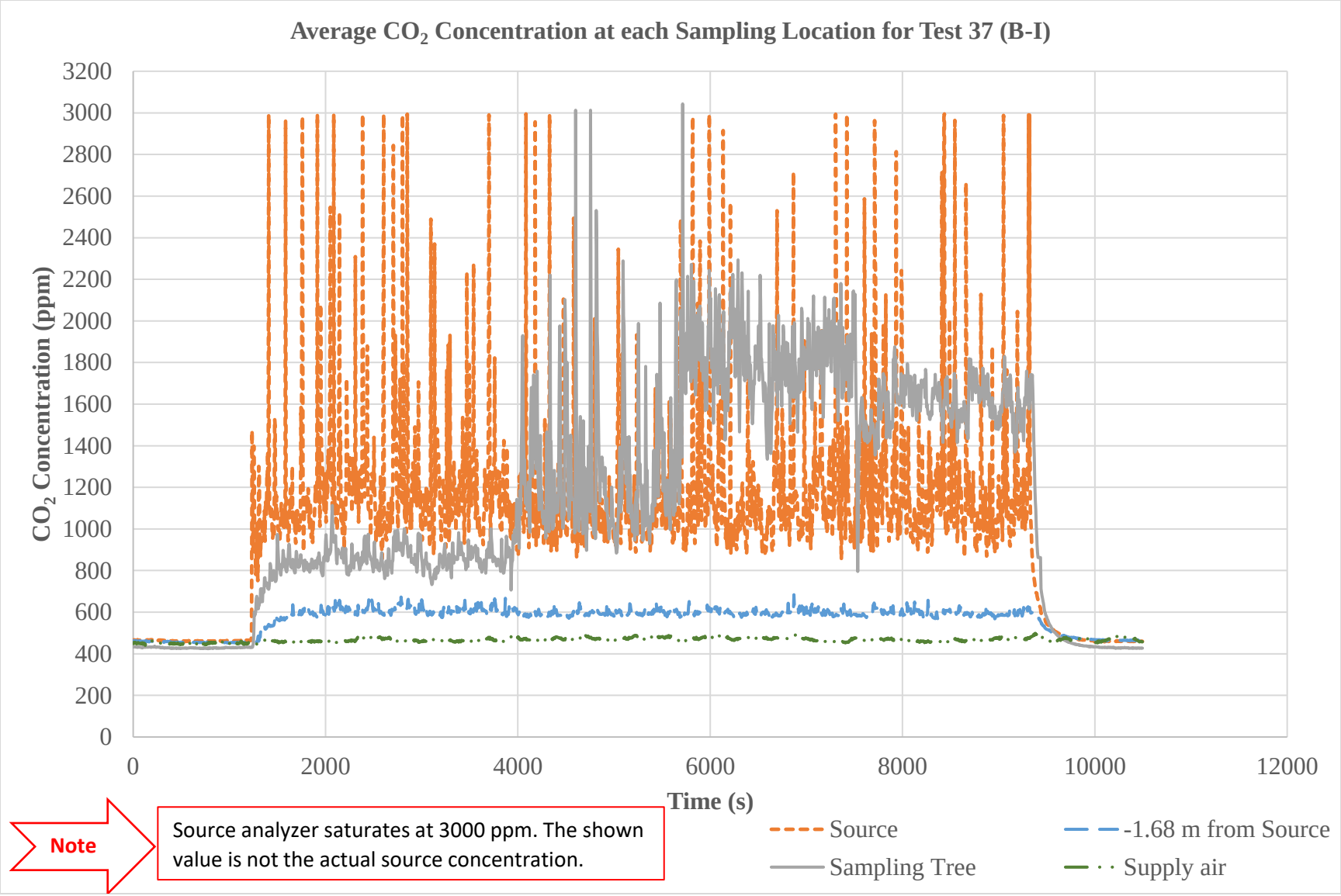

Figure C.93 Ininstantaneous CO_2 concentration at each sampling location for Test 37 (B-I) ISOPass undeployed.

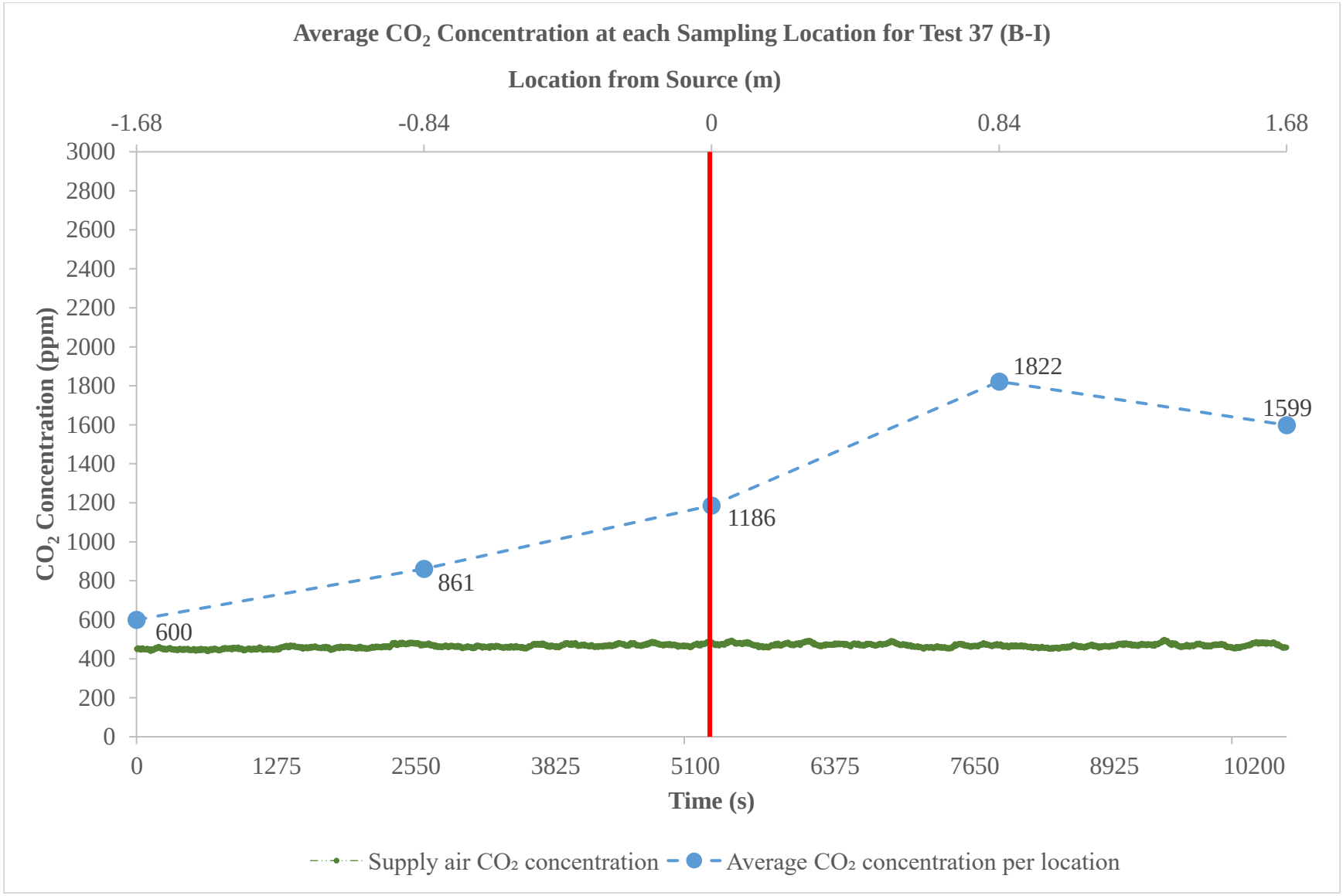

Figure C.94 Average CO_2 concentration at each sampling location for Test 37 (B-I) ISOPass undeployed.

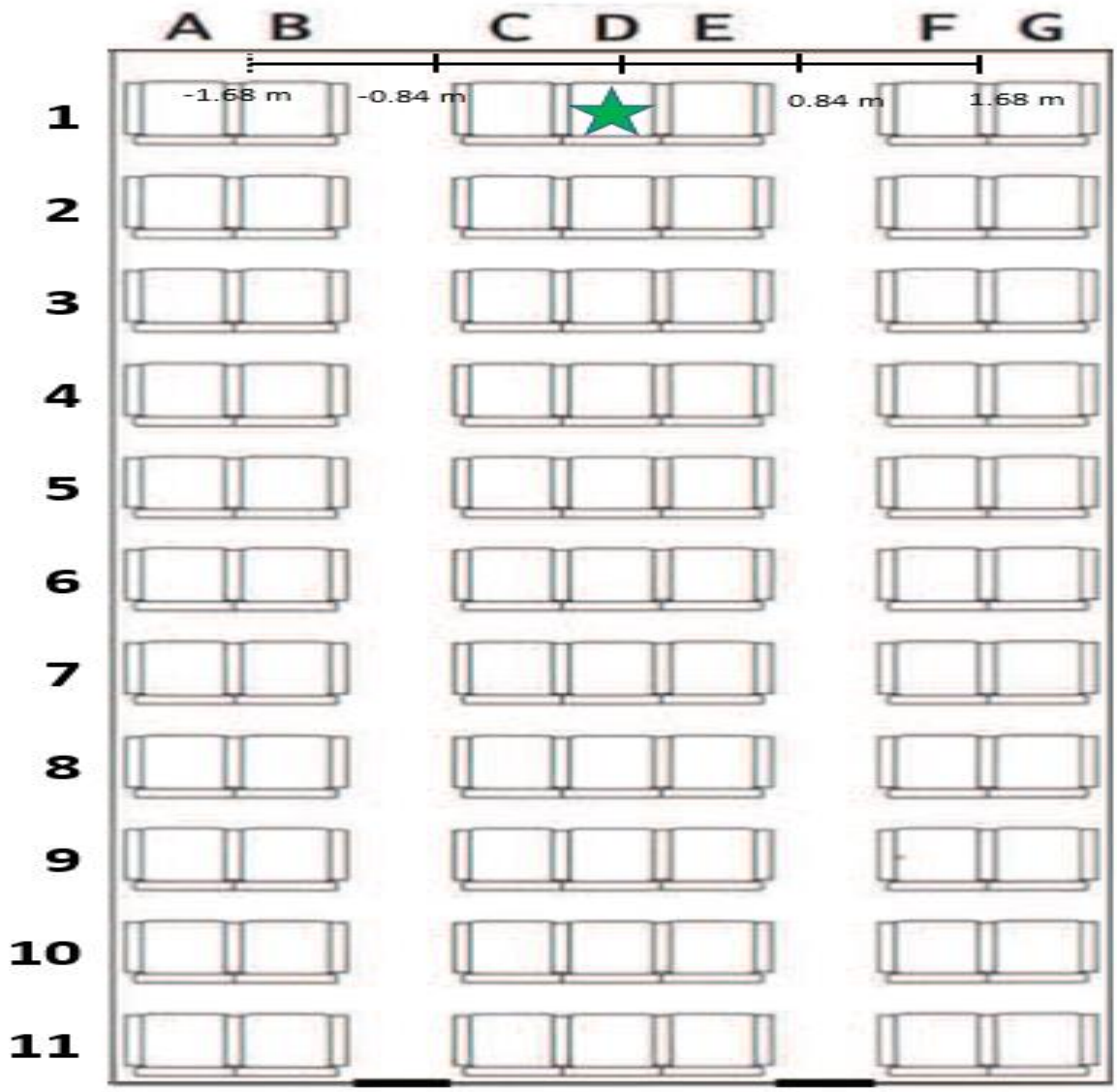

Figure C.95 Test 38 (B-I) ISOPass undeployed source location and sampling tree orientation.

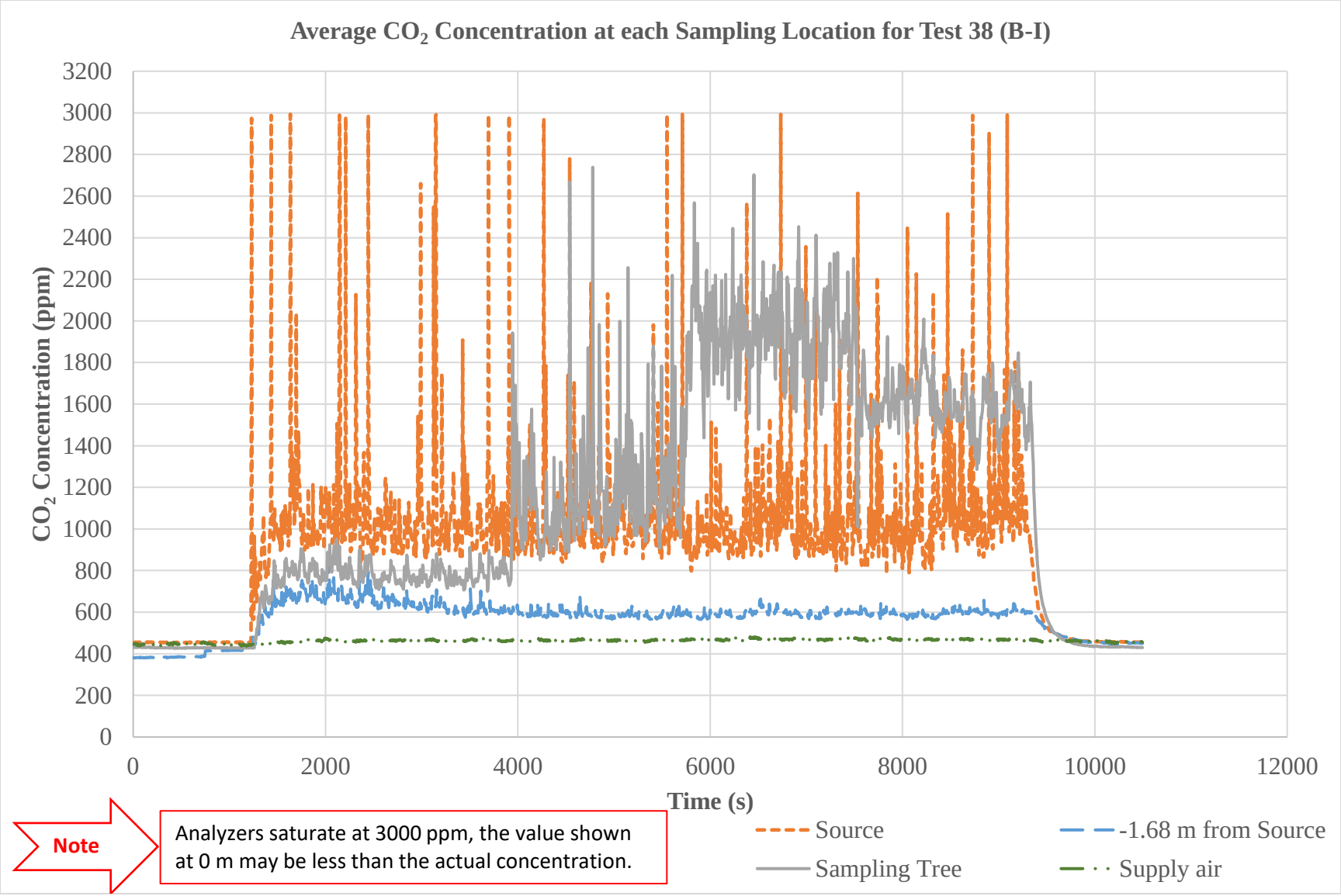

Figure C.96 Ininstantaneous CO_2 concentration at each sampling location for Test 38 (B-I) ISOPass undeployed.

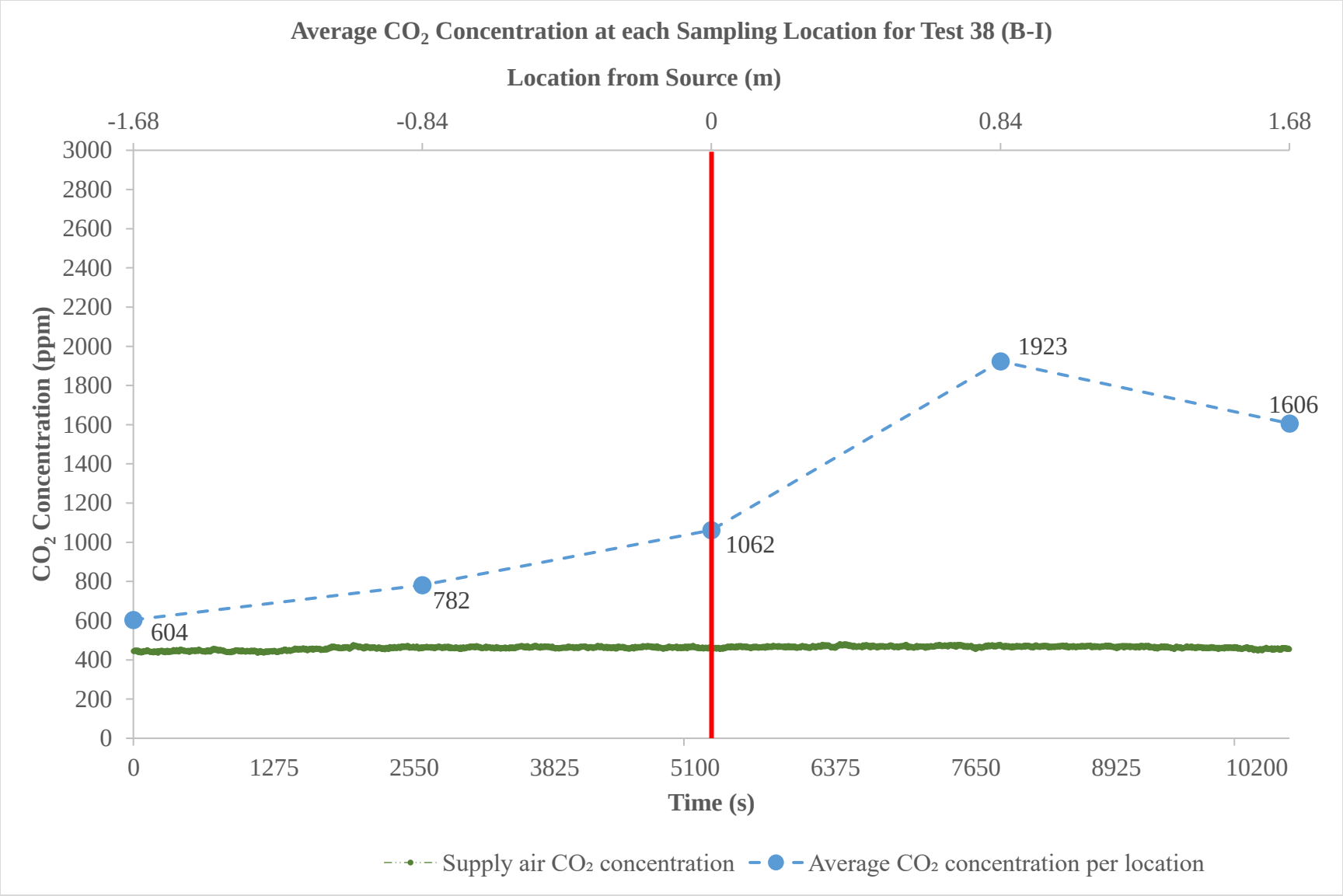

Figure C.97 Average CO_2 concentration at each sampling location for Test 38 (B-I) ISOPass undeployed.

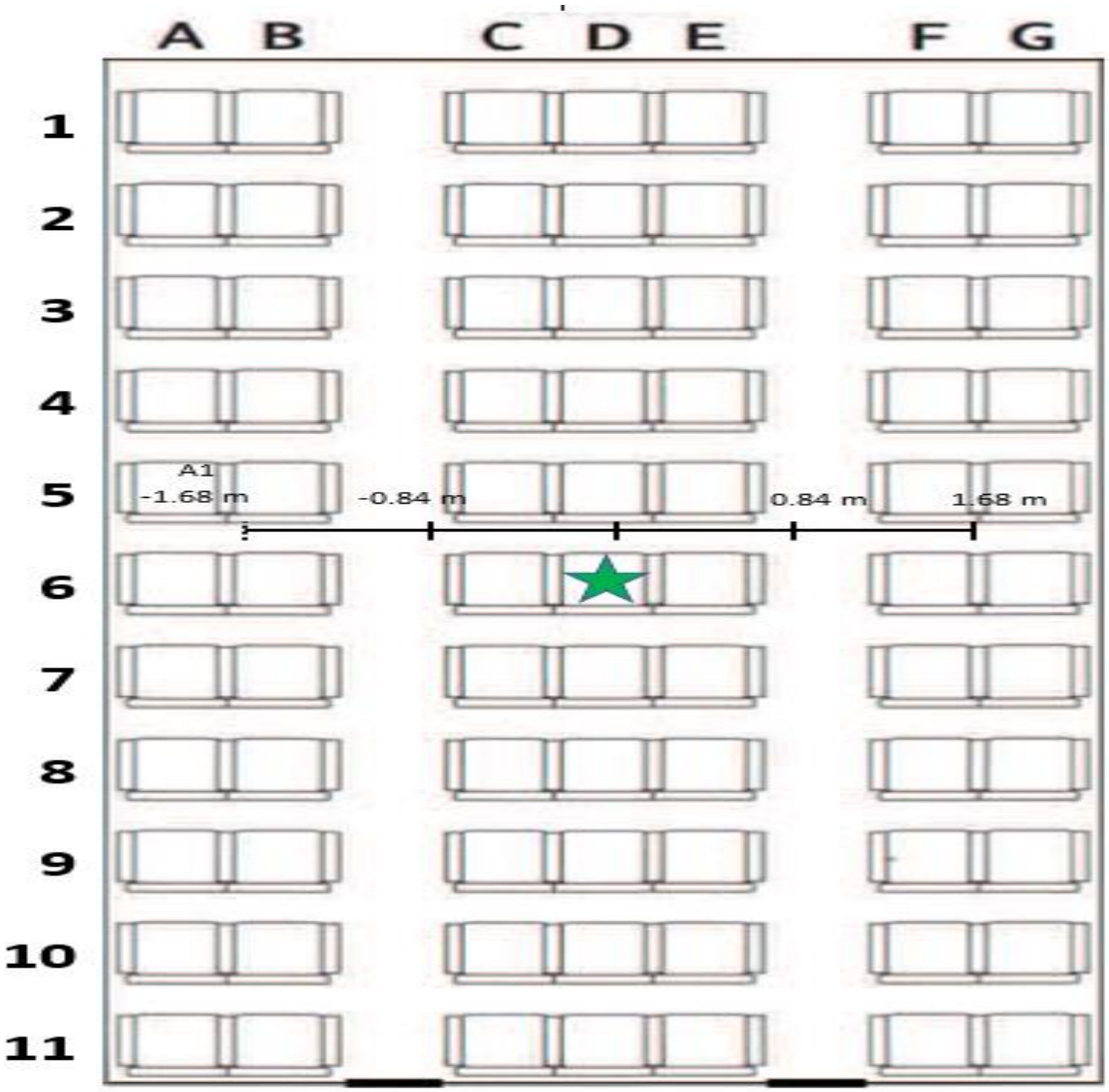

Figure C.98 Test 42 (B-I) ISOPass undeployed source location and sampling tree orientation.

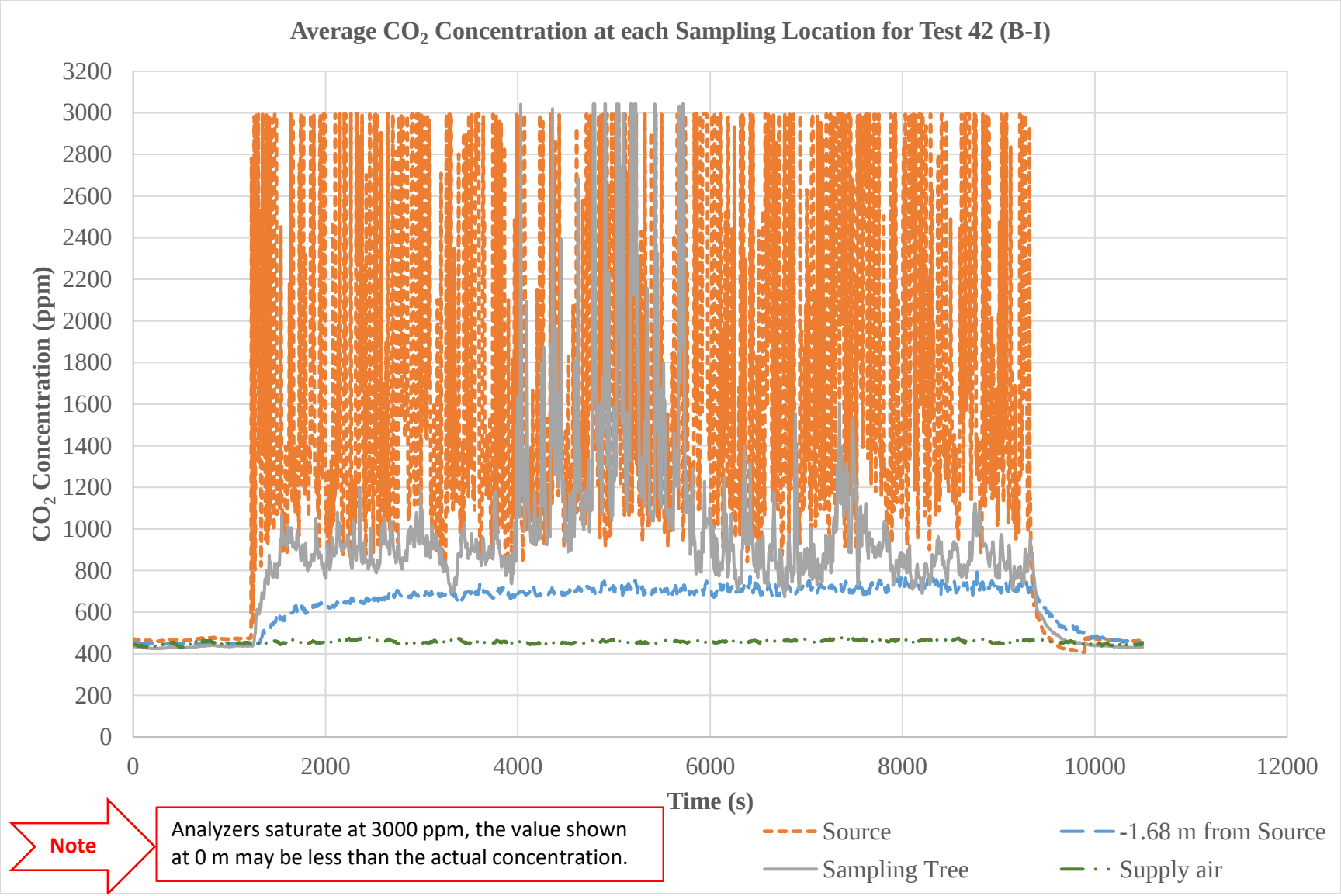

Figure C.99 Ininstantaneous CO_2 concentration at each sampling location for Test 42 (B-I) ISOPass undeployed.

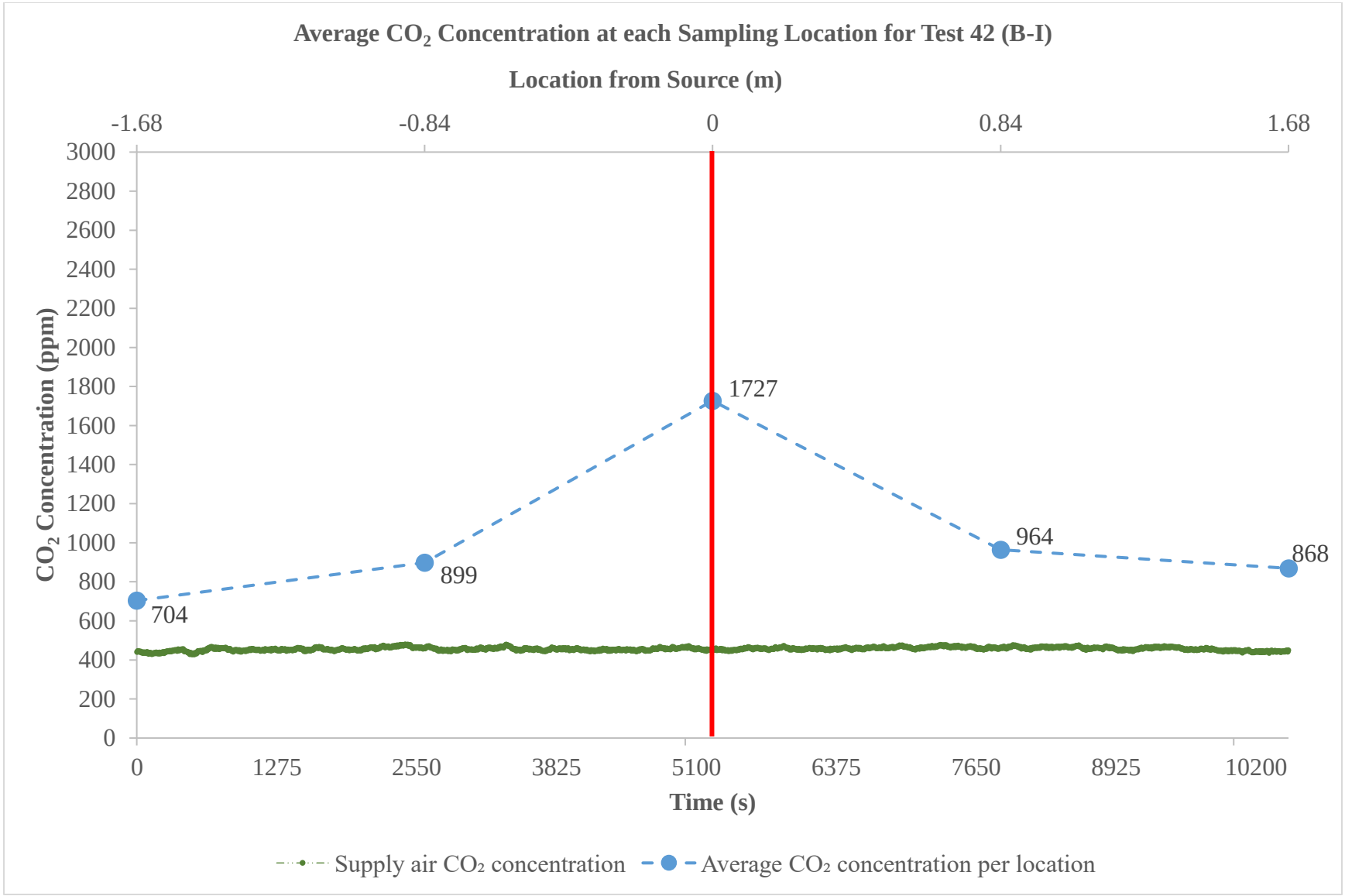

Figure C.100 Average CO_2 concentration at each sampling location for Test 42 (B-I) ISOPass undeployed.

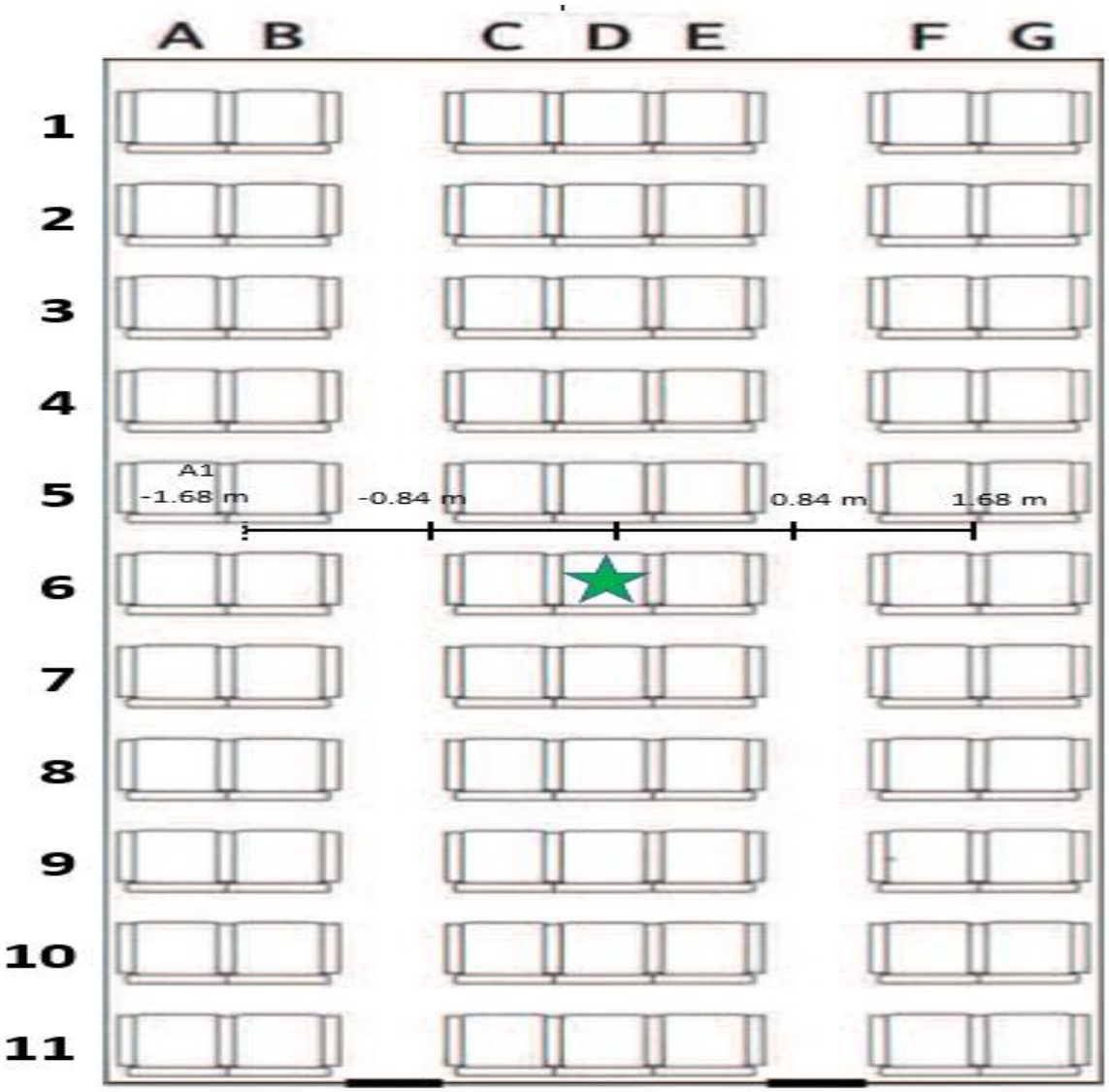

Figure C.101 Test 45 (B-I) ISOPass undeployed source location and sampling tree orientation.

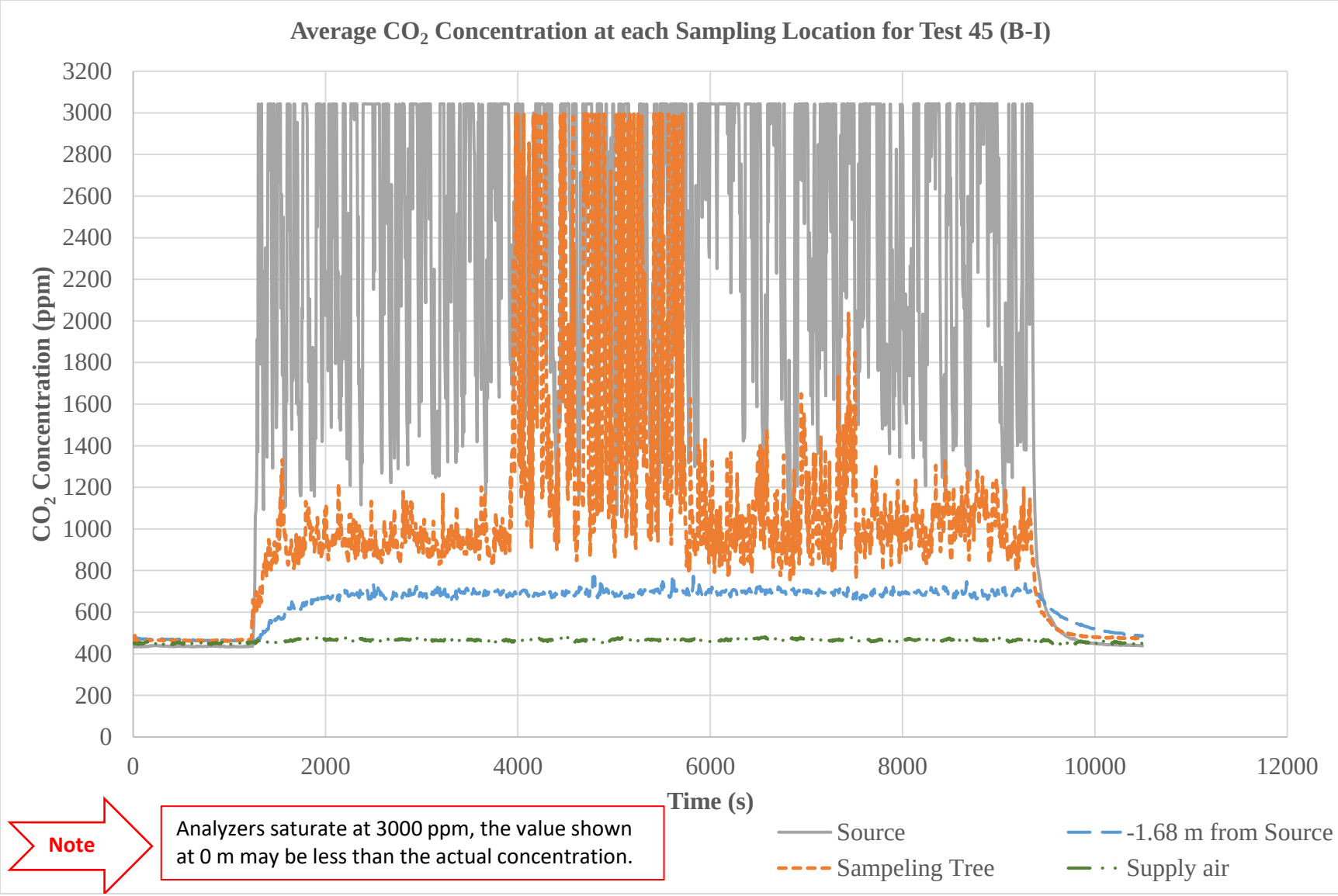

Figure C.102 Ininstantaneous CO_2 concentration at each sampling location for Test 45 (B-I) ISOPass undeployed.

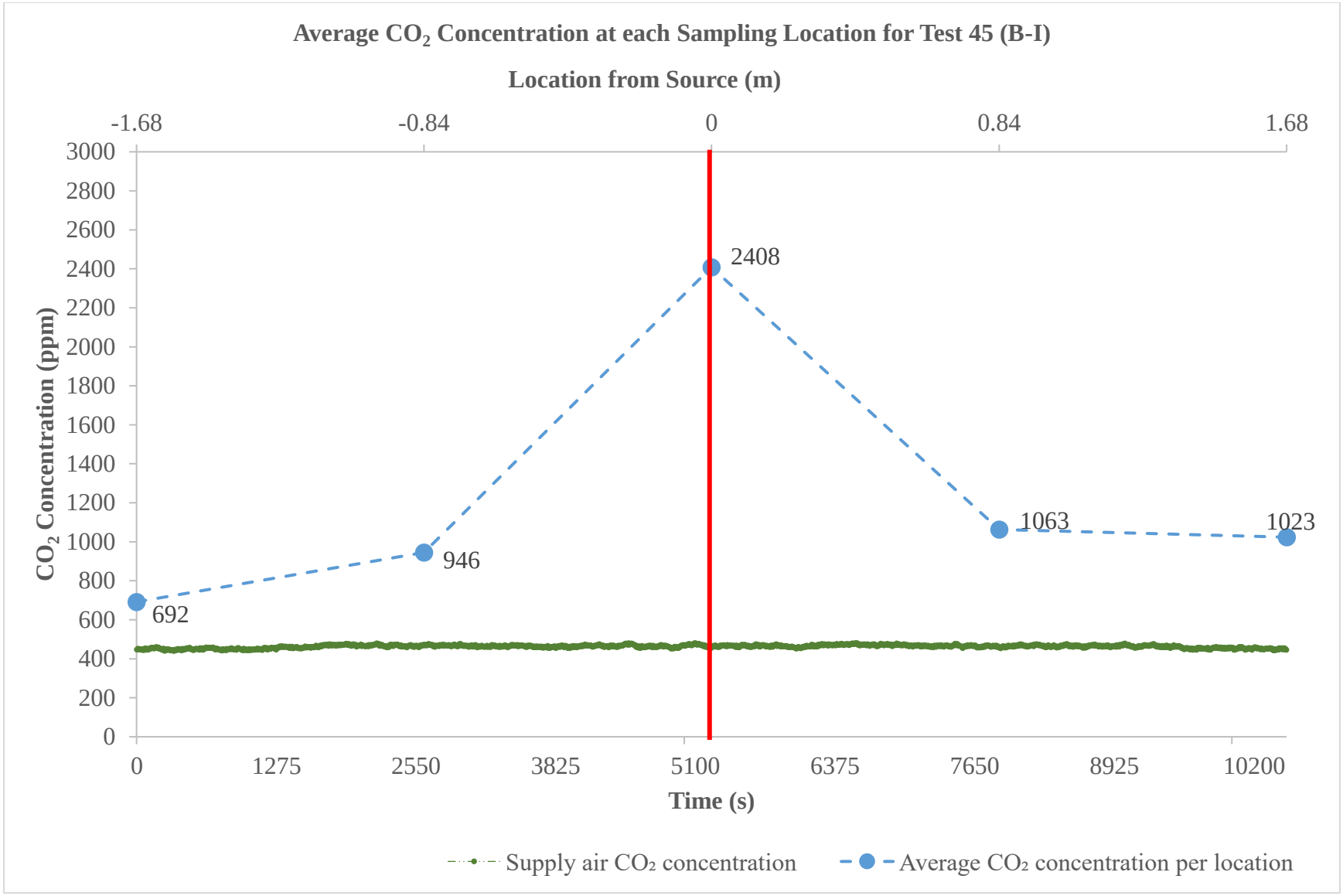

Figure C.103 Average CO_2 concentration at each sampling location for Test 45 (B-I) ISOPass undeployed.

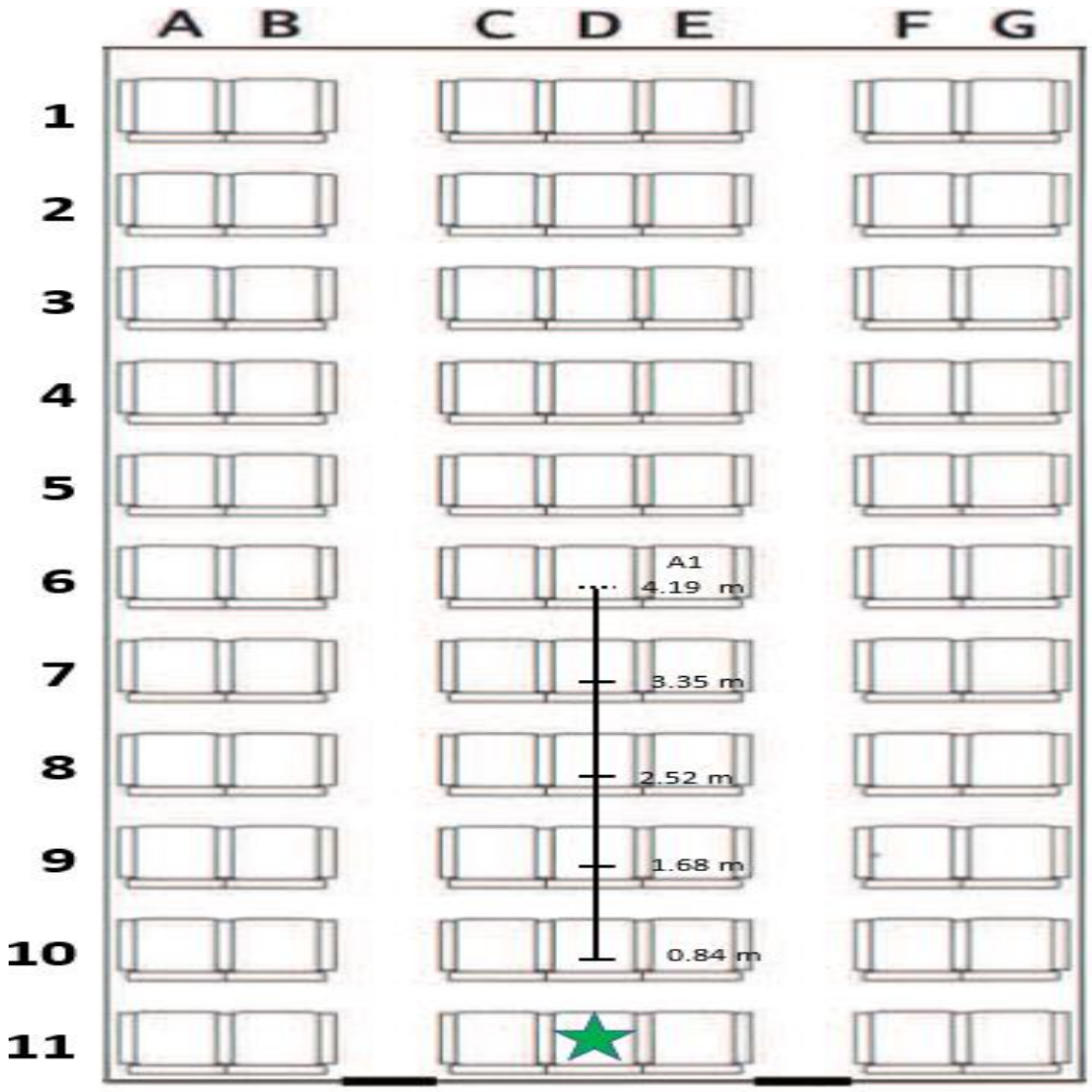

Figure C.104 Test 46 (B-I) ISOPass undeployed source location and sampling tree orientation.

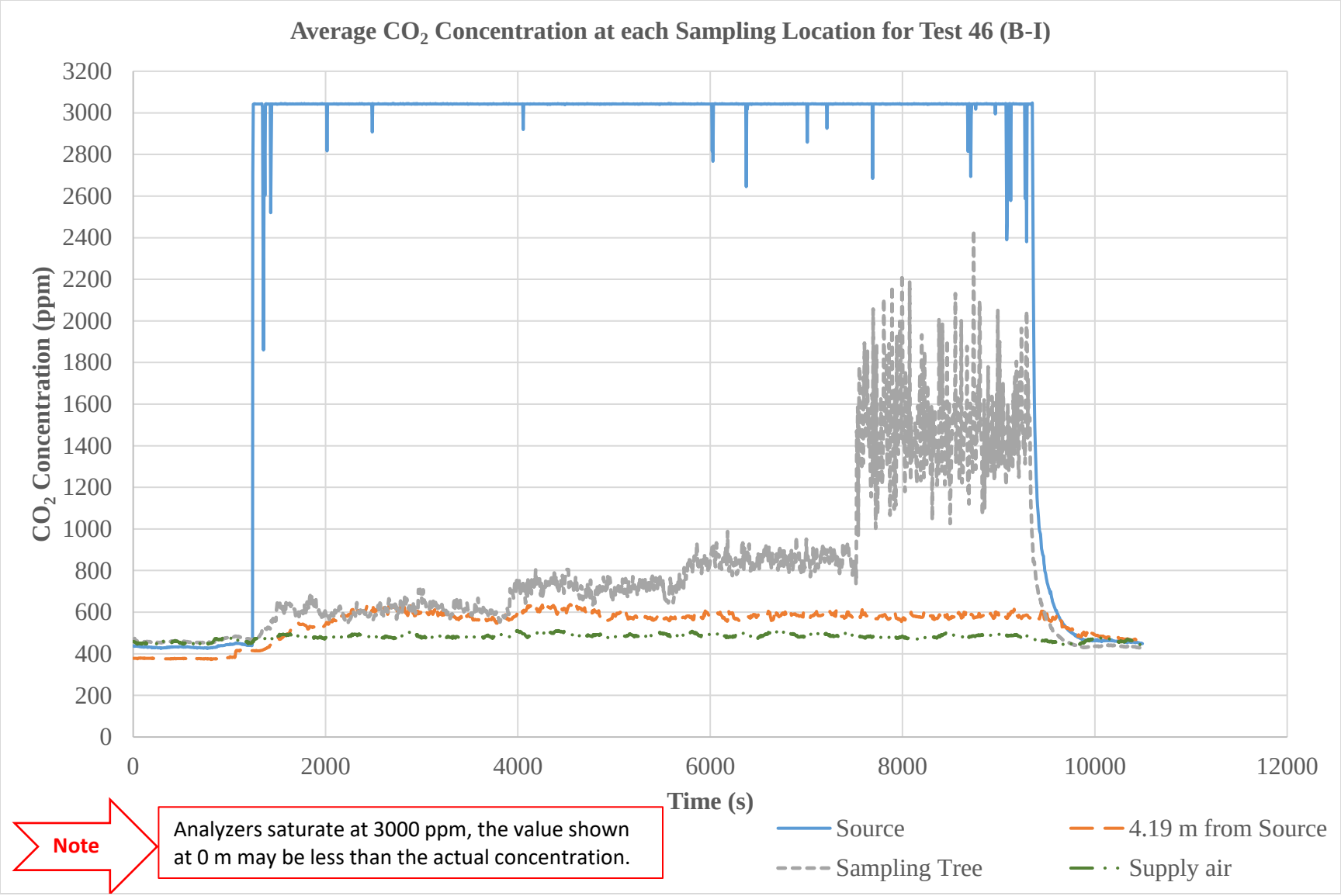

Figure C.105 Ininstantaneous CO_2 concentration at each sampling location for Test 46 (B-I) ISOPass undeployed.

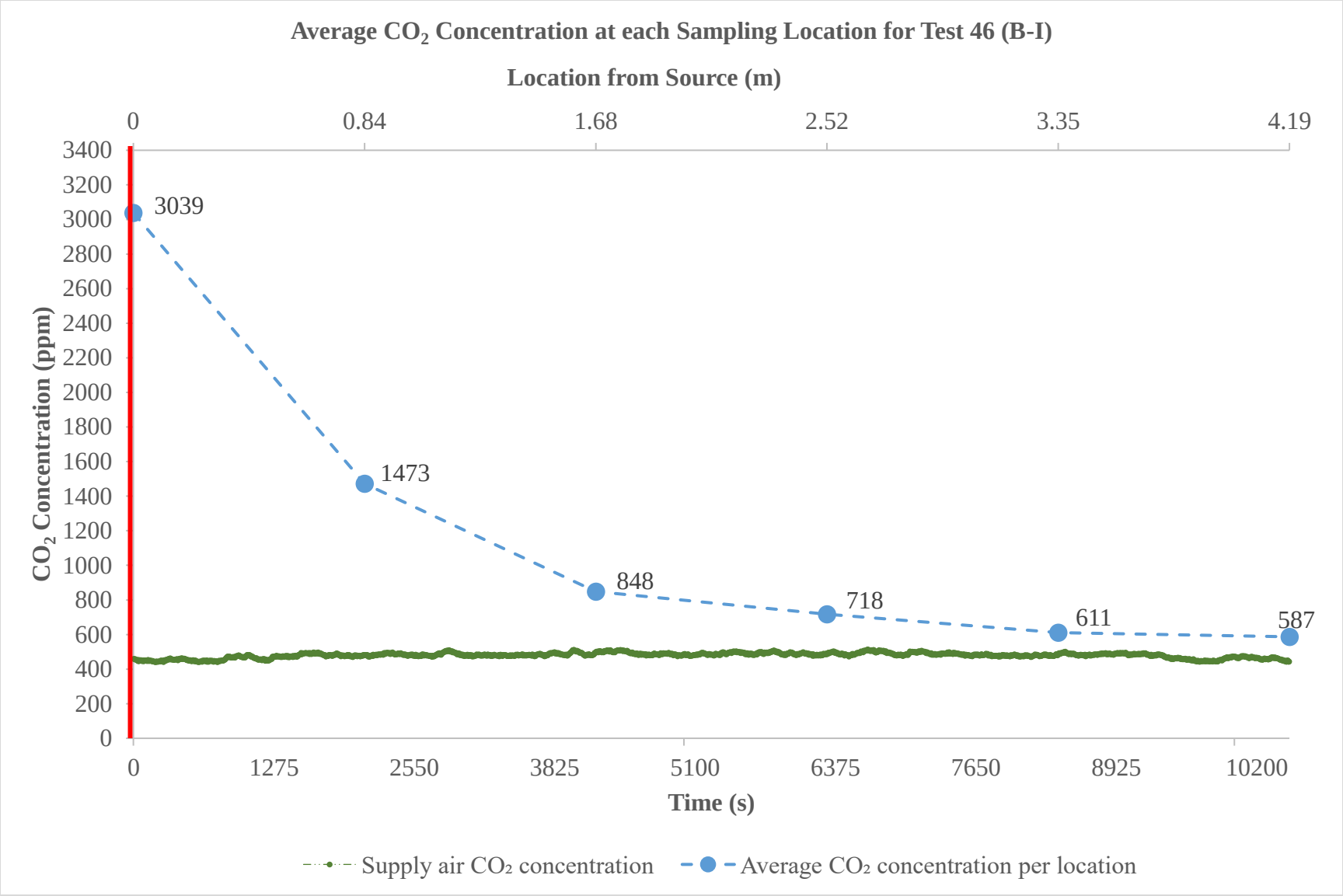

Figure C.106 Average CO_2 concentration at each sampling location for Test 46 (B-I) ISOPass undeployed.

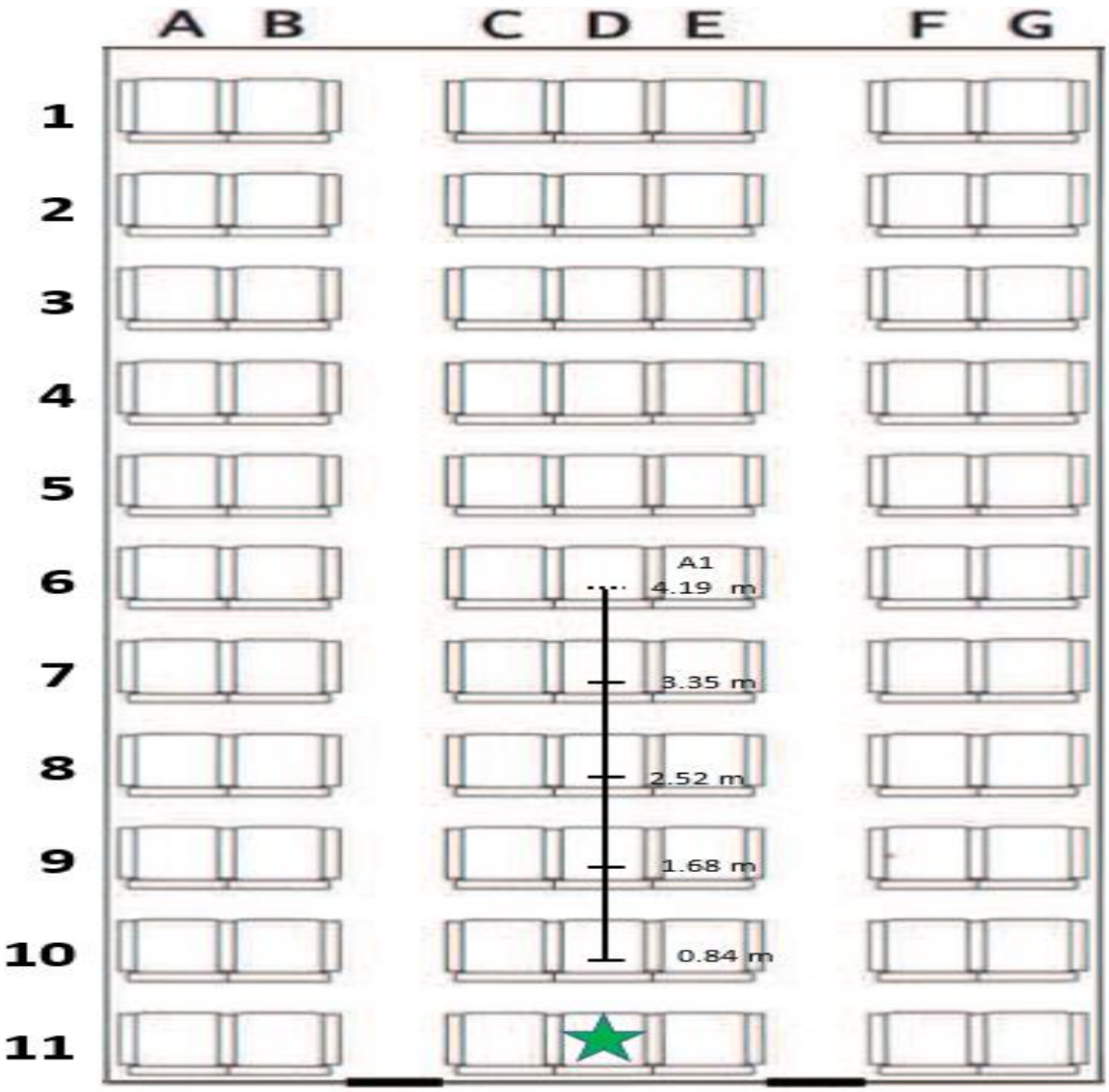

Figure C.107 Test 47 (B-I) ISOPass undeployed source location and sampling tree orientation.

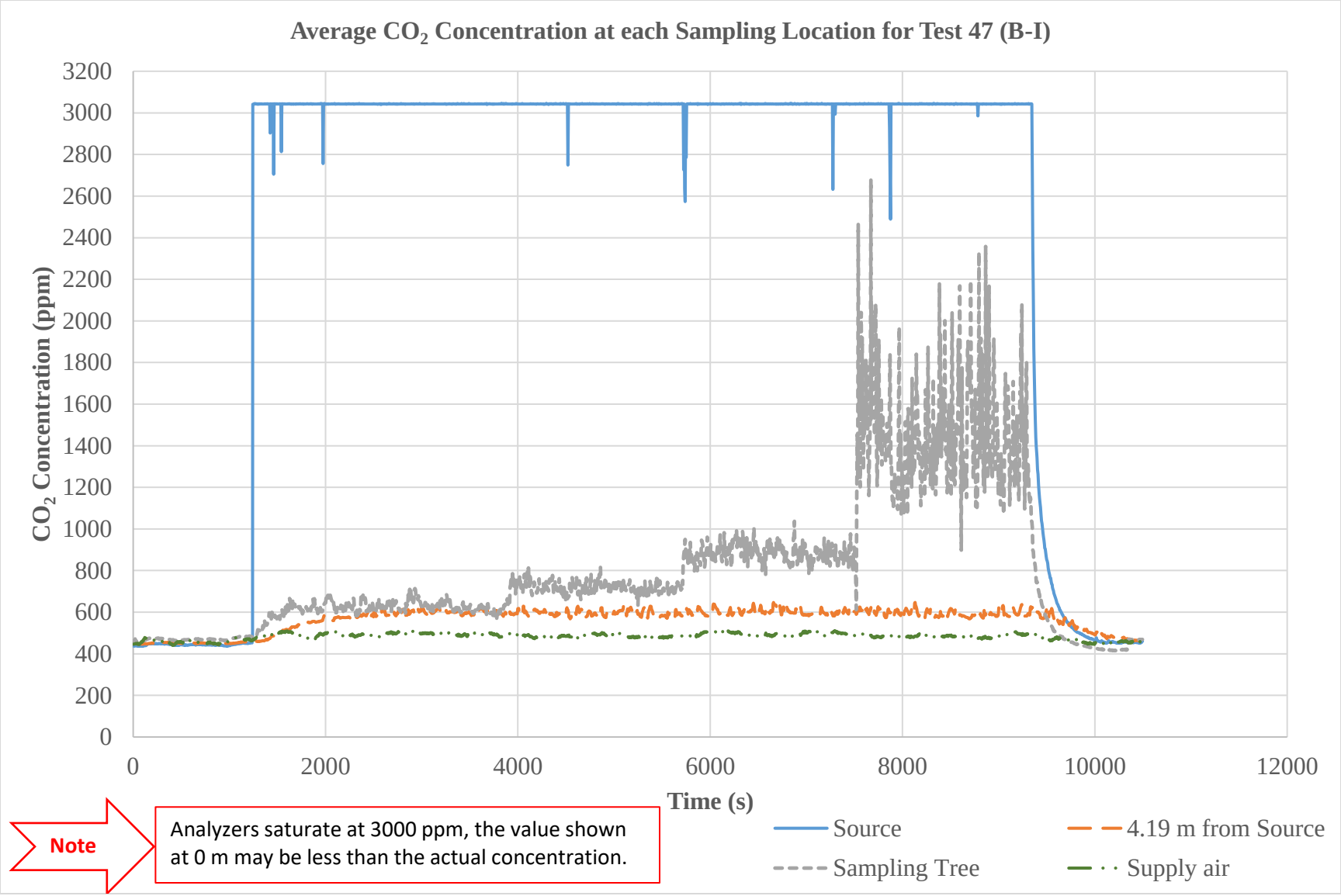

Figure C.108 Ininstantaneous CO_2 concentration at each sampling location for Test 47 (B-I) ISOPass undeployed.

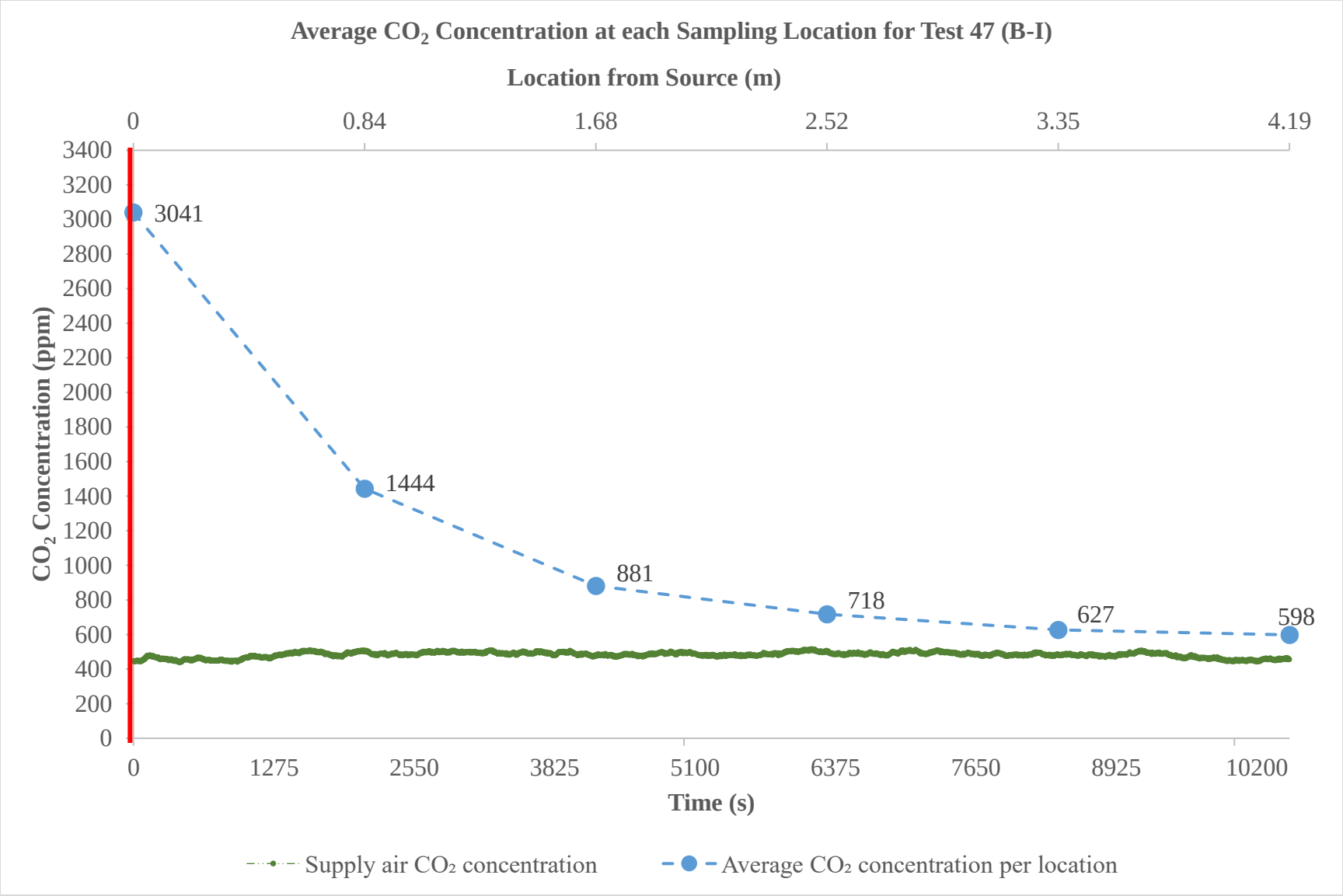

Figure C.109 Average CO_2 concentration at each sampling location for Test 47 (B-I) ISOPass undeployed.

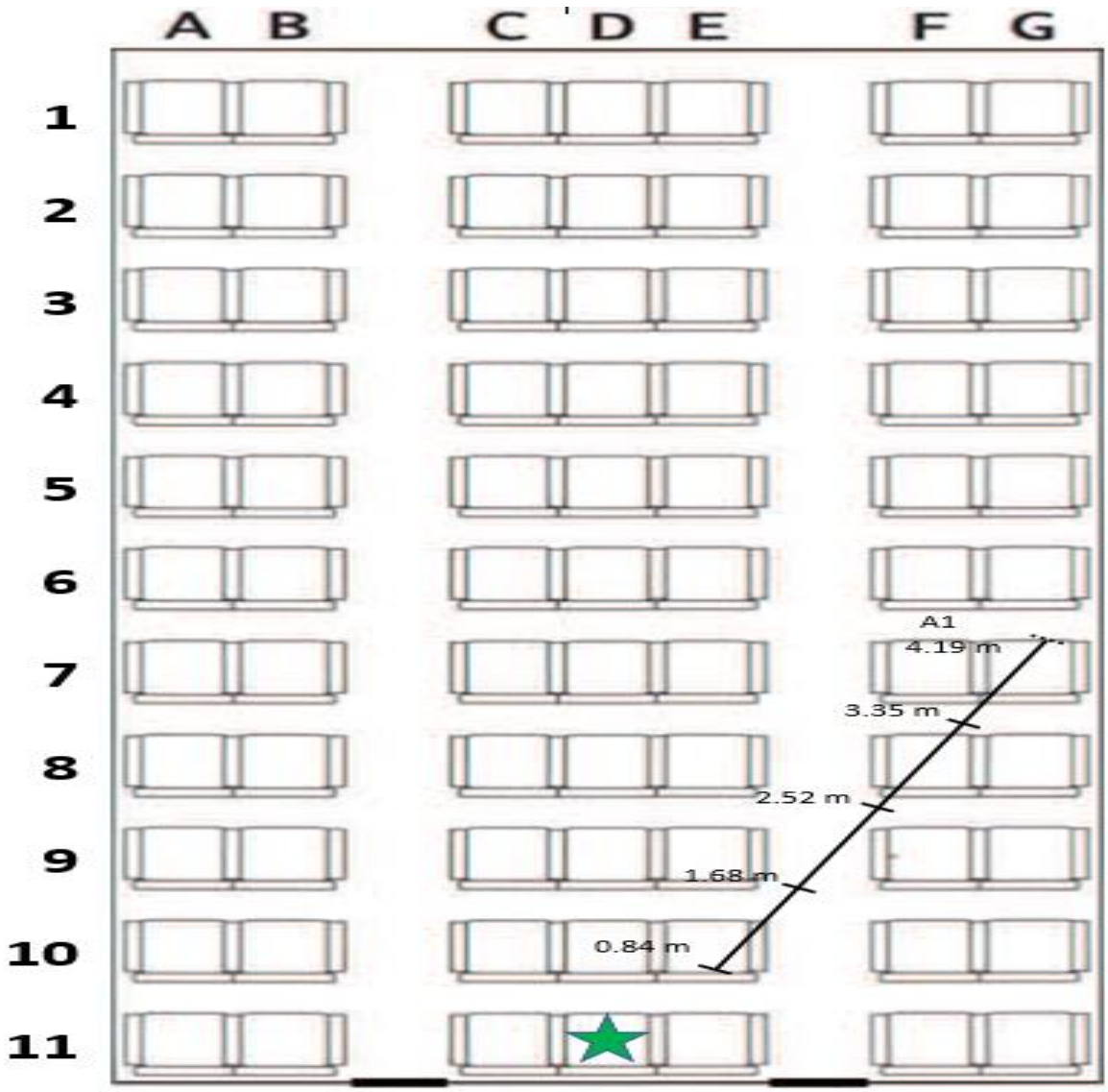

Figure C.110 Test 48 (B-I) ISOPass undeployed source location and sampling tree orientation.

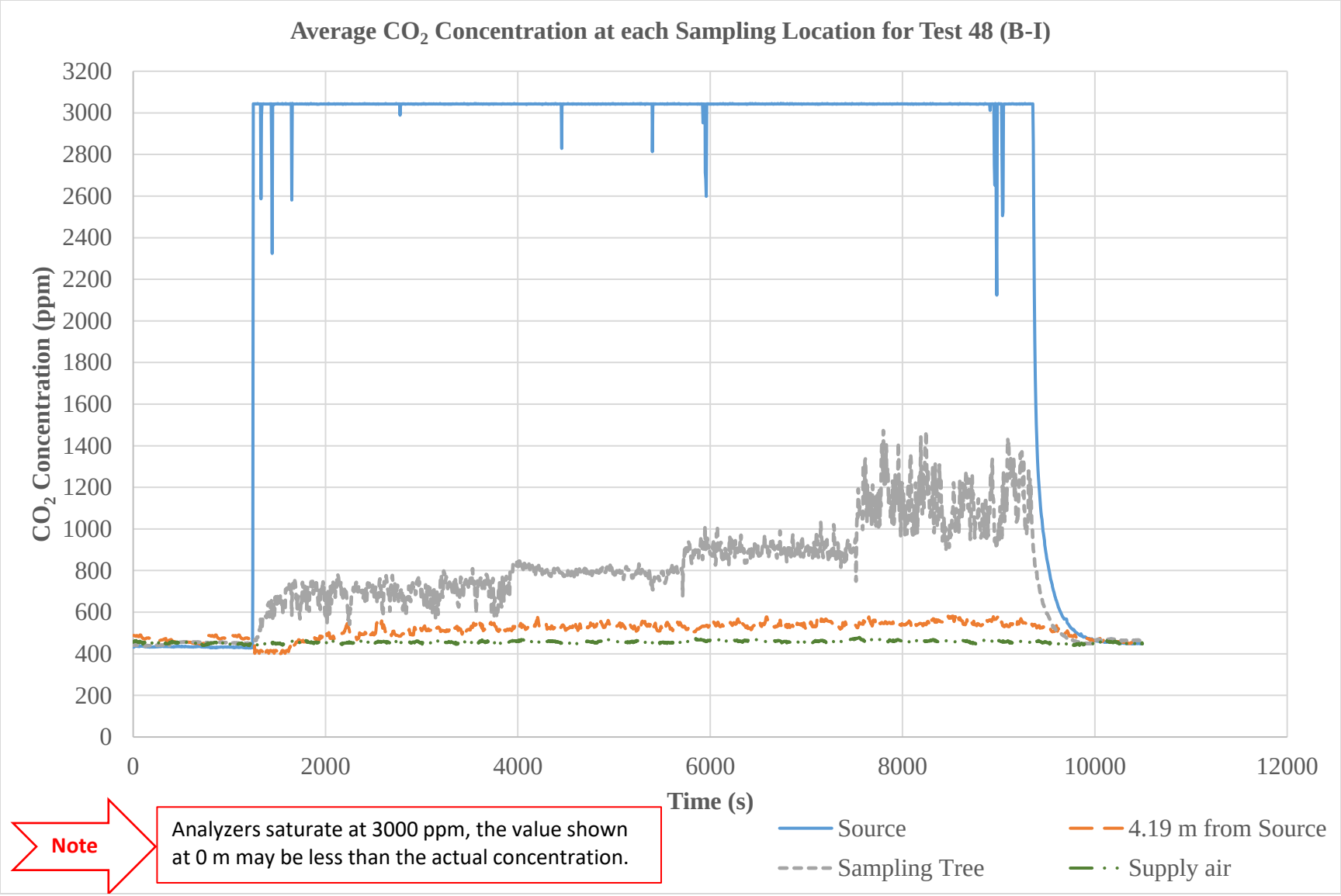

Figure C.111 Ininstantaneous CO_2 concentration at each sampling location for Test 48 (B-I) ISOPass undeployed.

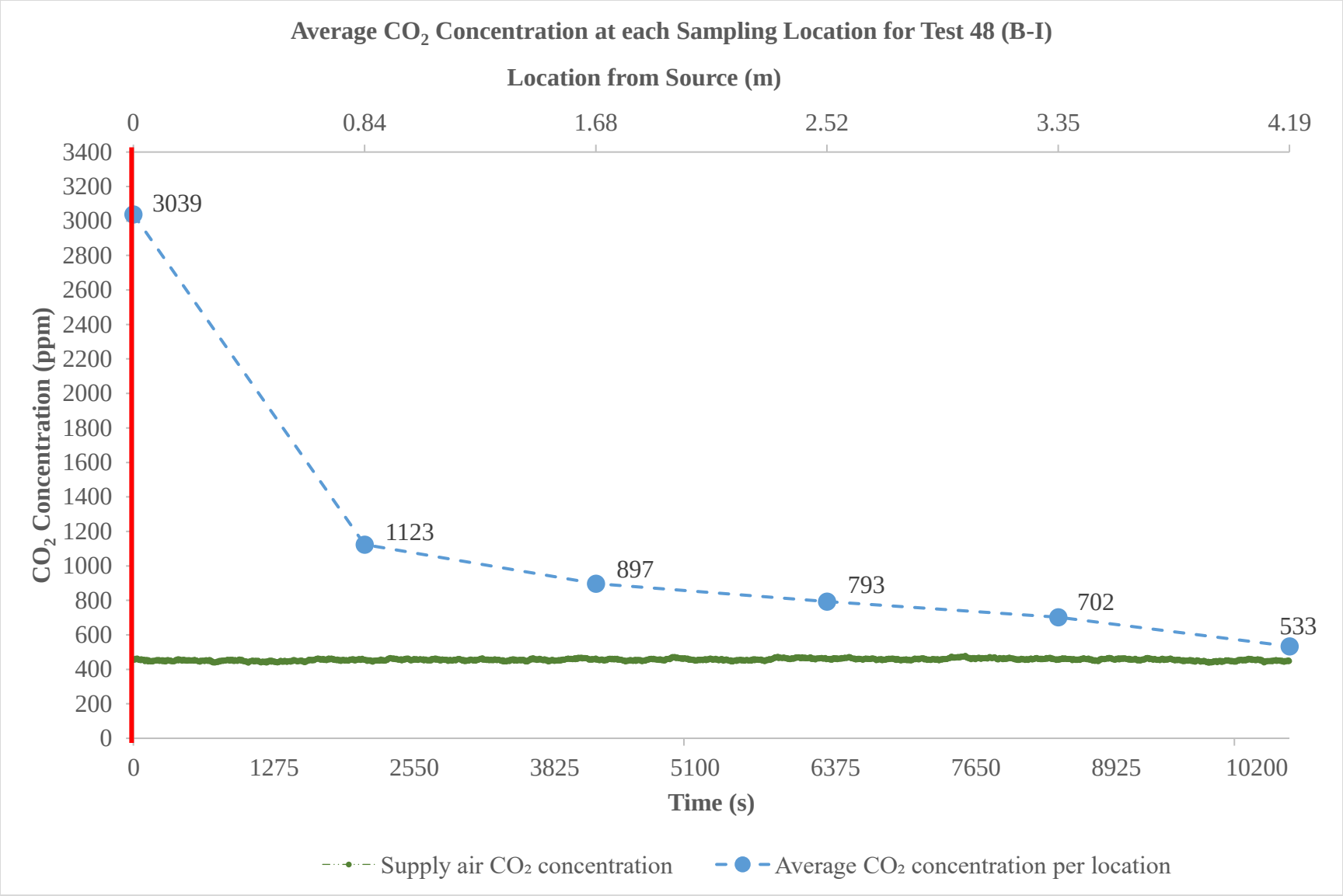

Figure C.112 Average CO_2 concentration at each sampling location for Test 48 (B-I) ISOPass undeployed.

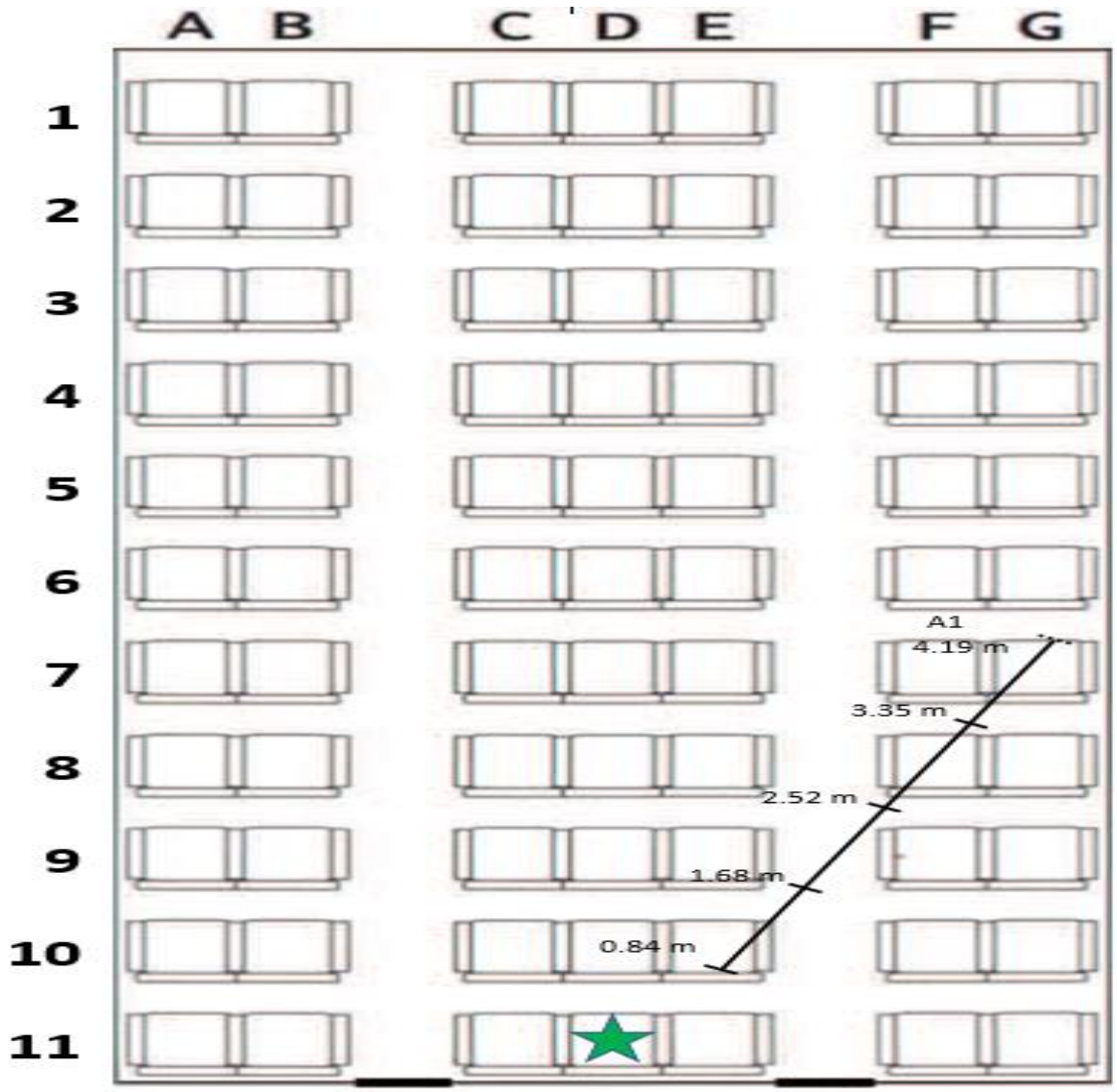

Figure C.113 Test 51 (B-I) ISOPass undeployed source location and sampling tree orientation.

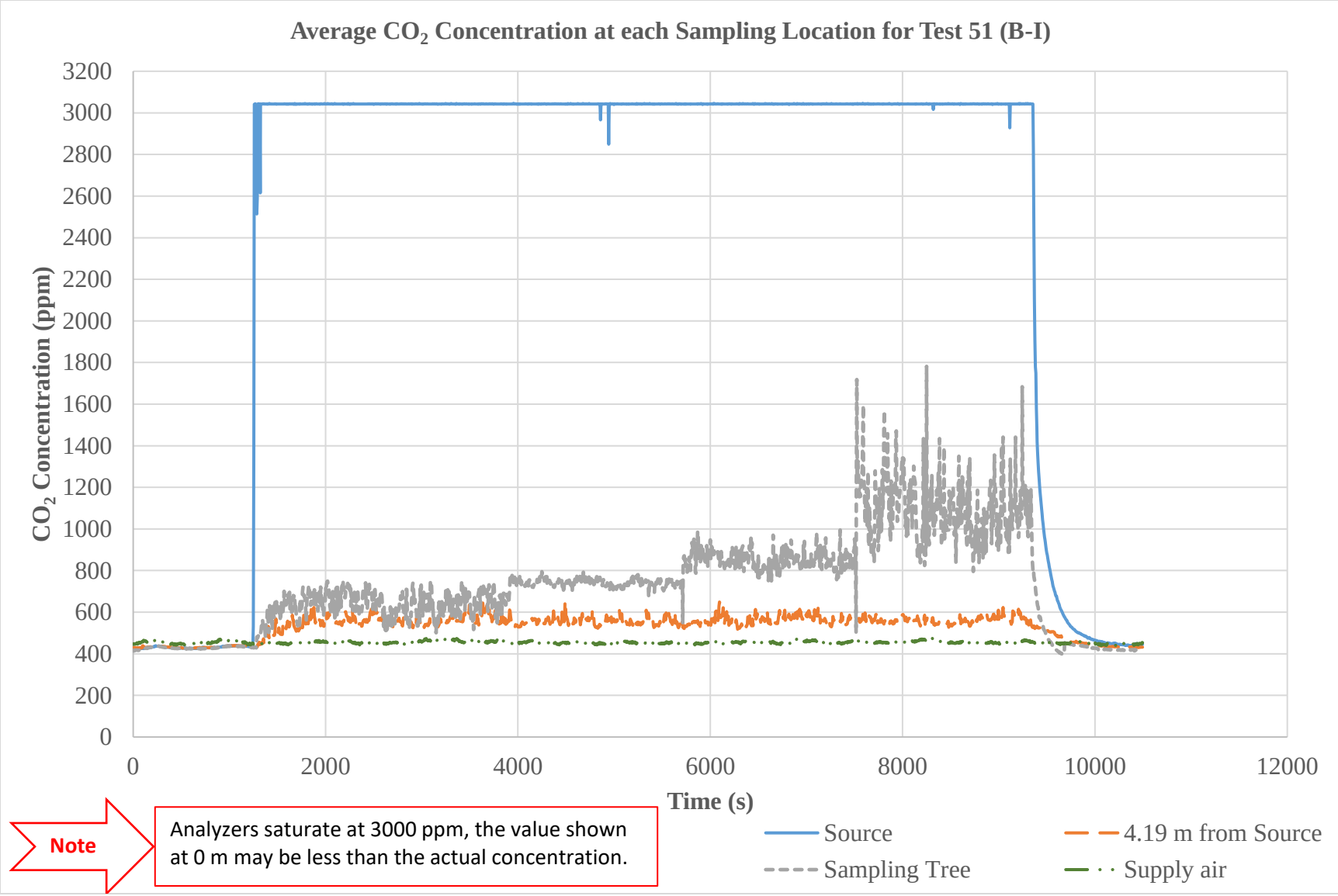

Figure C.114 Ininstantaneous CO_2 concentration at each sampling location for Test 51 (B-I) ISOPass undeployed.

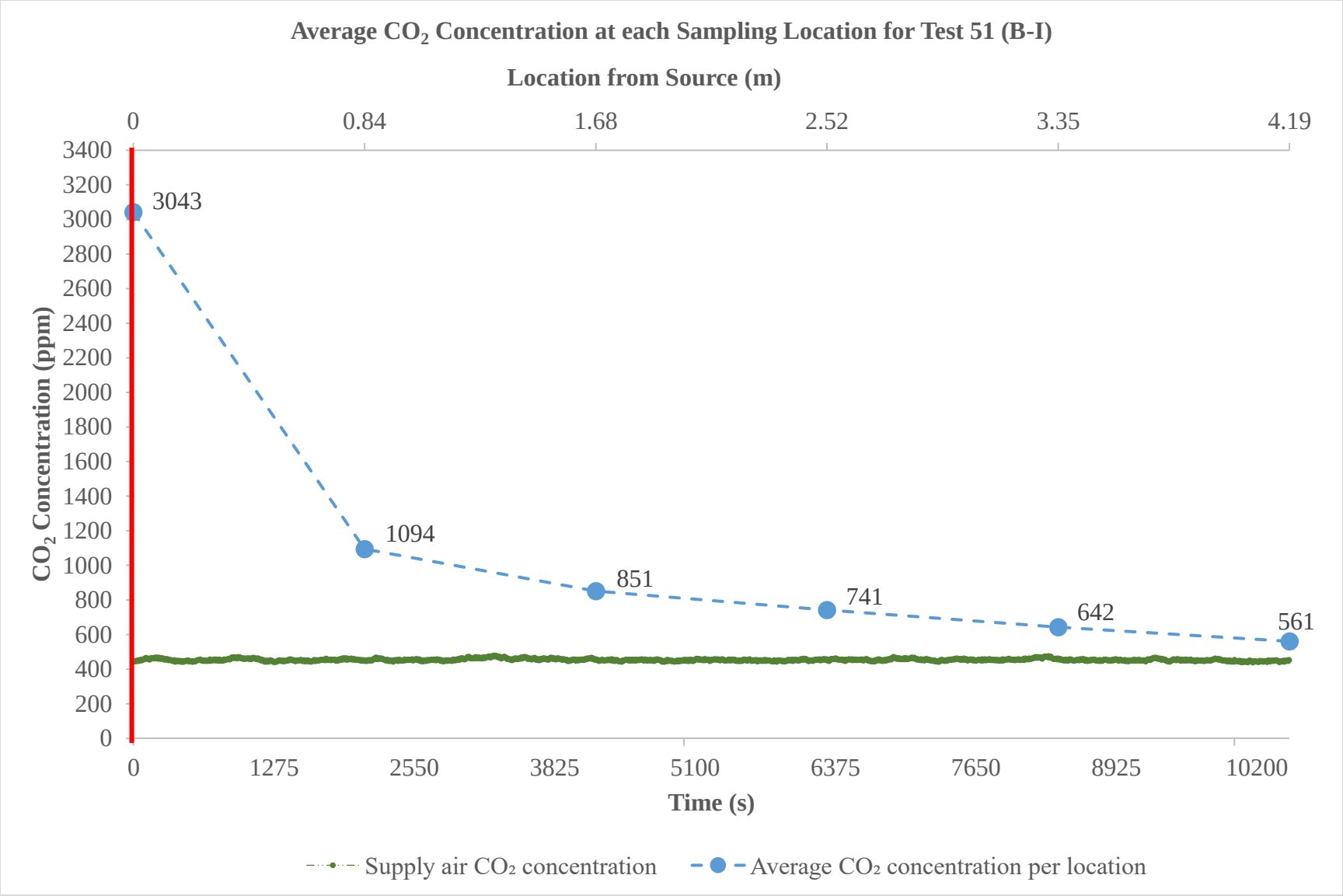

Figure C.115 Average CO_2 concentration at each sampling location for Test 51 (B-I) ISOPass undeployed.

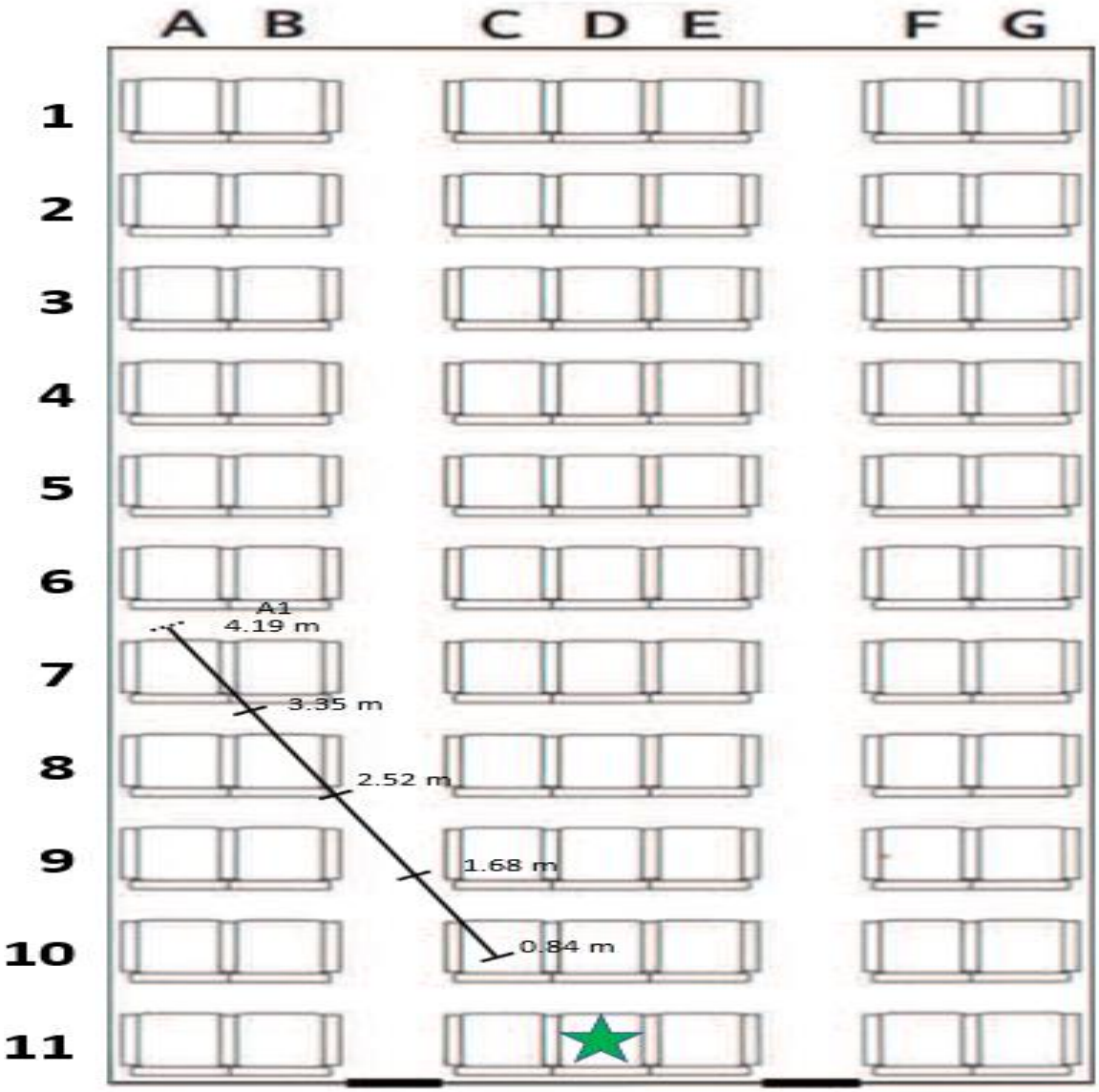

Figure C.116 Test 52 (B-I) ISOPass undeployed source location and sampling tree orientation.

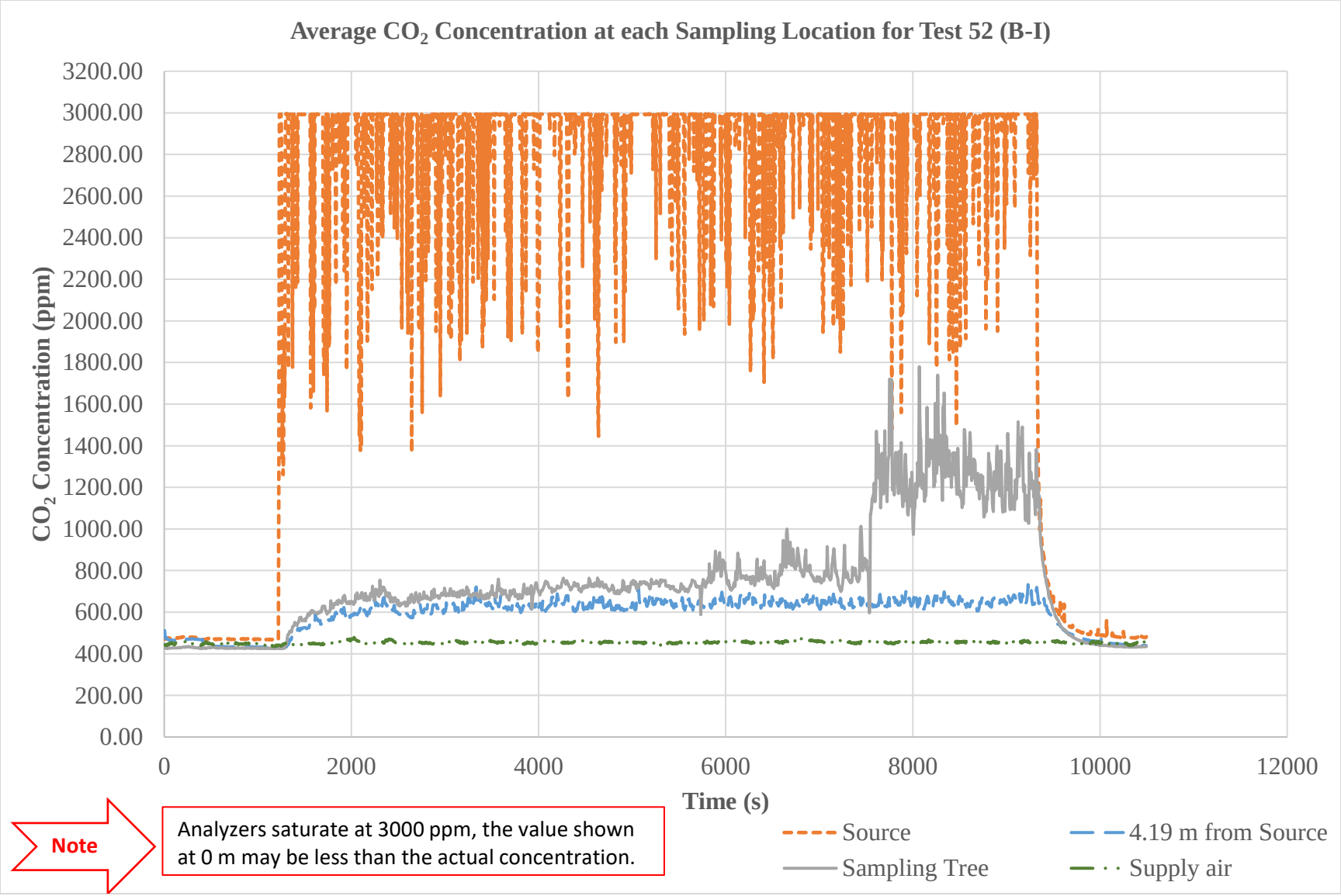

Figure C.117 Ininstantaneous CO_2 concentration at each sampling location for Test 52 (B-I) ISOPass undeployed.

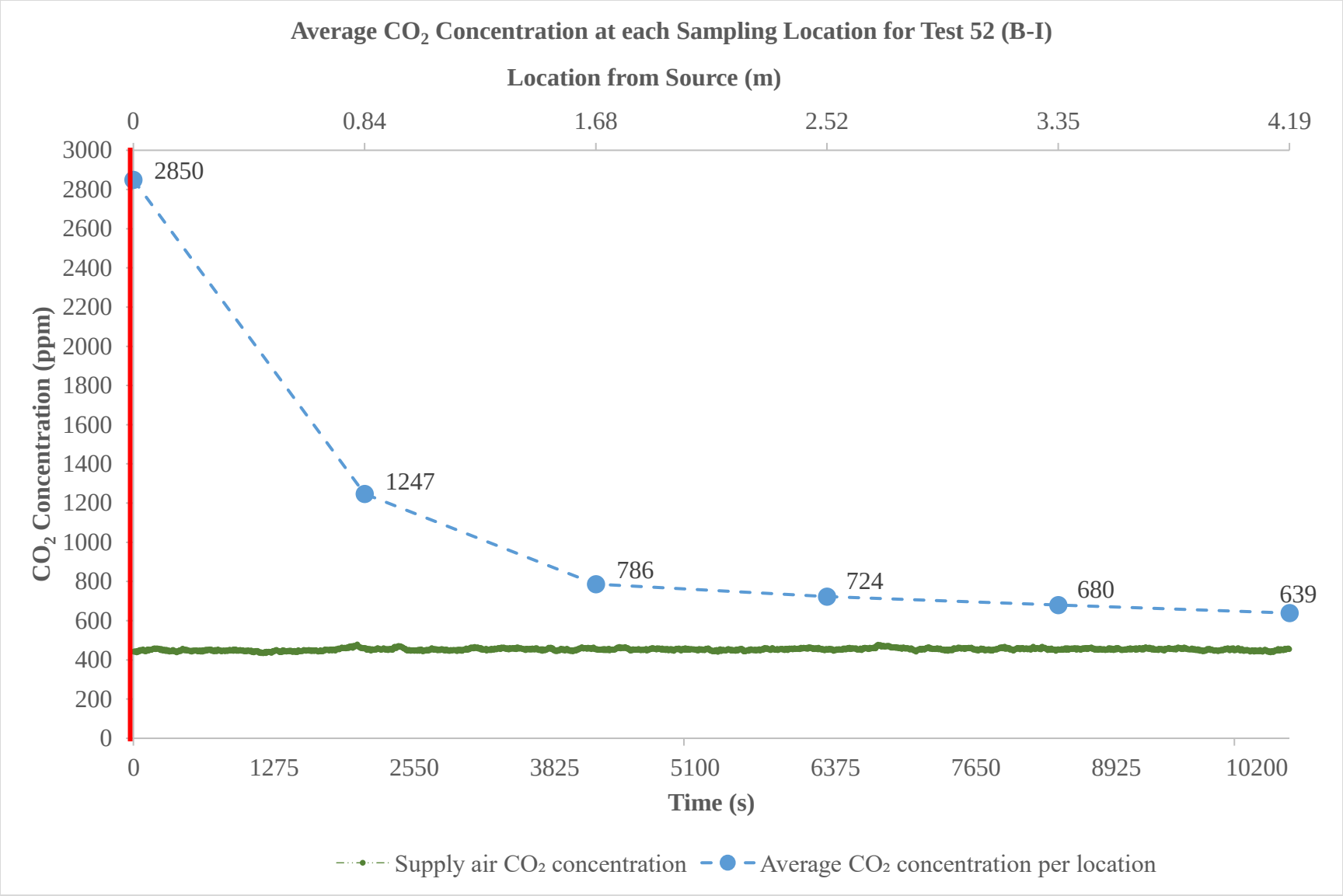

Figure C.118 Average CO_2 concentration at each sampling location for Test 52 (B-I) ISOPass undeployed.

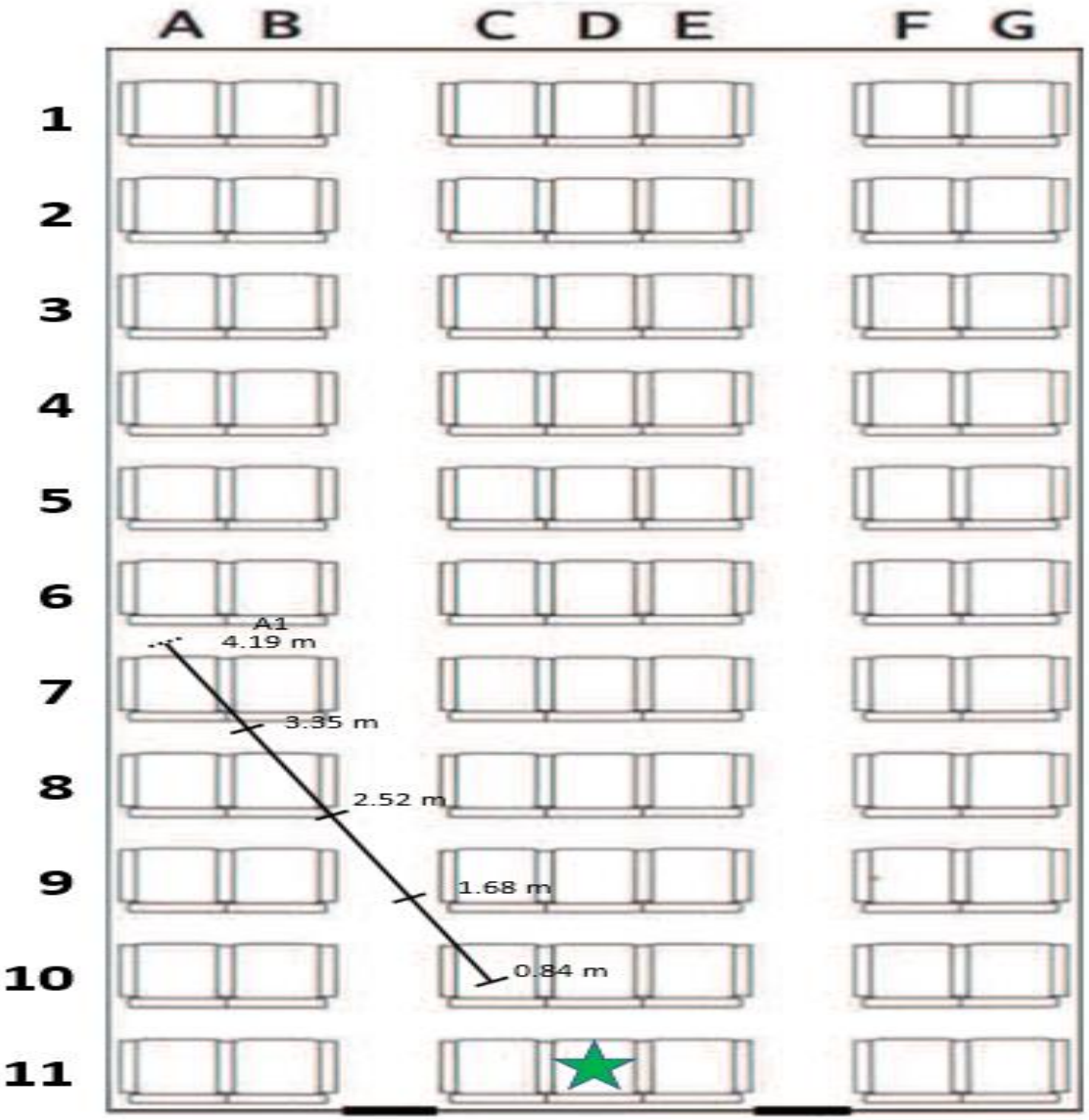

Figure C.119 Test 53 (B-I) ISOPass undeployed source location and sampling tree orientation.

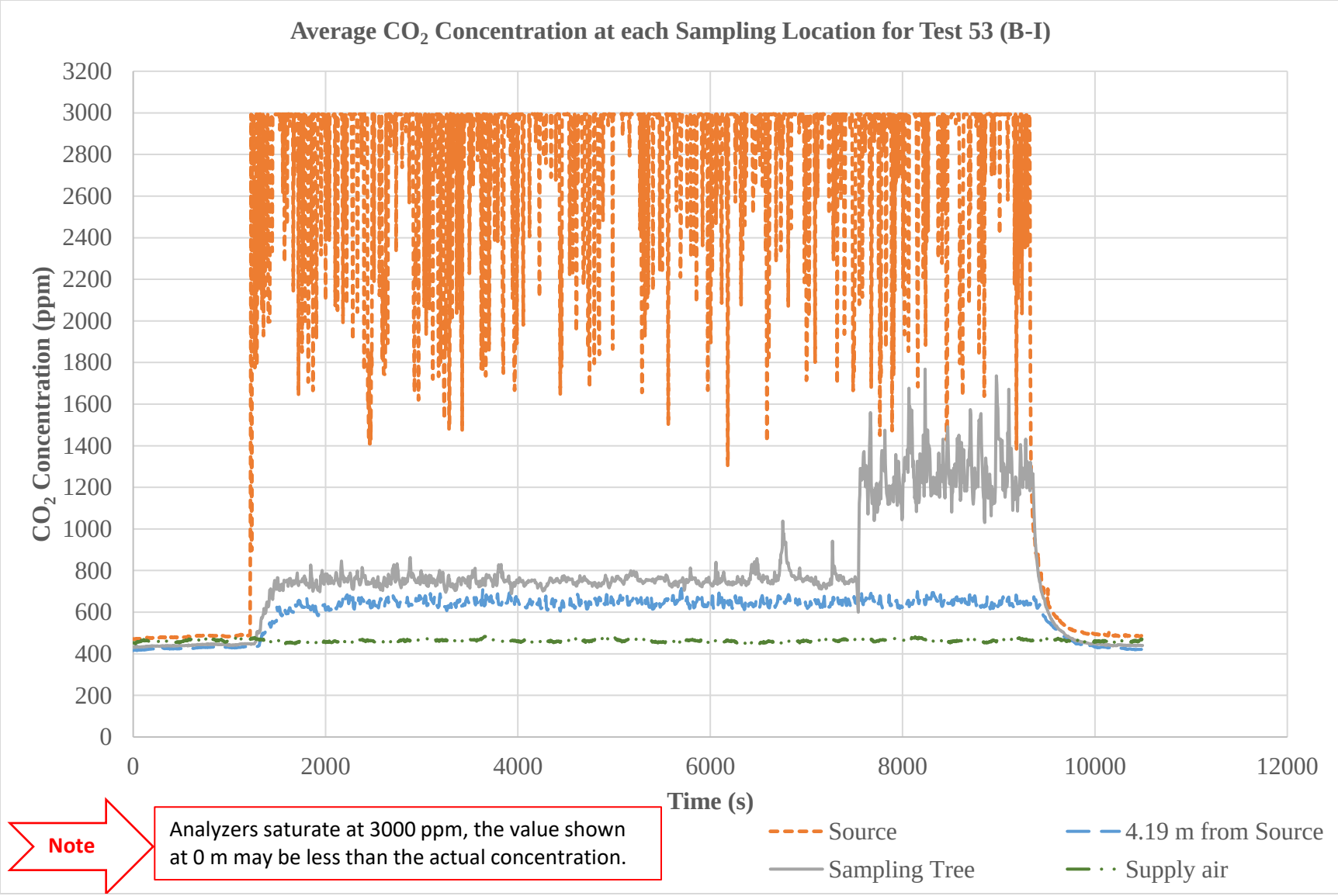

Figure C.120 Ininstantaneous CO_2 concentration at each sampling location for Test 53 (B-I) ISOPass undeployed.

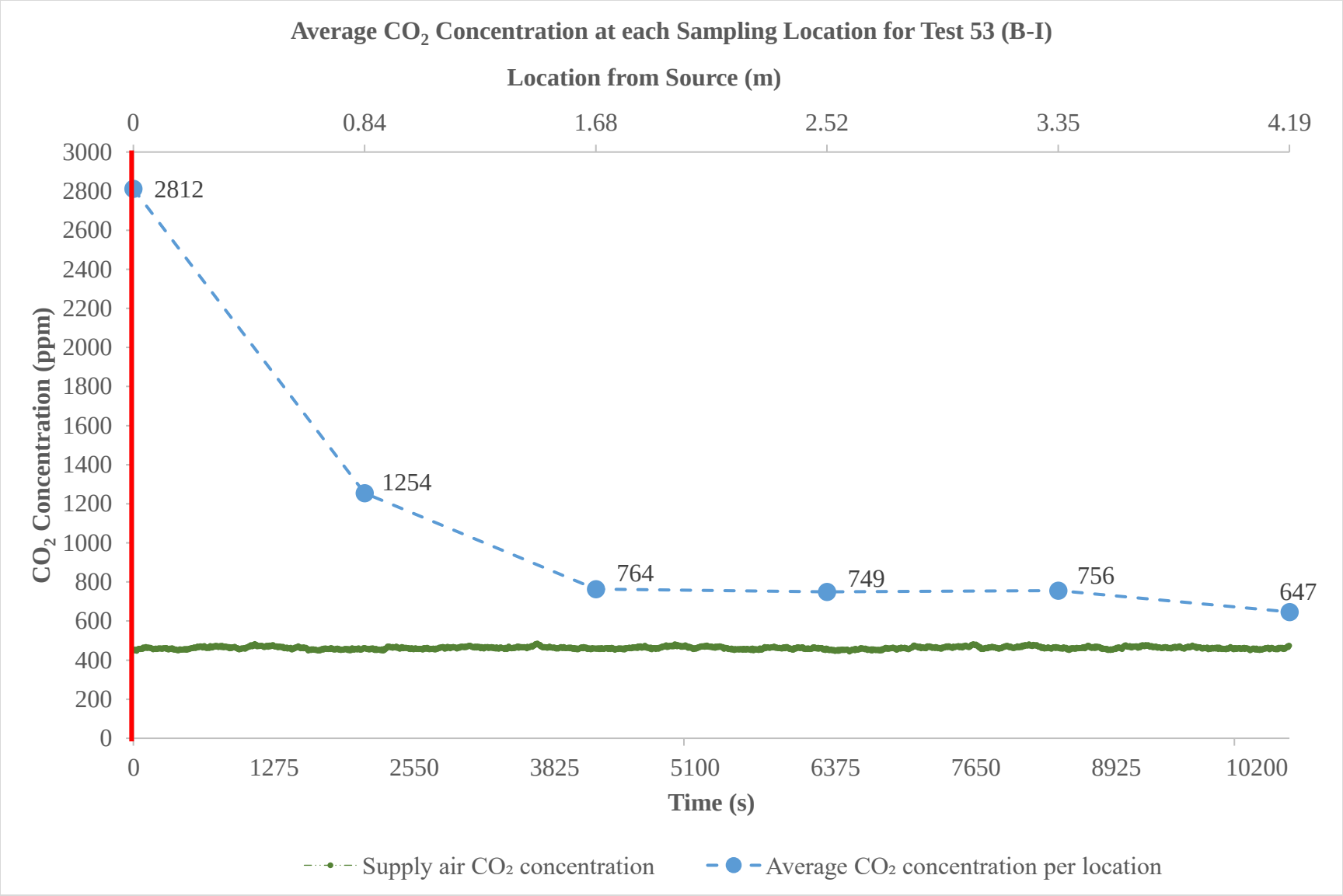

Figure C.121 Average CO_2 concentration at each sampling location for Test 53 (B-I) ISOPass undeployed.

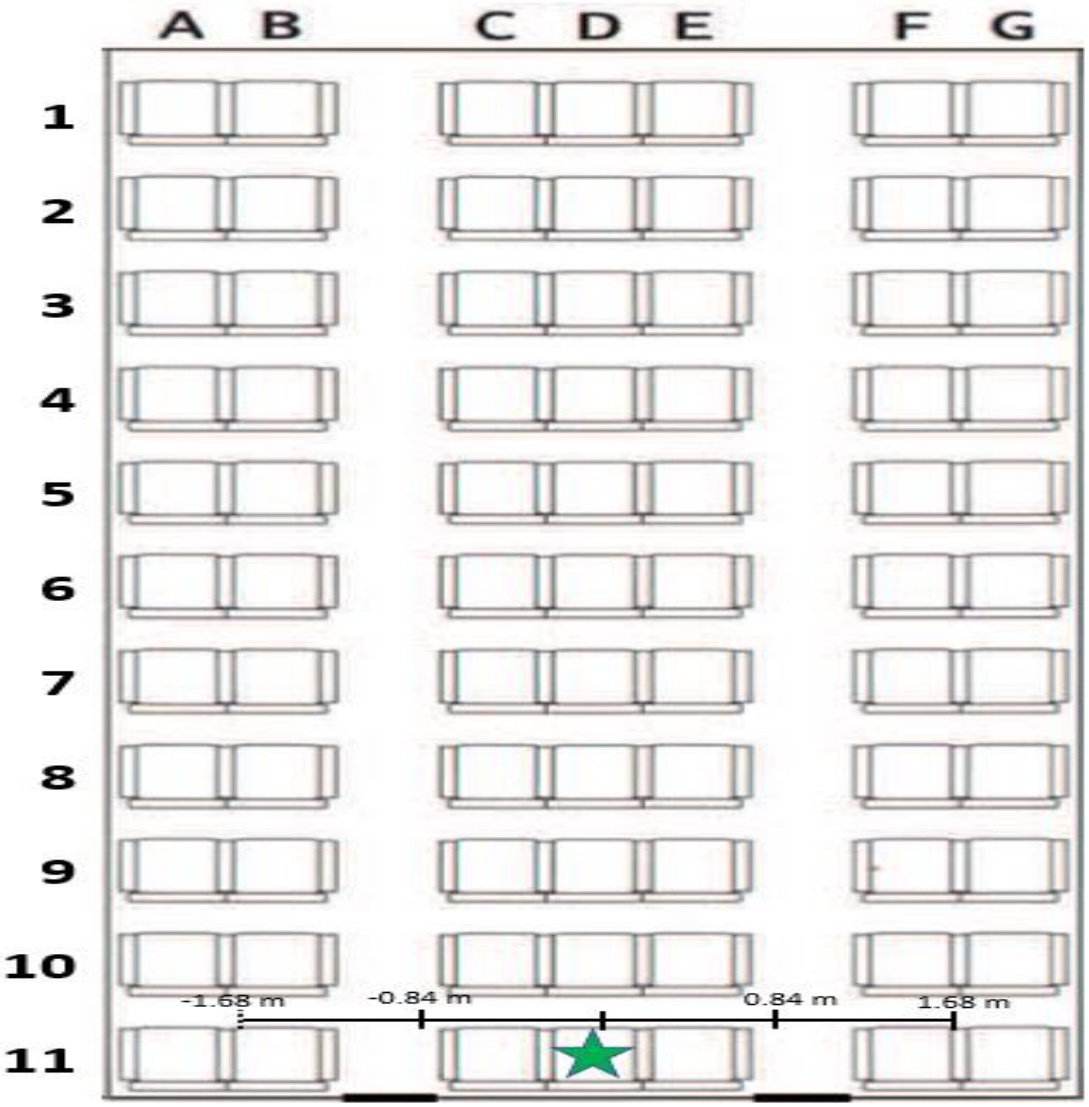

Figure C.122 Test 54 (B-I) ISOPass undeployed source location and sampling tree orientation.

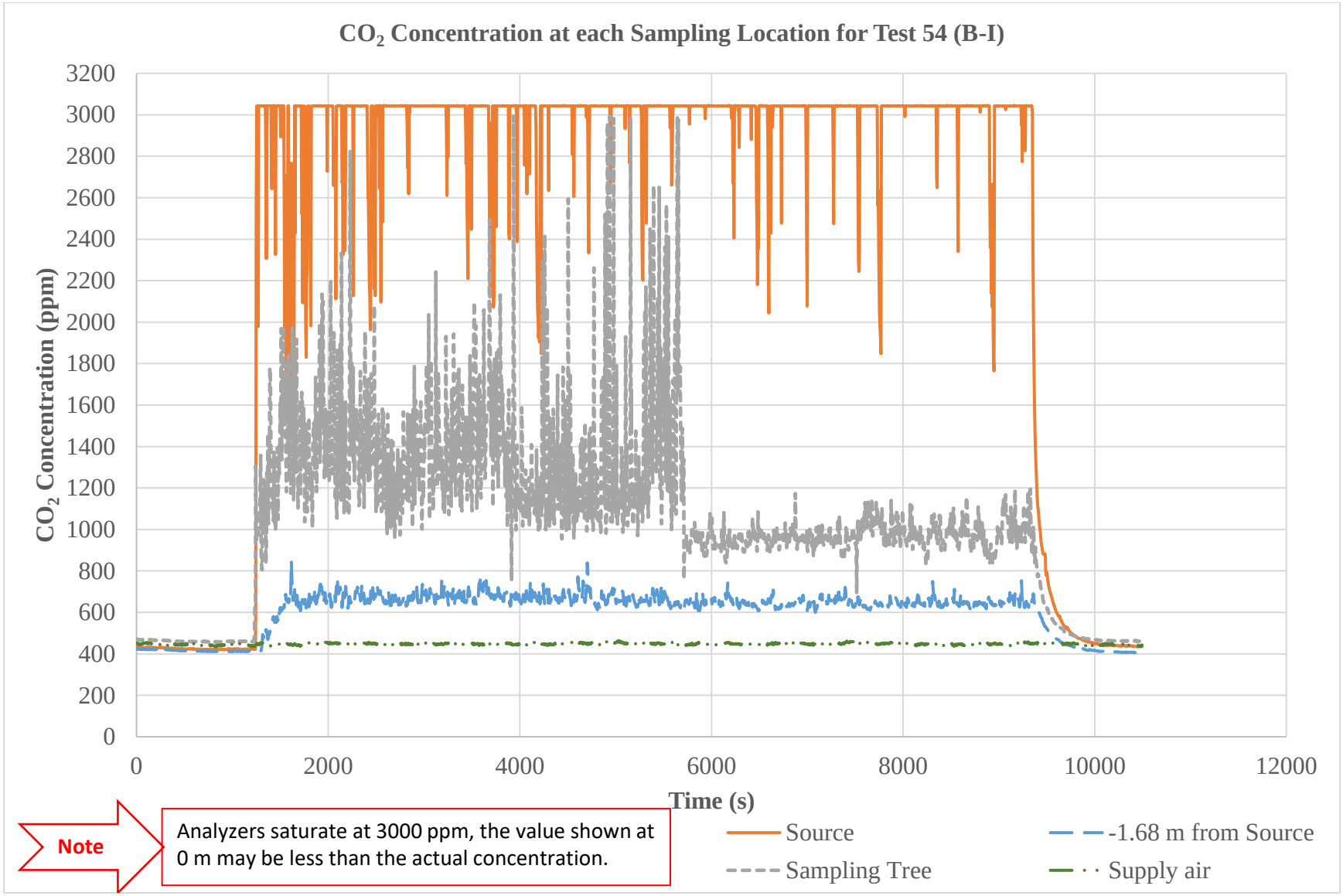

Figure C.123 Ininstantaneous CO_2 concentration at each sampling location for Test 54 (B-I) ISOPass undeployed.

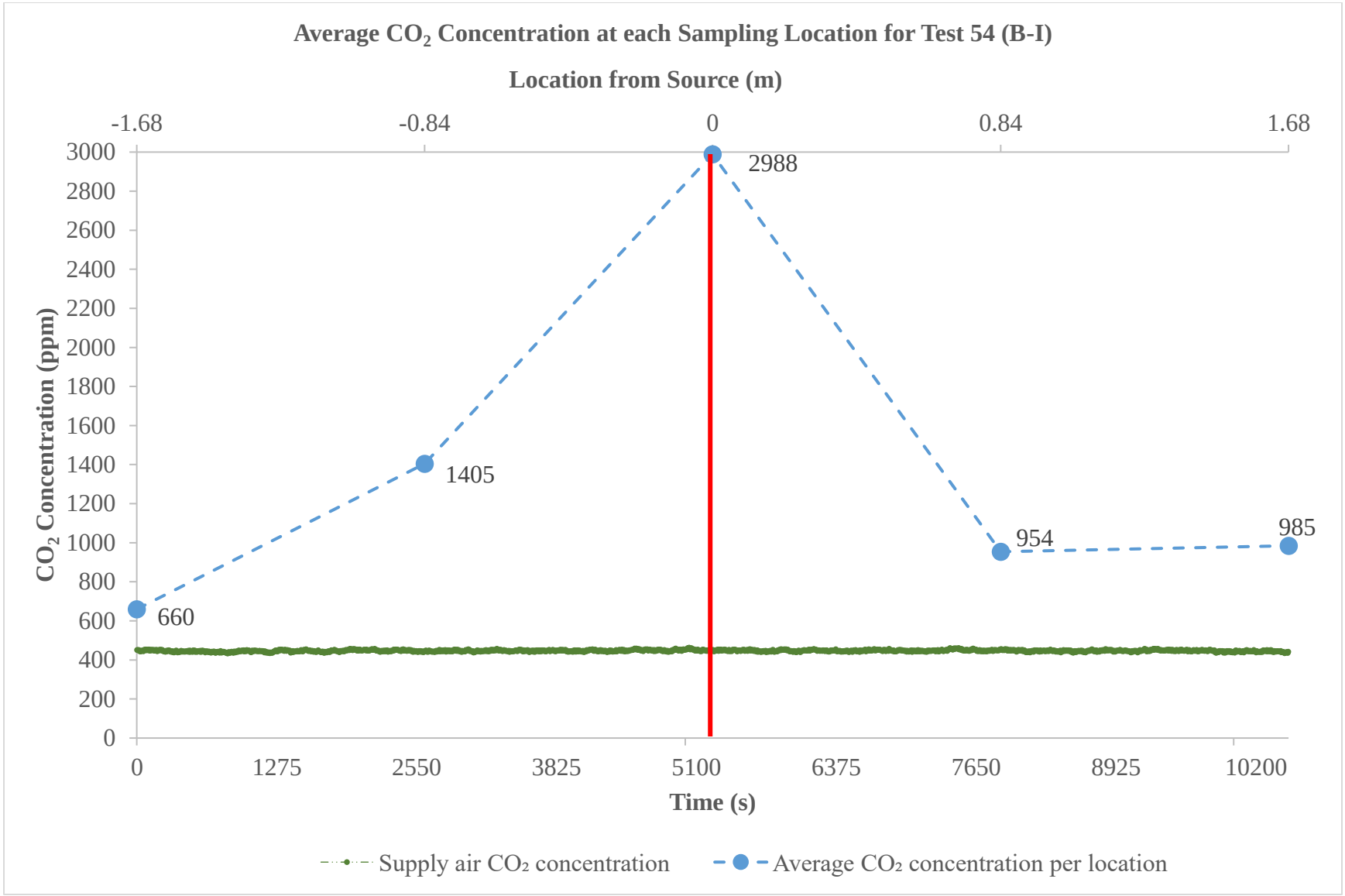

Figure C.124 Average CO_2 concentration at each sampling location for Test 54 (B-I) ISOPass undeployed.

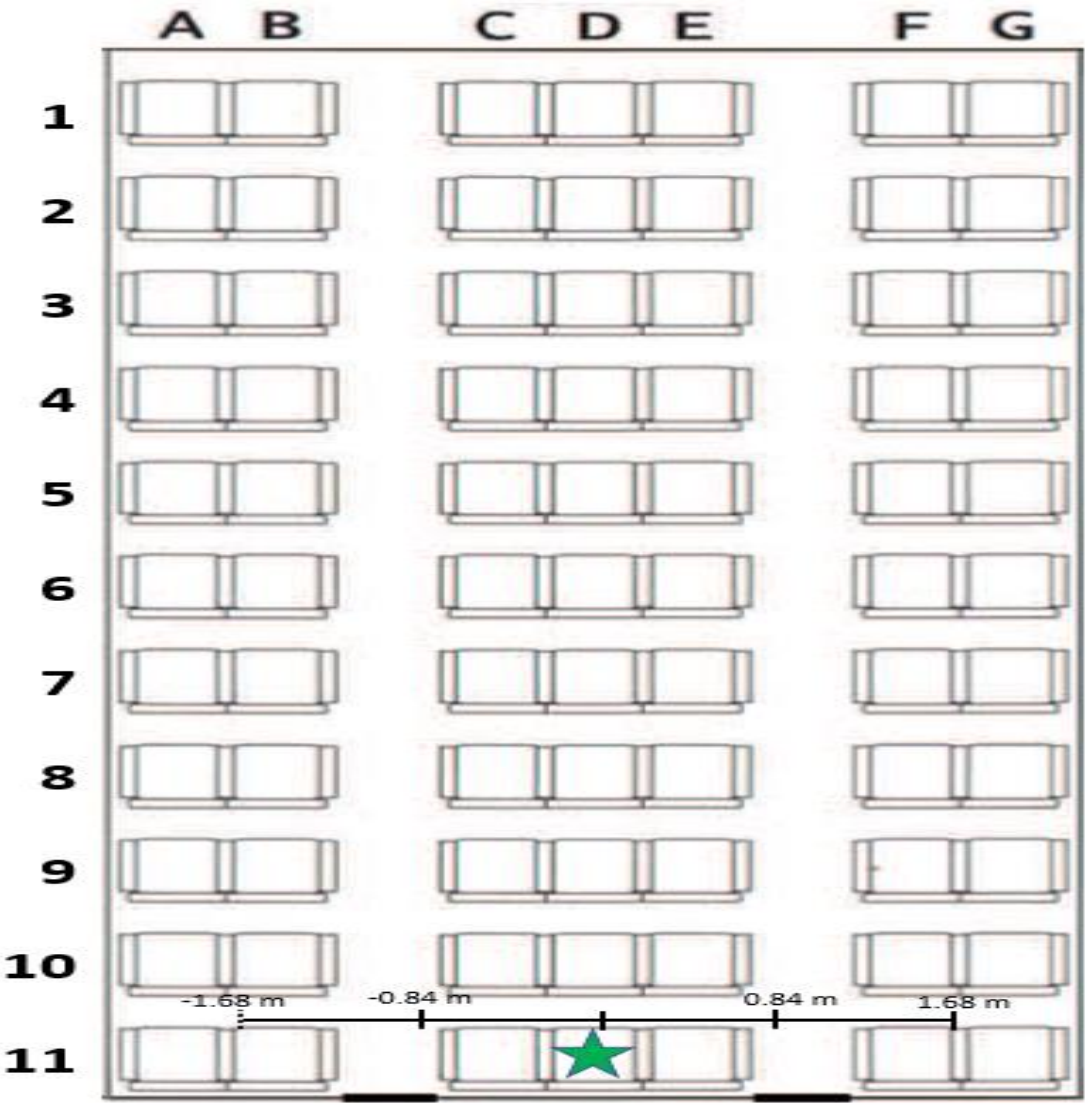

Figure C.125 Test 55 (B-I) ISOPass undeployed source location and sampling tree orientation.

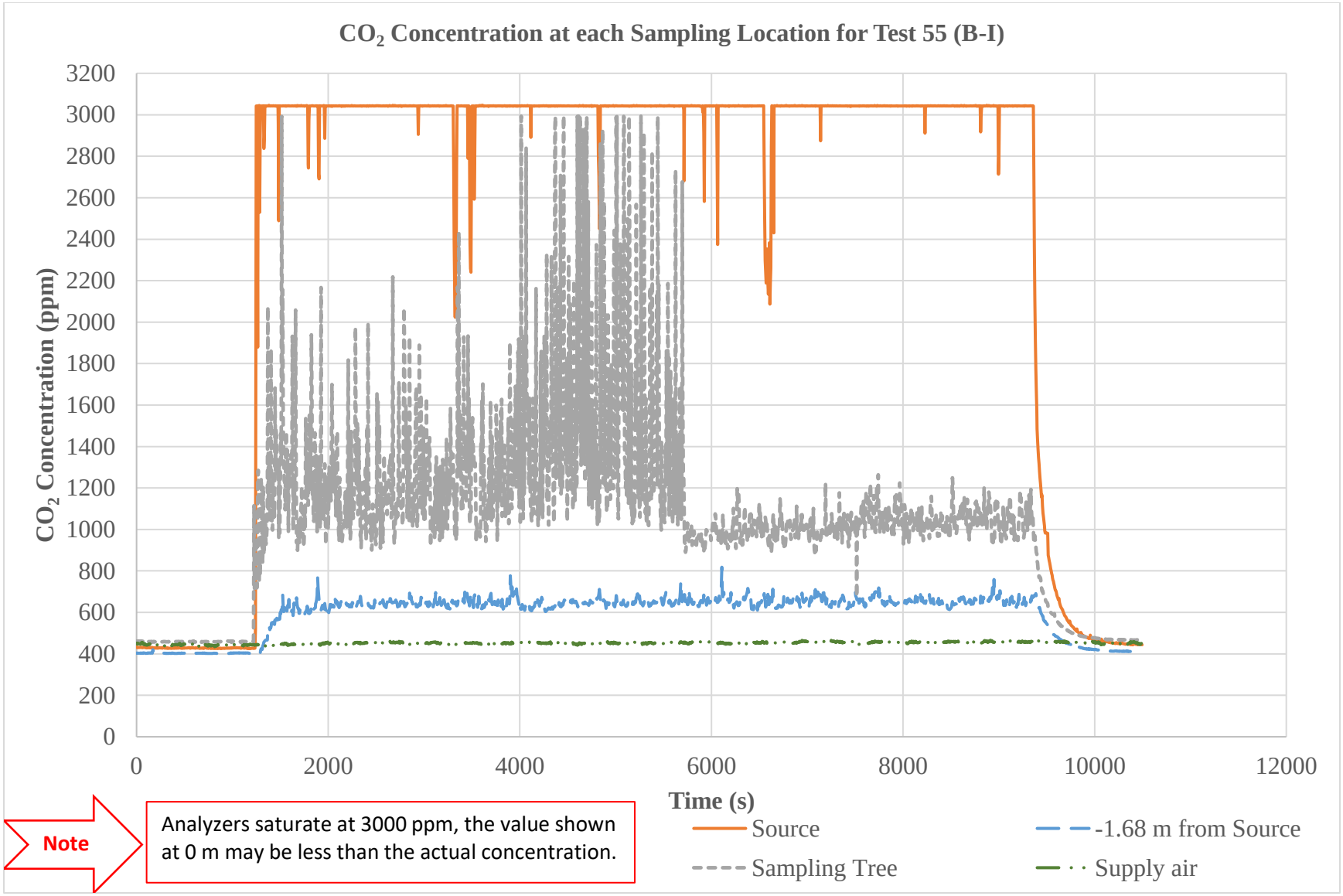

Figure C.126 Ininstantaneous CO_2 concentration at each sampling location for Test 55 (B-I) ISOPass undeployed.

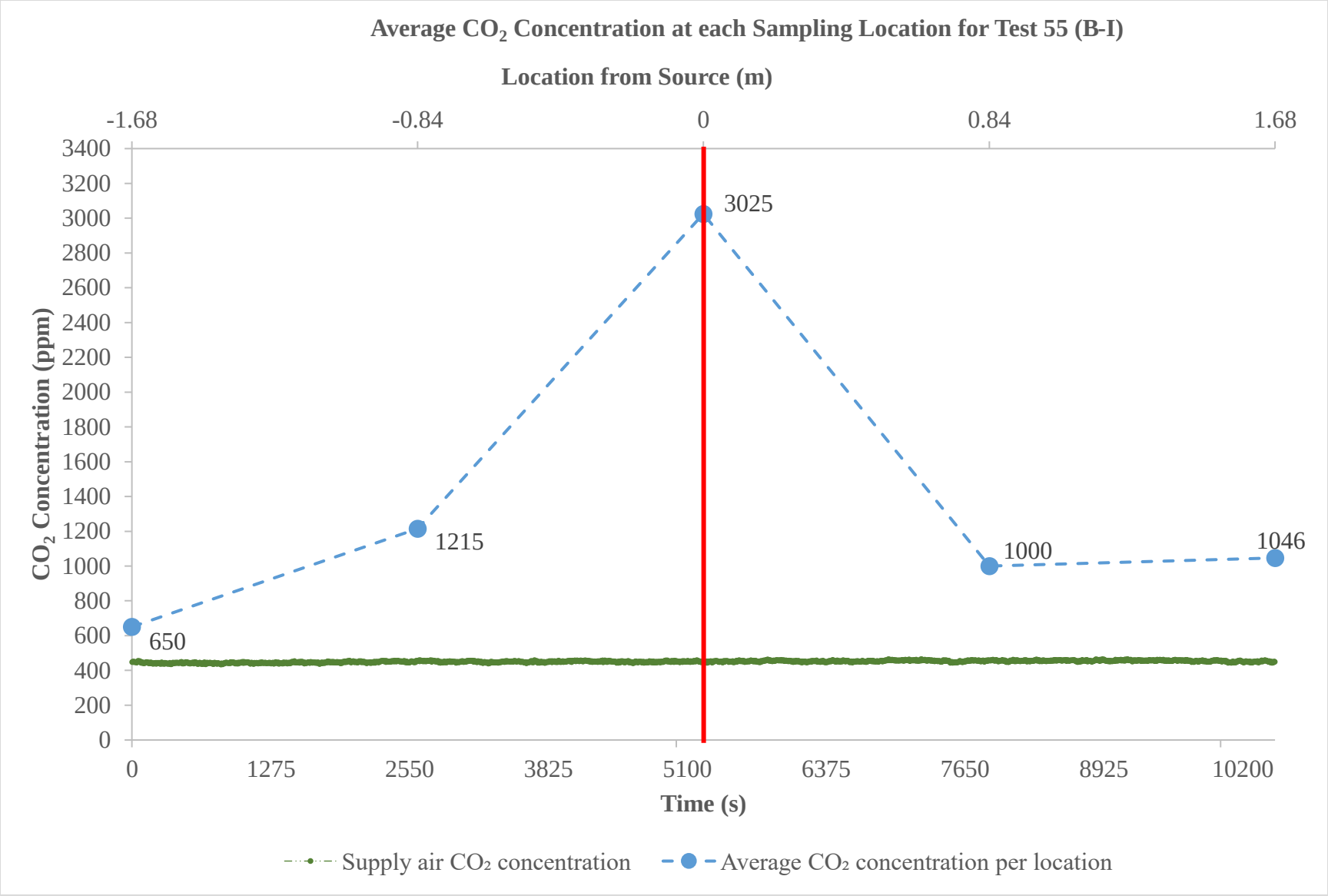

Figure C.127 Average CO_2 concentration at each sampling location for Test 55 (B-I) ISOPass undeployed.

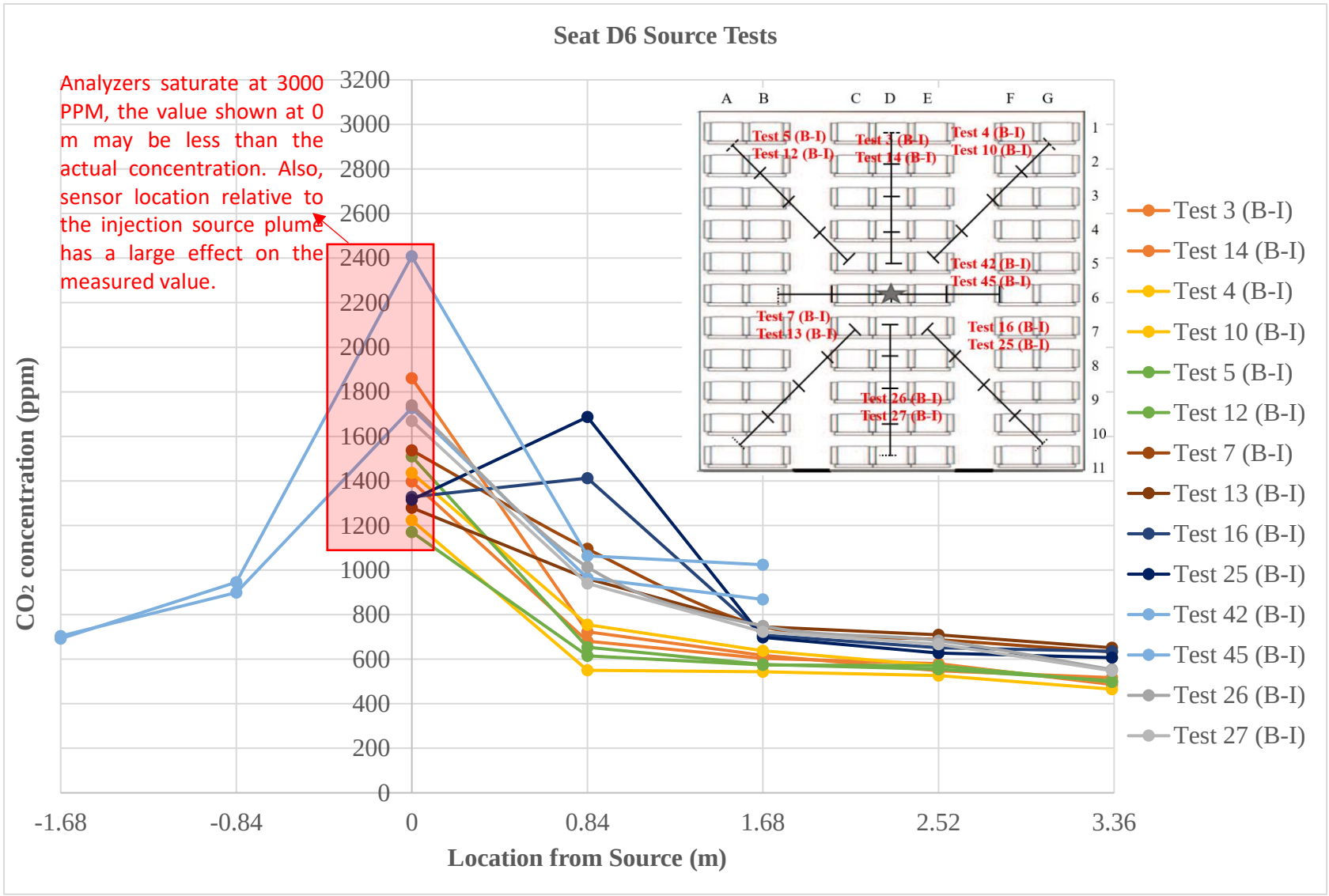

Figure C.128 Seat D6 continuous injection source tests in the Boeing 767 cabin mockup with the ISOPass undeployed.

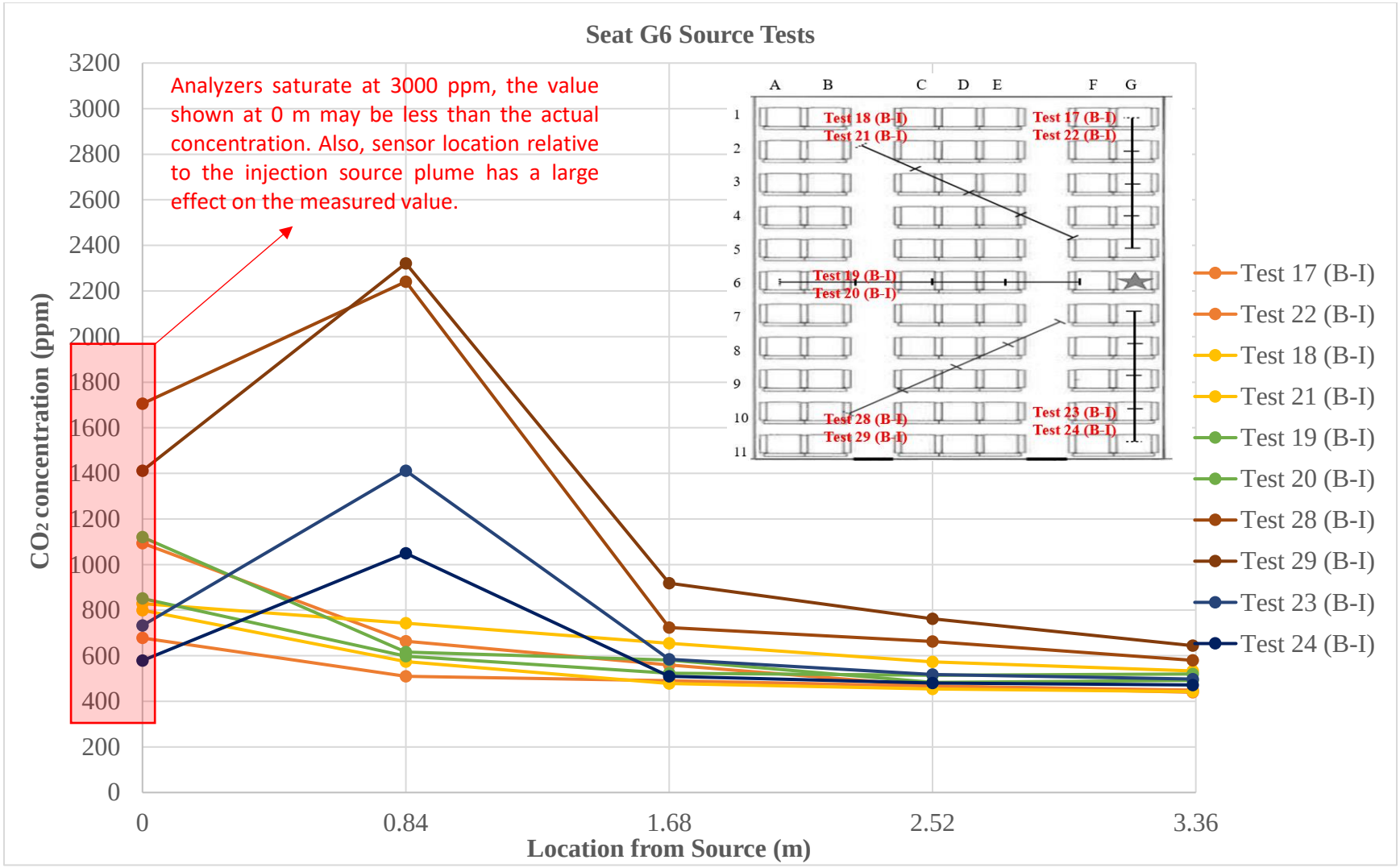

Figure C.129 Seat G6 continuous injection source tests in the Boeing 767 cabin mockup with the ISOPass undeployed.

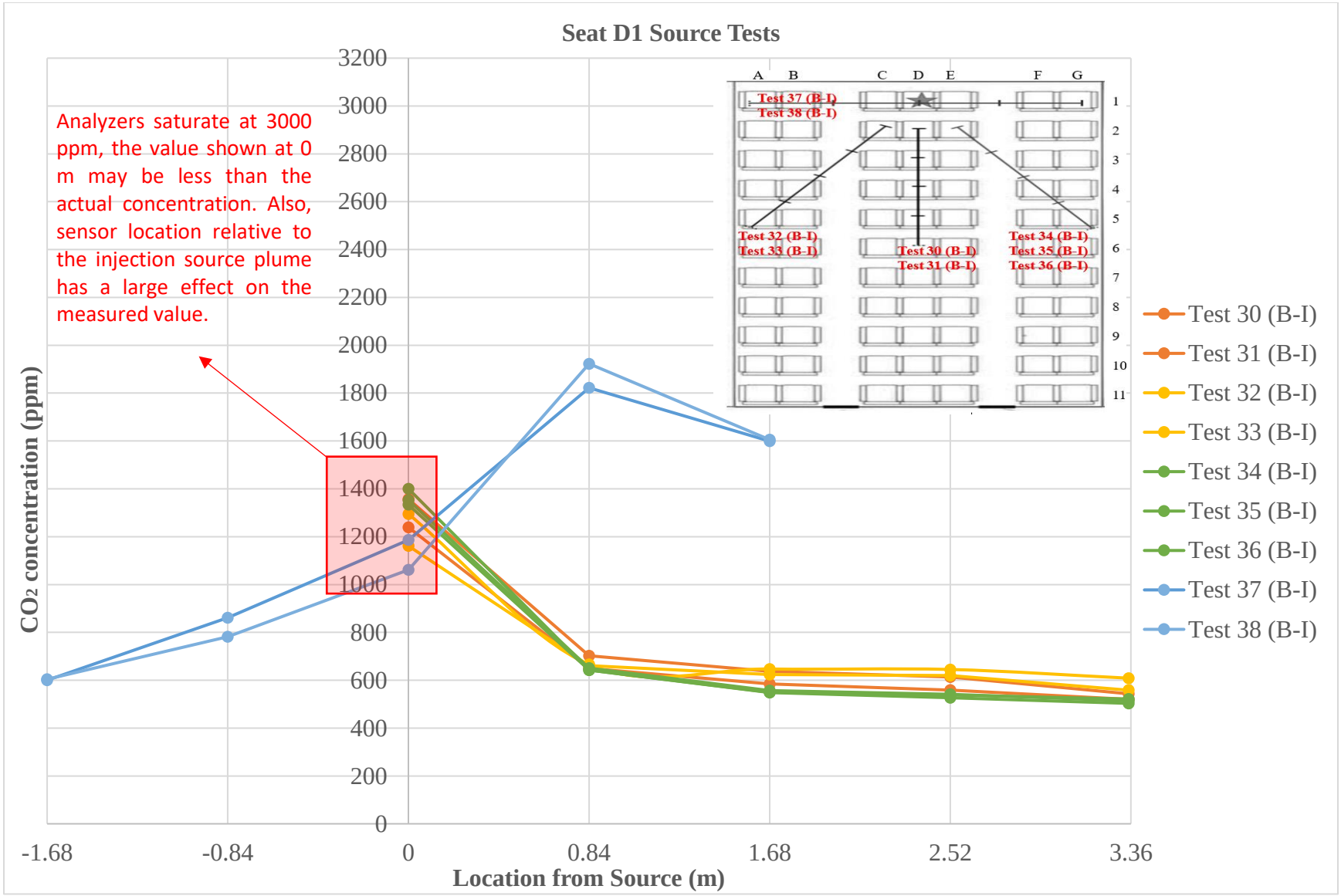

Figure C.130 Seat D1 continuous injection source tests in the Boeing 767 cabin mockup with the ISOPass undeployed.

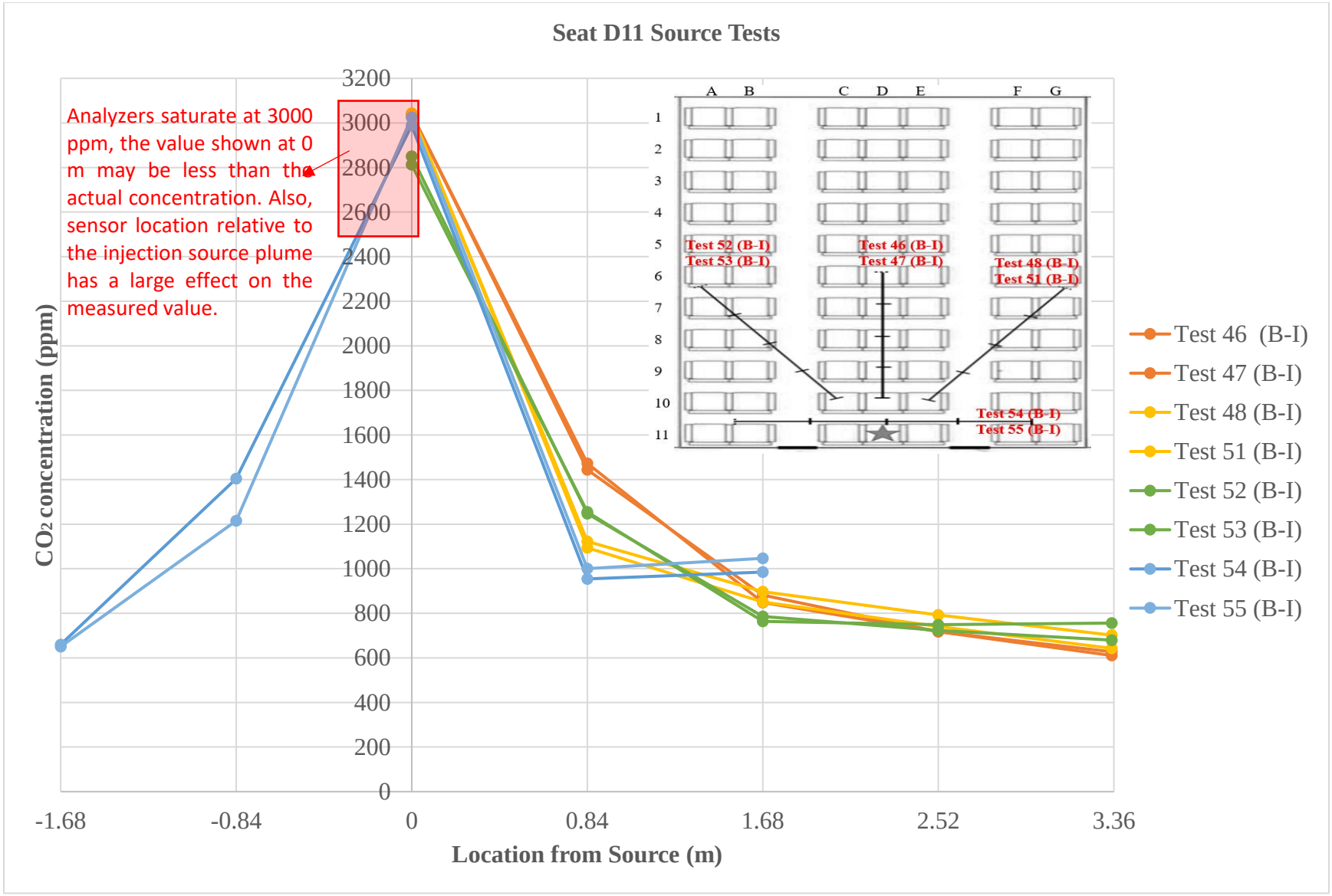

Figure C.131 Seat D11 continuous injection source tests in the Boeing 767 cabin mockup with the ISOPass undeployed.

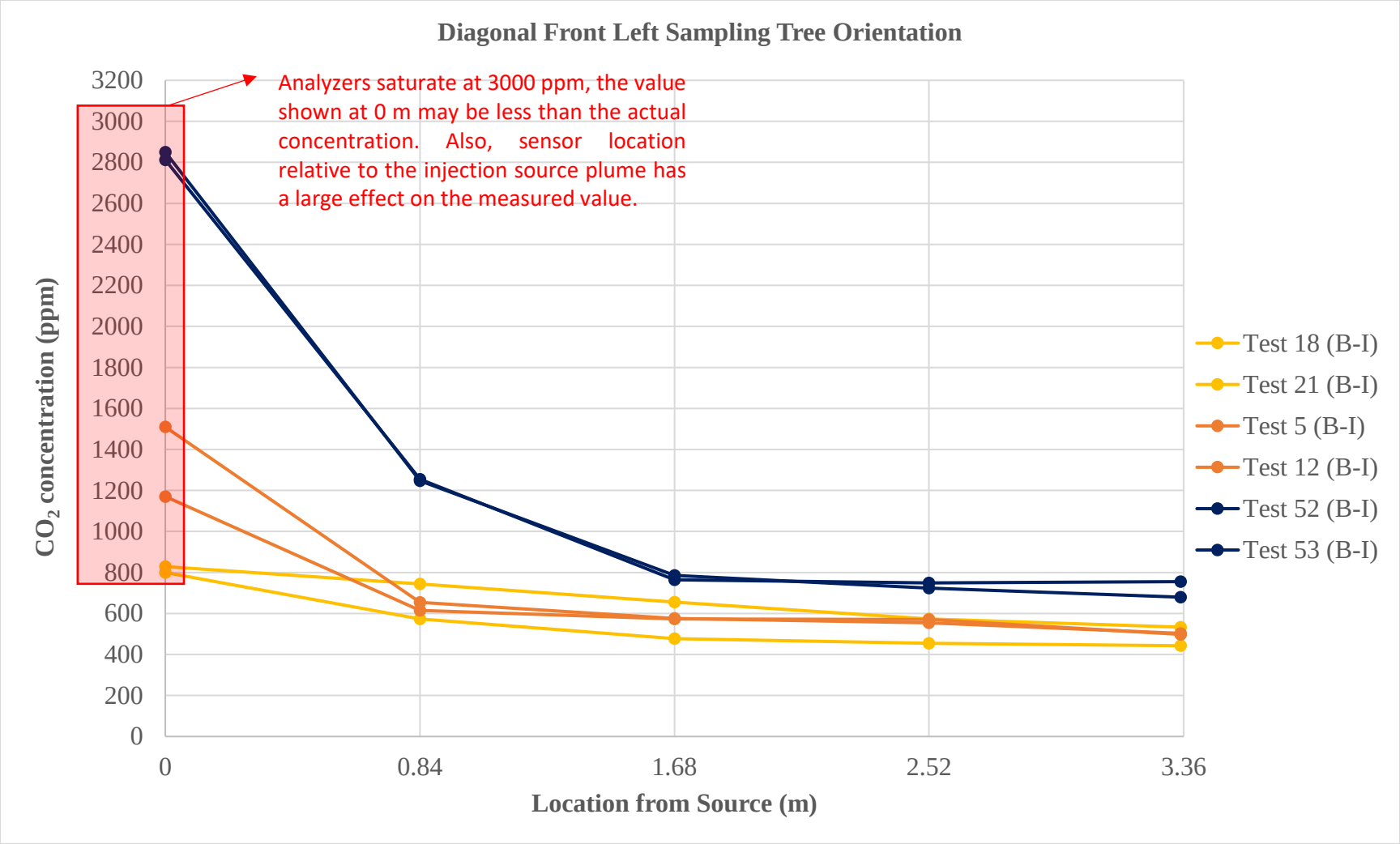

Figure C.132 Diagonal front left sampling tree orientation tests in the Boeing 767 cabin mockup with the ISOPass undeployed.

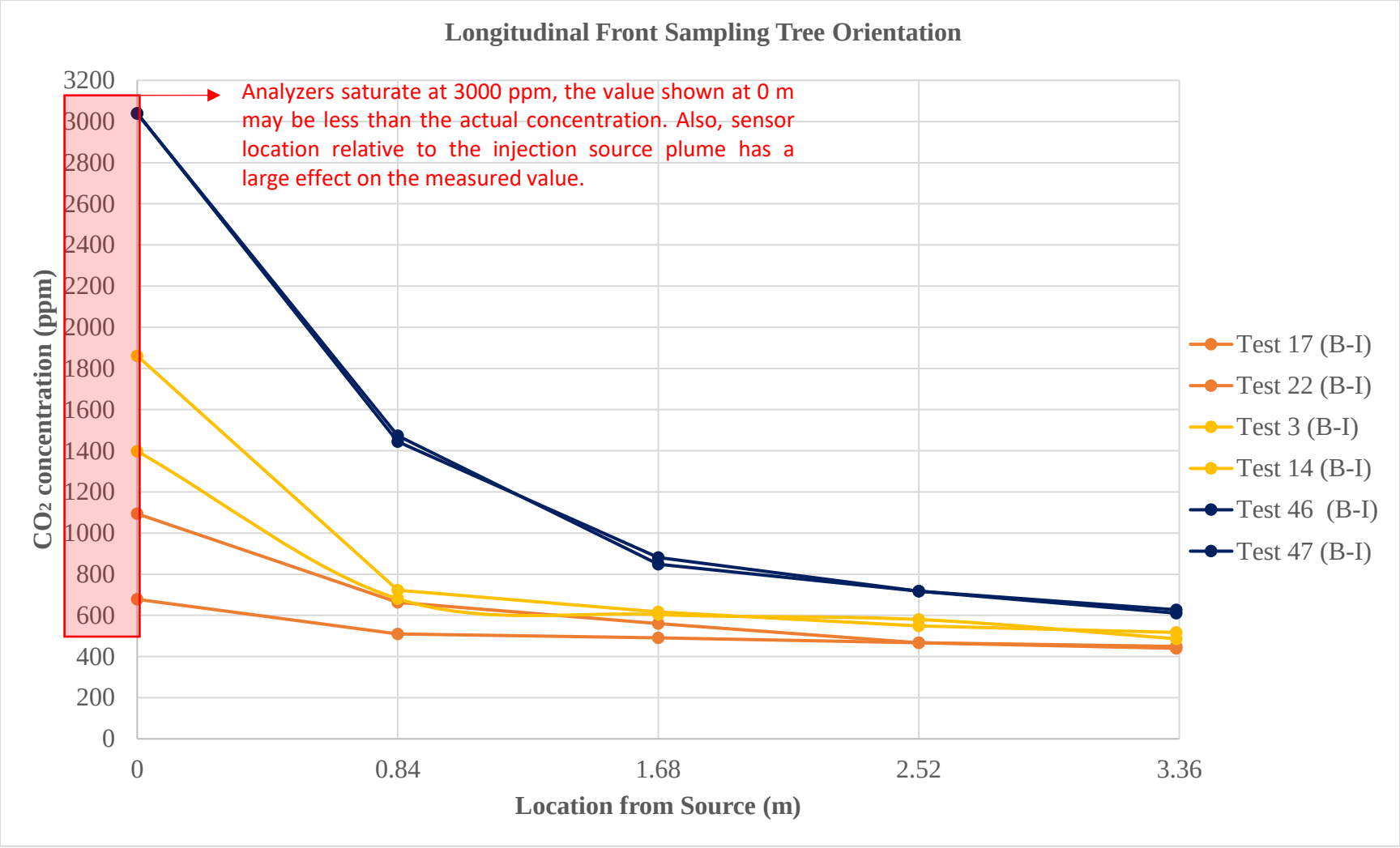

Figure C.133 Longitudinal front sampling tree orientation tests in the Boeing 767 cabin mockup with the ISOPass undeployed.

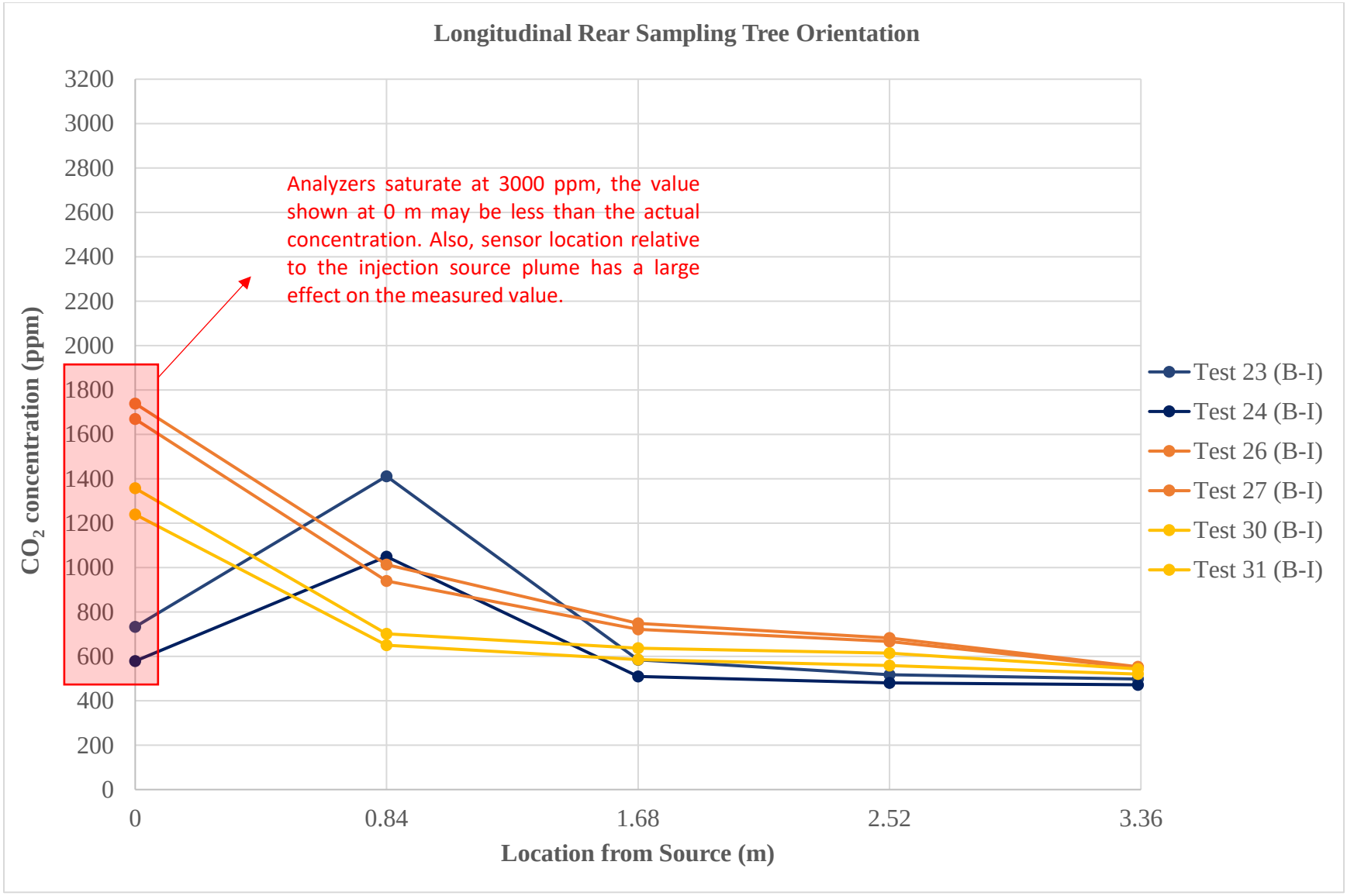

Figure C.134 Longitudinal rear sampling tree orientation tests in the Boeing 767 cabin mockup with the ISOPass undeployed.

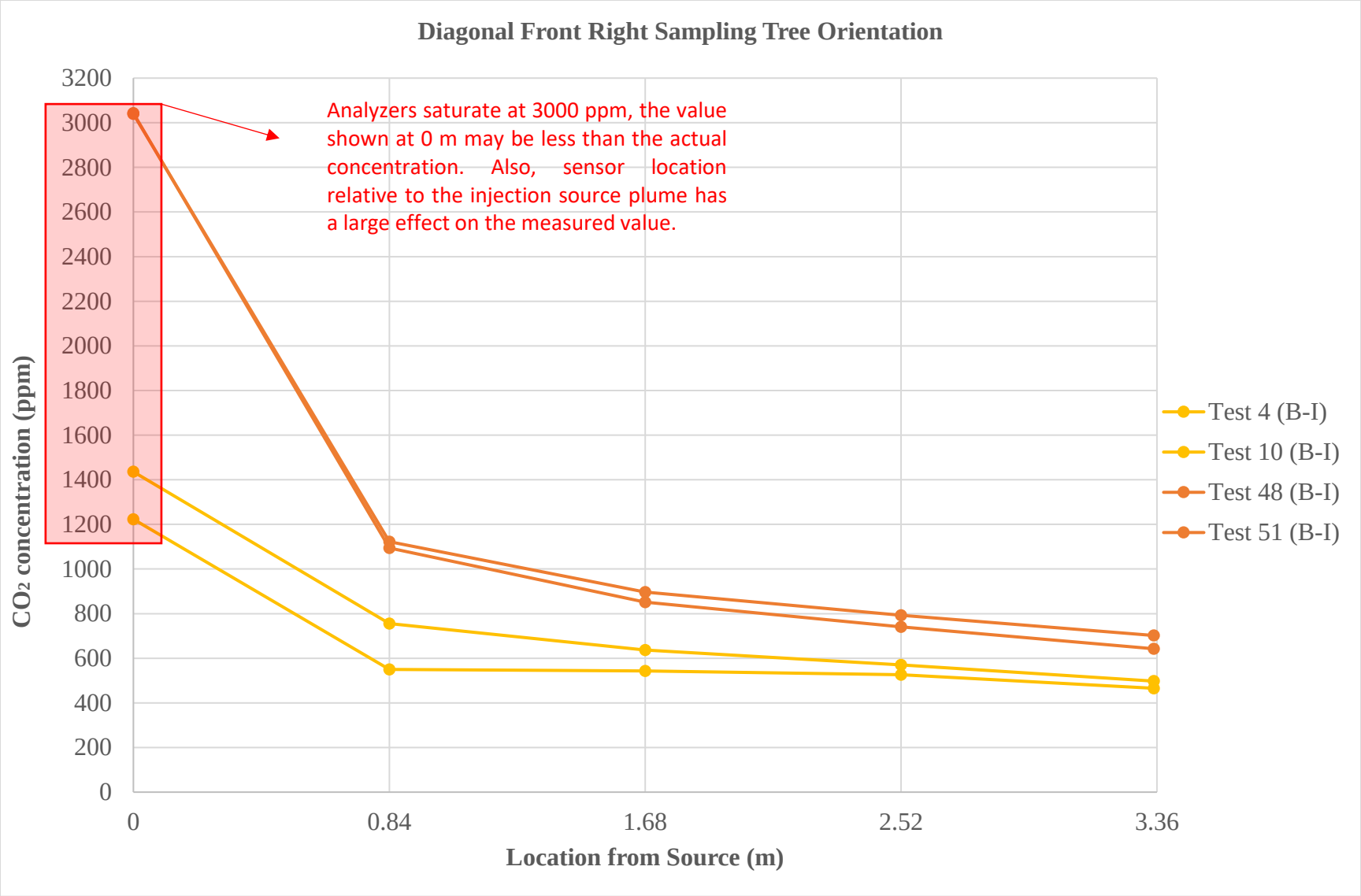

Figure C.135 Diagonal front right sampling tree orientation tests in the Boeing 767 cabin mockup with the ISOPass undeployed.

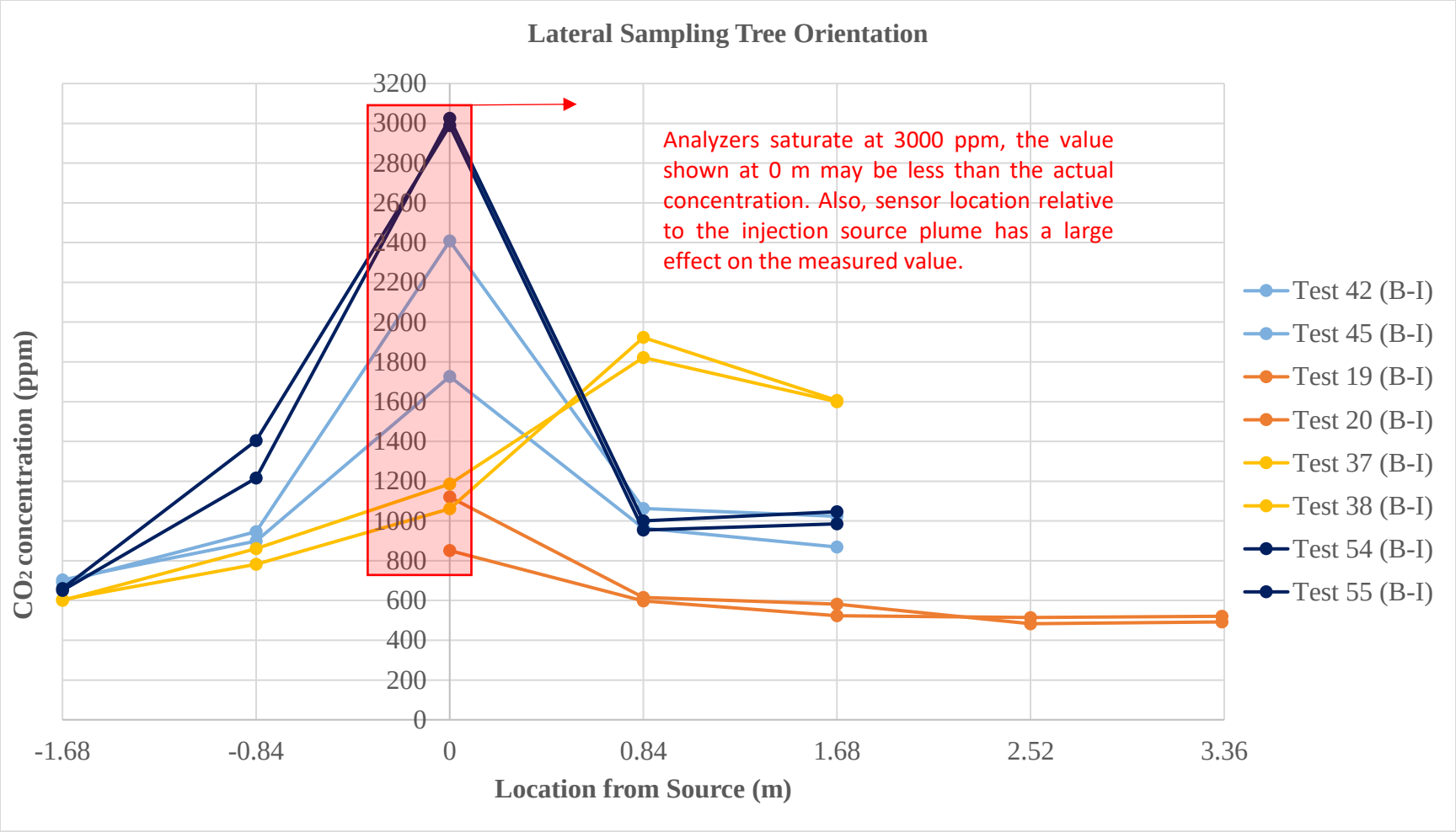

Figure C.136 Lateral sampling tree orientation tests in the Boeing 767 cabin mockup with the ISOPass undeployed.

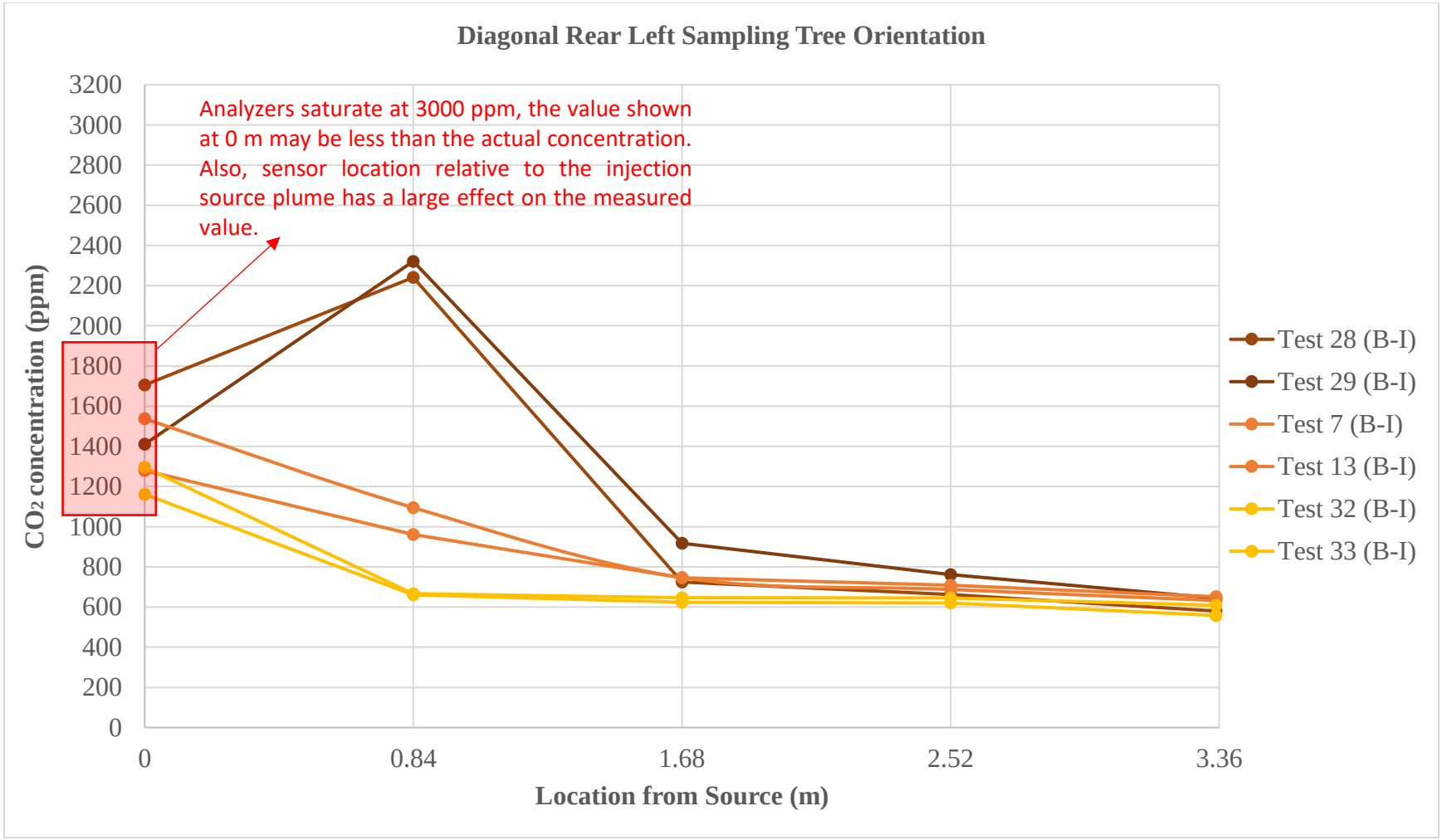

Figure C.137 Diagonal rear left sampling tree orientation tests in the Boeing 767 cabin mockup with the ISOPass undeployed.

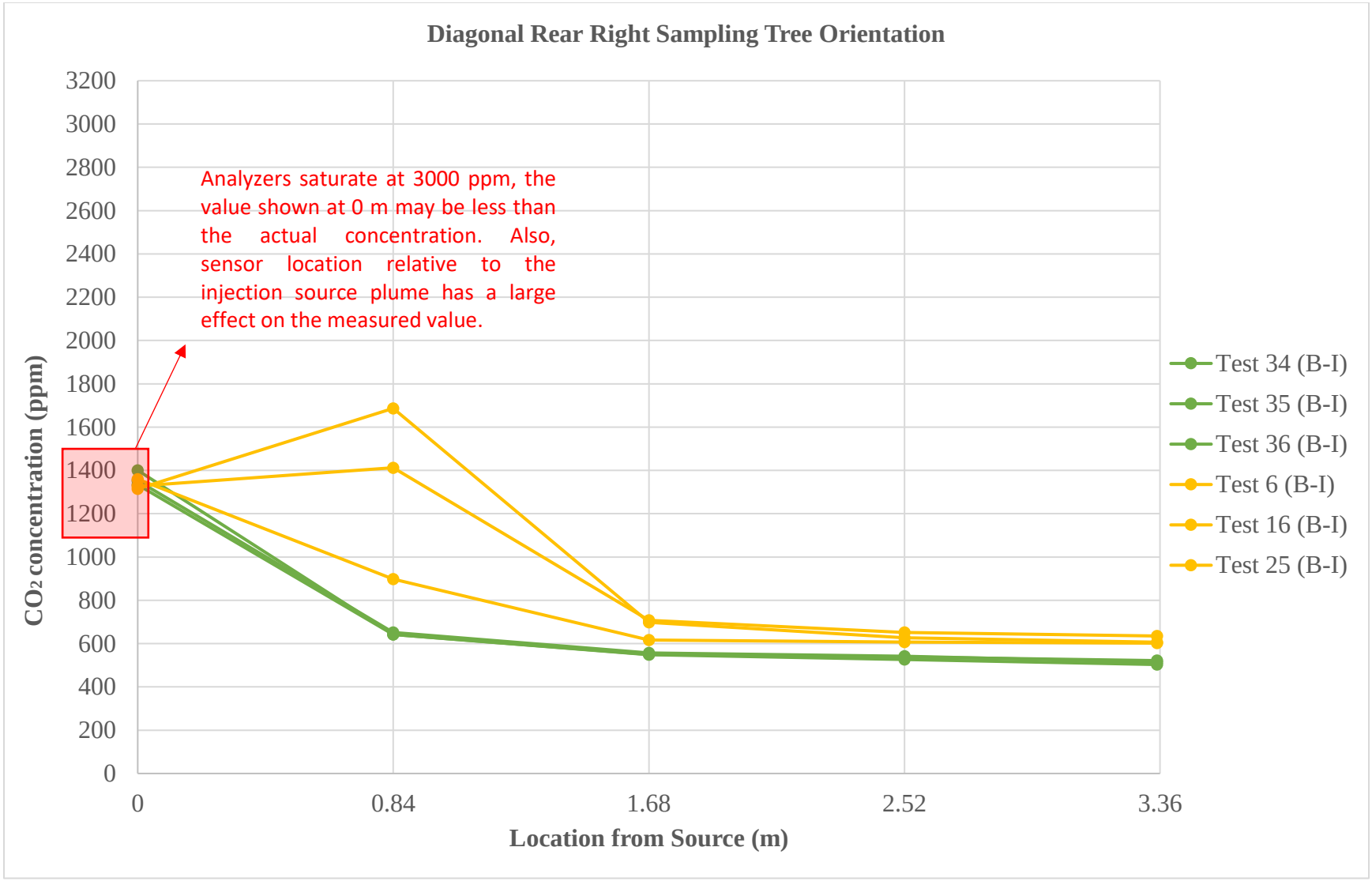

Figure C.138 Diagonal rear right sampling tree orientation tests in the Boeing 767 cabin mockup with the ISOPass undeployed.

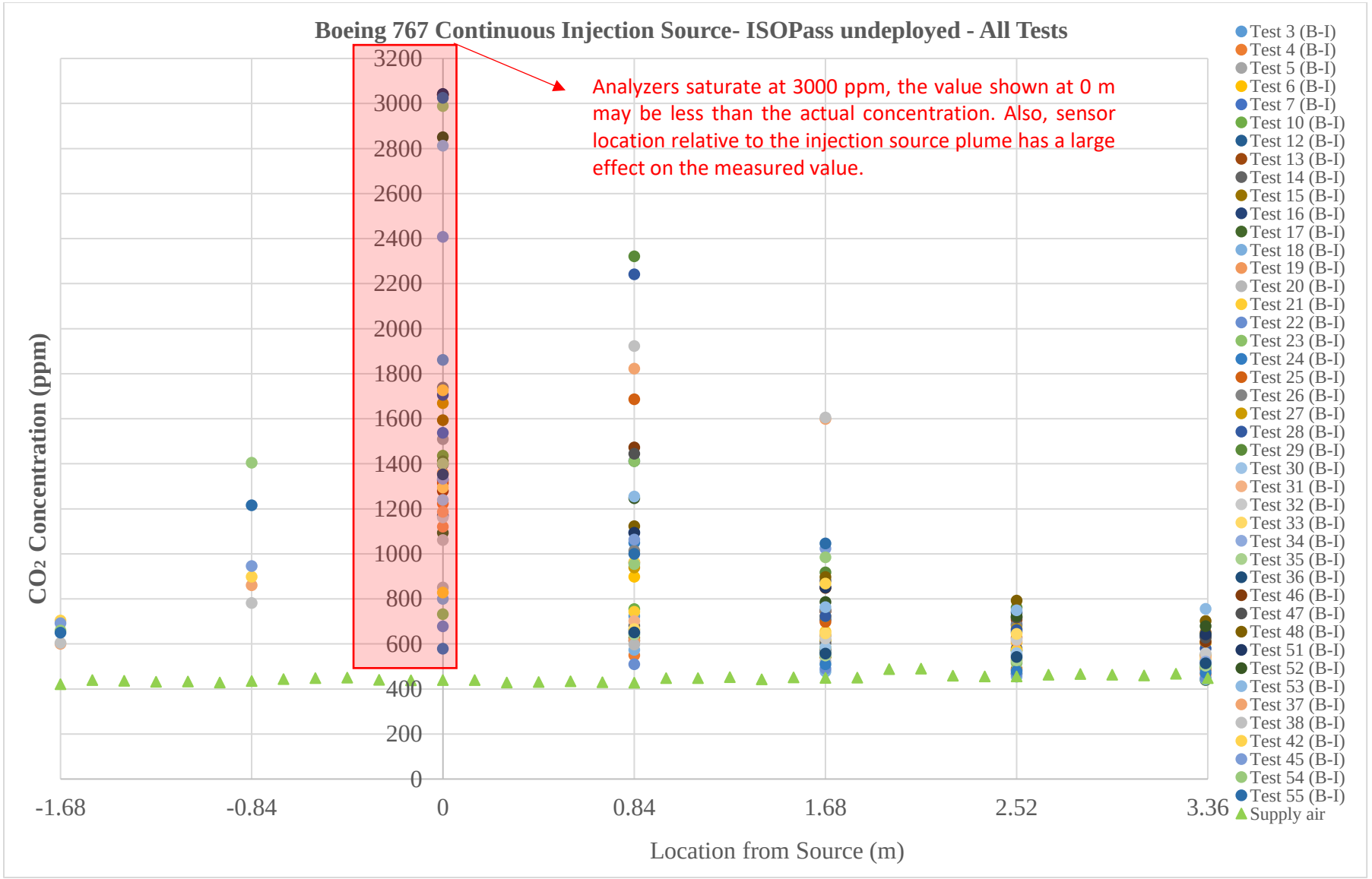

Figure C.139 Boeing 767 mockup cabin continuous injection source tests with the ISOPass undeployed.

Figure C.140 Boeing 767 mockup cabin continuous injection source tests with the ISOPass undeployed, Absolute distances from the source.

Appendix D - Boeing 767 ISOPass Deployed Continuous Injection Results

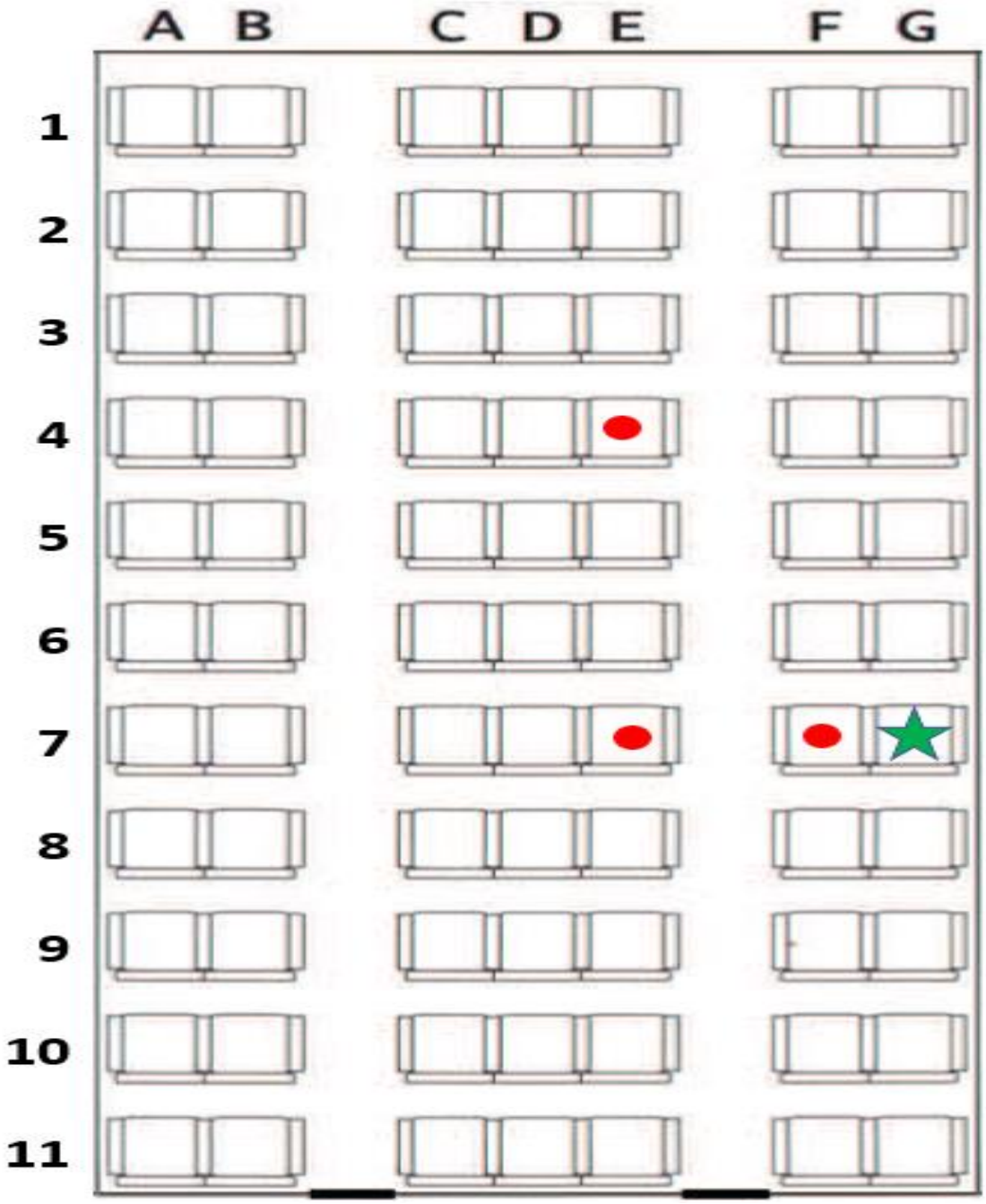

Figure D.1 Test 1 (B-I) ISOPass deployed source location and sampling tree orientation.

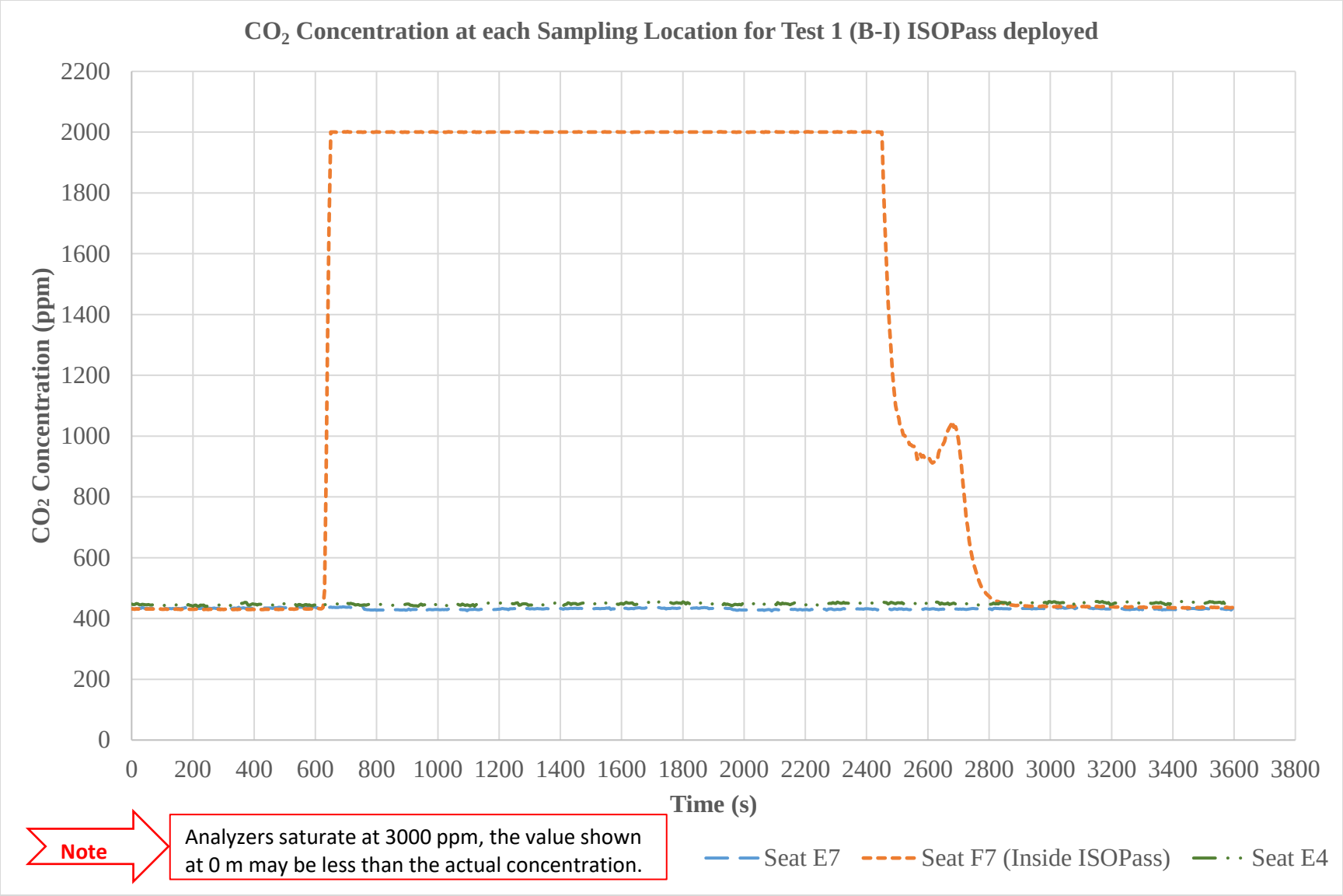

Figure D.2 Ininstantaneous CO_2 concentration at each sampling location for Test 1 (B-I) ISOPass deployed.

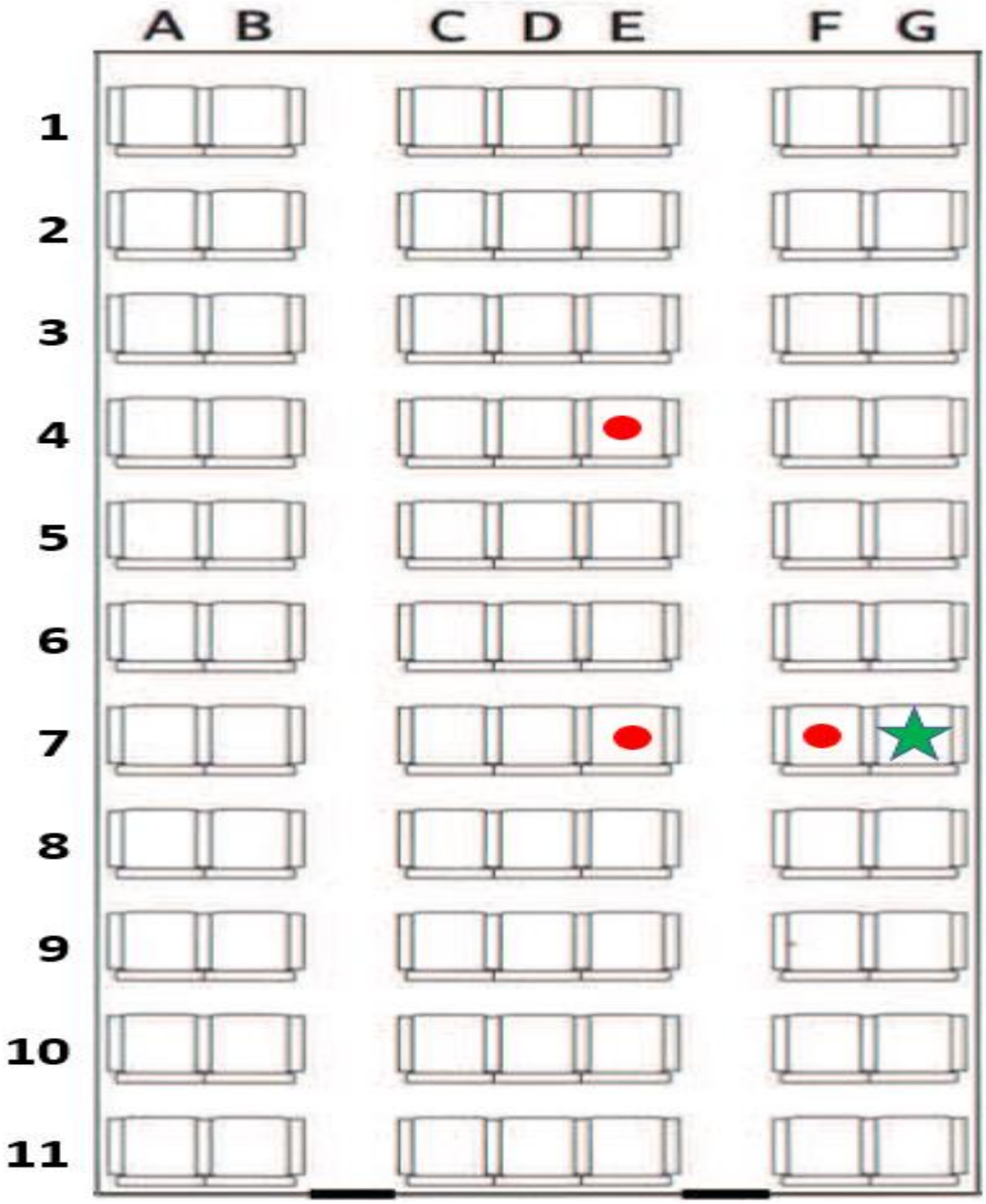

Figure D.3 Test 2 (B-I) ISOPass deployed source location and sampling tree orientation.

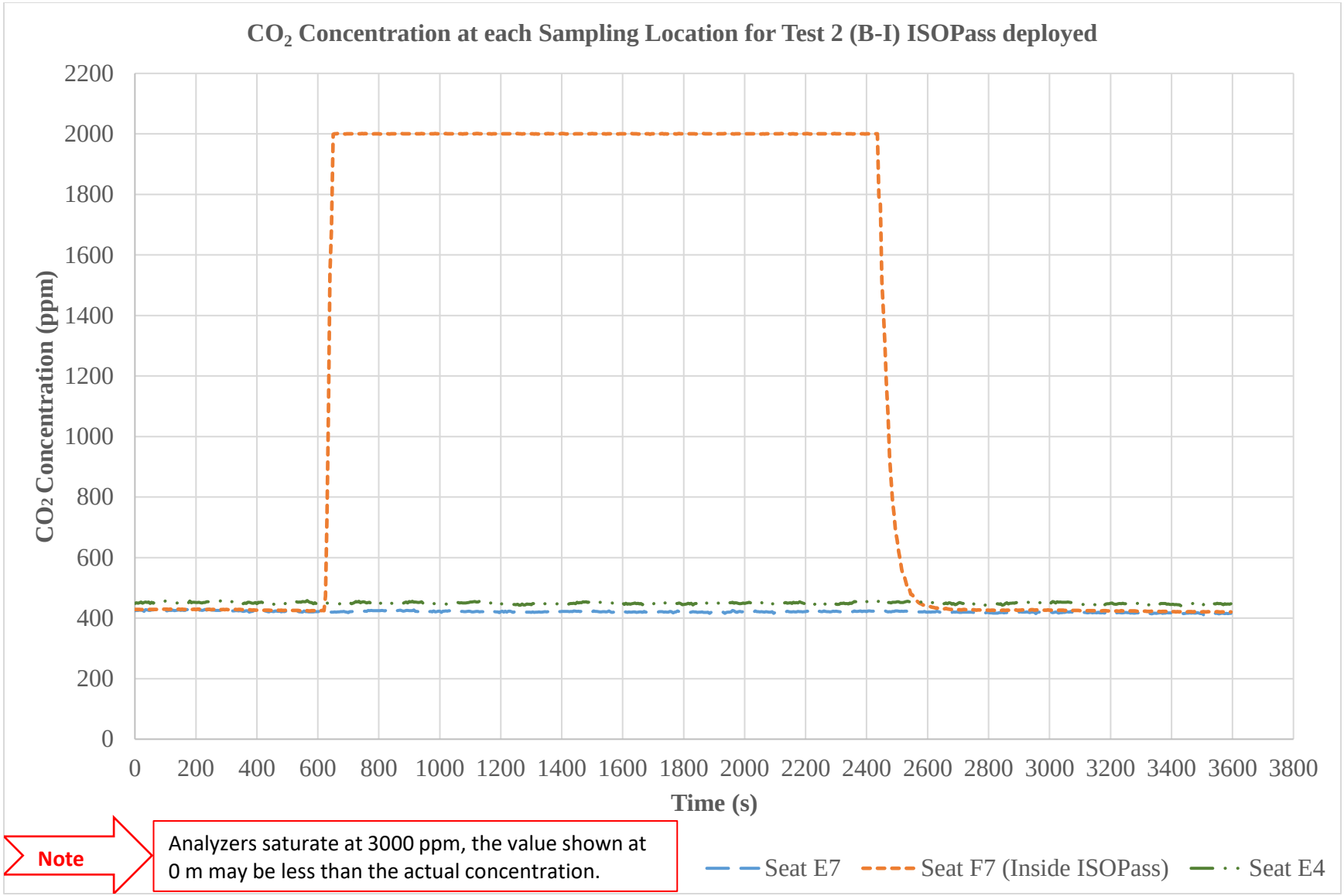

Figure D.4 Ininstantaneous CO_2 concentration at each sampling location for Test 2 (B-I) ISOPass deployed.

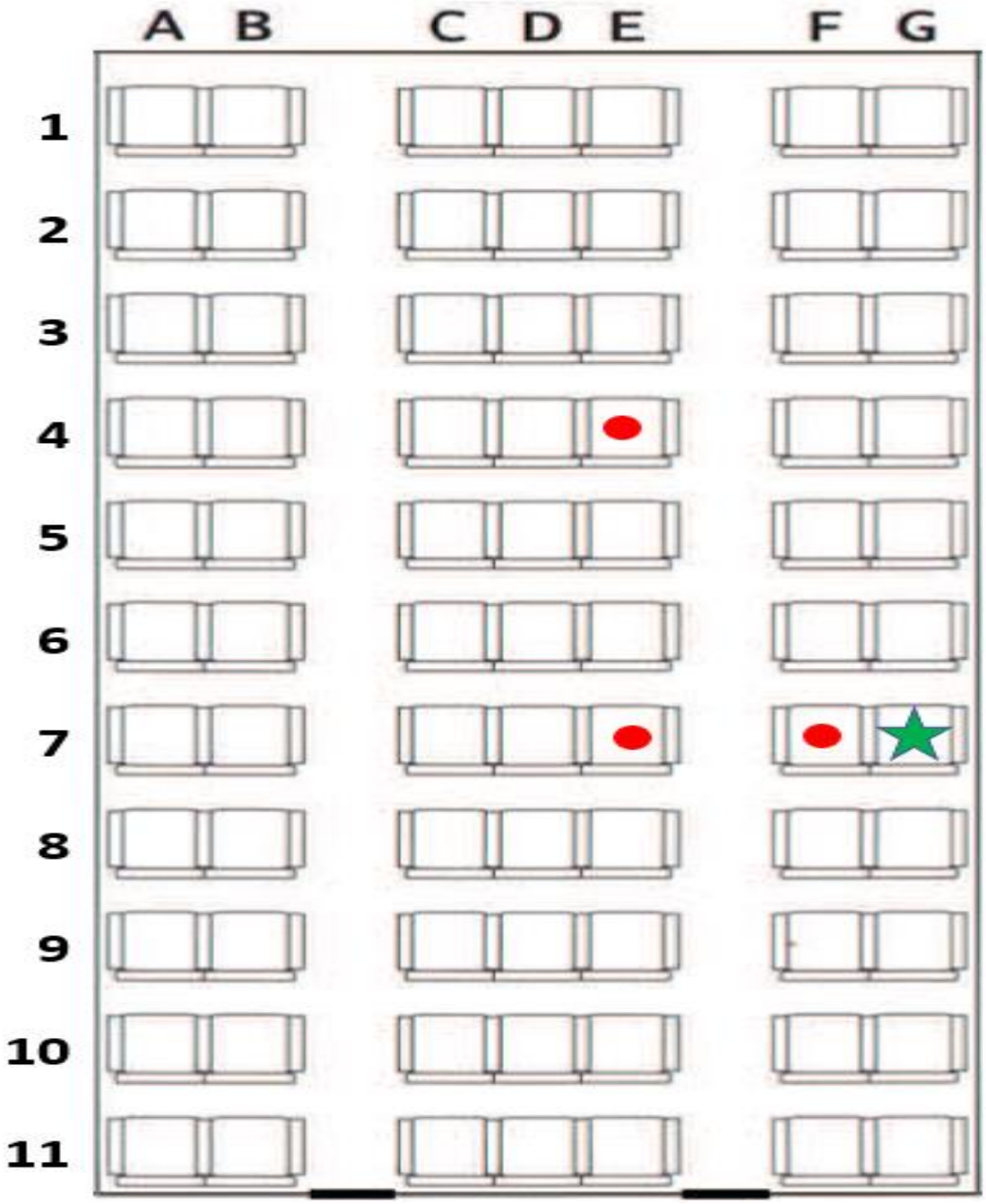

Figure D.5 Test 3 (B-I) ISOPass deployed source location and sampling tree orientation.

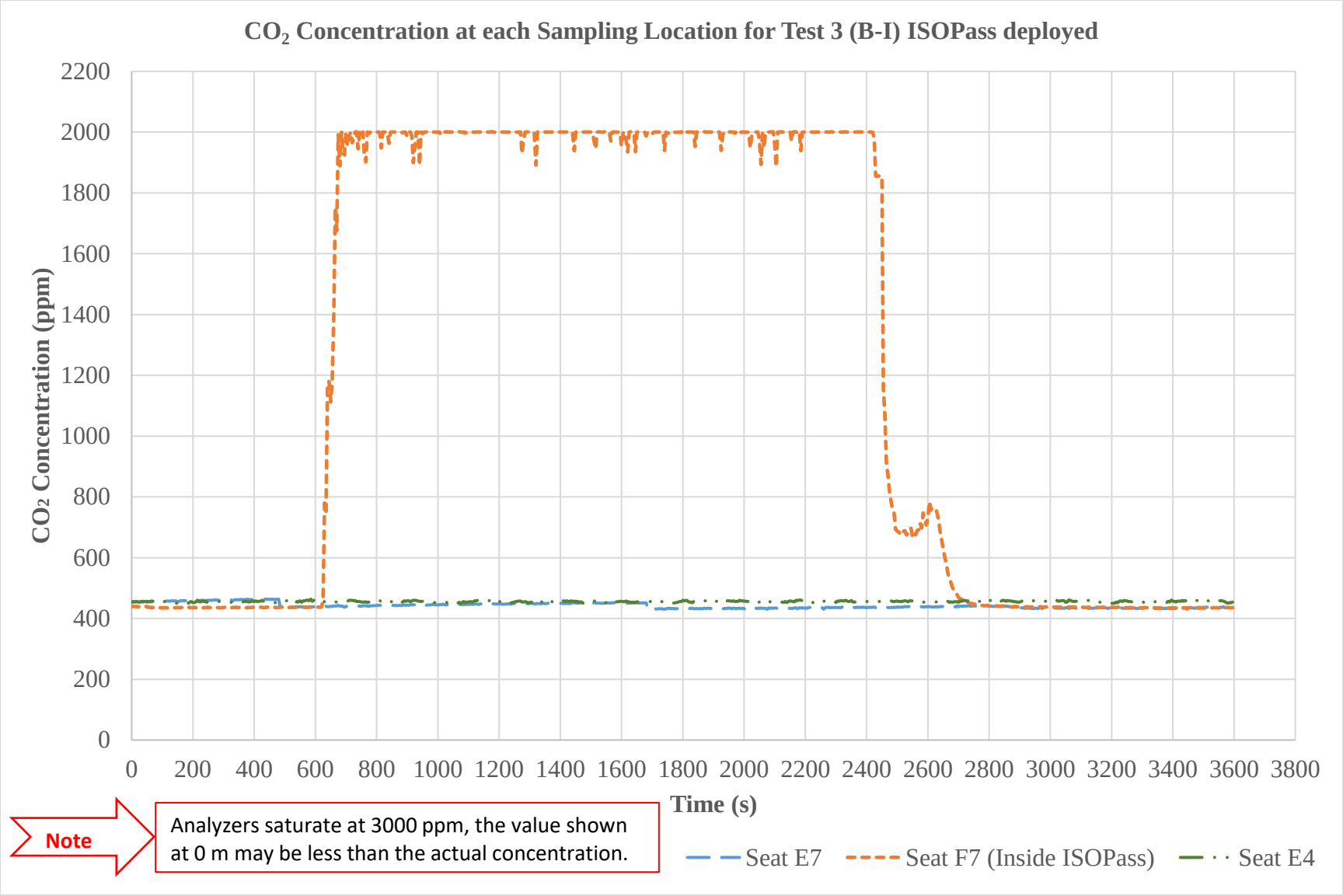

Figure D.6 Ininstantaneous CO_2 concentration at each sampling location for Test 3 (B-I) ISOPass deployed.

Appendix E - Modified Cabin ISOPass Undeployed Continuous Injection Results

Notes about this appendix:

- The positive direction is the one pointing from the source to the sampling tree solenoid valves block in the tests conducted with a longitudinal or a diagonal sampling tree directions.
- The positive direction was taken as the right direction from the source in the tests performed with a lateral sampling tree direction similar to a typical coordinate system.
- The letter "A" after the test number indicates that the test was done in the modified mockup cabin and the letter "I" indicates that it was done using a continuous injection source.
- The sampling tree is a metal rod that has 4 ports controlled by solenoid valves. The measurements are collected sequentially from each of the ports. The tree is connected to a single gas analyzer to measure the concentration of the tracer gas from the opened port.
- The solenoid valves block is marked by a dashed line crossing the sampling tree.
- In addition to the sampling tree, additional tracer gas analyzers are placed in the cabin to collect measurements at the cabin supply air, injection source seat, and other locations of interest.
- The tracer gas analyzers are not of the same model or calibration and hence, the accuracy of the readings is not identical. For the tracer gas measurements accuracy, refer to chapter 4.4. Uncertainty Analysis of this dissertation.

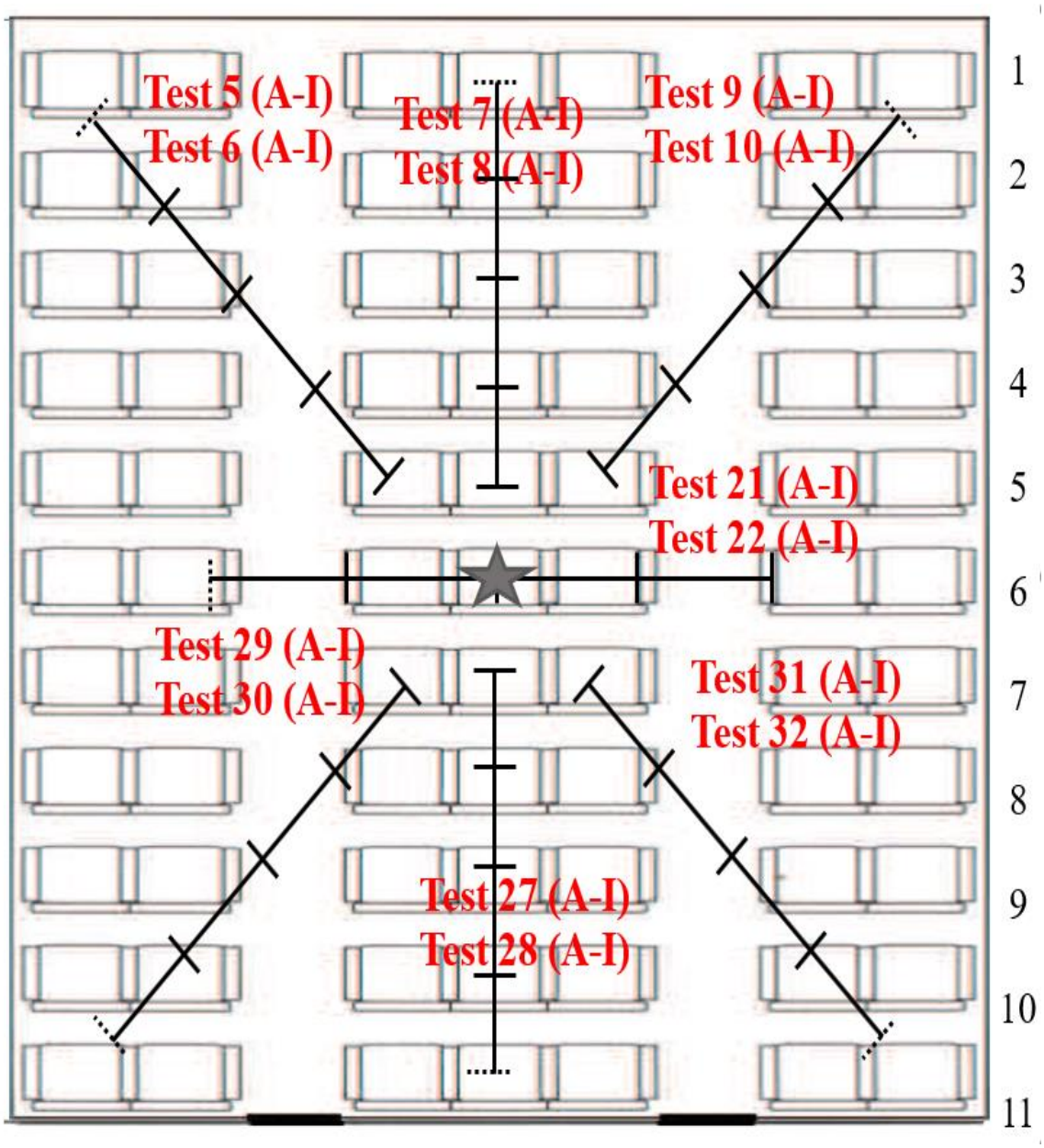

Figure E.1 Seat D6 ISOPass undeployed continuous injection tracer gas test numbers and sampling tree orientations in the modified cabin mockup.

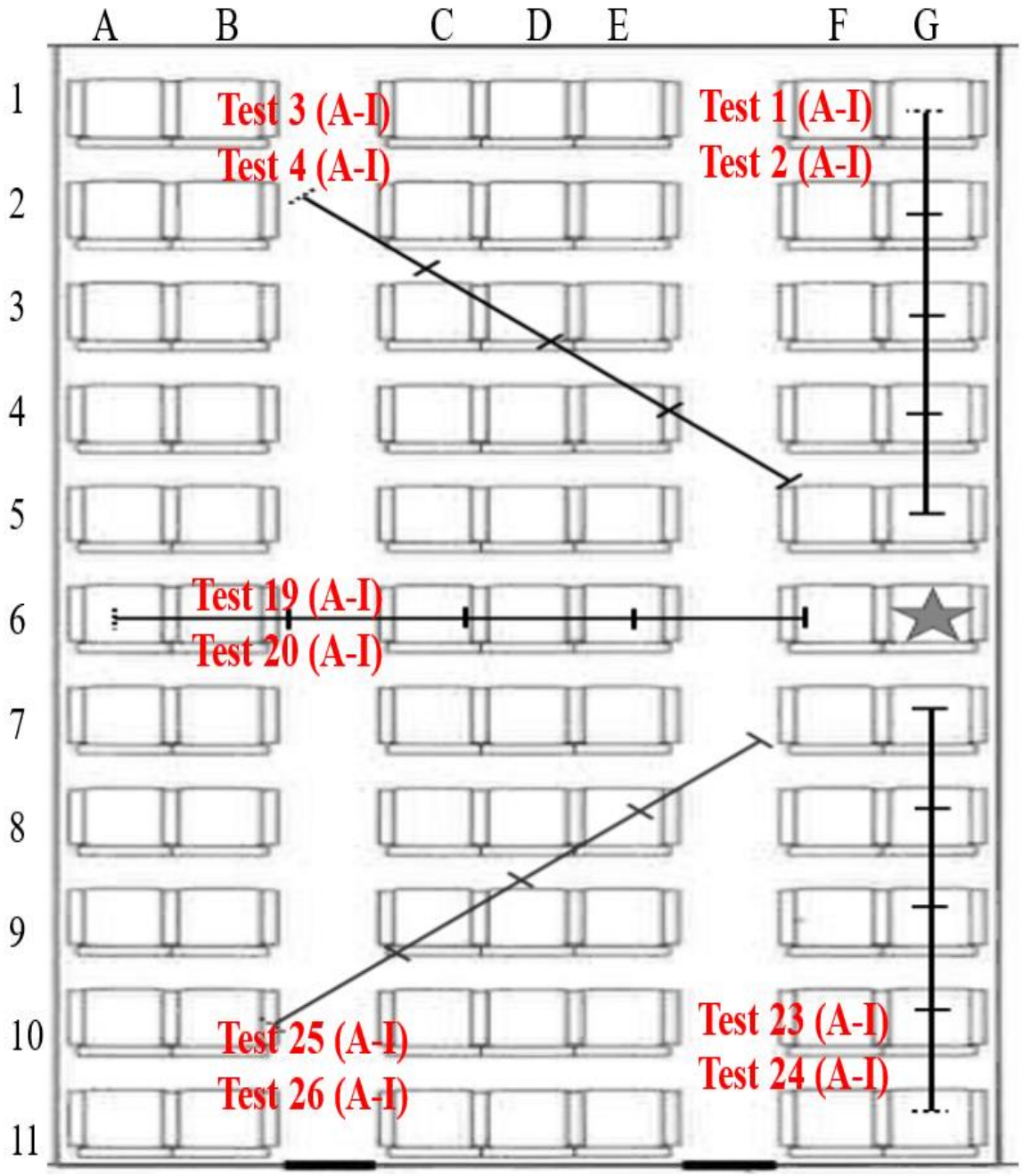

Figure E.2 Seat G6 ISOPass undeployed continuous injection tracer gas test numbers and sampling tree orientations in the modified cabin mockup.

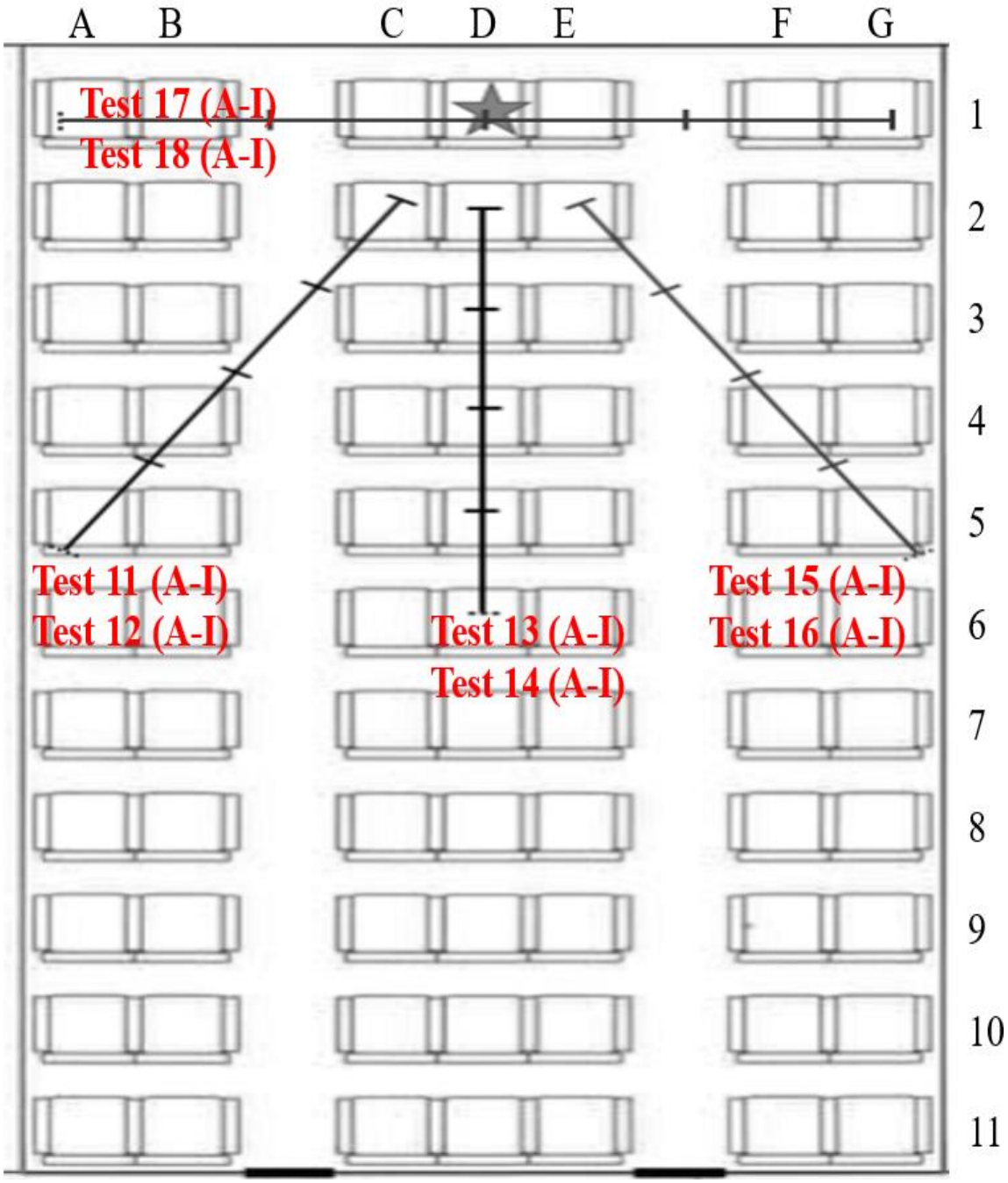

Figure E.3 Seat D1 ISOPass undeployed continuous injection tracer gas test numbers and sampling tree orientations in the modified cabin mockup.

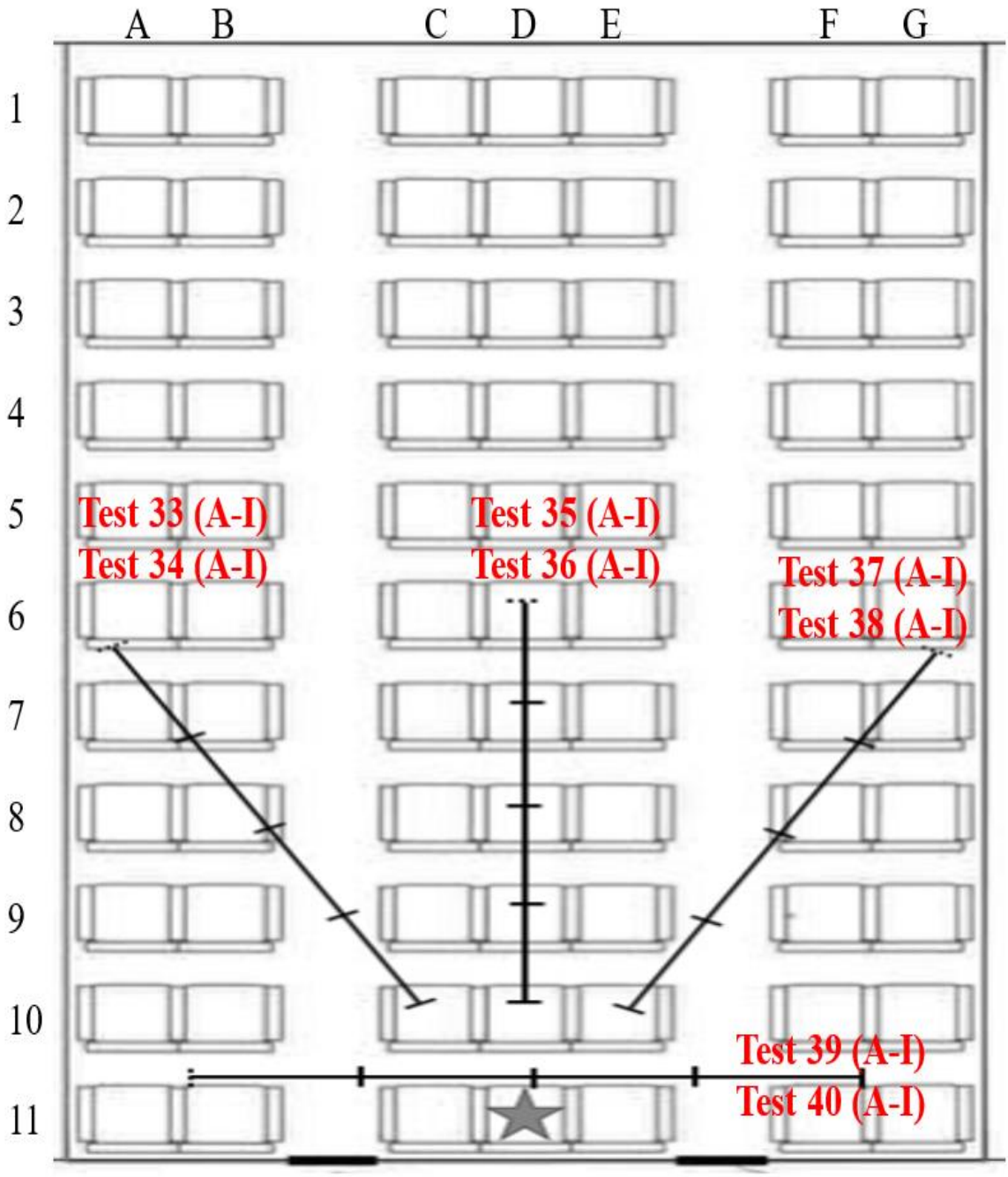

Figure E.4 Seat D11 ISOPass undeployed continuous injection tracer gas test numbers and sampling tree orientations in the modified cabin mockup.

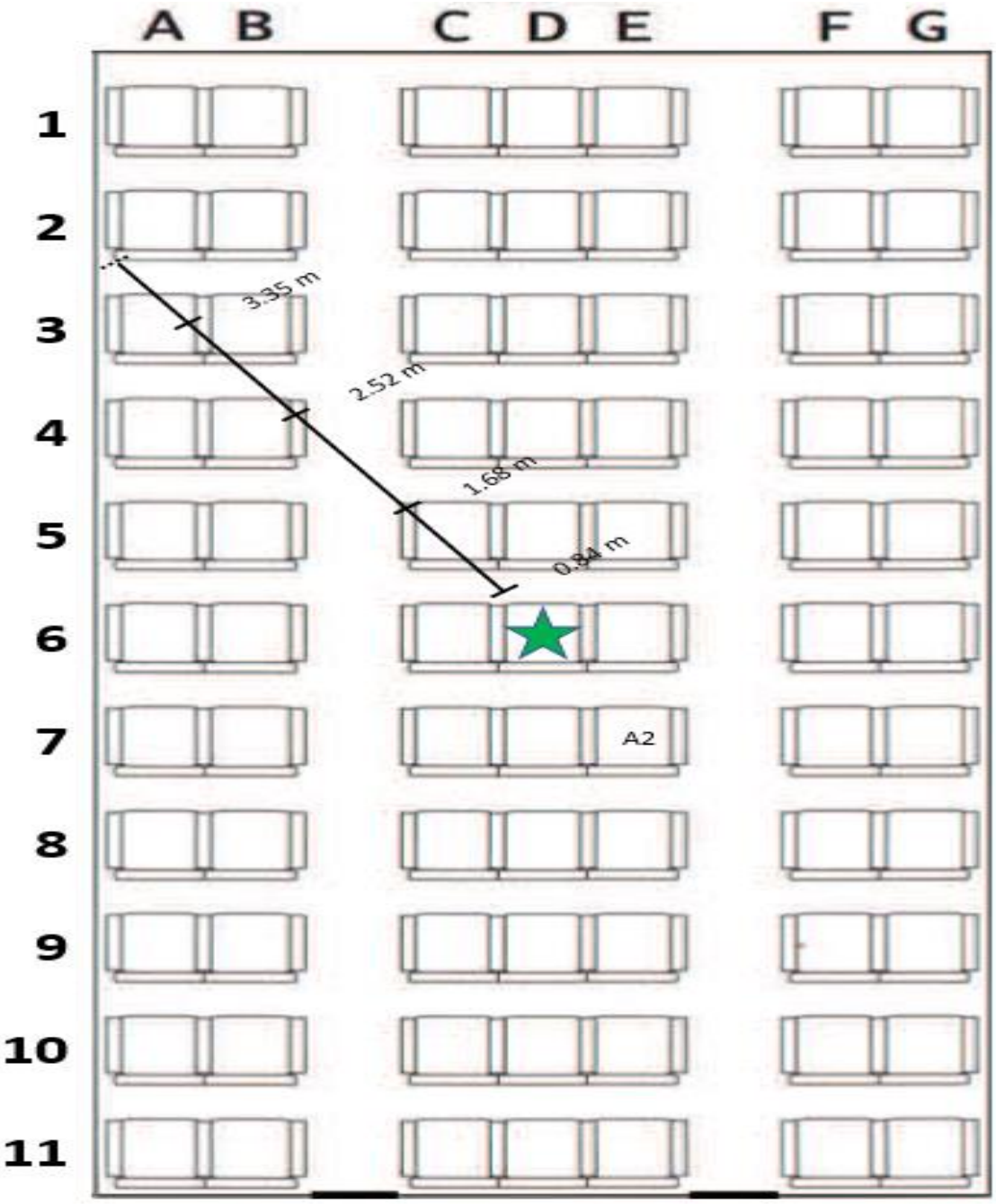

Figure E.5 Test 5 (A-I) ISOPass undeployed source location and sampling tree orientation.

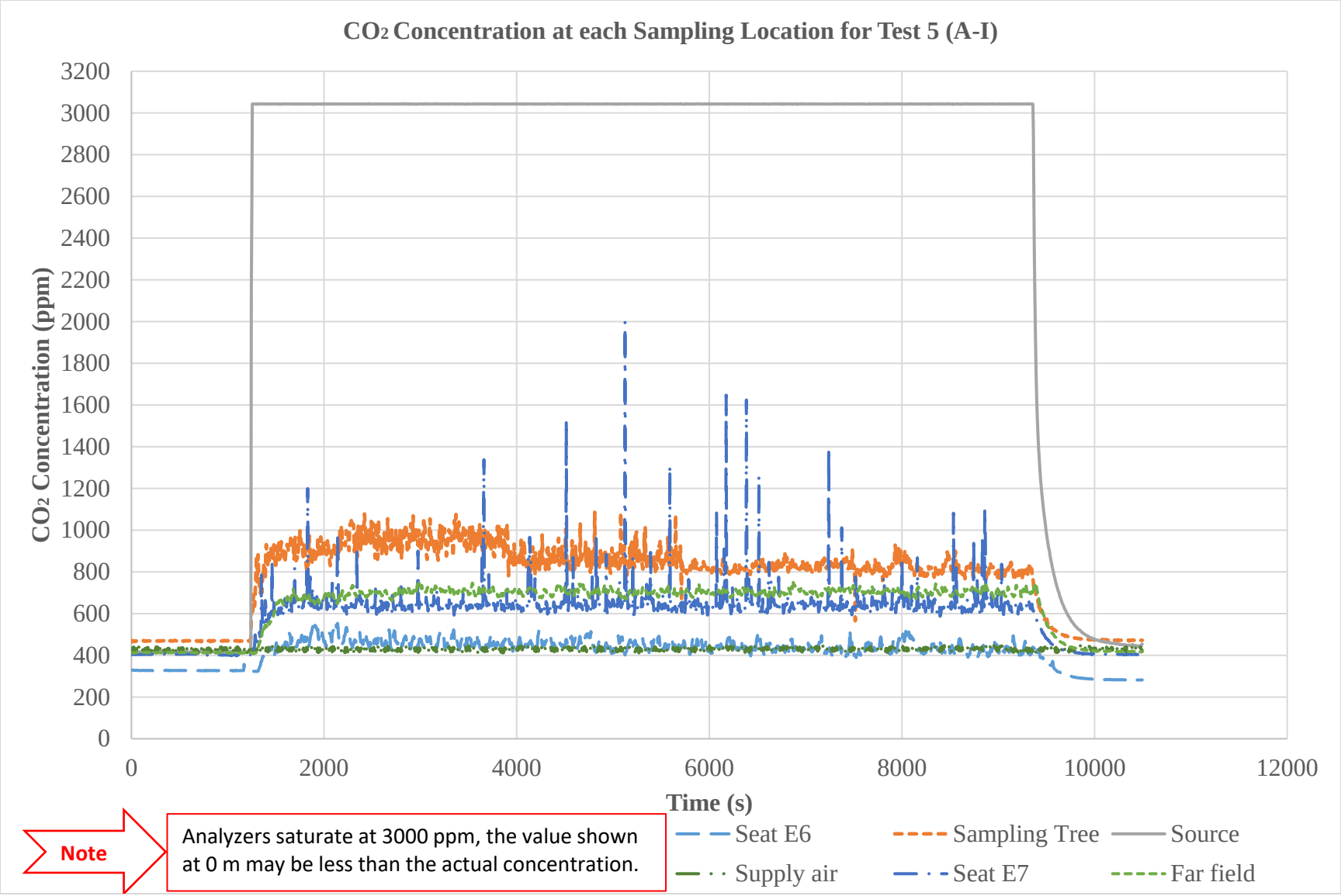

Figure E.6 Ininstantaneous CO_2 concentration at each sampling location for Test 5 (A-I) ISOPass undeployed.

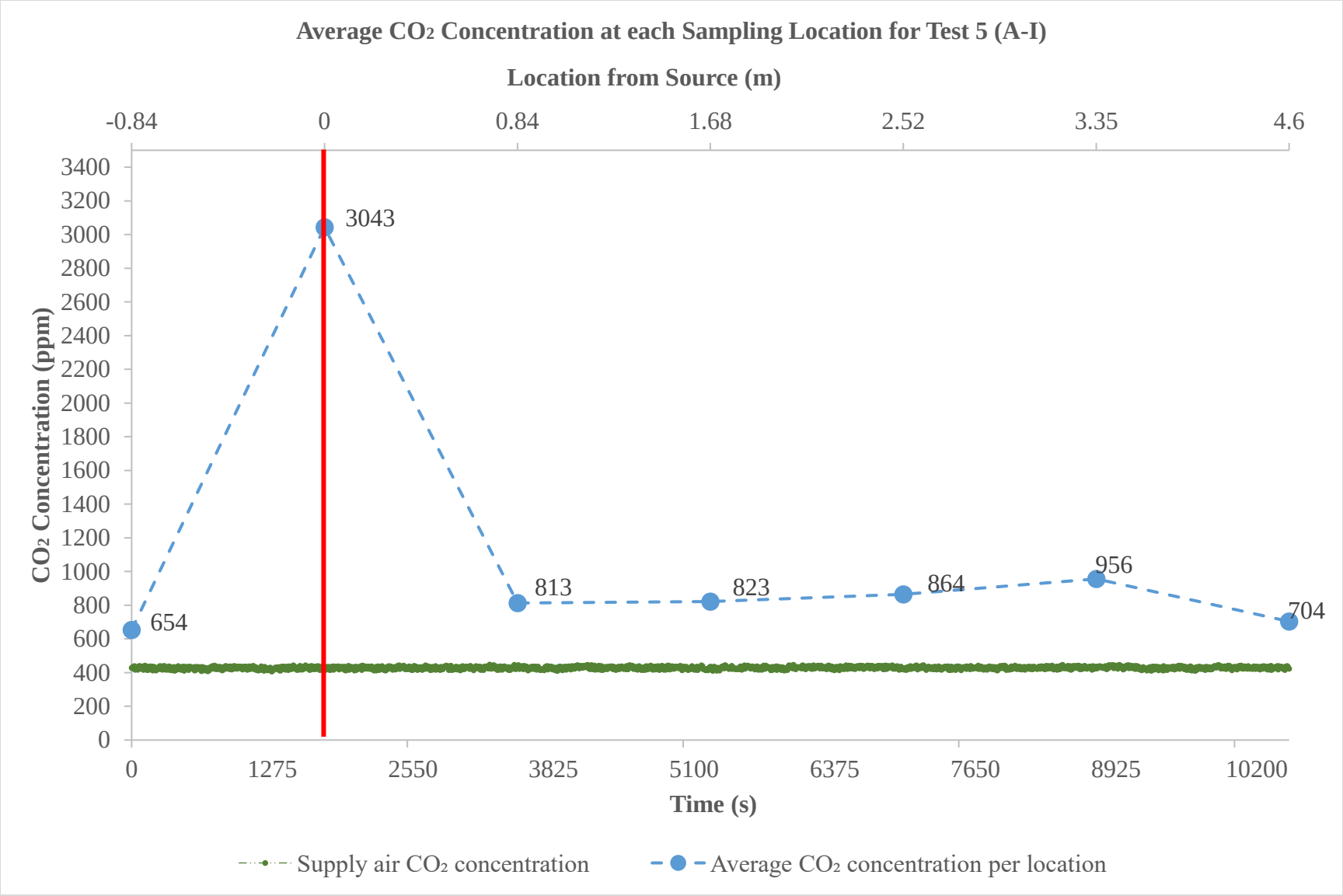

Figure E.7 Average CO_2 concentration at each sampling location for Test 5 (A-I) ISOPass undeployed.

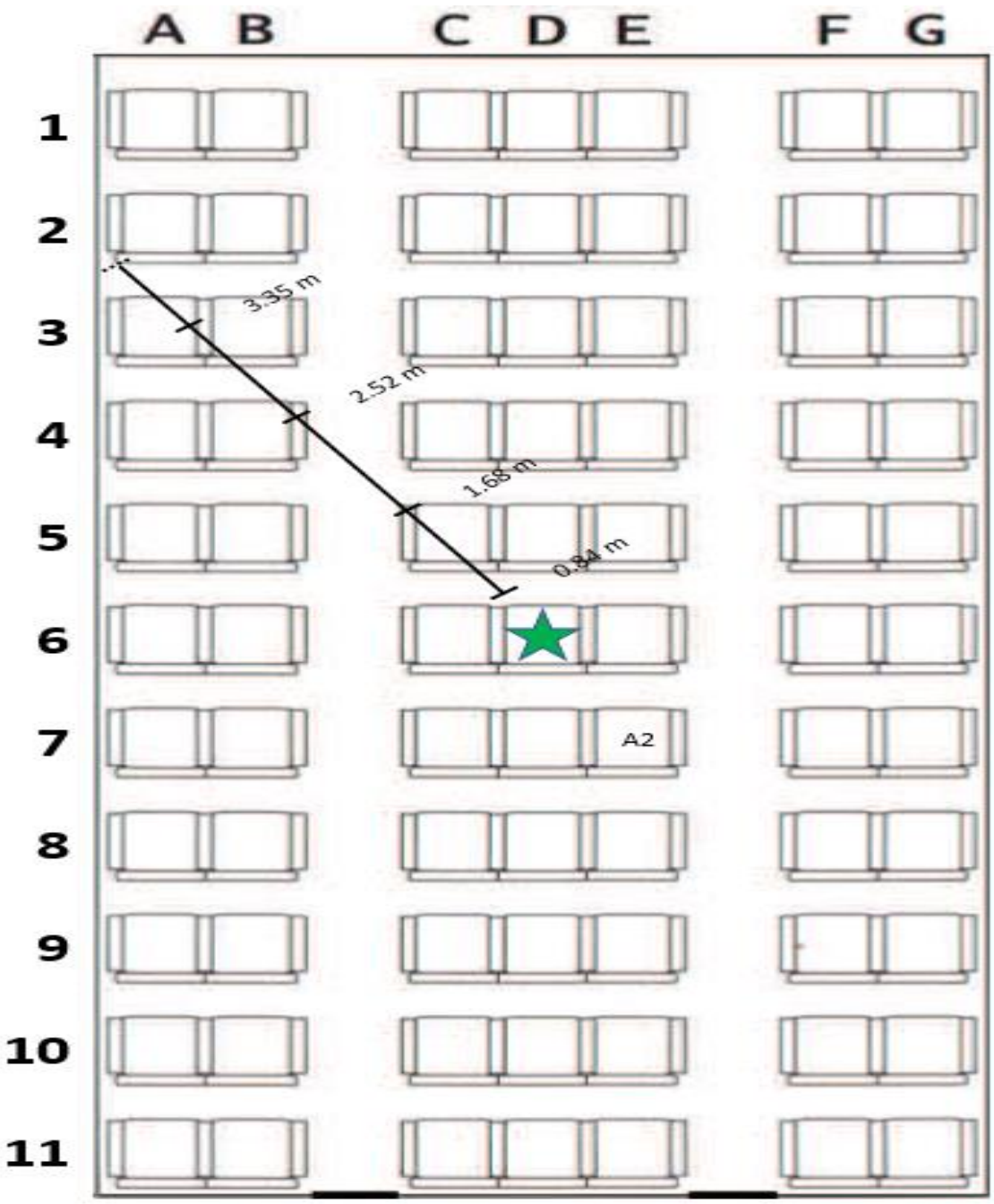

Figure E.8 Test 6 (A-I) ISOPass undeployed source location and sampling tree orientation.

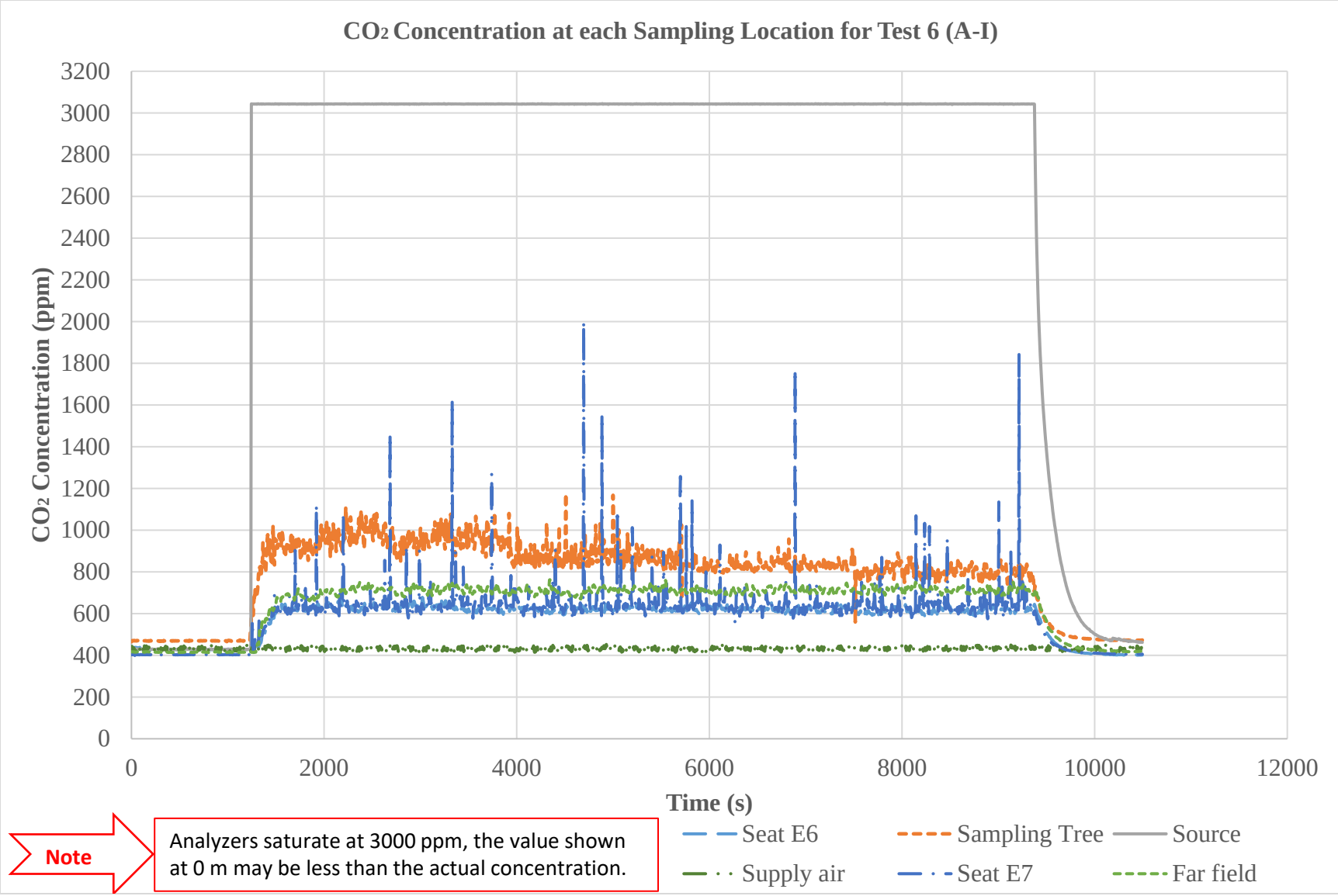

Figure E.9 Ininstantaneous CO_2 concentration at each sampling location for Test 6 (A-I) ISOPass undeployed.

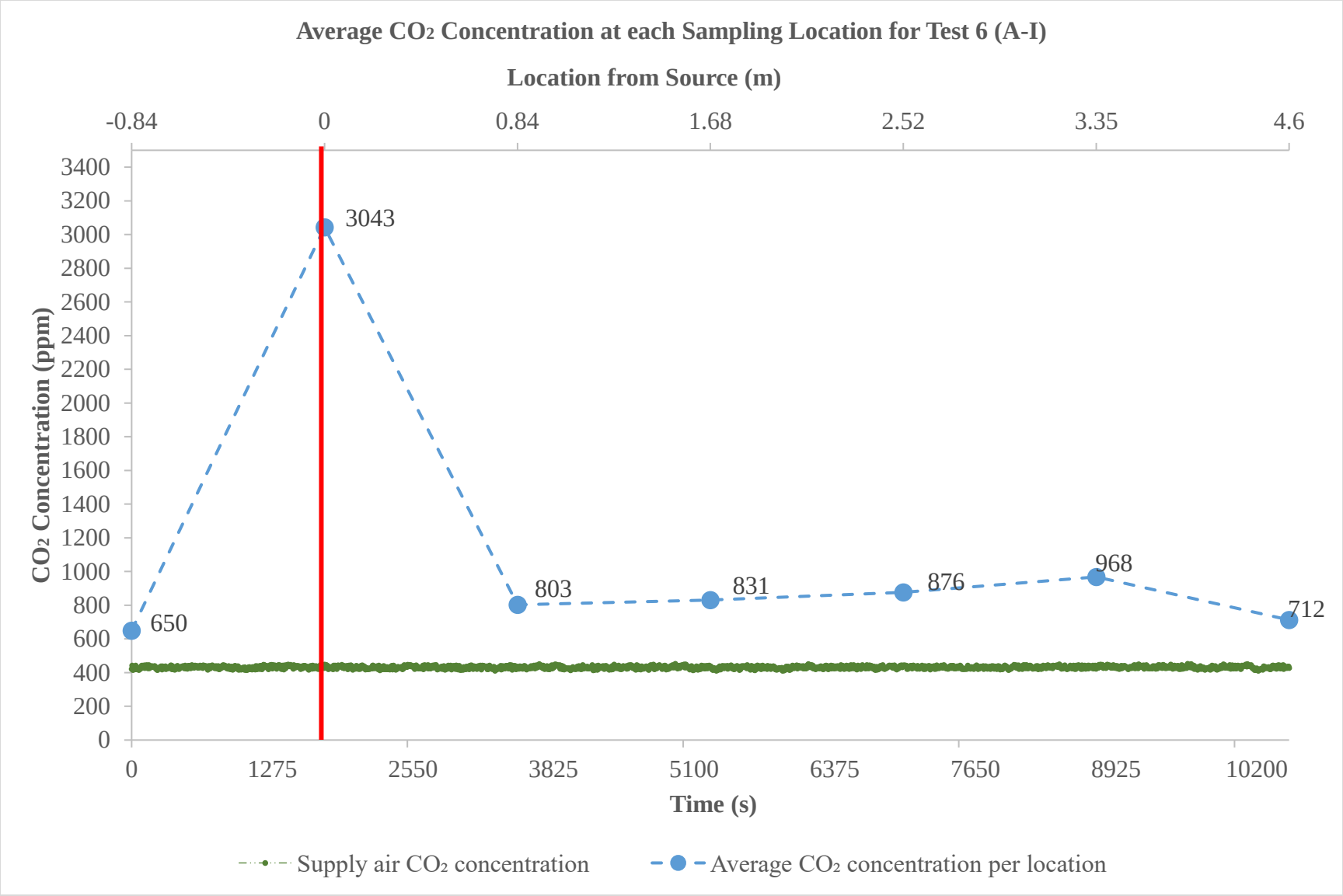

Figure E.10 Average CO_2 concentration at each sampling location for Test 6 (A-I) ISOPass undeployed.

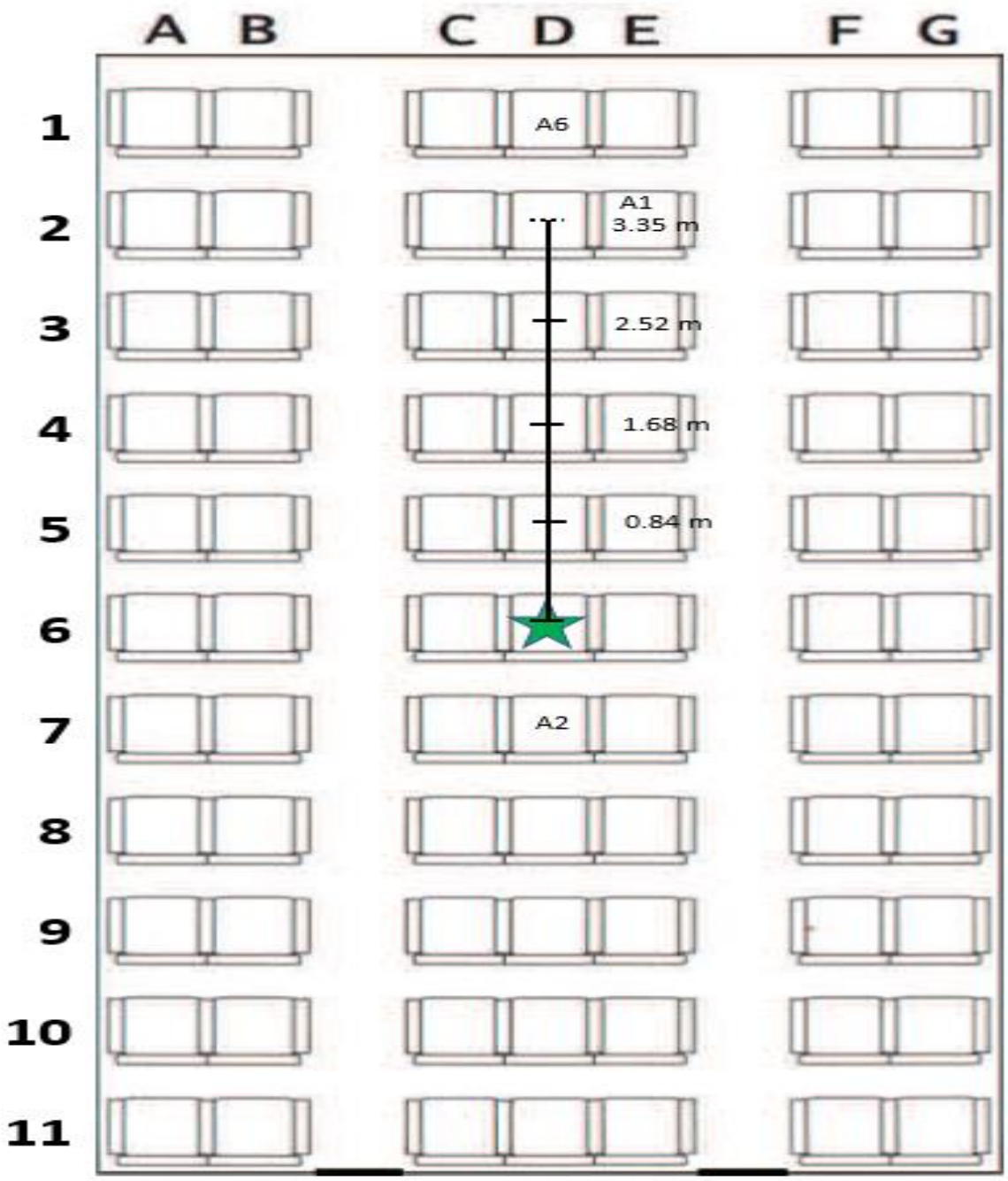

Figure E.11 Test 7 (A-I) ISOPass undeployed source location and sampling tree orientation.

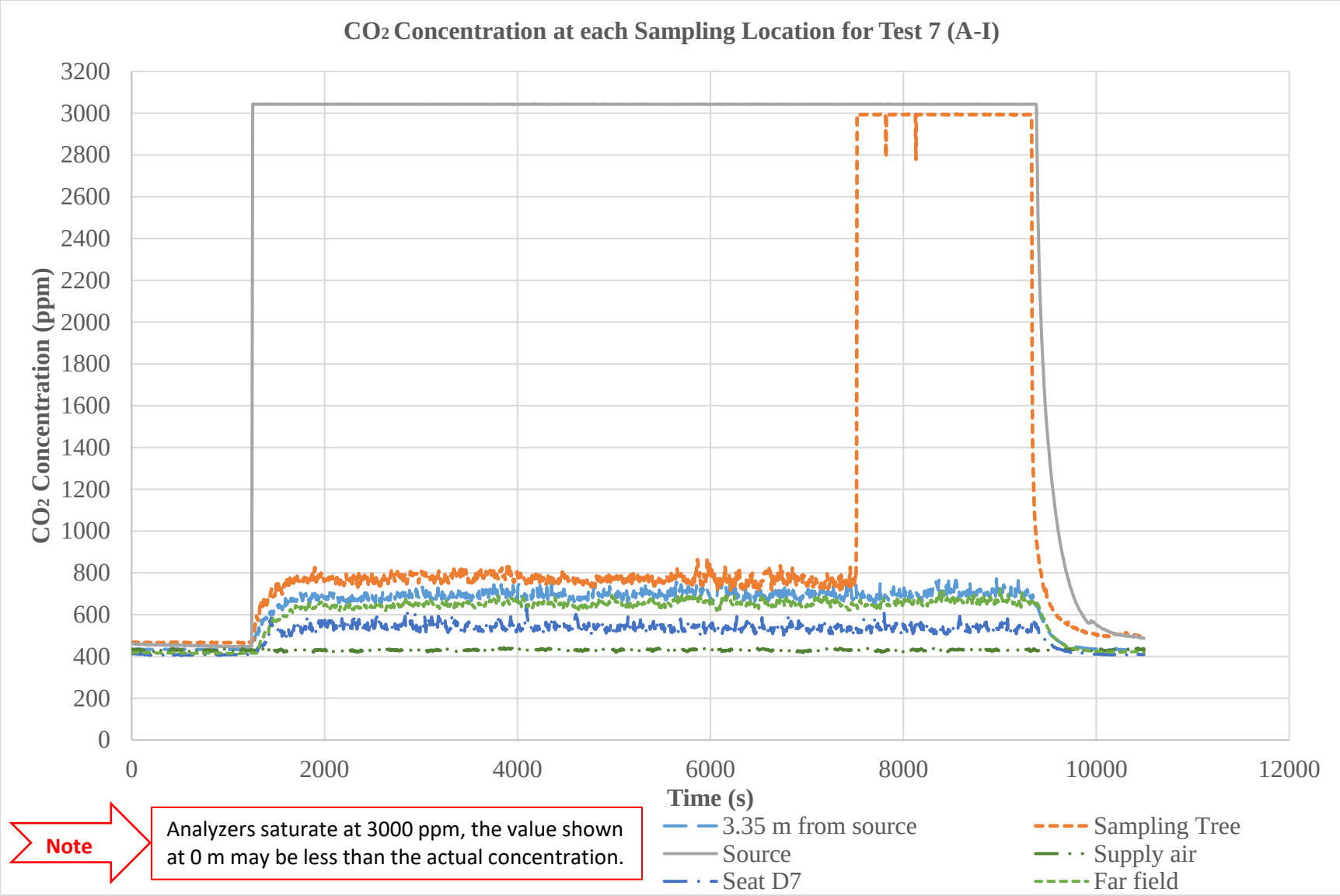

Figure E.12 Ininstantaneous CO_2 concentration at each sampling location for Test 7 (A-I) ISOPass undeployed.

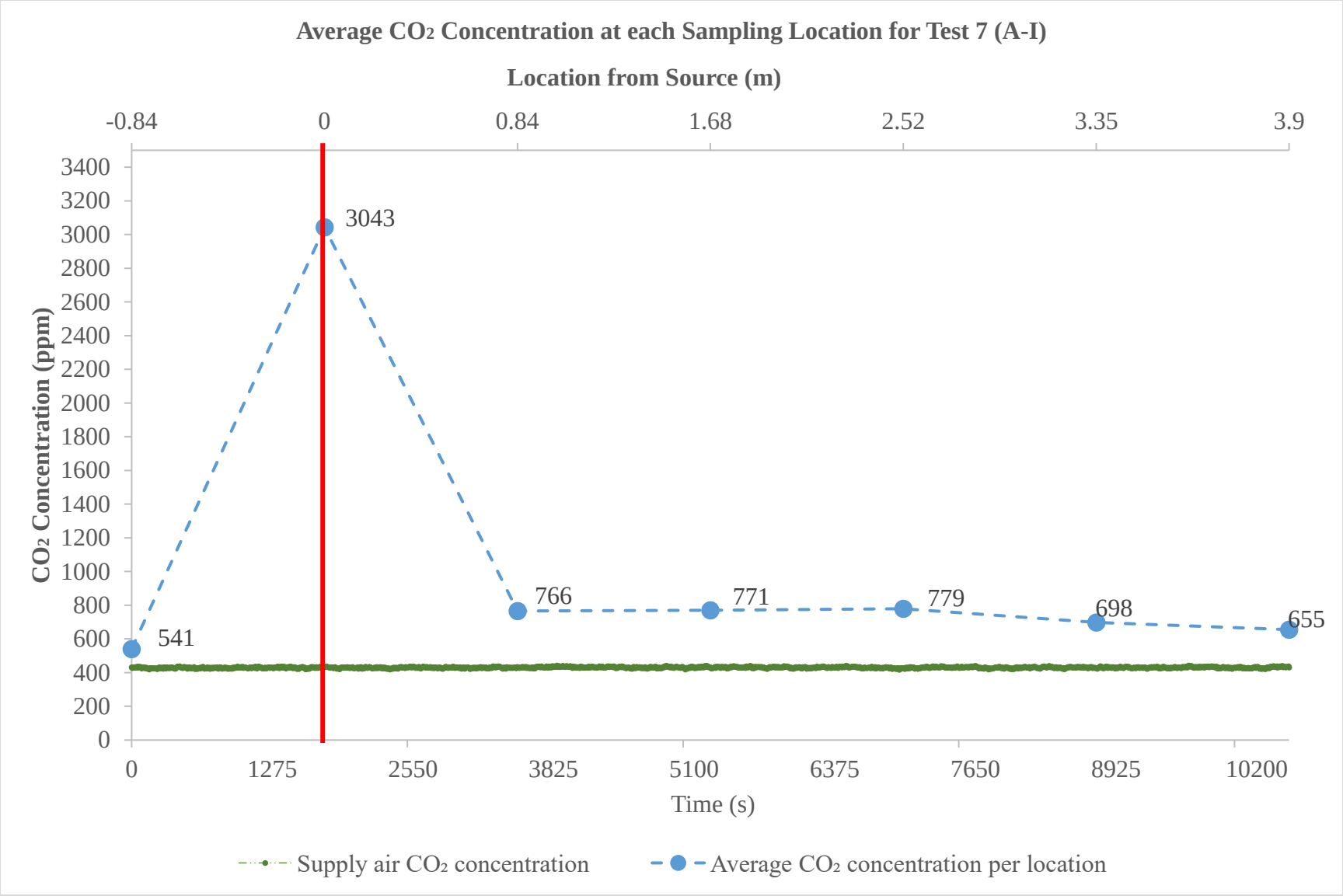

Figure E.13 Average CO_2 concentration at each sampling location for Test 7 (A-I) ISOPass undeployed.

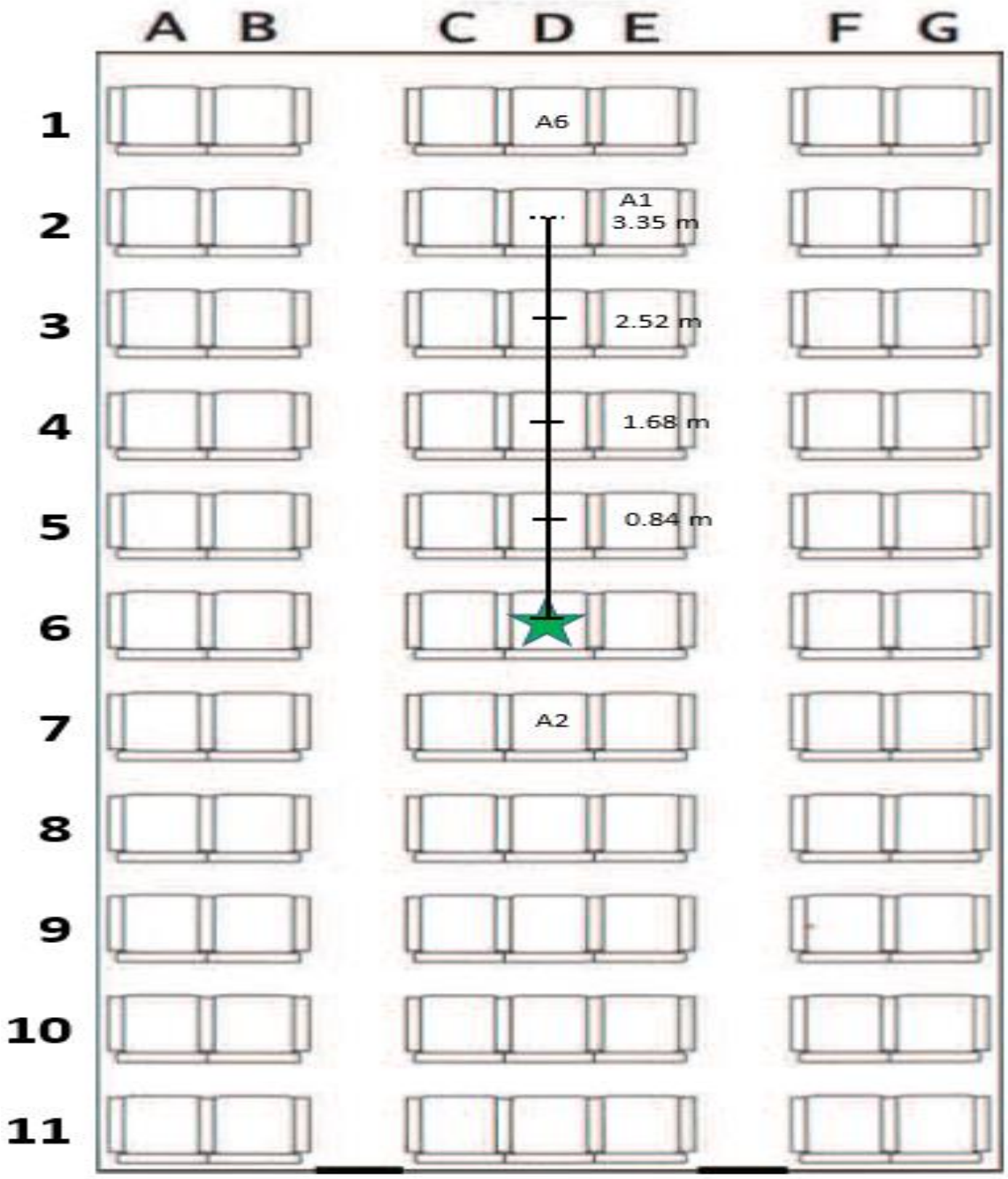

Figure E.14 Test 8 (A-I) ISOPass undeployed source location and sampling tree orientation.

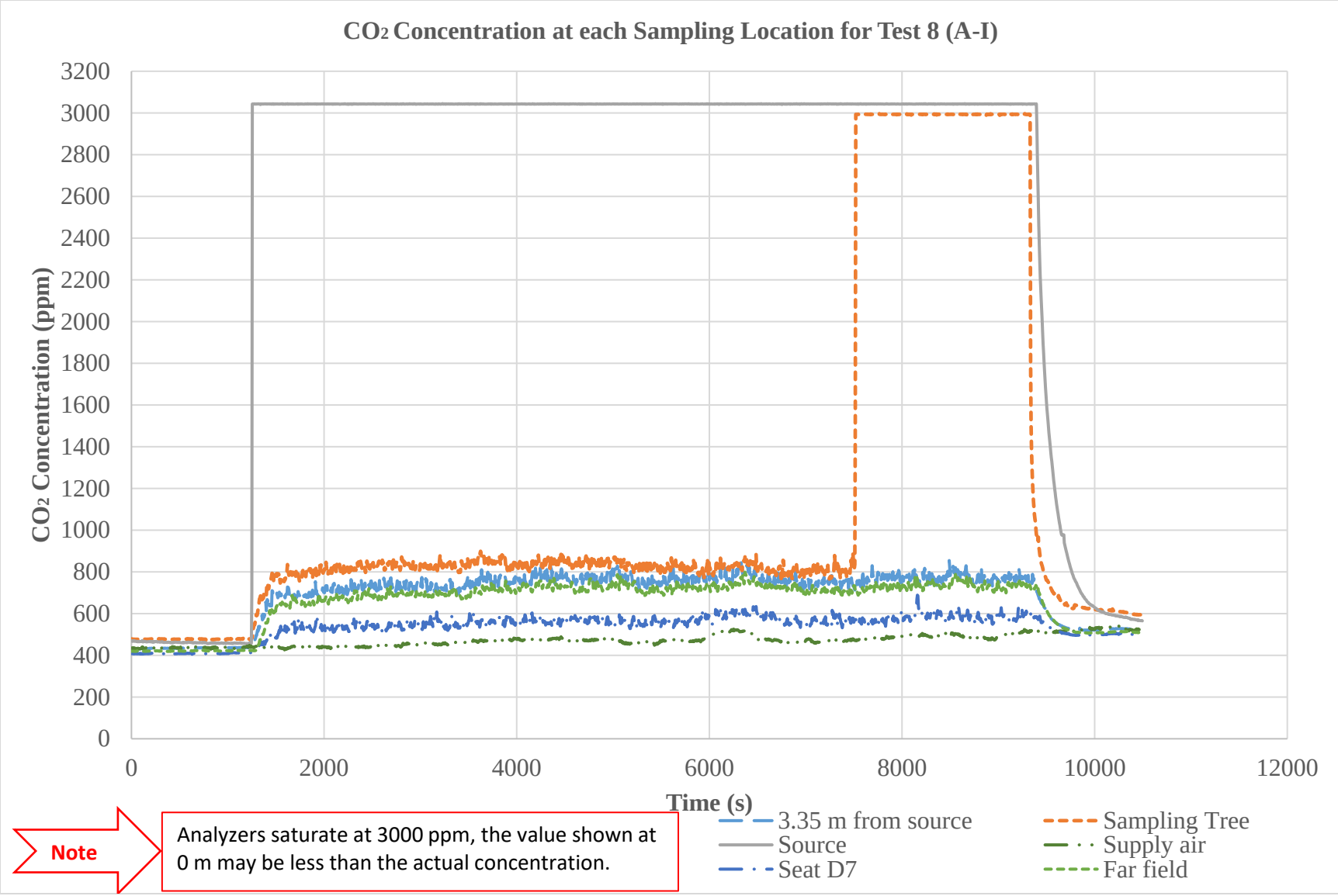

Figure E.15 Ininstantaneous CO_2 concentration at each sampling location for Test 8 (A-I) ISOPass undeployed.

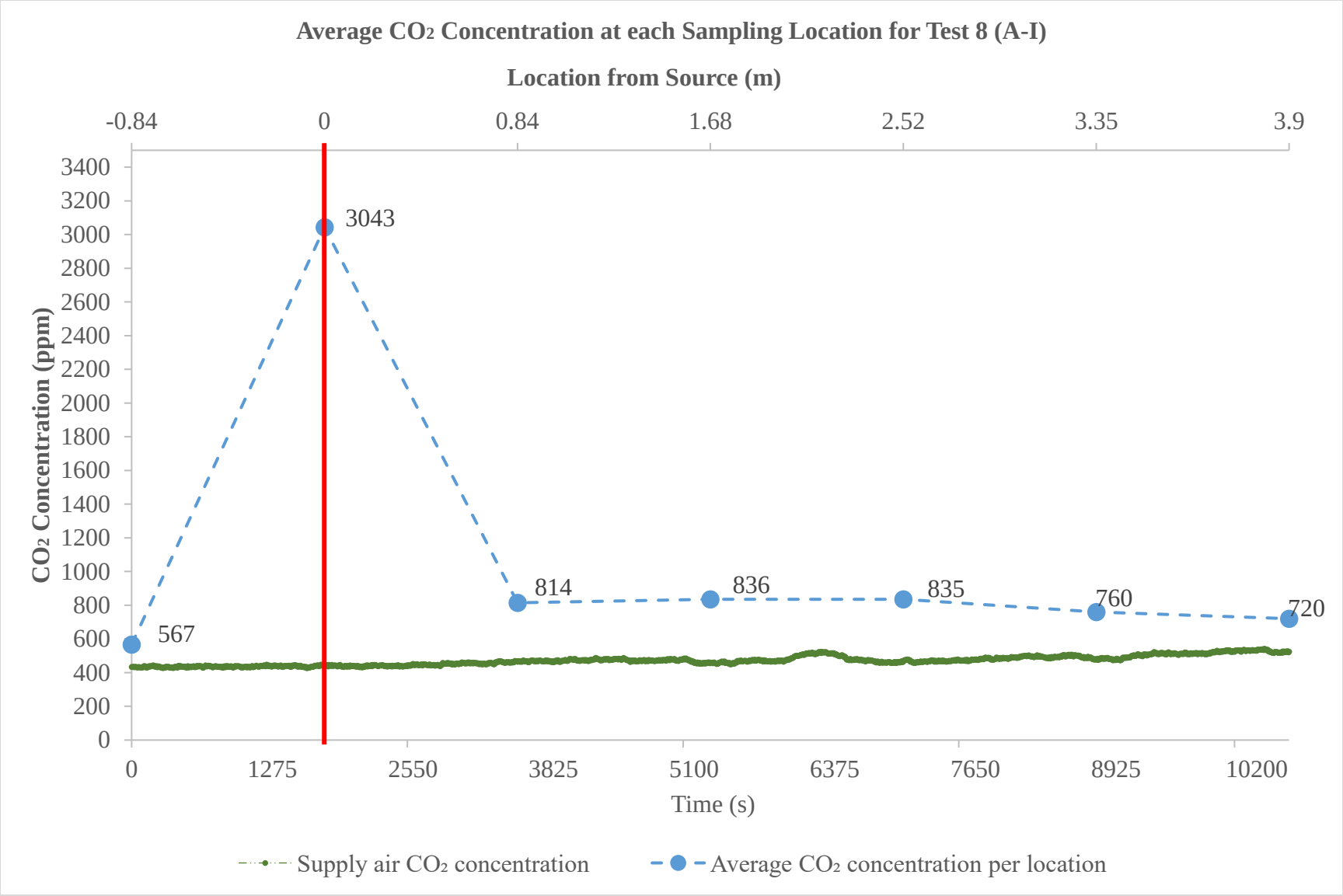

Figure E.16 Average CO_2 concentration at each sampling location for Test 8 (A-I) ISOPass undeployed.

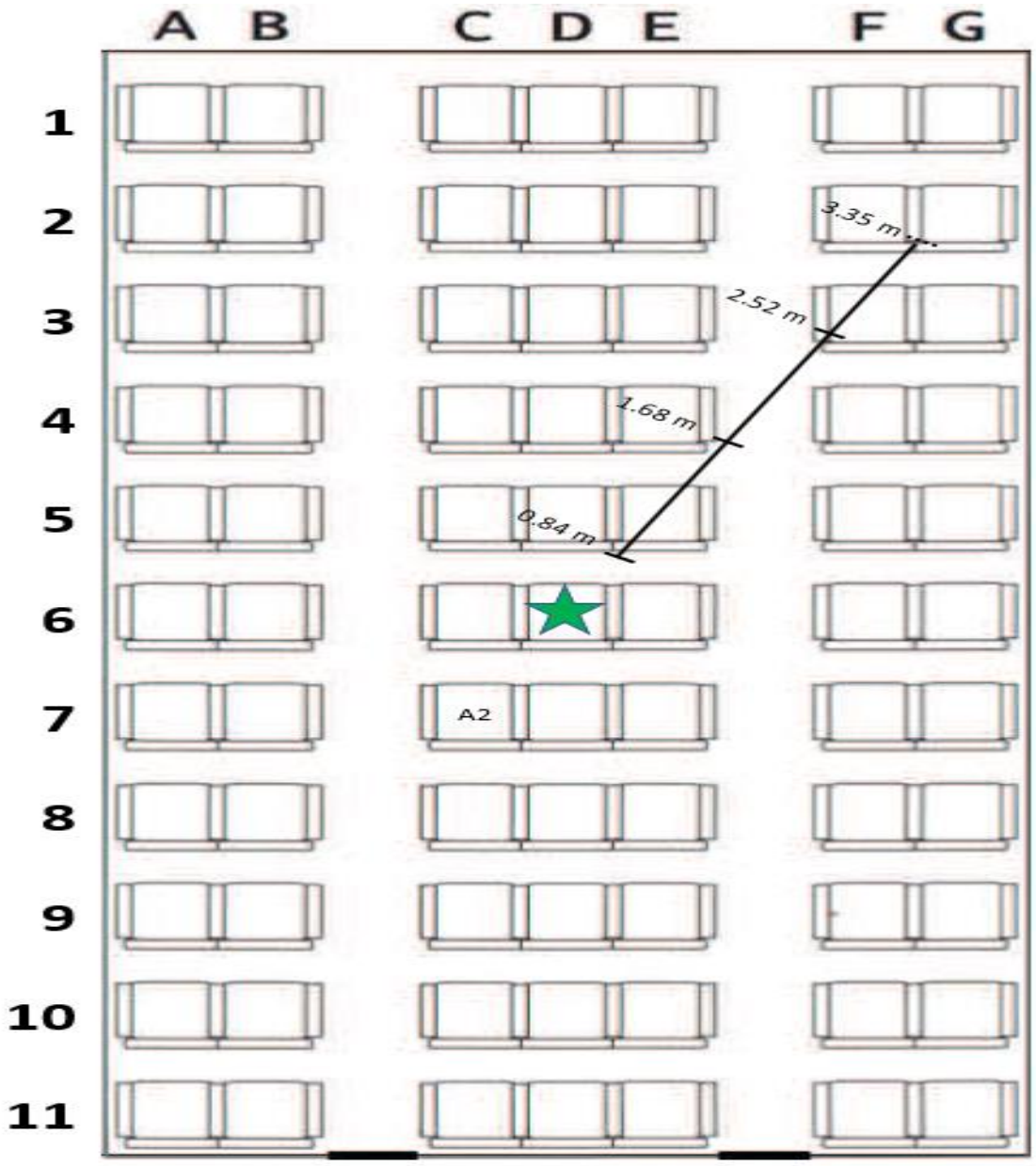

Figure E.17 Test 9 (A-I) ISOPass undeployed source location and sampling tree orientation.

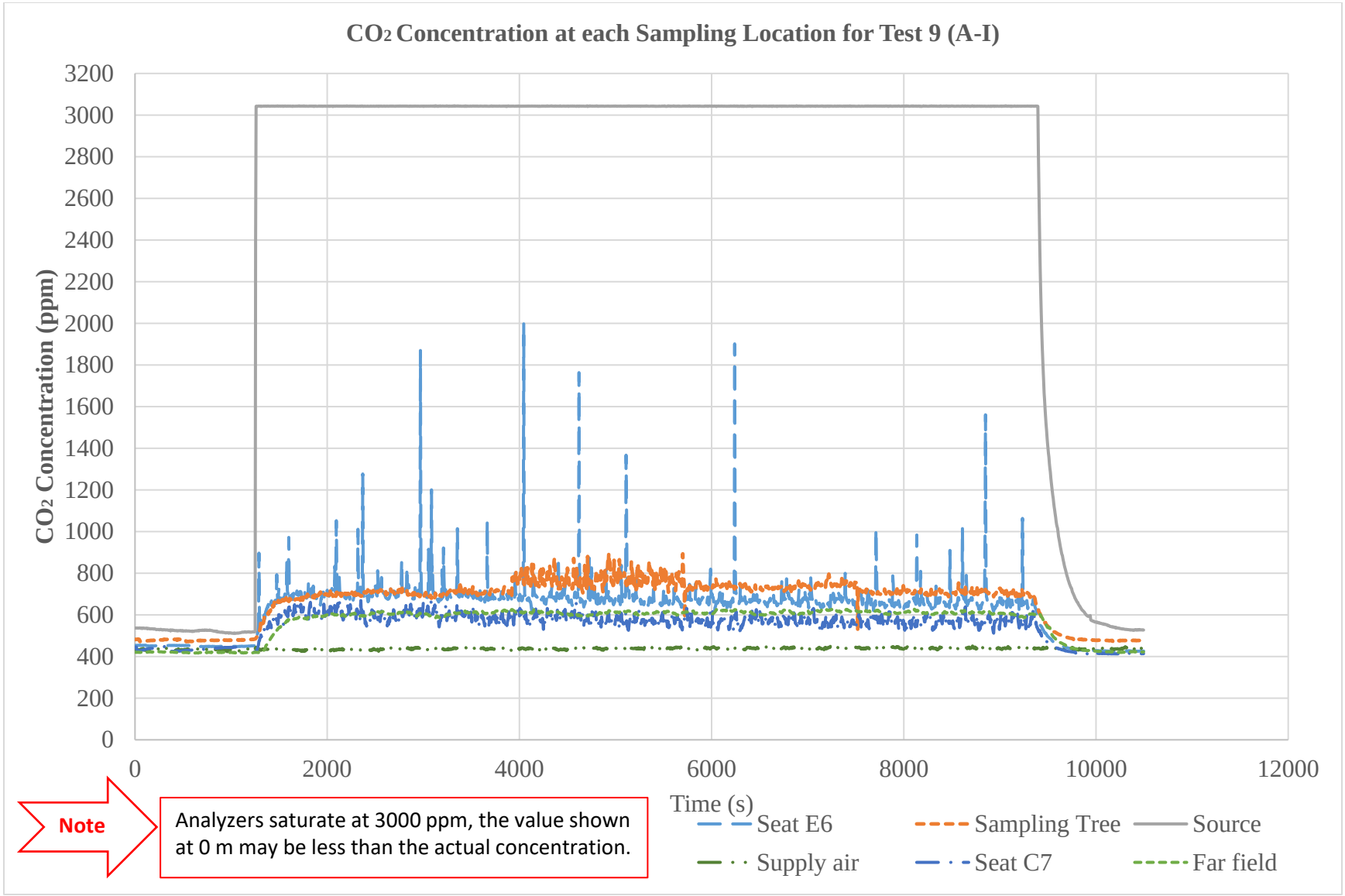

Figure E.18 Ininstantaneous CO_2 concentration at each sampling location for Test 9 (A-I) ISOPass undeployed.

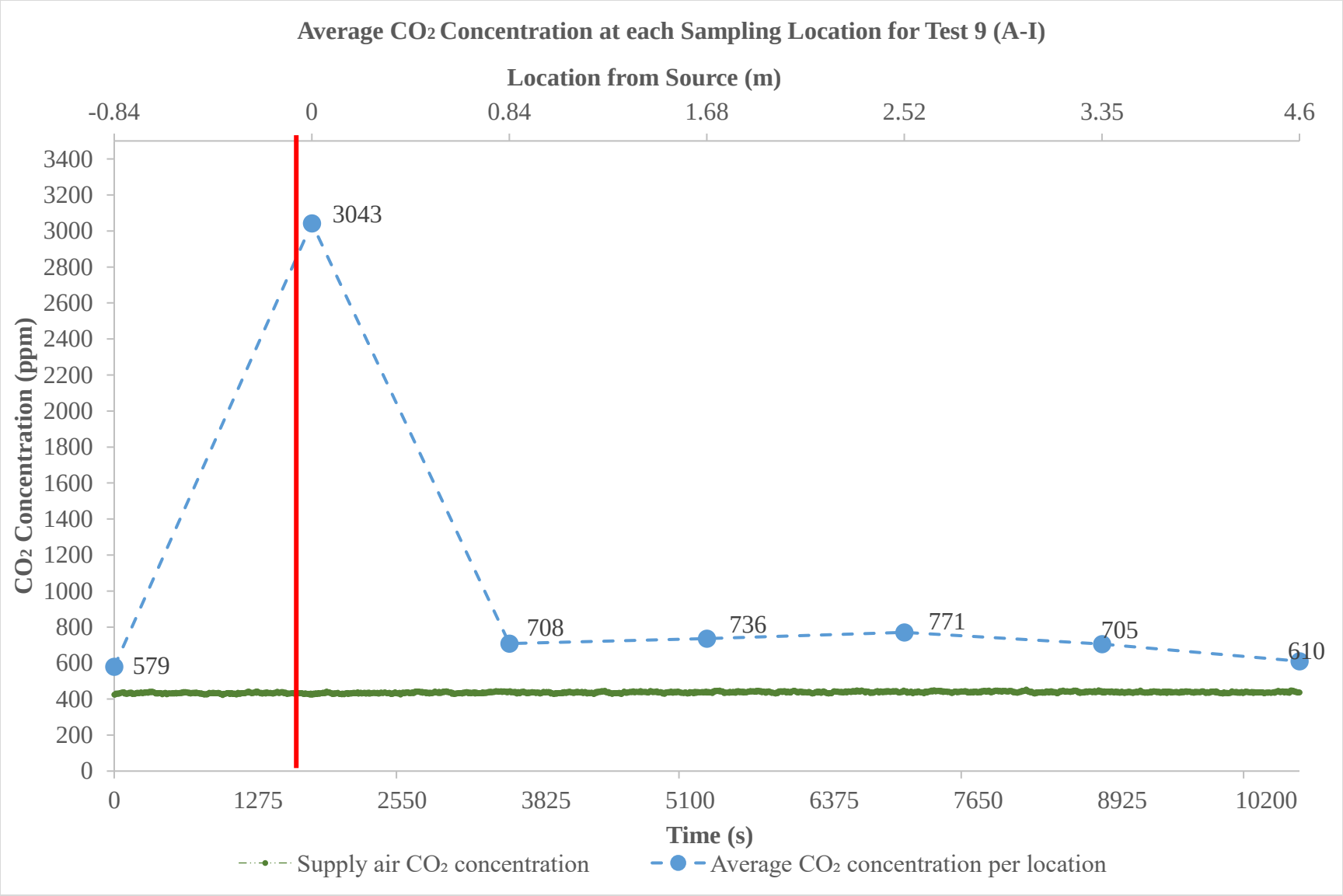

Figure E.19 Average CO_2 concentration at each sampling location for Test 9 (A-I) ISOPass undeployed.

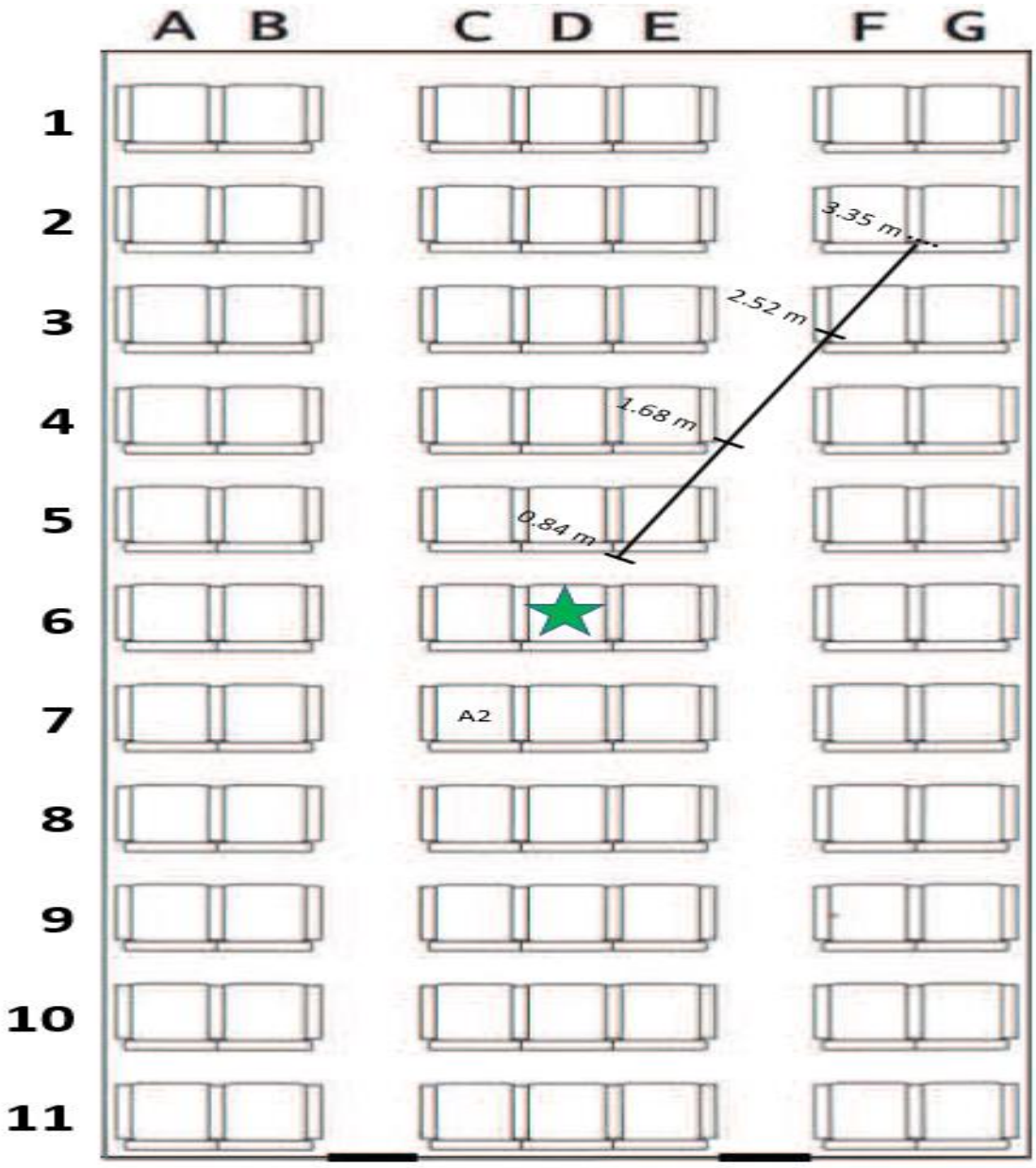

Figure E.20 Test 10 (A-I) ISOPass undeployed source location and sampling tree orientation.

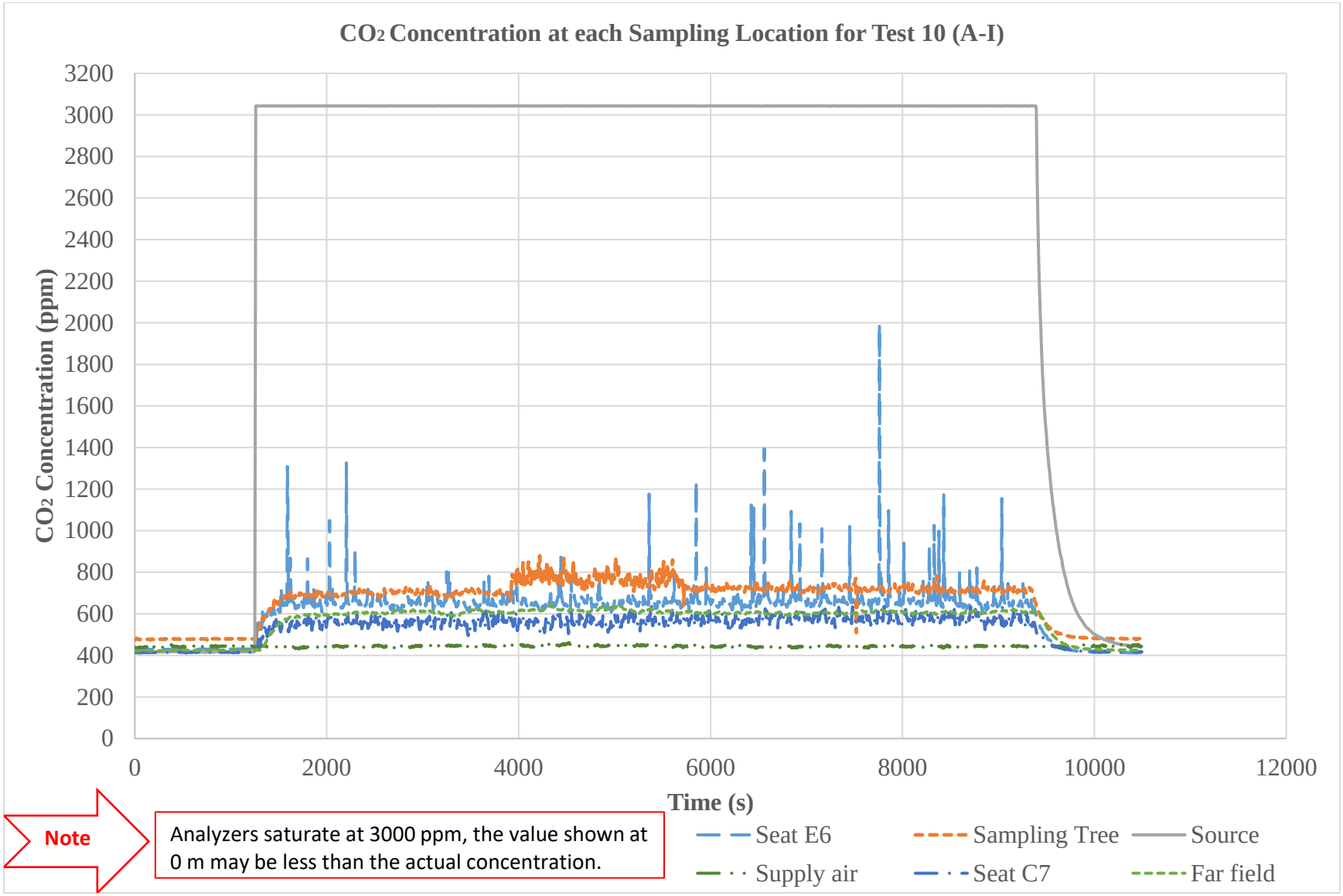

Figure E.21 Ininstantaneous CO_2 concentration at each sampling location for Test 10 (A-I) ISOPass undeployed.

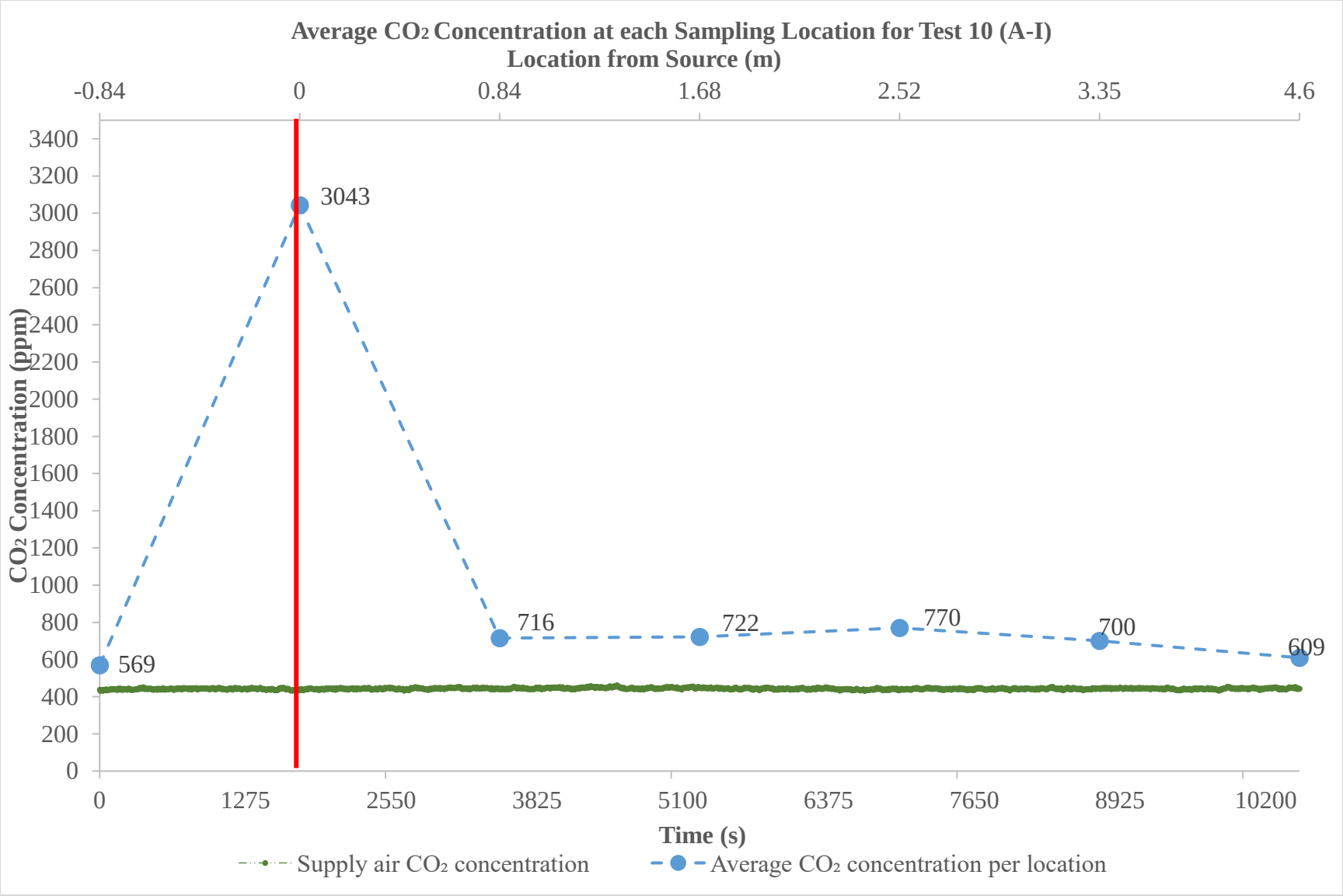

Figure E.22 Average CO_2 concentration at each sampling location for Test 10 (A-I) ISOPass undeployed.

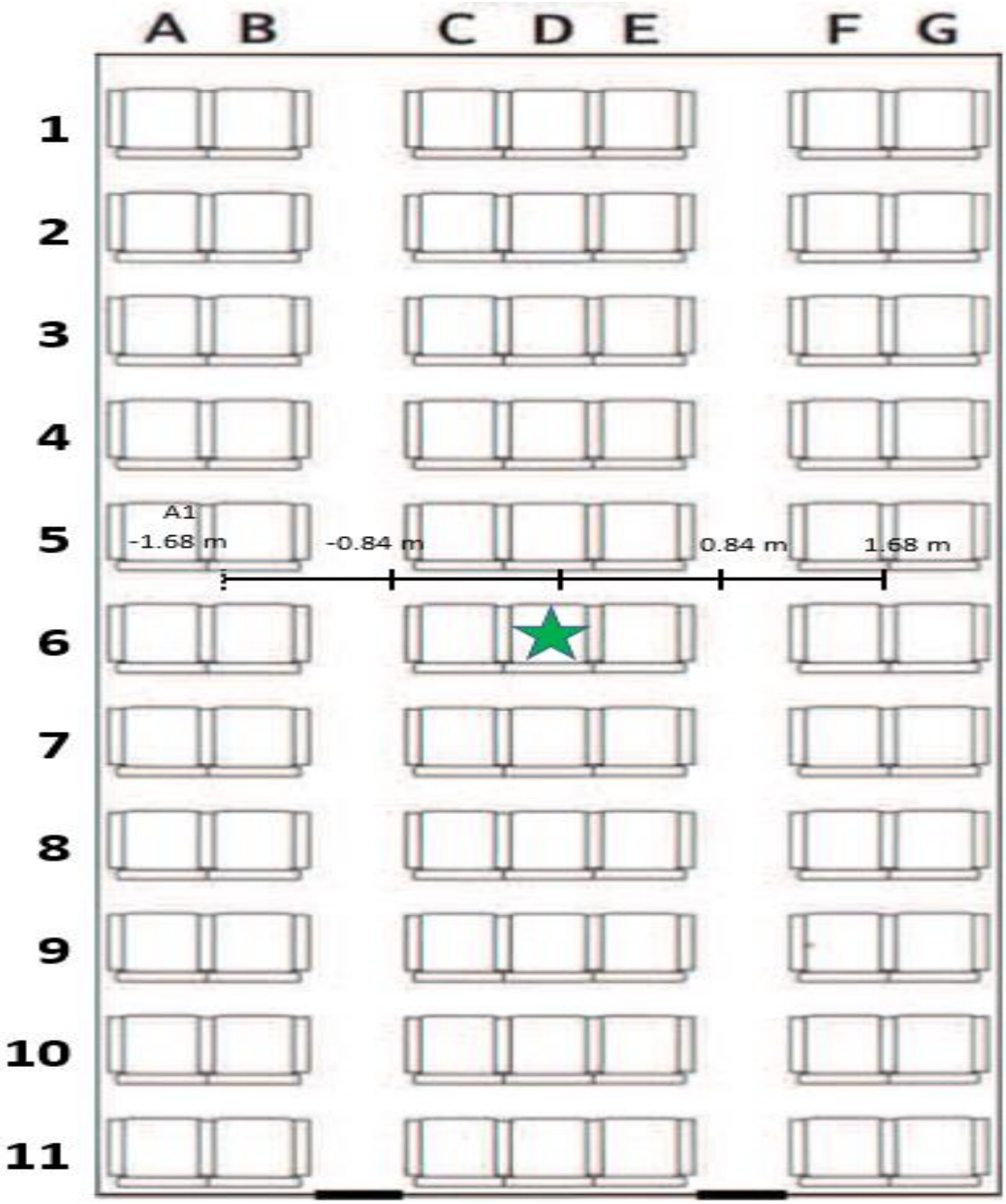

Figure E.23 Test 21 (A-I) ISOPass undeployed source location and sampling tree orientation.

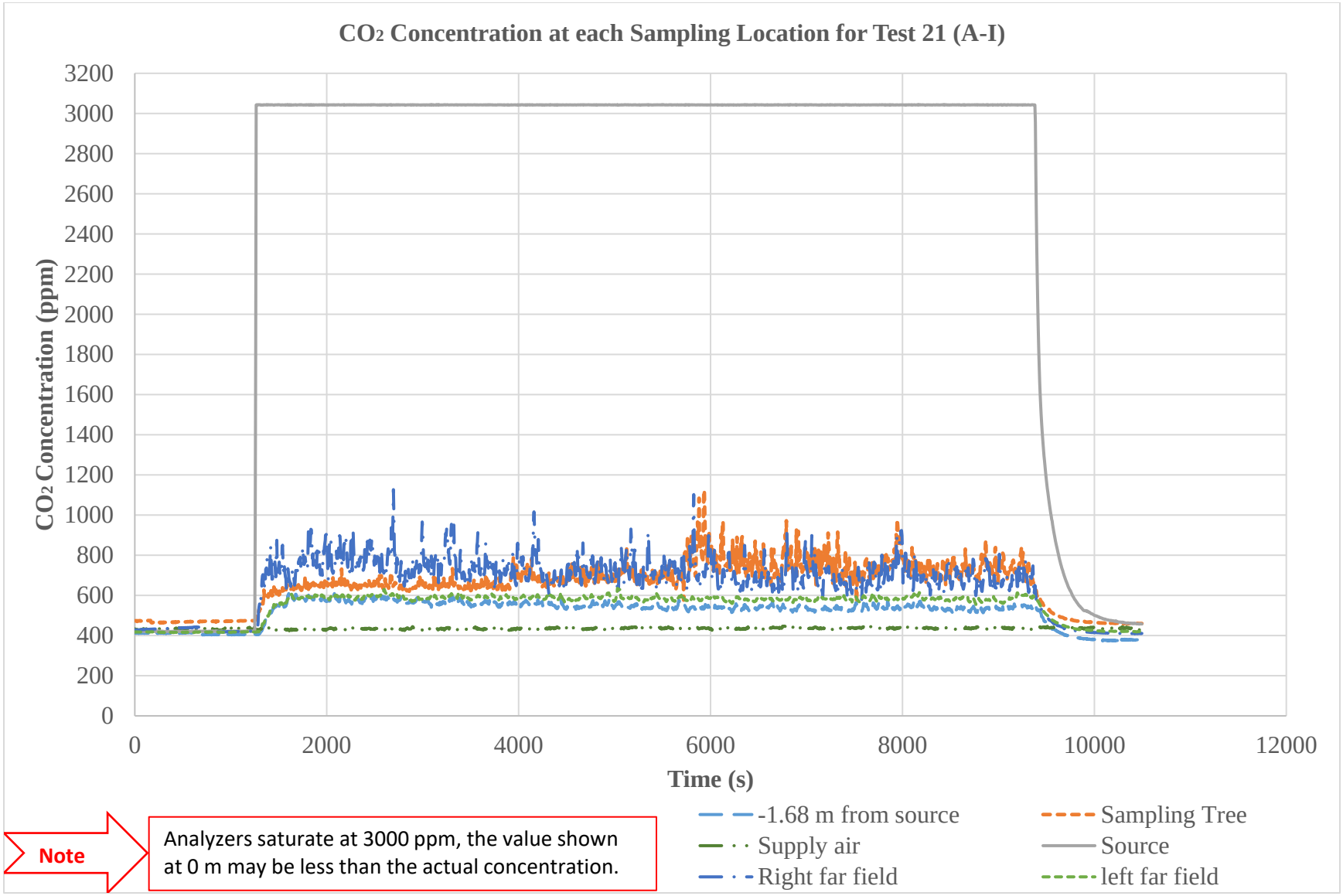

Figure E.24 Ininstantaneous CO_2 concentration at each sampling location for Test 21 (A-I) ISOPass undeployed.

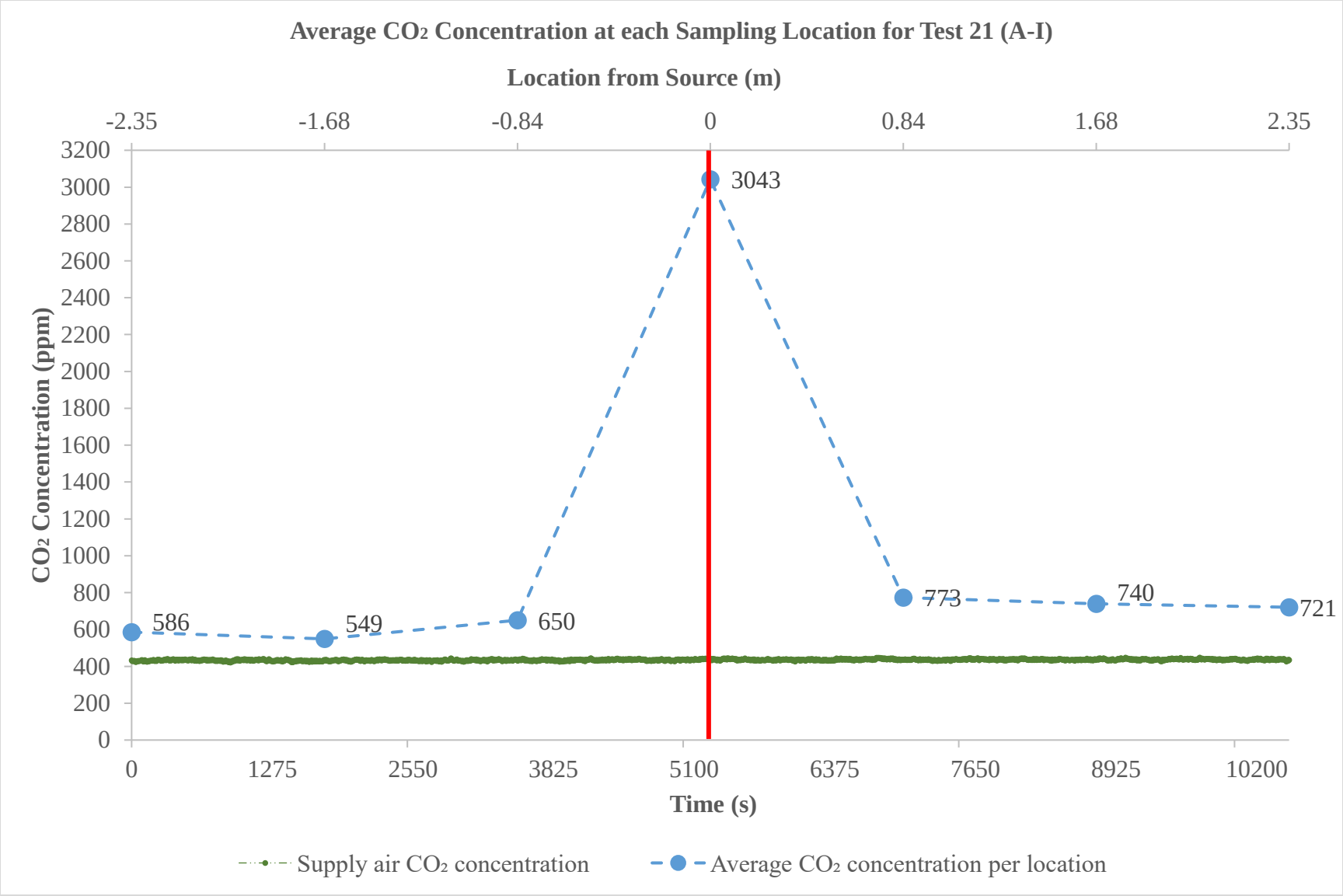

Figure E.25 Average CO_2 concentration at each sampling location for Test 21 (A-I) ISOPass undeployed.

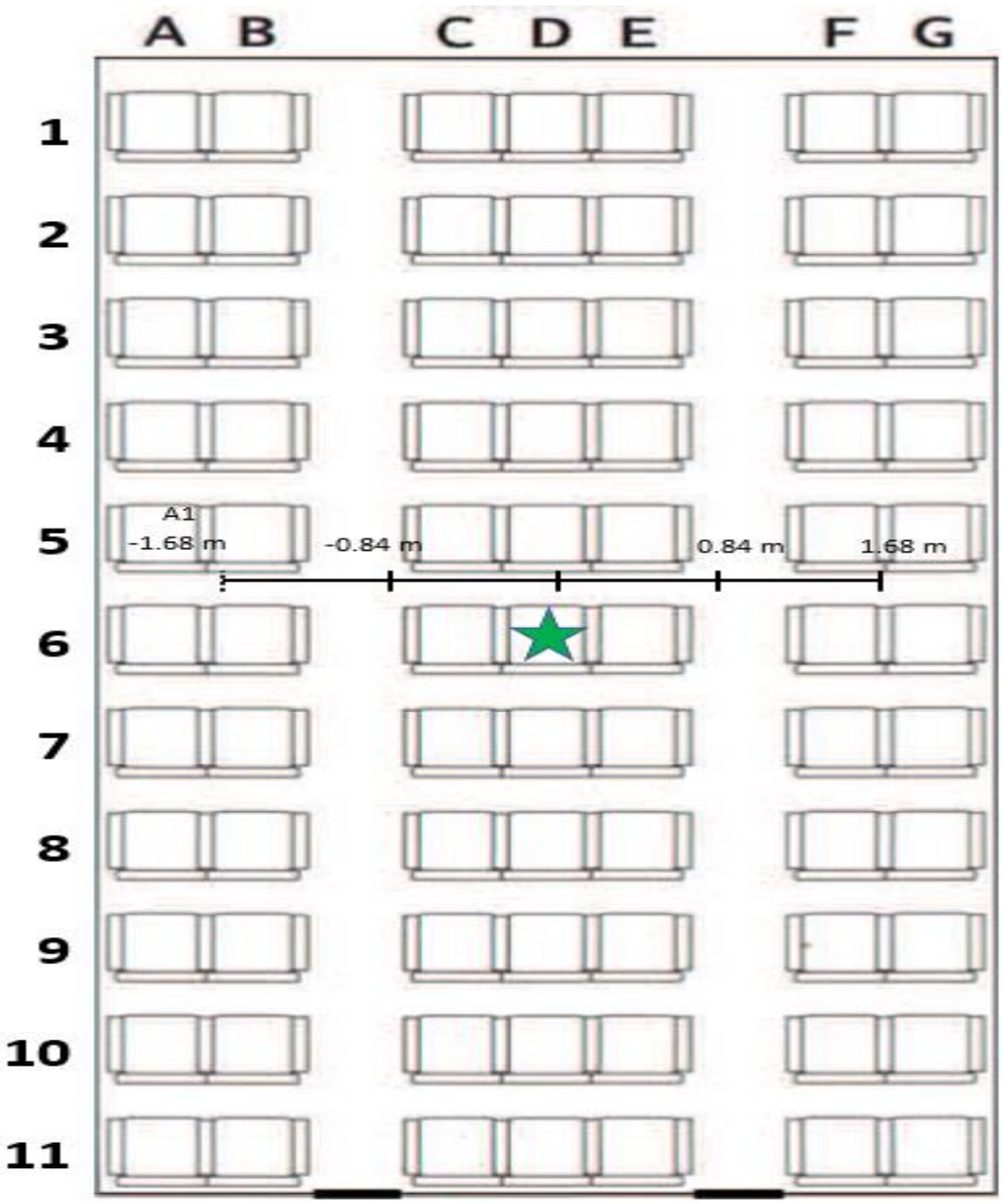

Figure E.26 Test 22 (A-I) ISOPass undeployed source location and sampling tree orientation.

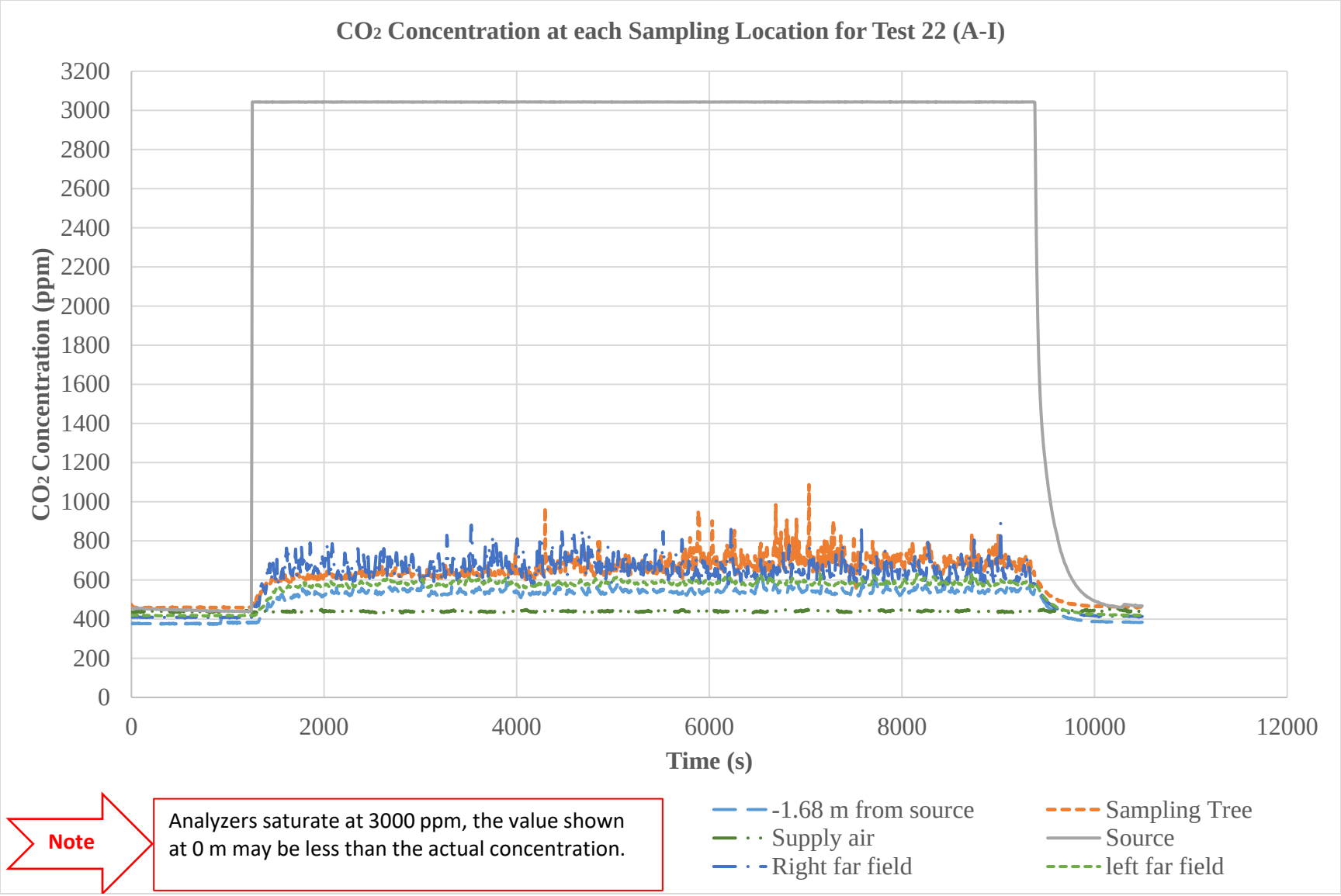

Figure E.27 Ininstantaneous CO_2 concentration at each sampling location for Test 22 (A-I) ISOPass undeployed.

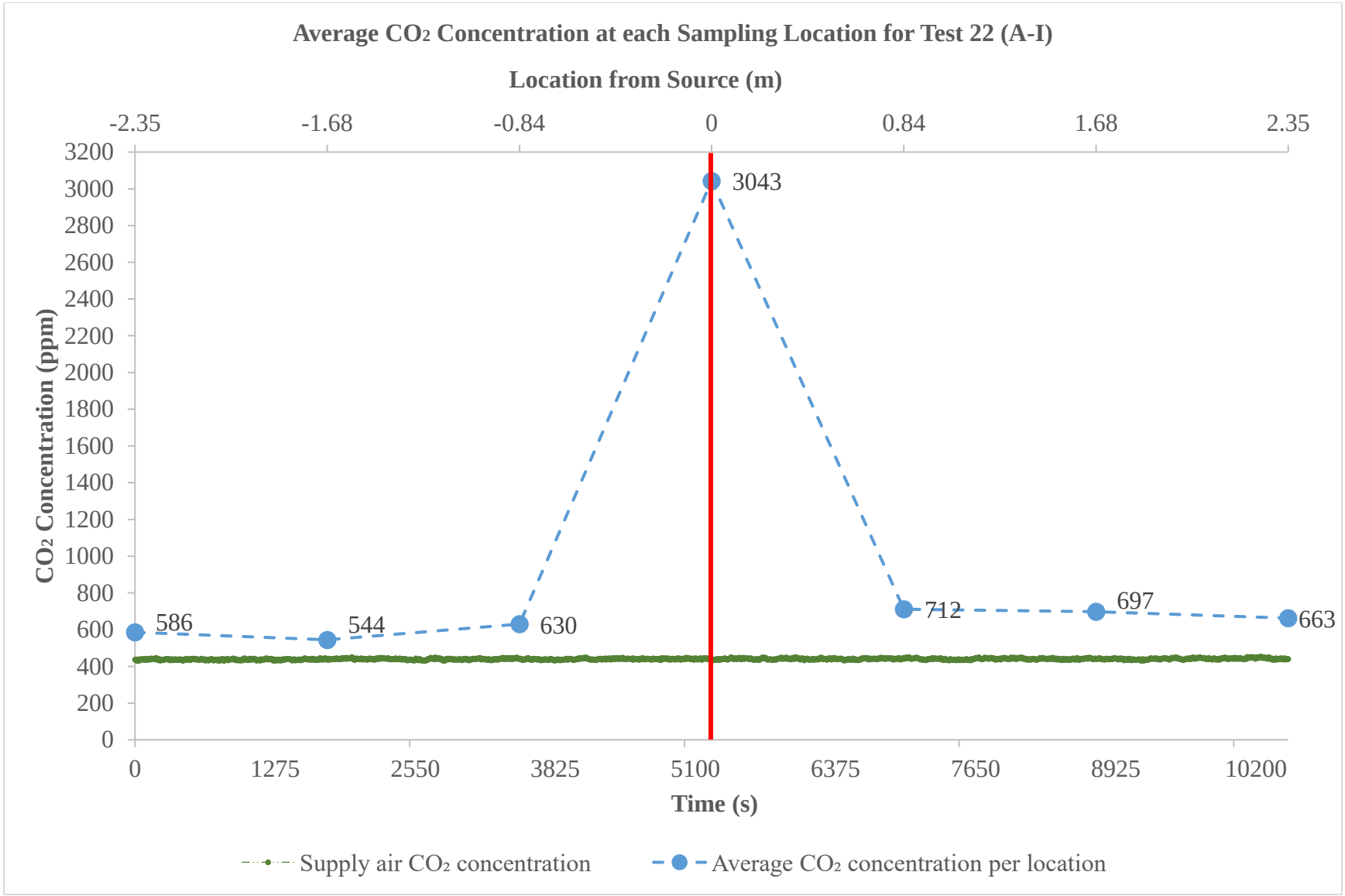

Figure E.28 Average CO_2 concentration at each sampling location for Test 22 (A-I) ISOPass undeployed.

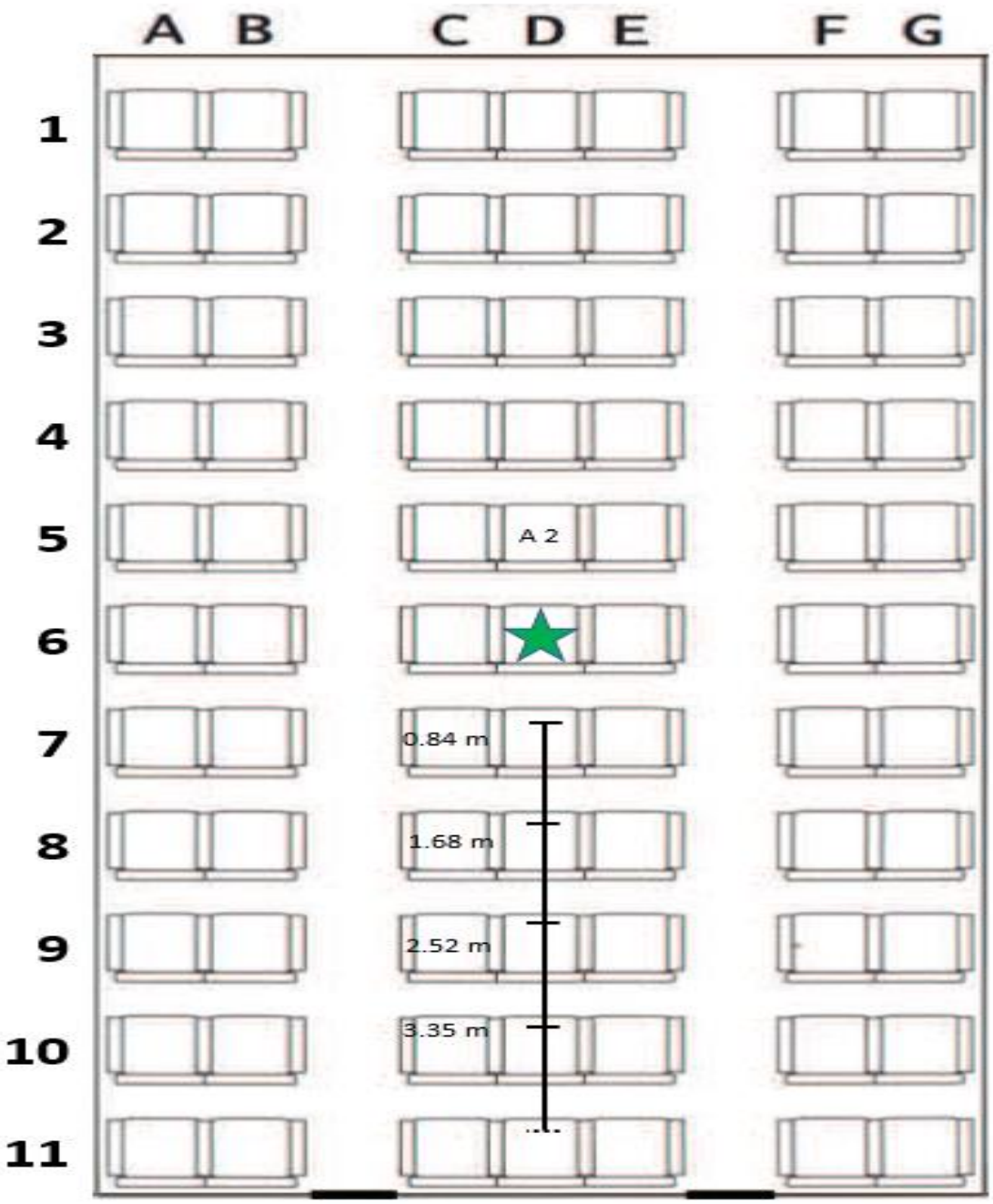

Figure E.29 Test 27 (A-I) ISOPass undeployed source location and sampling tree orientation.

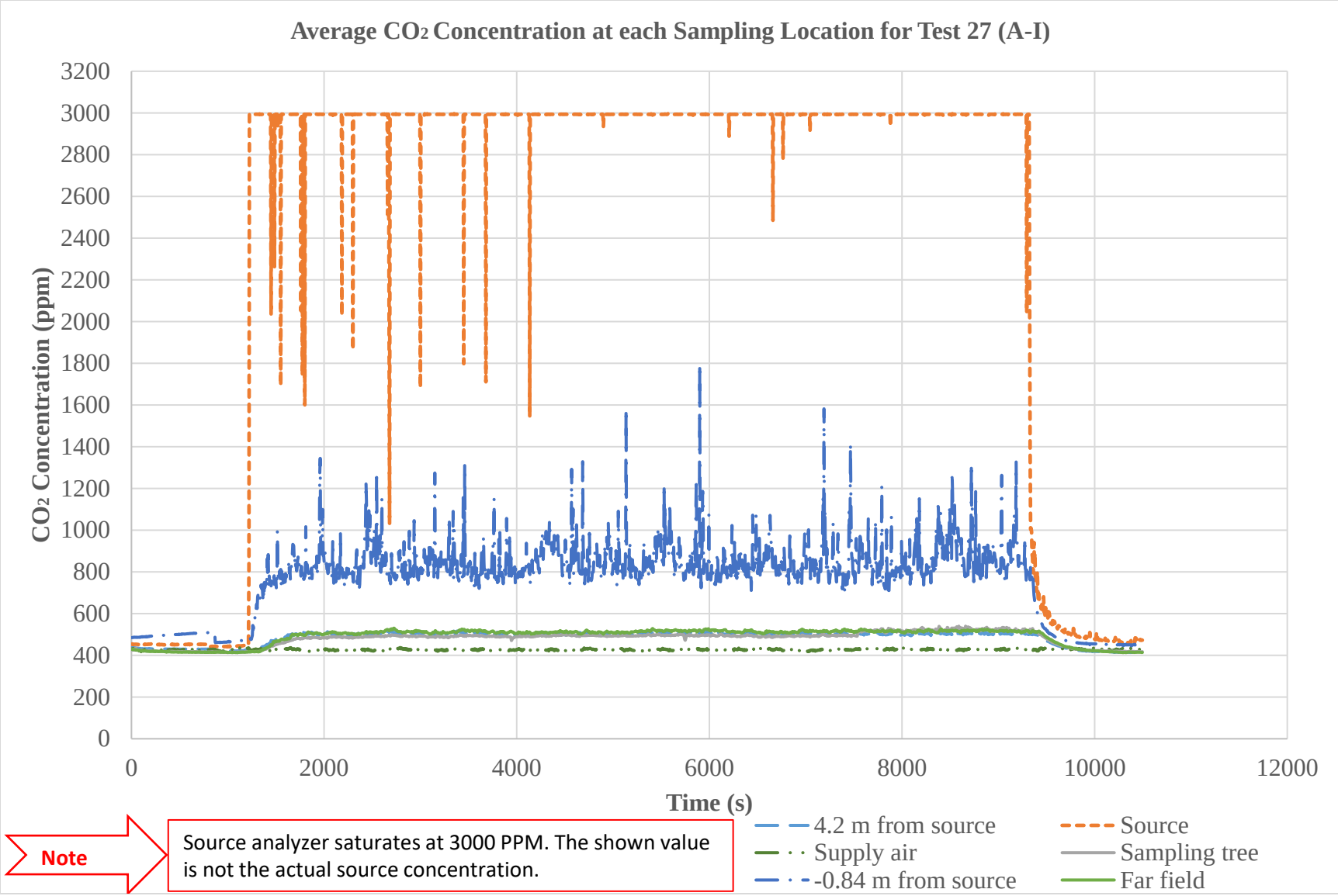

Figure E.30 Ininstantaneous CO_2 concentration at each sampling location for Test 27 (A-I) ISOPass undeployed.

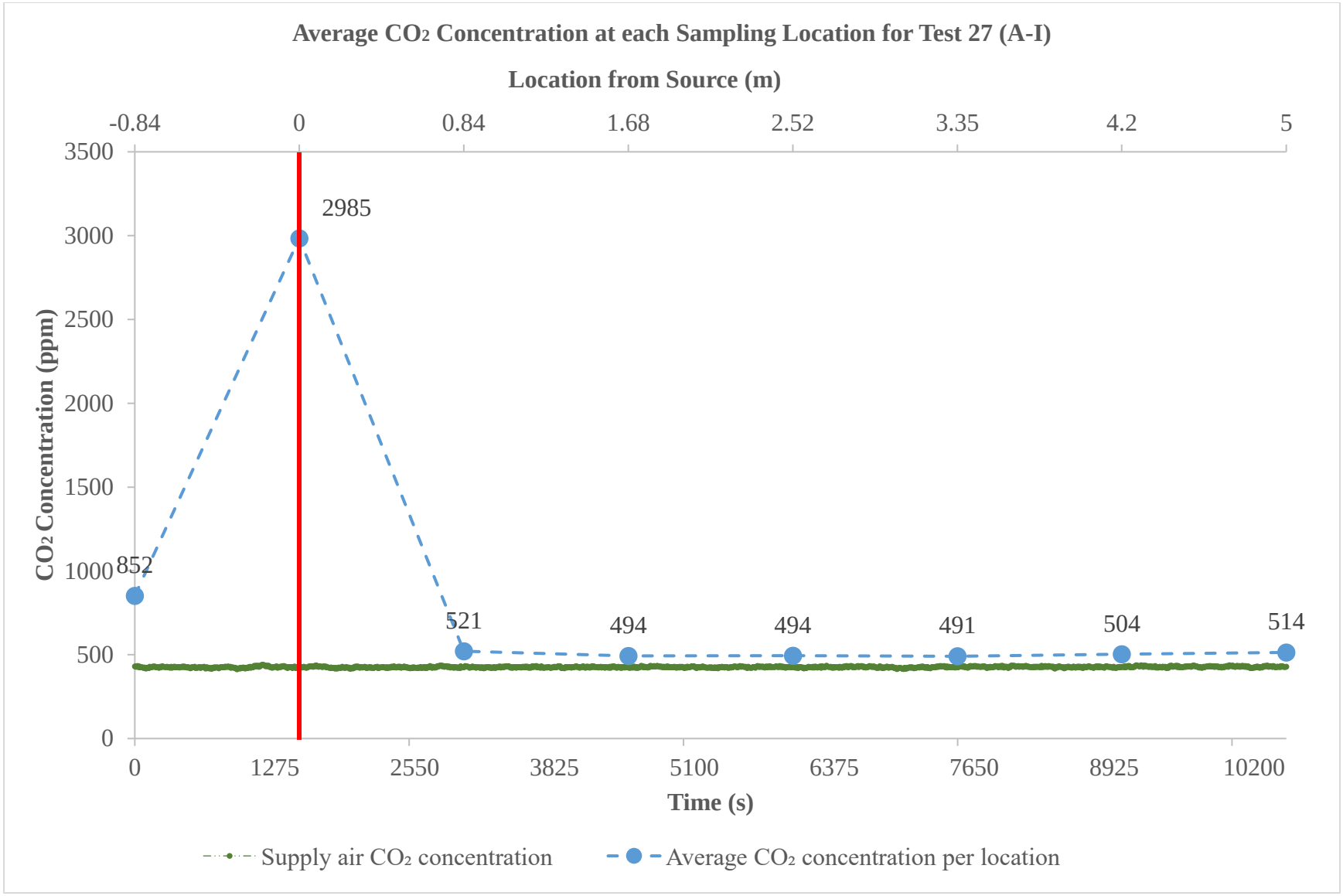

Figure E.31 Average CO_2 concentration at each sampling location for Test 27 (A-I) ISOPass undeployed.

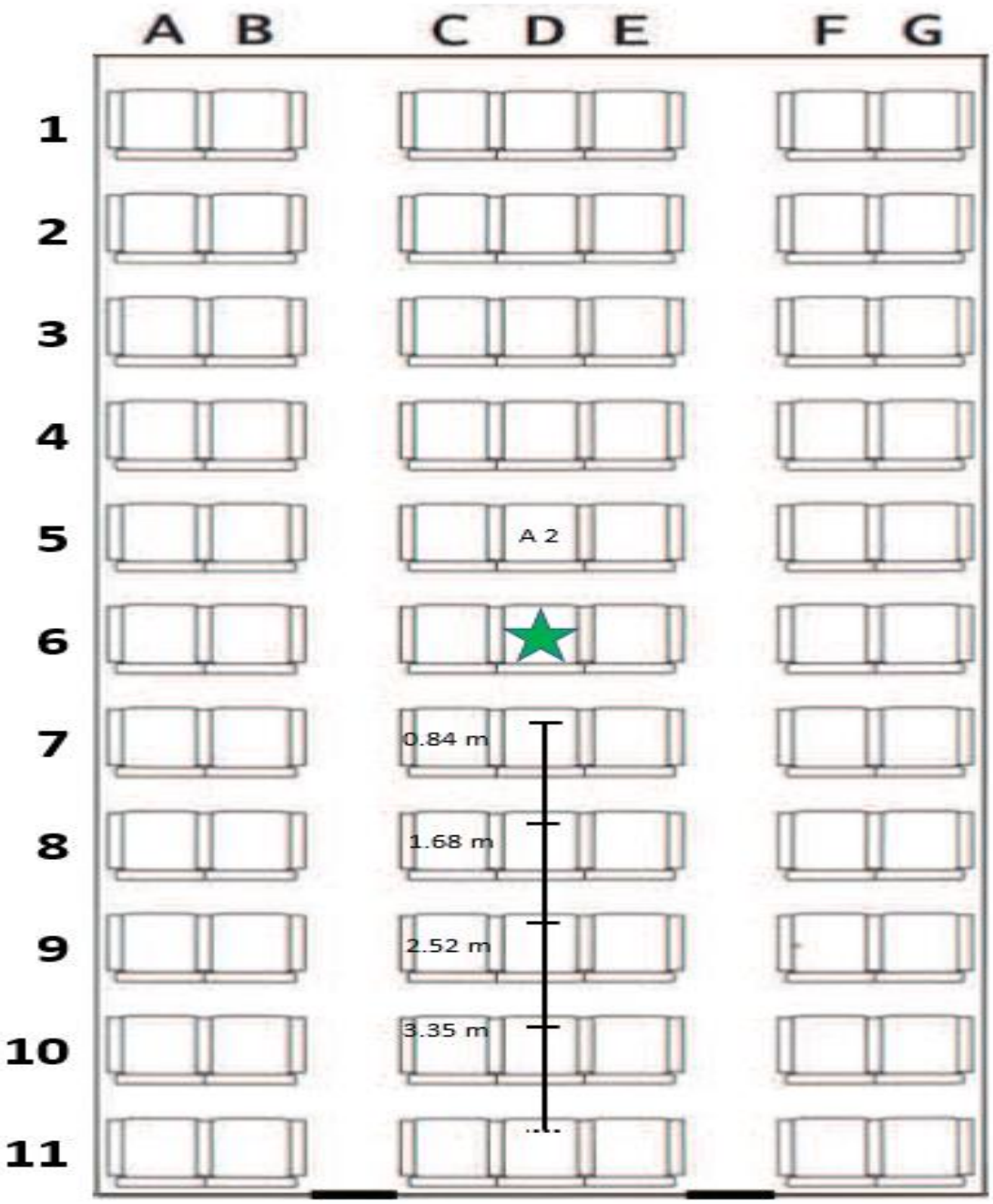

Figure E.32 Test 28 (A-I) ISOPass undeployed source location and sampling tree orientation.

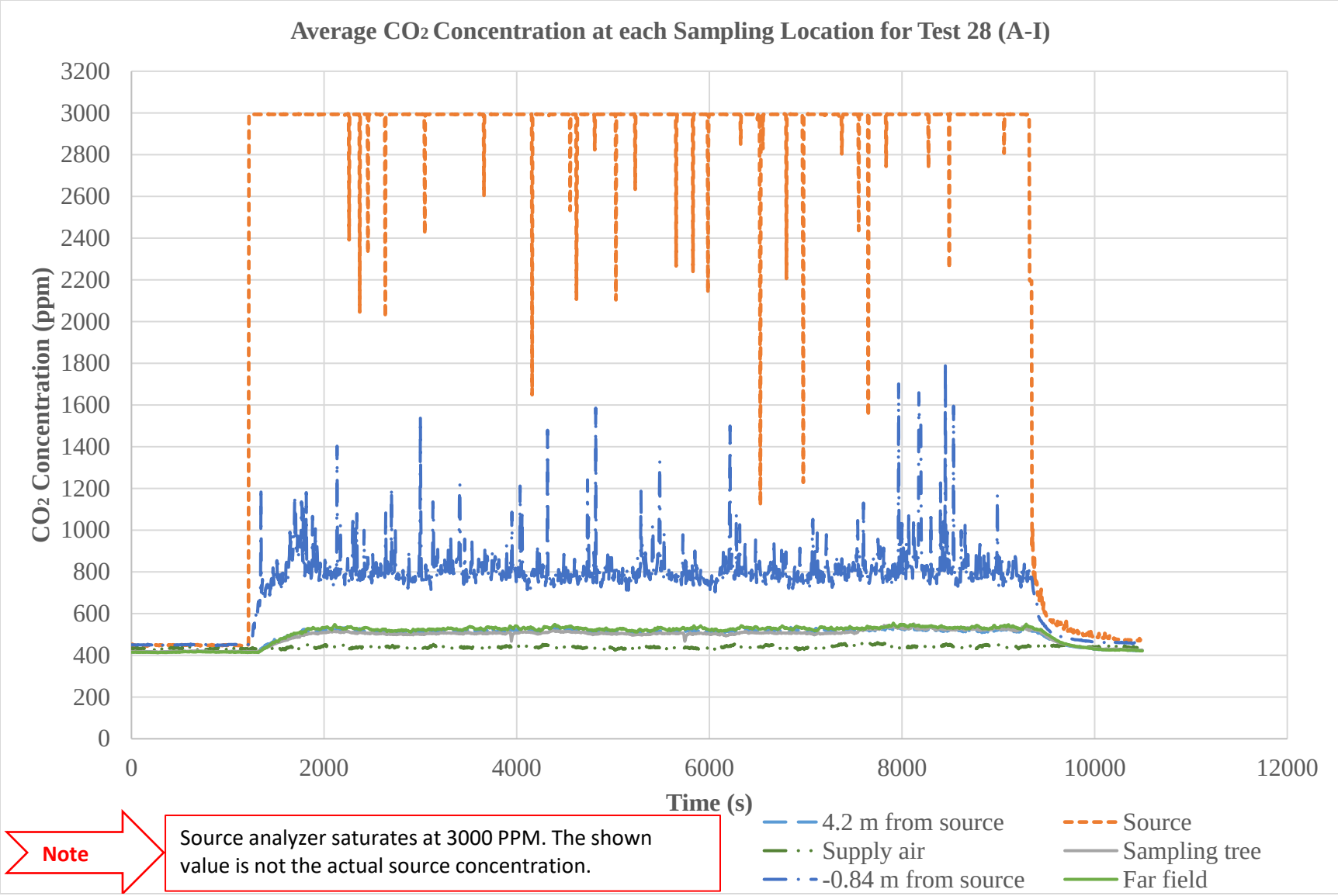

Figure E.33 Ininstantaneous CO_2 concentration at each sampling location for Test 28 (A-I) ISOPass undeployed.

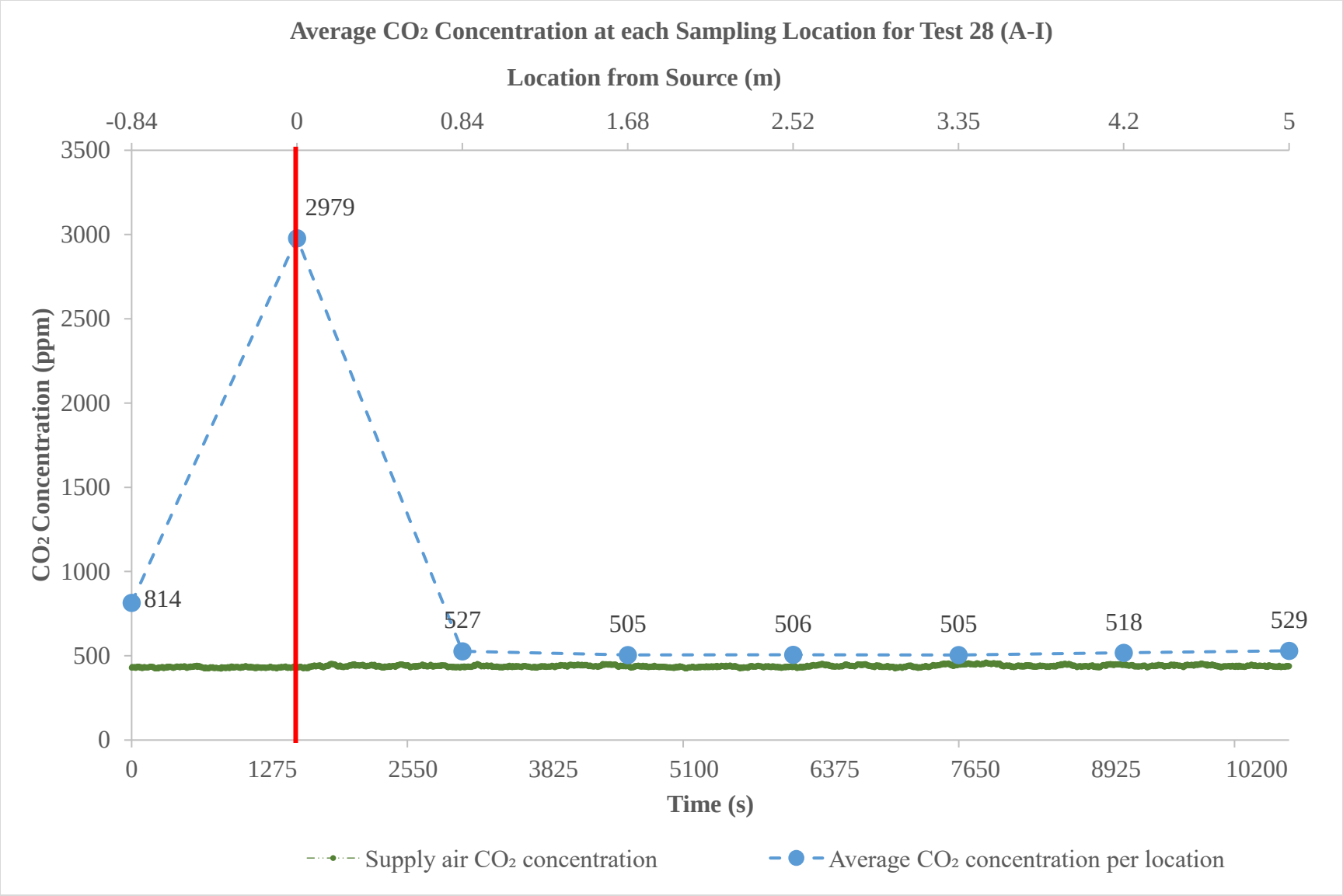

Figure E.34 Average CO_2 concentration at each sampling location for Test 28 (A-I) ISOPass undeployed.

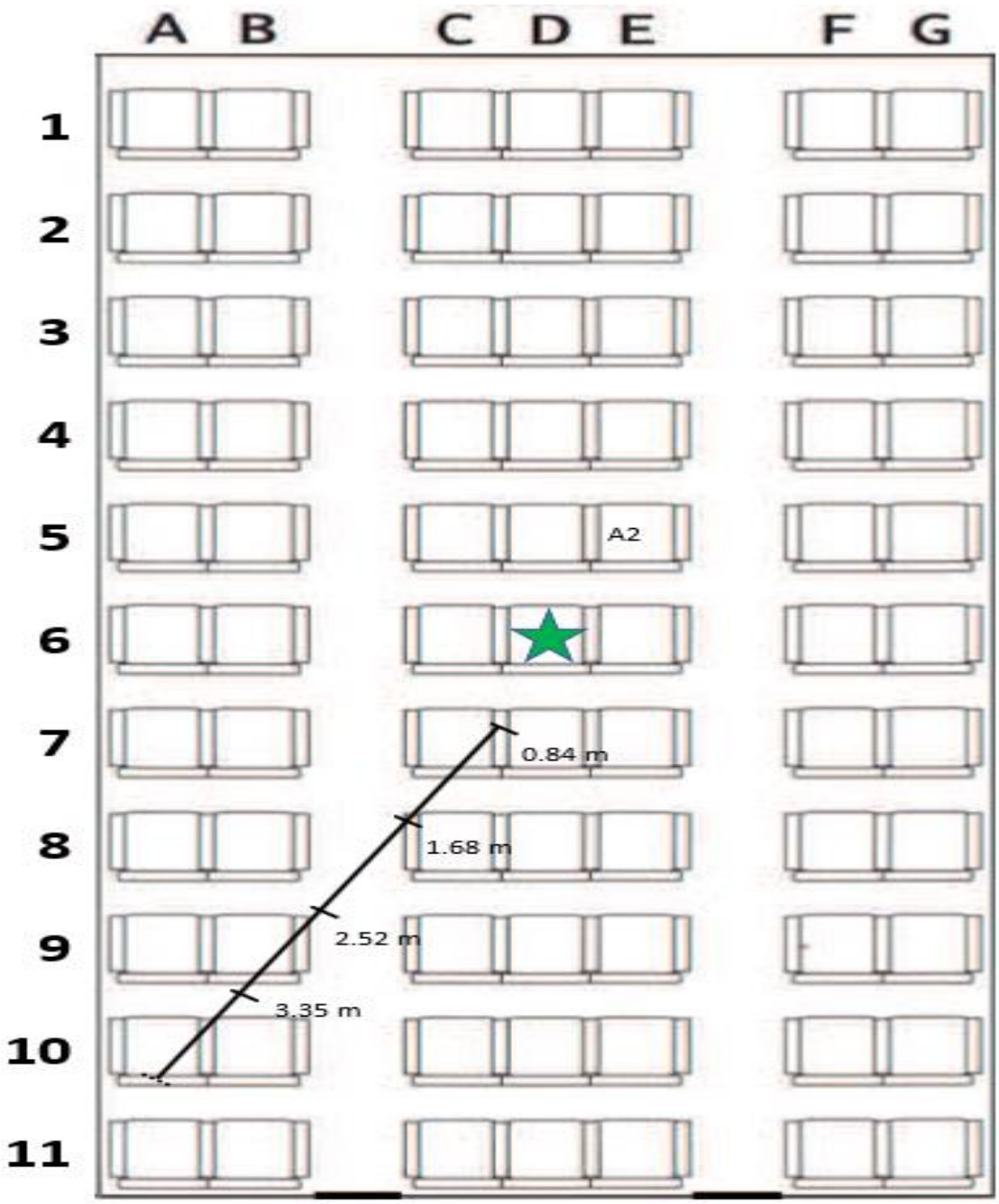

Figure E.35 Test 29 (A-I) ISOPass undeployed source location and sampling tree orientation.

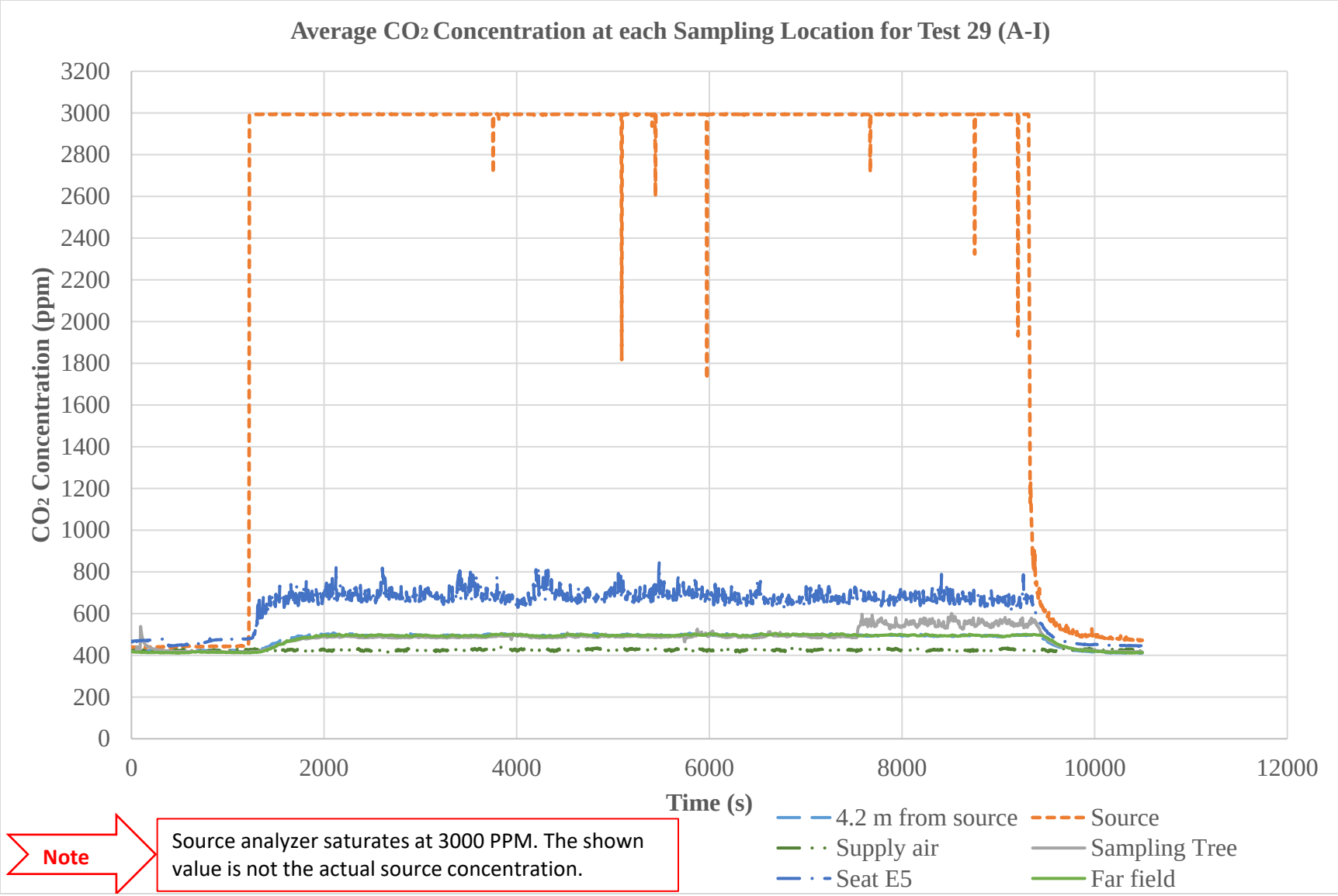

Figure E.36 Ininstantaneous CO_2 concentration at each sampling location for Test 29 (A-I) ISOPass undeployed.

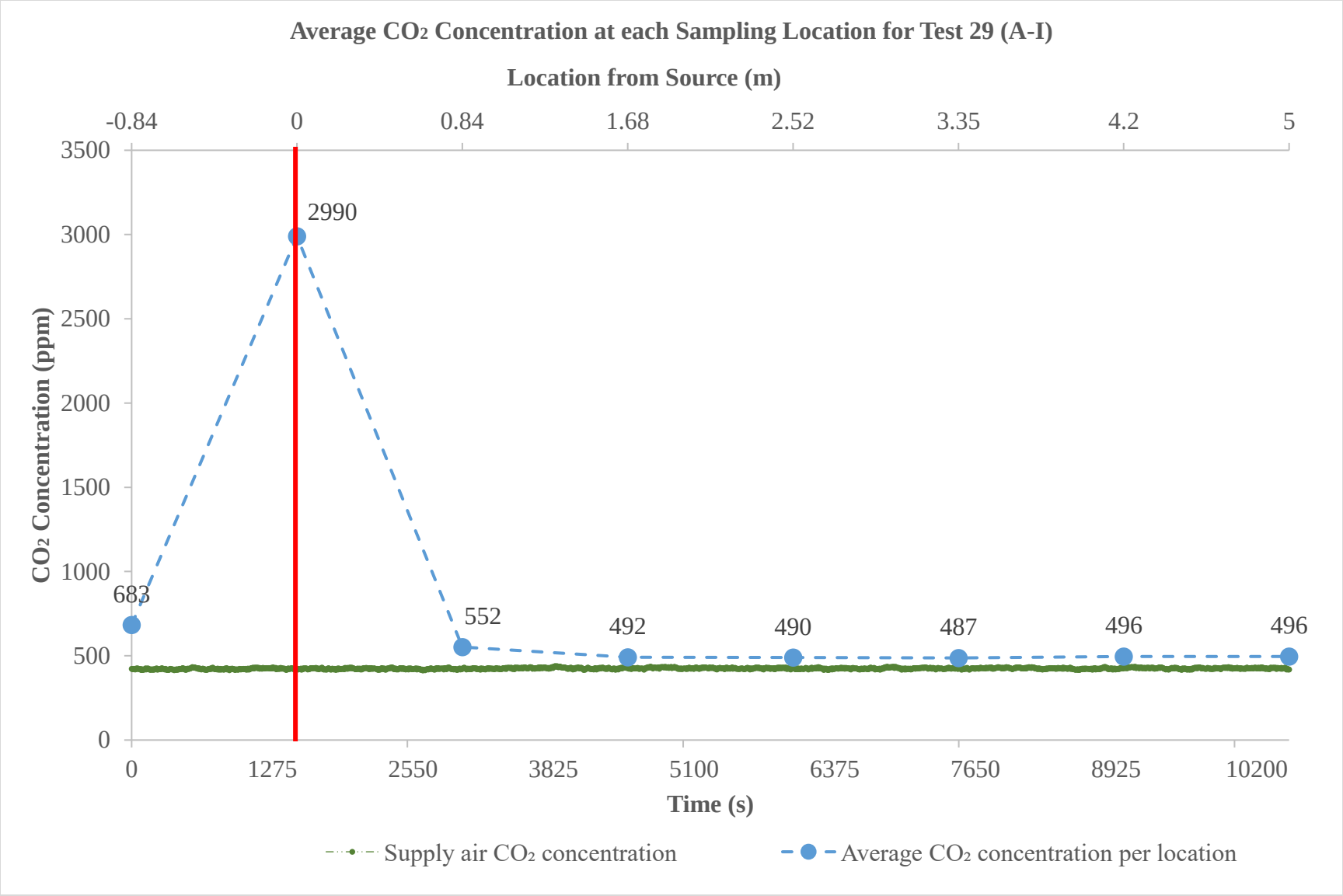

Figure E.37 Average CO_2 concentration at each sampling location for Test 29 (A-I) ISOPass undeployed.

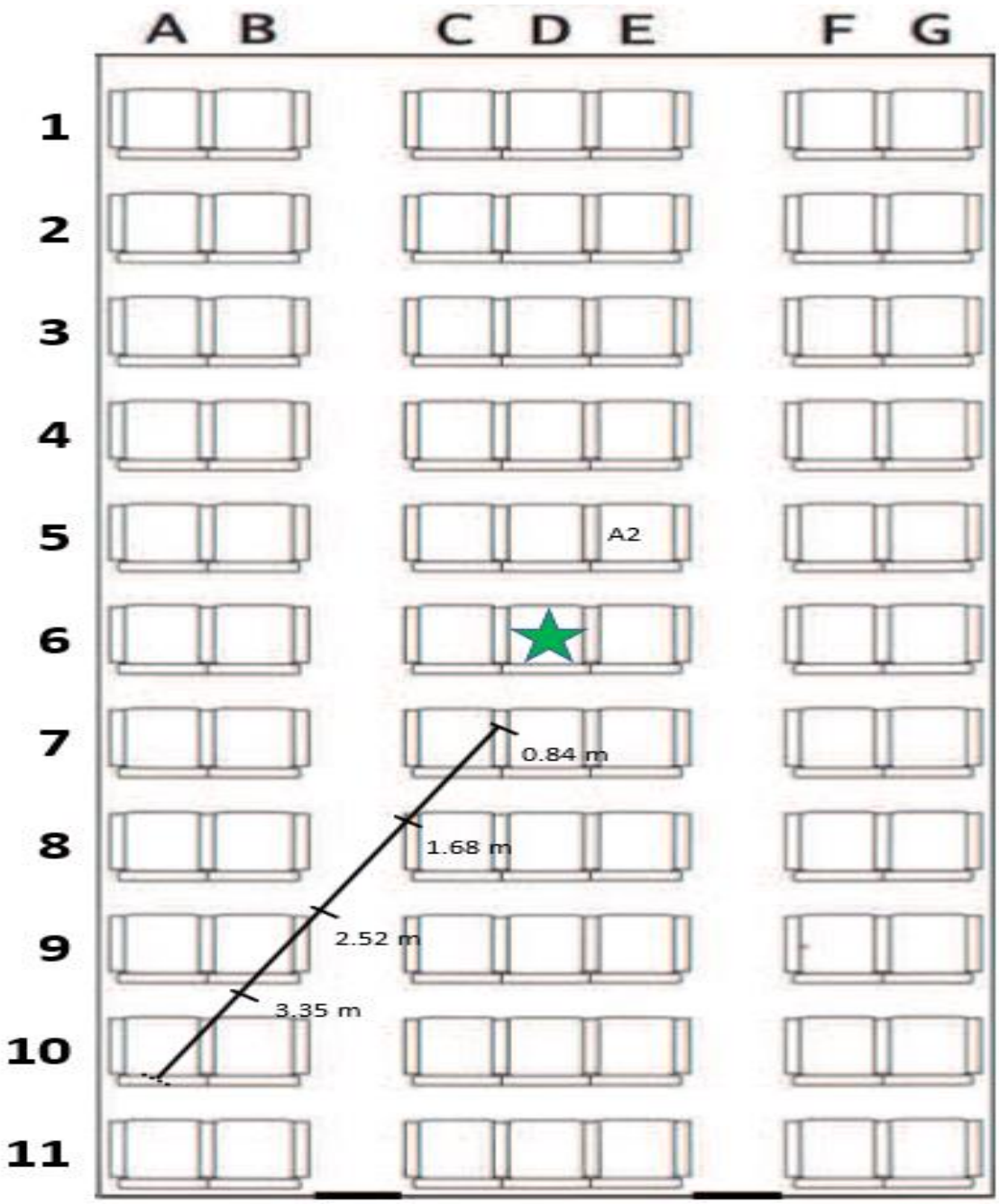

Figure E.38 Test 30 (A-I) ISOPass undeployed source location and sampling tree orientation.

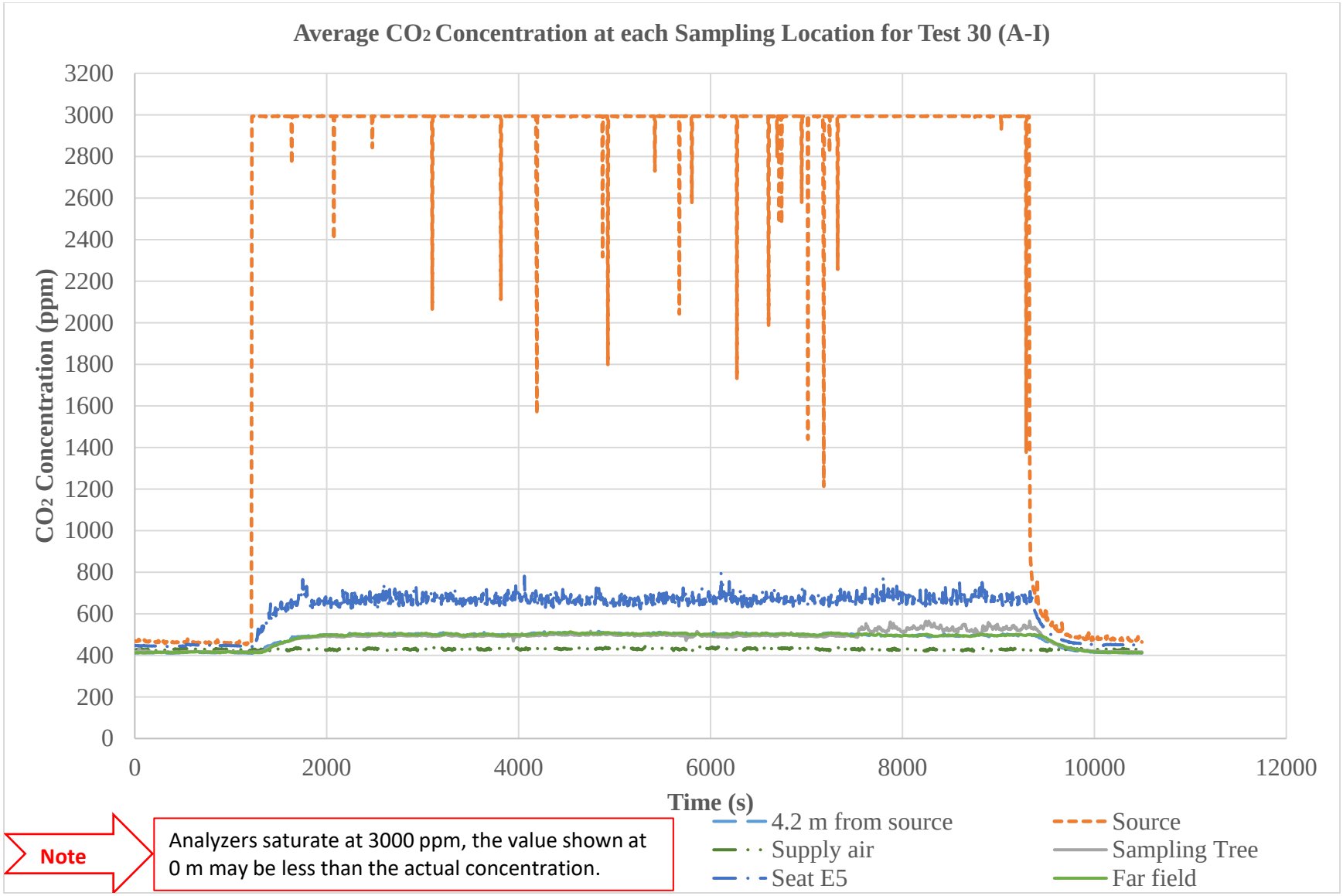

Figure E.39 Ininstantaneous CO_2 concentration at each sampling location for Test 30 (A-I) ISOPass undeployed.

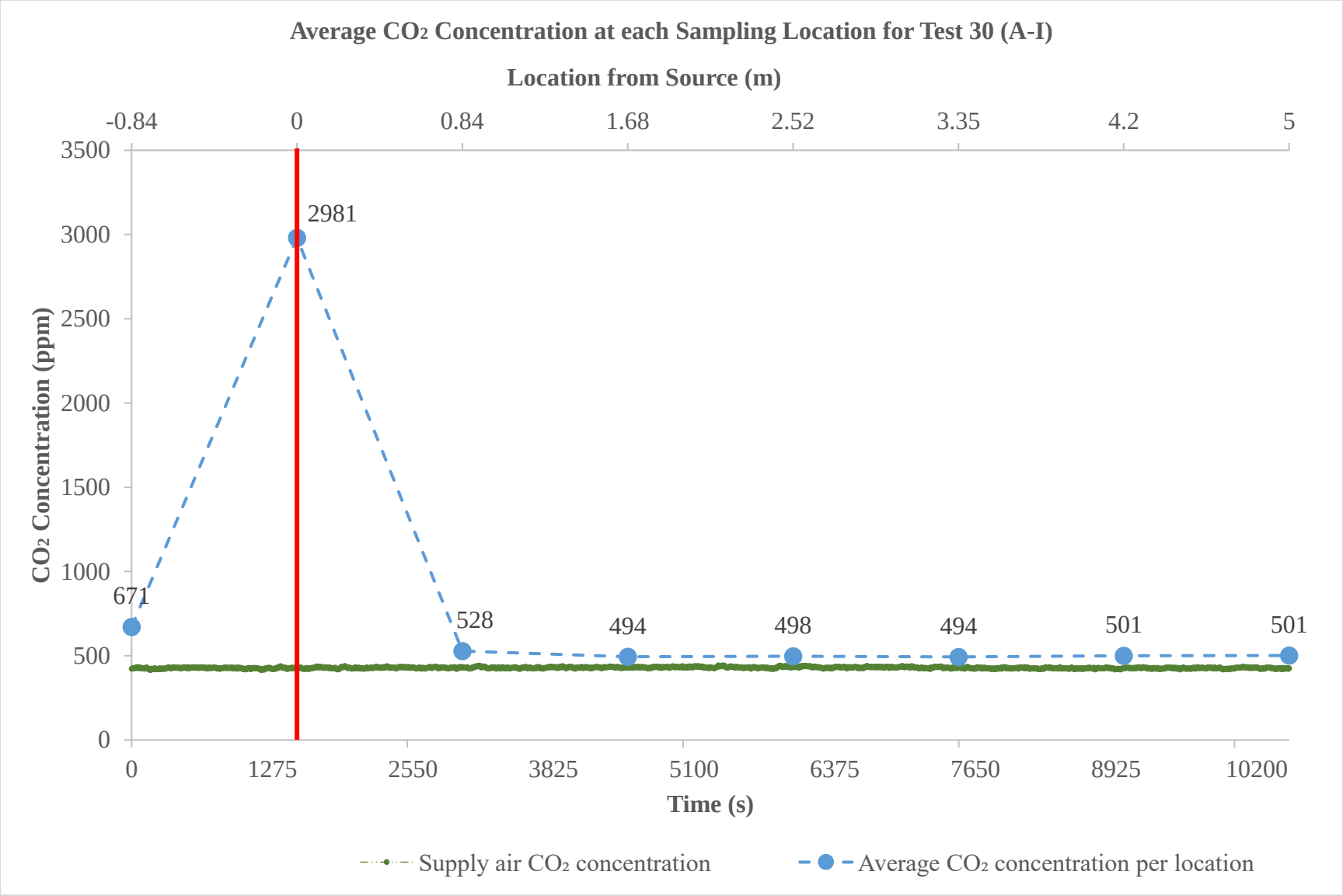

Figure E.40 Average CO_2 concentration at each sampling location for Test 30 (A-I) ISOPass undeployed.

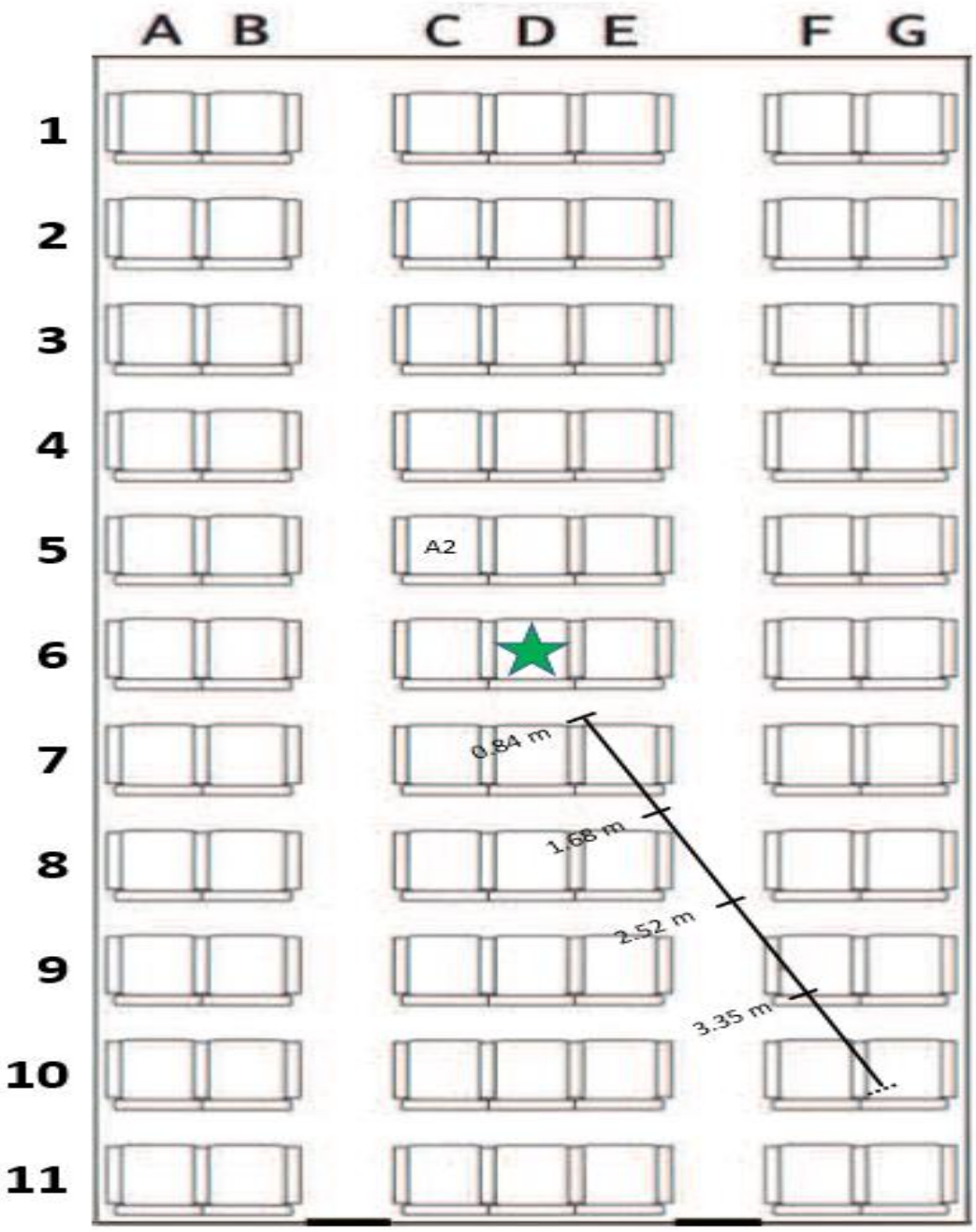

Figure E.41 Test 31 (A-I) ISOPass undeployed source location and sampling tree orientation.

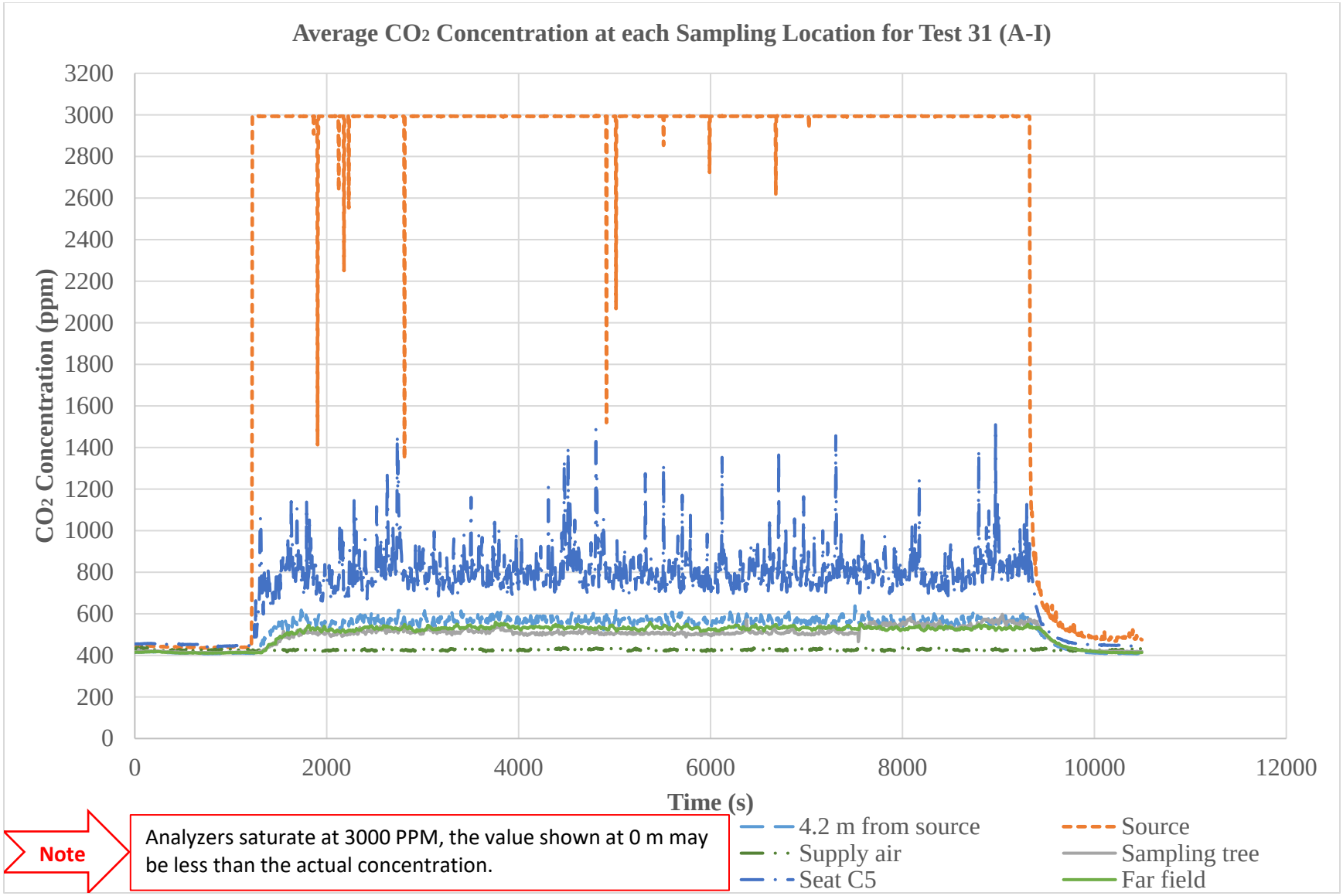

Figure E.42 Ininstantaneous CO_2 concentration at each sampling location for Test 31 (A-I) ISOPass undeployed.

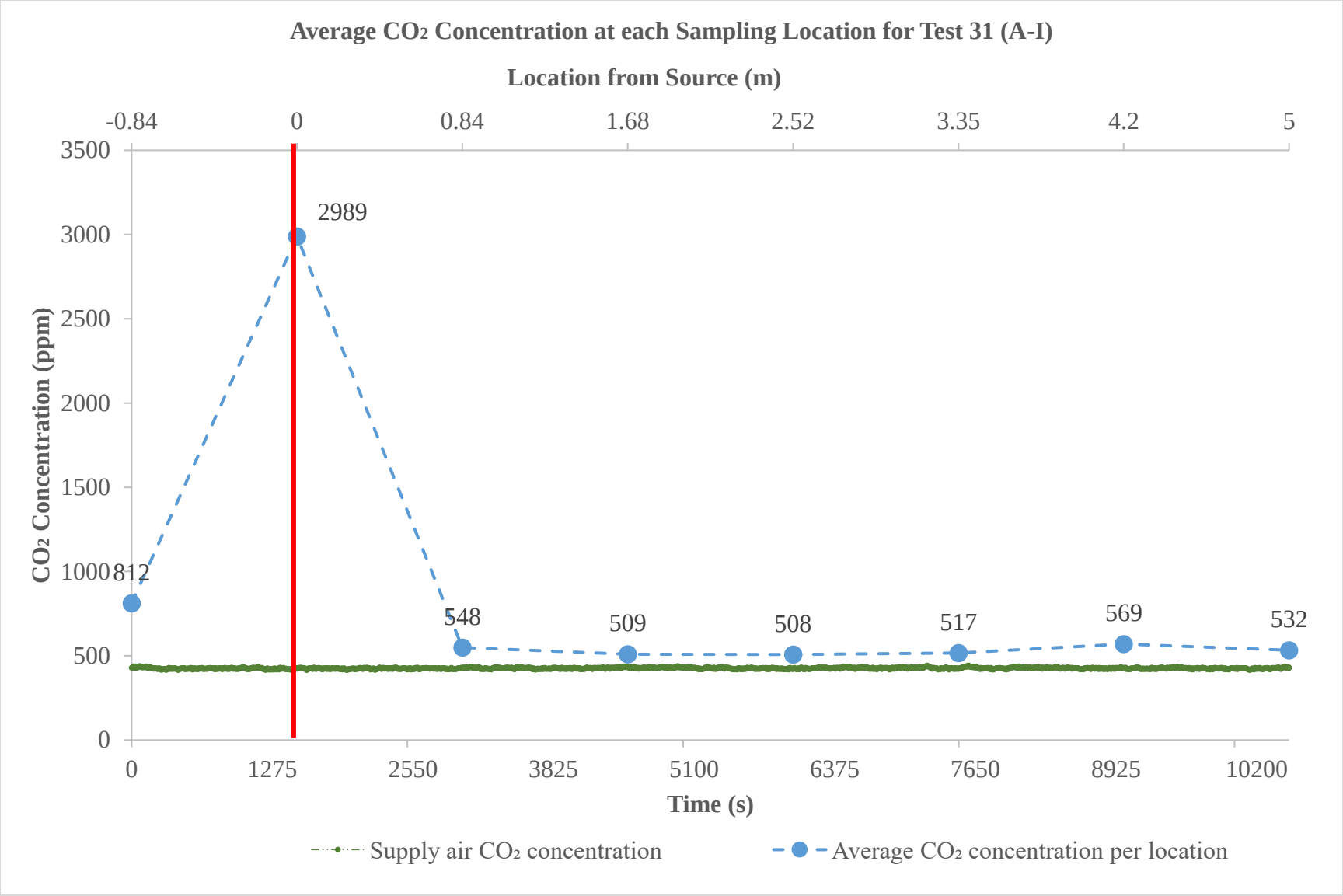

Figure E.43 Average CO_2 concentration at each sampling location for Test 31 (A-I) ISOPass undeployed.

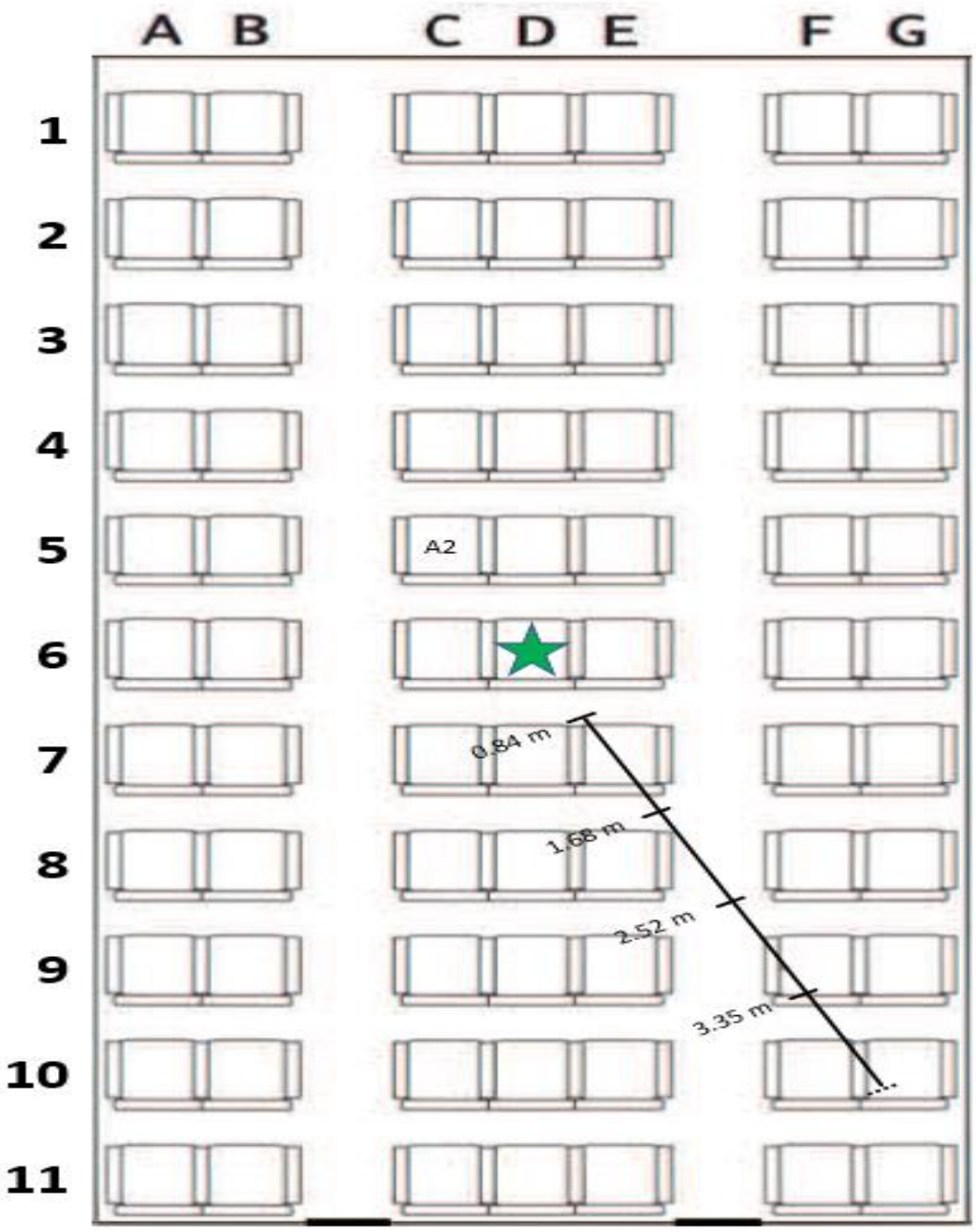

Figure E.44 Test 32 (A-I) ISOPass undeployed source location and sampling tree orientation.

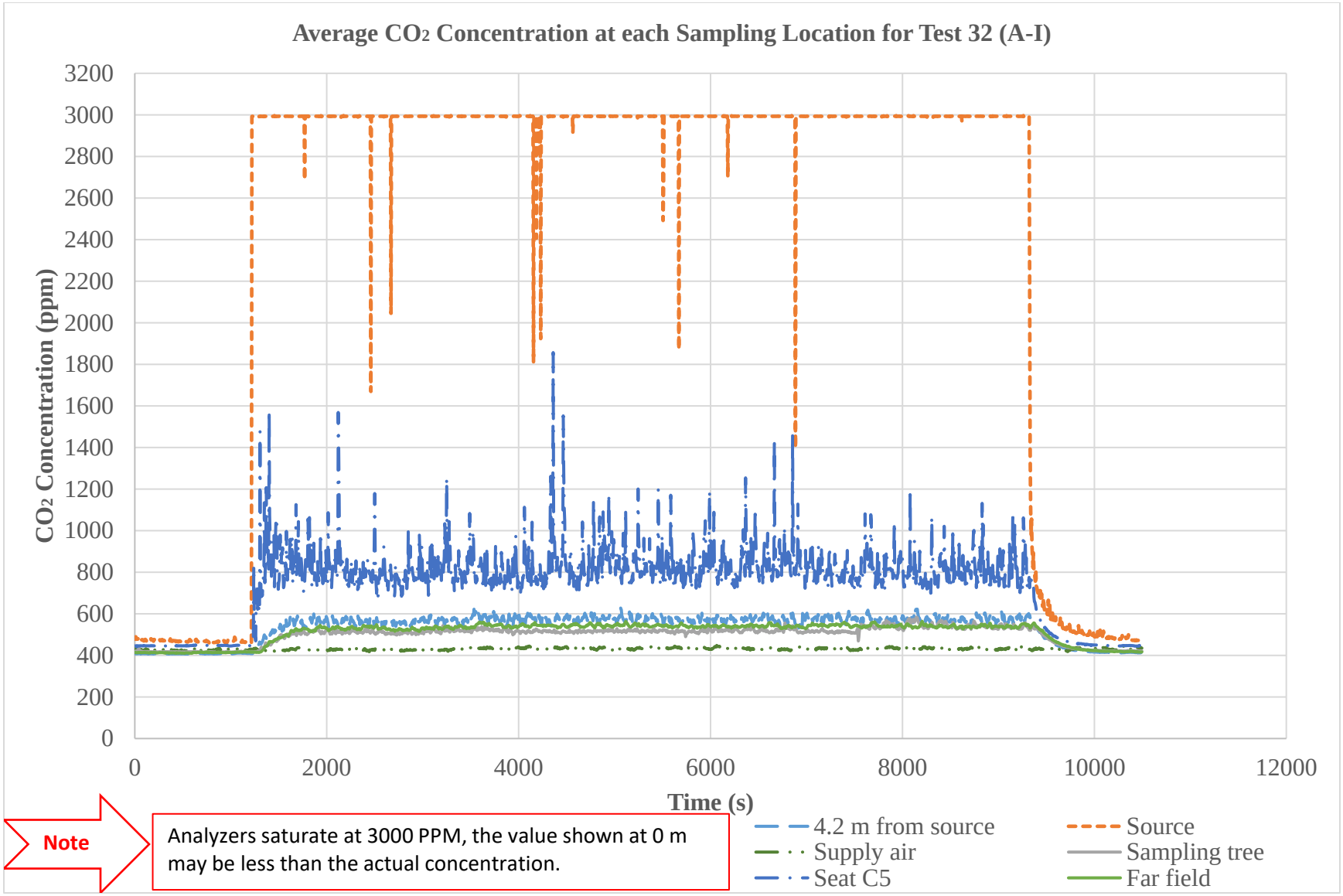

Figure E.45 Ininstantaneous CO_2 concentration at each sampling location for Test 32 (A-I) ISOPass undeployed.

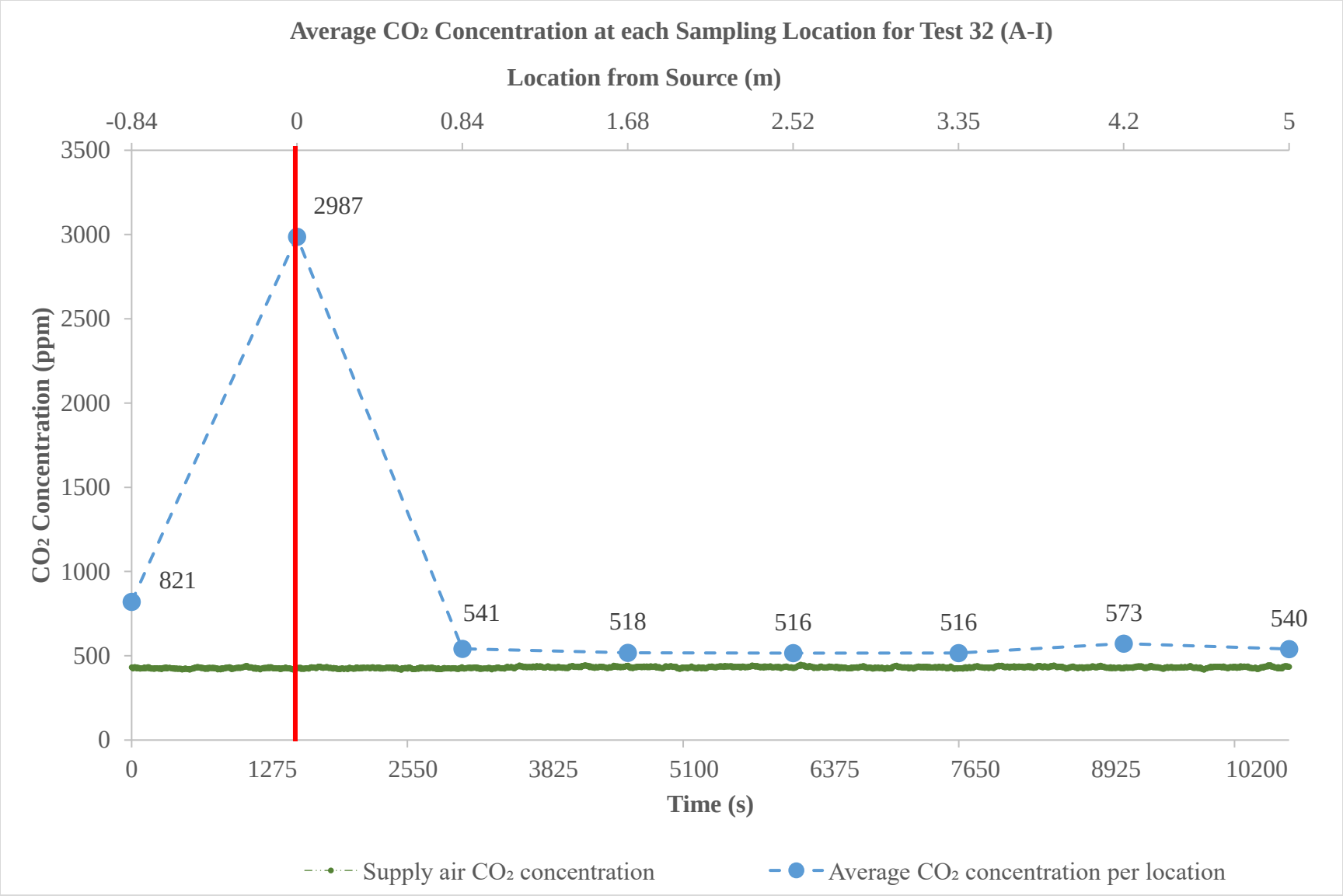

Figure E.46 Average CO_2 concentration at each sampling location for Test 32 (A-I) ISOPass undeployed.

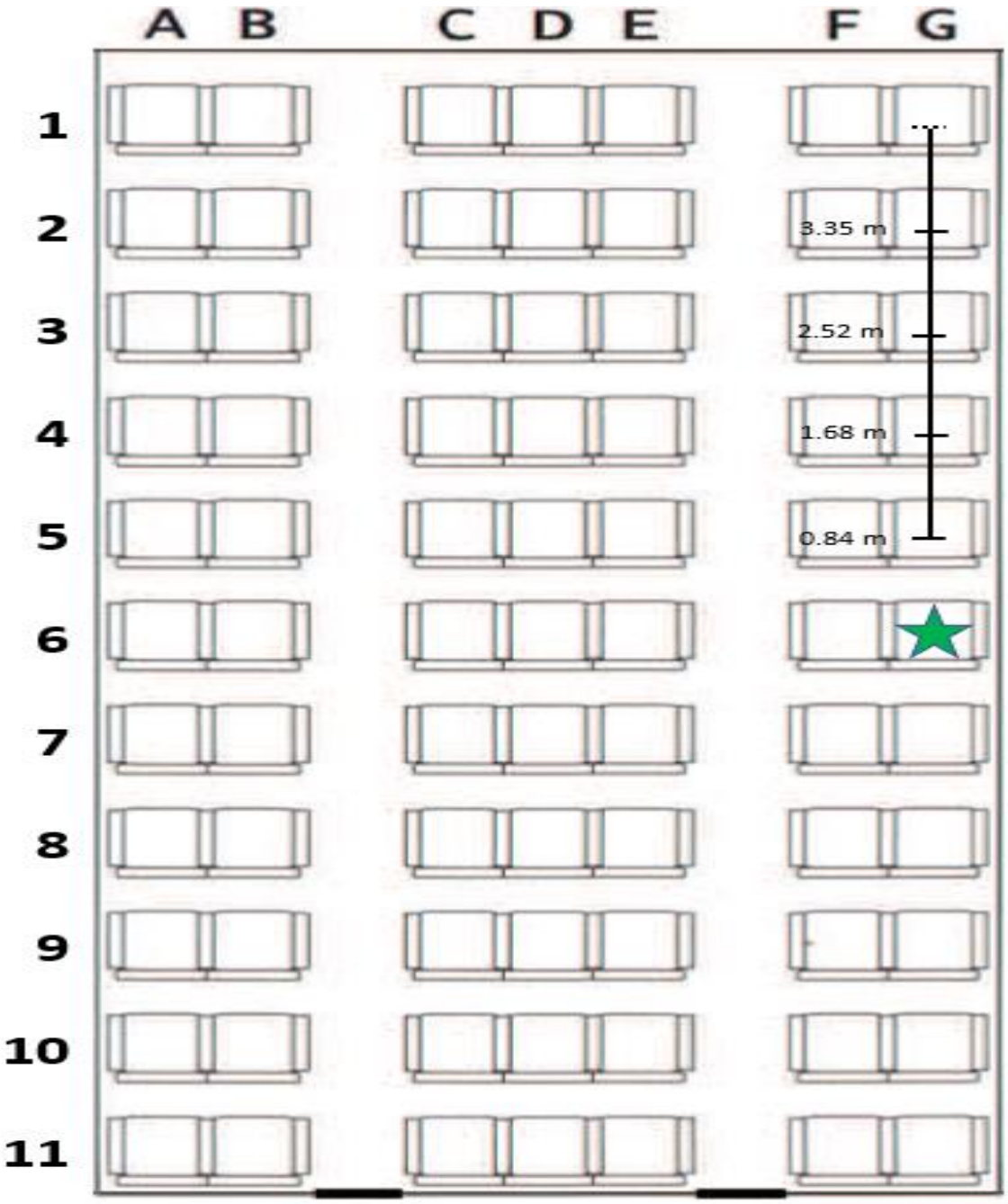

Figure E.47 Test 1 (A-I) ISOPass undeployed source location and sampling tree orientation.

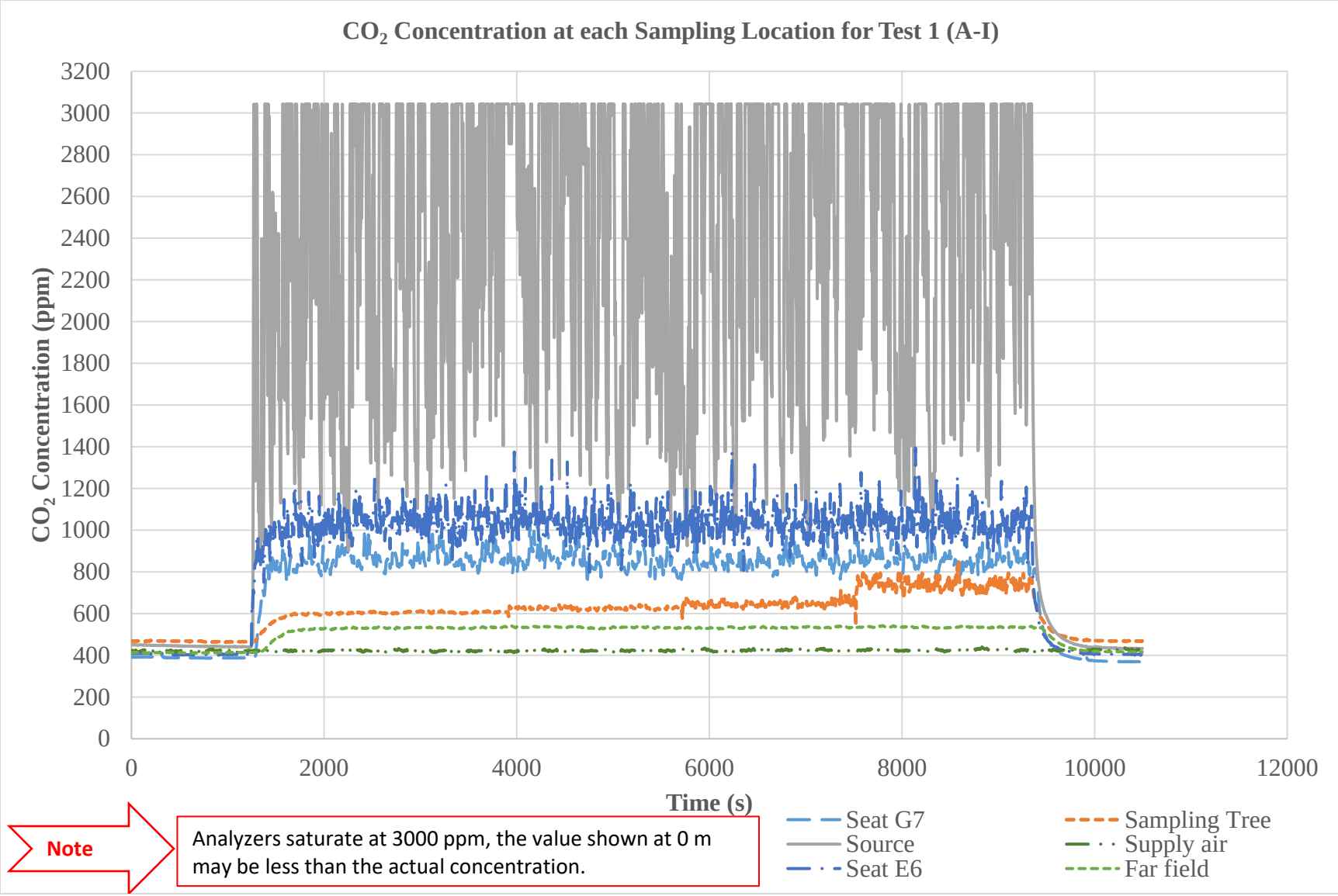

Figure E.48 Ininstantaneous CO_2 concentration at each sampling location for Test 1 (A-I) ISOPass undeployed.

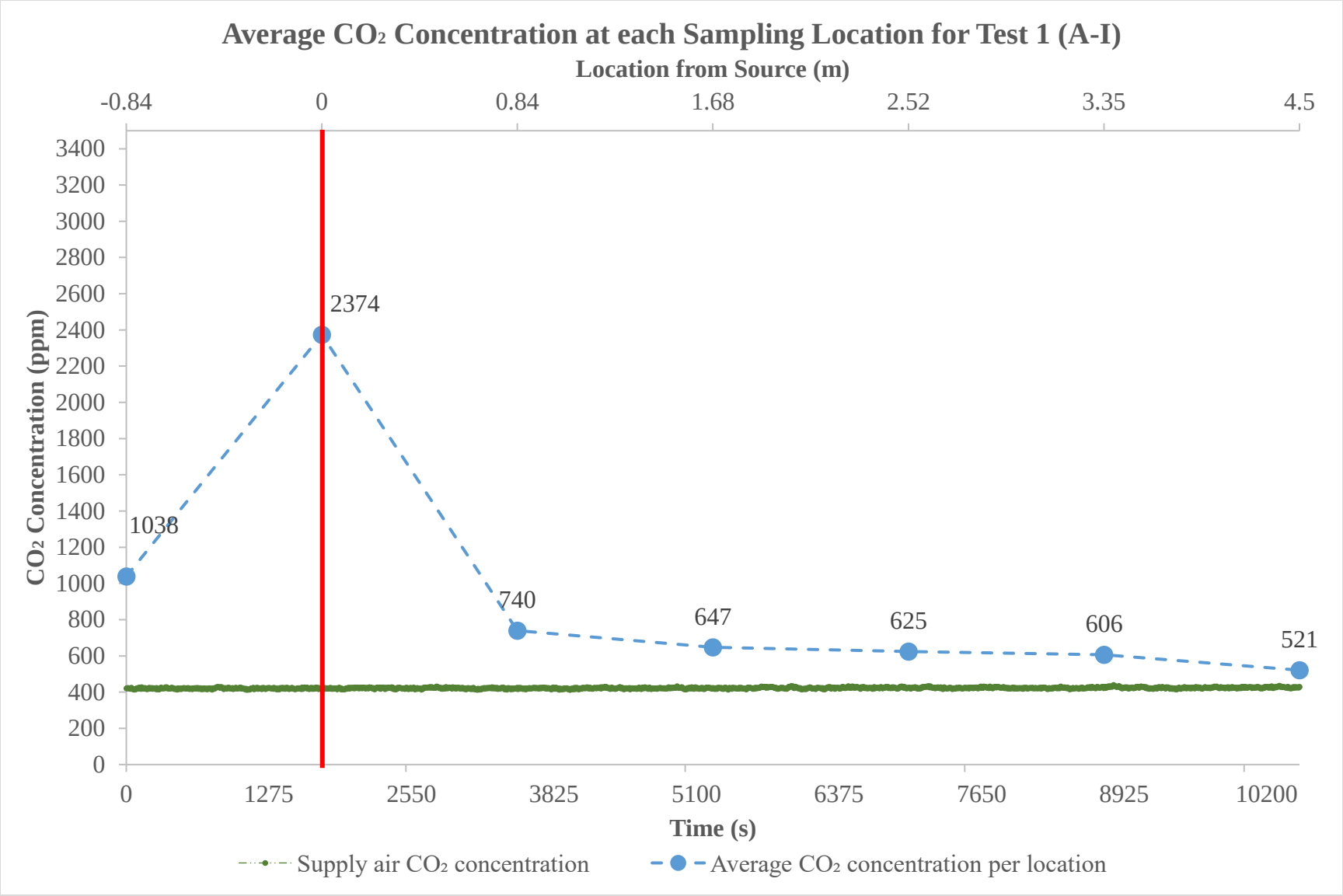

Figure E.49 Average CO_2 concentration at each sampling location for Test 1 (A-I) ISOPass undeployed.

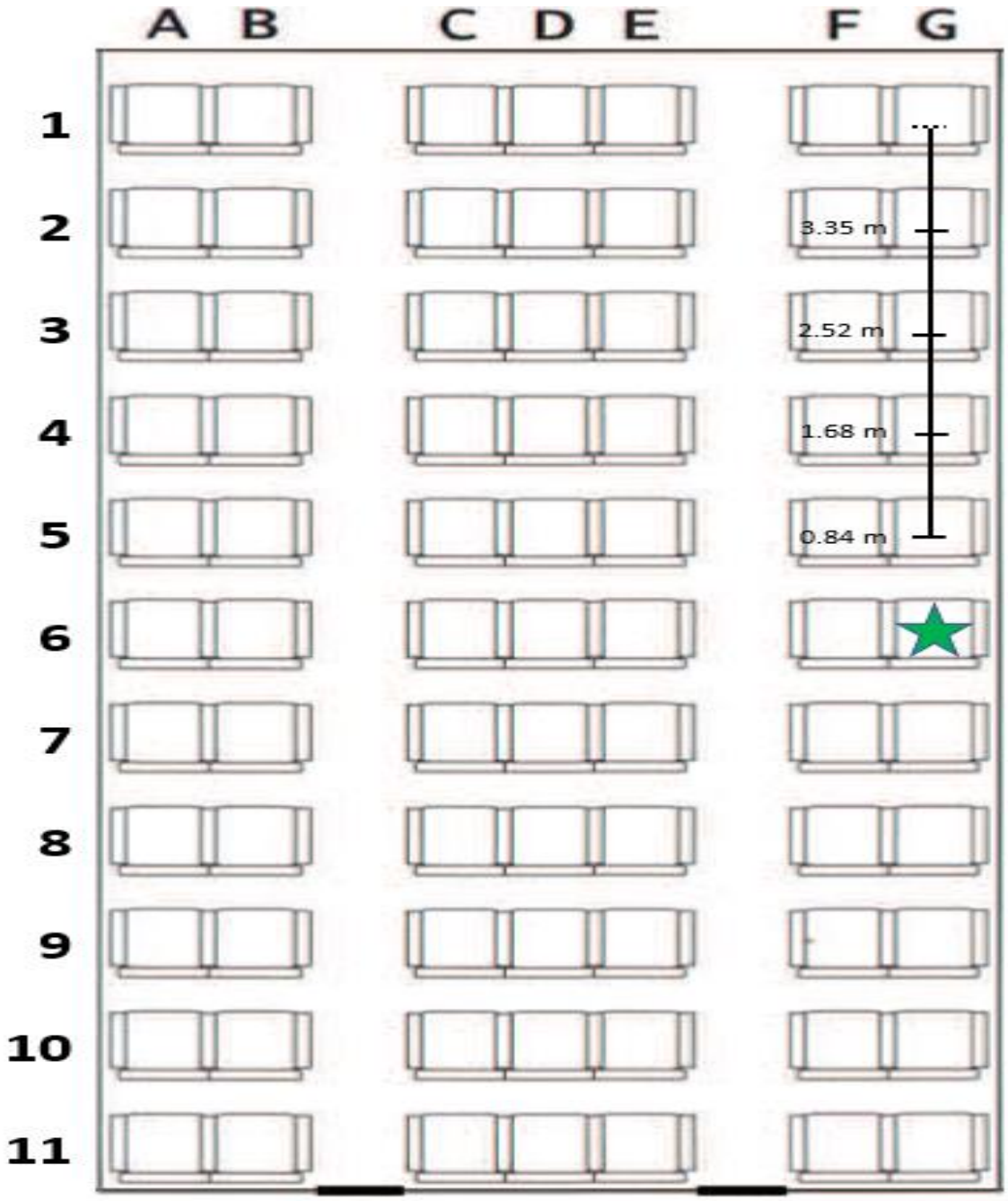

Figure E.50 Test 2 (A-I) ISOPass undeployed source location and sampling tree orientation.

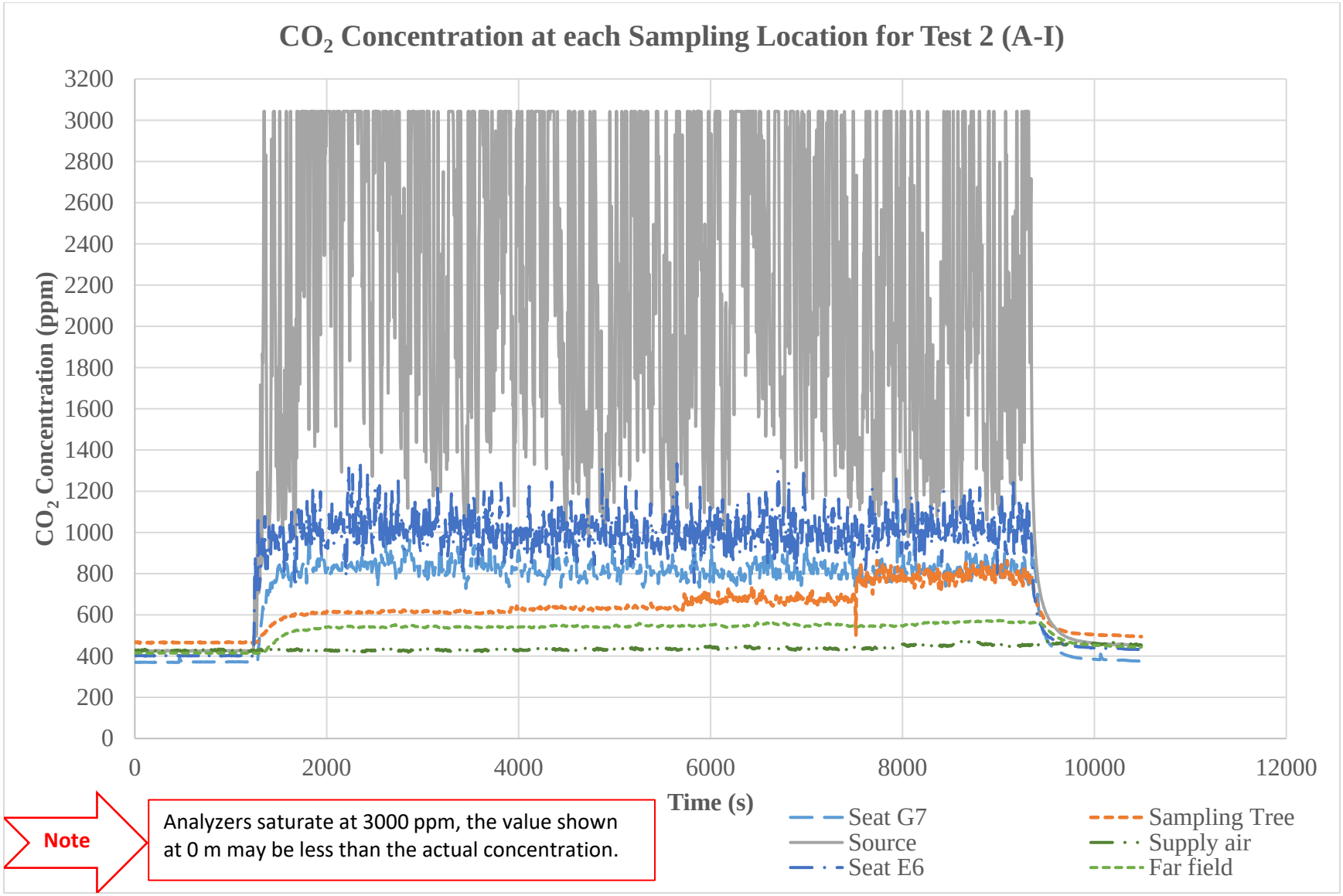

Figure E.51 Ininstantaneous CO_2 concentration at each sampling location for Test 2 (A-I) ISOPass undeployed.

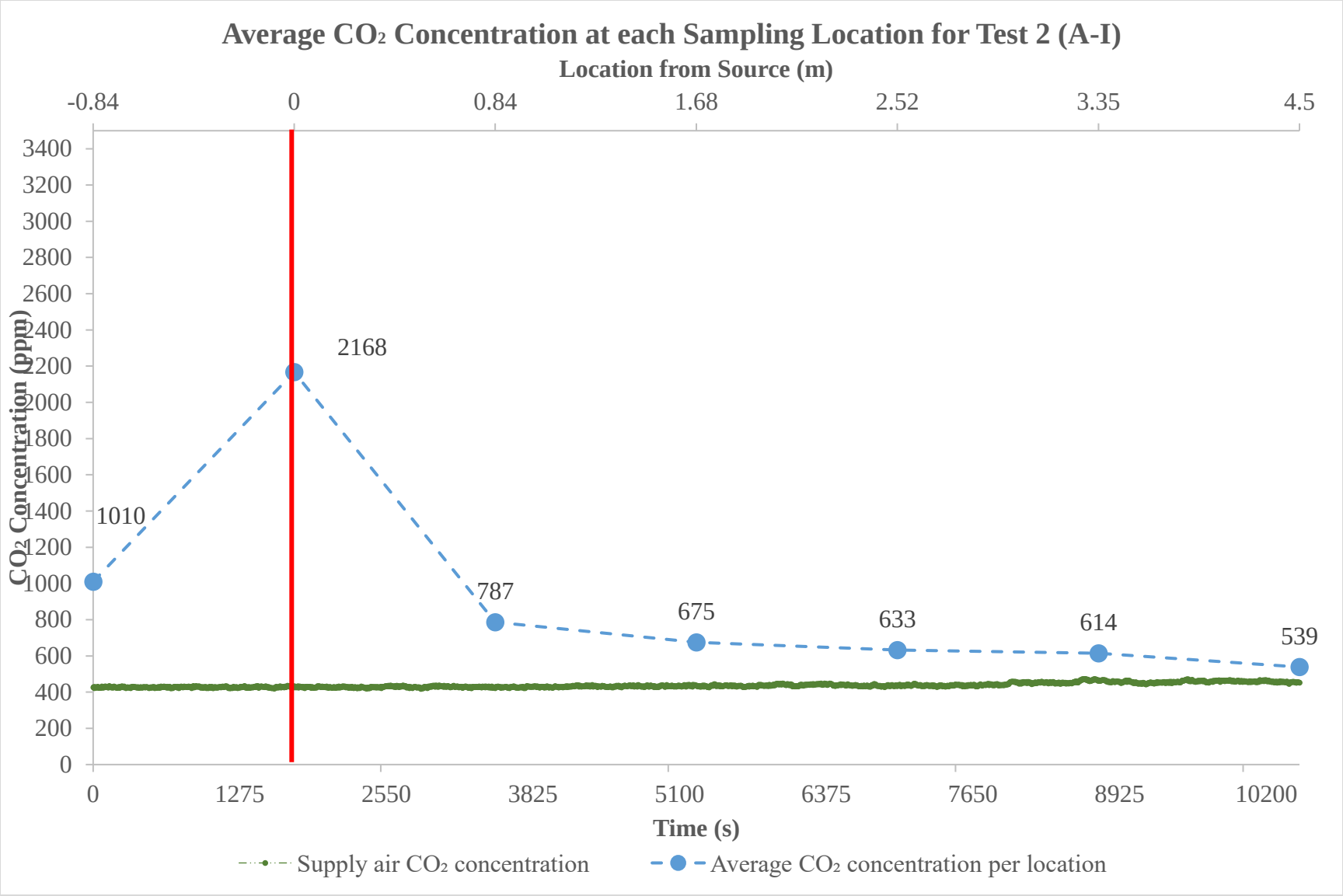

Figure E.52 Average CO_2 concentration at each sampling location for Test 2 (A-I) ISOPass undeployed.

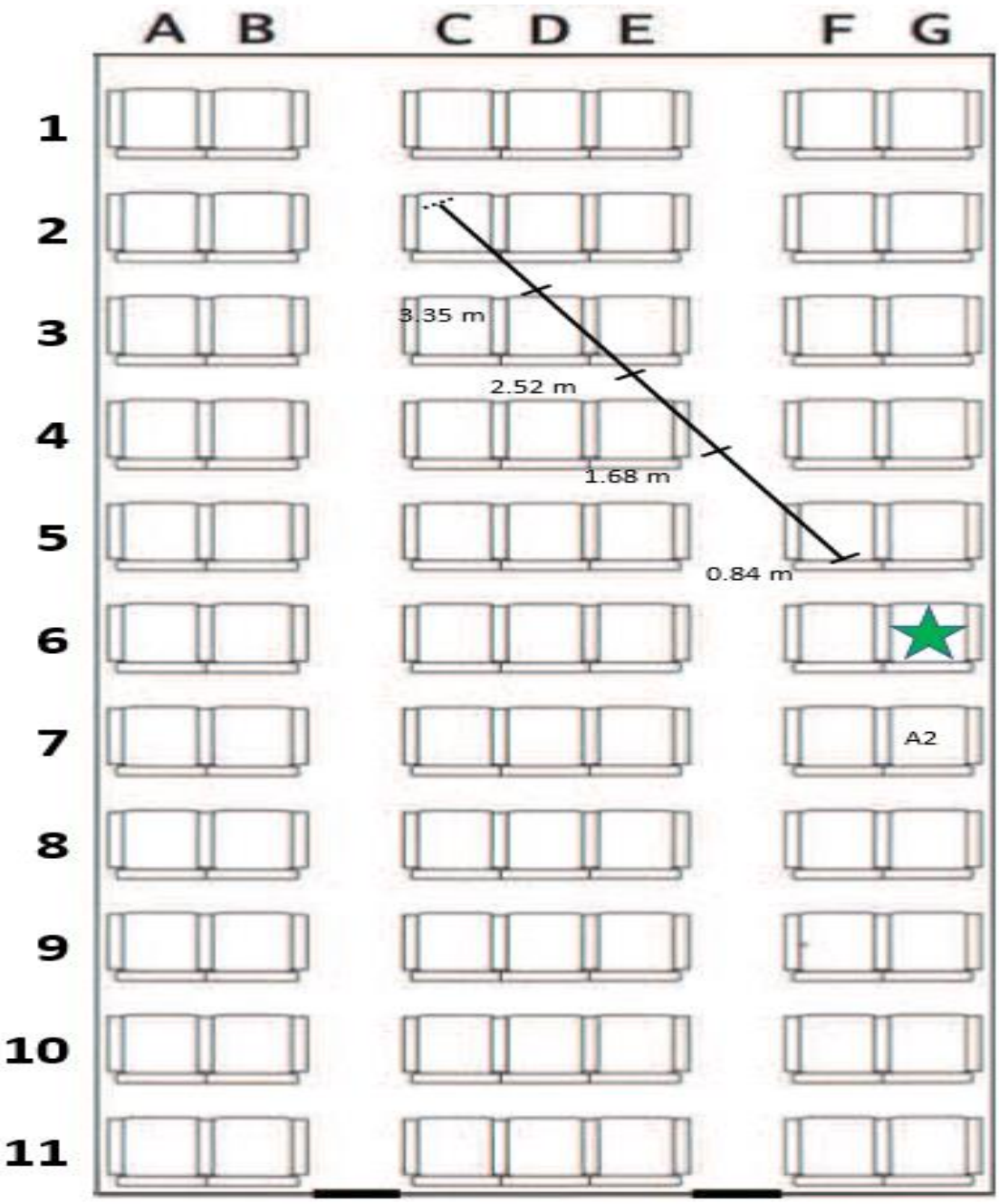

Figure E.53 Test 3 (A-I) ISOPass undeployed source location and sampling tree orientation.

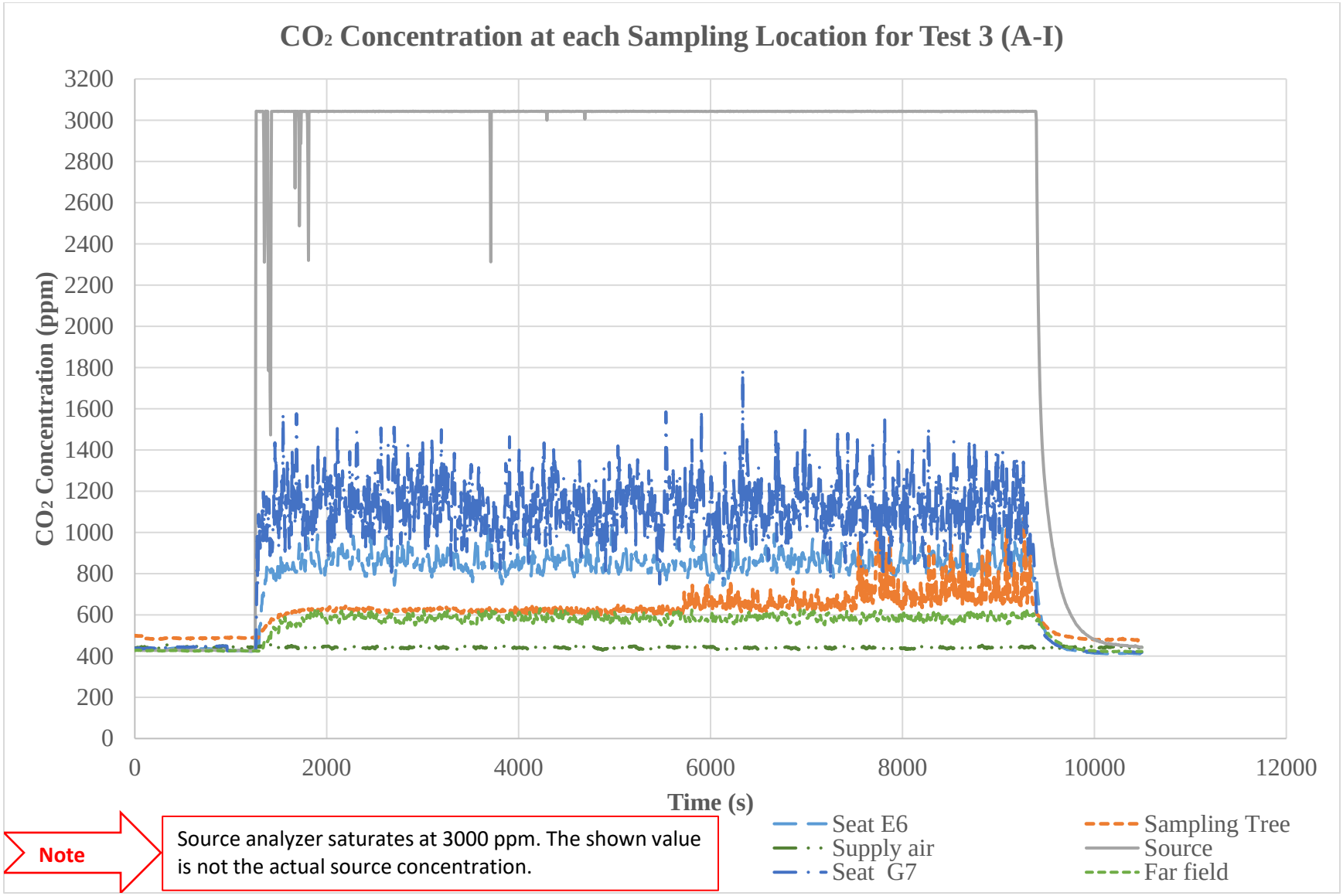

Figure E.54 Ininstantaneous CO_2 concentration at each sampling location for Test 3 (A-I) ISOPass undeployed.

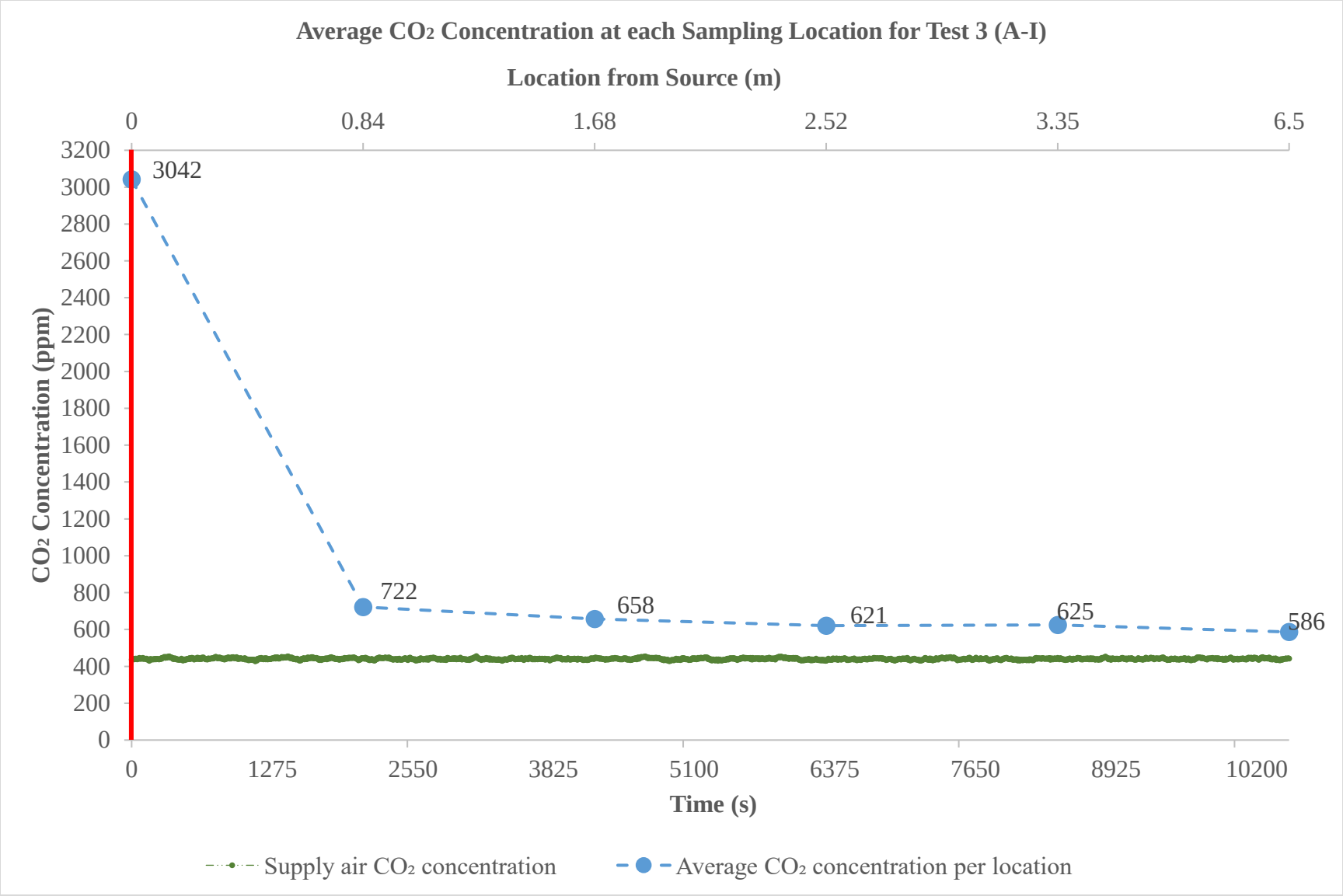

Figure E.55 Average CO_2 concentration at each sampling location for Test 3 (A-I) ISOPass undeployed.

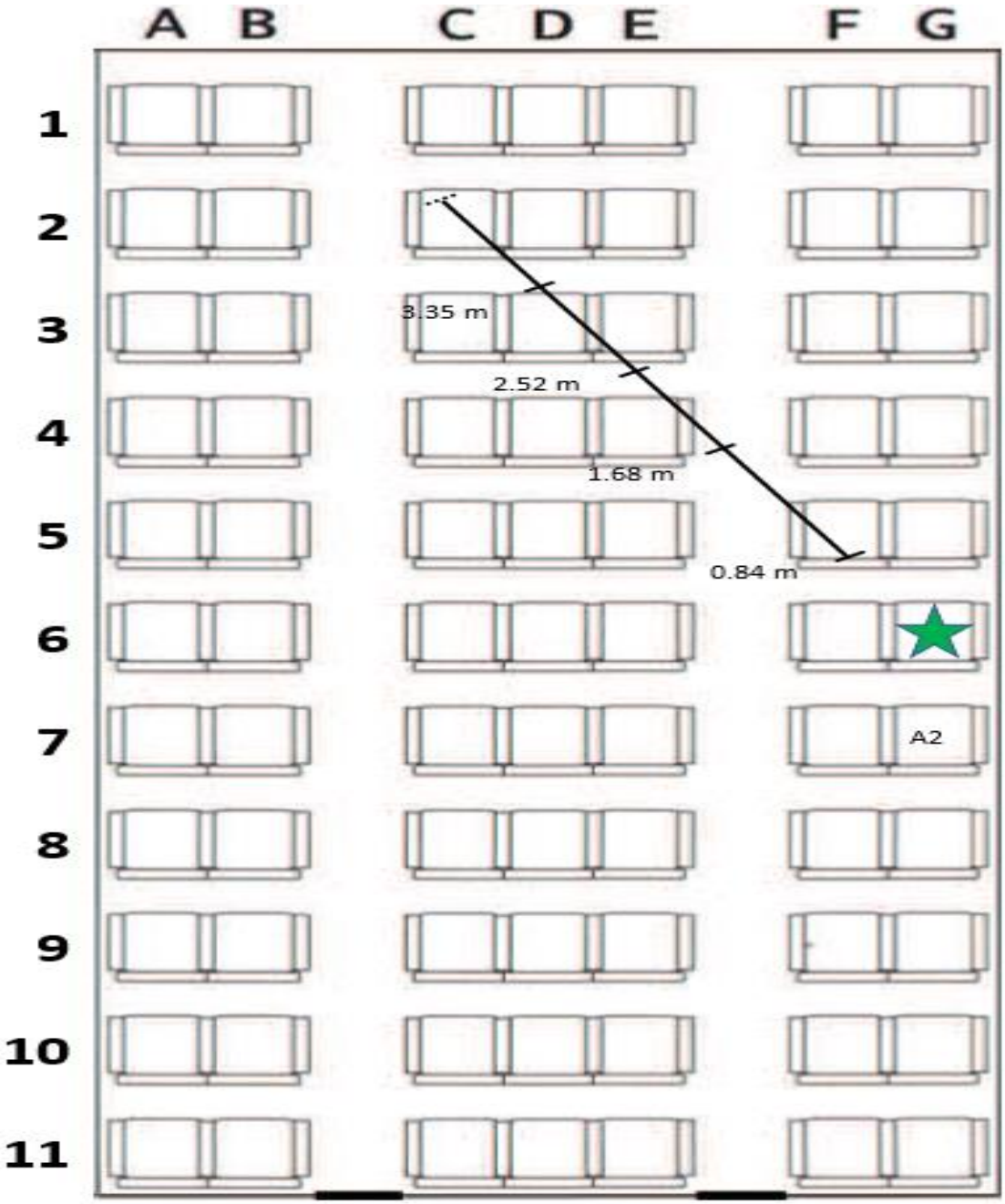

Figure E.56 Test 4 (A-I) ISOPass undeployed source location and sampling tree orientation.

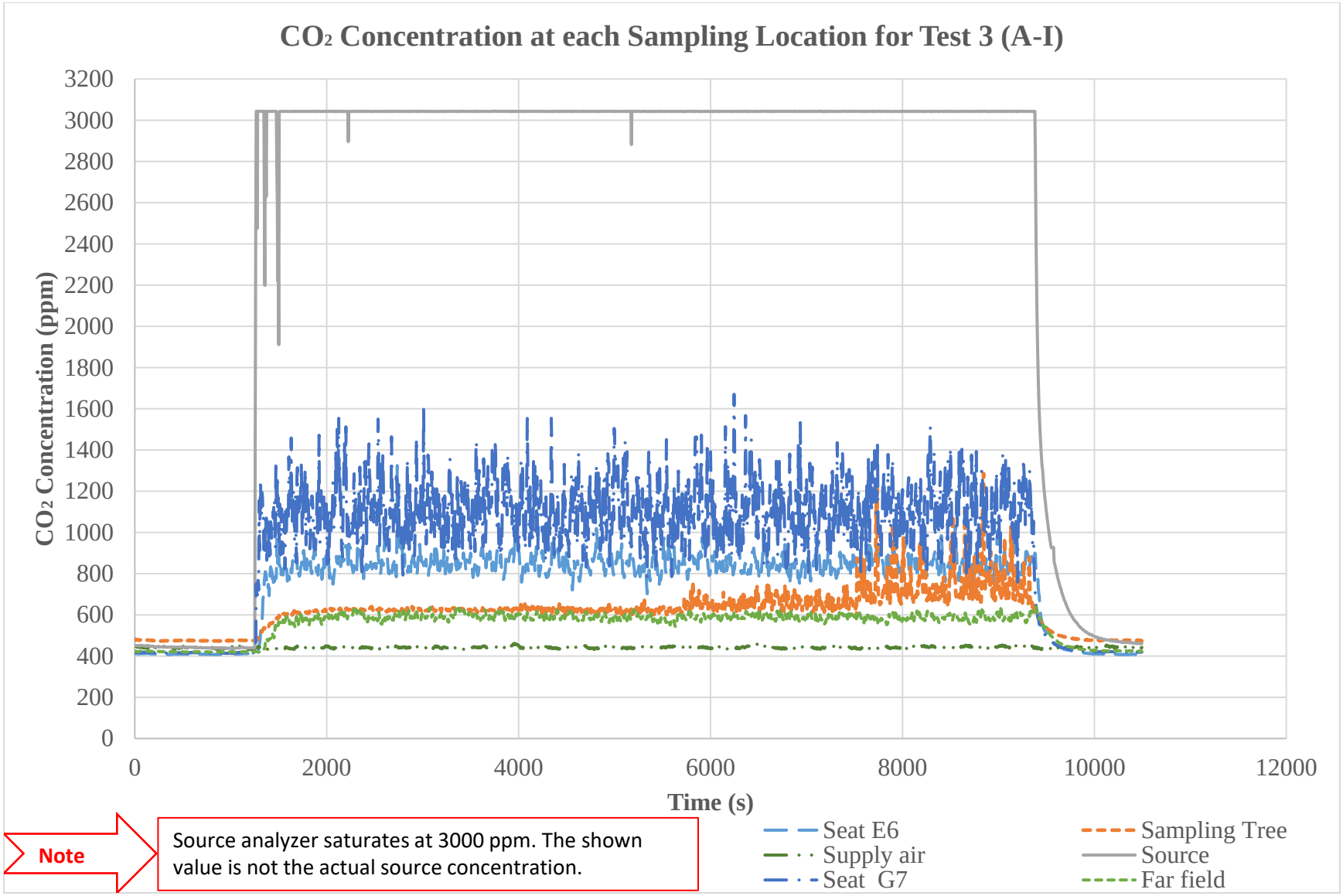

Figure E.57 Ininstantaneous CO_2 concentration at each sampling location for Test 4 (A-I) ISOPass undeployed.

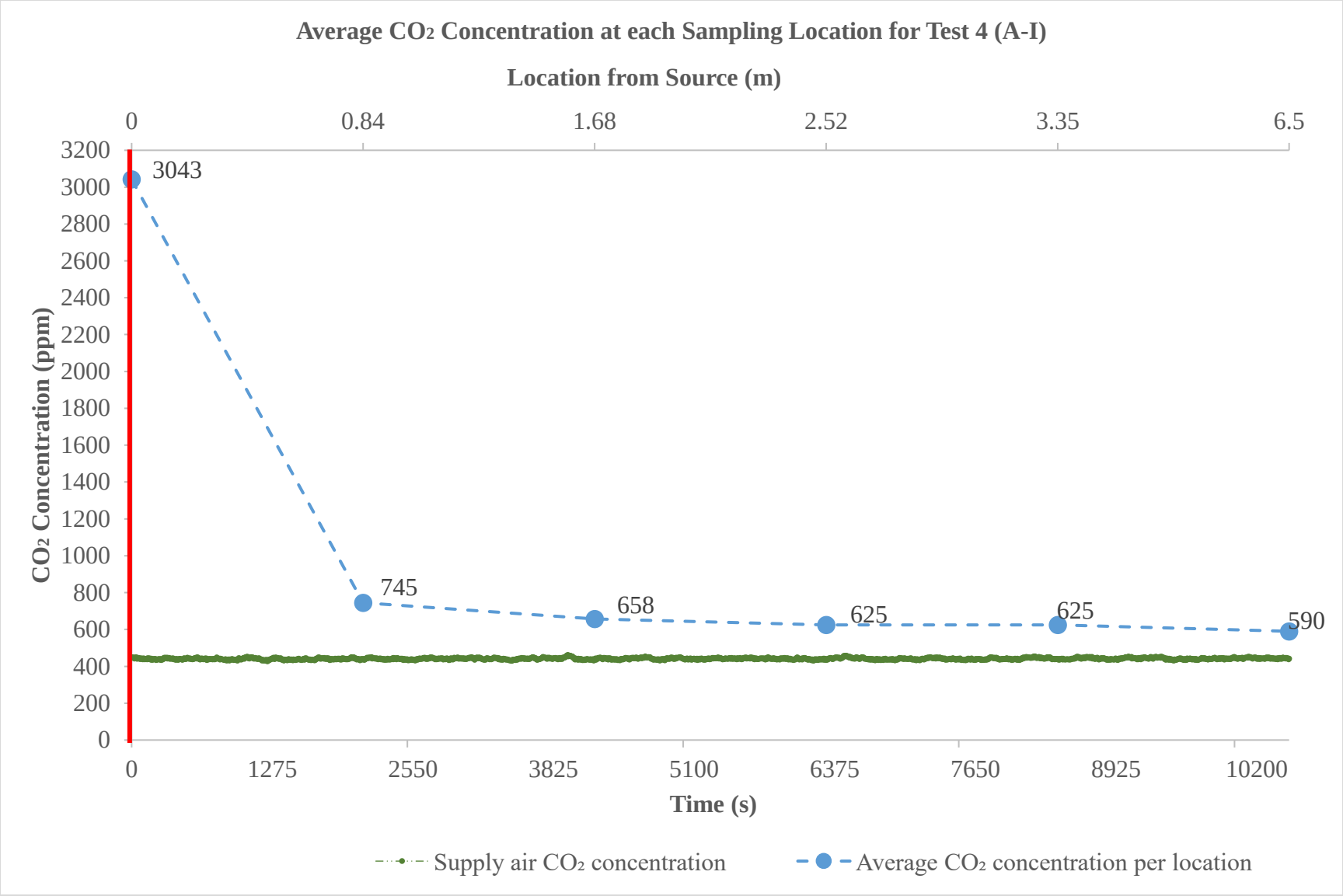

Figure E.58 Average CO_2 concentration at each sampling location for Test 4 (A-I) ISOPass undeployed.

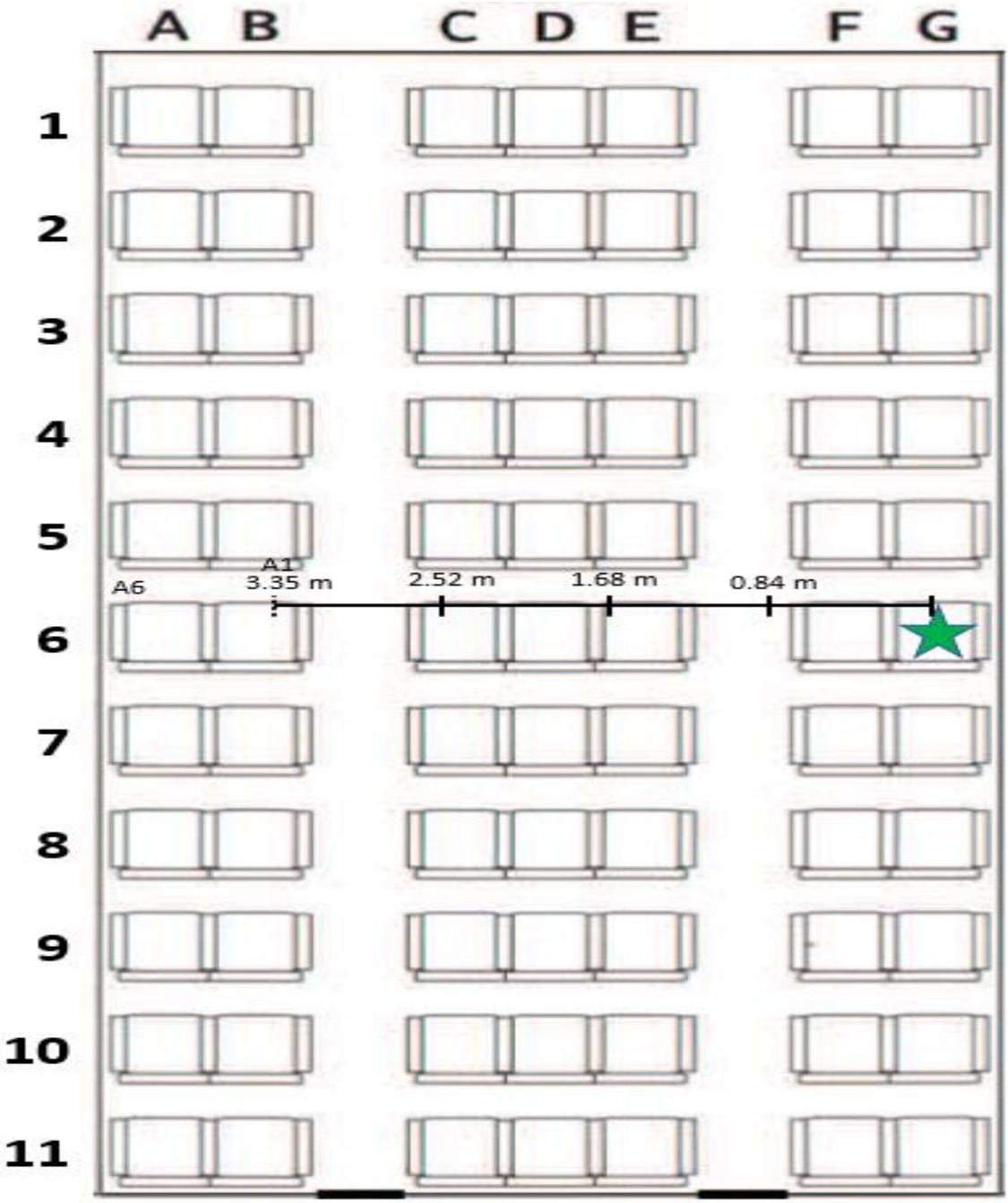

Figure E.59 Test 19 (A-I) ISOPass undeployed source location and sampling tree orientation.

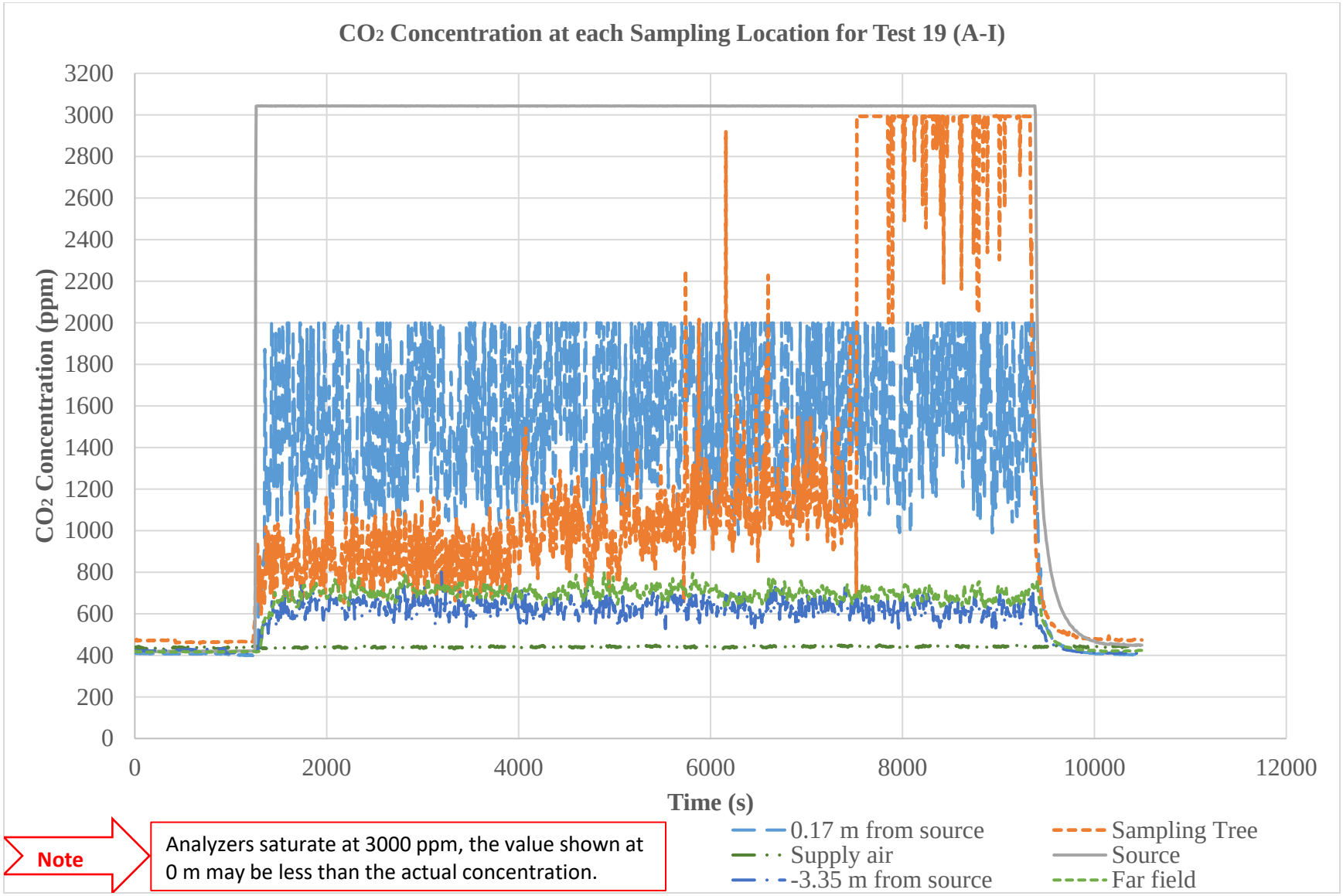

Figure E.60 Ininstantaneous CO_2 concentration at each sampling location for Test 19 (A-I) ISOPass undeployed.

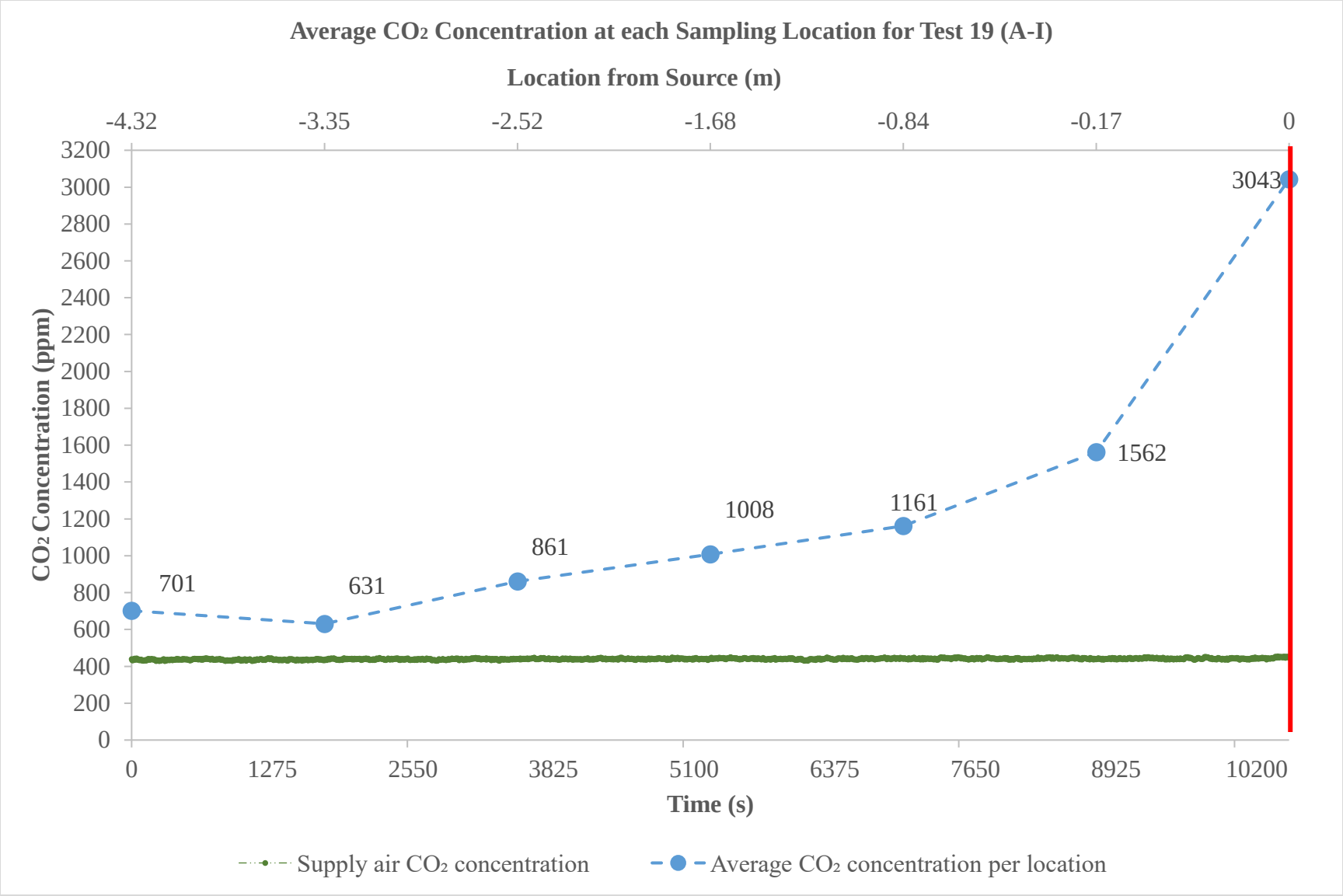

Figure E.61 Average CO_2 concentration at each sampling location for Test 19 (A-I) ISOPass undeployed.

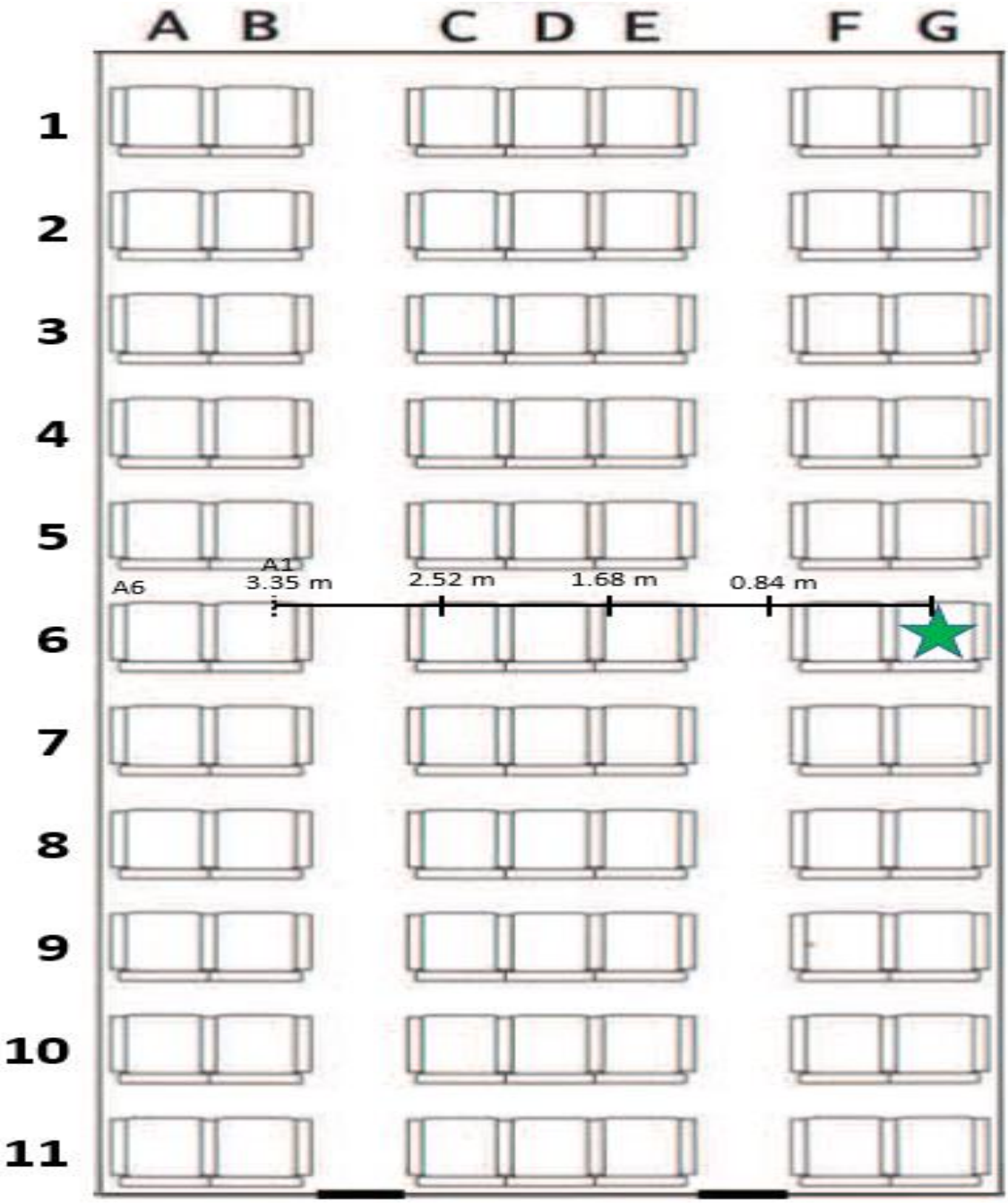

Figure E.62 Test 19 (A-I) ISOPass undeployed source location and sampling tree orientation.

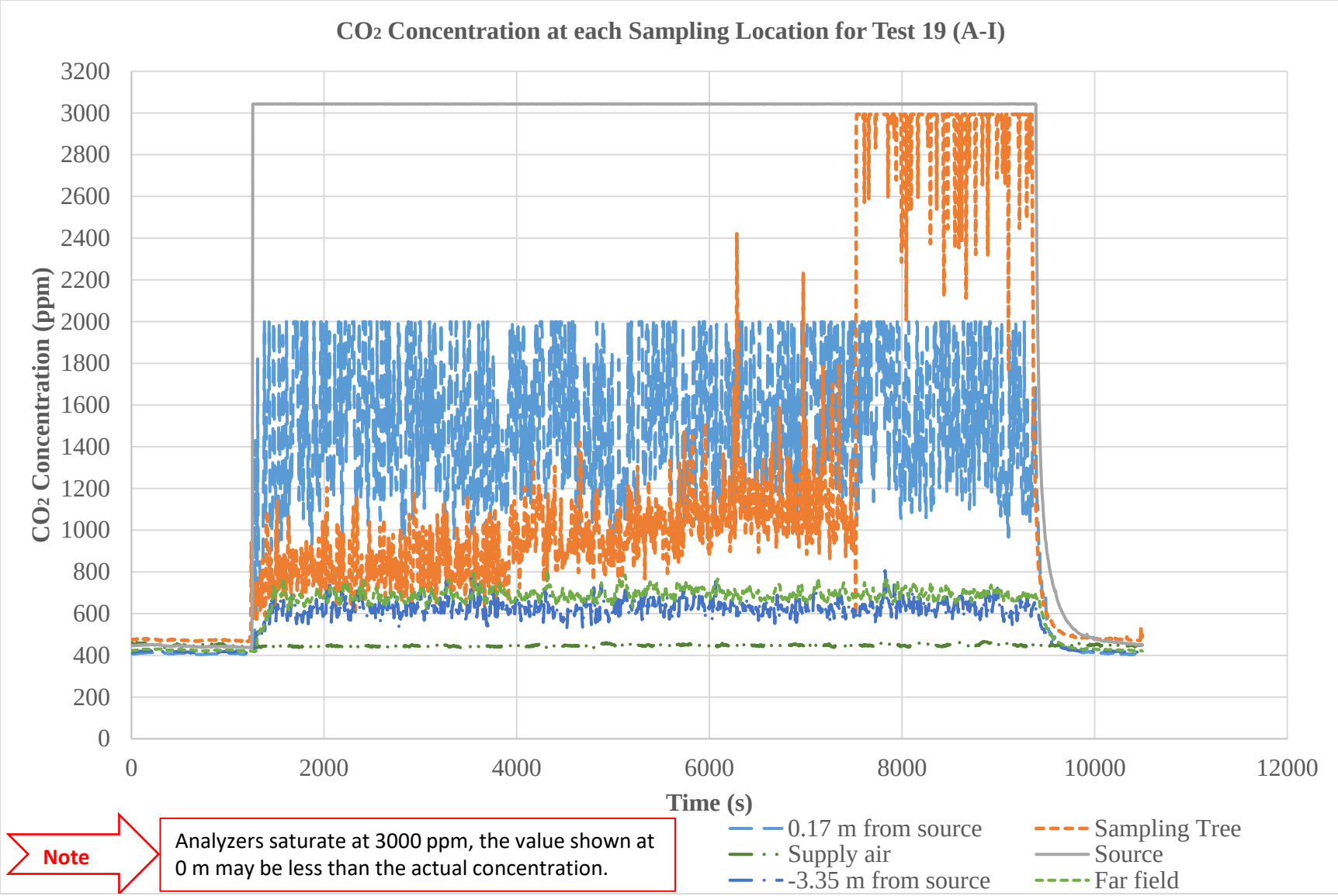

Figure E.63 Ininstantaneous CO_2 concentration at each sampling location for Test 19 (A-I) ISOPass undeployed.

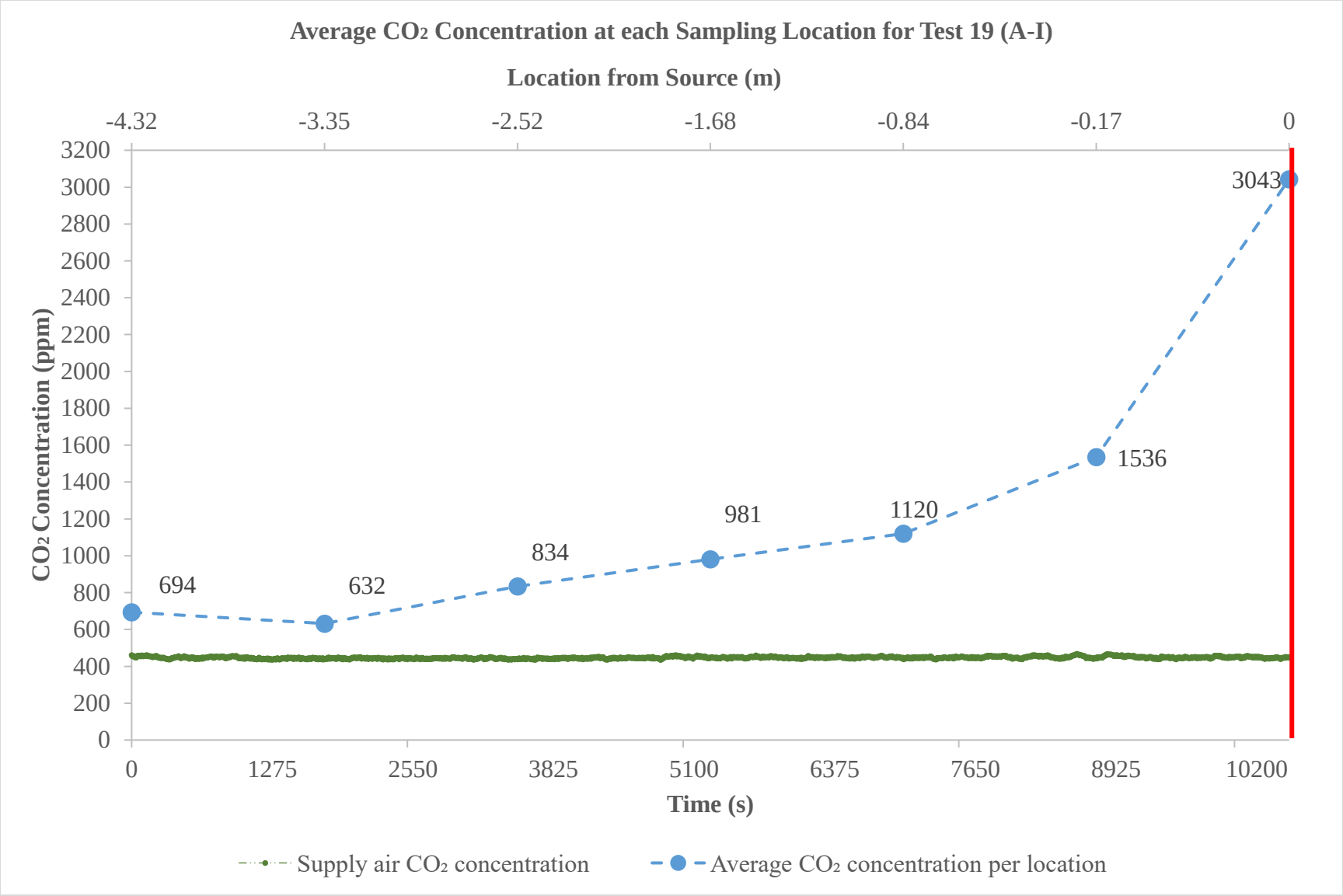

Figure E.64 Average CO_2 concentration at each sampling location for Test 19 (A-I) ISOPass undeployed.

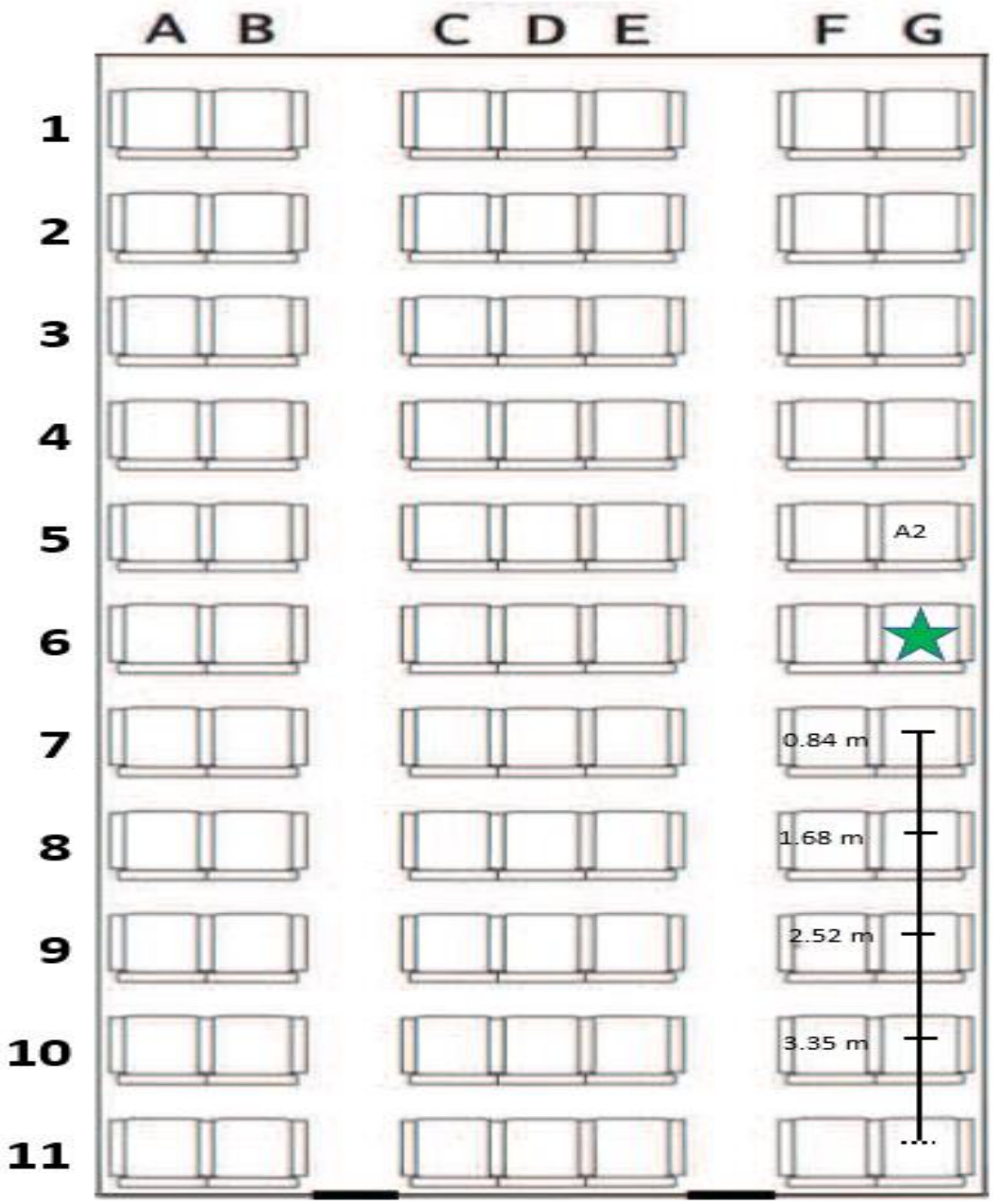

Figure E.65 Test 23 (A-I) ISOPass undeployed source location and sampling tree orientation.

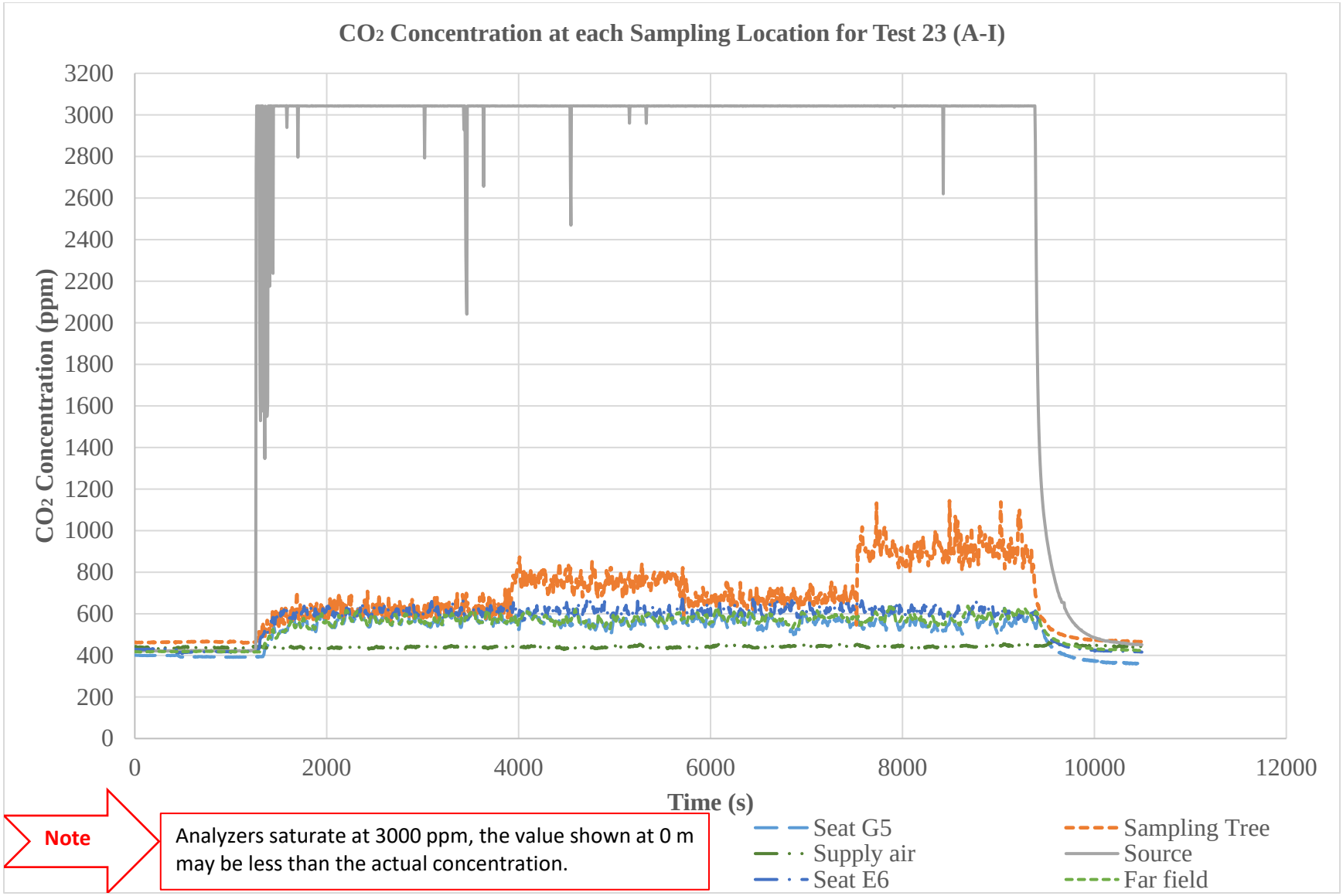

Figure E.66 Ininstantaneous CO_2 concentration at each sampling location for Test 23 (A-I) ISOPass undeployed.

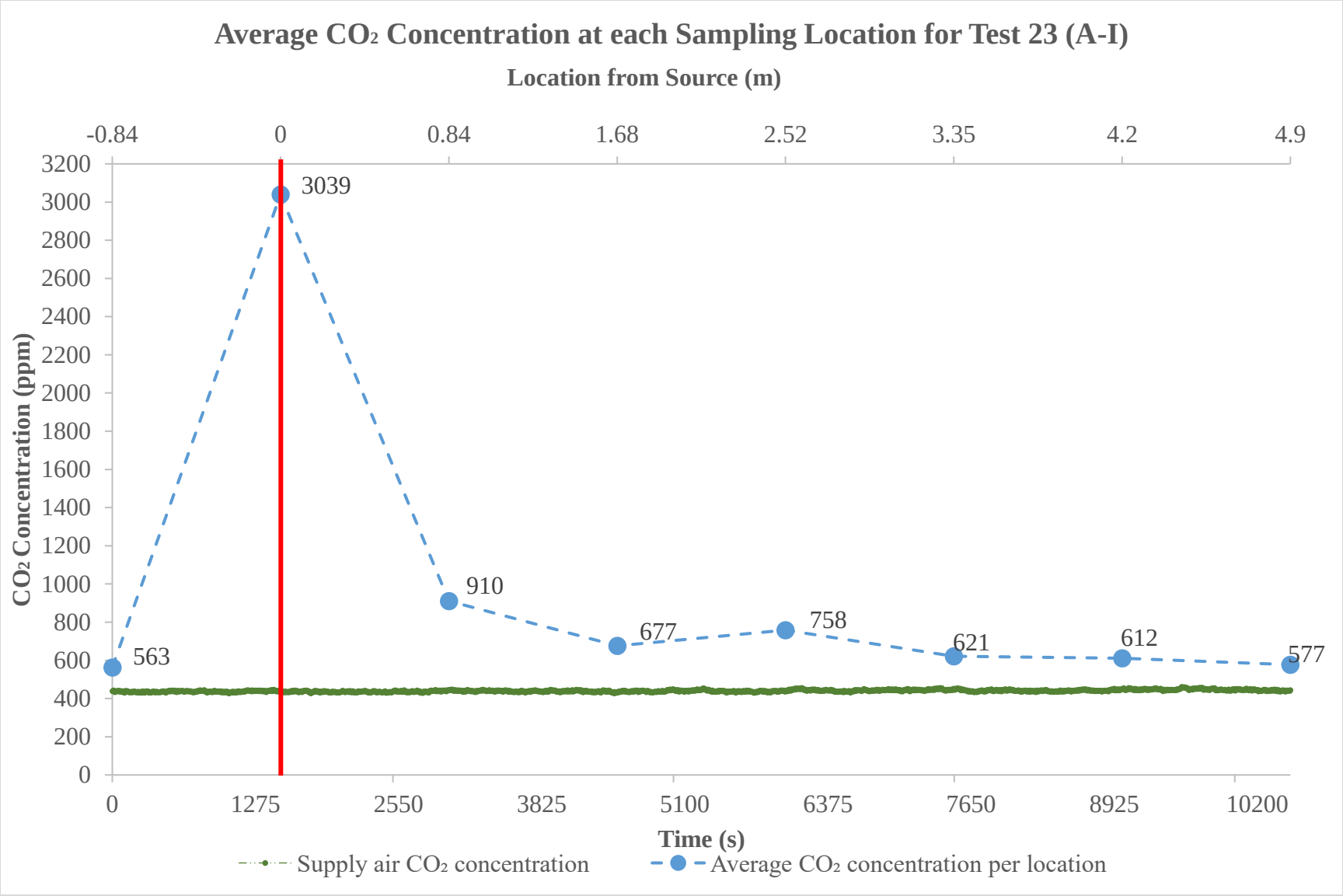

Figure E.67 Average CO_2 concentration at each sampling location for Test 23 (A-I) ISOPass undeployed.

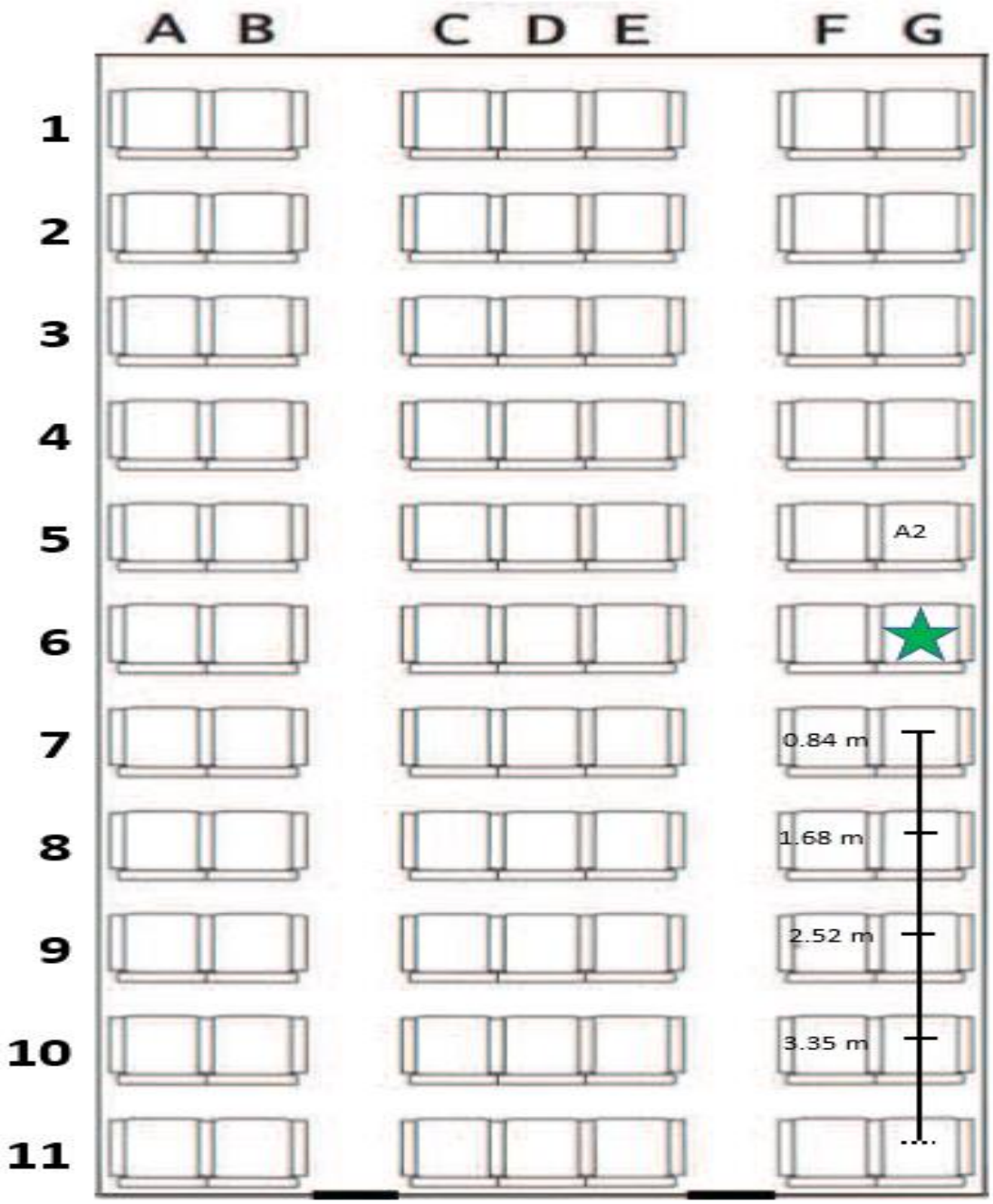

Figure E.68 Test 24 (A-I) ISOPass undeployed source location and sampling tree orientation.

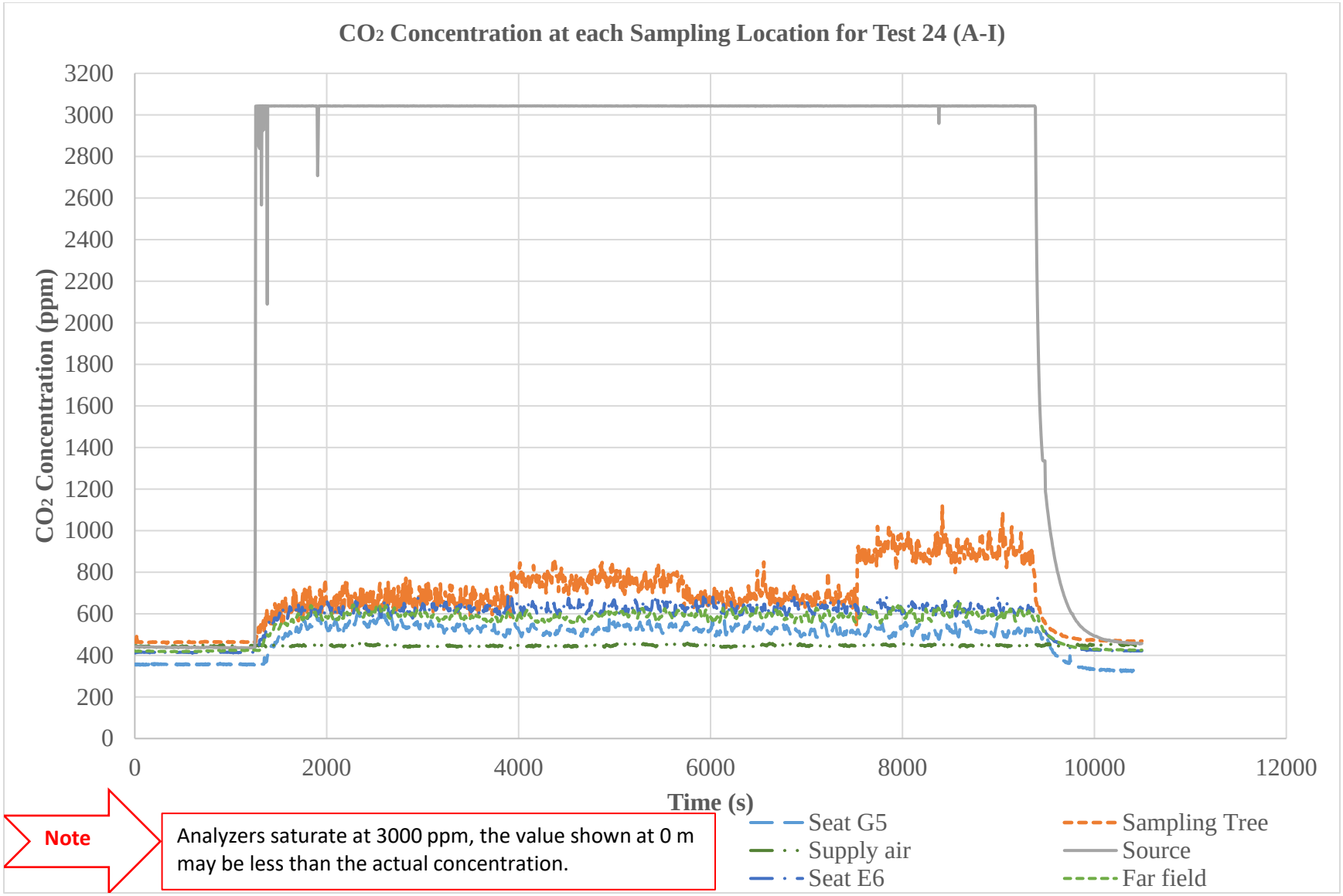

Figure E.69 Ininstantaneous CO_2 concentration at each sampling location for Test 24 (A-I) ISOPass undeployed.

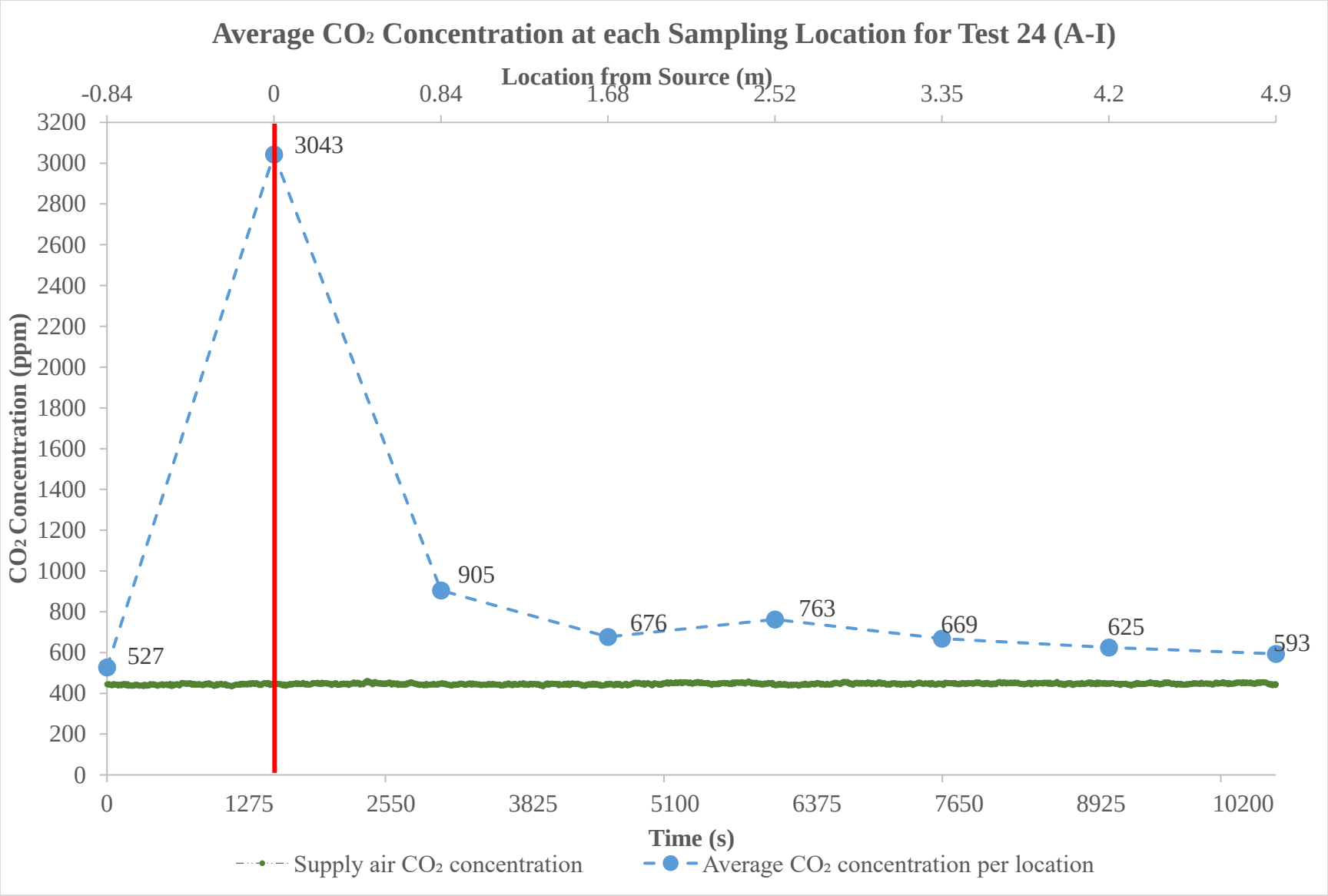

Figure E.70 Average CO_2 concentration at each sampling location for Test 24 (A-I) ISOPass undeployed.

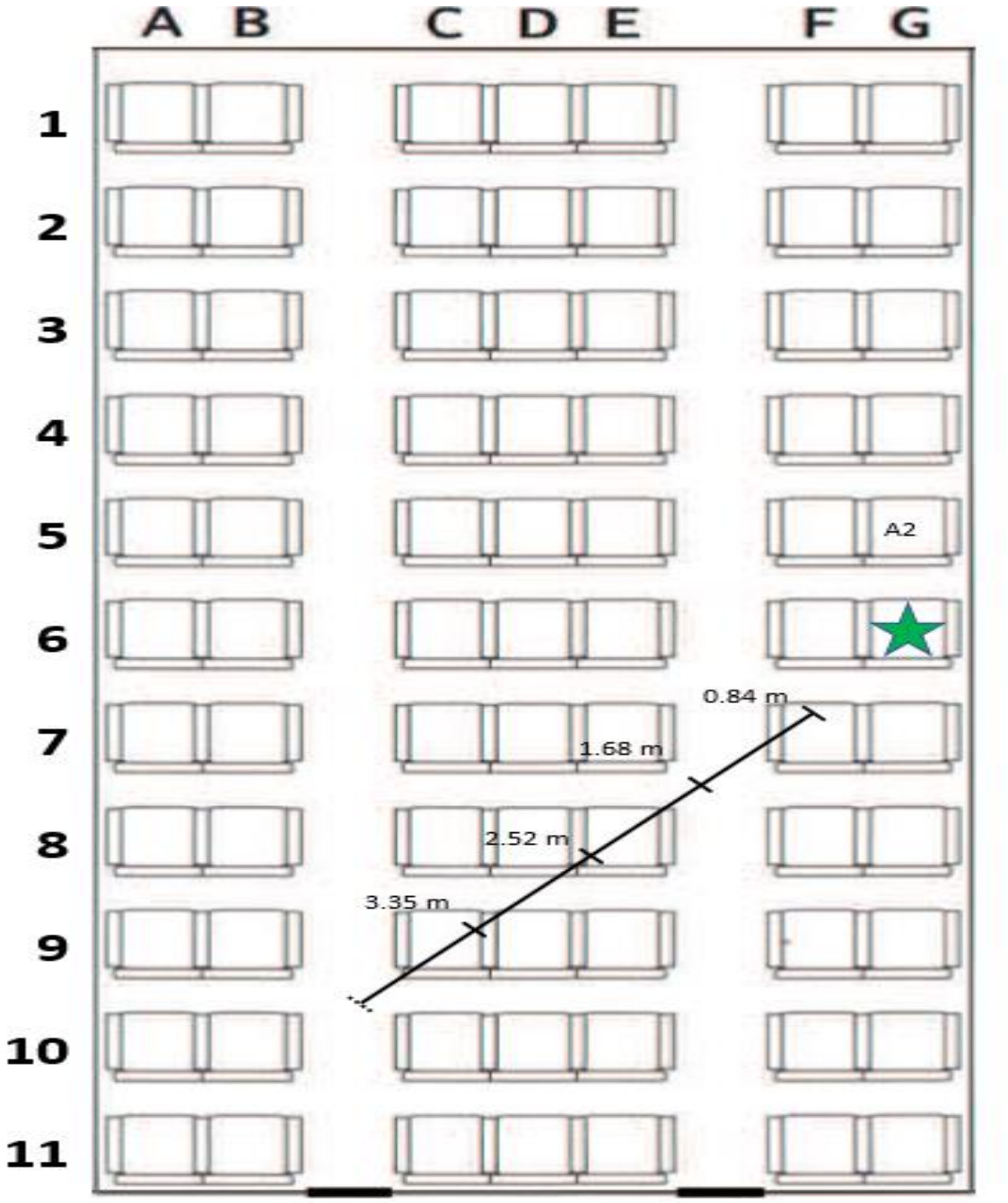

Figure E.71 Test 25 (A-I) ISOPass undeployed source location and sampling tree orientation.

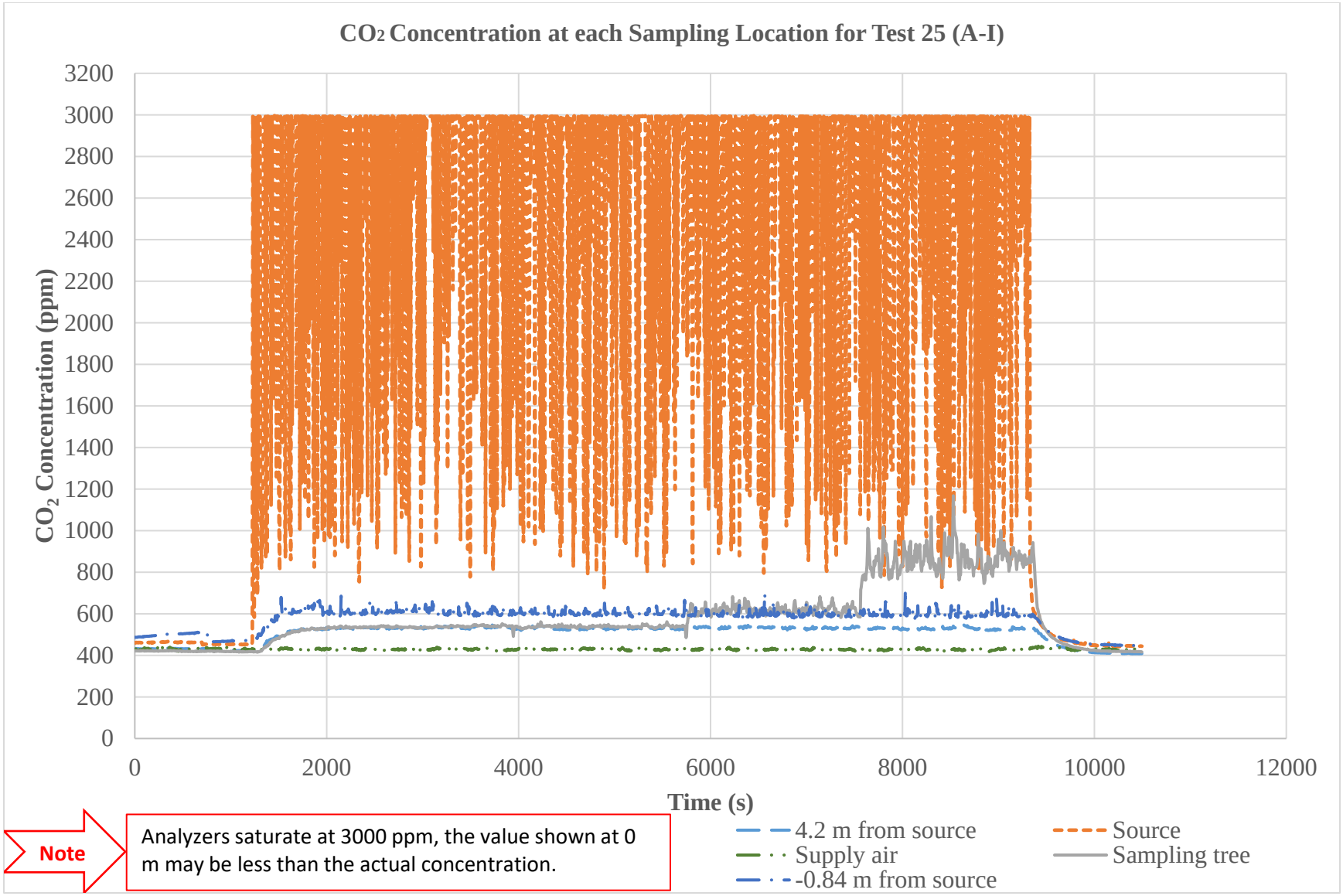

Figure E.72 Ininstantaneous CO_2 concentration at each sampling location for Test 25 (A-I) ISOPass undeployed.

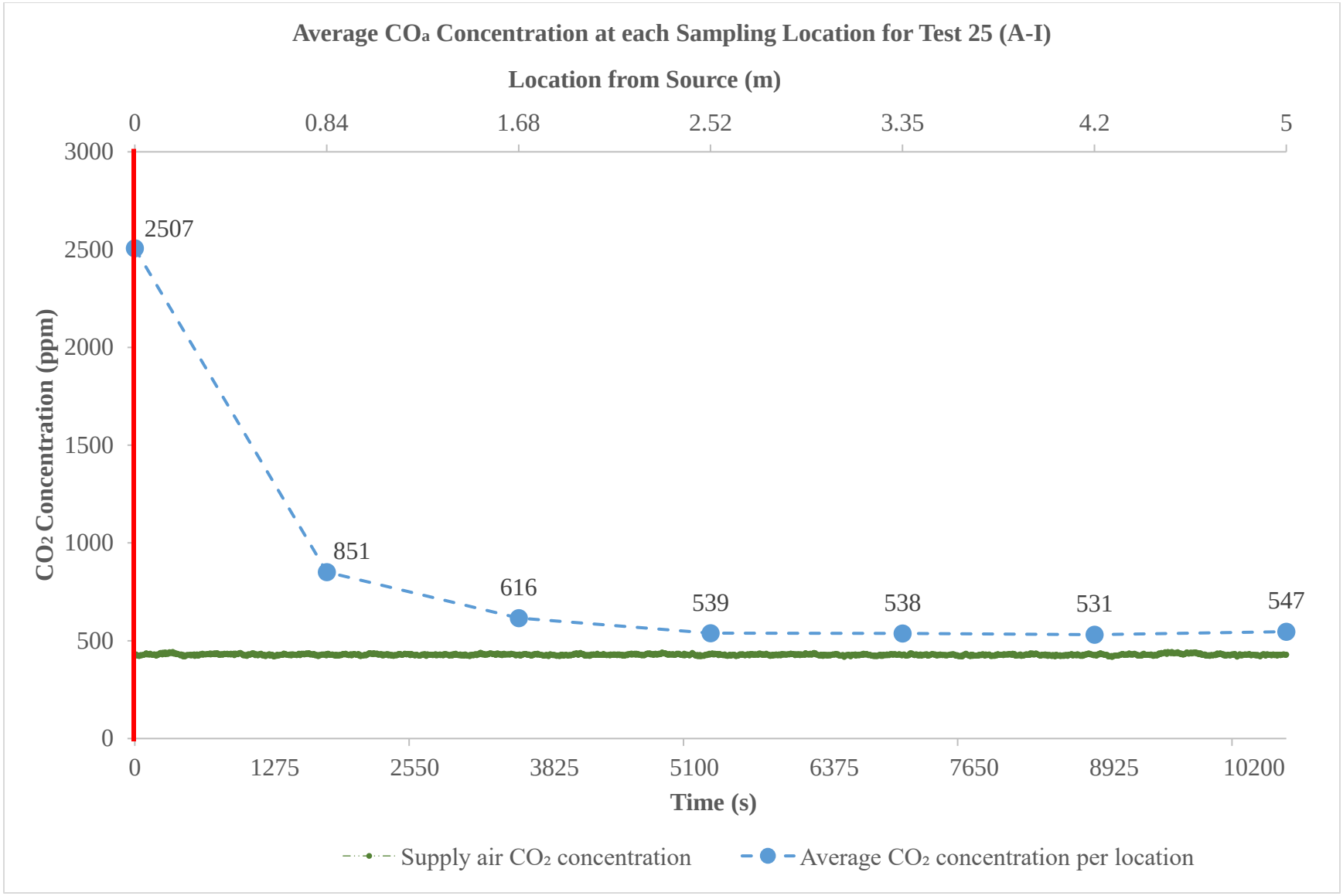

Figure E.73 Average CO_2 concentration at each sampling location for Test 25 (A-I) ISOPass undeployed.

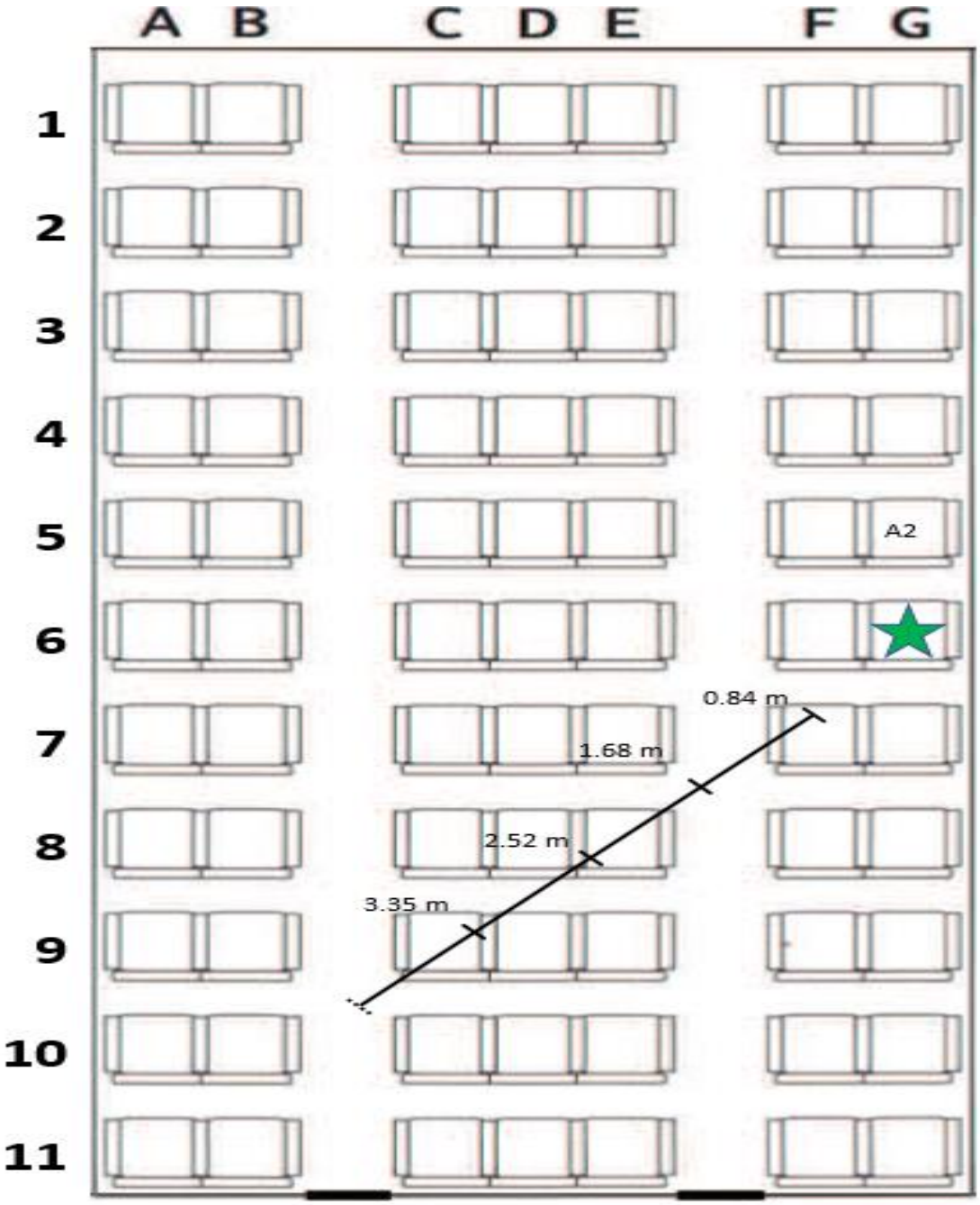

Figure E.74 Test 26 (A-I) ISOPass undeployed source location and sampling tree orientation.

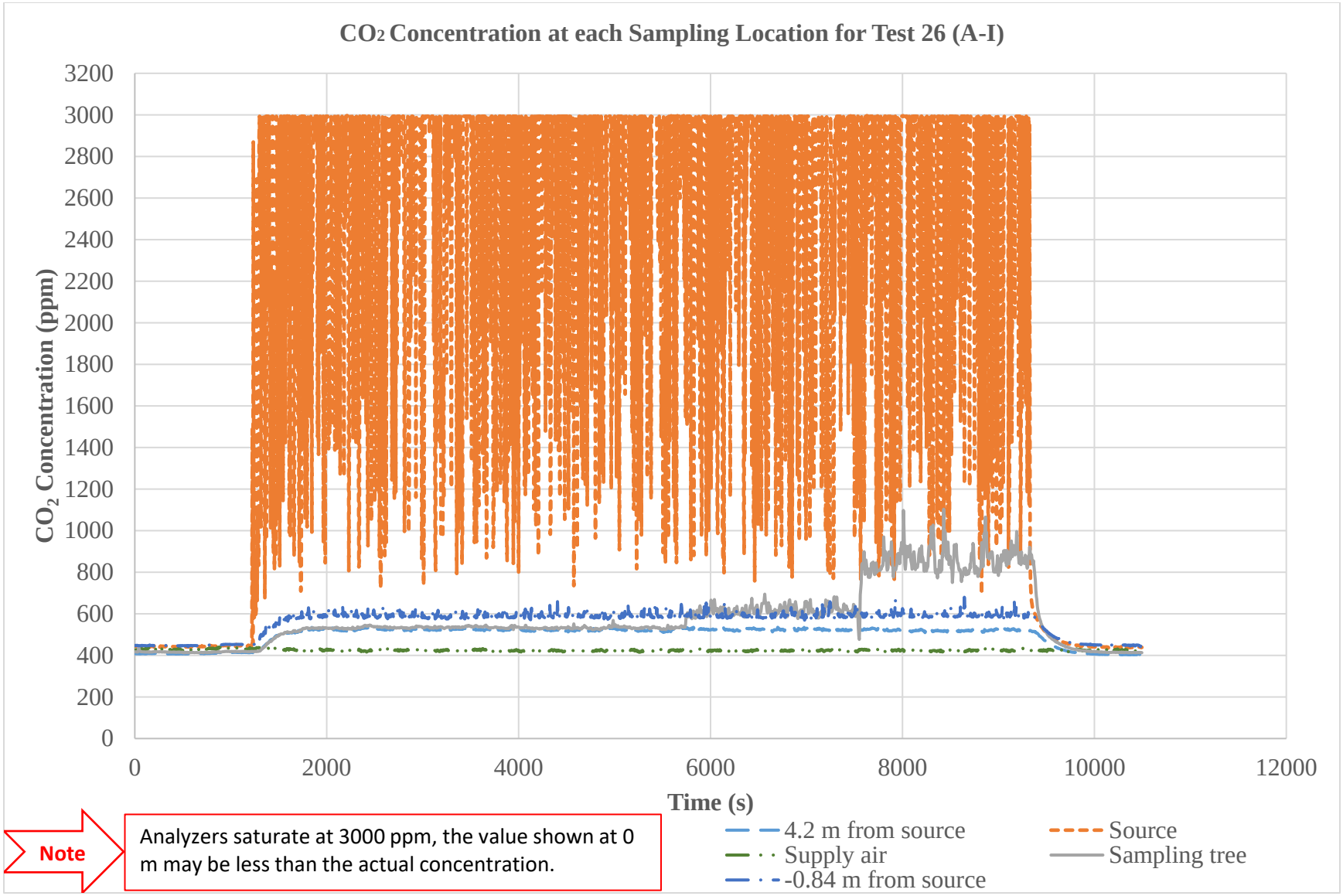

Figure E.75 Ininstantaneous CO_2 concentration at each sampling location for Test 26 (A-I) ISOPass undeployed.

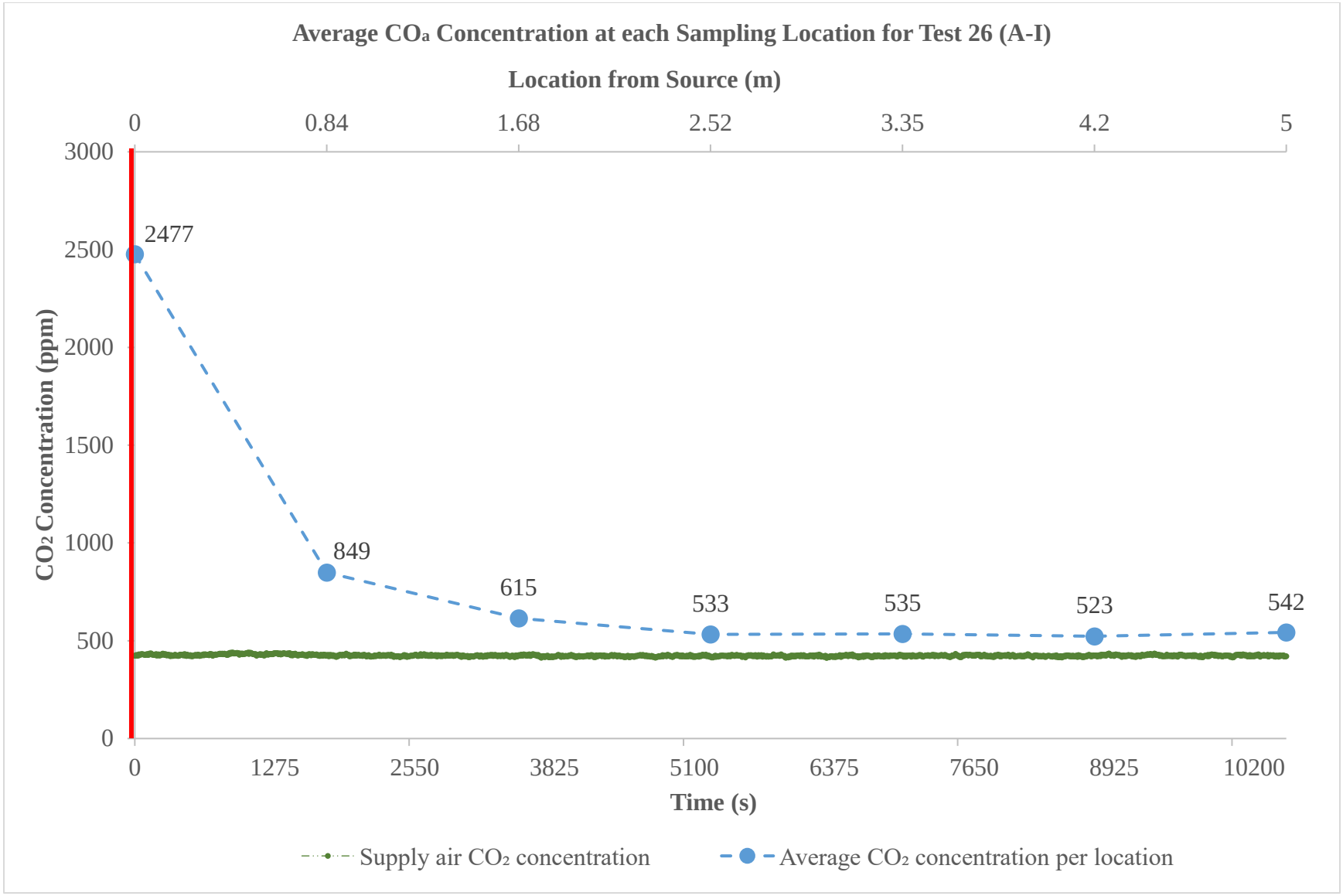

Figure E.76 Average CO_2 concentration at each sampling location for Test 26 (A-I) ISOPass undeployed.

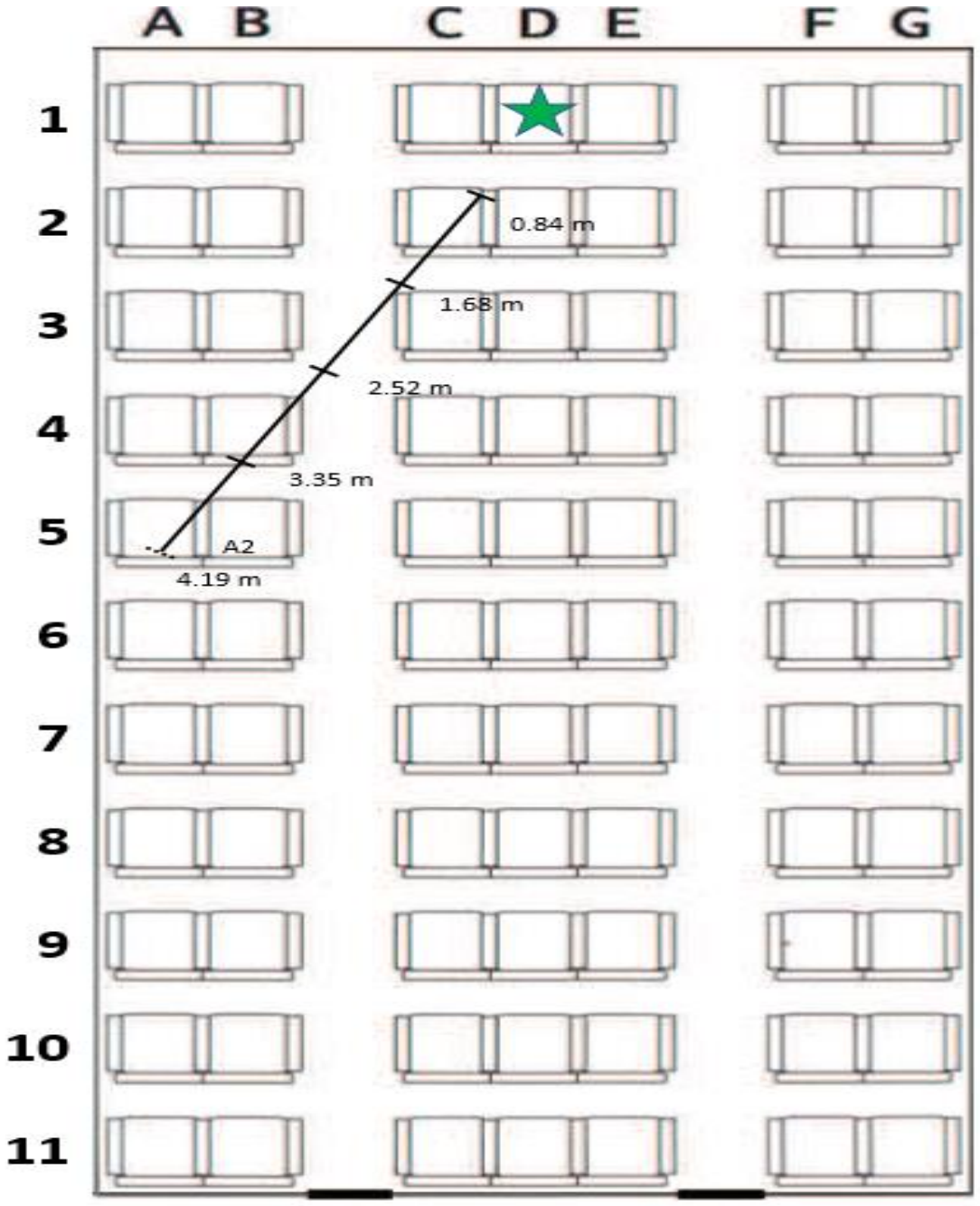

Figure E.77 Test 11 (A-I) ISOPass undeployed source location and sampling tree orientation.

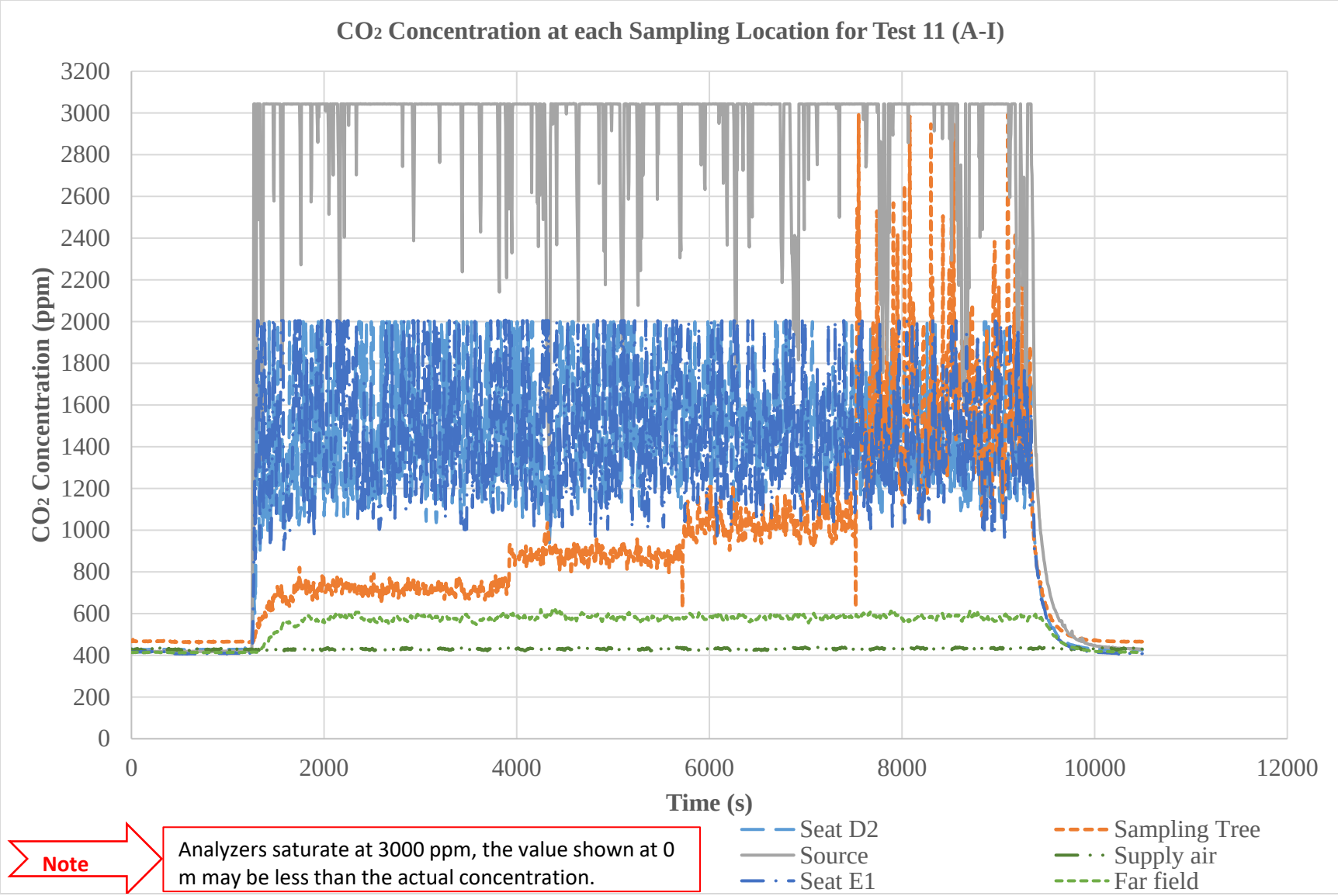

Figure E.78 Ininstantaneous CO_2 concentration at each sampling location for Test 11 (A-I) ISOPass undeployed.

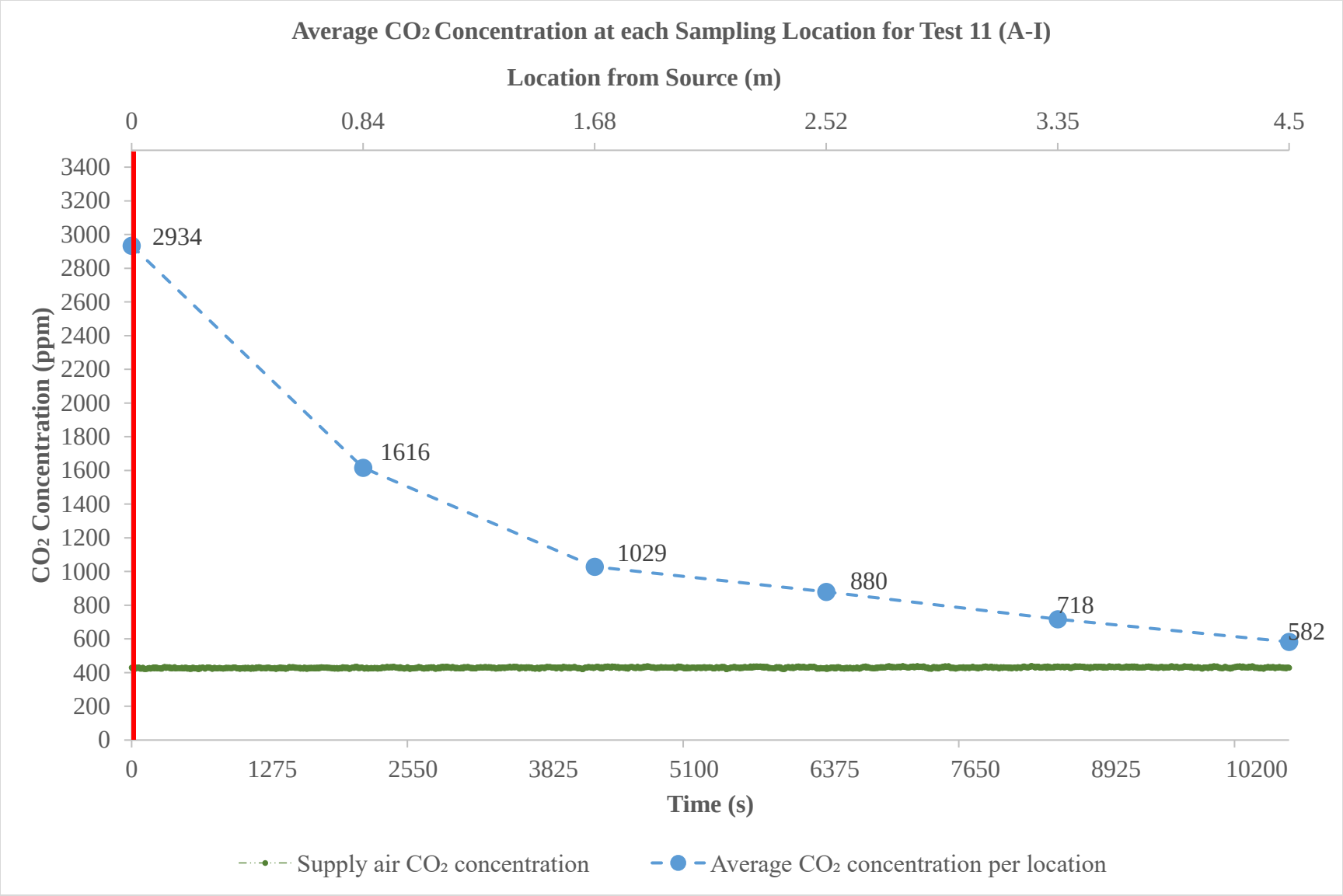

Figure E.79 Average CO_2 concentration at each sampling location for Test 11 (A-I) ISOPass undeployed.

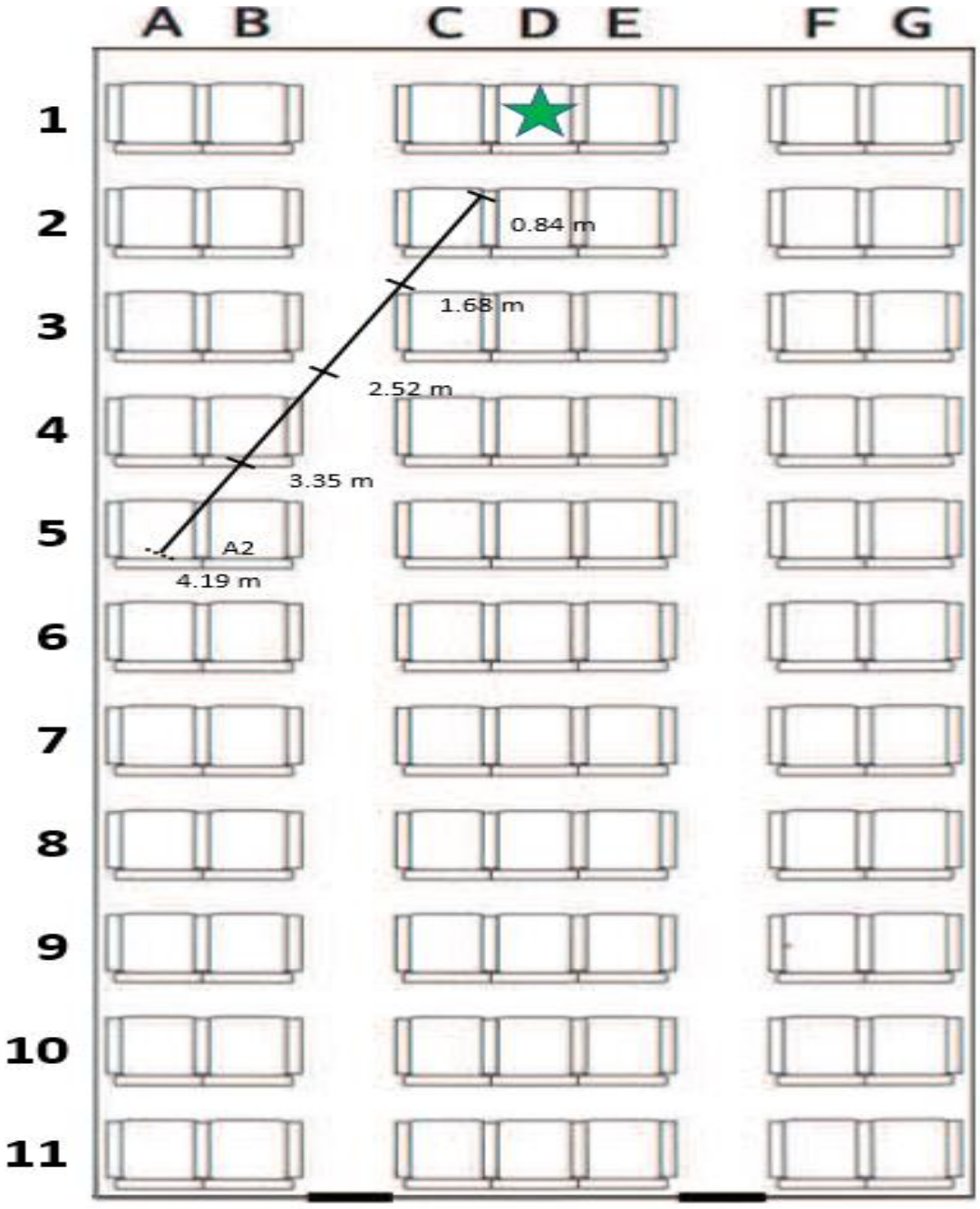

Figure E. 80 Test 12 (A-I) ISOPass undeployed source location and sampling tree orientation.

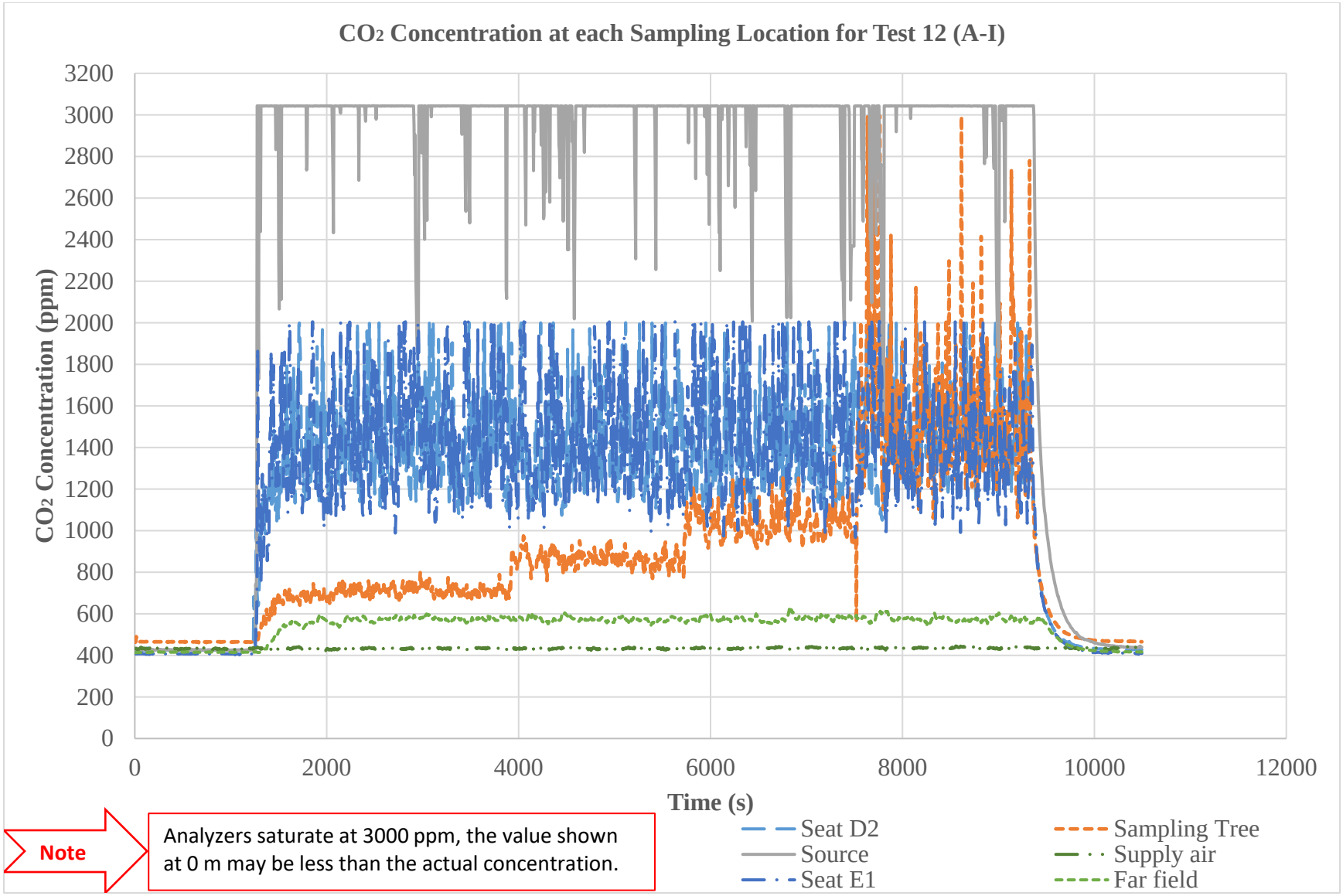

Figure E.81 Ininstantaneous CO_2 concentration at each sampling location for Test 12 (A-I) ISOPass undeployed.

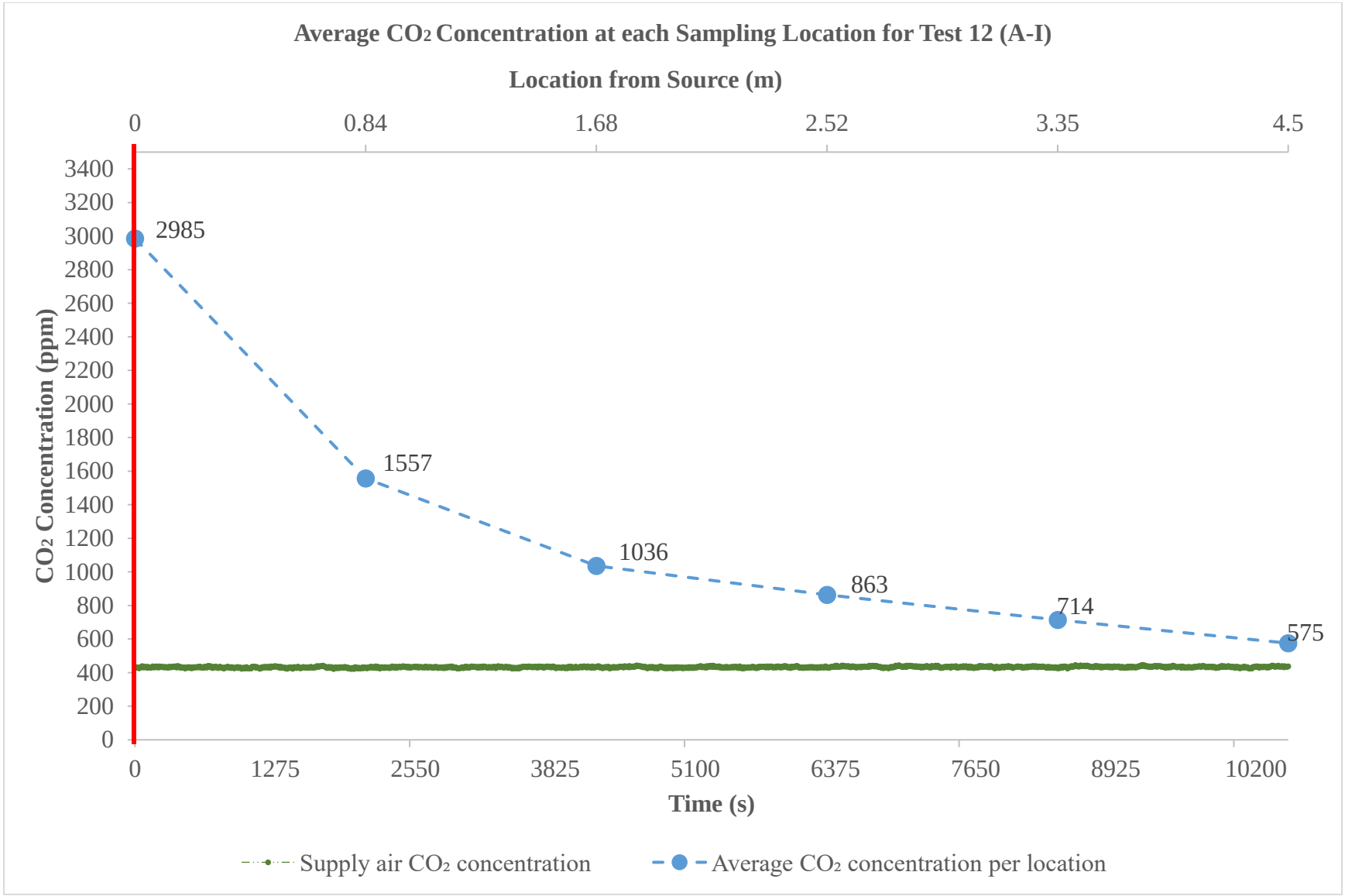

Figure E.82 Average CO_2 concentration at each sampling location for Test 12 (A-I) ISOPass undeployed.

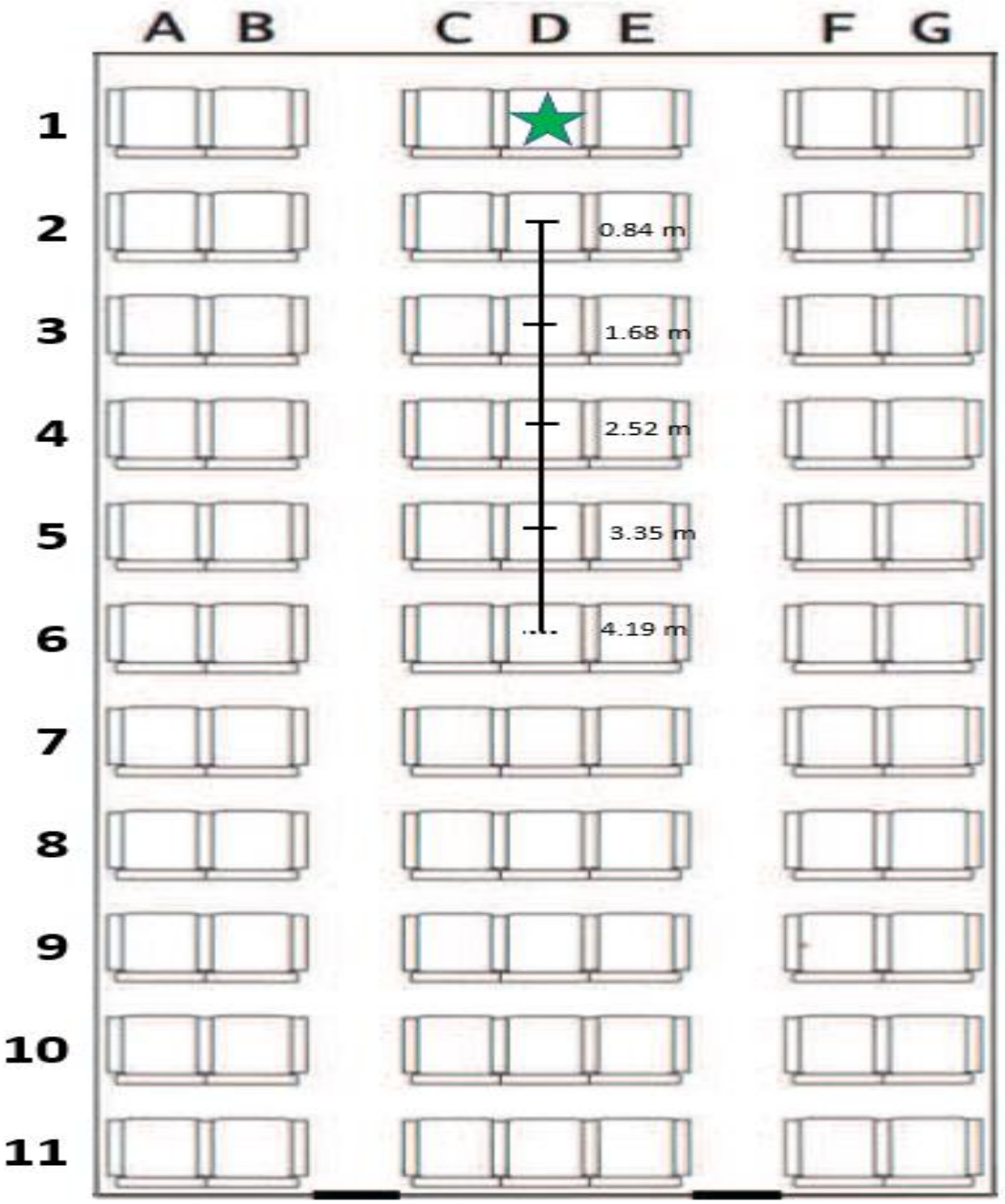

Figure E.83 Test 13 (A-I) ISOPass undeployed source location and sampling tree orientation.

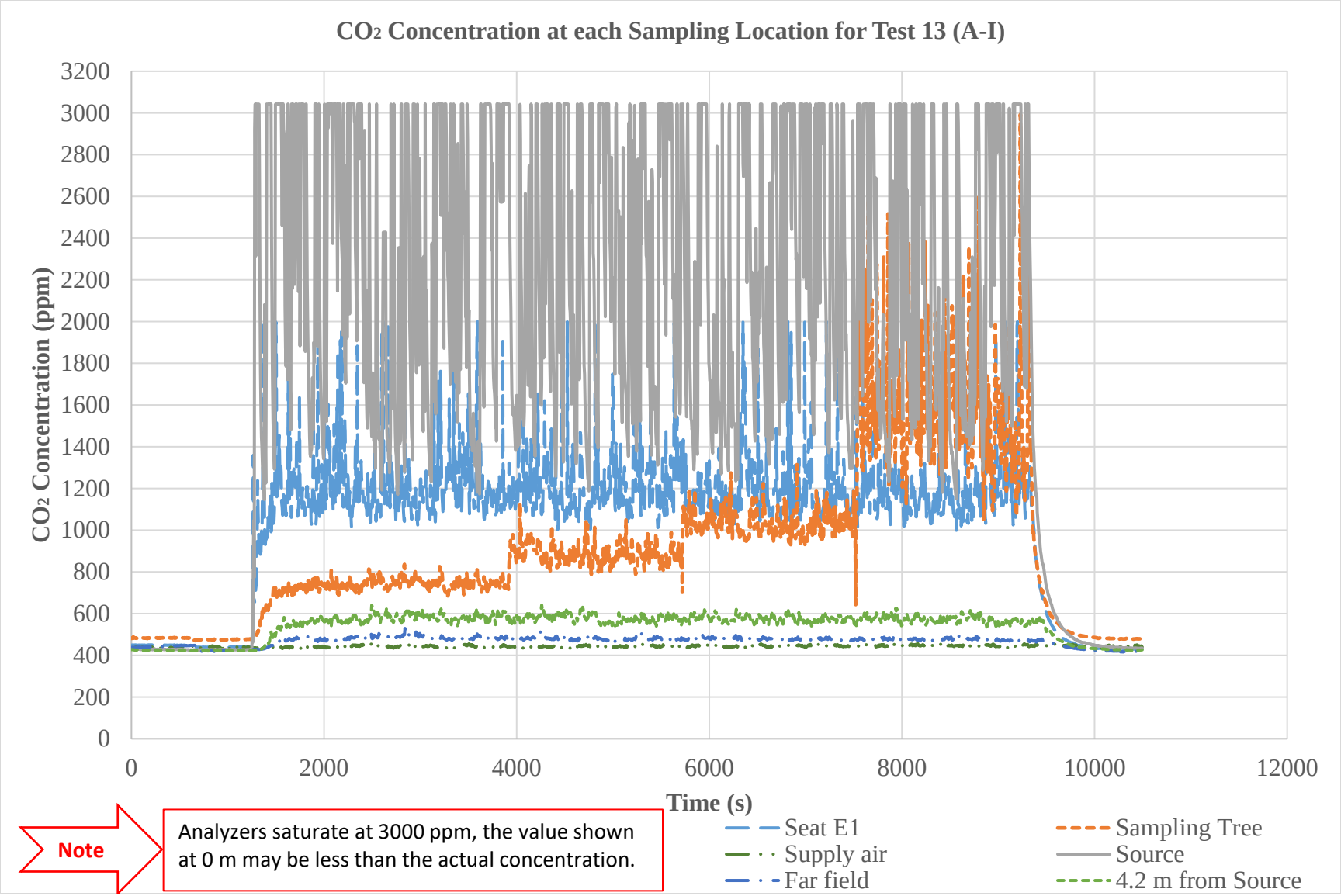

Figure E.84 Ininstantaneous CO_2 concentration at each sampling location for Test 13 (A-I) ISOPass undeployed.

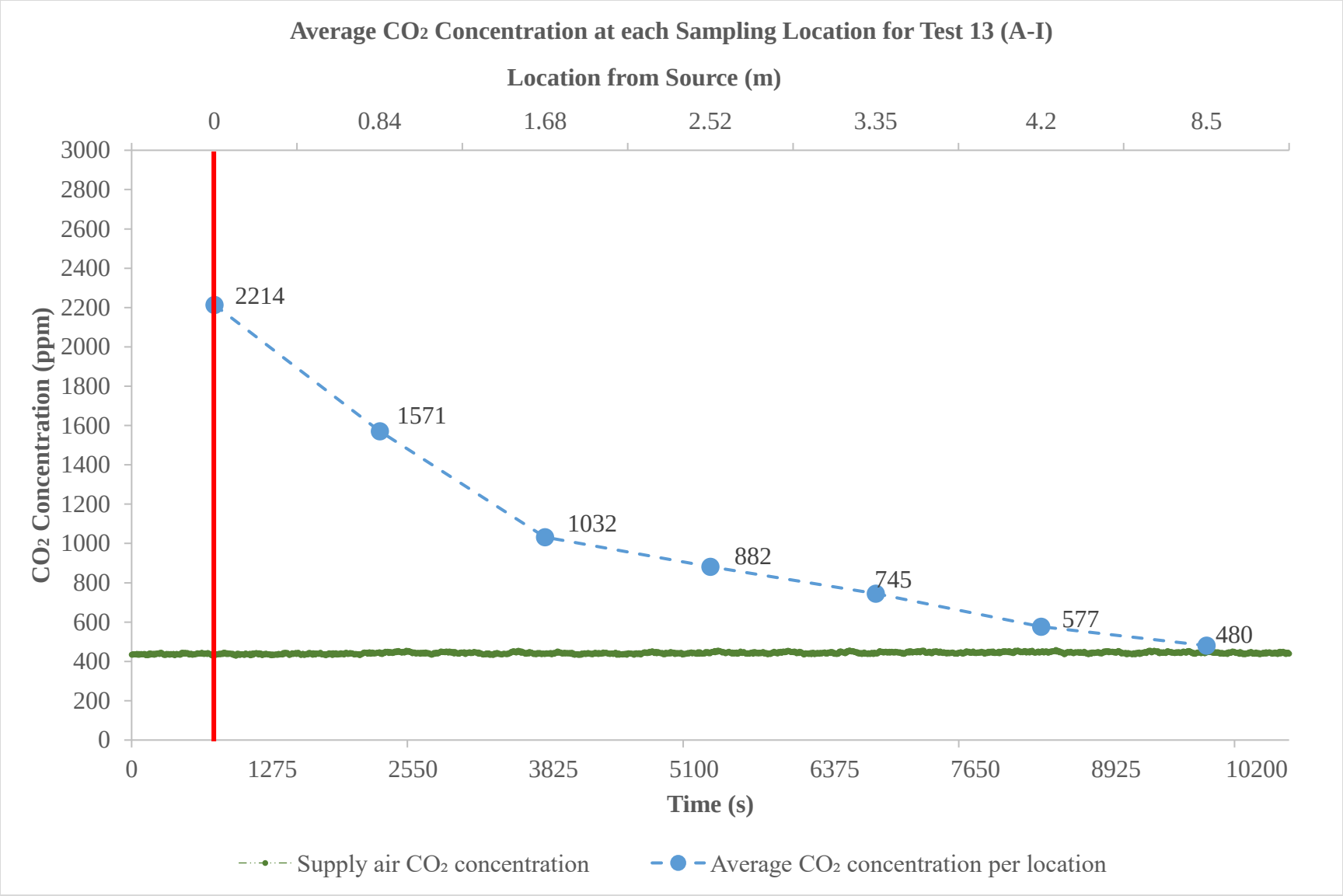

Figure E.85 Average CO_2 concentration at each sampling location for Test 13 (A-I) ISOPass undeployed.

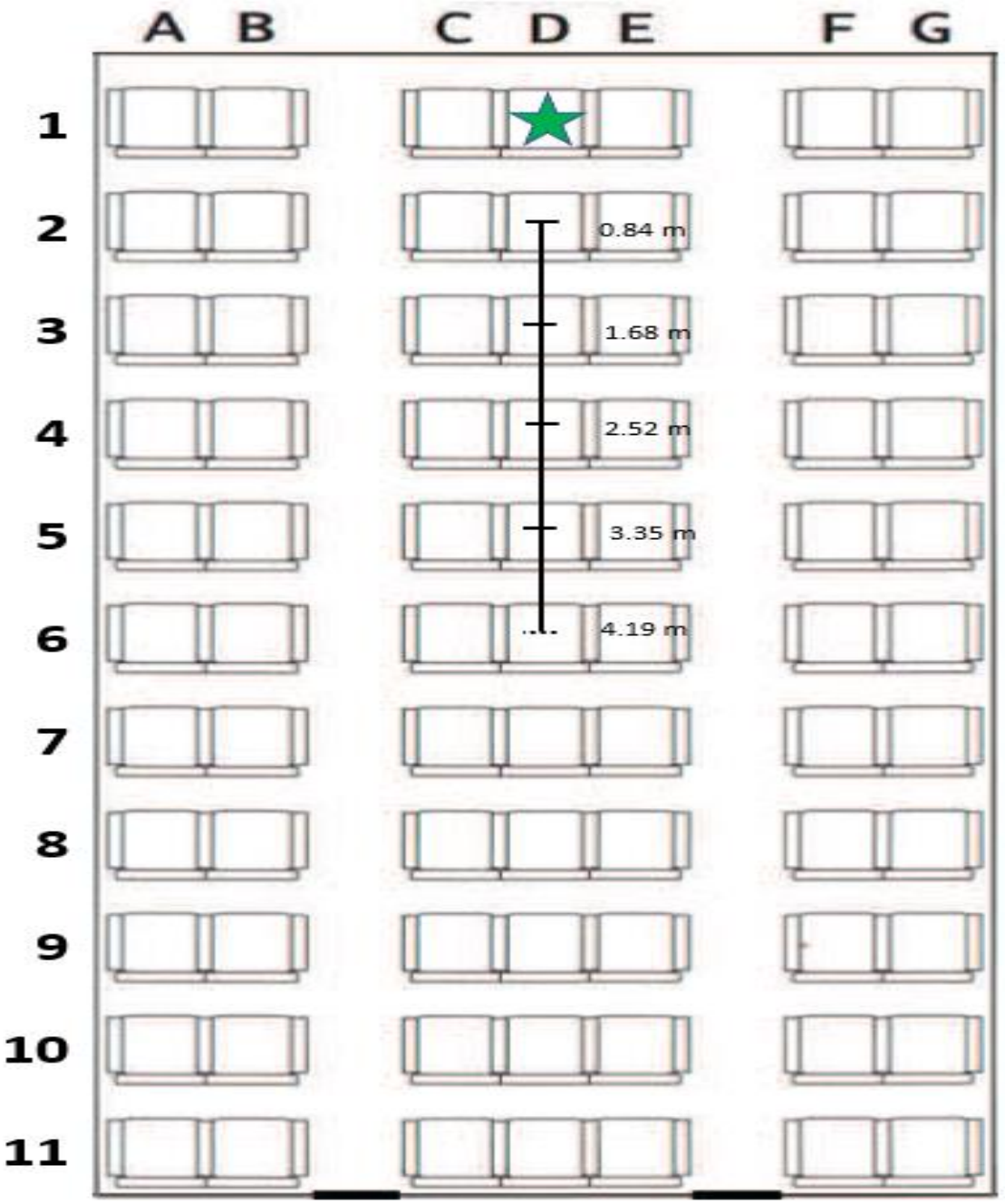

Figure E.86 Test 14 (A-I) ISOPass undeployed source location and sampling tree orientation.

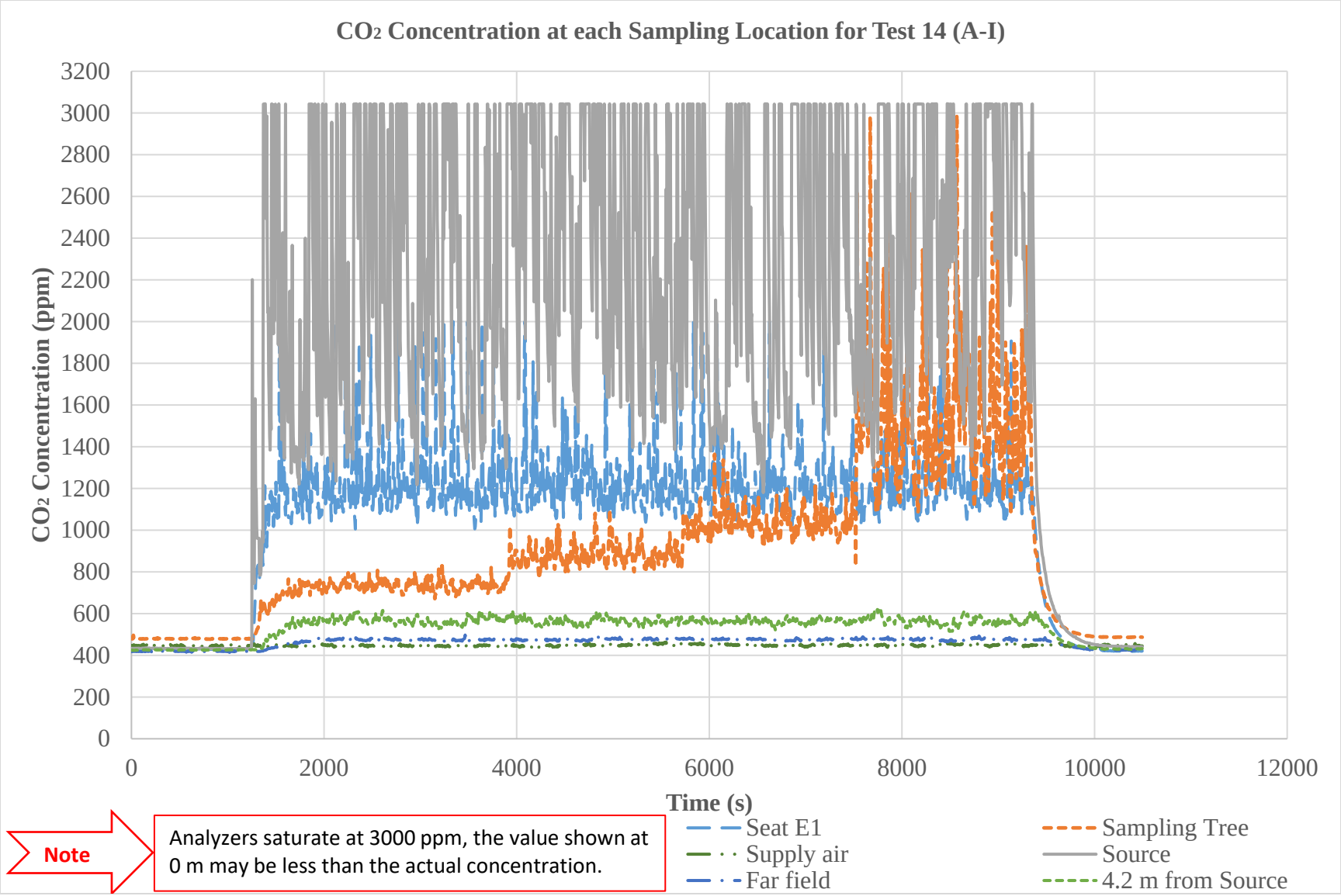

Figure E.87 Ininstantaneous CO_2 concentration at each sampling location for Test 14 (A-I) ISOPass undeployed.

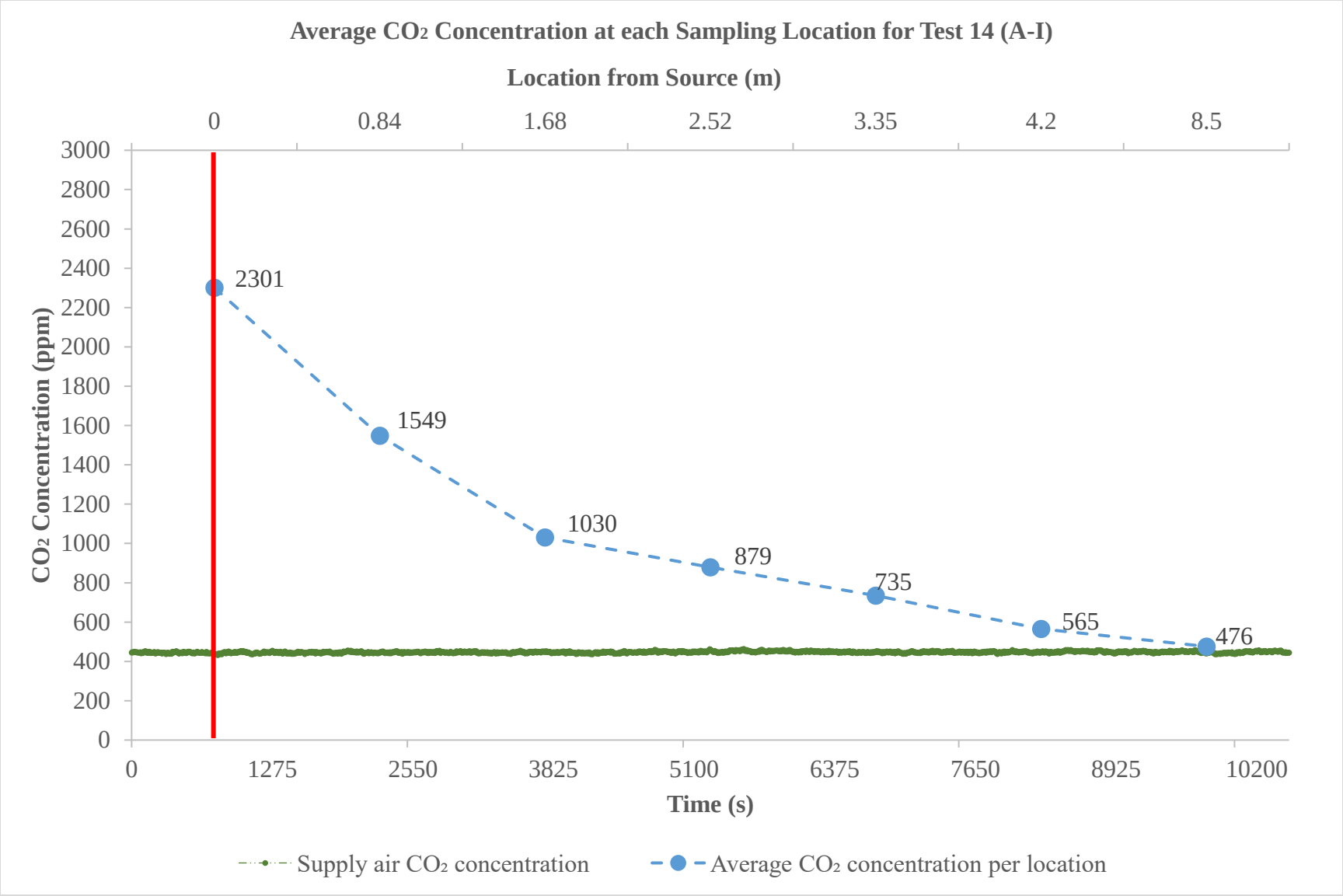

Figure E.88 Average CO_2 concentration at each sampling location for Test 14 (A-I) ISOPass undeployed.

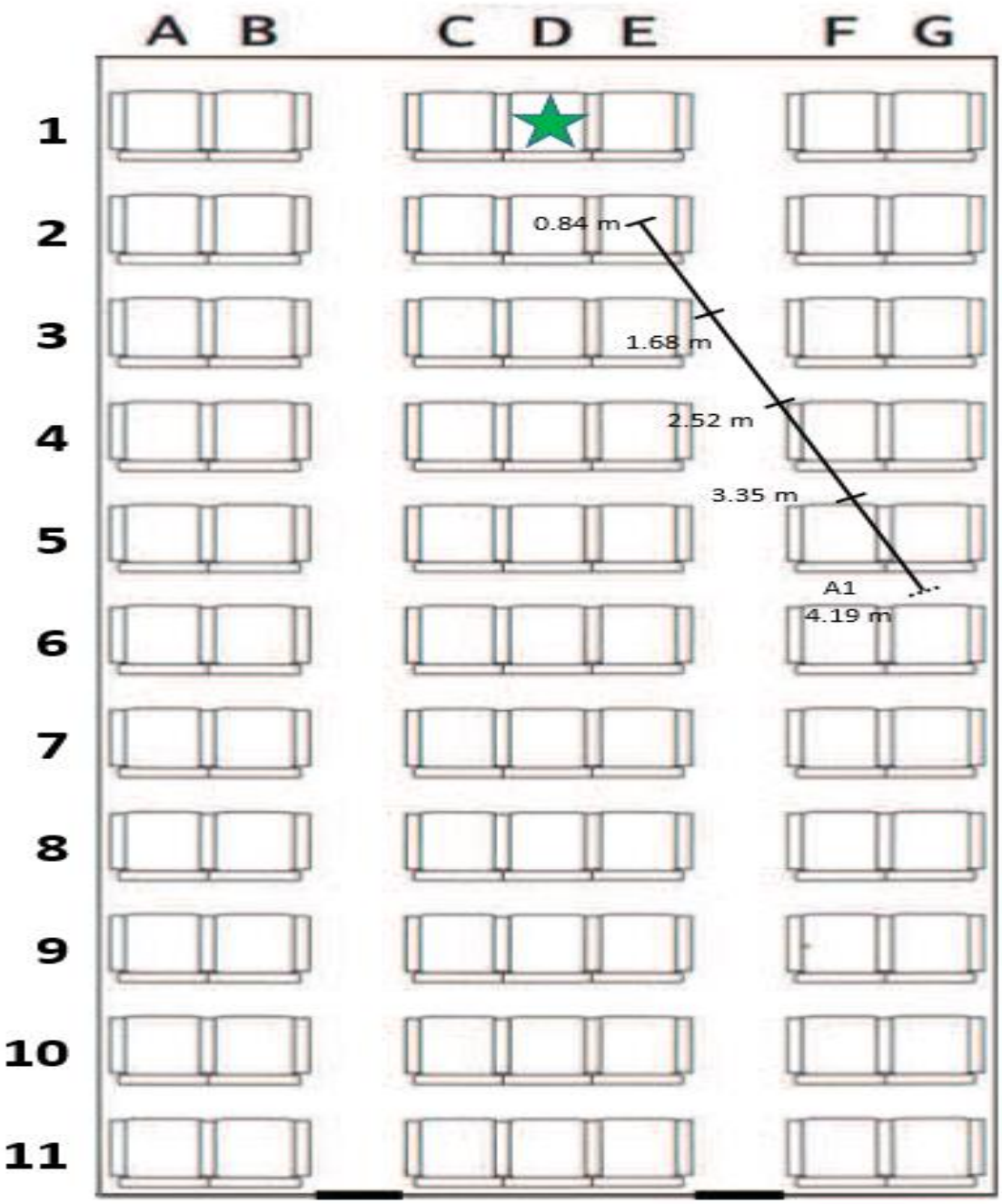

Figure E.89 Test 15 (A-I) ISOPass undeployed source location and sampling tree orientation.

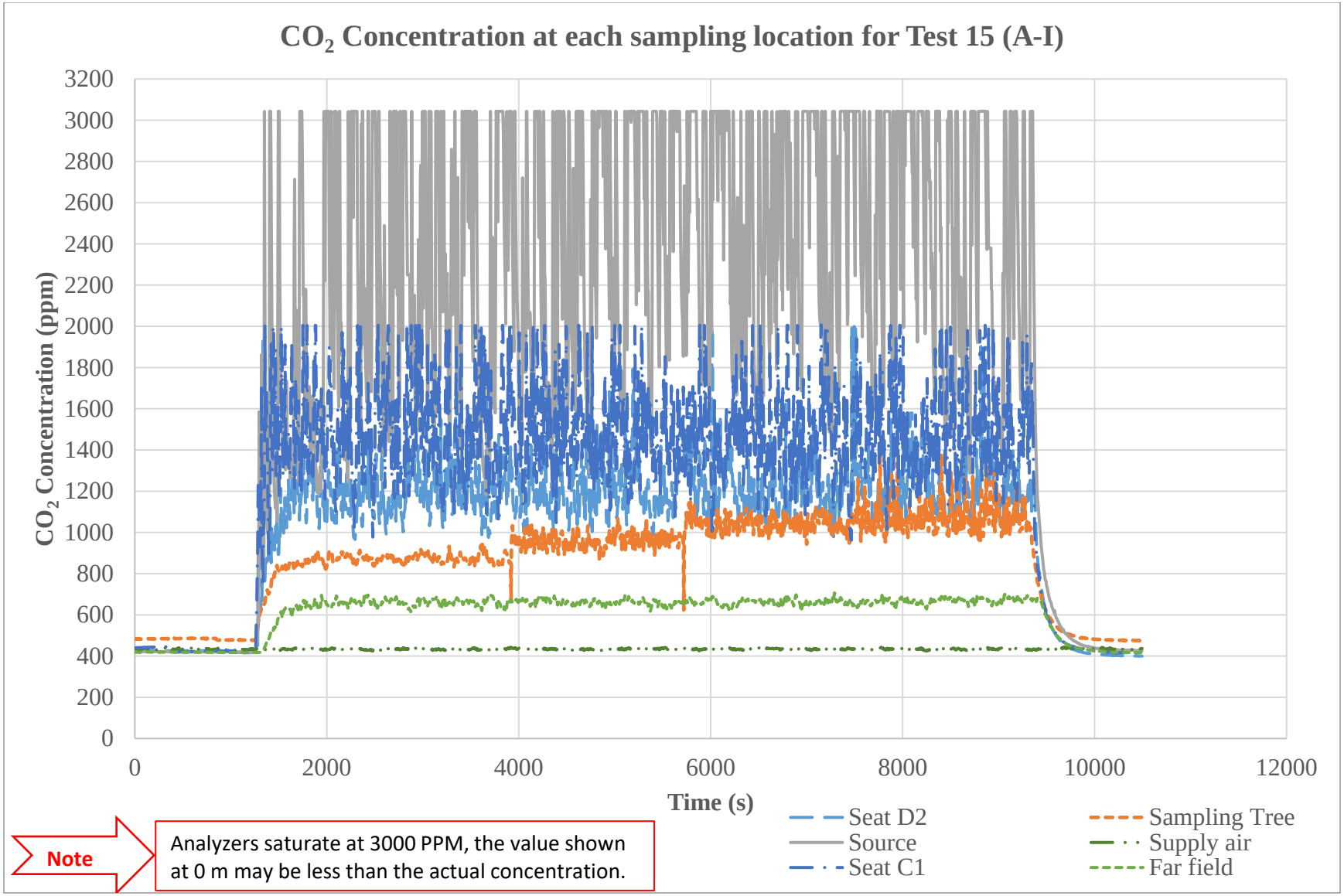

Figure E.90 Ininstantaneous CO_2 concentration at each sampling location for Test 15 (A-I) ISOPass undeployed.

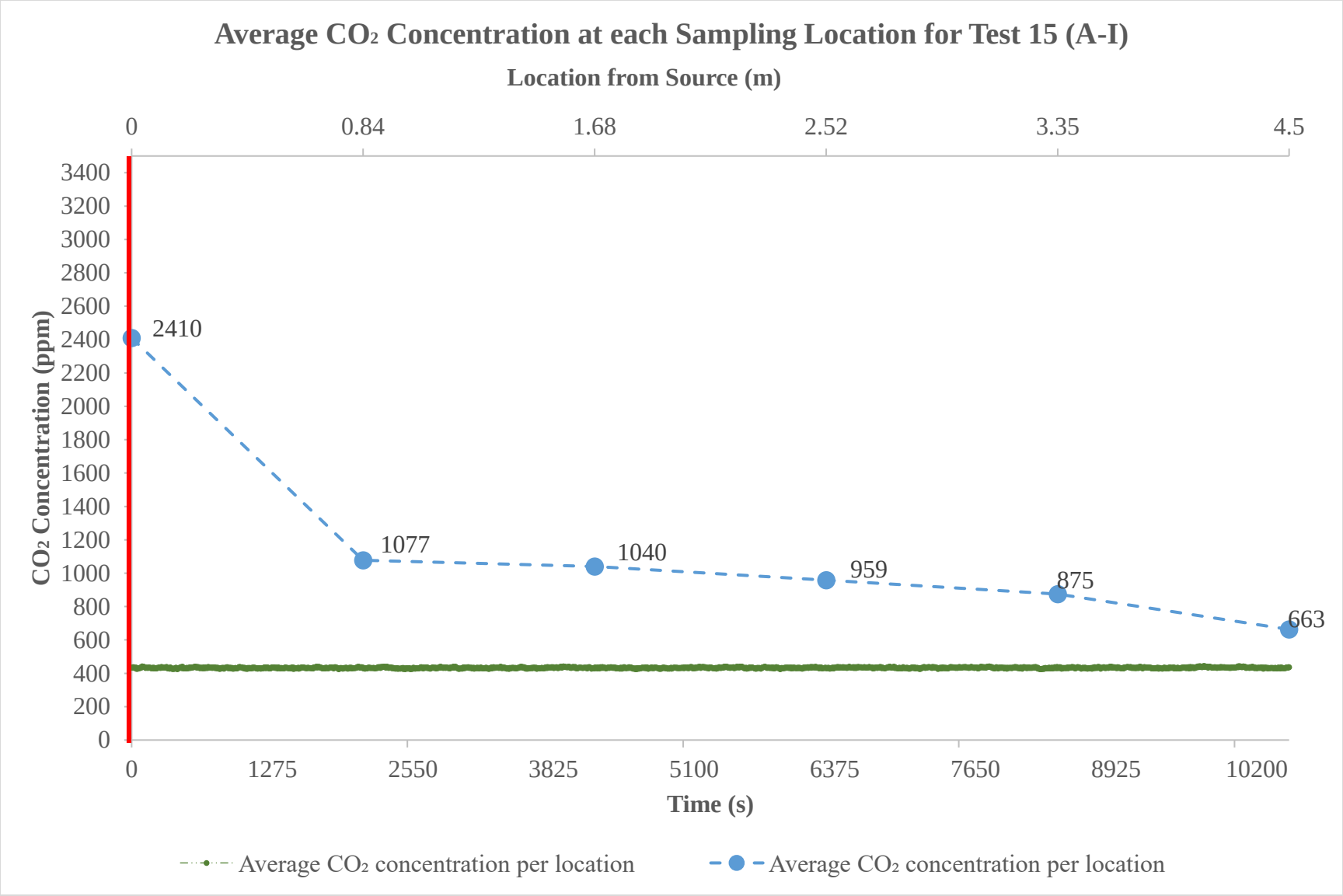

Figure E.91 Average CO_2 concentration at each sampling location for Test 15 (A-I) ISOPass undeployed.

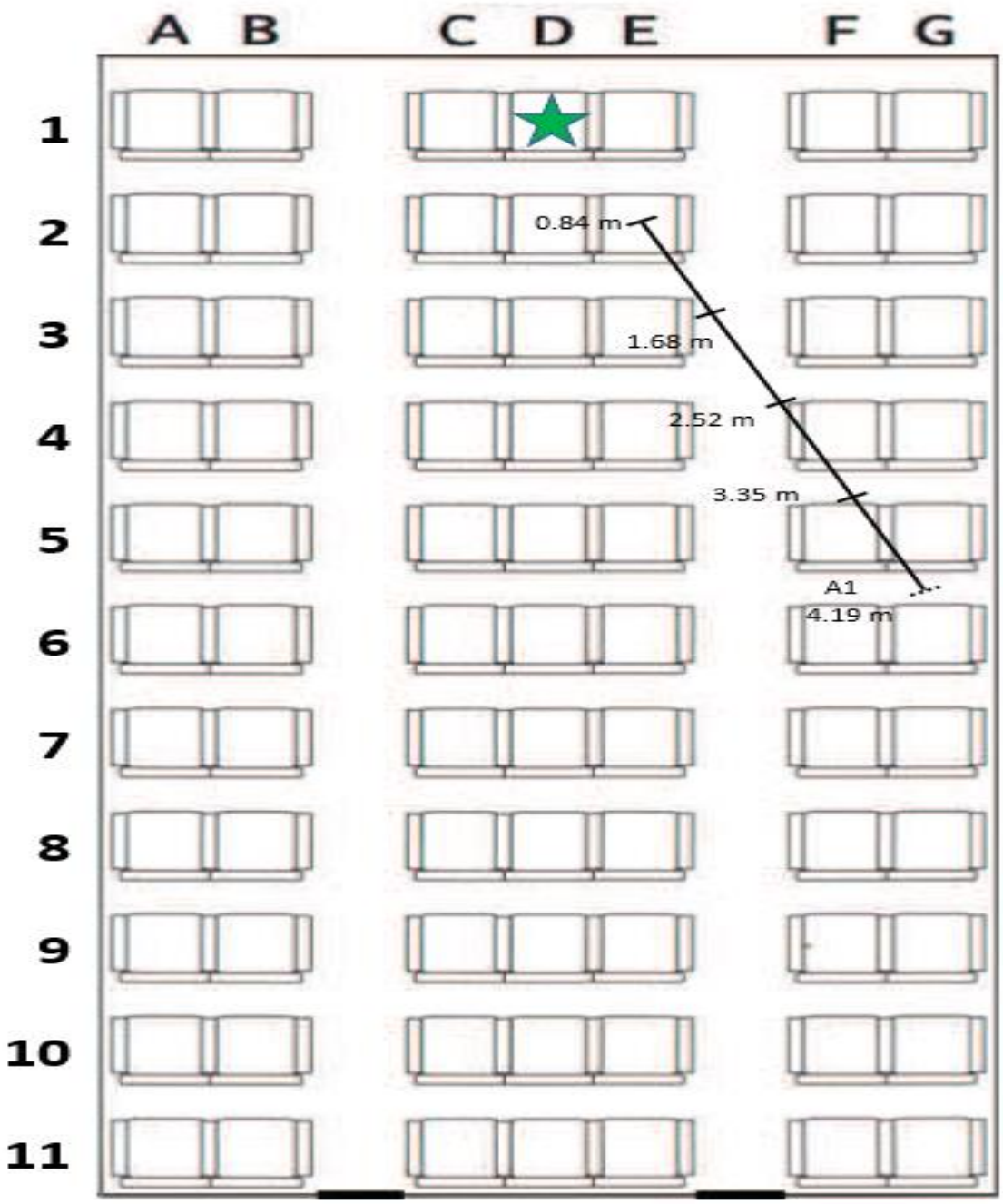

Figure E.92 Test 16 (A-I) ISOPass undeployed source location and sampling tree orientation.

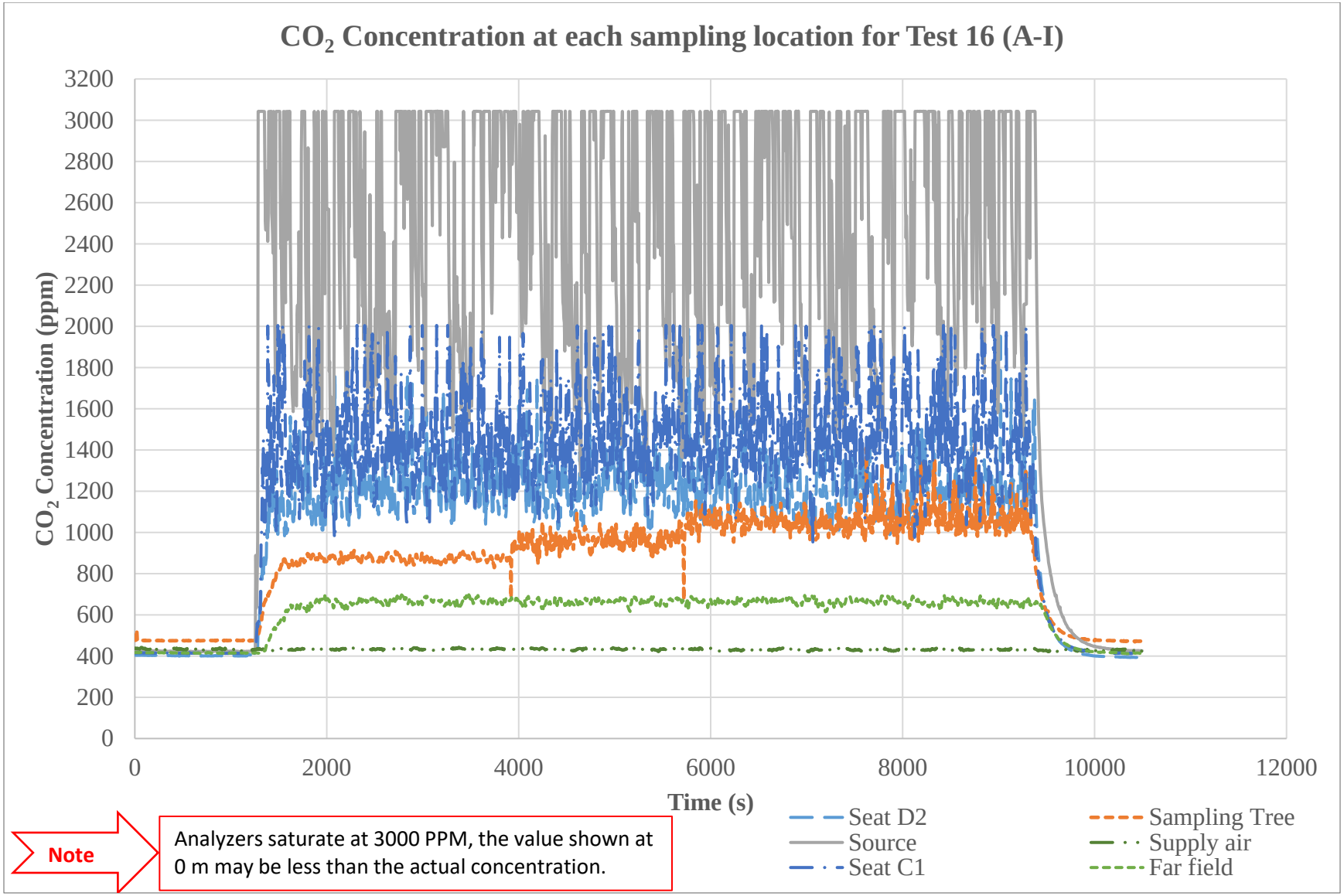

Figure E.93 Ininstantaneous CO_2 concentration at each sampling location for Test 16 (A-I) ISOPass undeployed.

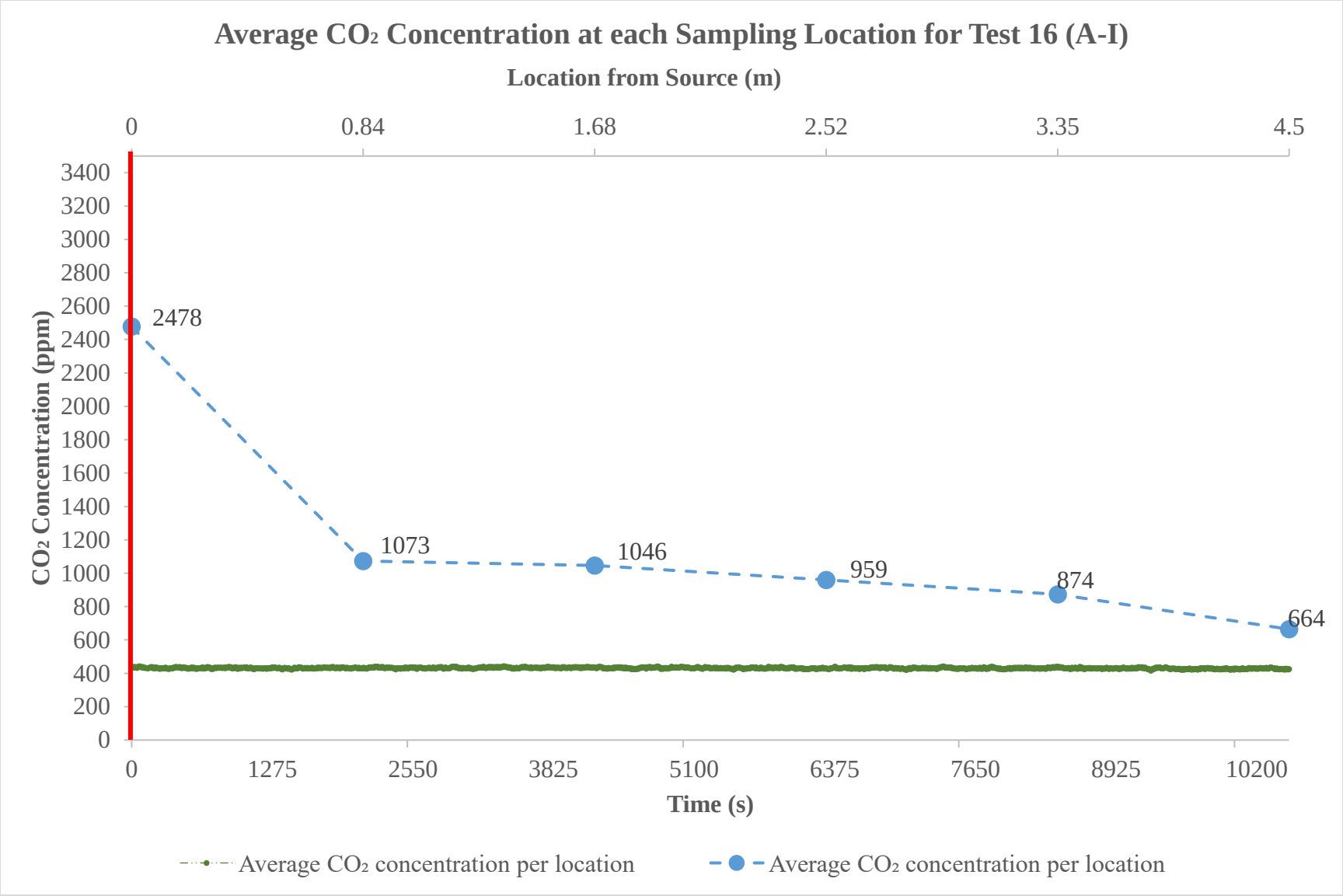

Figure E.94 Average CO_2 concentration at each sampling location for Test 16 (A-I) ISOPass undeployed.

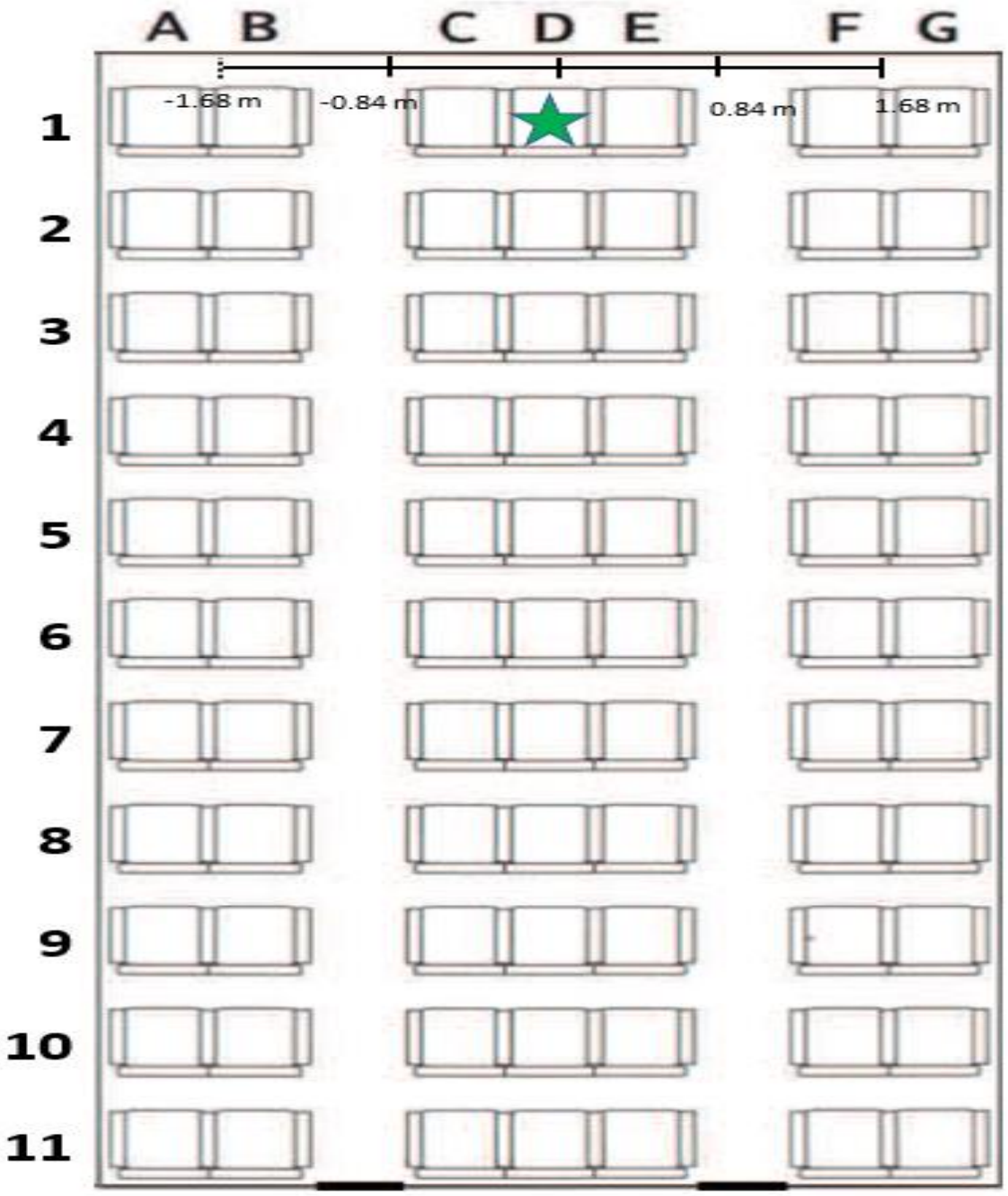

Figure E.95 Test 17 (A-I) ISOPass undeployed source location and sampling tree orientation.

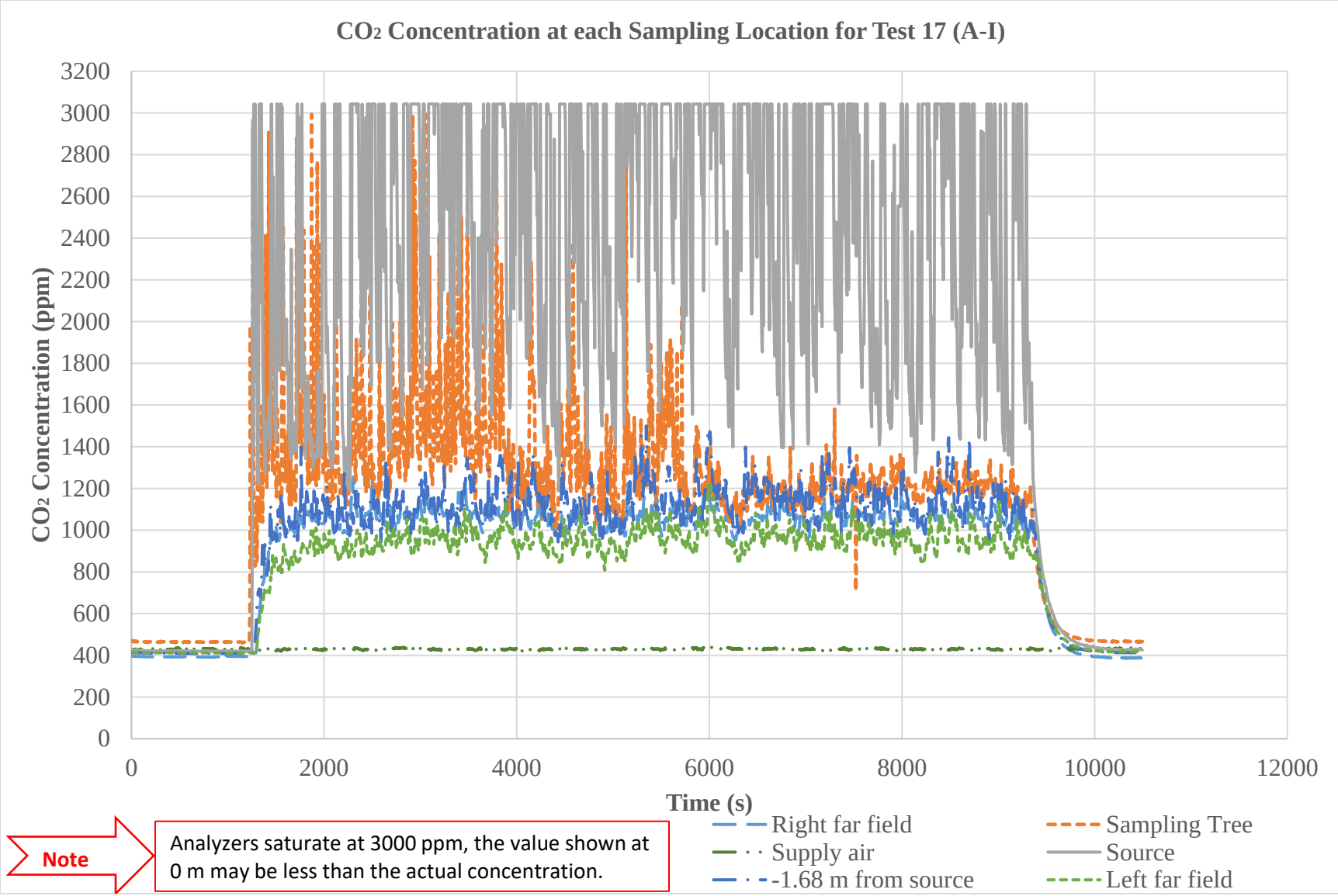

Figure E.96 Ininstantaneous CO_2 concentration at each sampling location for Test 17 (A-I) ISOPass undeployed.

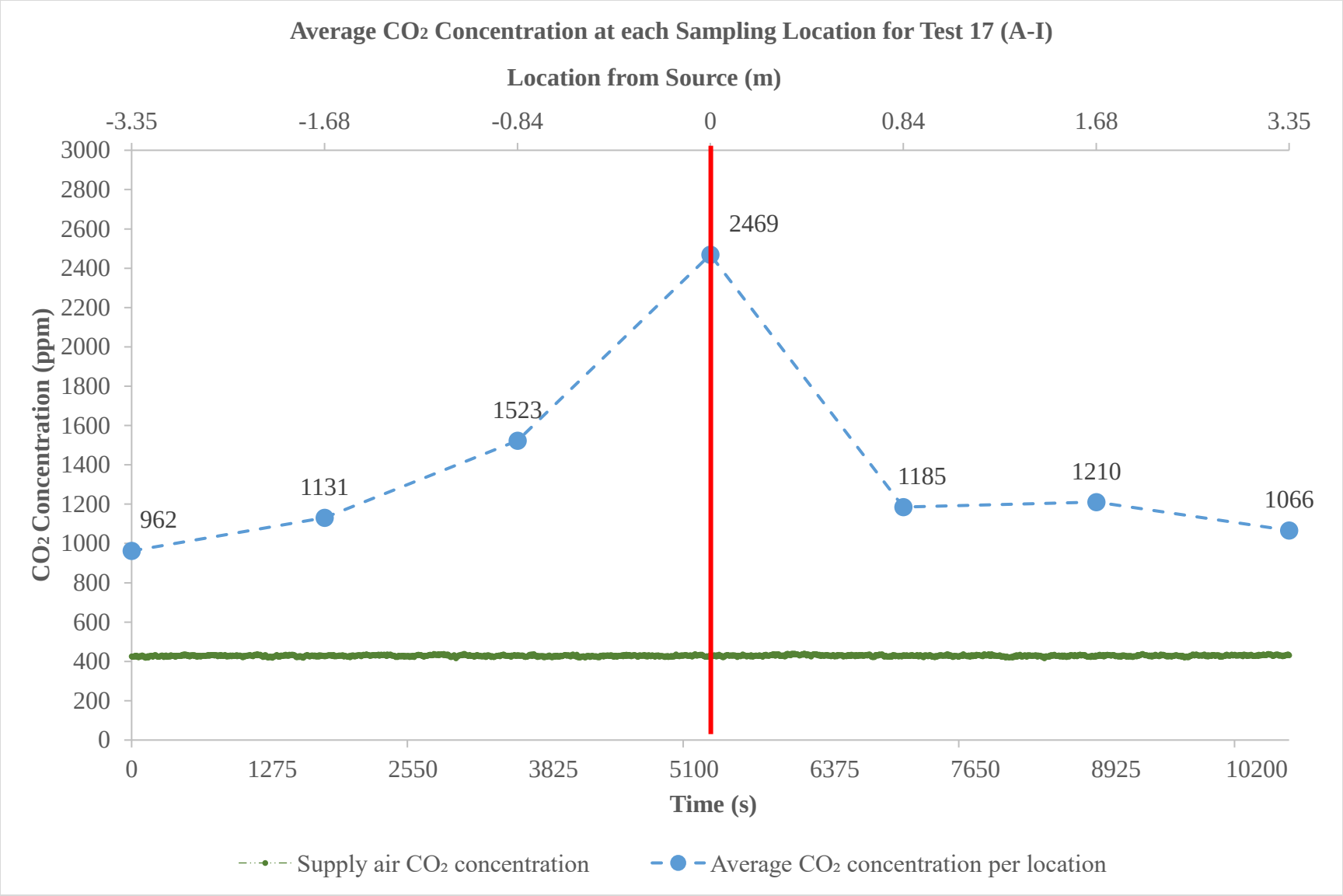

Figure E.97 Average CO_2 concentration at each sampling location for Test 17 (A-I) ISOPass undeployed.

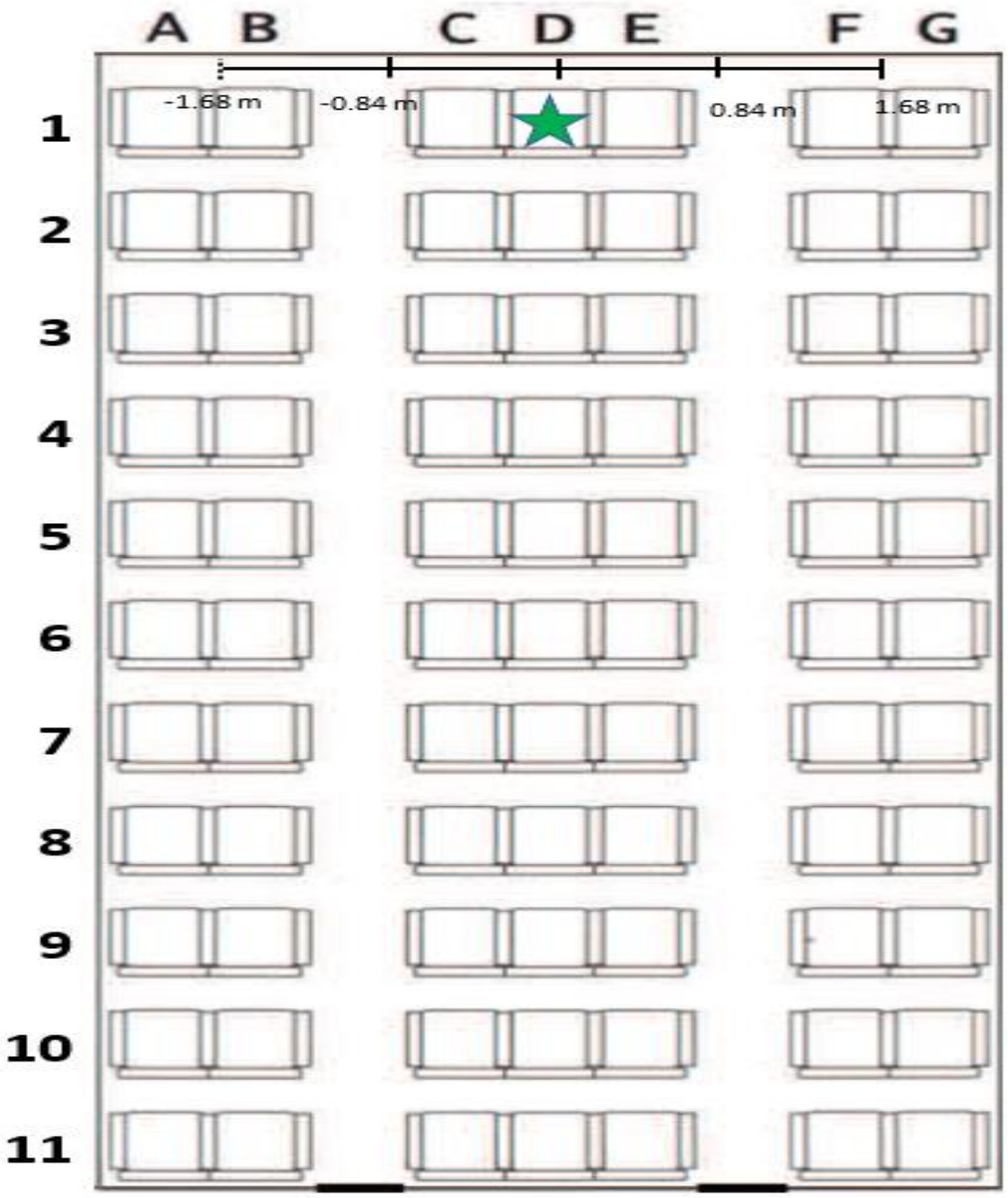

Figure E.98 Test 18 (A-I) ISOPass undeployed source location and sampling tree orientation.

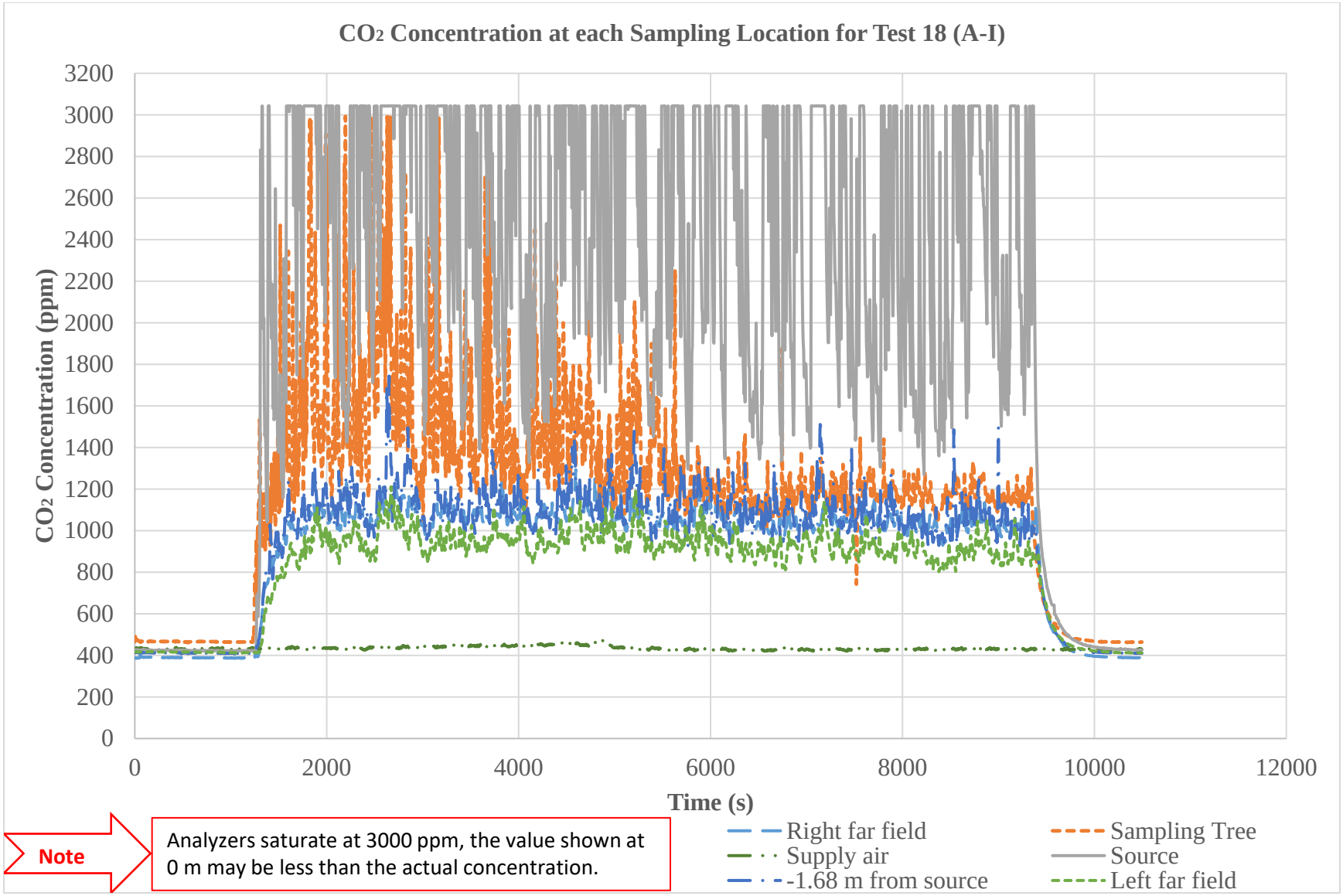

Figure E.99 Ininstantaneous CO_2 concentration at each sampling location for Test 18 (A-I) ISOPass undeployed.

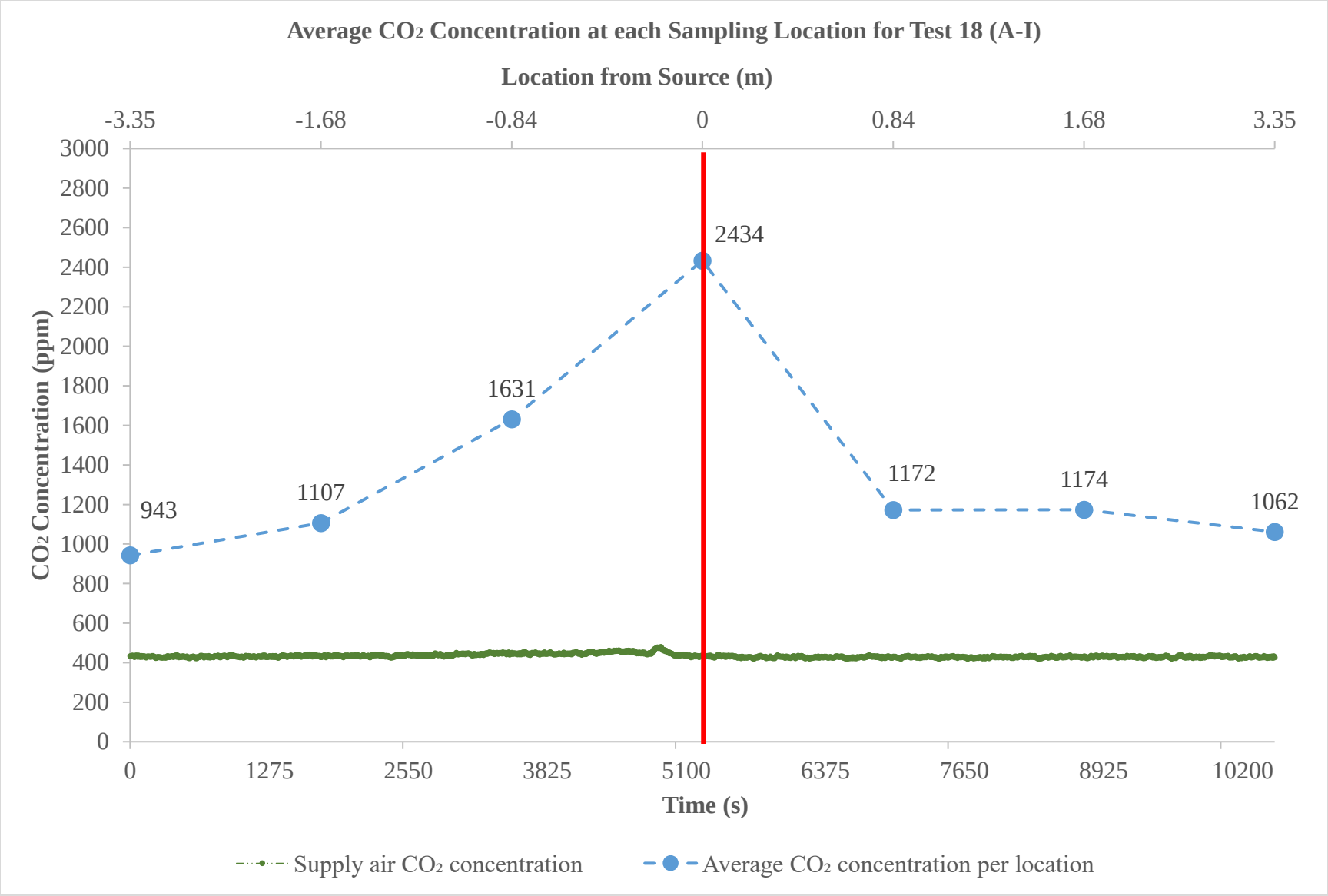

Figure E.100 Average CO_2 concentration at each sampling location for Test 18 (A-I) ISOPass undeployed.

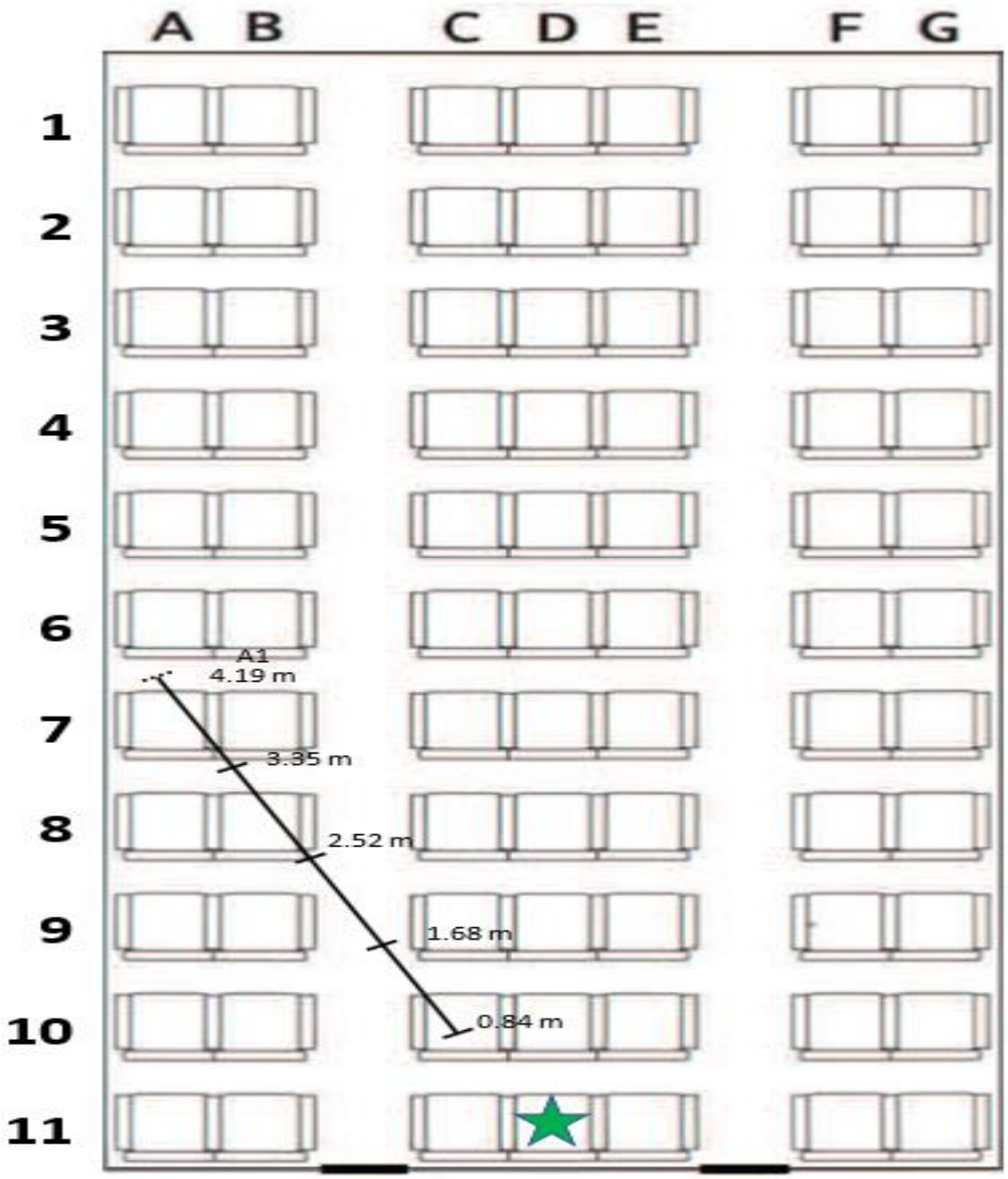

Figure E.101 Test 33 (A-I) ISOPass undeployed source location and sampling tree orientation.

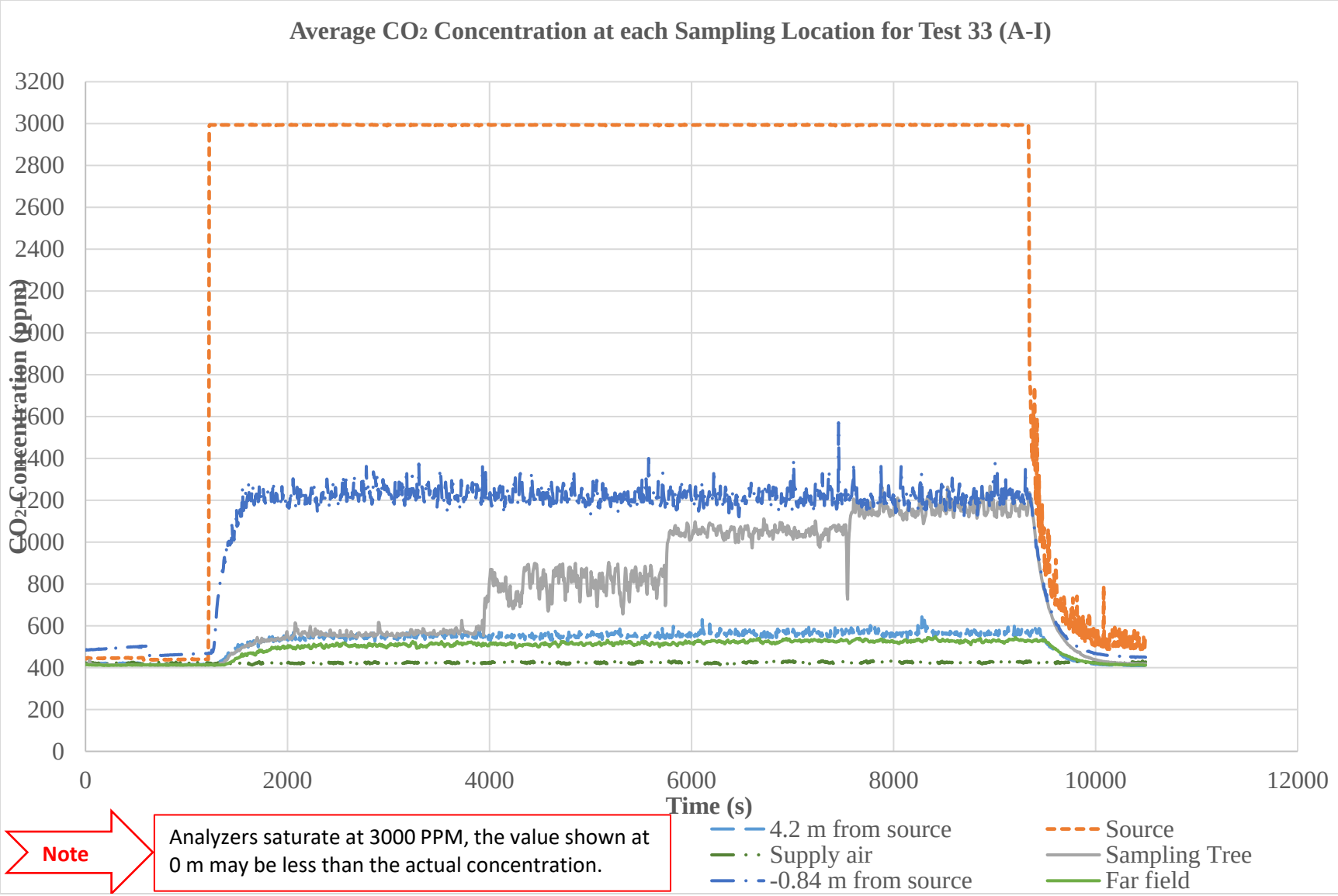

Figure E.102 Ininstantaneous CO_2 concentration at each sampling location for Test 33 (A-I) ISOPass undeployed.

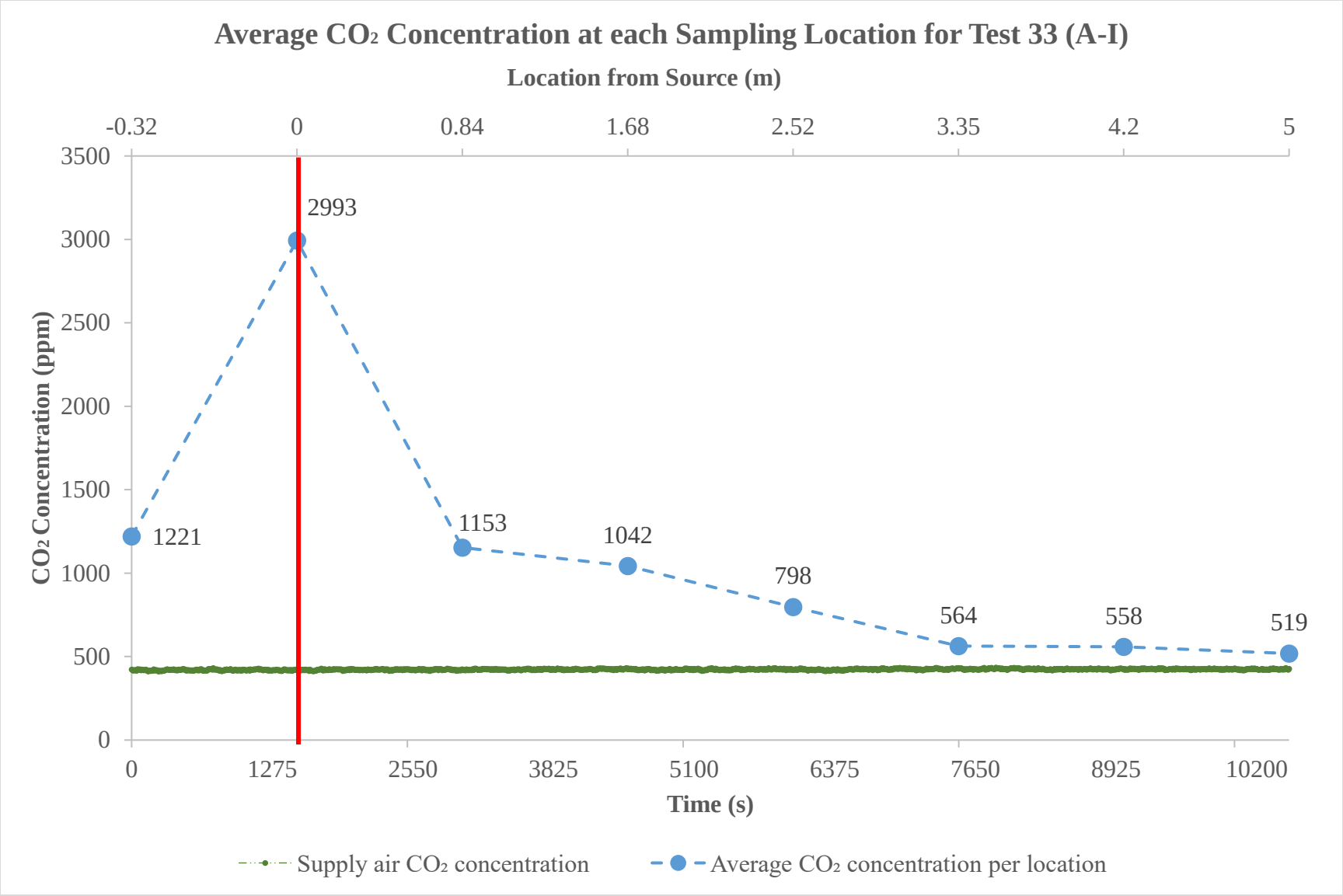

Figure E.103 Average CO_2 concentration at each sampling location for Test 33 (A-I) ISOPass undeployed.

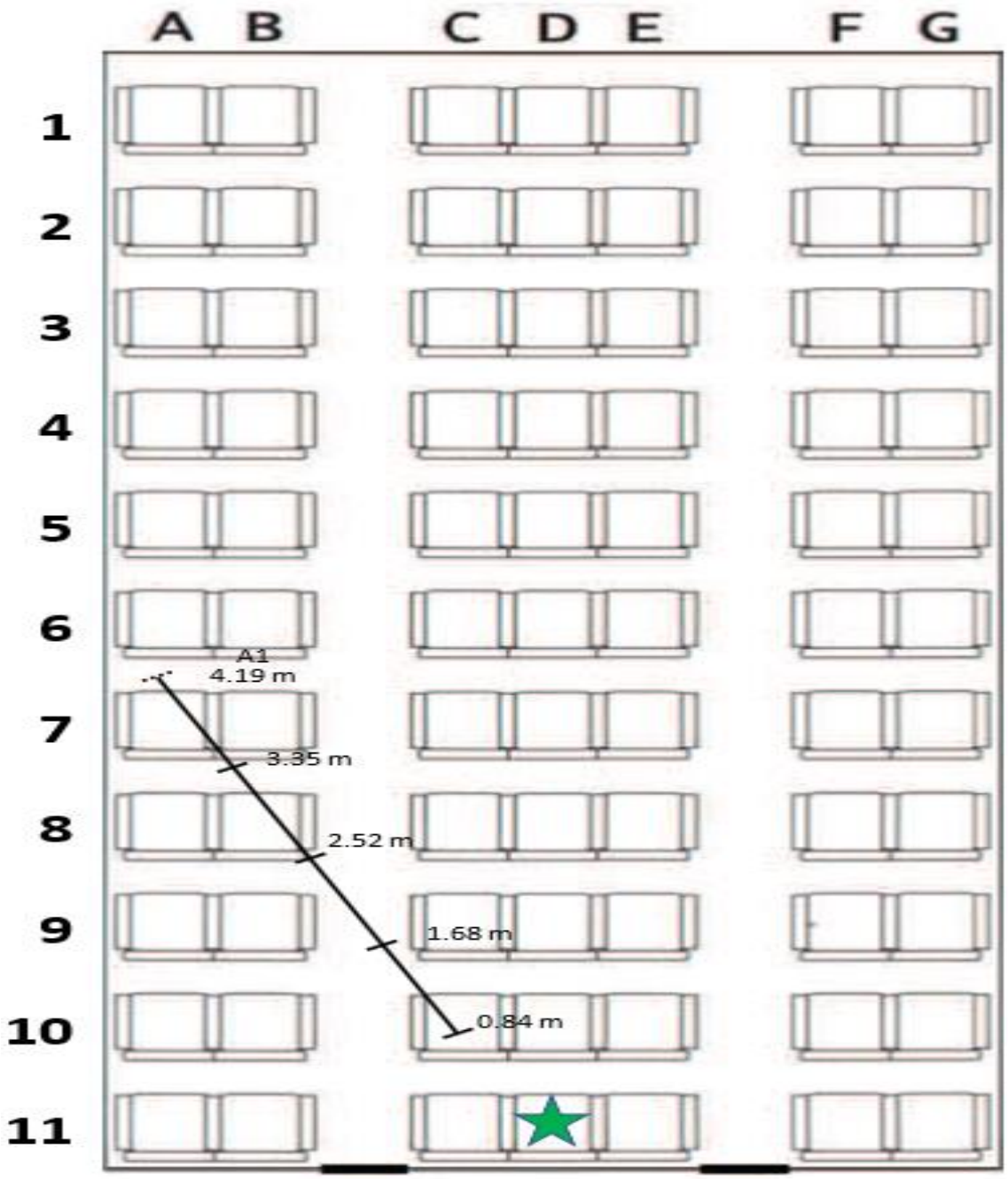

Figure E.104 Test 34 (A-I) ISOPass undeployed source location and sampling tree orientation.

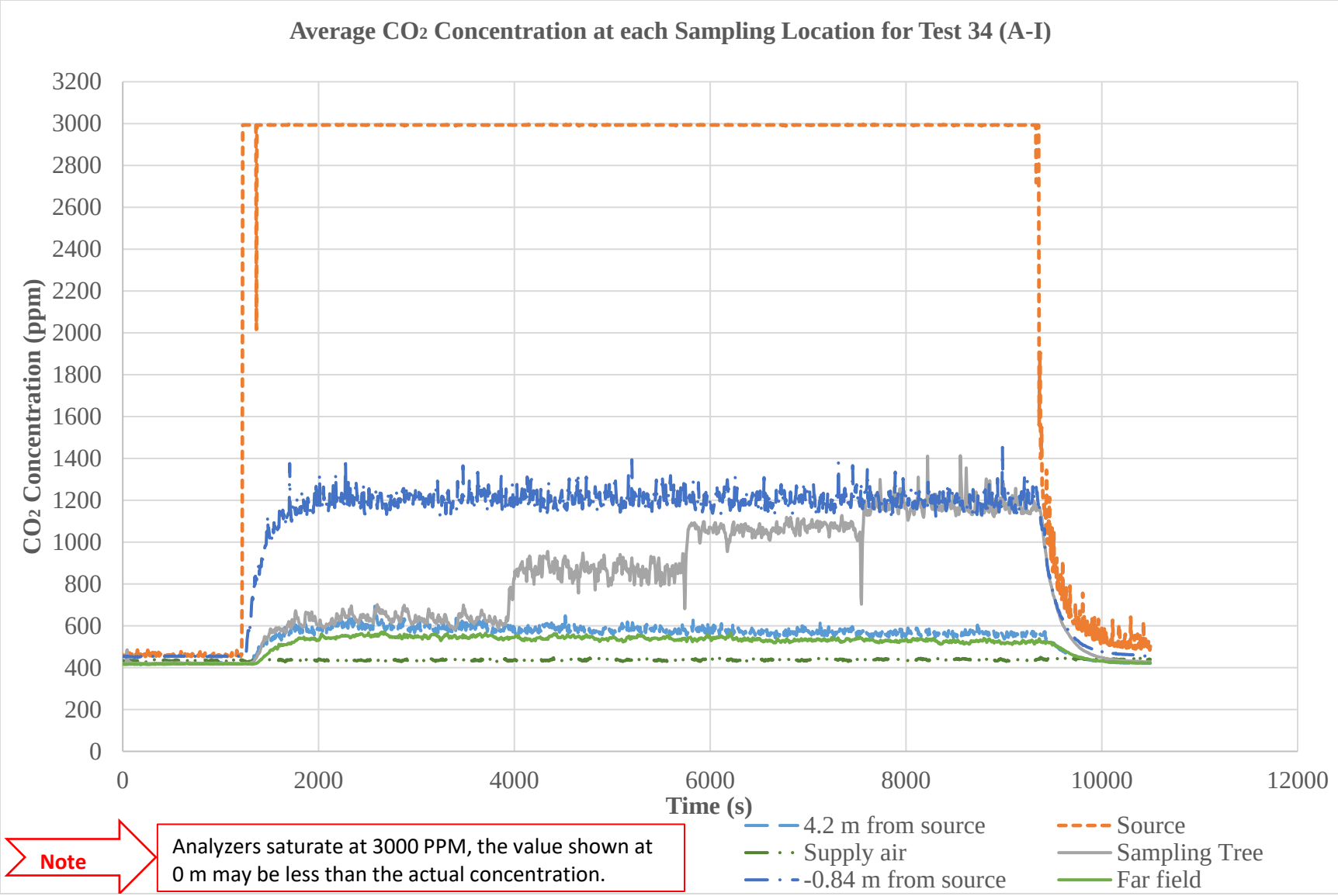

Figure E.105 Ininstantaneous CO_2 concentration at each sampling location for Test 34 (A-I) ISOPass undeployed.

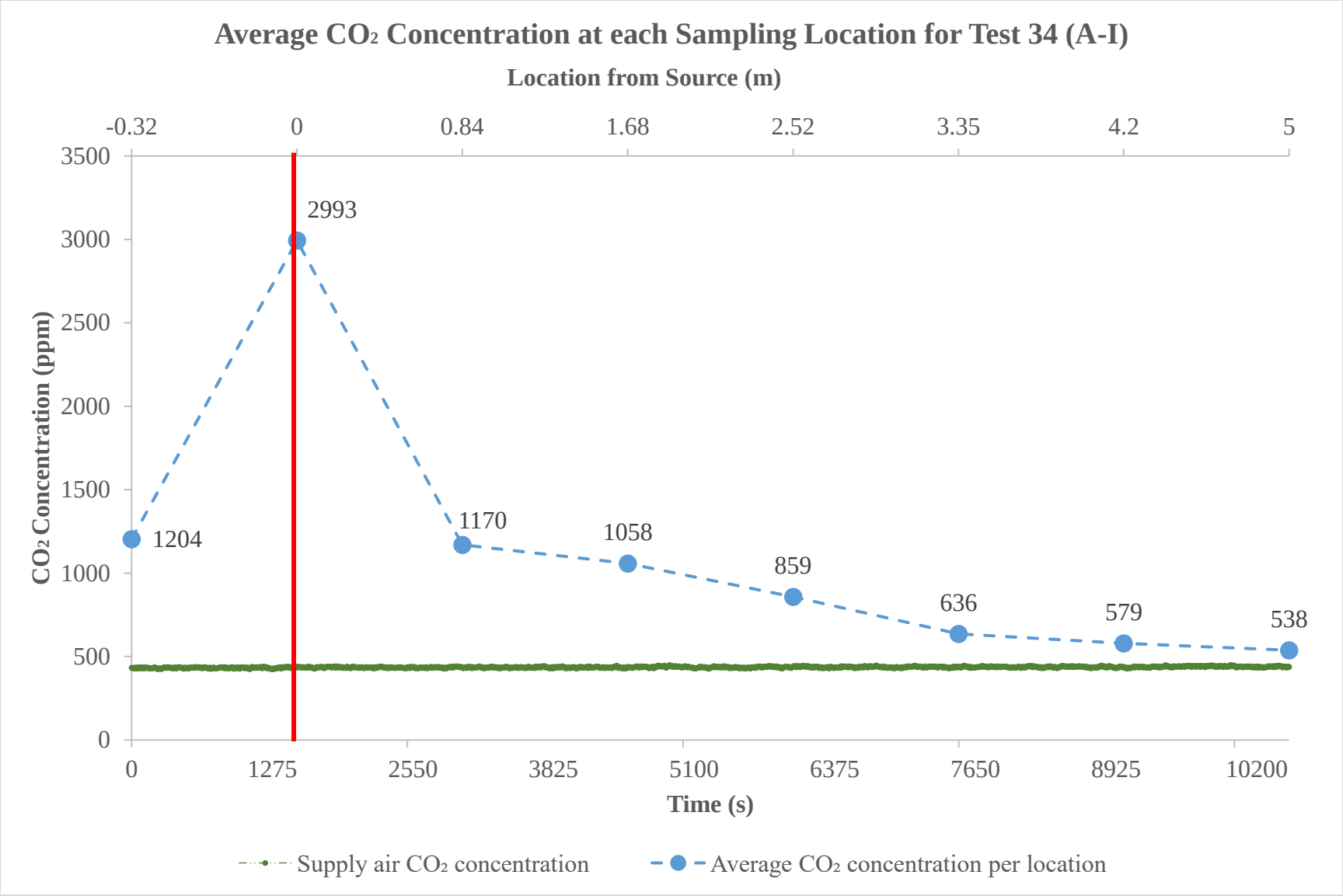

Figure E.106 Average CO_2 concentration at each sampling location for Test 34 (A-I) ISOPass undeployed.

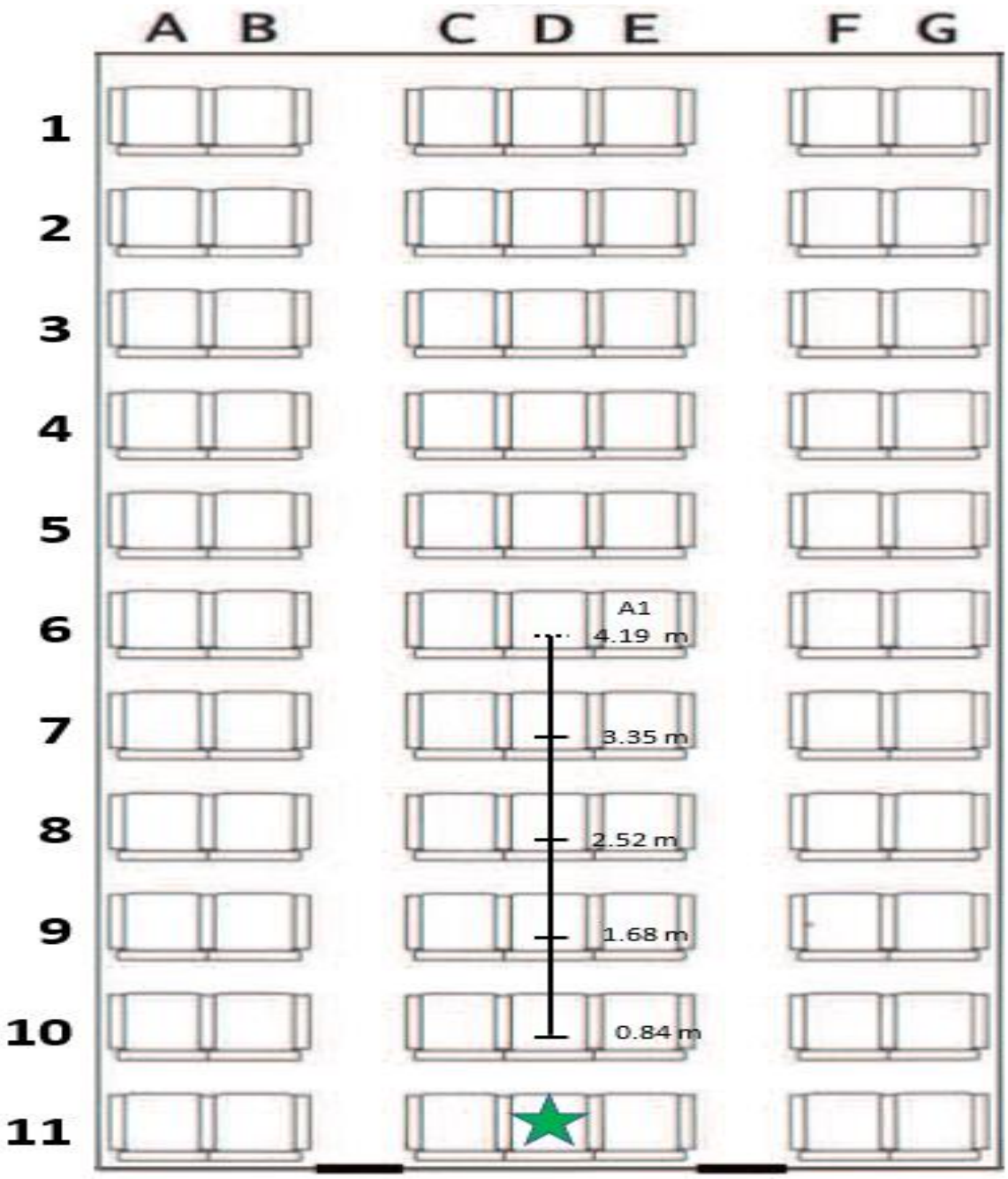

Figure E.107 Test 35 (A-I) ISOPass undeployed source location and sampling tree orientation.

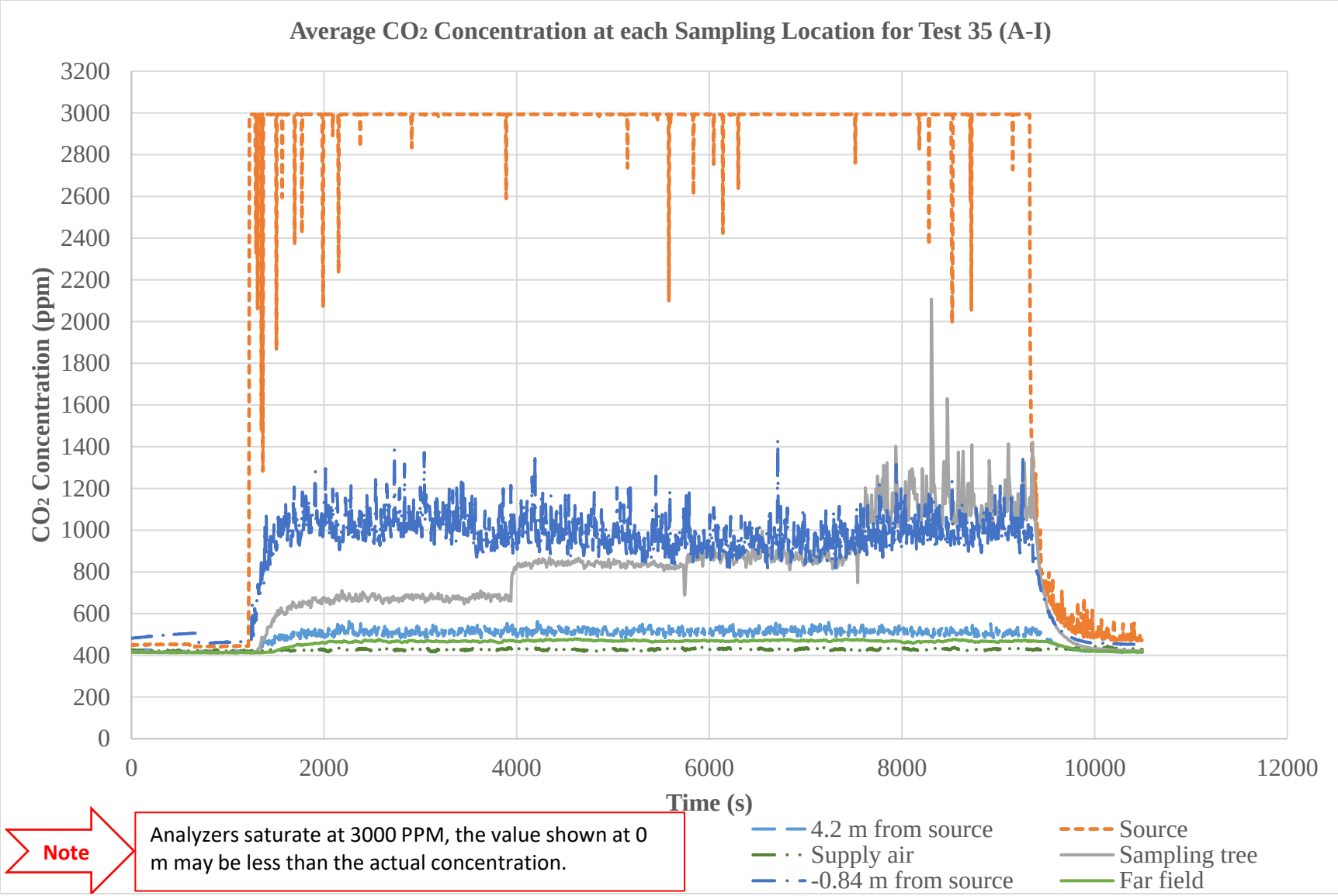

Figure E.108 Ininstantaneous CO_2 concentration at each sampling location for Test 35 (A-I) ISOPass undeployed.

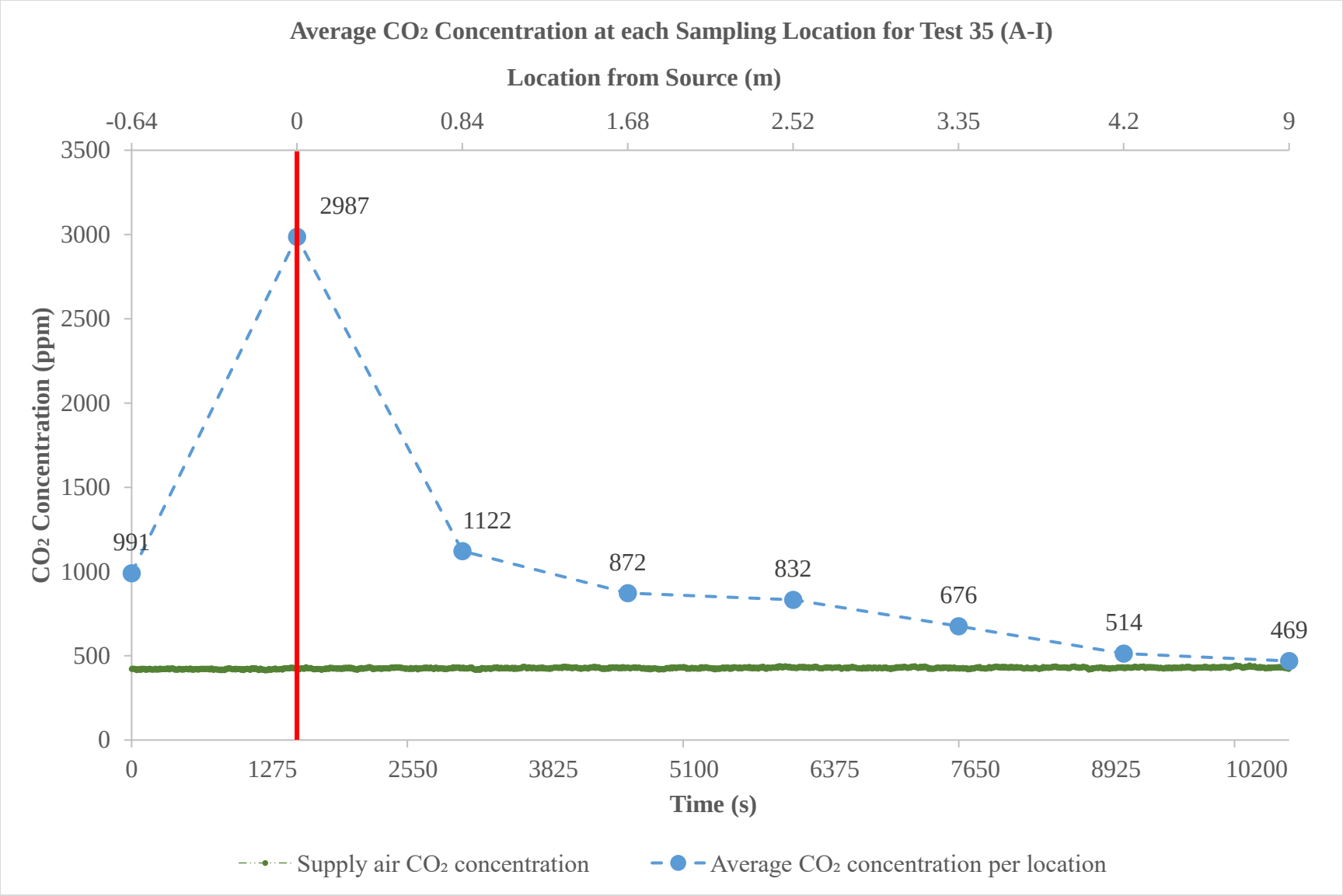

Figure E.109 Average CO_2 concentration at each sampling location for Test 35 (A-I) ISOPass undeployed.

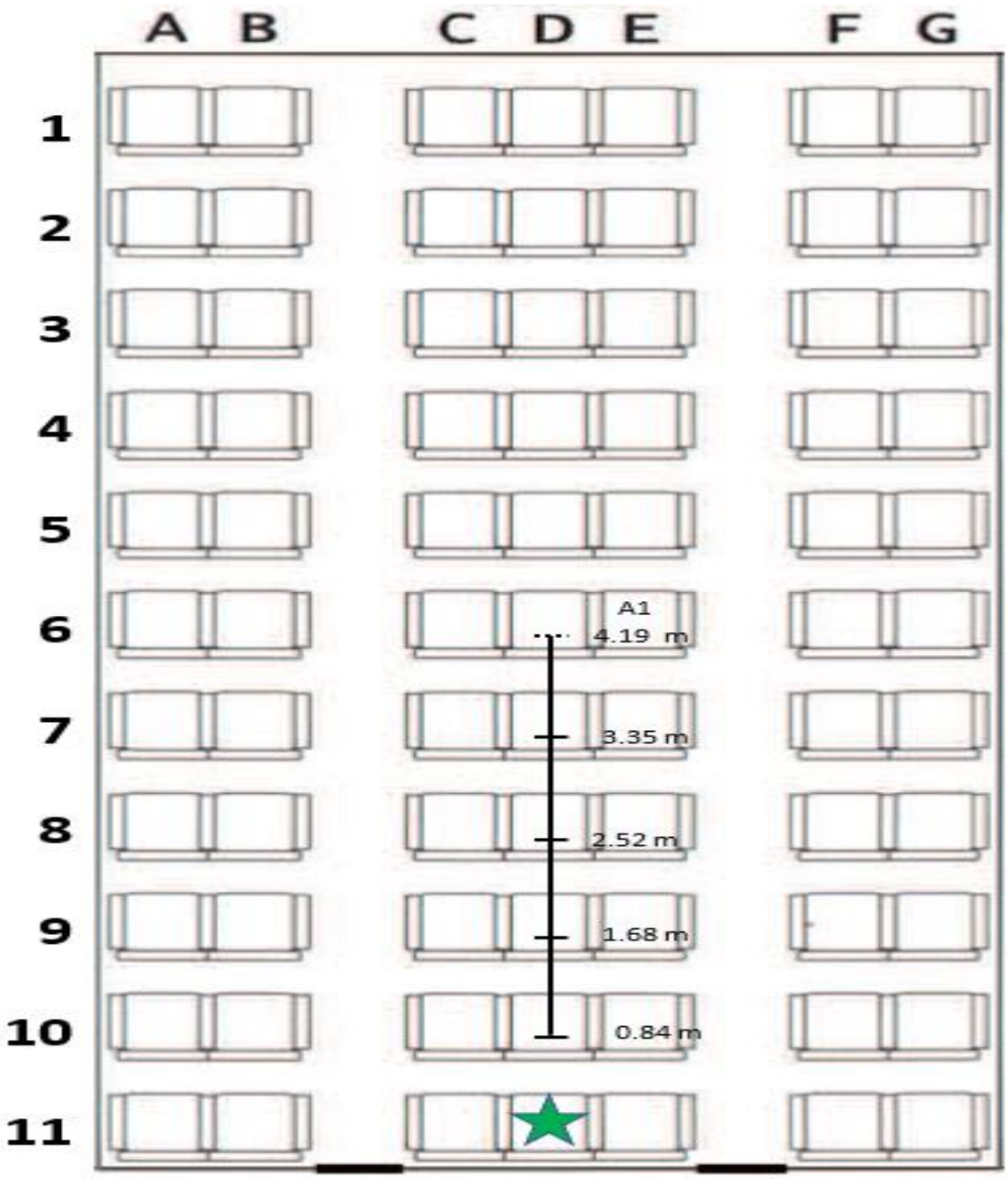

Figure E.110 Test 36 (A-I) ISOPass undeployed source location and sampling tree orientation.

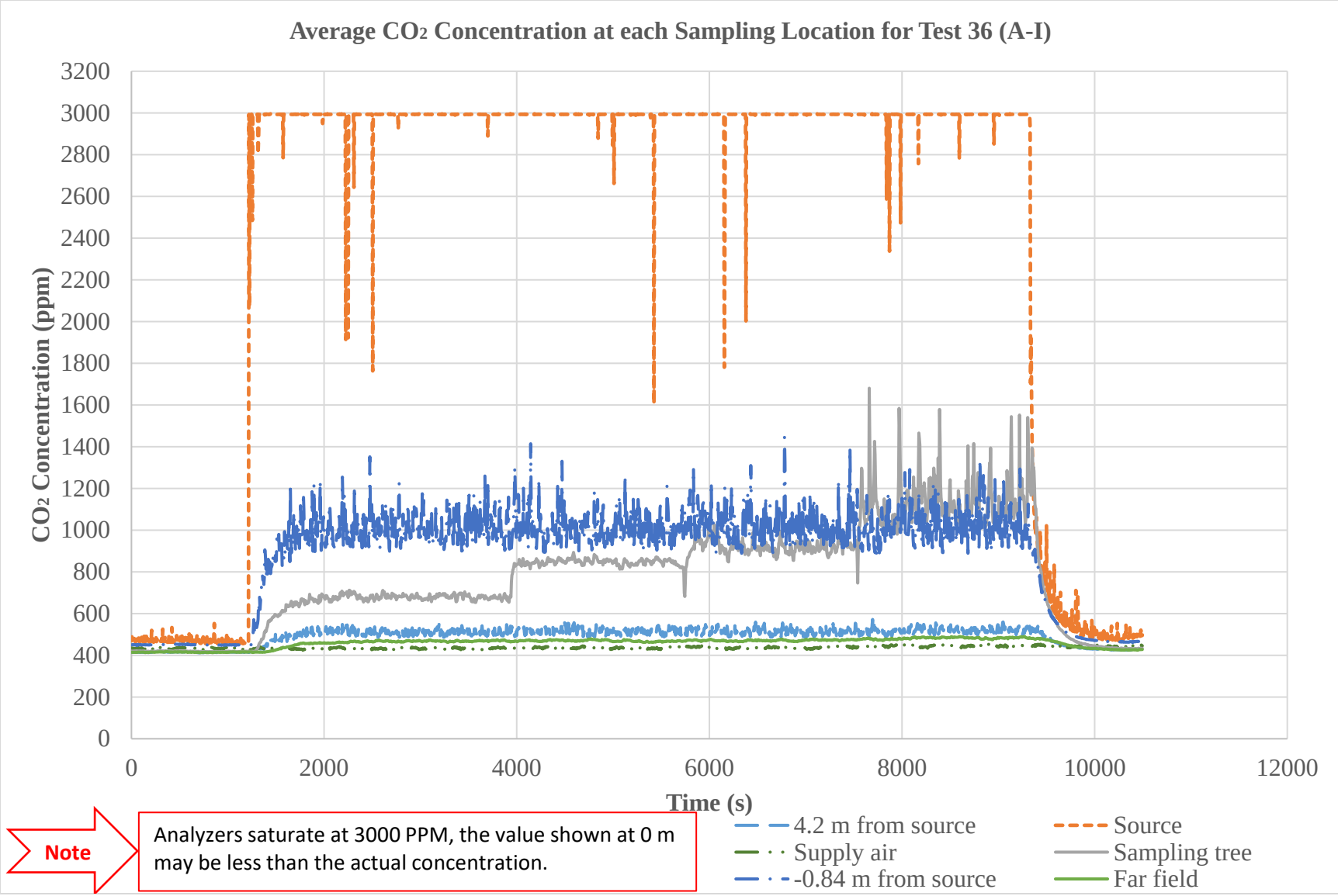

Figure E.111 Ininstantaneous CO_2 concentration at each sampling location for Test 36 (A-I) ISOPass undeployed.

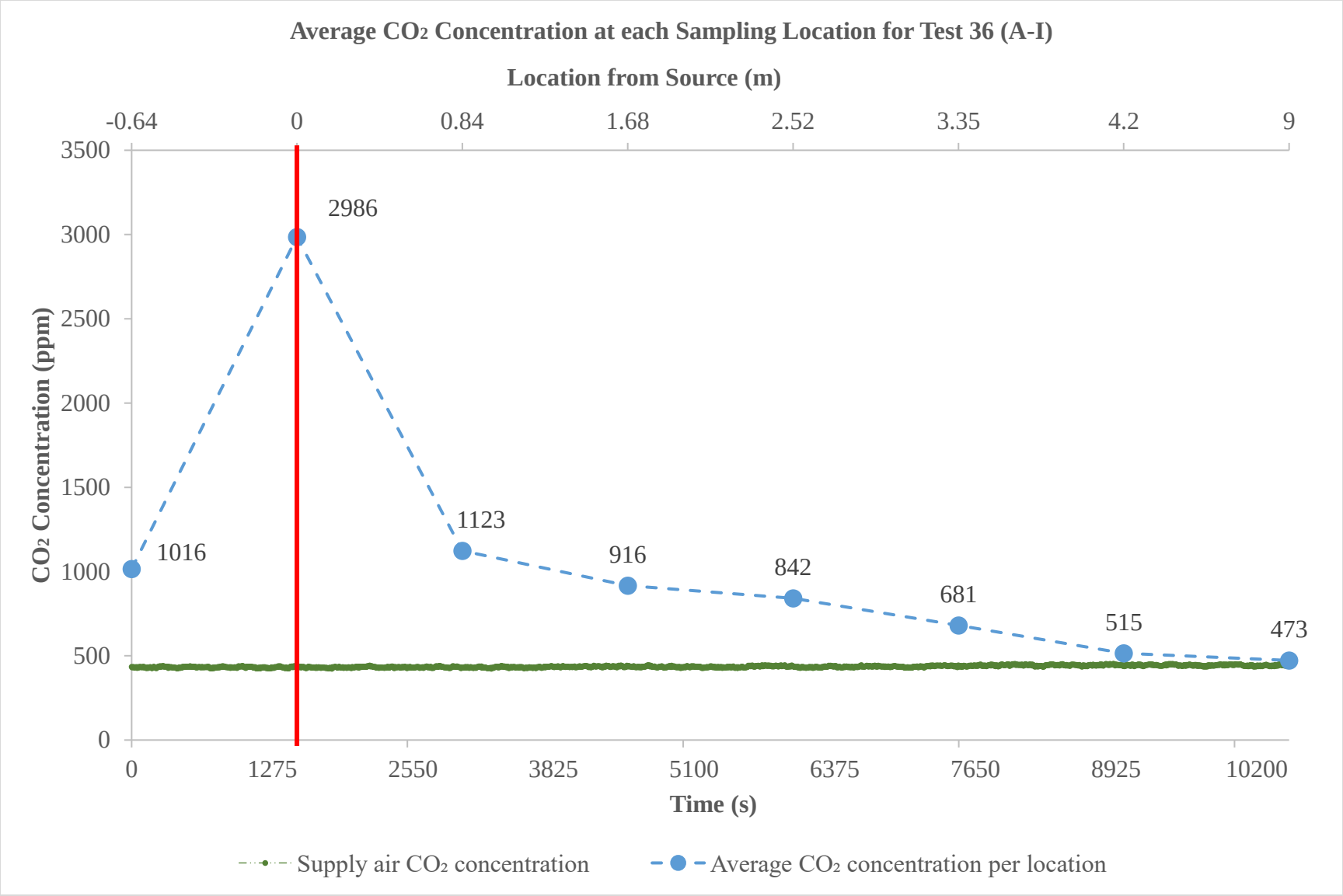

Figure E.112 Average CO_2 concentration at each sampling location for Test 36 (A-I) ISOPass undeployed.

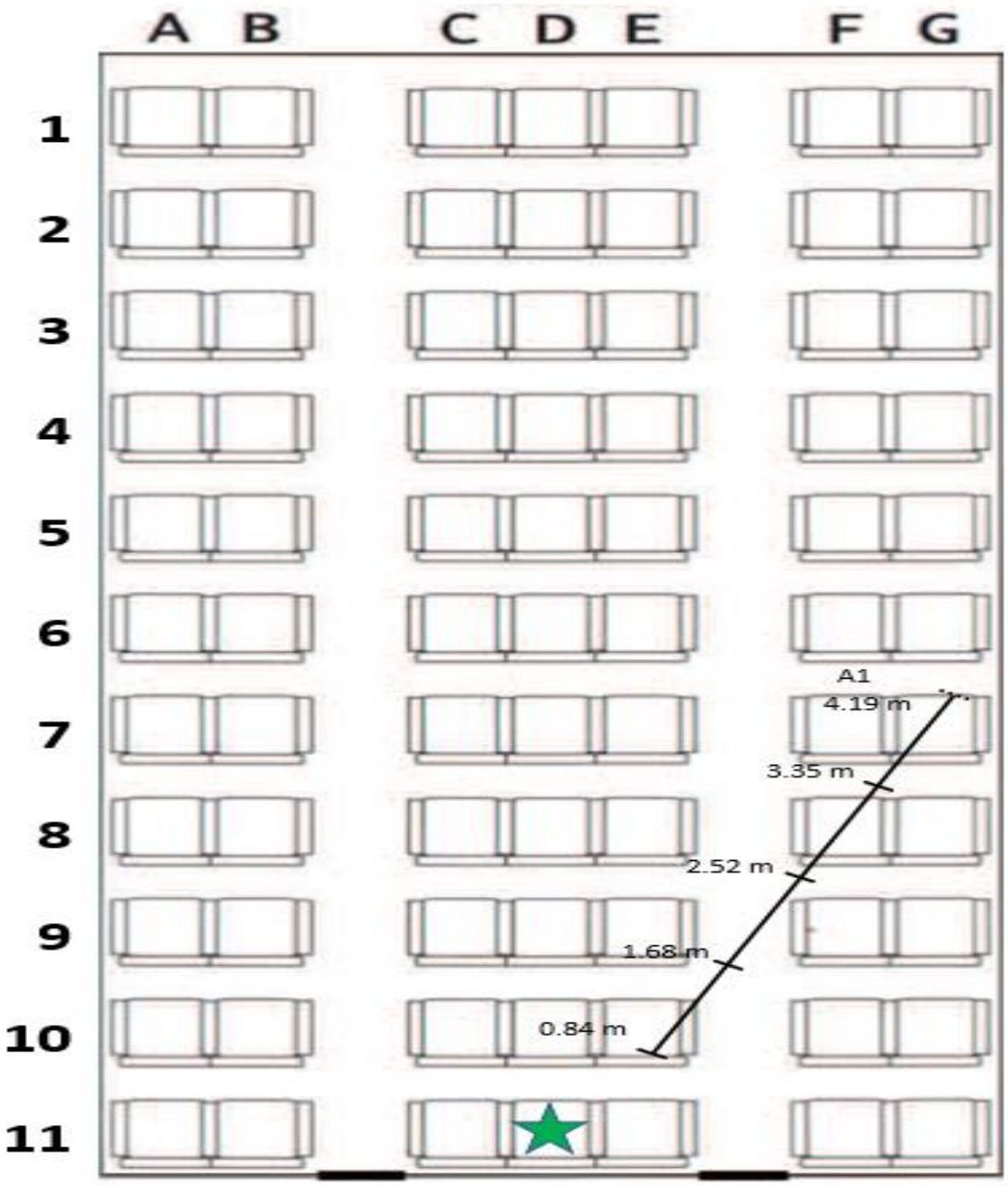

Figure E.113 Test 37 (A-I) ISOPass undeployed source location and sampling tree orientation.

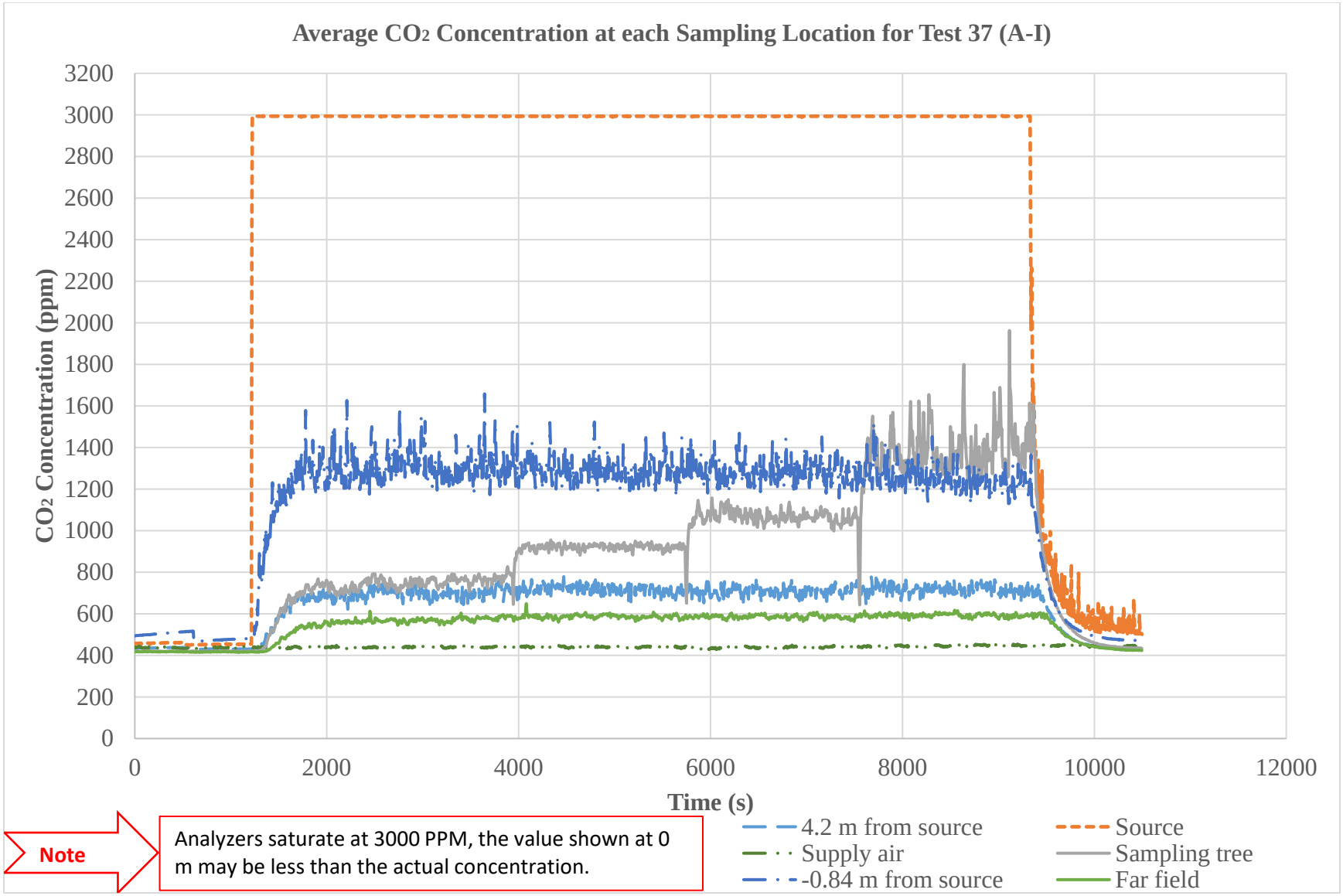

Figure E.114 Ininstantaneous CO_2 concentration at each sampling location for Test 37 (A-I) ISOPass undeployed.

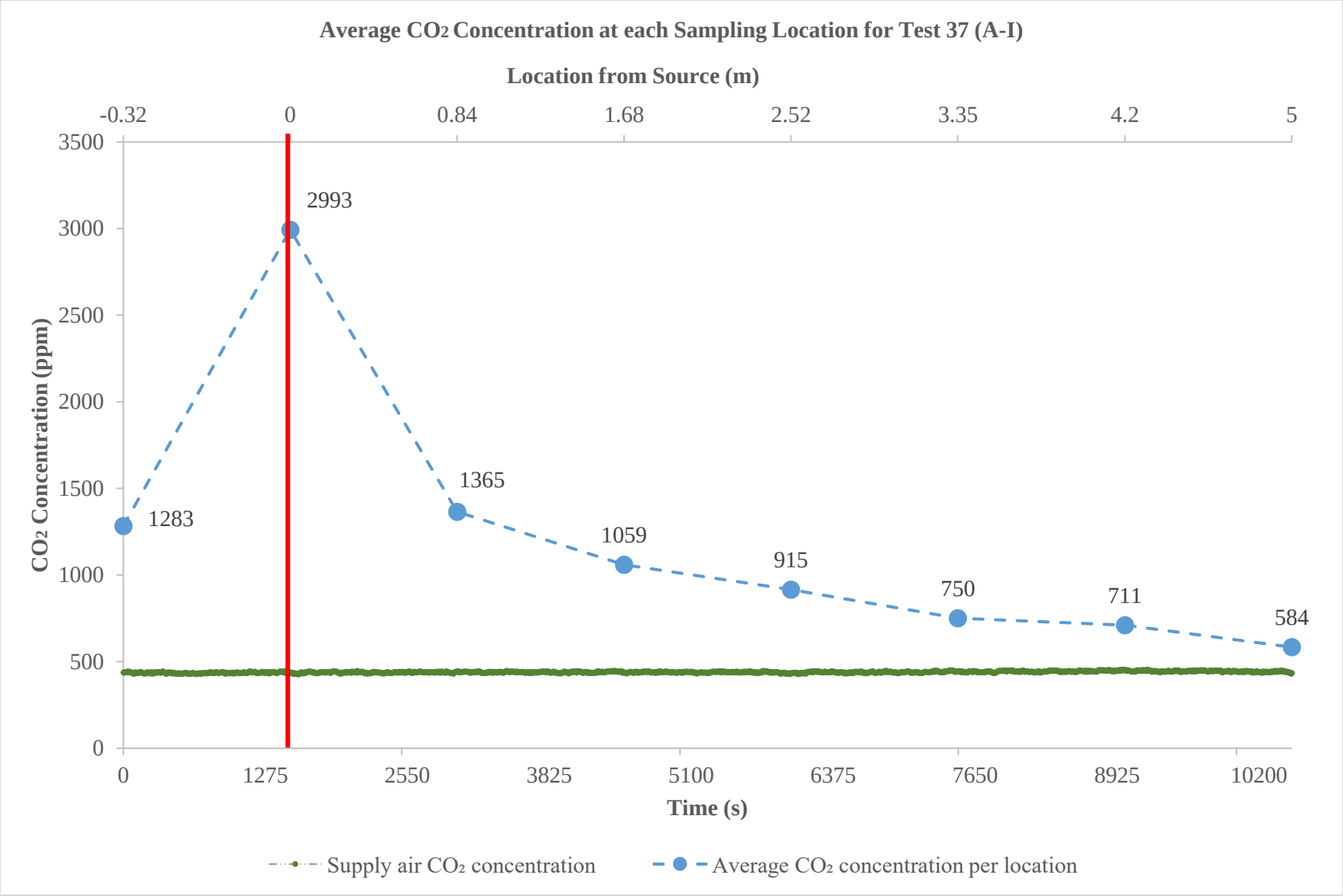

Figure E.115 Average CO_2 concentration at each sampling location for Test 37 (A-I) ISOPass undeployed.

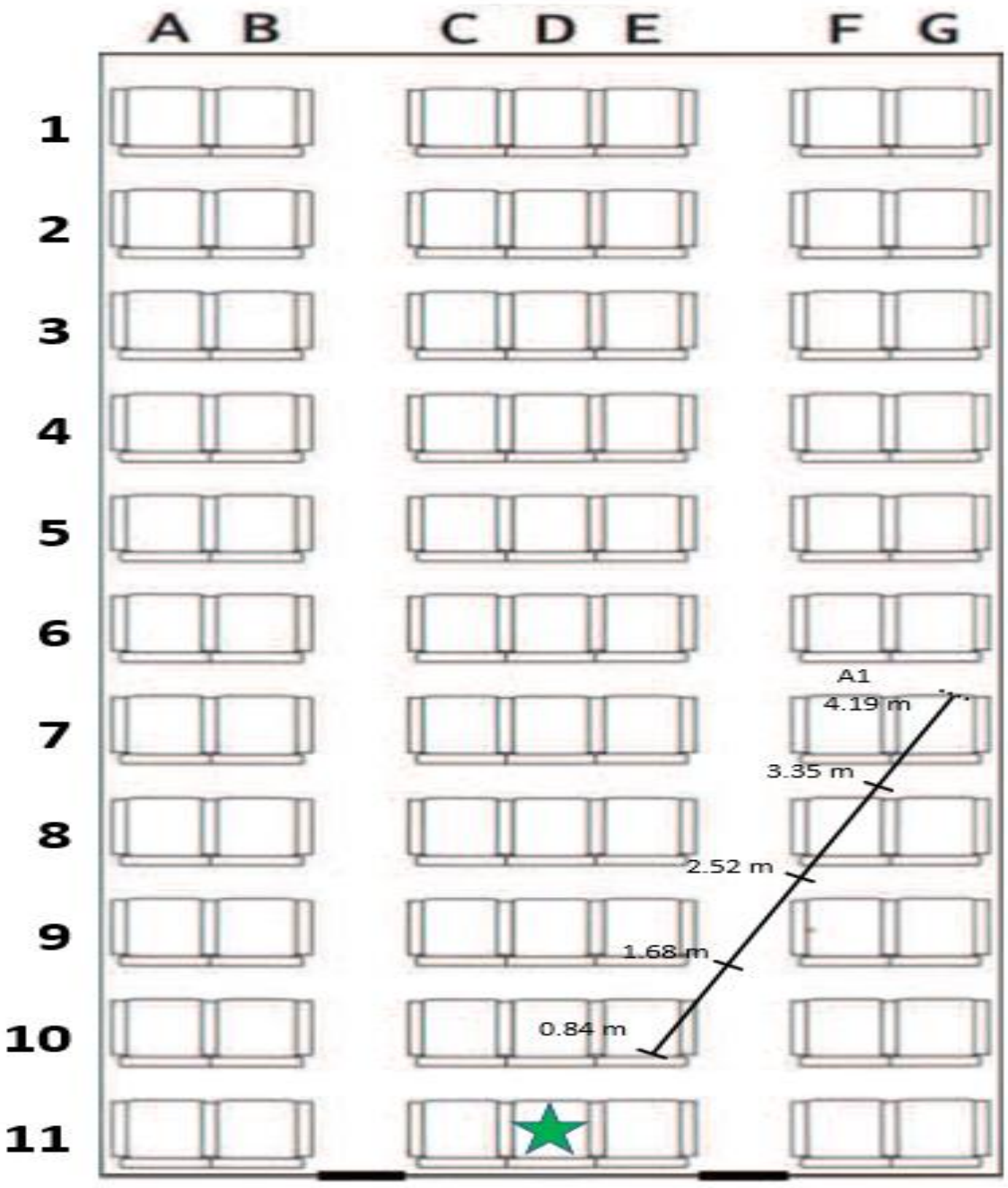

Figure E.116 Test 38 (A-I) ISOPass undeployed source location and sampling tree orientation.

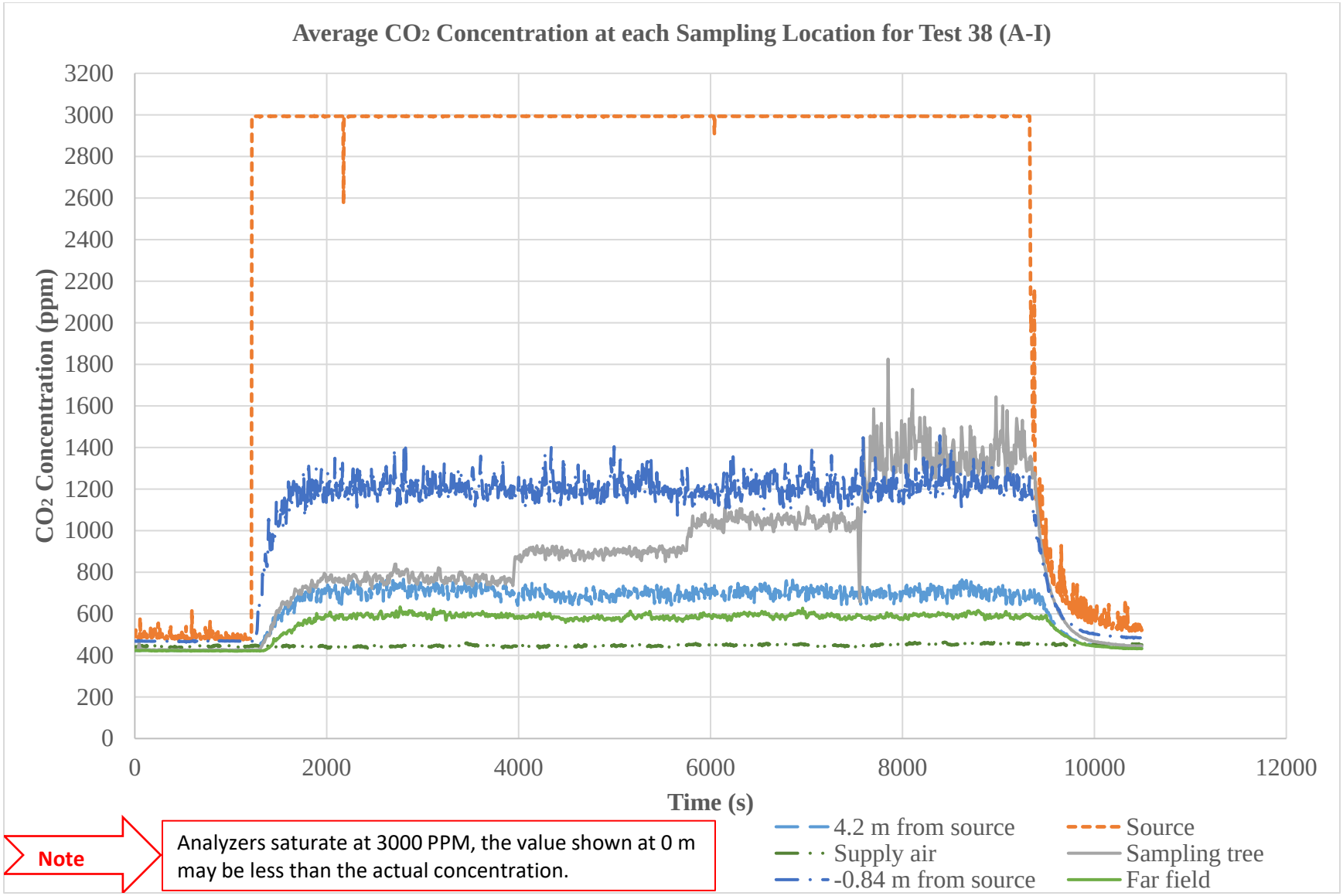

Figure E.117 Ininstantaneous CO_2 concentration at each sampling location for Test 38 (A-I) ISOPass undeployed.

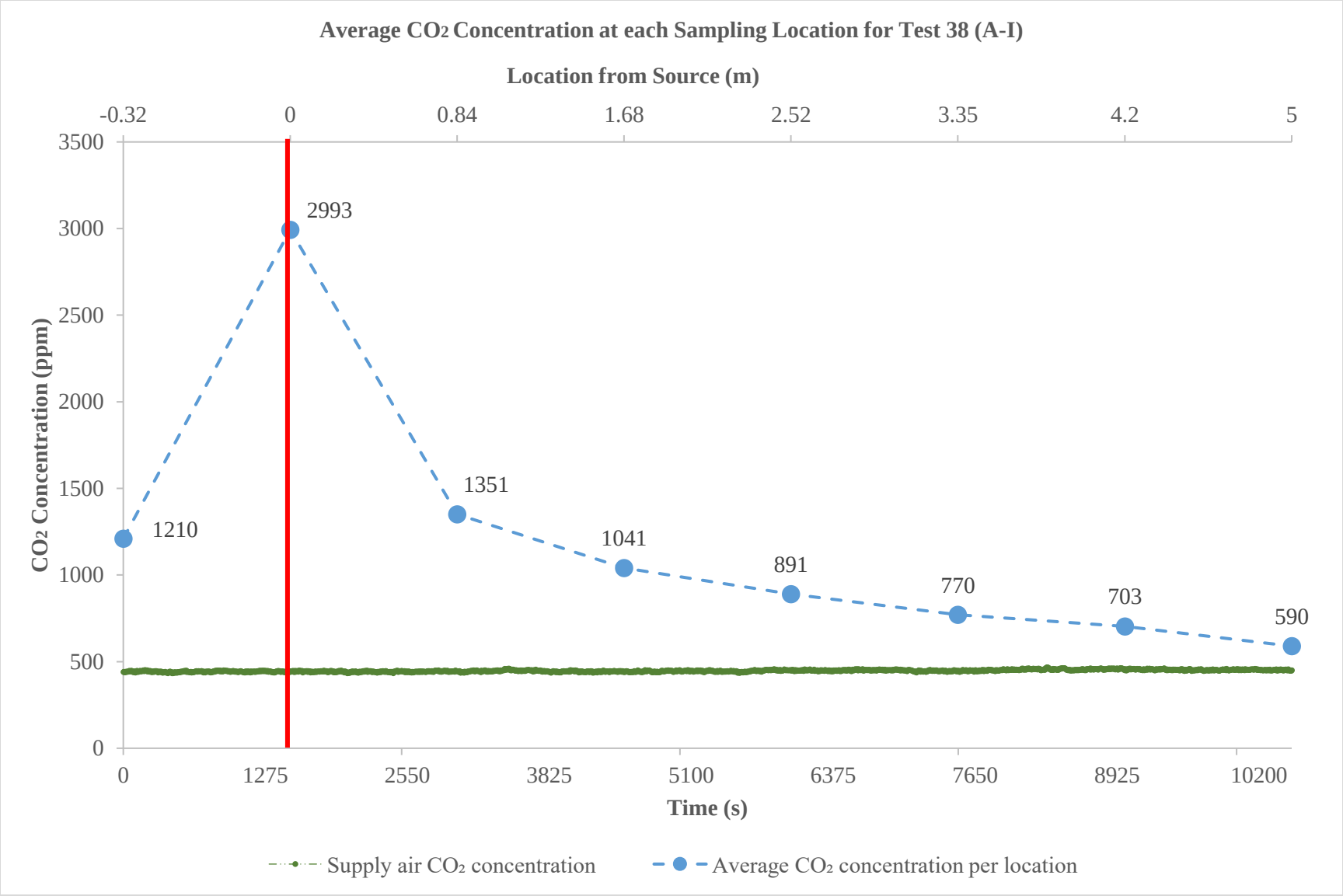

Figure E.118 Average CO_2 concentration at each sampling location for Test 38 (A-I) ISOPass undeployed.

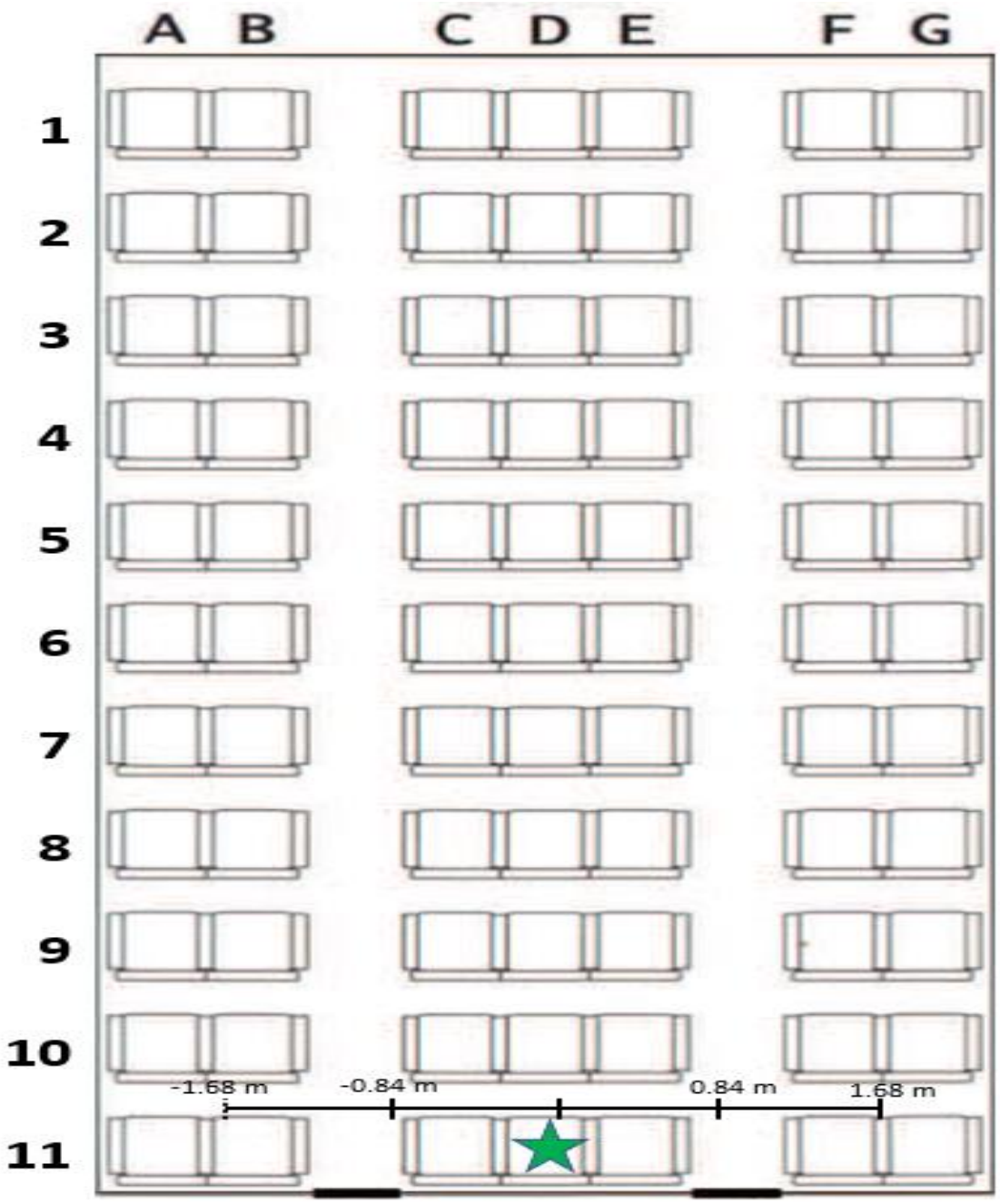

Figure E.119 Test 39 (A-I) ISOPass undeployed source location and sampling tree orientation.

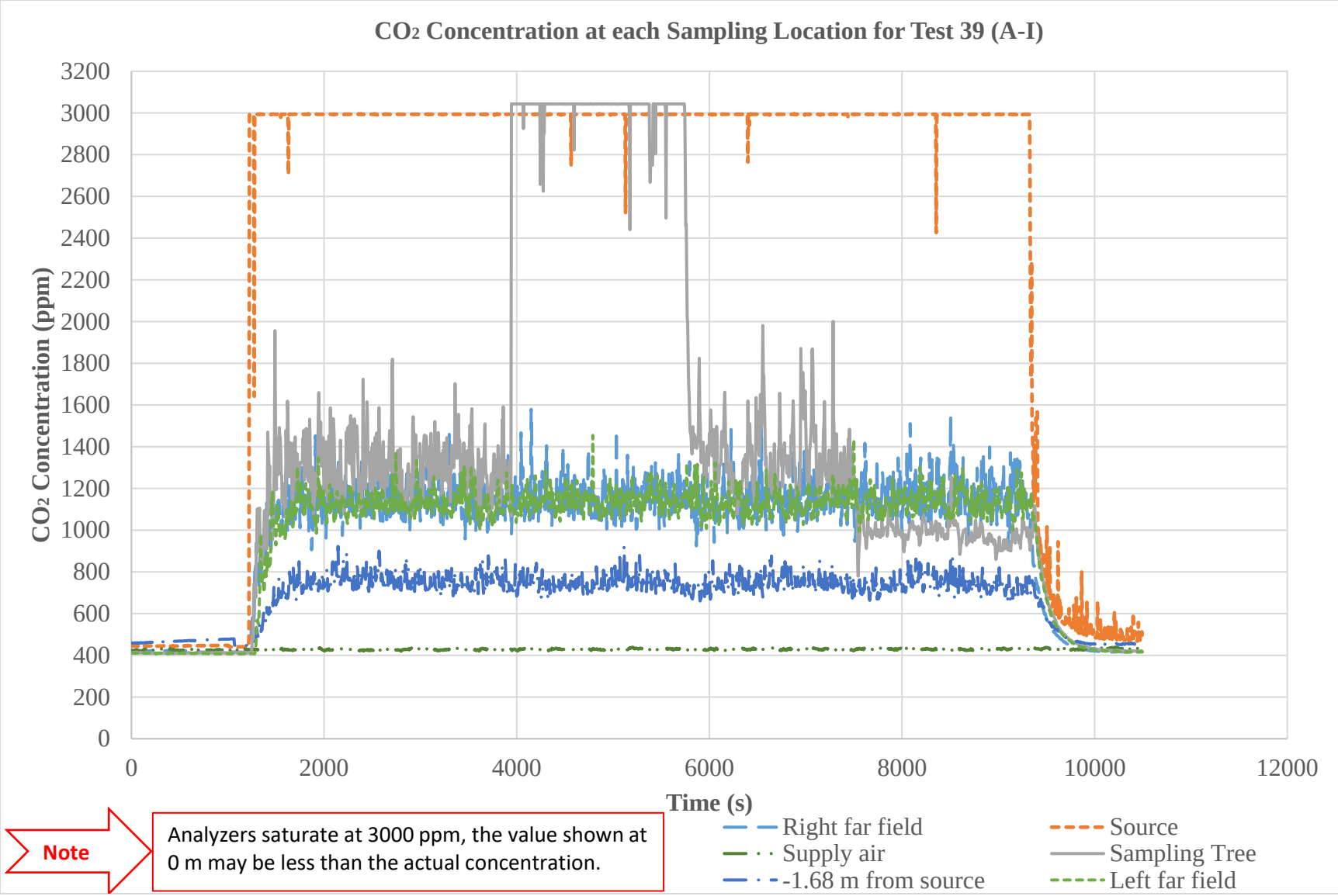

Figure E.120 Ininstantaneous CO_2 concentration at each sampling location for Test 39 (A-I) ISOPass undeployed.

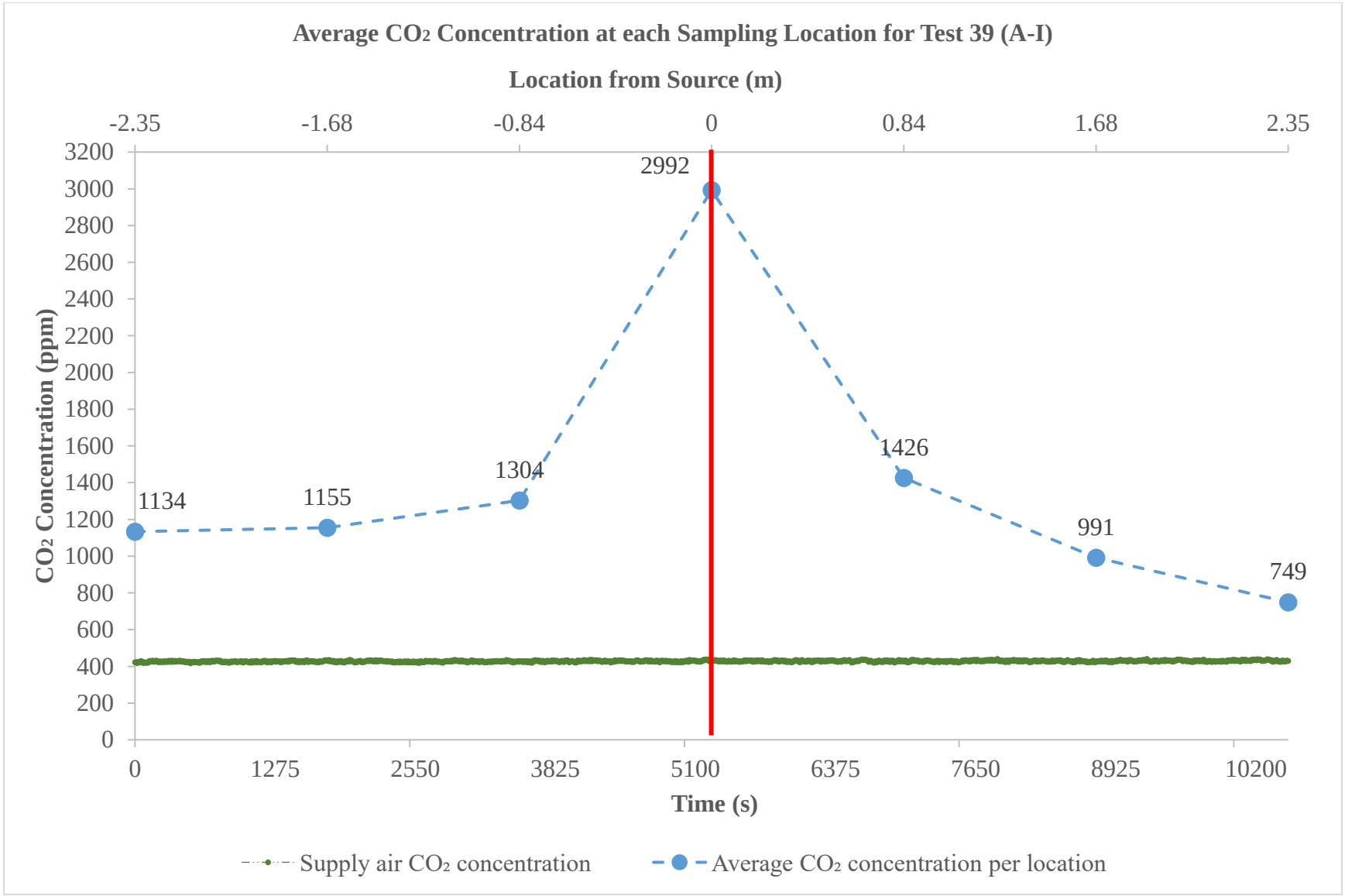

Figure E.121 Average CO_2 concentration at each sampling location for Test 39 (A-I) ISOPass undeployed.

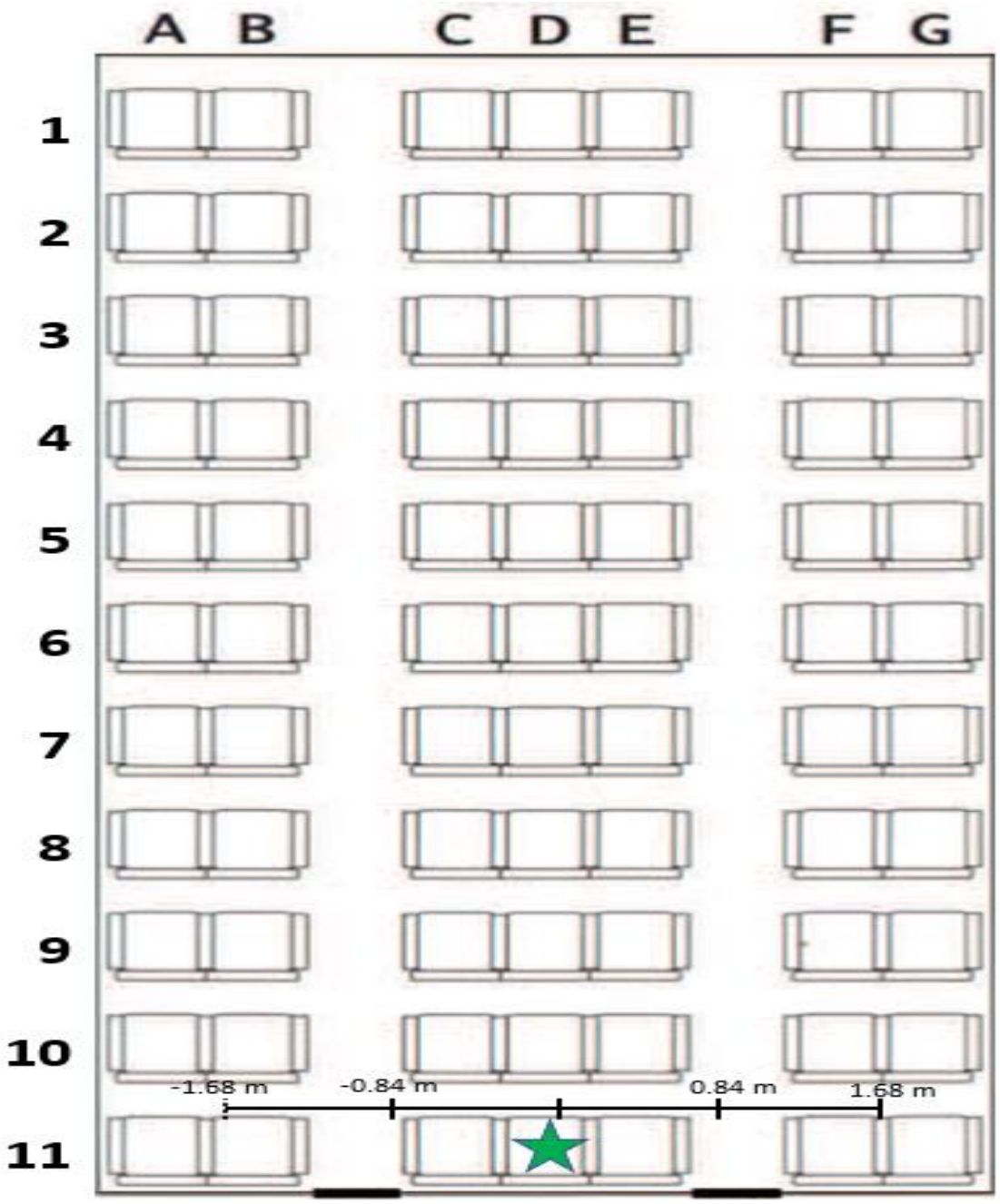

Figure E.122 Test 40 (A-I) ISOPass undeployed source location and sampling tree orientation.

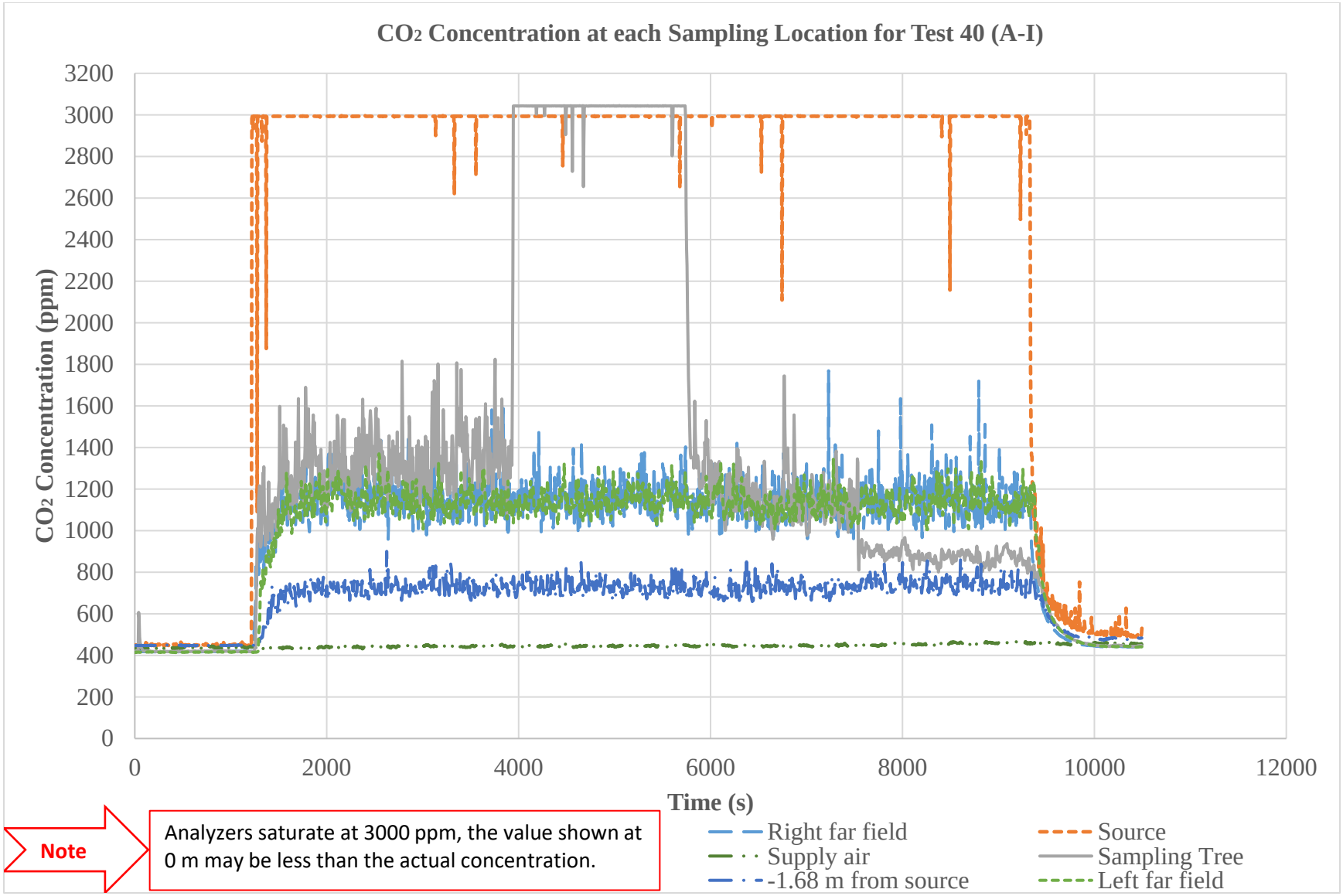

Figure E.123 Ininstantaneous CO_2 concentration at each sampling location for Test 40 (A-I) ISOPass undeployed.

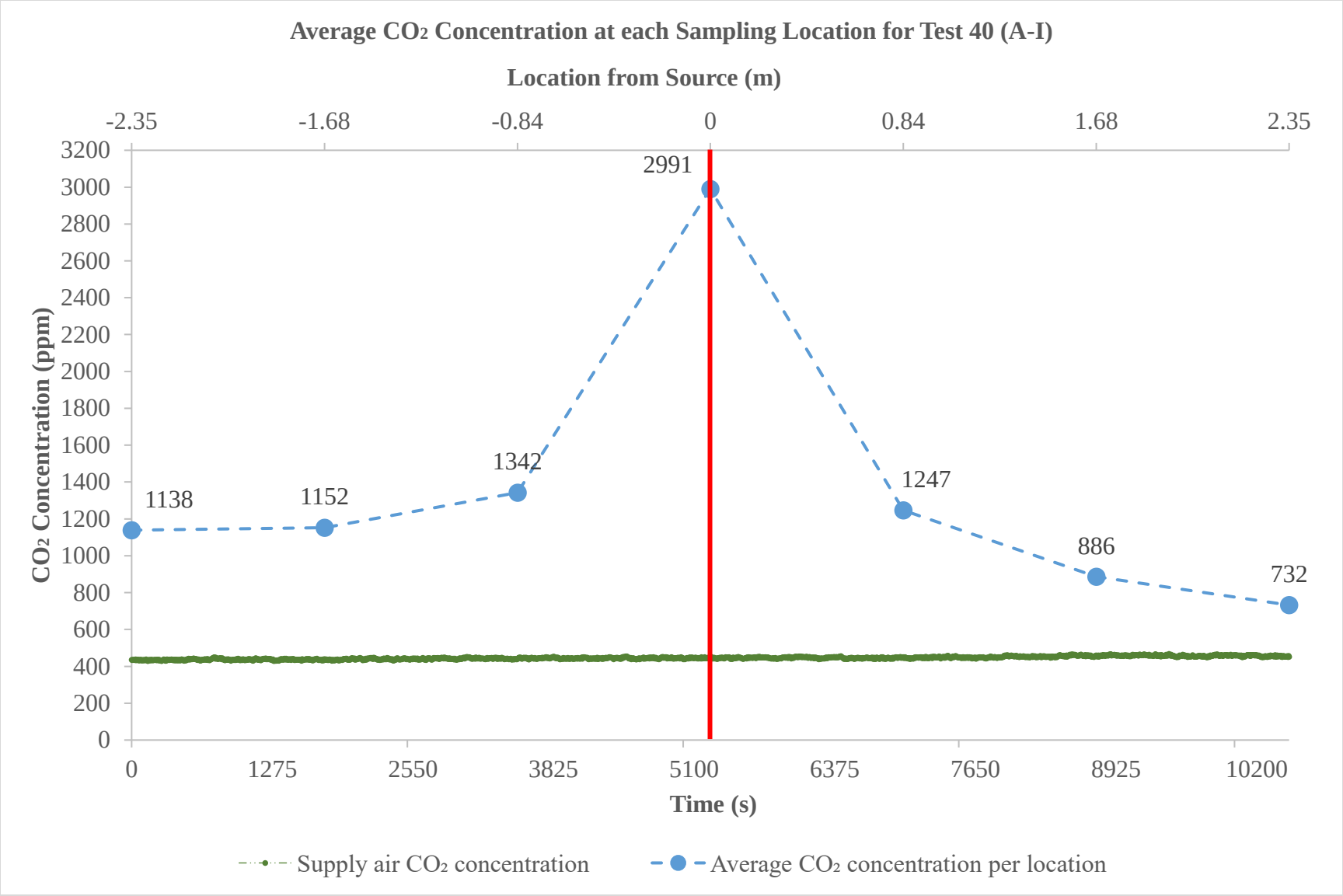

Figure E.124 Average CO_2 concentration at each sampling location for Test 40 (A-I) ISOPass undeployed.

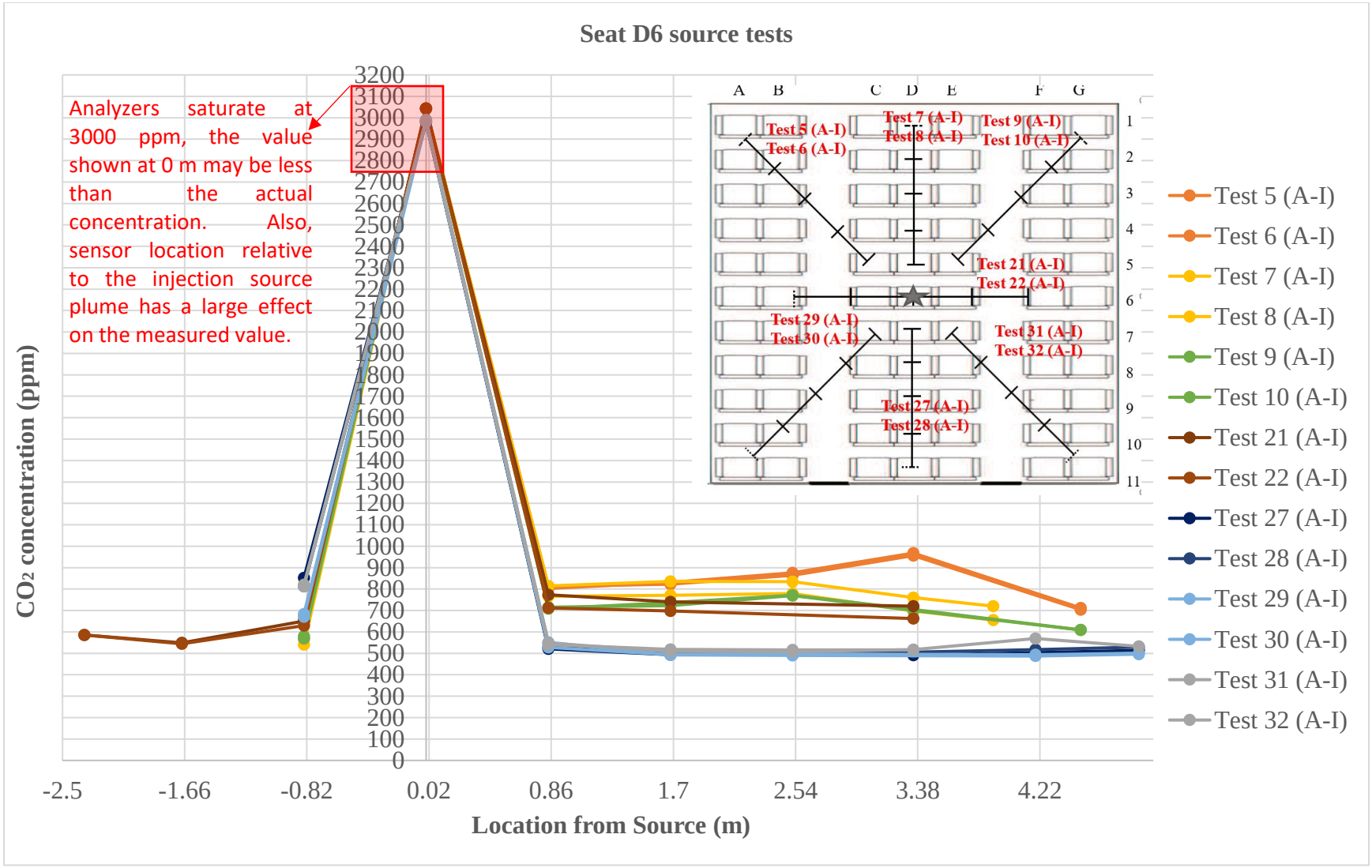

Figure E.125 Seat D6 continuous injection source tests in the modified cabin with the ISOPass undeployed.

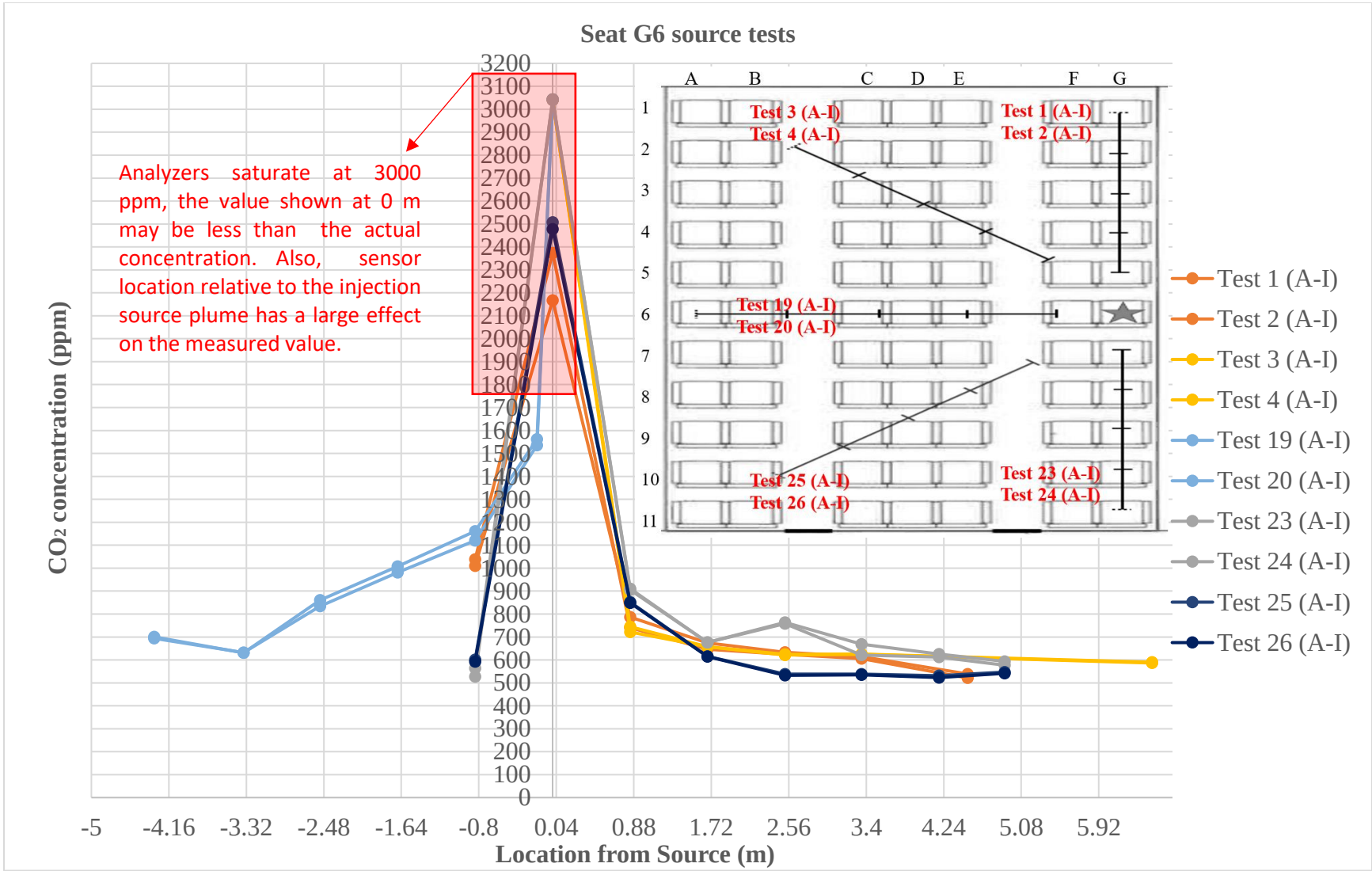

Figure E.126 Seat G6 continuous injection source tests in the modified cabin with the ISOPass undeployed.

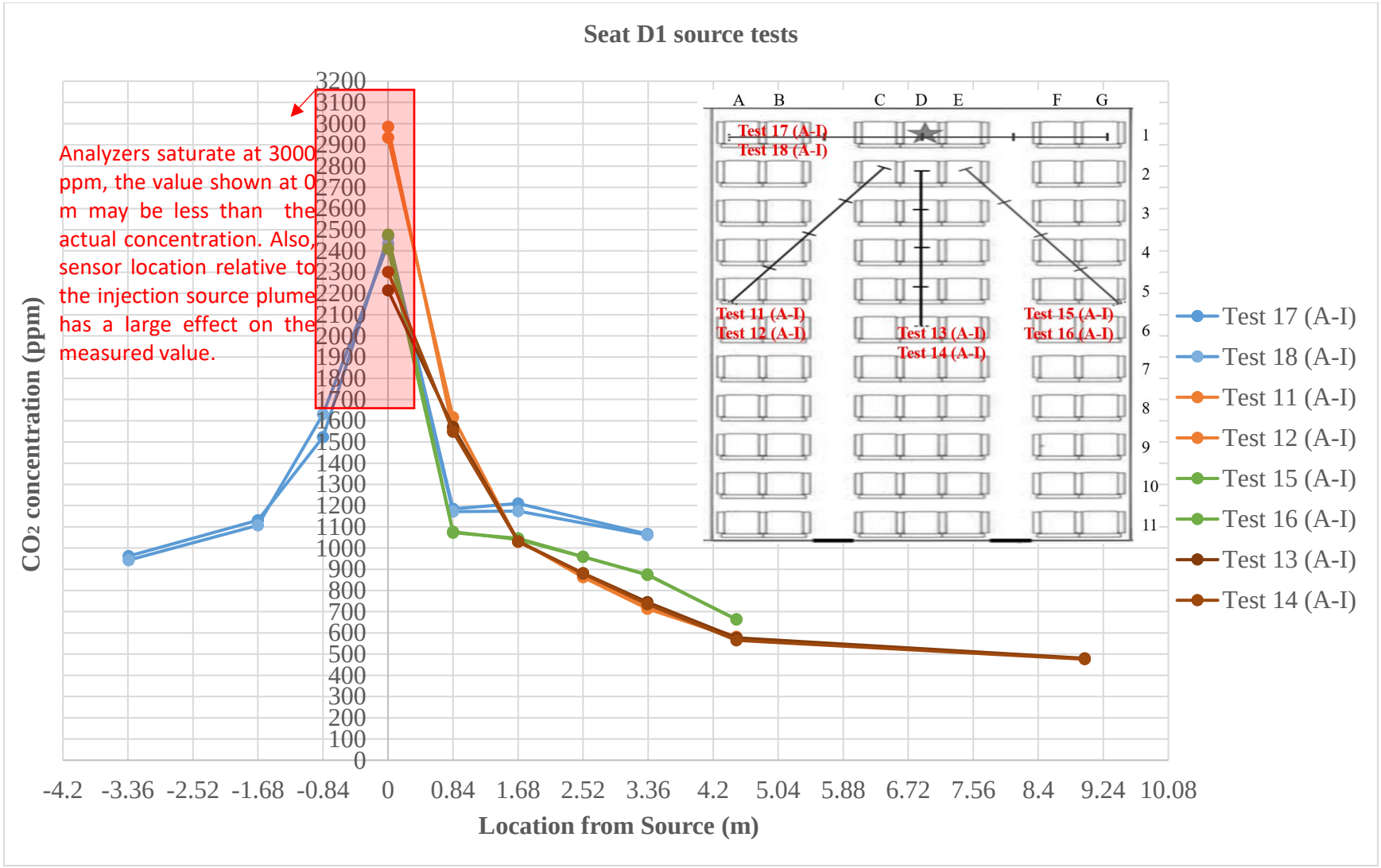

Figure E.127 Seat D1 continuous injection source tests in the modified cabin with the ISOPass undeployed.

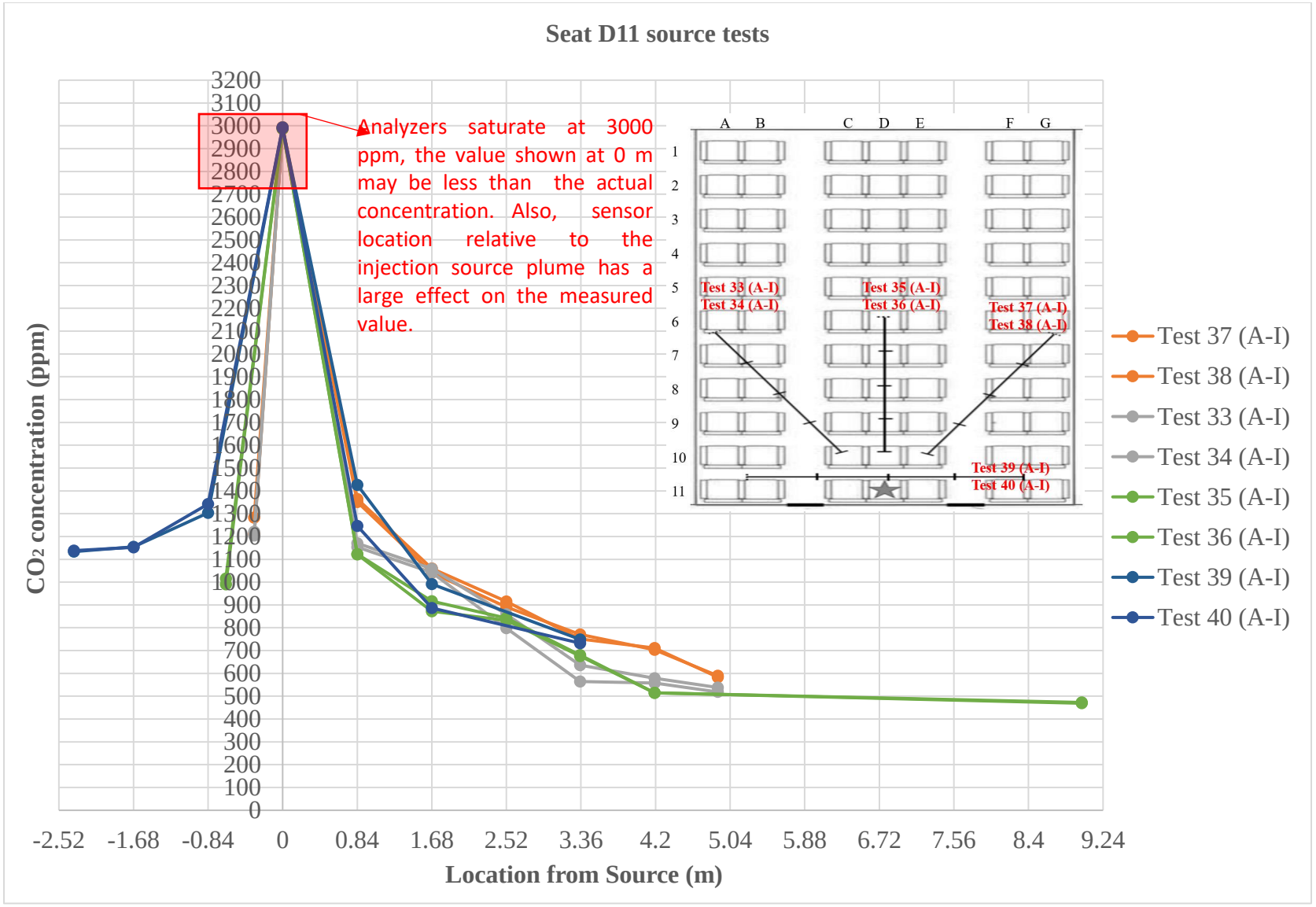

Figure E.128 Seat D11 continuous injection source tests in the modified cabin with the ISOPass undeployed.

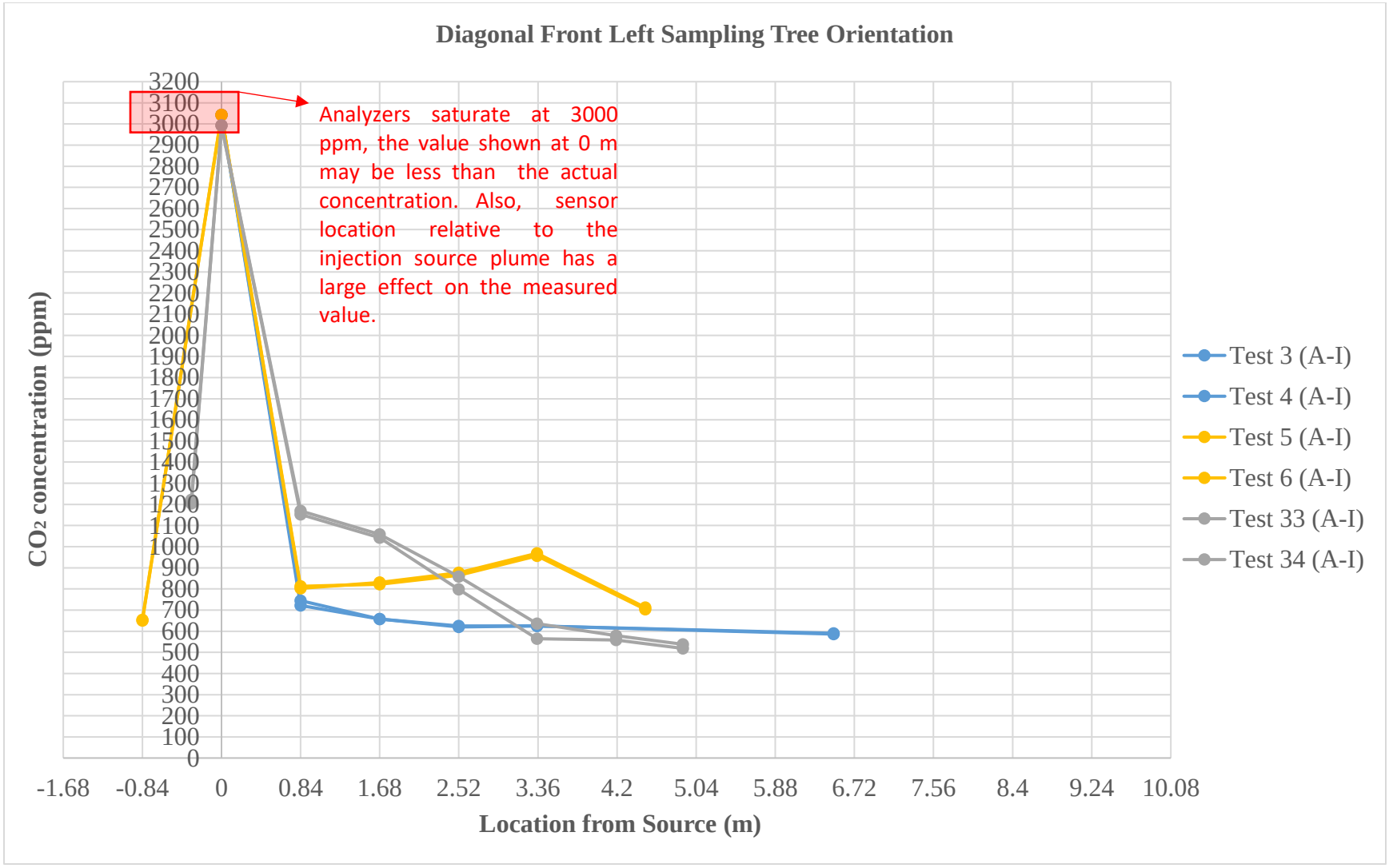

Figure E.129 Diagonal front left sampling tree orientation tests in the modified cabin with the ISOPass undeployed.

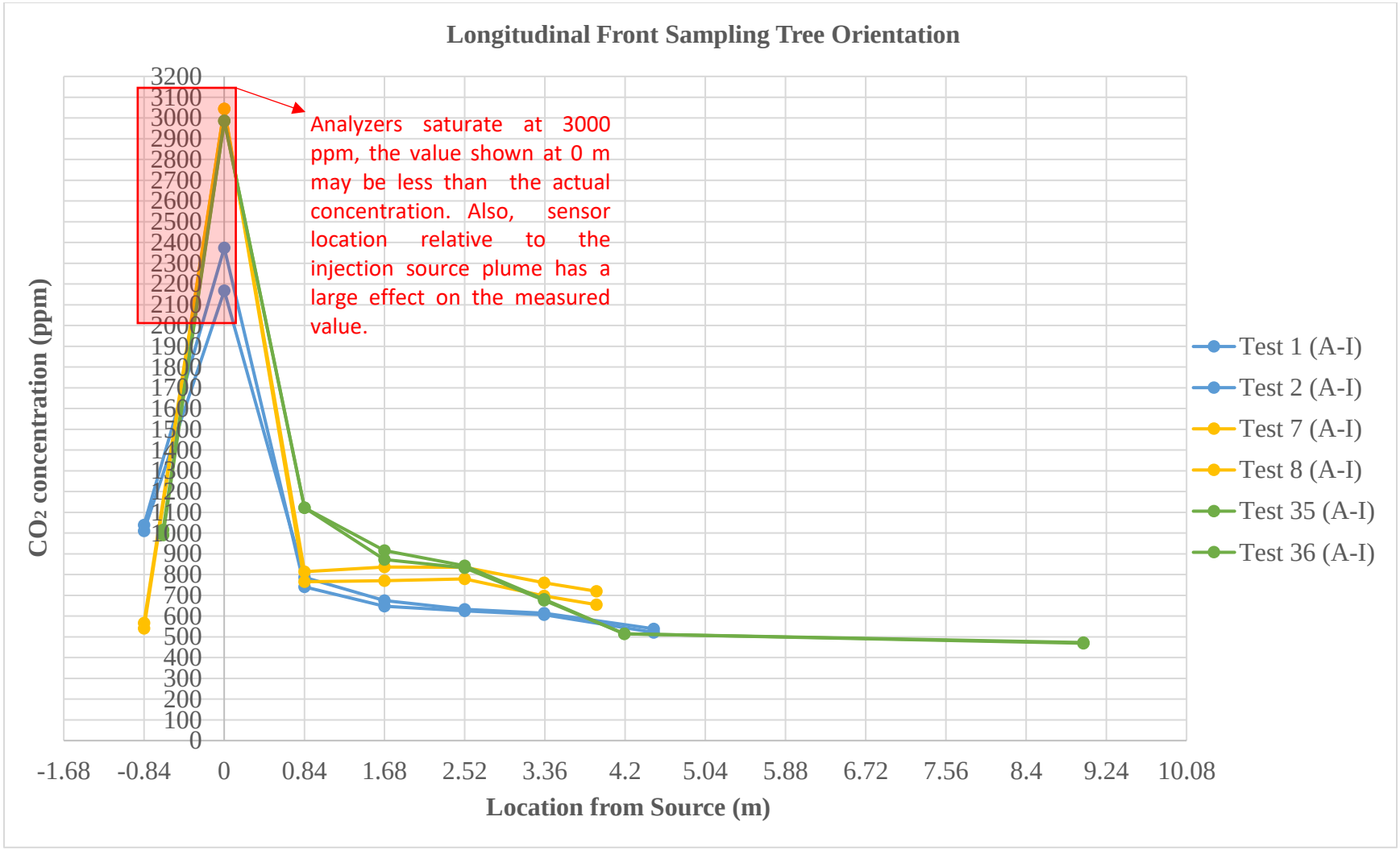

Figure E.130 Longitudinal front sampling tree orientation tests in the modified cabin with the ISOPass undeployed.

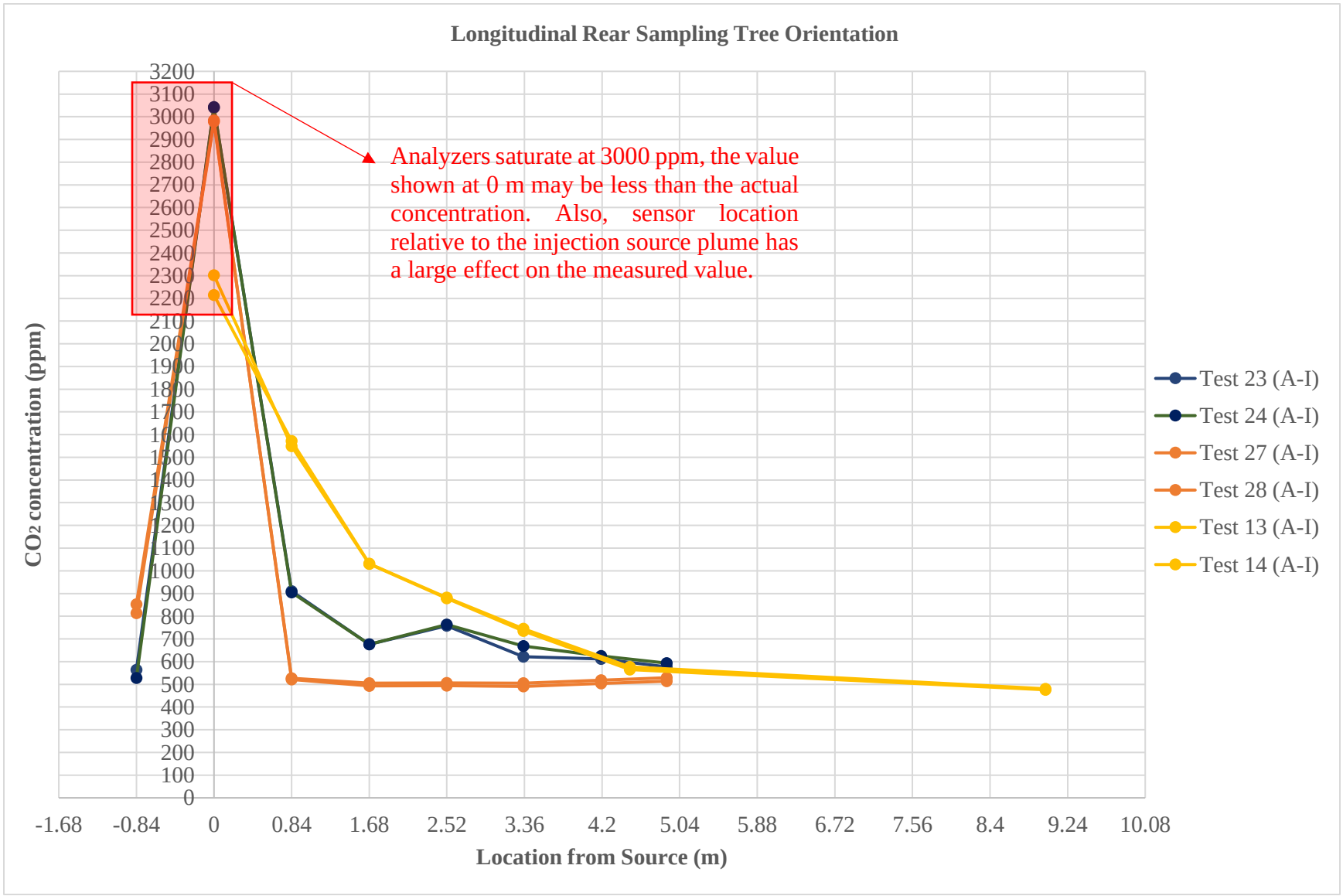

Figure E.131 Longitudinal rear sampling tree orientation tests in the modified cabin with the ISOPass undeployed.

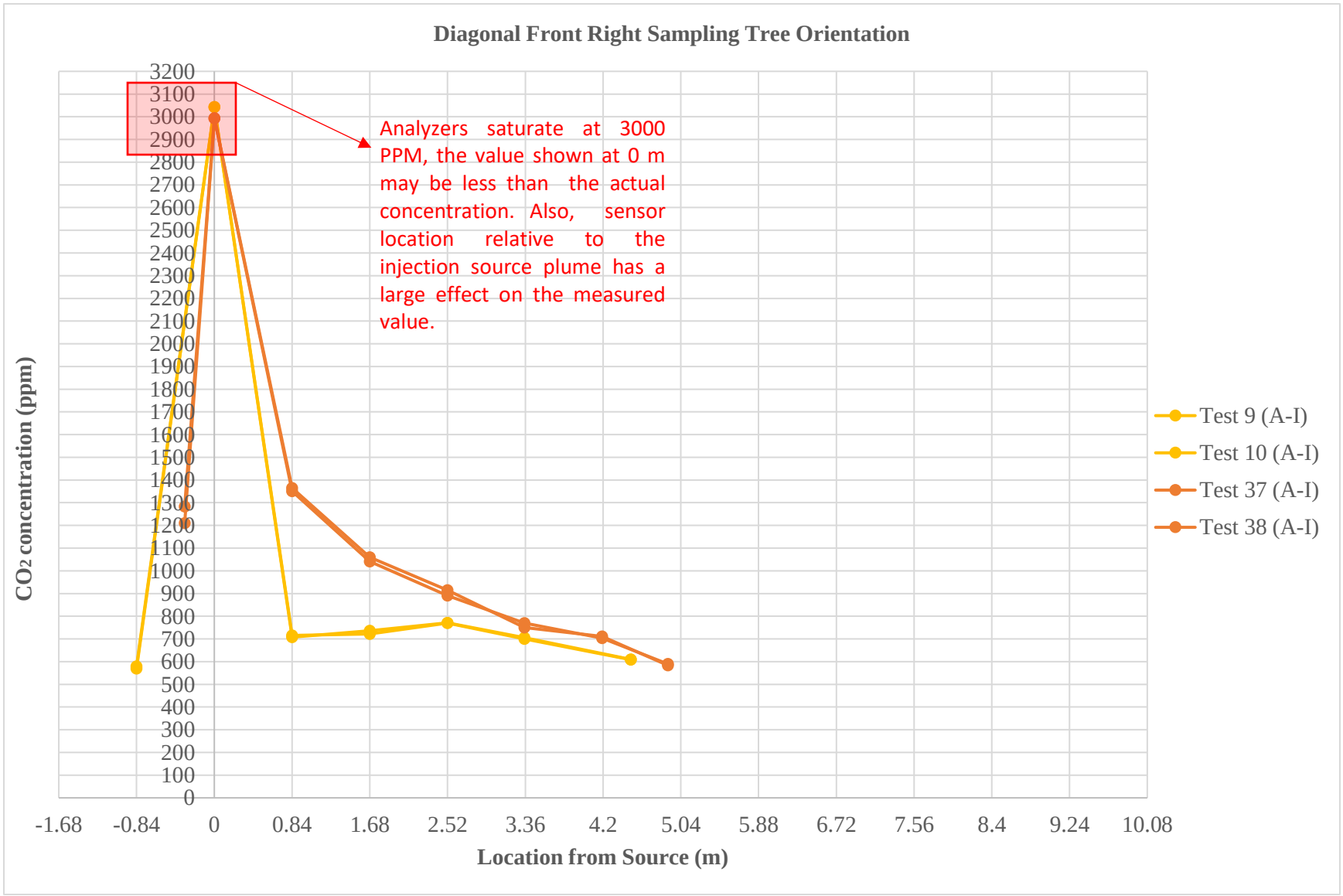

Figure E.132 Diagonal front right sampling tree orientation tests in the modified cabin with the ISOPass undeployed.

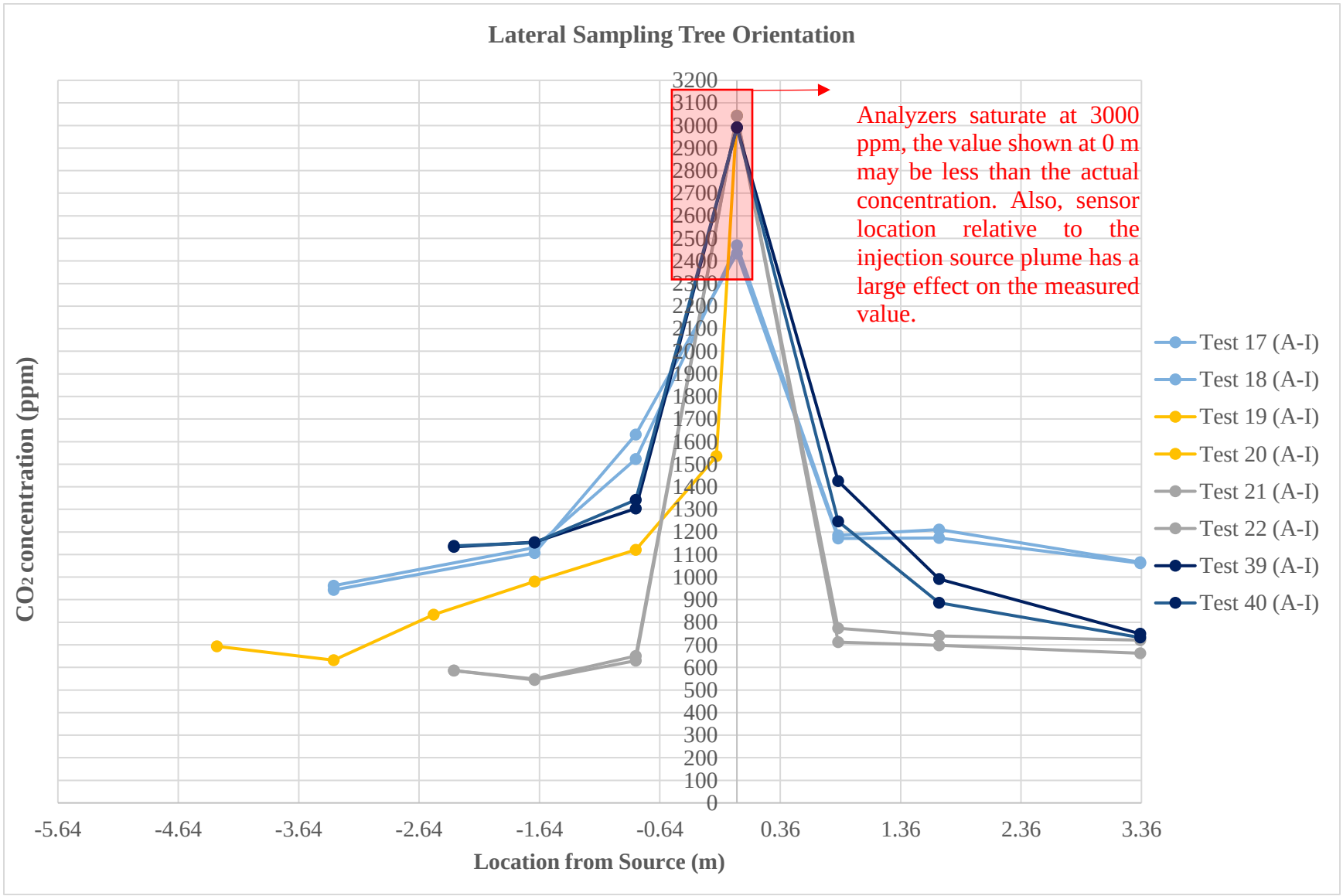

Figure E.133 Lateral sampling tree orientation tests in the modified cabin with the ISOPass undeployed.

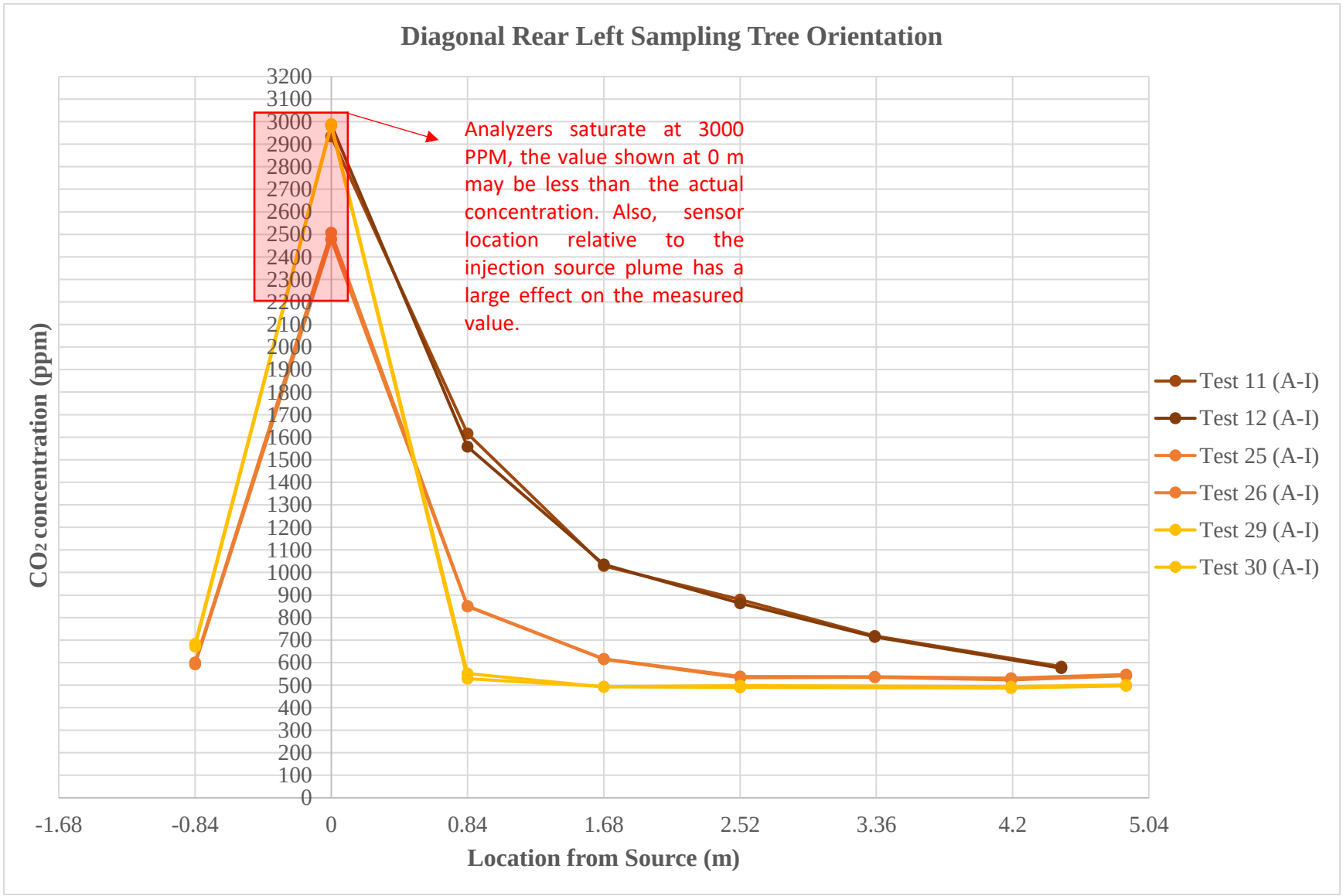

Figure E.134 Diagonal rear left sampling tree orientation tests in the modified cabin with the ISOPass undeployed.

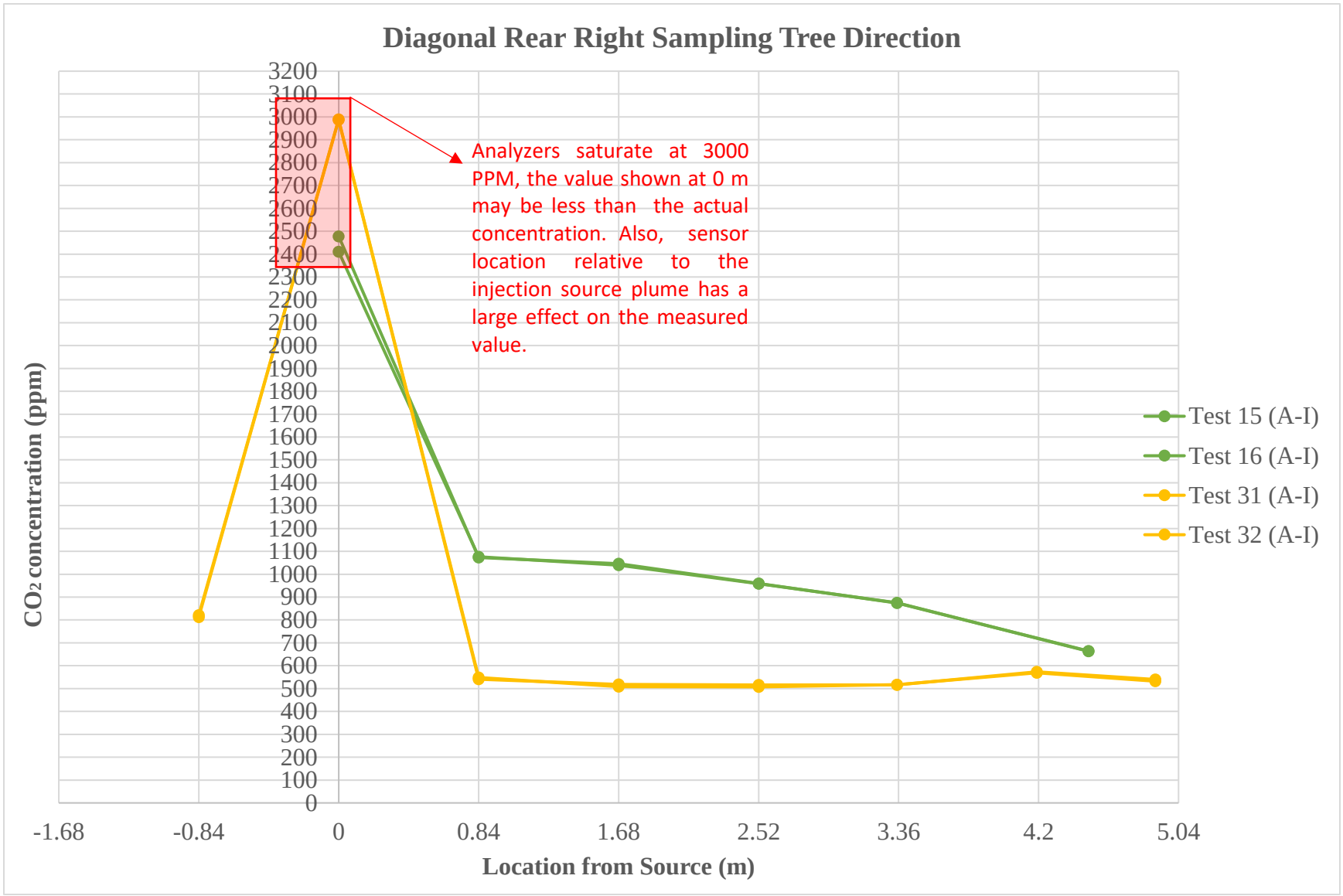

Figure E.135 Diagonal rear right sampling tree orientation tests in the modified cabin with the ISOPass undeployed.

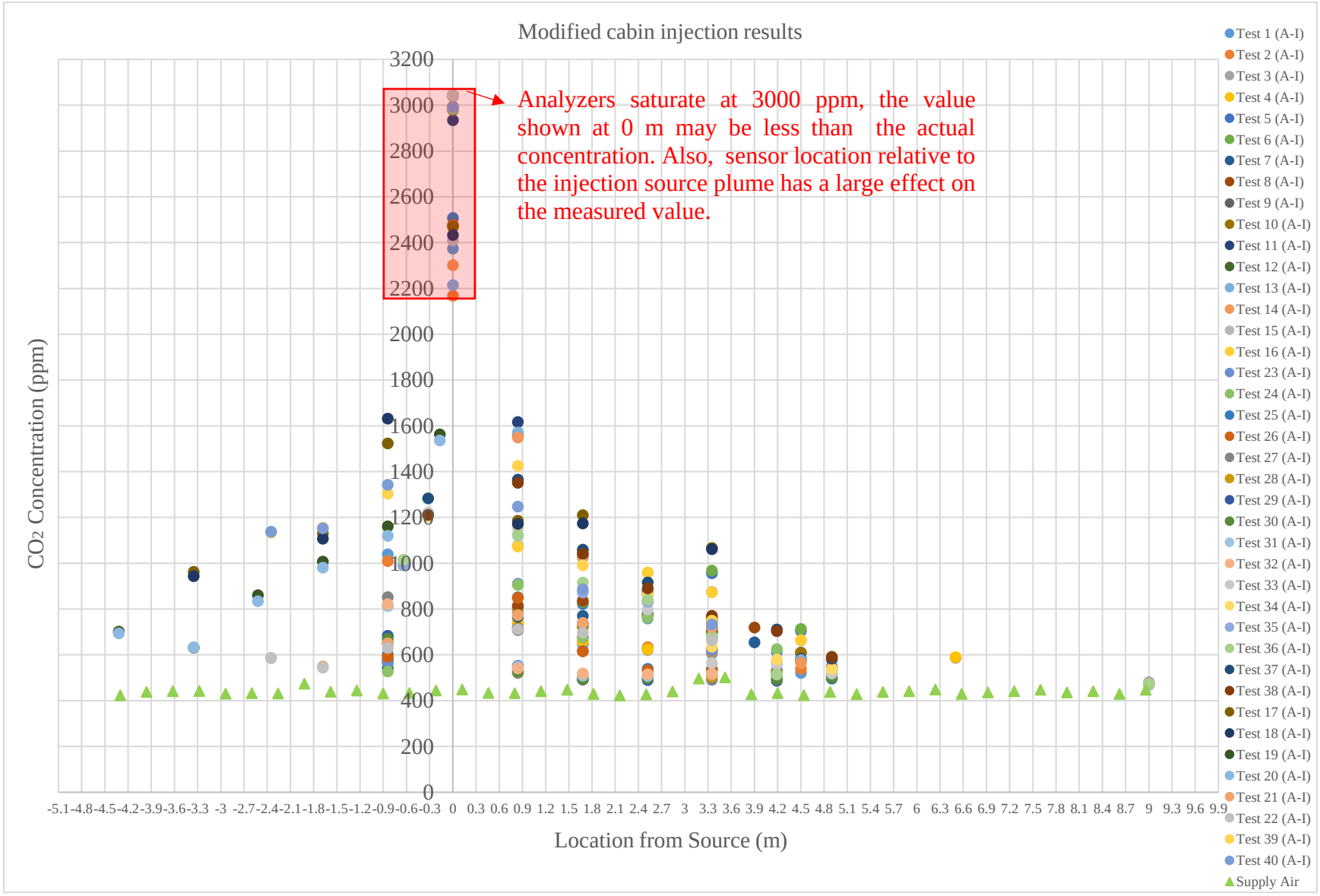

Figure E.136 Modified cabin continuous injection source tests with the ISOPass undeployed.

Figure E.137 Modified cabin continuous injection source tests with the ISOPass undeployed, Absolute distances from the source.

Appendix F - Boeing 737 ISOPass Undeployed Continuous Injection Results

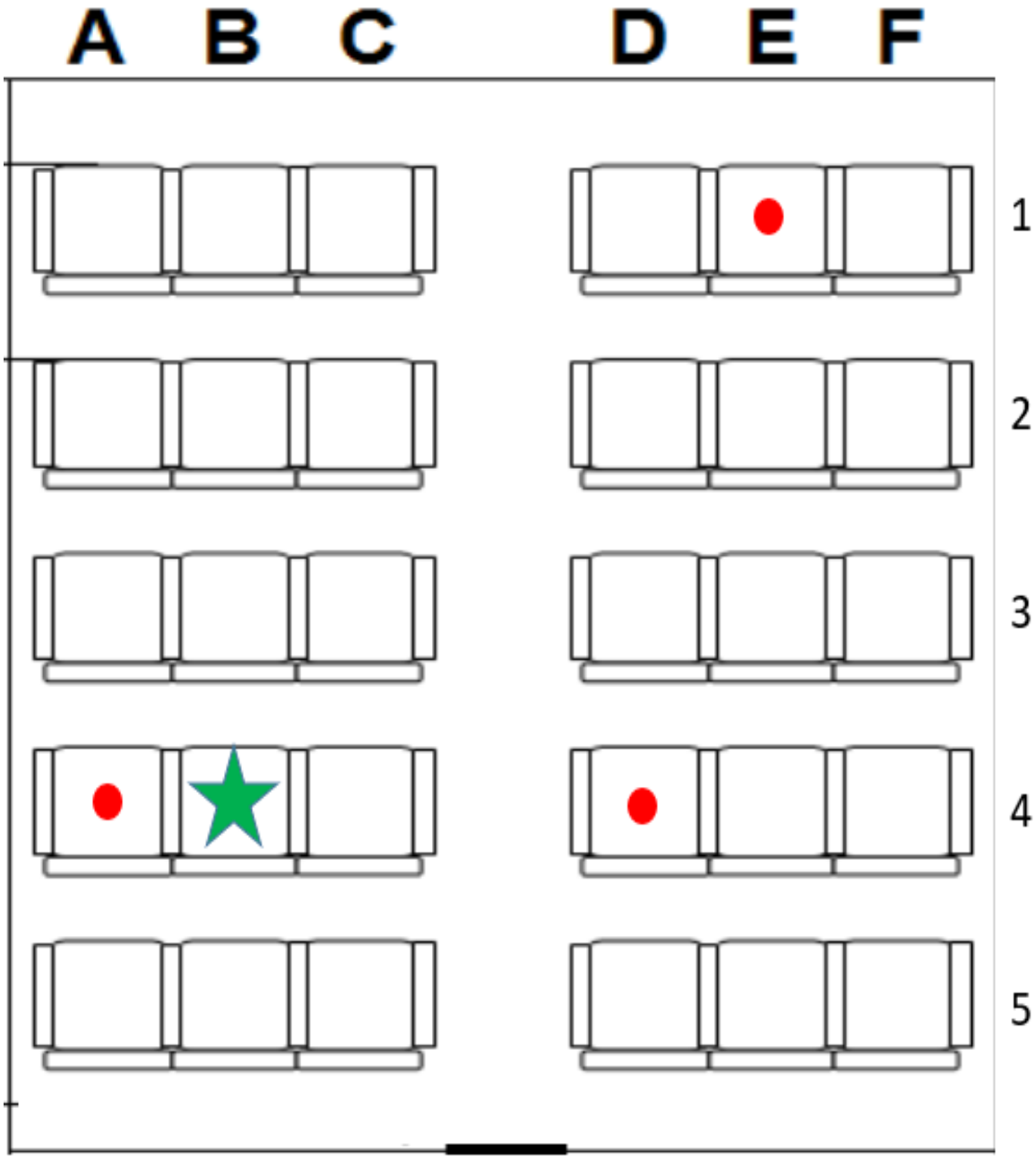

Figure F.1 Seat B4 ISOPass undeployed Test 1 (C-I) continuous injection tracer gas source and gas analyzers locations in the Boeing 737 cabin section.

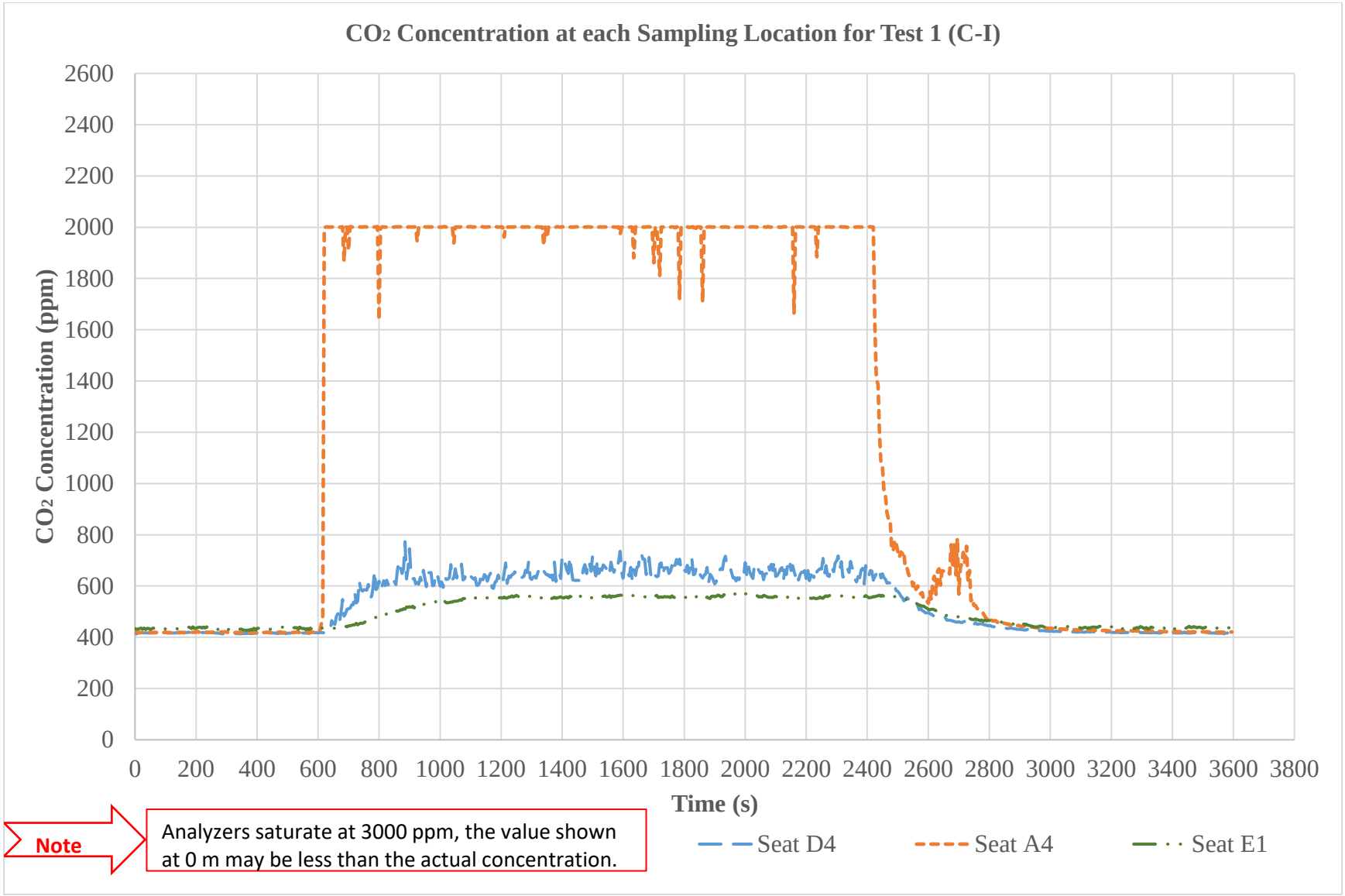

Figure F.2 Ininstantaneous CO_2 concentration at each sampling location for Test 1 (C-I) ISOPass undeployed.

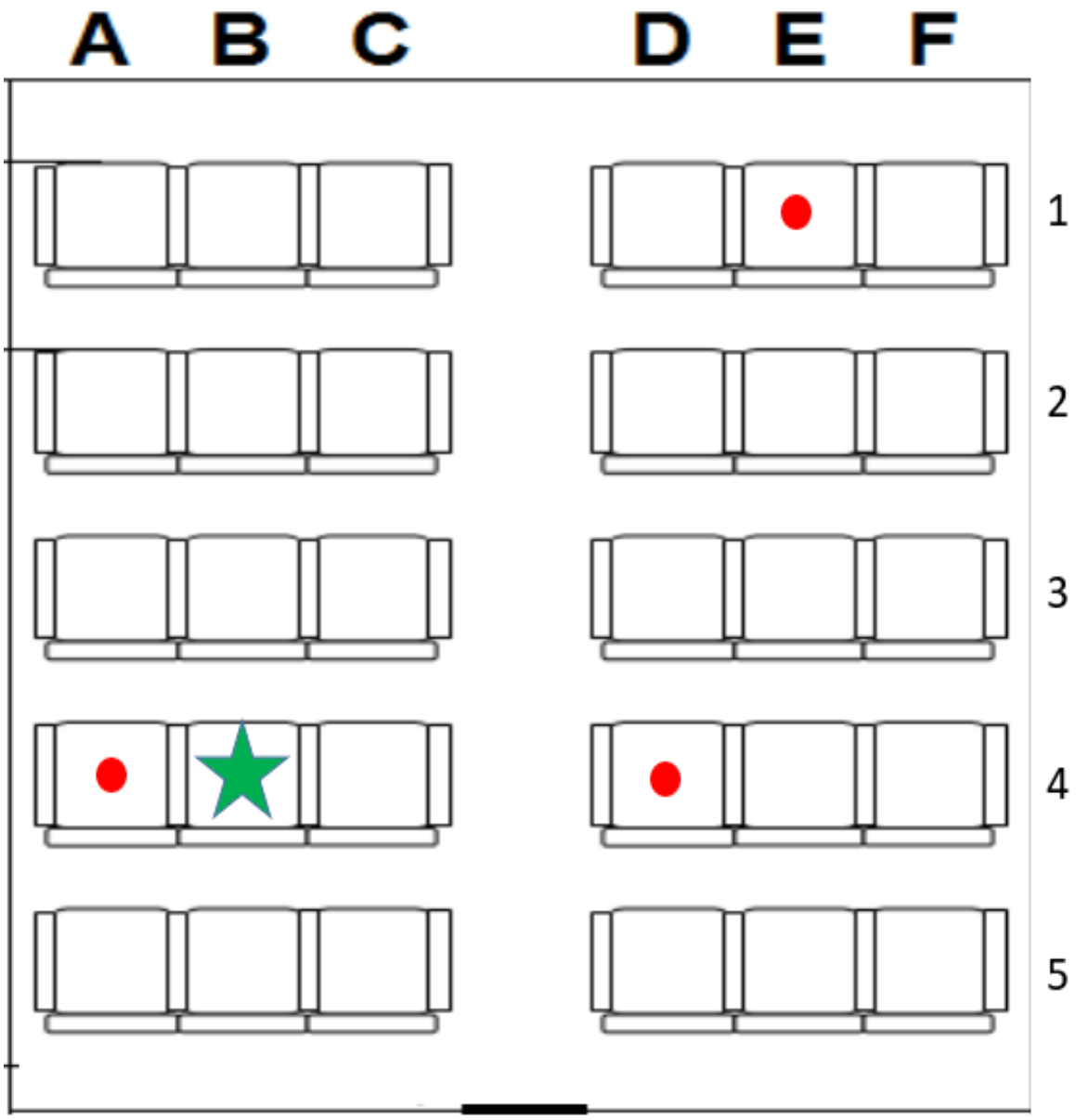

Figure F.3 Seat B4 ISOPass undeployed Test 2 (C-I) continuous injection tracer gas source and gas analyzers locations in the Boeing 737 cabin section.

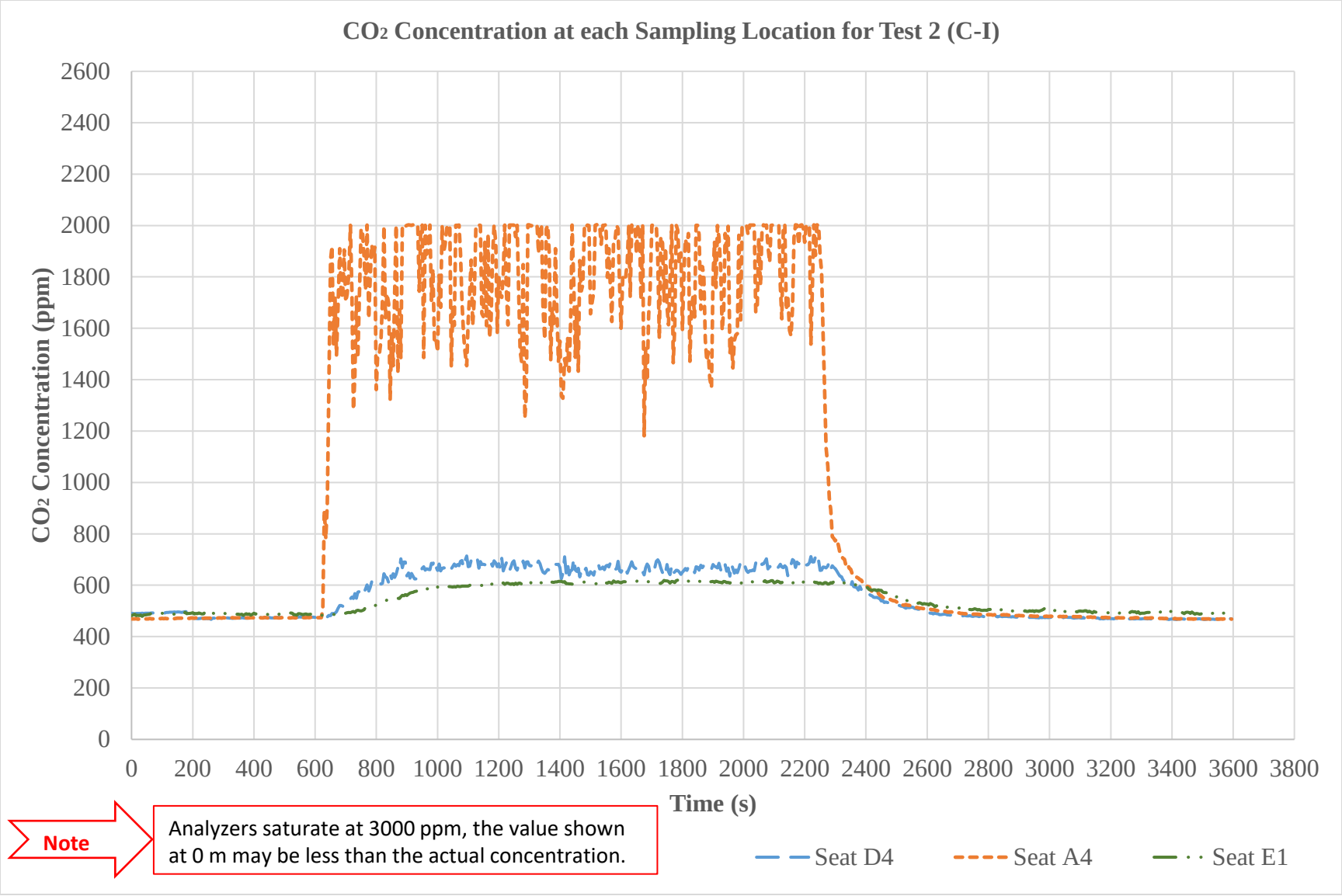

Figure F.4 Ininstantaneous CO_2 concentration at each sampling location for Test 2 (C-I) ISOPass undeployed.

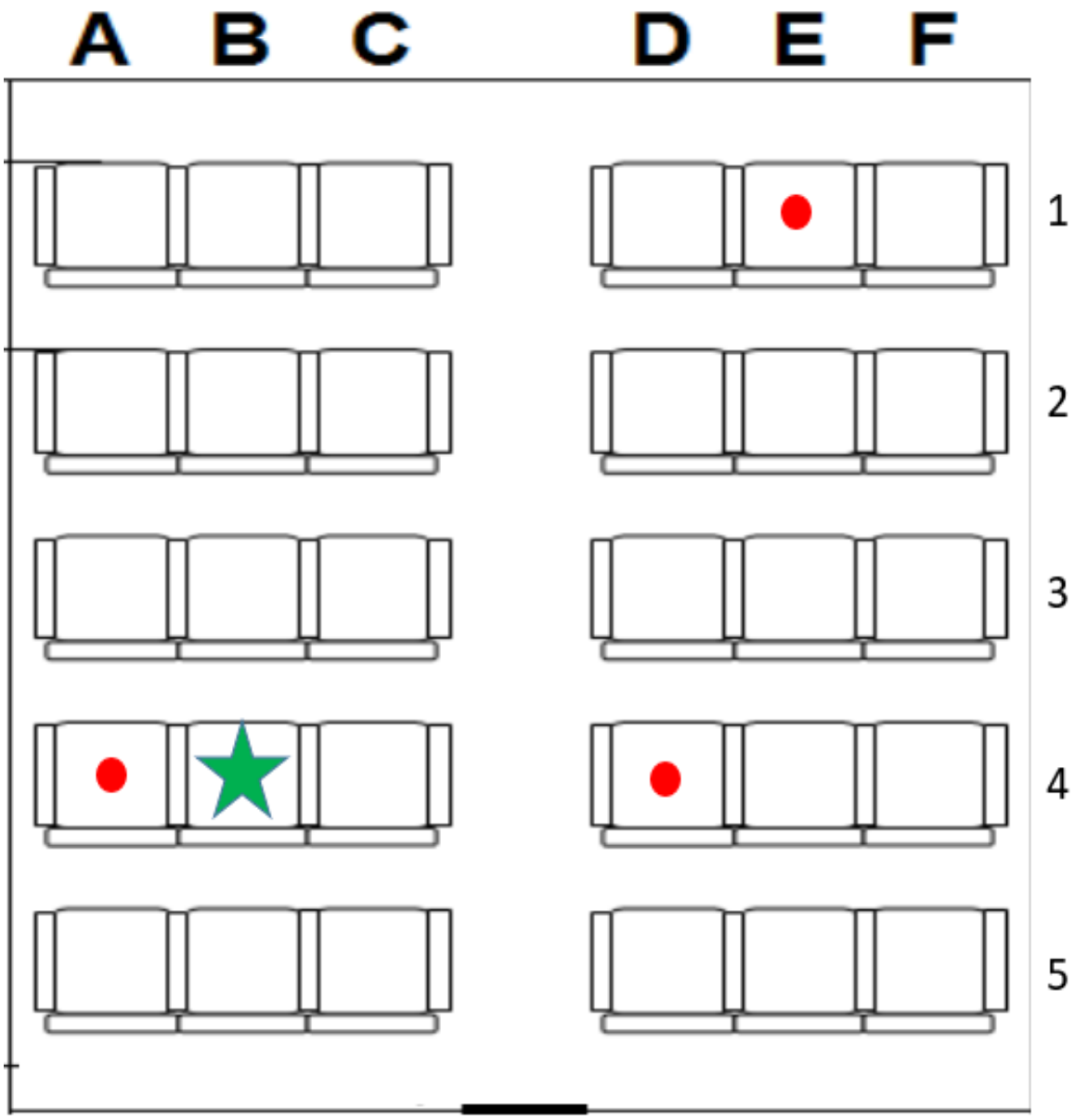

Figure F.5 Seat B4 ISOPass undeployed Test 3 (C-I) continuous injection tracer gas source and gas analyzers locations in the Boeing 737 cabin section.

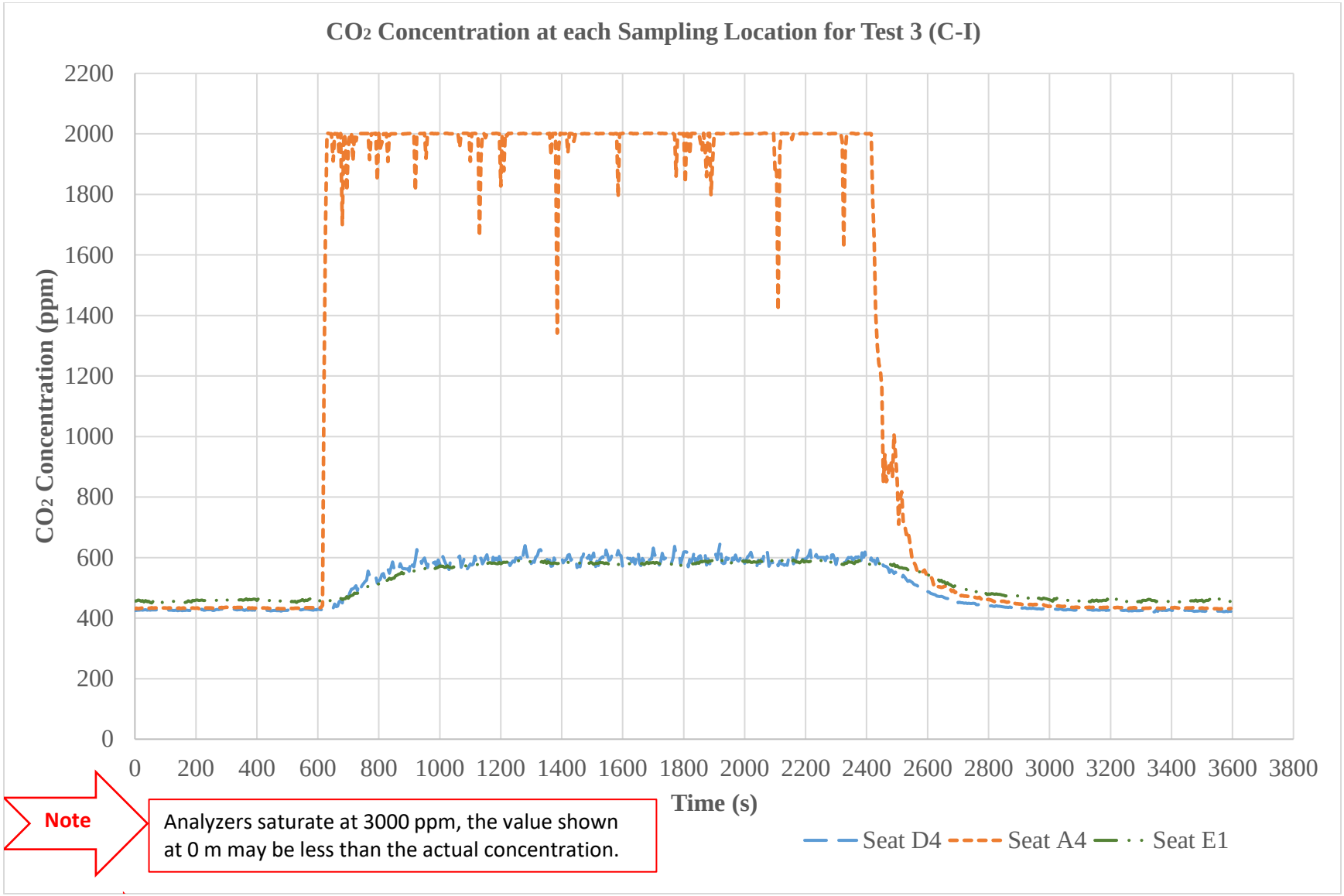

Figure F.6 Ininstantaneous CO_2 concentration at each sampling location for Test 3 (C-I) ISOPass undeployed.

Appendix G - Boeing 737 ISOPass Deployed Continuous Injection Results

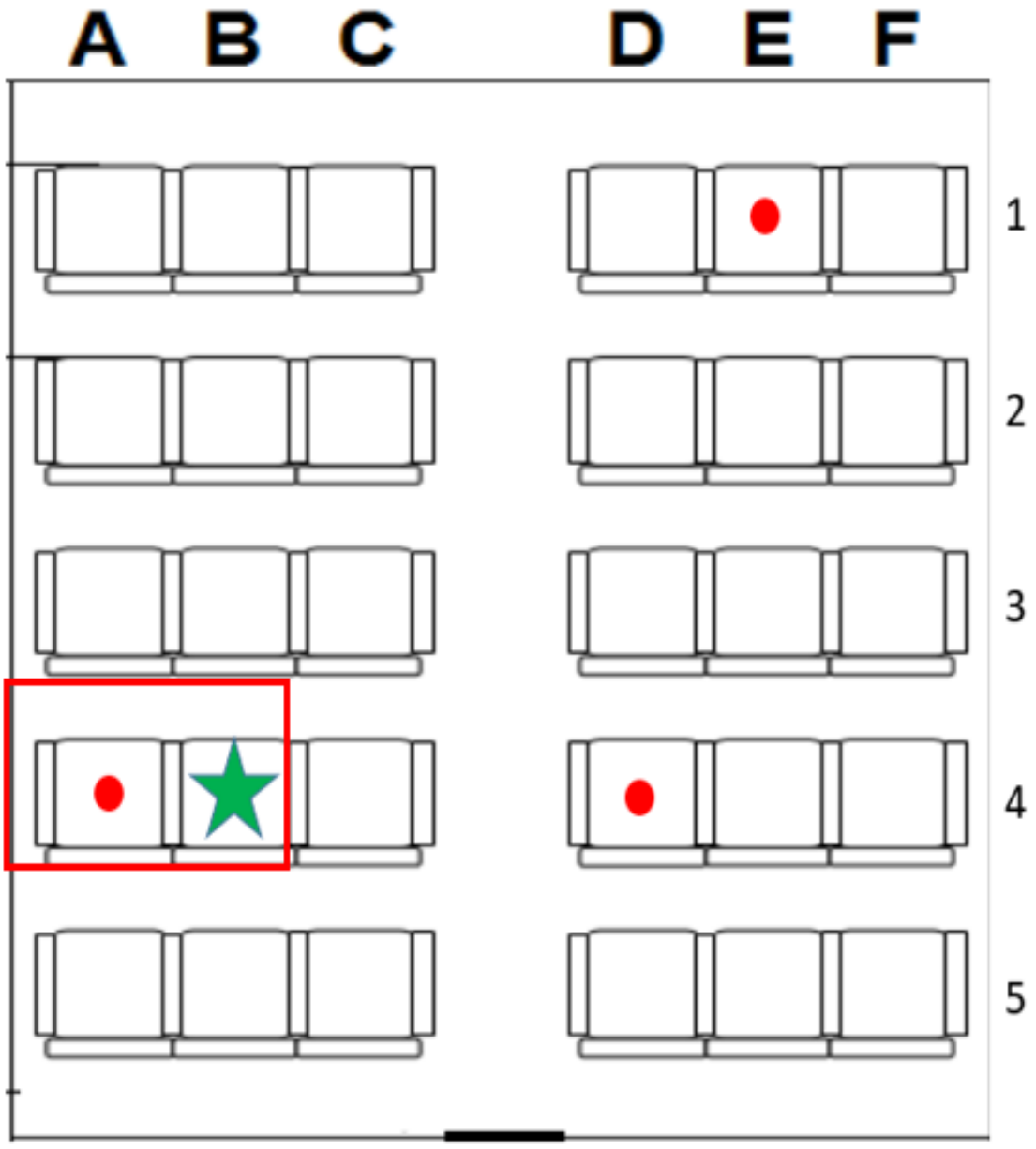

Figure G.1 Seat B4 ISOPass deployed Test 4 (C-I) continuous injection tracer gas source and gas analyzers locations in the Boeing 737 cabin section.

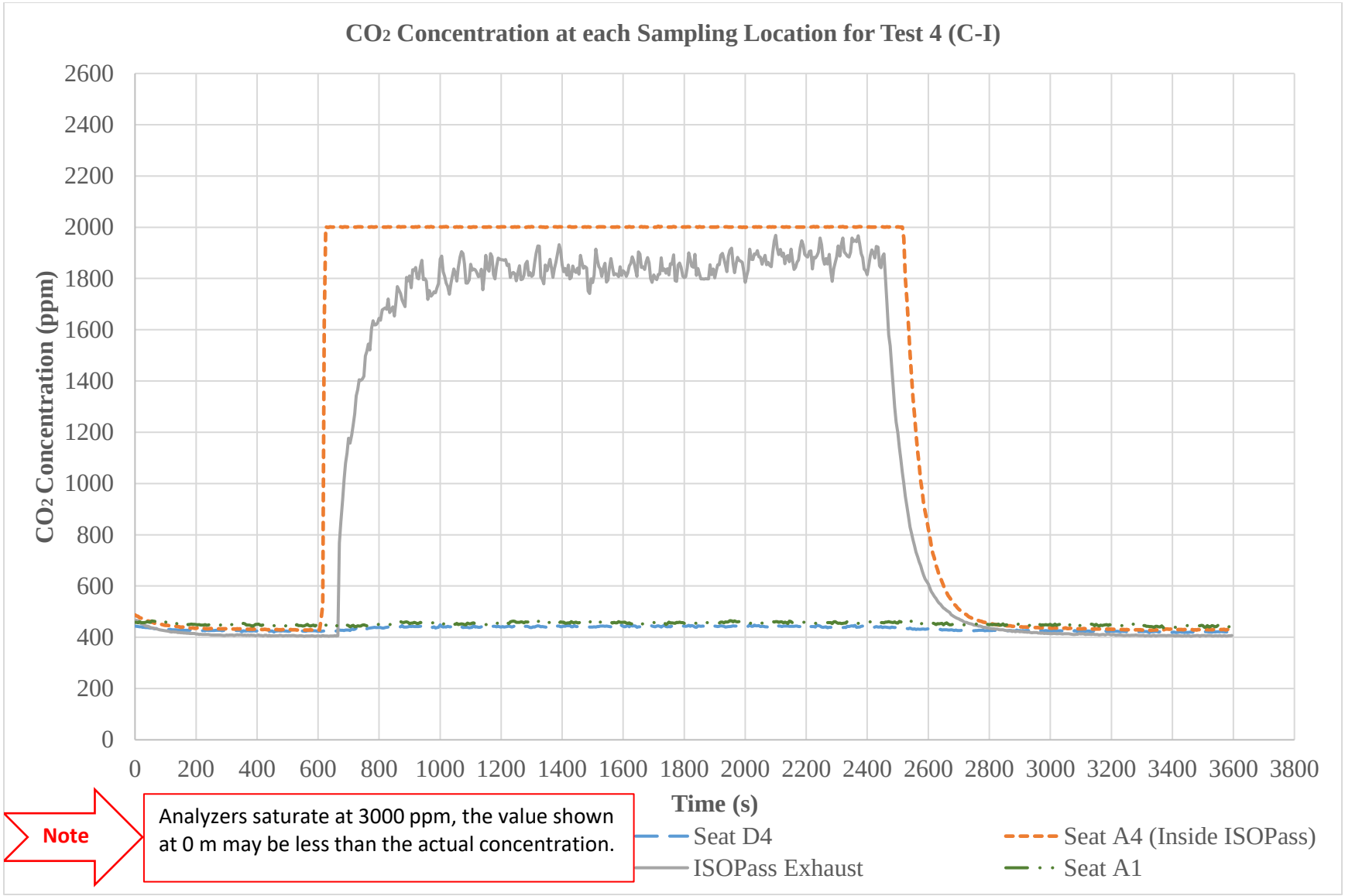

Figure G.2 Ininstantaneous CO_2 concentration at each sampling location for Test 4 (C-I) ISOPass deployed.

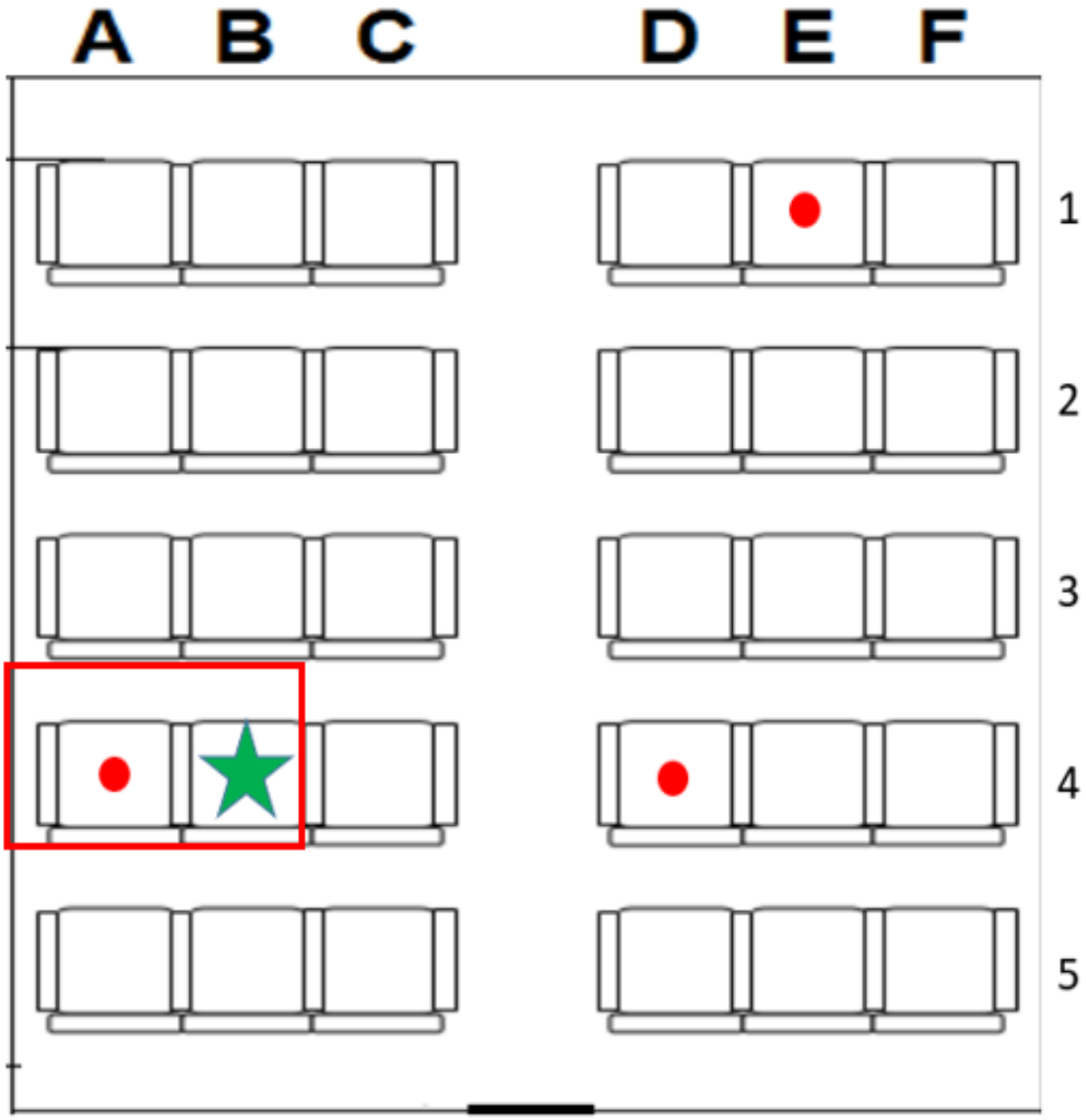

Figure G.3 Seat B4 ISOPass deployed Test 5 (C-I) continuous injection tracer gas source and gas analyzers locations in the Boeing 737 cabin section.

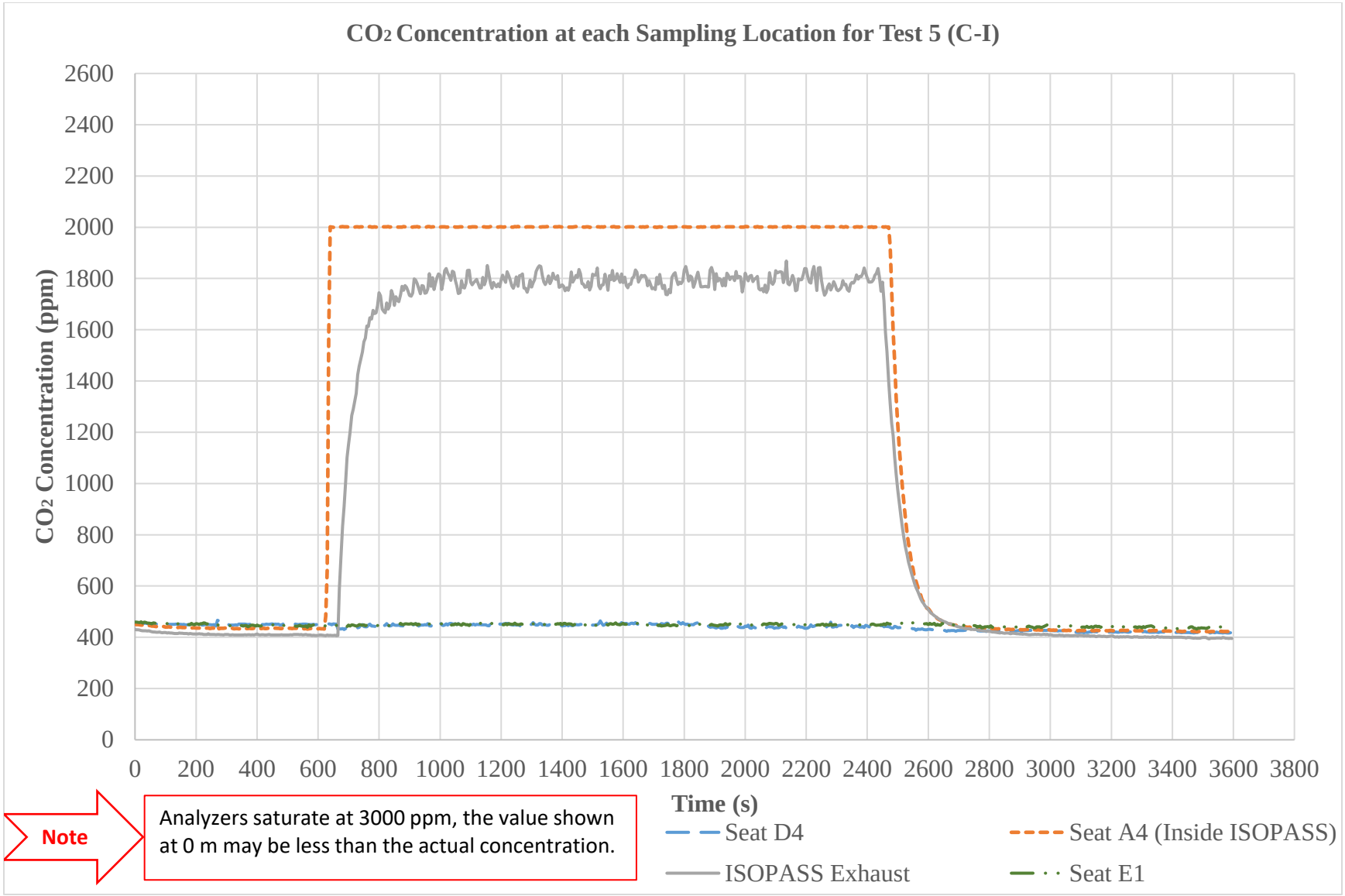

Figure G.4 Ininstantaneous CO_2 concentration at each sampling location for Test 5 (C-I) ISOPass deployed.

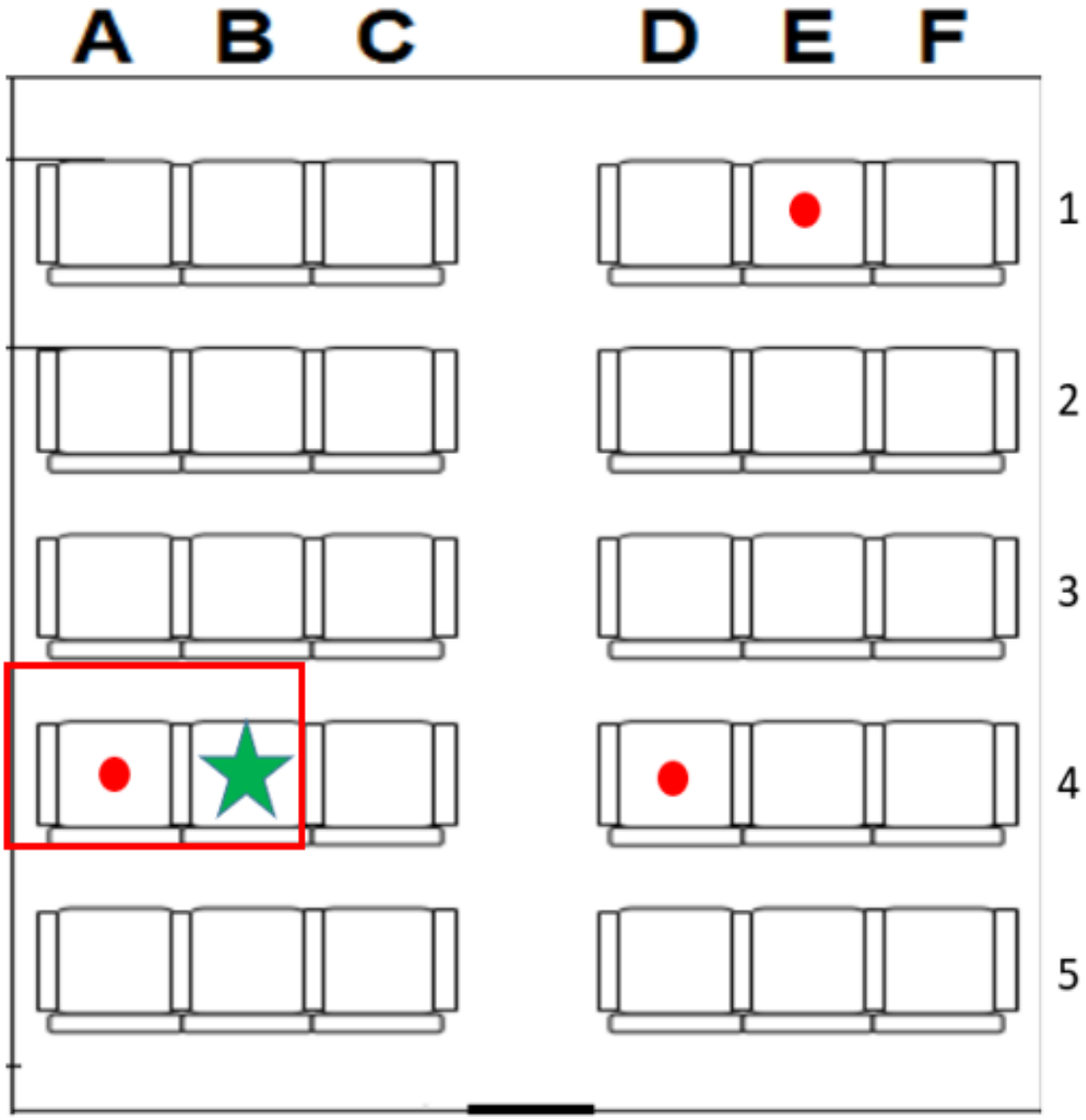

Figure G.5 Seat B4 ISOPass deployed Test 6 (C-I) continuous injection tracer gas source and gas analyzers locations in the Boeing 737 cabin section.

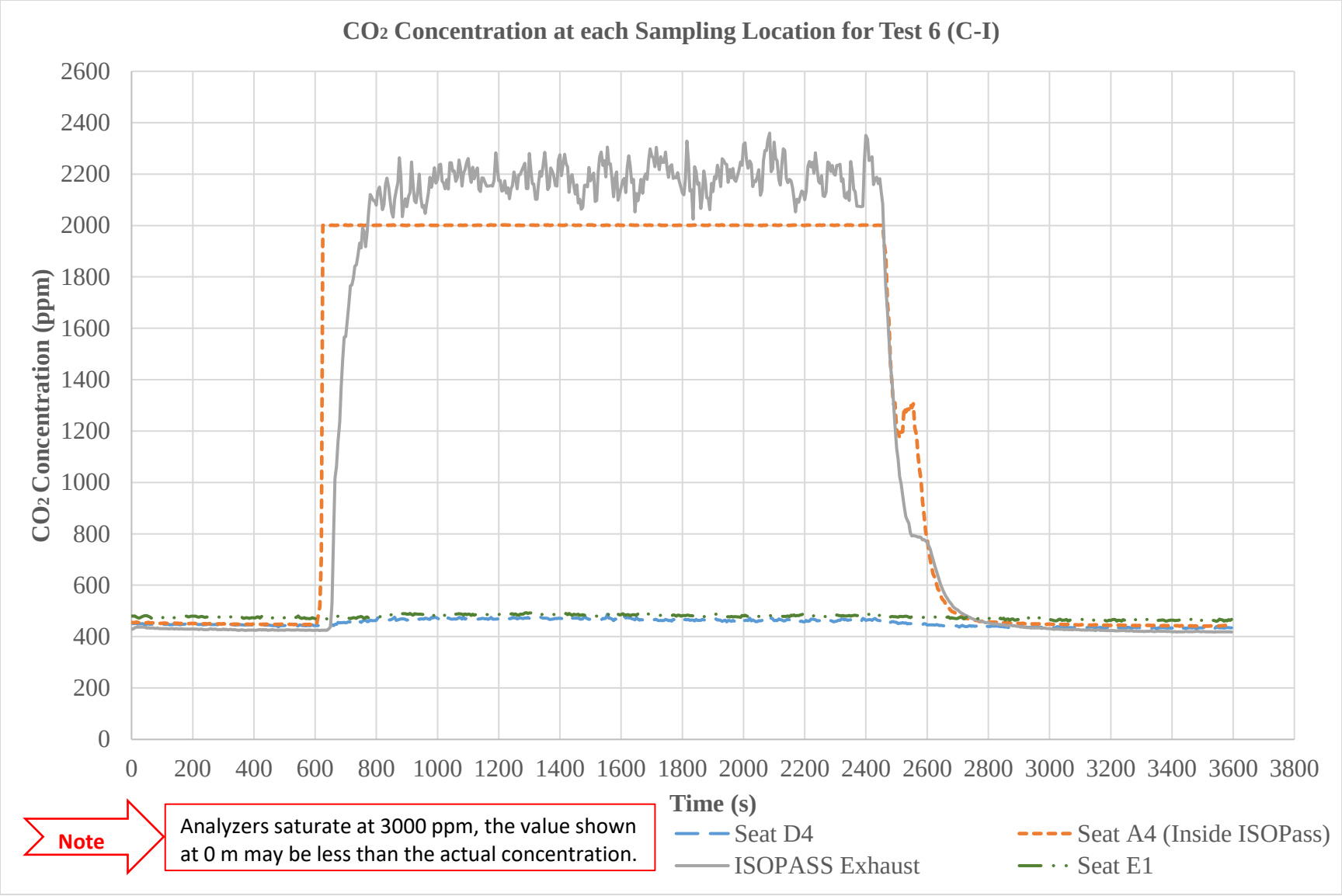

Figure G.6 Ininstantaneous CO_2 concentration at each sampling location for Test 6 (C-I) ISOPass deployed.

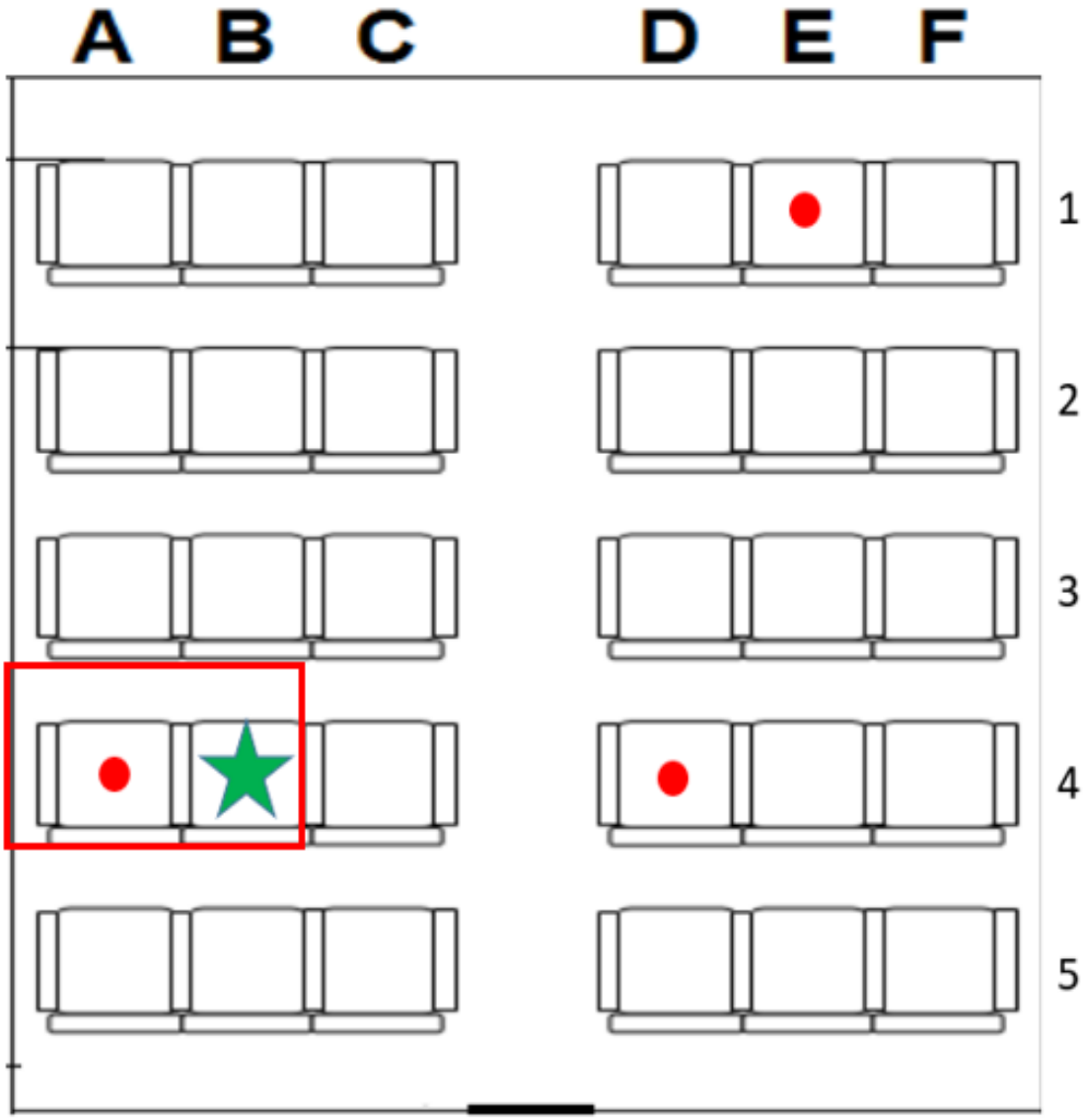

Figure G.7 Seat B4 ISOPass deployed Test 7 (C-I) continuous injection tracer gas source and gas analyzers locations in the Boeing 737 cabin section.

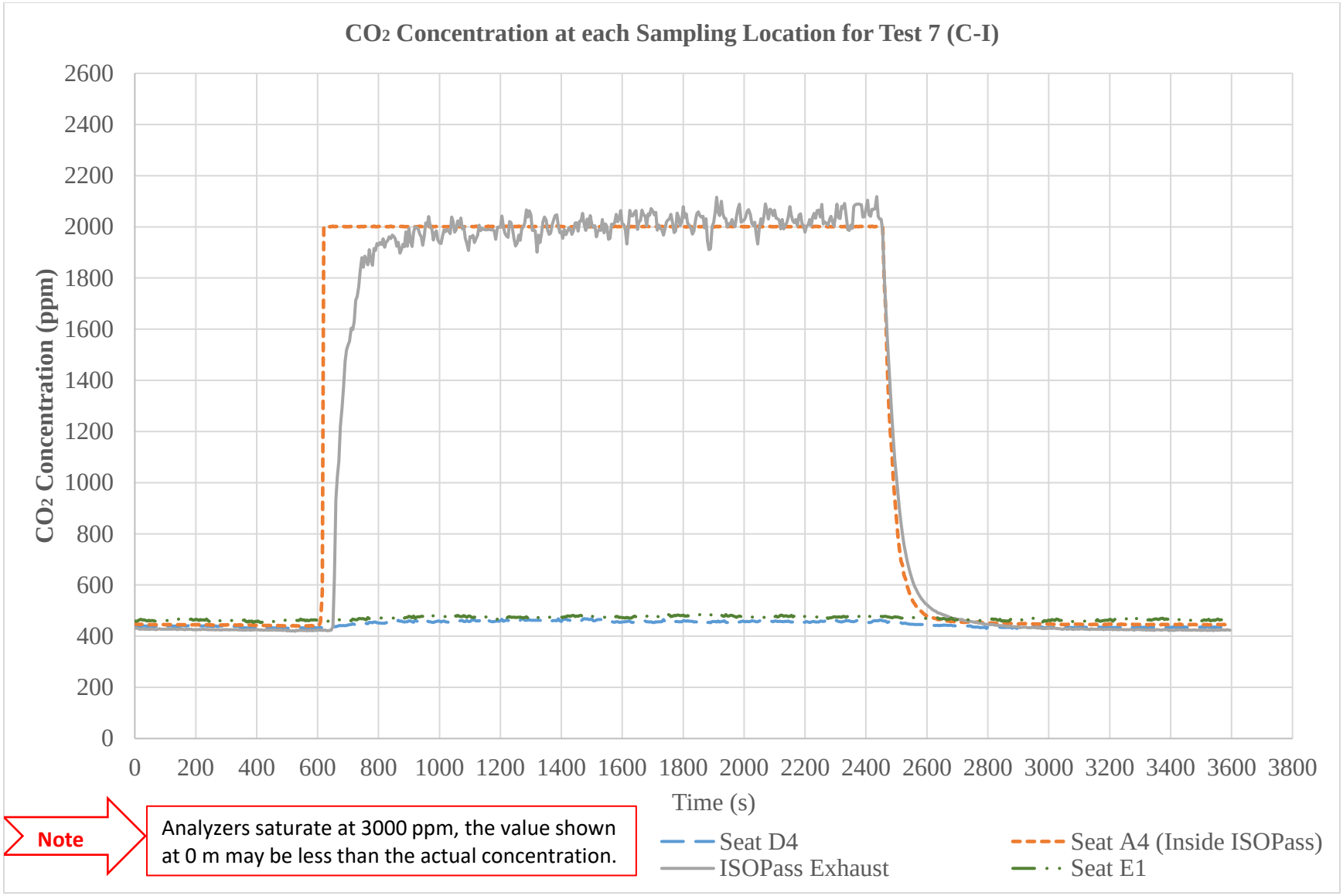

Figure G.8 Ininstantaneous CO_2 concentration at each sampling location for Test 7 (C-I) ISOPass deployed.

Appendix H - Boeing 767 ISOPass Undeployed Coughing Manikin Results

Notes about this appendix:

- The positive direction is the one pointing from the source to the sampling tree solenoid valves block in the tests conducted with a longitudinal or a diagonal sampling tree directions.
- The positive direction was taken as the right direction from the source in the tests performed with a lateral sampling tree direction similar to a typical coordinate system.
- The letter "B" after the test number indicates that the test was conducted in the Boeing 767 mockup cabin and the letter "M" indicates that it was conducted using a coughing manikin source.
- The sampling tree is a metal rod that has 4 ports controlled by solenoid valves. The measurements are collected sequentially from each of the ports. The tree is connected to a single gas analyzer to measure the concentration of the tracer gas from the opened port.
- The solenoid valves block is marked by a dashed line crossing the sampling tree.
- In addition to the sampling tree, additional tracer gas analyzers are placed in the cabin to collect measurements at the cabin supply air, source seat, and other locations of interest.
- The tracer gas analyzers are not of the same model or calibration and hence, the accuracy of the readings is not identical. For the tracer gas measurements accuracy, refer to chapter 4.4. Uncertainty Analysis of this dissertation.

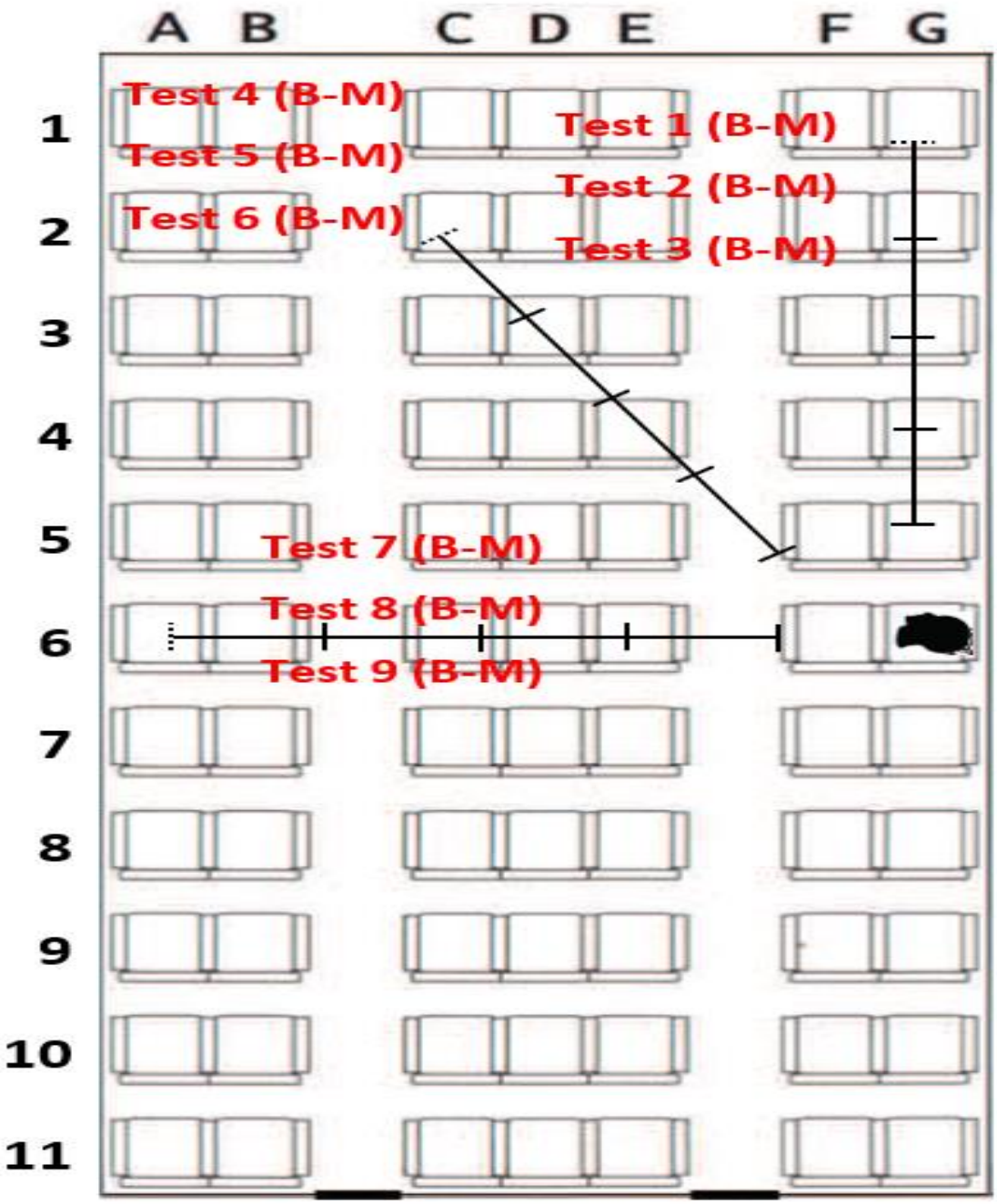

Figure H.1 Seat G6 ISOPass undeployed coughing manikin tracer gas test numbers and sampling tree orientations in the Boeing 767 cabin mockup.

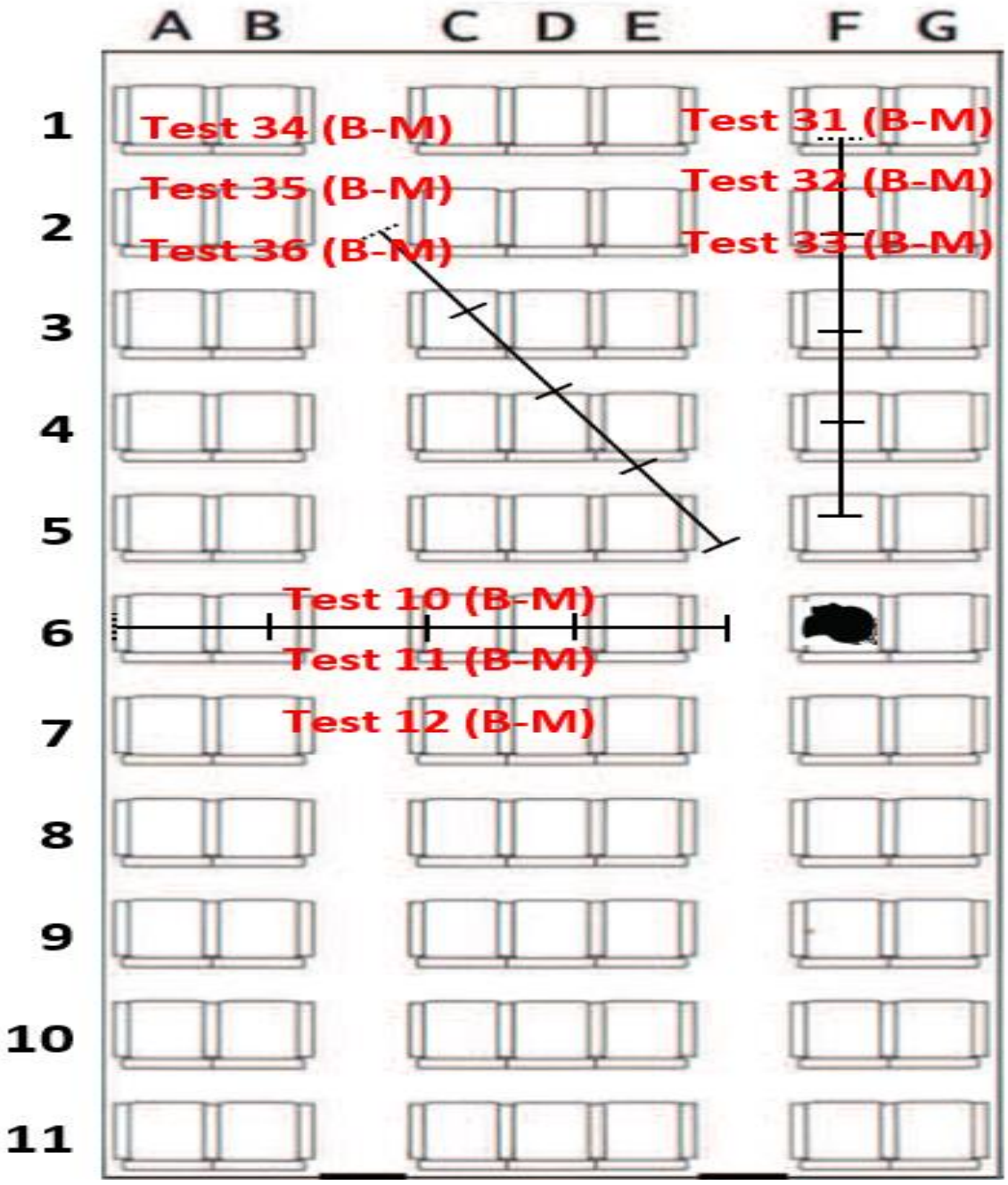

Figure H.2 Seat F6 ISOPass undeployed coughing manikin tracer gas test numbers and sampling tree orientations in the Boeing 767 cabin mockup.

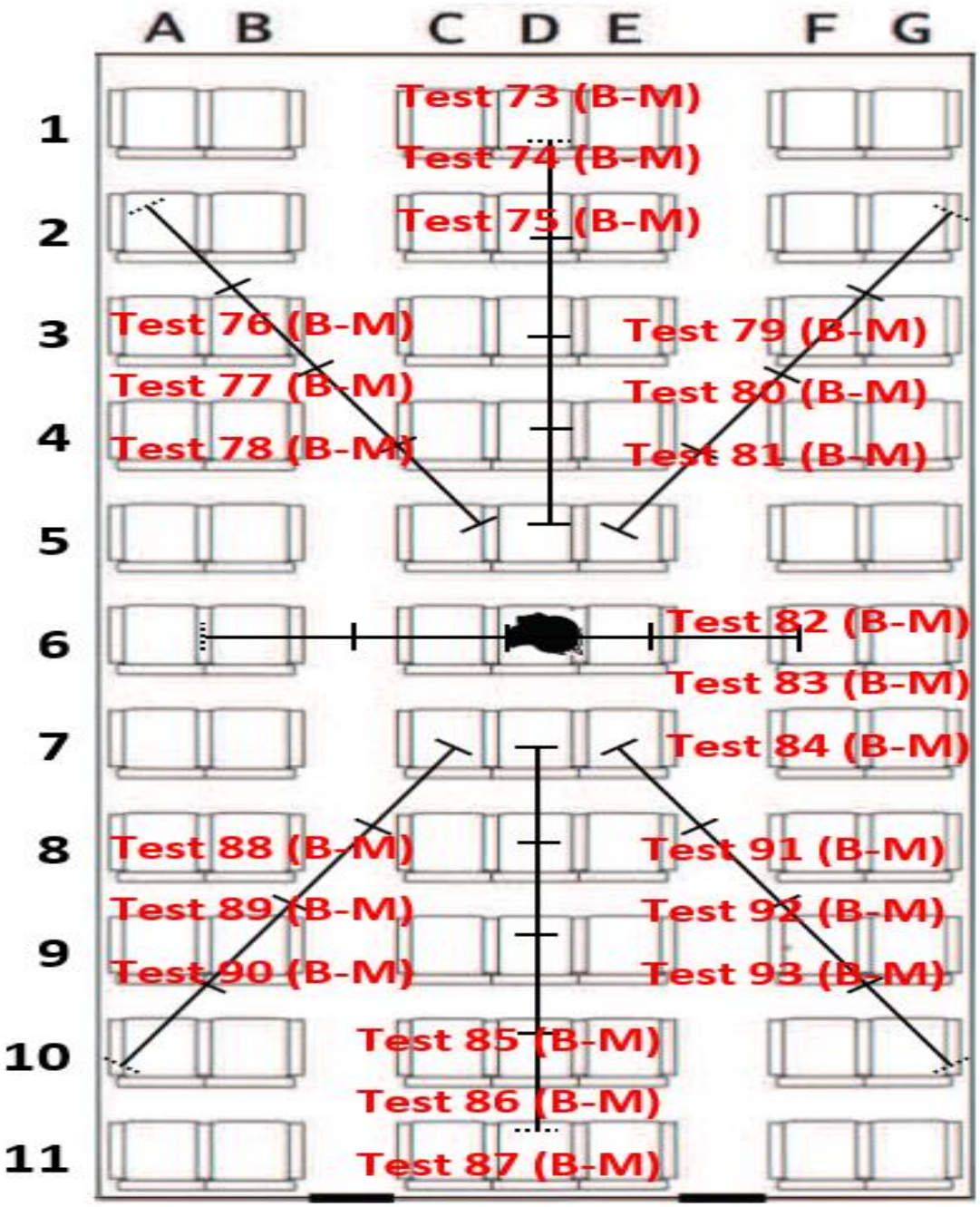

Figure H.3 Seat D6 ISOPass undeployed coughing manikin tracer gas test numbers and sampling tree orientations in the Boeing 767 cabin mockup.

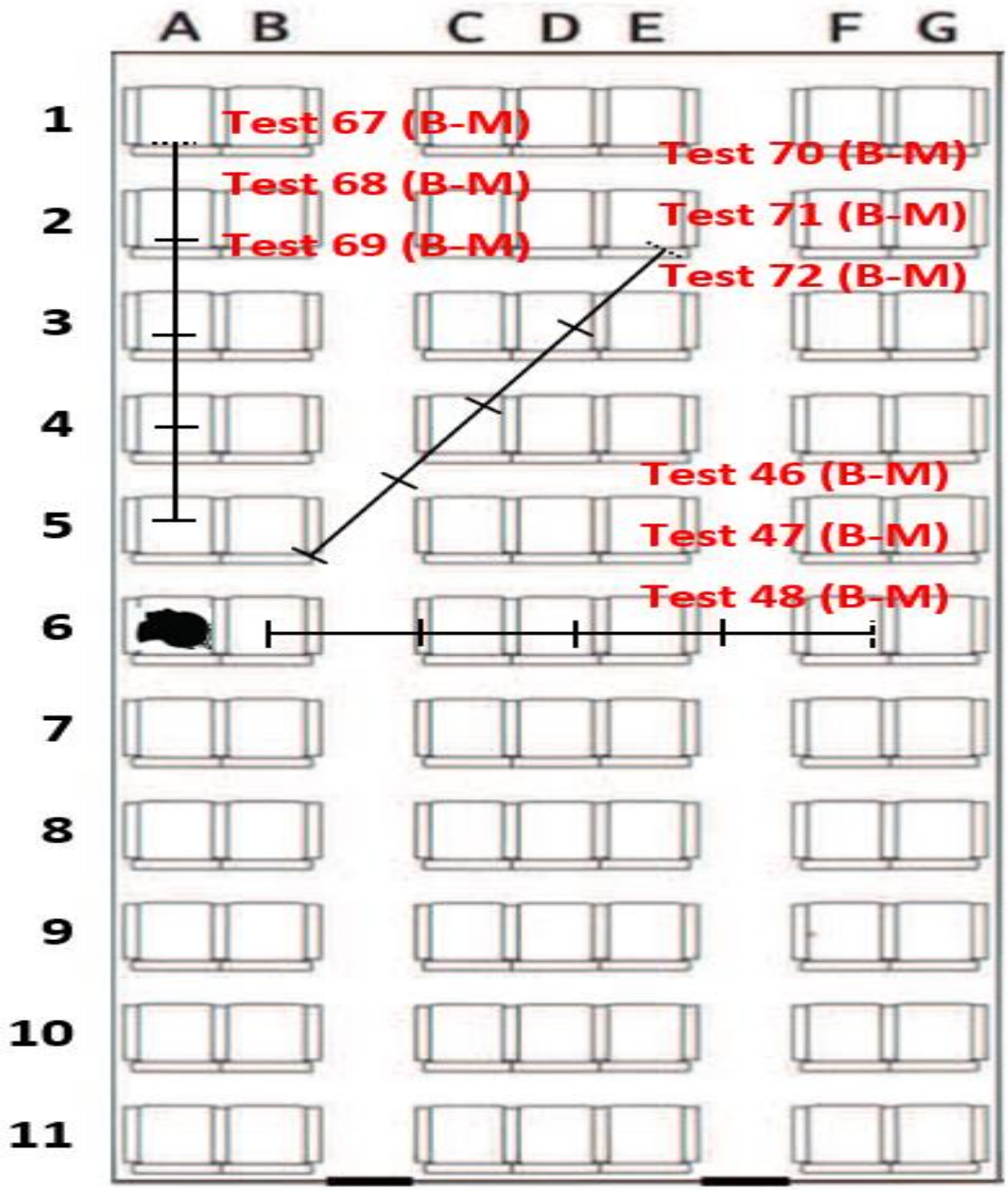

Figure H.4 Seat A6 ISOPass undeployed coughing manikin tracer gas test numbers and sampling tree orientations in the Boeing 767 cabin mockup.

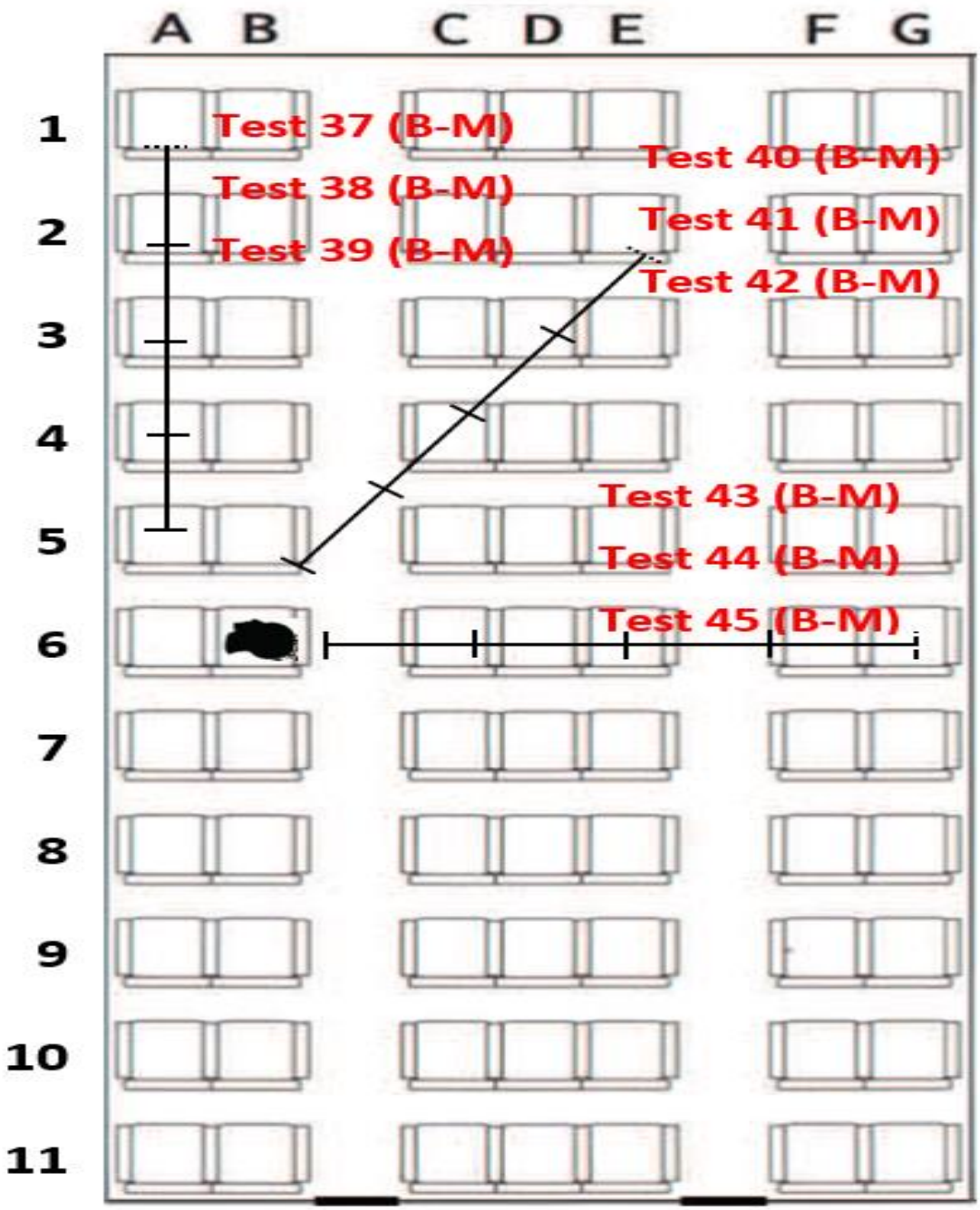

Figure H.5 Seat B6 ISOPass undeployed coughing manikin tracer gas test numbers and sampling tree orientations in the Boeing 767 cabin mockup.

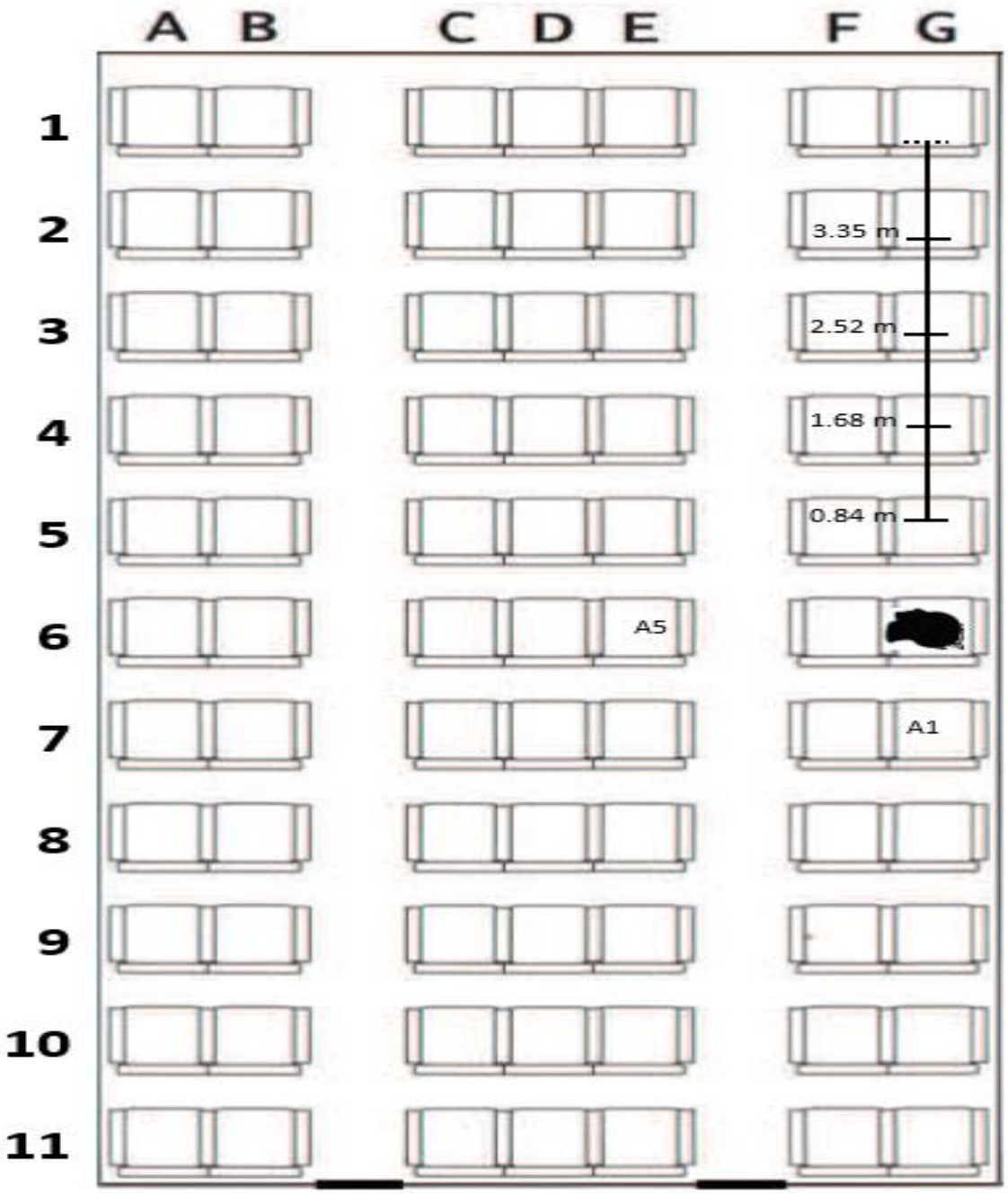

Figure H.6 Test 1 (B-M) ISOPass undeployed source location and sampling tree orientation.

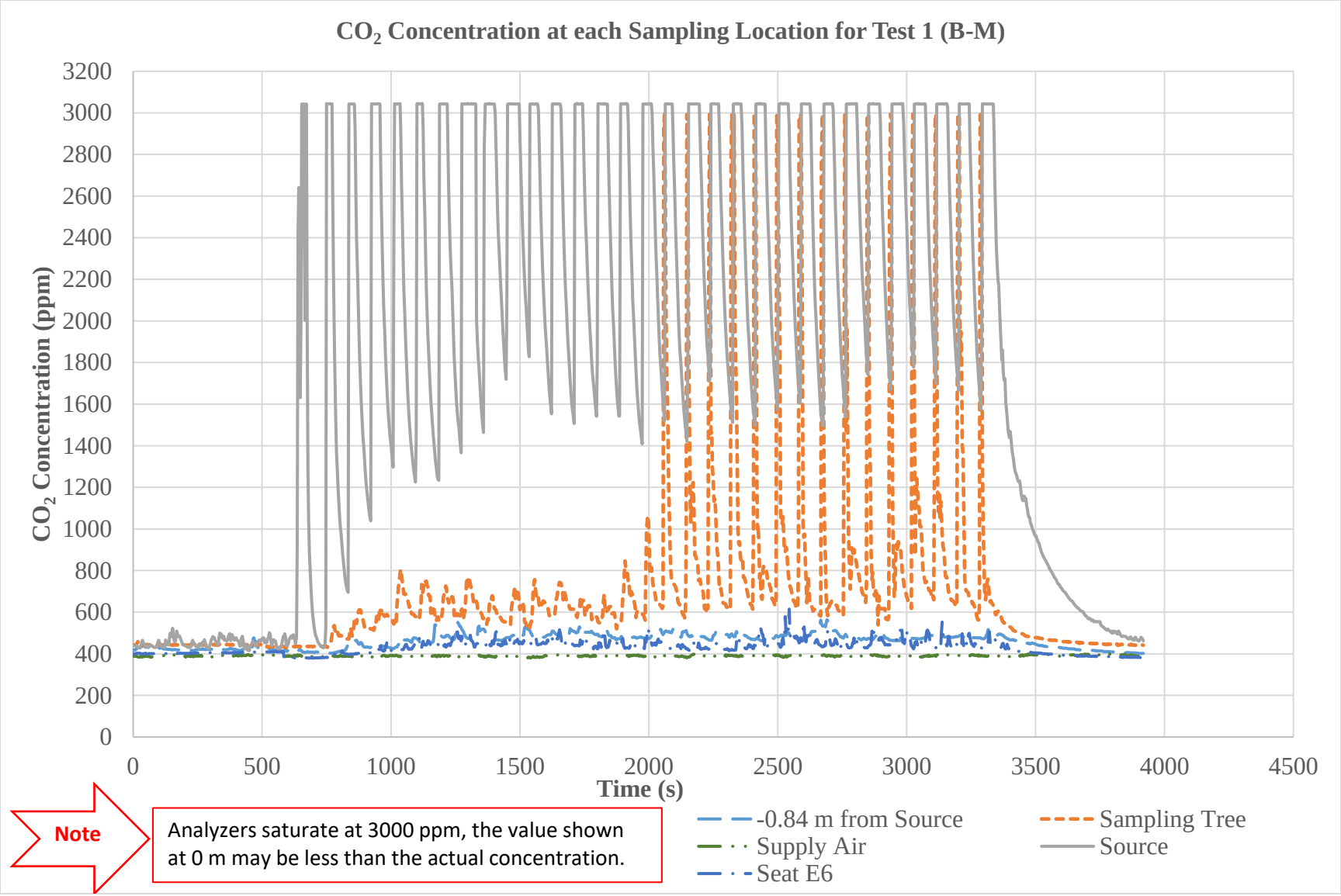

Figure H.7 Ininstantaneous CO_2 concentration at each sampling location for Test 1 (B-M) ISOPass undeployed.

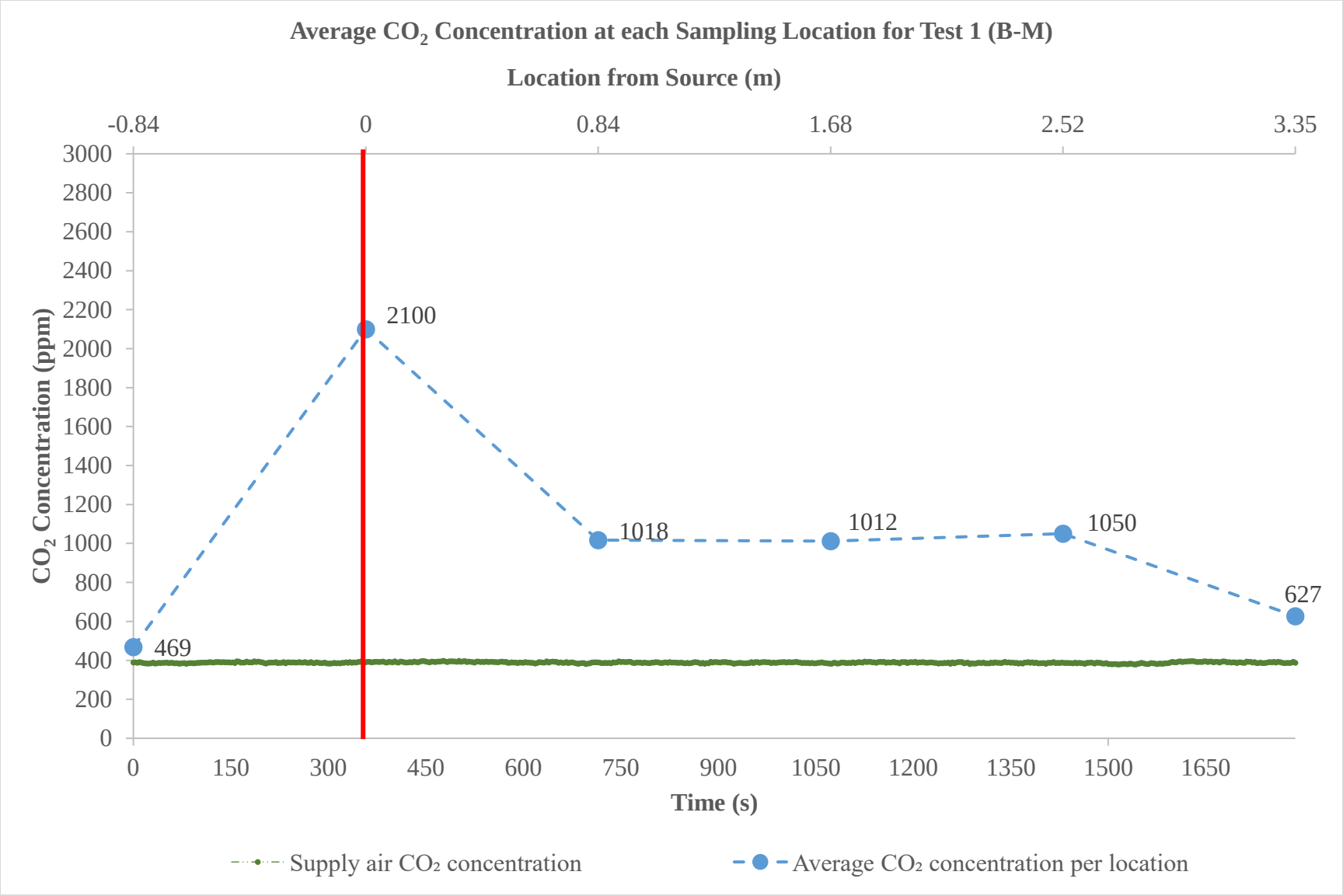

Figure H.8 Average CO_2 concentration at each sampling location for Test 1 (B-M) ISOPass undeployed.

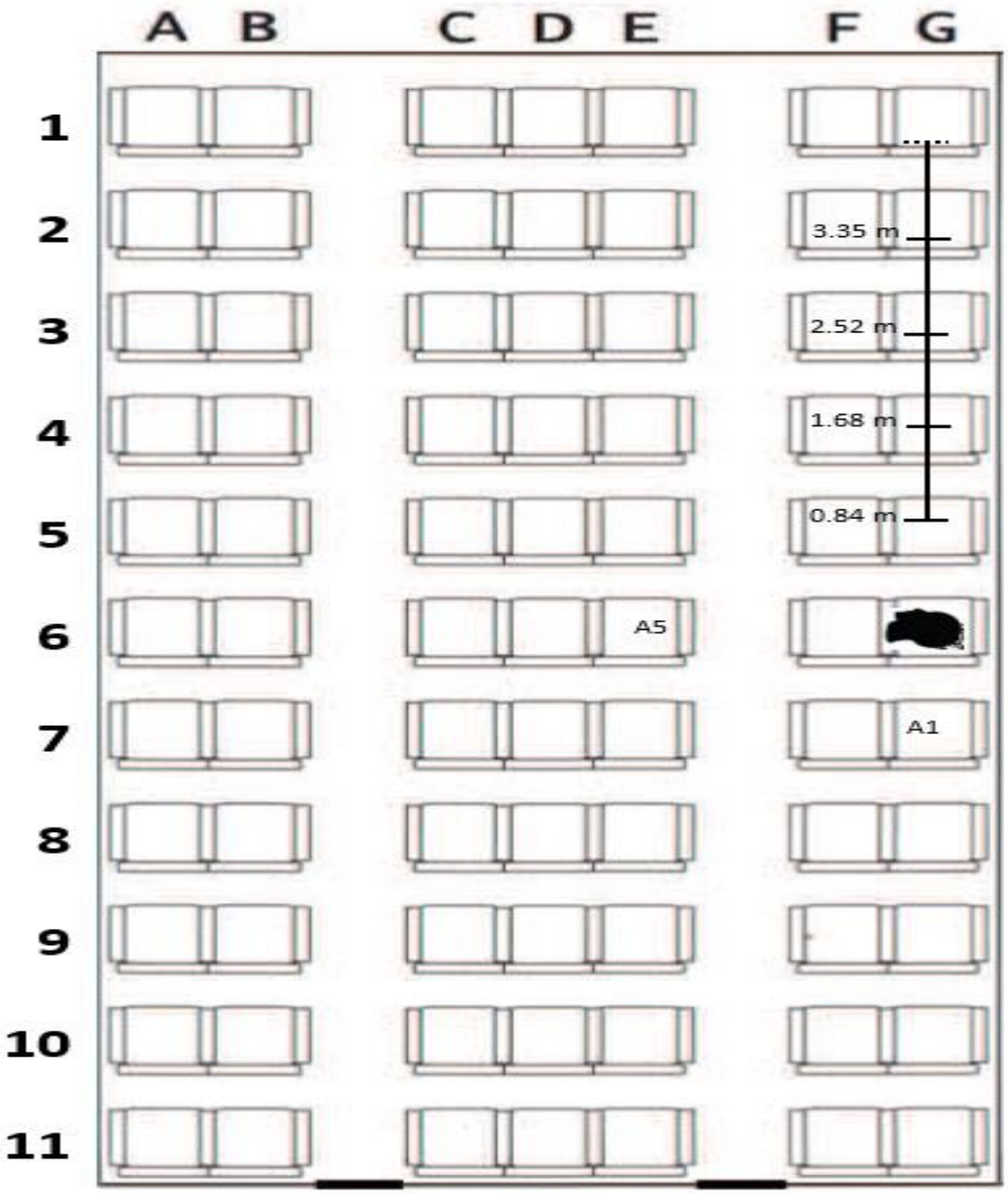

Figure H.9 Test 2 (B-M) ISOPass undeployed source location and sampling tree orientation.

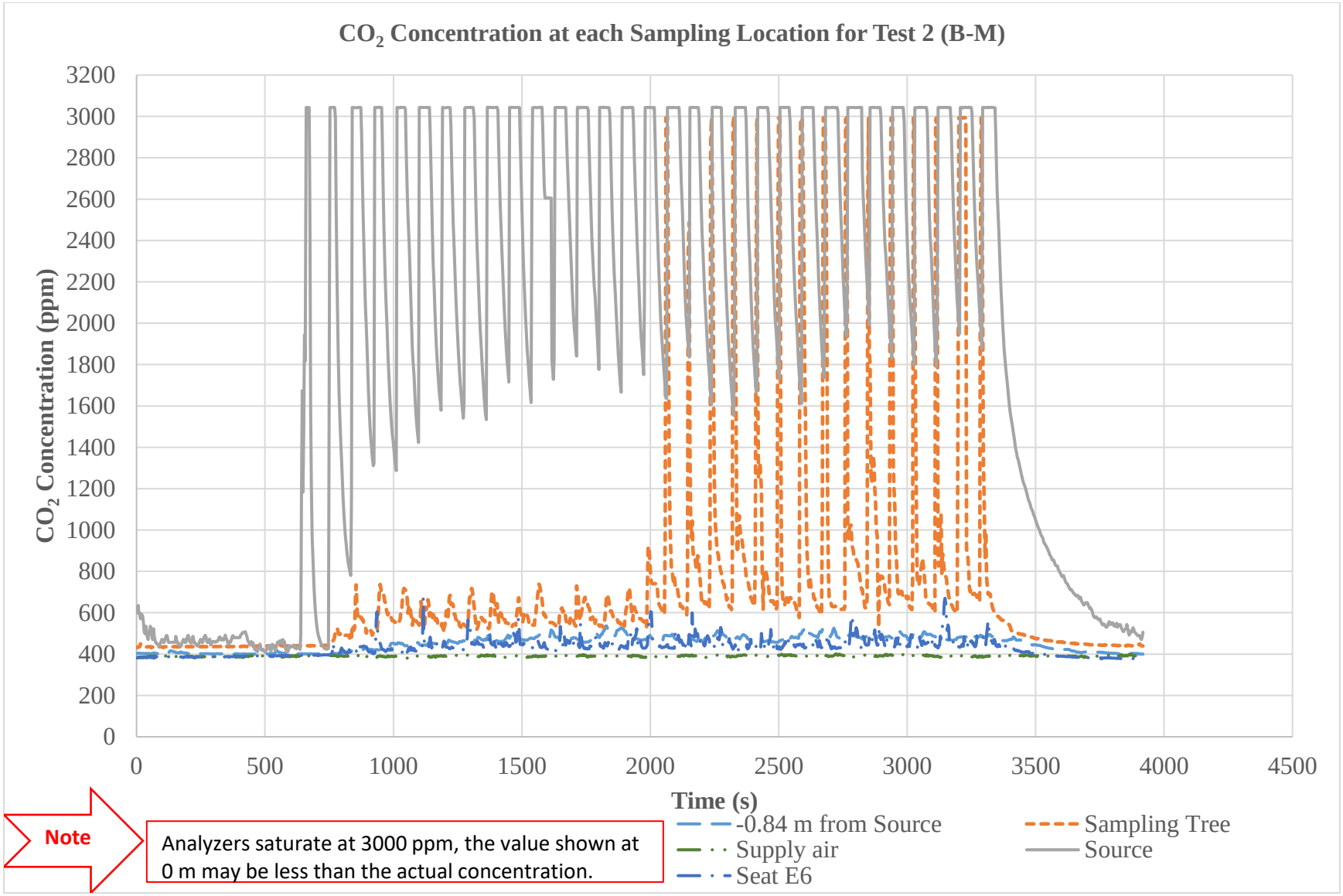

Figure H.10 Ininstantaneous CO_2 concentration at each sampling location for Test 2 (B-M) ISOPass undeployed.

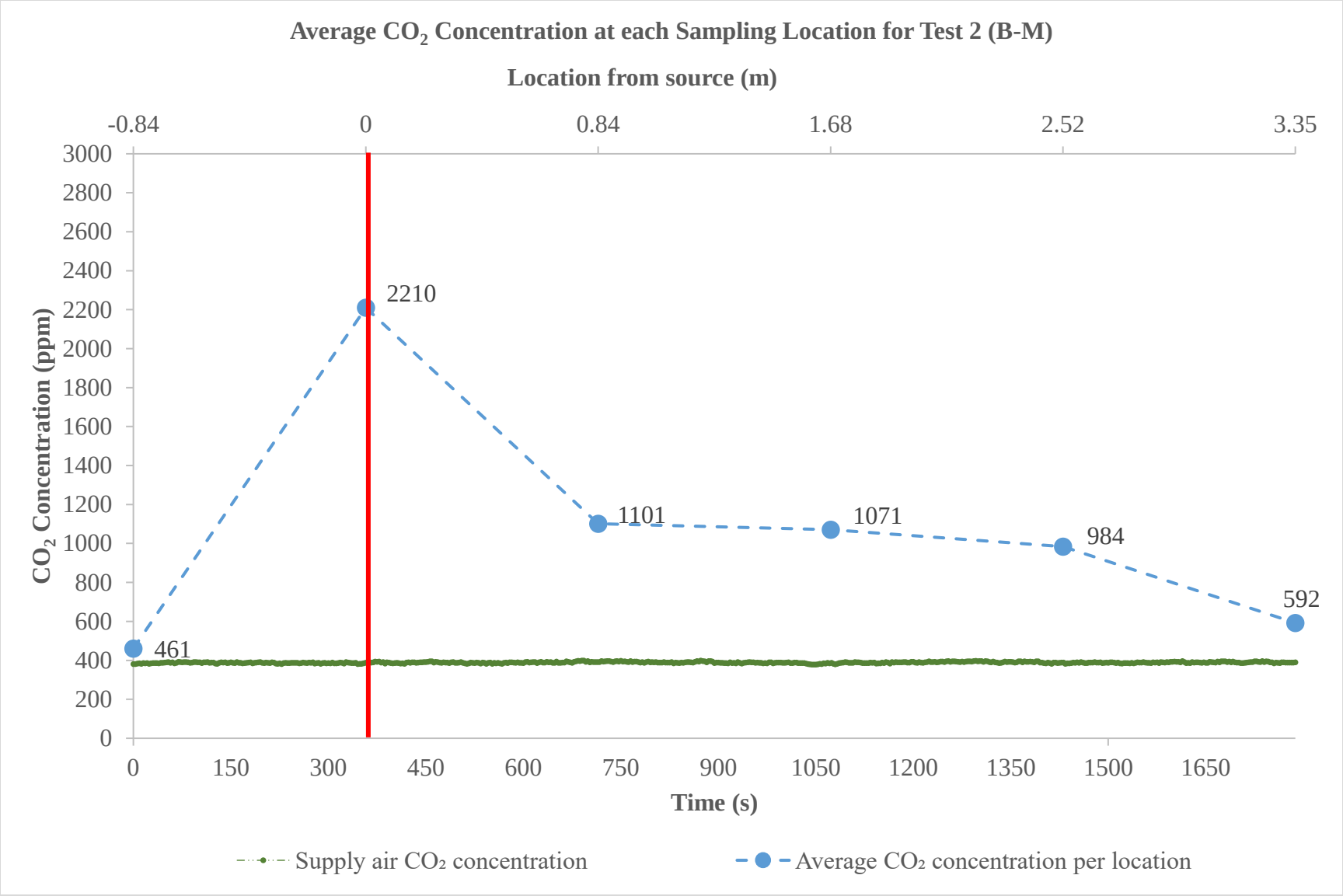

Figure H.11 Average CO_2 concentration at each sampling location for Test 2 (B-M) ISOPass undeployed.

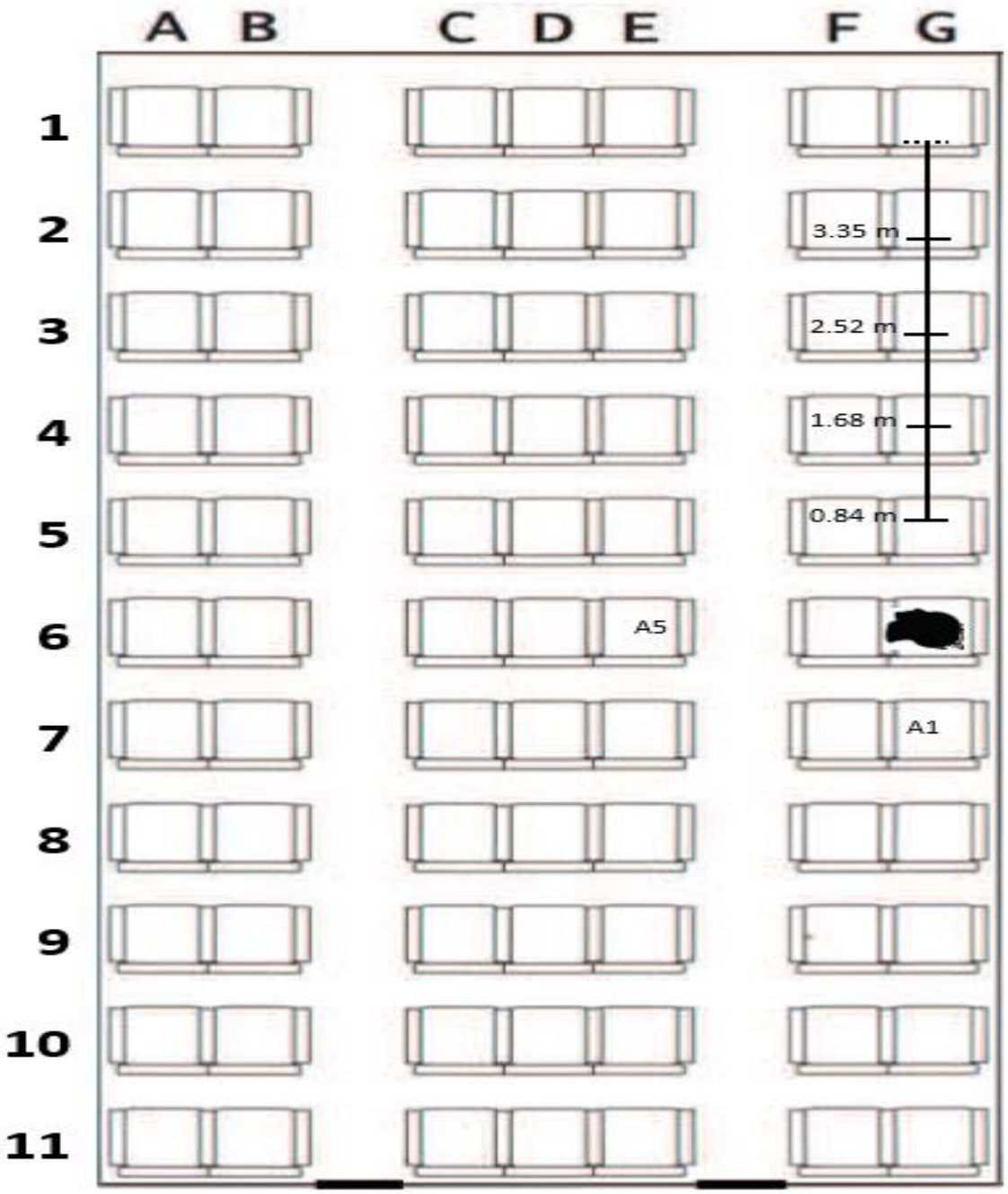

Figure H.12 Test 3 (B-M) ISOPass undeployed source location and sampling tree orientation.

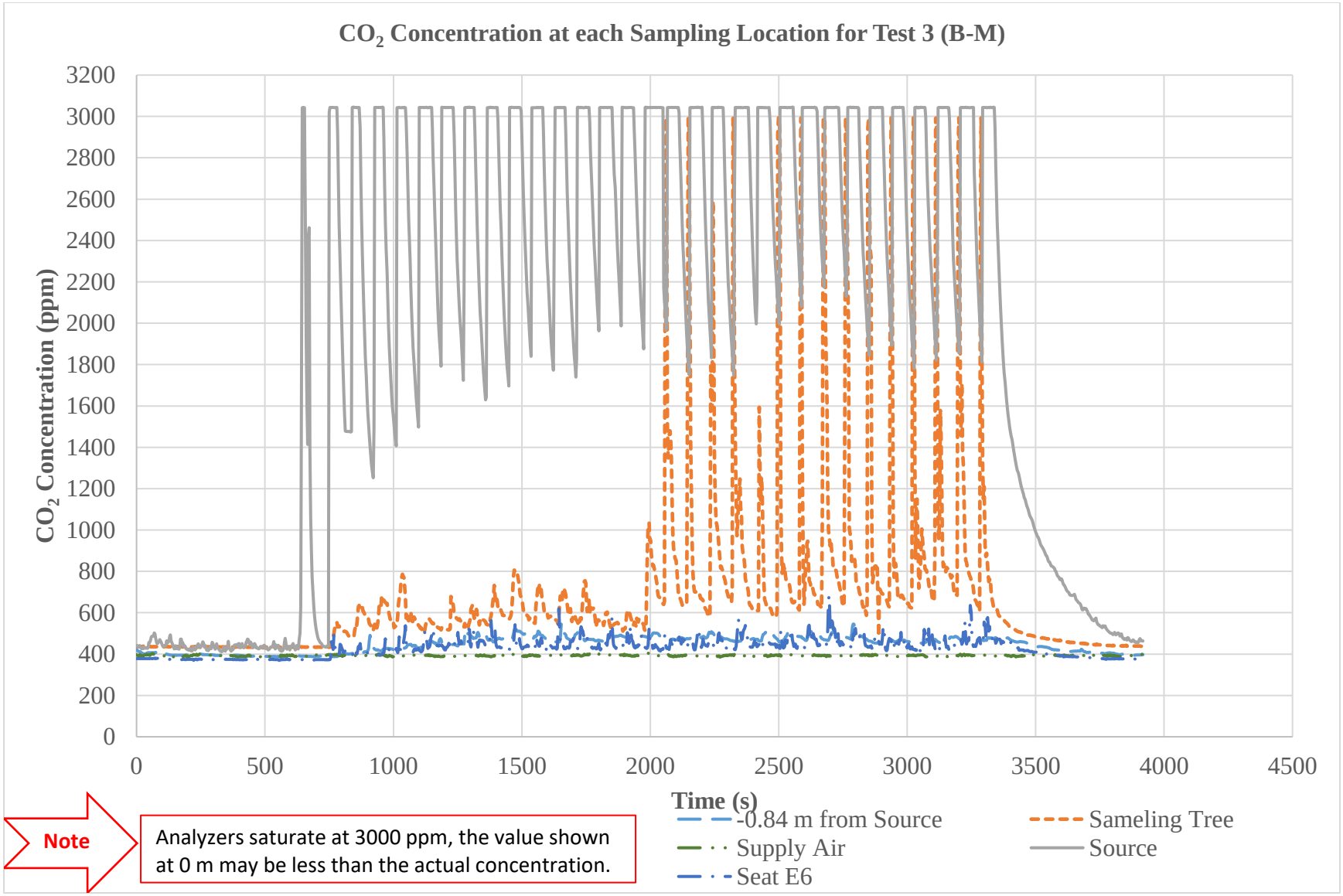

Figure H.13 Ininstantaneous CO_2 concentration at each sampling location for Test 3 (B-M) ISOPass undeployed.

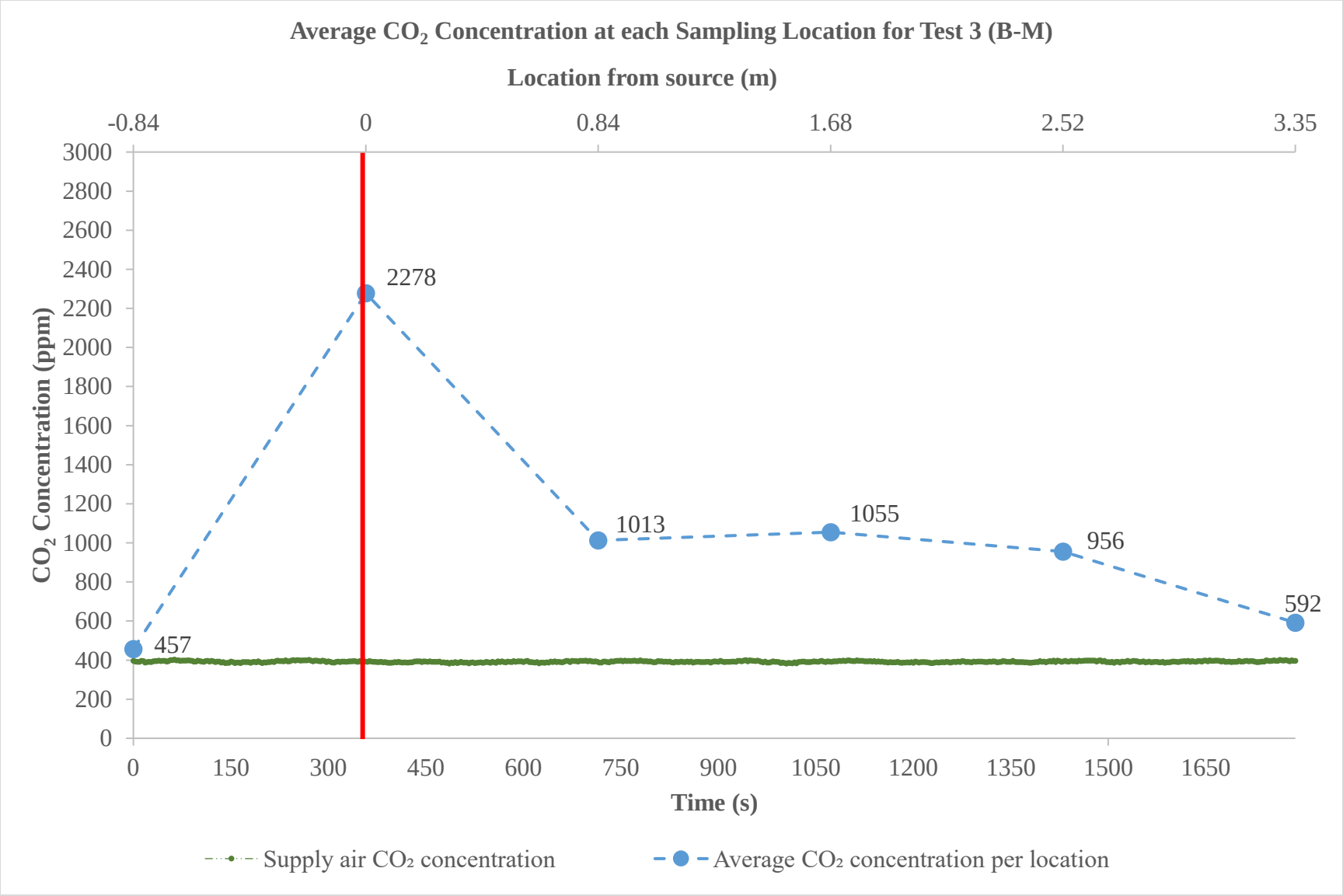

Figure H.14 Average CO_2 concentration at each sampling location for Test 3 (B-M) ISOPass undeployed.

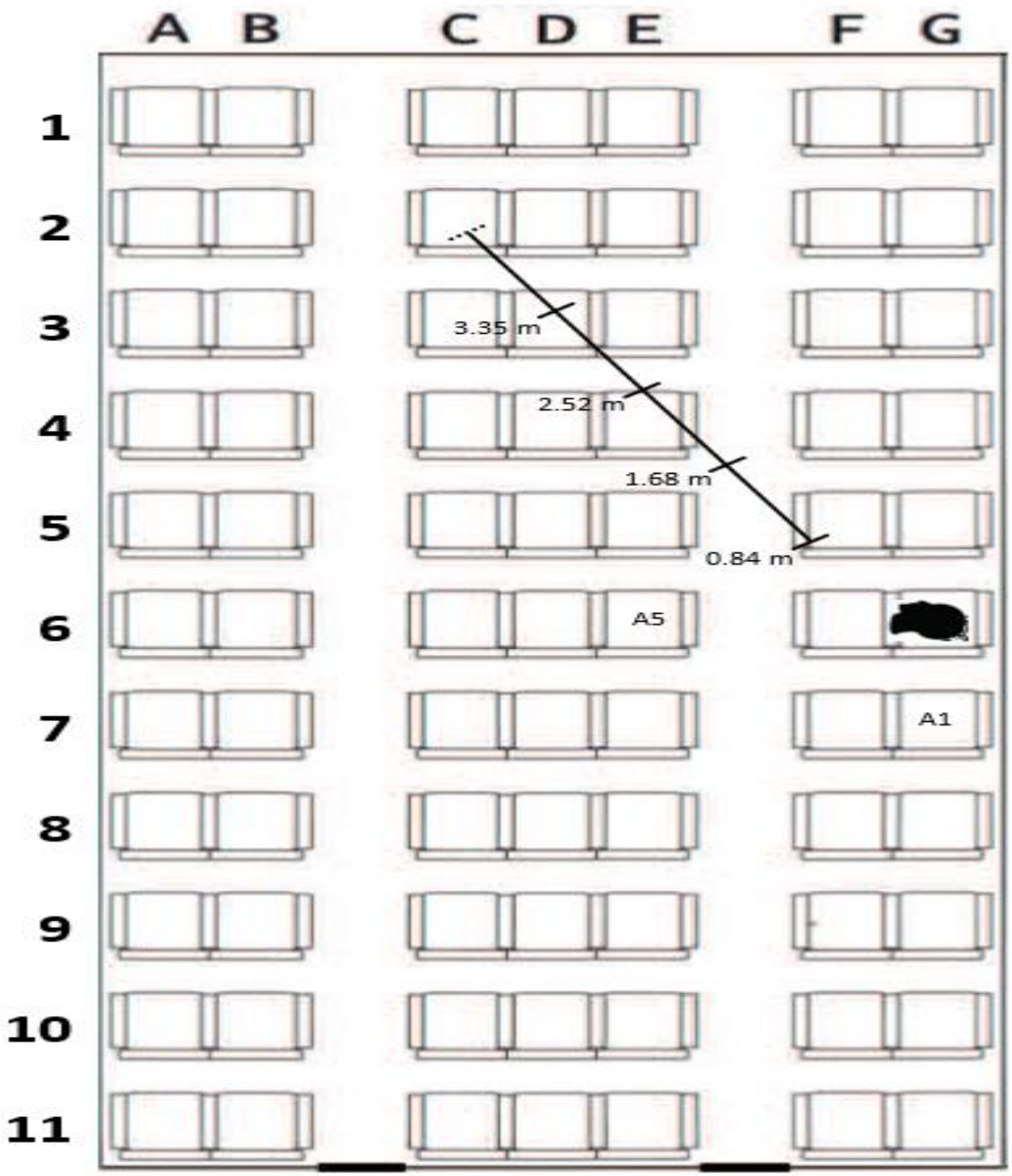

Figure H.15 Test 4 (B-M) ISOPass undeployed source location and sampling tree orientation.

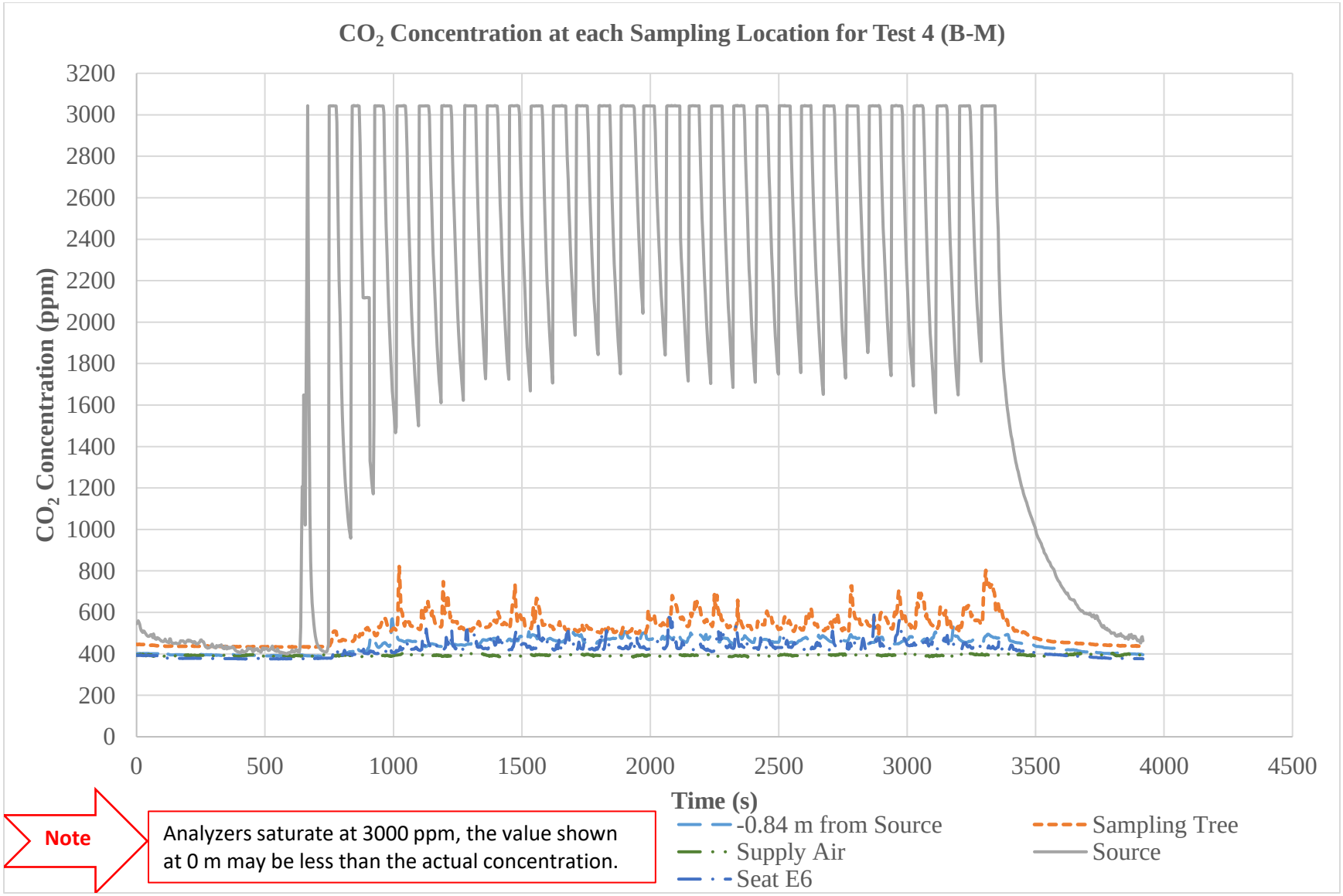

Figure H.16 Ininstantaneous CO_2 concentration at each sampling location for Test 4 (B-M) ISOPass undeployed.

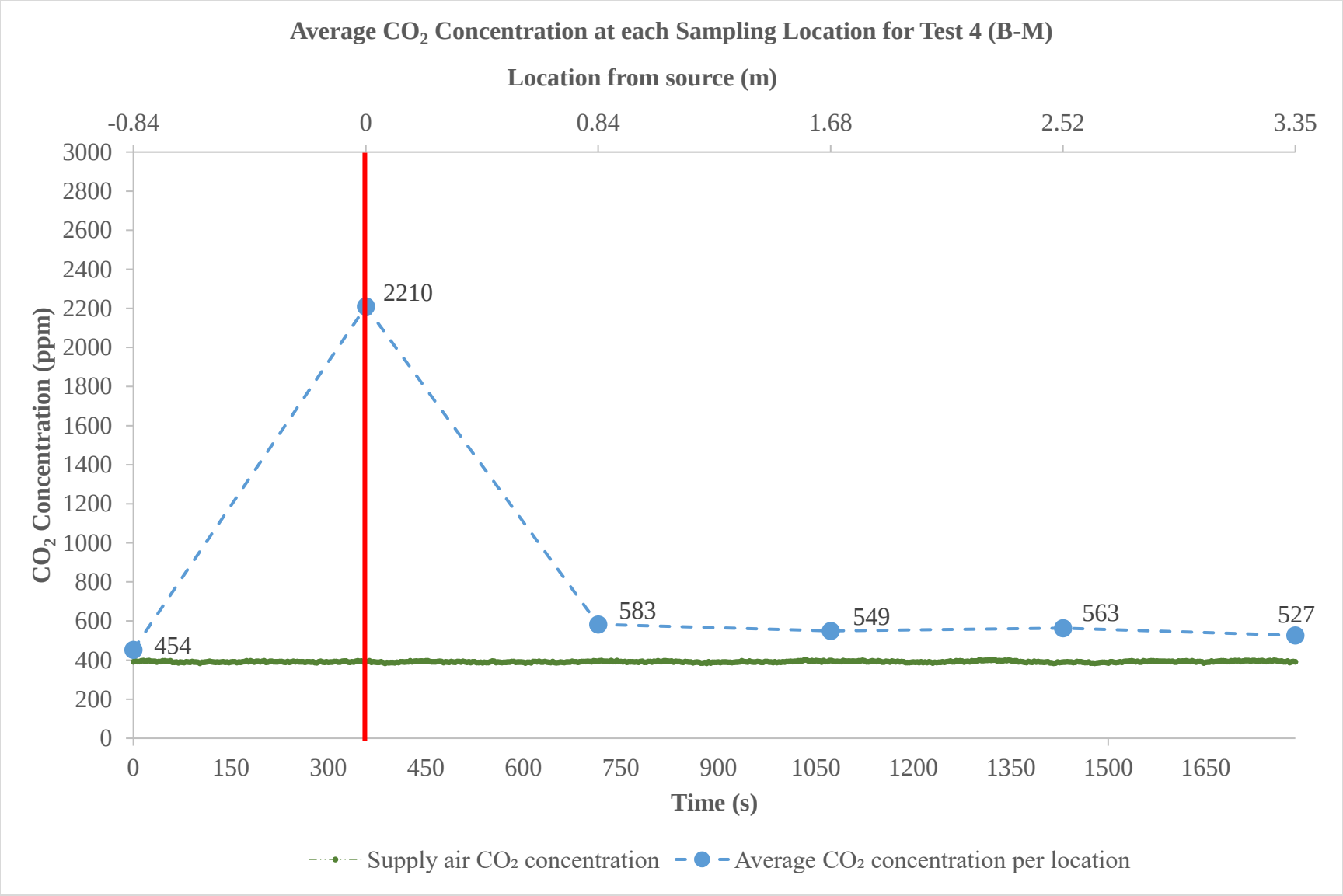

Figure H.17 Average CO_2 concentration at each sampling location for Test 4 (B-M) ISOPass undeployed.

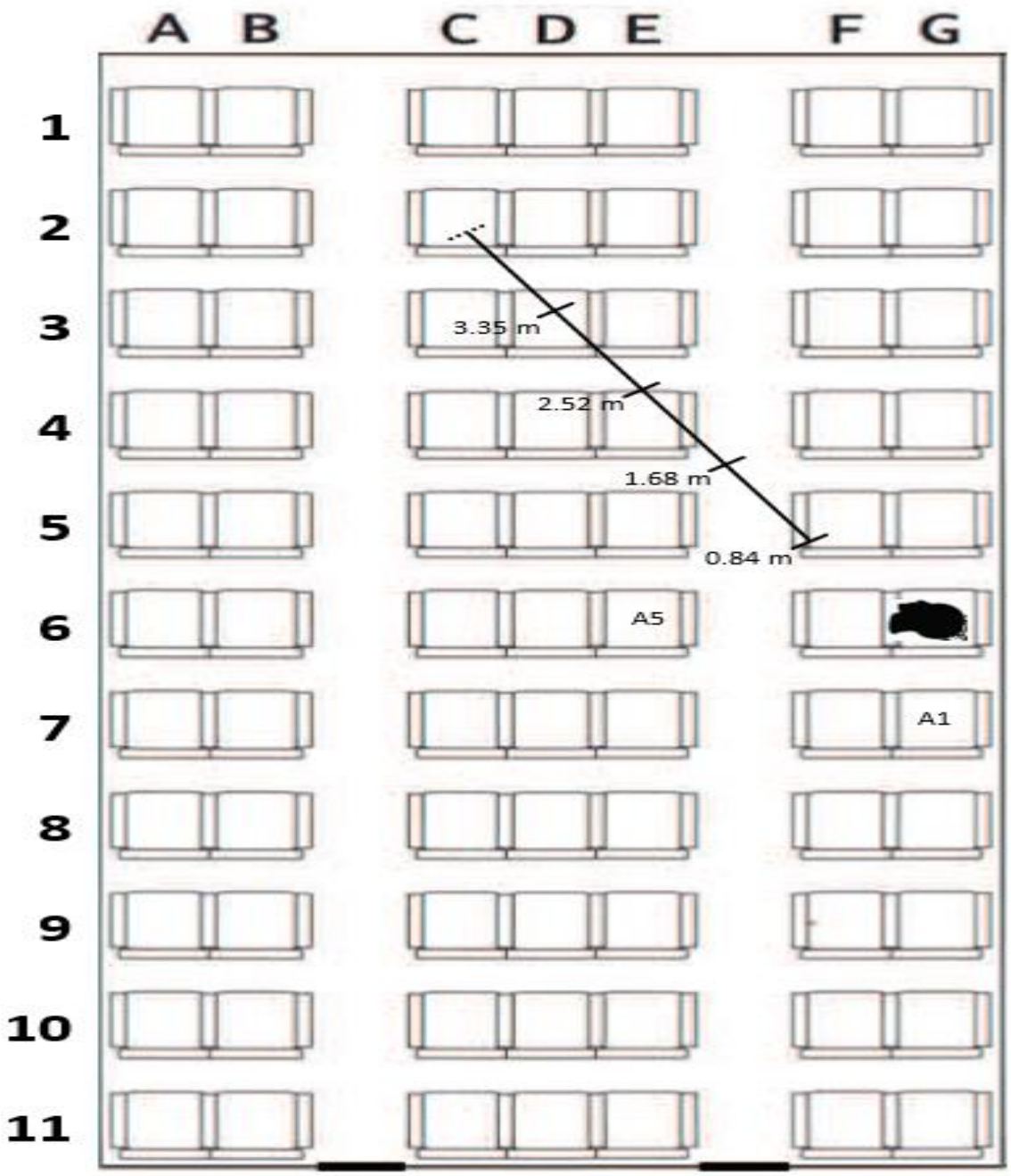

Figure H.18 Test 5 (B-M) ISOPass undeployed source location and sampling tree orientation.

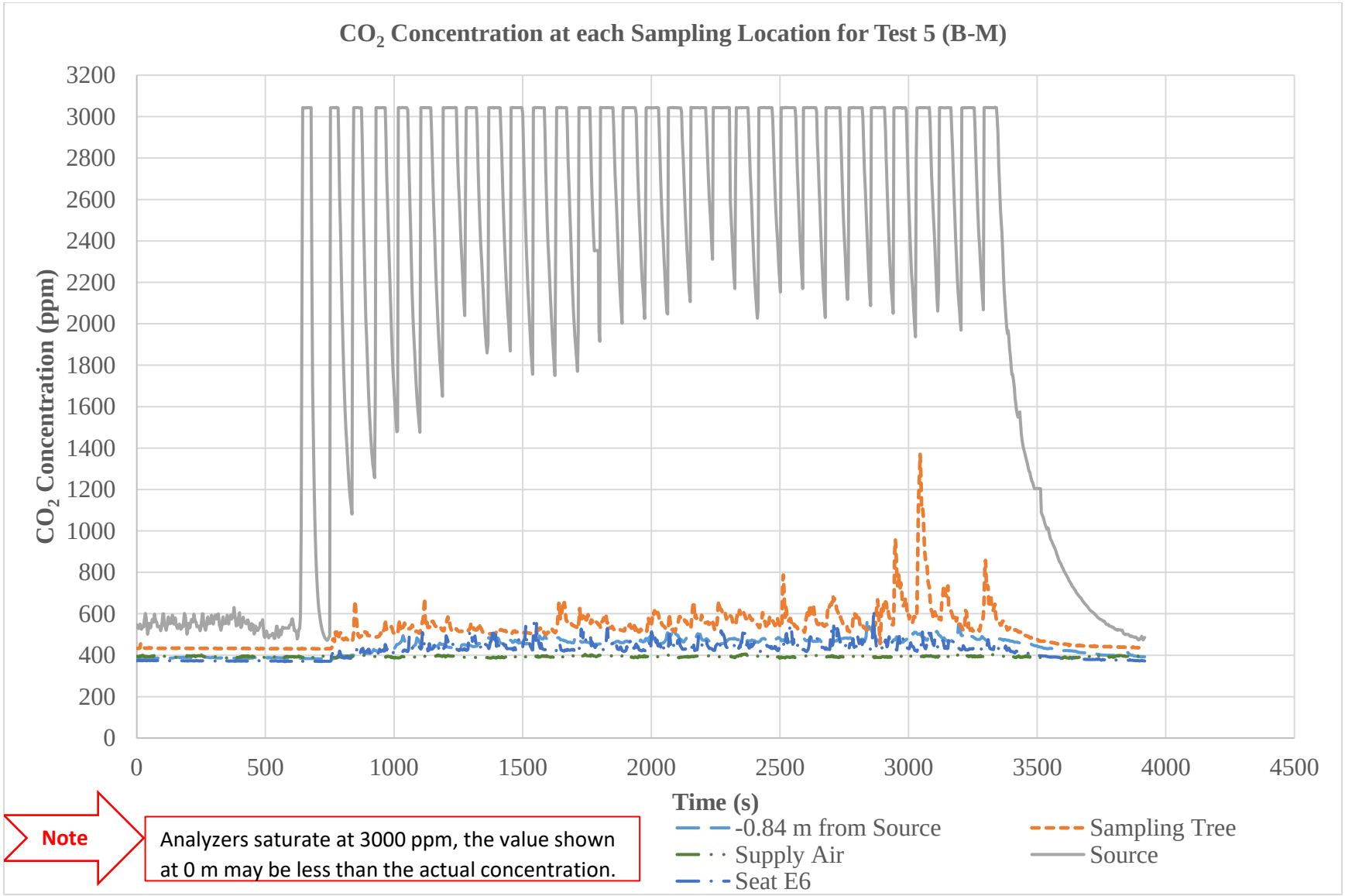

Figure H.19 Ininstantaneous CO_2 concentration at each sampling location for Test 5 (B-M) ISOPass undeployed.

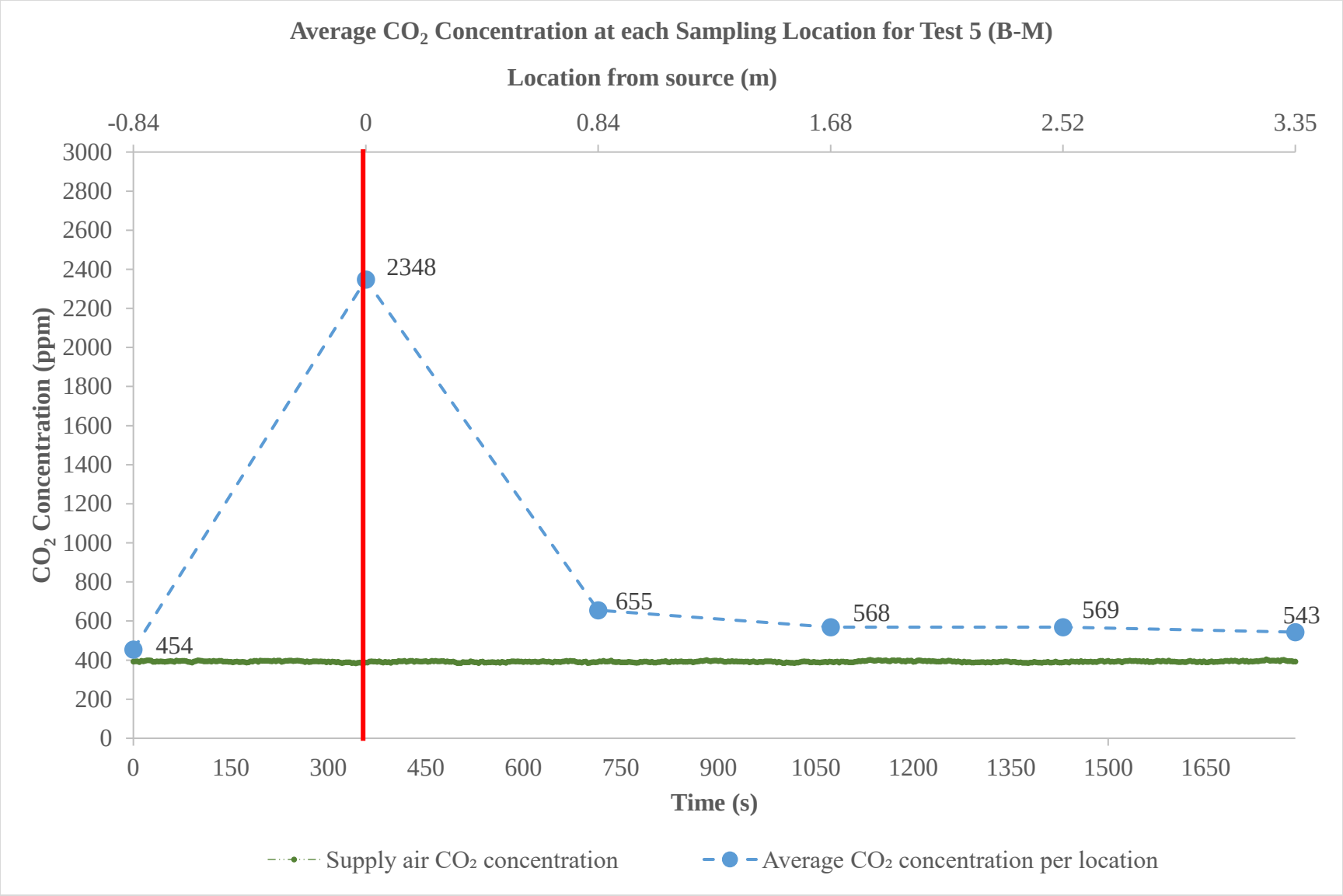

Figure H.20 Average CO_2 concentration at each sampling location for Test 5 (B-M) ISOPass undeployed.

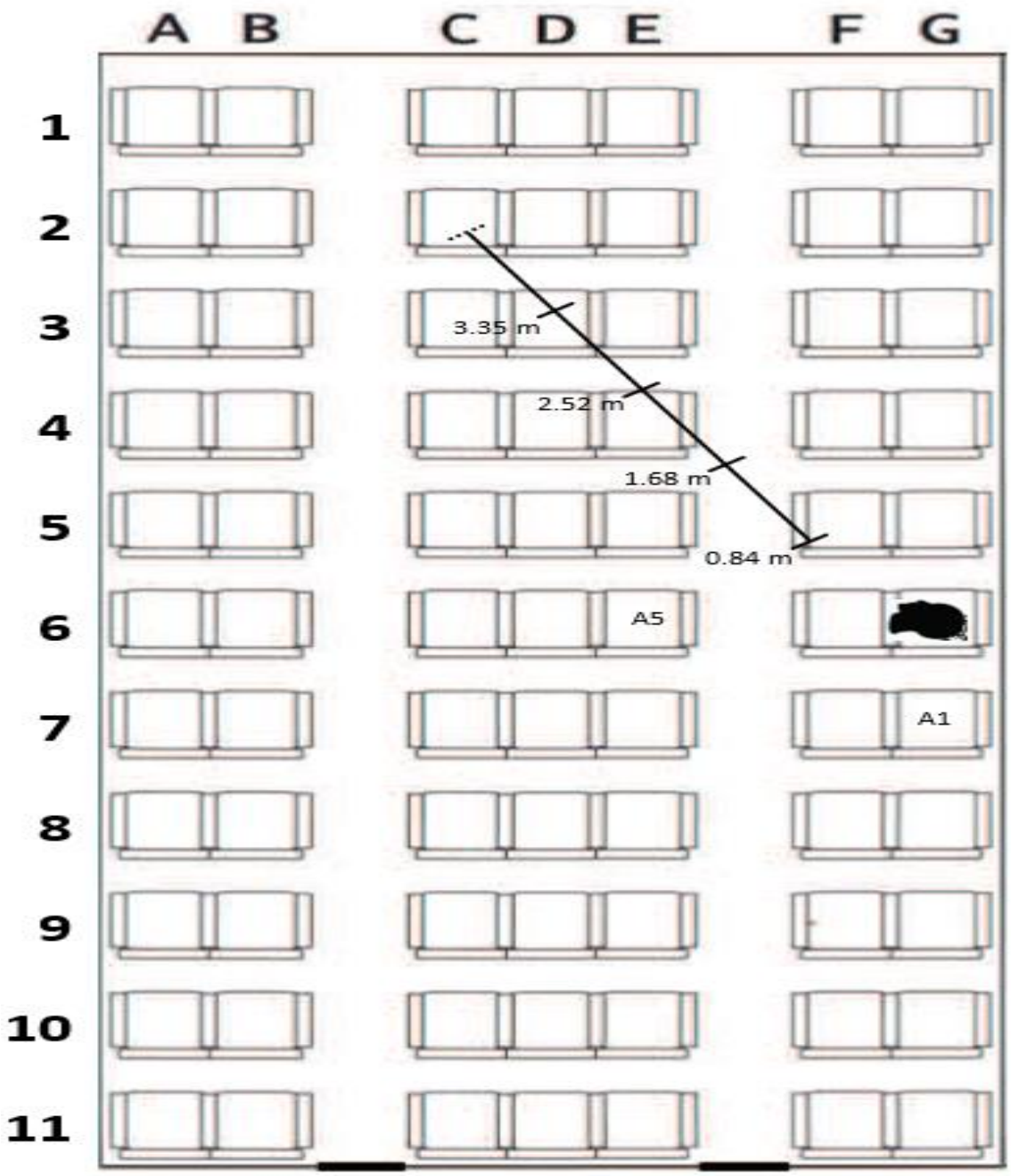

Figure H.21 Test 6 (B-M) ISOPass undeployed source location and sampling tree orientation.

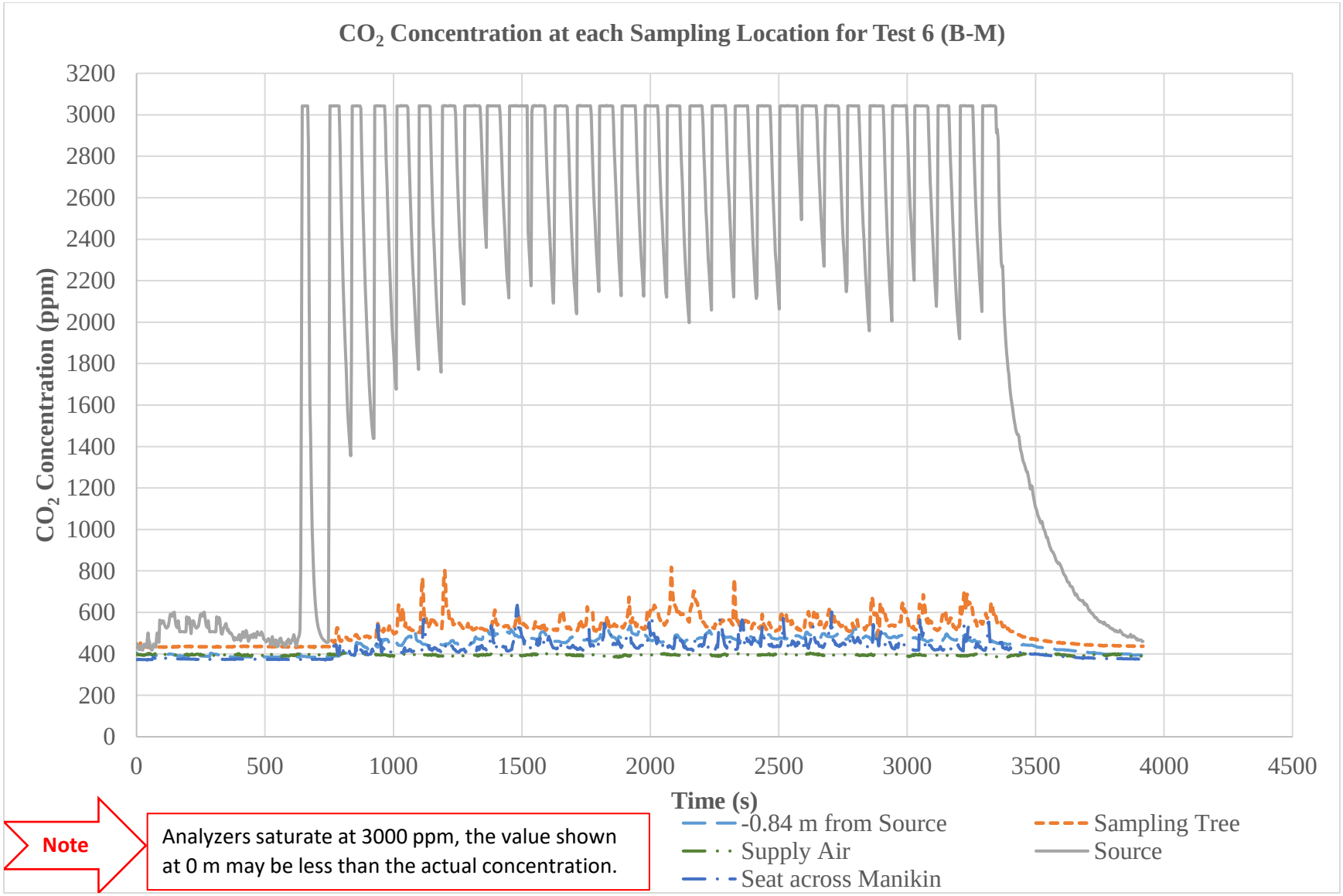

Figure H.22 Ininstantaneous CO_2 concentration at each sampling location for Test 6 (B-M) ISOPass undeployed.

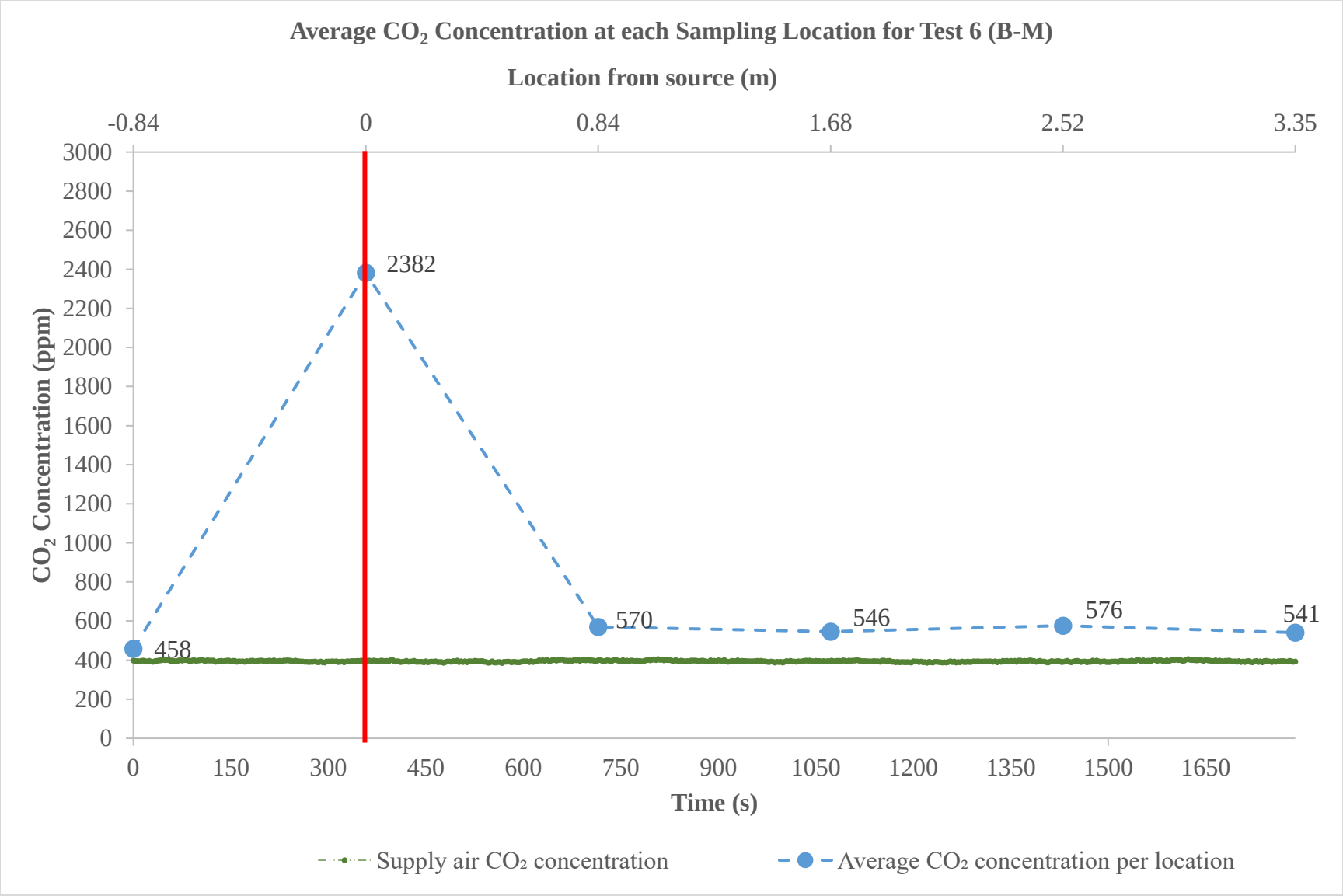

Figure H.23 Average CO_2 concentration at each sampling location for Test 6 (B-M) ISOPass undeployed.

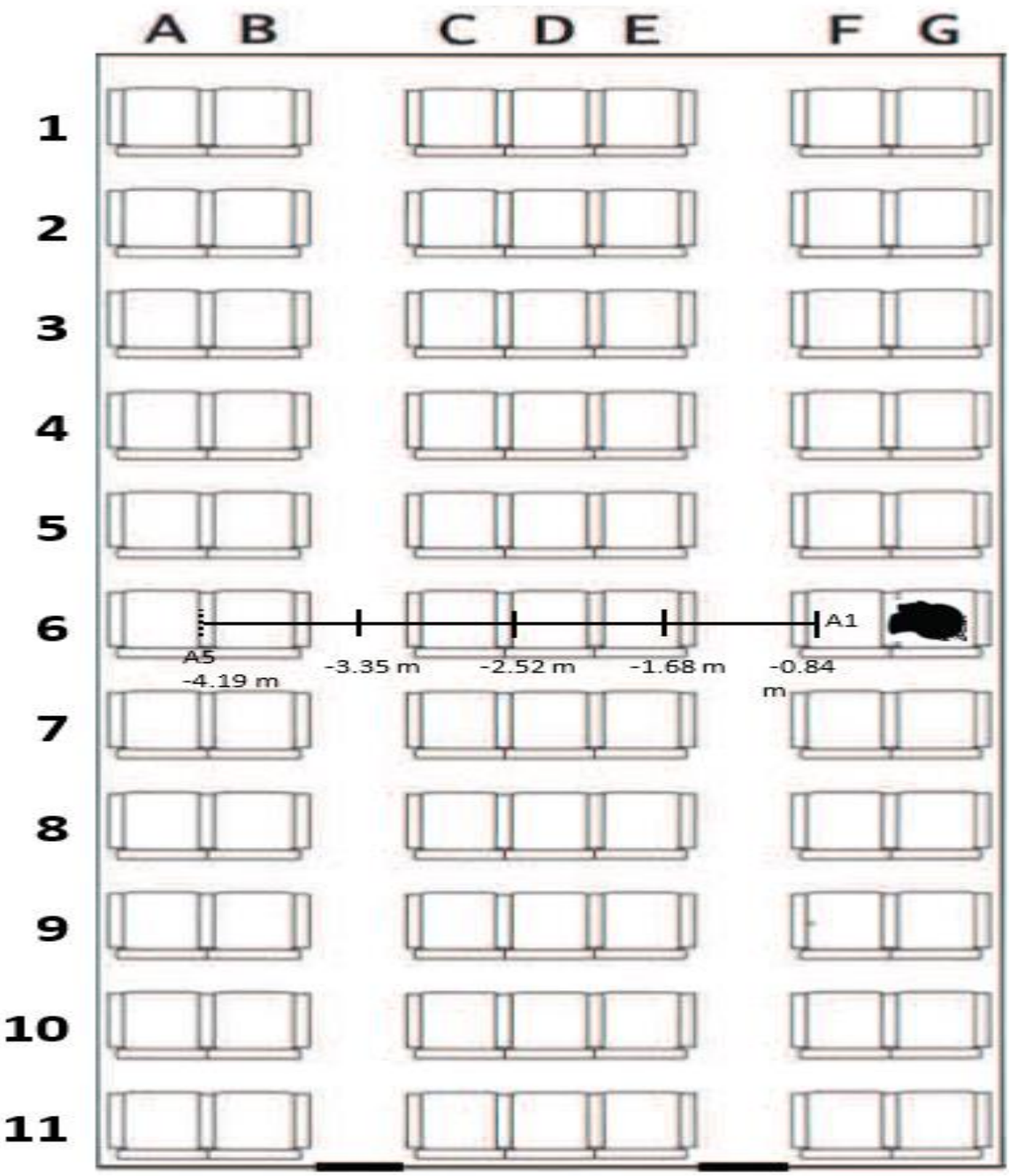

Figure H.24 Test 7 (B-M) ISOPass undeployed source location and sampling tree orientation.

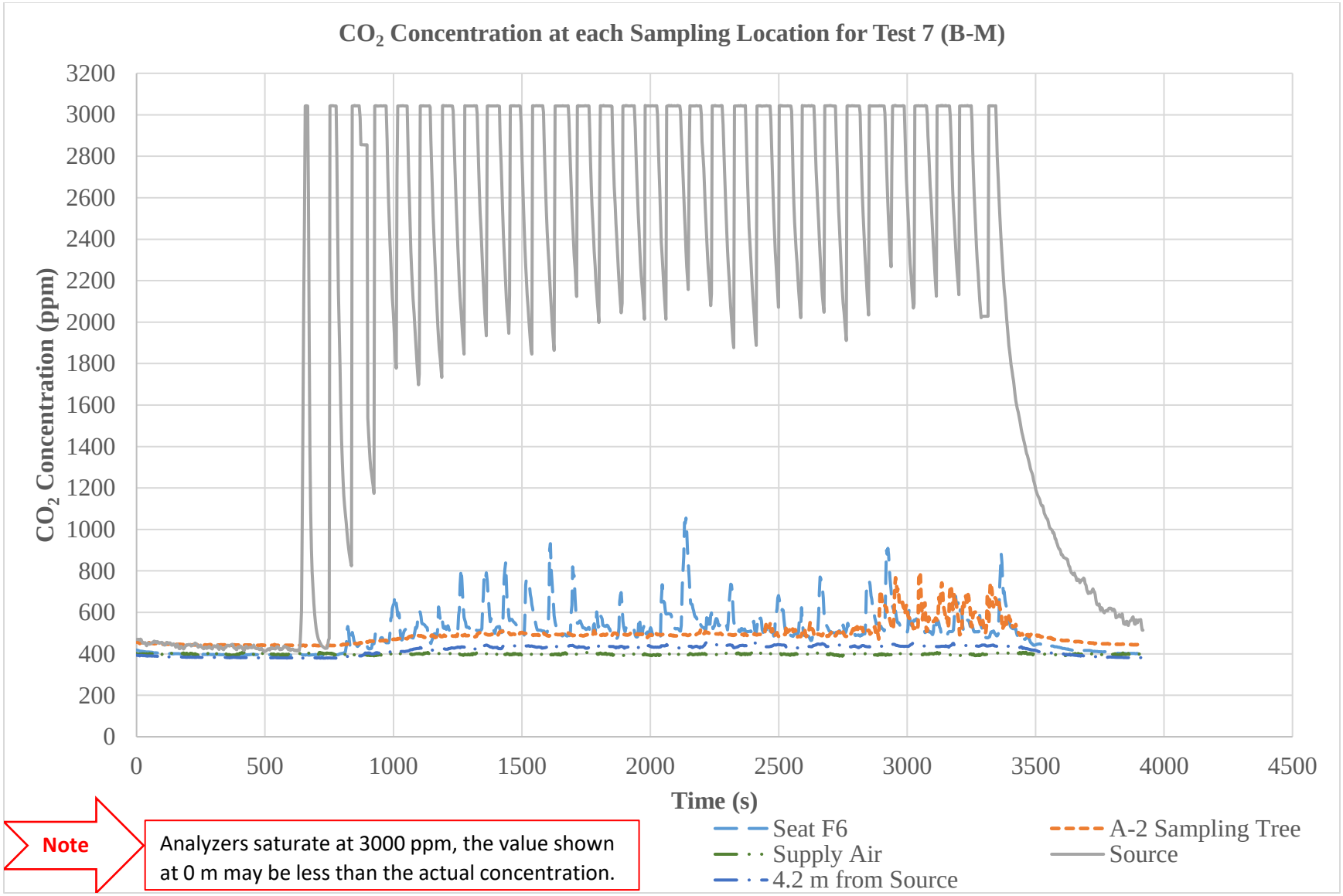

Figure H.25 Ininstantaneous CO_2 concentration at each sampling location for Test 7 (B-M) ISOPass undeployed.

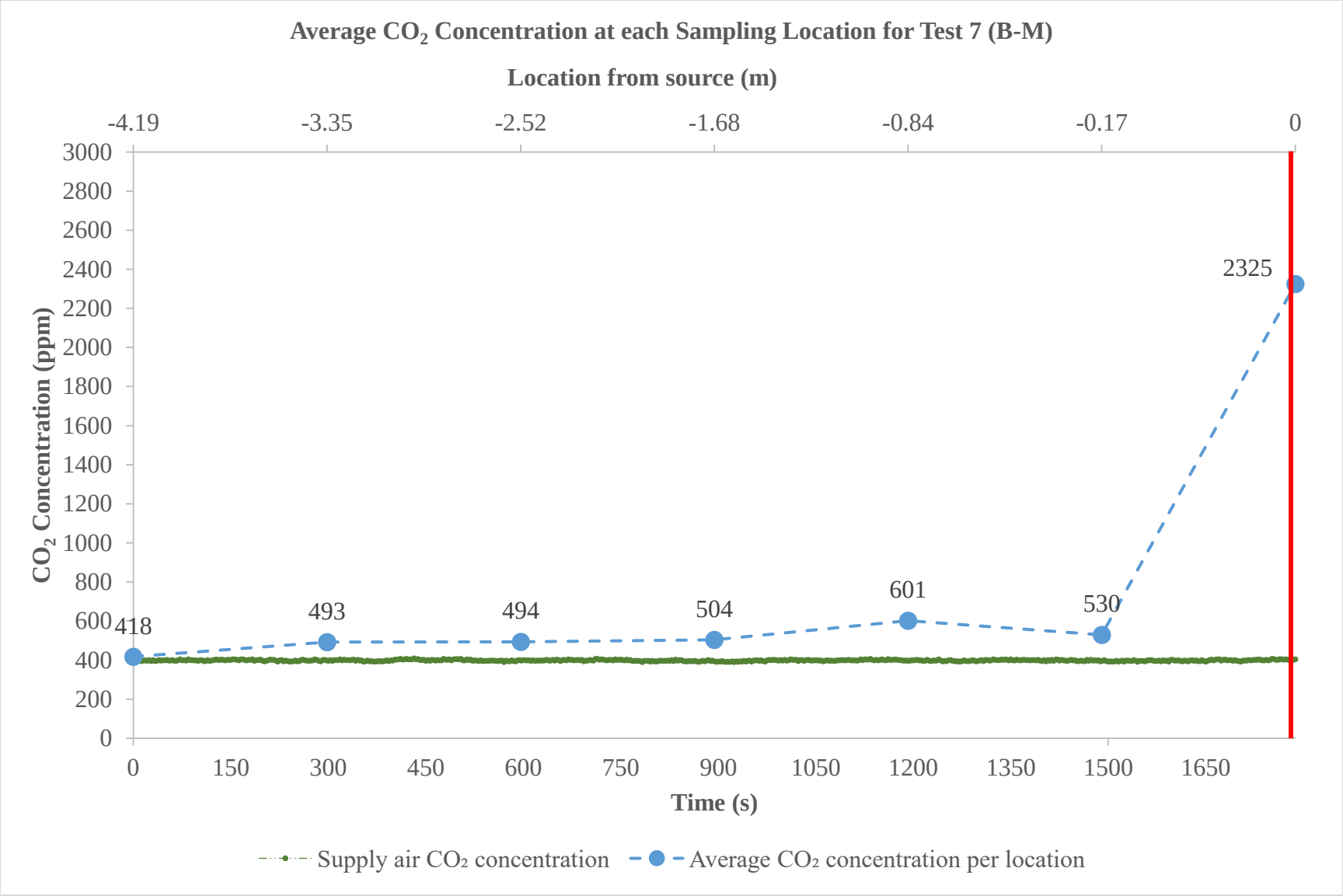

Figure H.26 Average CO_2 concentration at each sampling location for Test 7 (B-M) ISOPass undeployed.

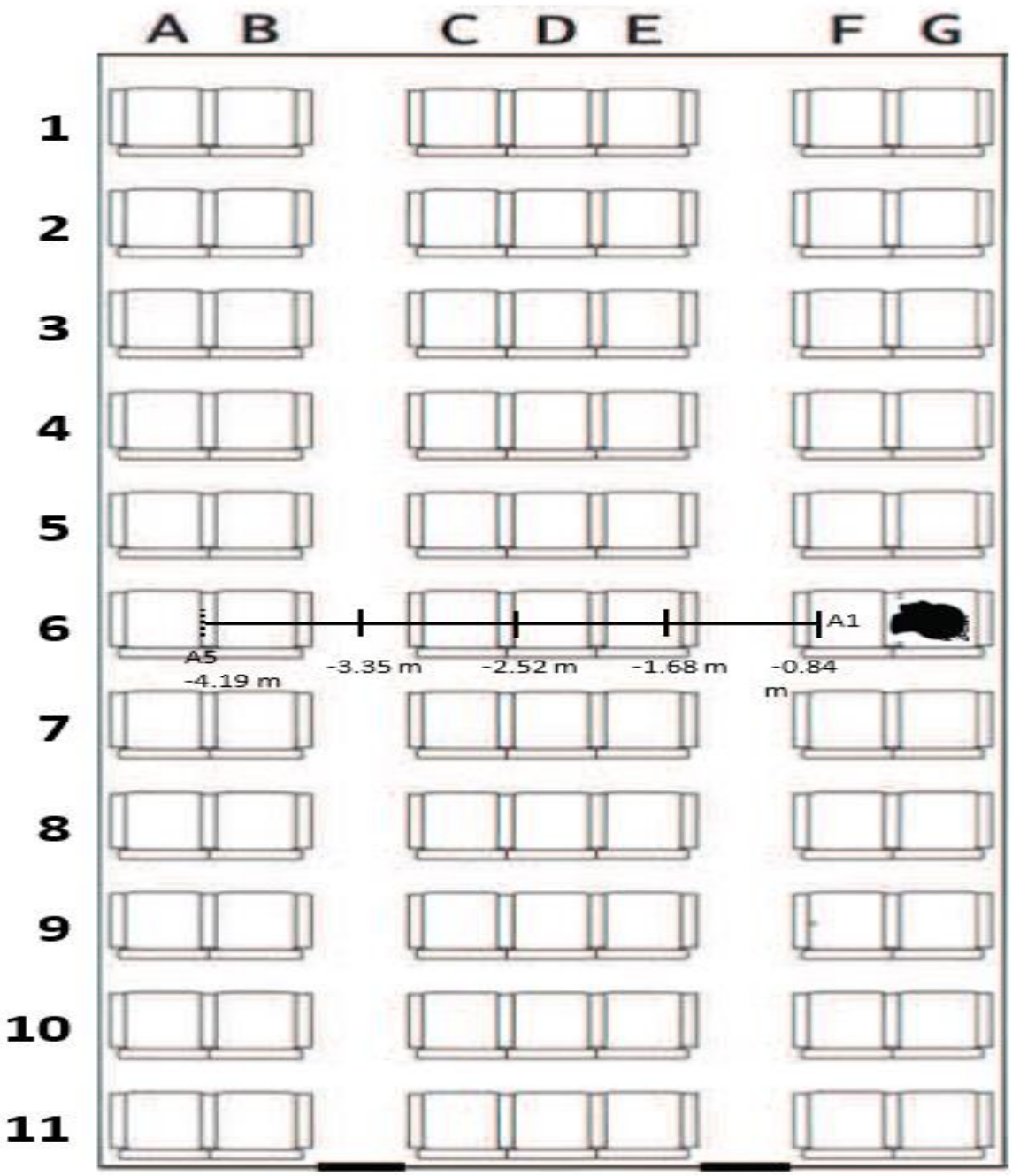

Figure H.27 Test 8 (B-M) ISOPass undeployed source location and sampling tree orientation.

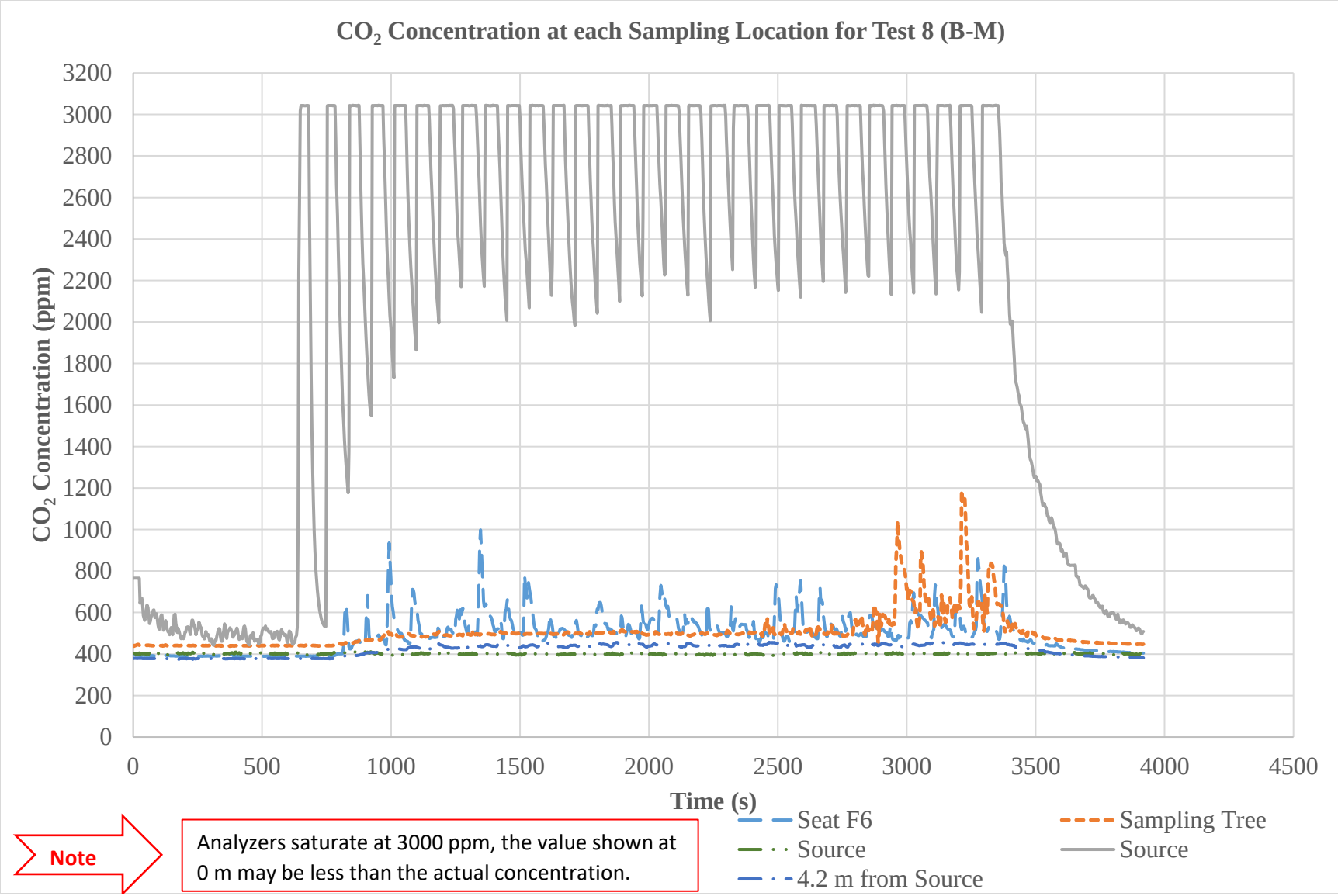

Figure H.28 Ininstantaneous CO_2 concentration at each sampling location for Test 8 (B-M) ISOPass undeployed.

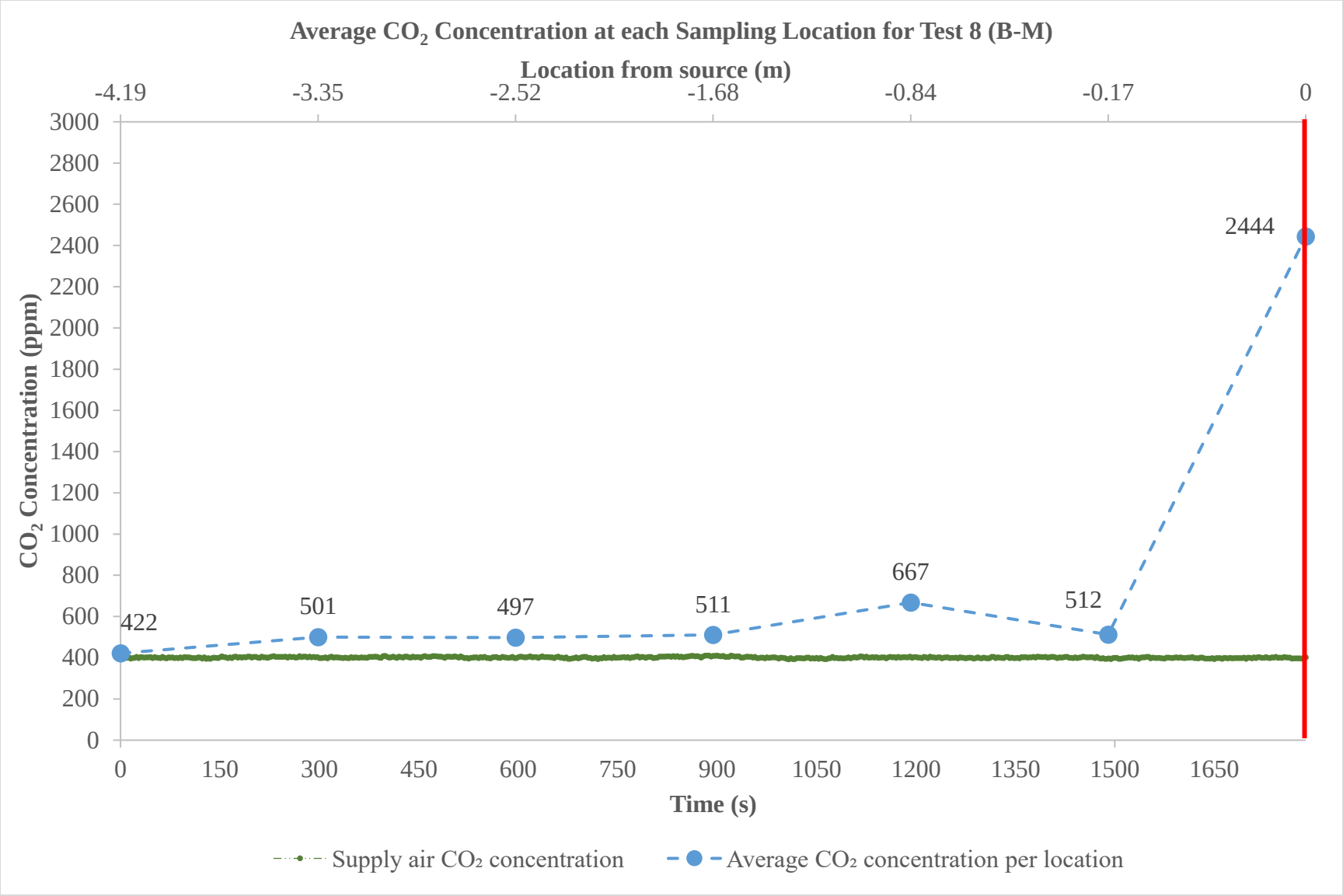

Figure H.29 Average CO_2 concentration at each sampling location for Test 8 (B-M) ISOPass undeployed.

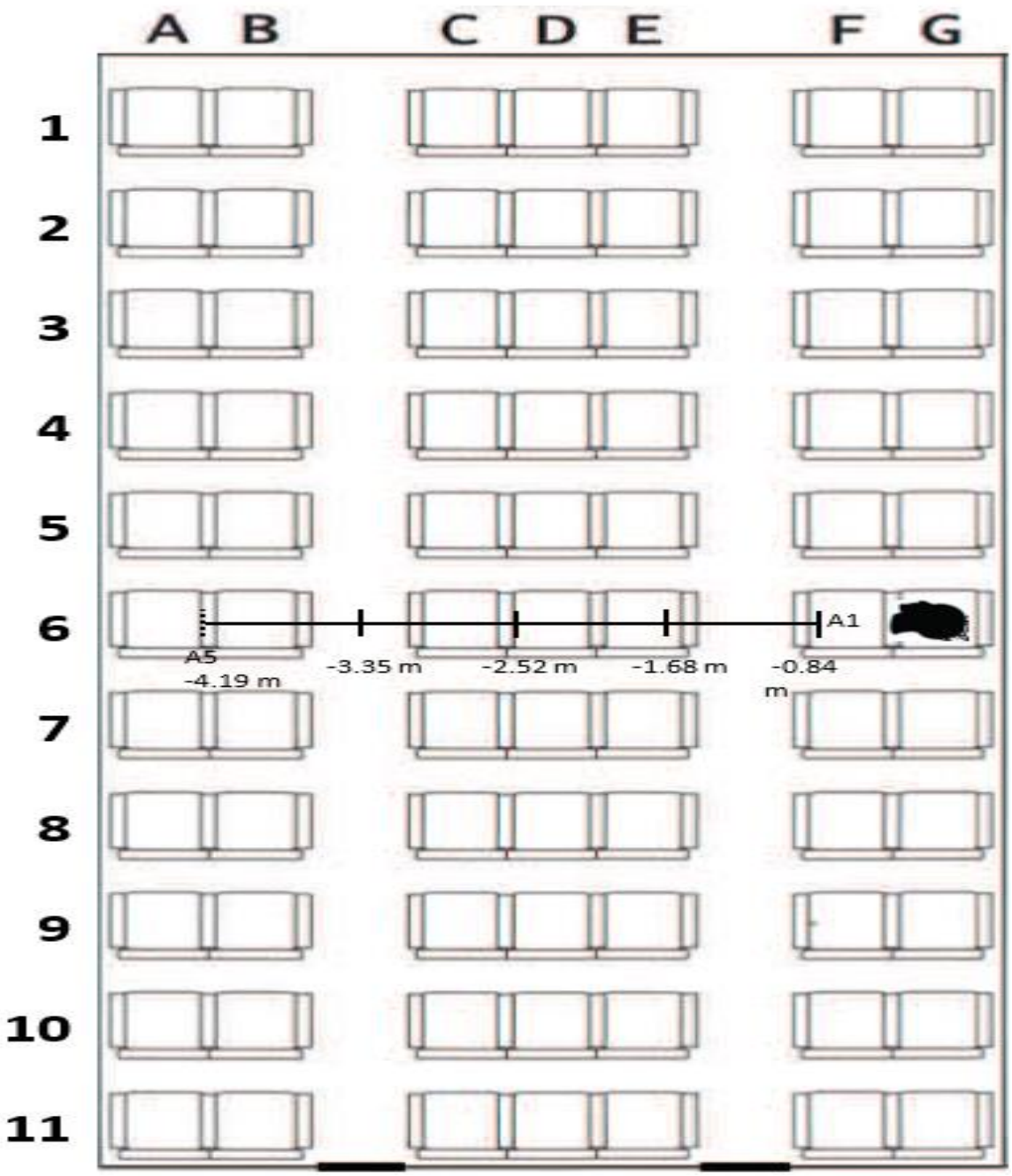

Figure H.30 Test 9 (B-M) ISOPass undeployed source location and sampling tree orientation.

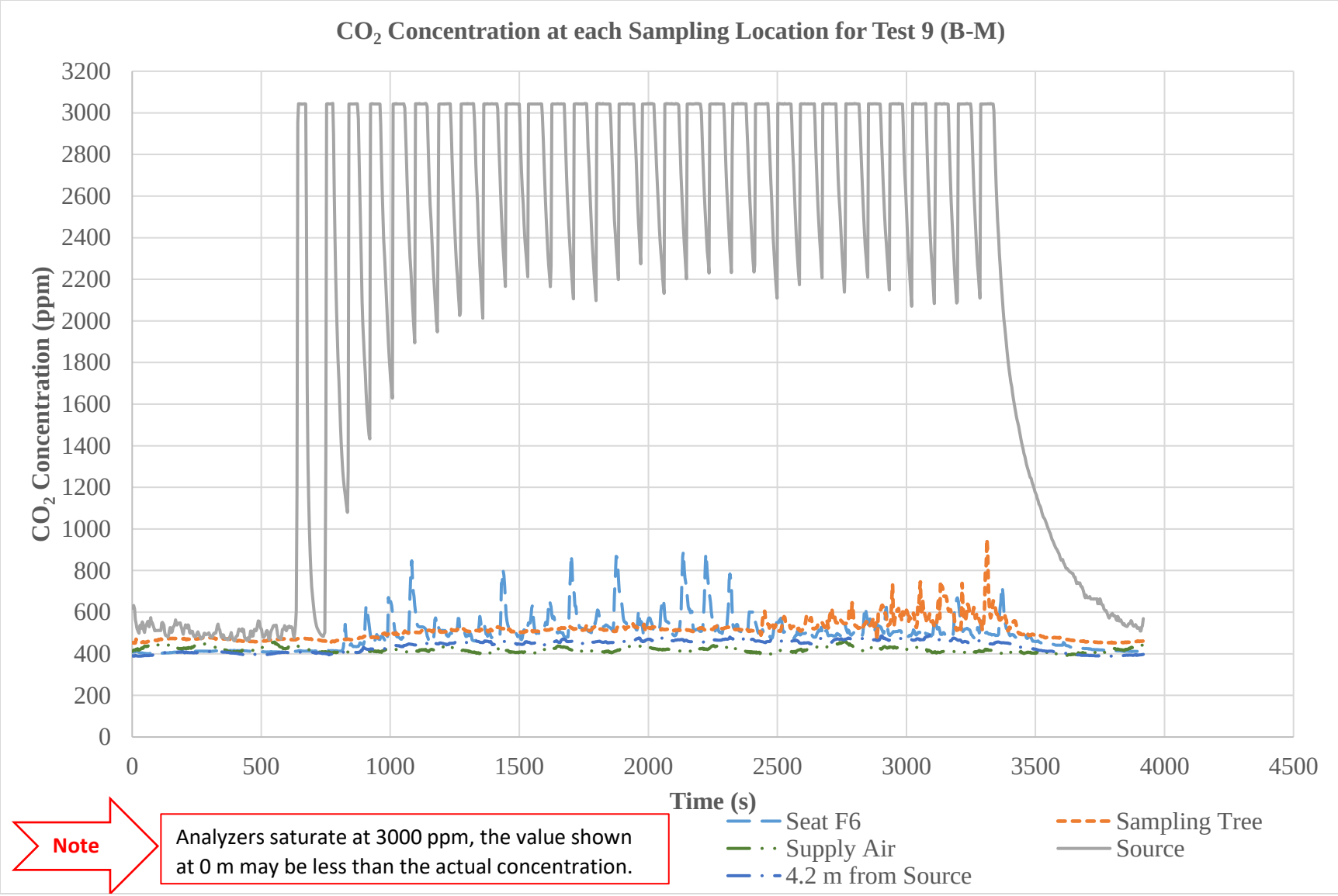

Figure H.31 Ininstantaneous CO_2 concentration at each sampling location for Test 9 (B-M) ISOPass undeployed.

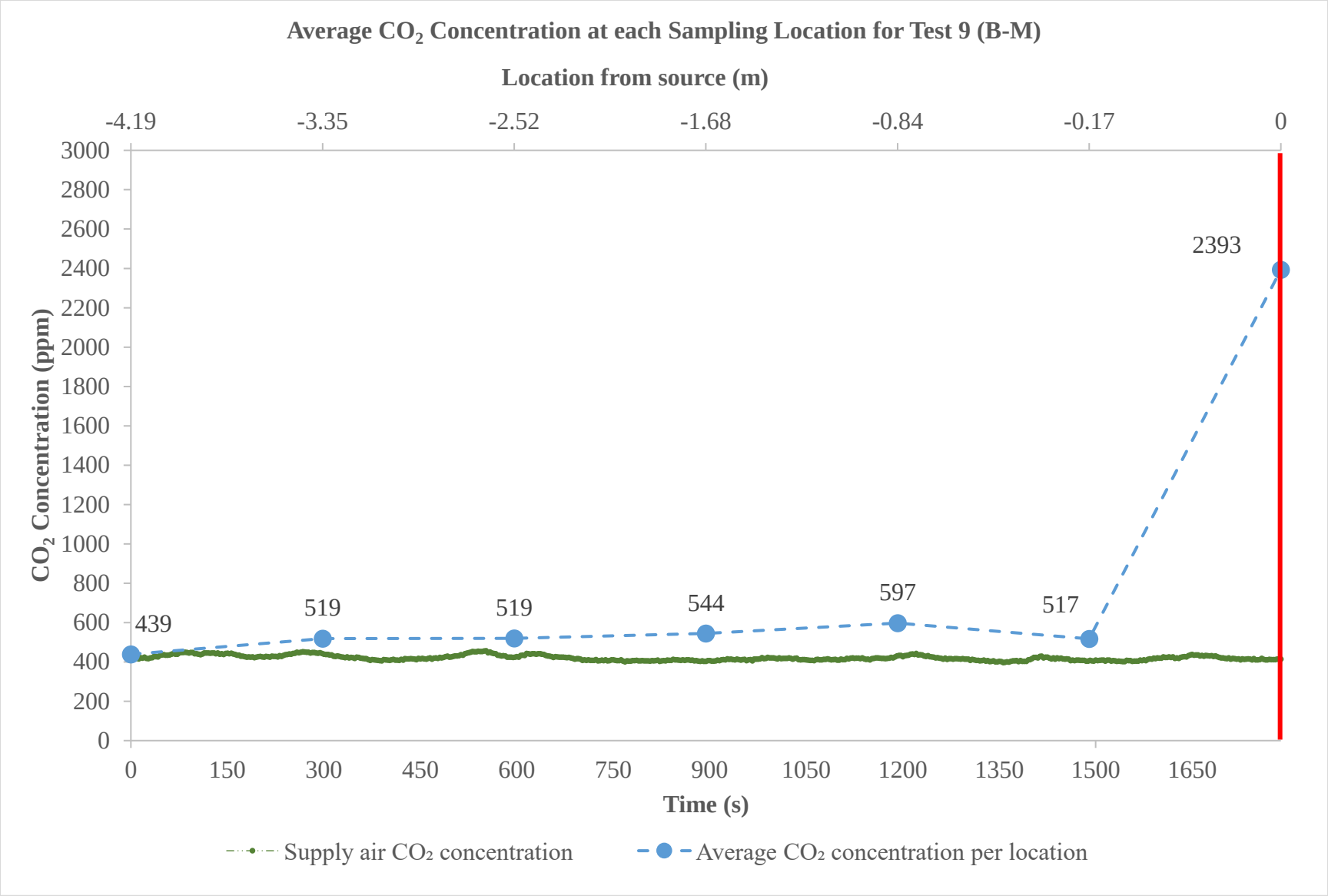

Figure H.32 Average CO_2 concentration at each sampling location for Test 9 (B-M) ISOPass undeployed.

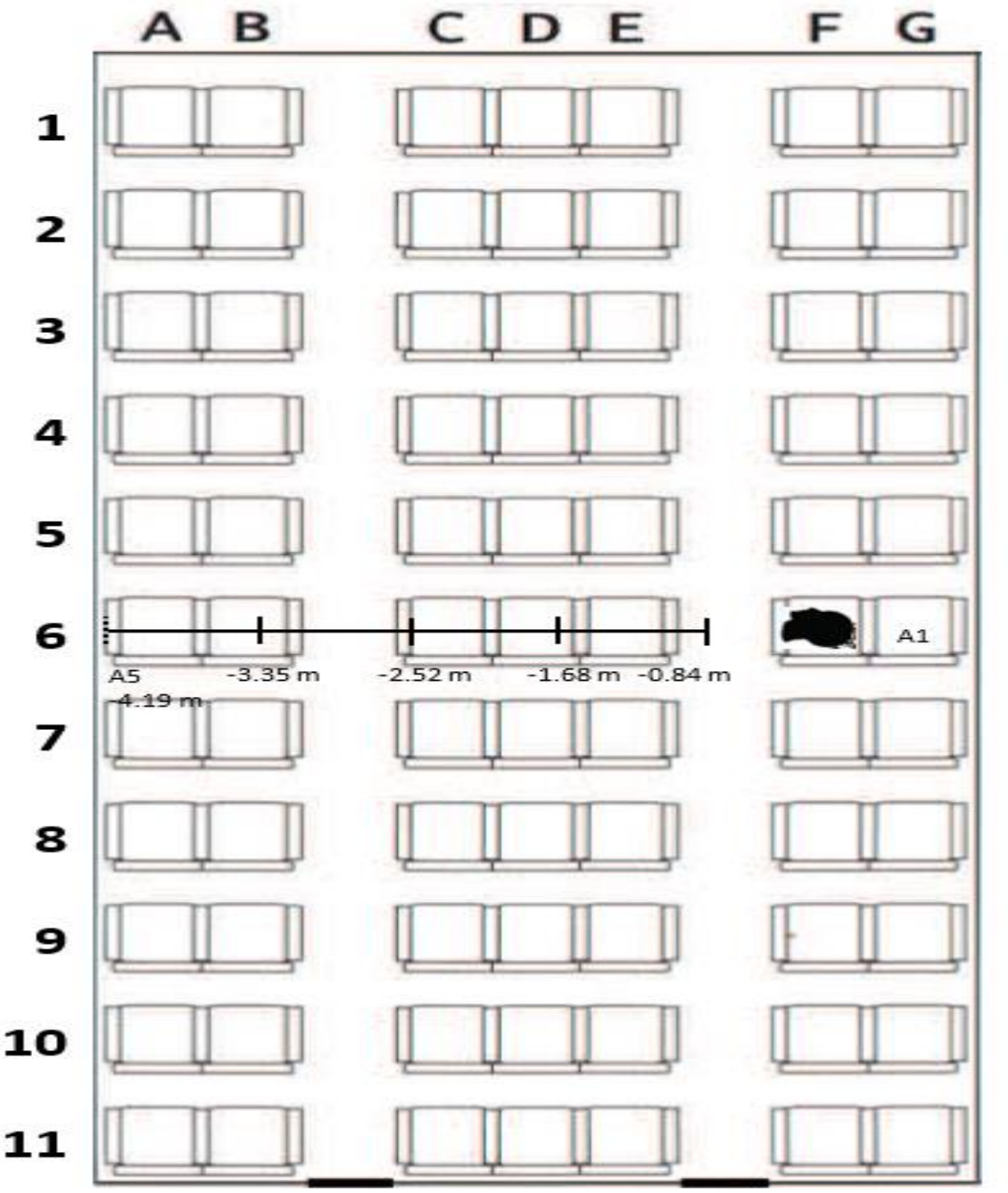

Figure H.33 Test 10 (B-M) ISOPass undeployed source location and sampling tree orientation.

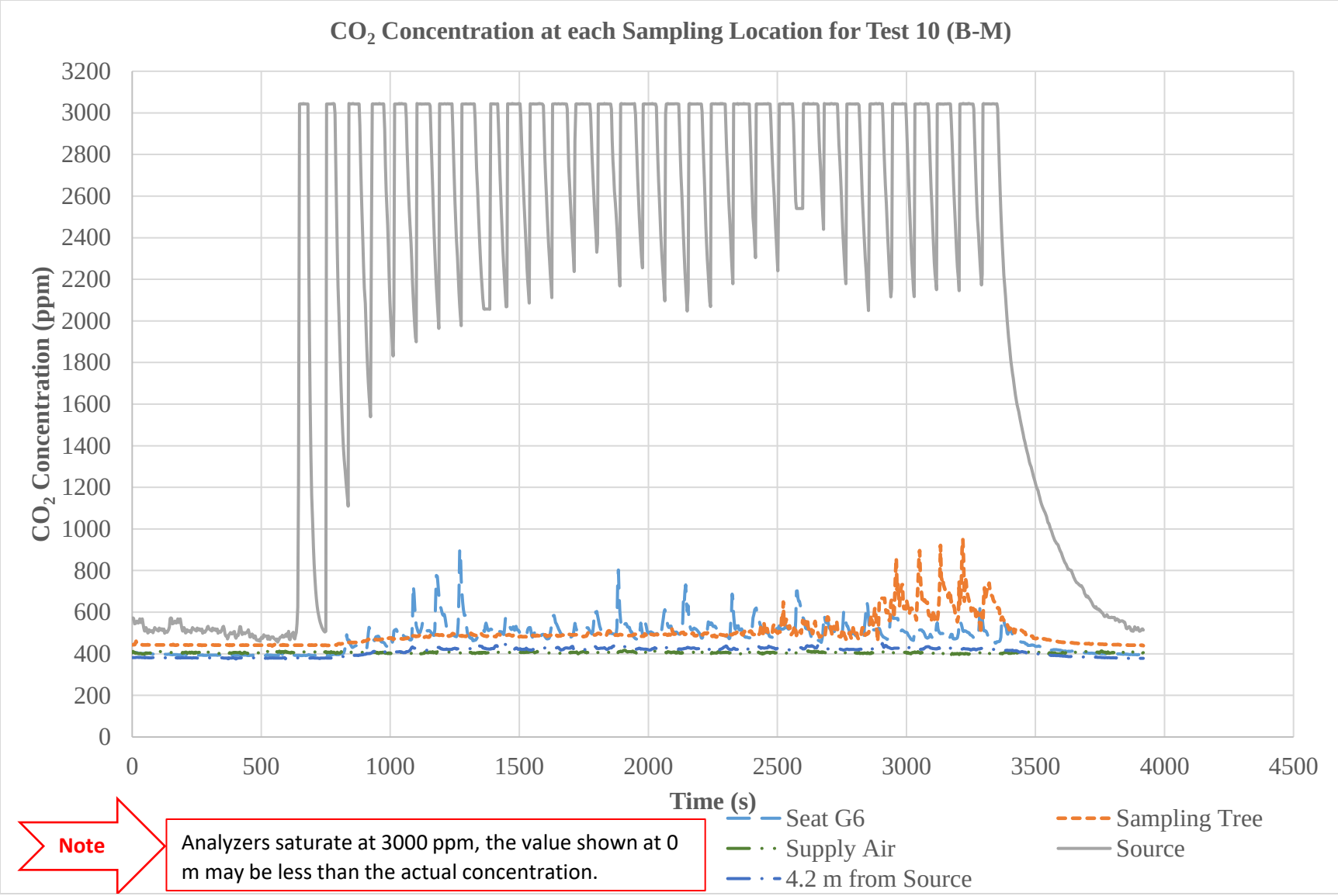

Figure H.34 Ininstantaneous CO_2 concentration at each sampling location for Test 10 (B-M) ISOPass undeployed.

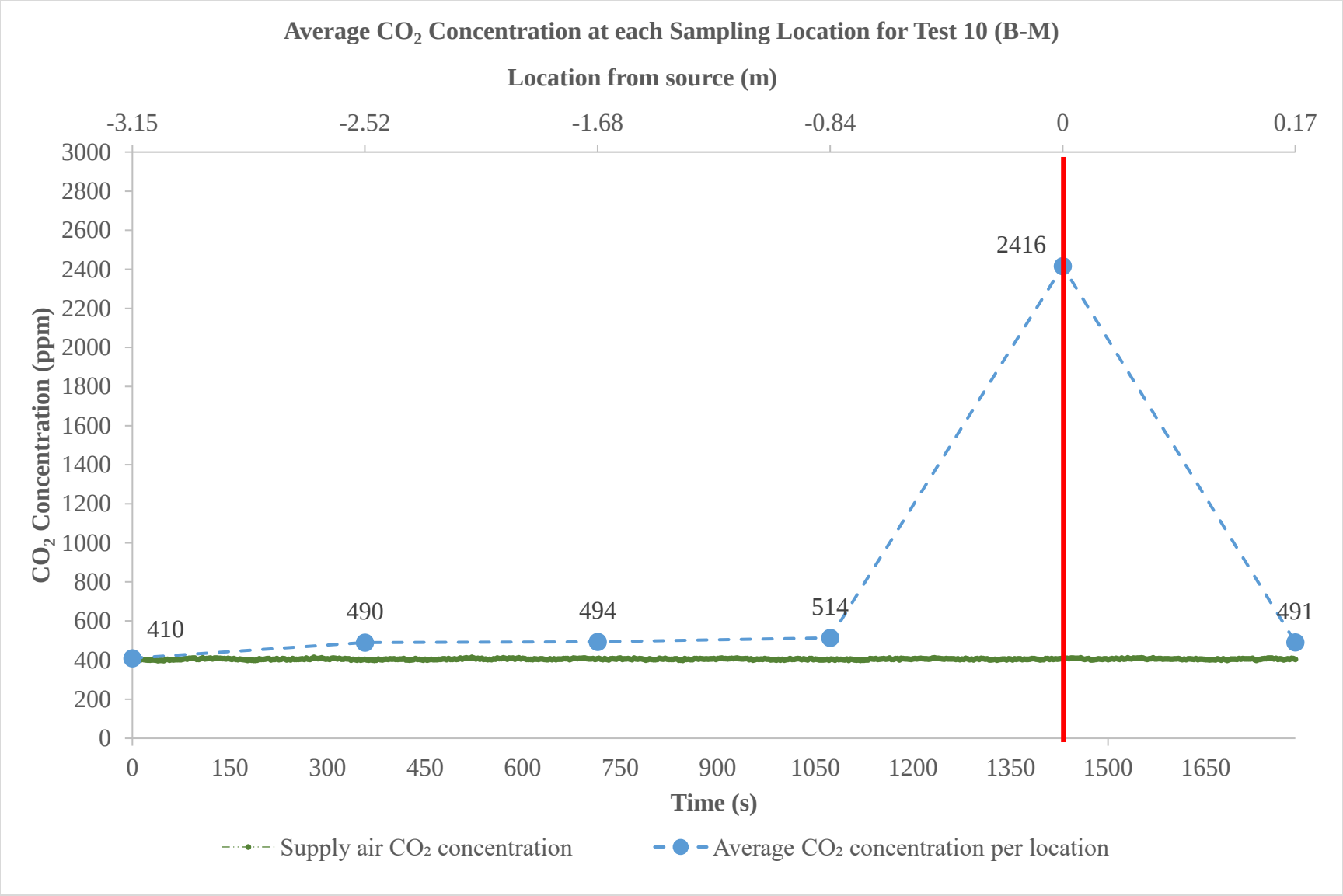

Figure H.35 Average CO_2 concentration at each sampling location for Test 10 (B-M) ISOPass undeployed.

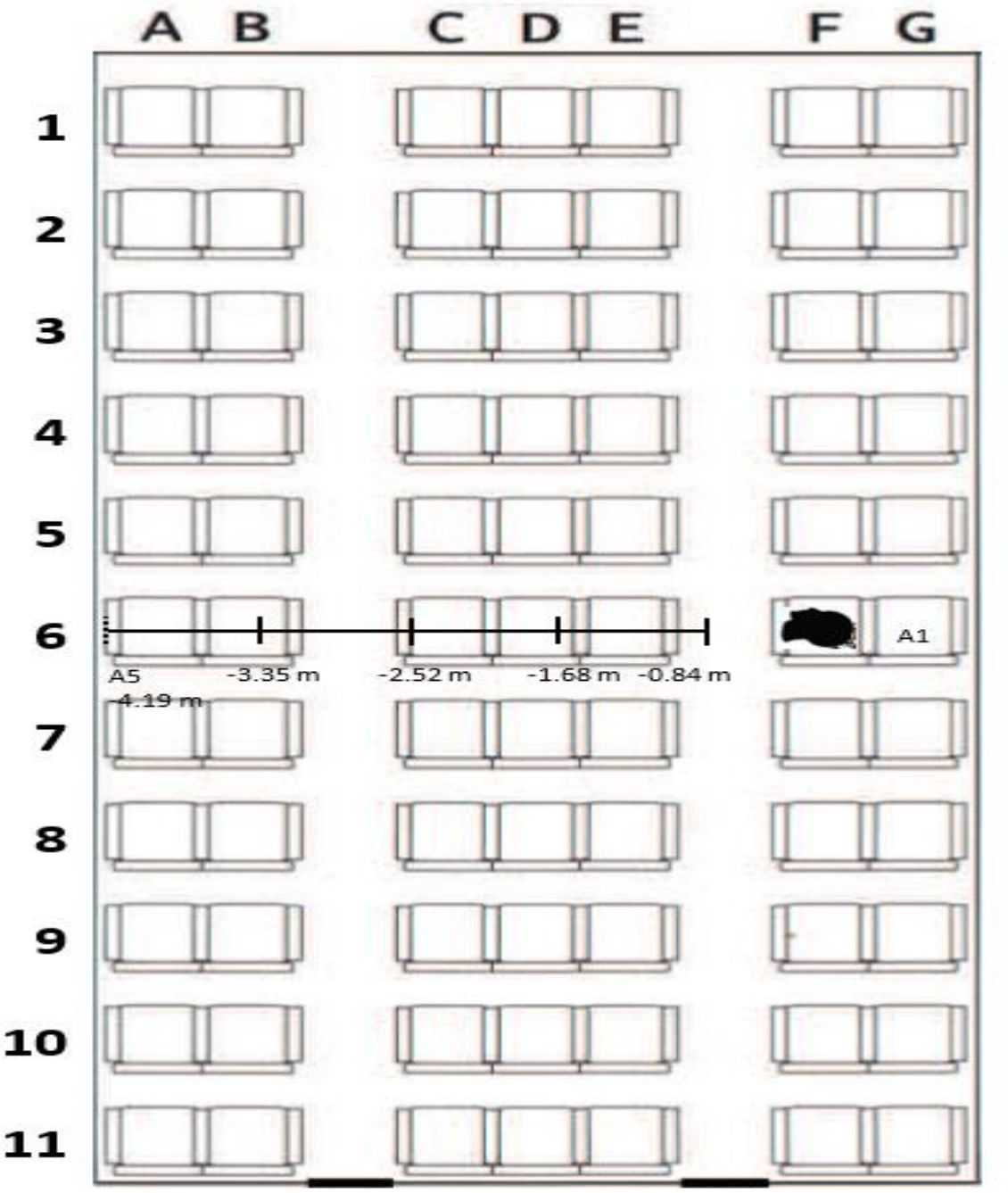

Figure H.36 Test 11 (B-M) ISOPass undeployed source location and sampling tree orientation.

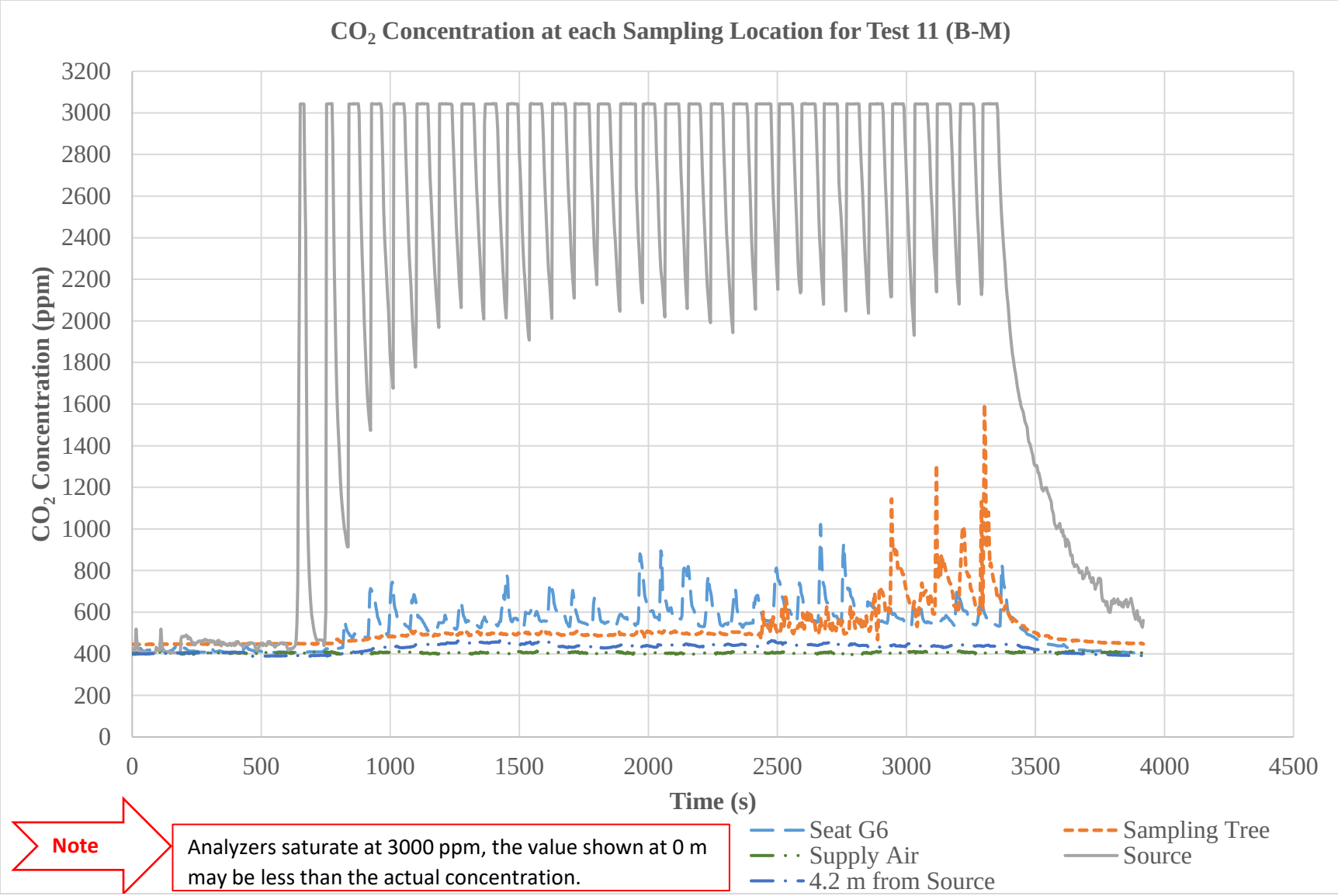

Figure H.37 Ininstantaneous CO_2 concentration at each sampling location for Test 11 (B-M) ISOPass undeployed.

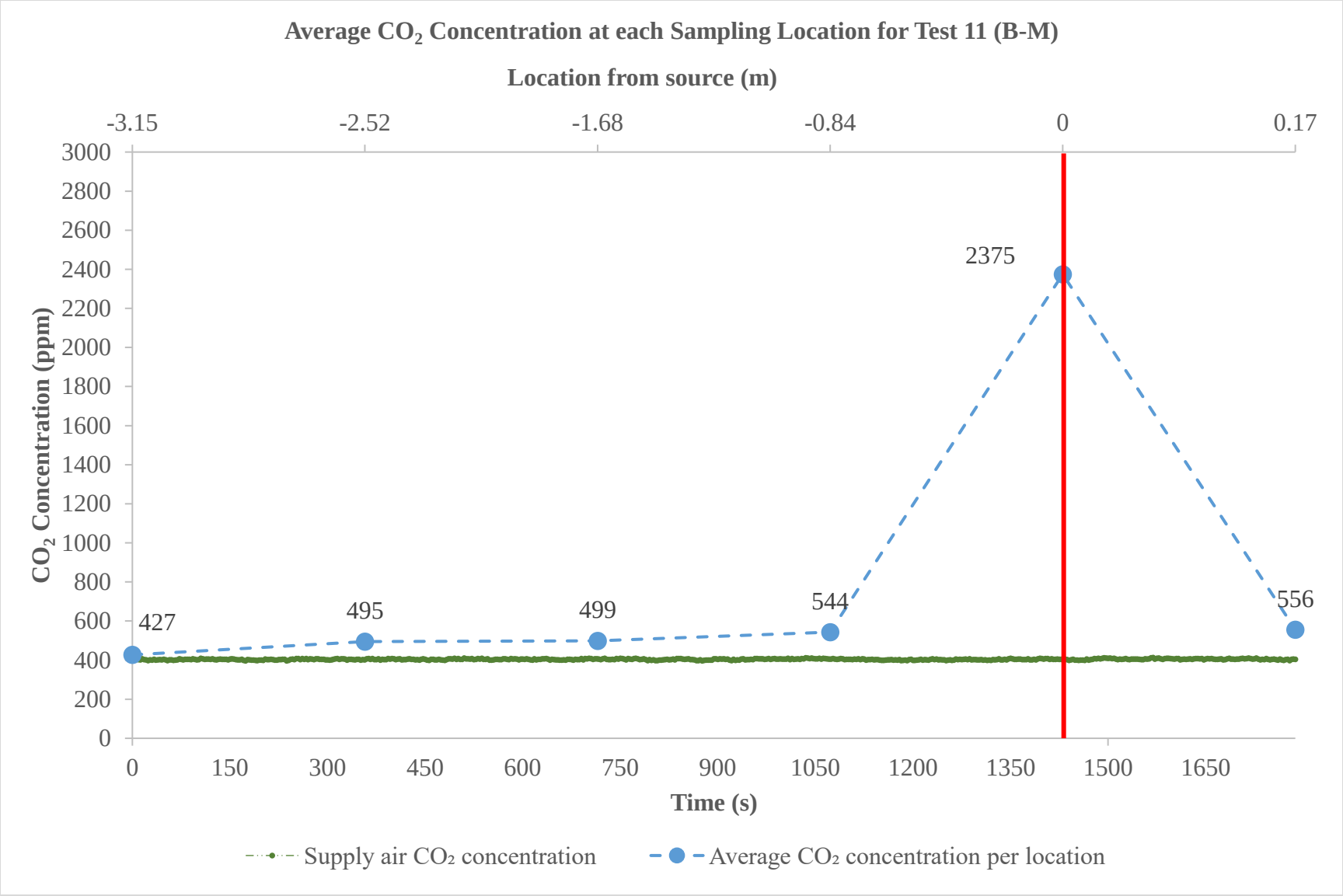

Figure H.38 Average CO_2 concentration at each sampling location for Test 11 (B-M) ISOPass undeployed.

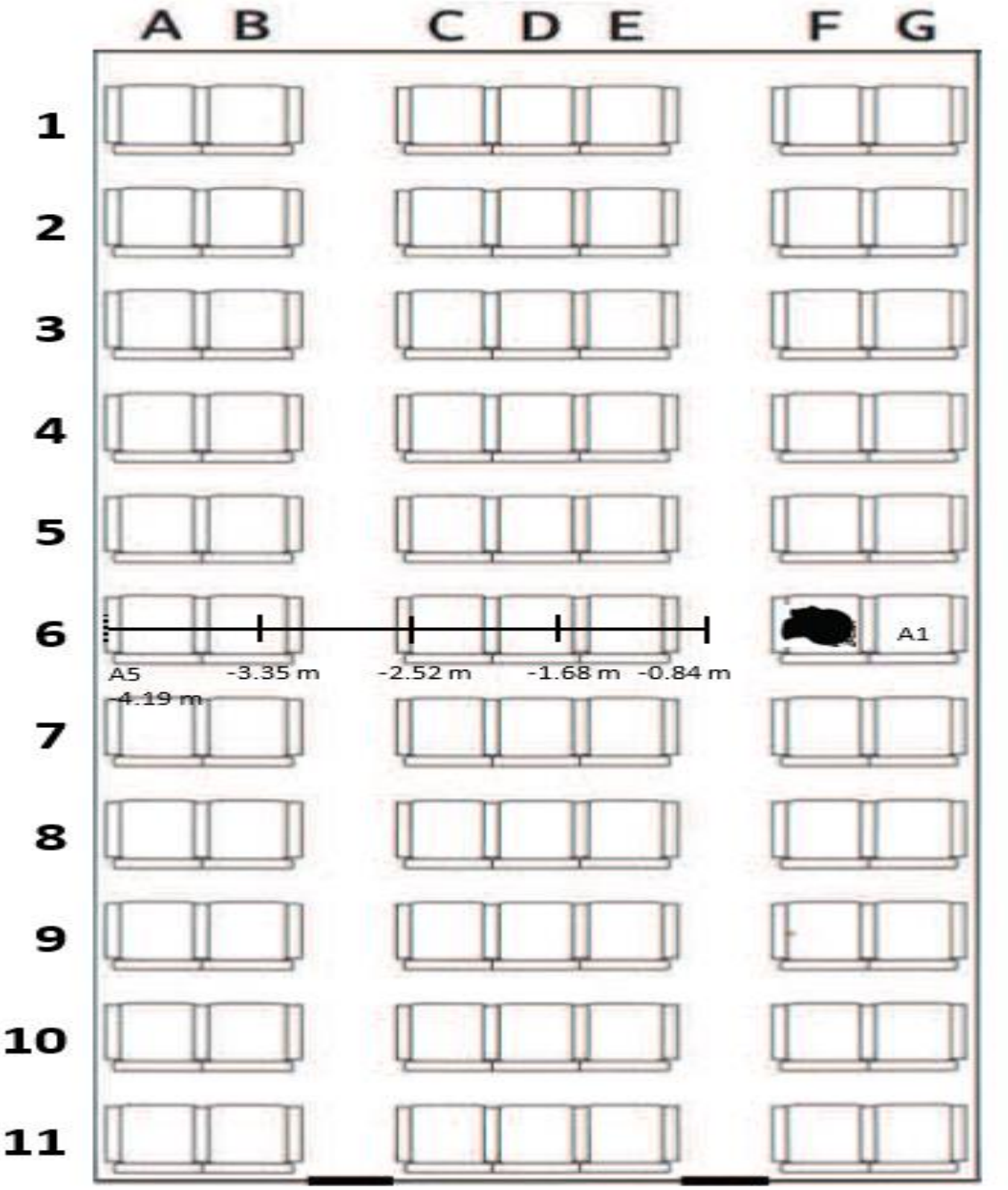

Figure H.39 Test 12 (B-M) ISOPass undeployed source location and sampling tree orientation.

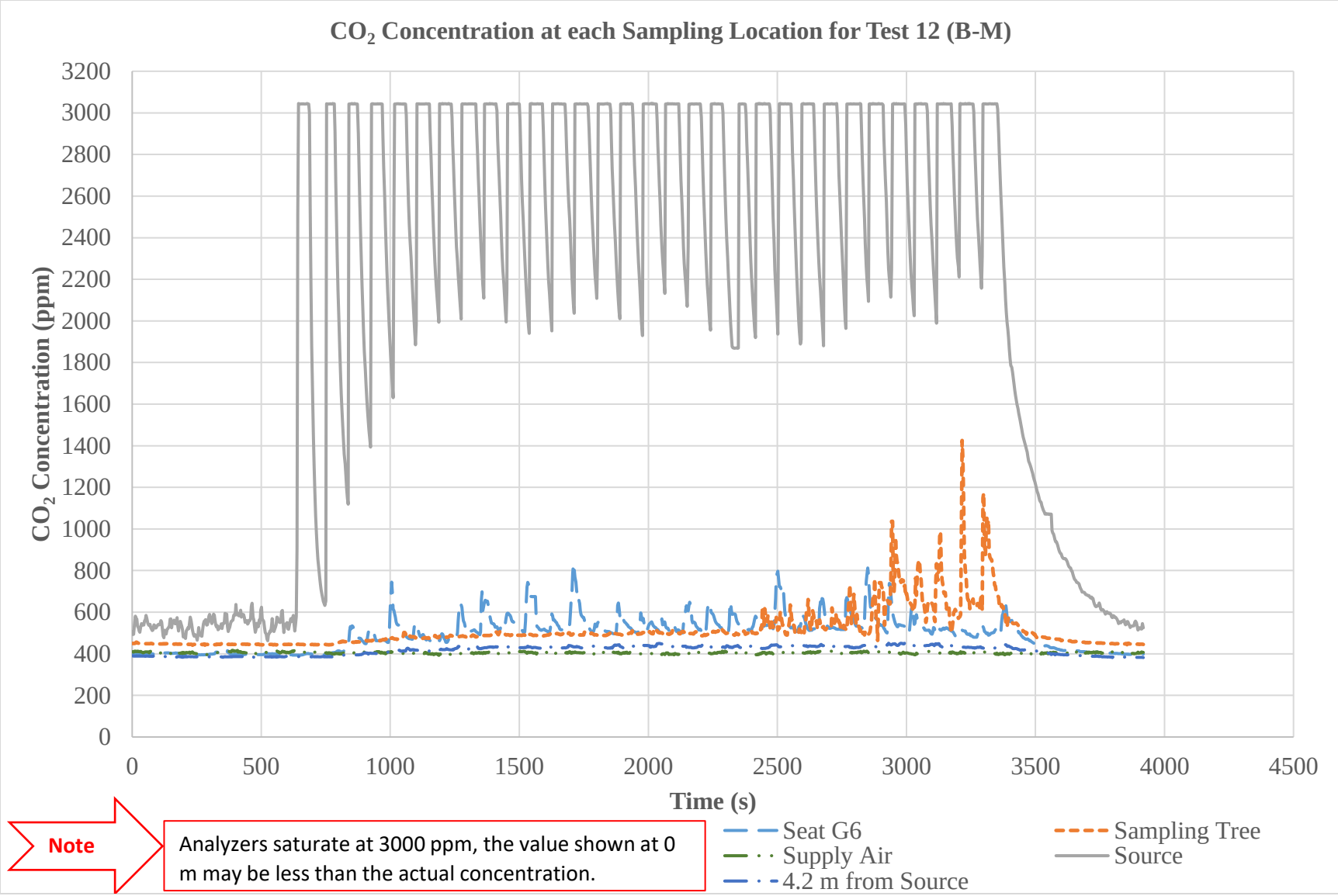

Figure H.40 Ininstantaneous CO_2 concentration at each sampling location for Test 12 (B-M) ISOPass undeployed.

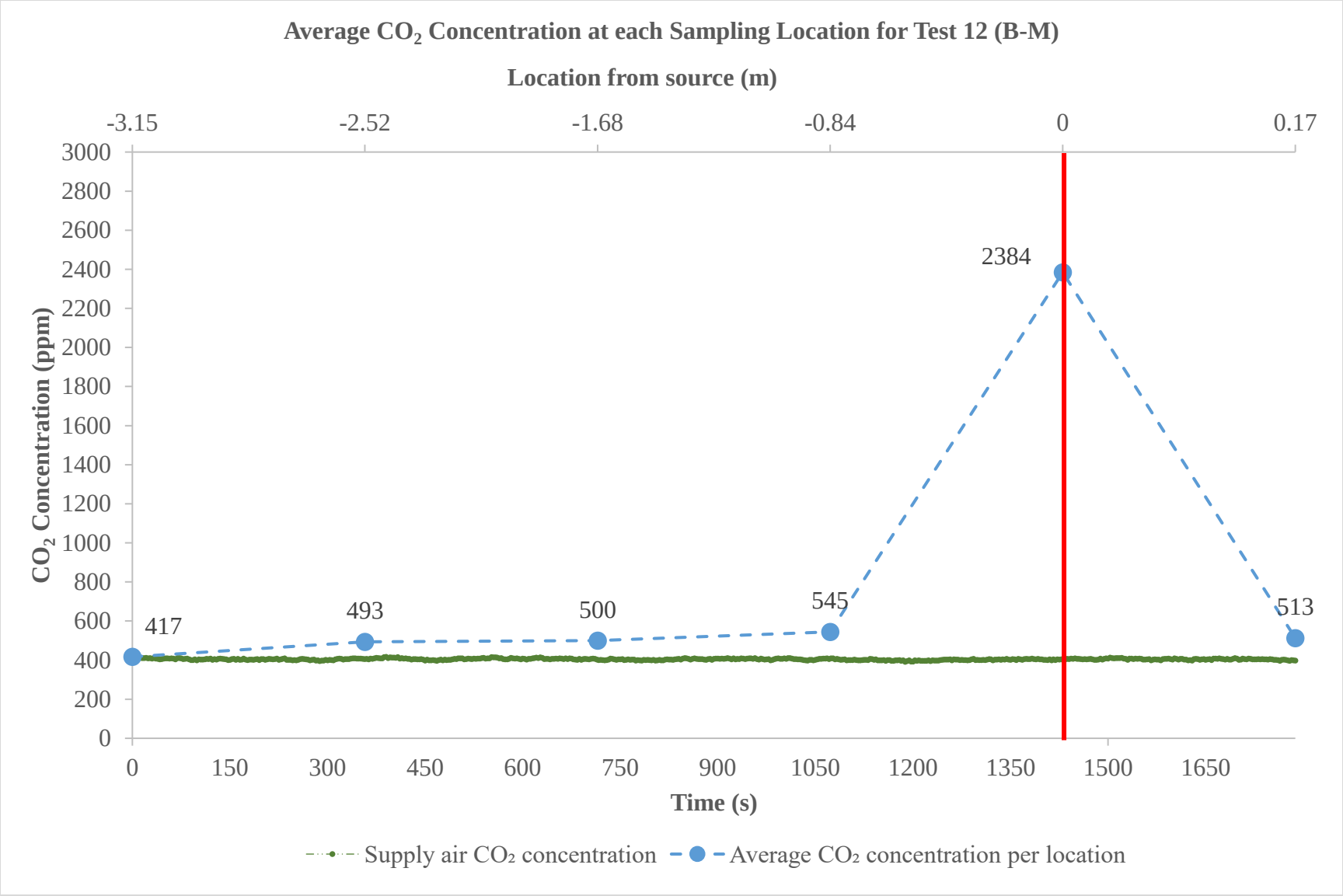

Figure H.41 Average CO_2 concentration at each sampling location for Test 12 (B-M) ISOPass undeployed.

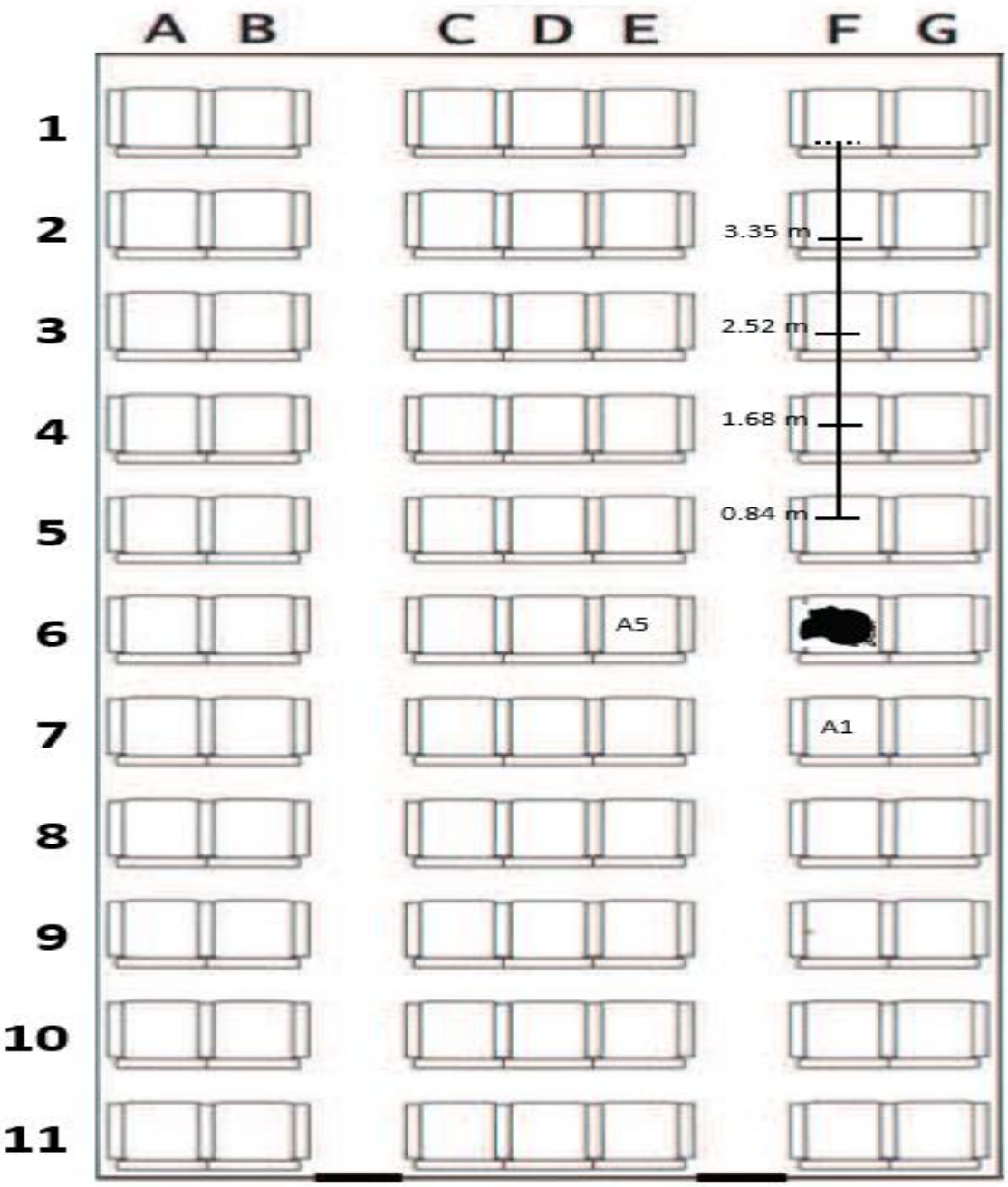

Figure H.42 Test 31 (B-M) ISOPass undeployed source location and sampling tree orientation.

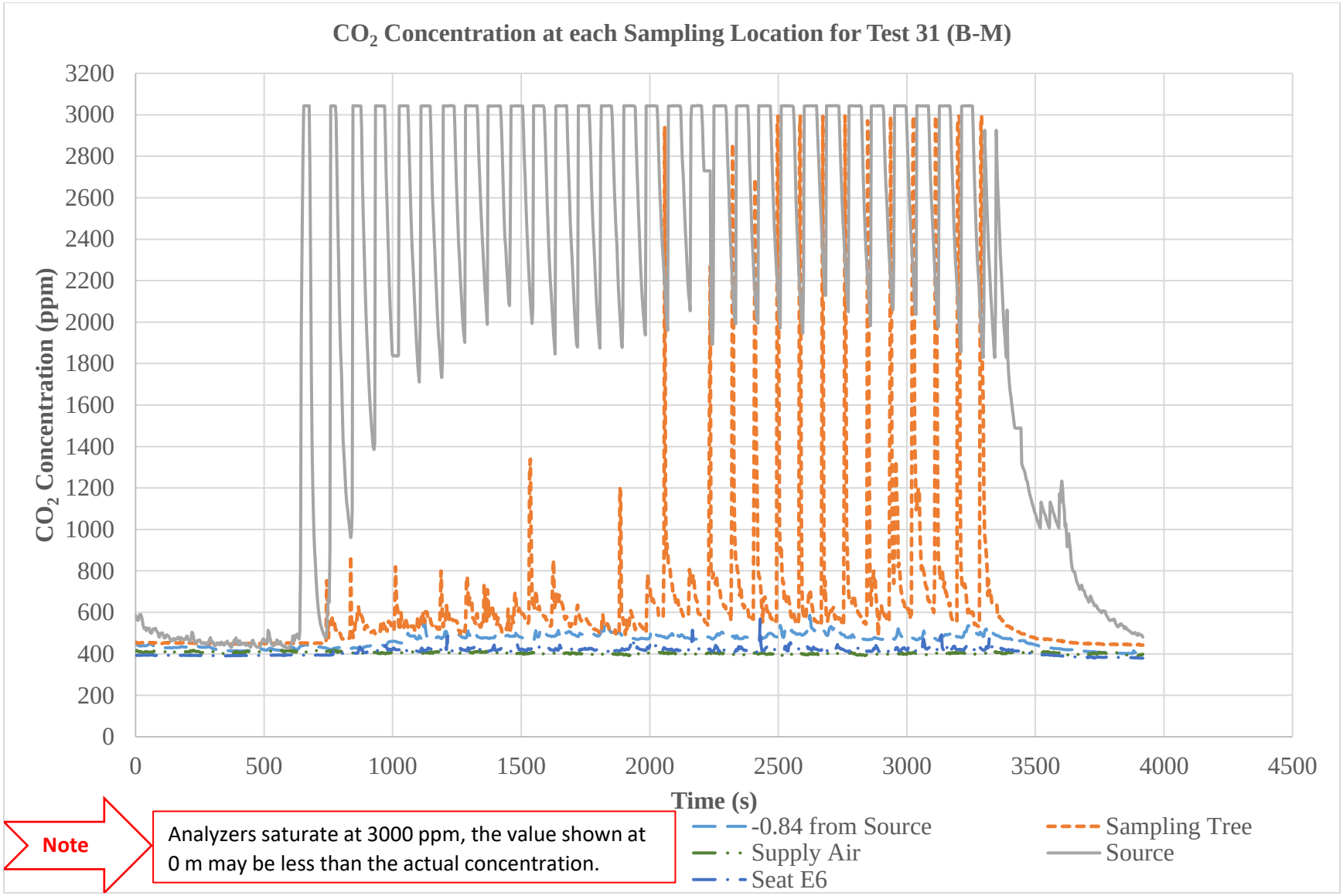

Figure H.43 Ininstantaneous CO_2 concentration at each sampling location for Test 31 (B-M) ISOPass undeployed.

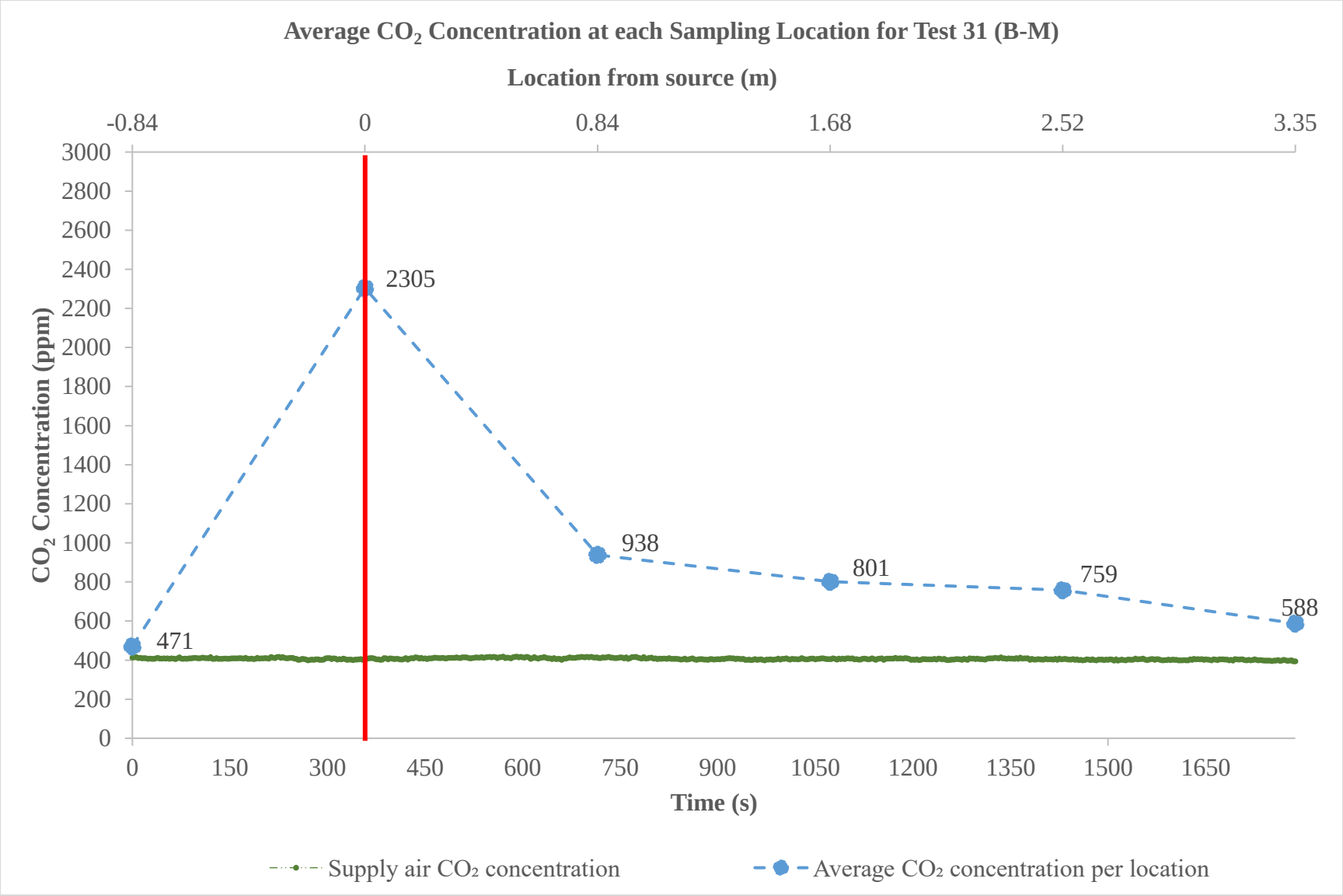

Figure H.44 Average CO_2 concentration at each sampling location for Test 31 (B-M) ISOPass undeployed.

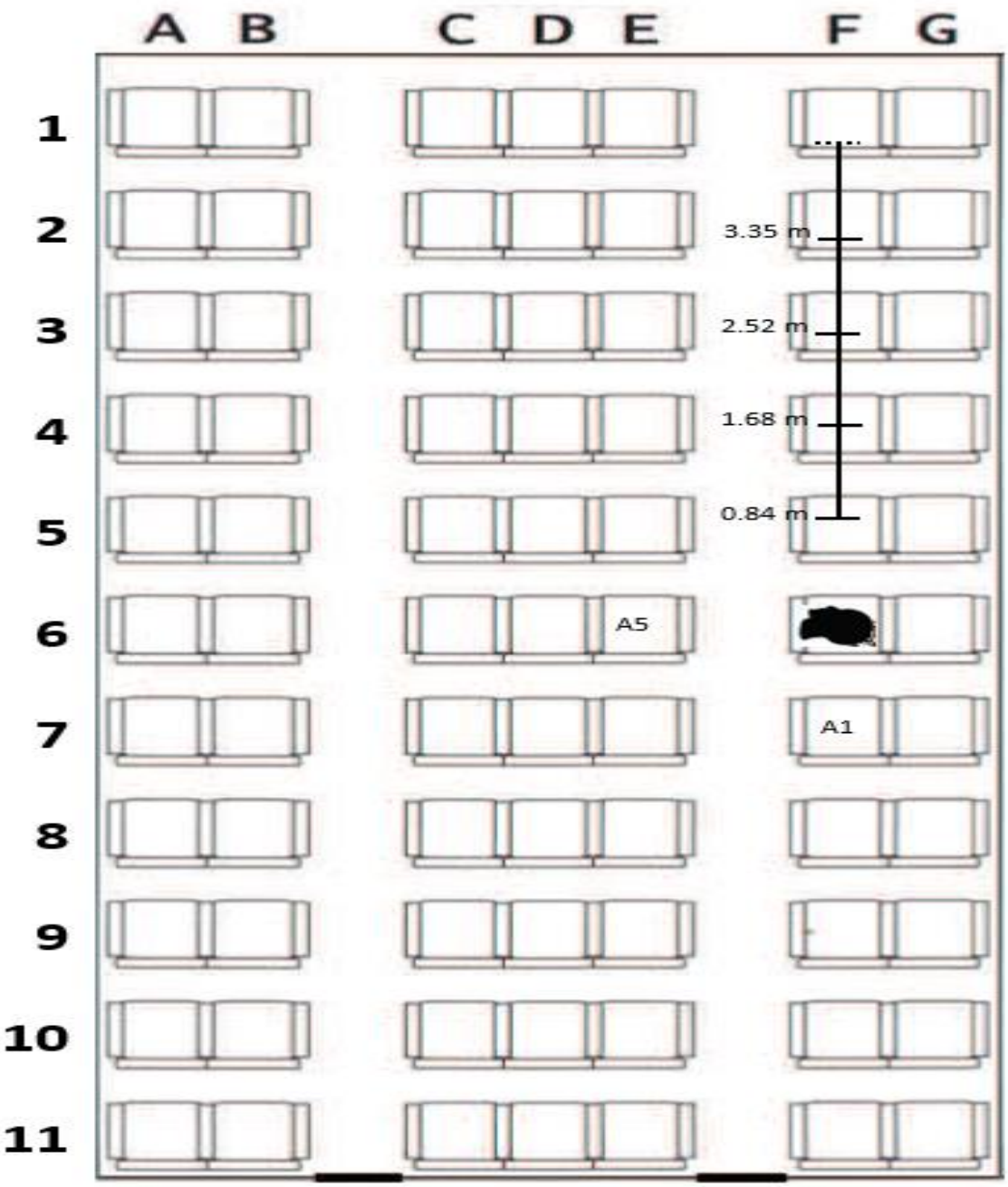

Figure H.45 Test 32 (B-M) ISOPass undeployed source location and sampling tree orientation.

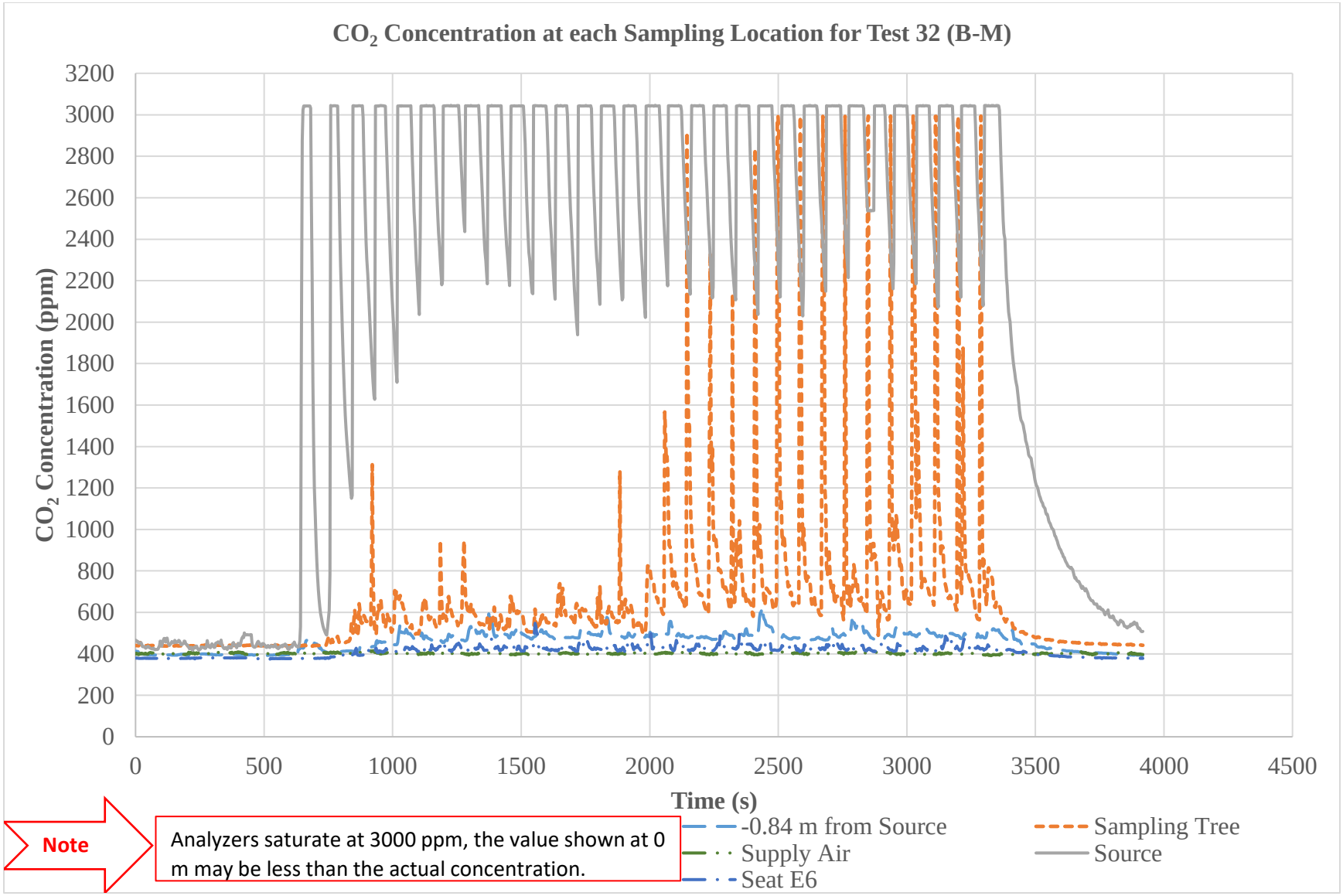

Figure H.46 Ininstantaneous CO_2 concentration at each sampling location for Test 32 (B-M) ISOPass undeployed.

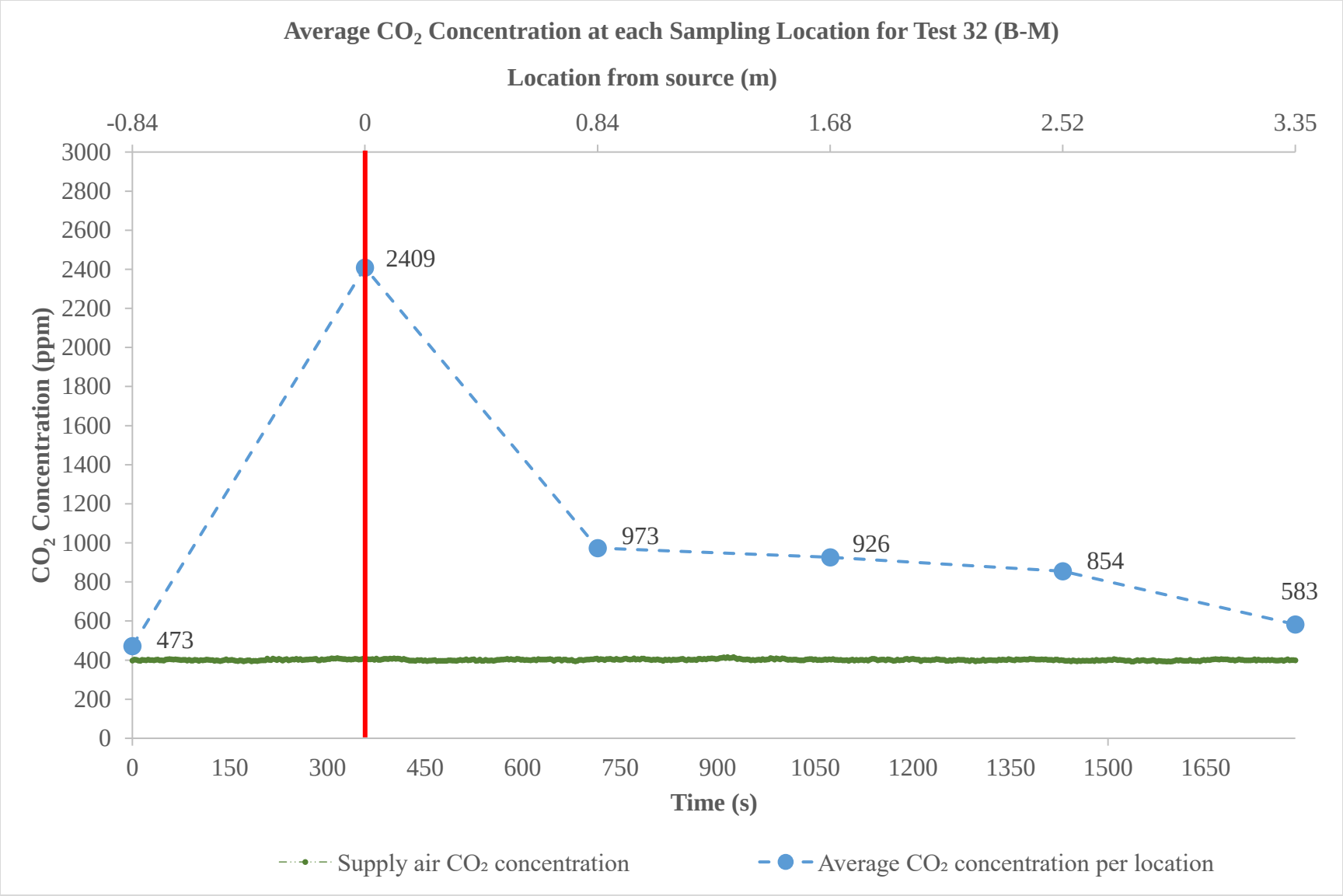

Figure H.47 Average CO_2 concentration at each sampling location for Test 32 (B-M) ISOPass undeployed.

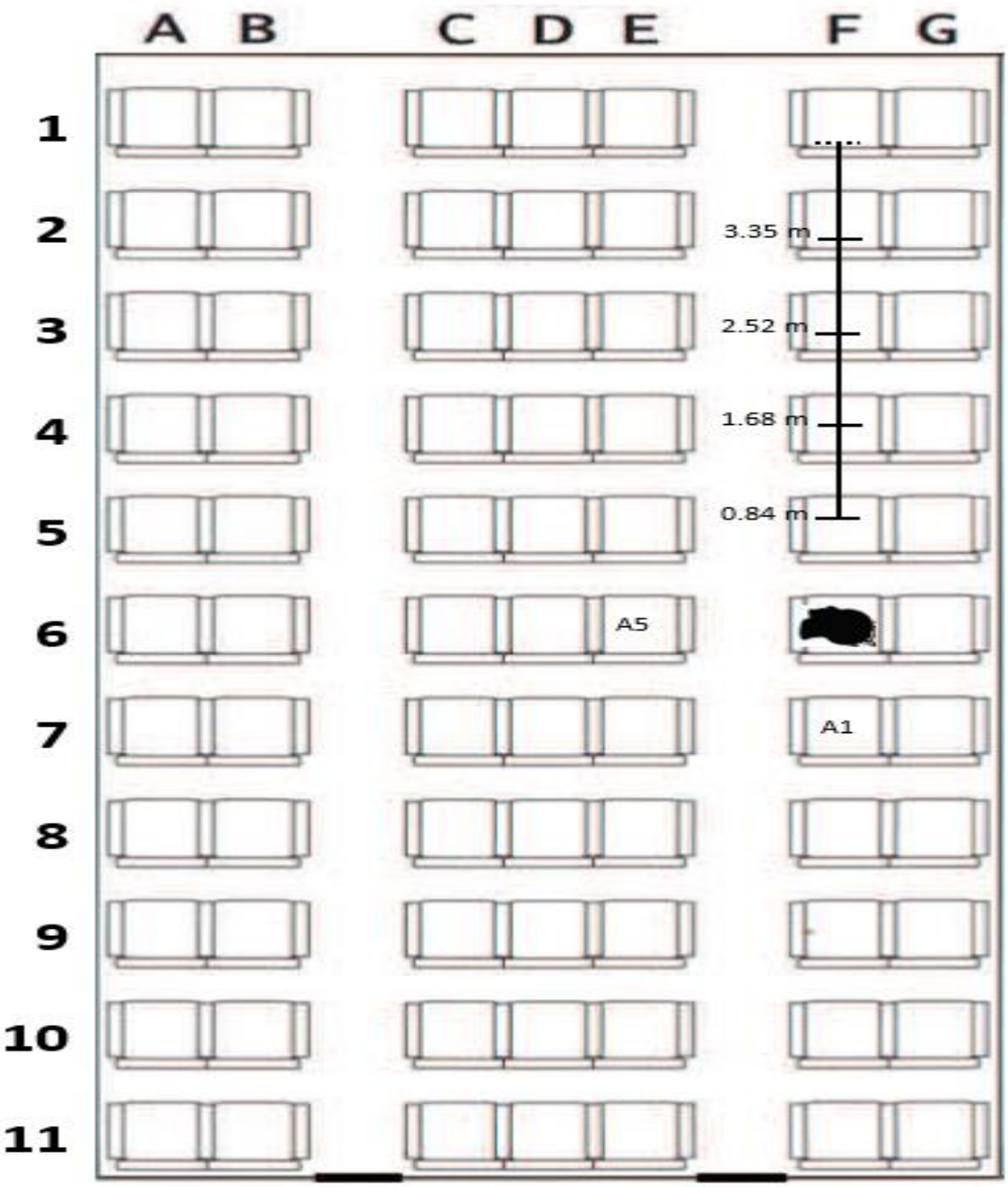

Figure H.48 Test 33 (B-M) ISOPass undeployed source location and sampling tree orientation.

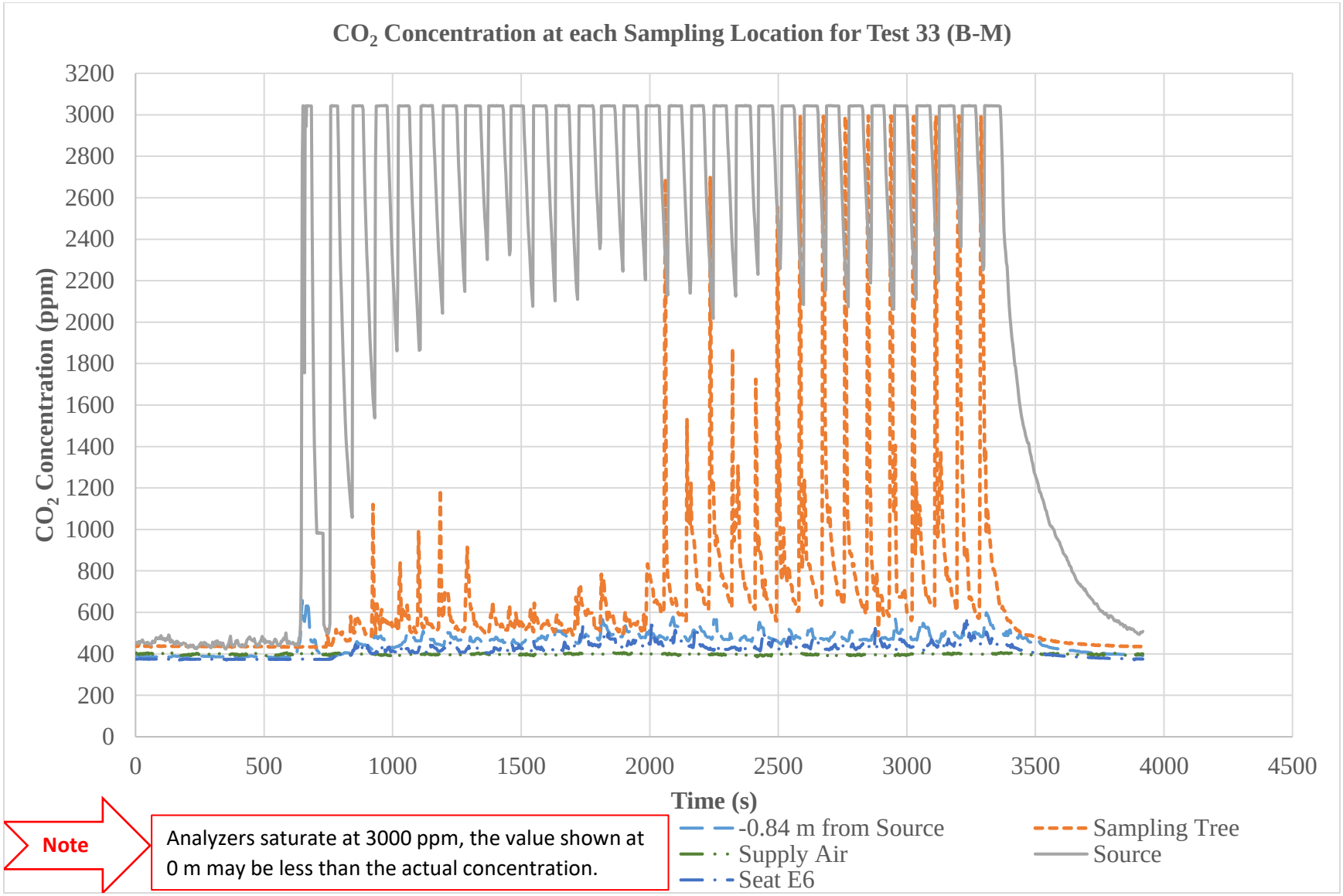

Figure H.49 Ininstantaneous CO_2 concentration at each sampling location for Test 33 (B-M) ISOPass undeployed.

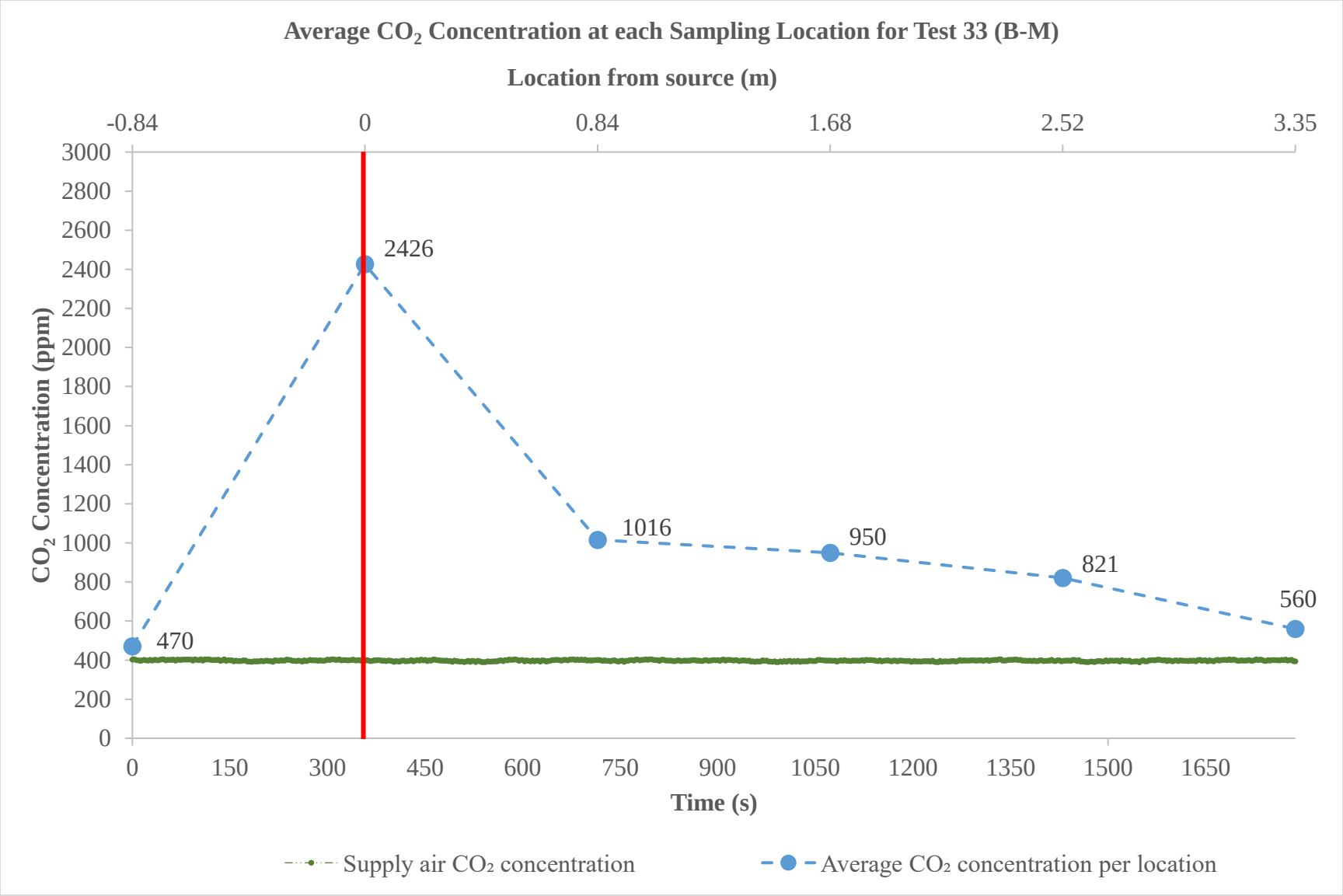

Figure H.50 Average CO_2 concentration at each sampling location for Test 33 (B-M) ISOPass undeployed.

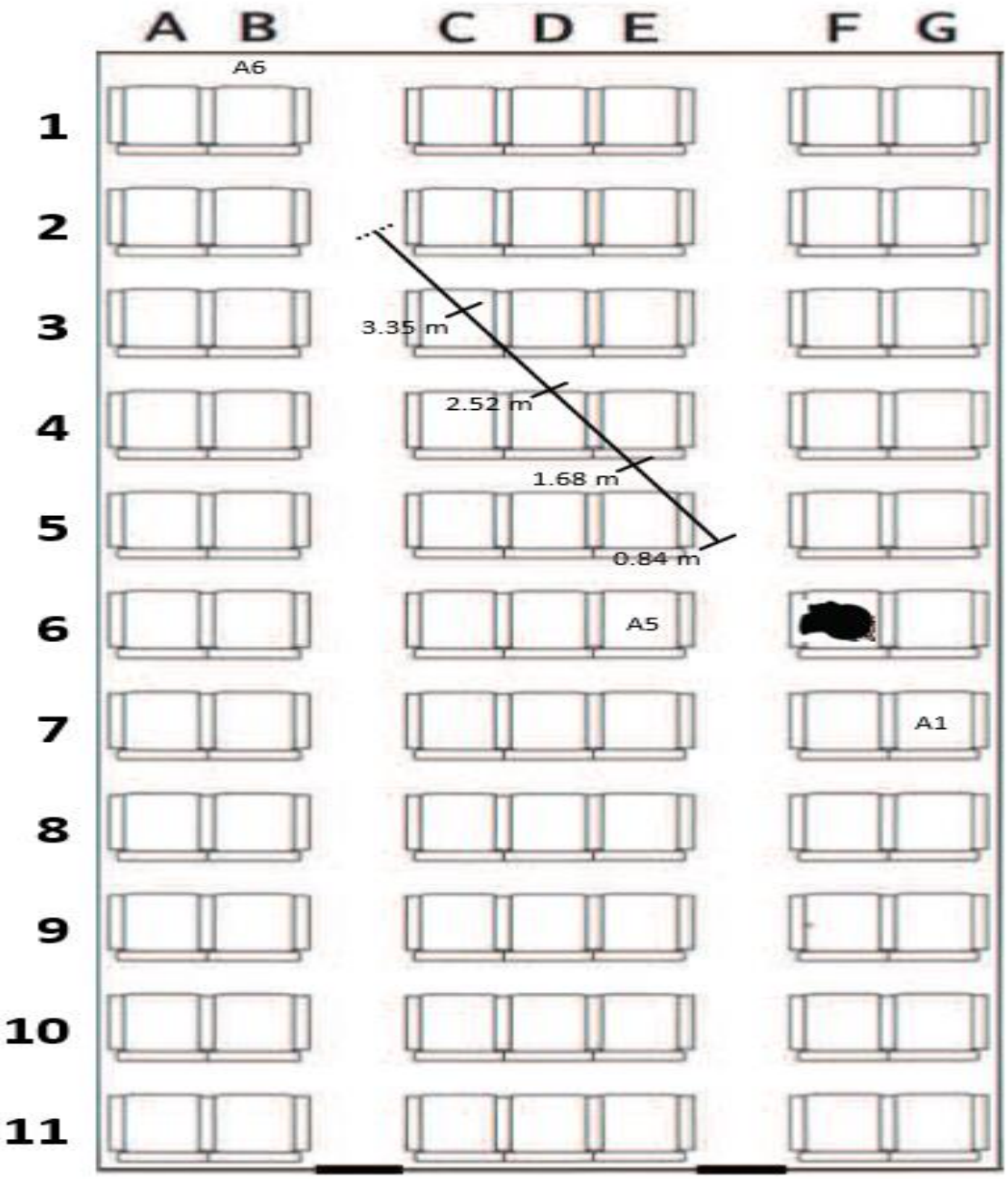

Figure H.51 Test 34 (B-M) ISOPass undeployed source location and sampling tree orientation.

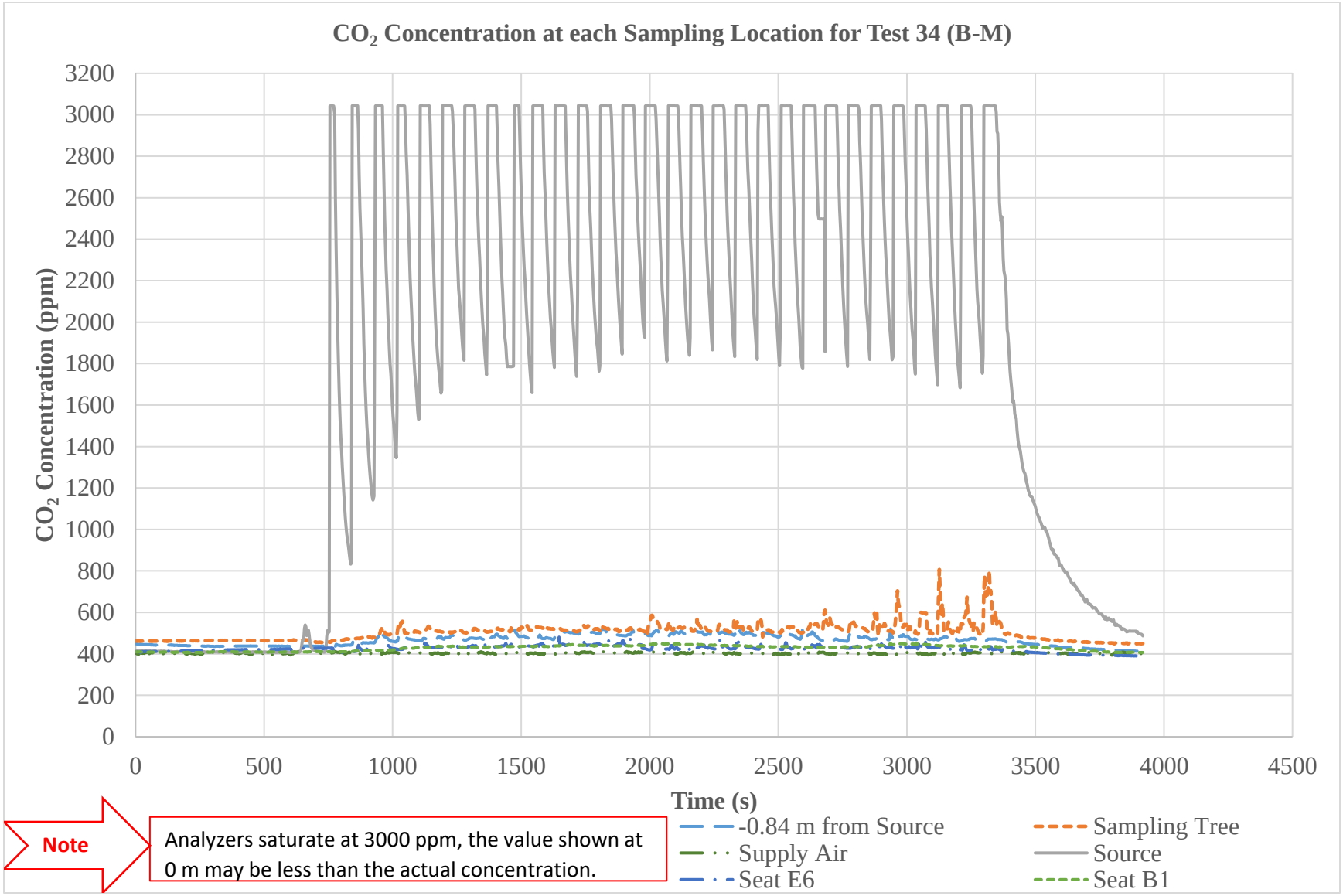

Figure H.52 Ininstantaneous CO_2 concentration at each sampling location for Test 34 (B-M) ISOPass undeployed.

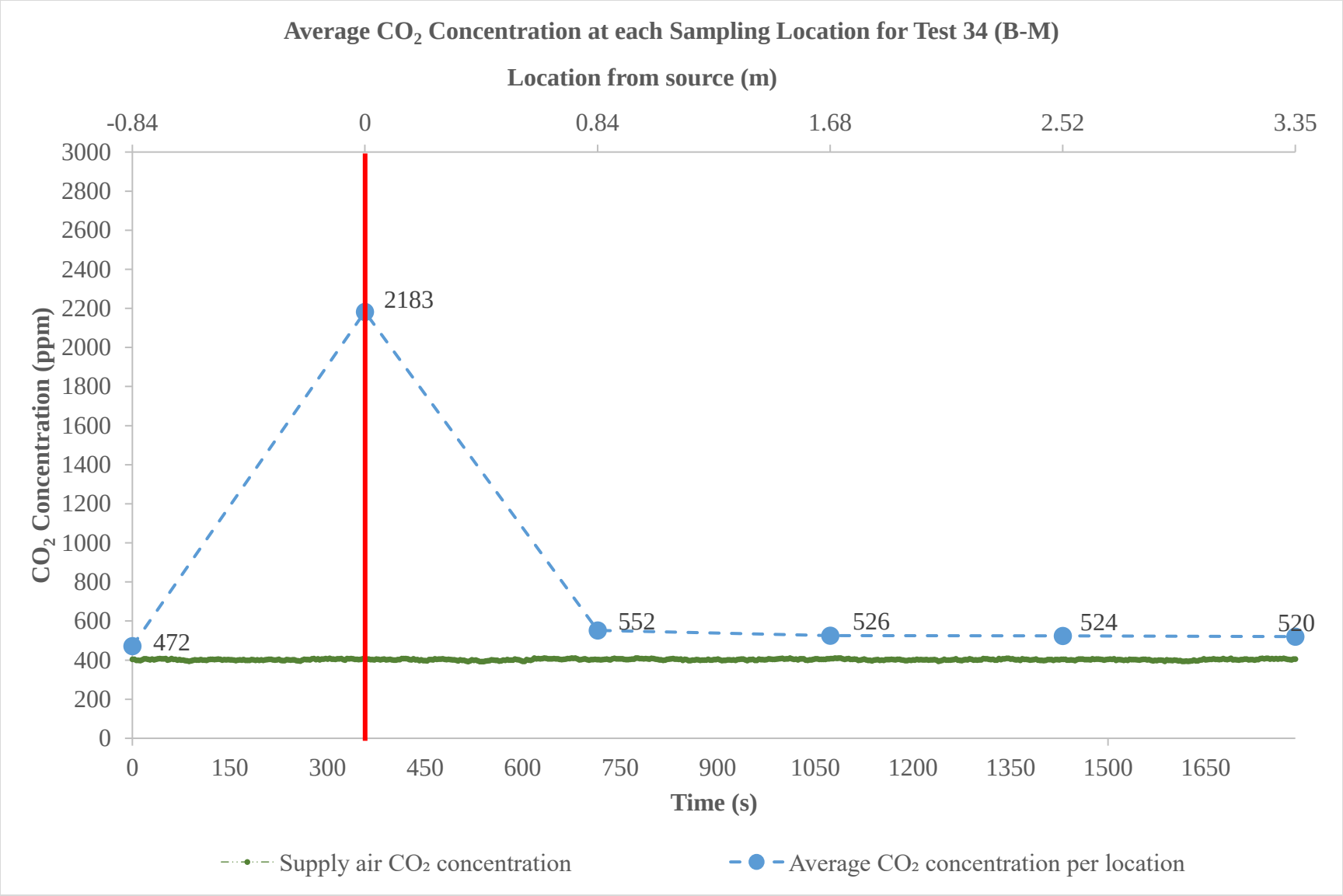

Figure H.53 Average CO_2 concentration at each sampling location for Test 34 (B-M) ISOPass undeployed.

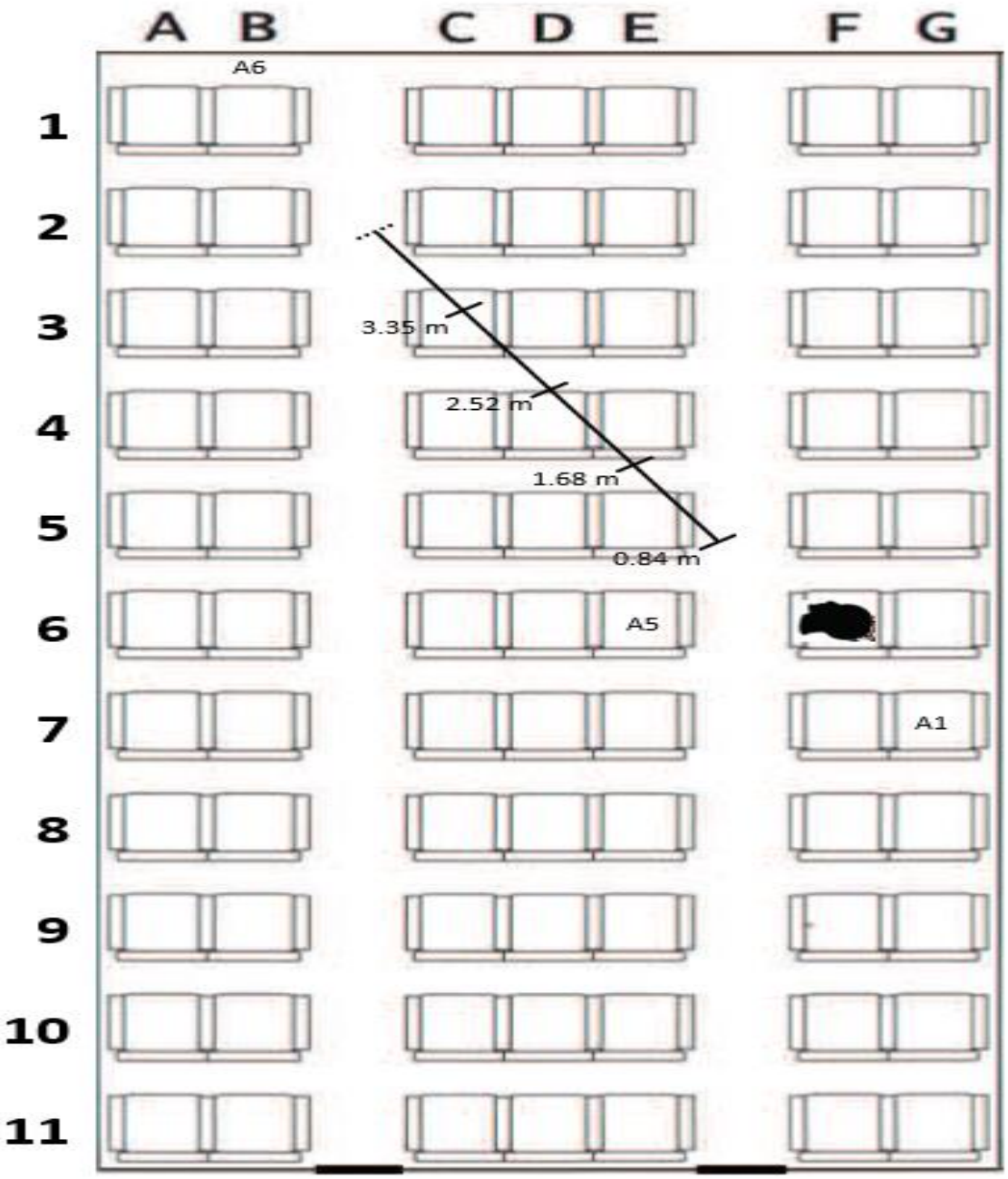

Figure H.54 Test 35 (B-M) ISOPass undeployed source location and sampling tree orientation.

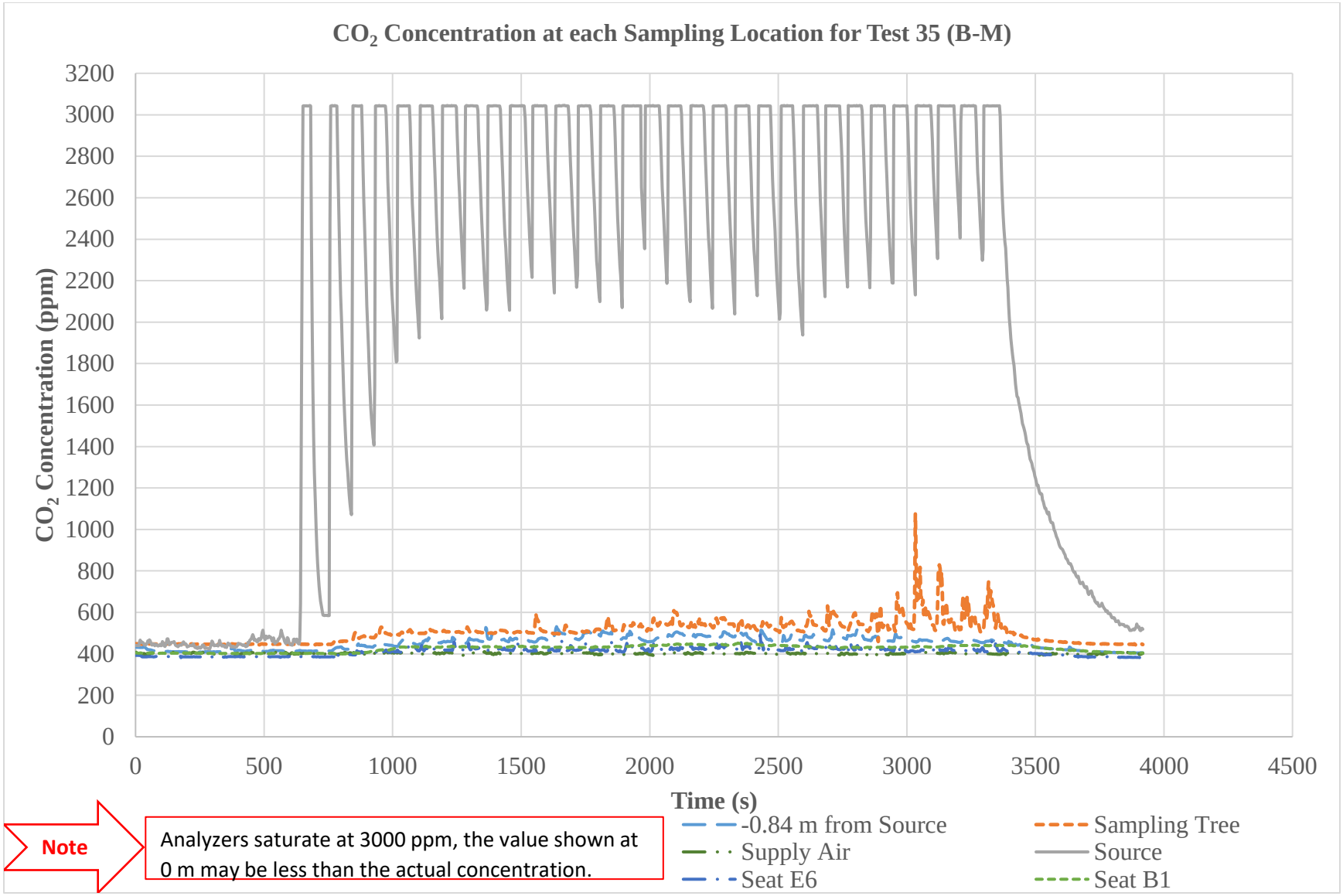

Figure H.55 Ininstantaneous CO_2 concentration at each sampling location for Test 35 (B-M) ISOPass undeployed.

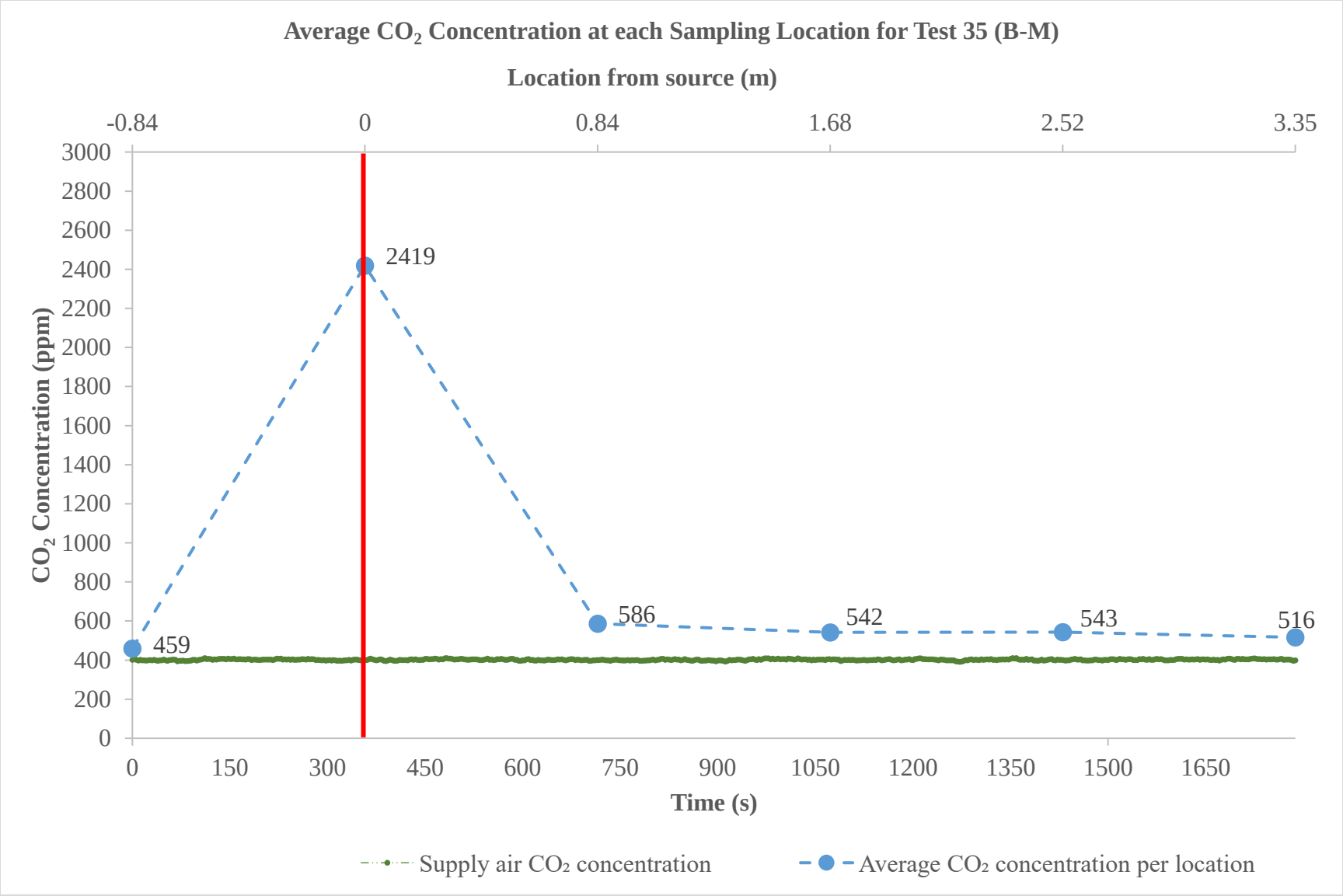

Figure H.56 Average CO_2 concentration at each sampling location for Test 35 (B-M) ISOPass undeployed.

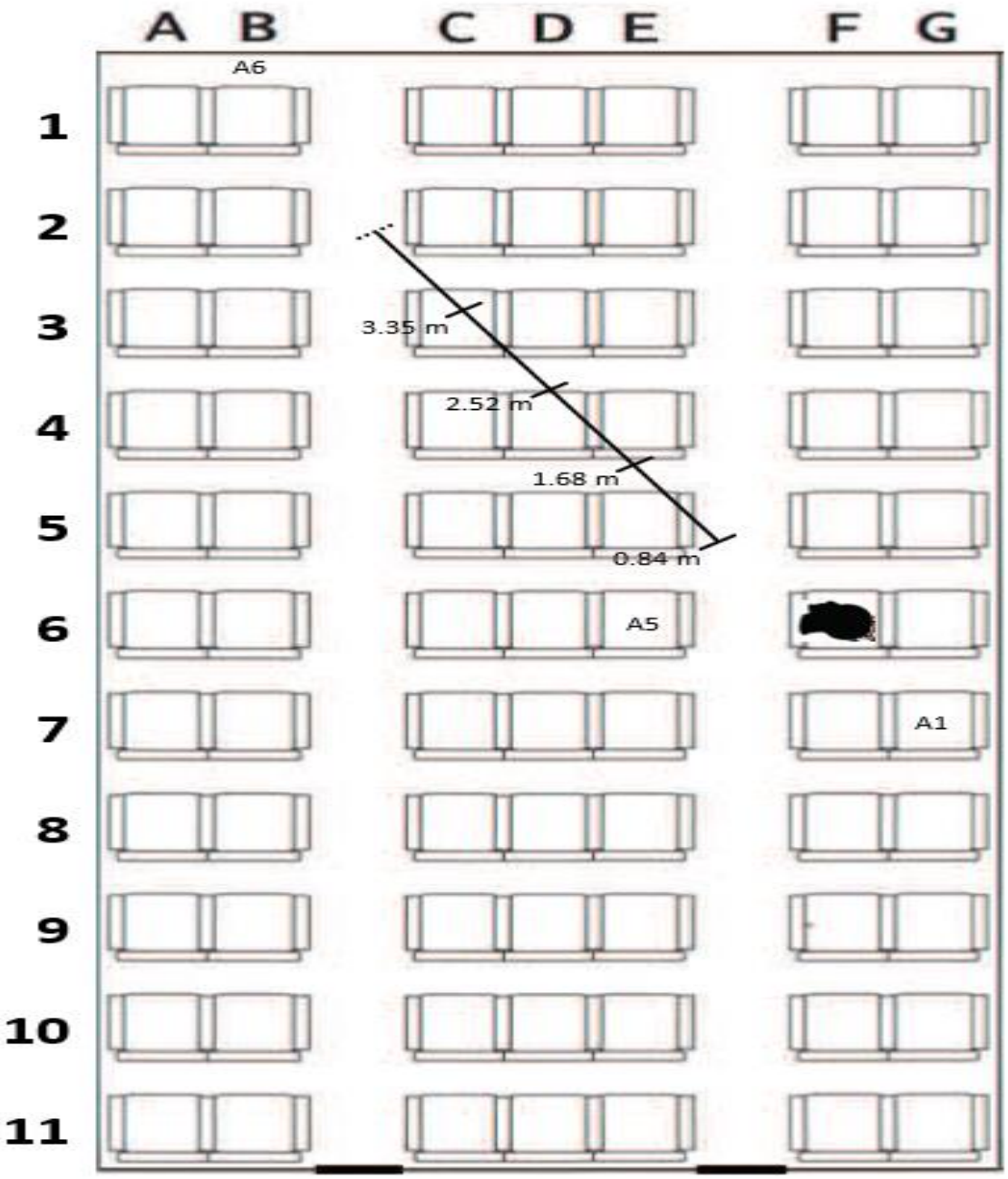

Figure H.57 Test 36 (B-M) ISOPass undeployed source location and sampling tree orientation.

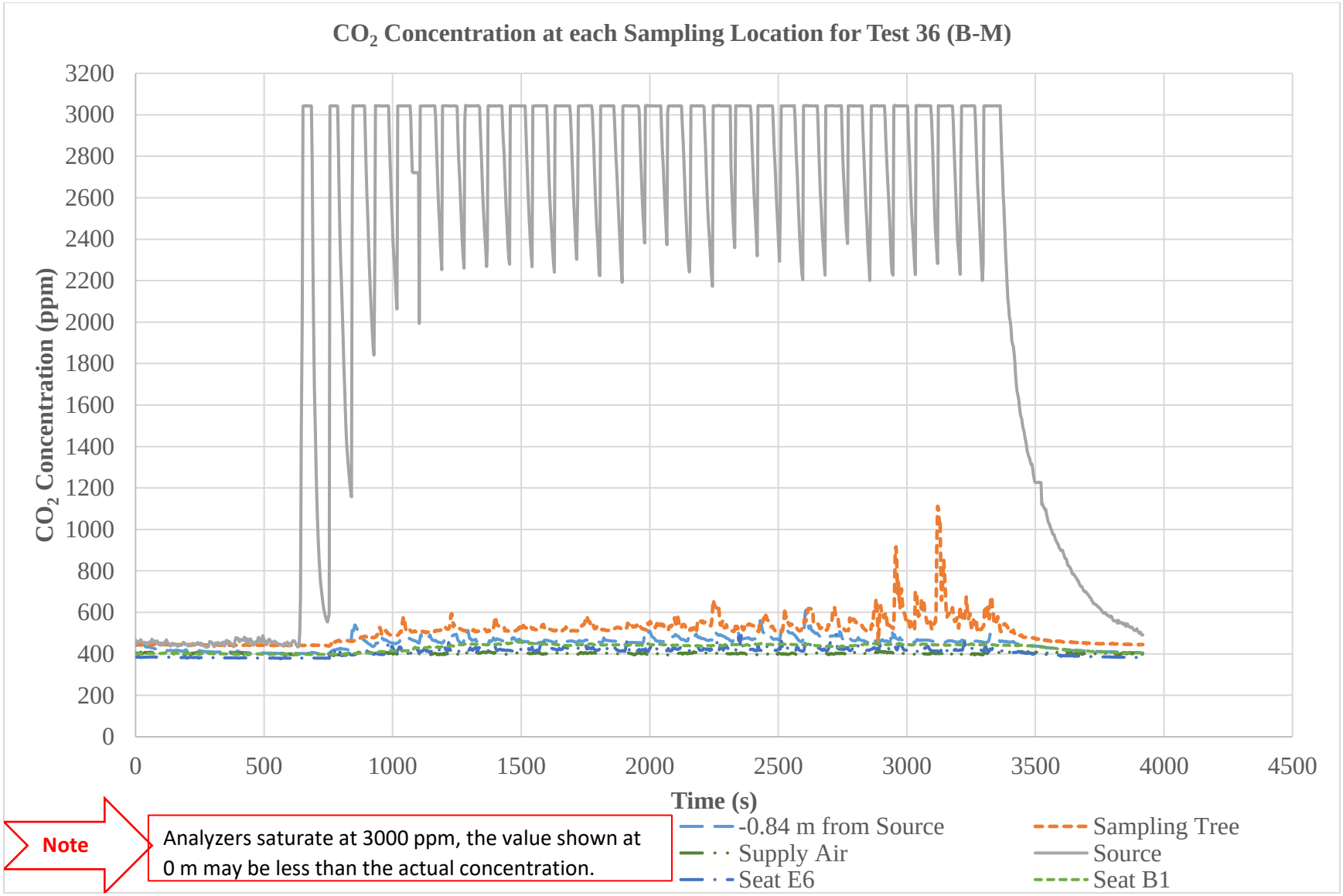

Figure H.58 Ininstantaneous CO_2 concentration at each sampling location for Test 36 (B-M) ISOPass undeployed.

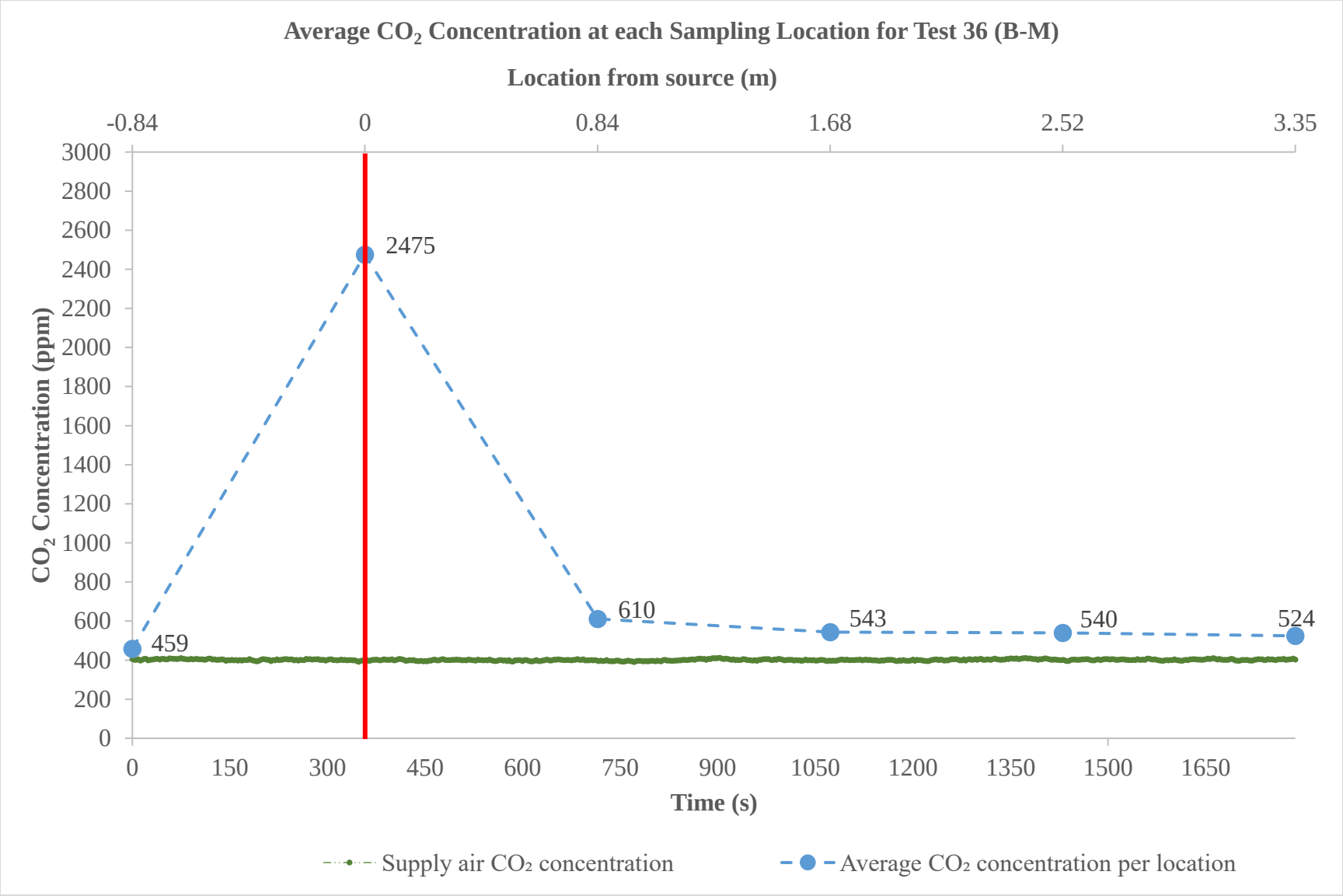

Figure H.59 Average CO_2 concentration at each sampling location for Test 36 (B-M) ISOPass undeployed.

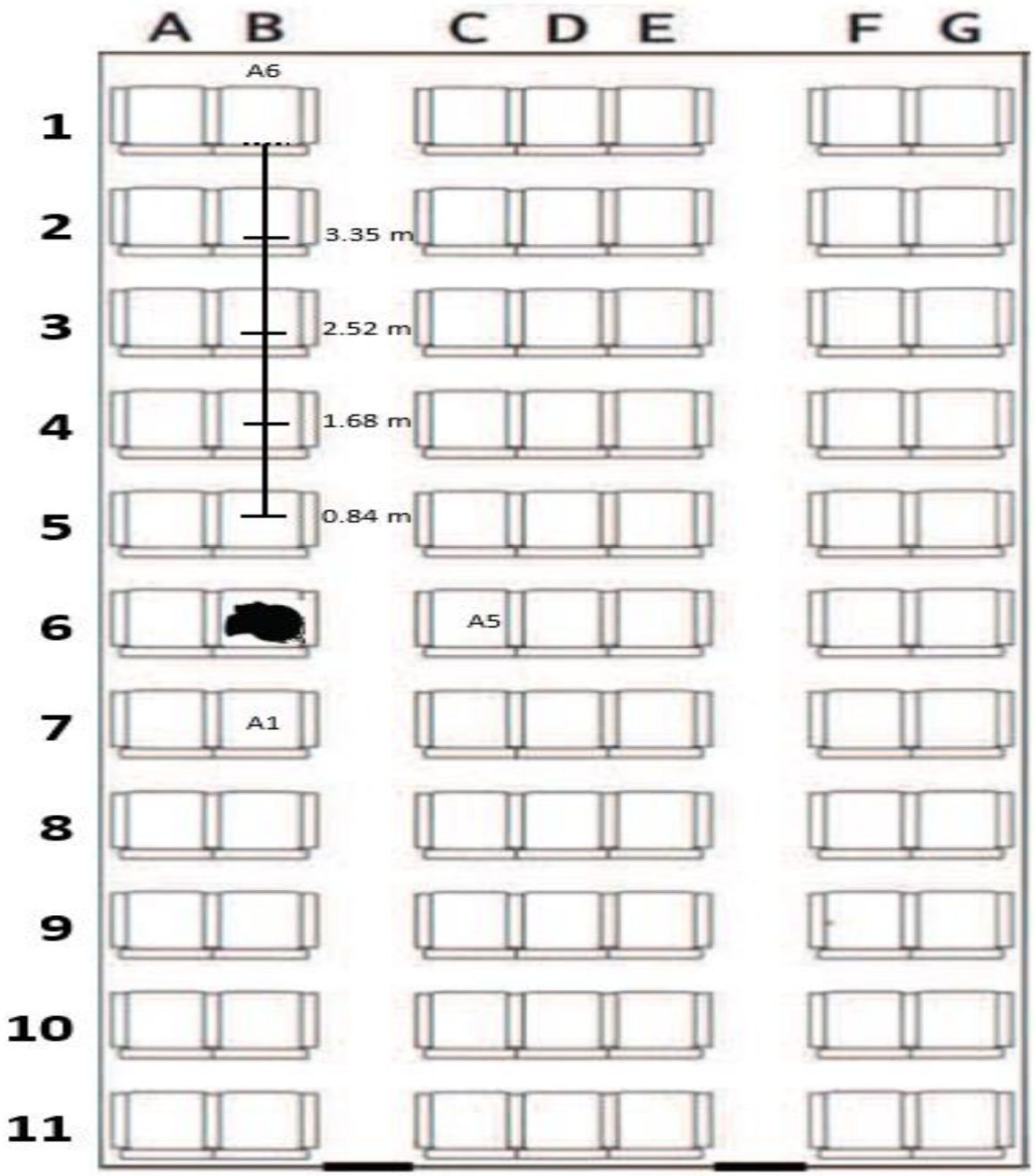

Figure H.60 Test 37 (B-M) ISOPass undeployed source location and sampling tree orientation.

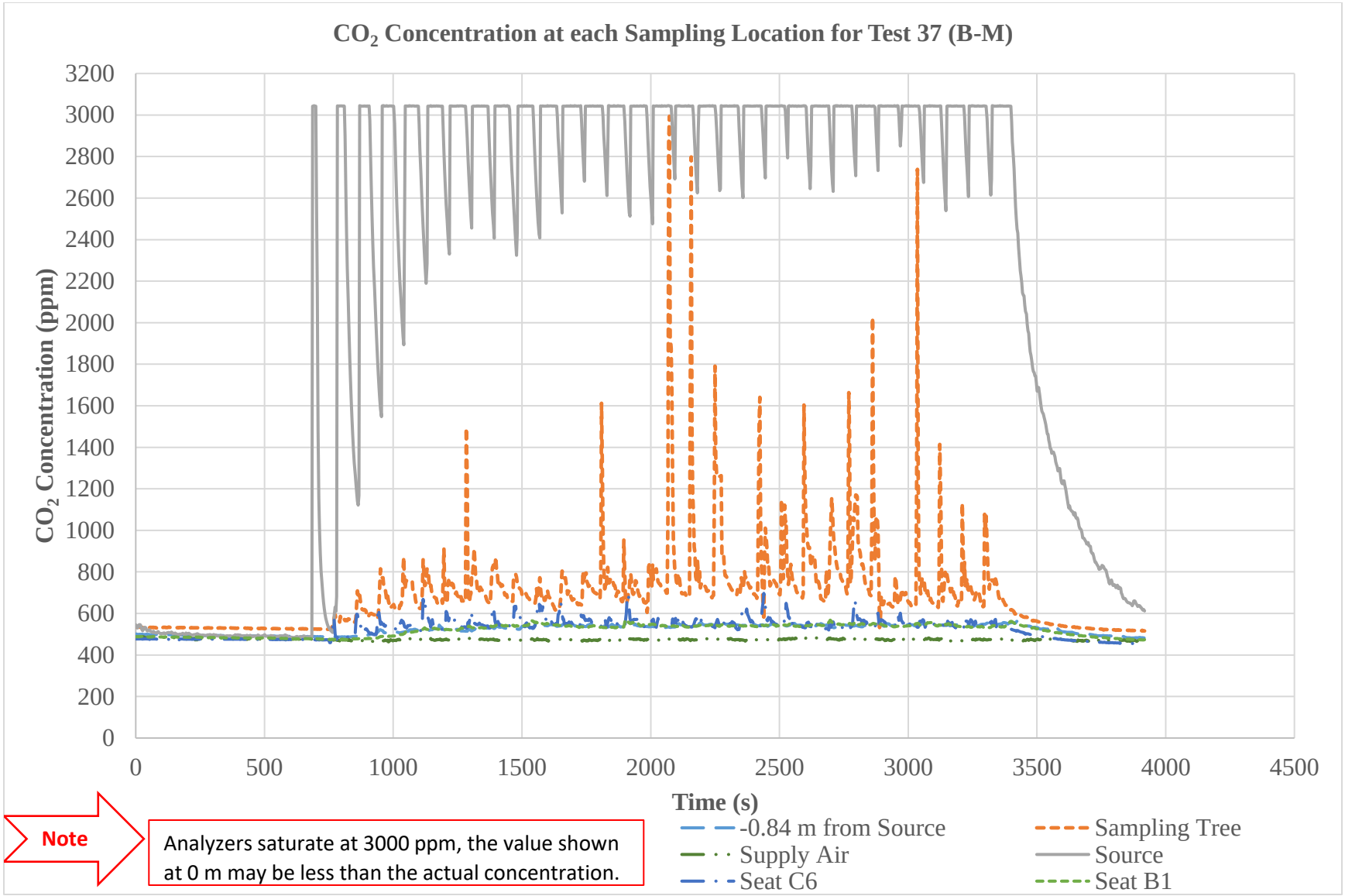

Figure H.61 Ininstantaneous CO_2 concentration at each sampling location for Test 37 (B-M) ISOPass undeployed.

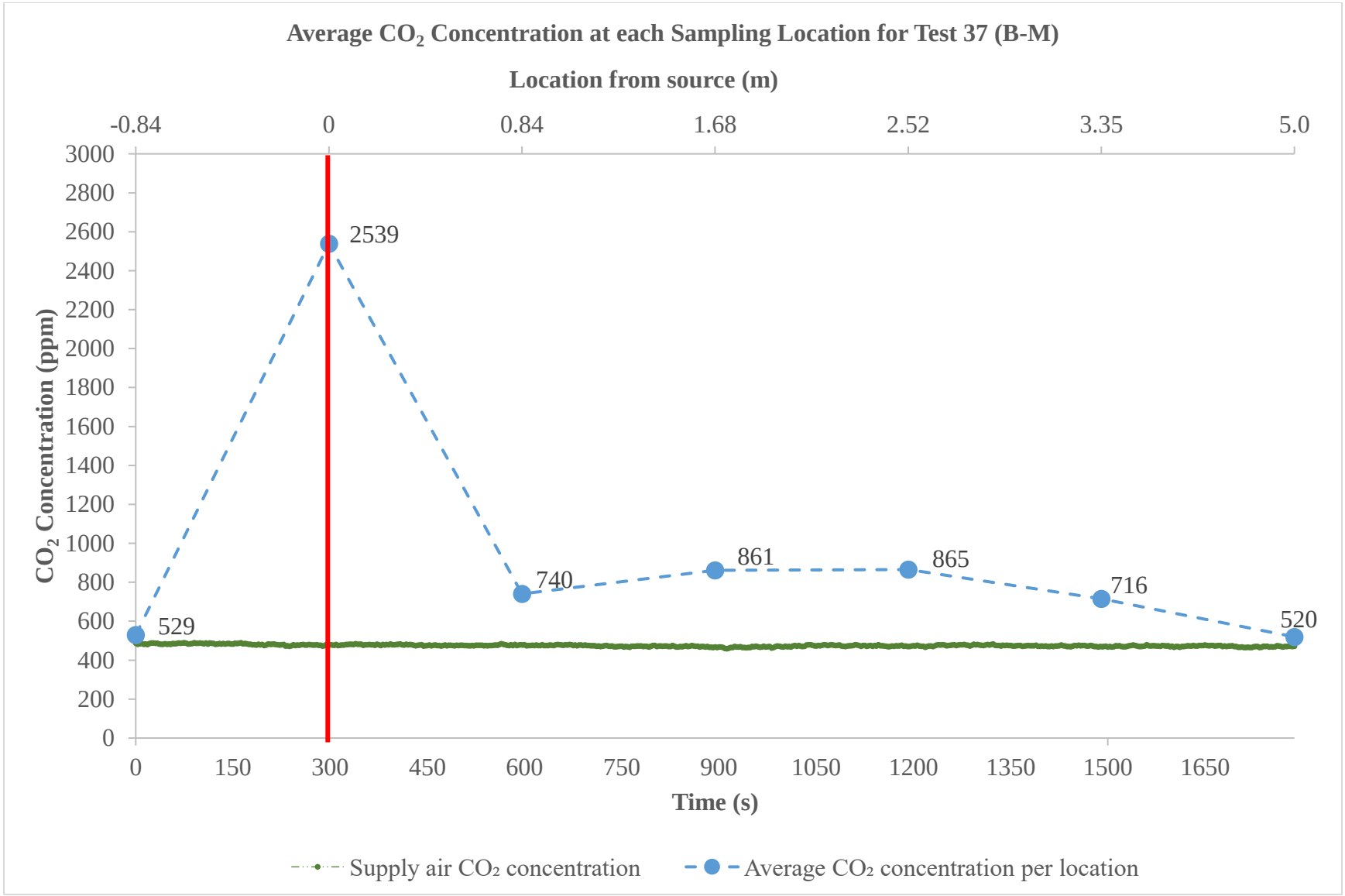

Figure H.62 Average CO_2 concentration at each sampling location for Test 37 (B-M) ISOPass undeployed.

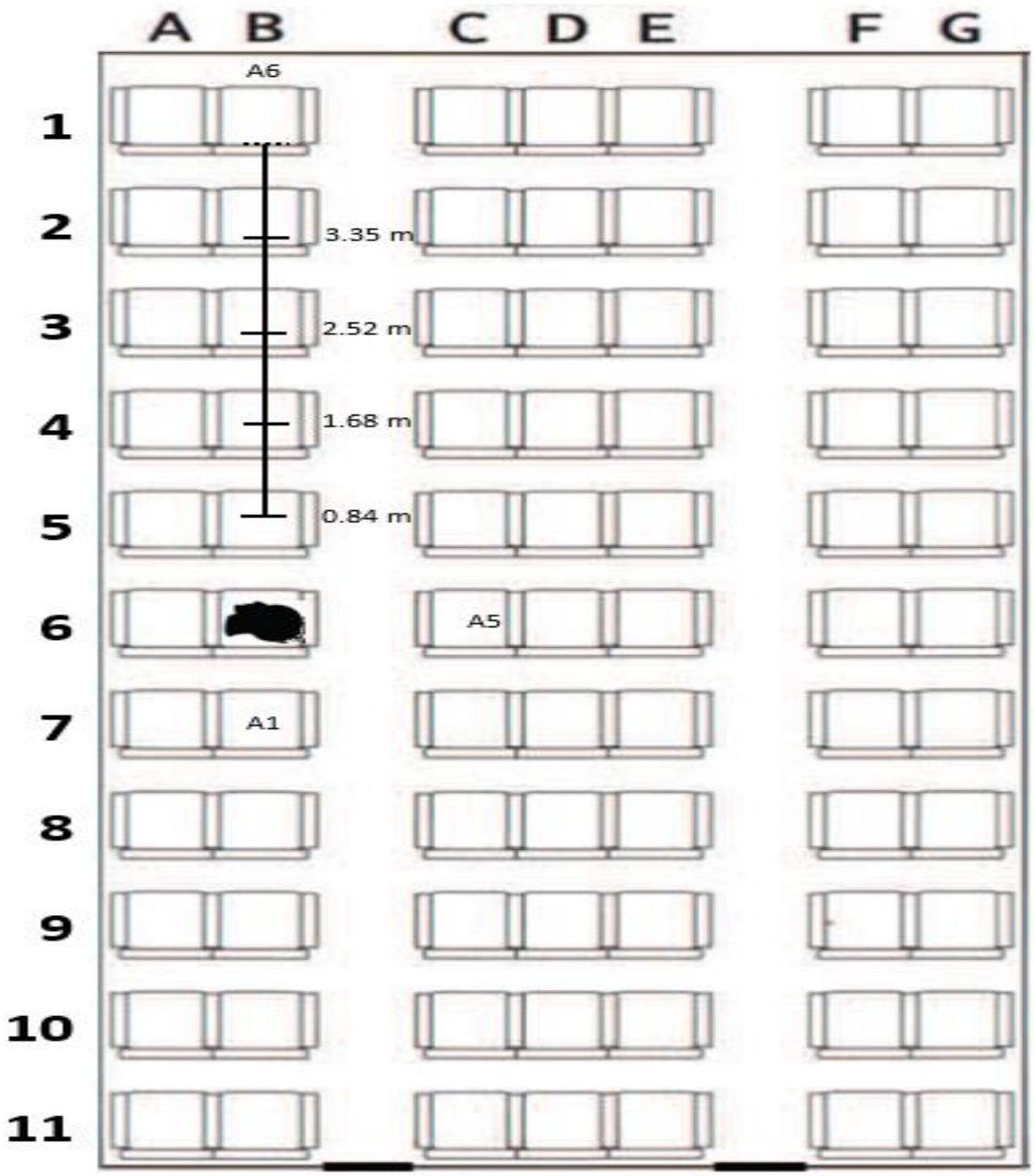

Figure H.63 Test 38 (B-M) ISOPass undeployed source location and sampling tree orientation.

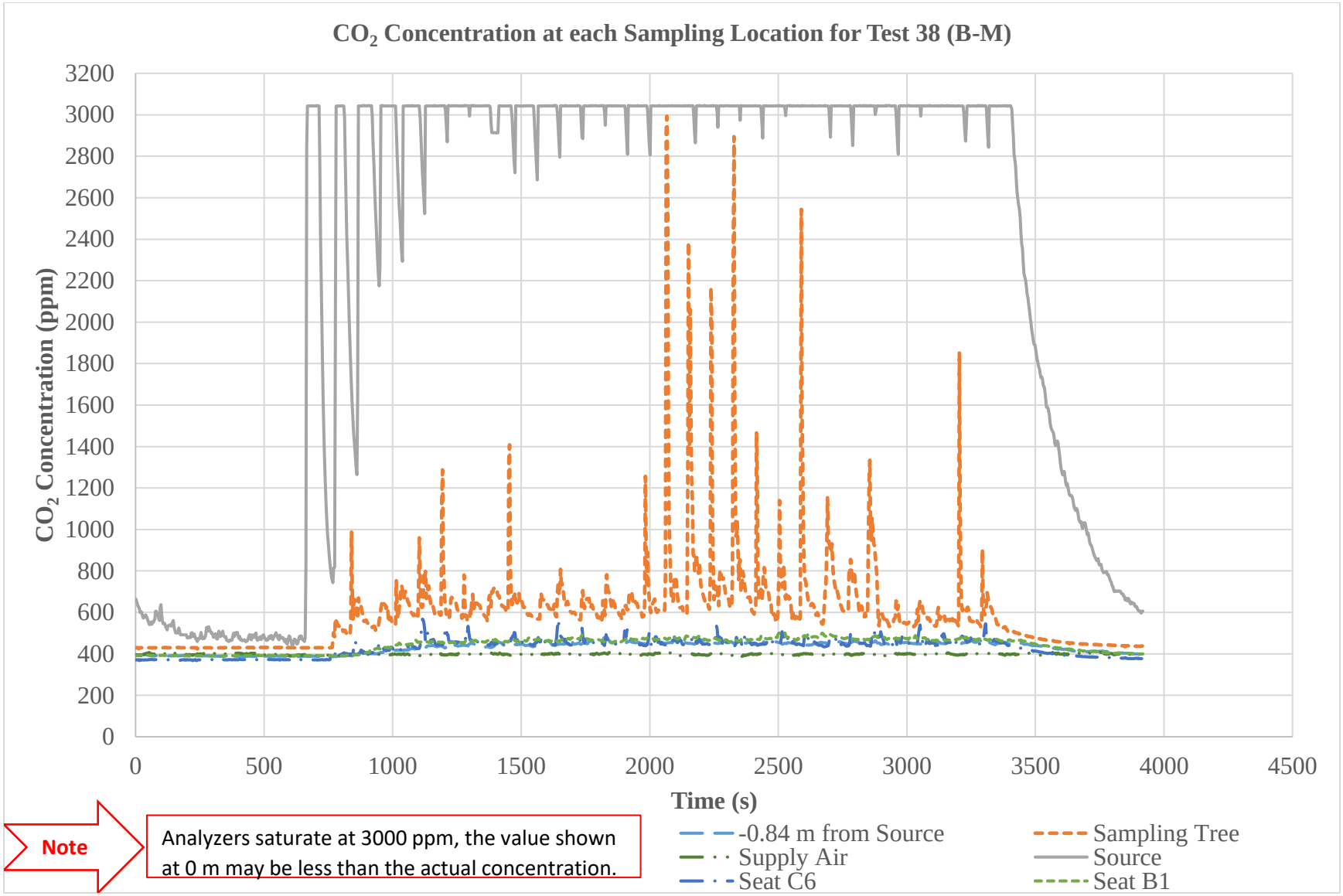

Figure H.64 Ininstantaneous CO_2 concentration at each sampling location for Test 38 (B-M) ISOPass undeployed.

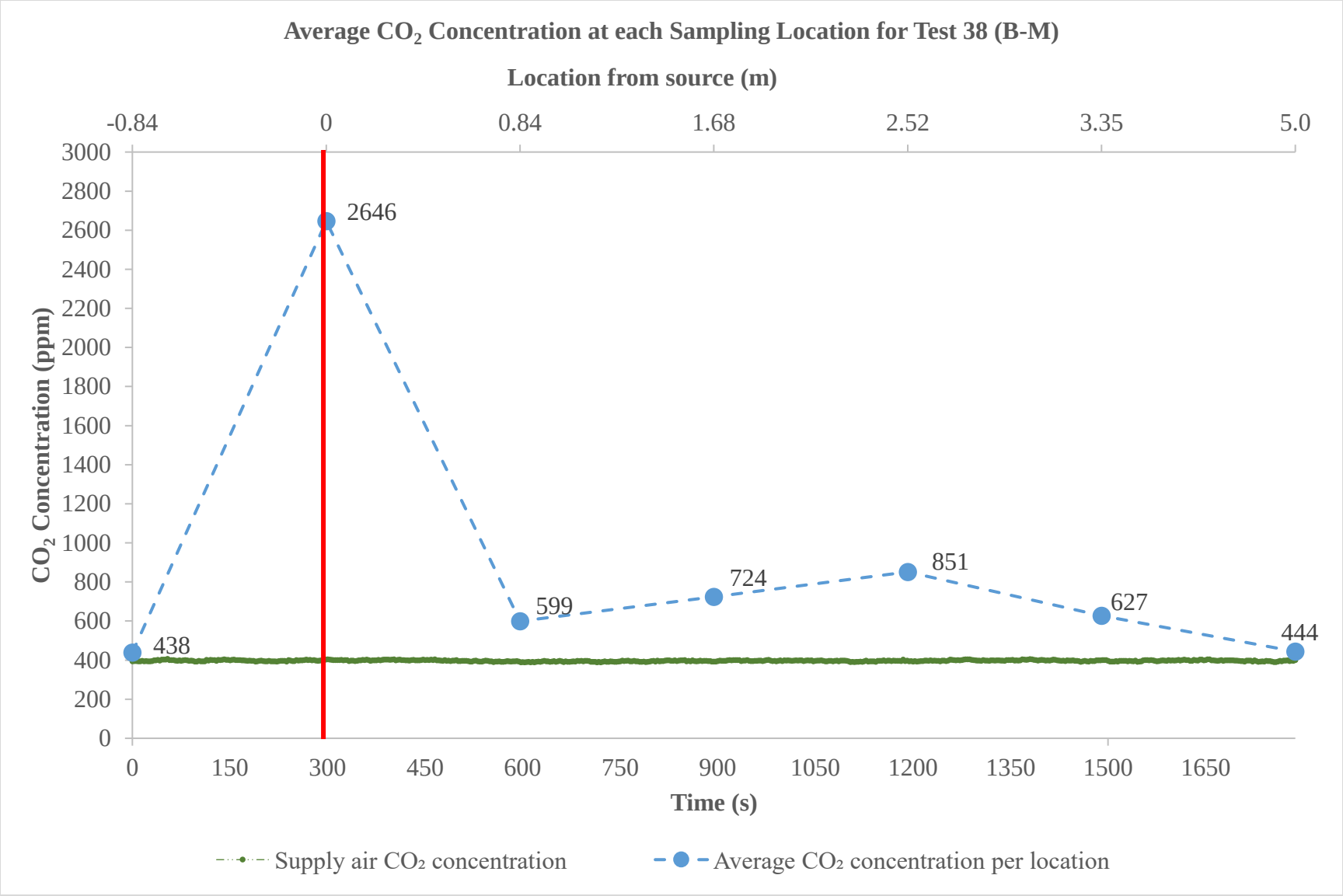

Figure H.65 Average CO_2 concentration at each sampling location for Test 38 (B-M) ISOPass undeployed.

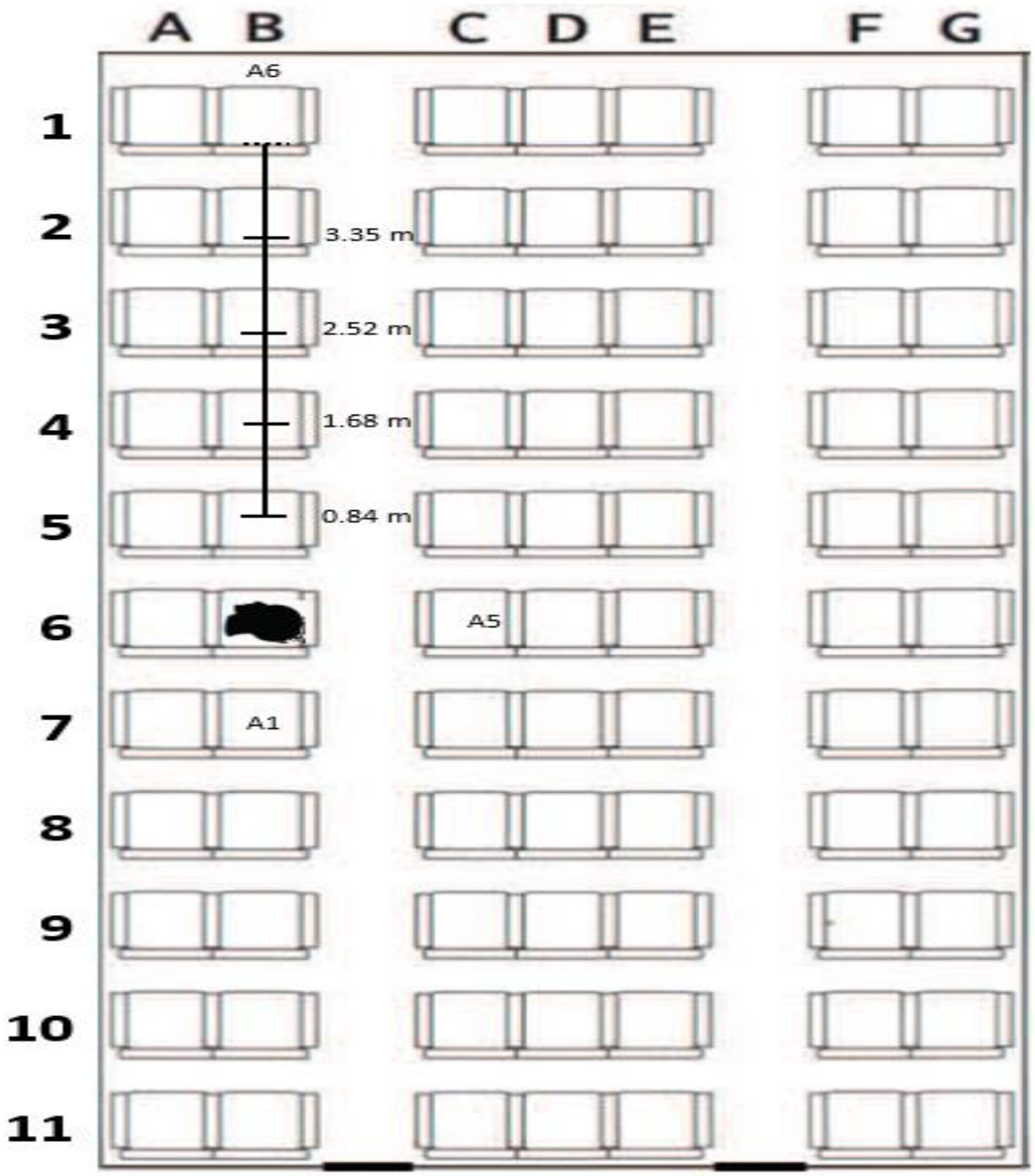

Figure H.66 Test 39 (B-M) ISOPass undeployed source location and sampling tree orientation.

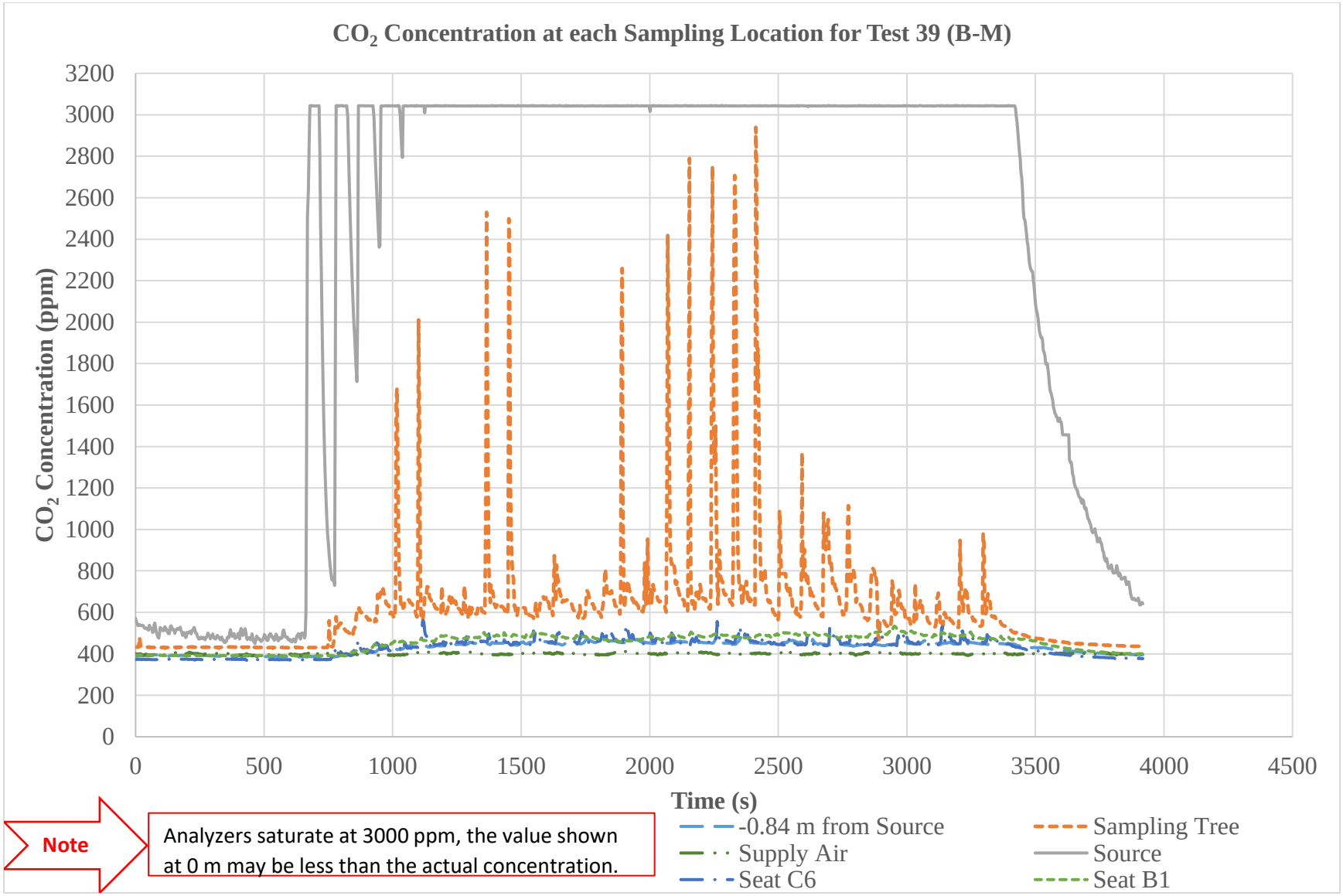

Figure H.67 Ininstantaneous CO_2 concentration at each sampling location for Test 39 (B-M) ISOPass undeployed.

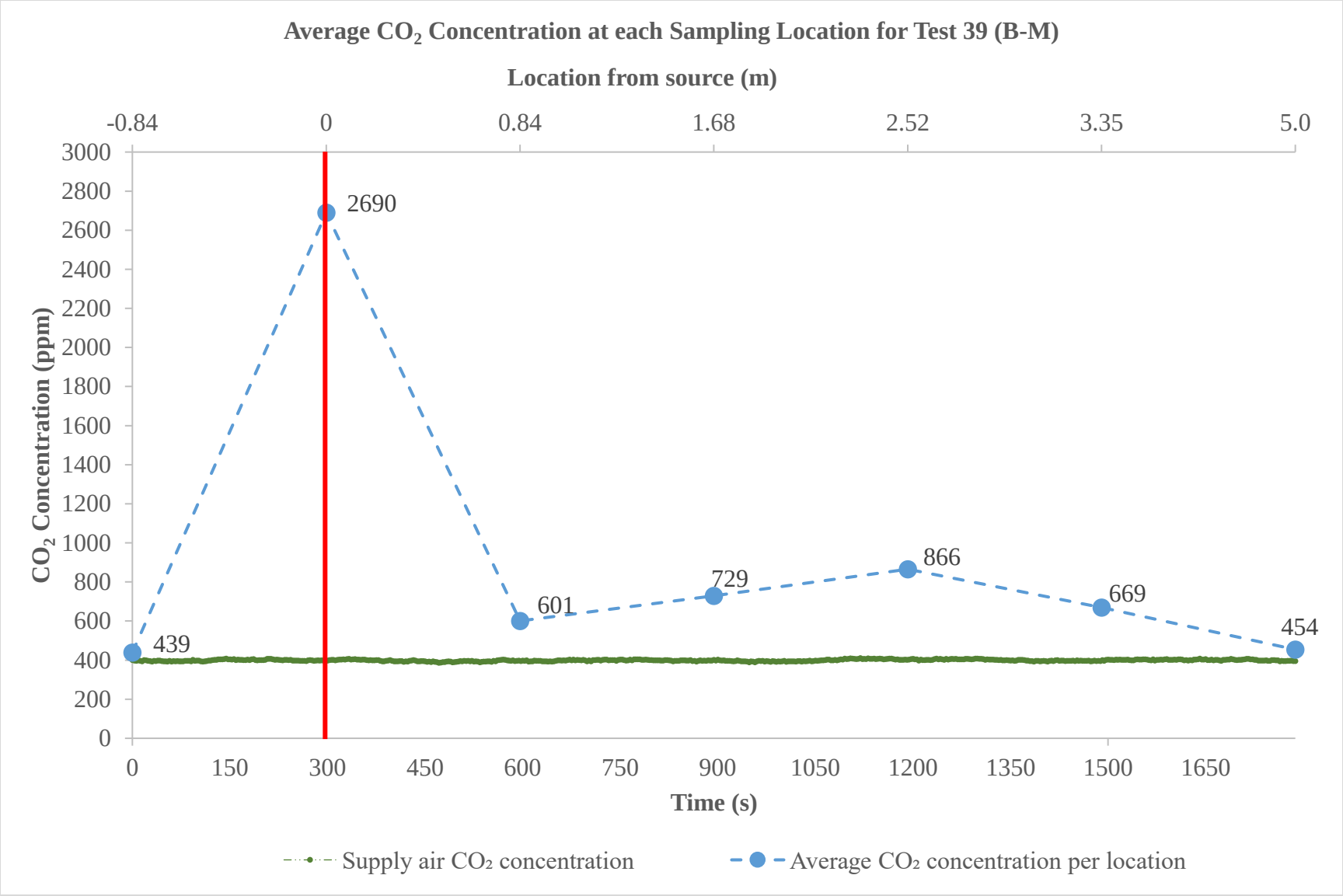

Figure H.68 Average CO_2 concentration at each sampling location for Test 39 (B-M) ISOPass undeployed.

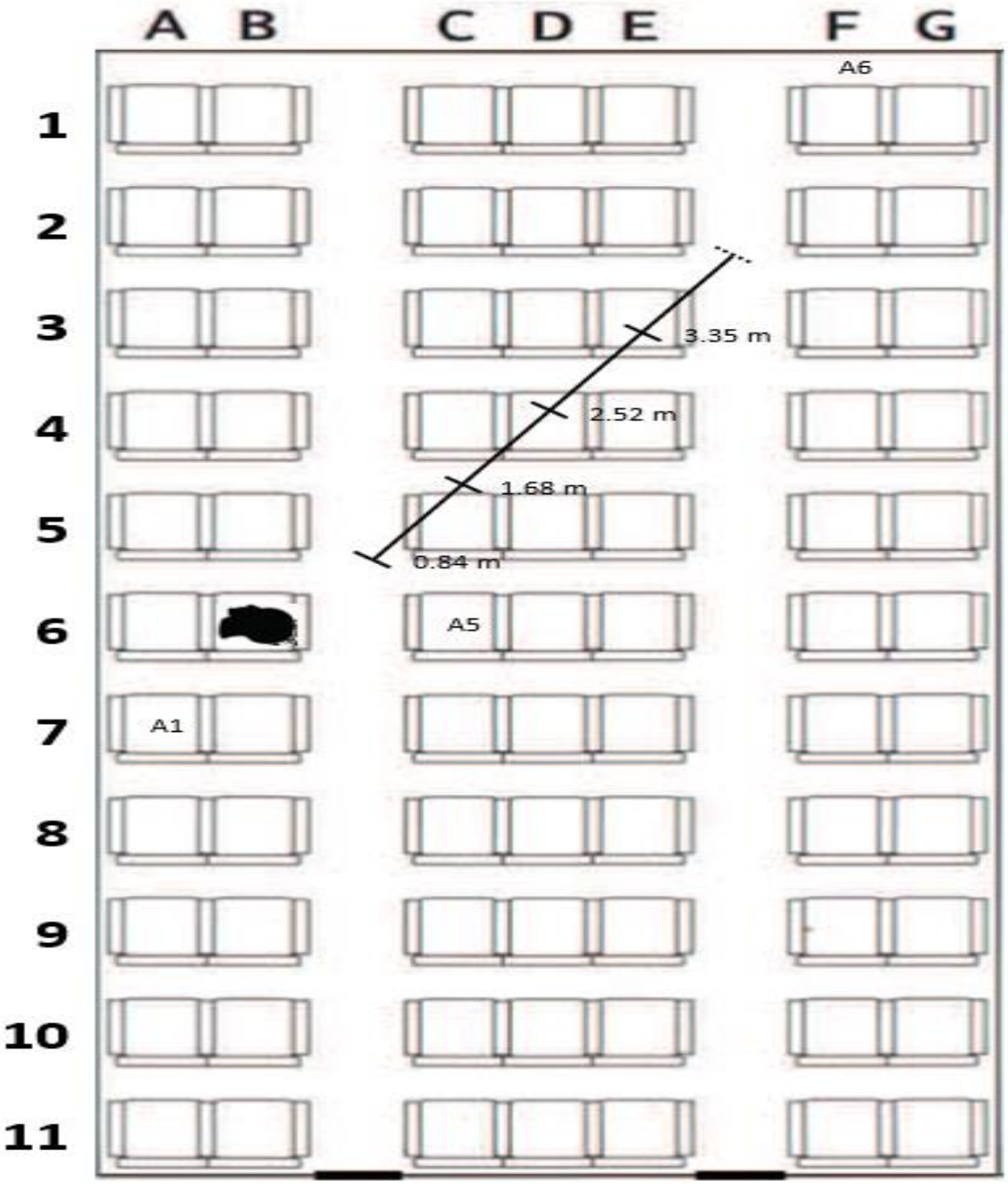

Figure H.69 Test 40 (B-M) ISOPass undeployed source location and sampling tree orientation.

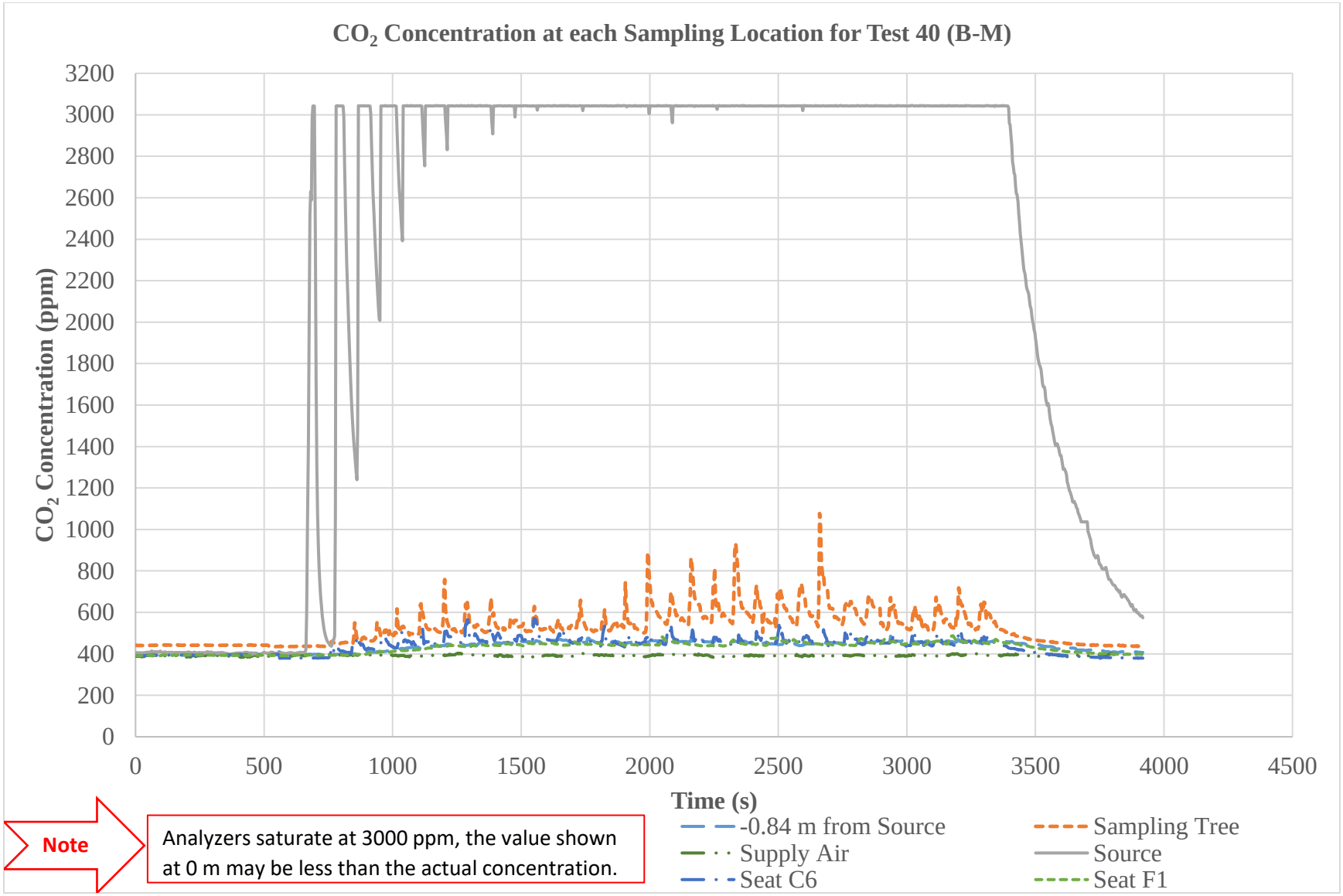

Figure H.70 Ininstantaneous CO_2 concentration at each sampling location for Test 40 (B-M) ISOPass undeployed.

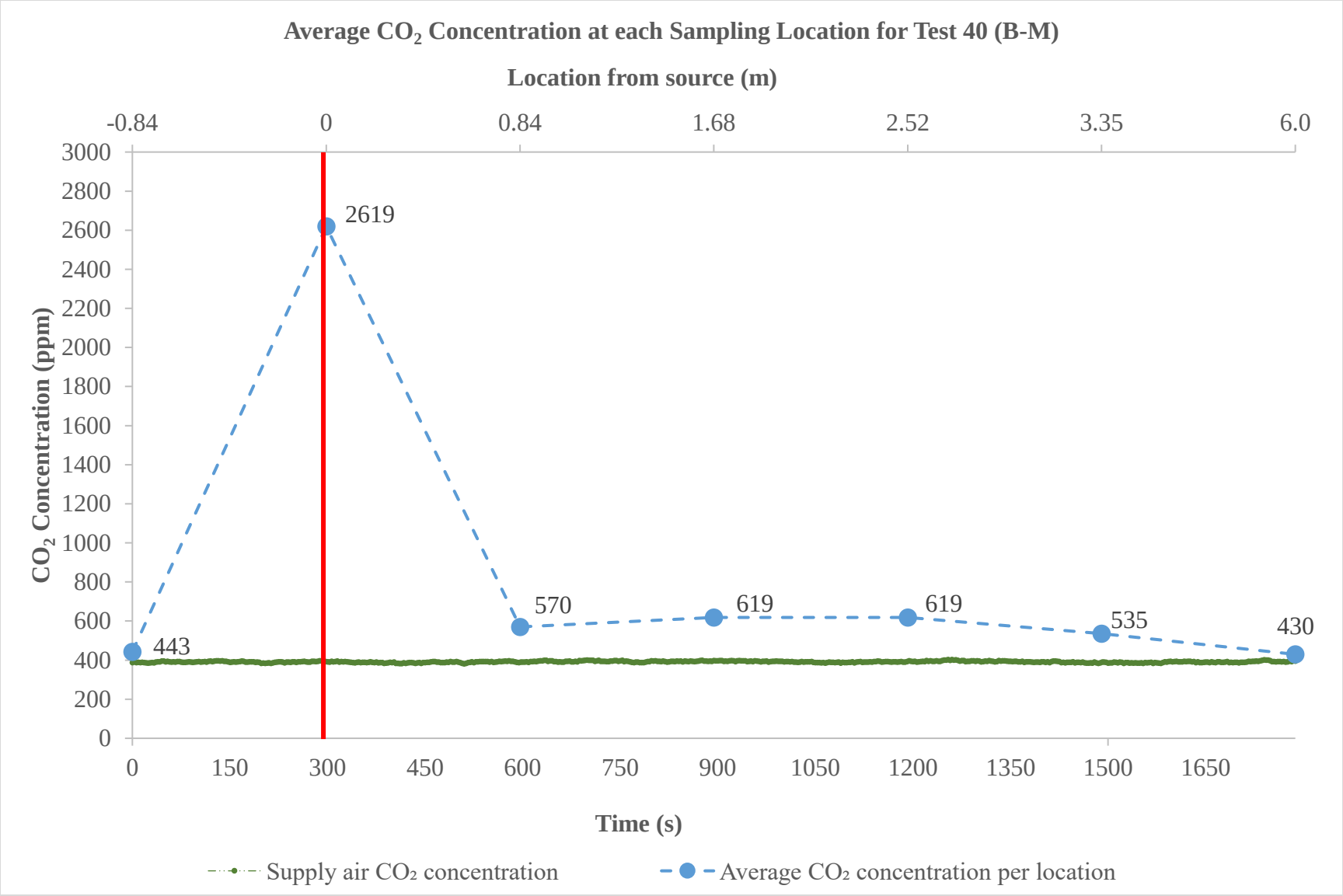

Figure H.71 Average CO_2 concentration at each sampling location for Test 40 (B-M) ISOPass undeployed.

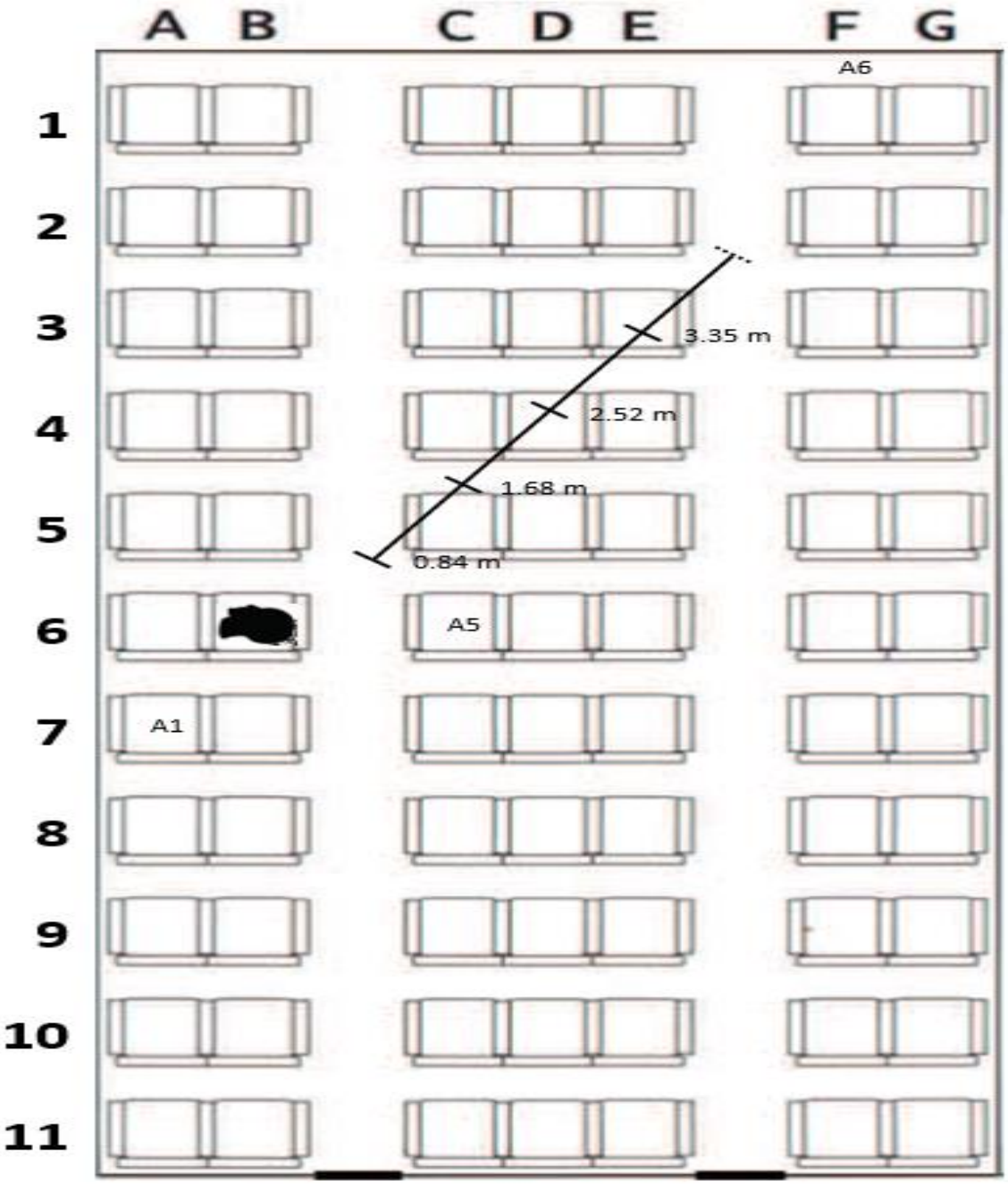

Figure H.72 Test 41 (B-M) ISOPass undeployed source location and sampling tree orientation.

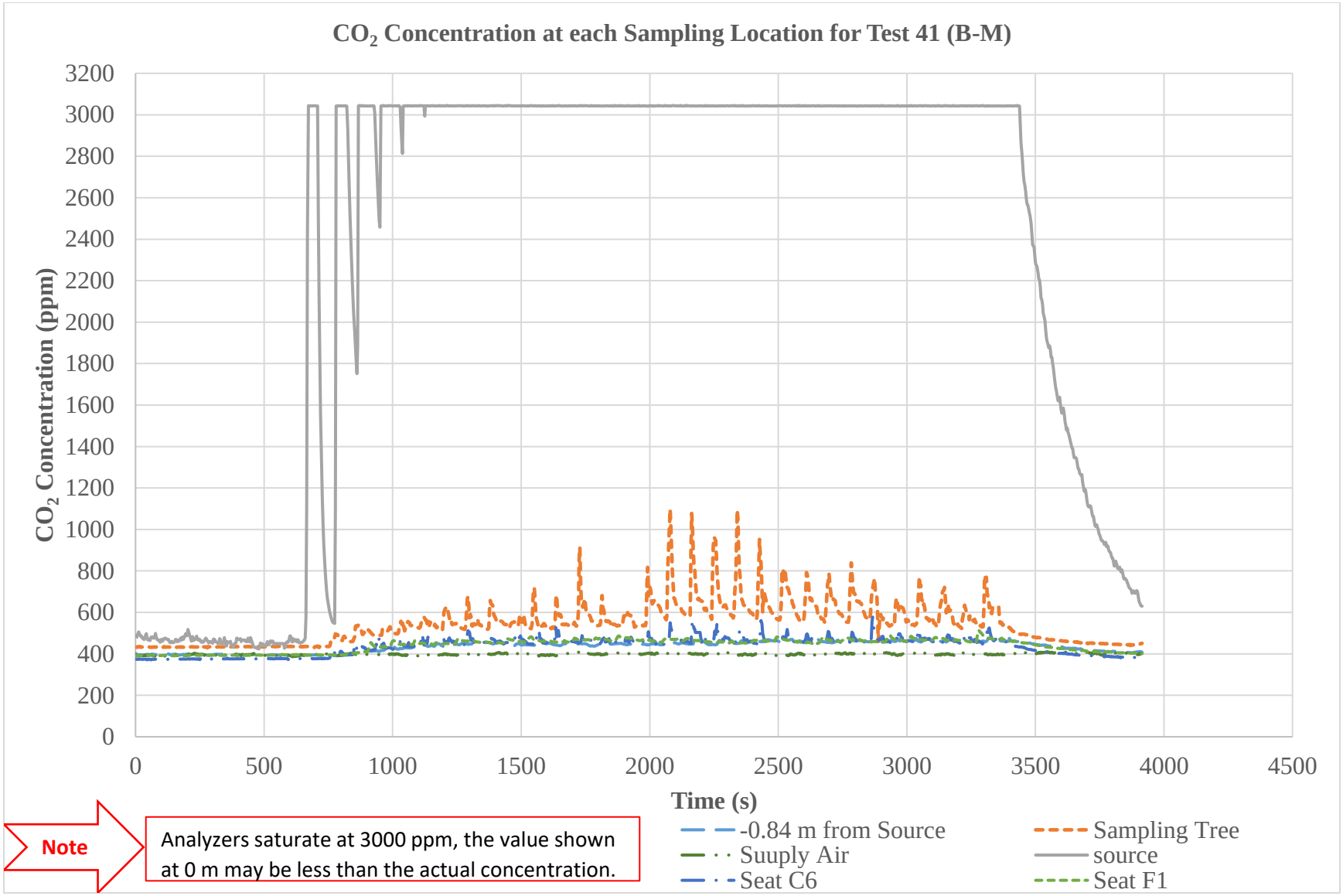

Figure H.73 Ininstantaneous CO_2 concentration at each sampling location for Test 41 (B-M) ISOPass undeployed.

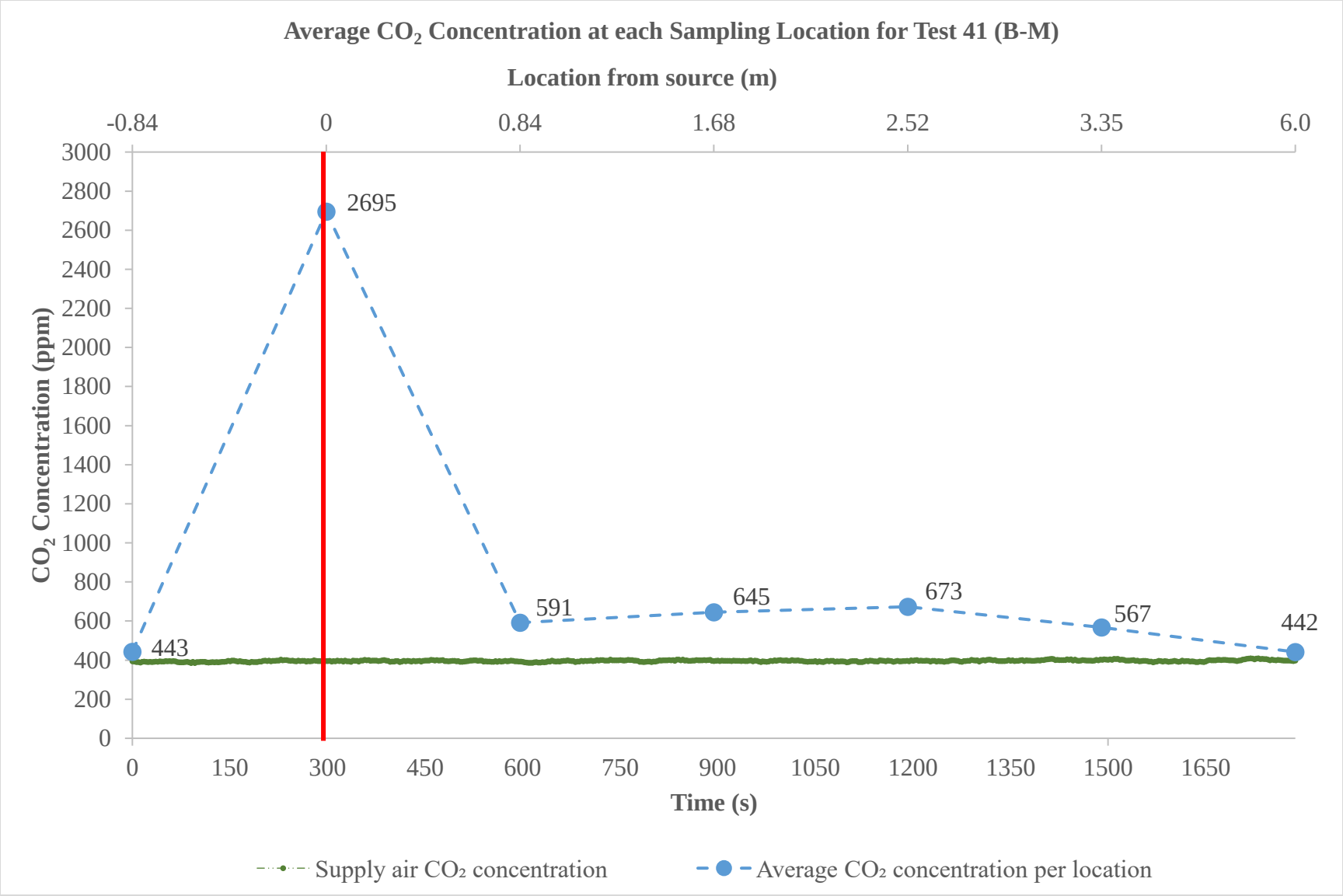

Figure H.74 Average CO_2 concentration at each sampling location for Test 41 (B-M) ISOPass undeployed.

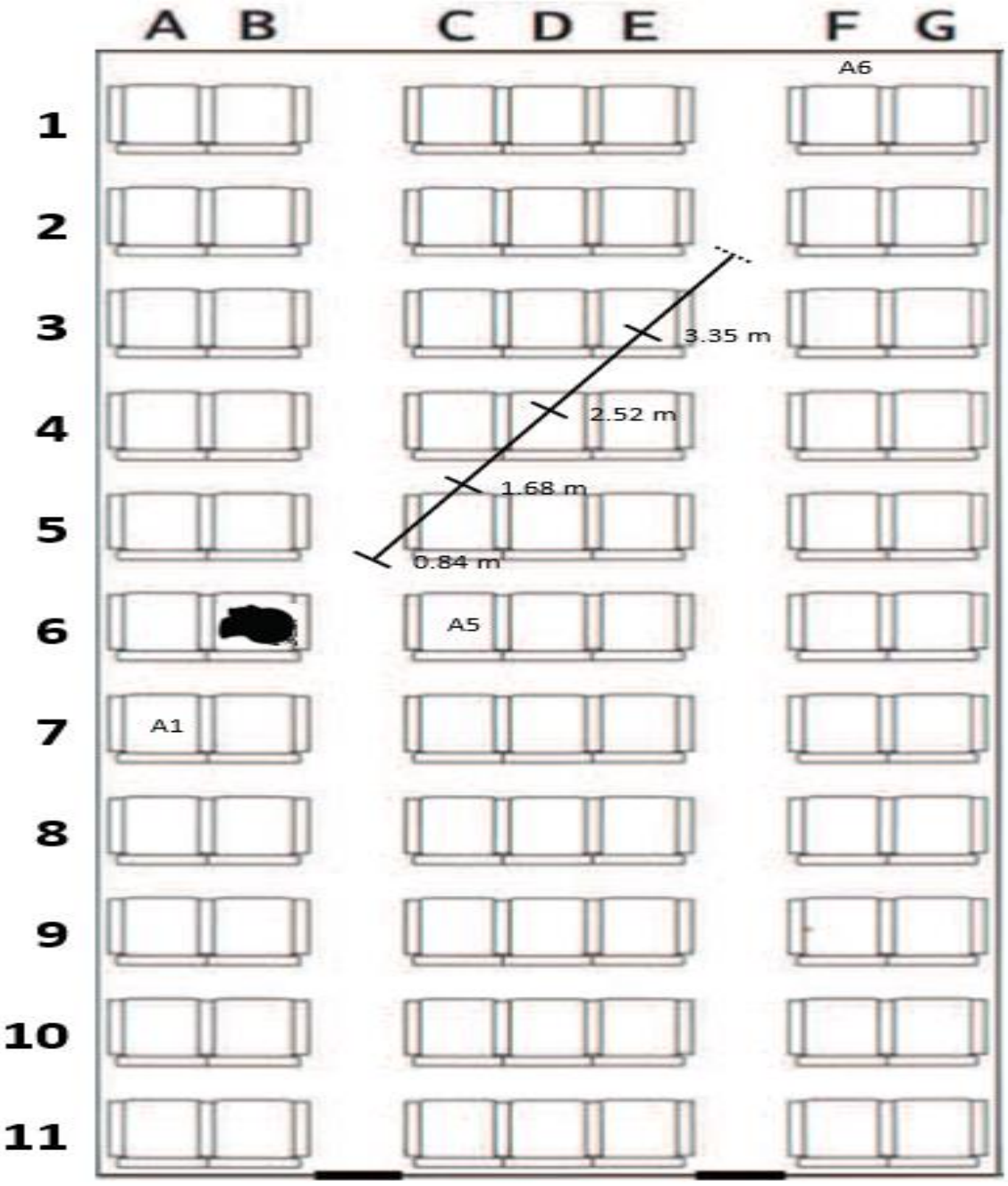

Figure H.75 Test 42 (B-M) ISOPass undeployed source location and sampling tree orientation.

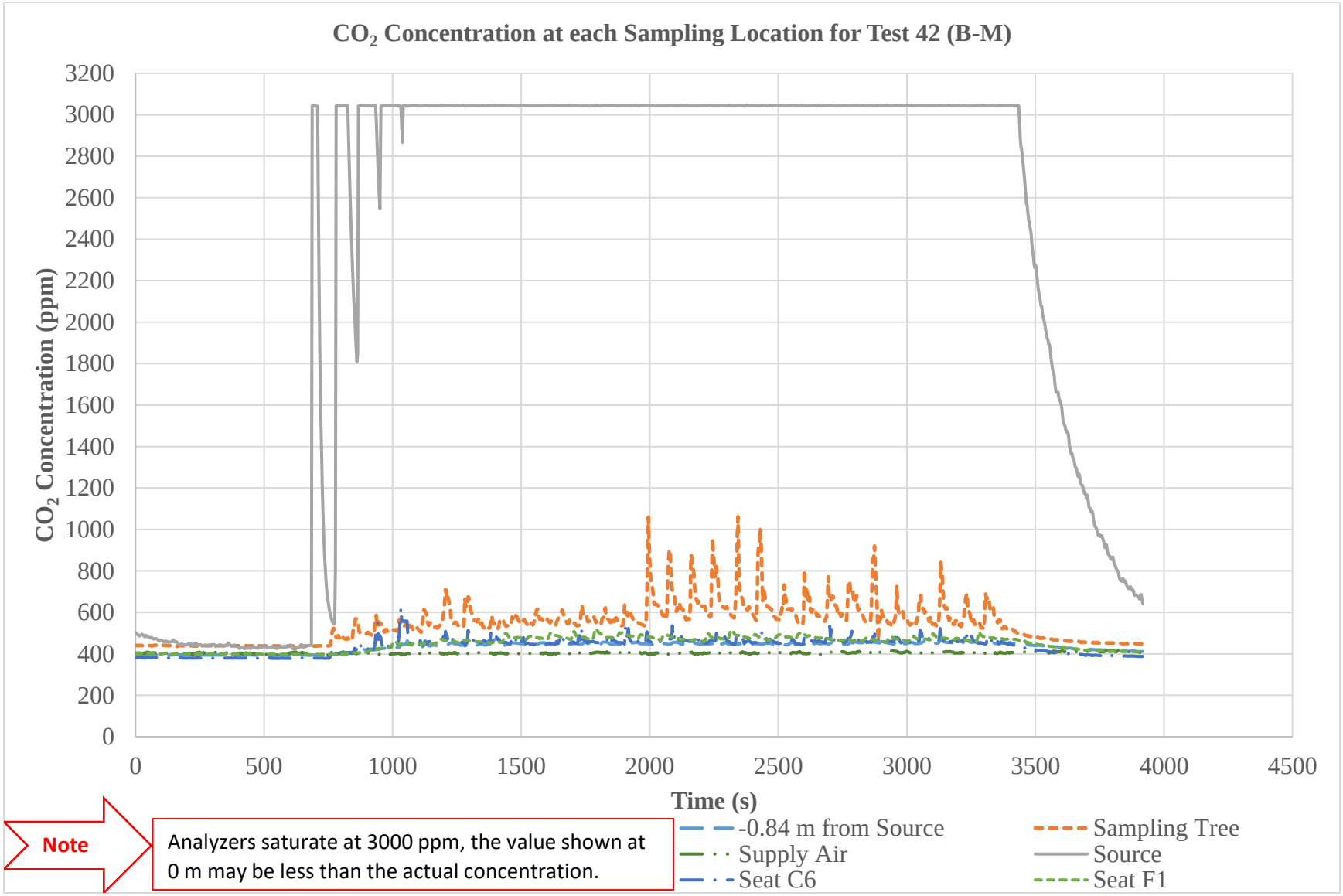

Figure H.76 Ininstantaneous CO_2 concentration at each sampling location for Test 42 (B-M) ISOPass undeployed.

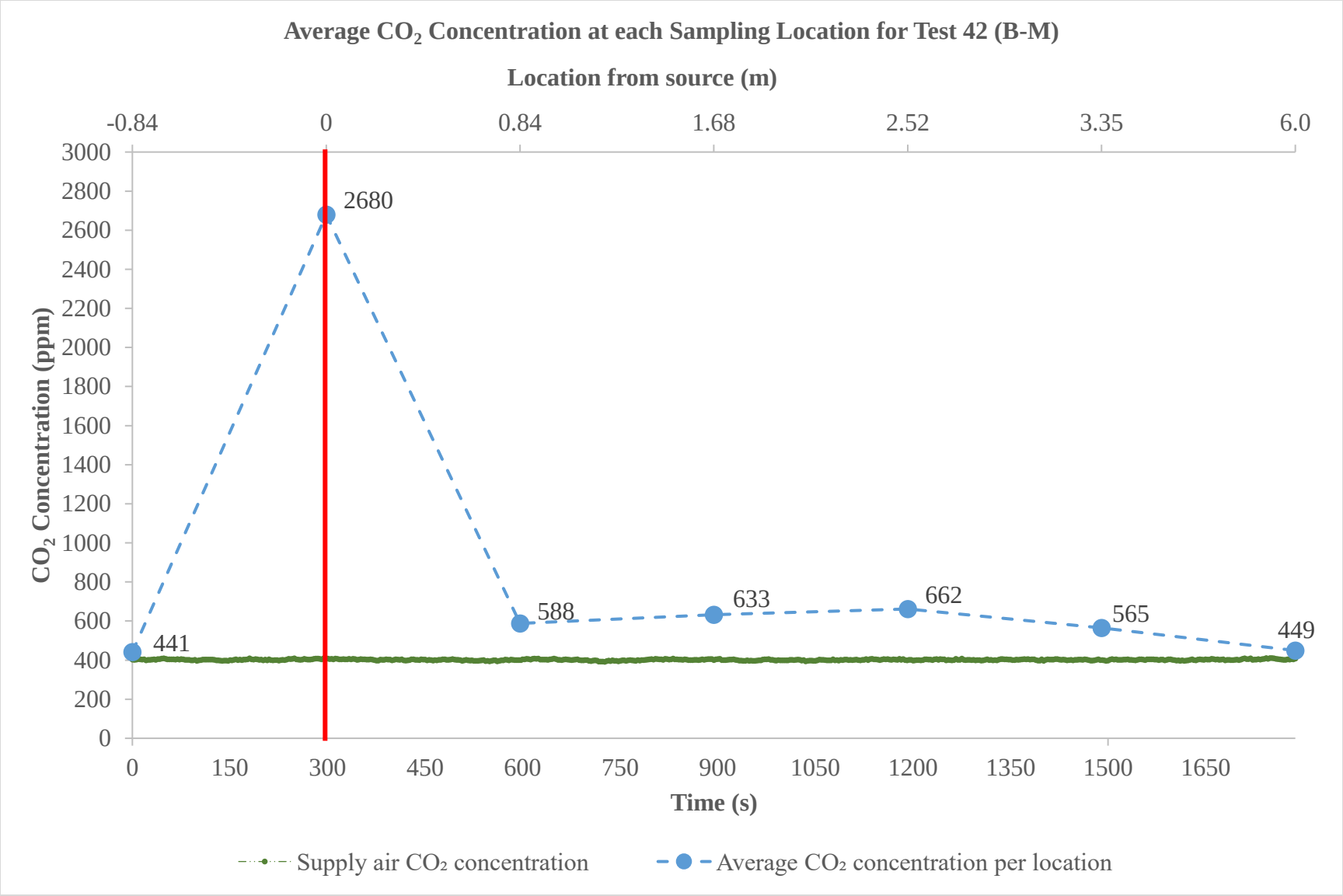

Figure H.77 Average CO_2 concentration at each sampling location for Test 42 (B-M) ISOPass undeployed.

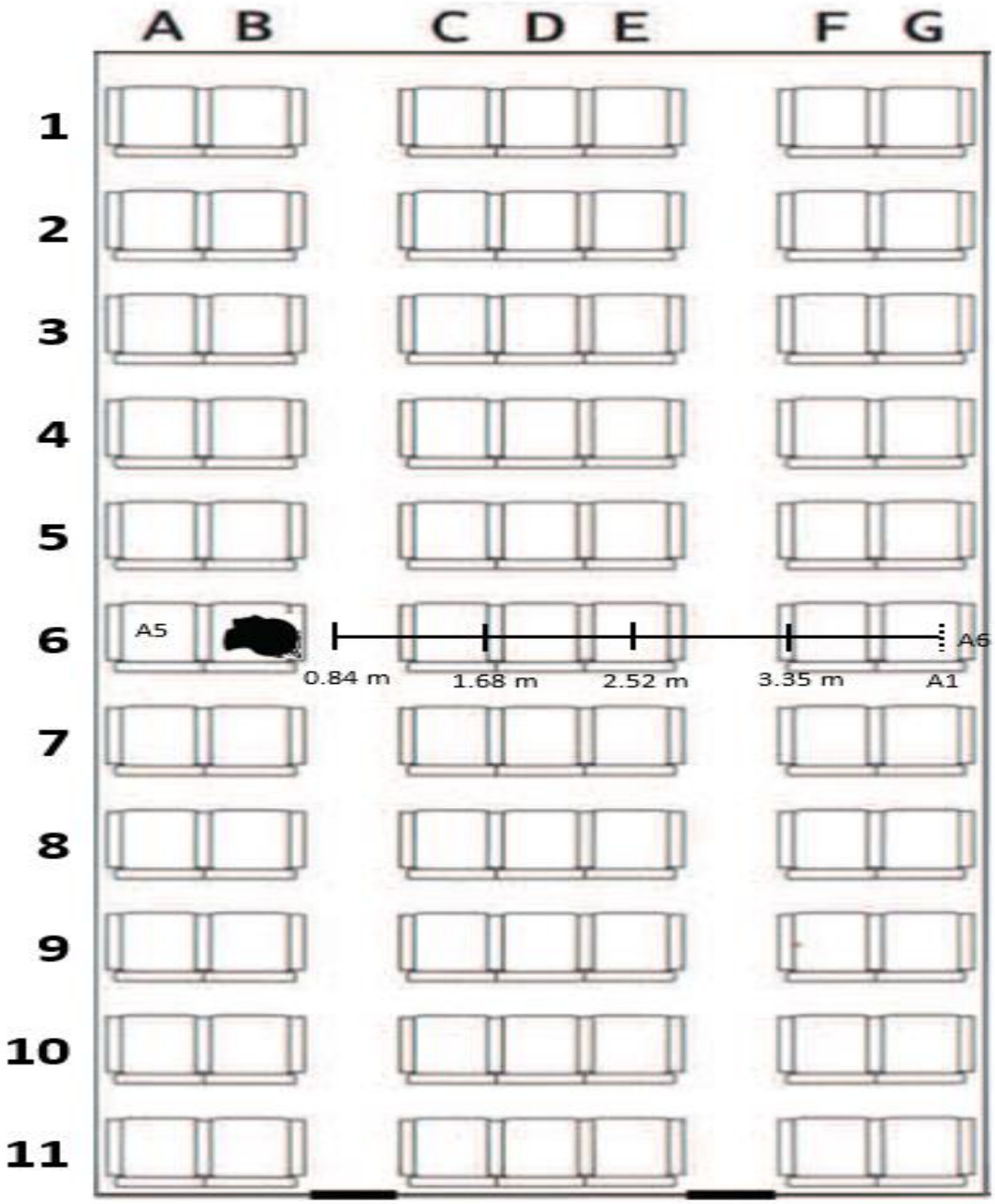

Figure H.78 Test 43 (B-M) ISOPass undeployed source location and sampling tree orientation.

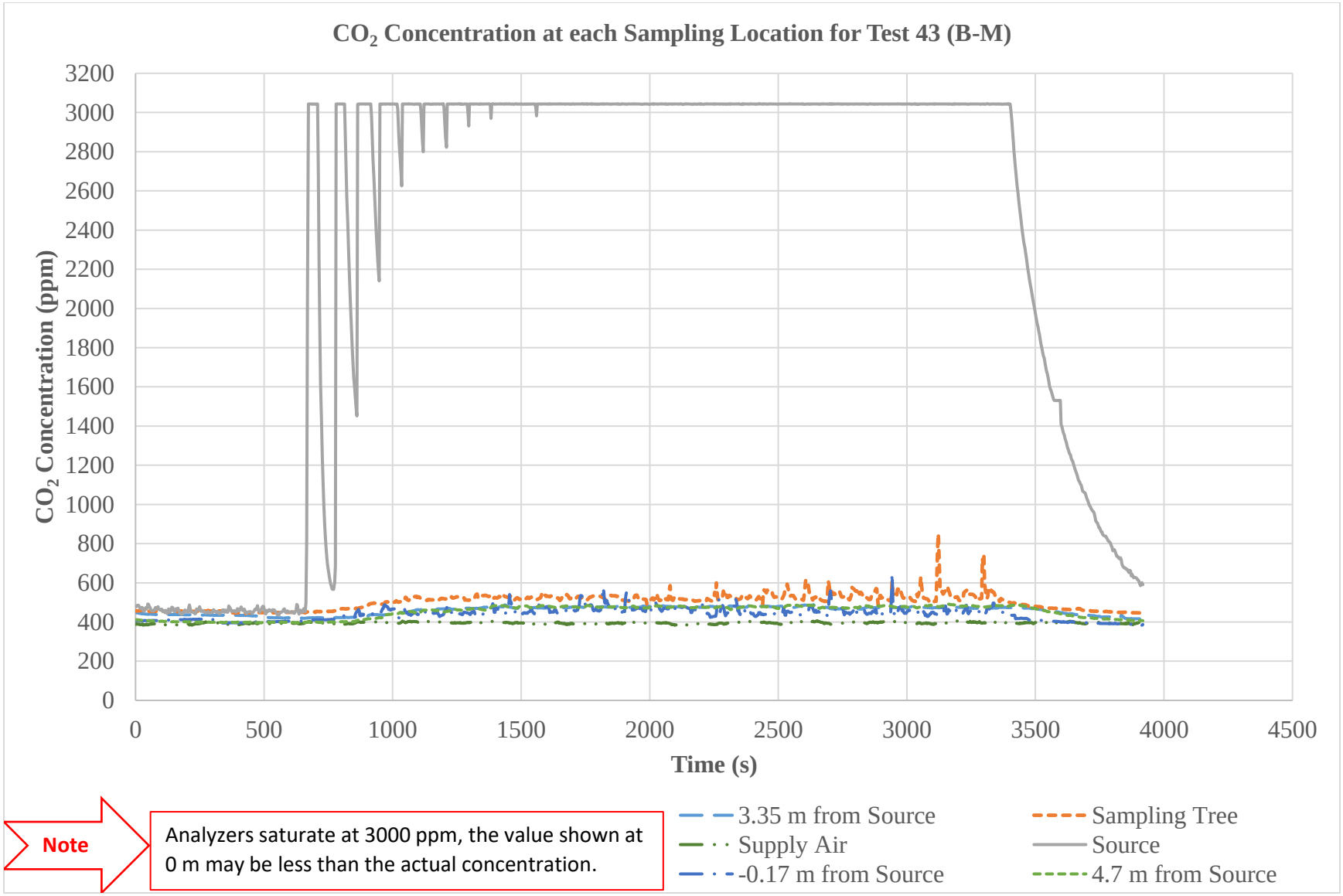

Figure H.79 Ininstantaneous CO_2 concentration at each sampling location for Test 43 (B-M) ISOPass undeployed.

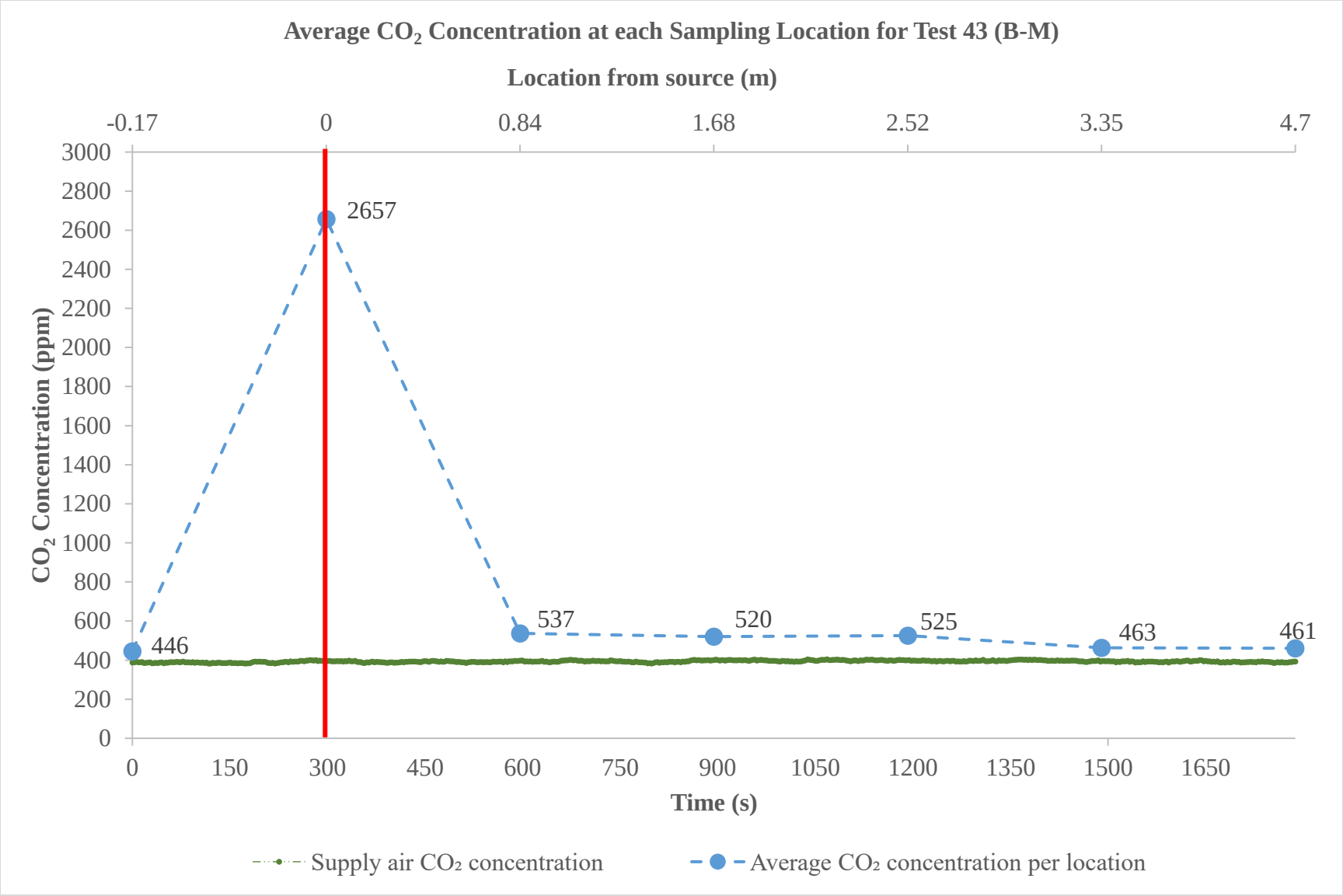

Figure H.80 Average CO_2 concentration at each sampling location for Test 43 (B-M) ISOPass undeployed.

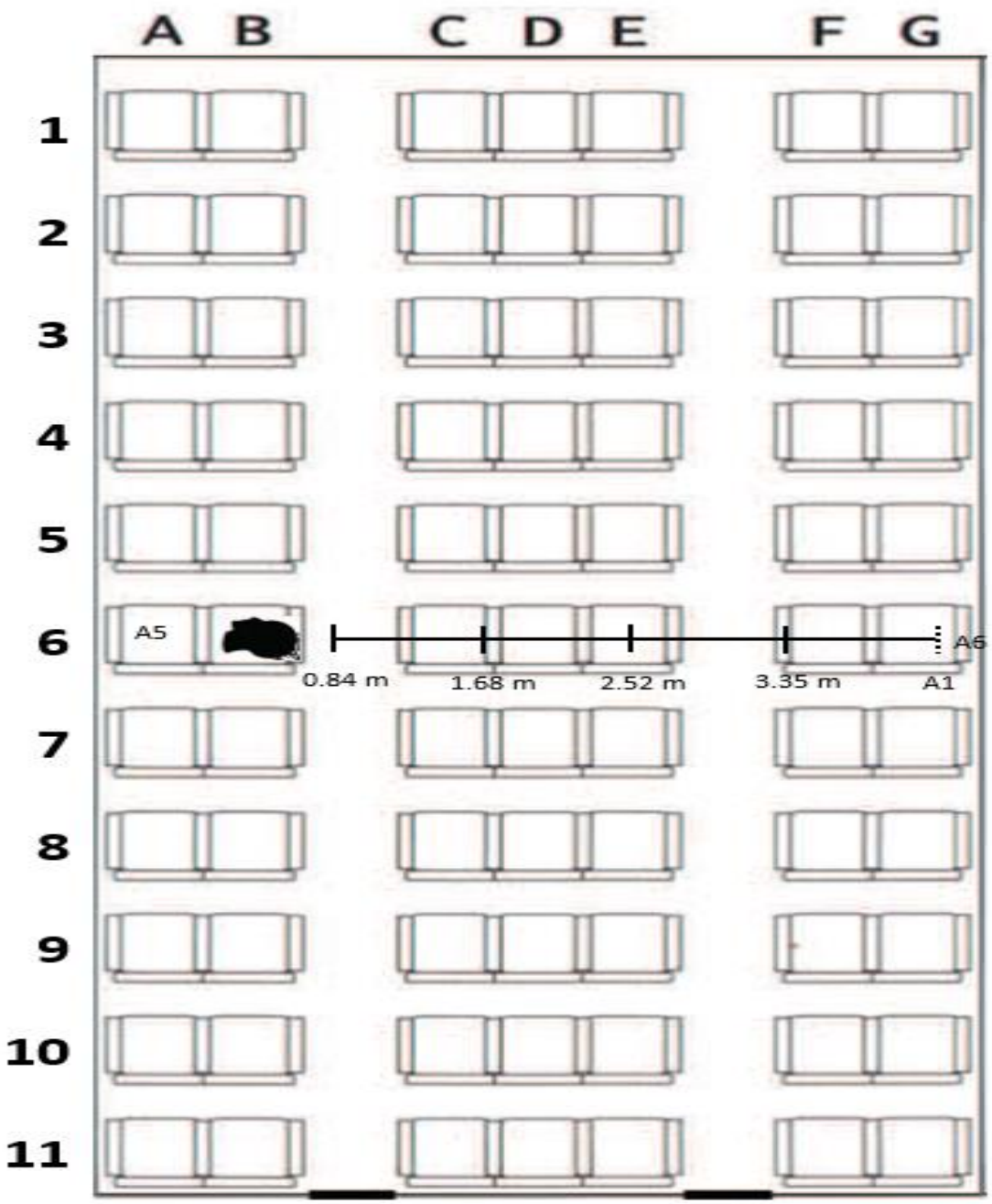

Figure H.81 Test 44 (B-M) ISOPass undeployed source location and sampling tree orientation.

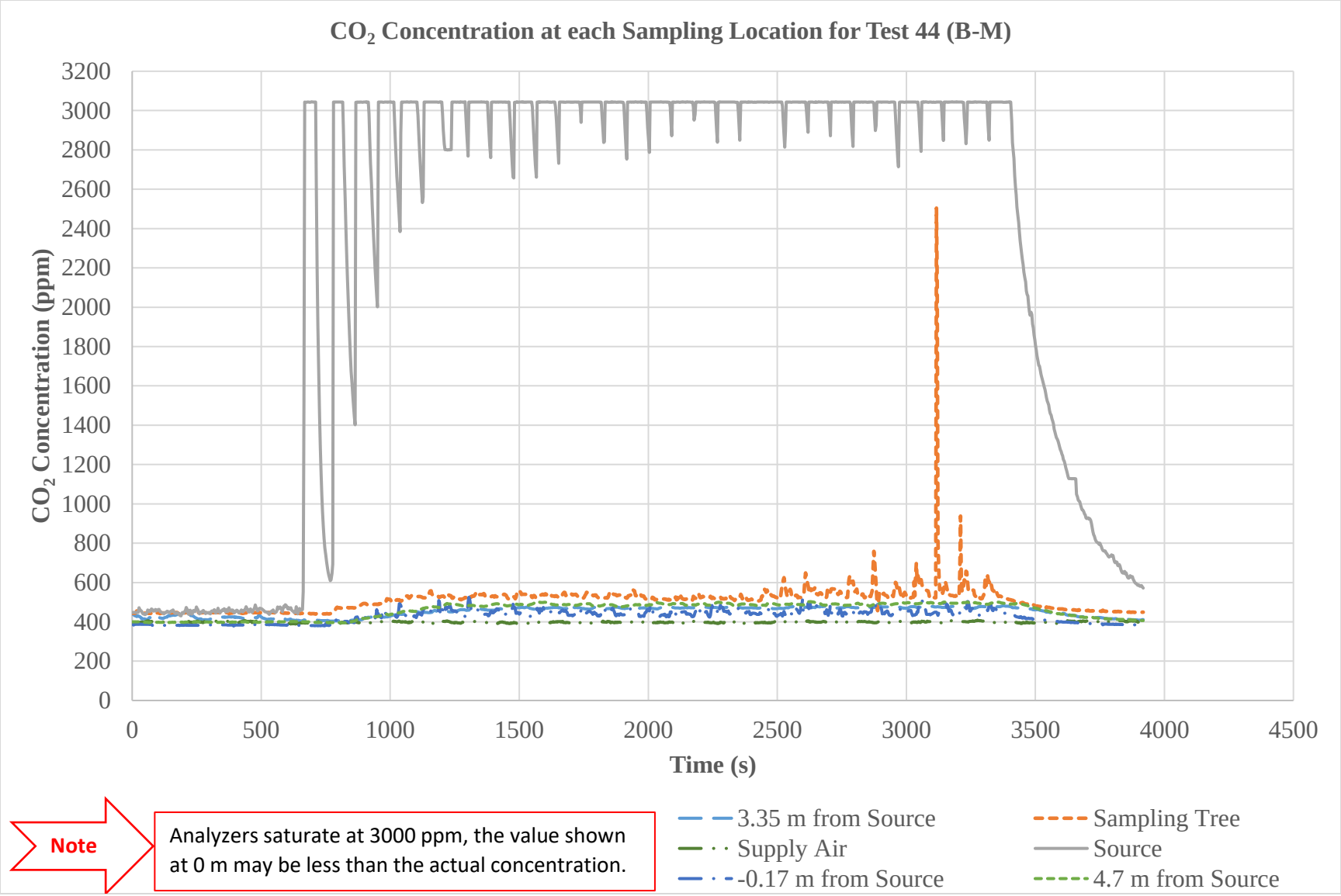

Figure H.82 Ininstantaneous CO_2 concentration at each sampling location for Test 44 (B-M) ISOPass undeployed.

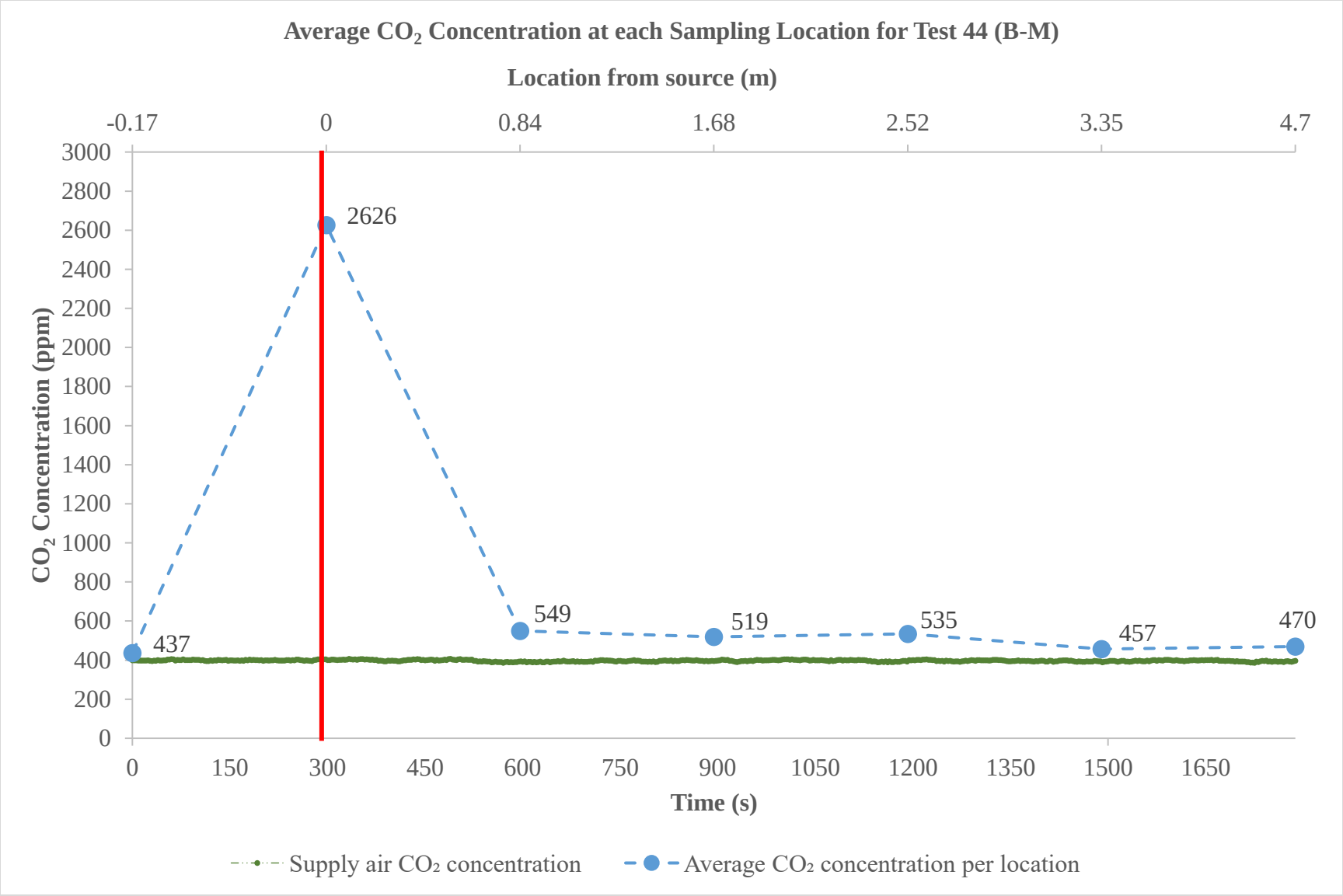

Figure H.83 Average CO_2 concentration at each sampling location for Test 44 (B-M) ISOPass undeployed.

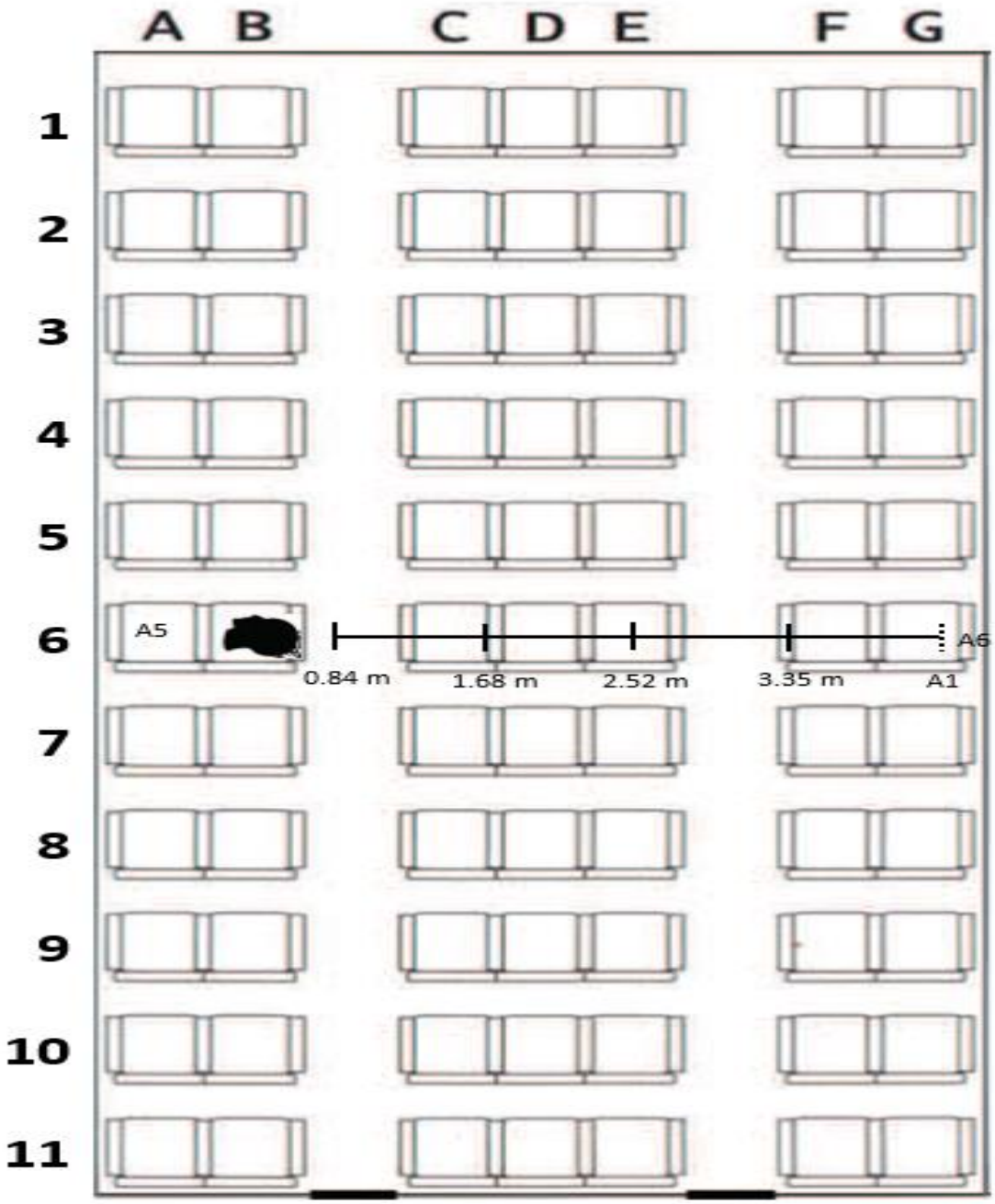

Figure H.84 Test 45 (B-M) ISOPass undeployed source location and sampling tree orientation.

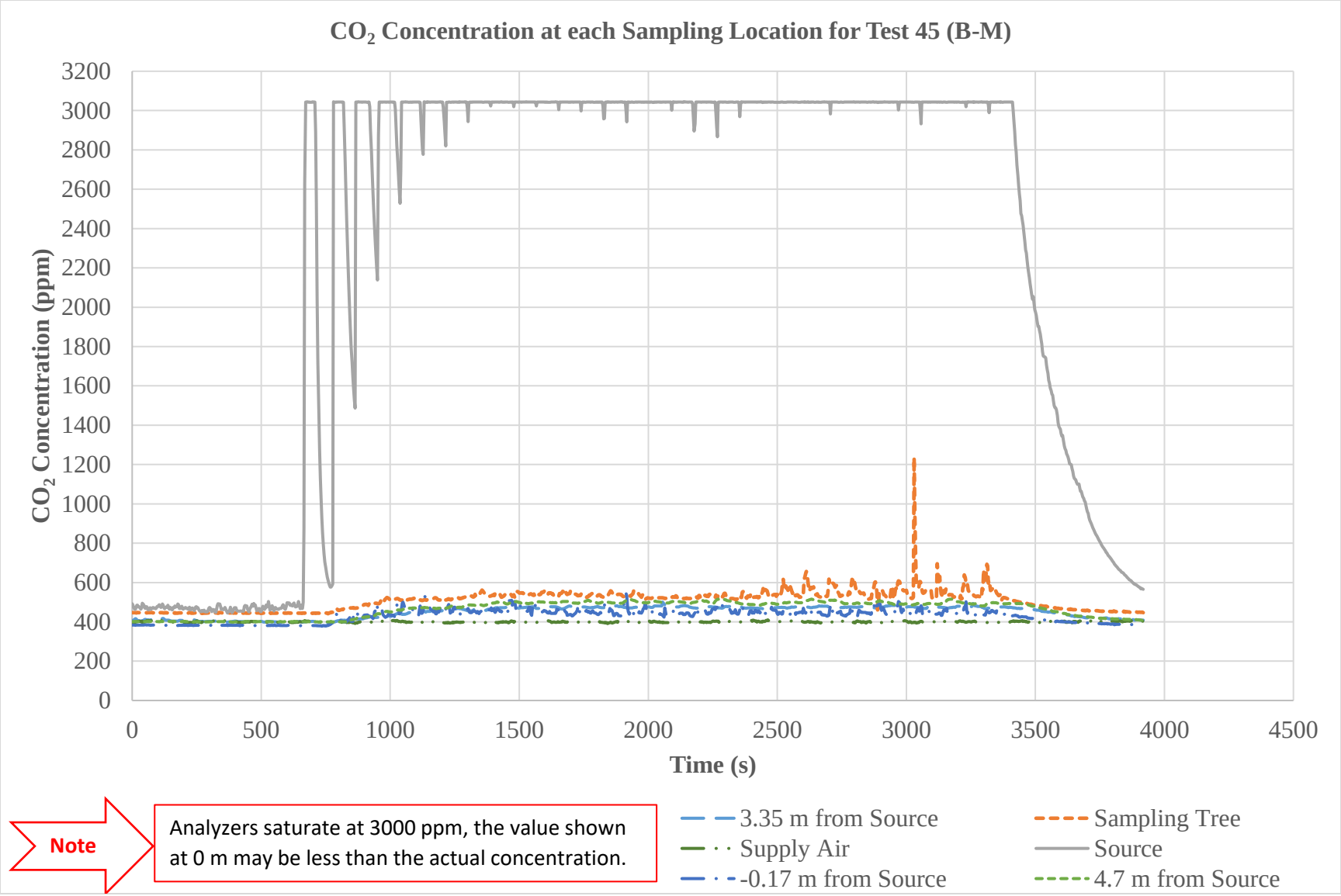

Figure H.85 Ininstantaneous CO_2 concentration at each sampling location for Test 45 (B-M) ISOPass undeployed.

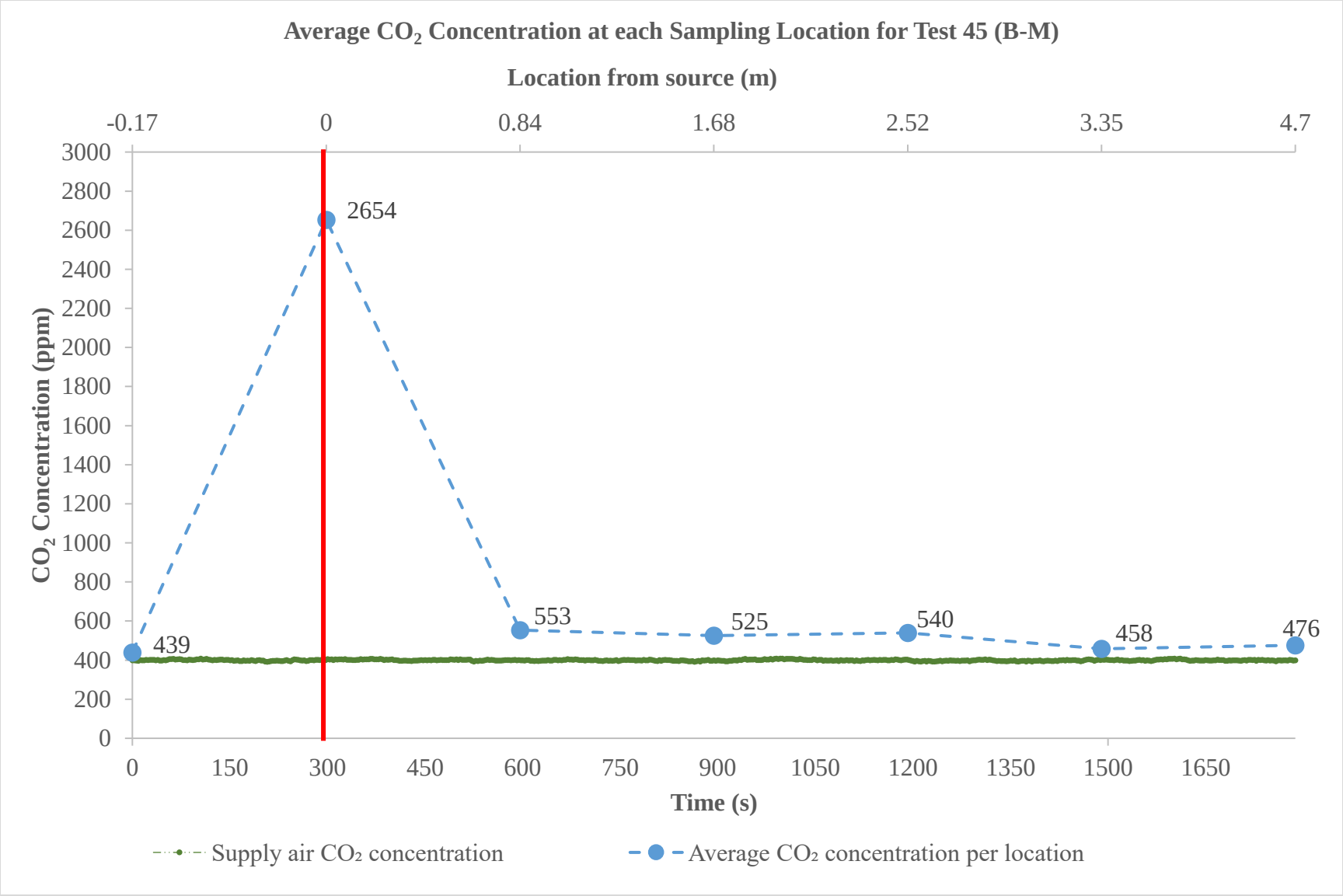

Figure H.86 Average CO_2 concentration at each sampling location for Test 45 (B-M) ISOPass undeployed.

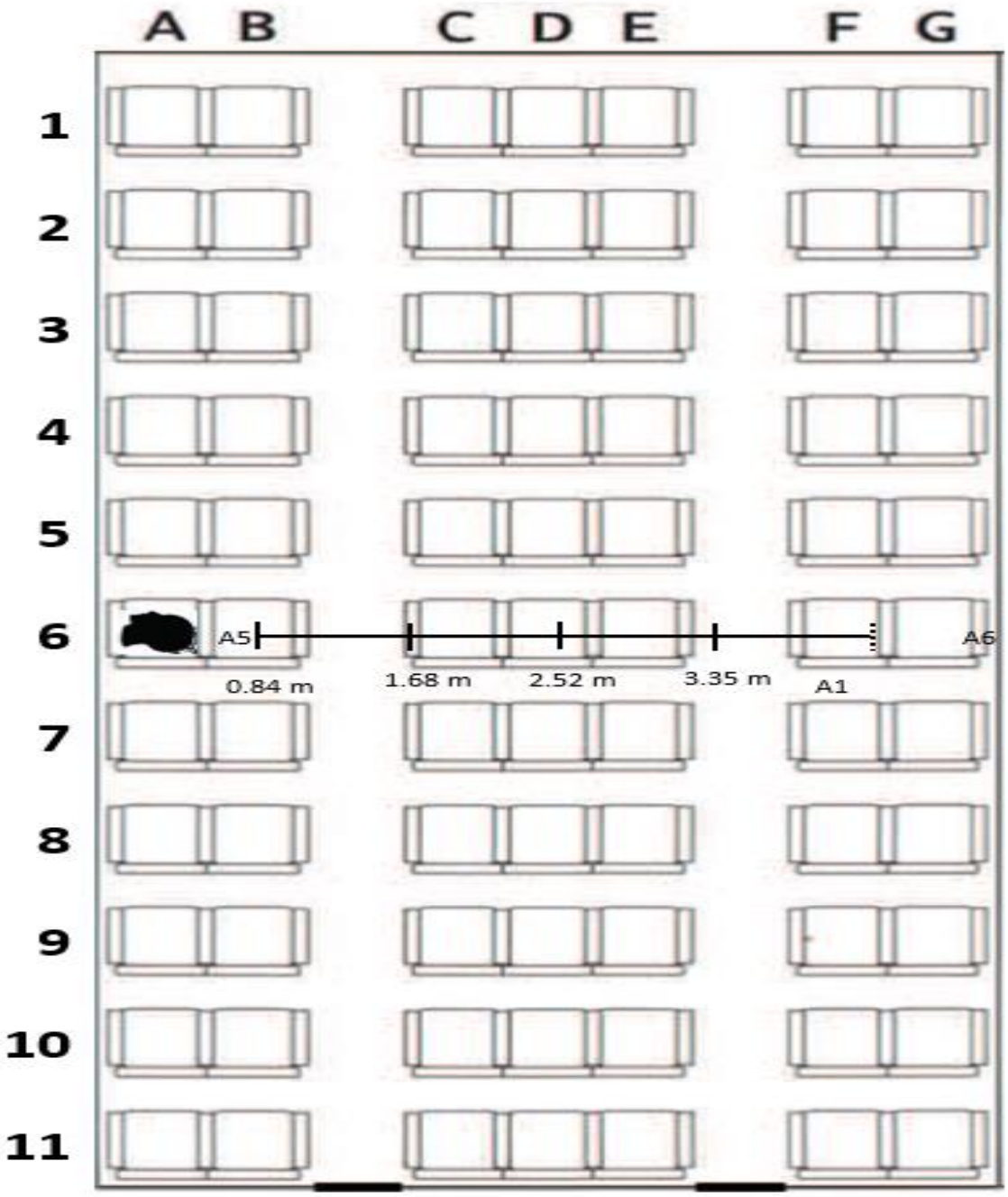

Figure H.87 Test 46 (B-M) ISOPass undeployed source location and sampling tree orientation.

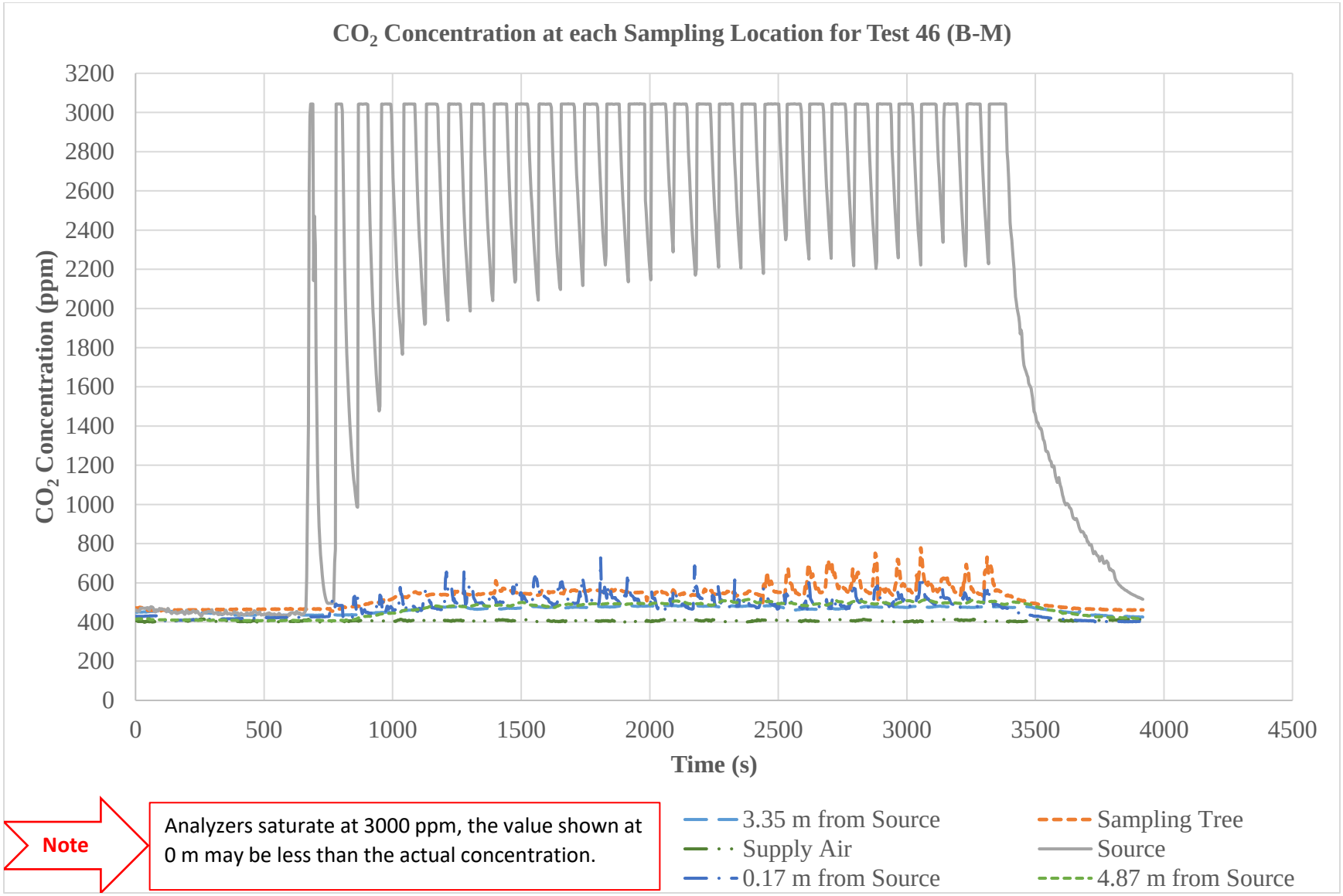

Figure H.88 Ininstantaneous CO_2 concentration at each sampling location for Test 46 (B-M) ISOPass undeployed.

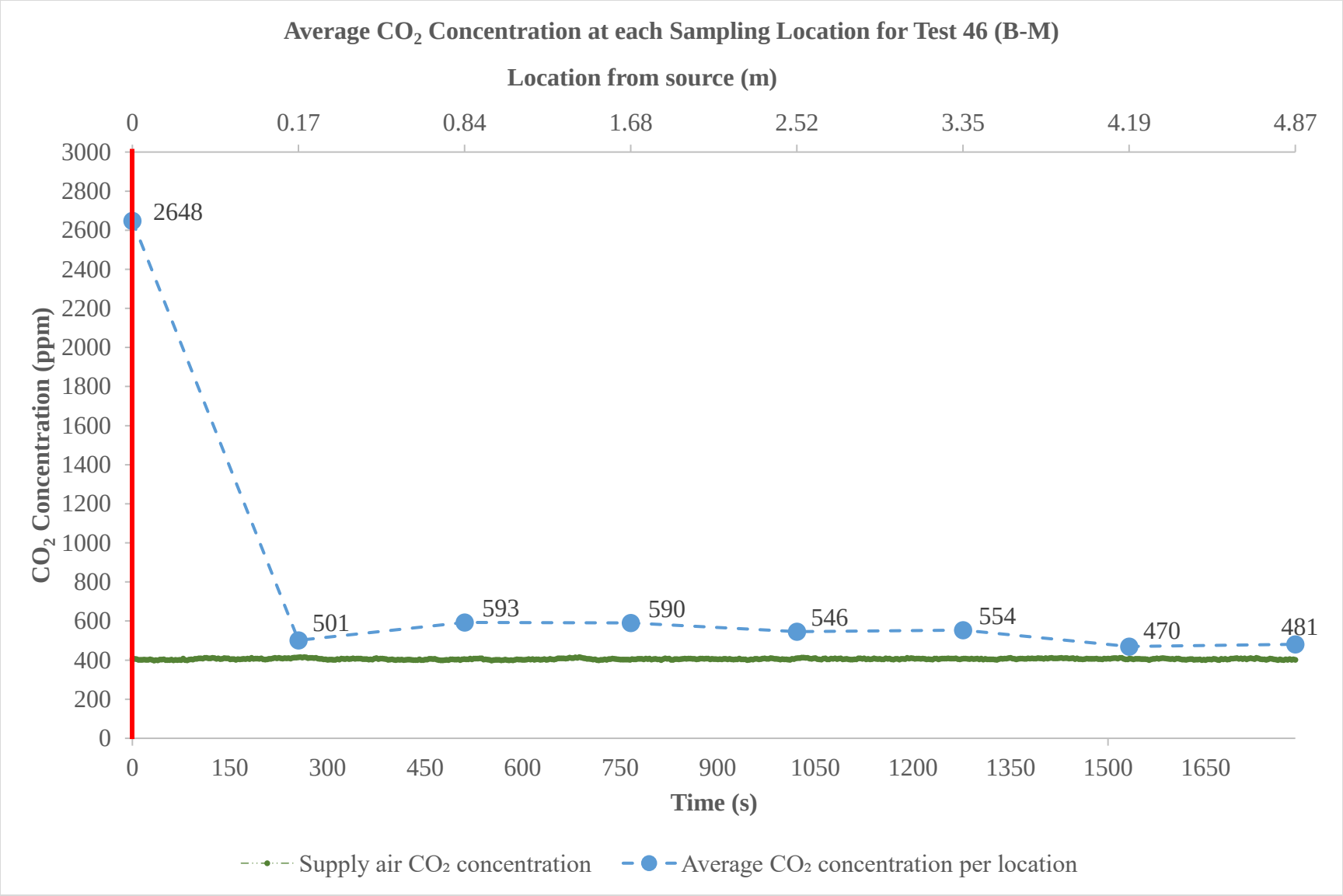

Figure H.89 Average CO_2 concentration at each sampling location for Test 46 (B-M) ISOPass undeployed.

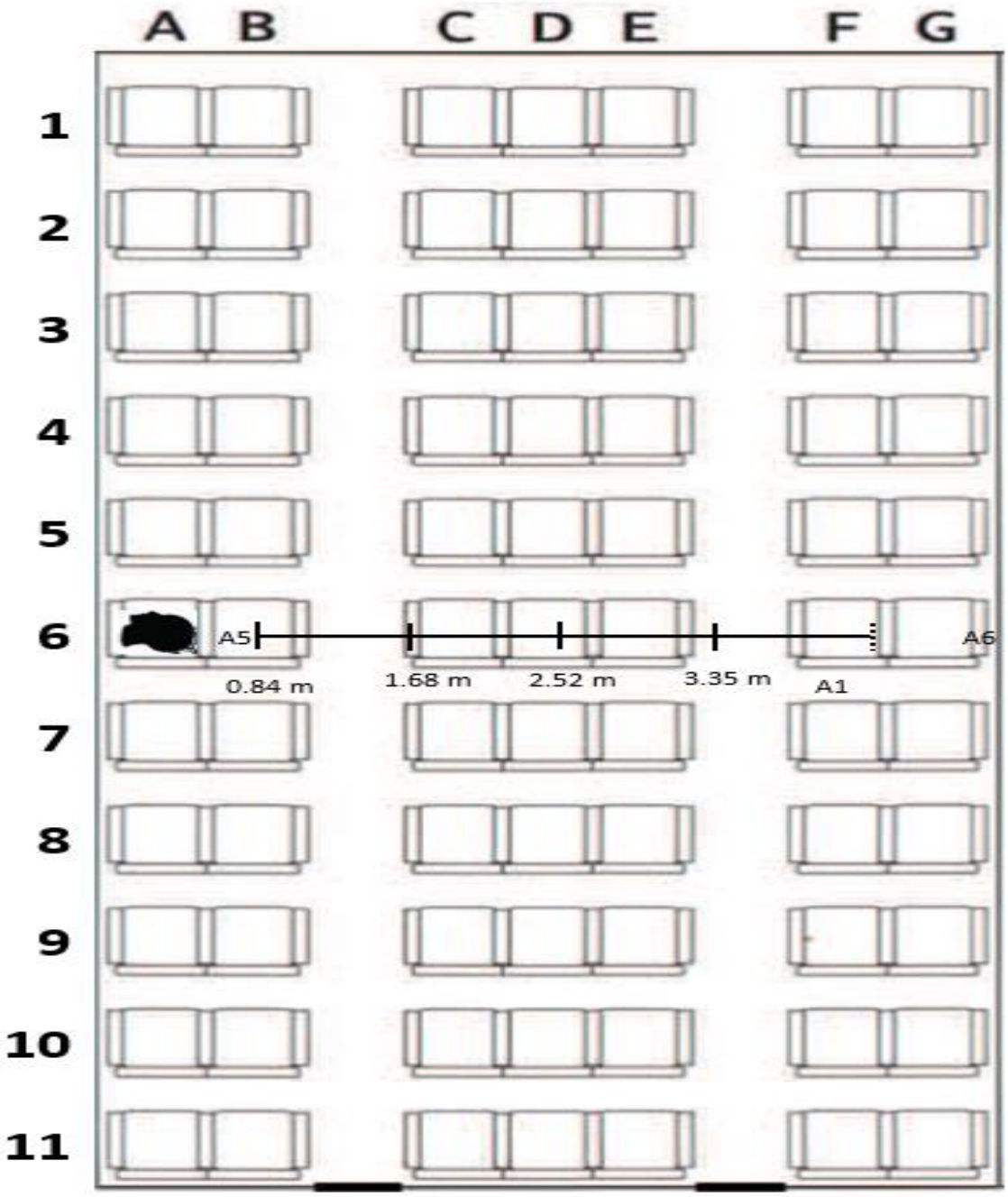

Figure H.90 Test 47 (B-M) ISOPass undeployed source location and sampling tree orientation.

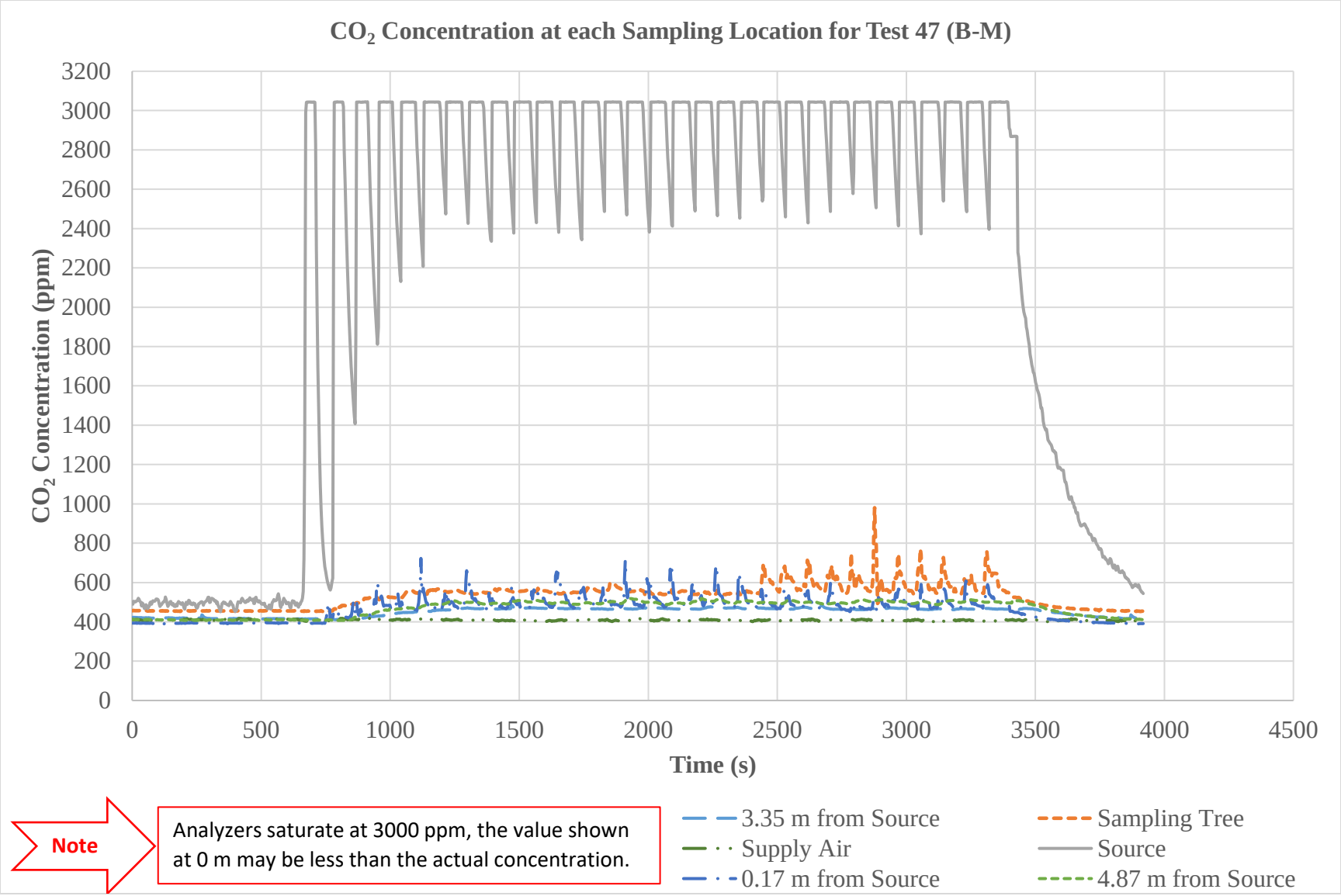

Figure H.91 Ininstantaneous CO_2 concentration at each sampling location for Test 47 (B-M) ISOPass undeployed.

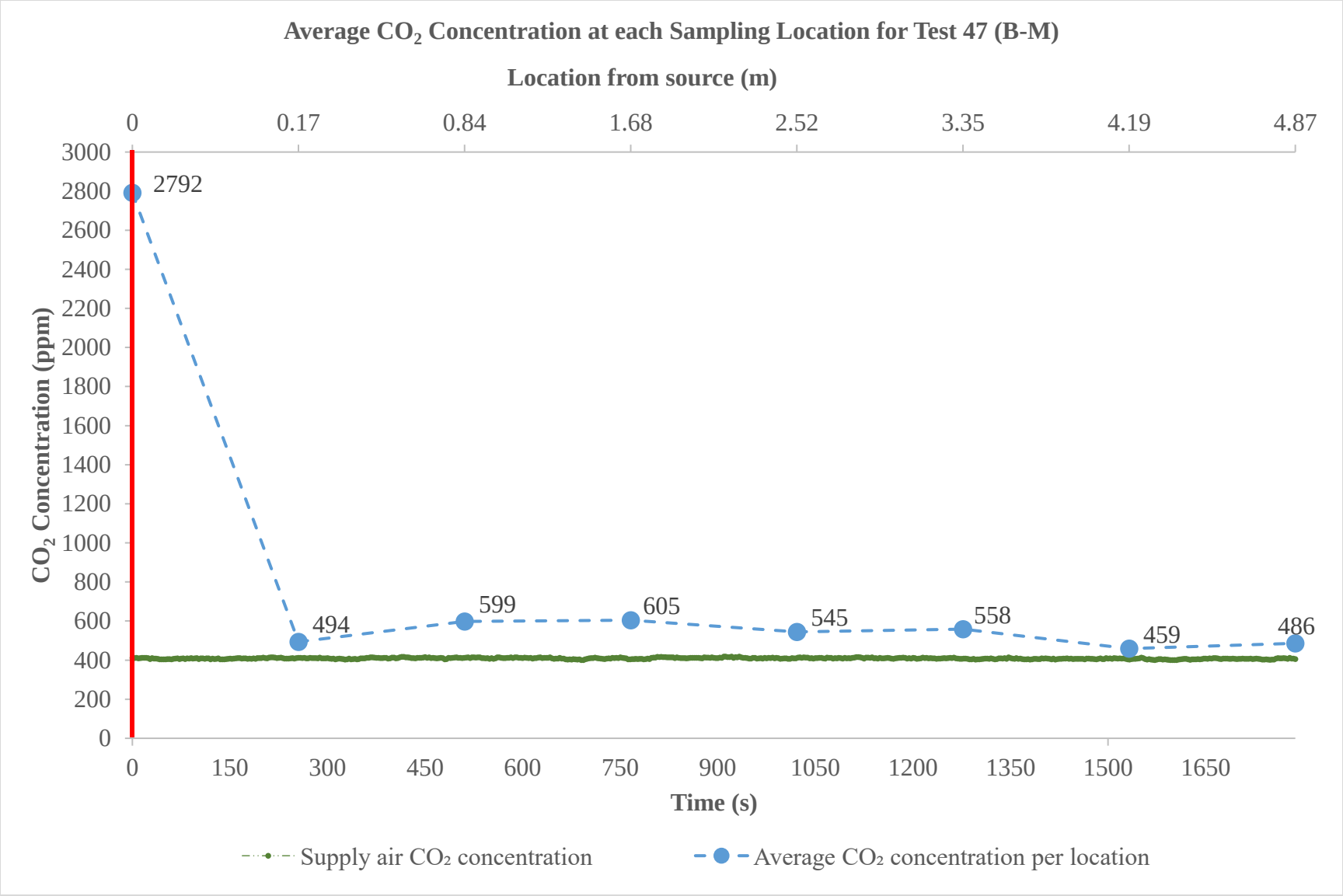

Figure H.92 Average CO_2 concentration at each sampling location for Test 47 (B-M) ISOPass undeployed.

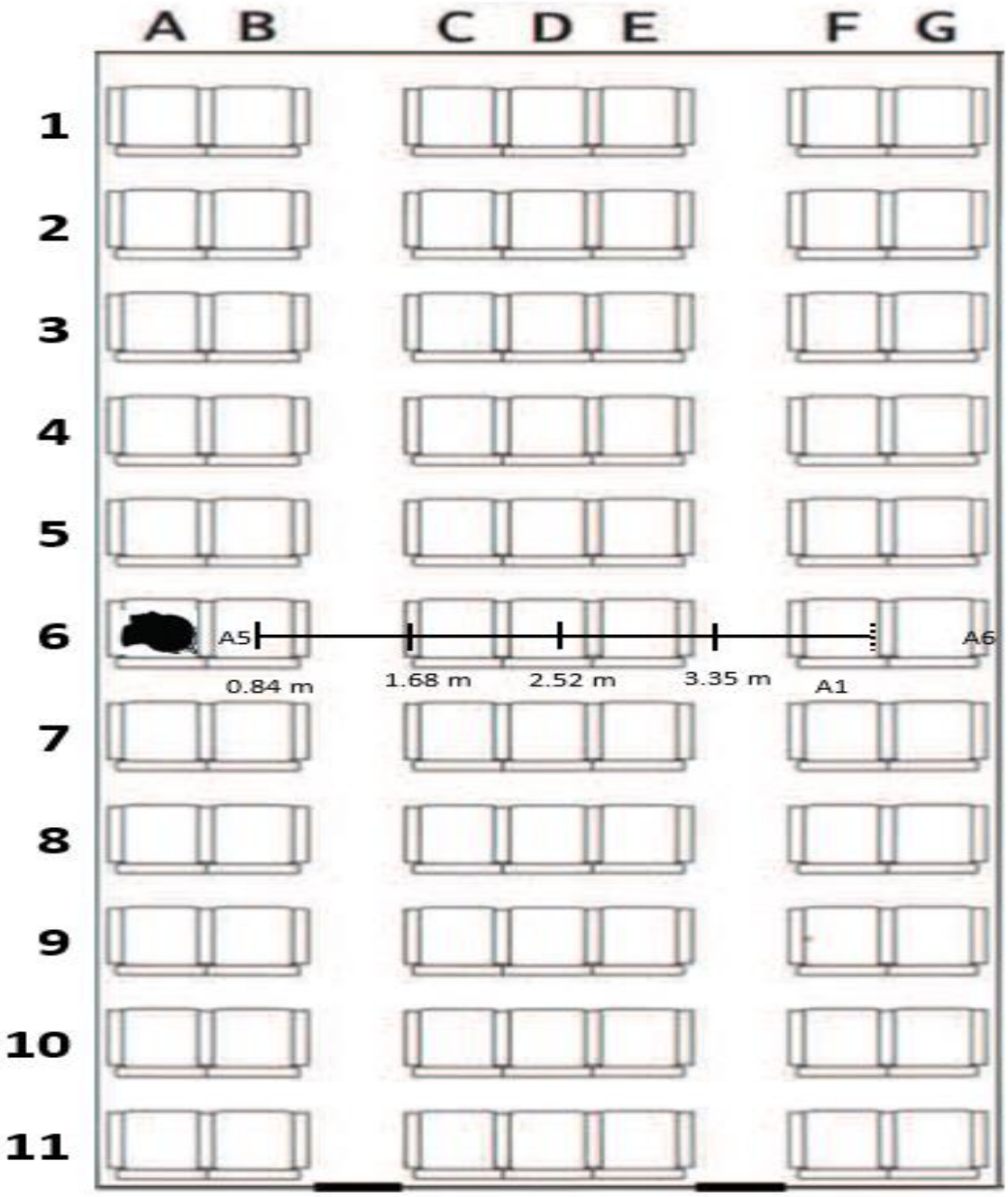

Figure H.93 Test 48 (B-M) ISOPass undeployed source location and sampling tree orientation.

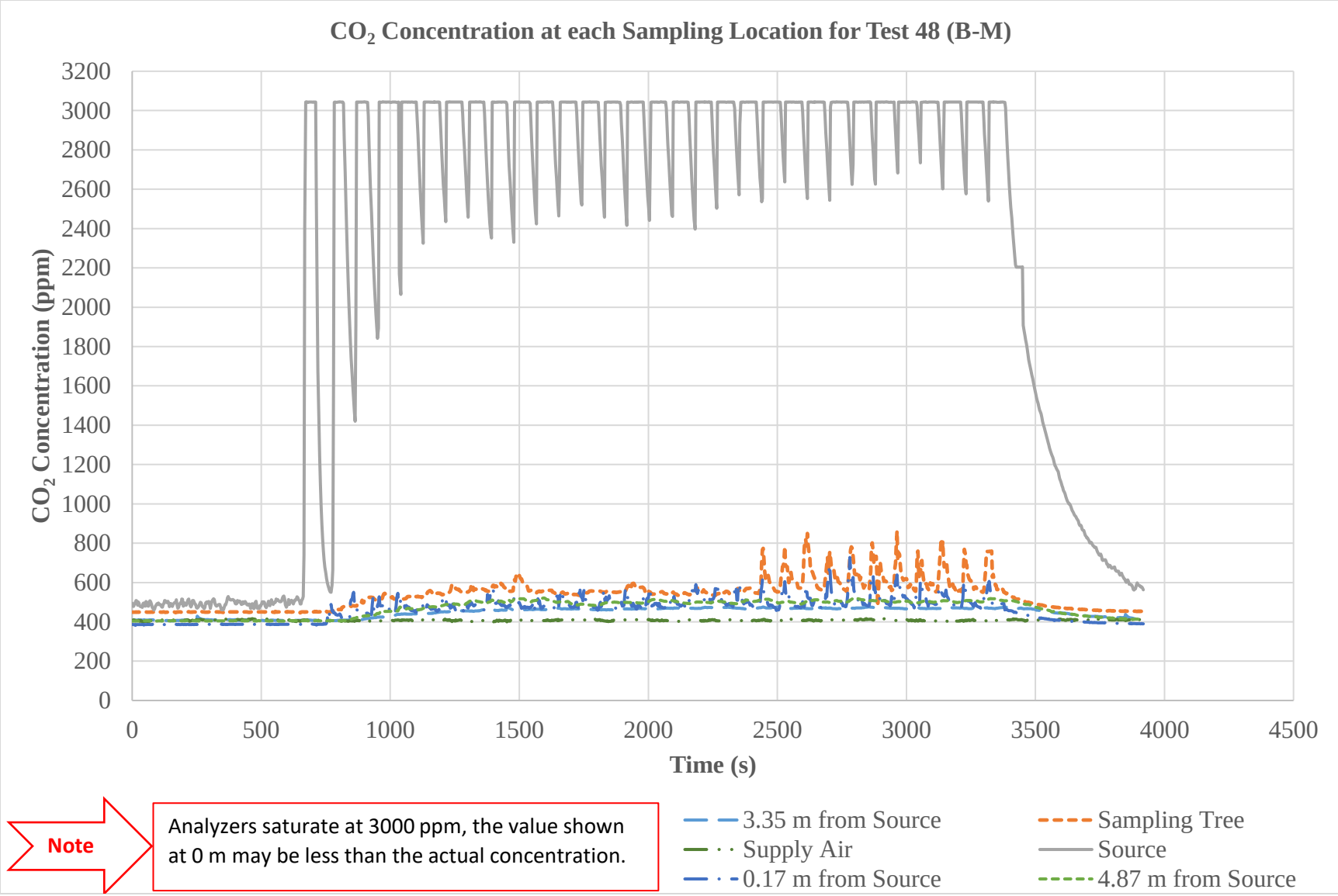

Figure H.94 Ininstantaneous CO_2 concentration at each sampling location for Test 48 (B-M) ISOPass undeployed.

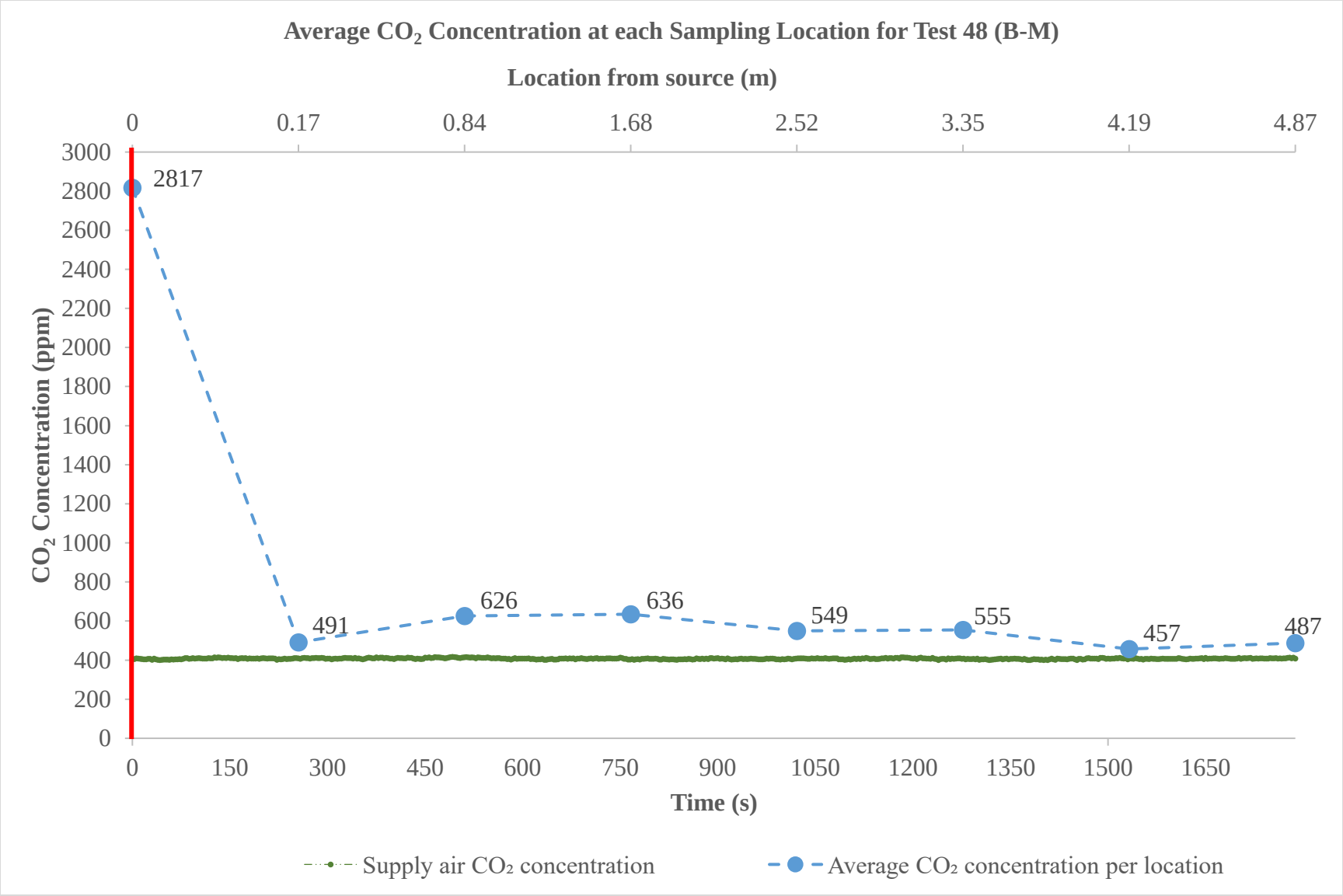

Figure H.95 Average CO_2 concentration at each sampling location for Test 48 (B-M) ISOPass undeployed.

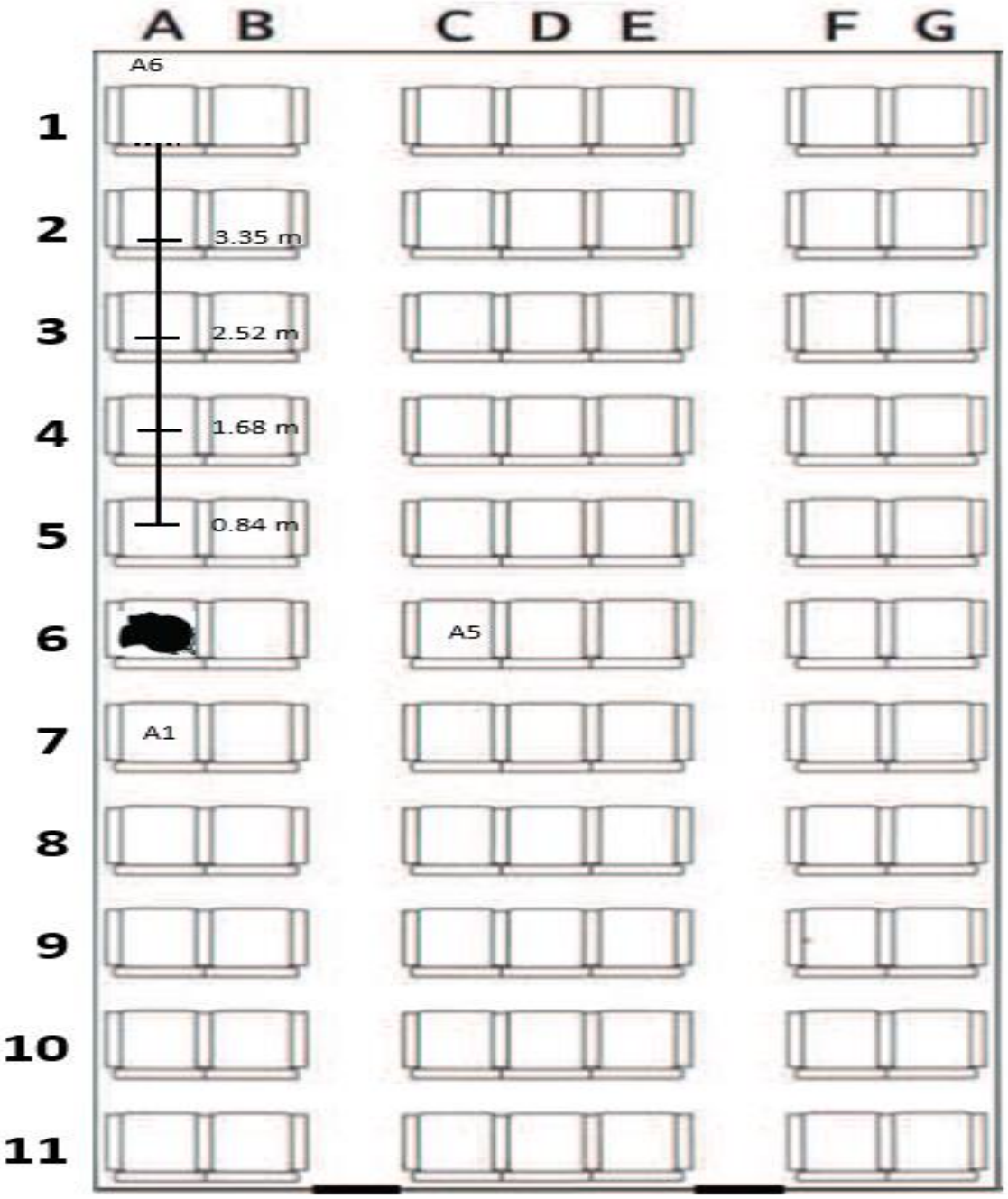

Figure H.96 Test 67 (B-M) ISOPass undeployed source location and sampling tree orientation.

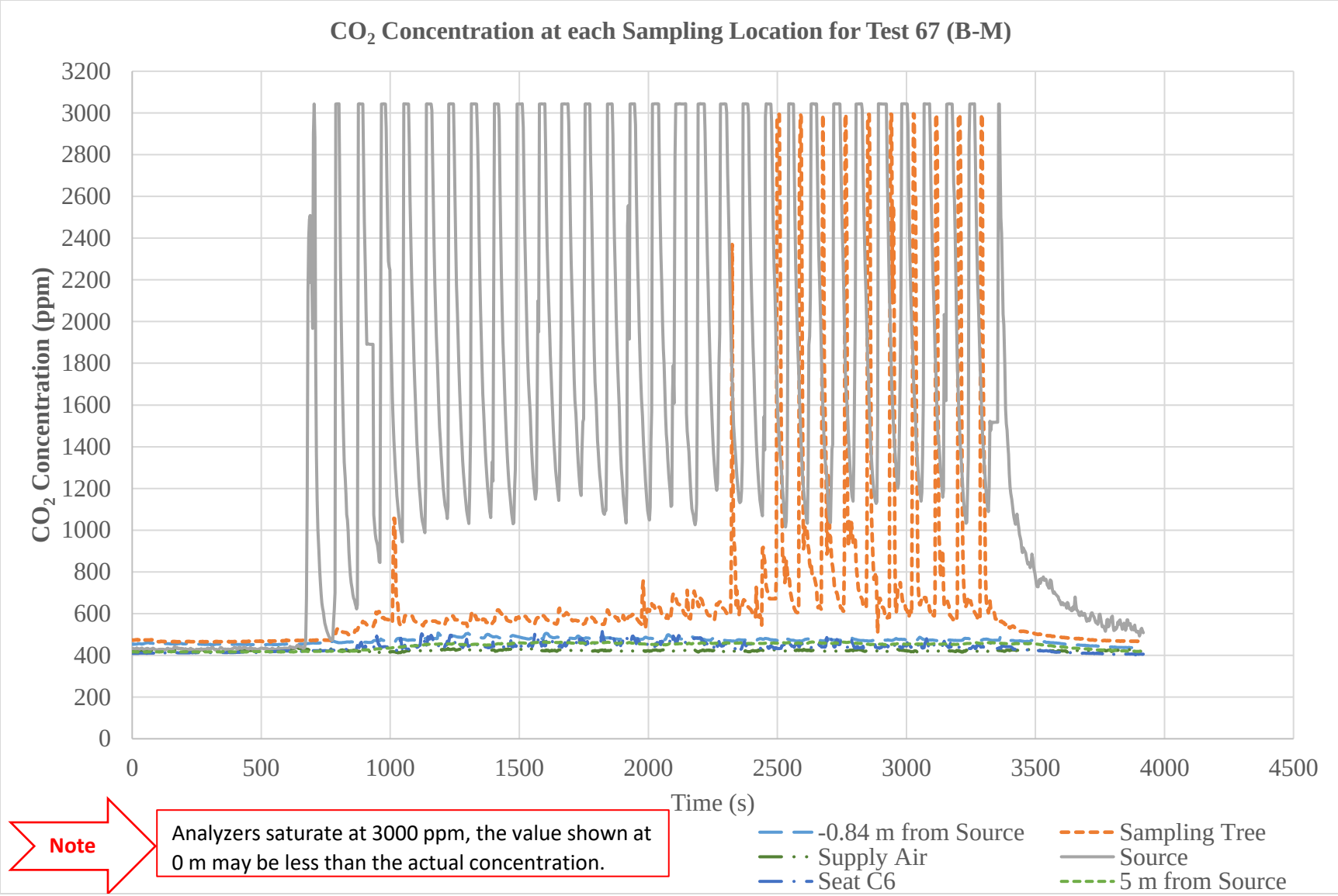

Figure H.97 Ininstantaneous CO_2 concentration at each sampling location for Test 67 (B-M) ISOPass undeployed.

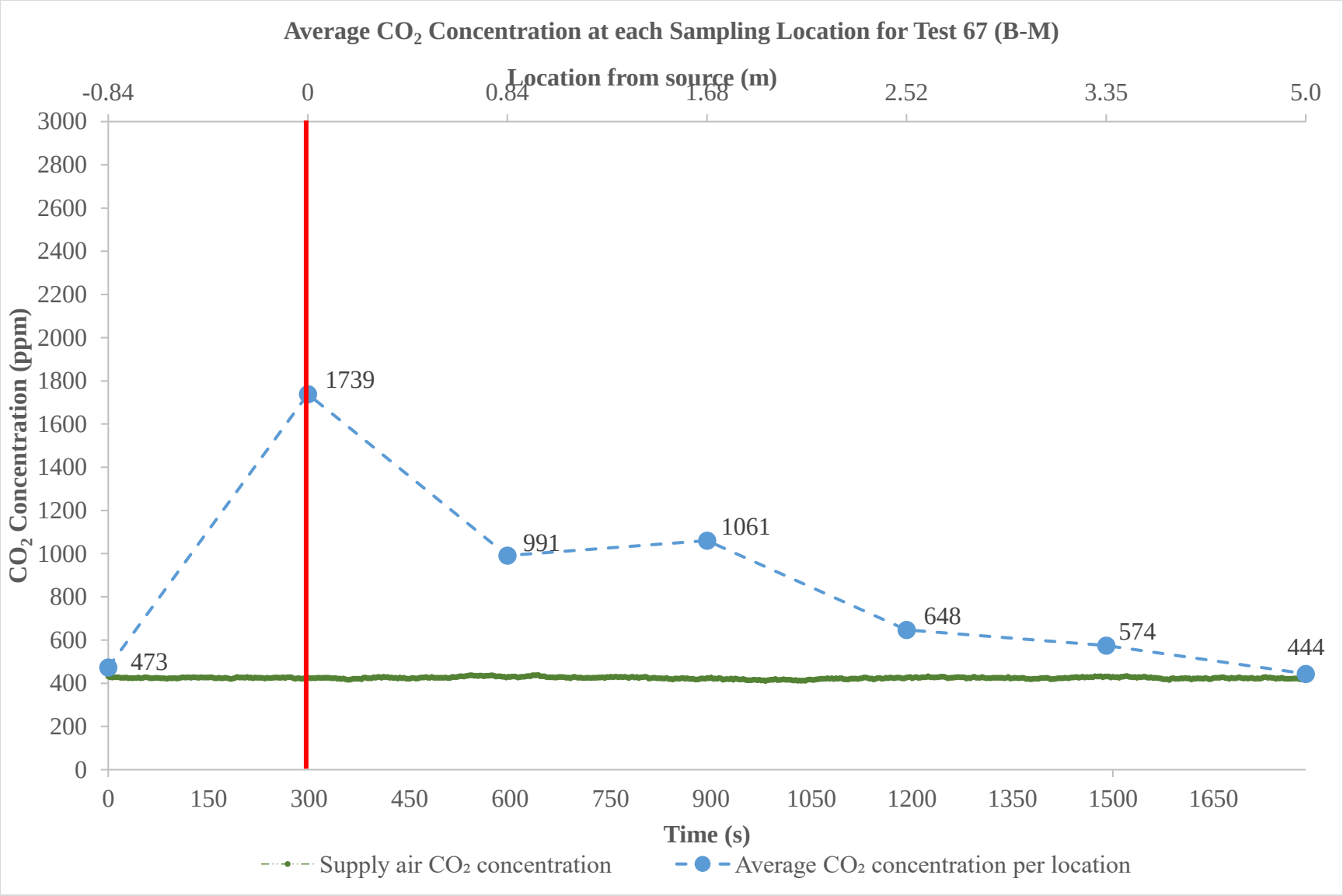

Figure H.98 Average CO_2 concentration at each sampling location for Test 67 (B-M) ISOPass undeployed.

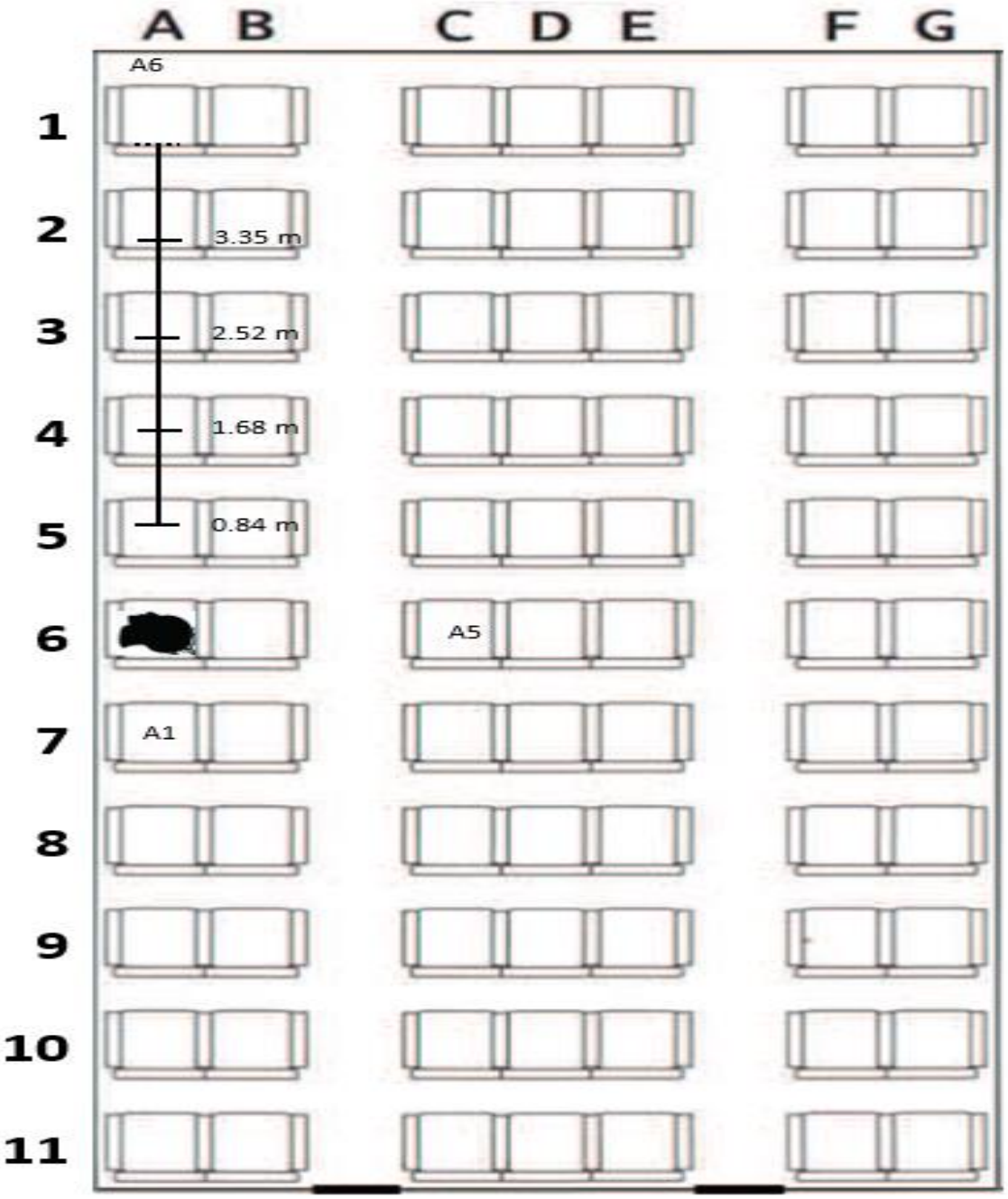

Figure H.99 Test 68 (B-M) ISOPass undeployed source location and sampling tree orientation.

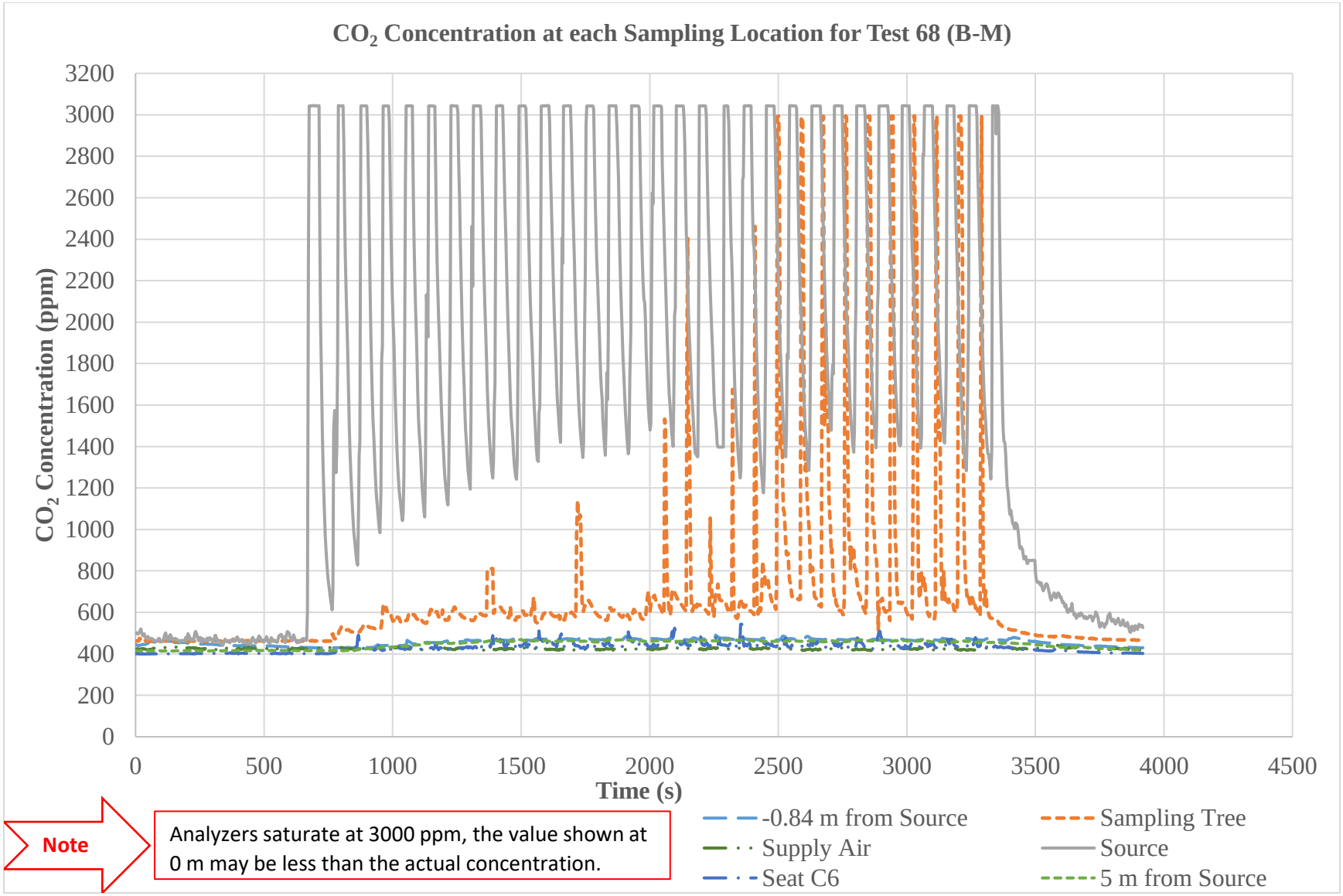

Figure H.100 Ininstantaneous CO_2 concentration at each sampling location for Test 68 (B-M) ISOPass undeployed.

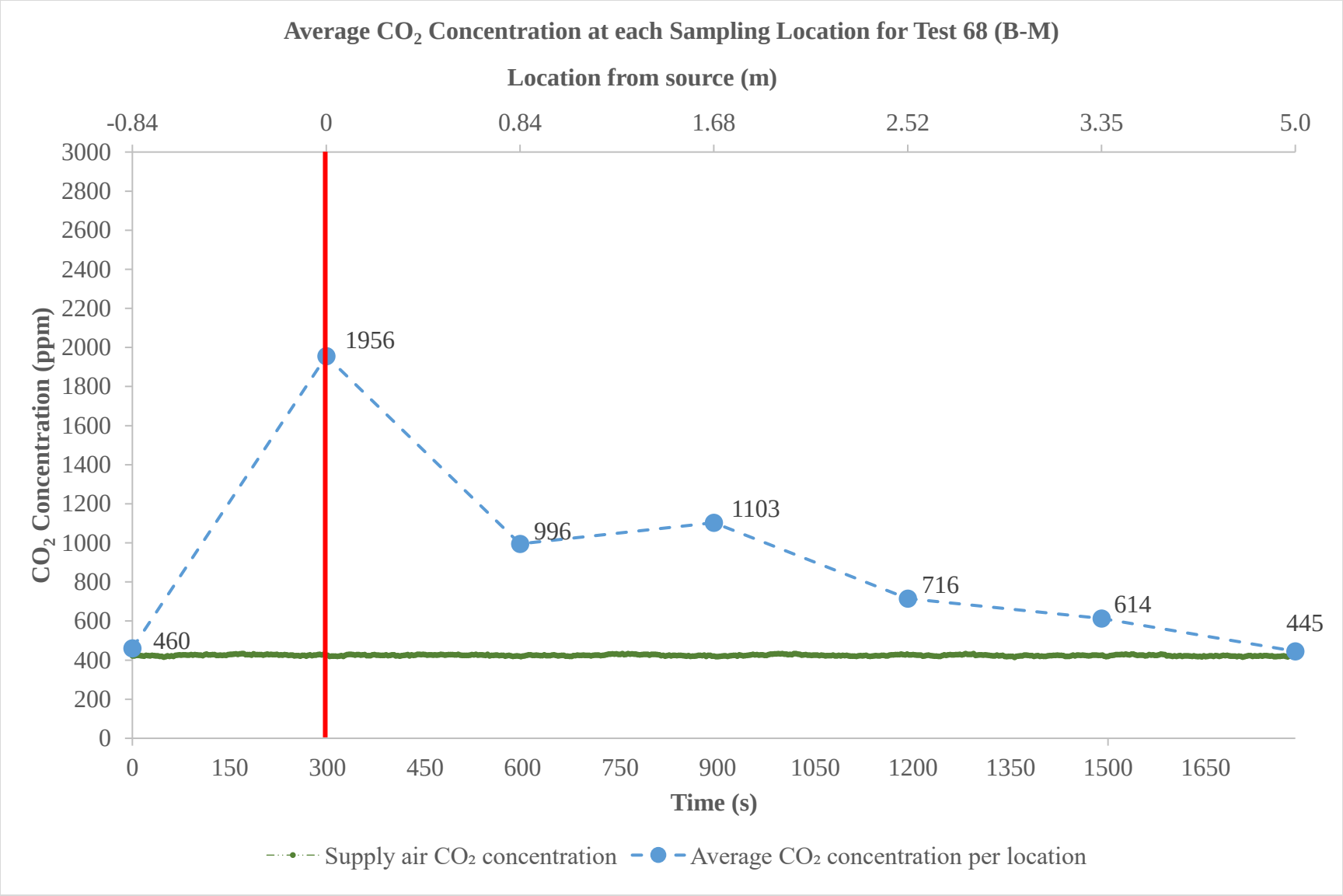

Figure H.101 Average CO_2 concentration at each sampling location for Test 68 (B-M) ISOPass undeployed.

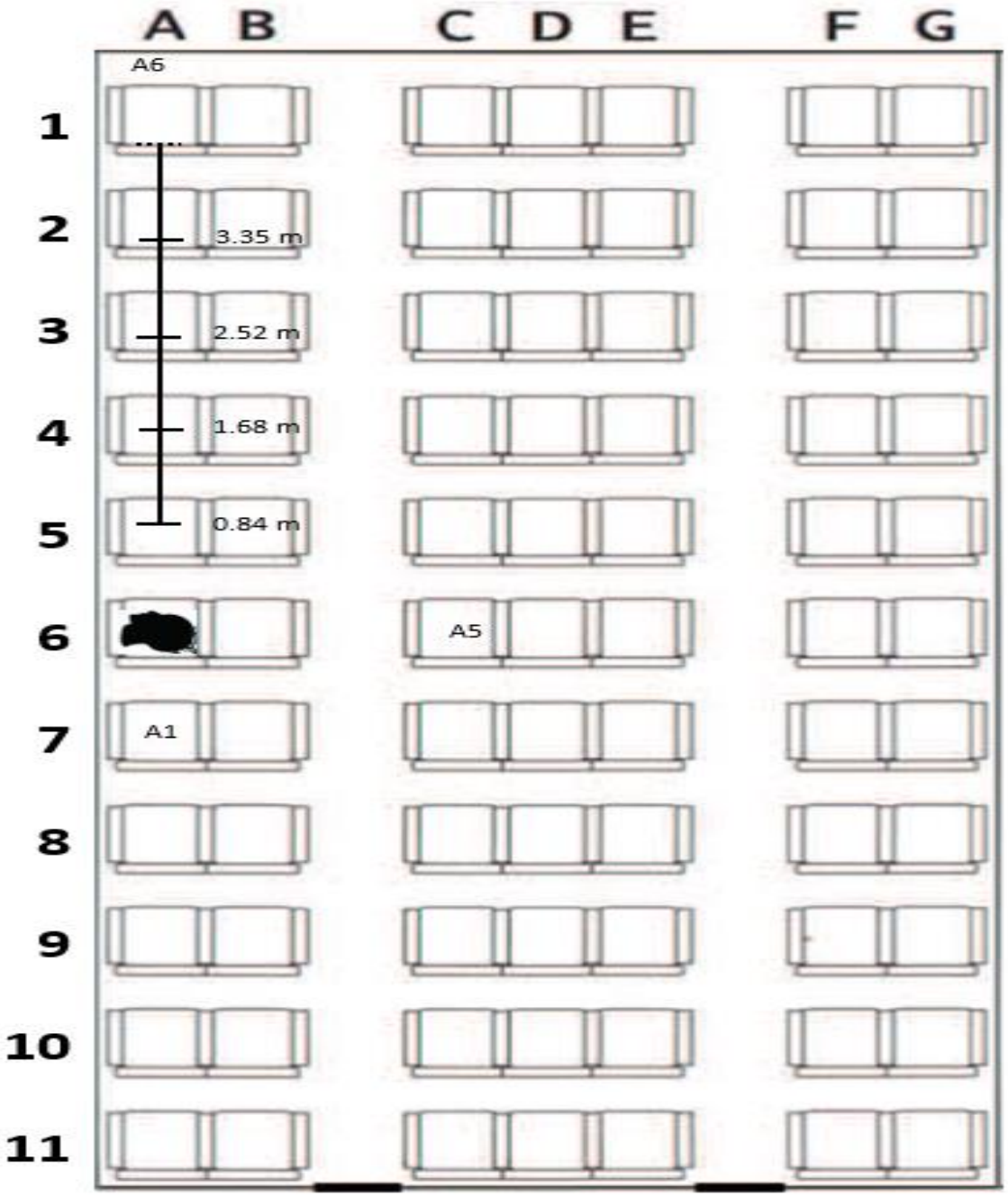

Figure H.102 Test 69 (B-M) ISOPass undeployed source location and sampling tree orientation.

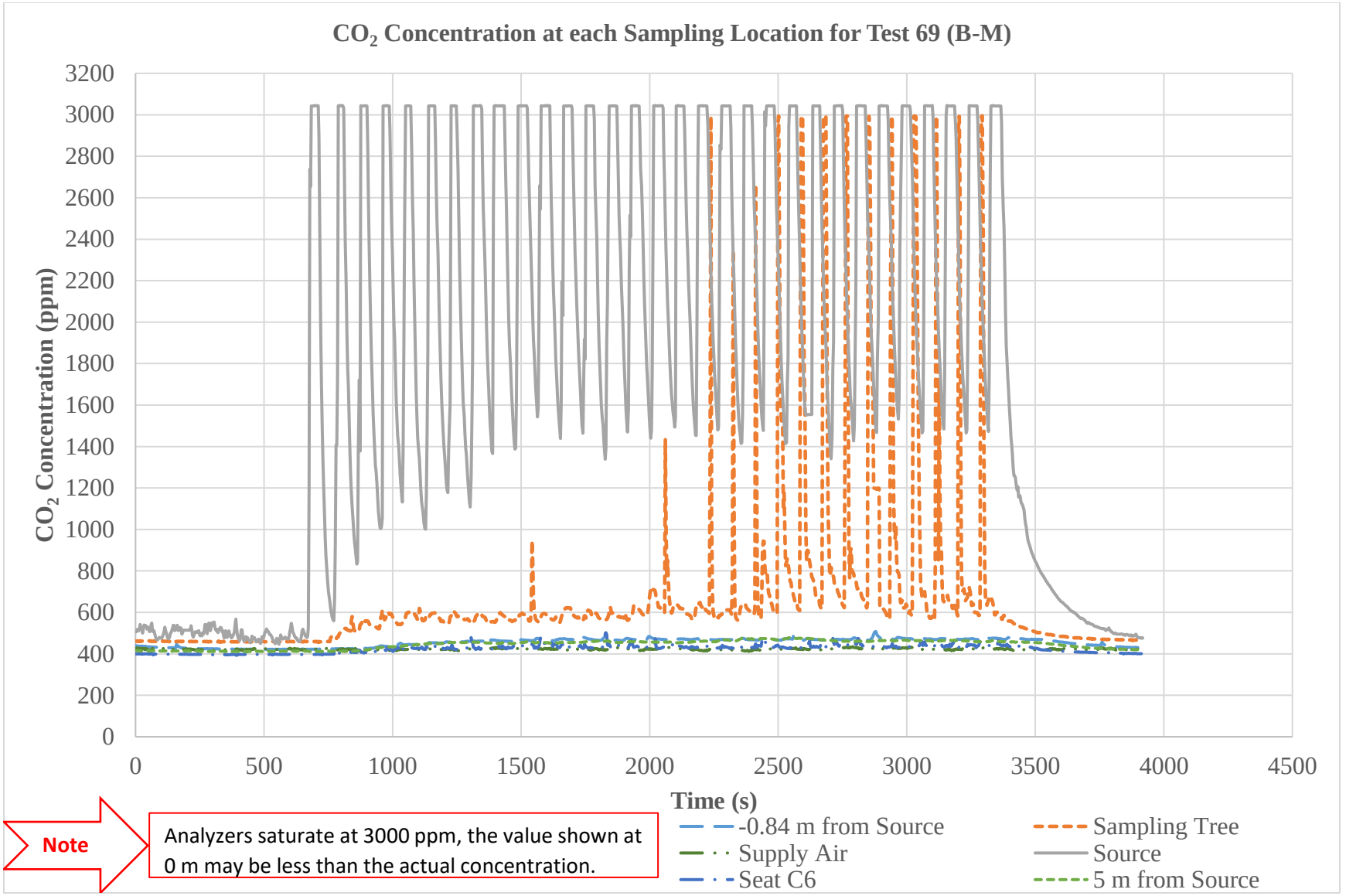

Figure H.103 Ininstantaneous CO_2 concentration at each sampling location for Test 69 (B-M) ISOPass undeployed.

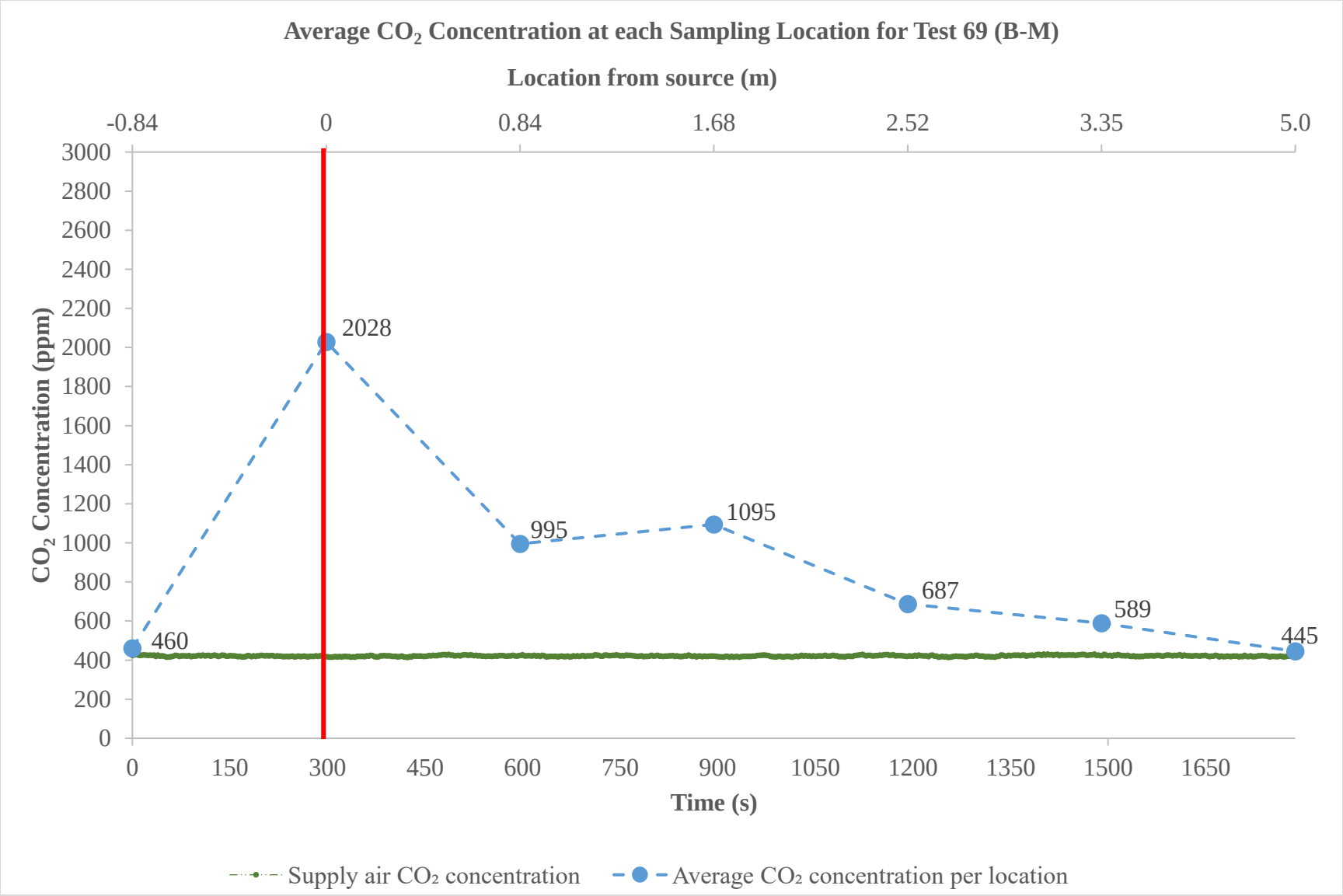

Figure H.104 Average CO_2 concentration at each sampling location for Test 69 (B-M) ISOPass undeployed.

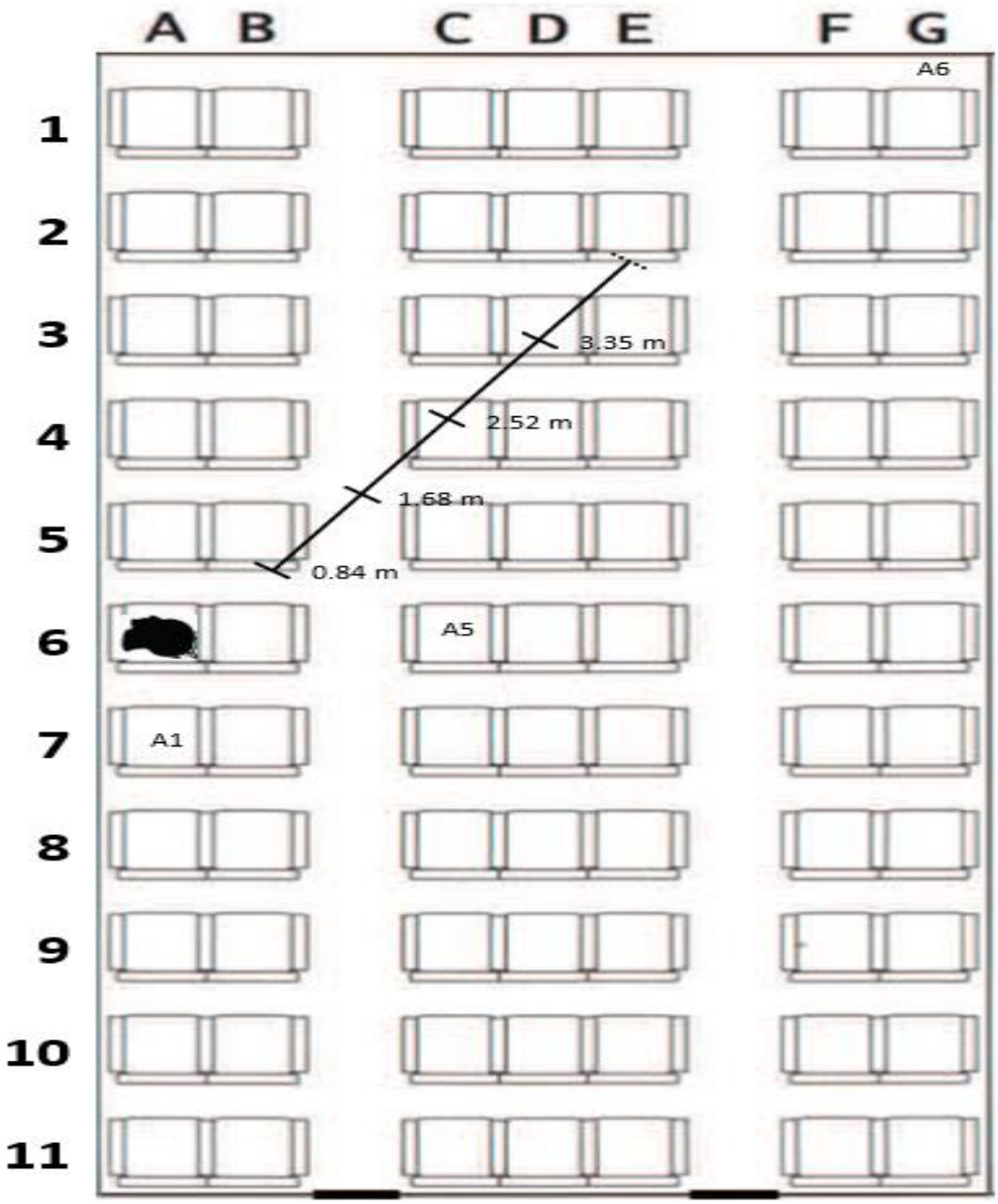

Figure H.105 Test 70 (B-M) ISOPass undeployed source location and sampling tree orientation.

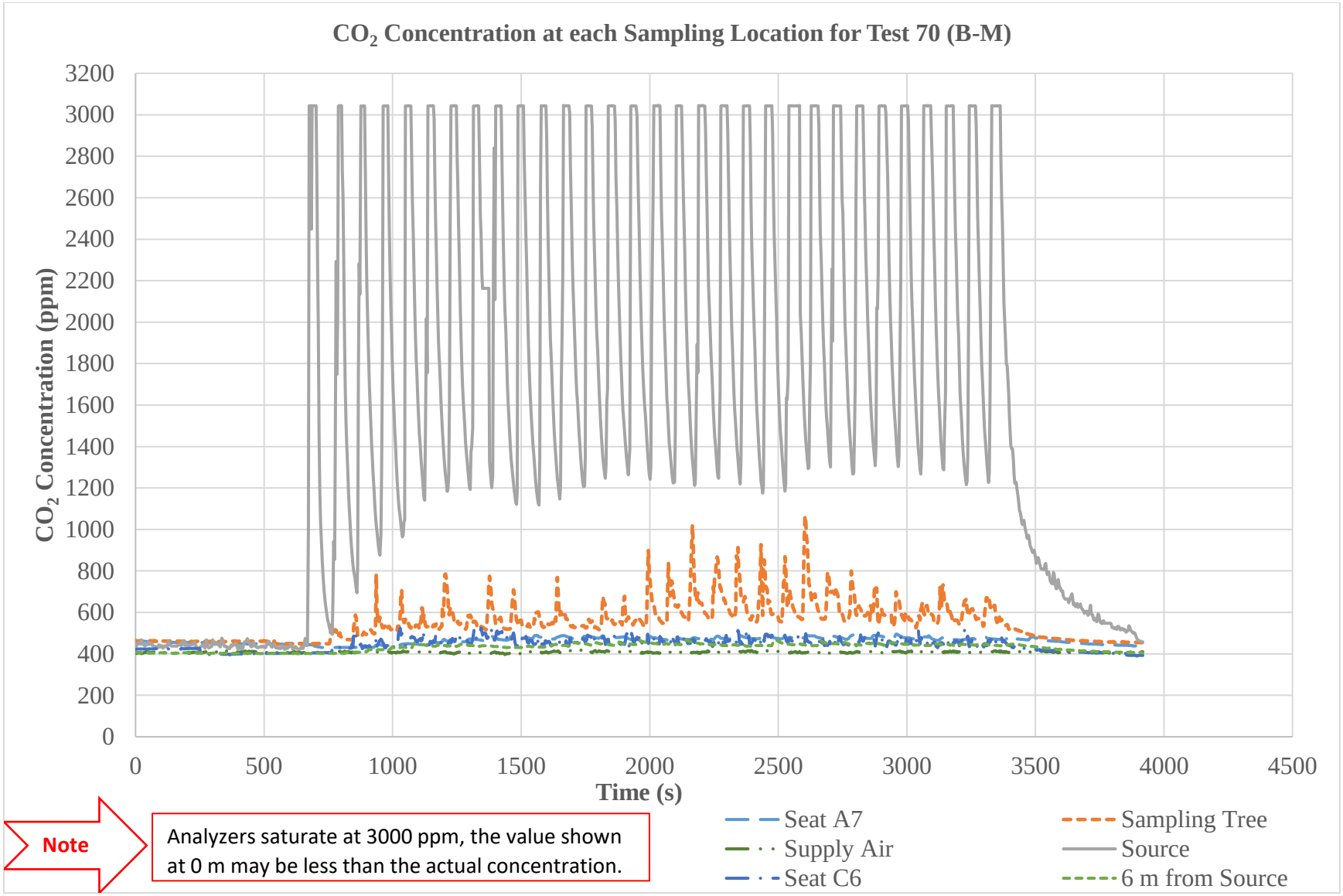

Figure H.106 Ininstantaneous CO_2 concentration at each sampling location for Test 70 (B-M) ISOPass undeployed.

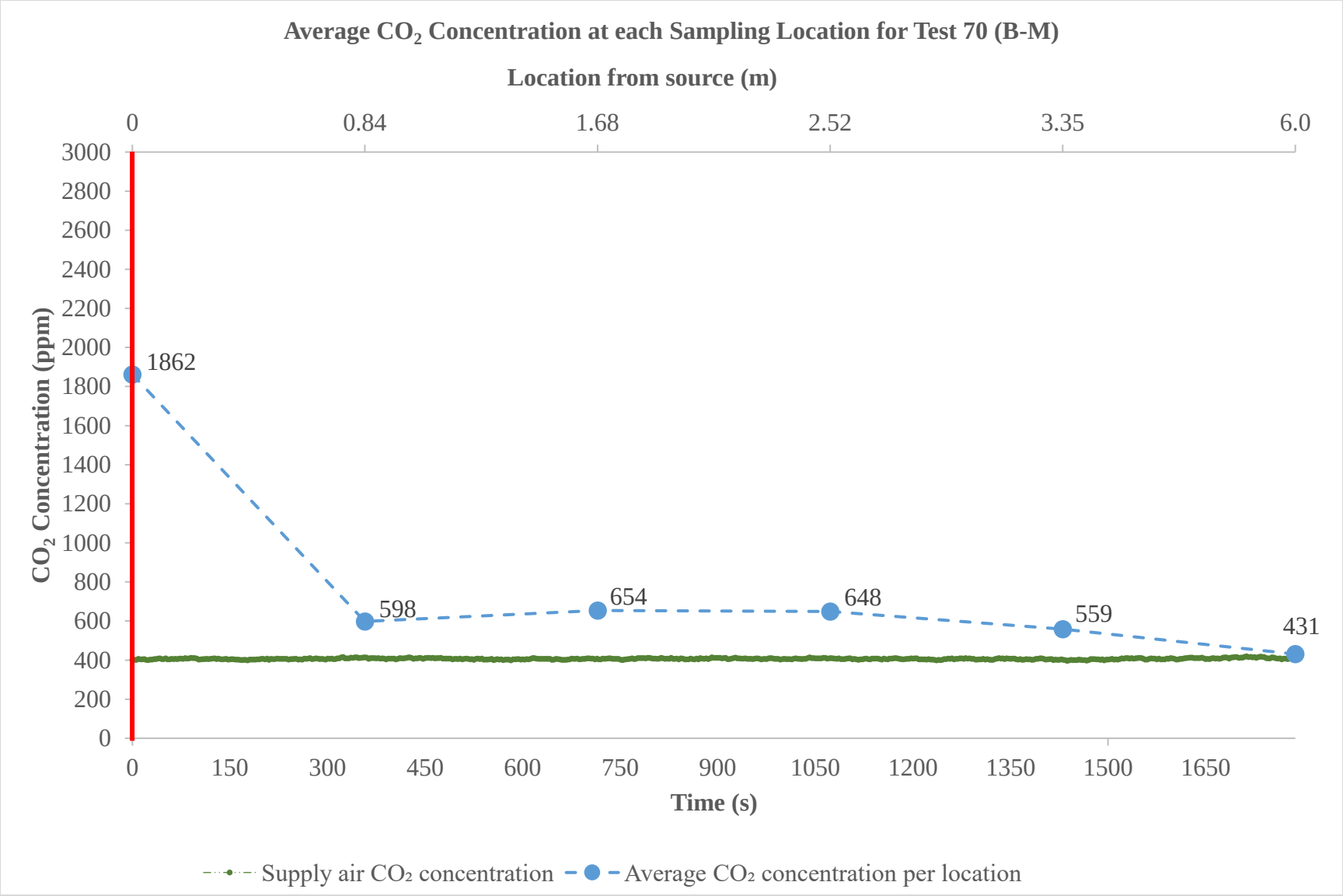

Figure H.107 Average CO_2 concentration at each sampling location for Test 70 (B-M) ISOPass undeployed.

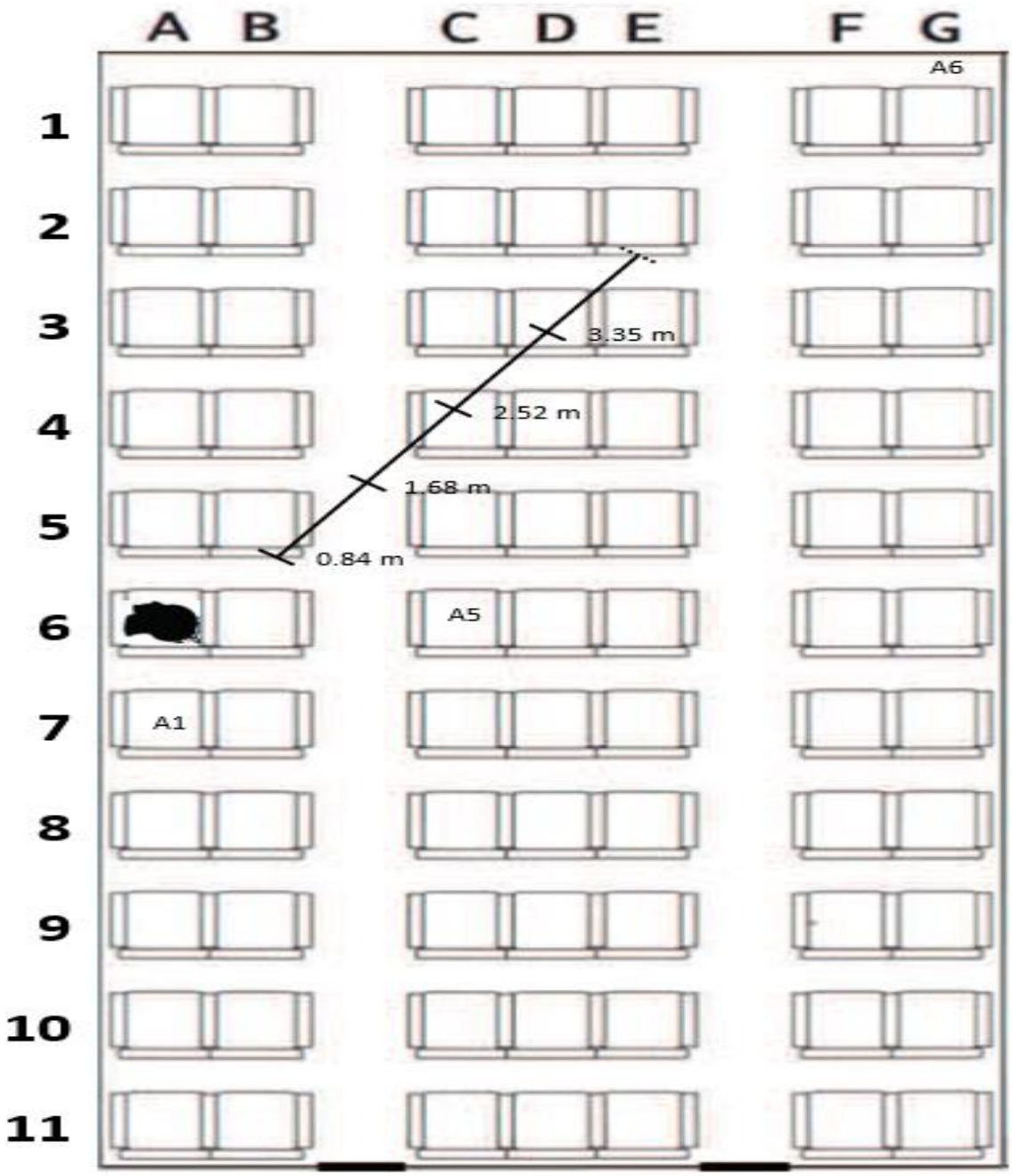

Figure H.108 Test 71 (B-M) ISOPass undeployed source location and sampling tree orientation.

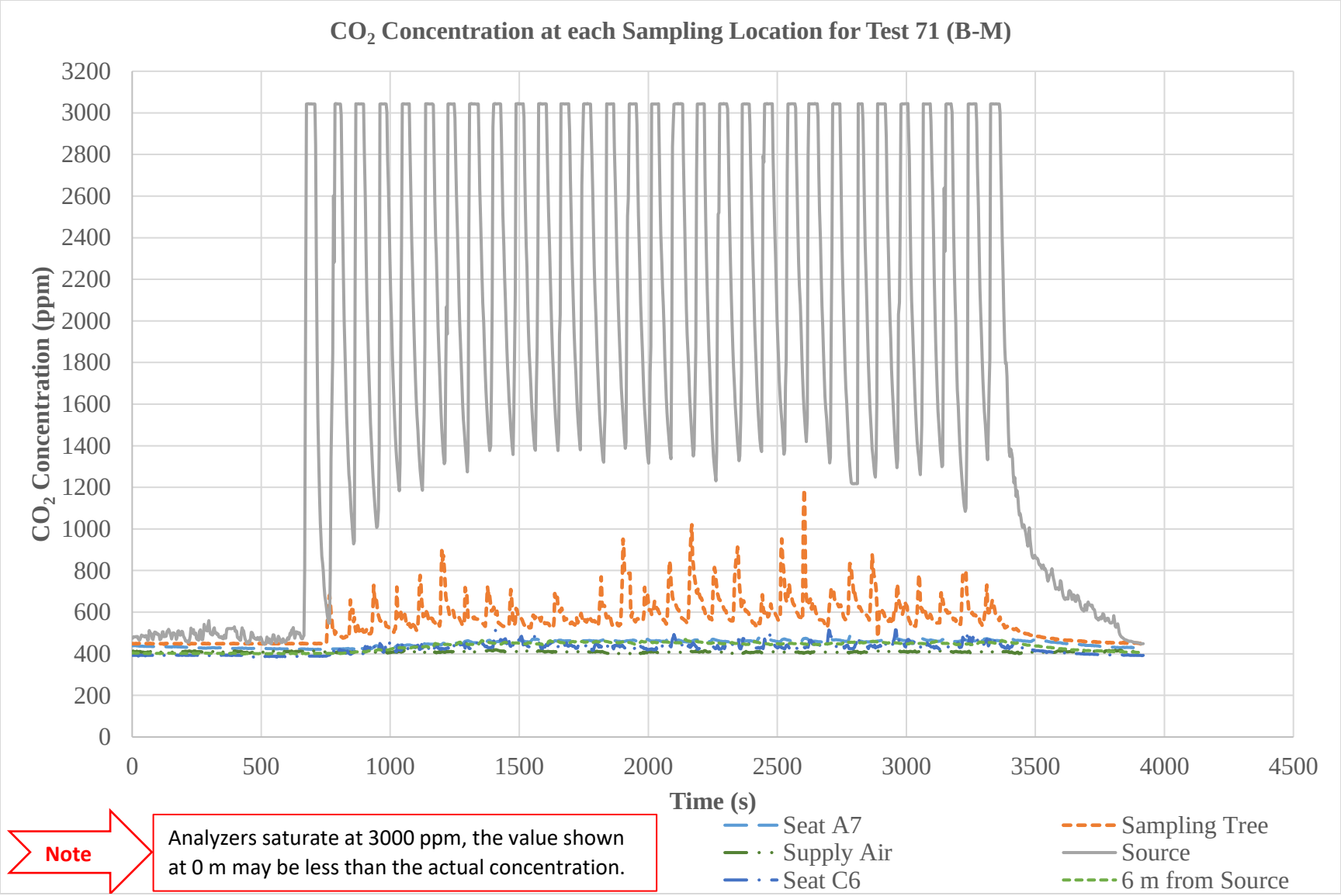

Figure H.109 Ininstantaneous CO_2 concentration at each sampling location for Test 71 (B-M) ISOPass undeployed.

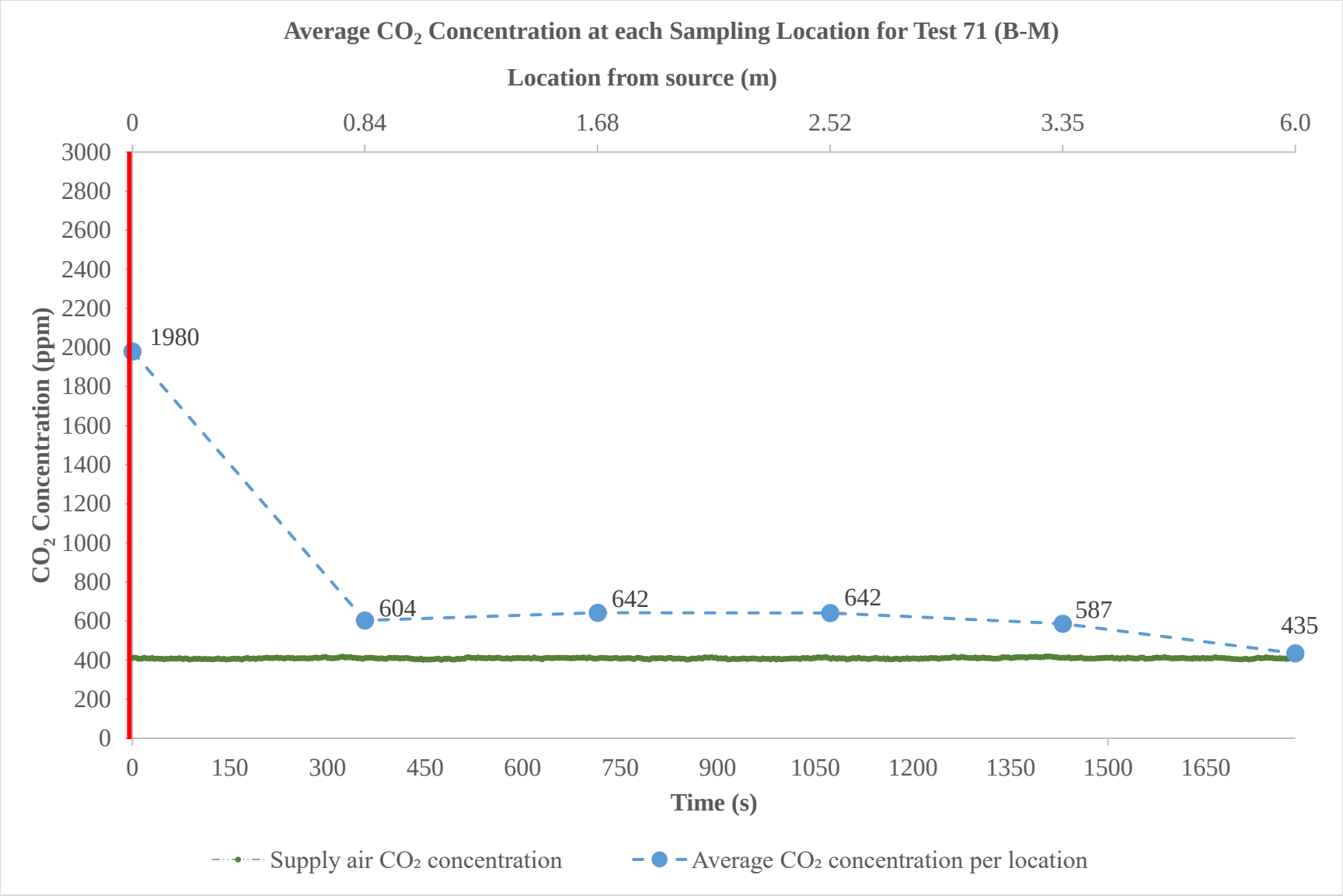

Figure H.110 Average CO_2 concentration at each sampling location for Test 71 (B-M) ISOPass undeployed.

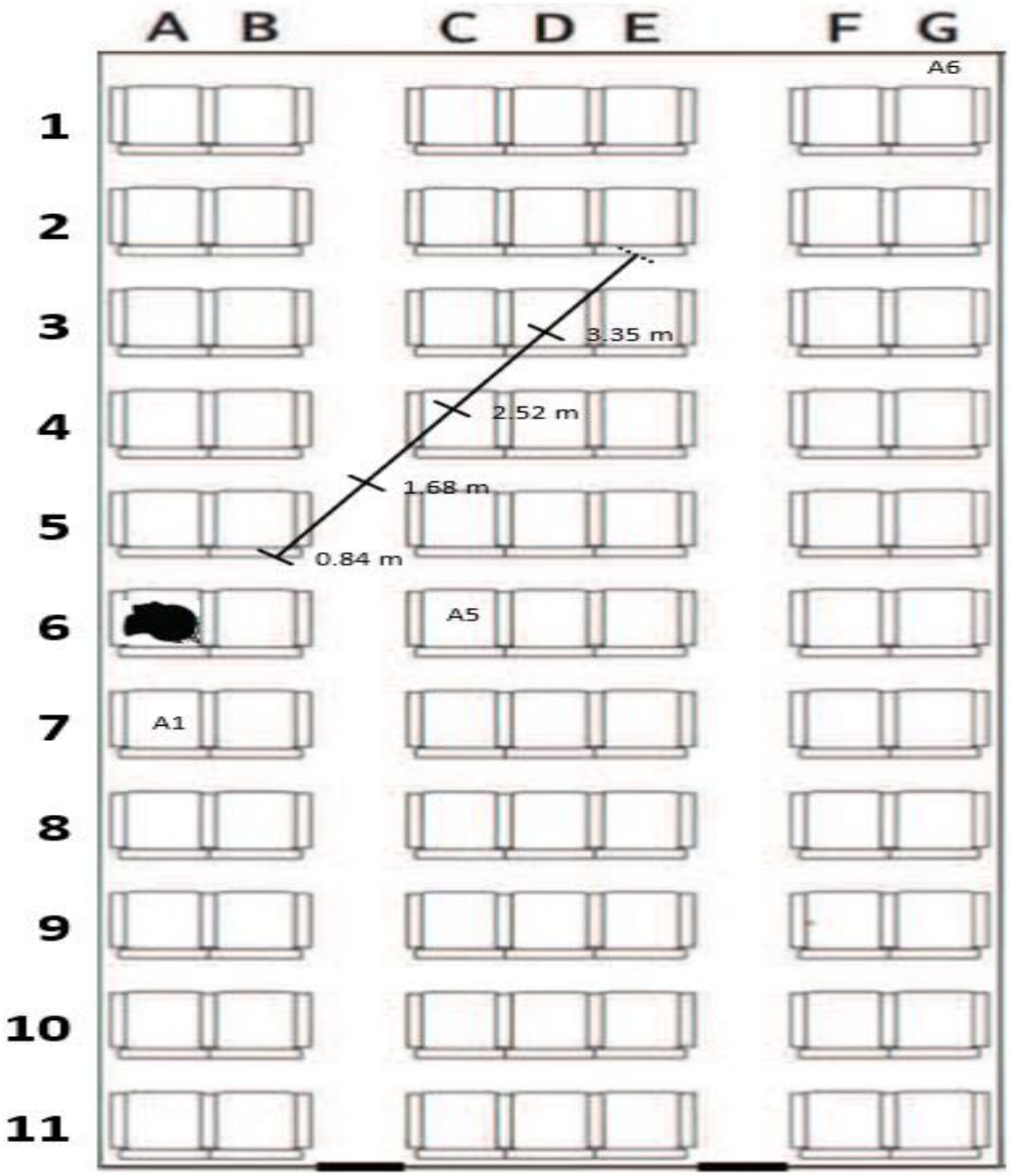

Figure H.111 Test 72 (B-M) ISOPass undeployed source location and sampling tree orientation.

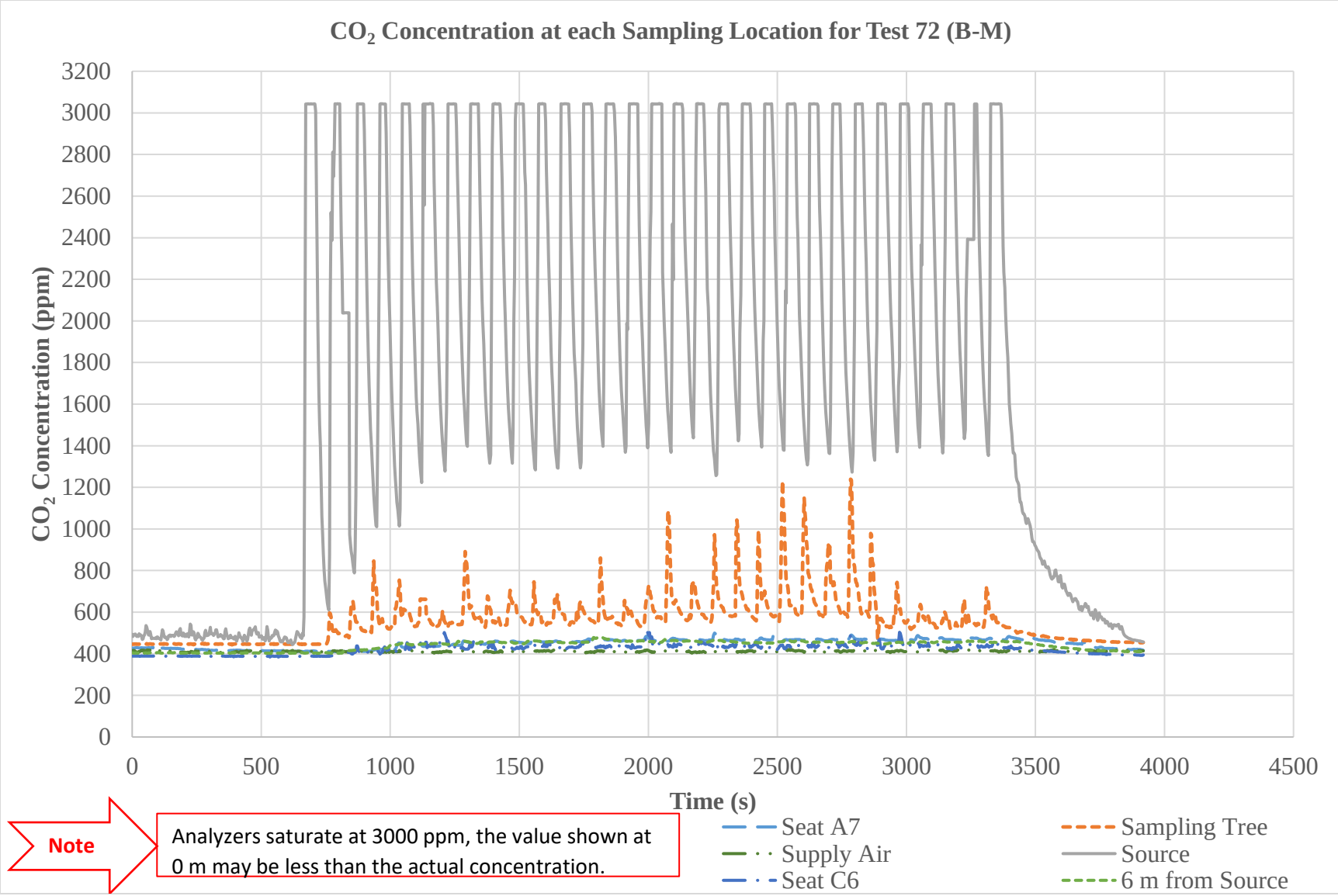

Figure H.112 Ininstantaneous CO_2 concentration at each sampling location for Test 72 (B-M) ISOPass undeployed.

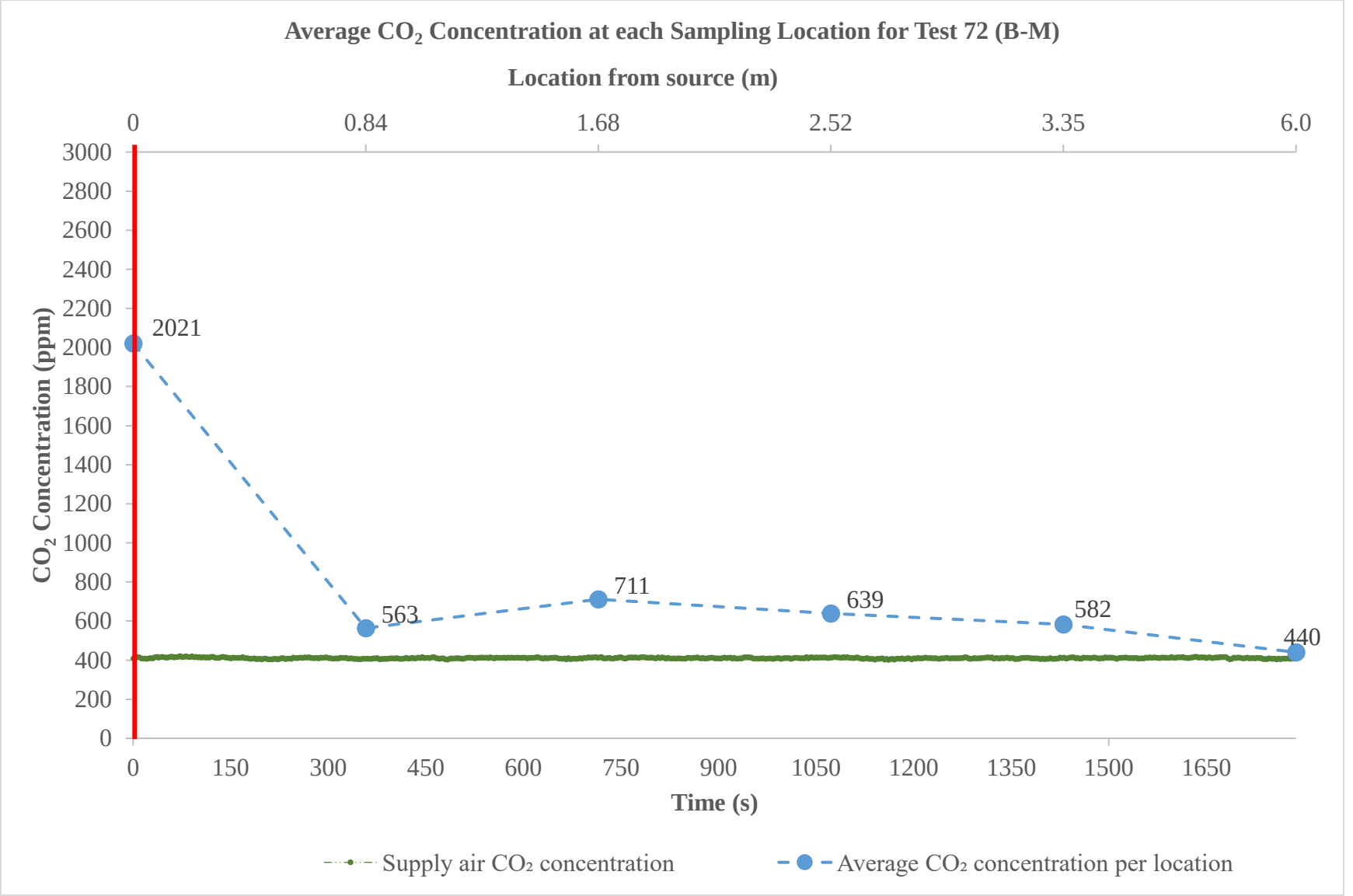

Figure H.113 Average CO_2 concentration at each sampling location for Test 72 (B-M) ISOPass undeployed.

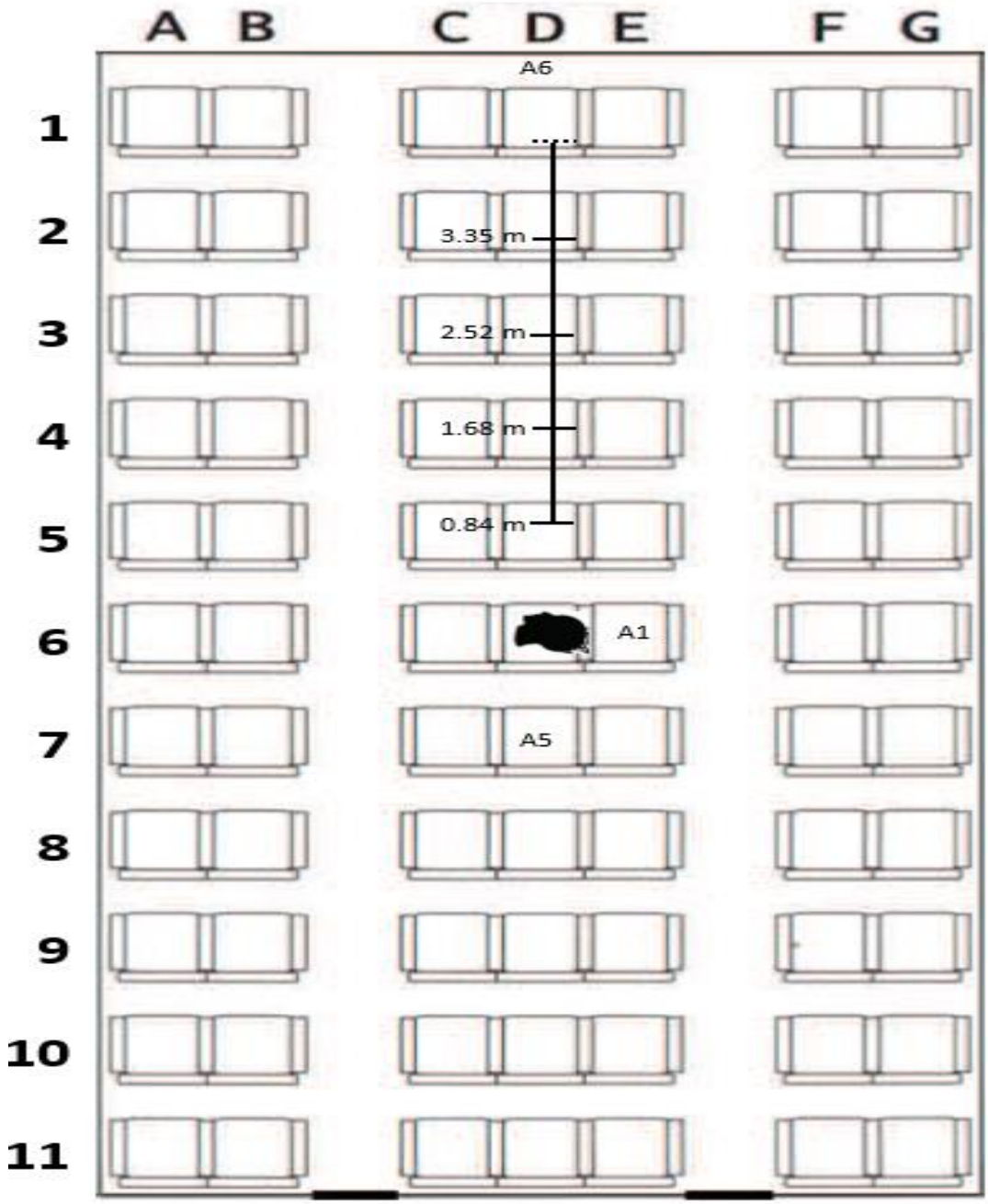

Figure H.114 Test 73 (B-M) ISOPass undeployed source location and sampling tree orientation.

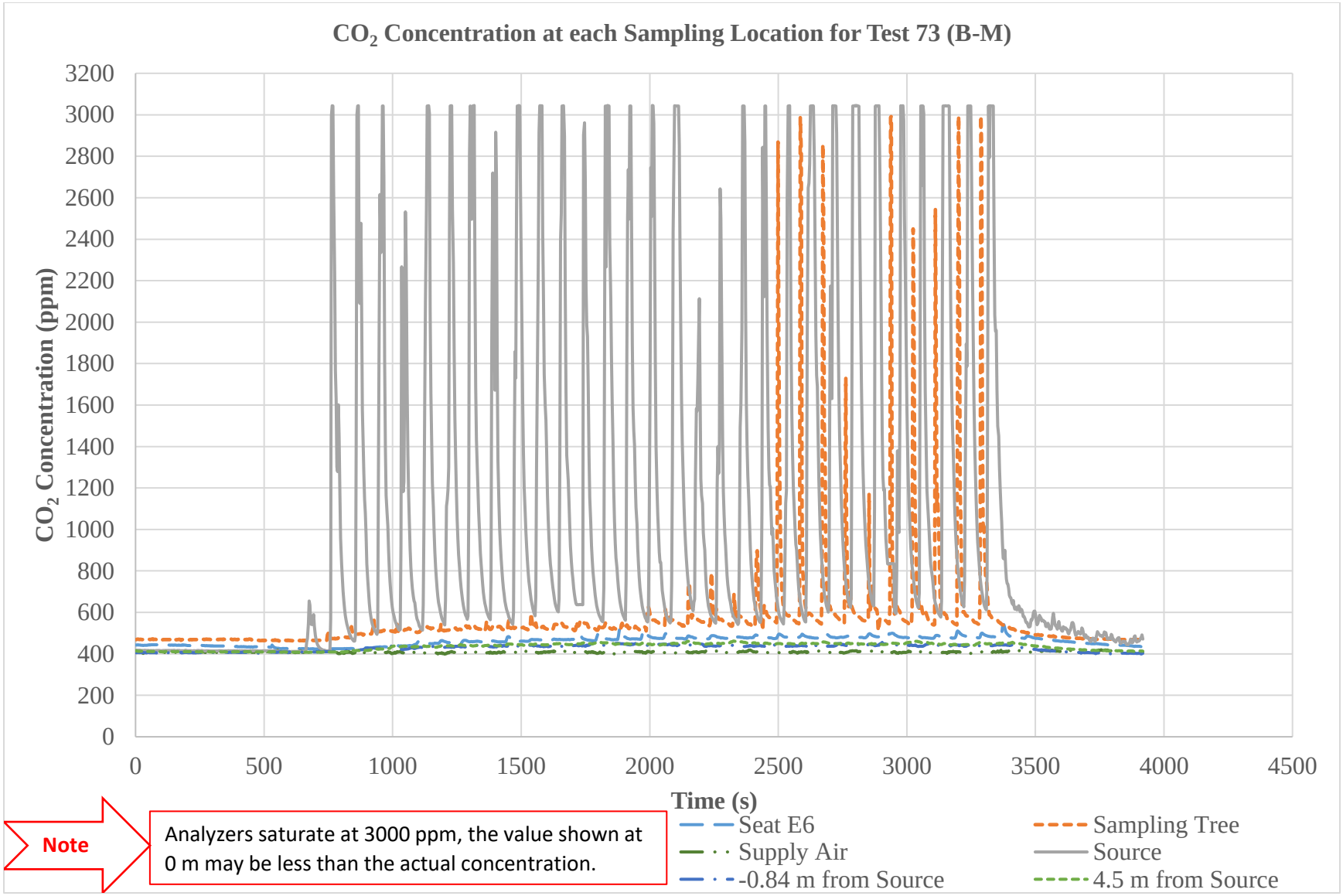

Figure H.115 Ininstantaneous CO_2 concentration at each sampling location for Test 73 (B-M) ISOPass undeployed.

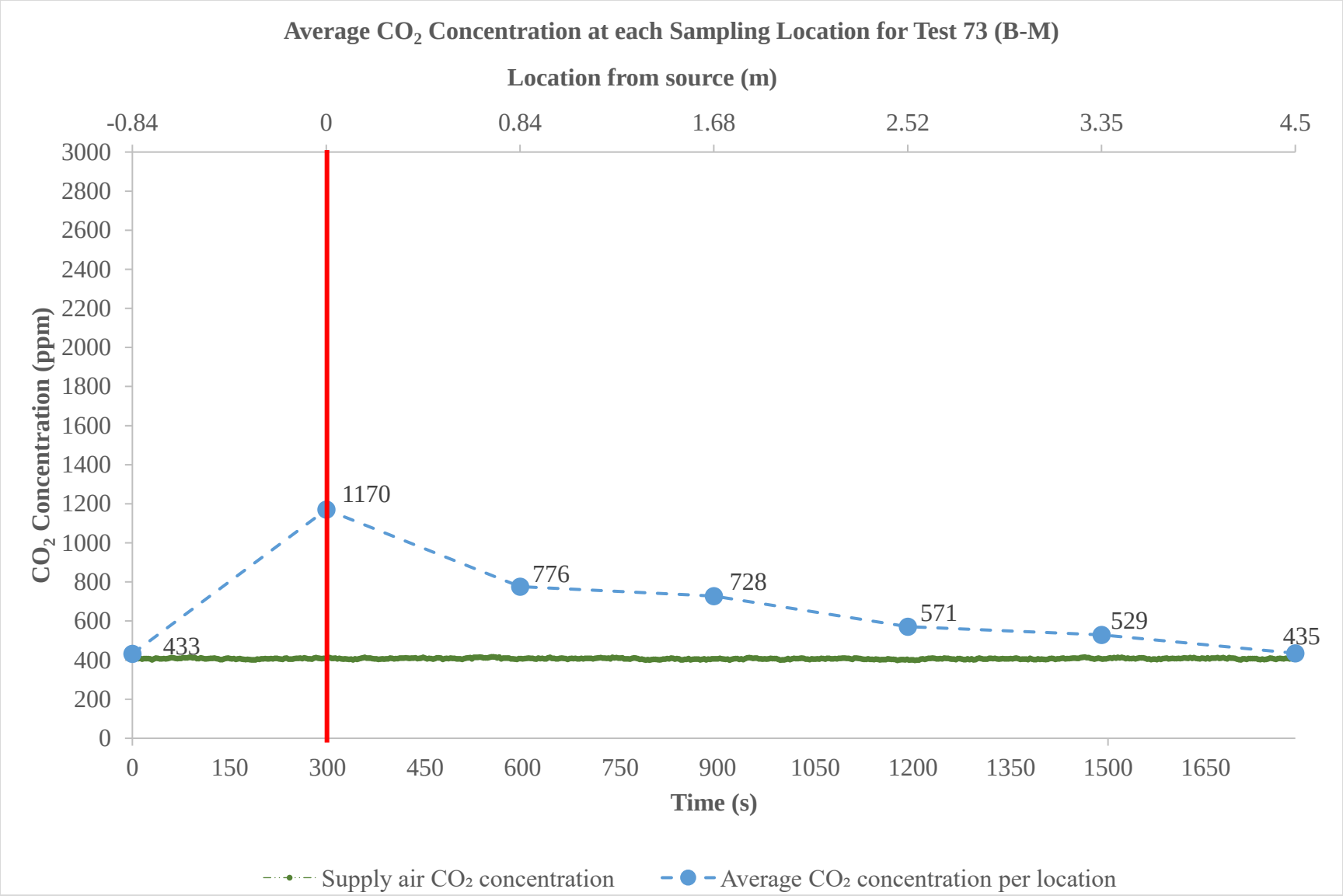

Figure H.116 Average CO_2 concentration at each sampling location for Test 73 (B-M) ISOPass undeployed.

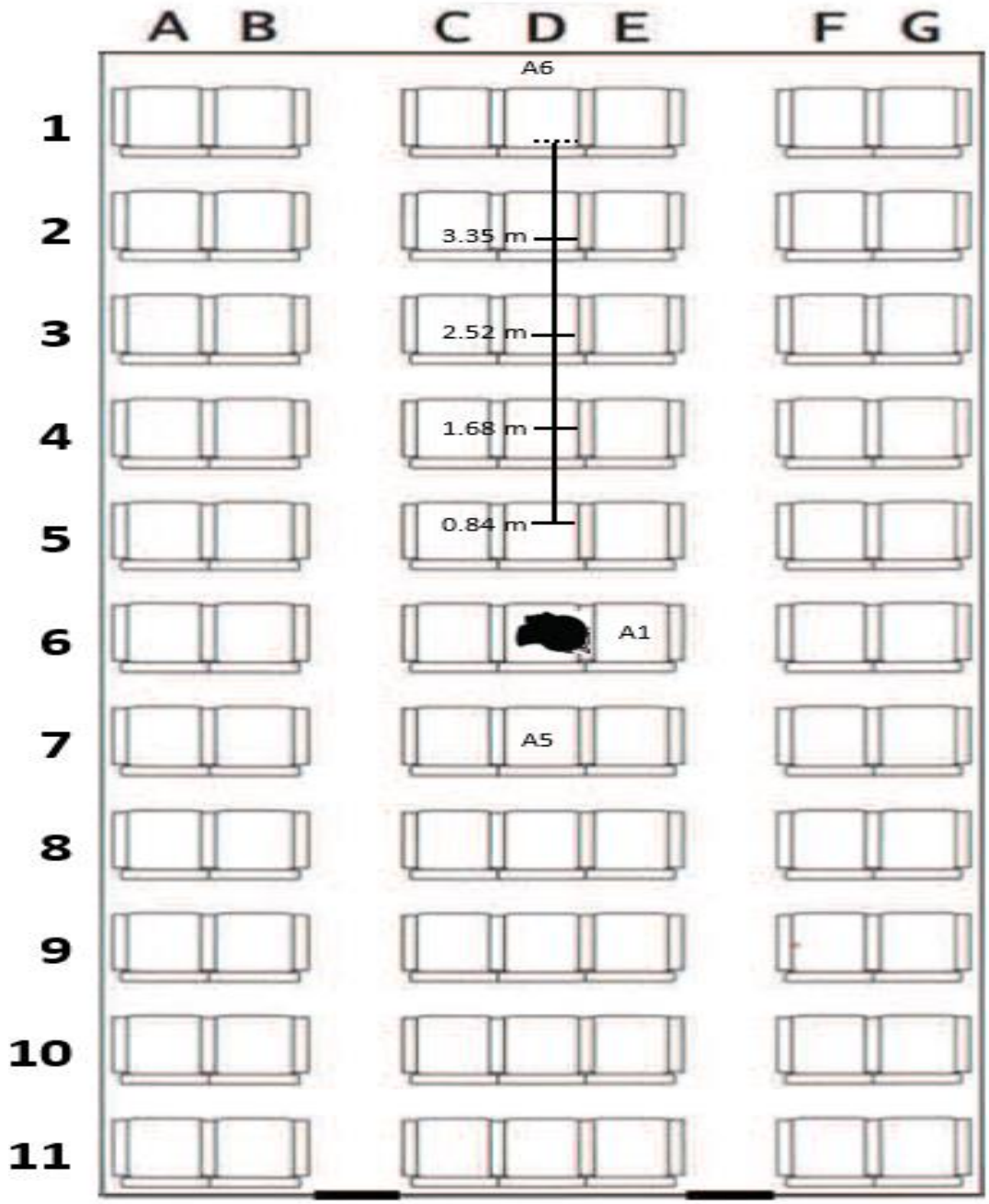

Figure H.117 Test 74 (B-M) ISOPass undeployed source location and sampling tree orientation.

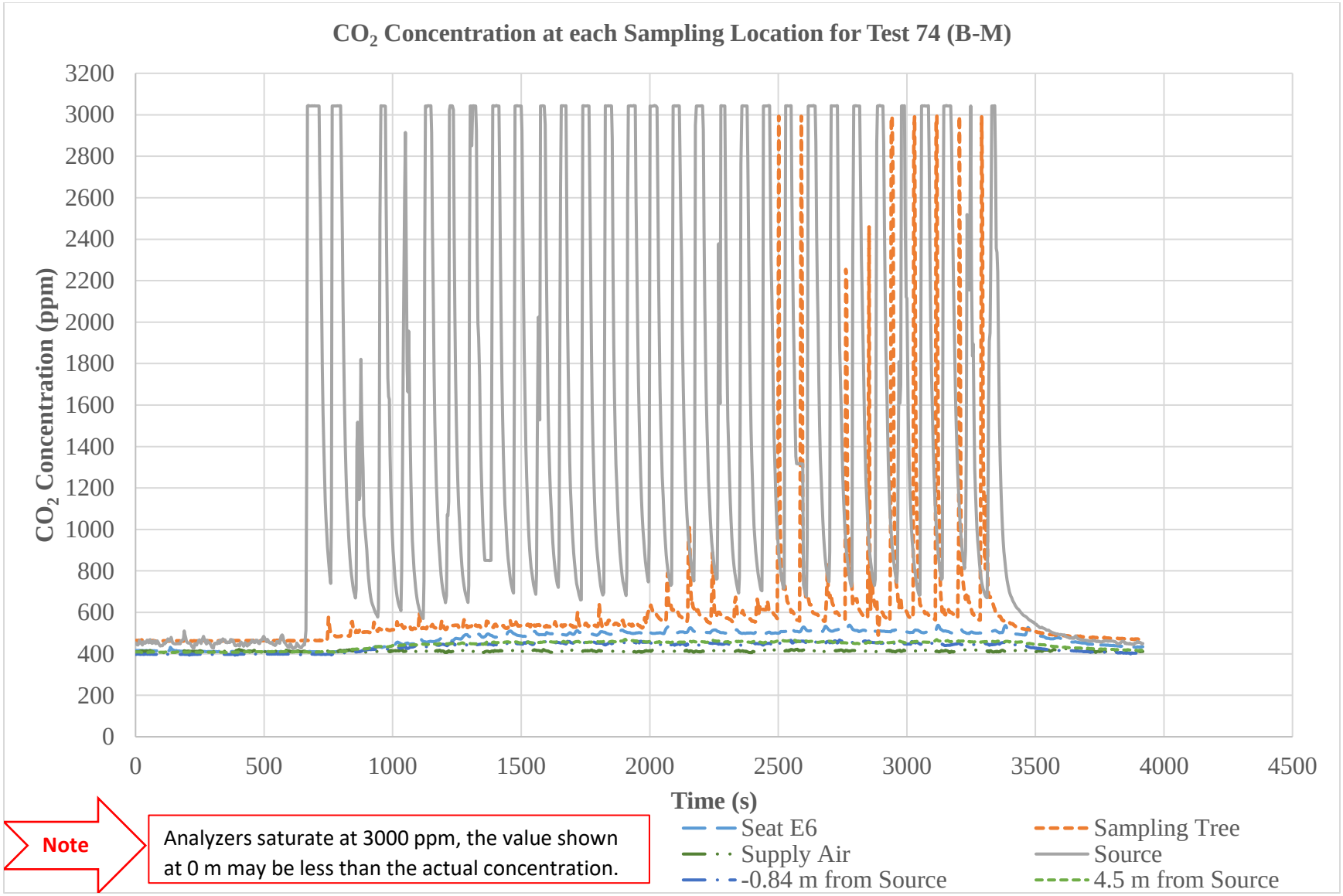

Figure H.118 Ininstantaneous CO_2 concentration at each sampling location for Test 74 (B-M) ISOPass undeployed.

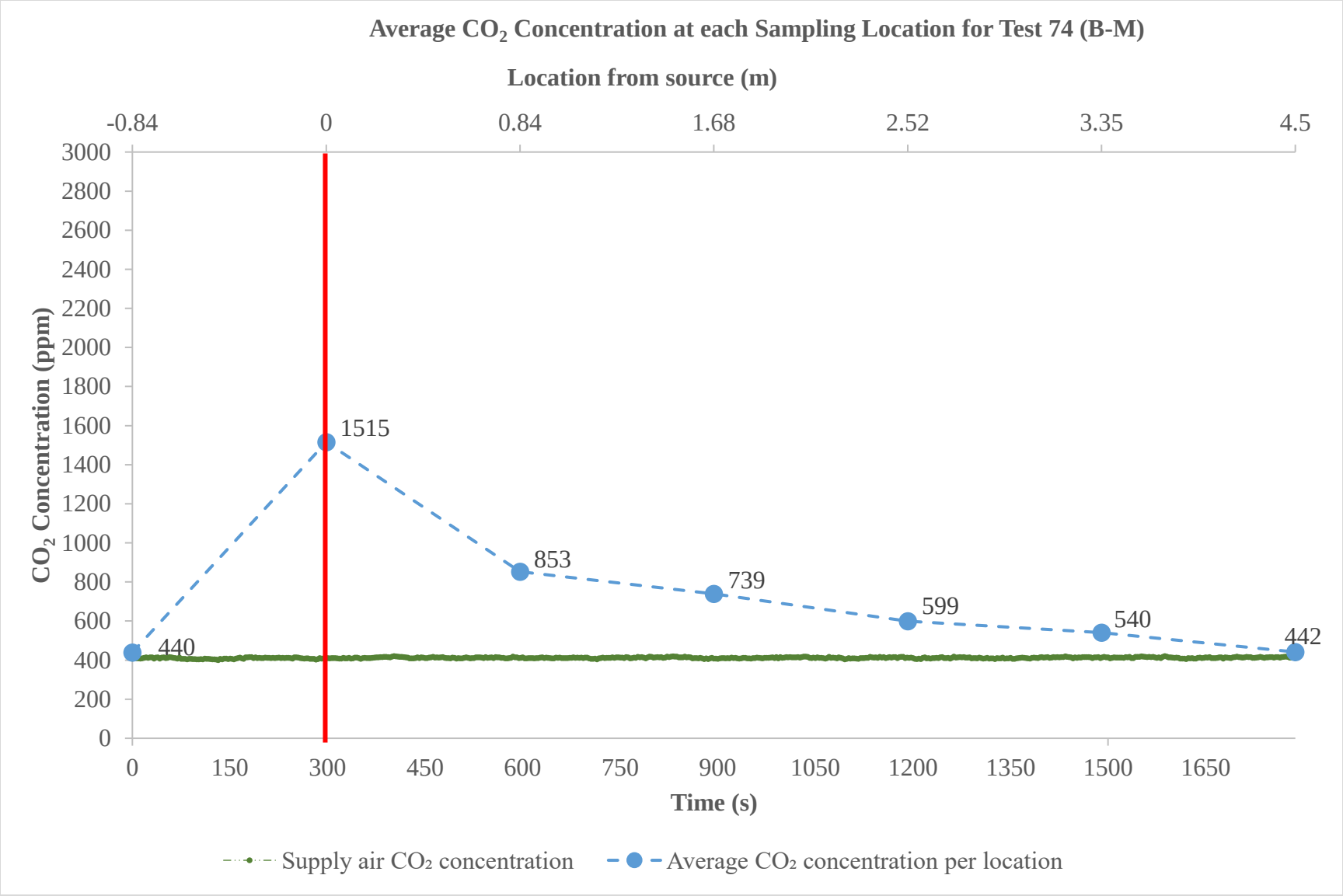

Figure H.119 Average CO_2 concentration at each sampling location for Test 74 (B-M) ISOPass undeployed.

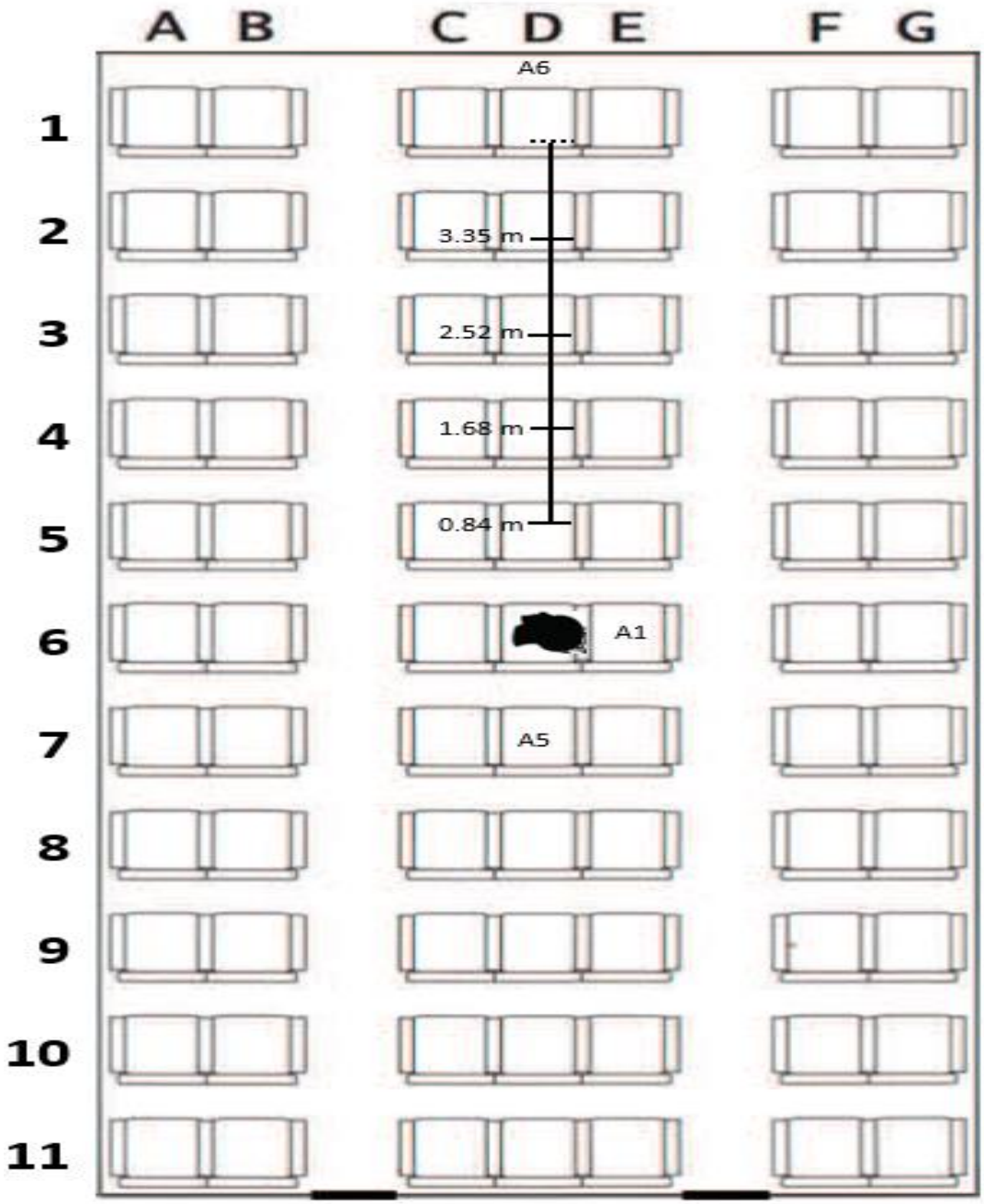

Figure H.120 Test 75 (B-M) ISOPass undeployed source location and sampling tree orientation.

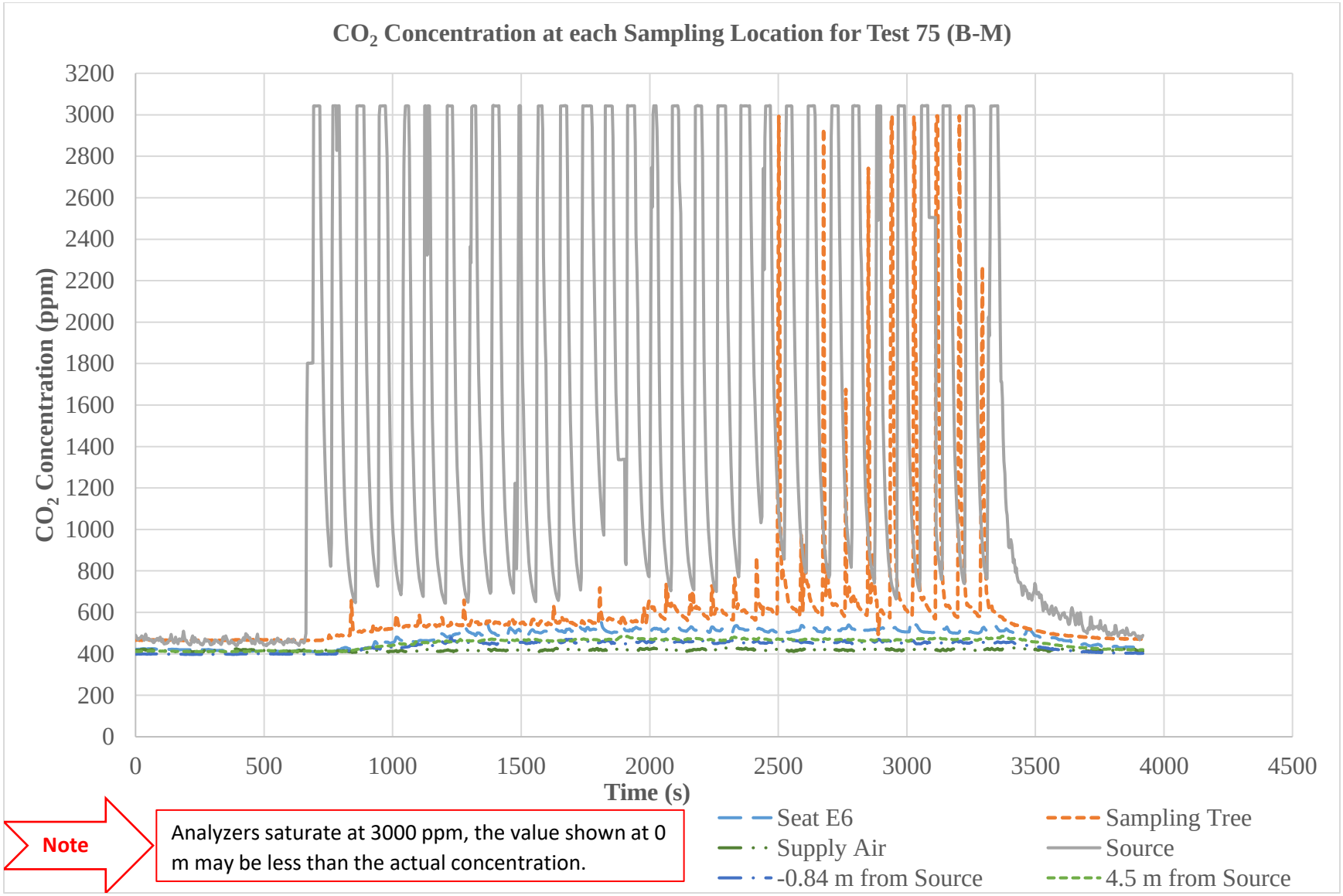

Figure H.121 Ininstantaneous CO_2 concentration at each sampling location for Test 75 (B-M) ISOPass undeployed.

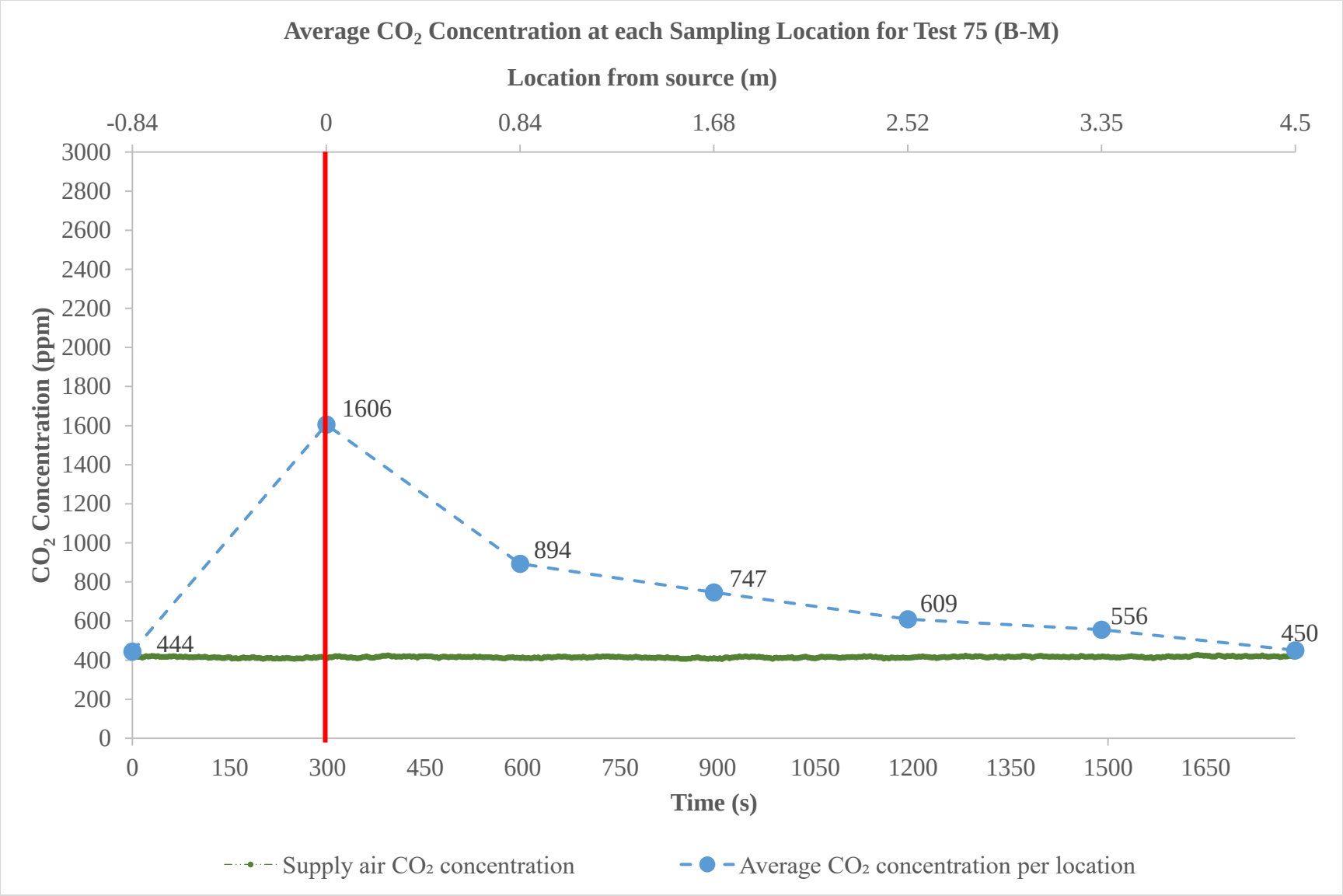

Figure H.122 Average CO_2 concentration at each sampling location for Test 75 (B-M) ISOPass undeployed.

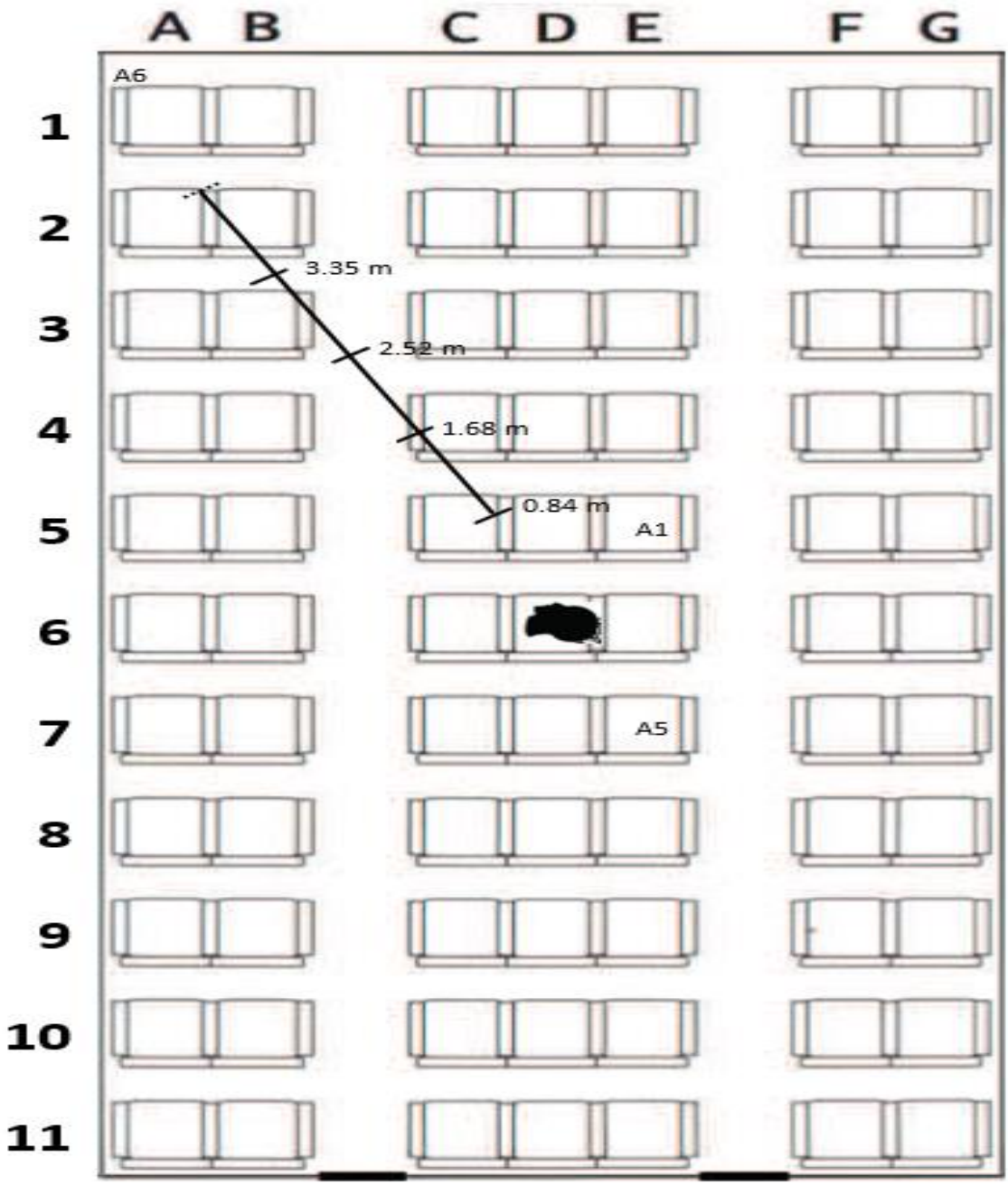

Figure H.123 Test 76 (B-M) ISOPass undeployed source location and sampling tree orientation.

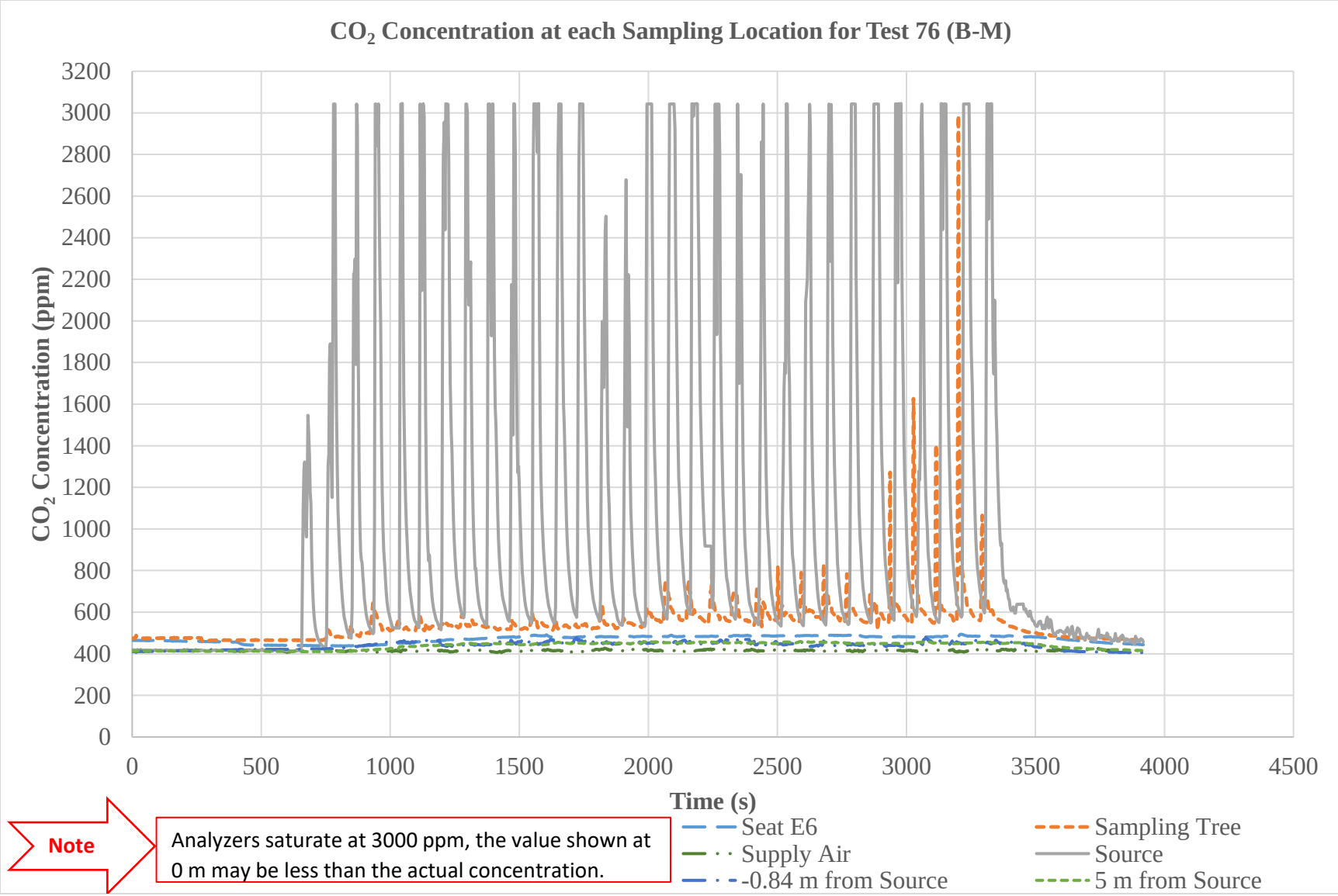

Figure H.124 Ininstantaneous CO_2 concentration at each sampling location for Test 76 (B-M) ISOPass undeployed.

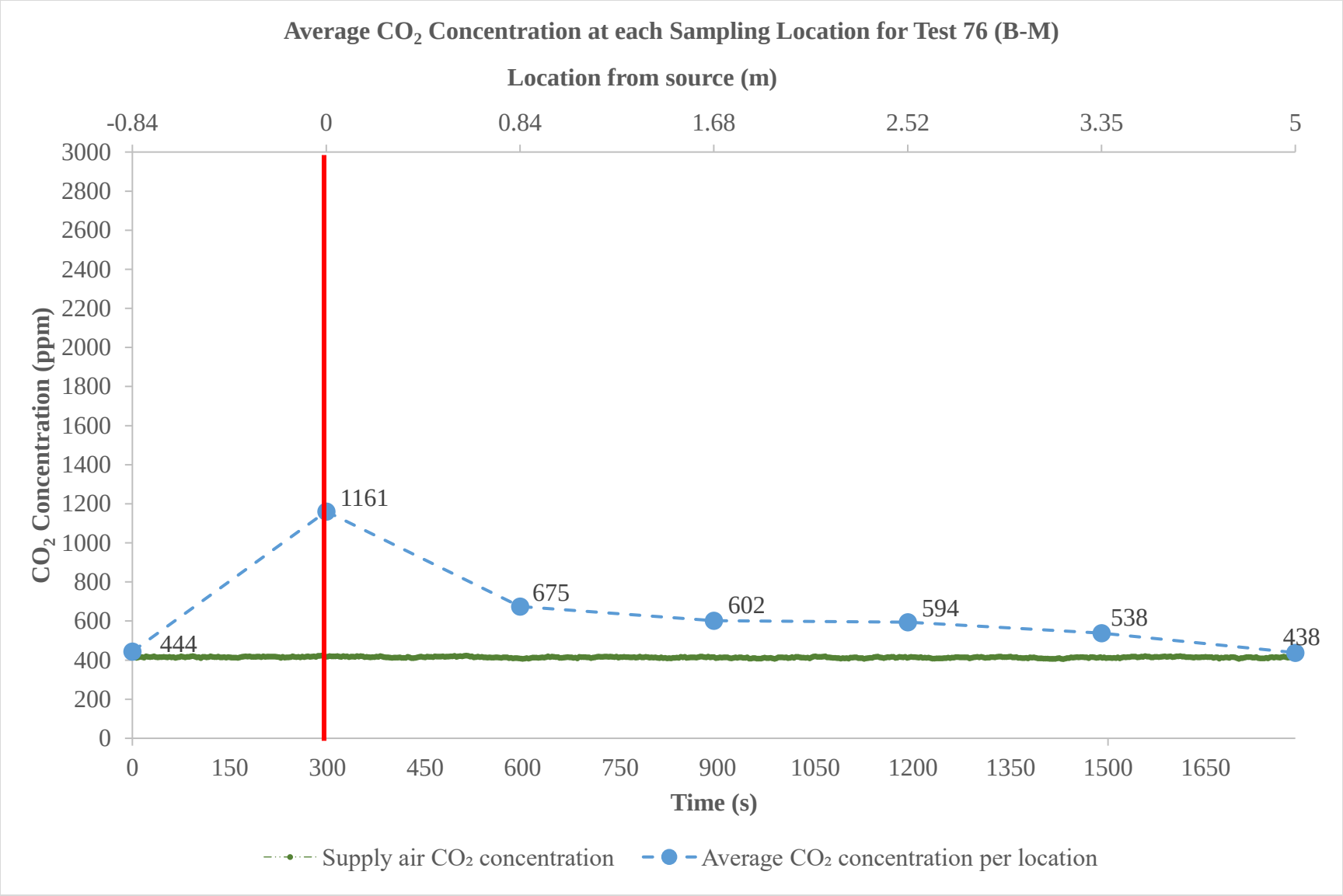

Figure H.125 Average CO_2 concentration at each sampling location for Test 76 (B-M) ISOPass undeployed.

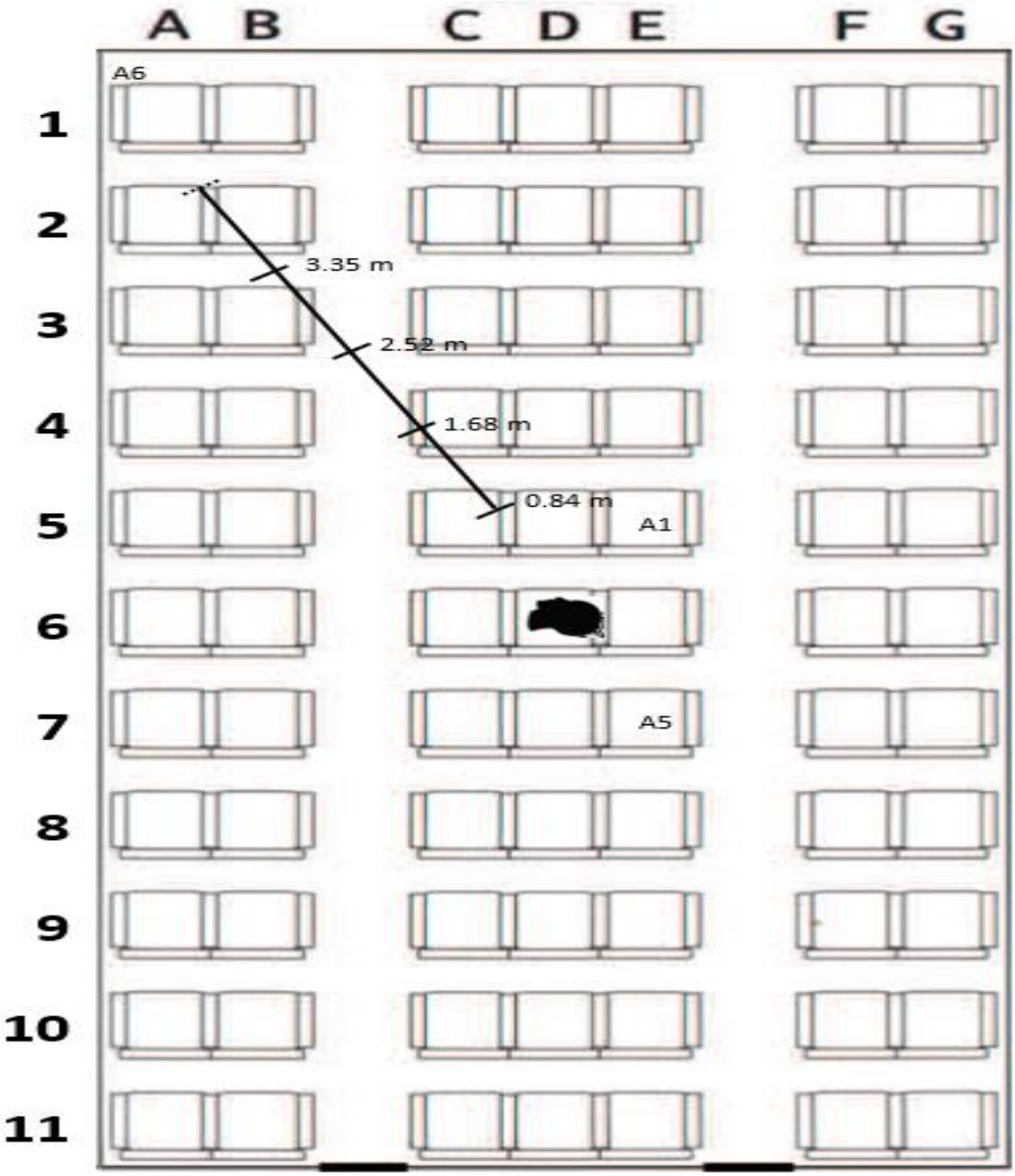

Figure H.126 Test 77 (B-M) ISOPass undeployed source location and sampling tree orientation.

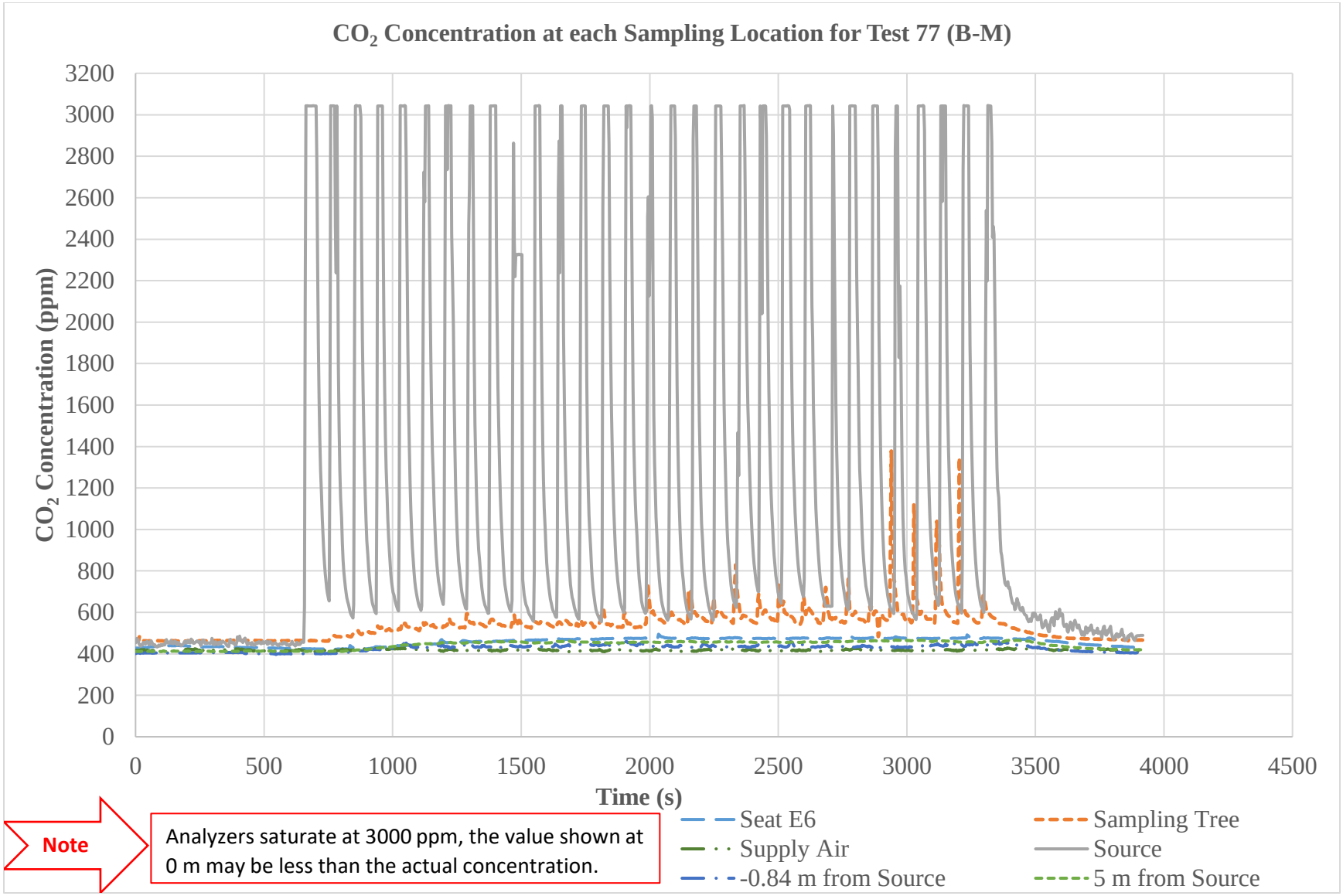

Figure H.127 Ininstantaneous CO_2 concentration at each sampling location for Test 77 (B-M) ISOPass undeployed.

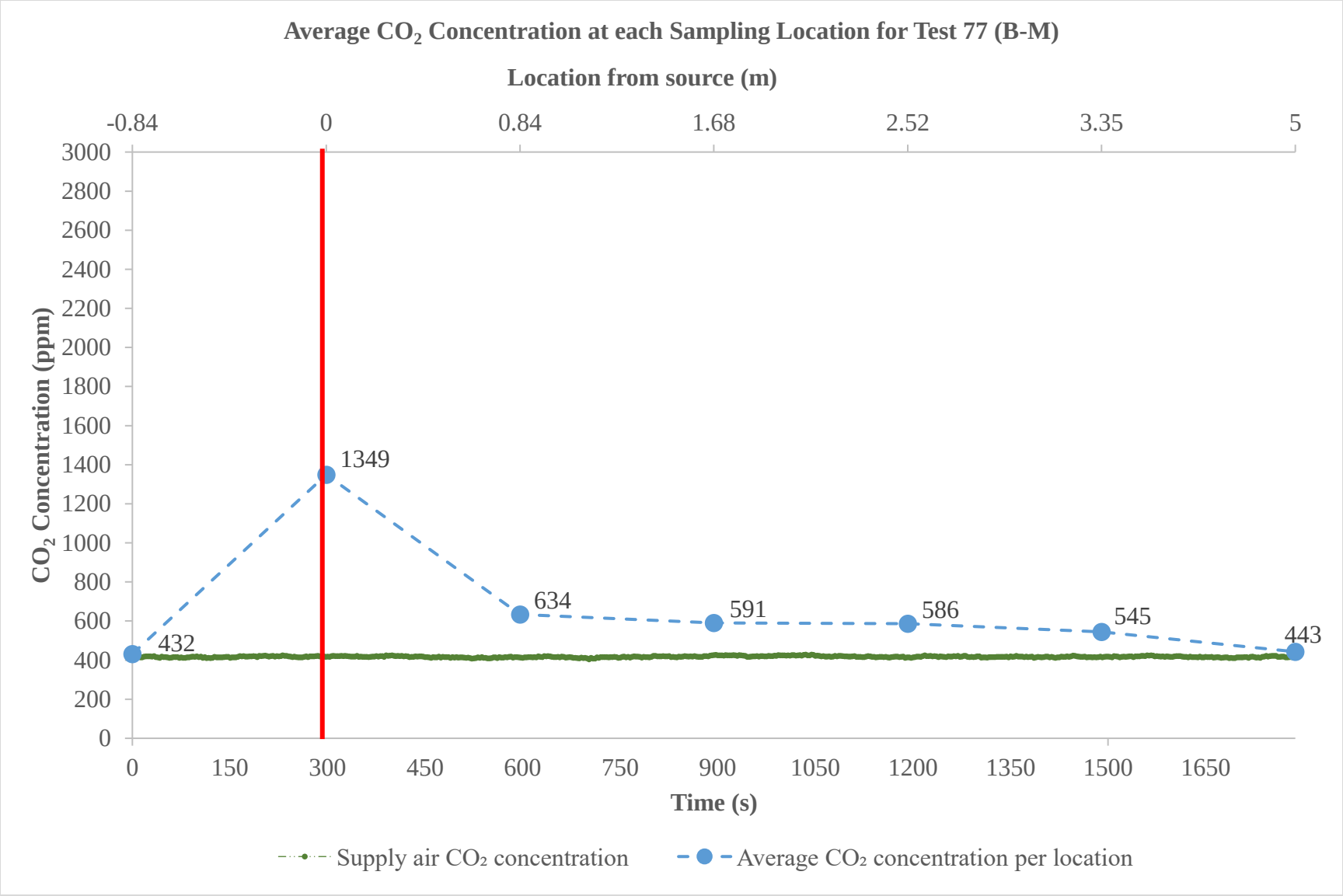

Figure H.128 Average CO_2 concentration at each sampling location for Test 77 (B-M) ISOPass undeployed.

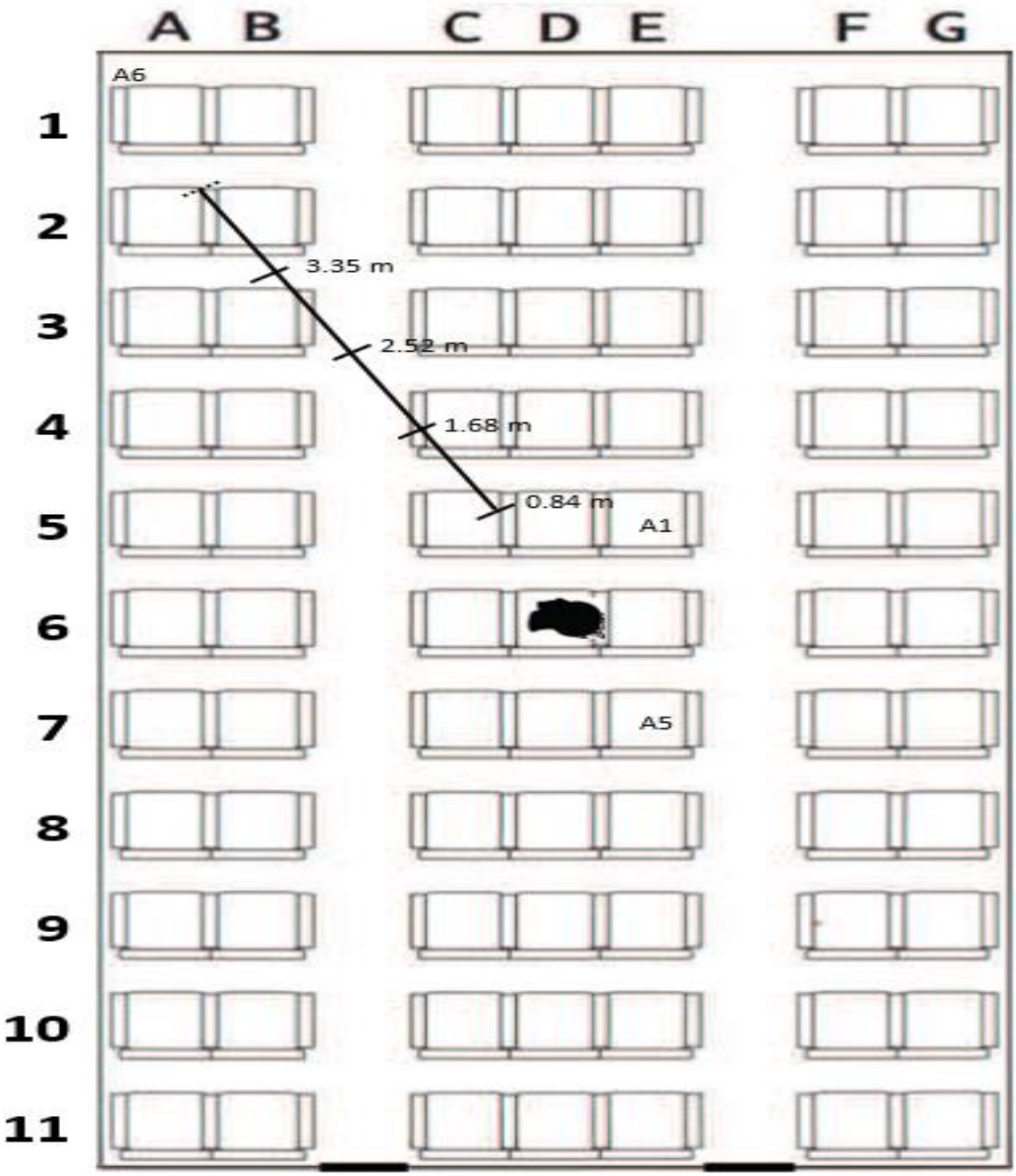

Figure H.129 Test 78 (B-M) ISOPass undeployed source location and sampling tree orientation.

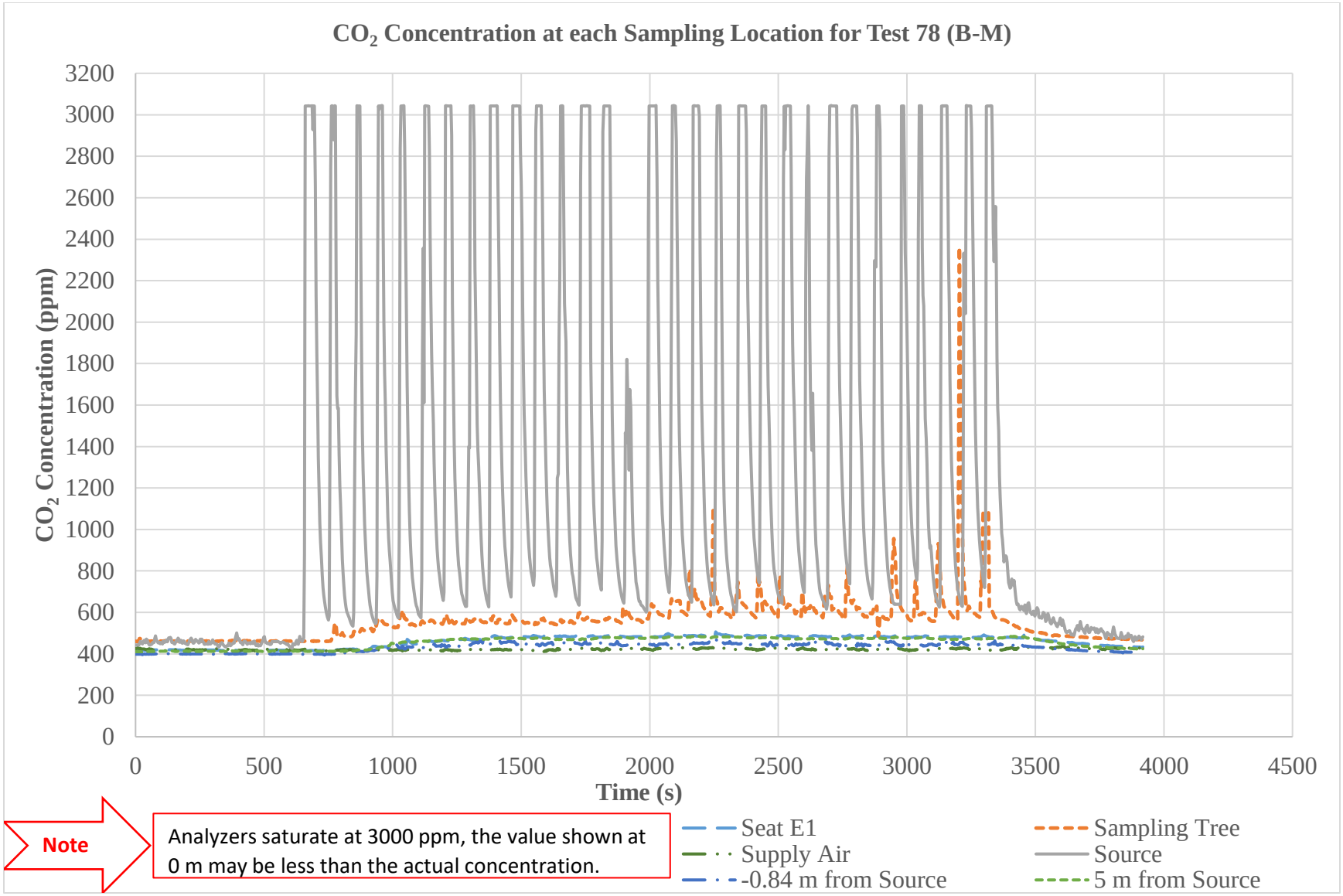

Figure H.130 Ininstantaneous CO_2 concentration at each sampling location for Test 78 (B-M) ISOPass undeployed.

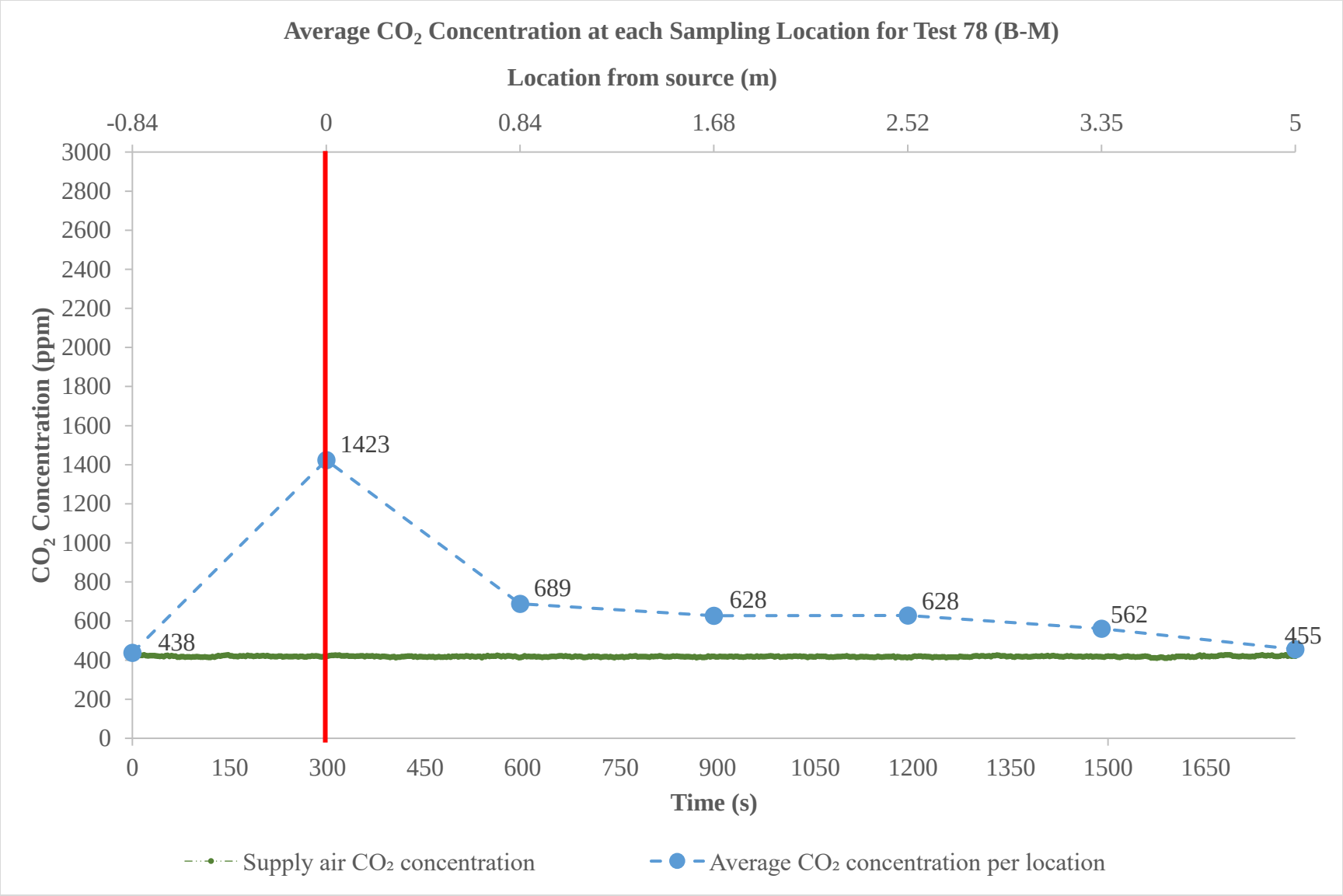

Figure H.131 Average CO_2 concentration at each sampling location for Test 78 (B-M) ISOPass undeployed.

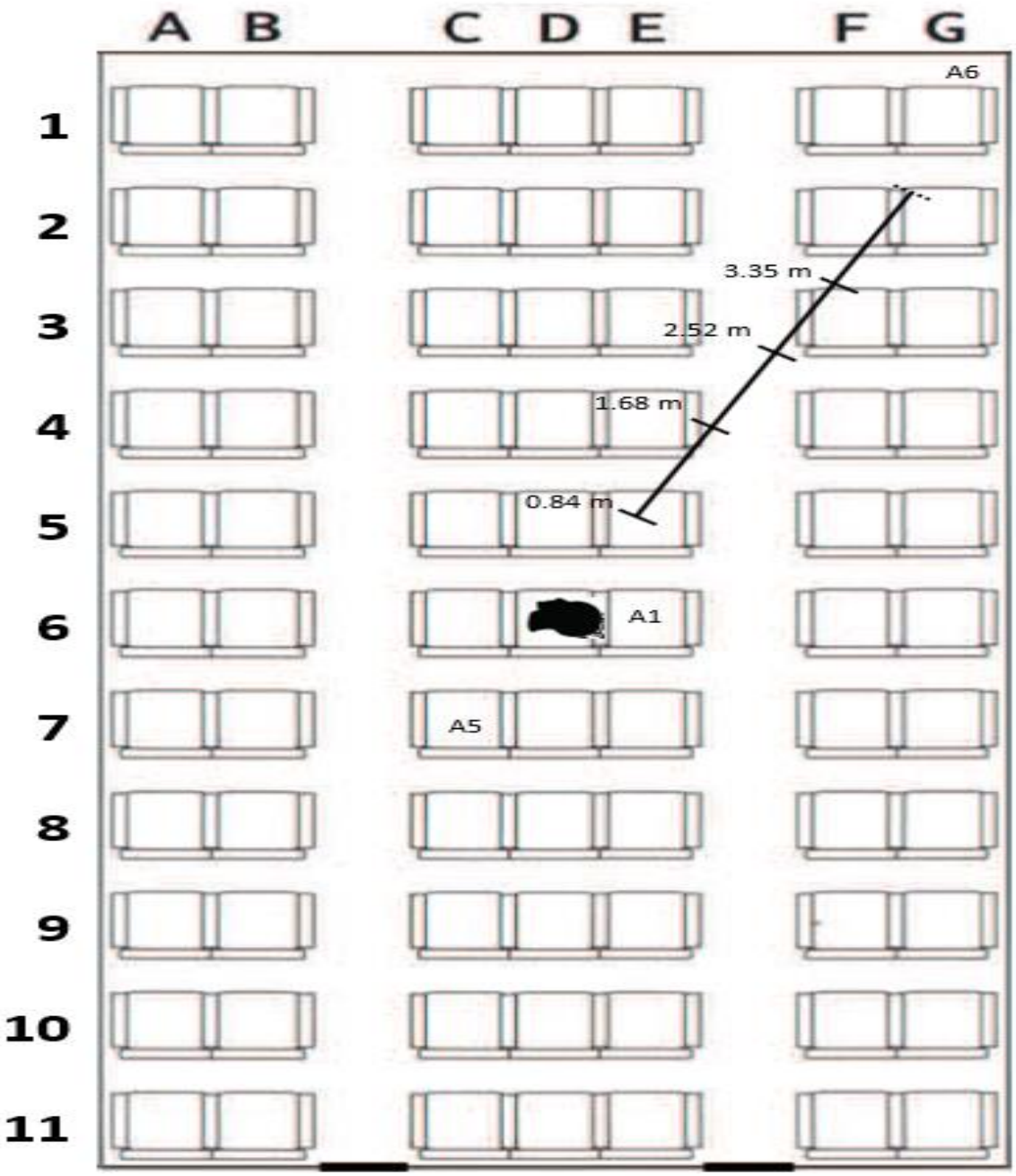

Figure H.132 Test 79 (B-M) ISOPass undeployed source location and sampling tree orientation.

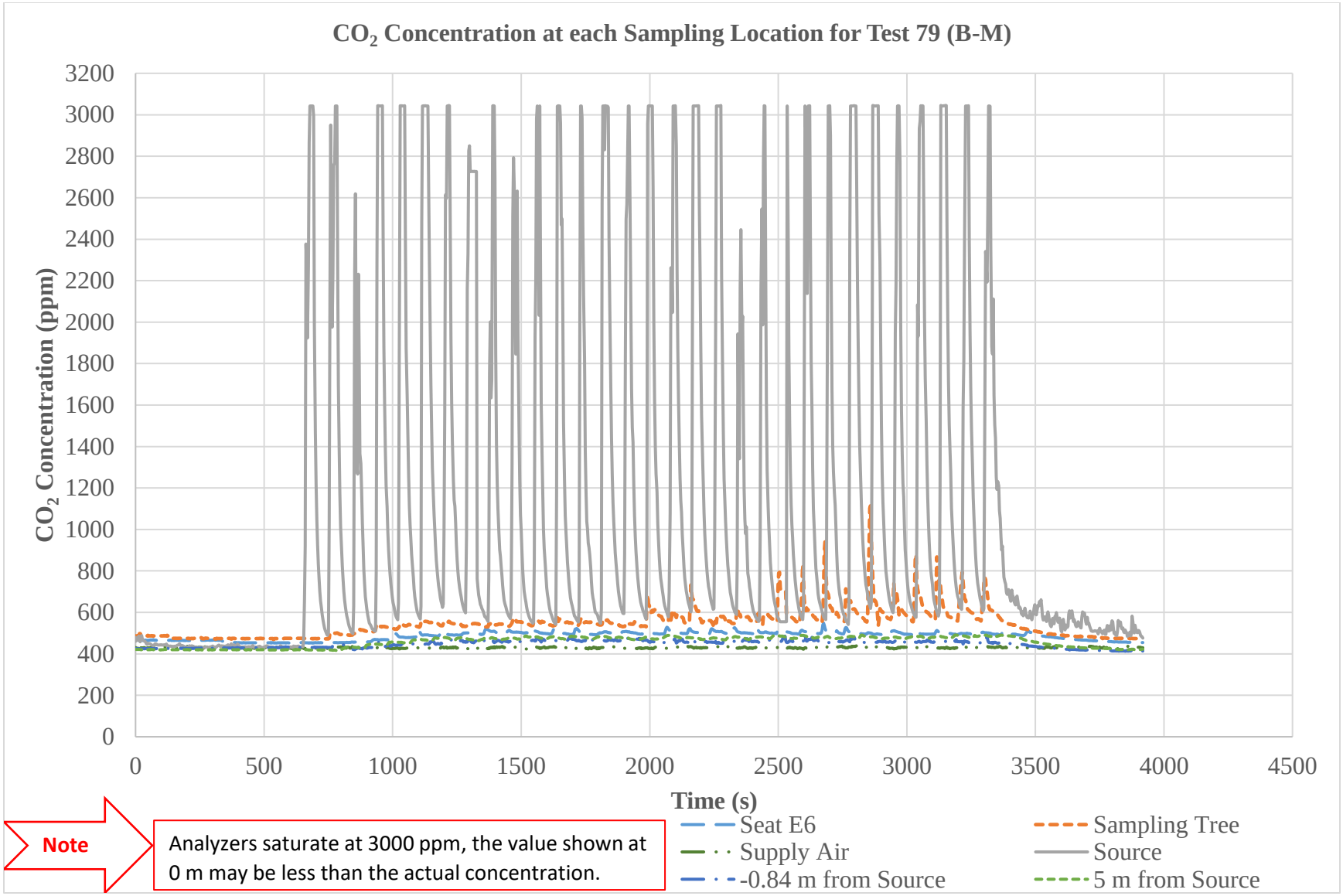

Figure H.133 Ininstantaneous CO_2 concentration at each sampling location for Test 79 (B-M) ISOPass undeployed.

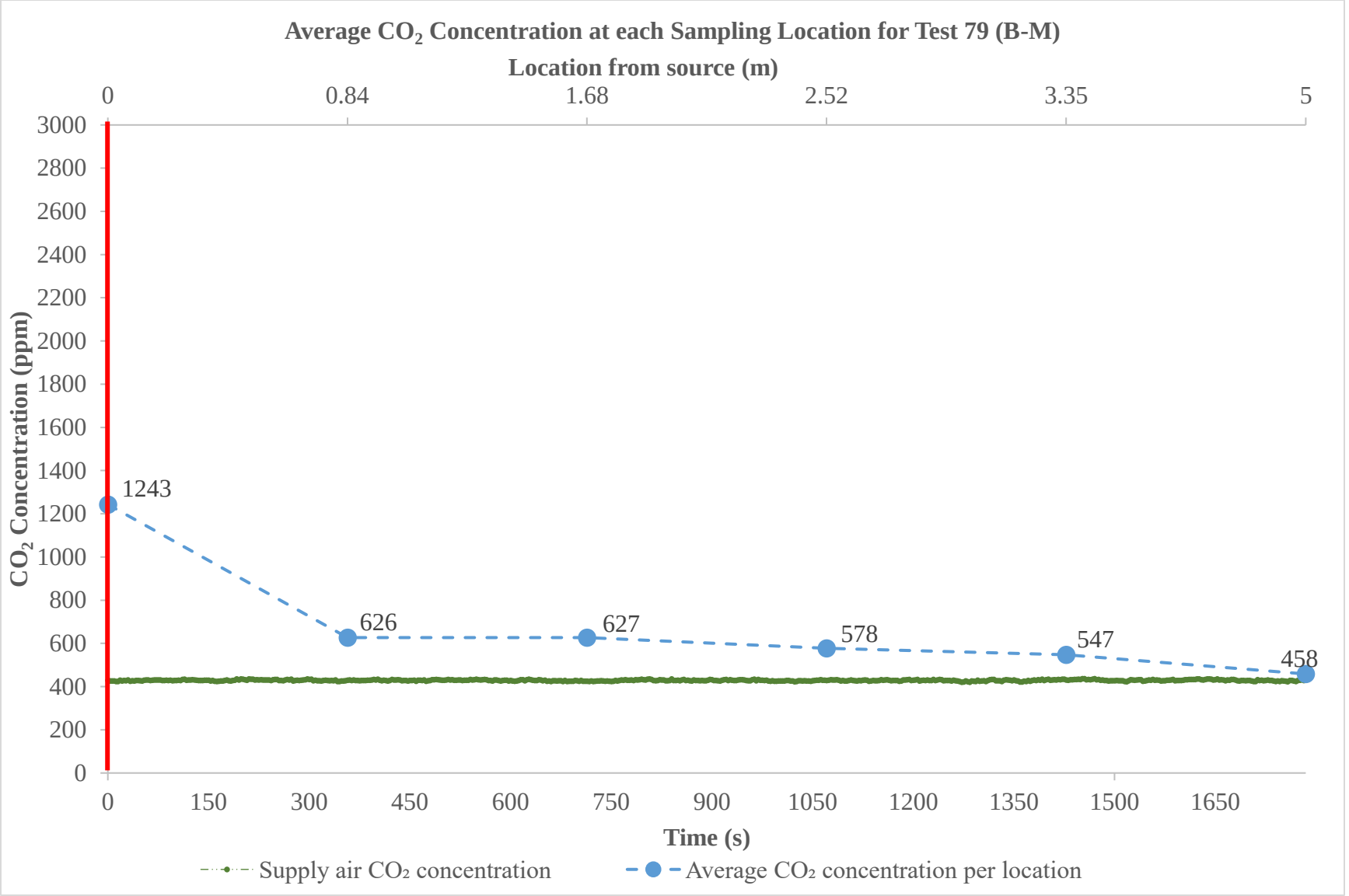

Figure H.134 Average CO_2 concentration at each sampling location for Test 79 (B-M) ISOPass undeployed.

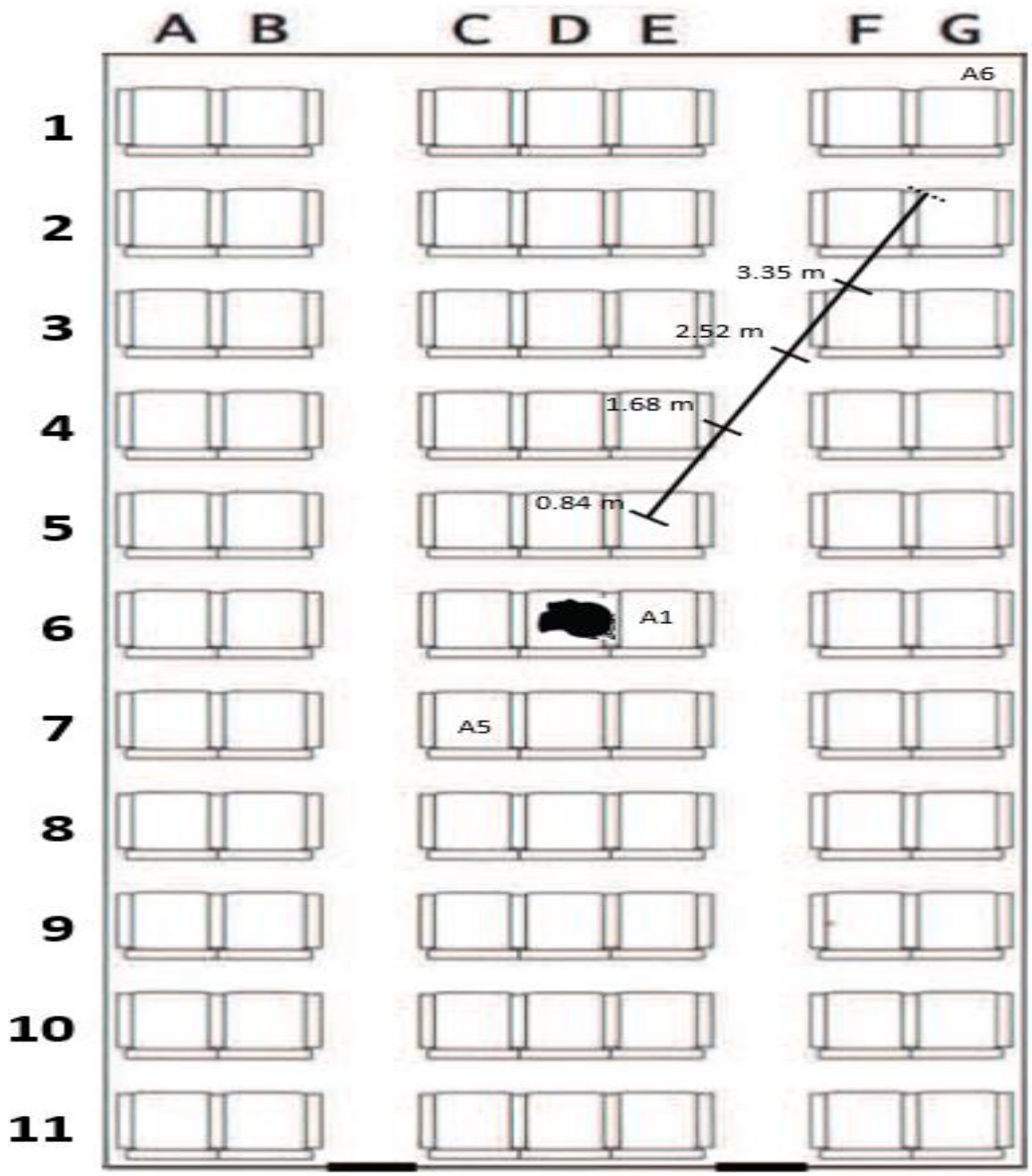

Figure H.135 Test 80 (B-M) ISOPass undeployed source location and sampling tree orientation.

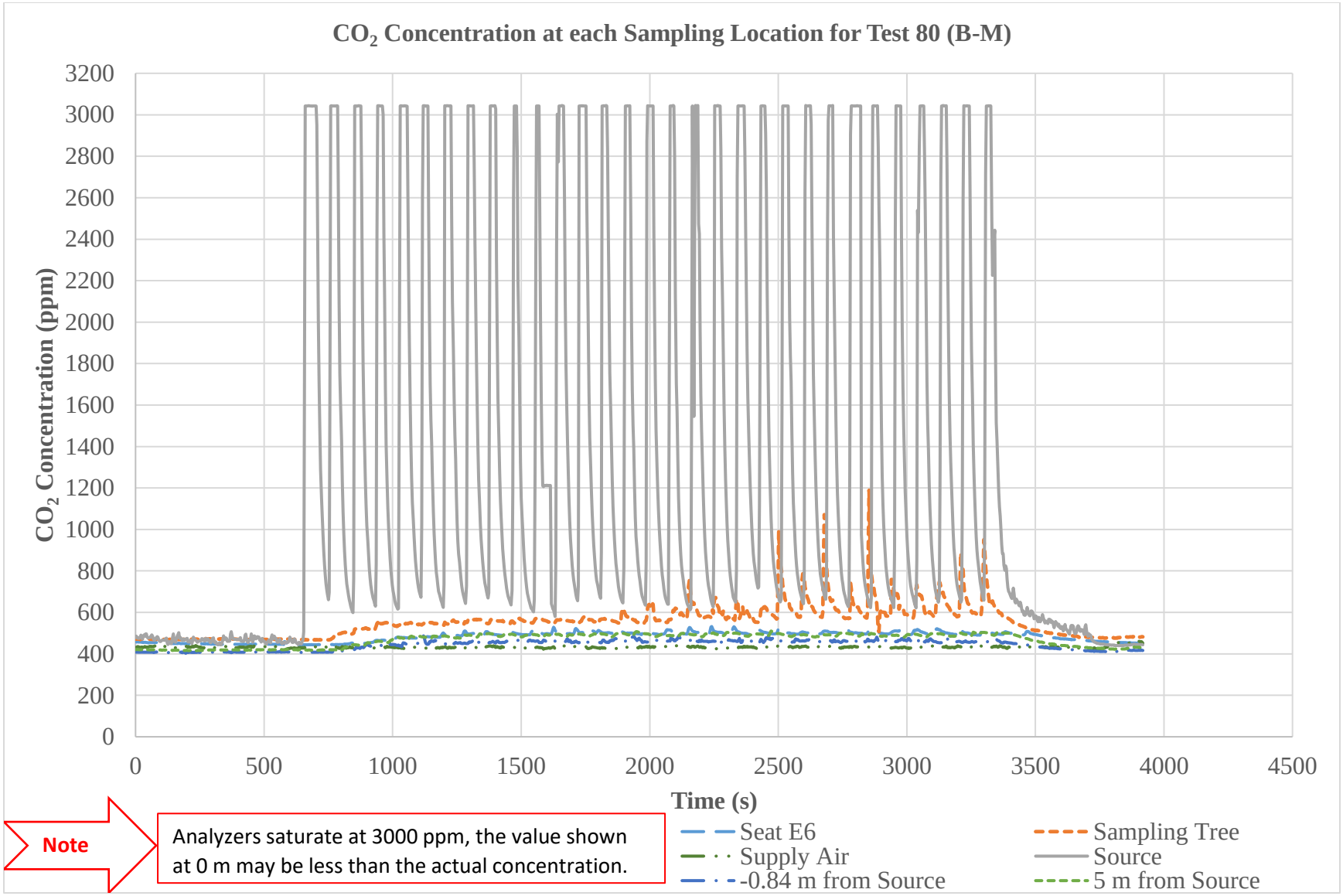

Figure H.136 Ininstantaneous CO_2 concentration at each sampling location for Test 80 (B-M) ISOPass undeployed.

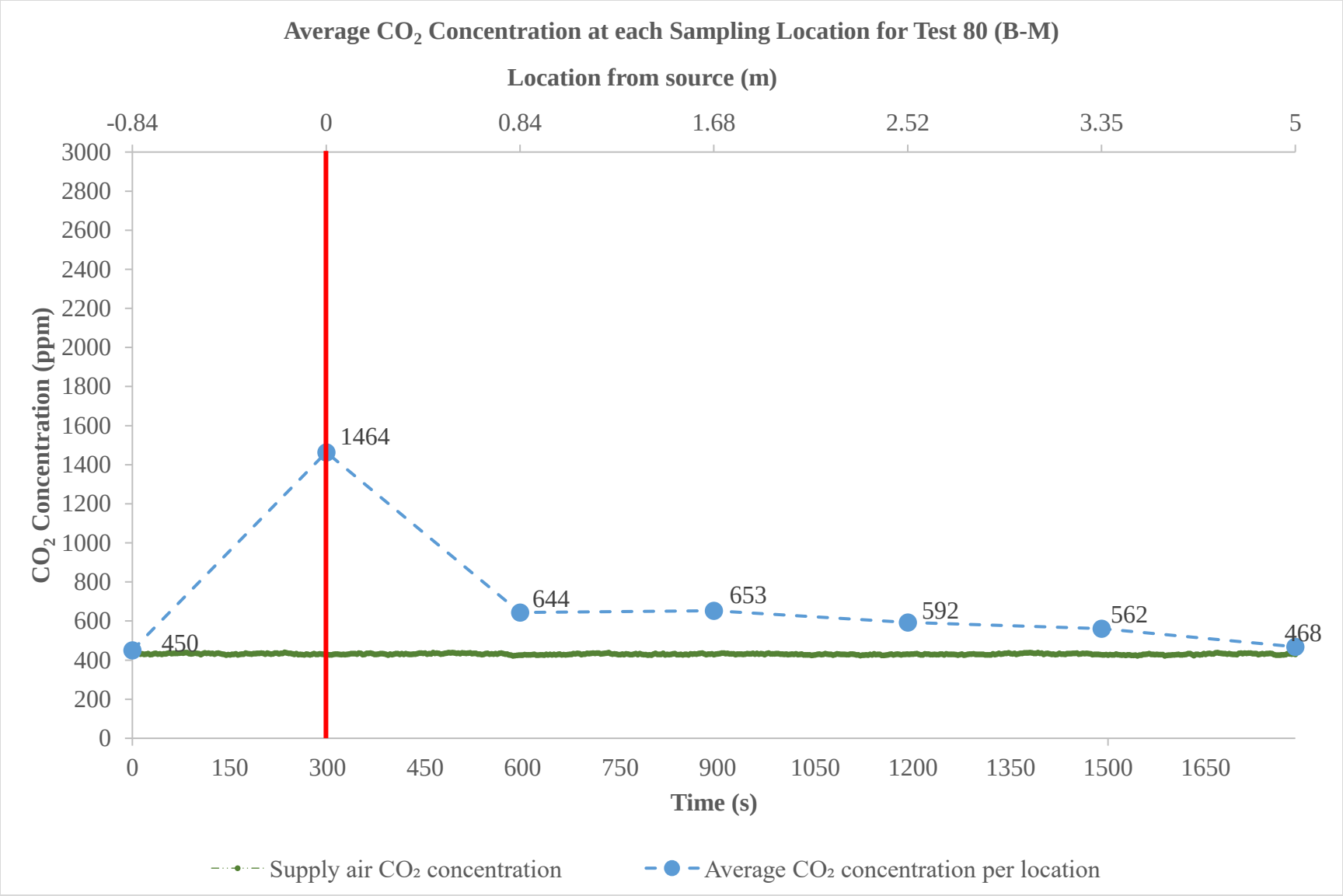

Figure H.137 Average CO_2 concentration at each sampling location for Test 80 (B-M) ISOPass undeployed.

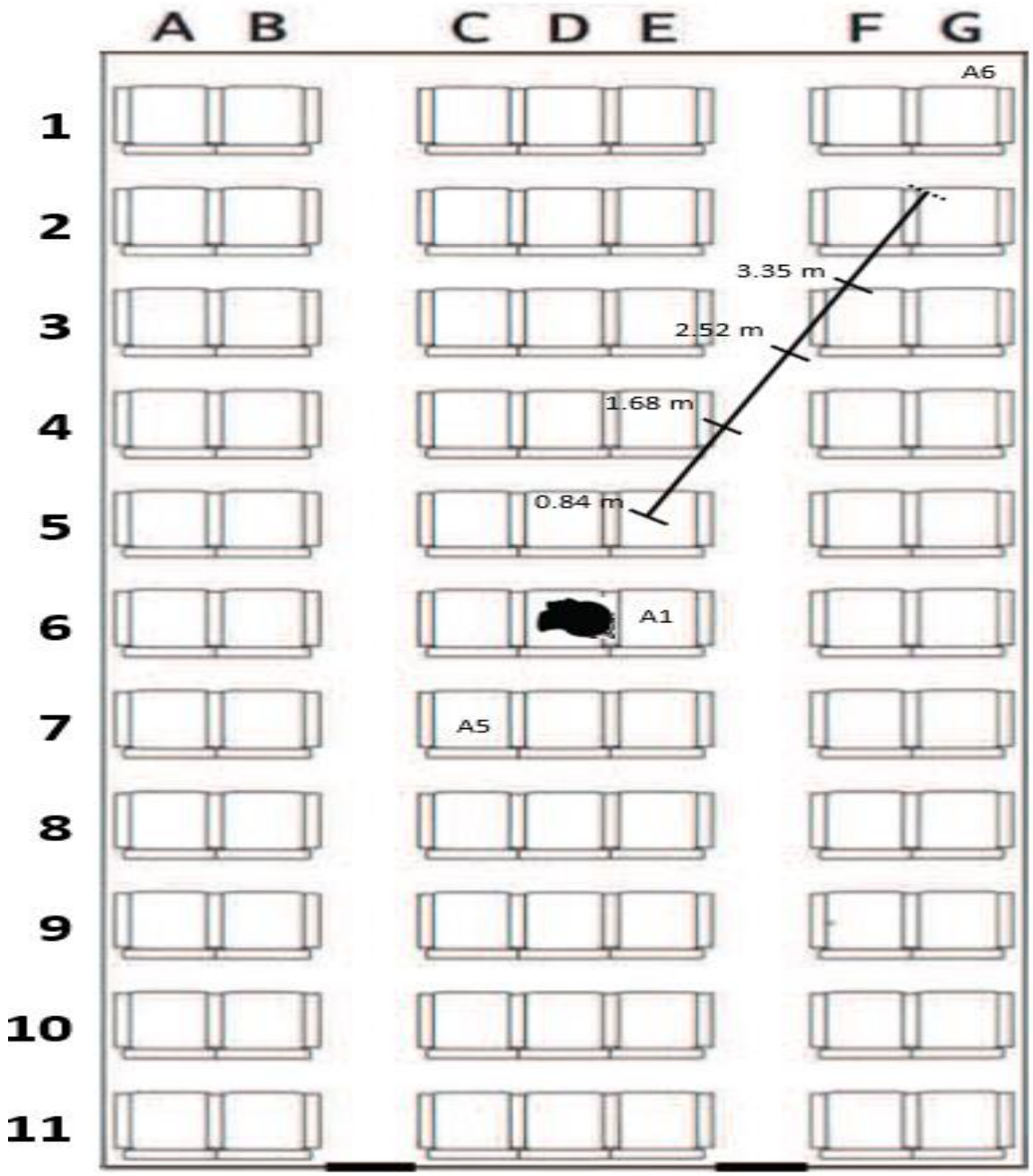

Figure H.138 Test 81 (B-M) ISOPass undeployed source location and sampling tree orientation.

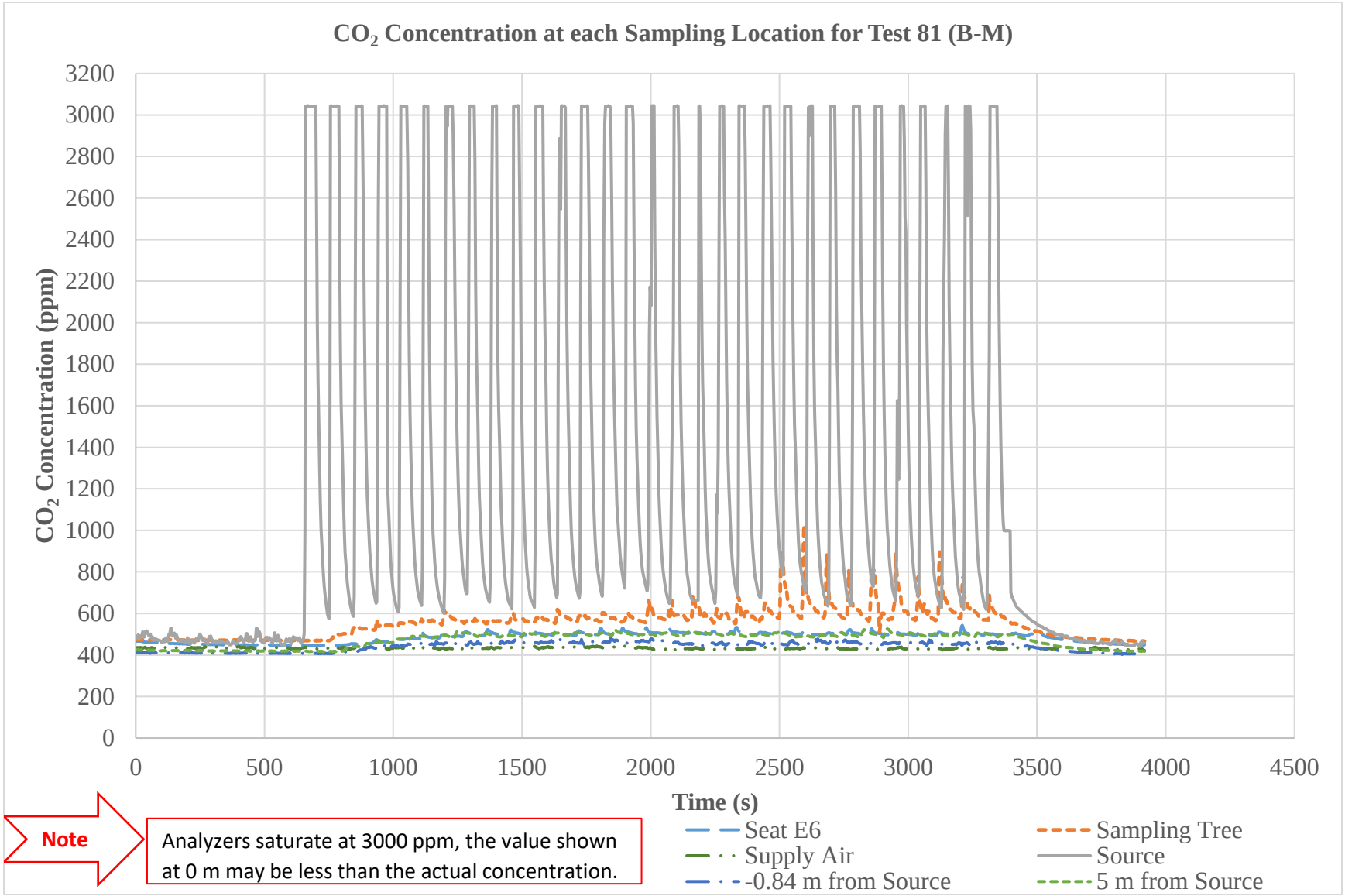

Figure H.139 Ininstantaneous CO_2 concentration at each sampling location for Test 81 (B-M) ISOPass undeployed.

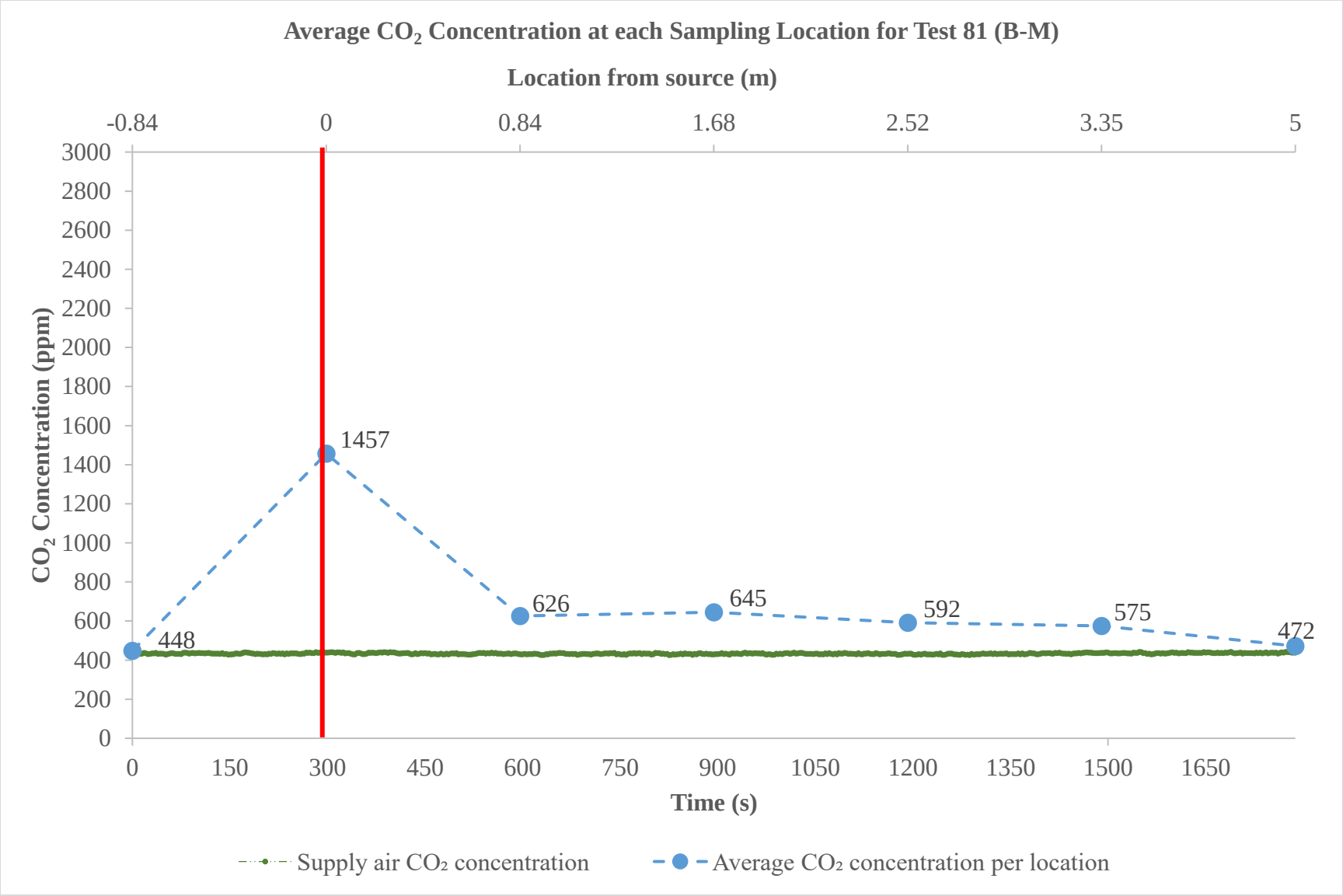

Figure H.140 Average CO_2 concentration at each sampling location for Test 81 (B-M) ISOPass undeployed.

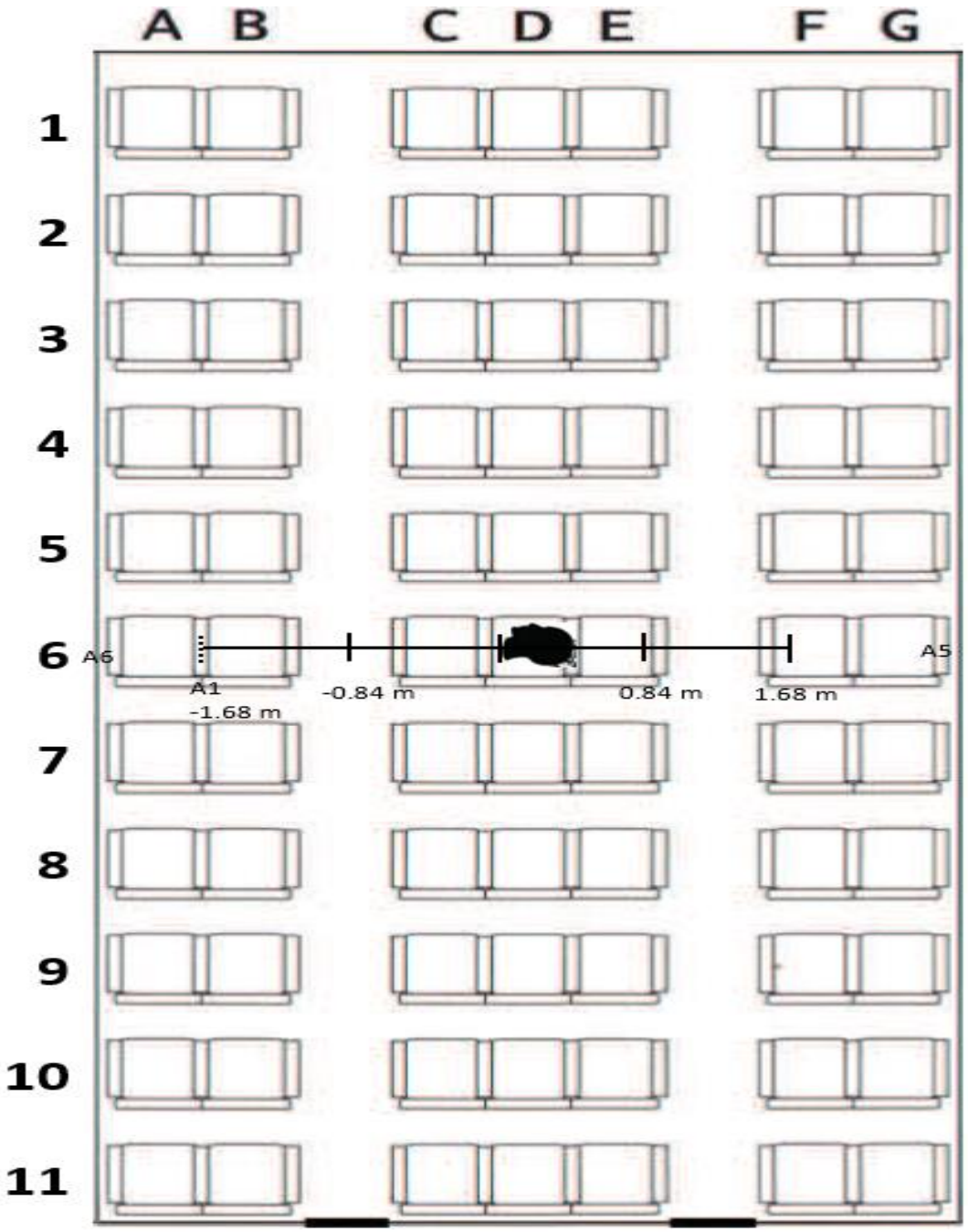

Figure H.141 Test 82 (B-M) ISOPass undeployed source location and sampling tree orientation.

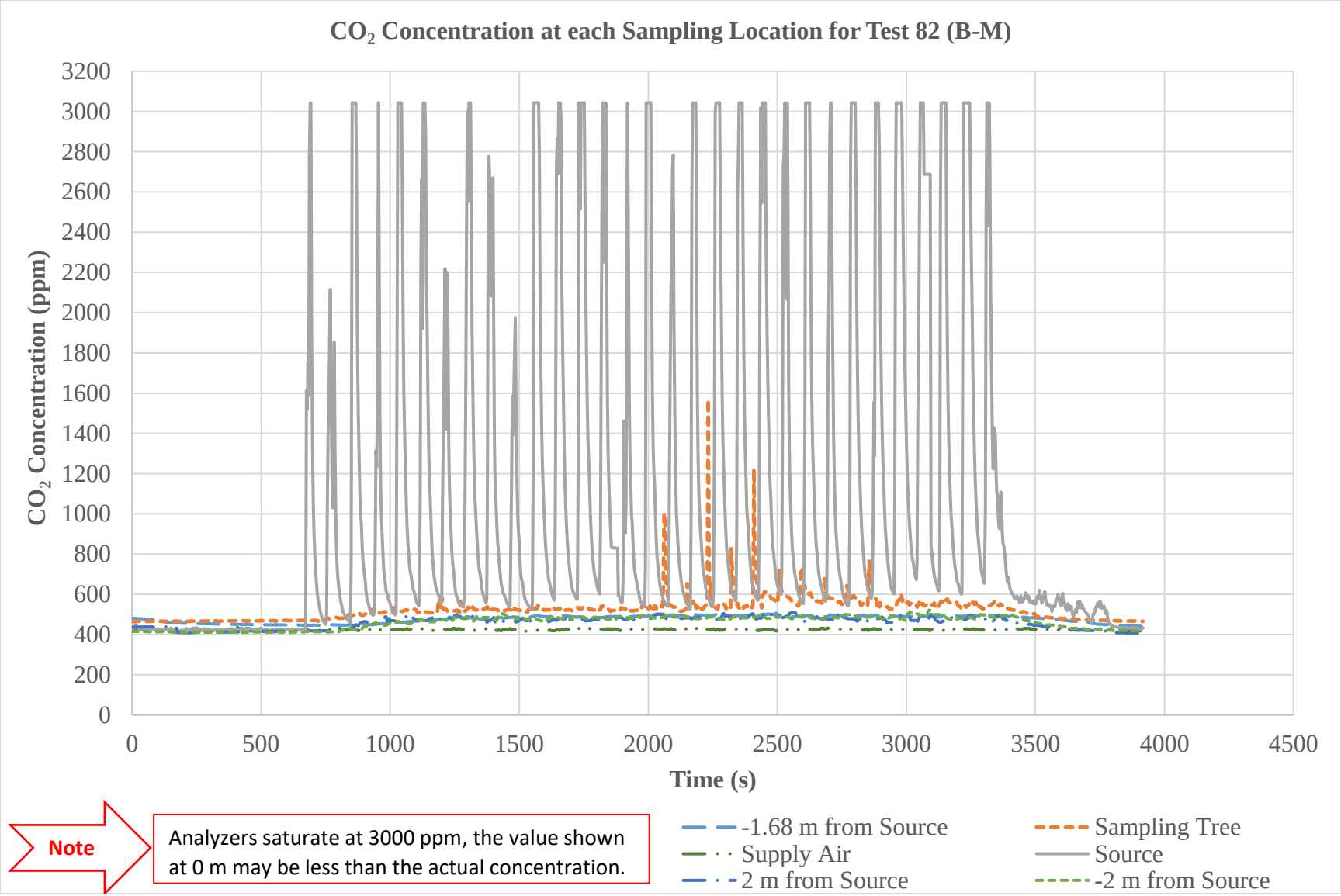

Figure H.142 Ininstantaneous CO_2 concentration at each sampling location for Test 82 (B-M) ISOPass undeployed.

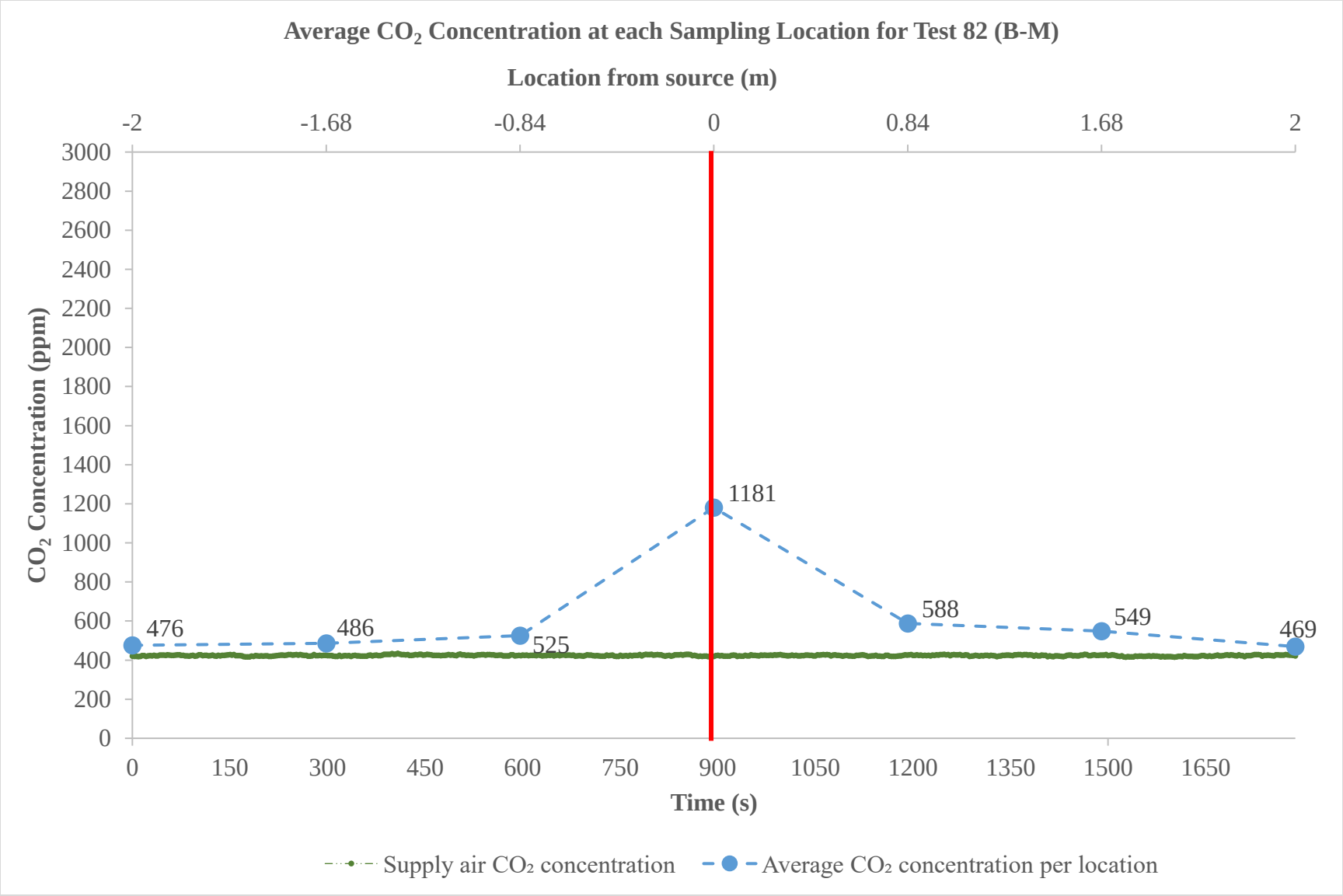

Figure H.143 Average CO_2 concentration at each sampling location for Test 82 (B-M) ISOPass undeployed.

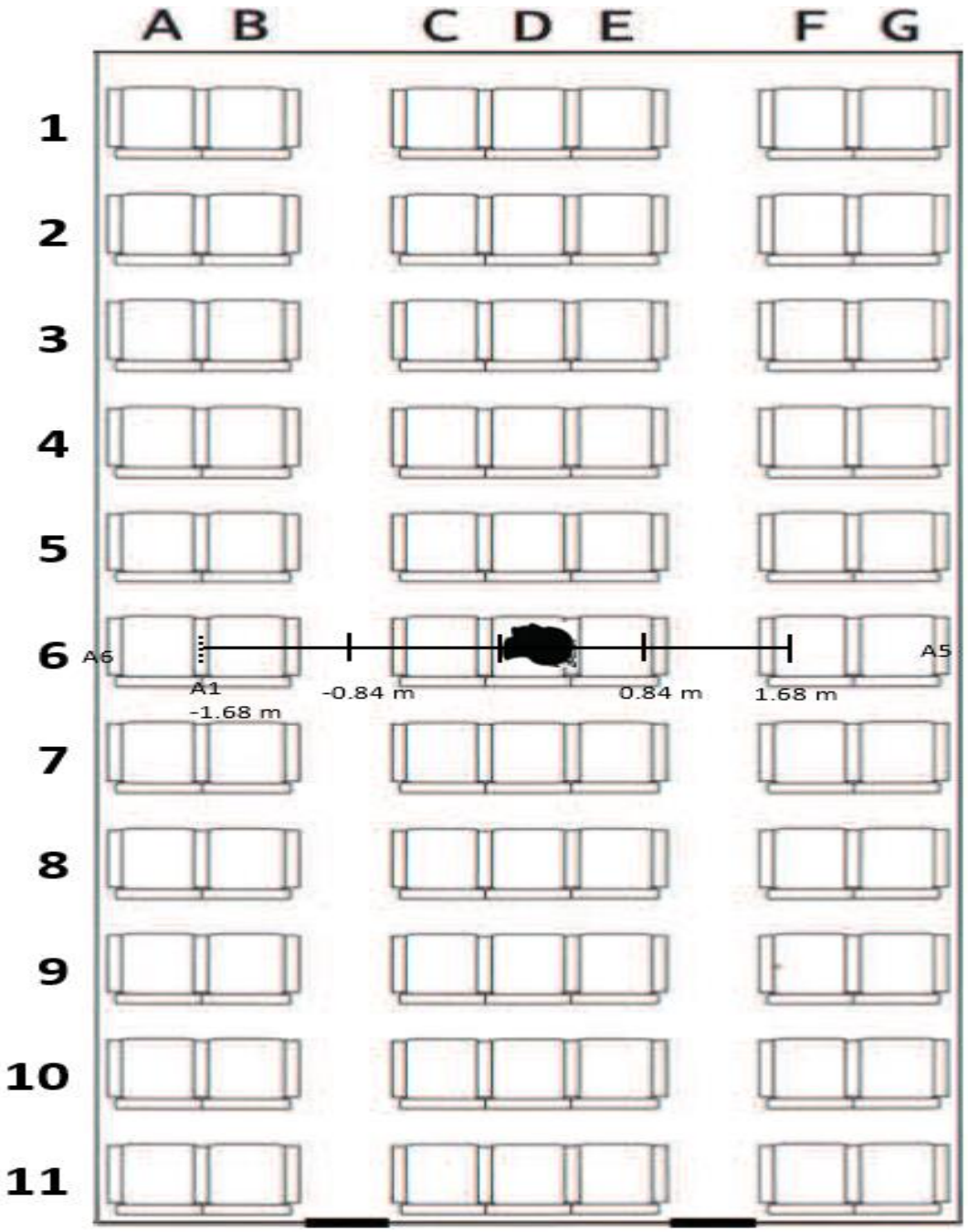

Figure H.144 Test 83 (B-M) ISOPass undeployed source location and sampling tree orientation.

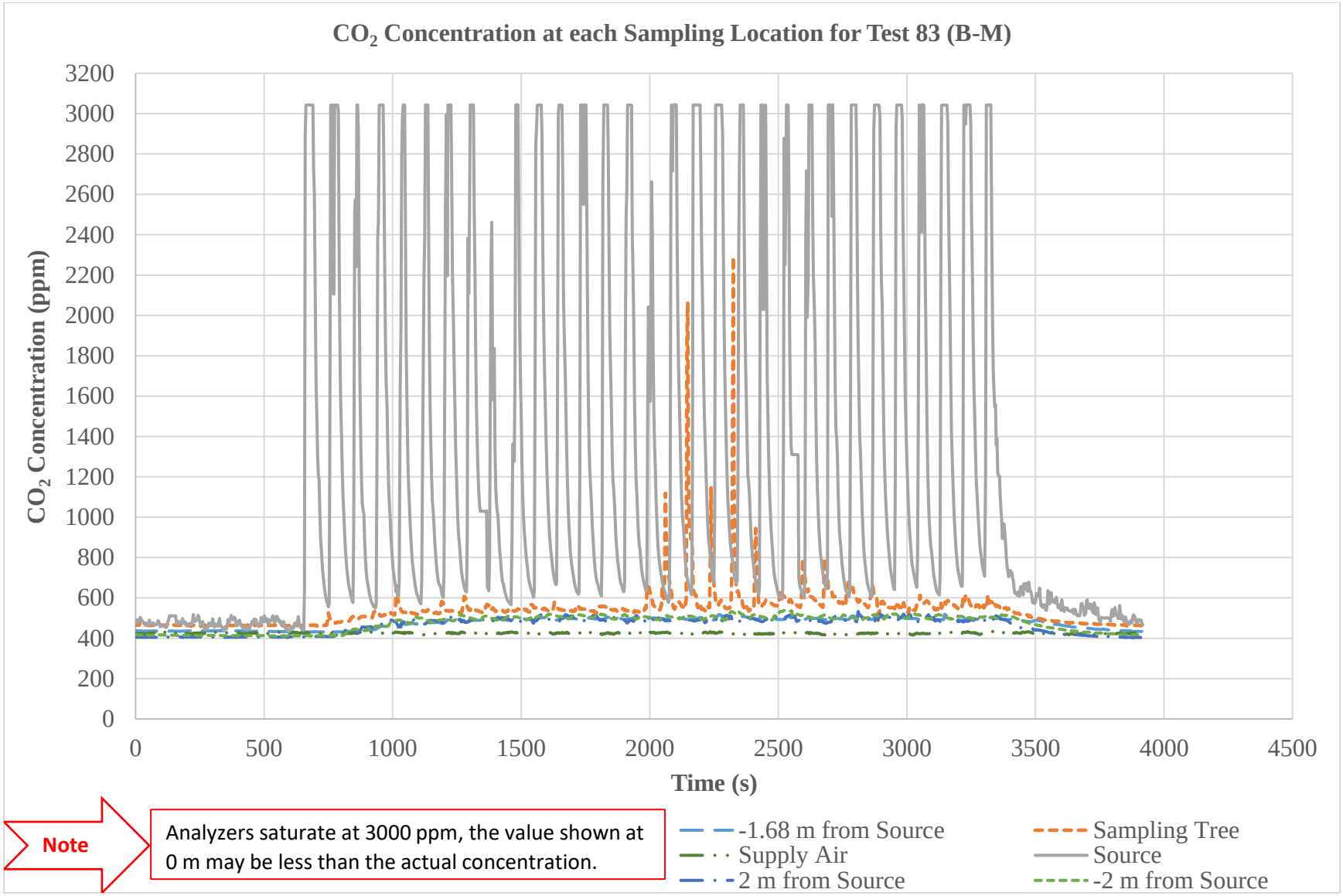

Figure H.145 Ininstantaneous CO_2 concentration at each sampling location for Test 83 (B-M) ISOPass undeployed.

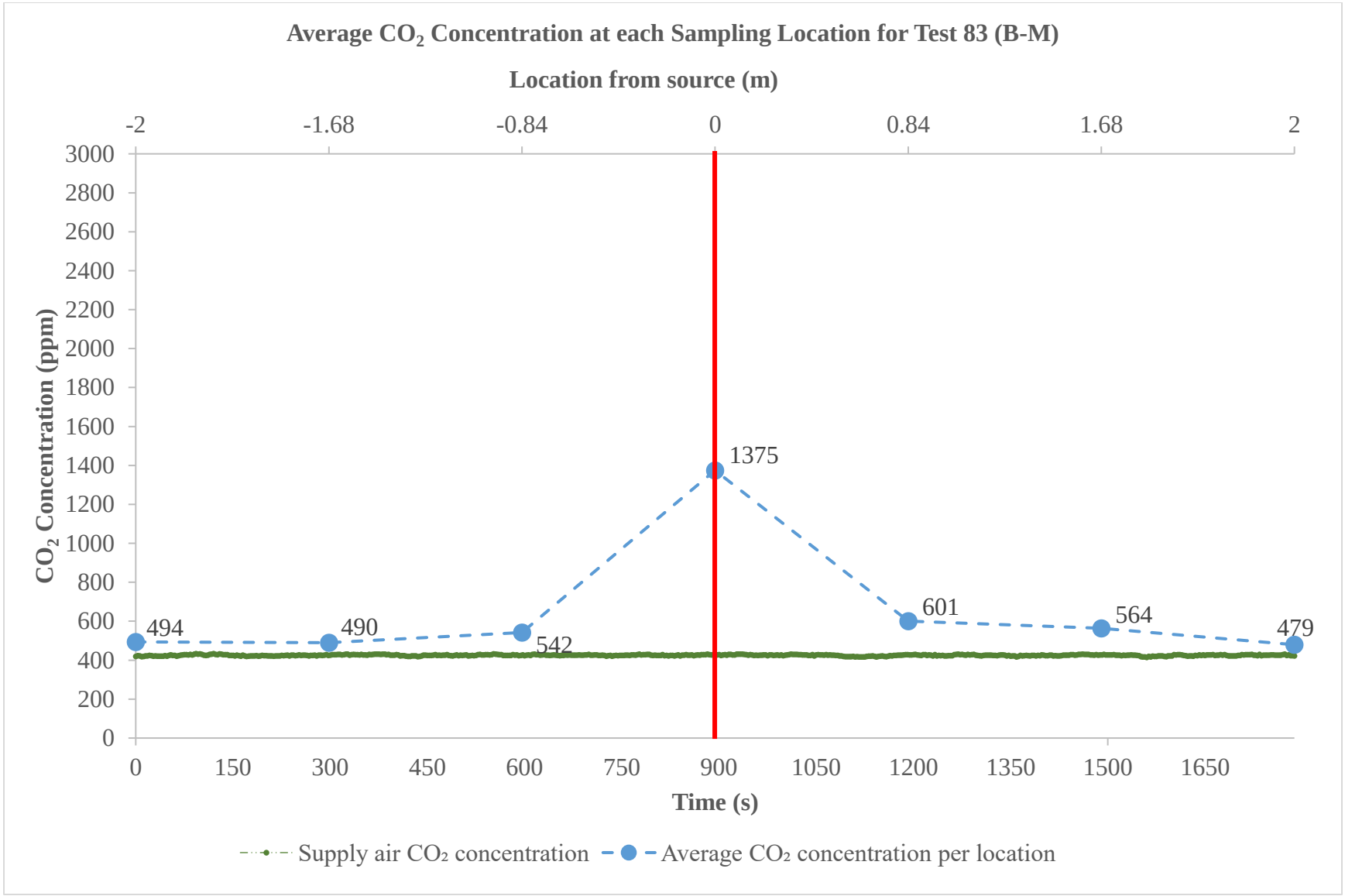

Figure H.146 Average CO_2 concentration at each sampling location for Test 83 (B-M) ISOPass undeployed.

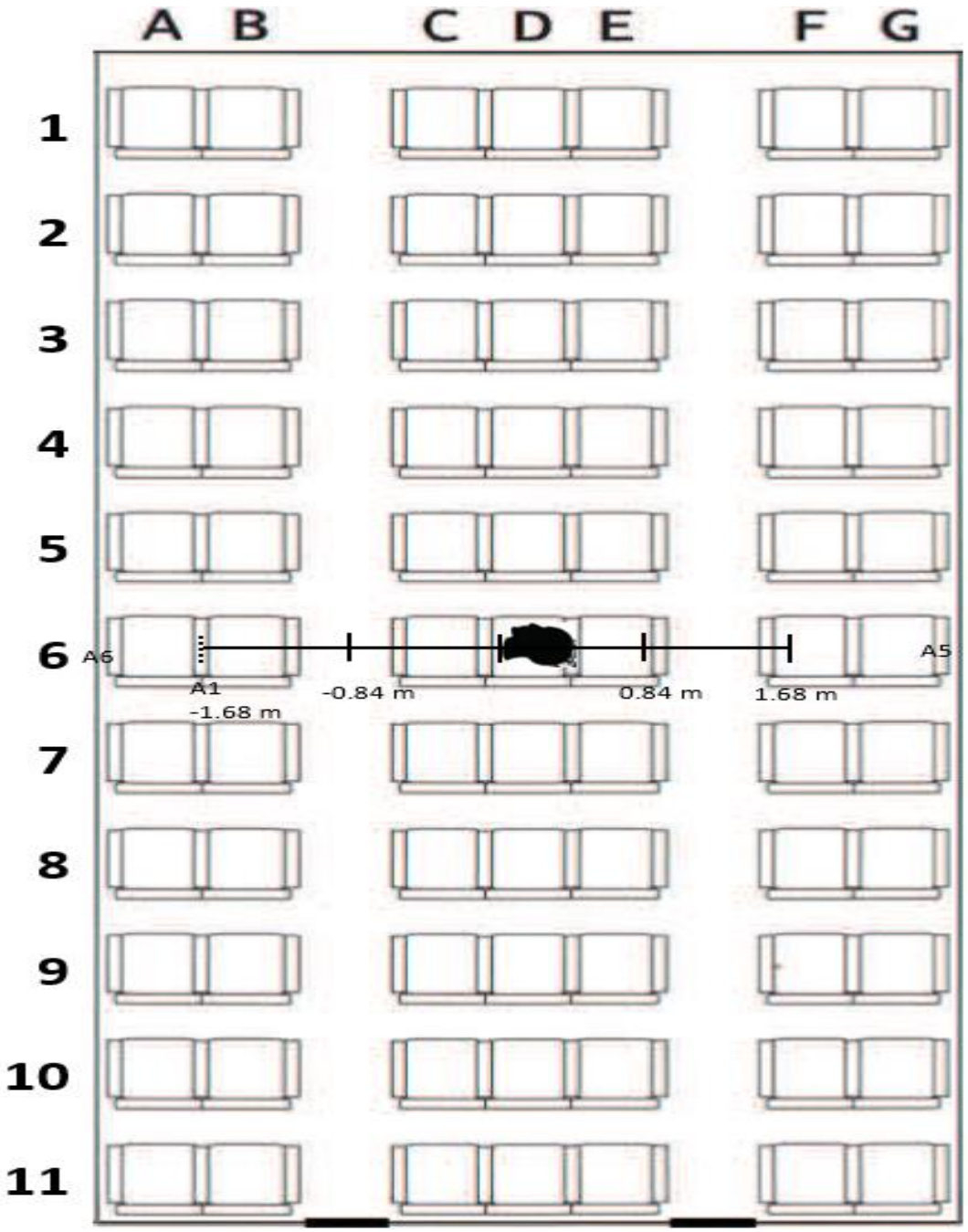

Figure H.147 Test 84 (B-M) ISOPass undeployed source location and sampling tree orientation.

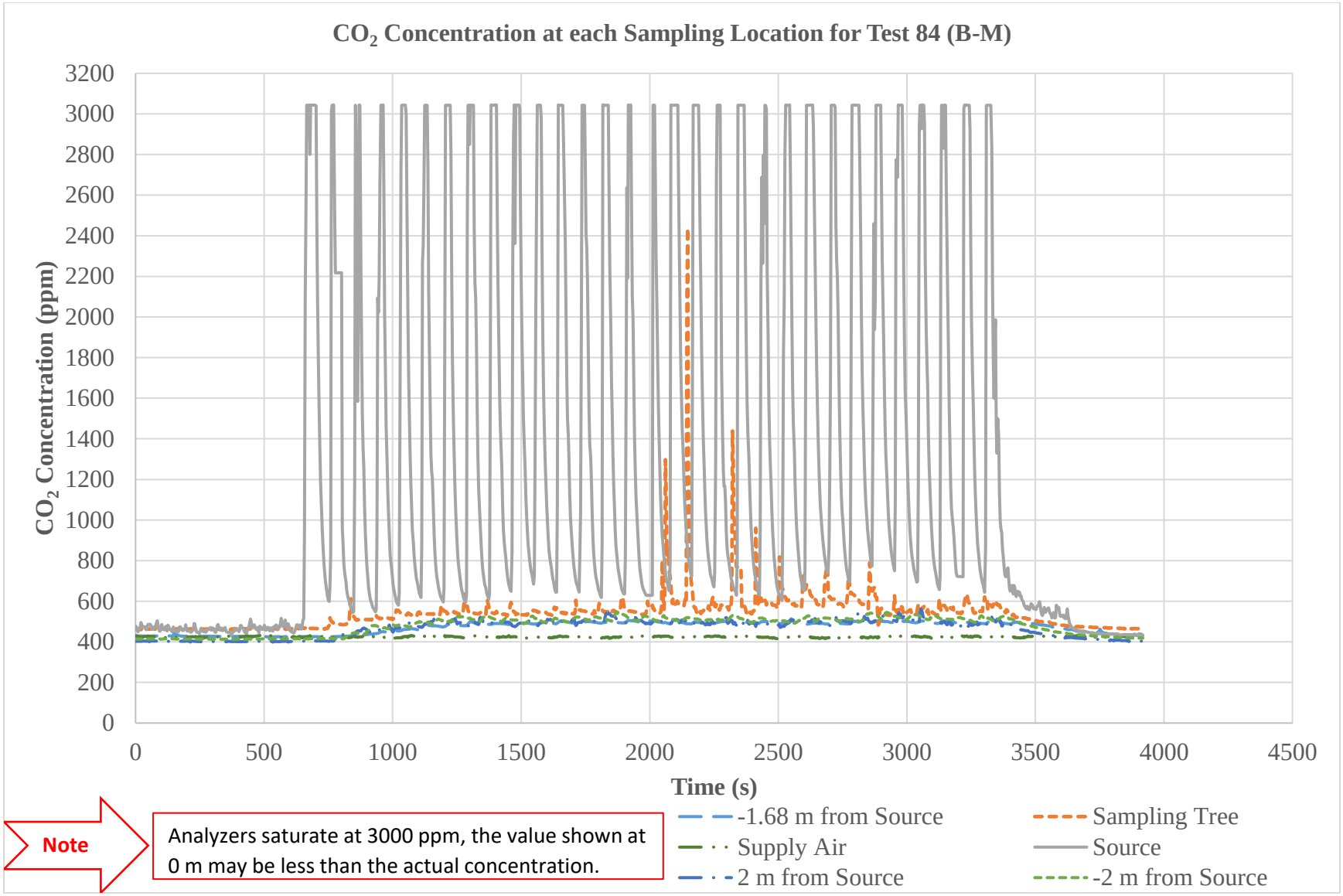

Figure H.148 Ininstantaneous CO_2 concentration at each sampling location for Test 84 (B-M) ISOPass undeployed.

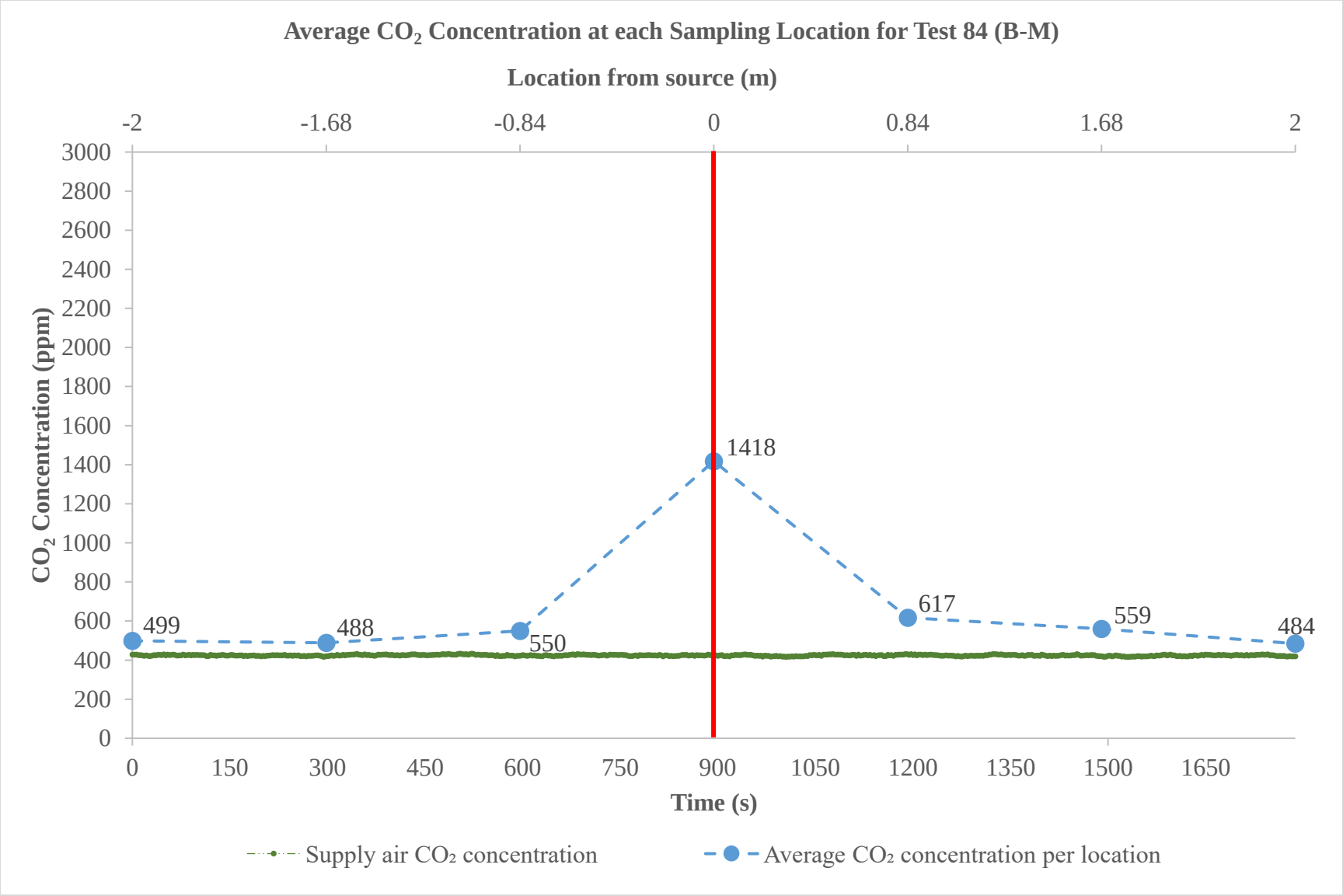

Figure H.149 Average CO_2 concentration at each sampling location for Test 84 (B-M) ISOPass undeployed.

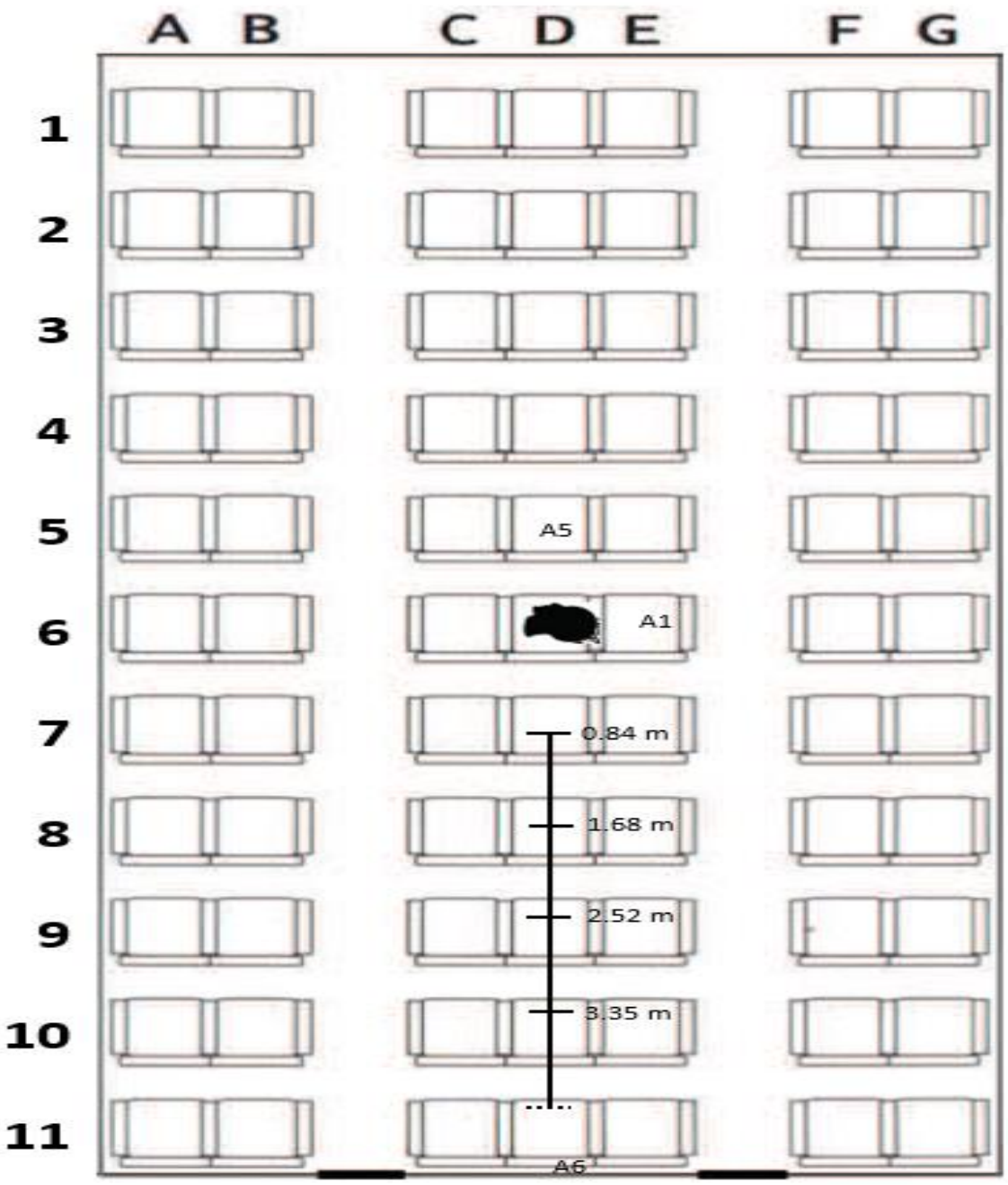

Figure H.150 Test 85 (B-M) ISOPass undeployed source location and sampling tree orientation.

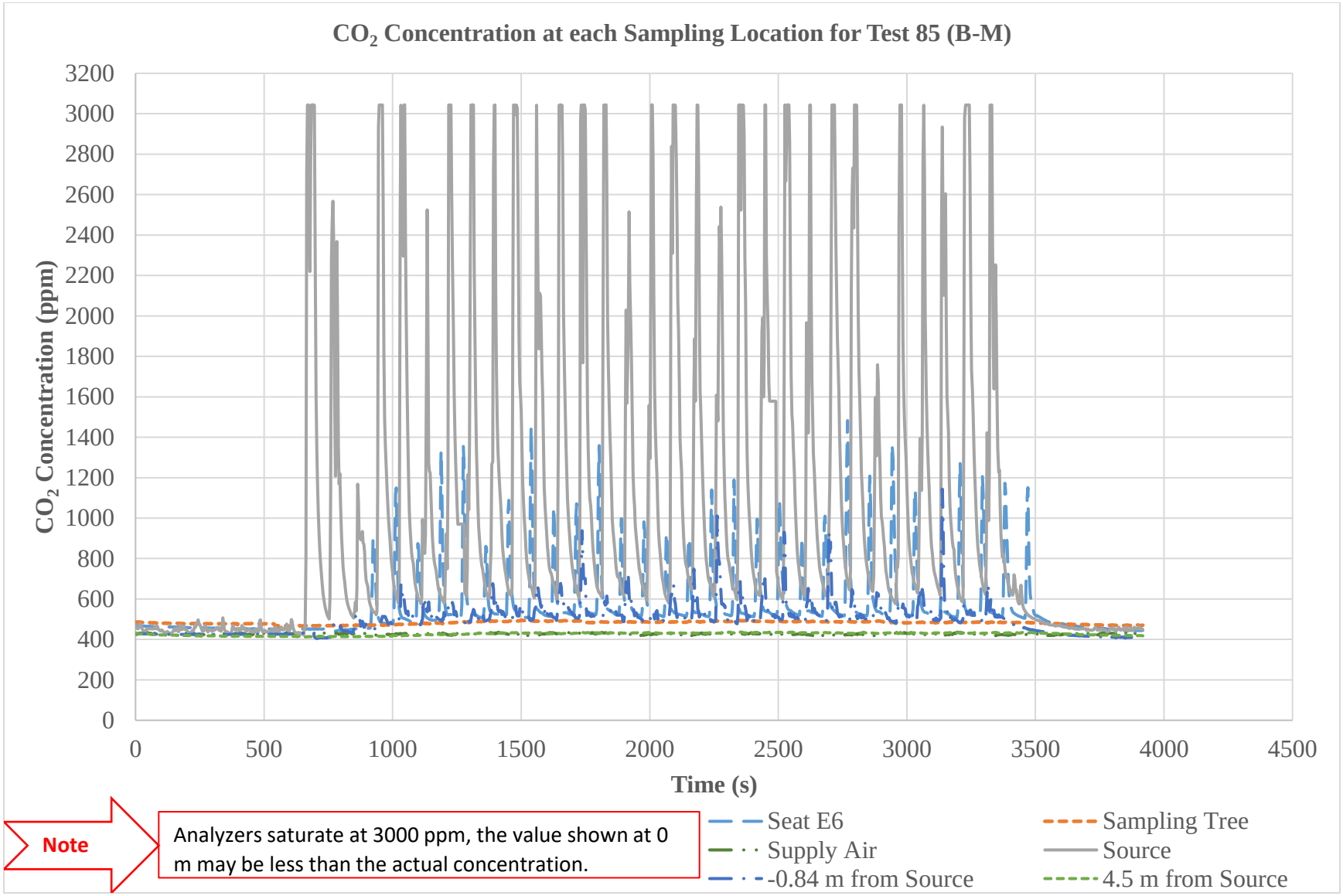

Figure H.151 Ininstantaneous CO_2 concentration at each sampling location for Test 85 (B-M) ISOPass undeployed.

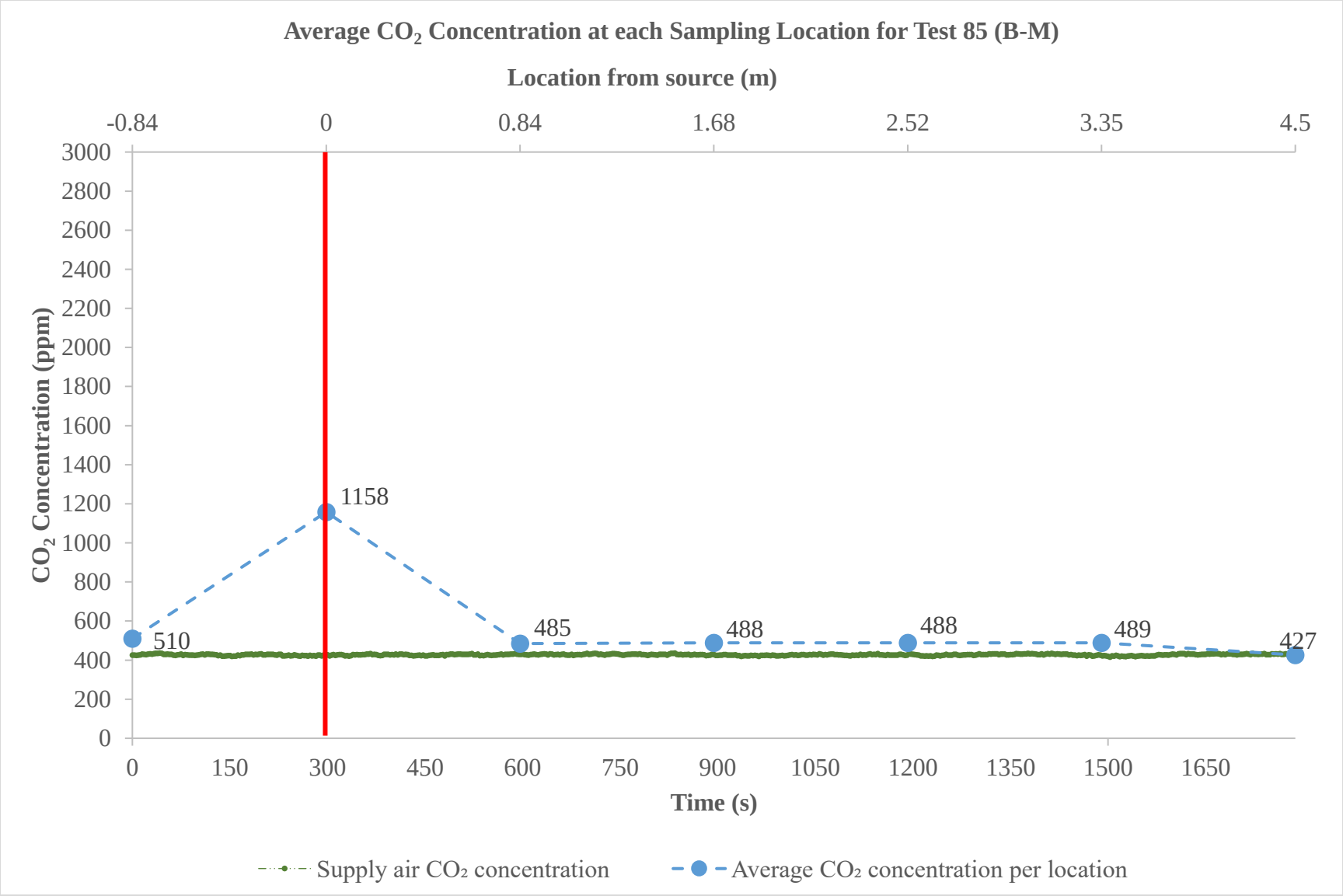

Figure H.152 Average CO_2 concentration at each sampling location for Test 85 (B-M) ISOPass undeployed.

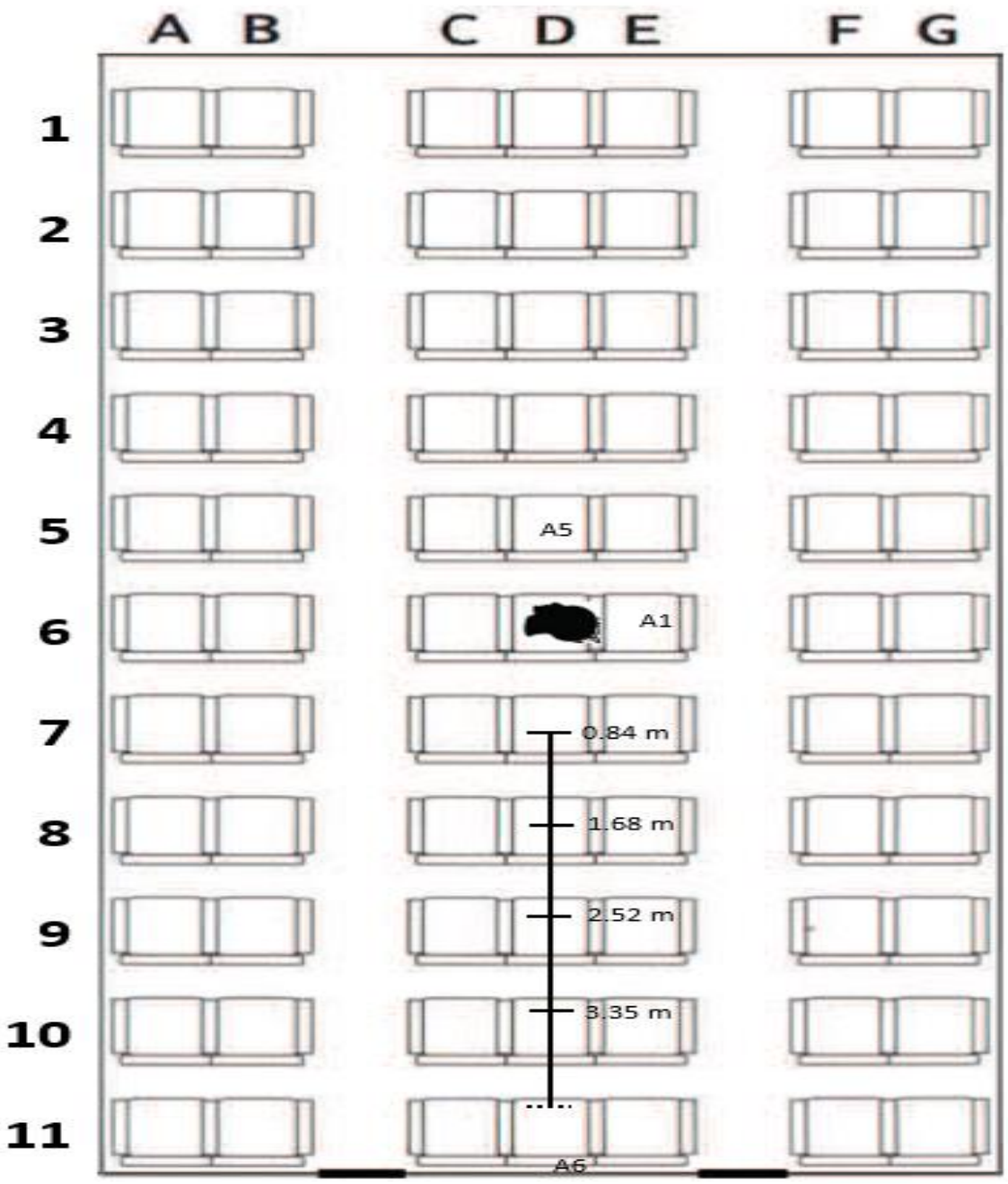

Figure H.153 Test 86 (B-M) ISOPass undeployed source location and sampling tree orientation.

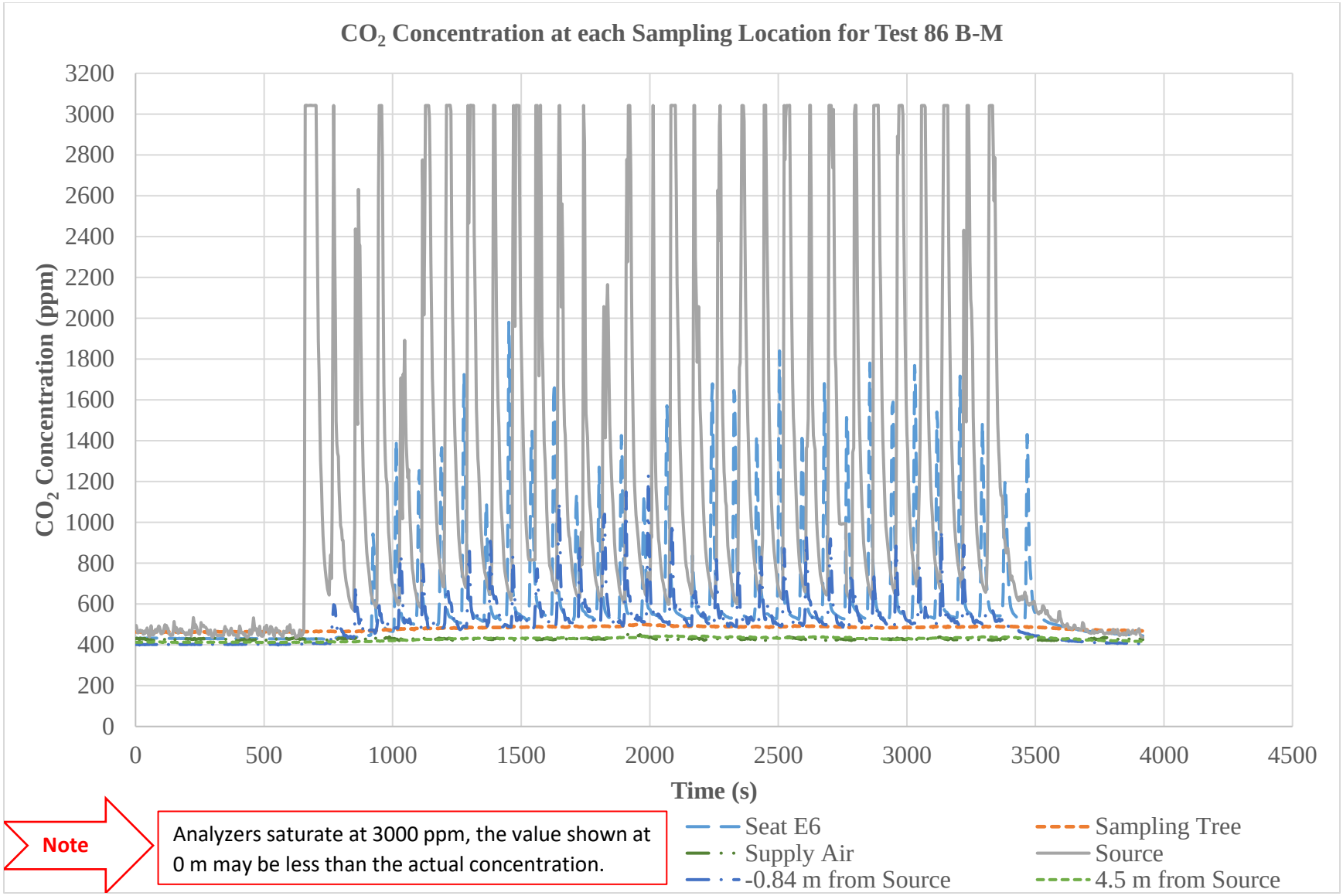

Figure H.154 Ininstantaneous CO_2 concentration at each sampling location for Test 86 (B-M) ISOPass undeployed.

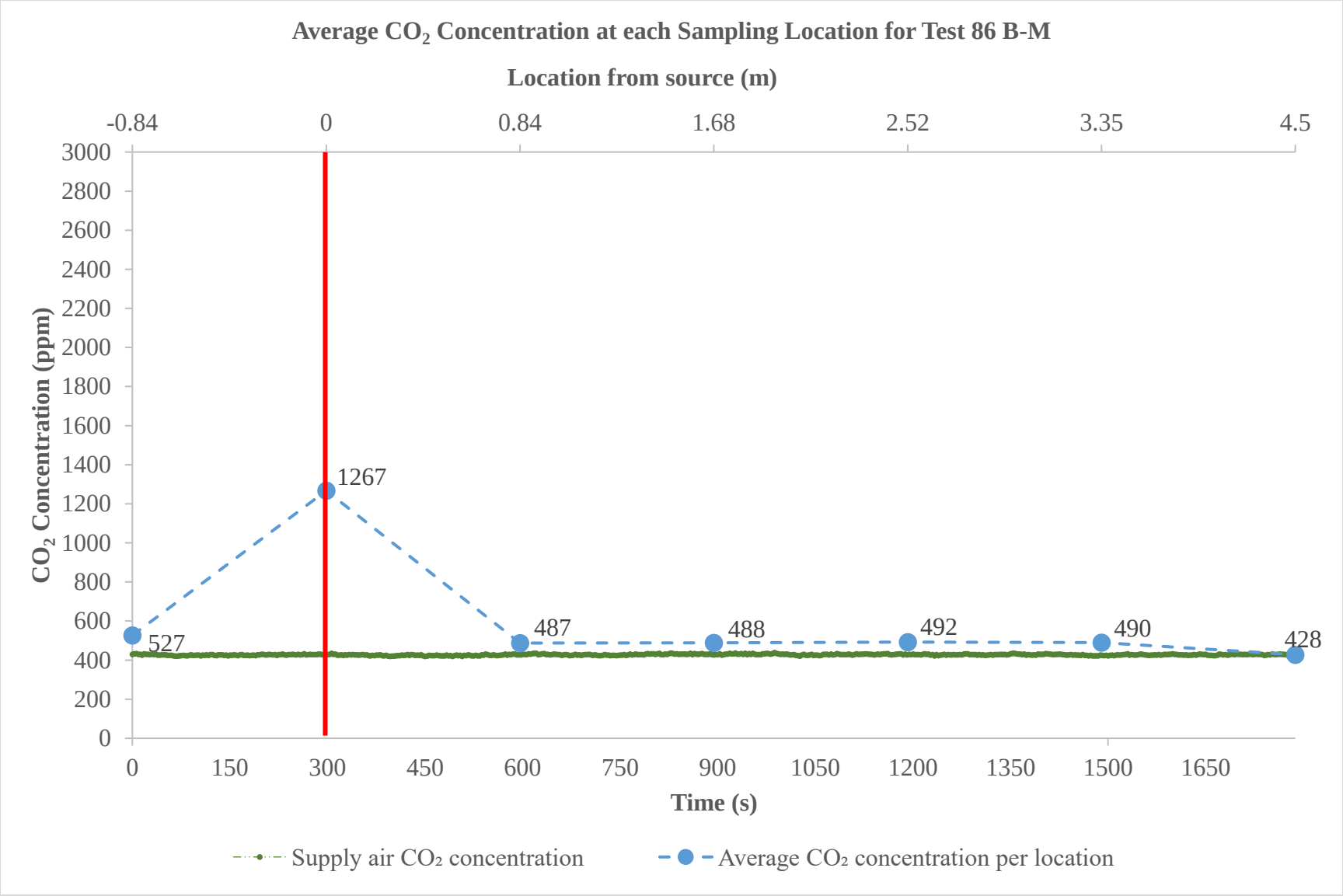

Figure H.155 Average CO_2 concentration at each sampling location for Test 86 (B-M) ISOPass undeployed.

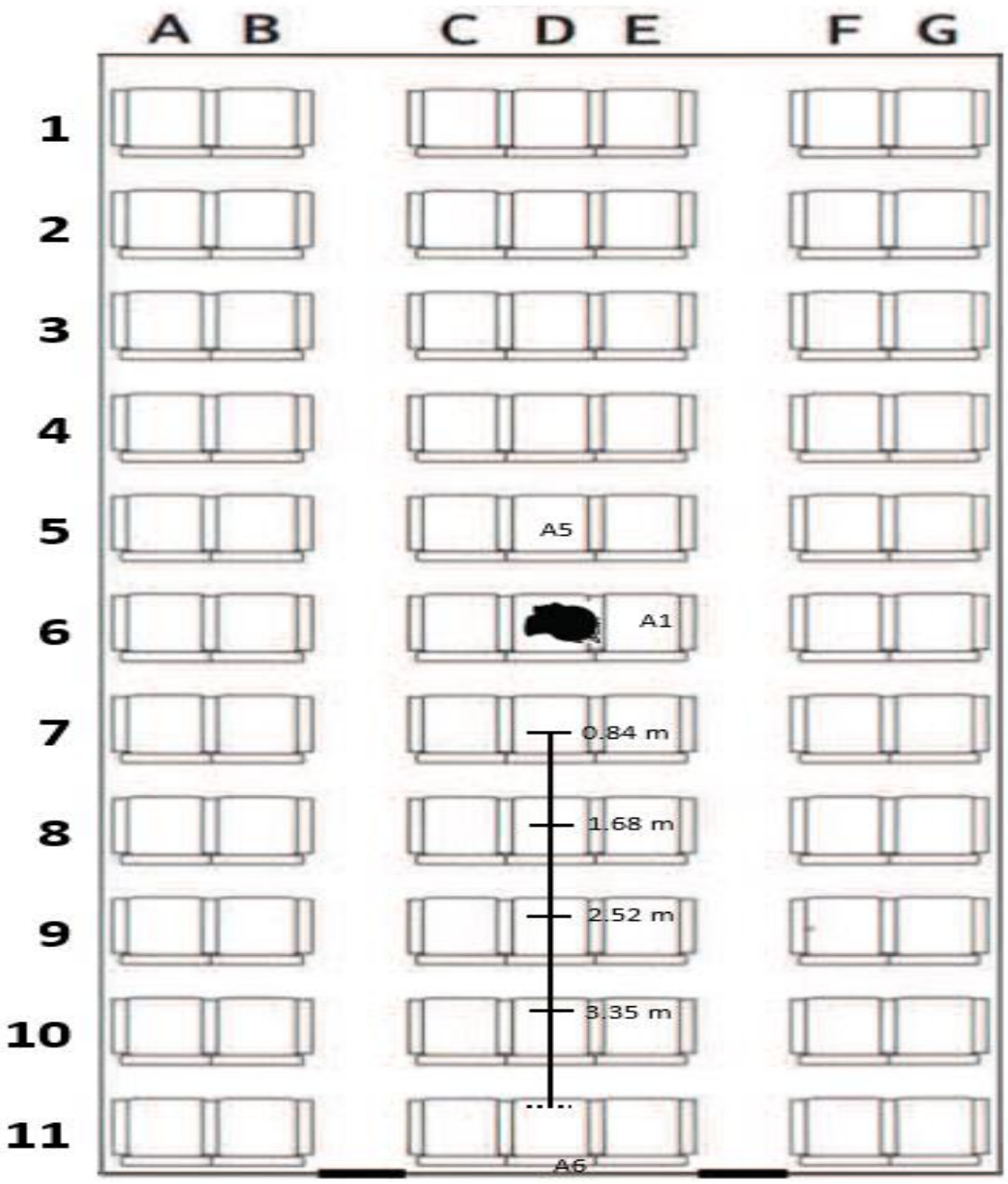

Figure H.156 Test 87 (B-M) ISOPass undeployed source location and sampling tree orientation.

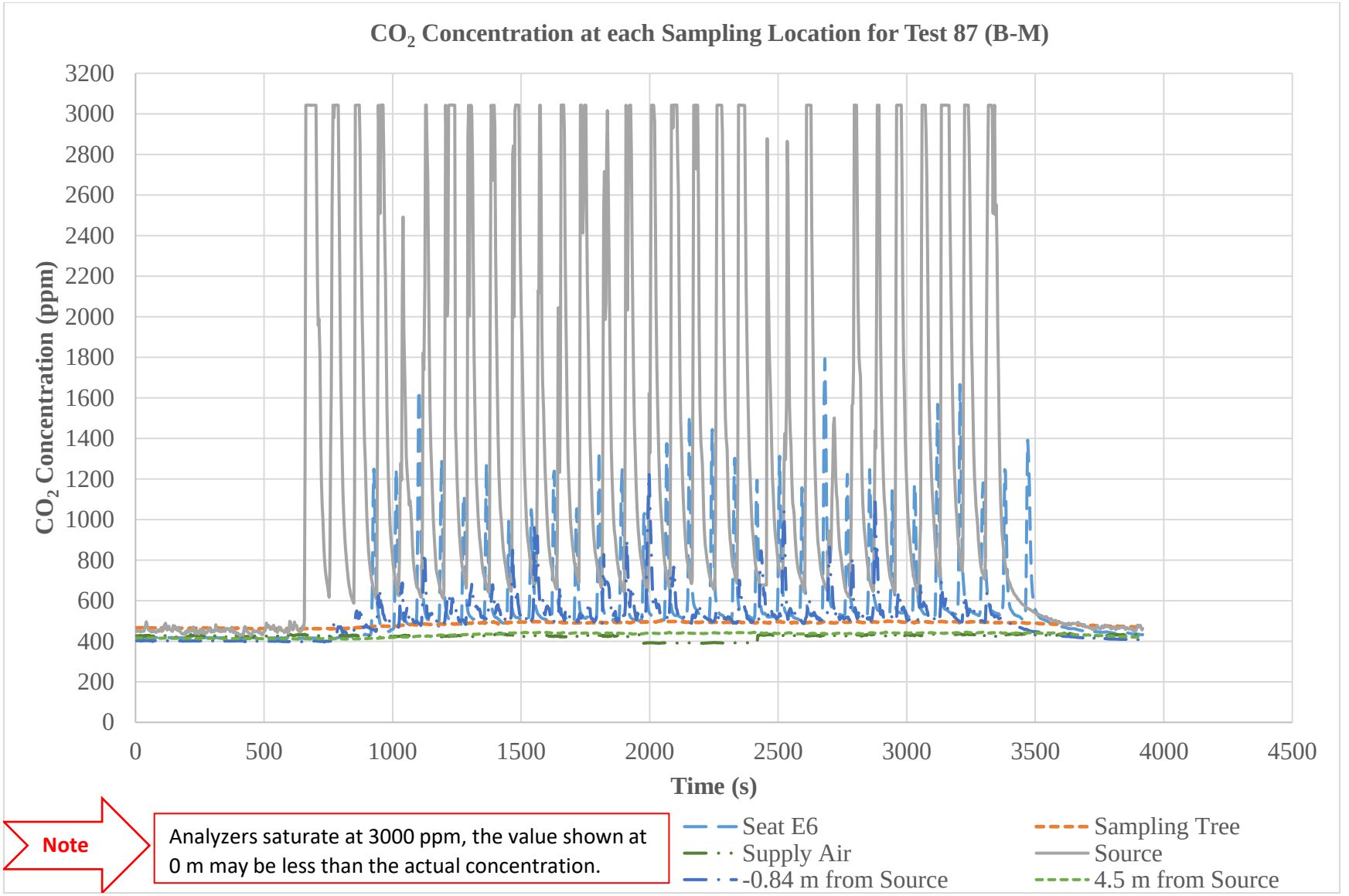

Figure H.157 Ininstantaneous CO_2 concentration at each sampling location for Test 87 (B-M) ISOPass undeployed.

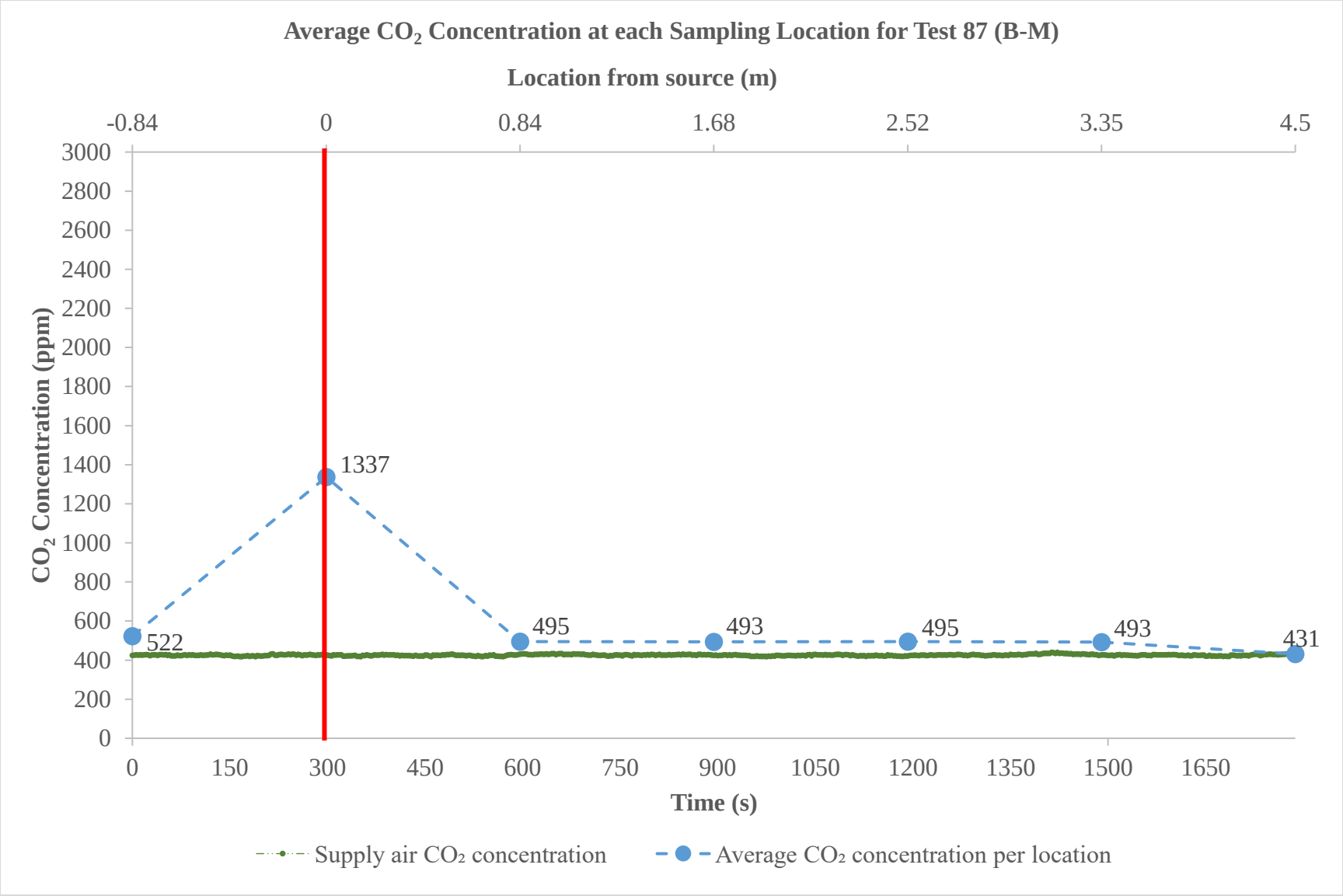

Figure H.158 Average CO_2 concentration at each sampling location for Test 87 (B-M) ISOPass undeployed.

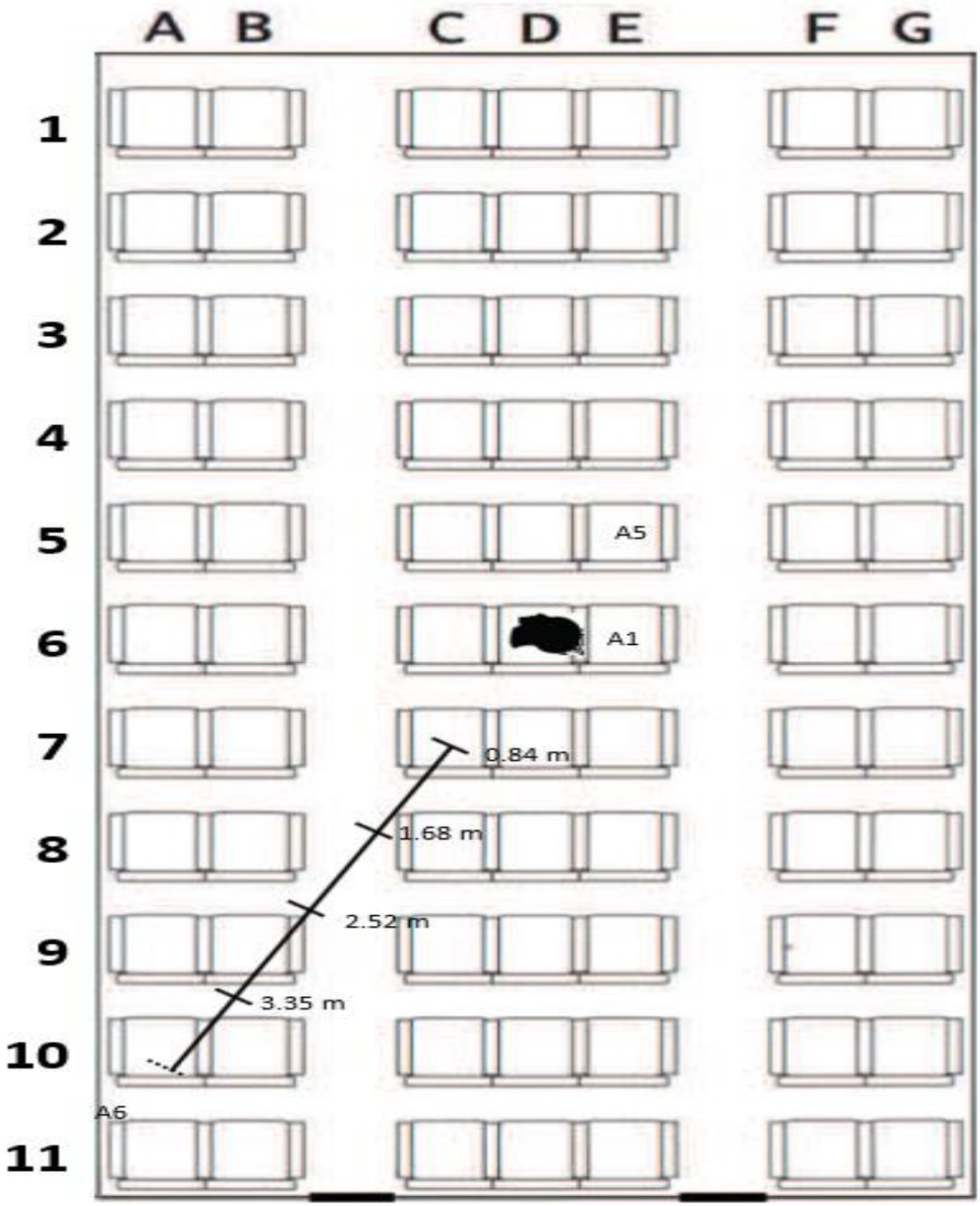

Figure H.159 Test 88 (B-M) ISOPass undeployed source location and sampling tree orientation.

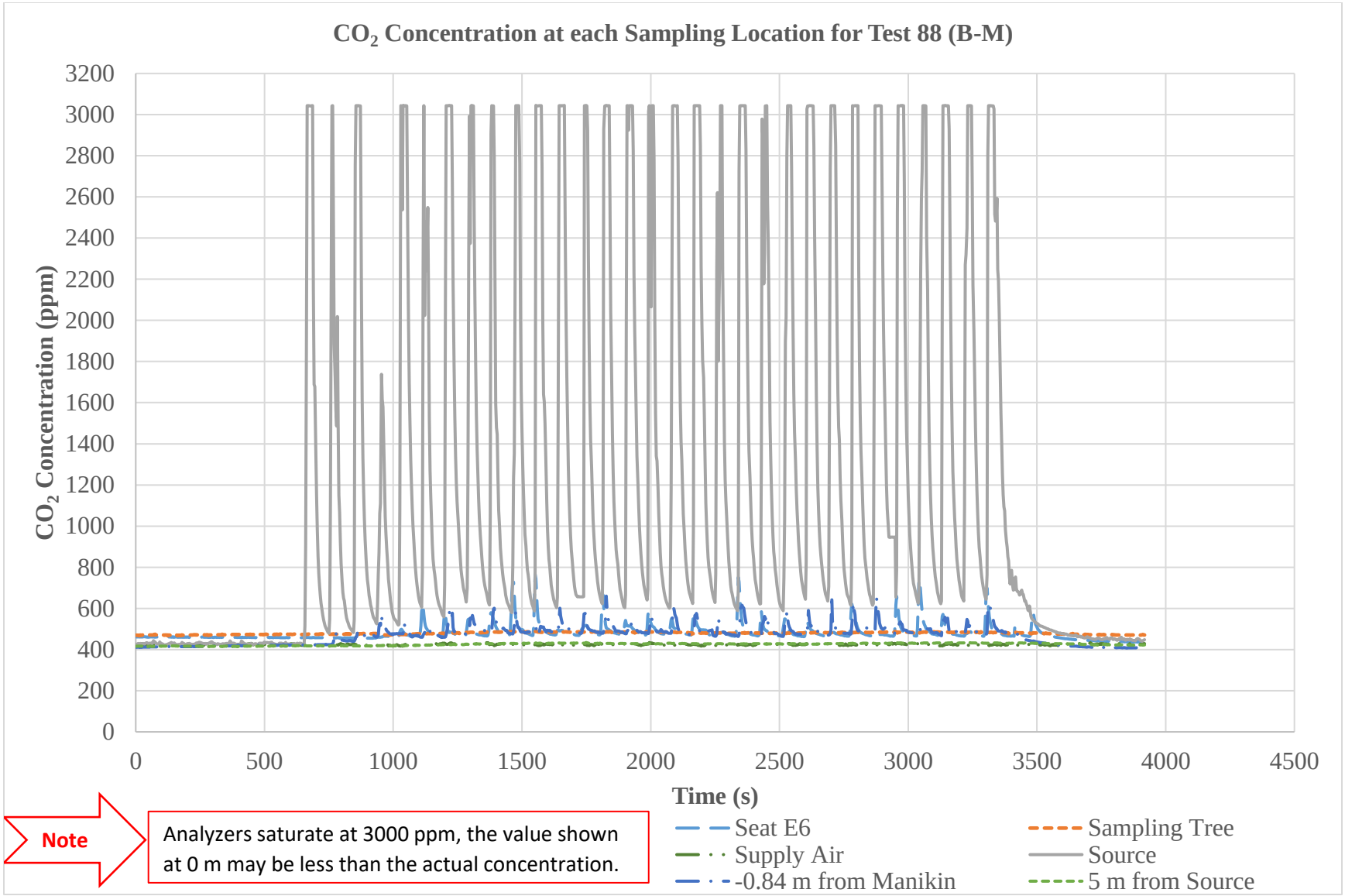

Figure H.160 Ininstantaneous CO_2 concentration at each sampling location for Test 88 (B-M) ISOPass undeployed.

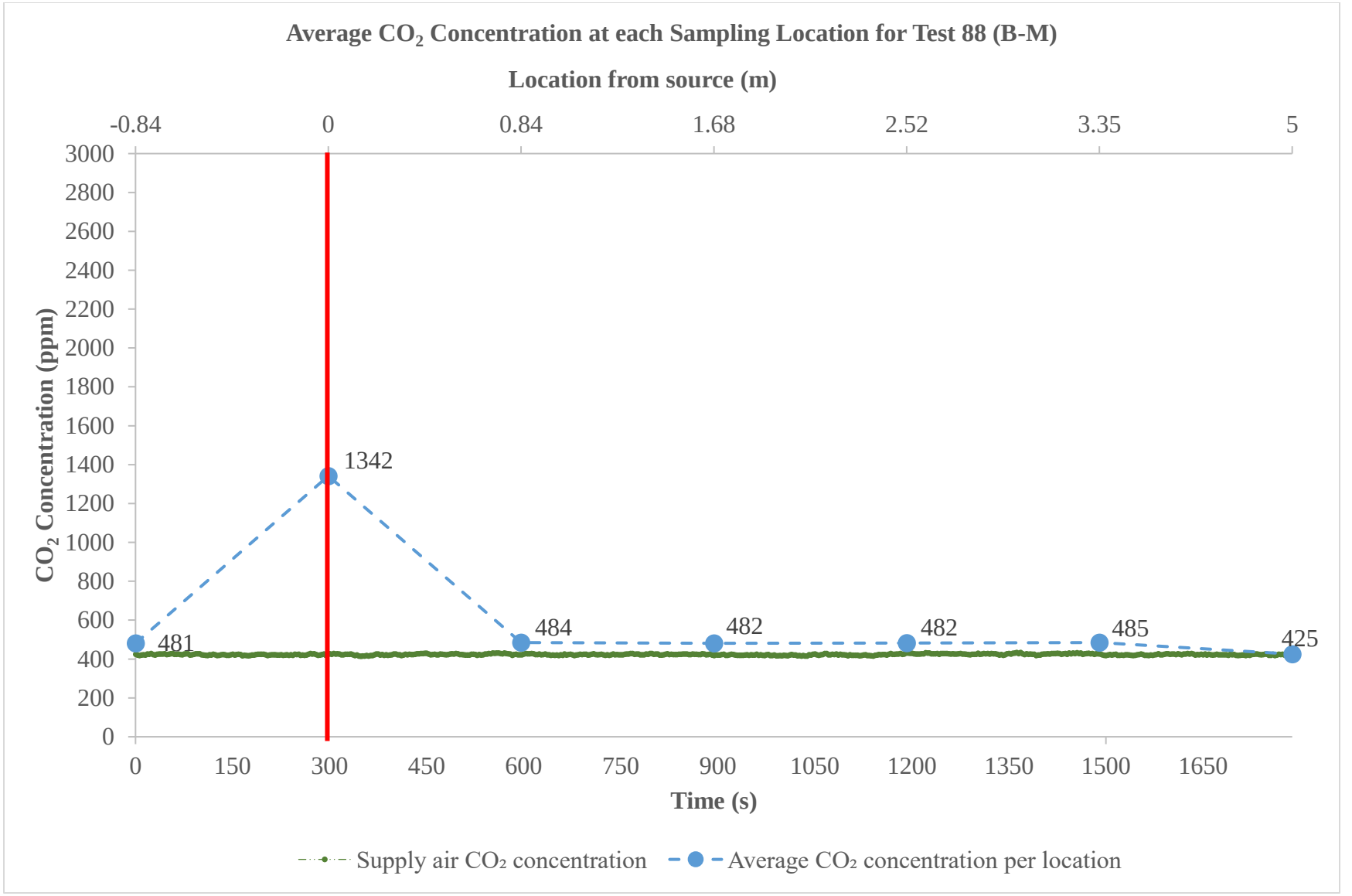

Figure H.161 Average CO_2 concentration at each sampling location for Test 88 (B-M) ISOPass undeployed.

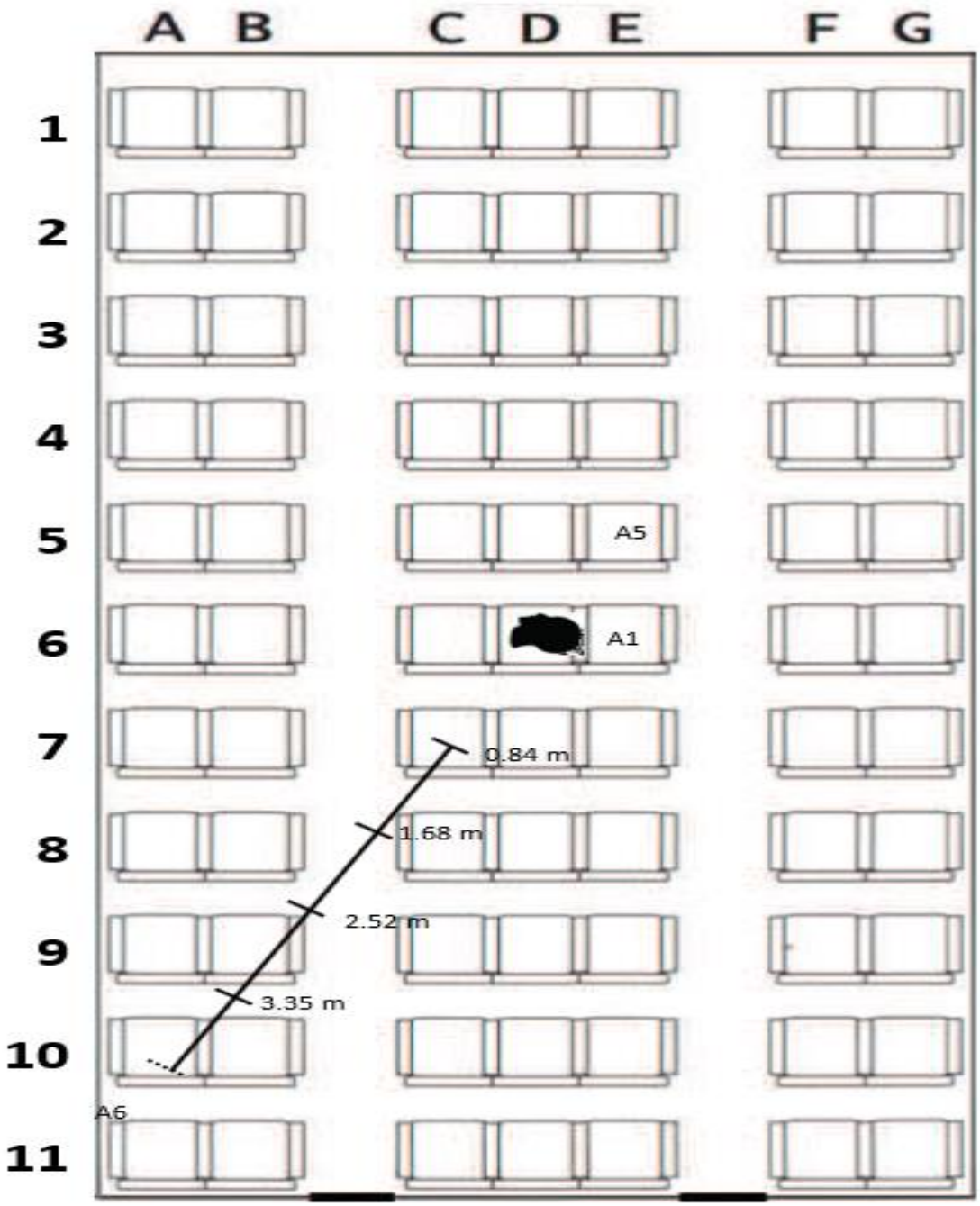

Figure H.162 Test 89 (B-M) ISOPass undeployed source location and sampling tree orientation.

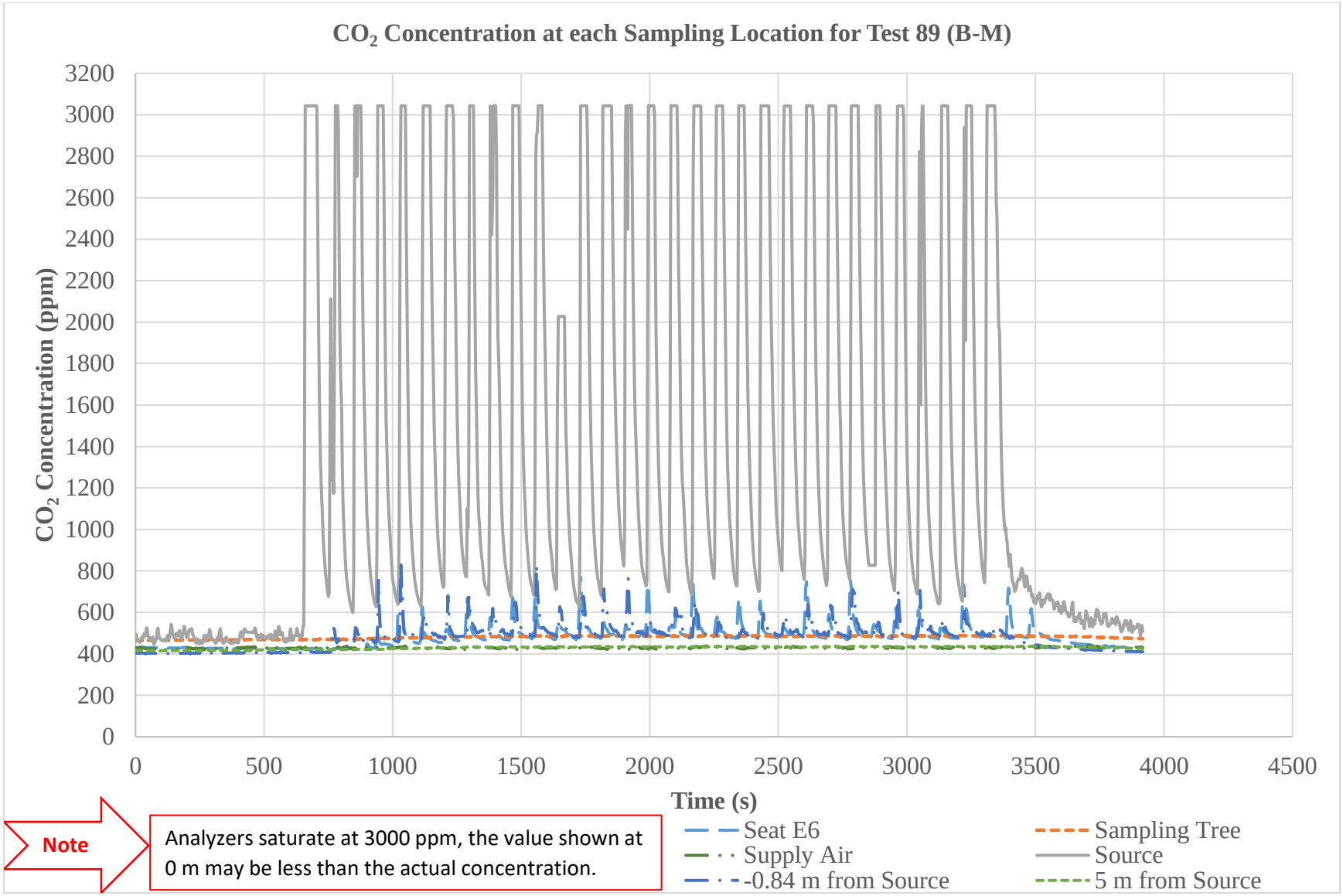

Figure H.163 Ininstantaneous CO_2 concentration at each sampling location for Test 89 (B-M) ISOPass undeployed.

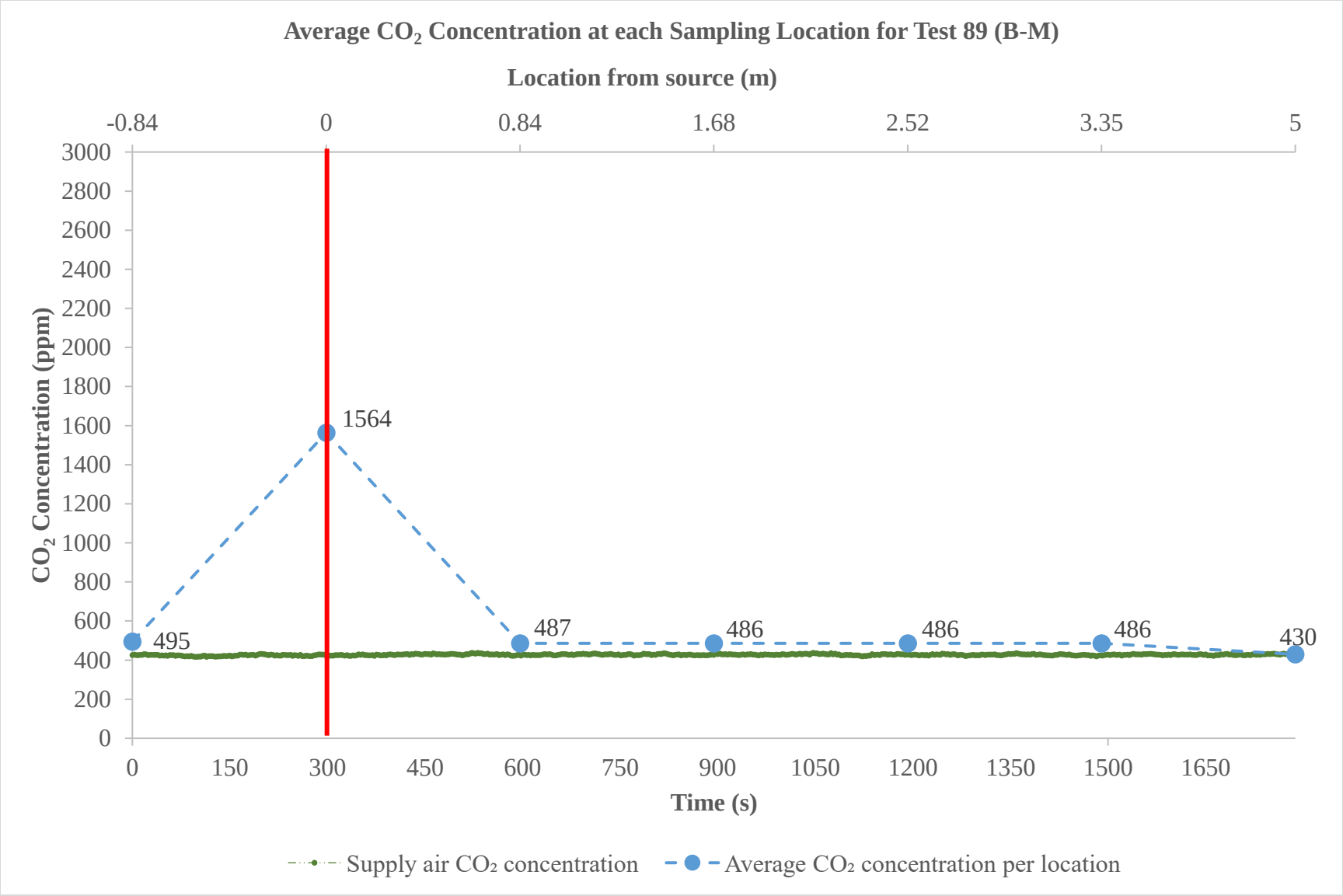

Figure H.164 Average CO_2 concentration at each sampling location for Test 89 (B-M) ISOPass undeployed.

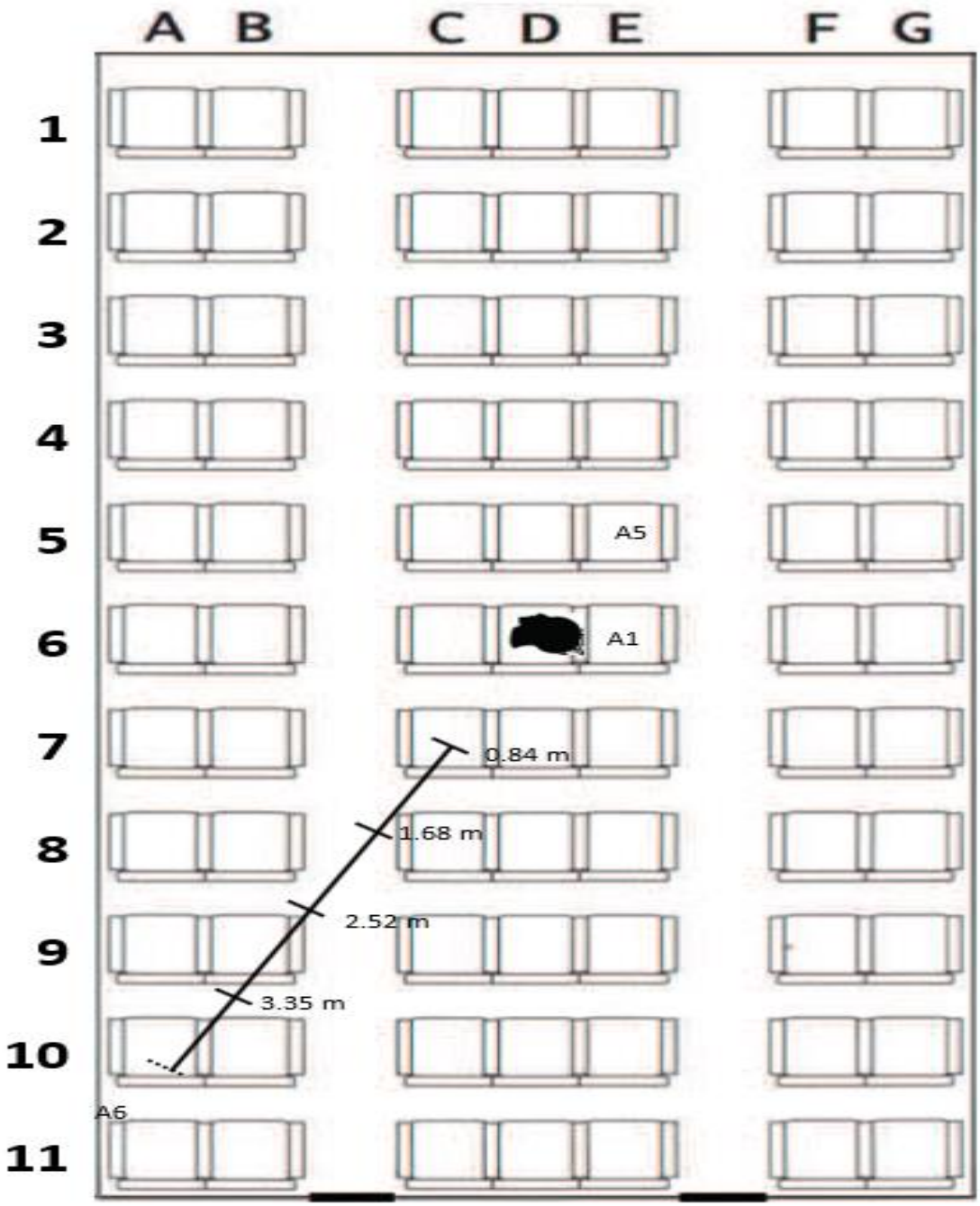

Figure H.165 Test 90 (B-M) ISOPass undeployed source location and sampling tree orientation.

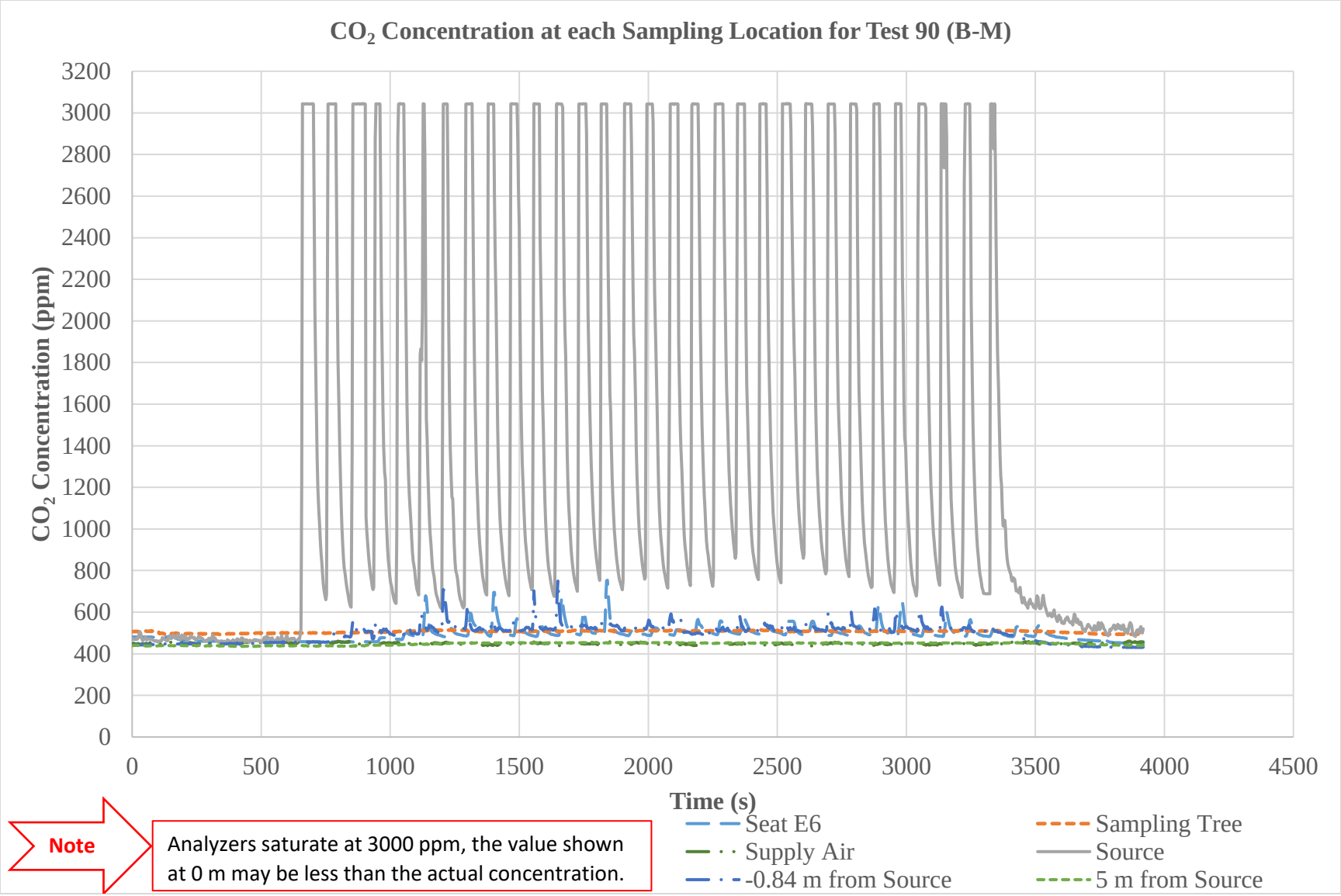

Figure H.166 Ininstantaneous CO_2 concentration at each sampling location for Test 90 (B-M) ISOPass undeployed.

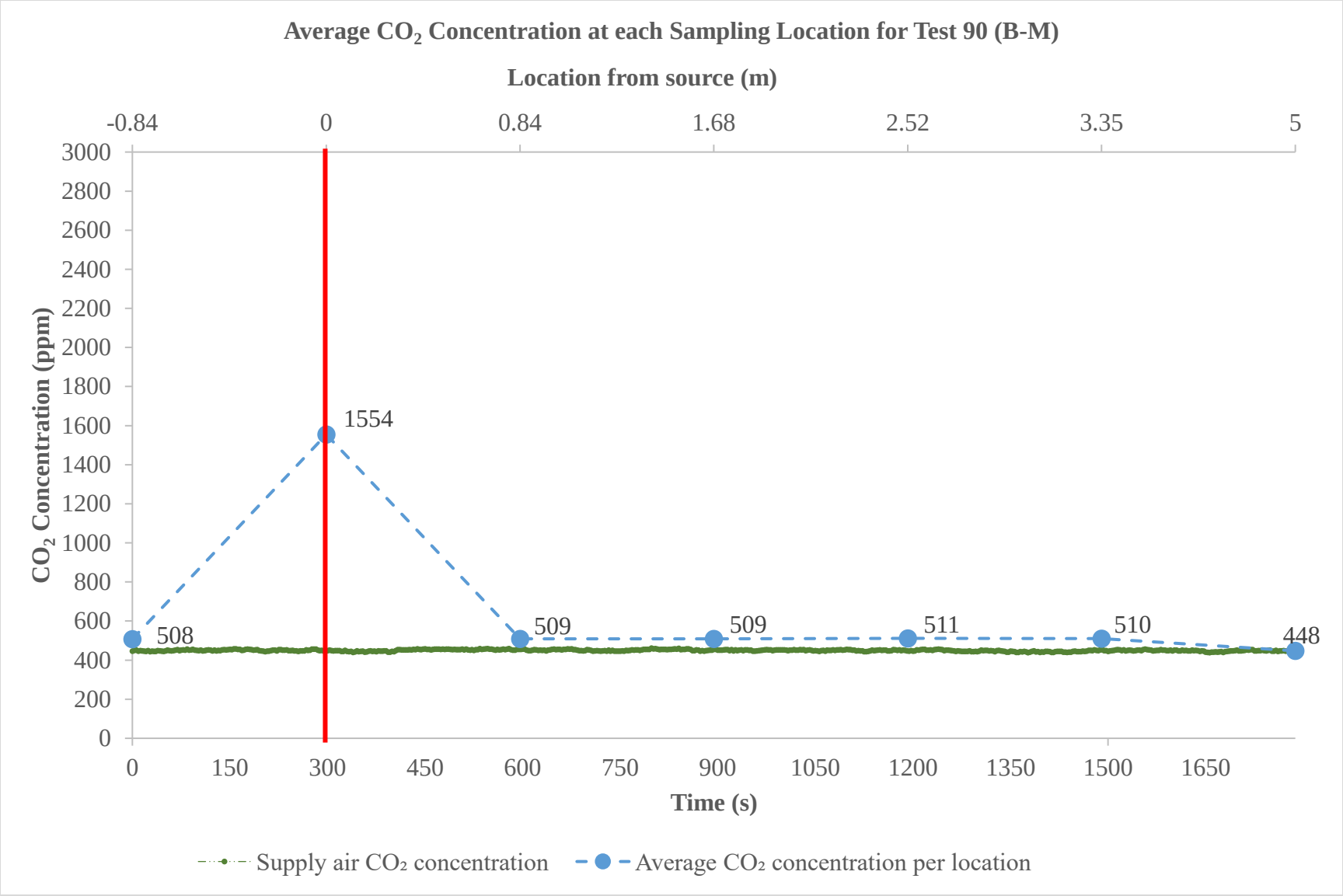

Figure H.167 Average CO_2 concentration at each sampling location for Test 90 (B-M) ISOPass undeployed.

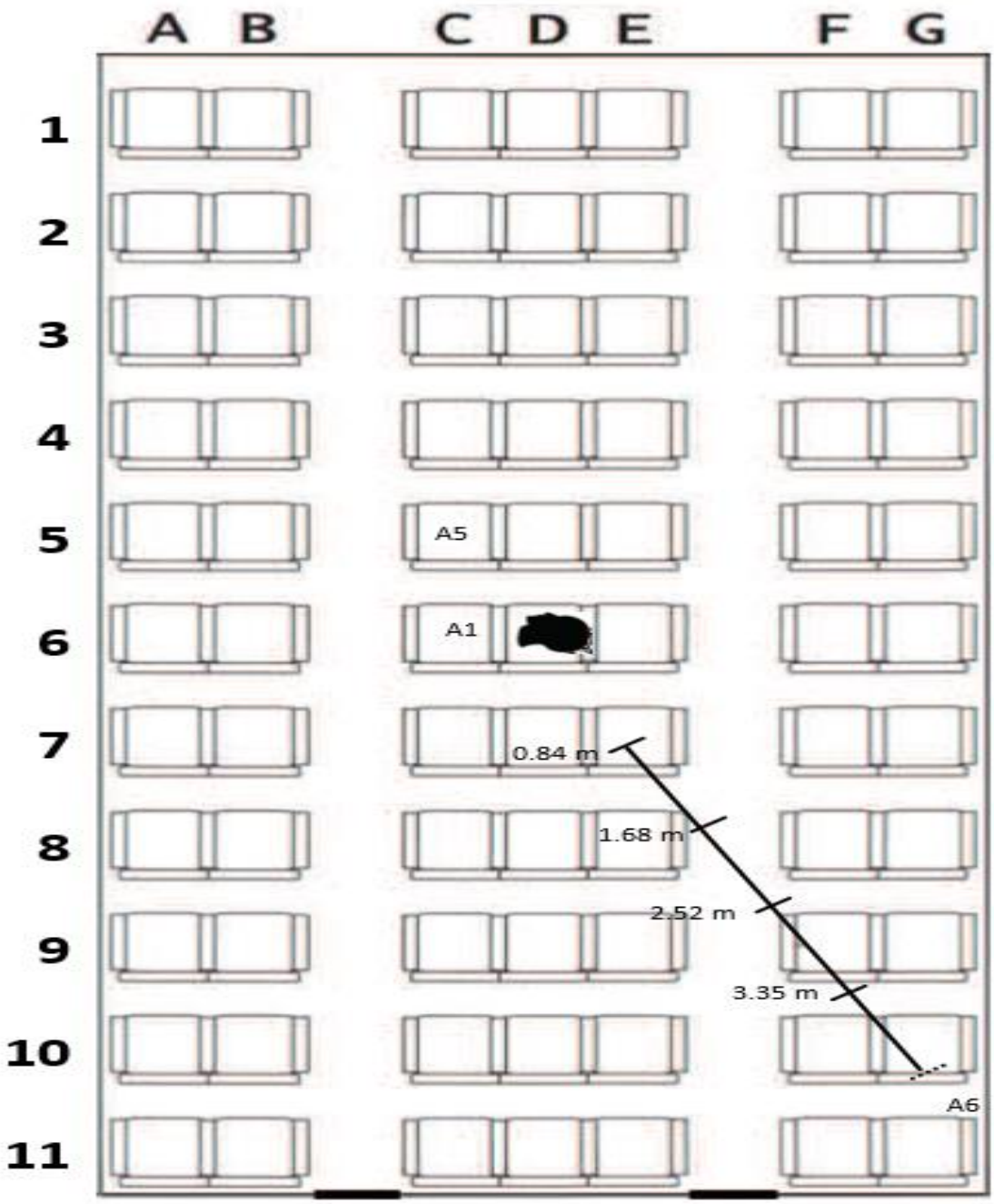

Figure H.168 Test 91 (B-M) ISOPass undeployed source location and sampling tree orientation.

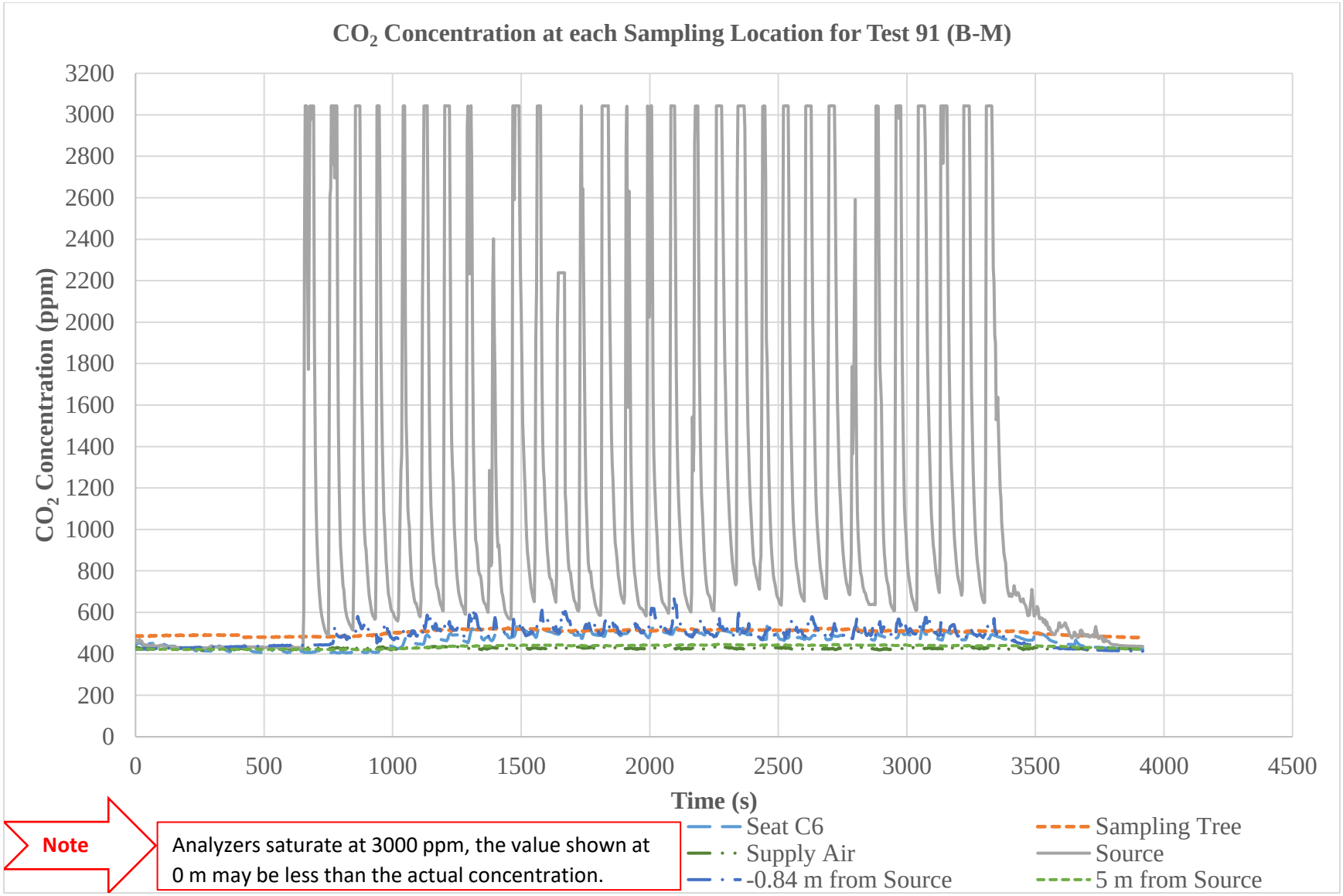

Figure H.169 Ininstantaneous CO_2 concentration at each sampling location for Test 91 (B-M) ISOPass undeployed.

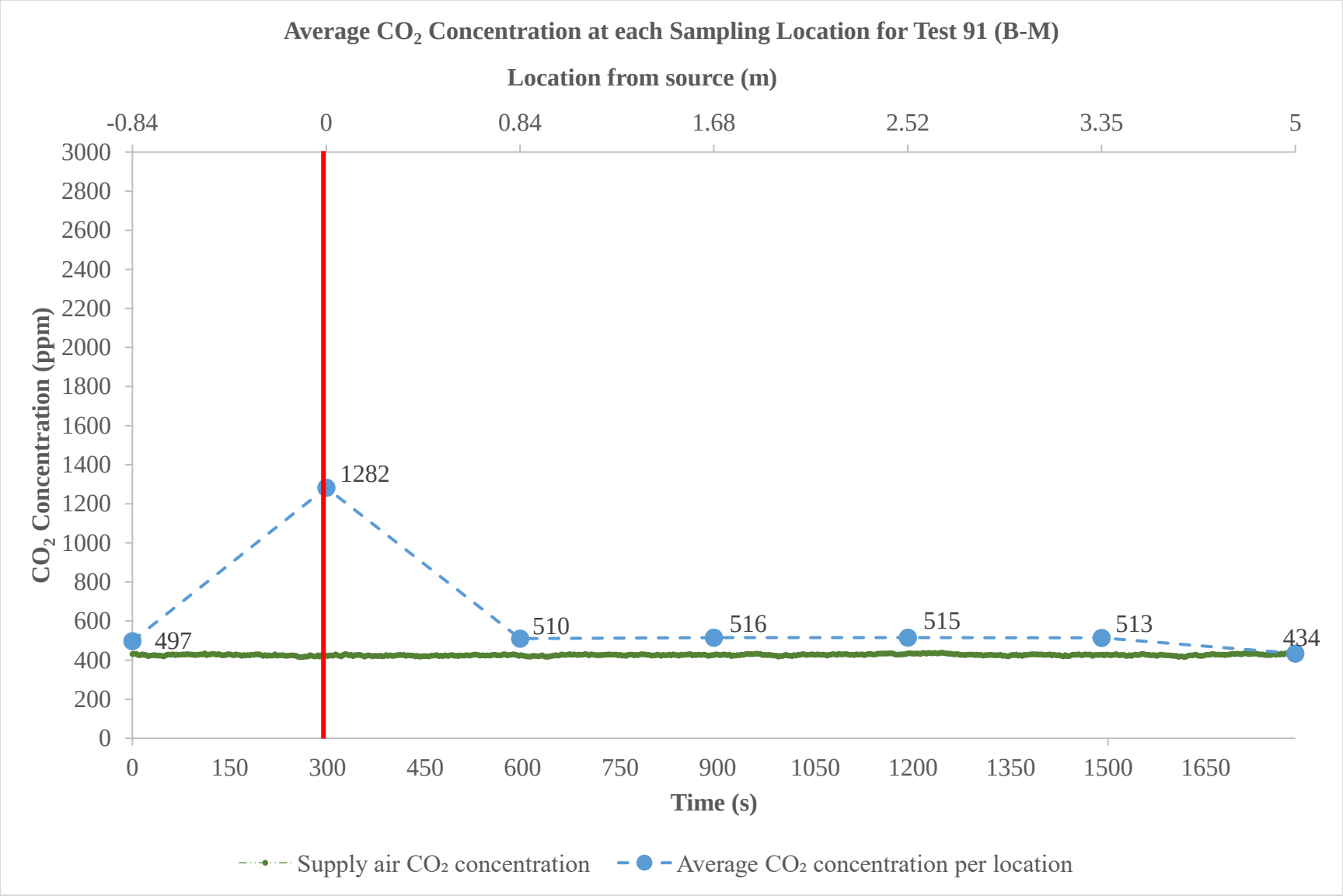

Figure H.170 Average CO_2 concentration at each sampling location for Test 91 (B-M) ISOPass undeployed.

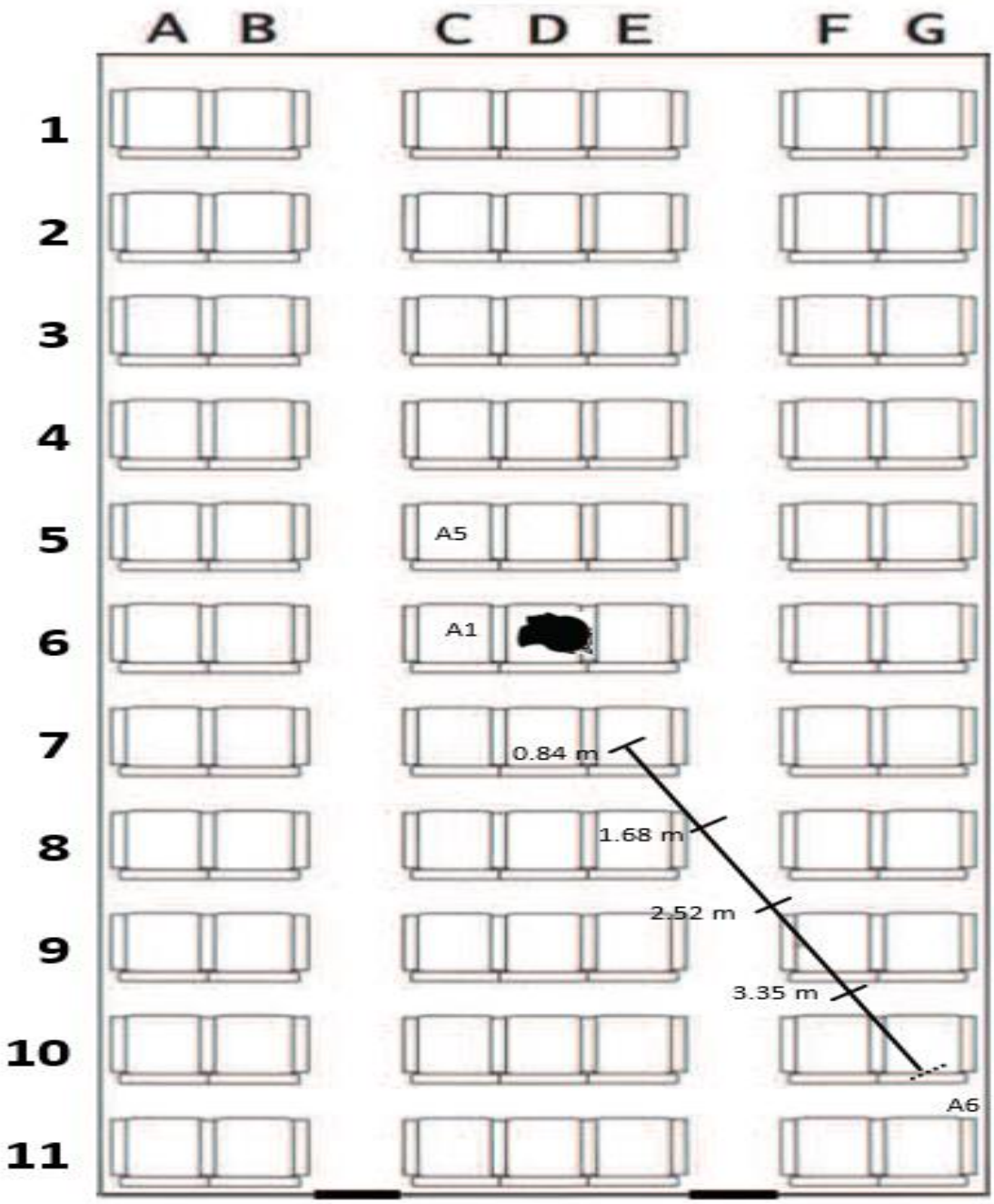

Figure H.171 Test 92 (B-M) ISOPass undeployed source location and sampling tree orientation.

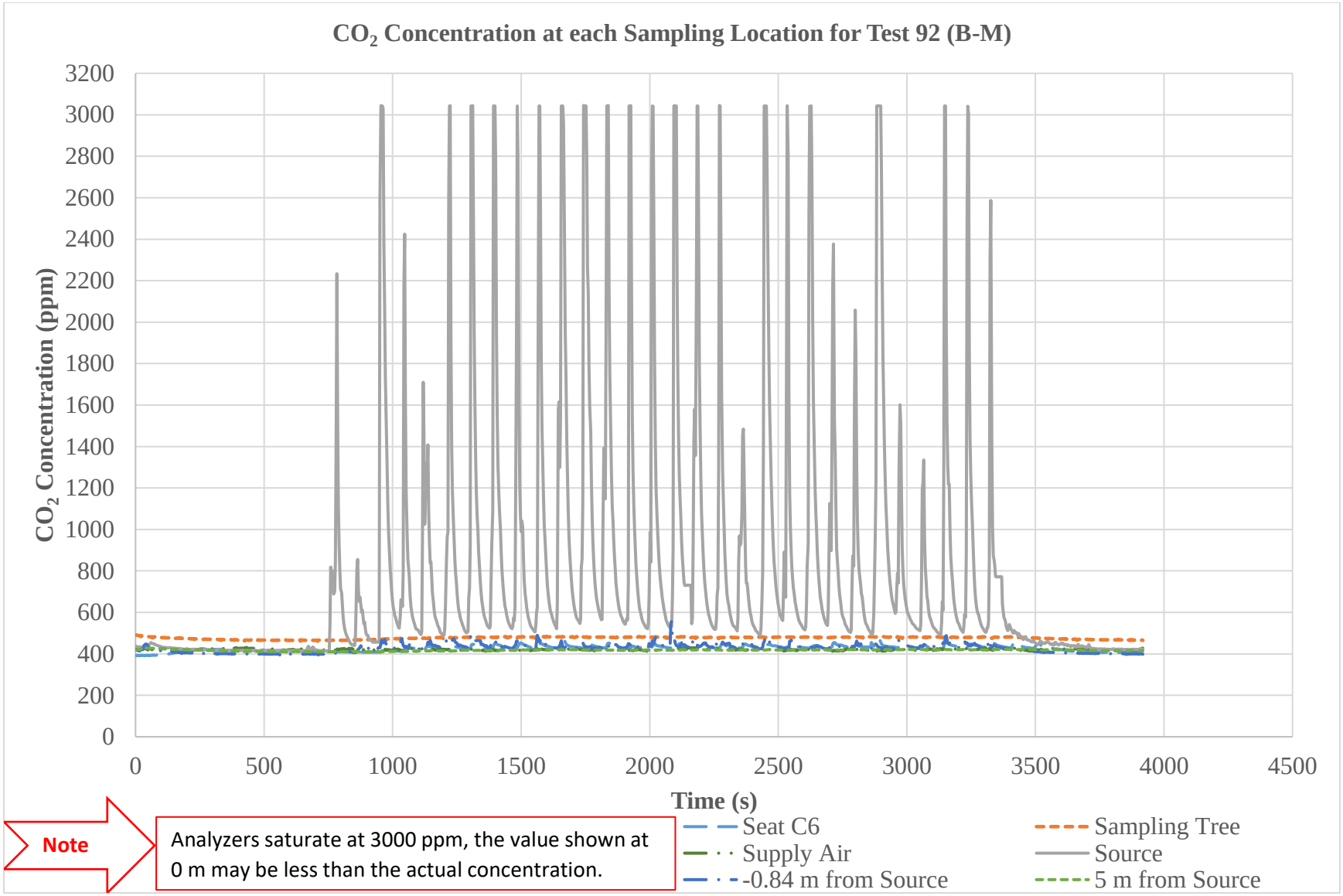

Figure H.172 Ininstantaneous CO_2 concentration at each sampling location for Test 92 (B-M) ISOPass undeployed.

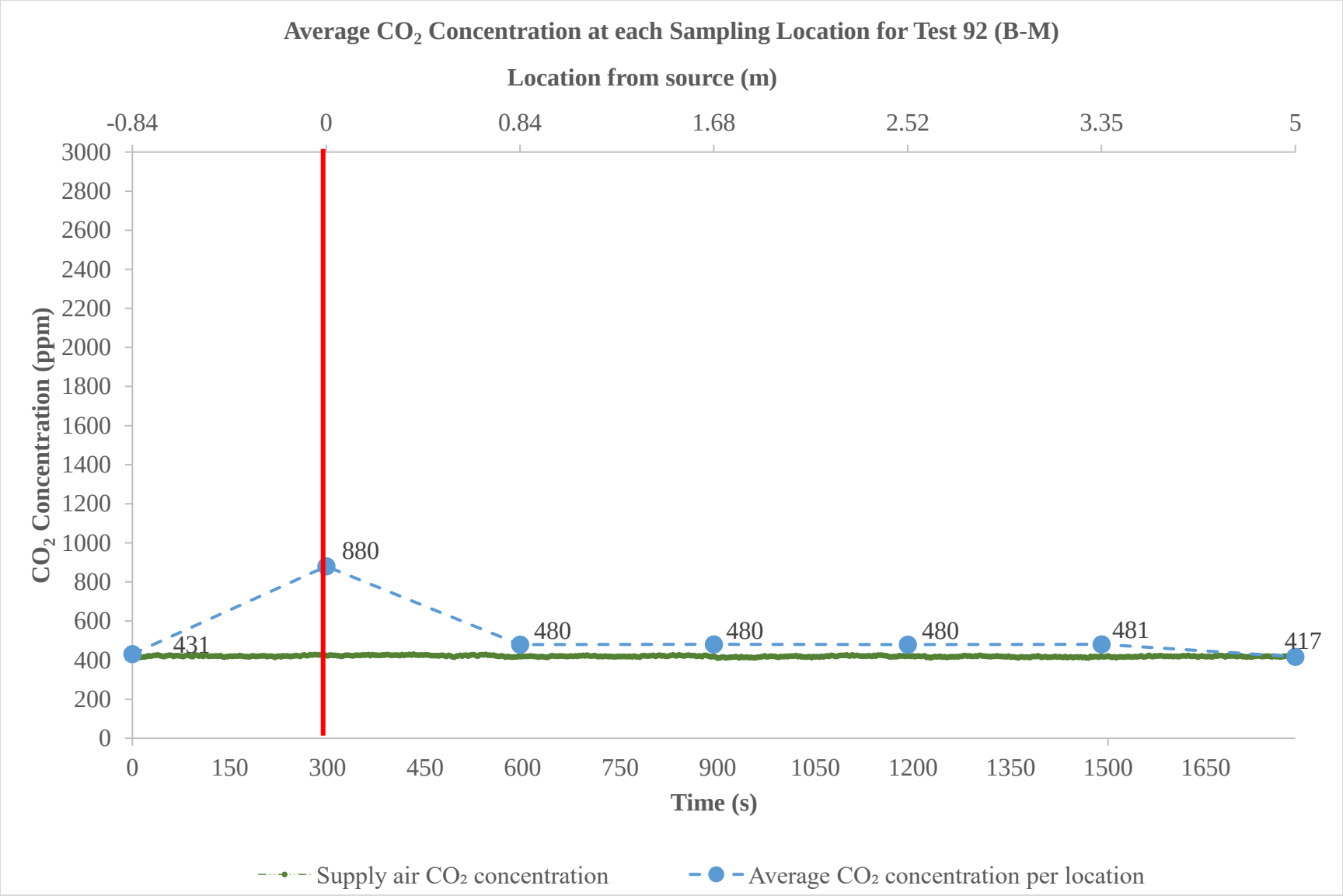

Figure H.173 Average CO_2 concentration at each sampling location for Test 92 (B-M) ISOPass undeployed.

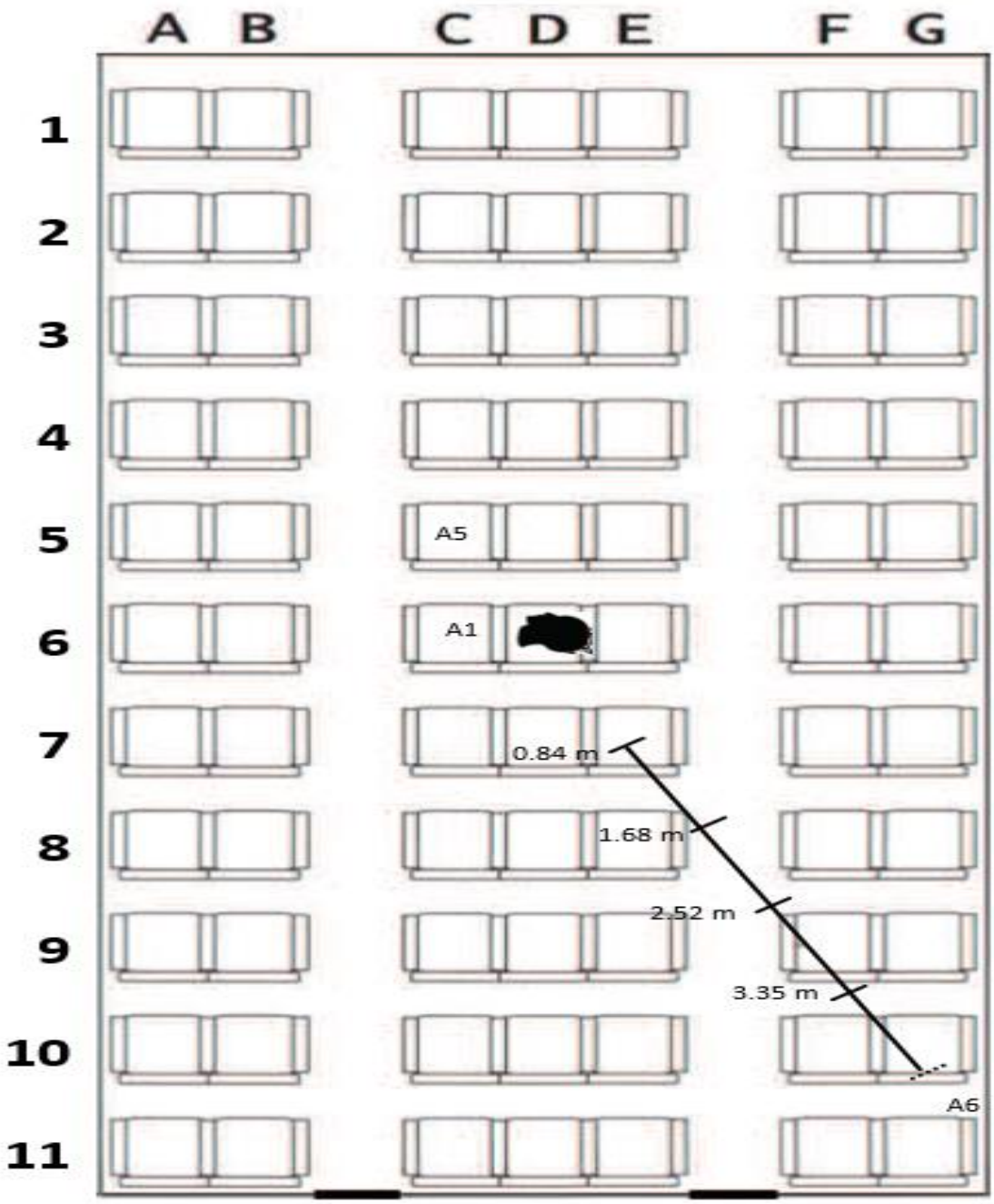

Figure H.174 Test 93 (B-M) ISOPass undeployed source location and sampling tree orientation.

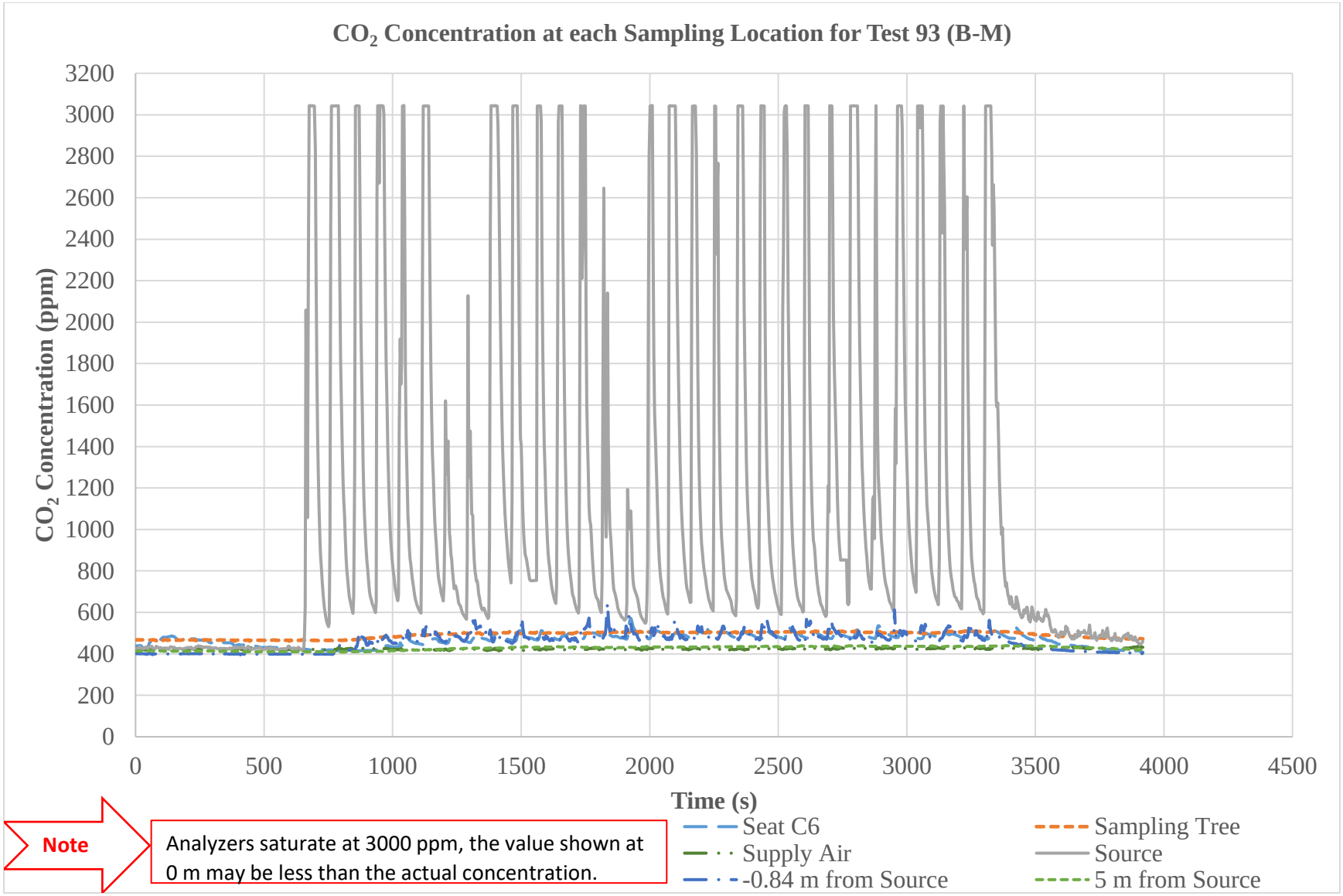

Figure H.175 Ininstantaneous CO_2 concentration at each sampling location for Test 93 (B-M) ISOPass undeployed.

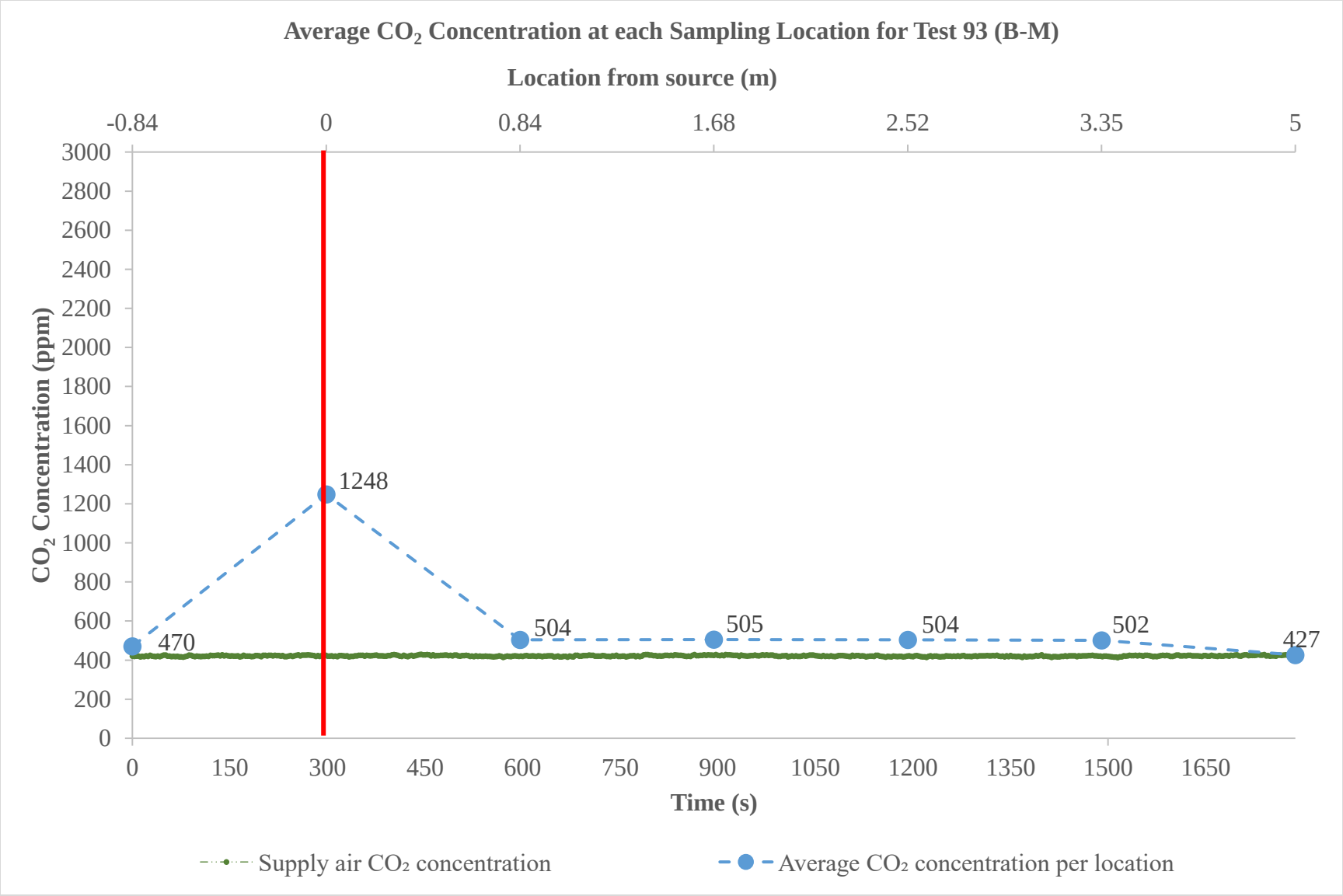

Figure H.176 Average CO_2 concentration at each sampling location for Test 93 (B-M) ISOPass undeployed.

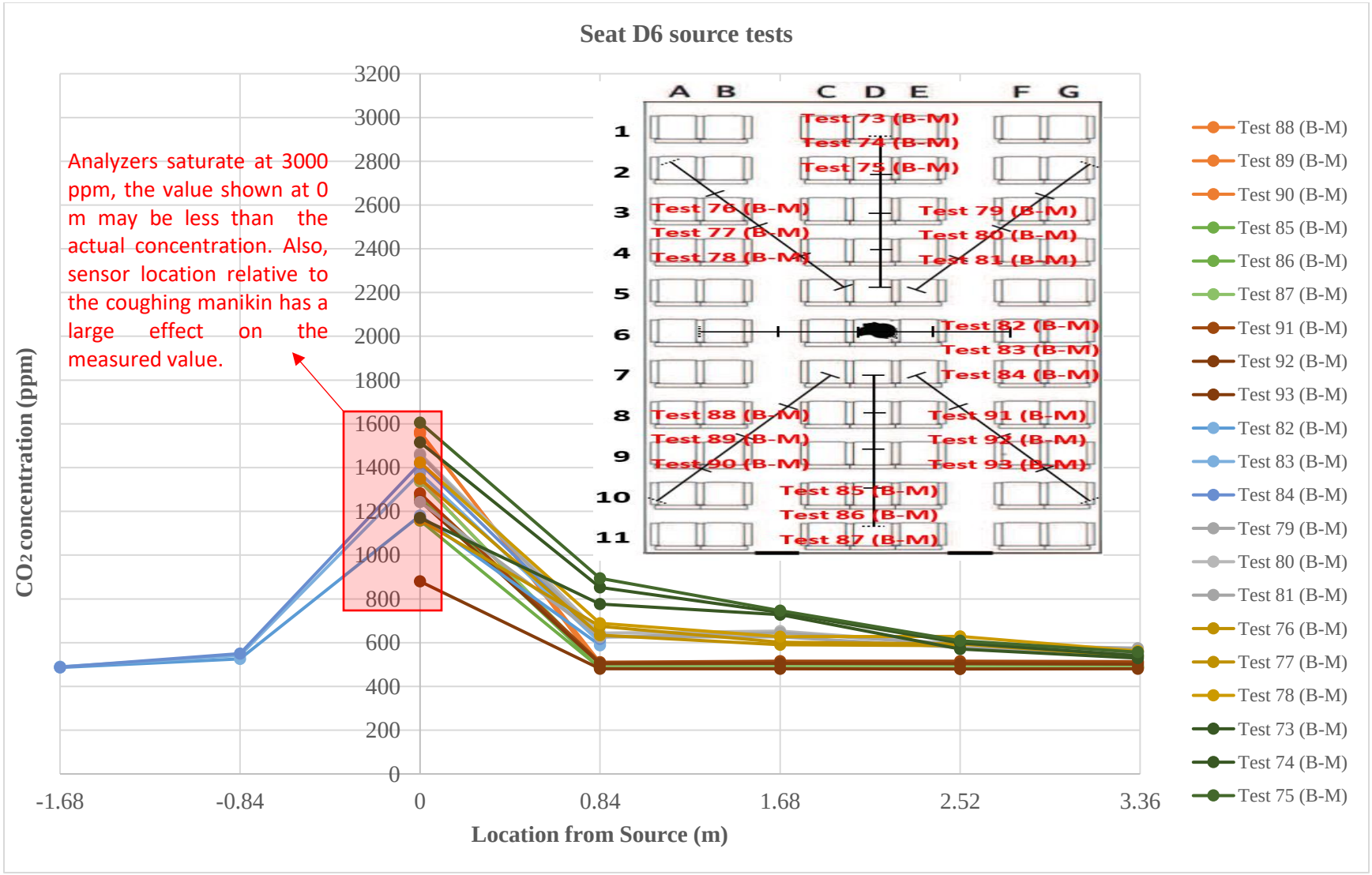

Figure H.177 Seat D6 coughing manikin source tests in the Boeing 767 cabin mockup with the ISOPass undeployed.

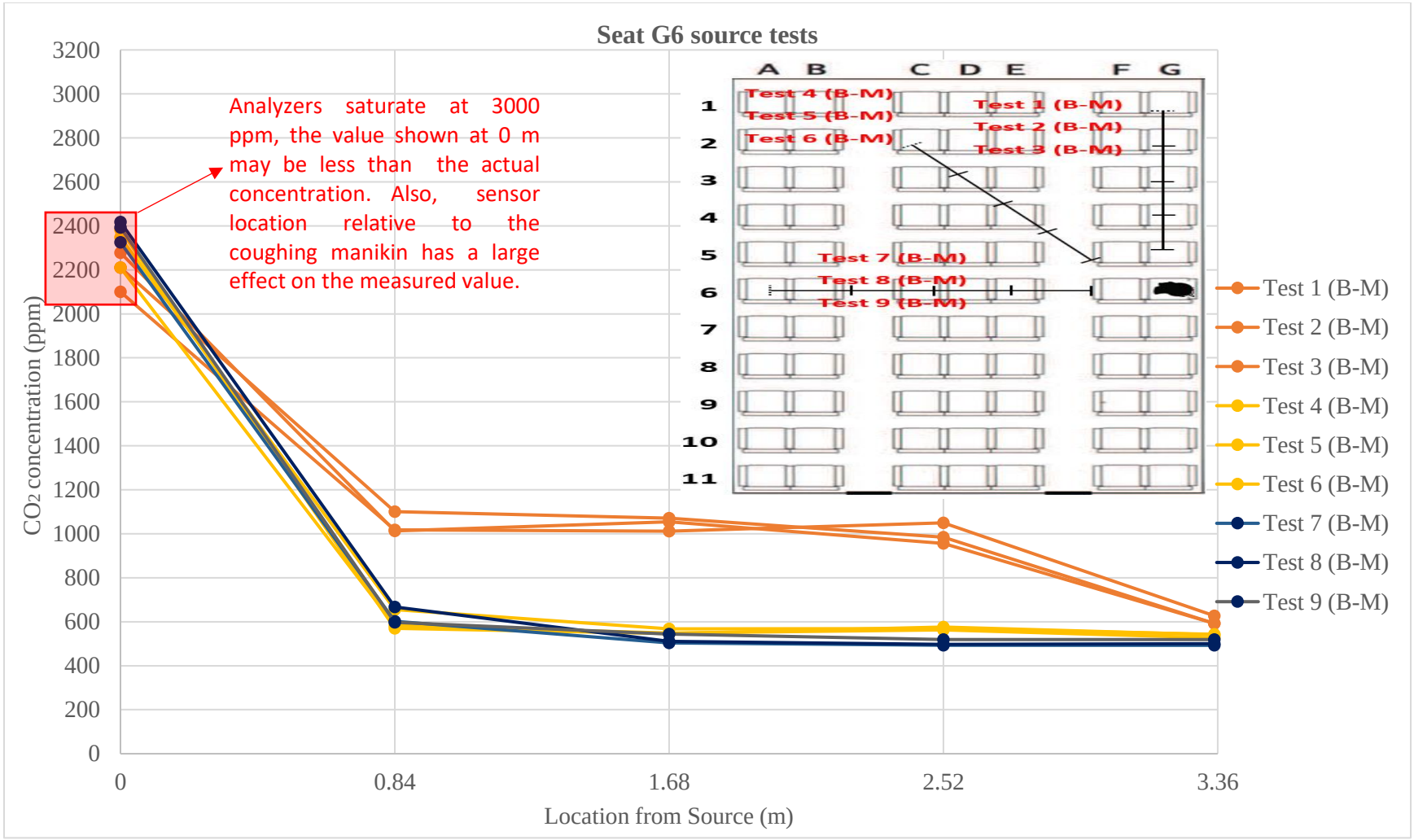

Figure H.178 Seat G6 coughing manikin source tests in the Boeing 767 cabin mockup with the ISOPass undeployed.

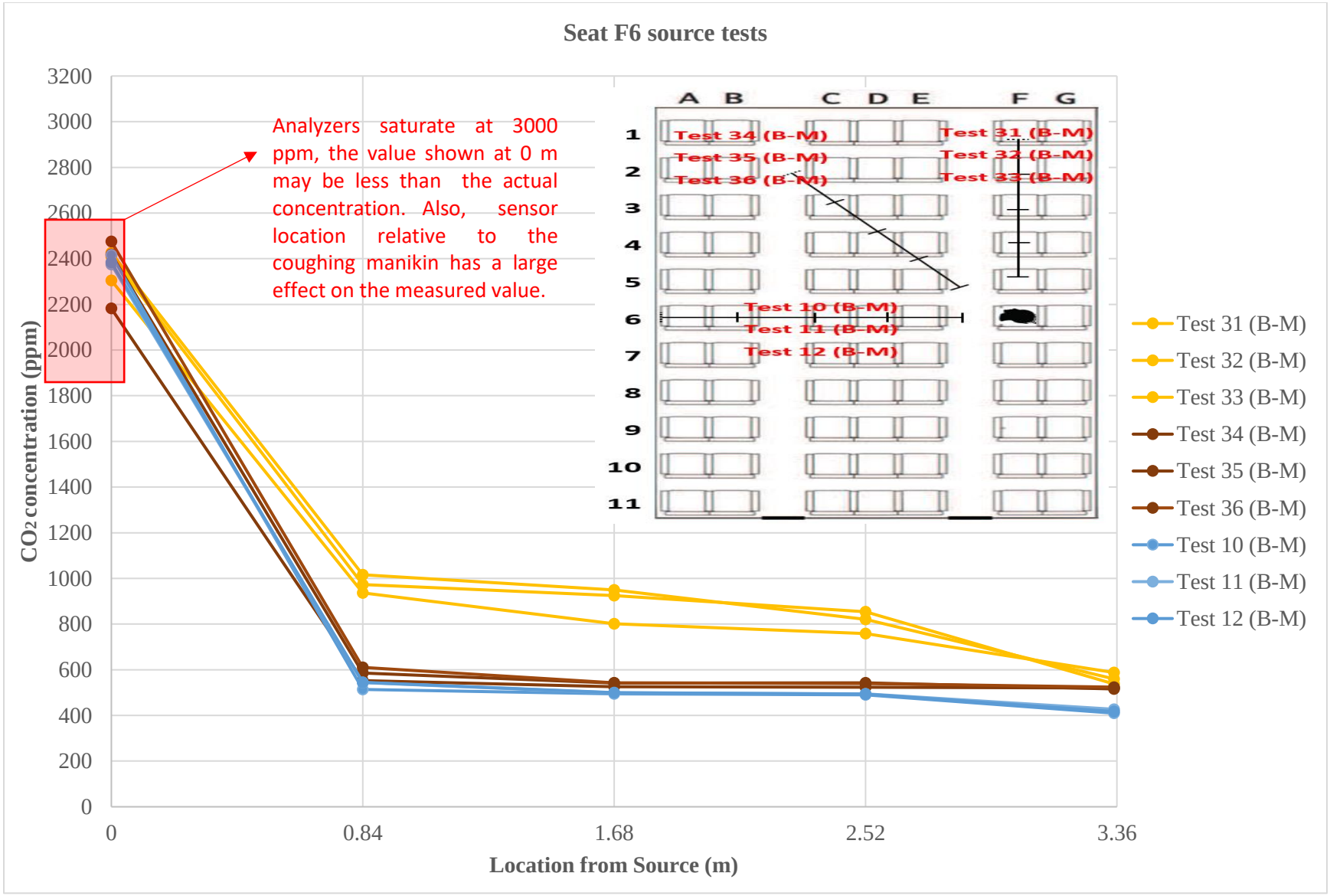

Figure H.179 Seat F6 coughing manikin source tests in the Boeing 767 cabin mockup with the ISOPass undeployed.

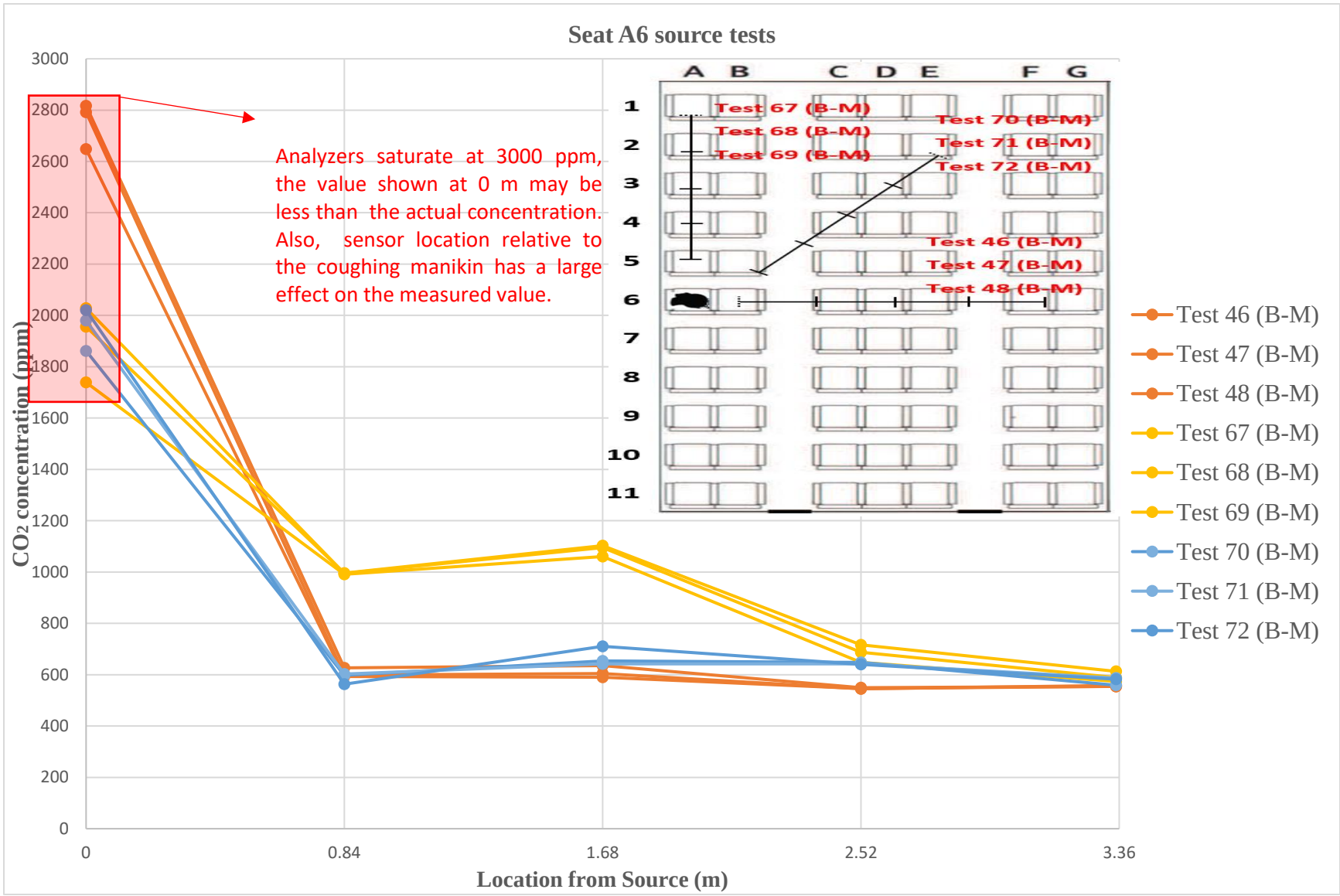

H. 180 Seat A6 coughing manikin source tests in the Boeing 767 cabin mockup with the ISOPass undeployed.

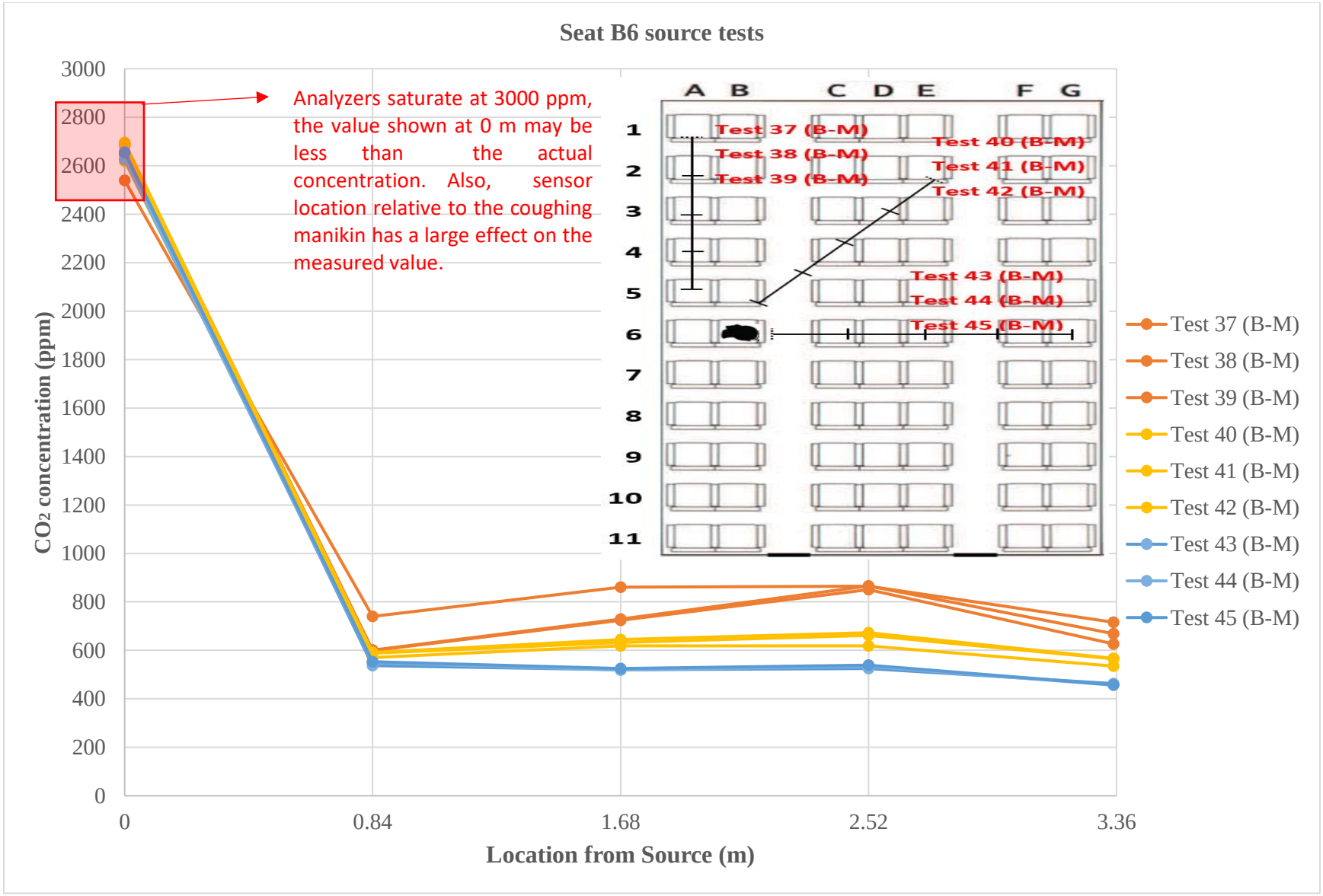

Figure H.181 Seat B6 coughing manikin source tests in the Boeing 767 cabin mockup with the ISOPass undeployed.

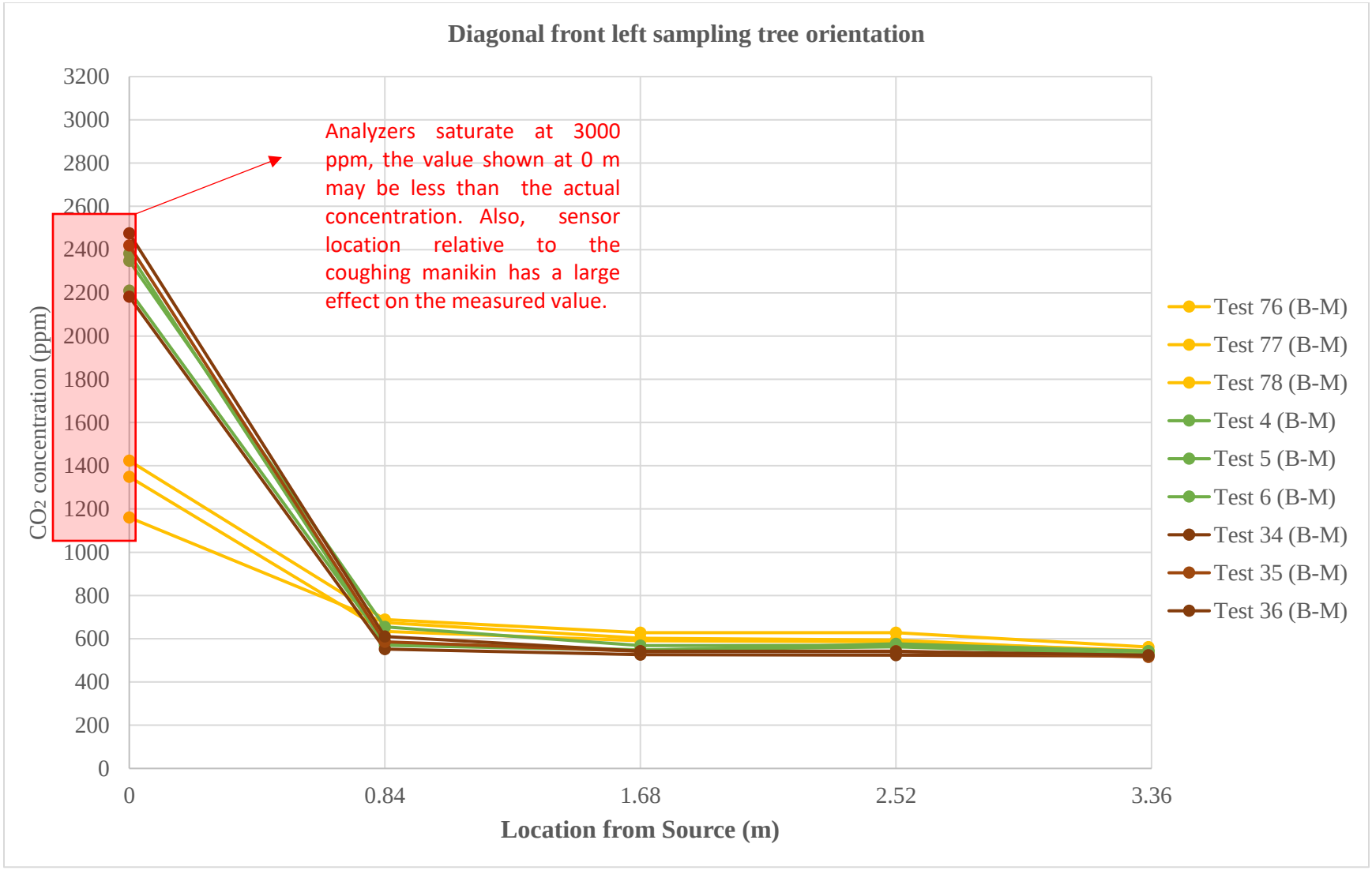

Figure H.182 Diagonal front left sampling tree orientation coughing manikin source tests in the Boeing 767 cabin mockup with the ISOPass undeployed.

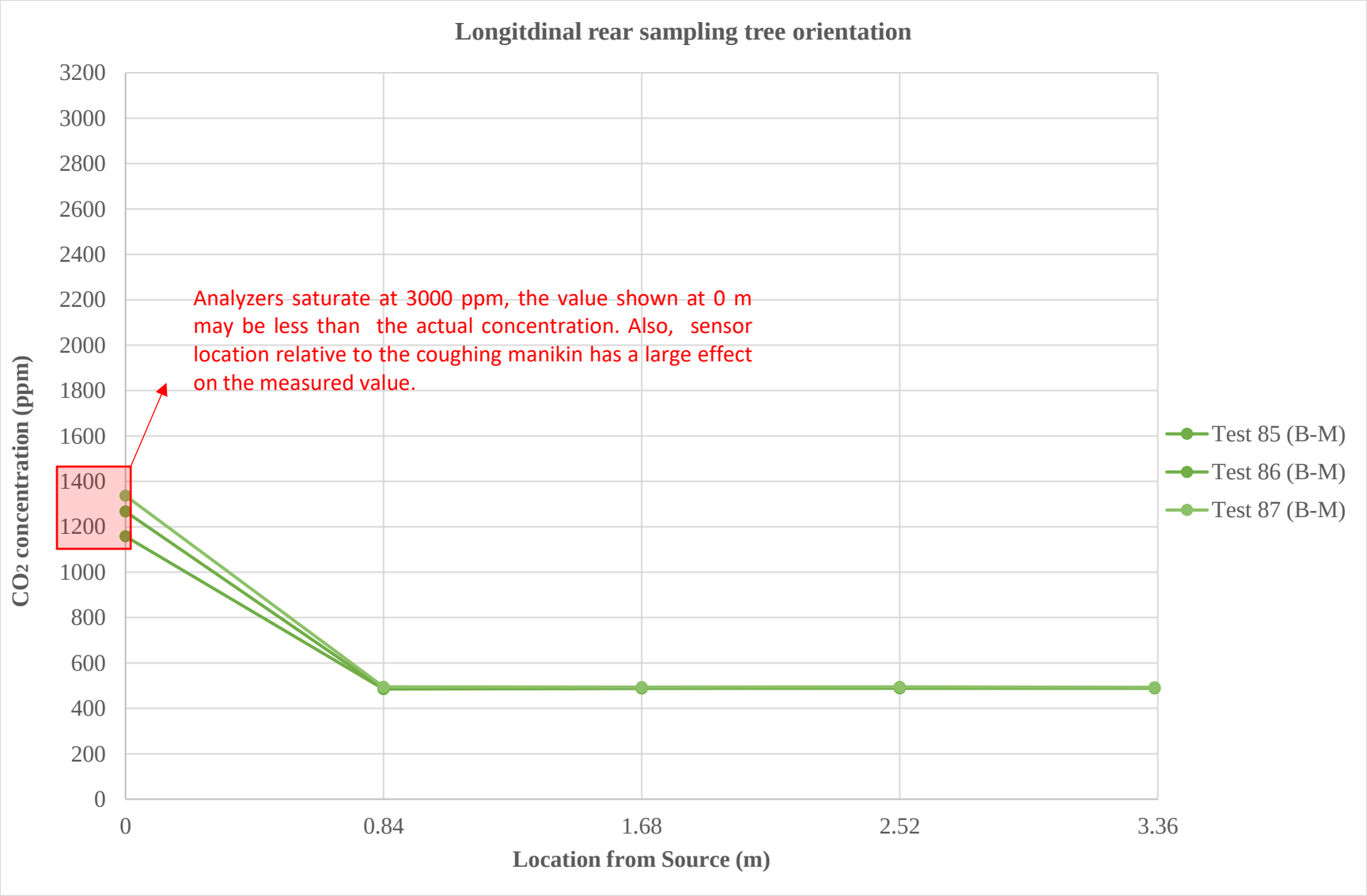

Figure H.183 Longitudinal rear sampling tree orientation coughing manikin source tests in the Boeing 767 cabin mockup with the ISOPass undeployed.

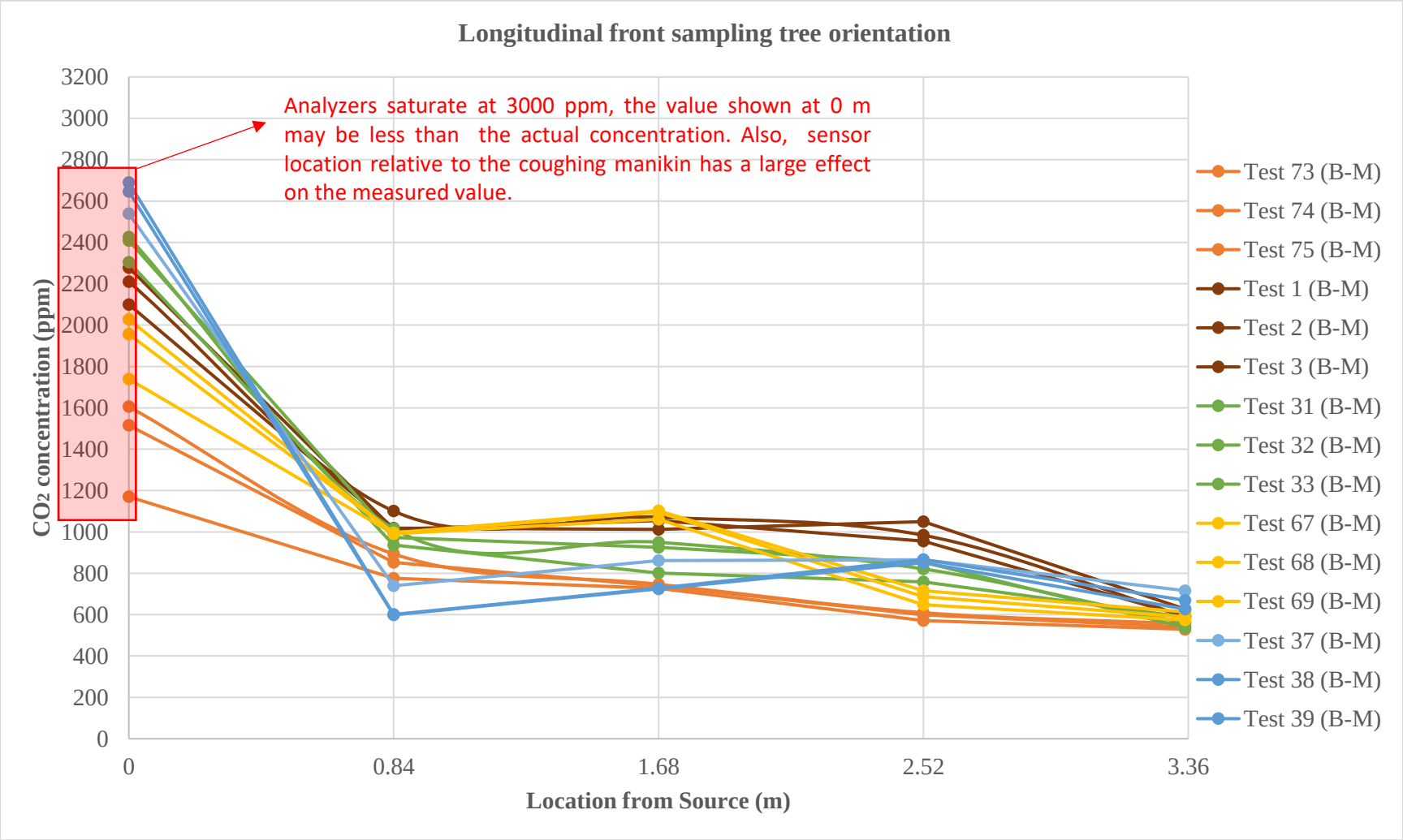

Figure H.184 Longitudinal front sampling tree orientation coughing manikin source tests in the Boeing 767 cabin mockup with the ISOPass undeployed.

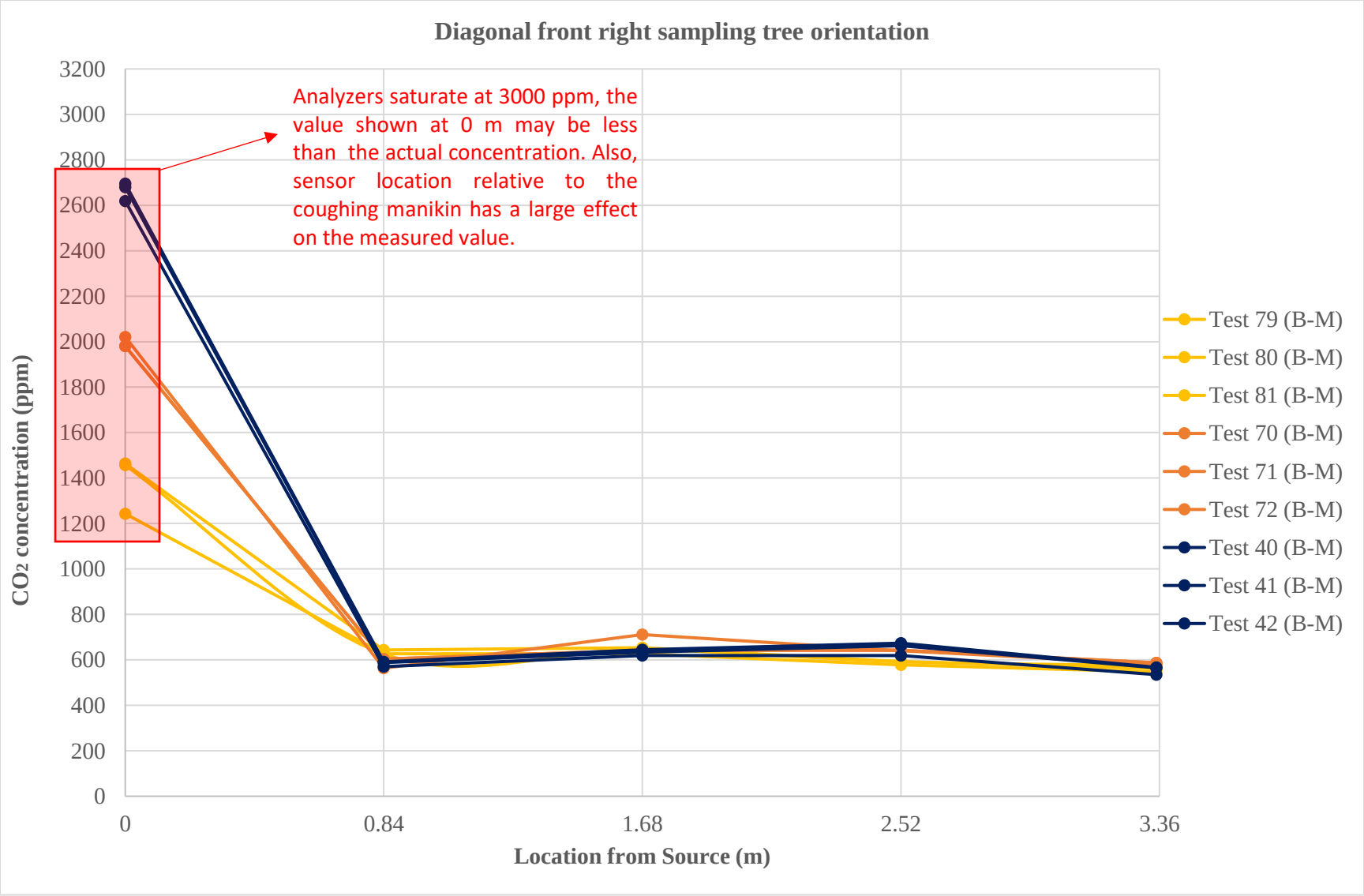

Figure H.185 Diagonal front right sampling tree orientation coughing manikin source tests in the Boeing 767 cabin mockup with the ISOPass undeployed.

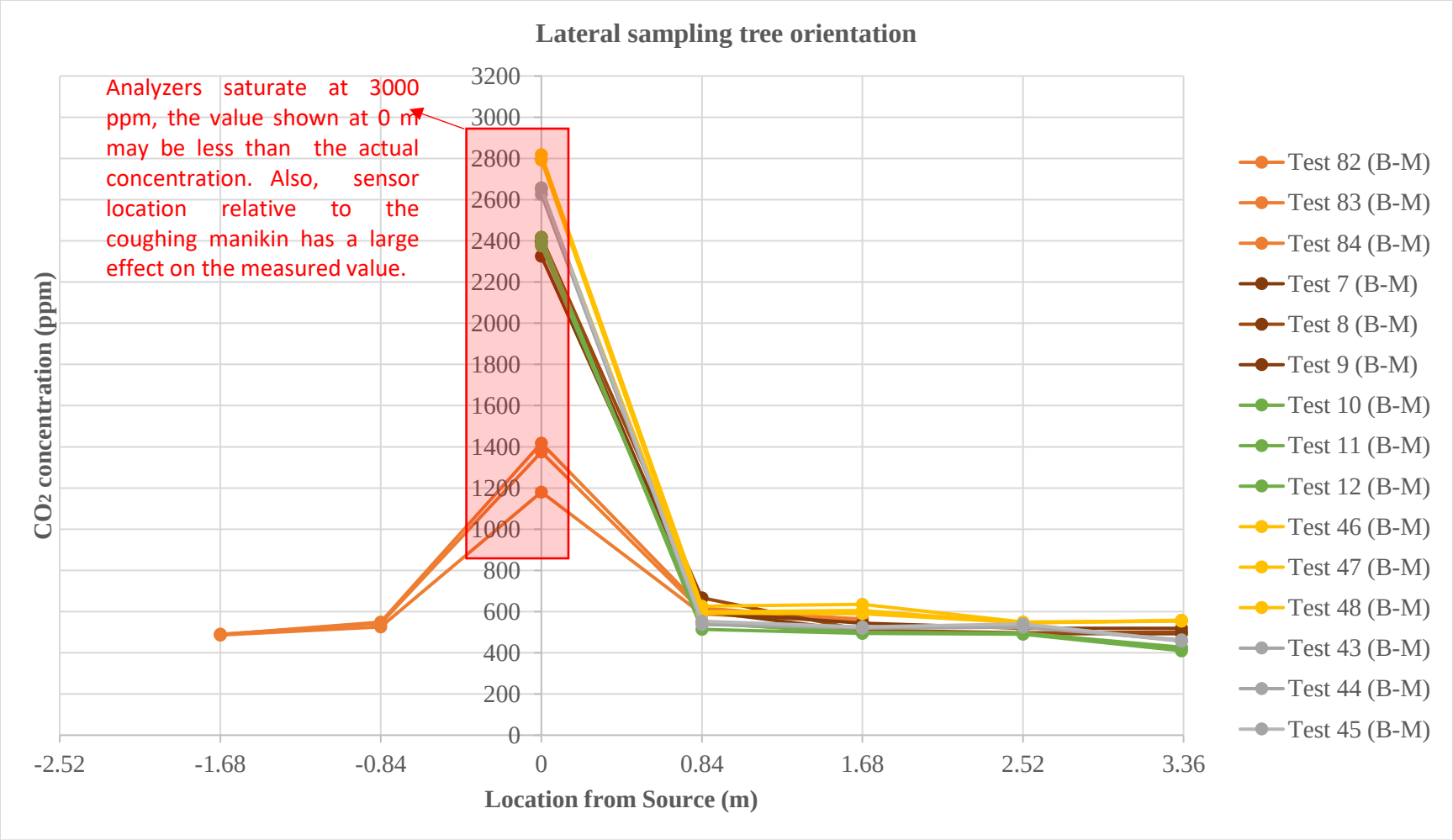

Figure H.186 Lateral sampling tree orientation coughing manikin source tests in the Boeing 767 cabin mockup with the ISOPass undeployed.

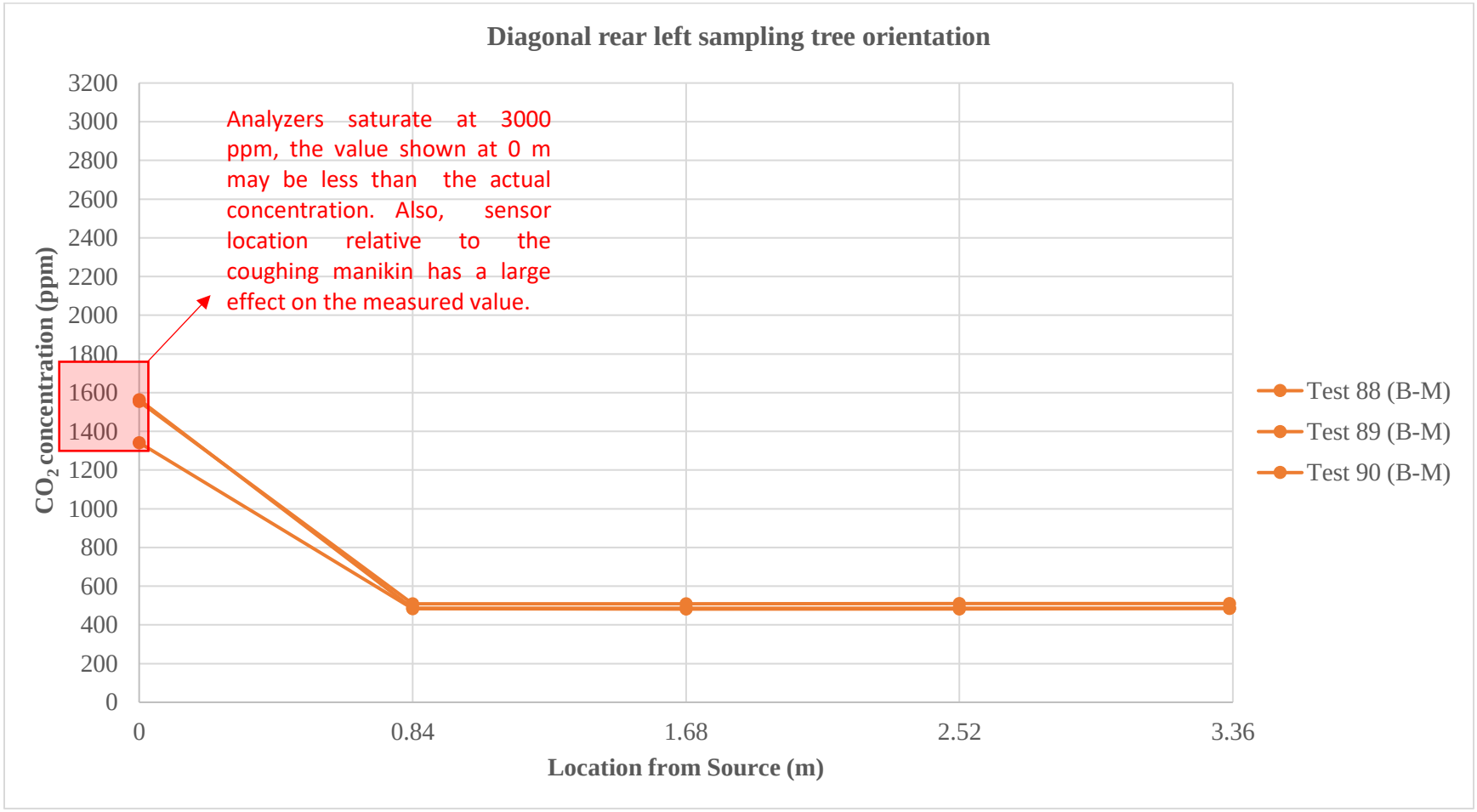

Figure H.187 Diagonal rear left sampling tree orientation coughing manikin source tests in the Boeing 767 cabin mockup with the ISOPass undeployed.

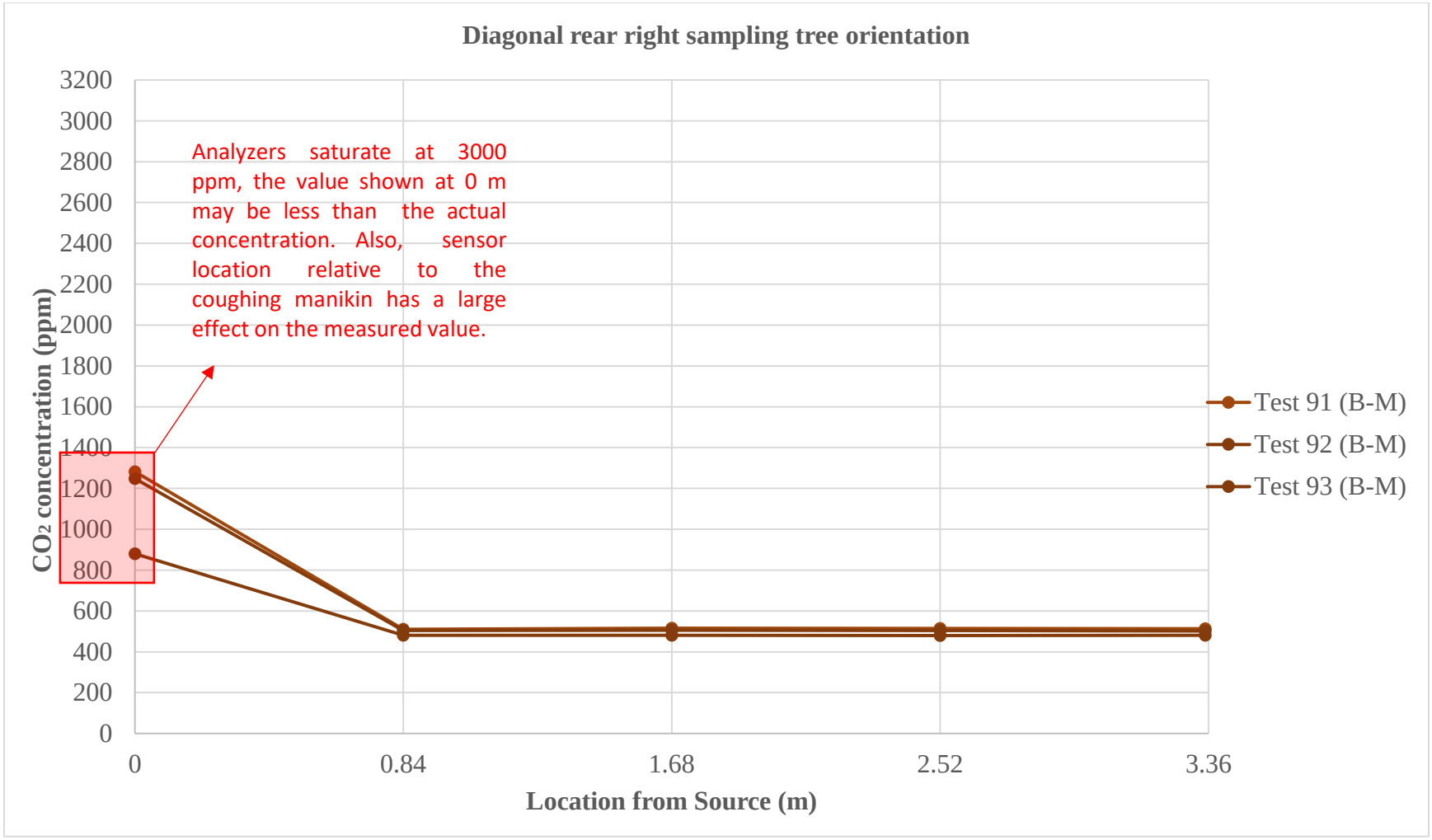

Figure H.188 Diagonal rear right sampling tree orientation coughing manikin source tests in the Boeing 767 cabin mockup with the ISOPass undeployed.

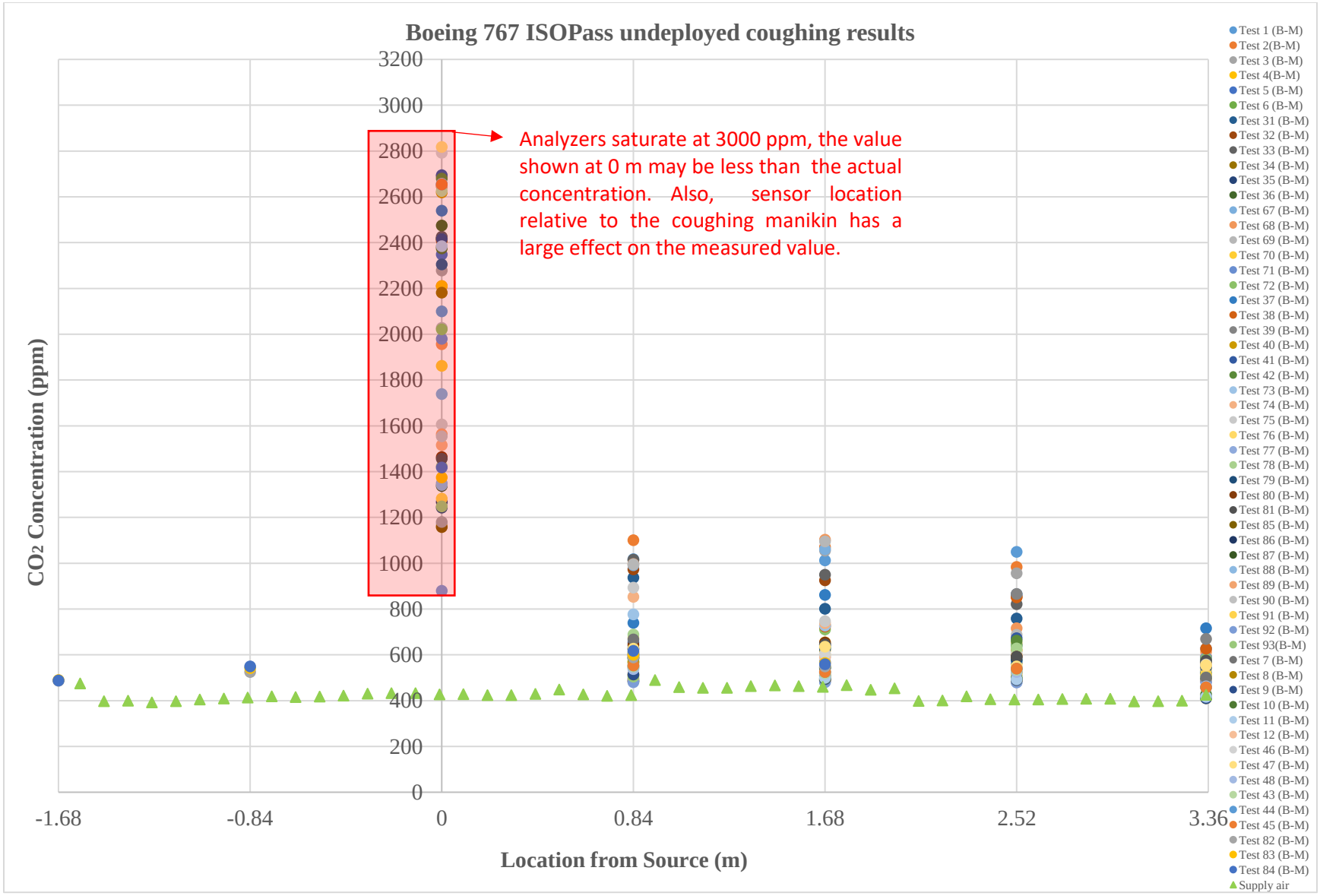

Figure H.189 Boeing 767 cabin mockup coughing manikin source tests with the ISOPass undeployed.

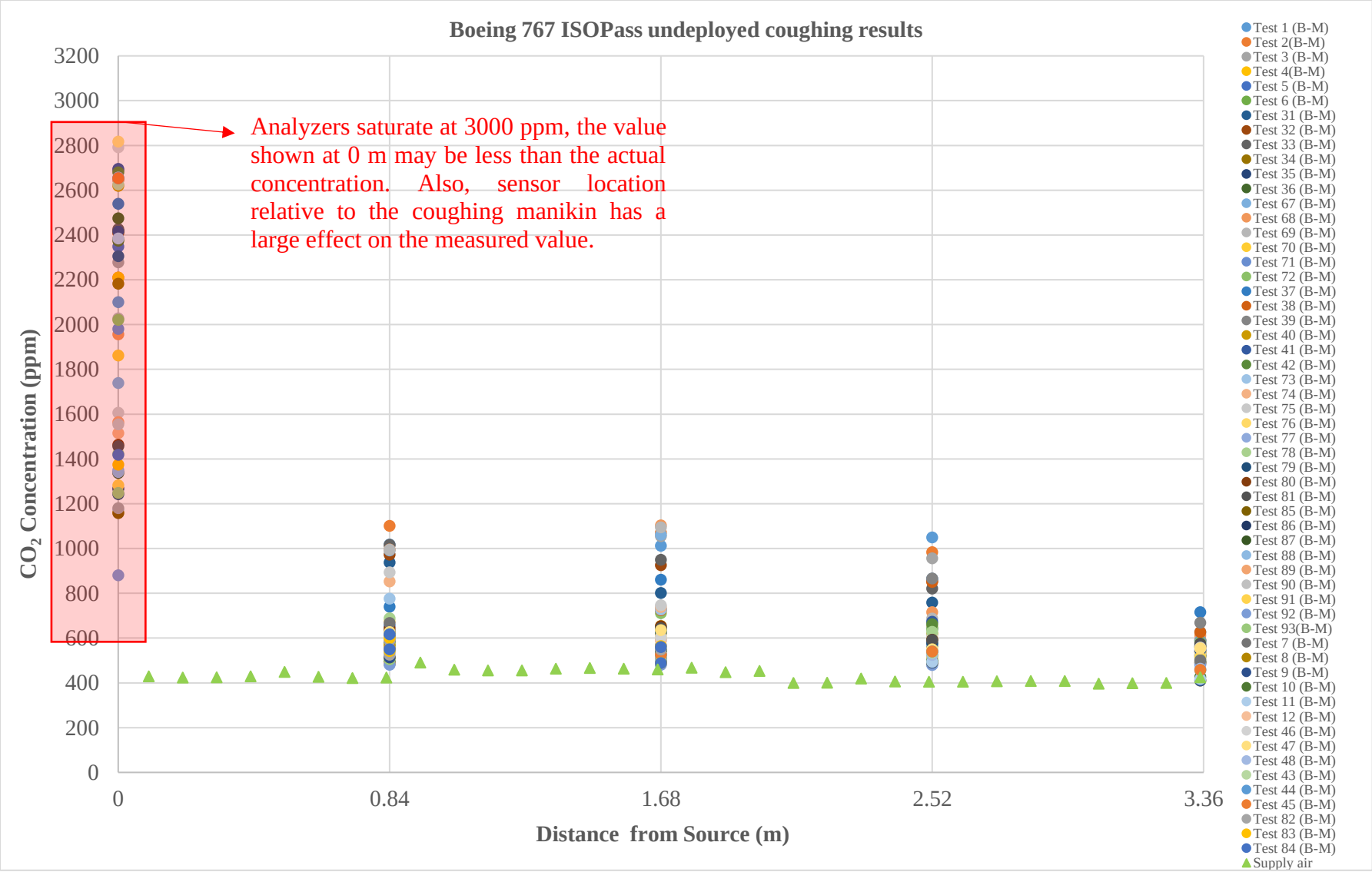

Figure H.190 Boeing 767 cabin mockup coughing manikin source tests with the ISOPass undeployed, Absolute distances from the source.

Appendix I - Boeing 767 ISOPass Deployed Coughing Manikin Results

Notes about this appendix:

- The positive direction is the one pointing from the source to the sampling tree solenoid valves block in the tests conducted with a longitudinal or a diagonal sampling tree directions.
- The positive direction was taken as the right direction from the source in the tests performed with a lateral sampling tree direction similar to a typical coordinate system.
- The letter "B" after the test number indicates that the test was conducted in the Boeing 767 mockup cabin and the letter "M" indicates that it was conducted using a coughing manikin source.
- The sampling tree is a metal rod that has 4 ports controlled by solenoid valves. The measurements are collected sequentially from each of the ports. The tree is connected to a single gas analyzer to measure the concentration of the tracer gas from the opened port.
- The solenoid valves block is marked by a dashed line crossing the sampling tree.
- In addition to the sampling tree, additional tracer gas analyzers are placed in the cabin to collect measurements at the cabin supply air, source seat, and other locations of interest.
- The tracer gas analyzers are not of the same model or calibration and hence, the accuracy of the readings is not identical. For the tracer gas measurements accuracy, refer to chapter 4.4. Uncertainty Analysis of this dissertation.

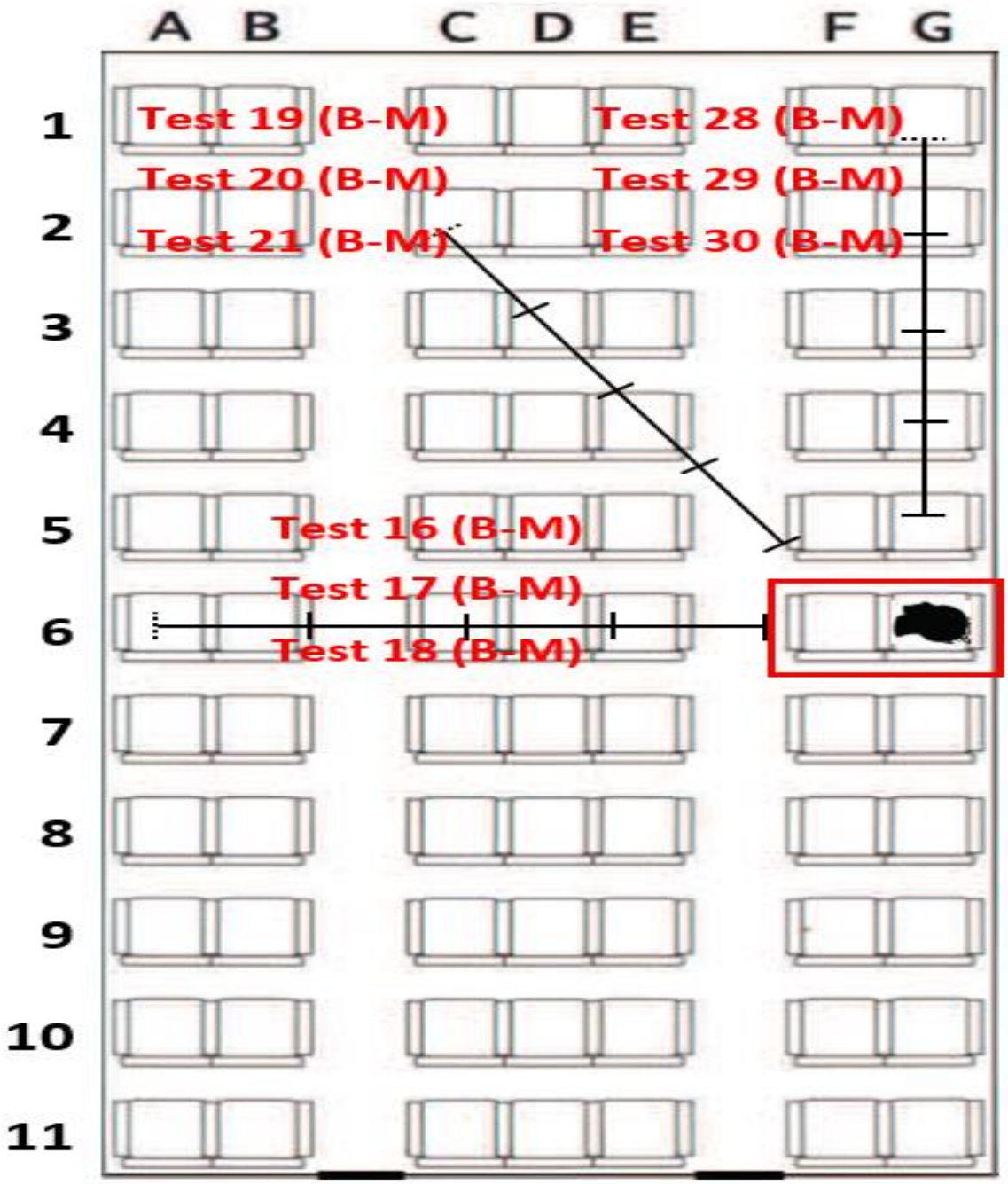

Figure I.1 Seat G6 ISOPass deployed coughing manikin tracer gas test numbers and sampling tree orientations in the Boeing 767 cabin mockup.

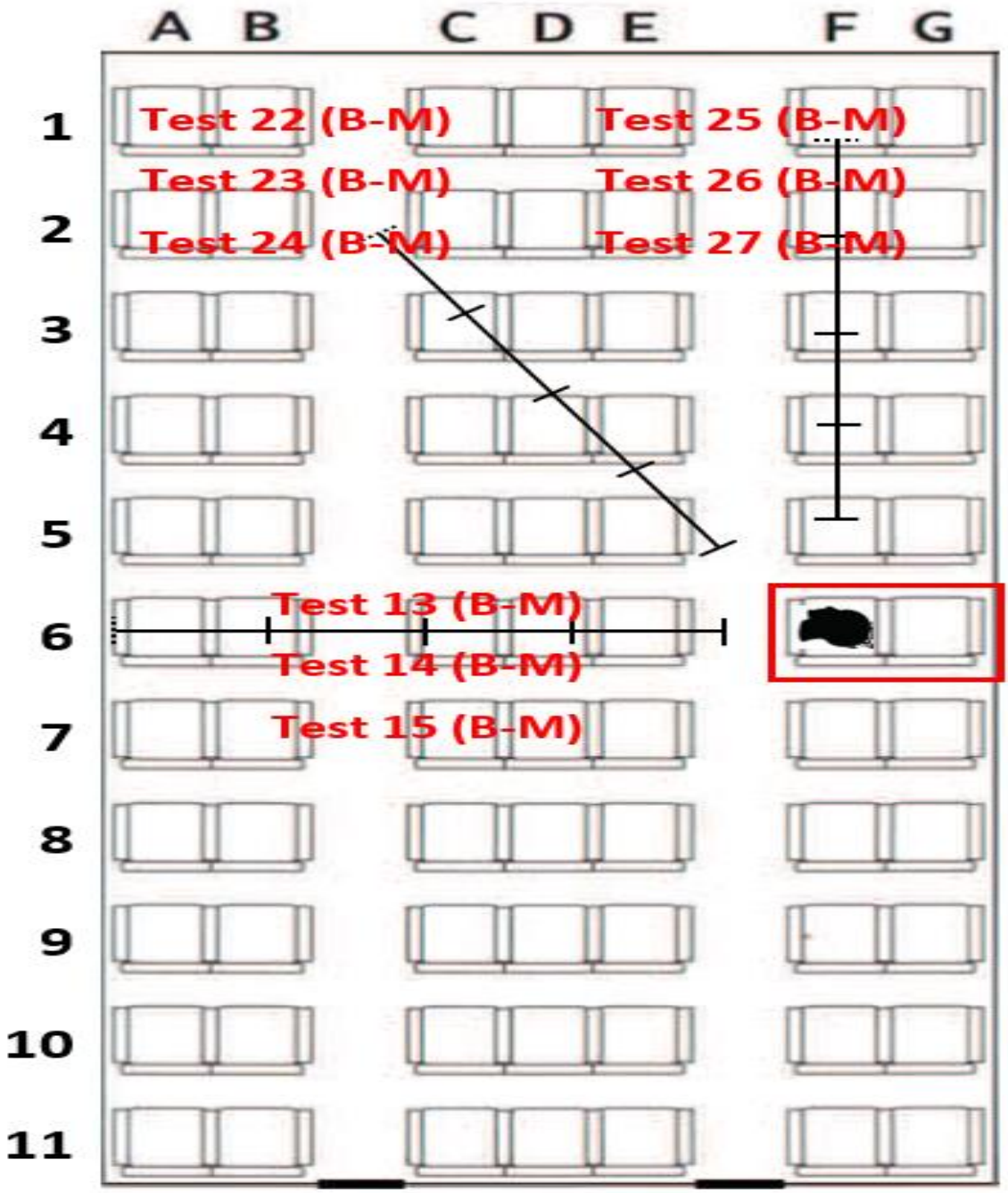

Figure I.2 Seat F6 ISOPass deployed coughing manikin tracer gas test numbers and sampling tree orientations in the Boeing 767 cabin mockup.

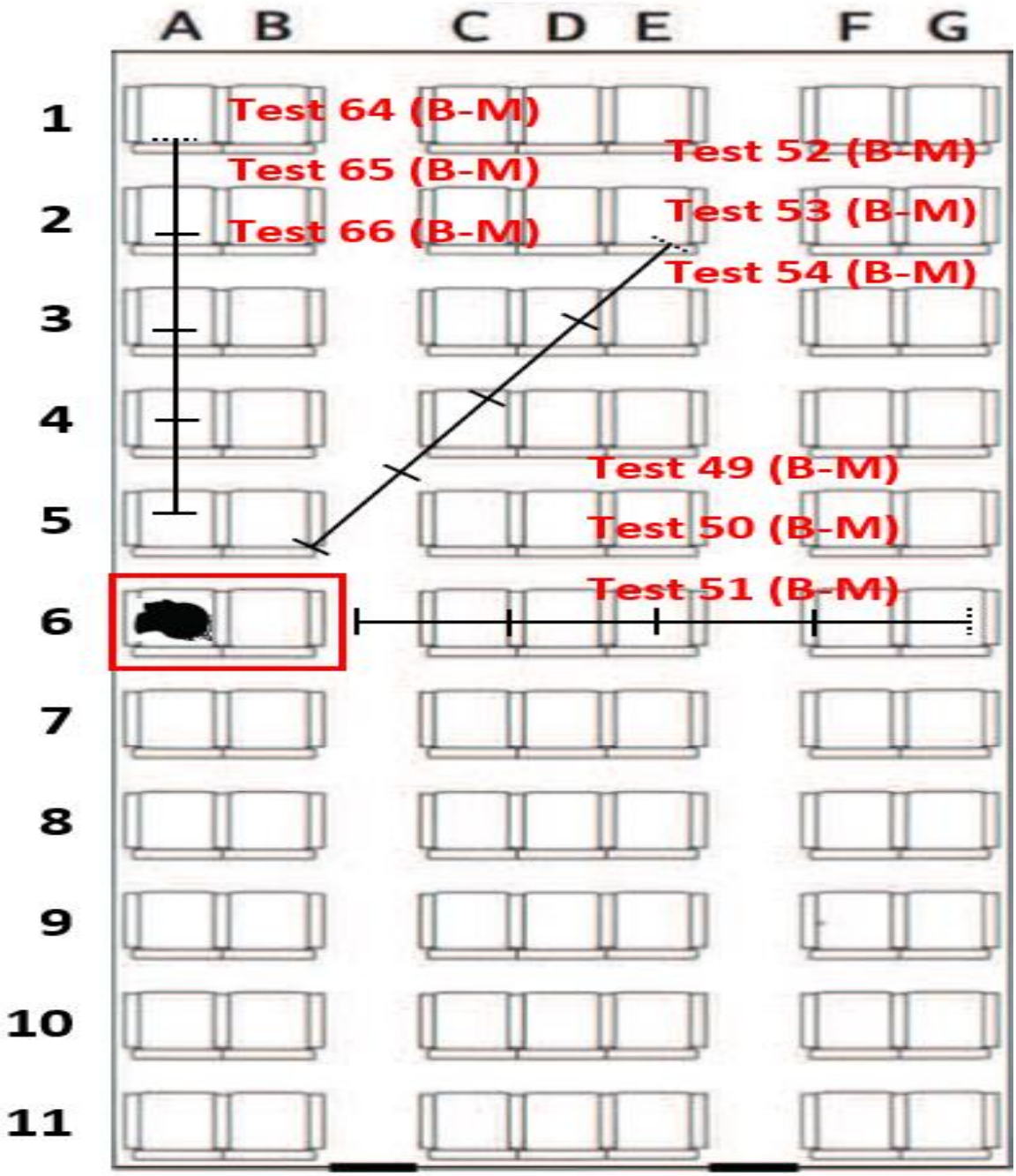

Figure I.3 Seat A6 ISOPass deployed coughing manikin tracer gas test numbers and sampling tree orientations in the Boeing 767 cabin mockup.

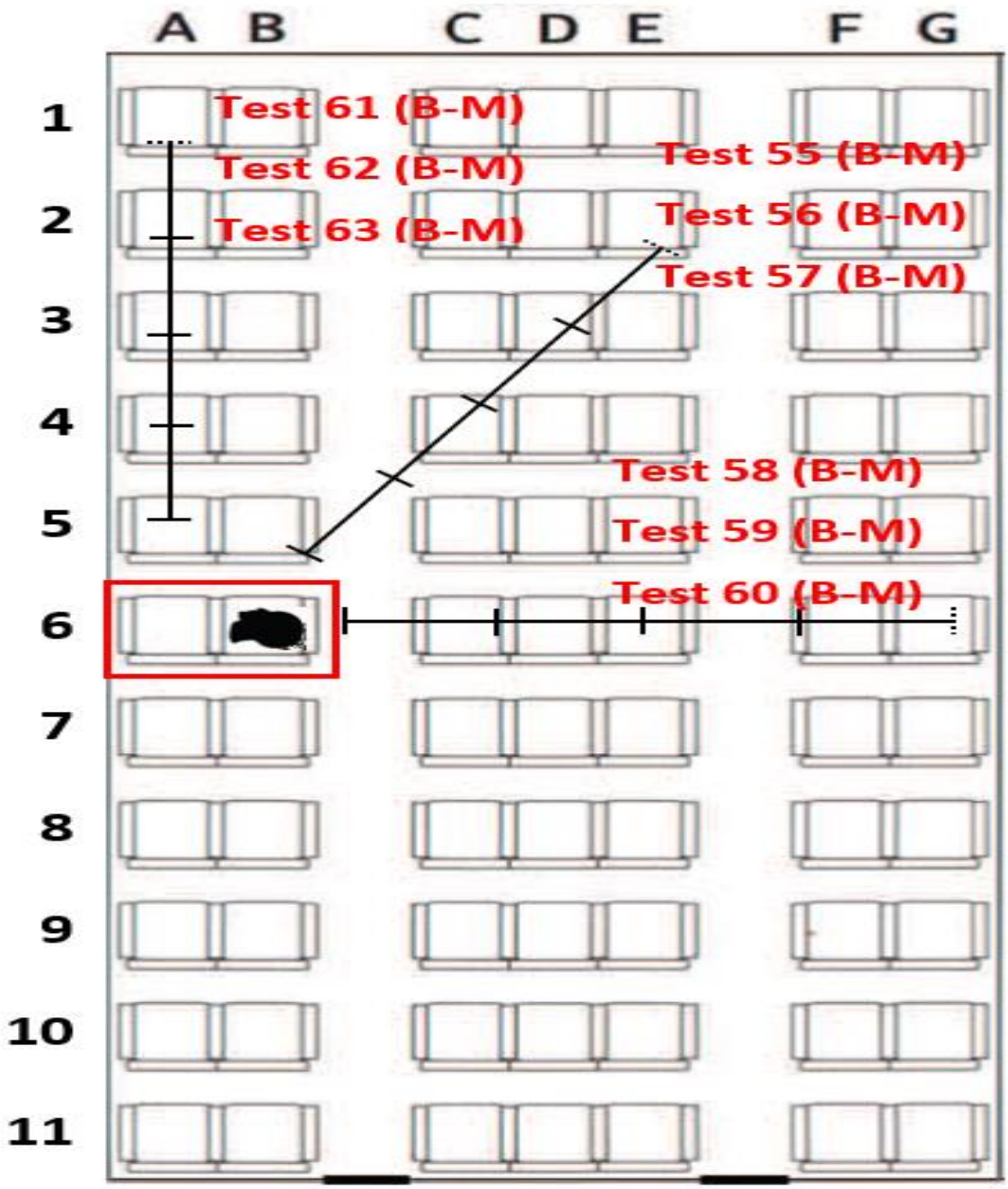

Figure I.4 Seat B6 ISOPass deployed coughing manikin tracer gas test numbers and sampling tree orientations in the Boeing 767 cabin mockup.

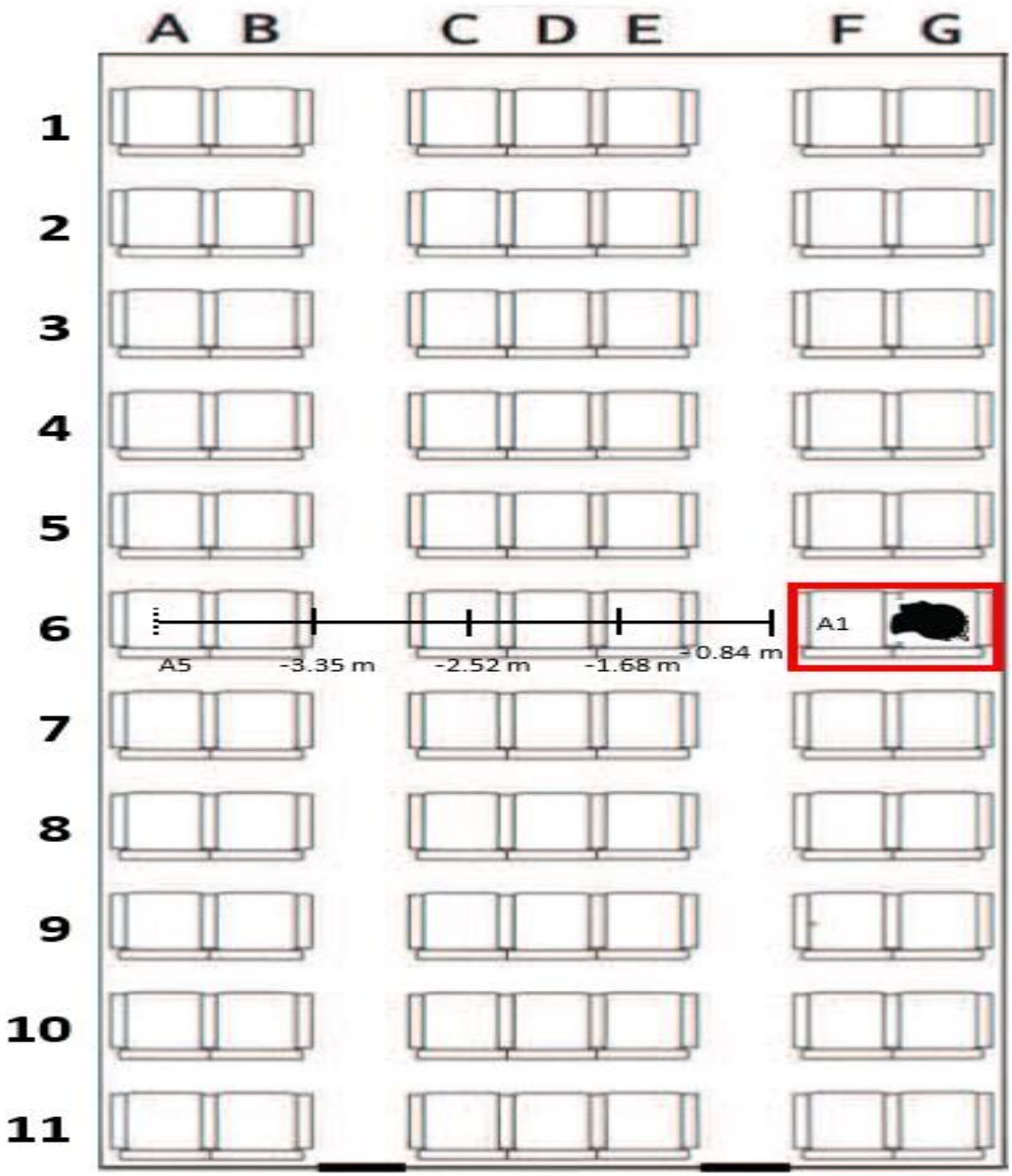

Figure I.5 Test 16 (B-M) ISOPass deployed source location and sampling tree orientation.

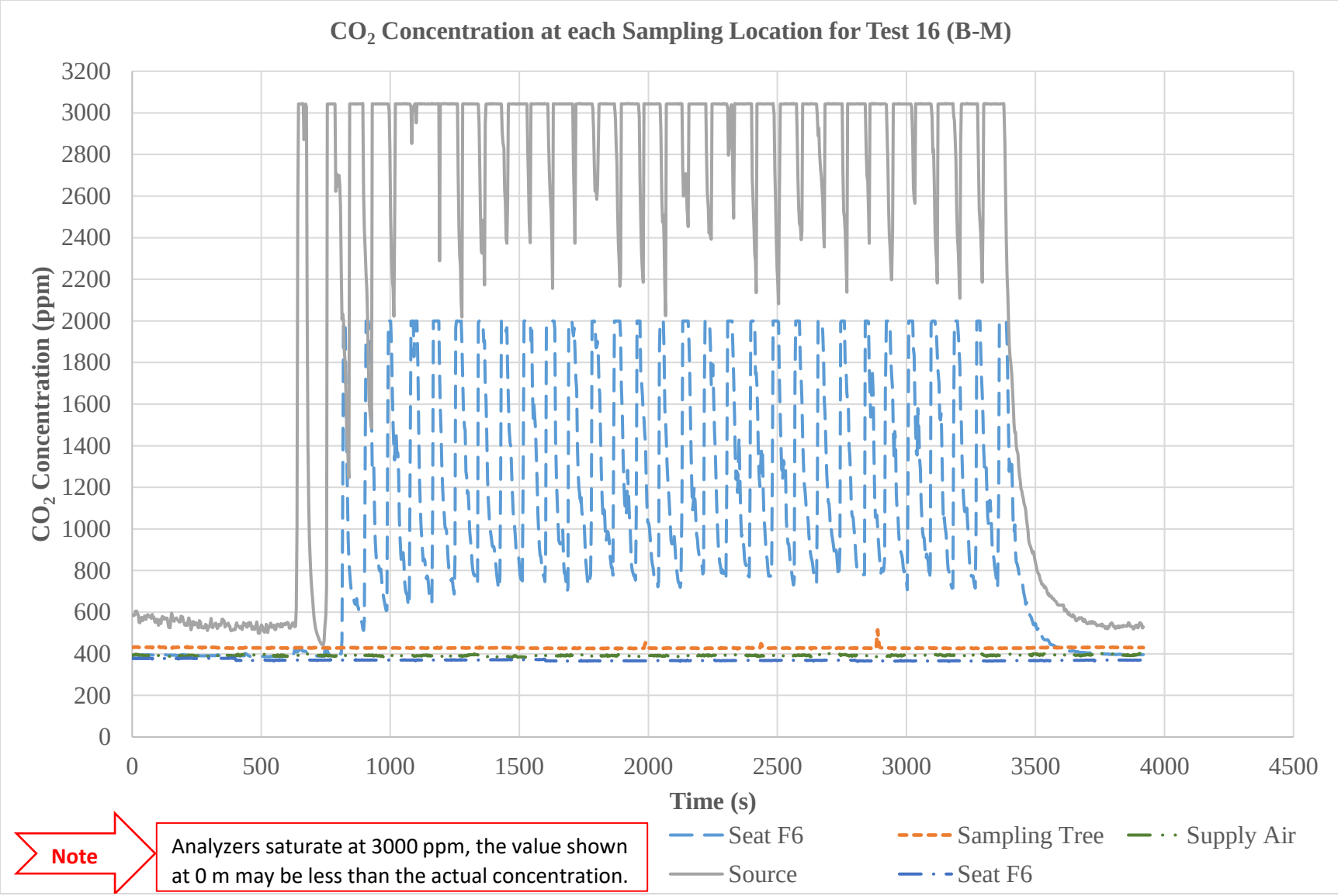

Figure I.6 Ininstantaneous CO_2 concentration at each sampling location for Test 16 (B-M) ISOPass deployed.

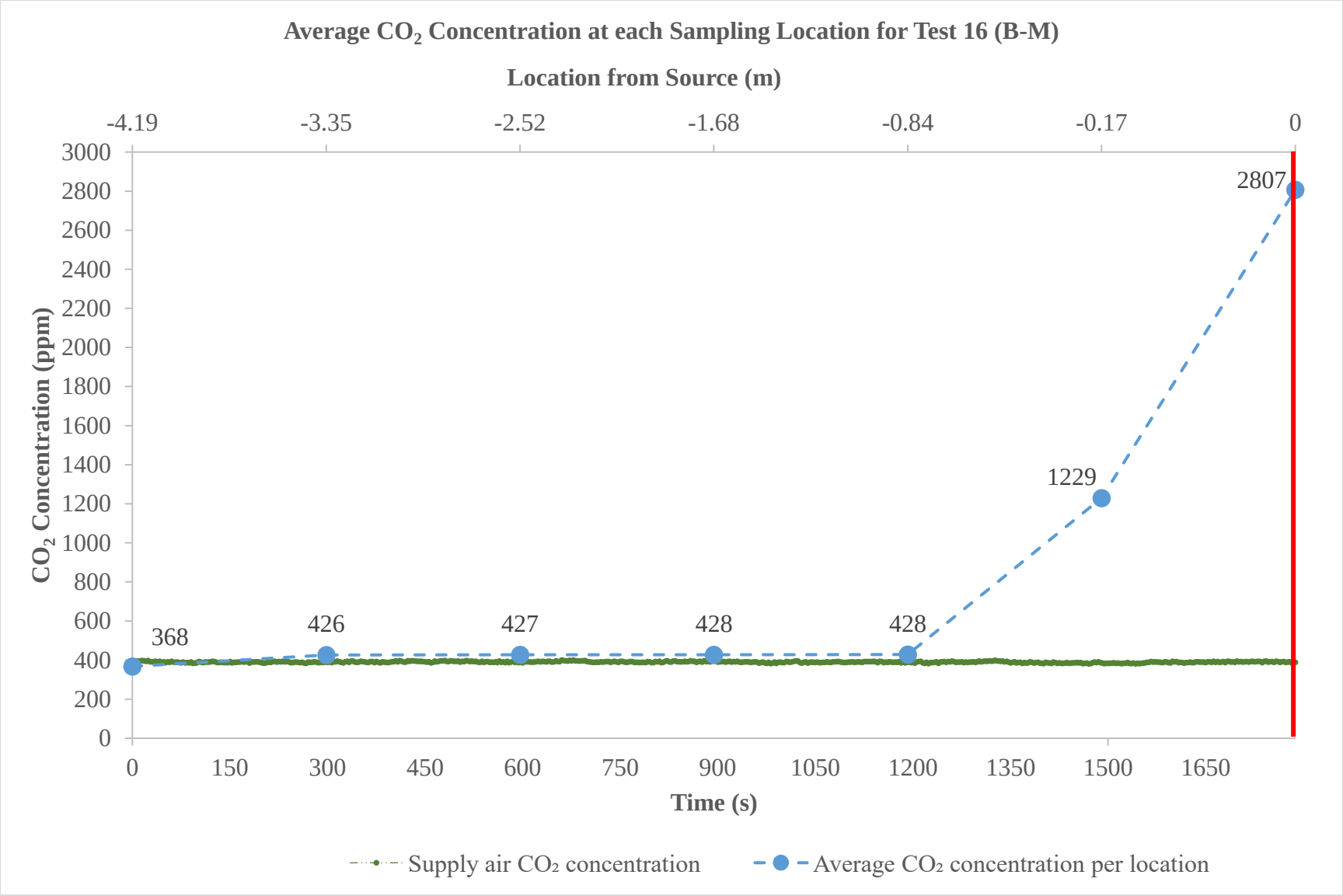

Figure I.7 Average CO_2 concentration at each sampling location for Test 16 (B-M) ISOPass deployed.

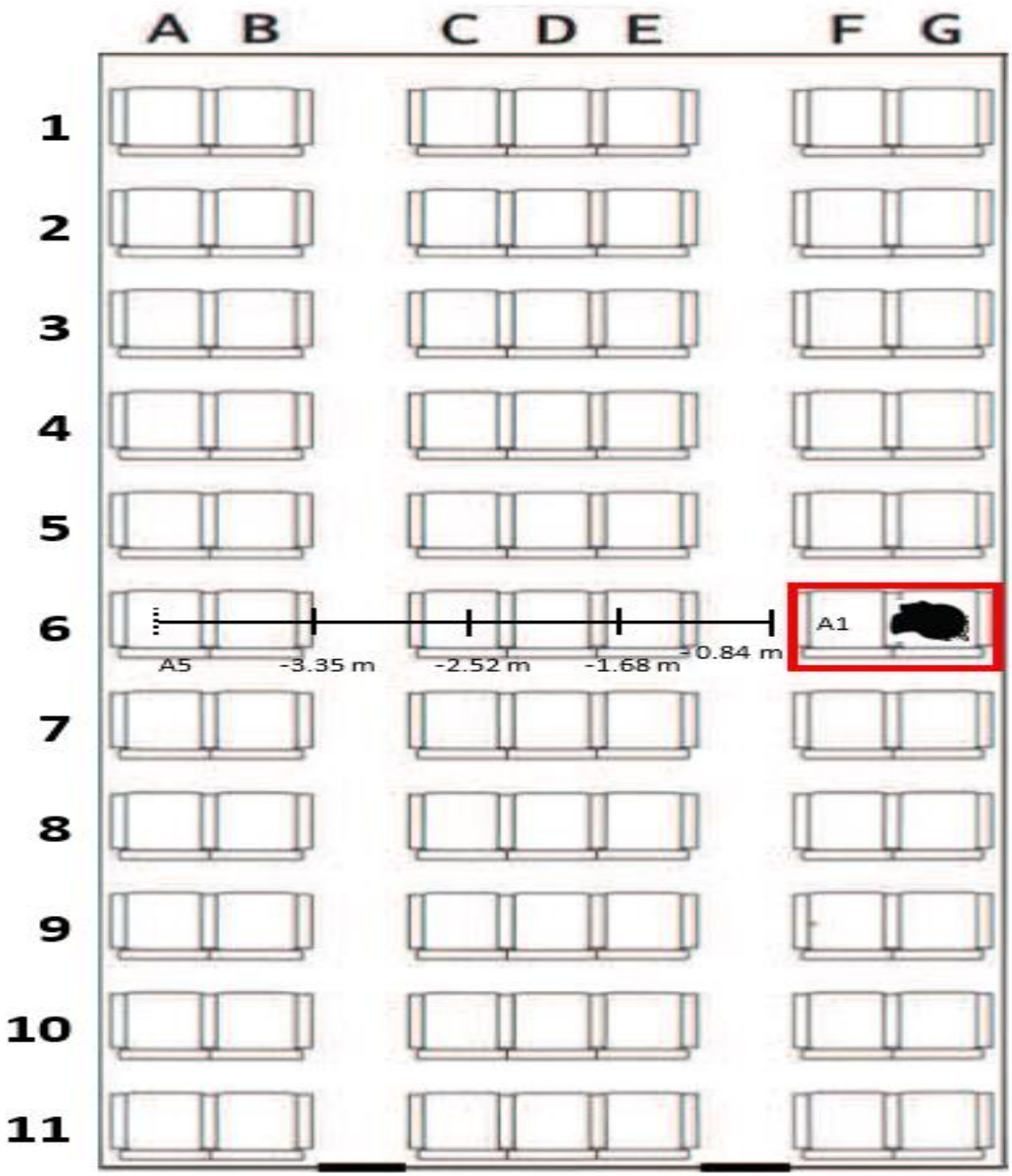

Figure I.8 Test 17 (B-M) ISOPass deployed source location and sampling tree orientation.

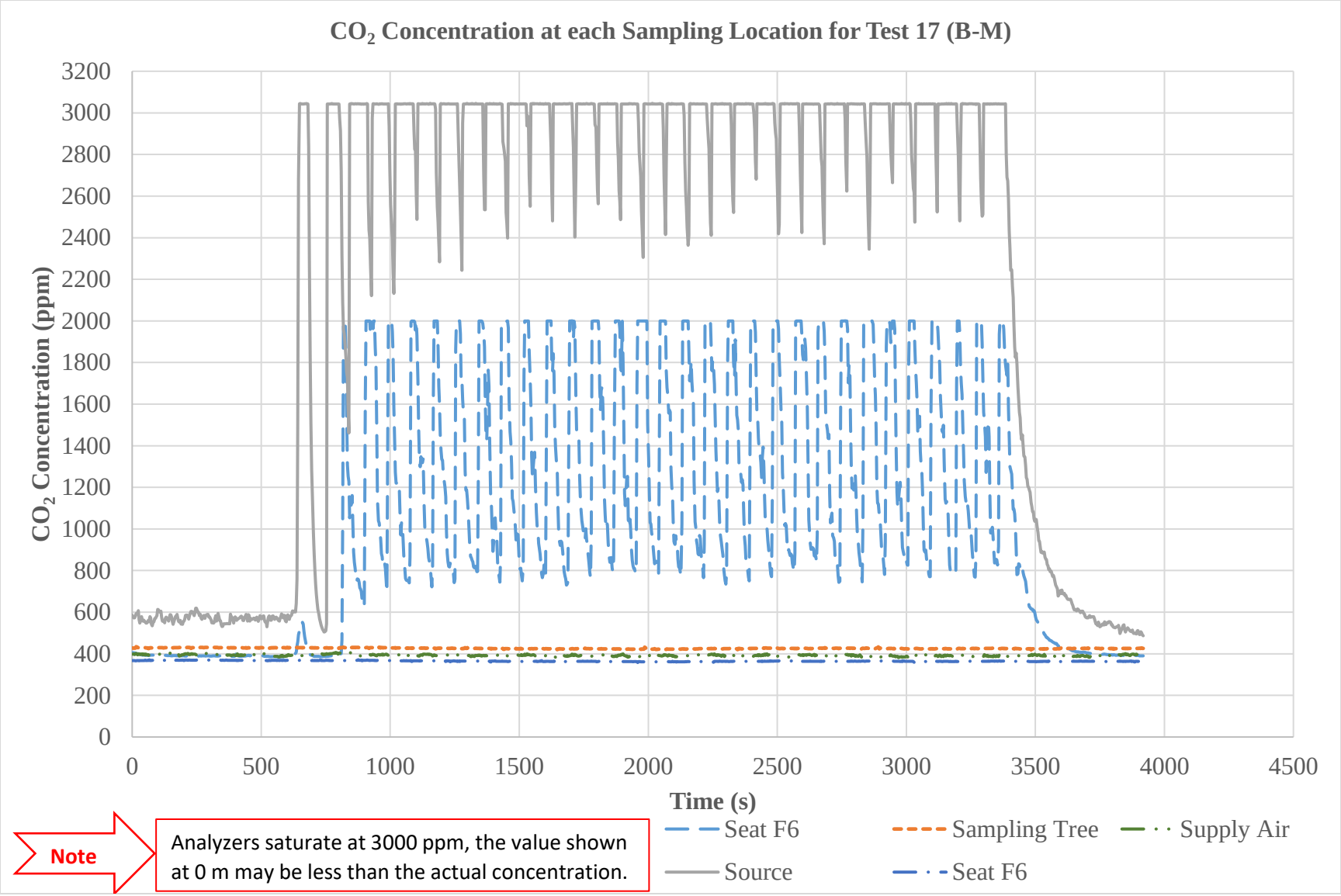

Figure I.9 Ininstantaneous CO_2 concentration at each sampling location for Test 17 (B-M) ISOPass deployed.

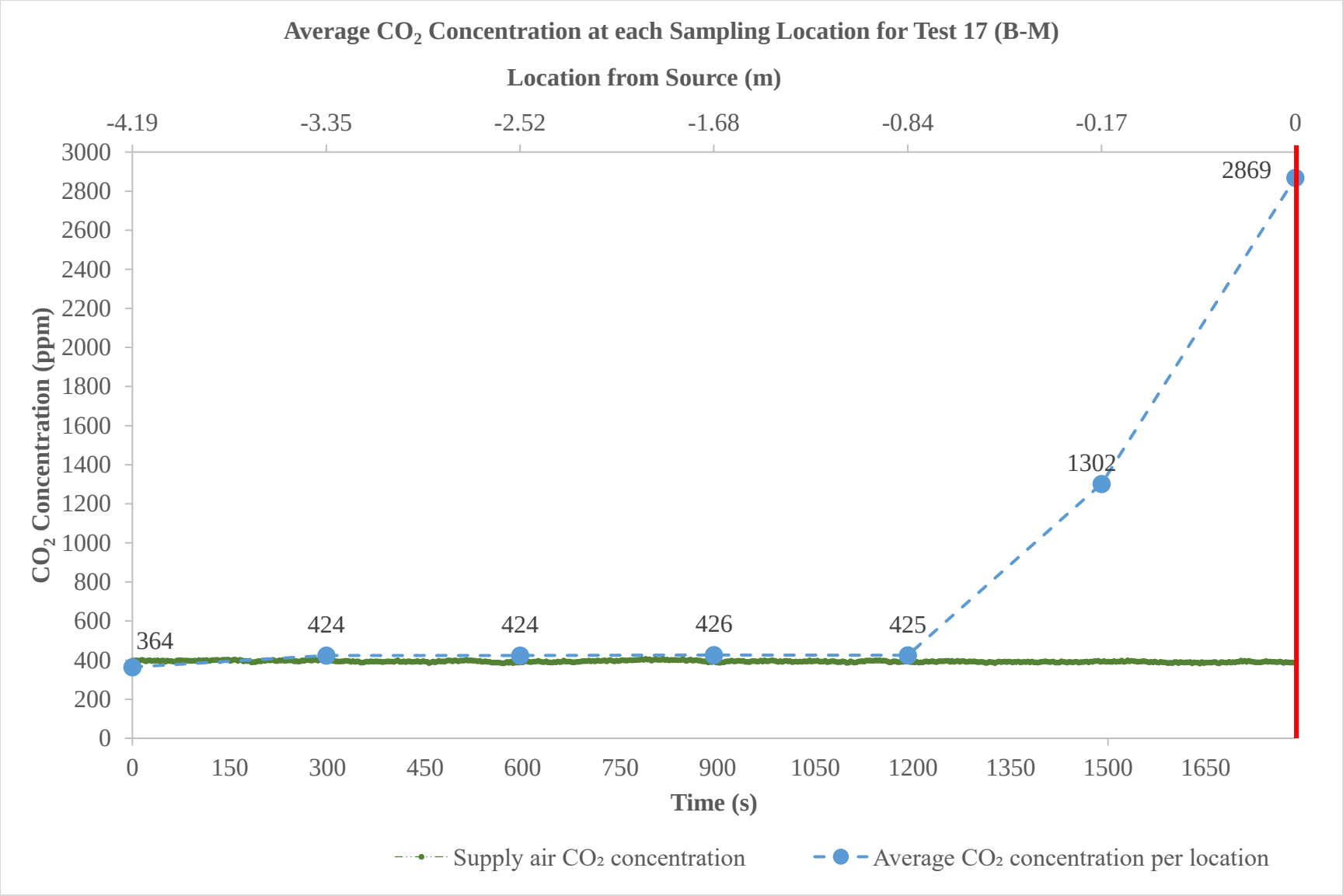

Figure I.10 Average CO_2 concentration at each sampling location for Test 17 (B-M) ISOPass deployed.

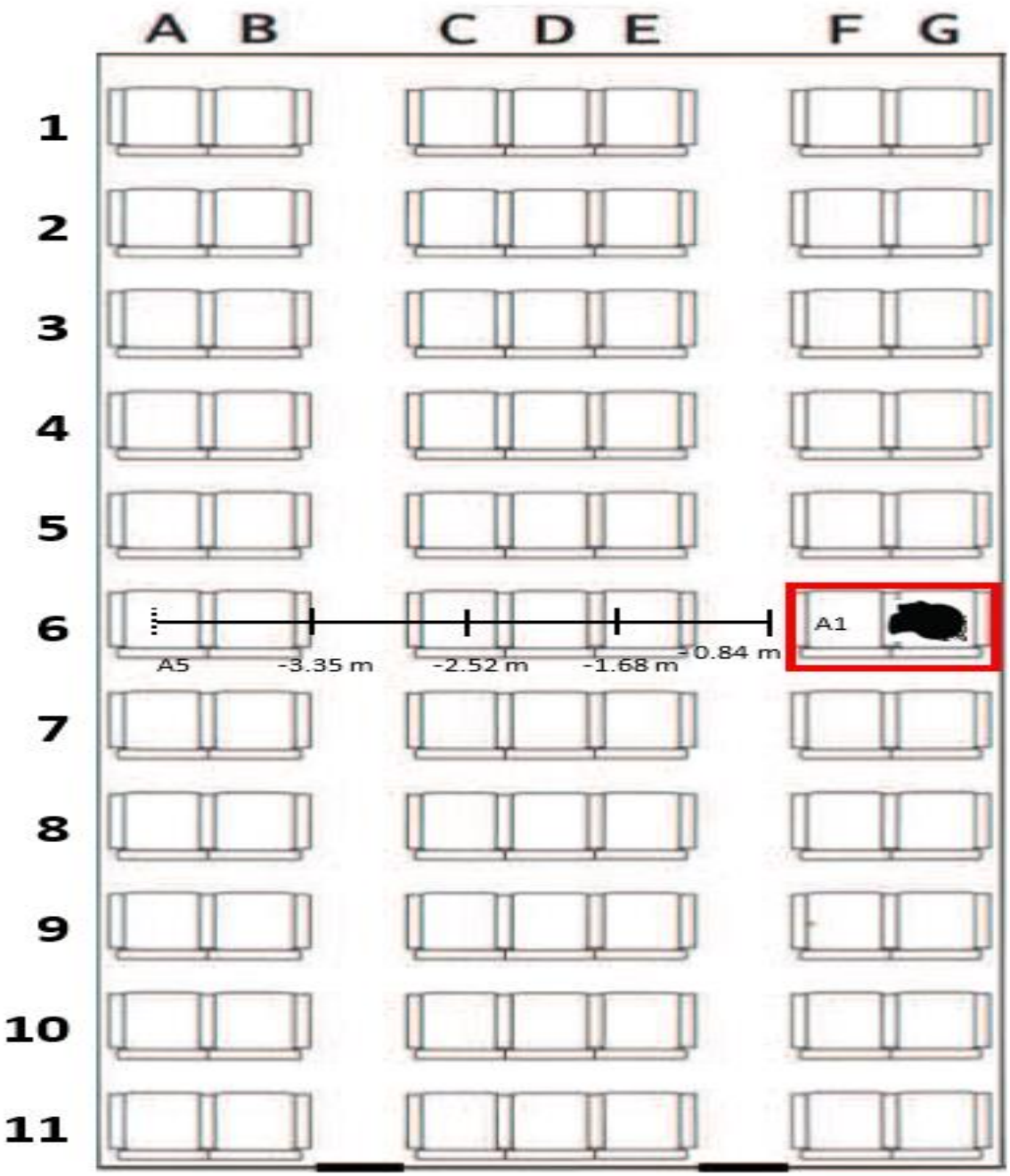

Figure I.11 Test 18 (B-M) ISOPass deployed source location and sampling tree orientation.

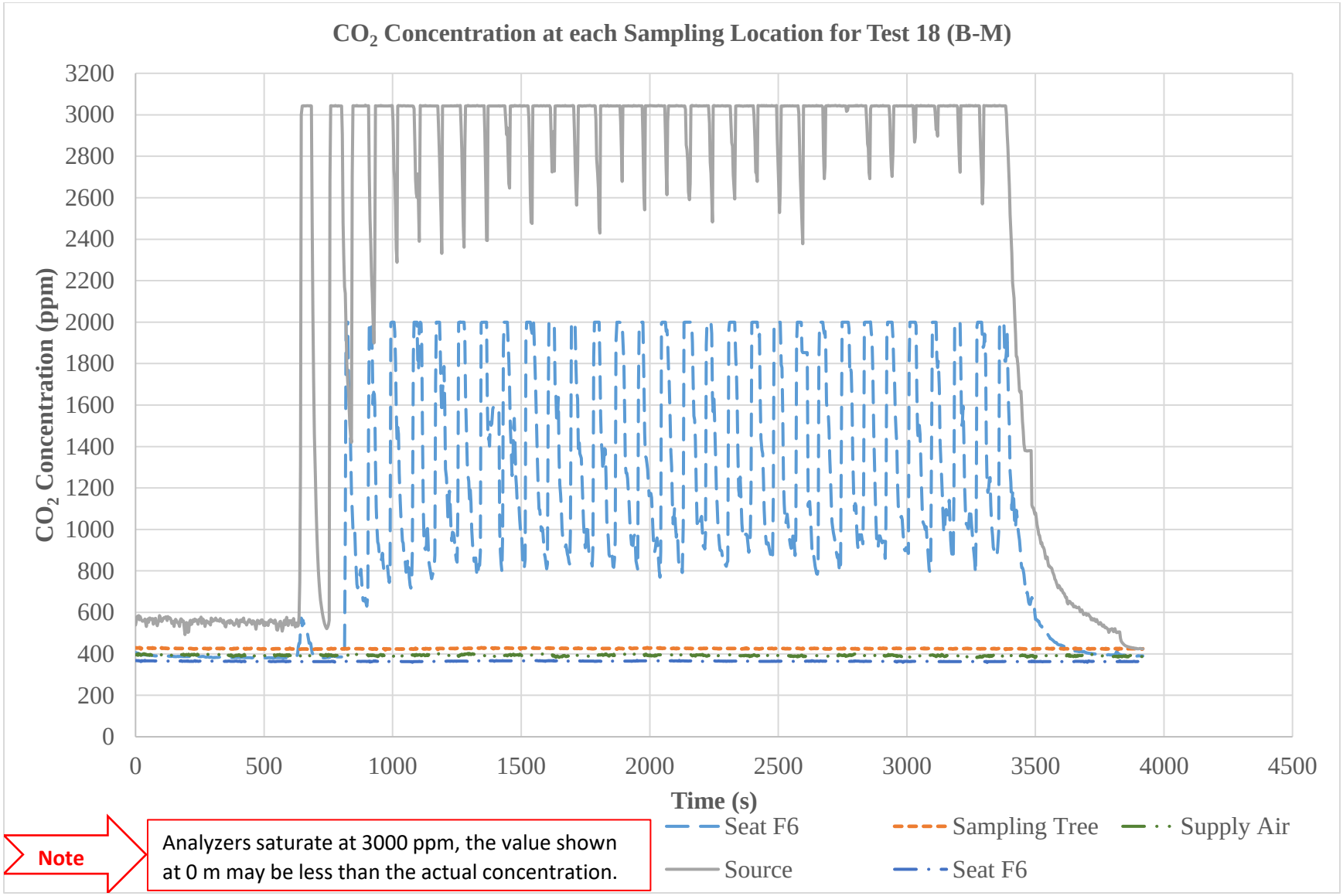

Figure I.12 Ininstantaneous CO_2 concentration at each sampling location for Test 18 (B-M) ISOPass deployed.

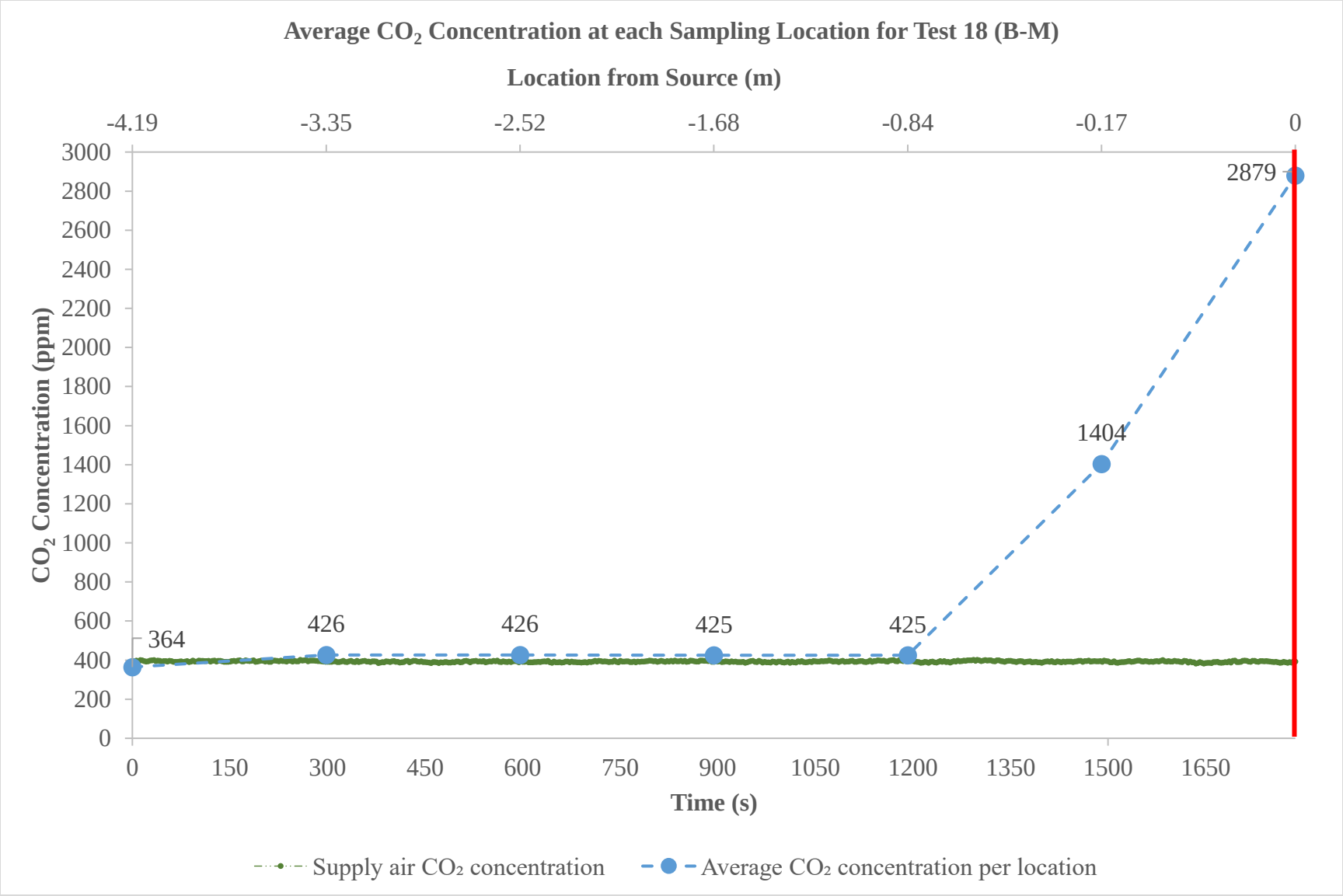

Figure I.13 Average CO_2 concentration at each sampling location for Test 18 (B-M) ISOPass deployed.

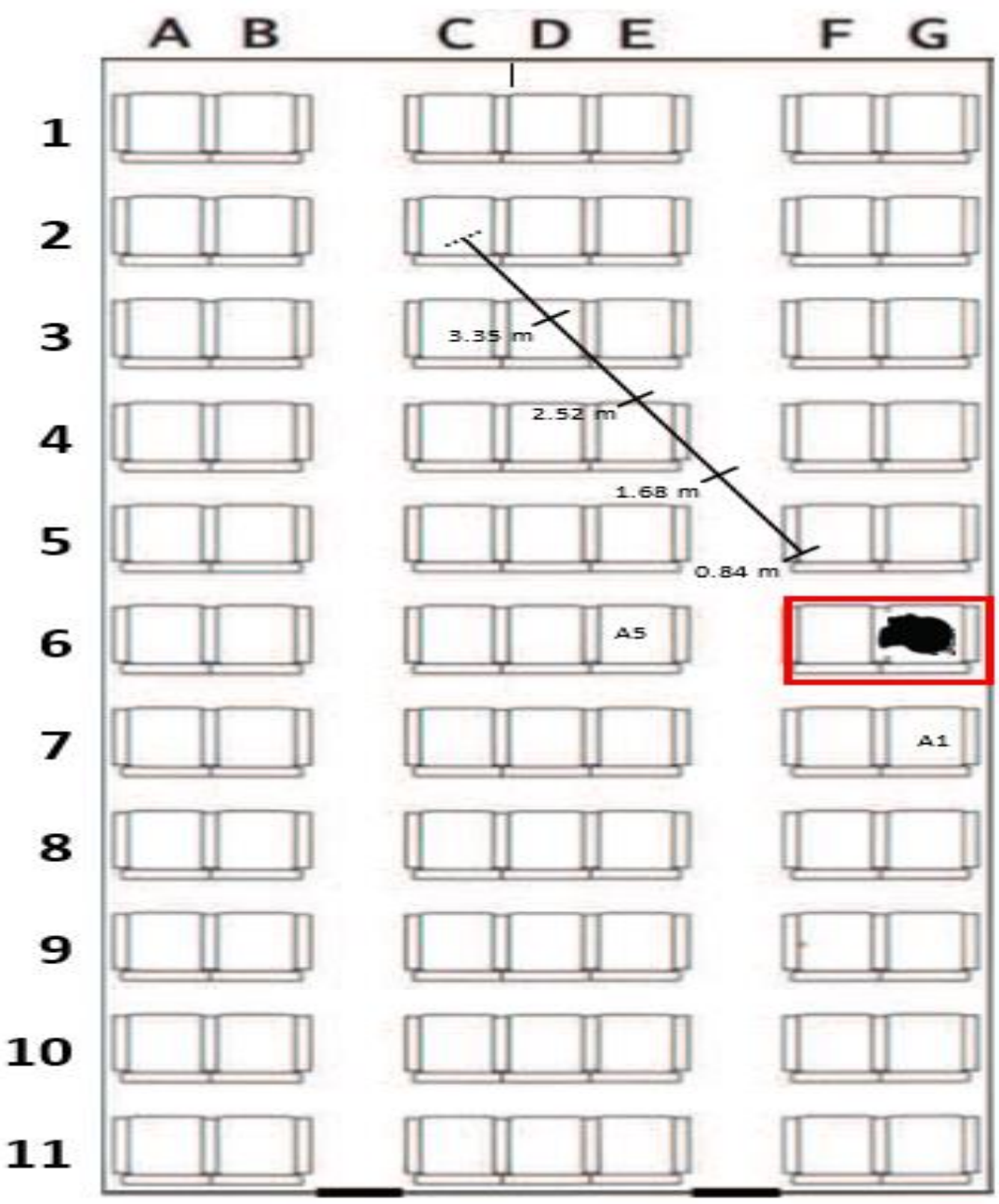

Figure I.14 Test 19 (B-M) ISOPass deployed source location and sampling tree orientation.

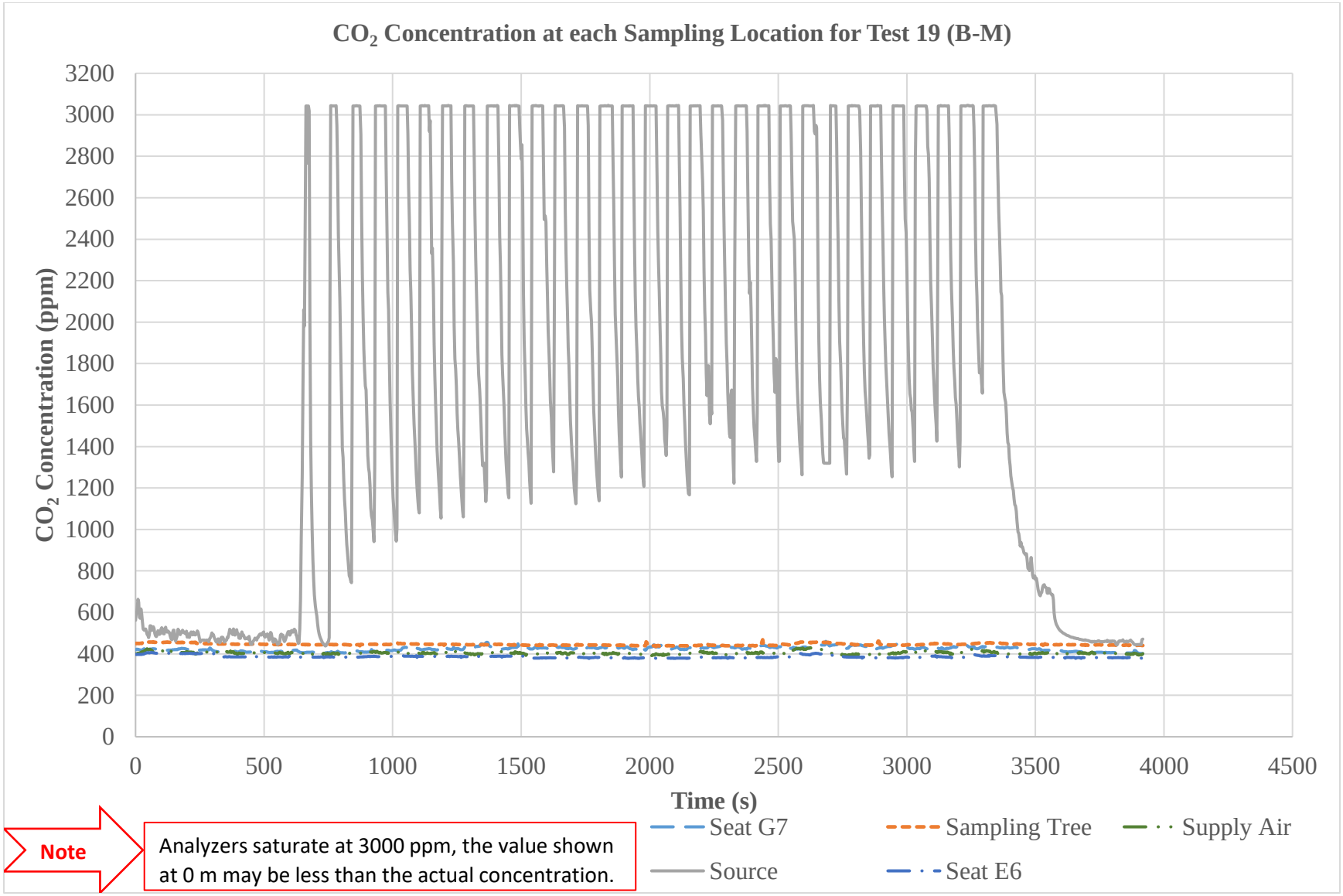

Figure I.15 Ininstantaneous CO_2 concentration at each sampling location for Test 19 (B-M) ISOPass deployed.

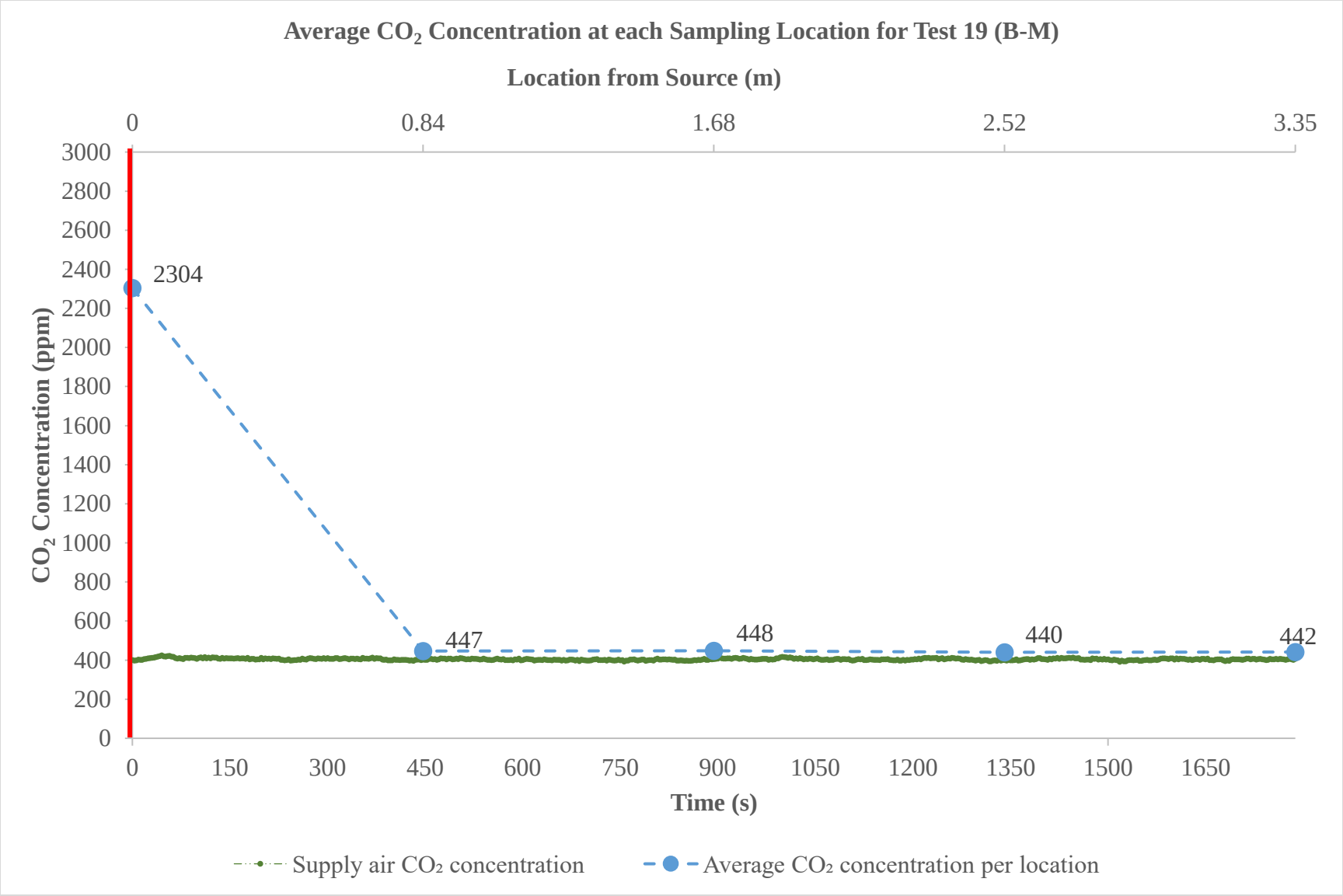

Figure I.16 Average CO_2 concentration at each sampling location for Test 19 (B-M) ISOPass deployed.

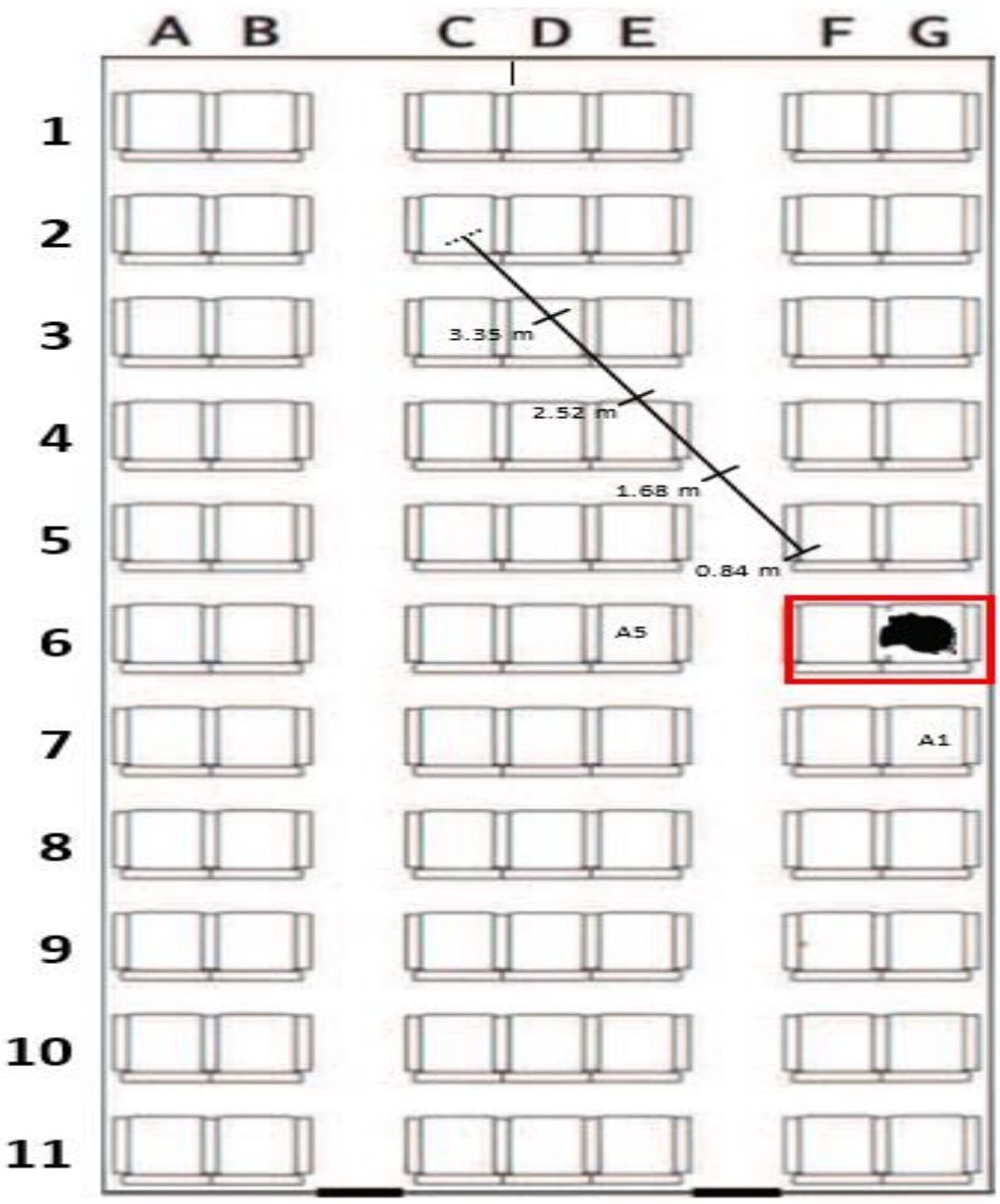

Figure I.17 Test 20 (B-M) ISOPass deployed source location and sampling tree orientation.

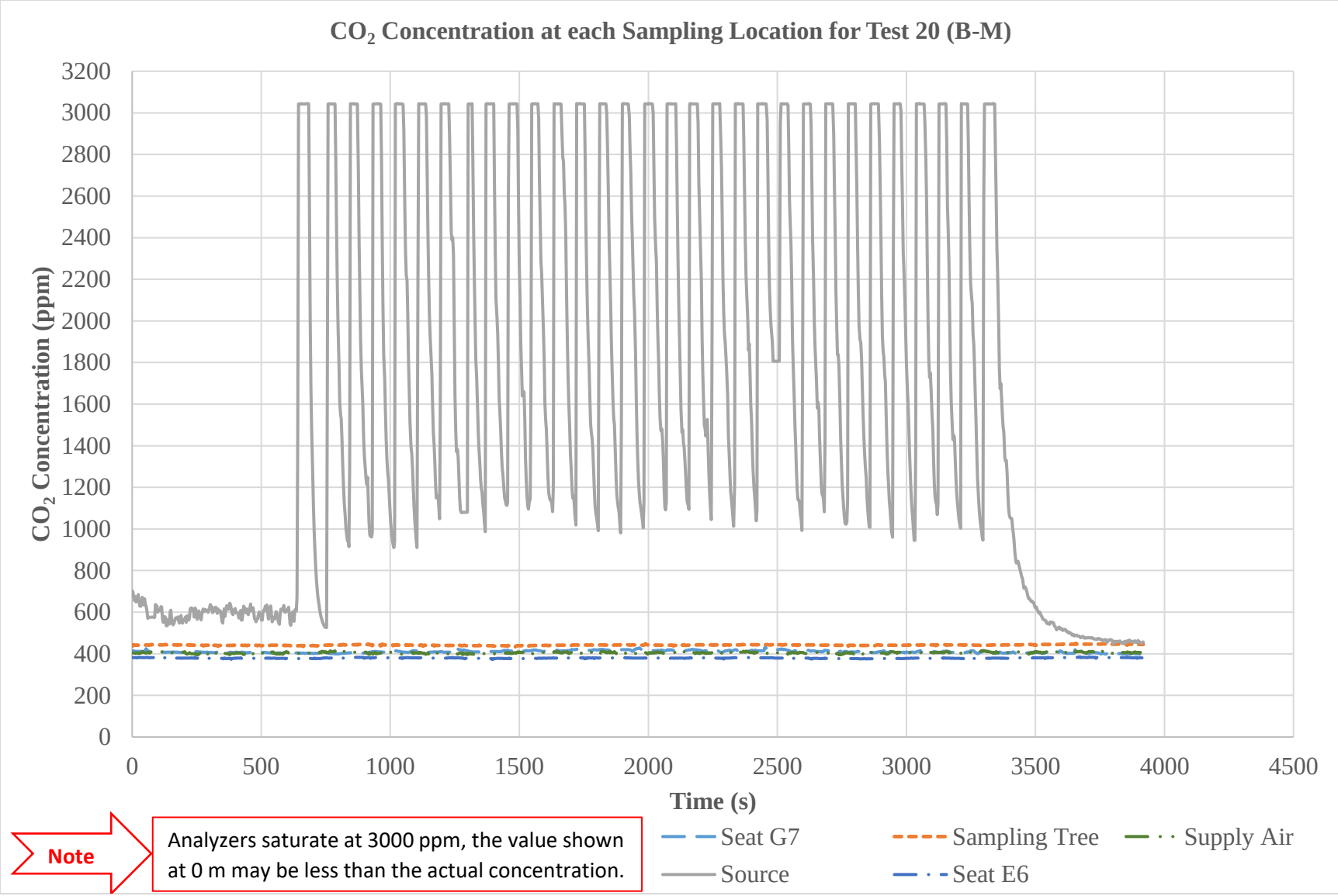

Figure I.18 Ininstantaneous CO_2 concentration at each sampling location for Test 20 (B-M) ISOPass deployed.

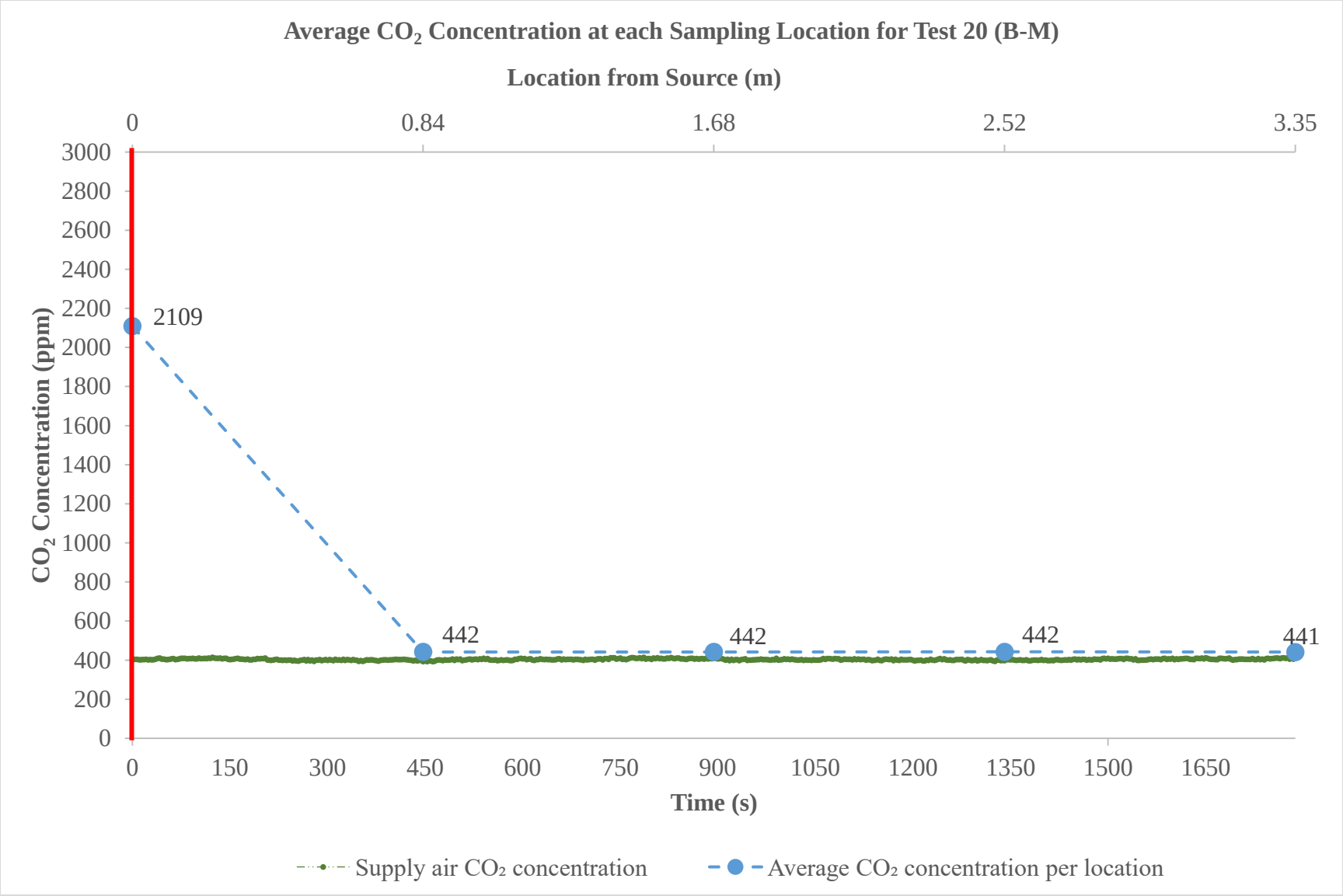

Figure I.19 Average CO_2 concentration at each sampling location for Test 20 (B-M) ISOPass deployed.

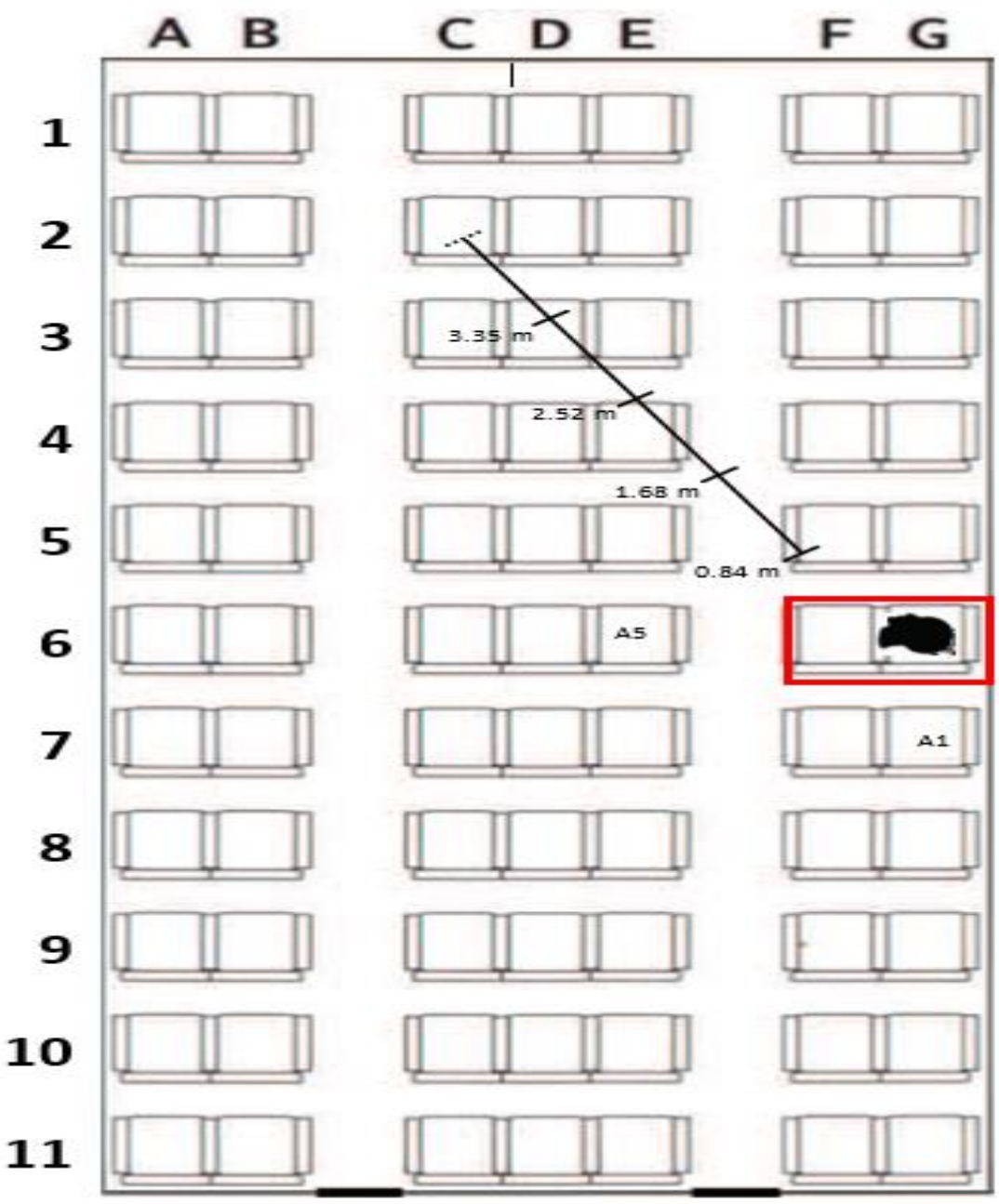

Figure I.20 Test 21 (B-M) ISOPass deployed source location and sampling tree orientation.

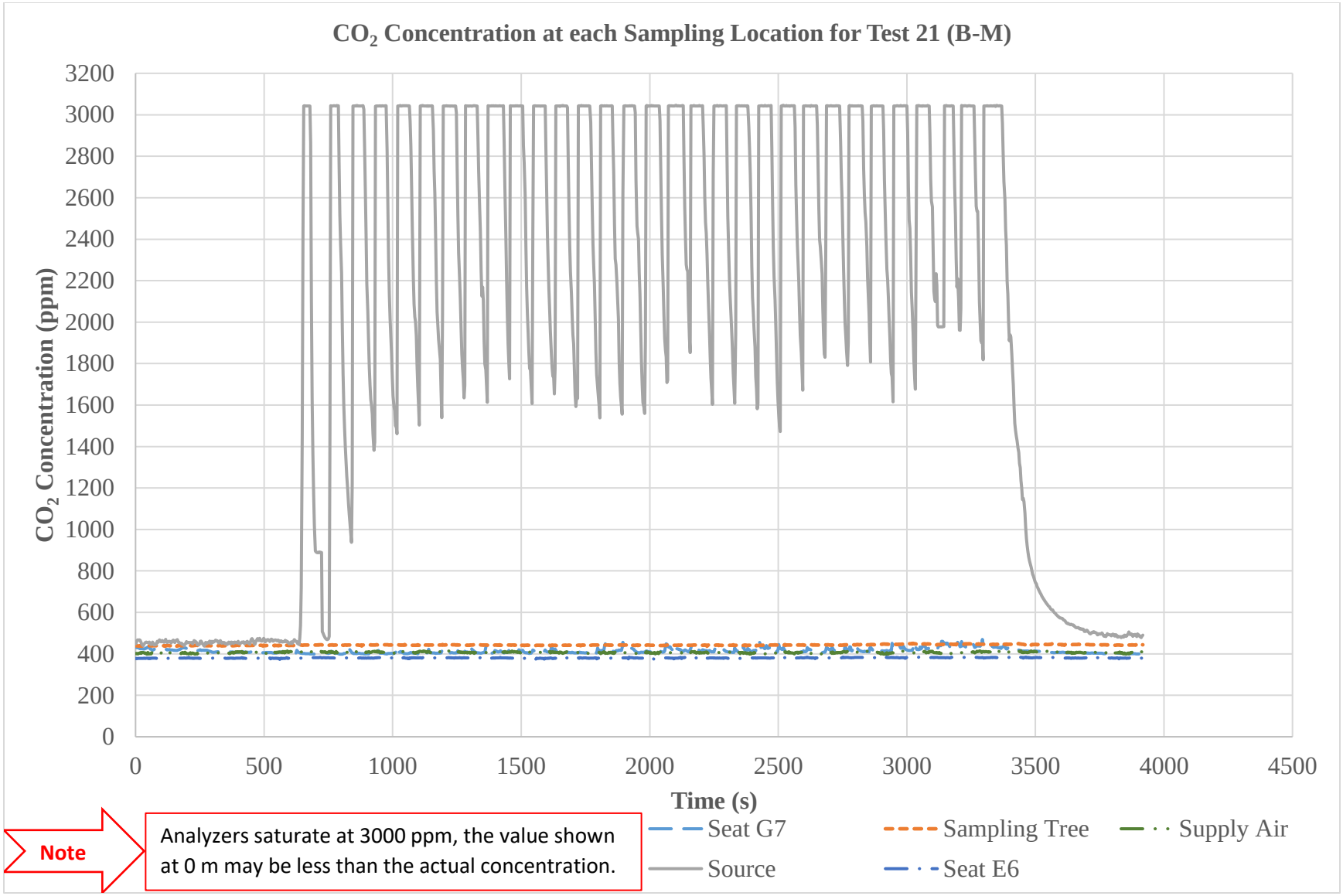

Figure I.21 Ininstantaneous CO_2 concentration at each sampling location for Test 21 (B-M) ISOPass deployed.

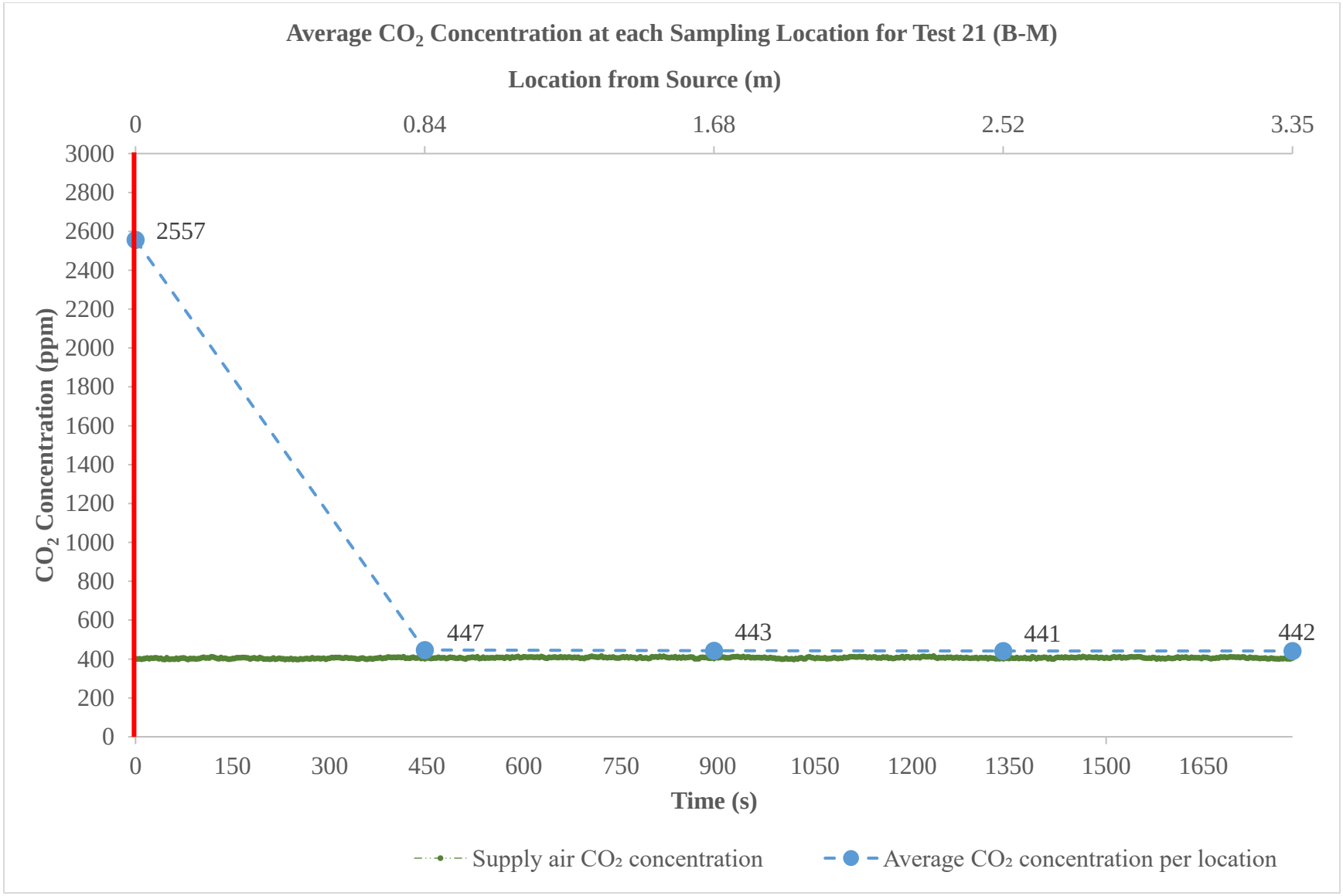

Figure I.22 Average CO_2 concentration at each sampling location for Test 21 (B-M) ISOPass deployed.

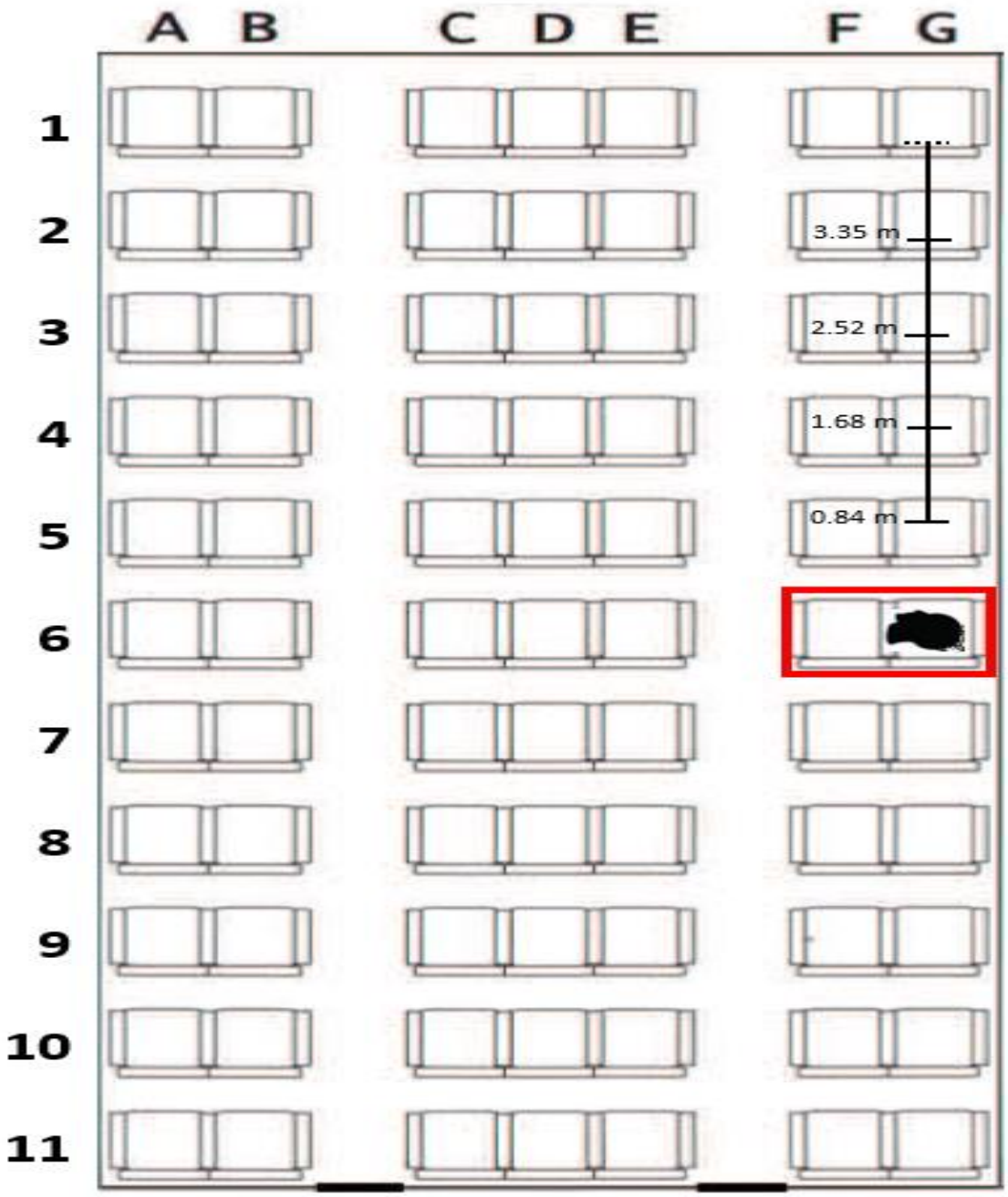

Figure I.23 Test 28 (B-M) ISOPass deployed source location and sampling tree orientation.

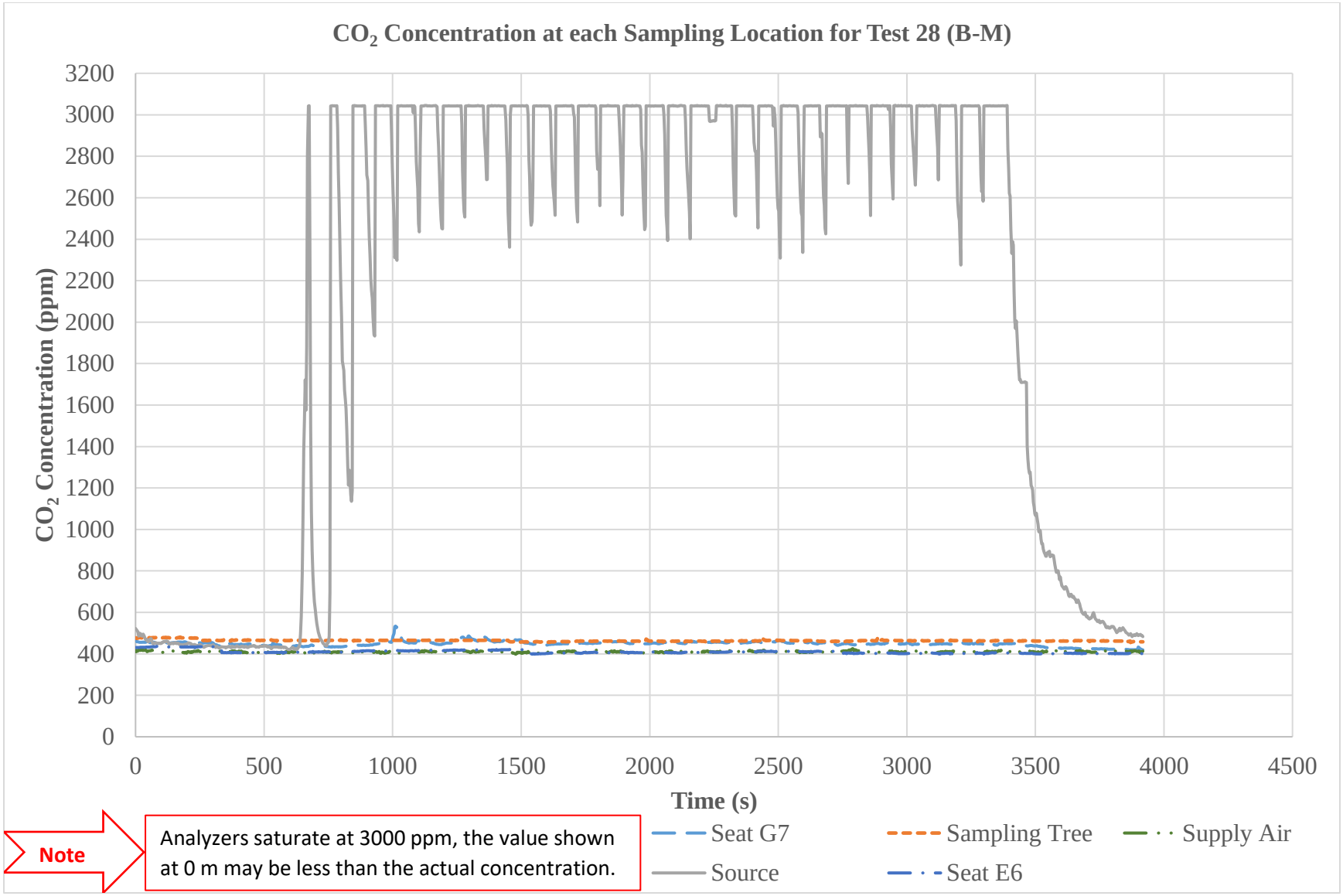

Figure I.24 Ininstantaneous CO_2 concentration at each sampling location for Test 28 (B-M) ISOPass deployed.

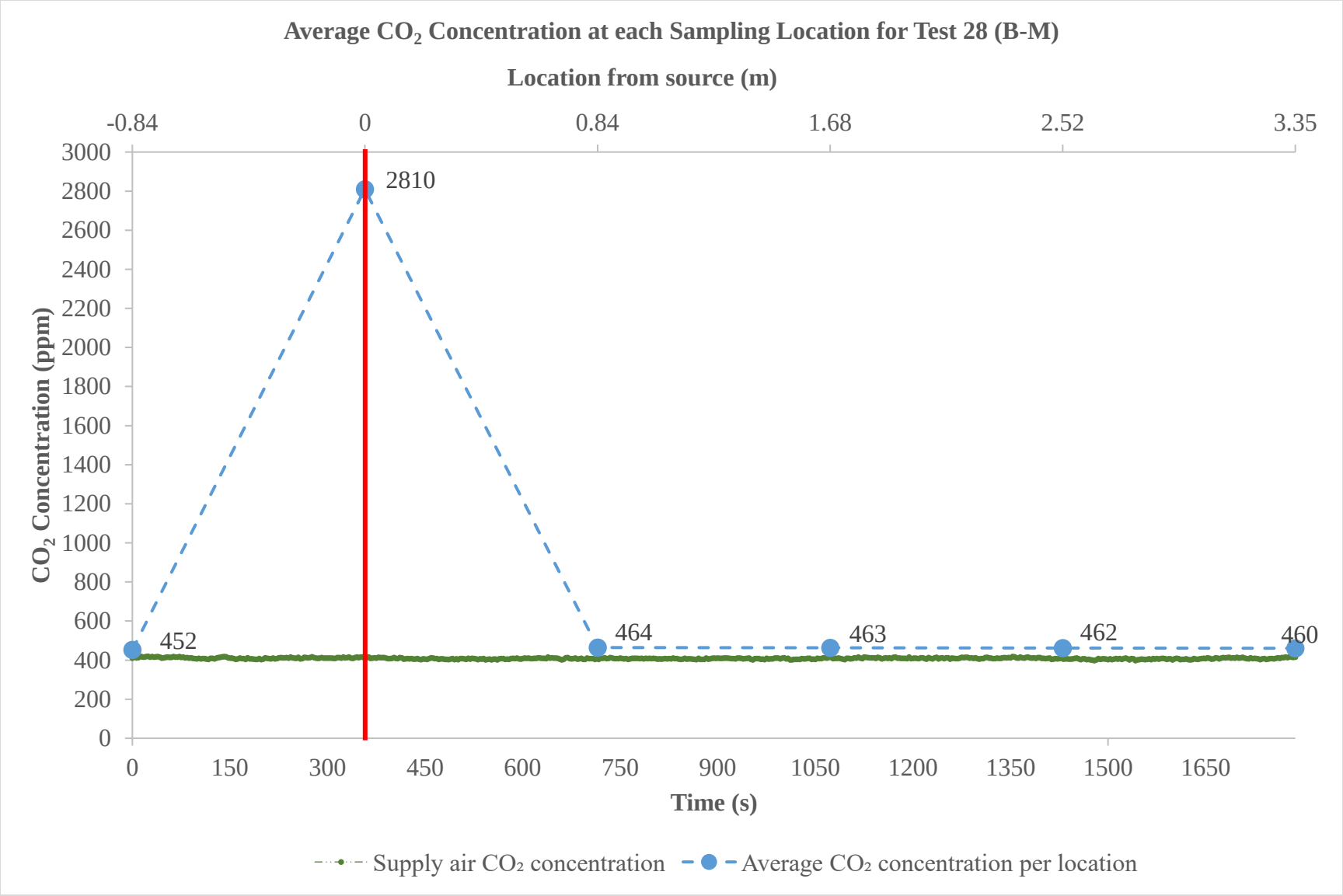

Figure I.25 Average CO_2 concentration at each sampling location for Test 28 (B-M) ISOPass deployed.

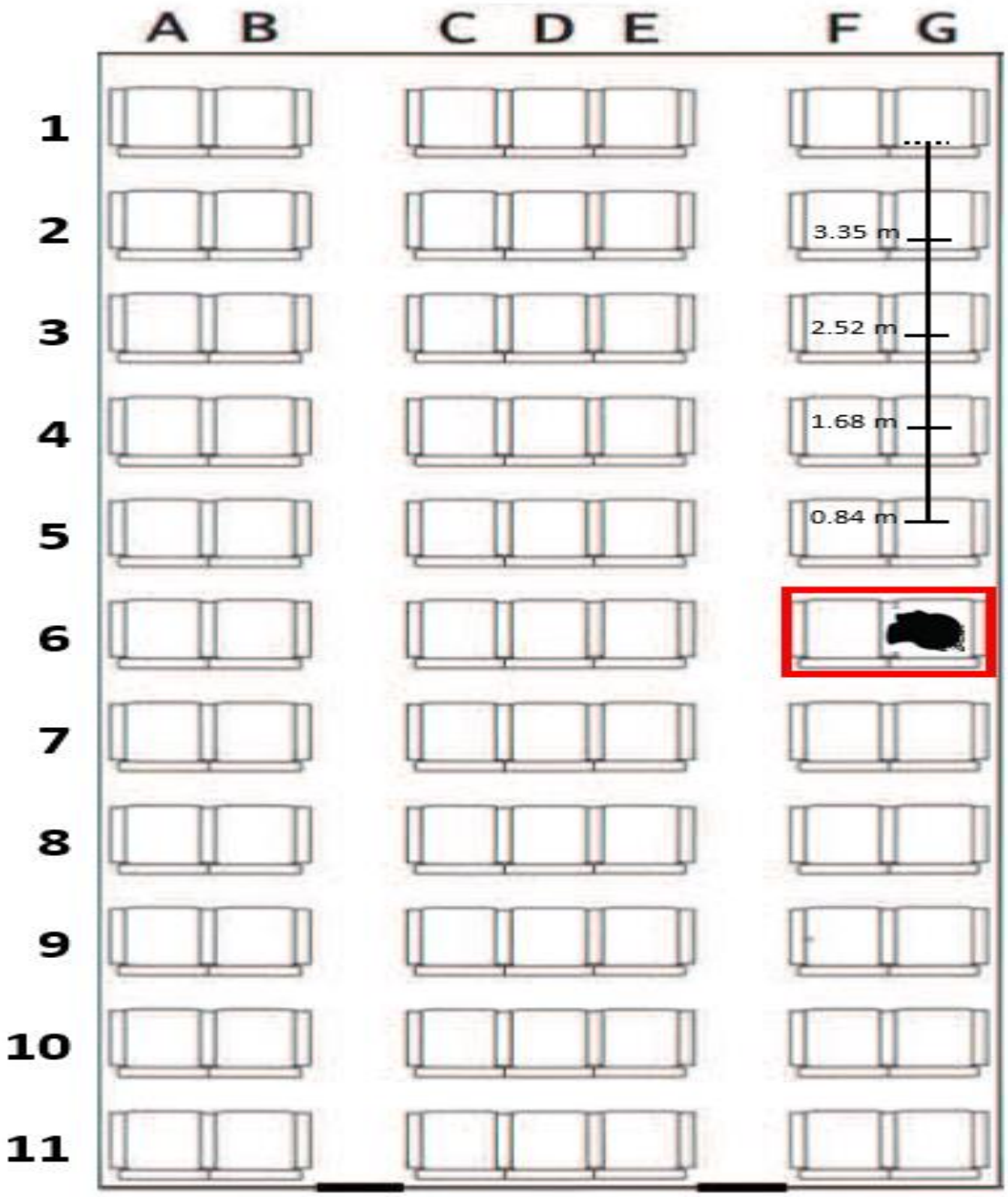

Figure I.26 Test 29 (B-M) ISOPass deployed source location and sampling tree orientation.

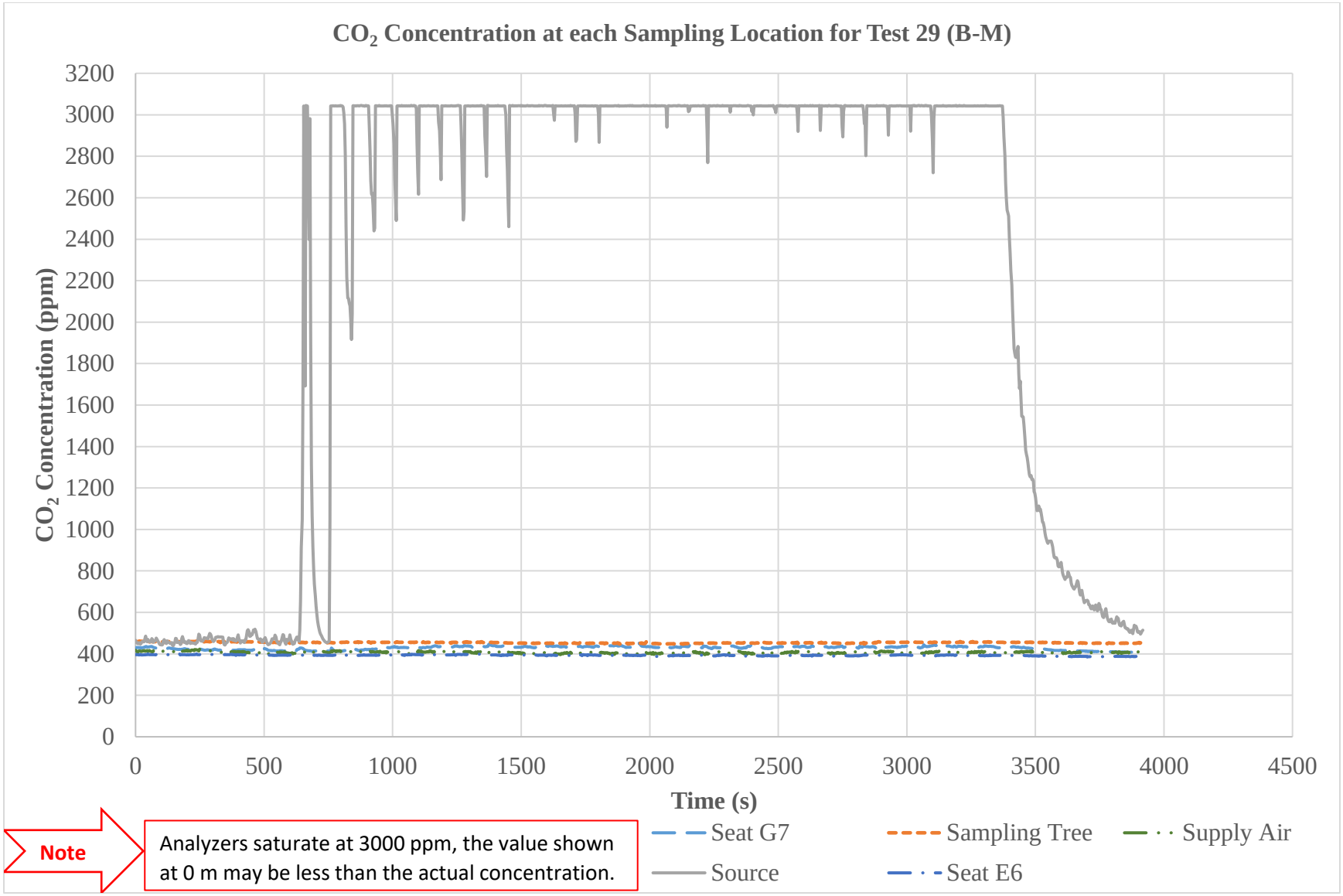

Figure I.27 Ininstantaneous CO_2 concentration at each sampling location for Test 29 (B-M) ISOPass deployed.

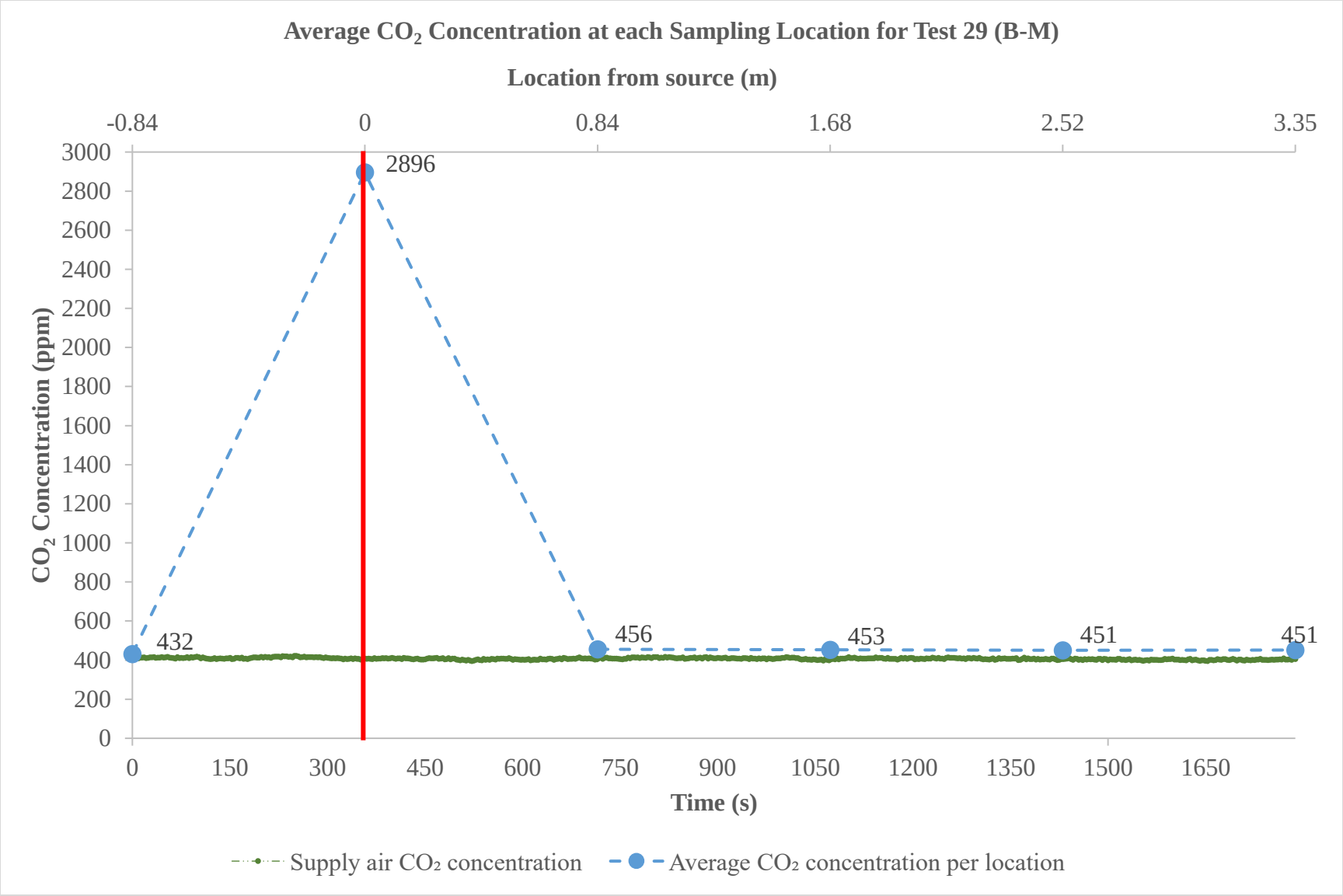

Figure I.28 Average CO_2 concentration at each sampling location for Test 29 (B-M) ISOPass deployed.

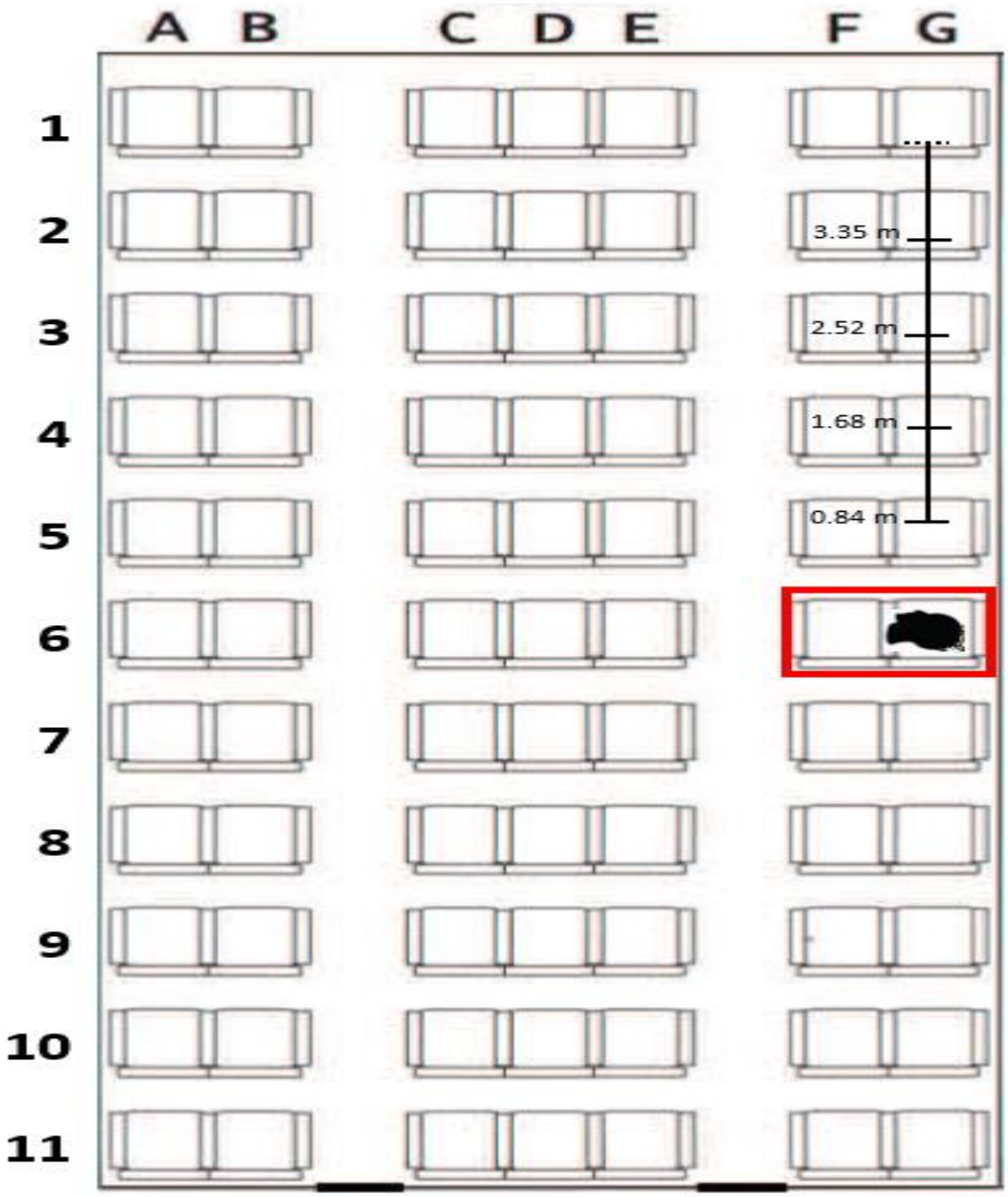

Figure I.29 Test 30 (B-M) ISOPass deployed source location and sampling tree orientation.

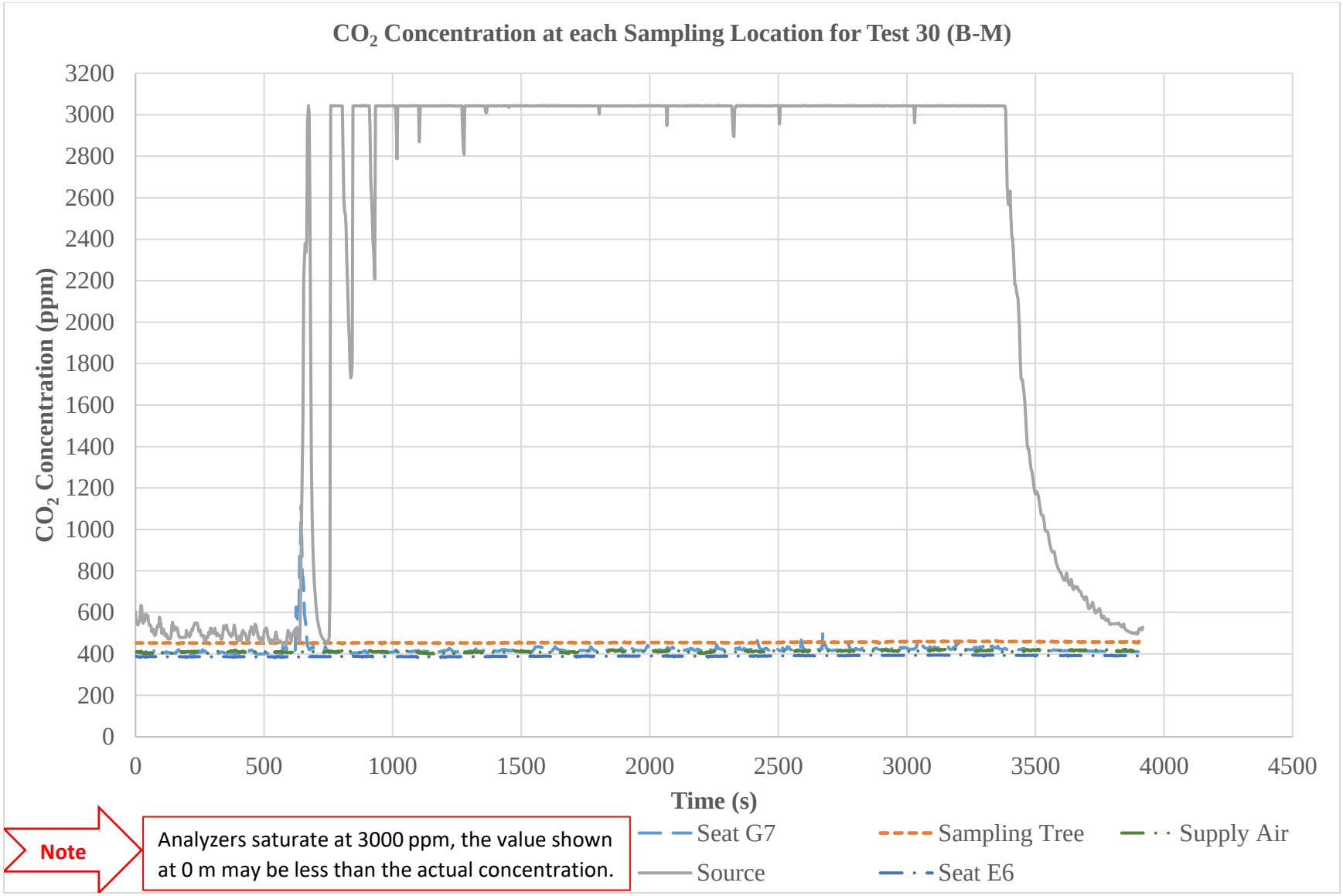

Figure I.30 Ininstantaneous CO_2 concentration at each sampling location for Test 30 (B-M) ISOPass deployed.

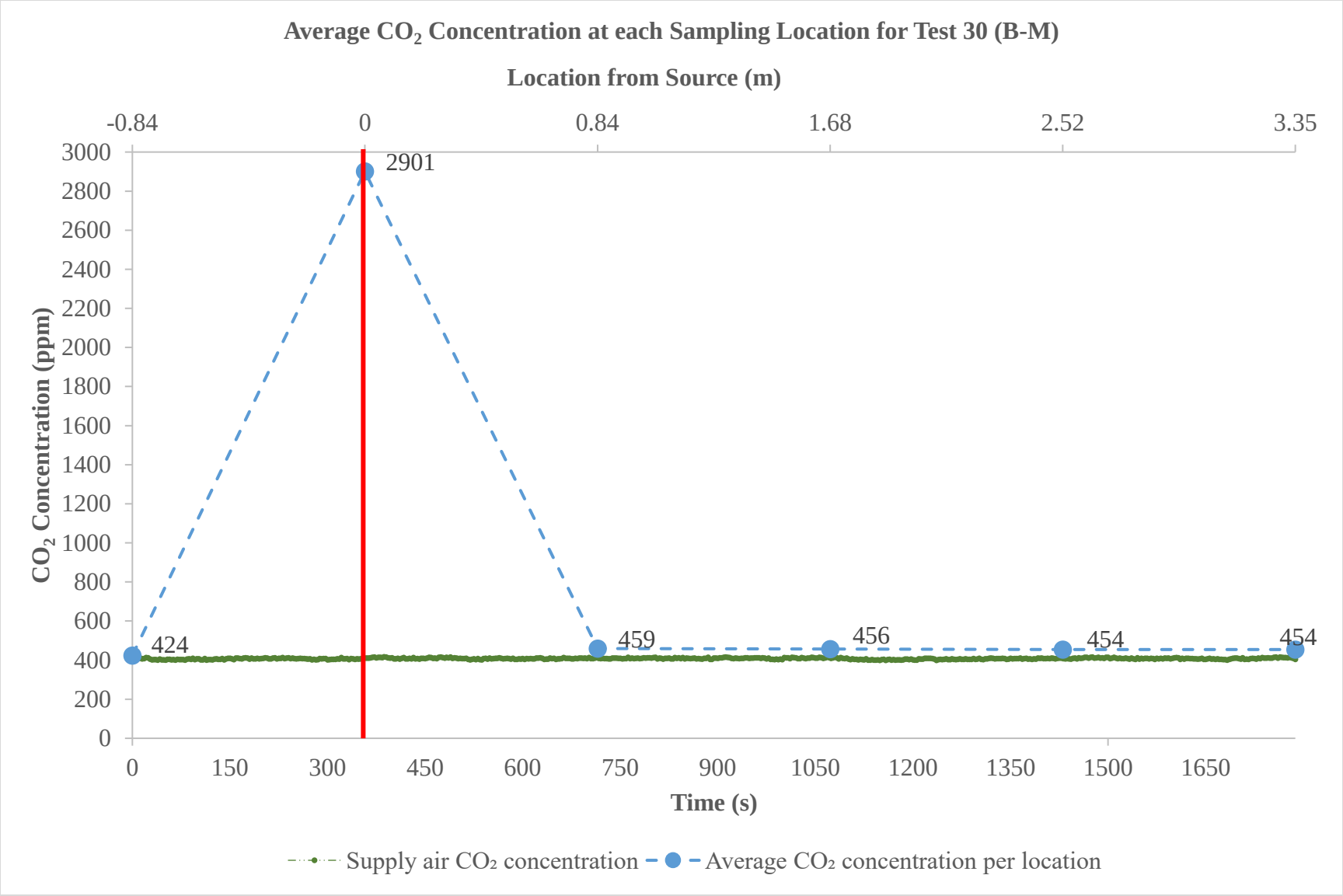

Figure I.31 Average CO_2 concentration at each sampling location for Test 30 (B-M) ISOPass deployed.

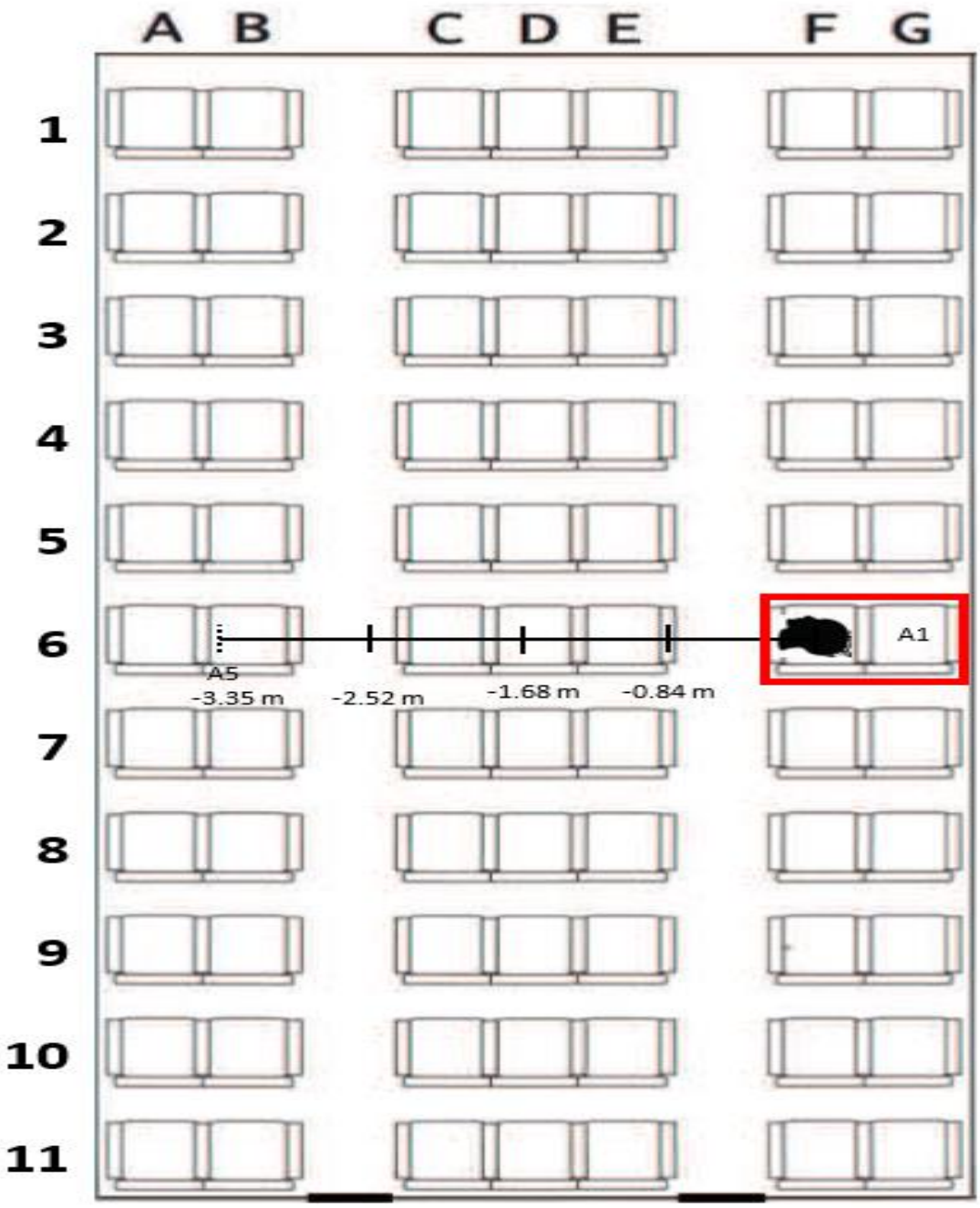

Figure I.32 Test 13 (B-M) ISOPass deployed source location and sampling tree orientation.

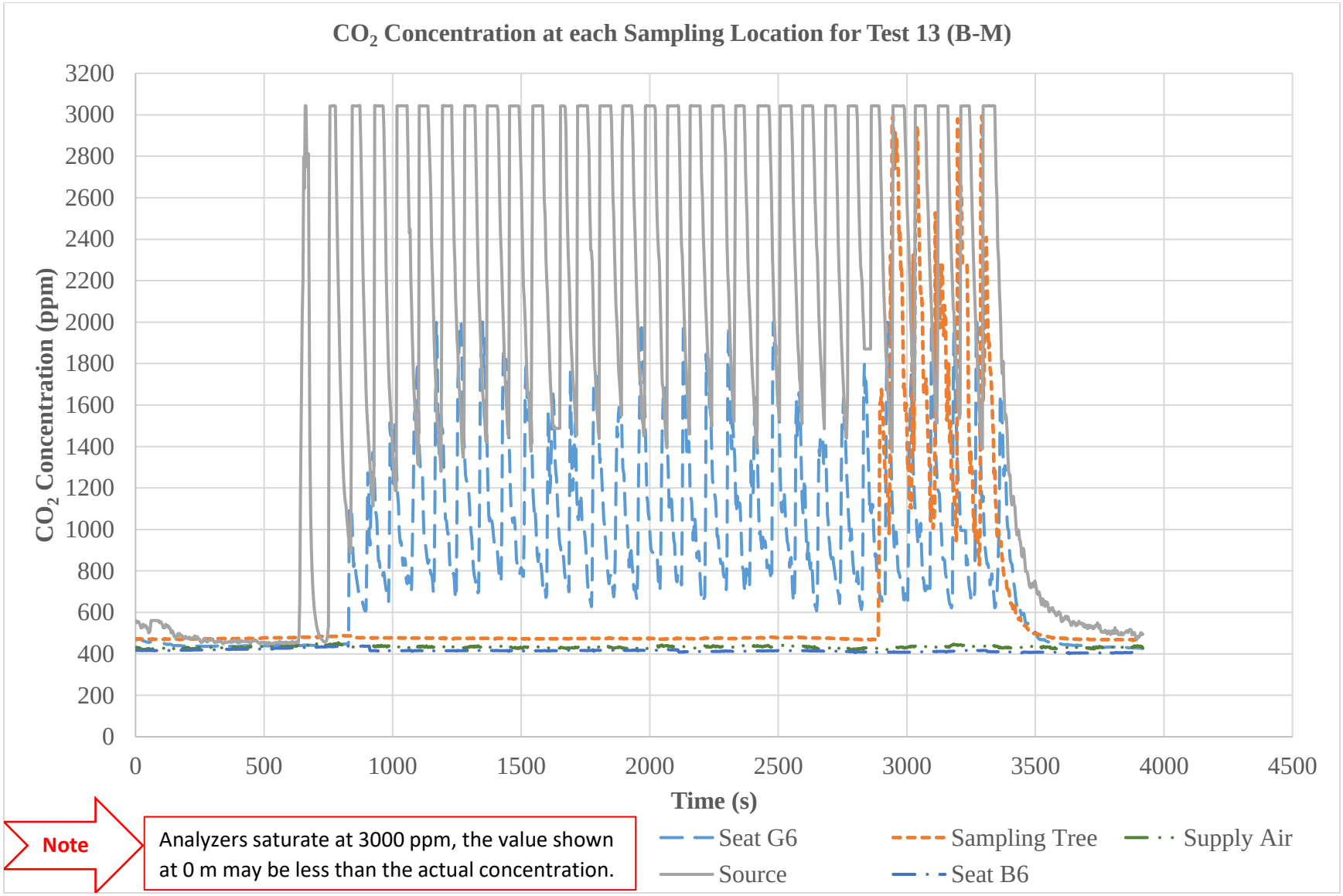

Figure I.33 Ininstantaneous CO_2 concentration at each sampling location for Test 13 (B-M) ISOPass deployed.

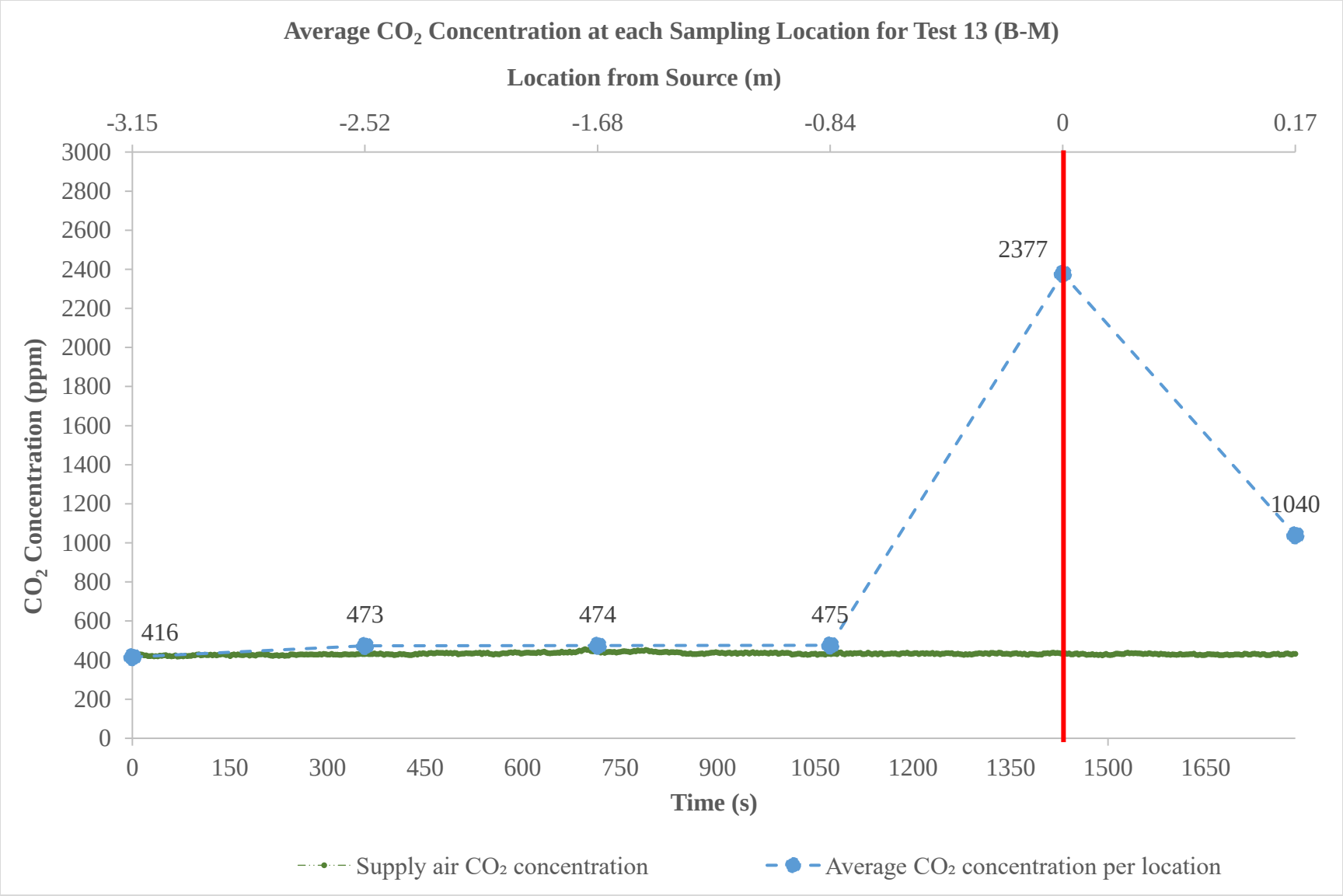

Figure I.34 Average CO_2 concentration at each sampling location for Test 13 (B-M) ISOPass deployed.

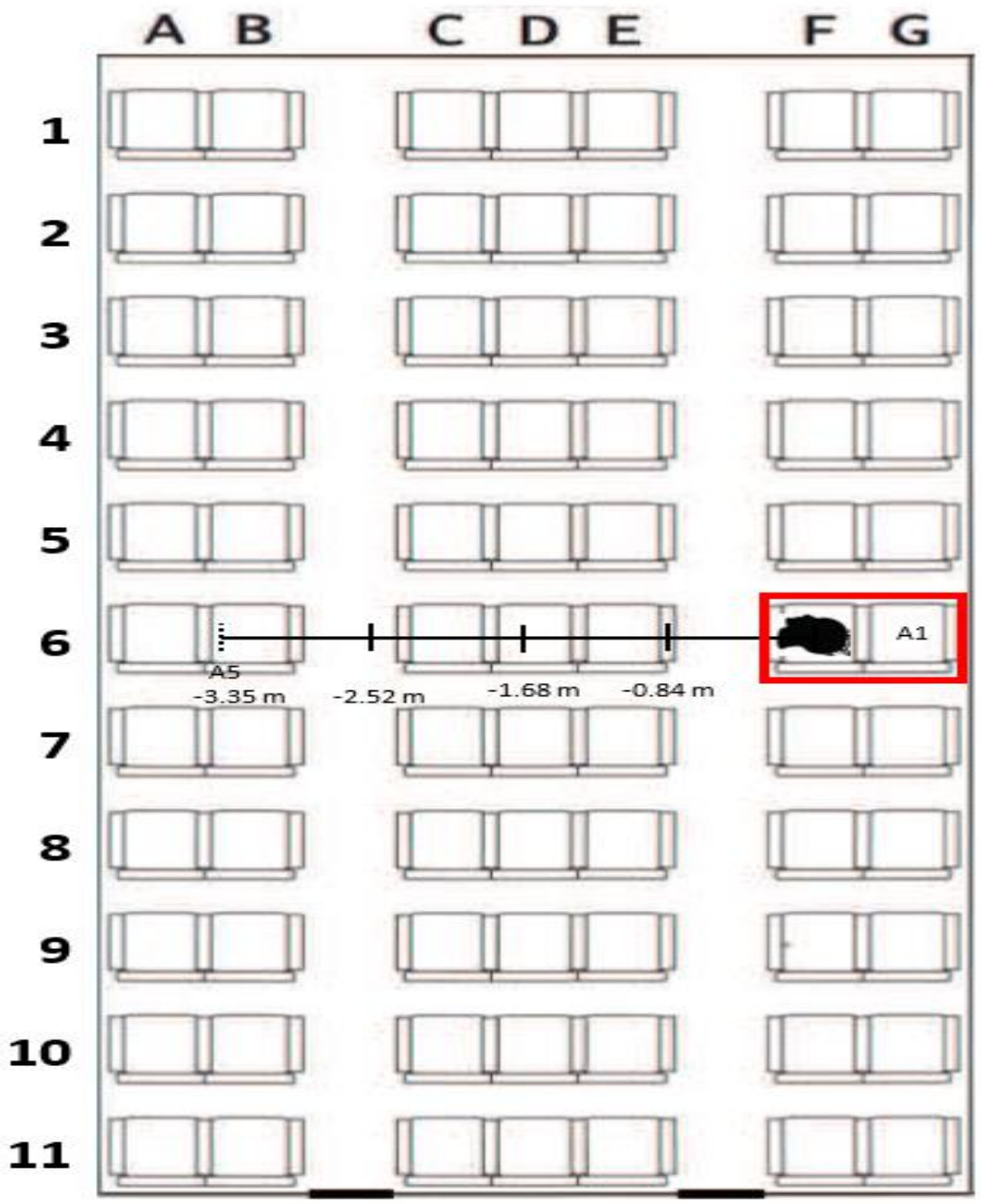

Figure I.35 Test 14 (B-M) ISOPass deployed source location and sampling tree orientation.

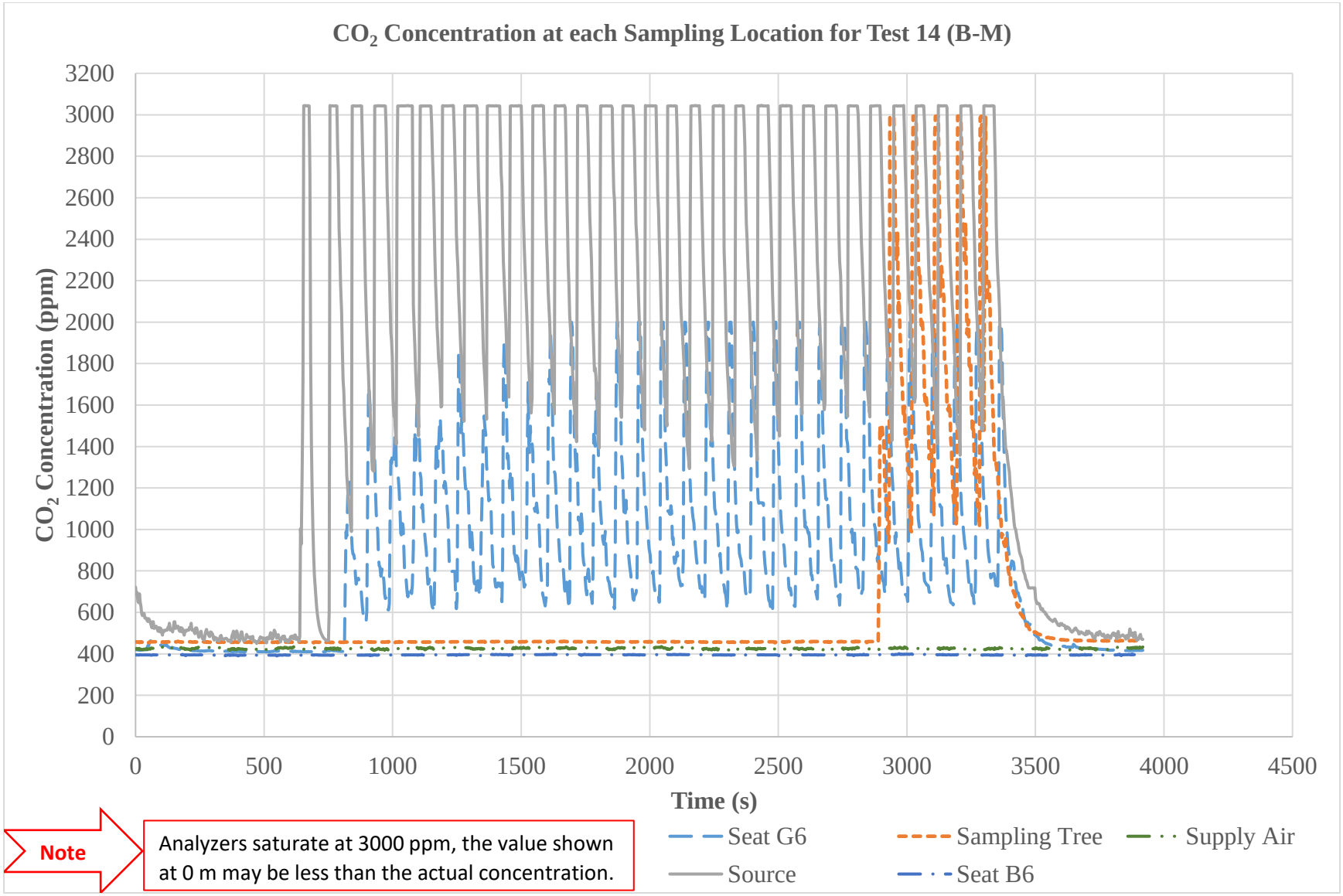

Figure I.36 Ininstantaneous CO_2 concentration at each sampling location for Test 14 (B-M) ISOPass deployed.

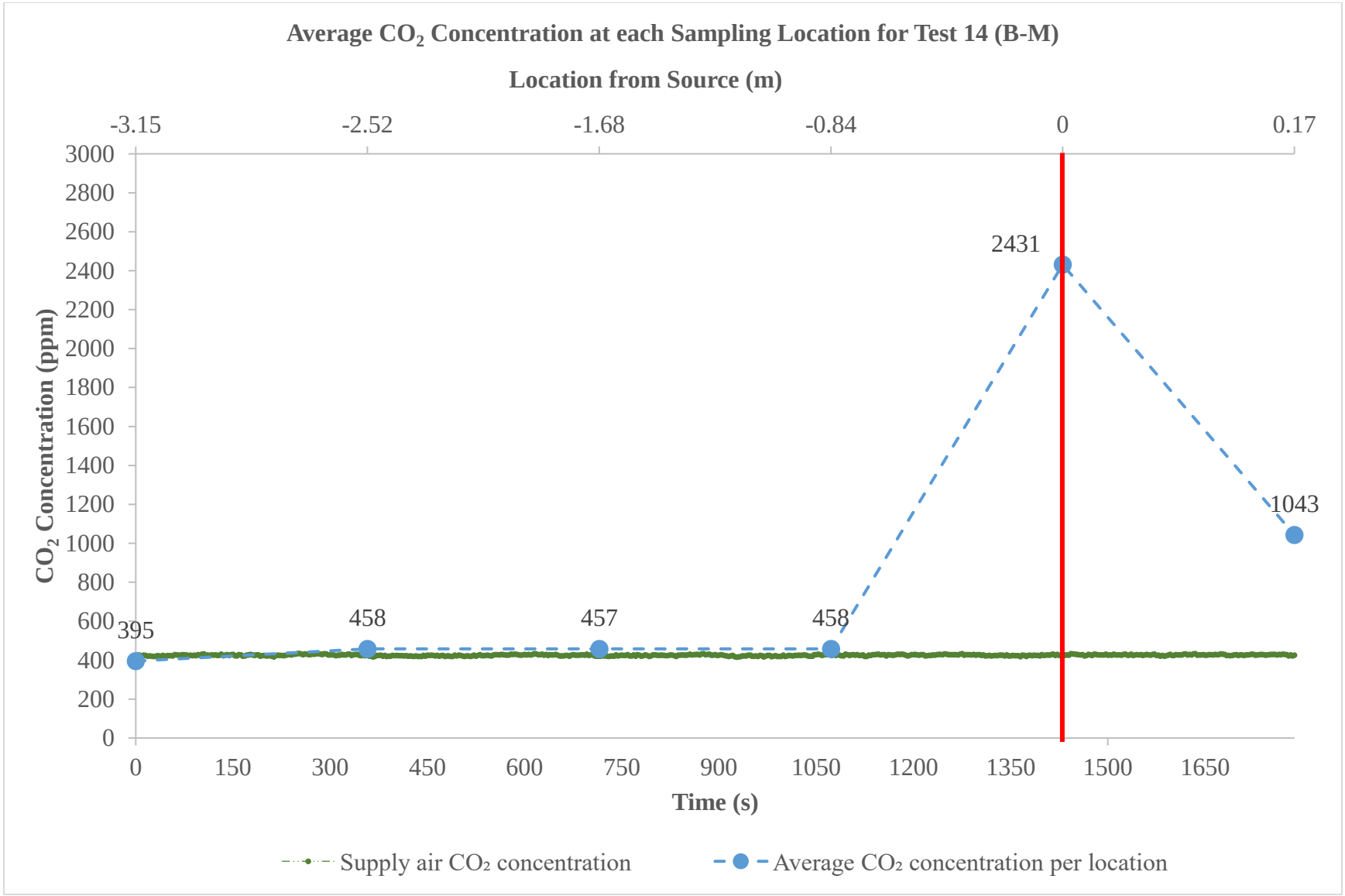

Figure I.37 Average CO_2 concentration at each sampling location for Test 14 (B-M) ISOPass deployed.

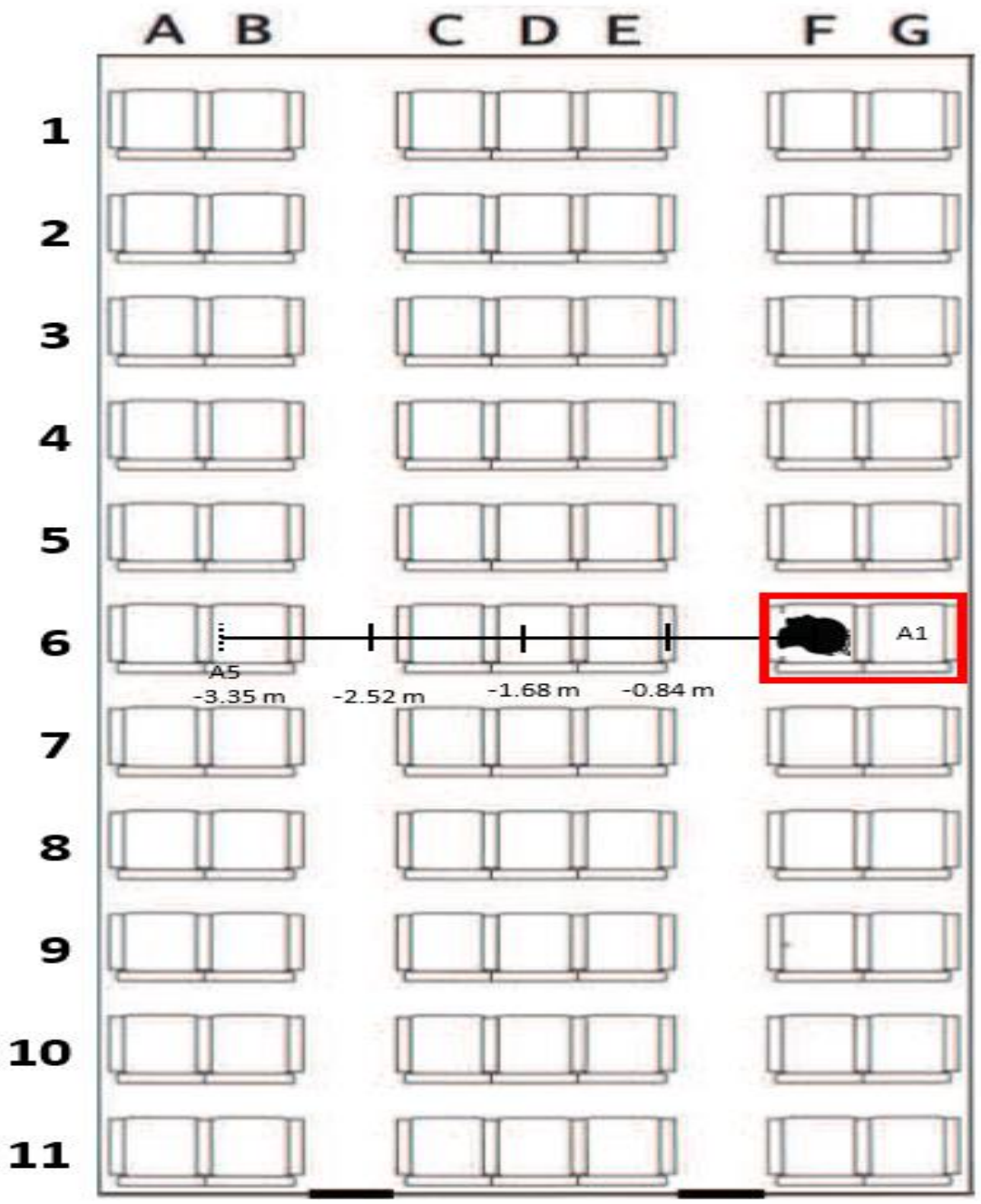

Figure I.38 Test 15 (B-M) ISOPass deployed source location and sampling tree orientation.

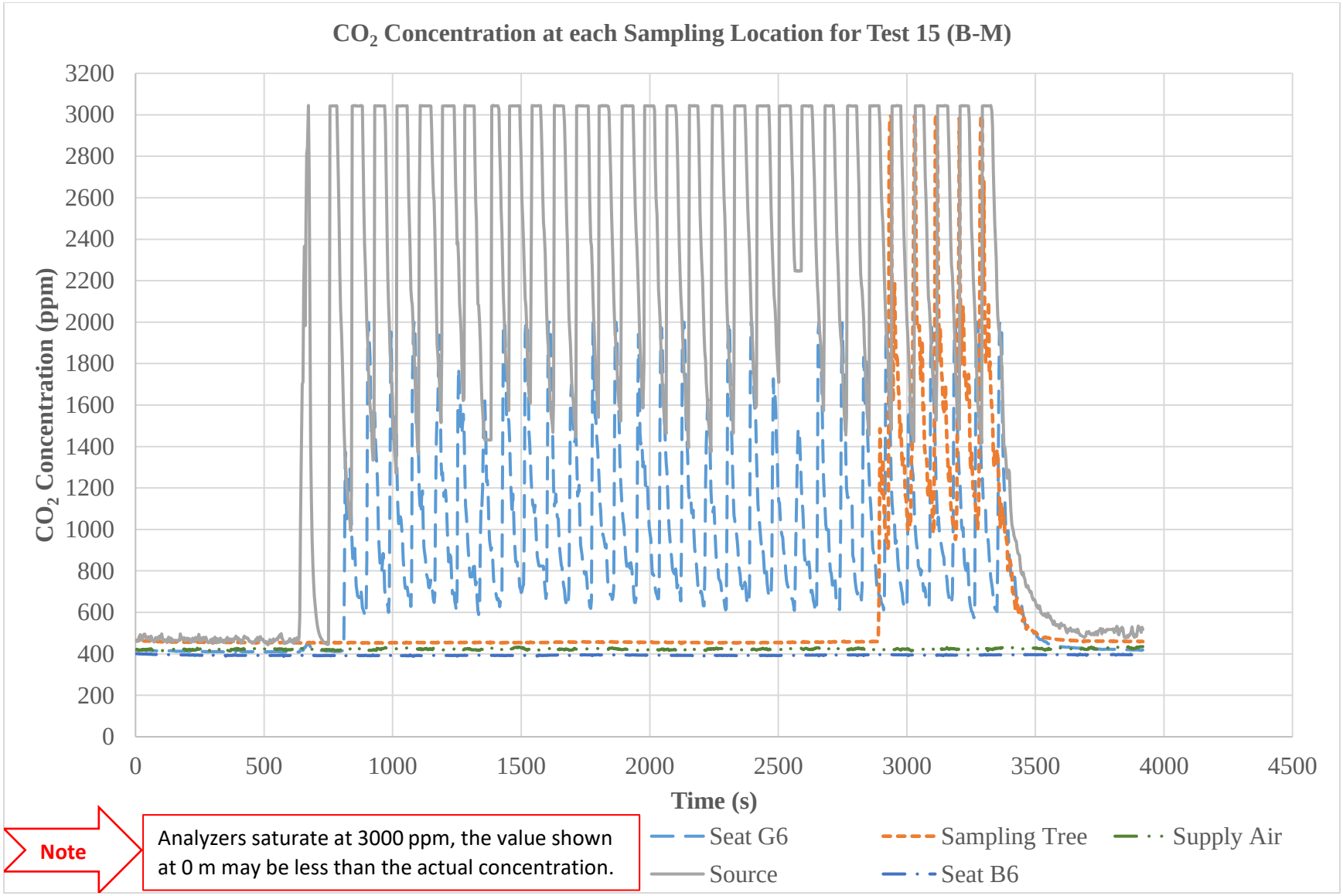

Figure I.39 Ininstantaneous CO_2 concentration at each sampling location for Test 15 (B-M) ISOPass deployed.

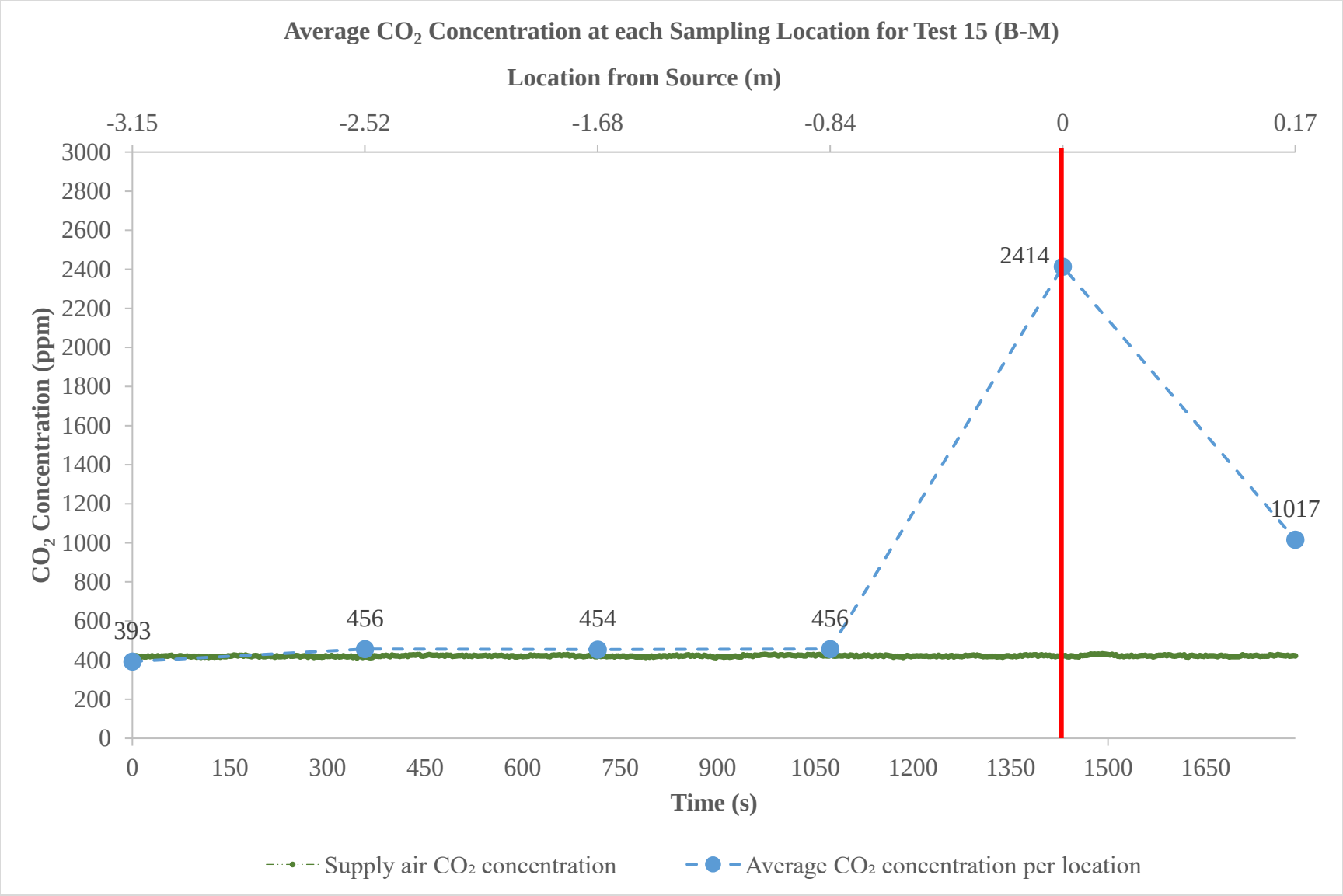

Figure I.40 Average CO_2 concentration at each sampling location for Test 15 (B-M) ISOPass deployed.

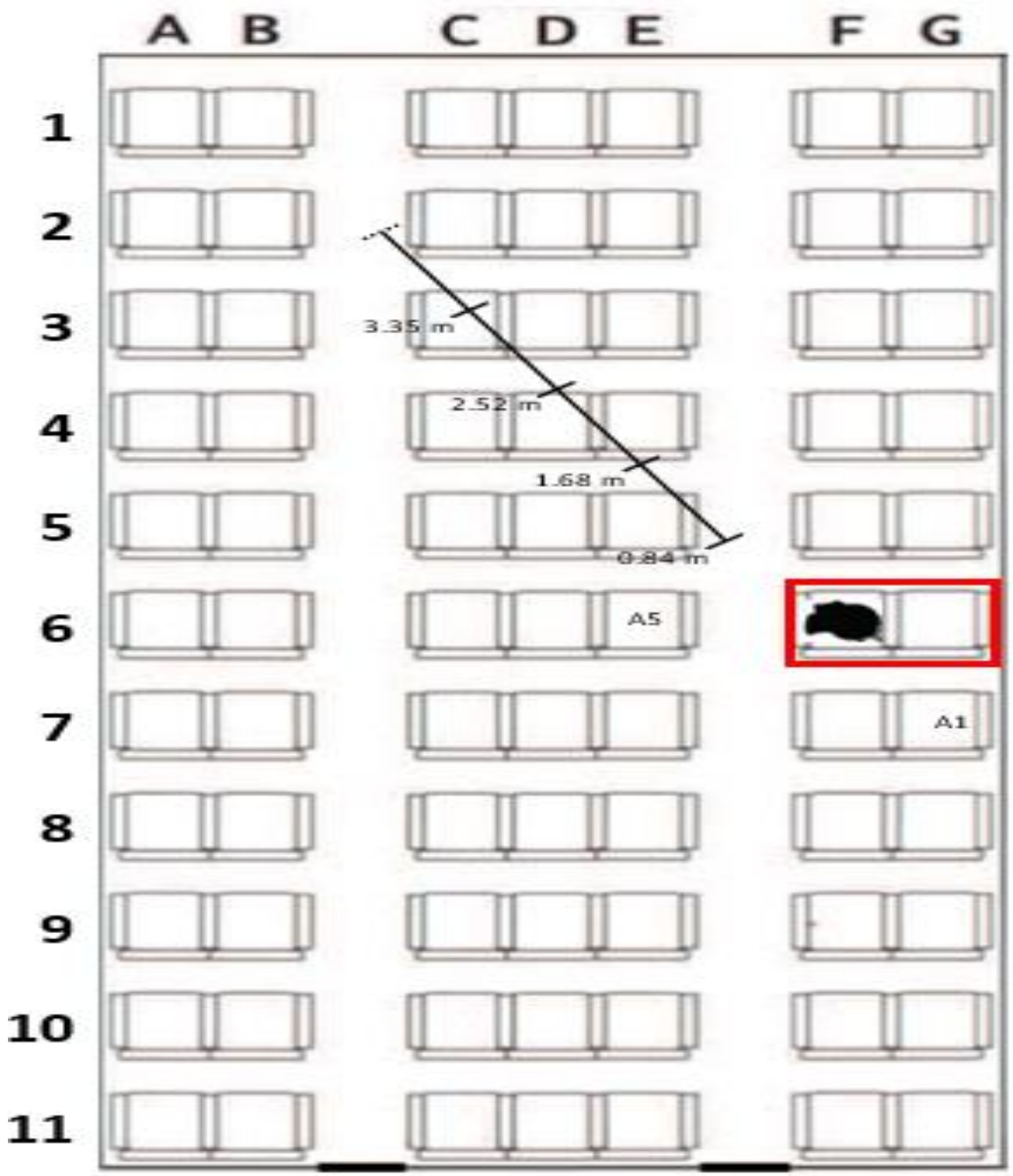

Figure I.41 Test 22 (B-M) ISOPass deployed source location and sampling tree orientation.

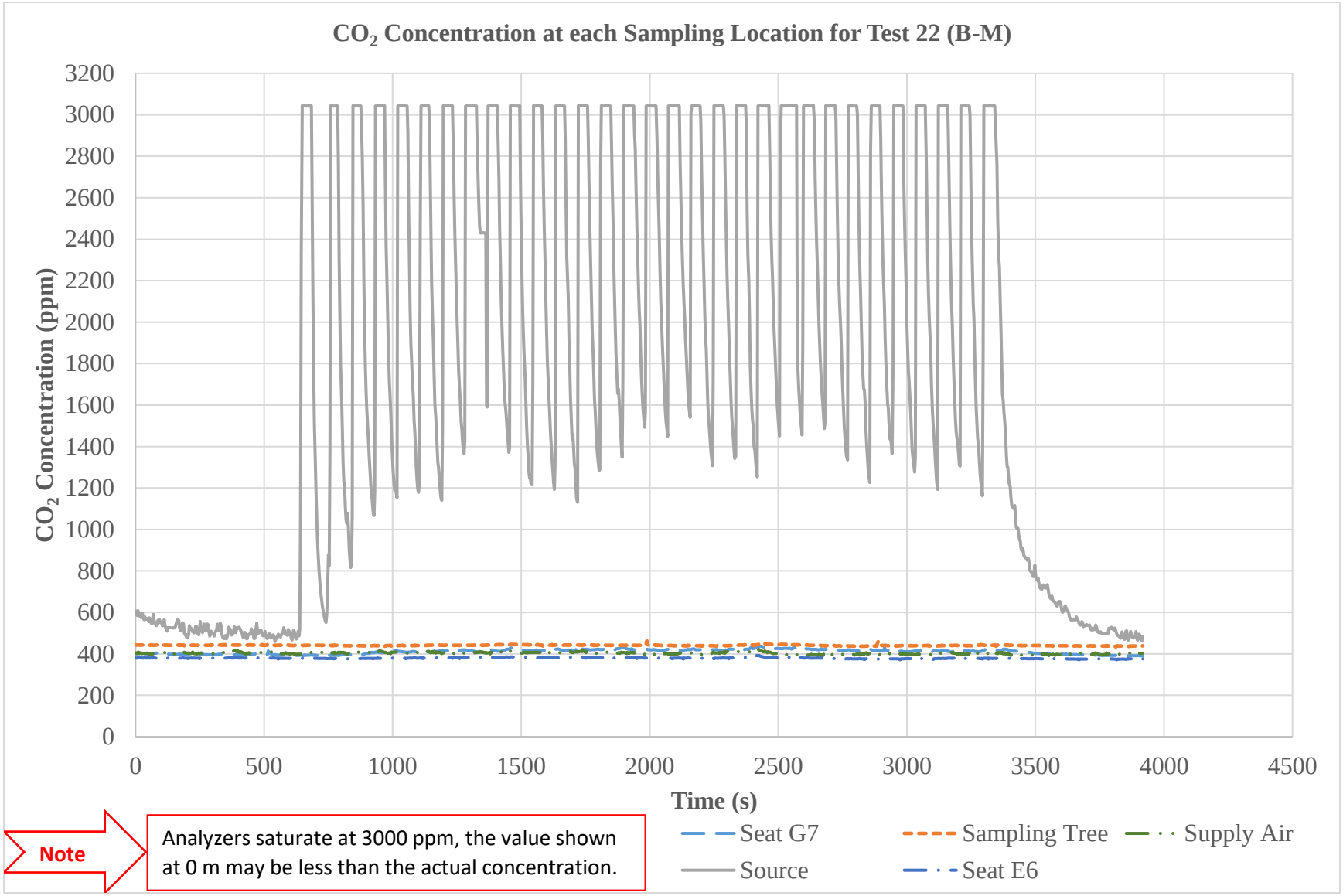

Figure I.42 Ininstantaneous CO_2 concentration at each sampling location for Test 22 (B-M) ISOPass deployed.

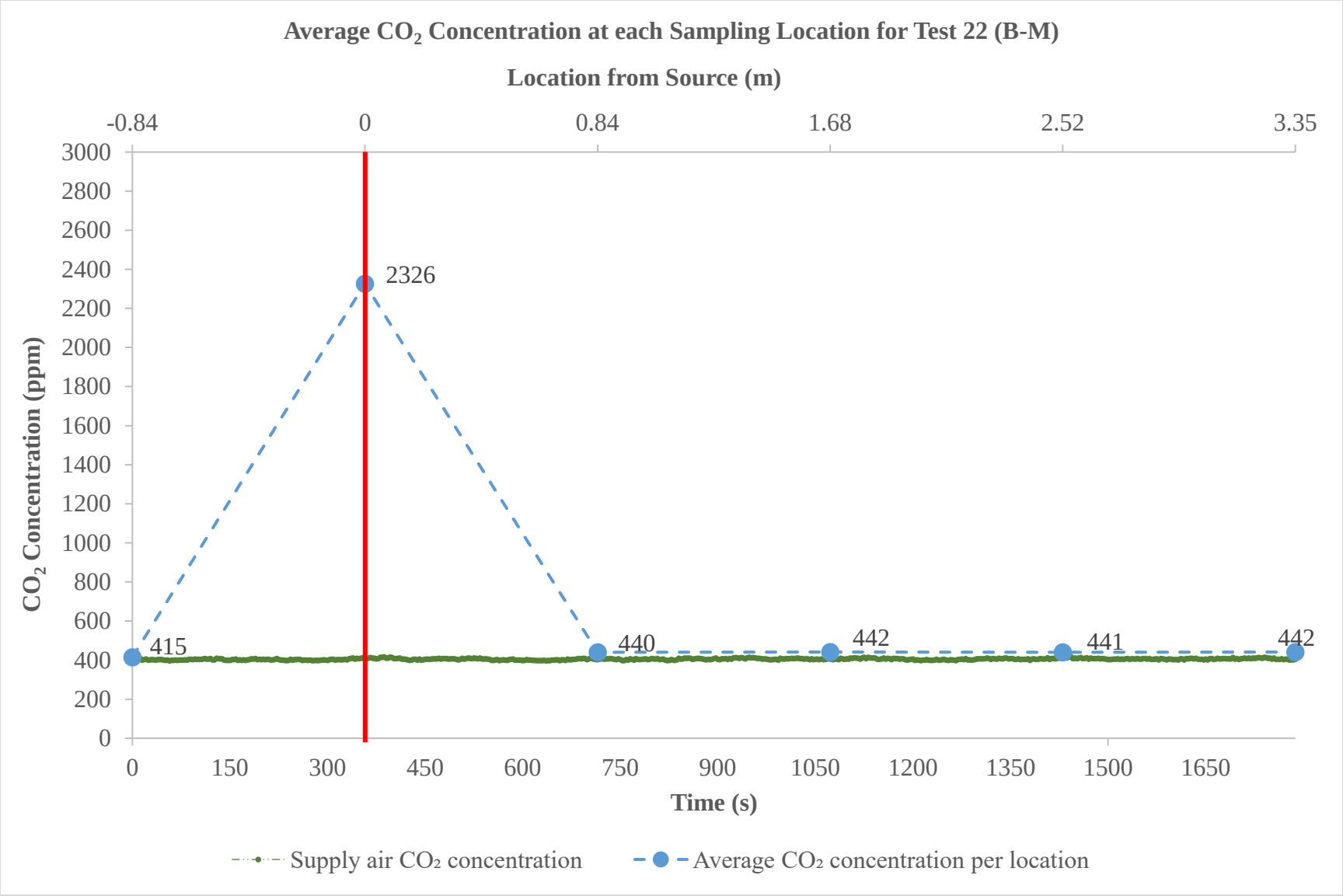

Figure I.43 Average CO_2 concentration at each sampling location for Test 22 (B-M) ISOPass deployed.

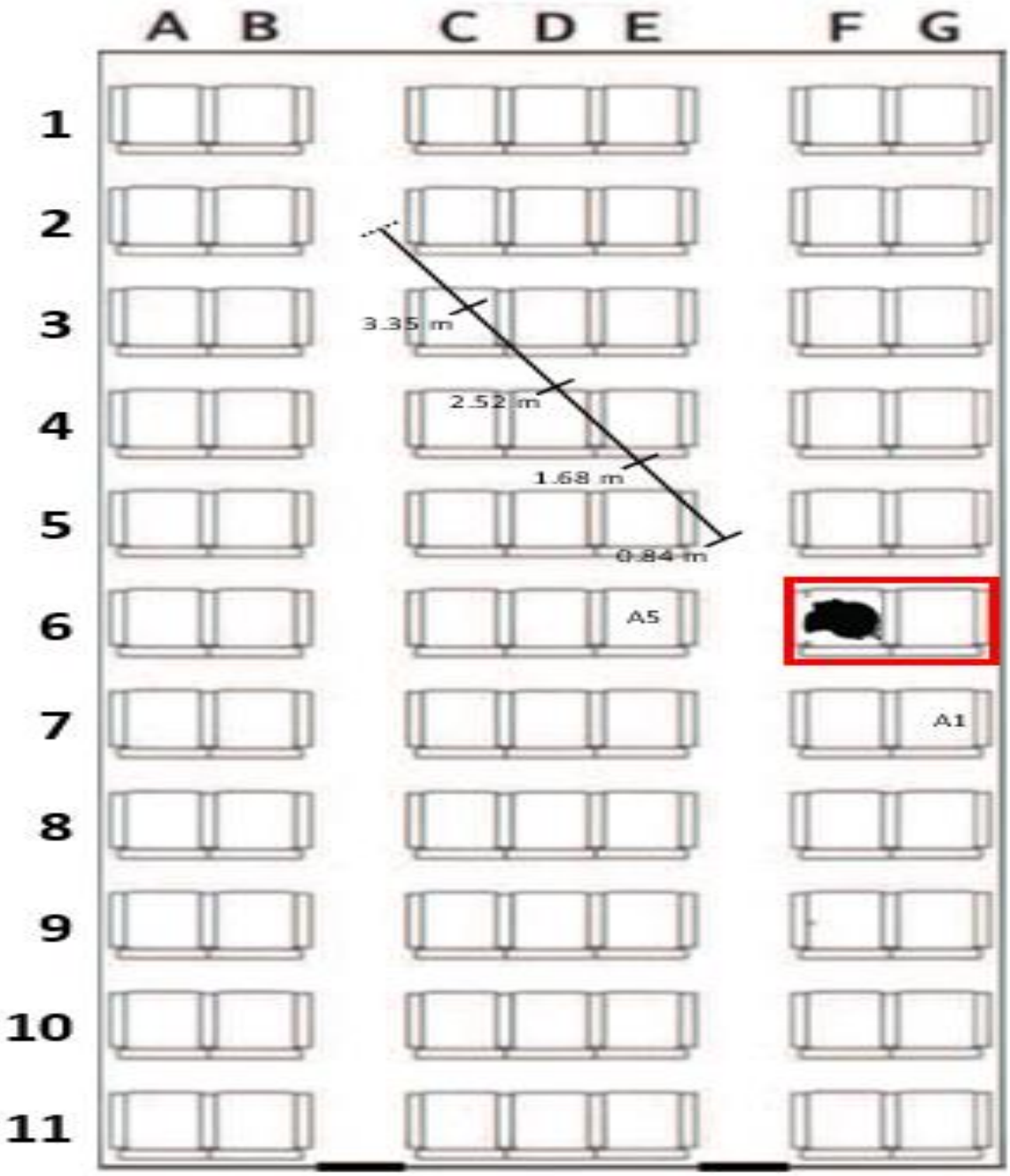

Figure I.44 Test 23 (B-M) ISOPass deployed source location and sampling tree orientation.

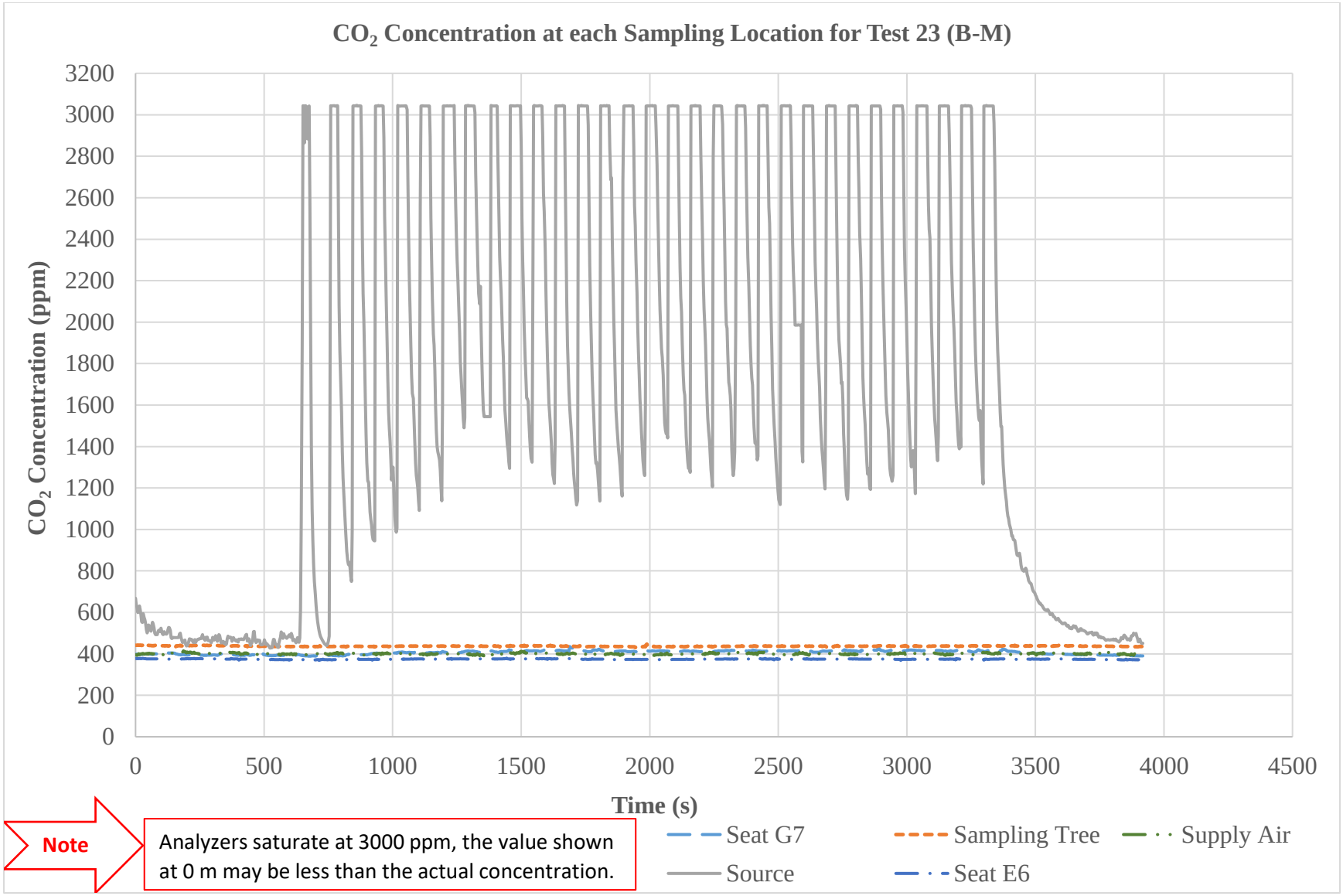

Figure I.45 Ininstantaneous CO_2 concentration at each sampling location for Test 23 (B-M) ISOPass deployed.

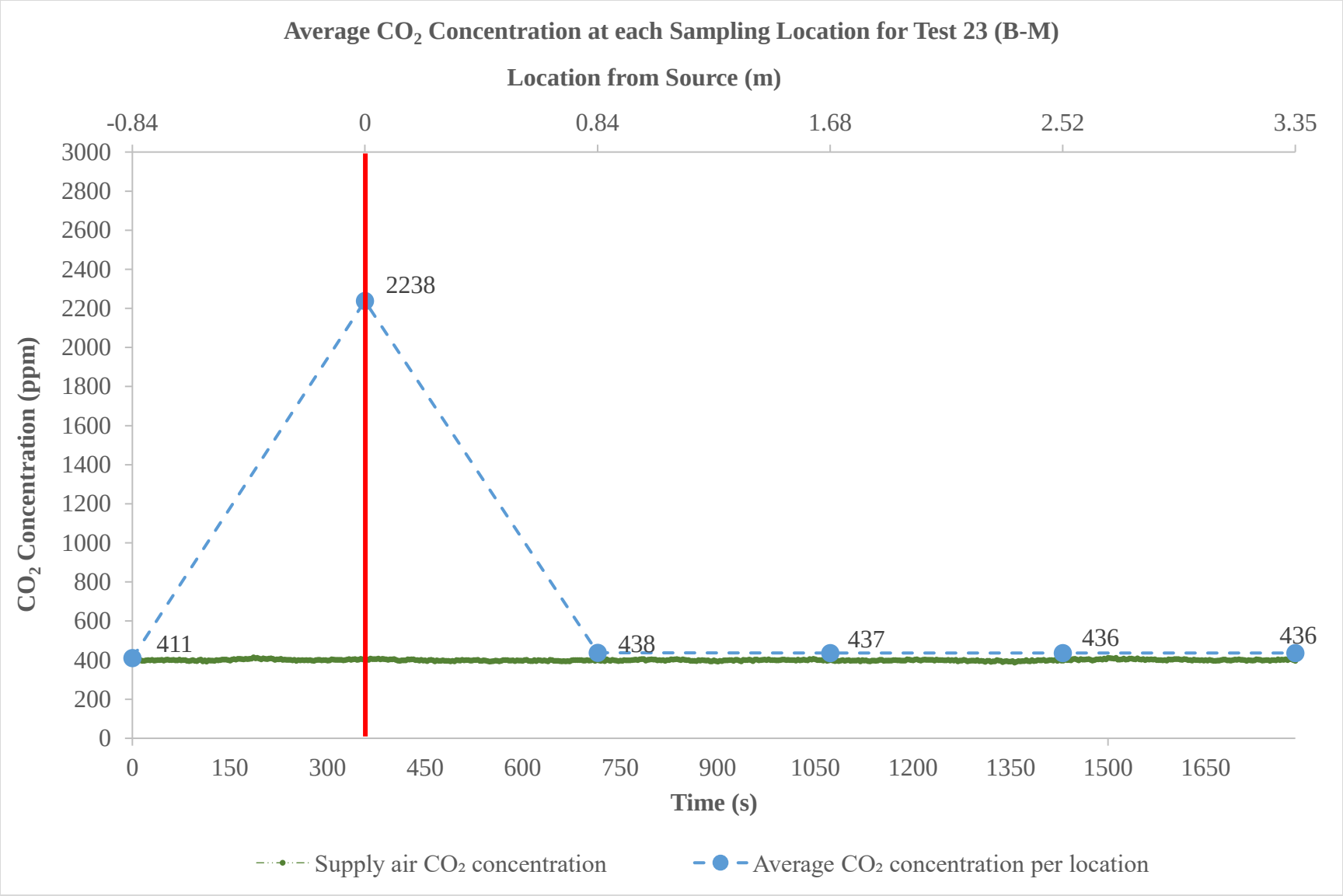

Figure I.46 Average CO_2 concentration at each sampling location for Test 23 (B-M) ISOPass deployed.

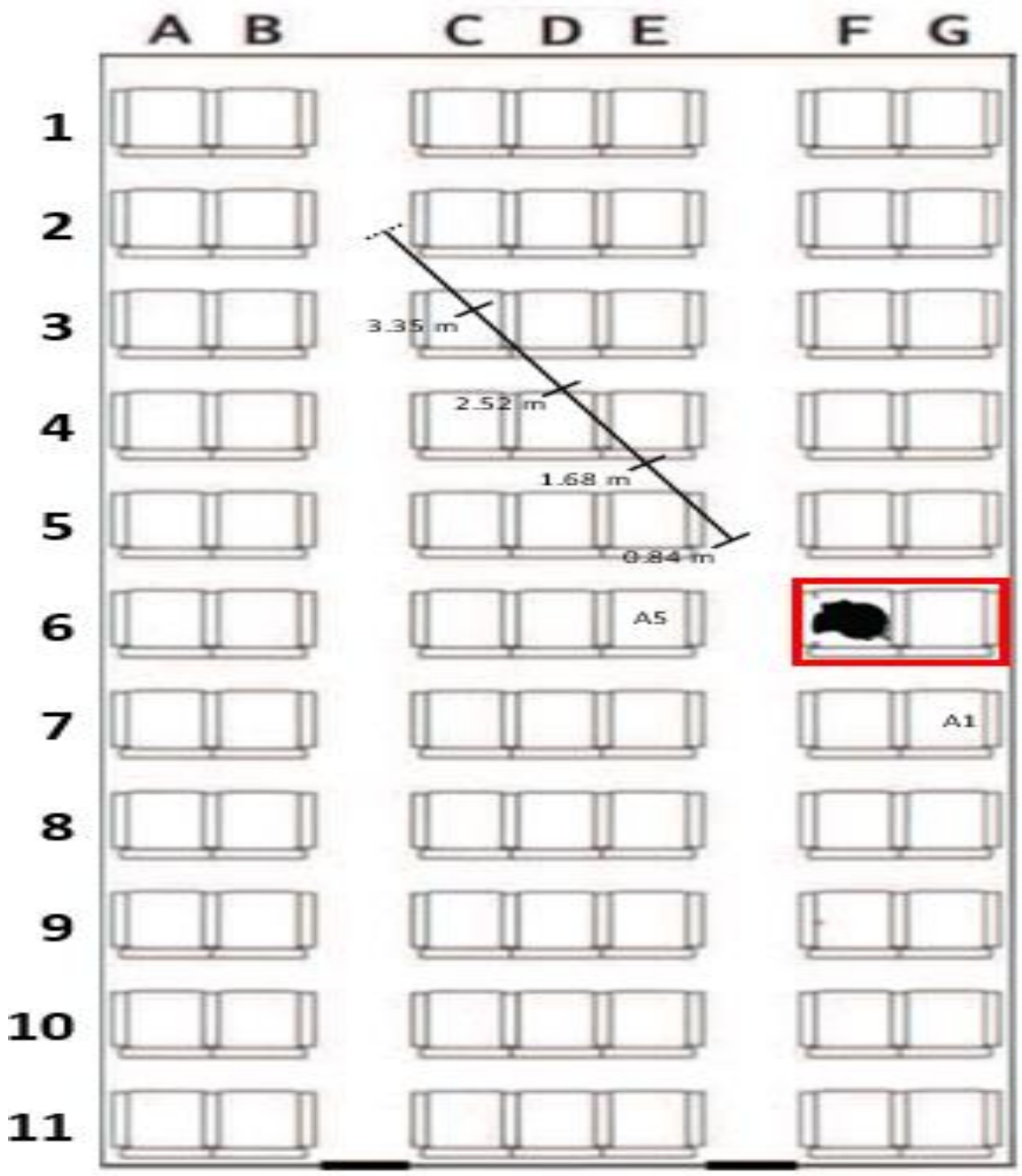

Figure I.47 Test 24 (B-M) ISOPass deployed source location and sampling tree orientation.

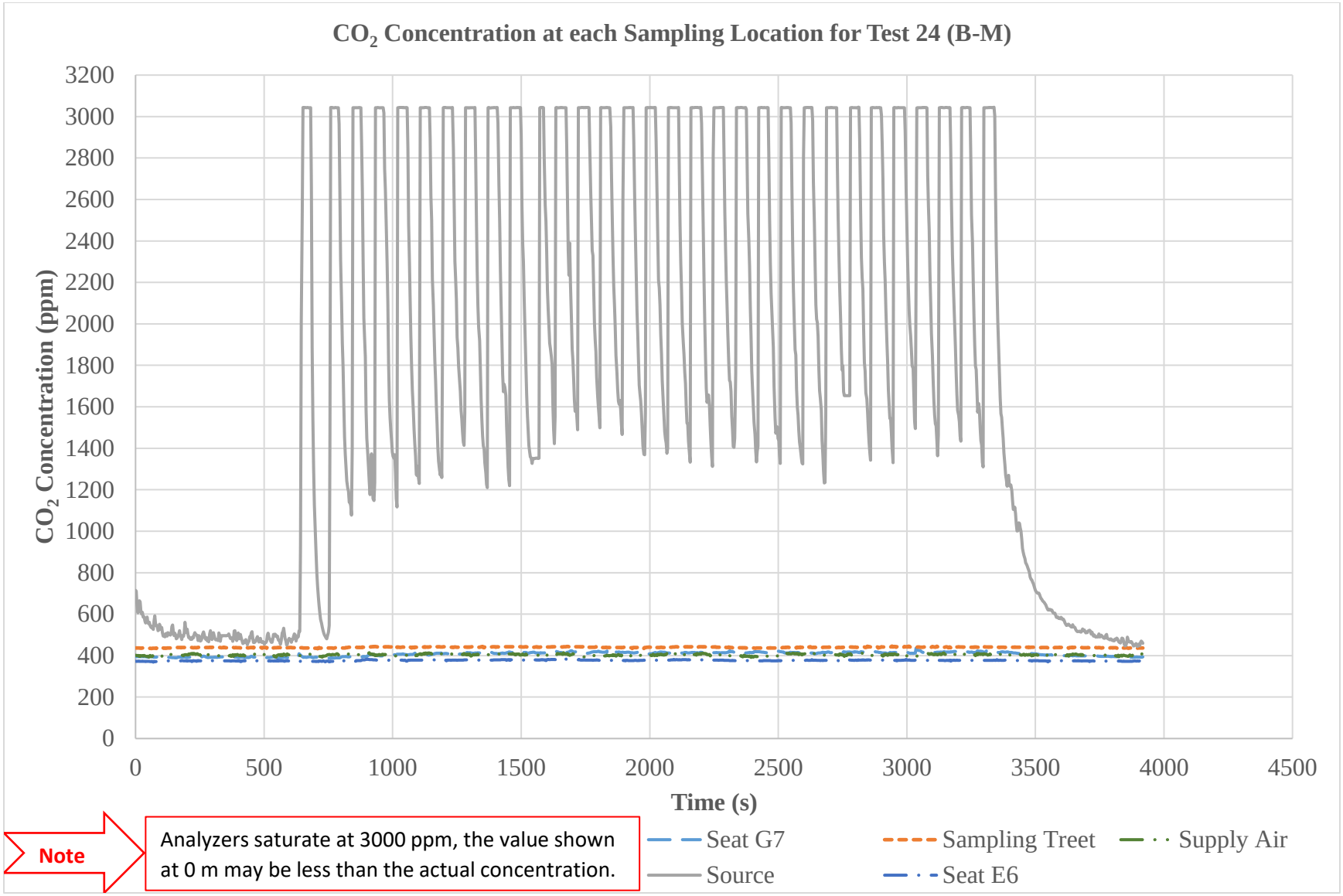

Figure I.48 Ininstantaneous CO_2 concentration at each sampling location for Test 24 (B-M) ISOPass deployed.

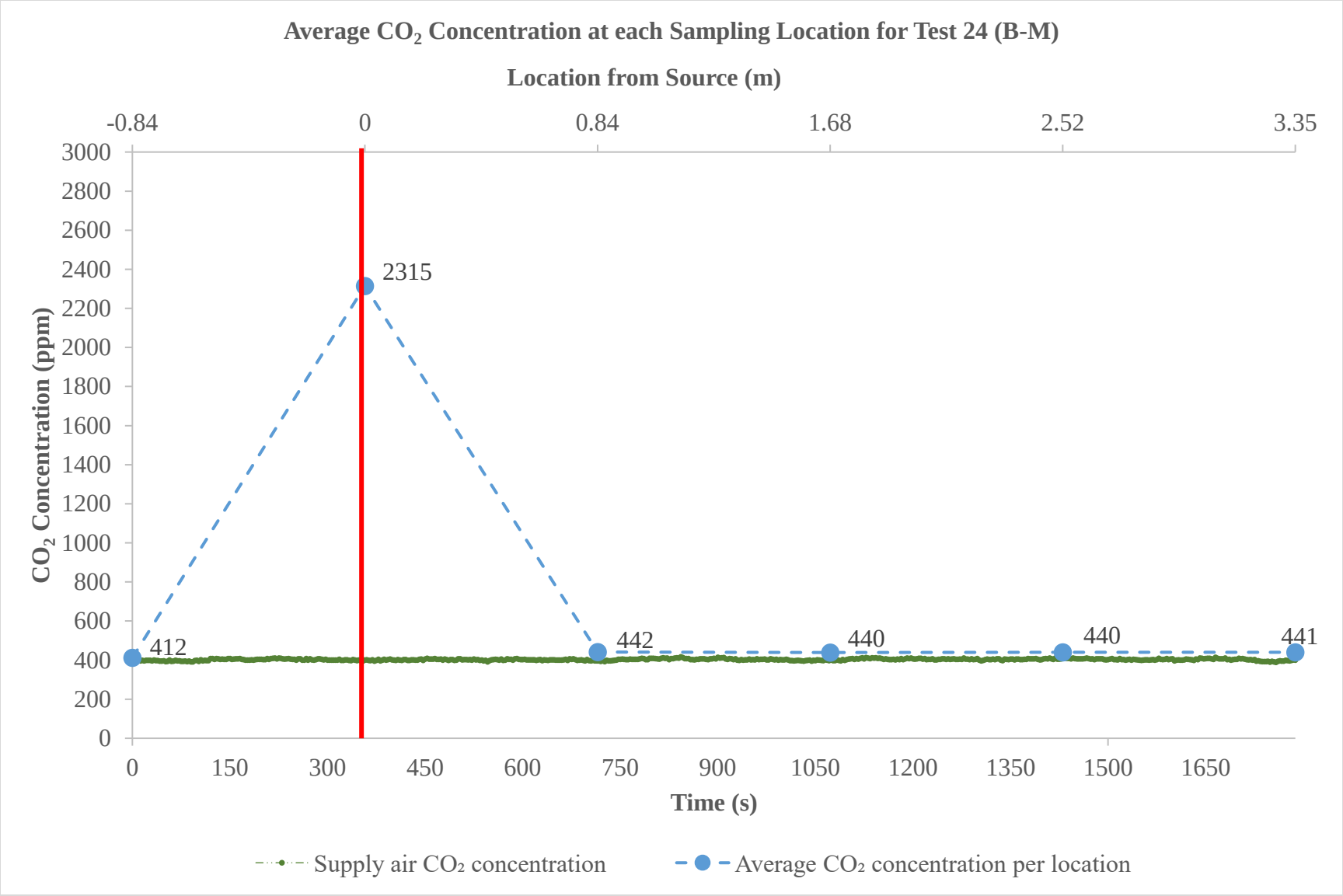

Figure I.49 Average CO_2 concentration at each sampling location for Test 24 (B-M) ISOPass deployed.

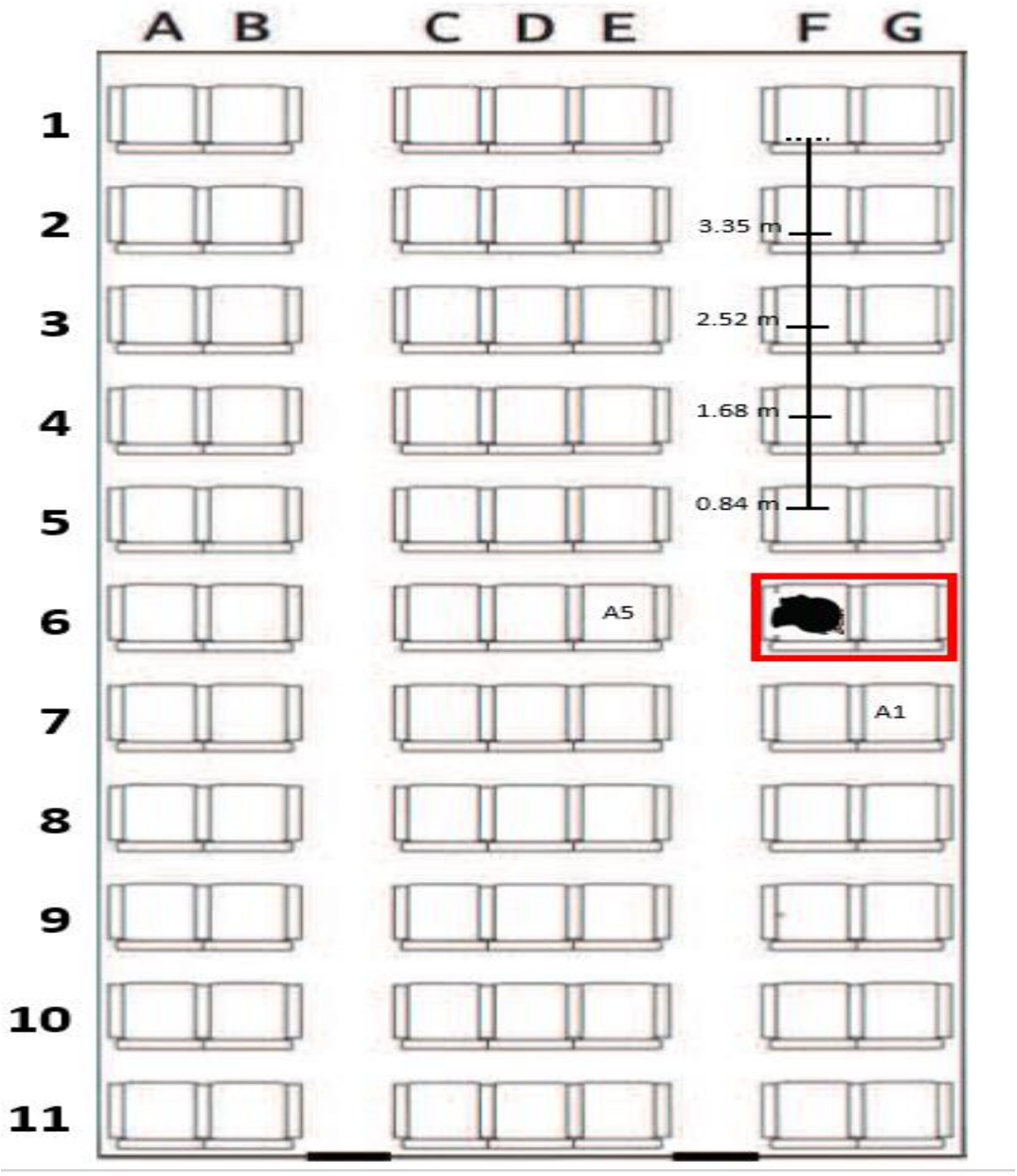

Figure I.50 Test 25 (B-M) ISOPass deployed source location and sampling tree orientation.

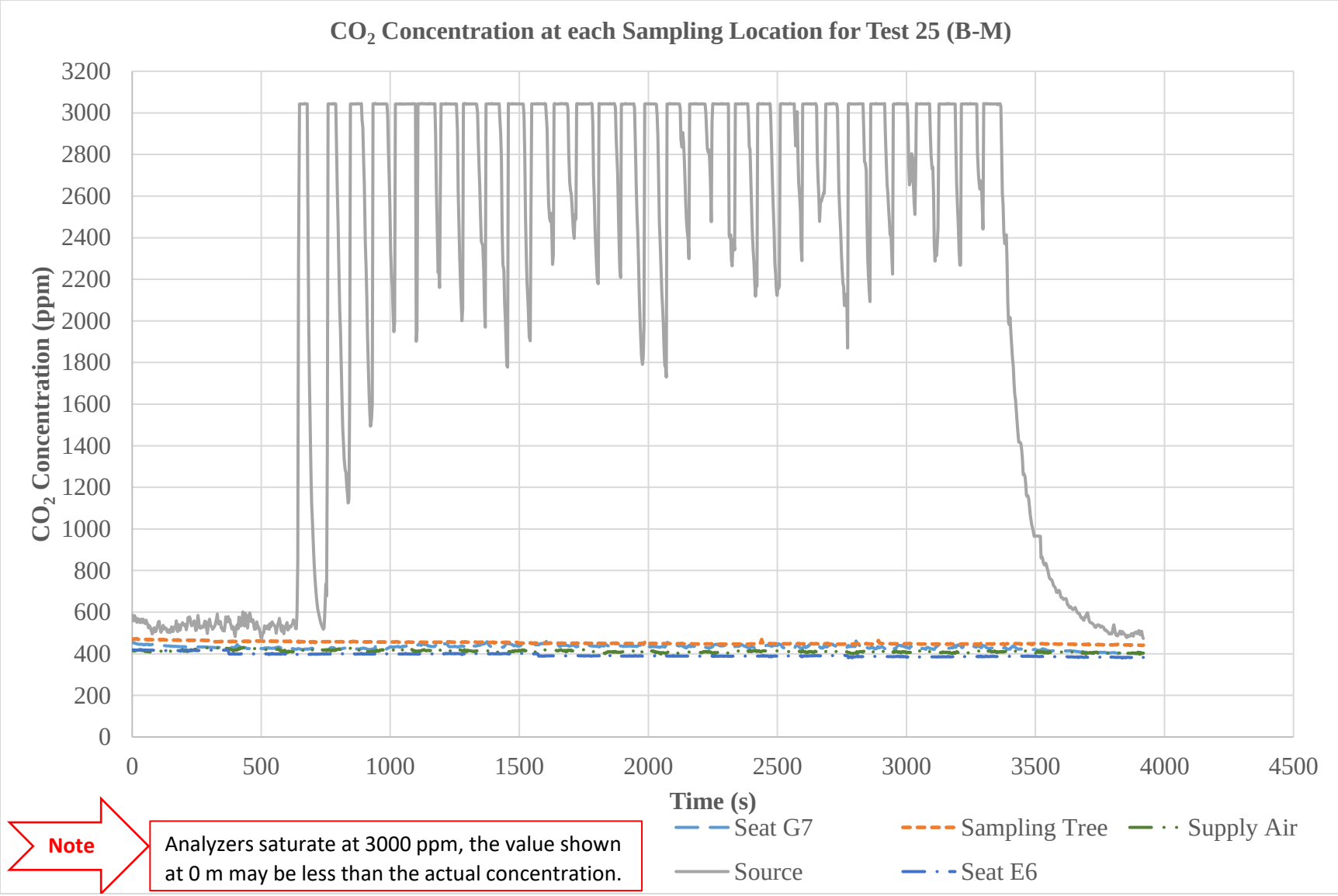

Figure I.51 Ininstantaneous CO_2 concentration at each sampling location for Test 25 (B-M) ISOPass deployed.

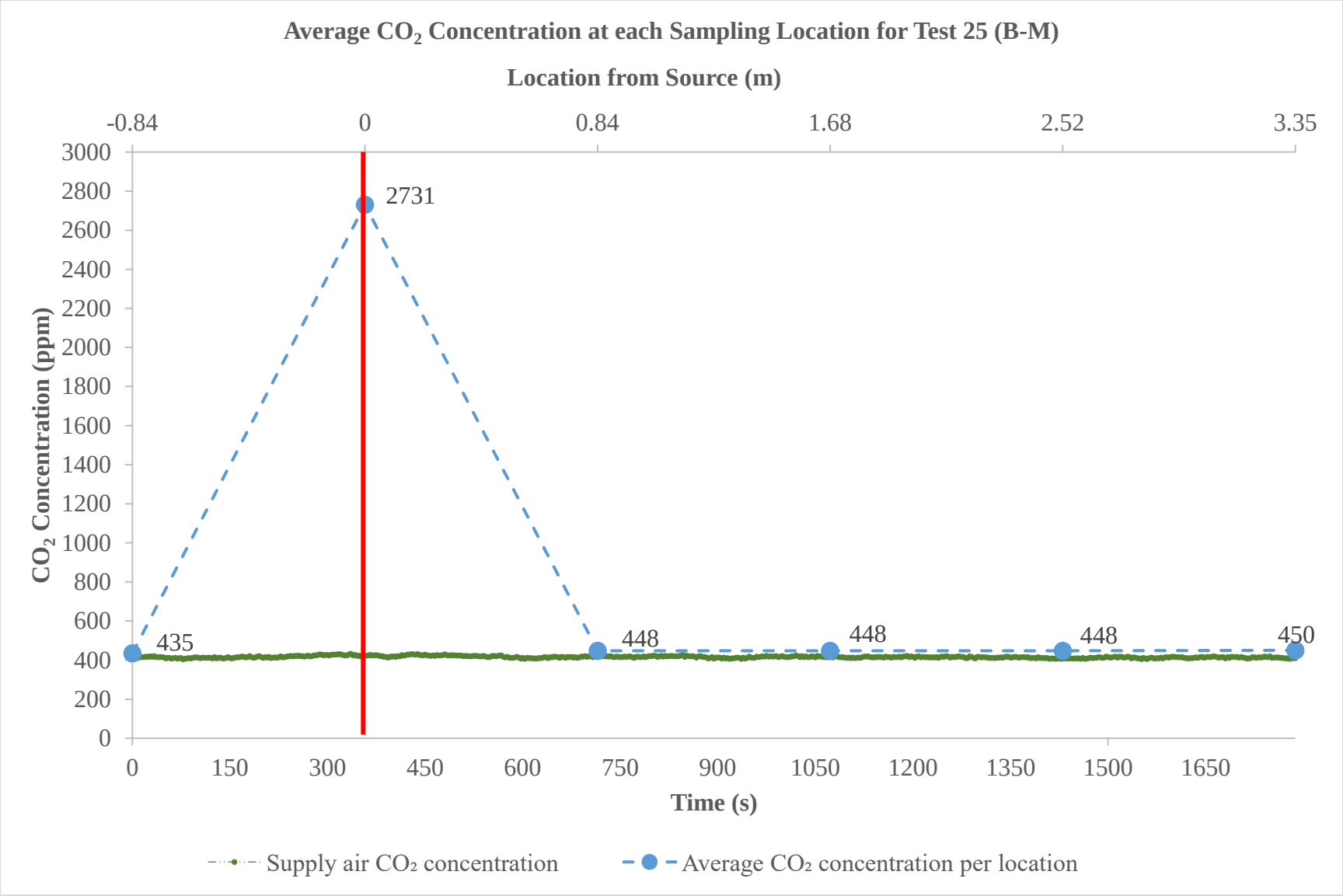

Figure I.52 Average CO_2 concentration at each sampling location for Test 25 (B-M) ISOPass deployed.

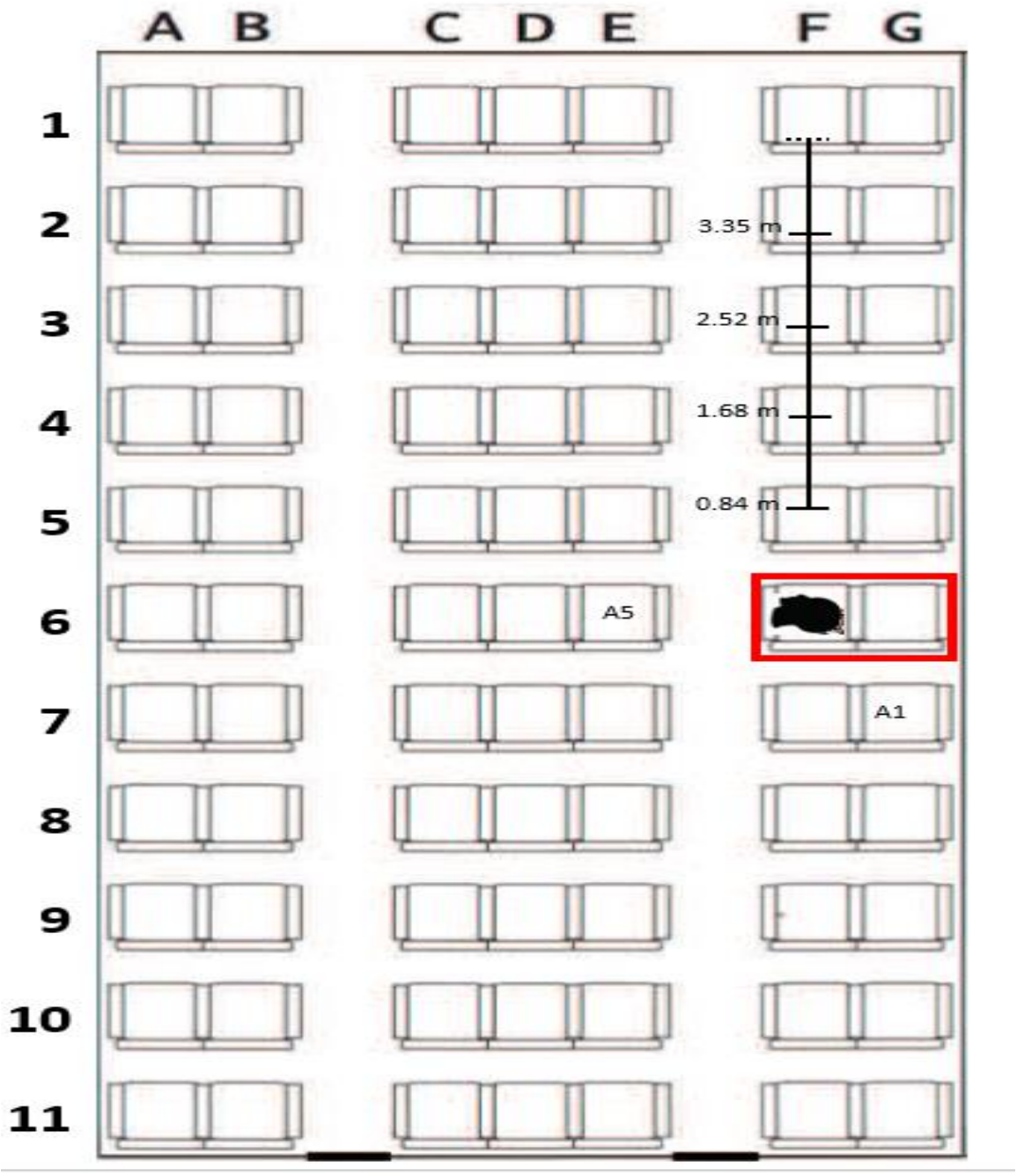

Figure I.53 Test 26 (B-M) ISOPass deployed source location and sampling tree orientation.

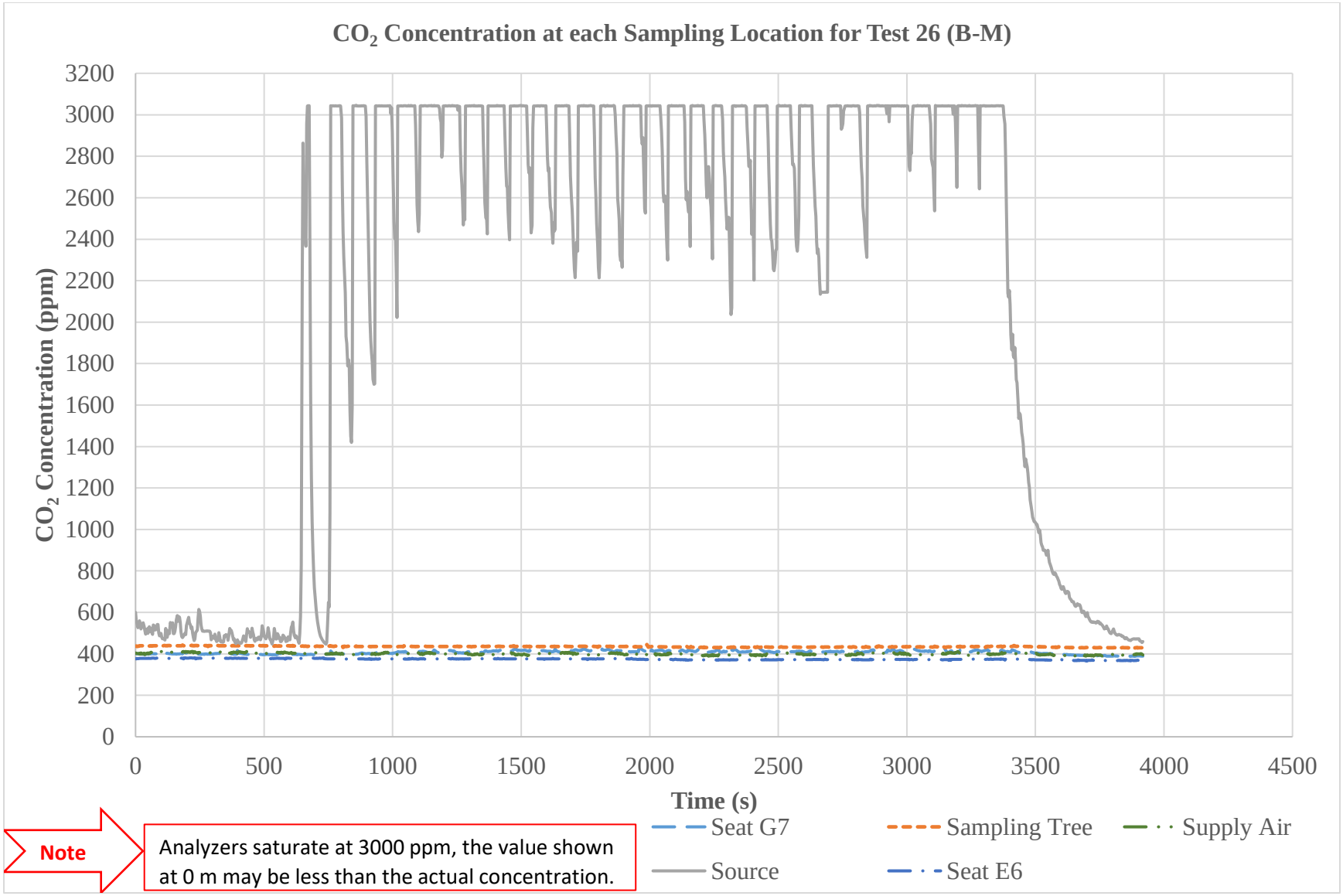

Figure I.54 Ininstantaneous CO_2 concentration at each sampling location for Test 26 (B-M) ISOPass deployed.

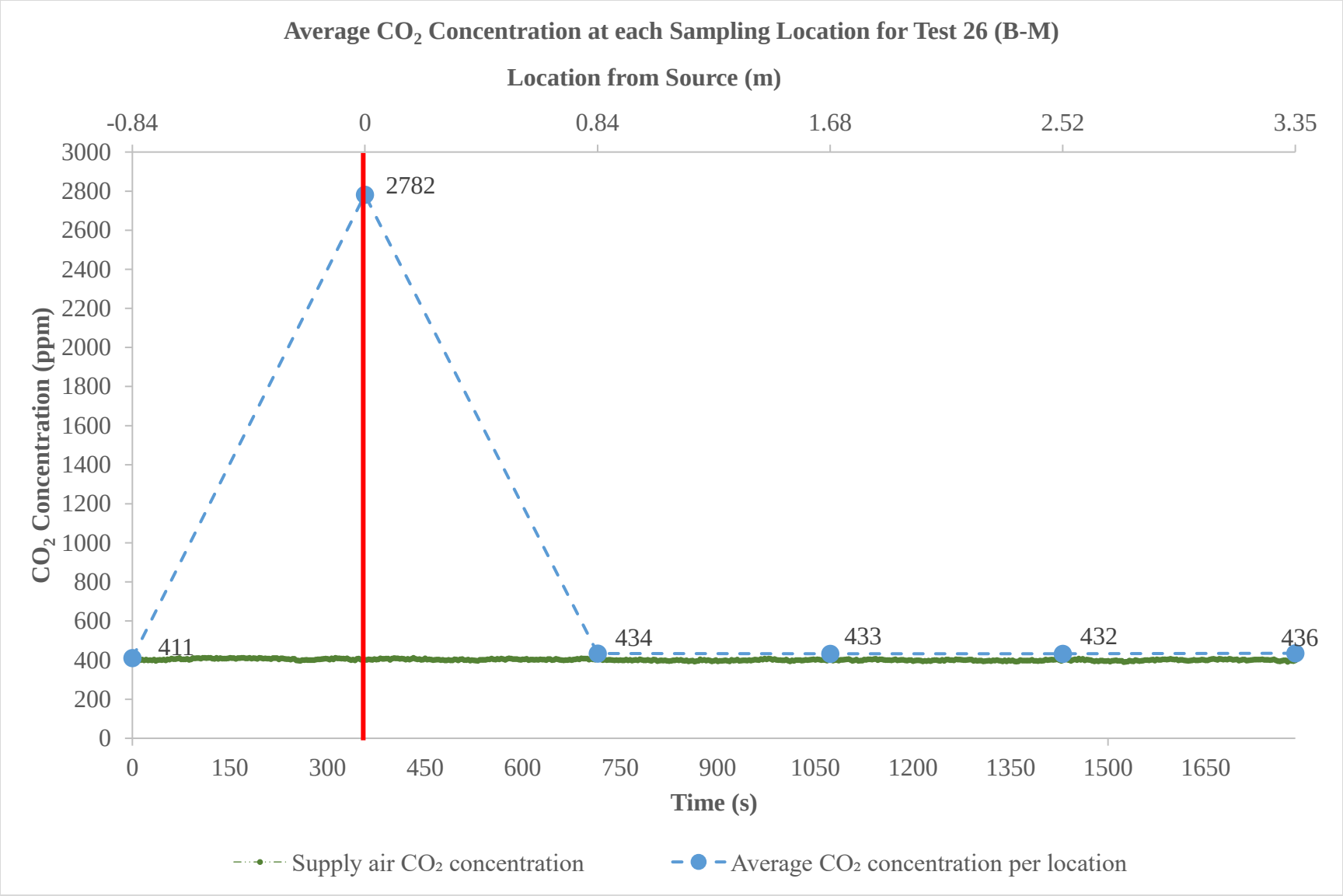

Figure I.55 Average CO_2 concentration at each sampling location for Test 26 (B-M) ISOPass deployed.

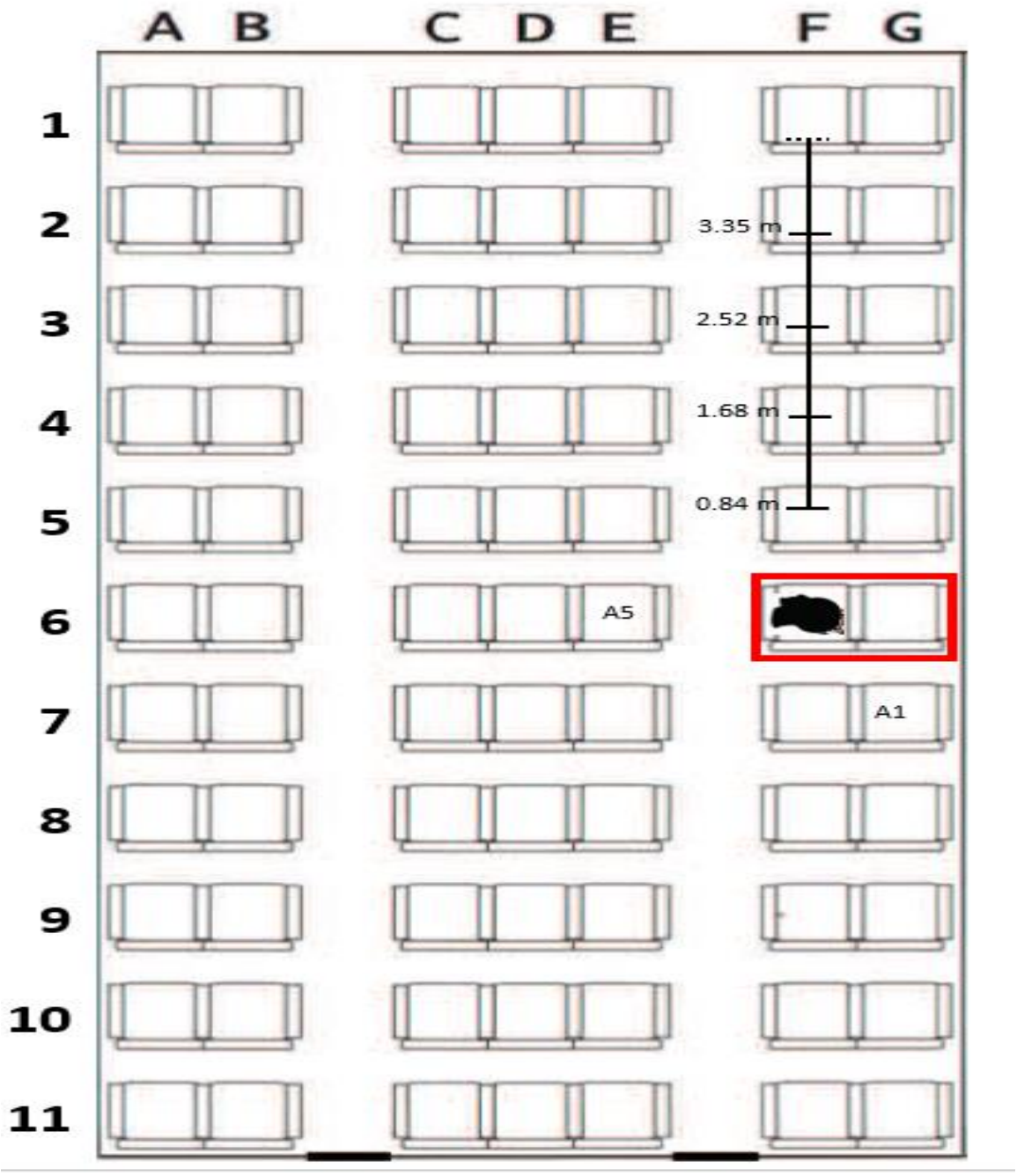

Figure I.56 Test 27 (B-M) ISOPass deployed source location and sampling tree orientation.

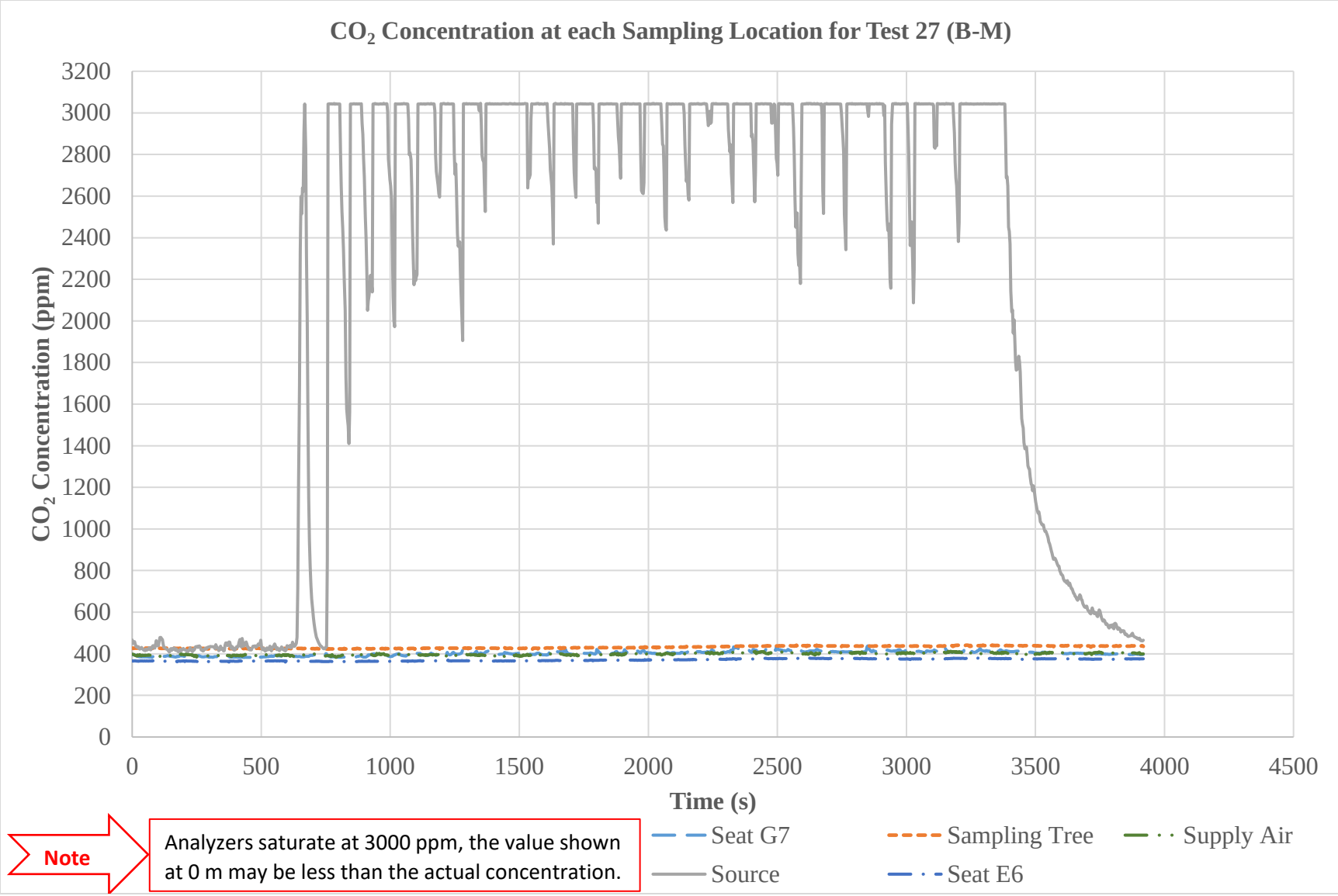

Figure I.57 Ininstantaneous CO_2 concentration at each sampling location for Test 27 (B-M) ISOPass deployed.

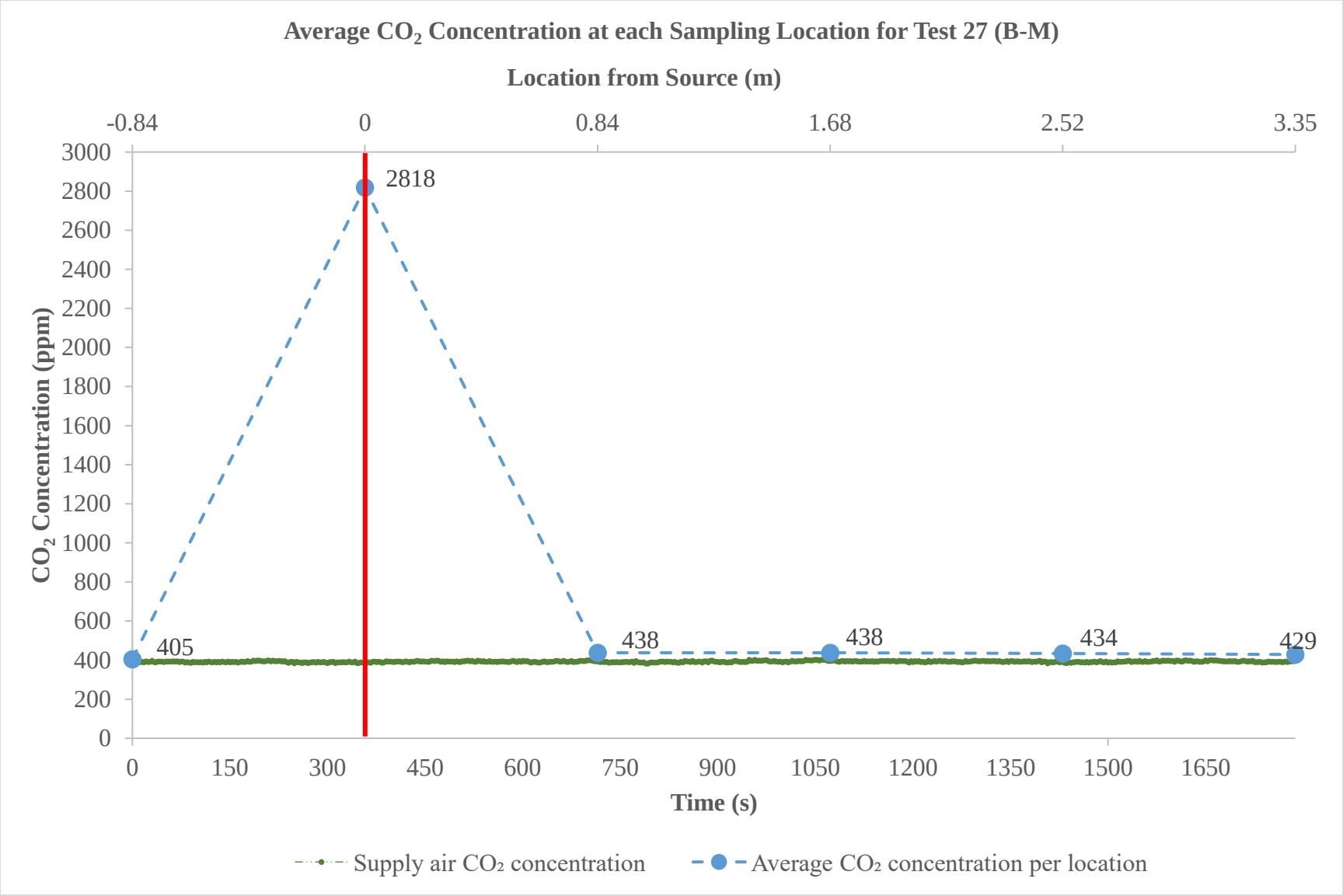

Figure I.58 Average CO_2 concentration at each sampling location for Test 27 (B-M) ISOPass deployed.

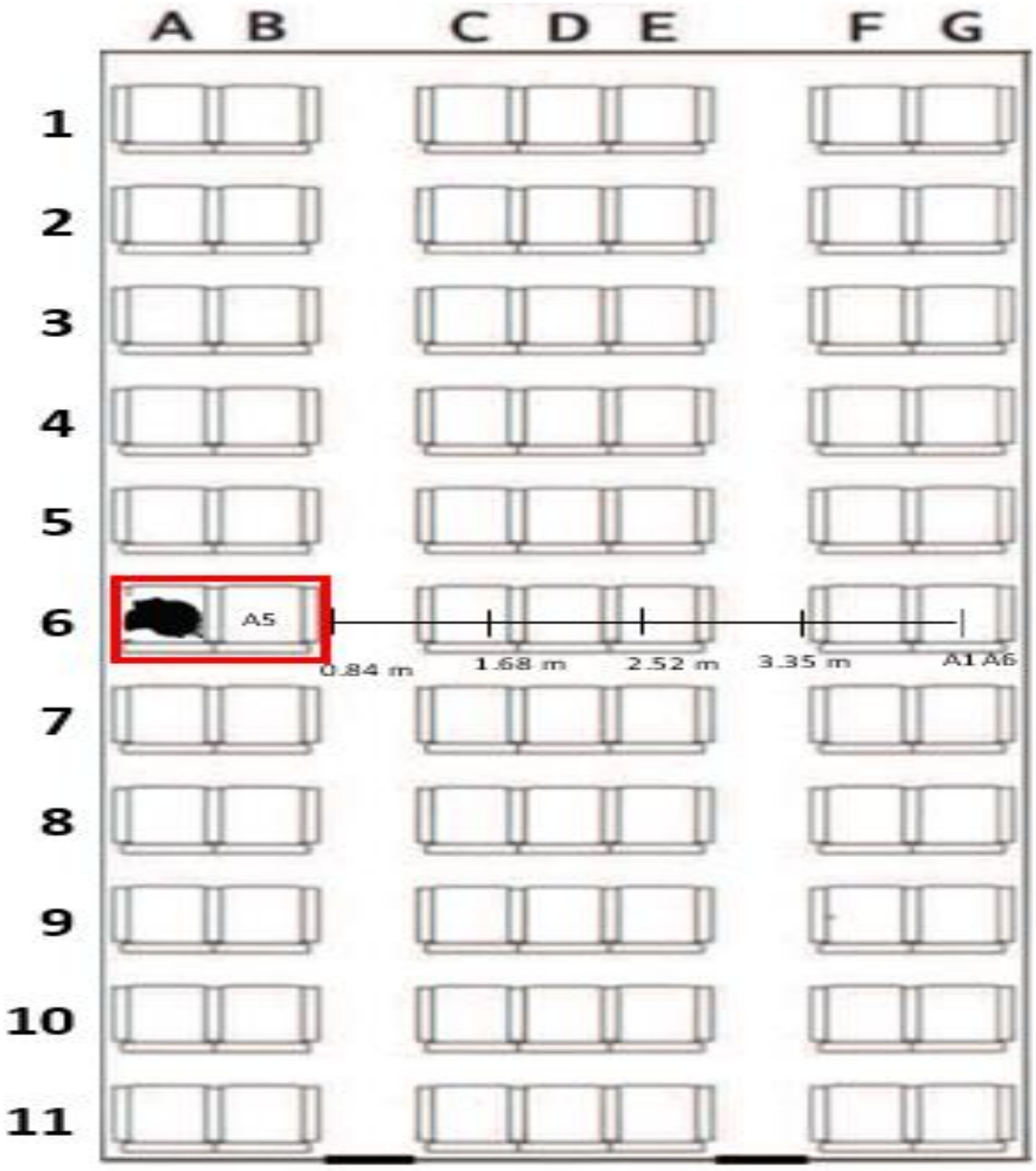

Figure I.59 Test 49 (B-M) ISOPass deployed source location and sampling tree orientation.

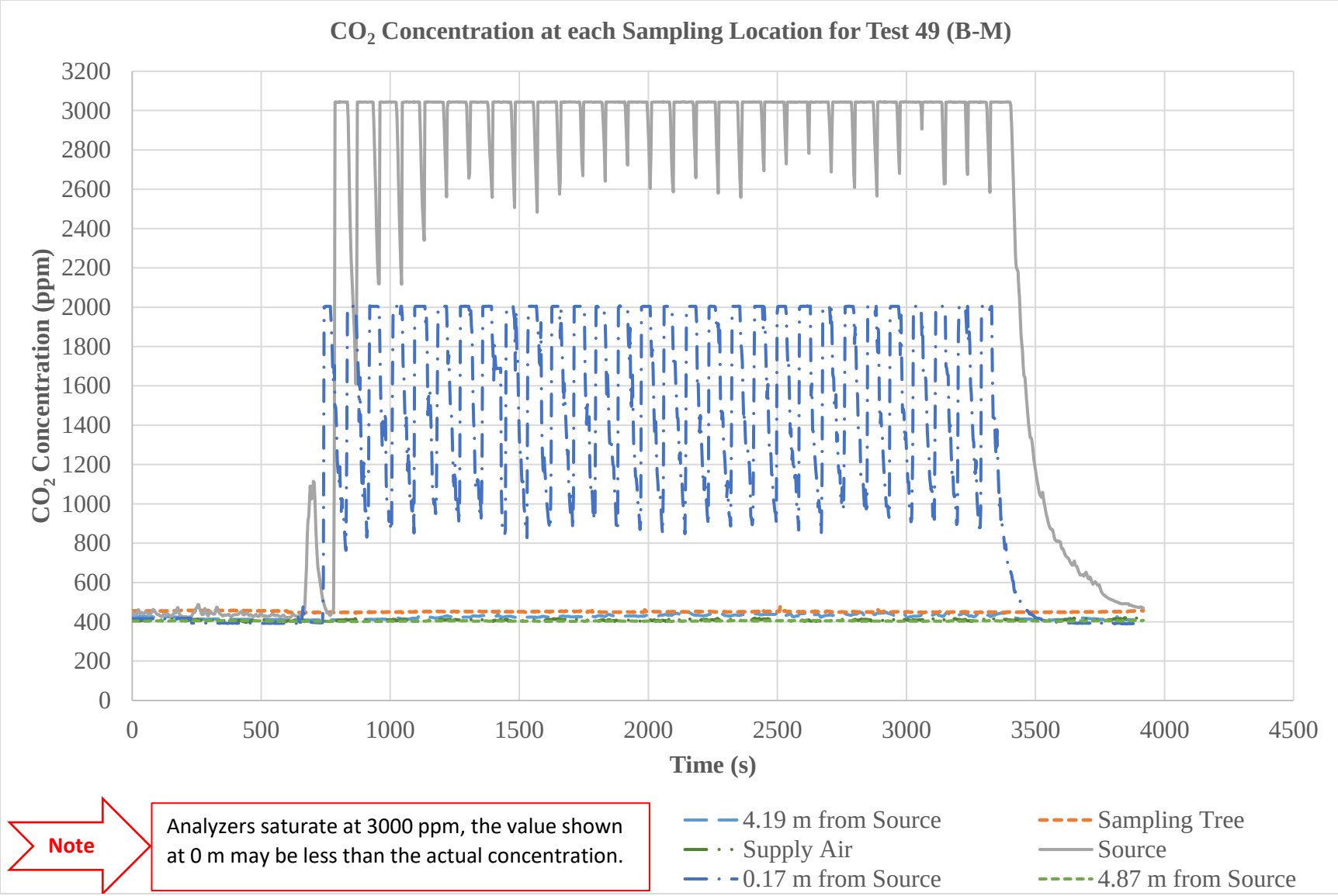

Figure I.60 Ininstantaneous CO_2 concentration at each sampling location for Test 49 (B-M) ISOPass deployed.

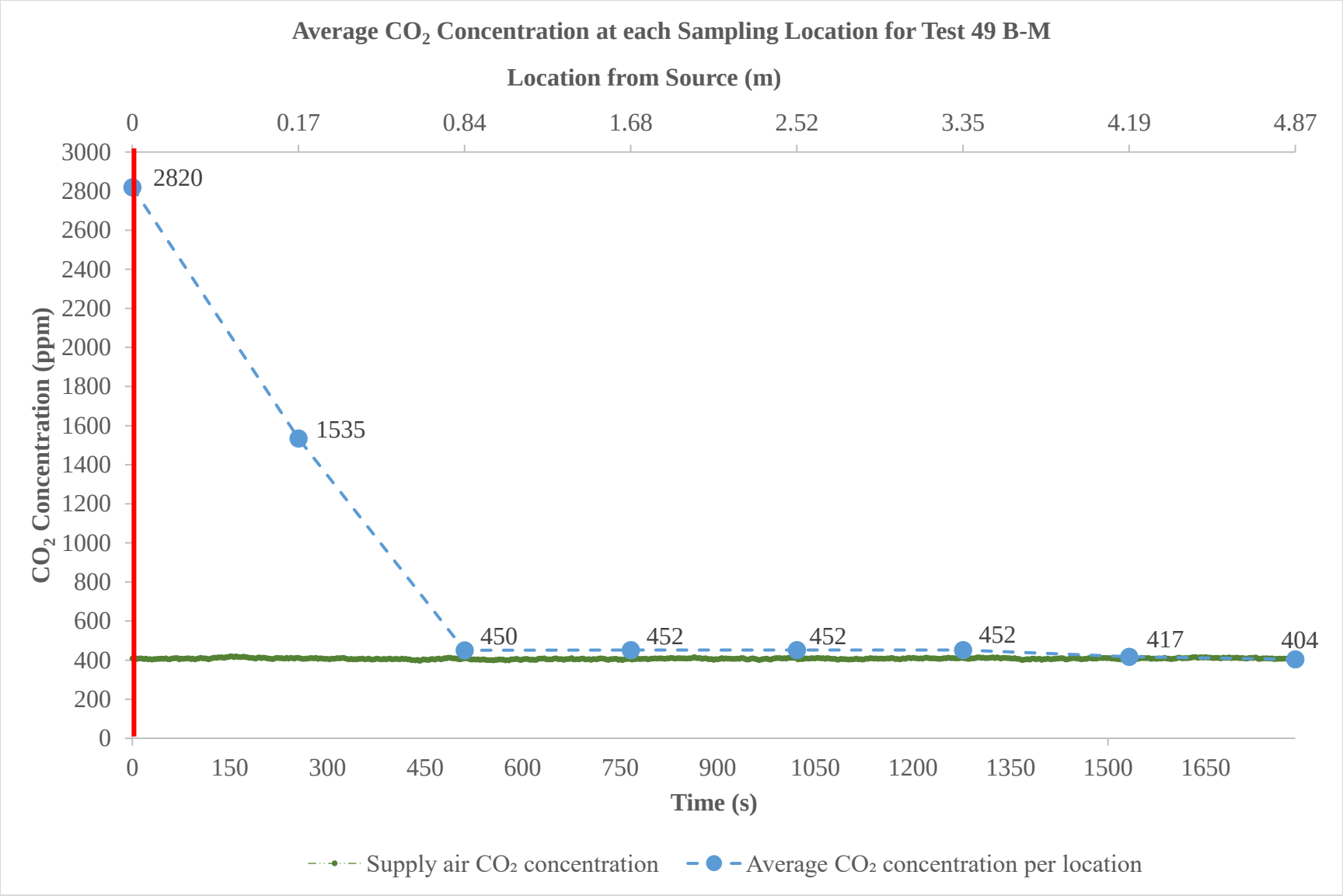

Figure I.61 Average CO_2 concentration at each sampling location for Test 49 (B-M) ISOPass deployed.

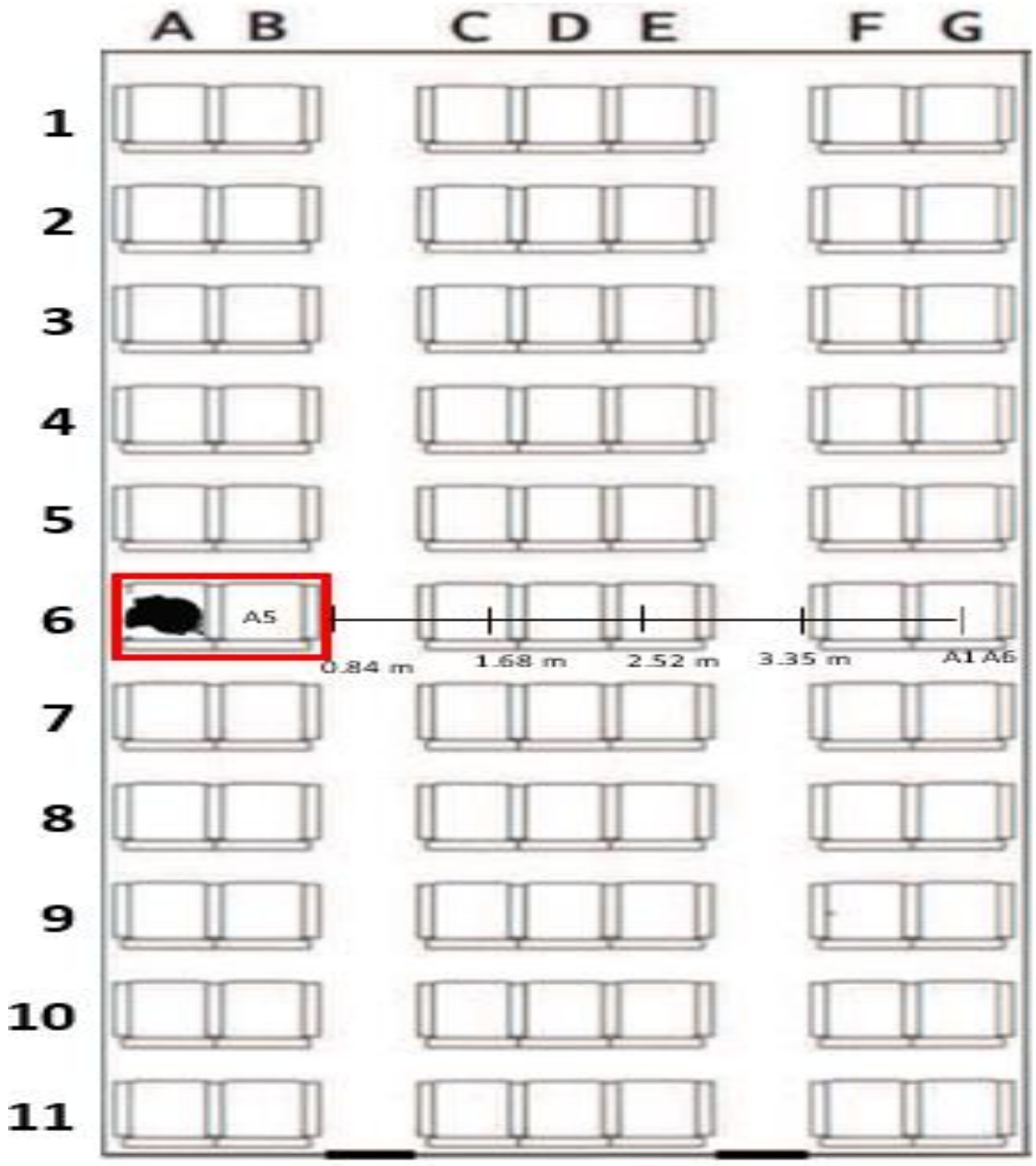

Figure I.62 Test 50 (B-M) ISOPass deployed source location and sampling tree orientation.

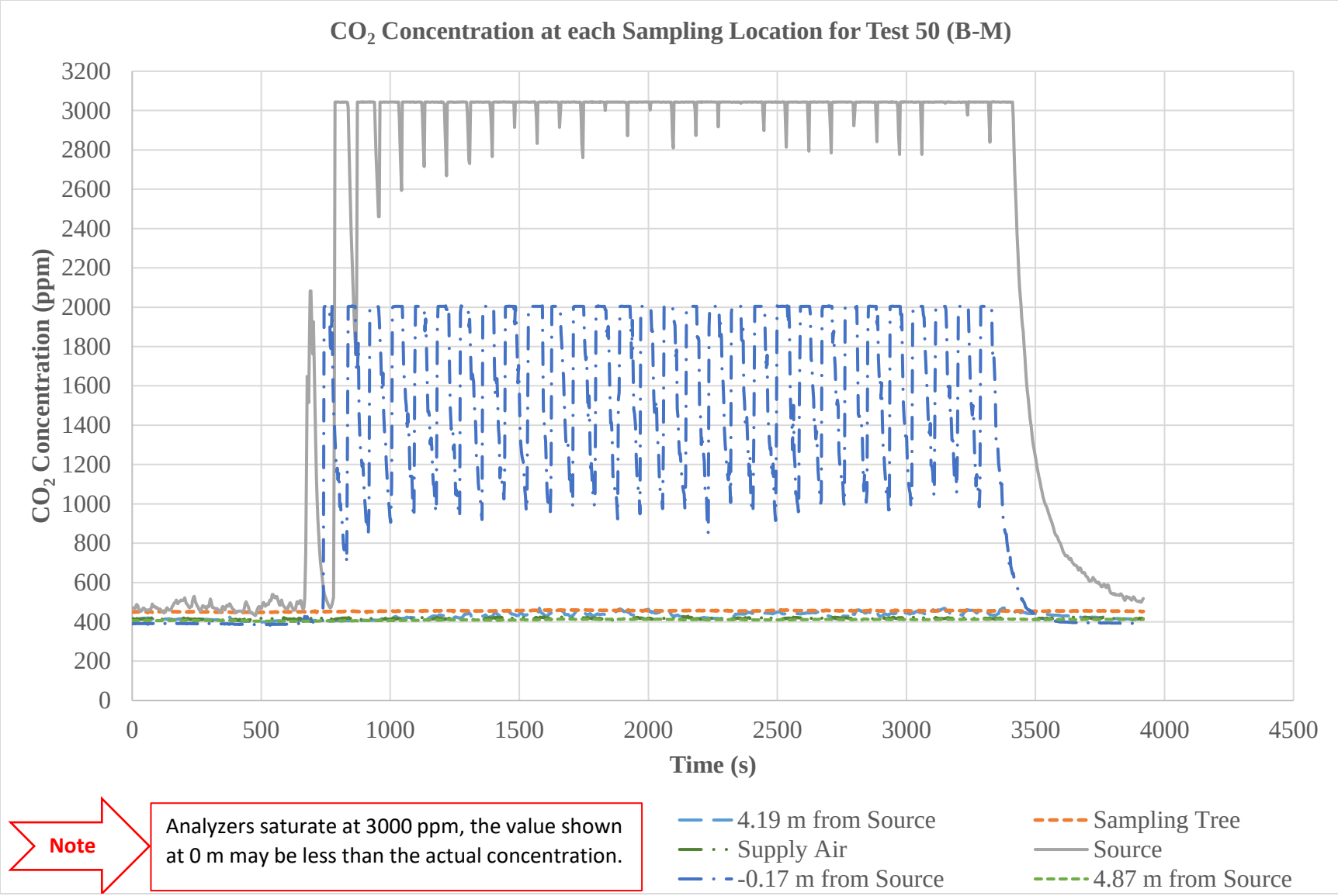

Figure I.63 Ininstantaneous CO_2 concentration at each sampling location for Test 50 (B-M) ISOPass deployed.

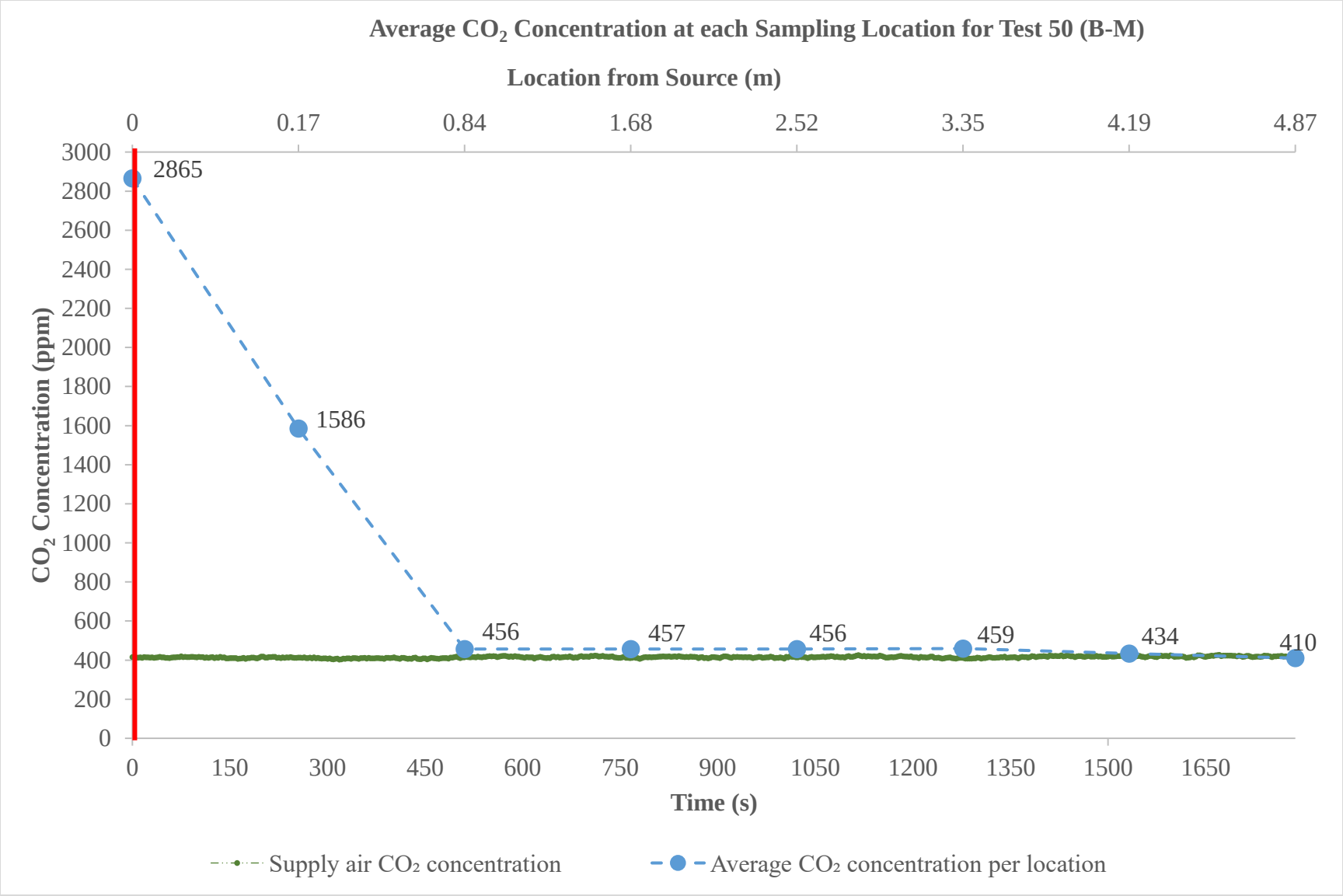

Figure I.64 Average CO_2 concentration at each sampling location for Test 50 (B-M) ISOPass deployed.

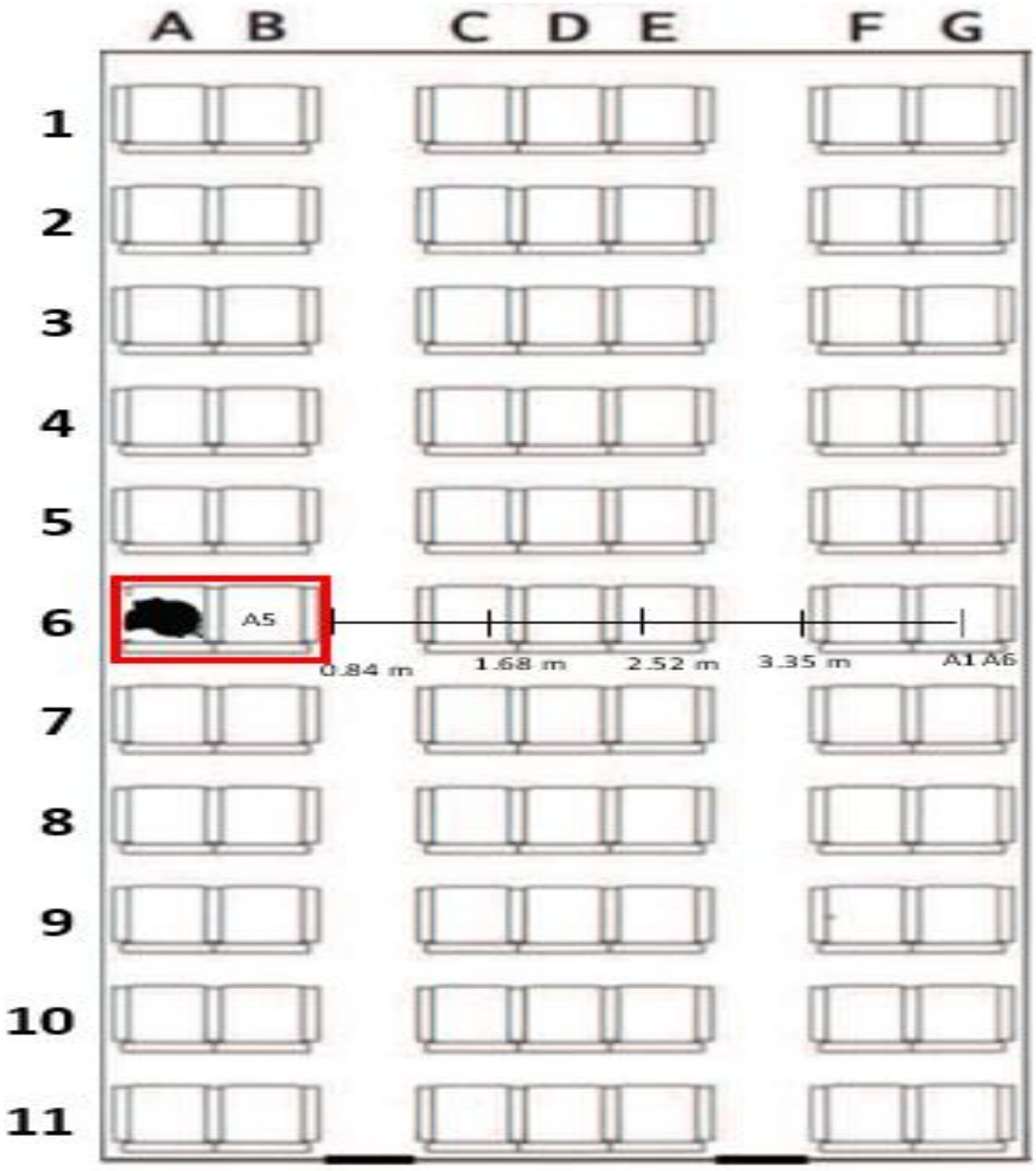

Figure I.65 Test 51 (B-M) ISOPass deployed source location and sampling tree orientation.

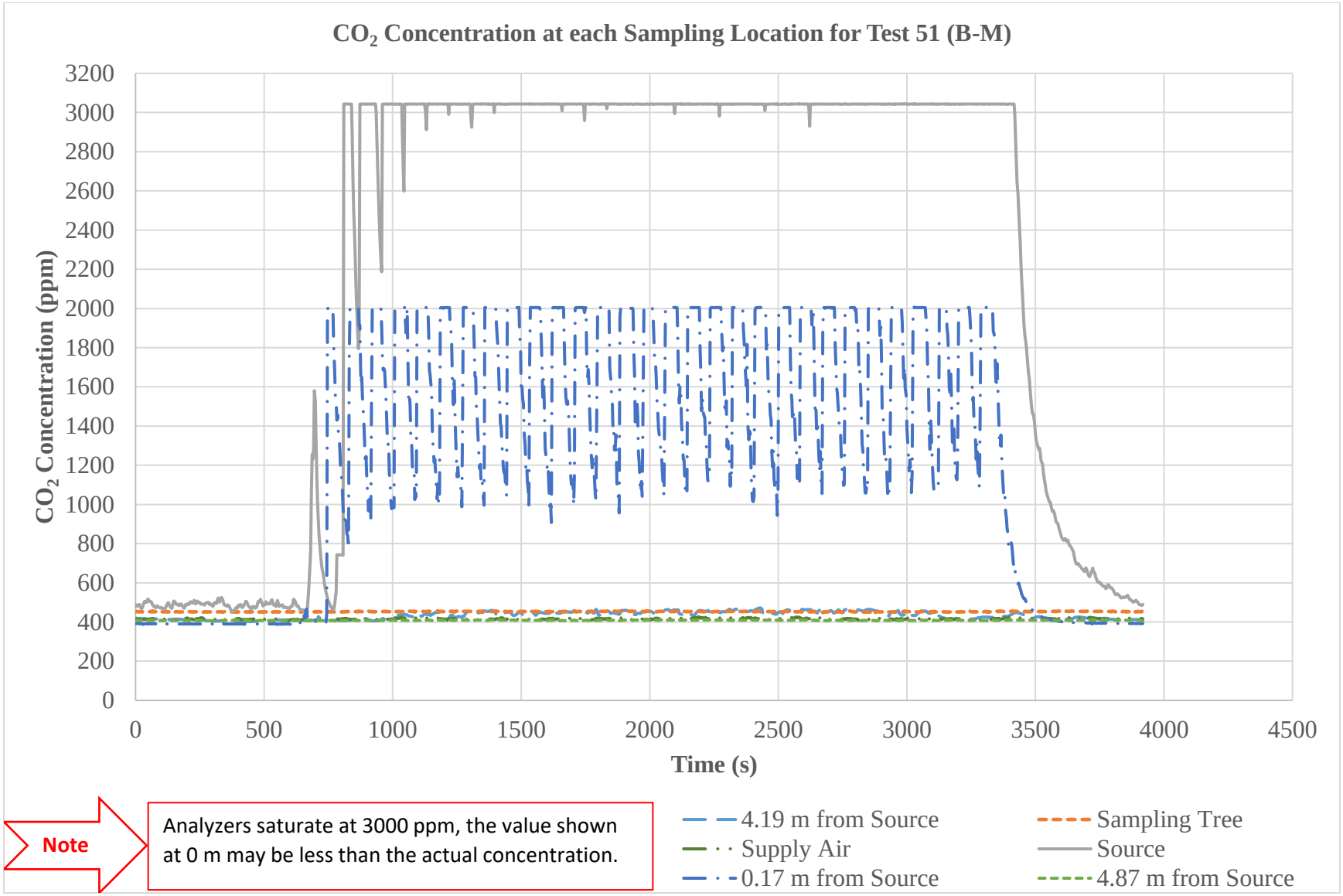

Figure I.66 Ininstantaneous CO_2 concentration at each sampling location for Test 51 (B-M) ISOPass deployed.

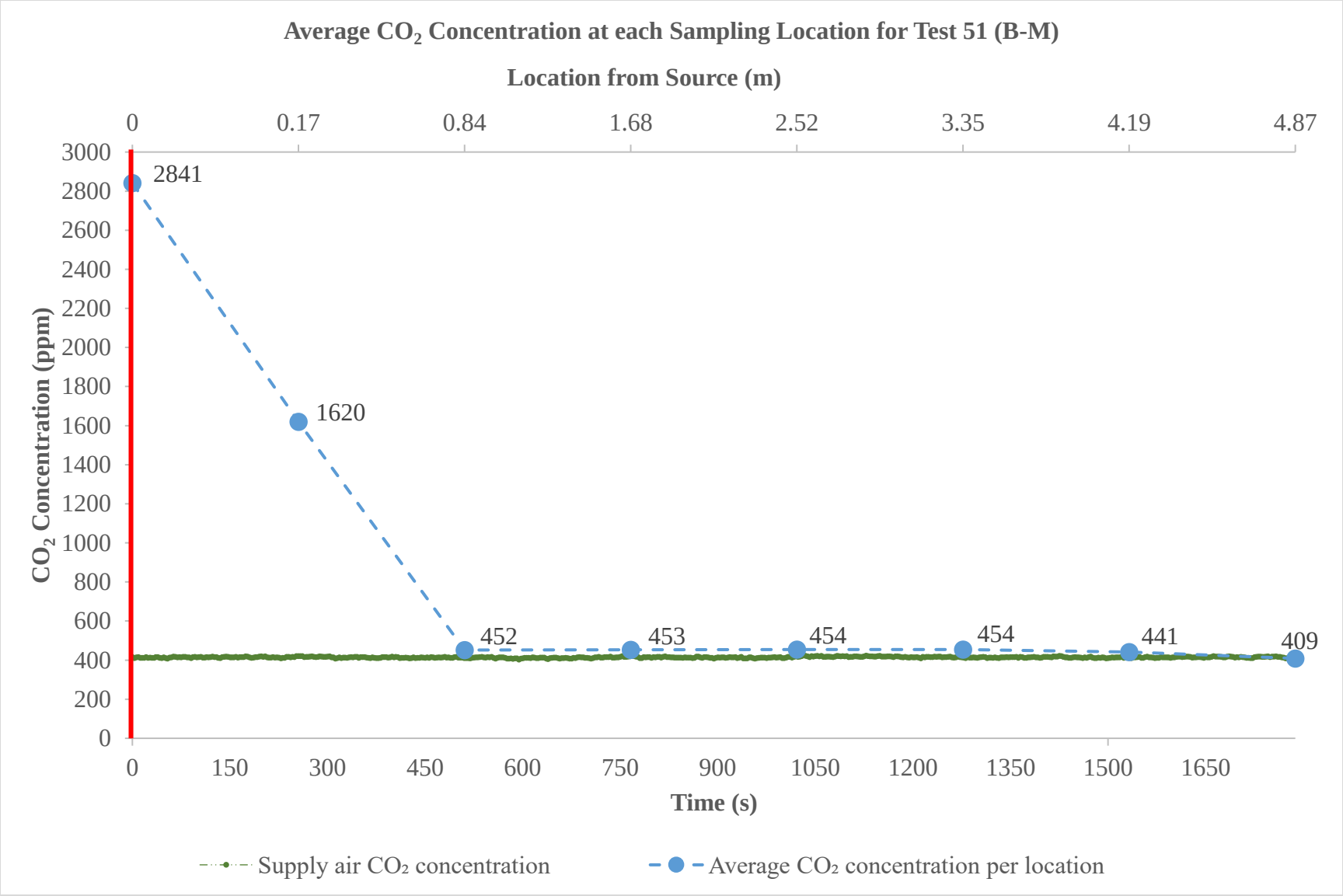

Figure I.67 Average CO_2 concentration at each sampling location for Test 51 (B-M) ISOPass deployed.

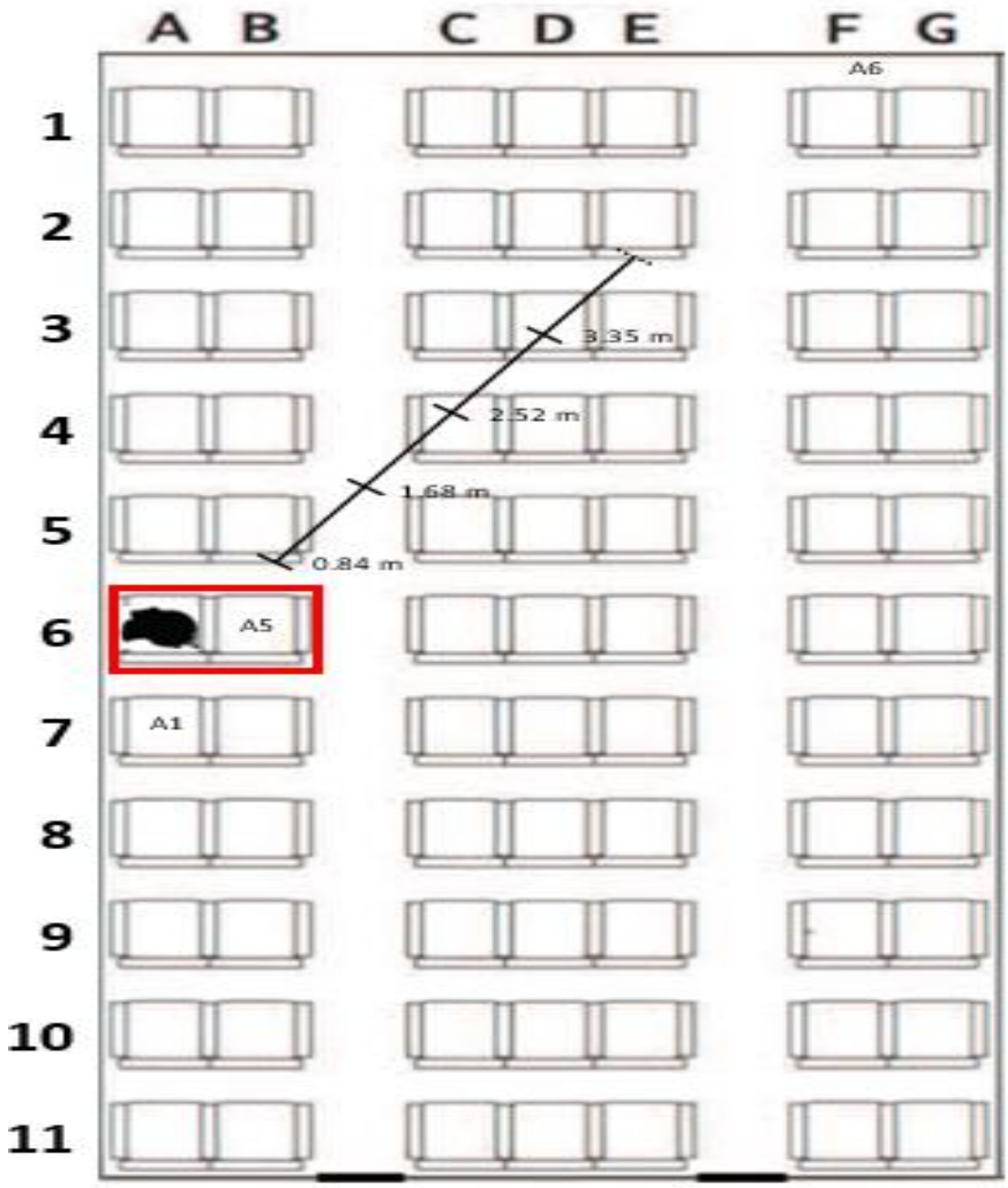

Figure I.68 Test 52 (B-M) ISOPass deployed source location and sampling tree orientation.

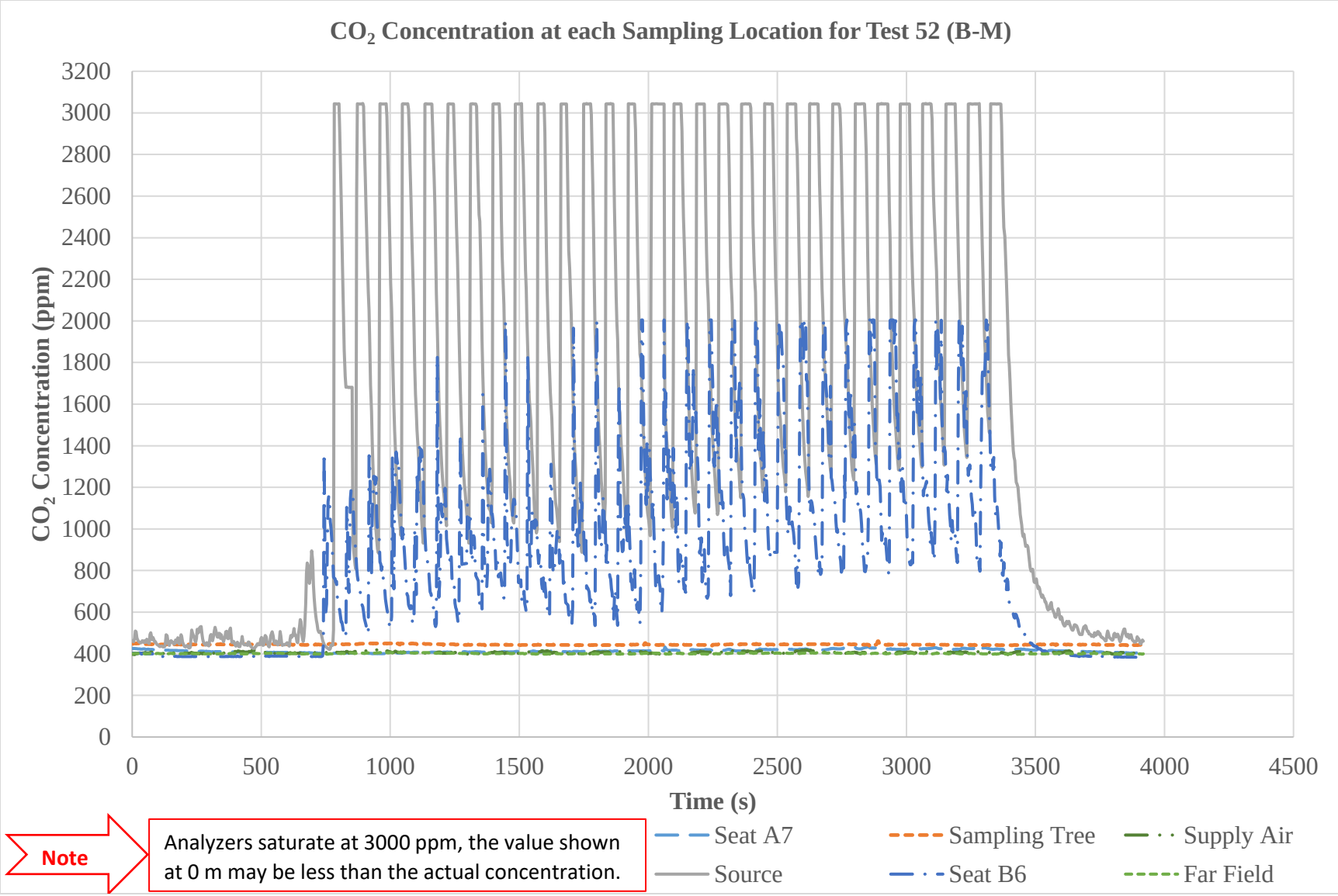

Figure I.69 Ininstantaneous CO_2 concentration at each sampling location for Test 52 (B-M) ISOPass deployed.

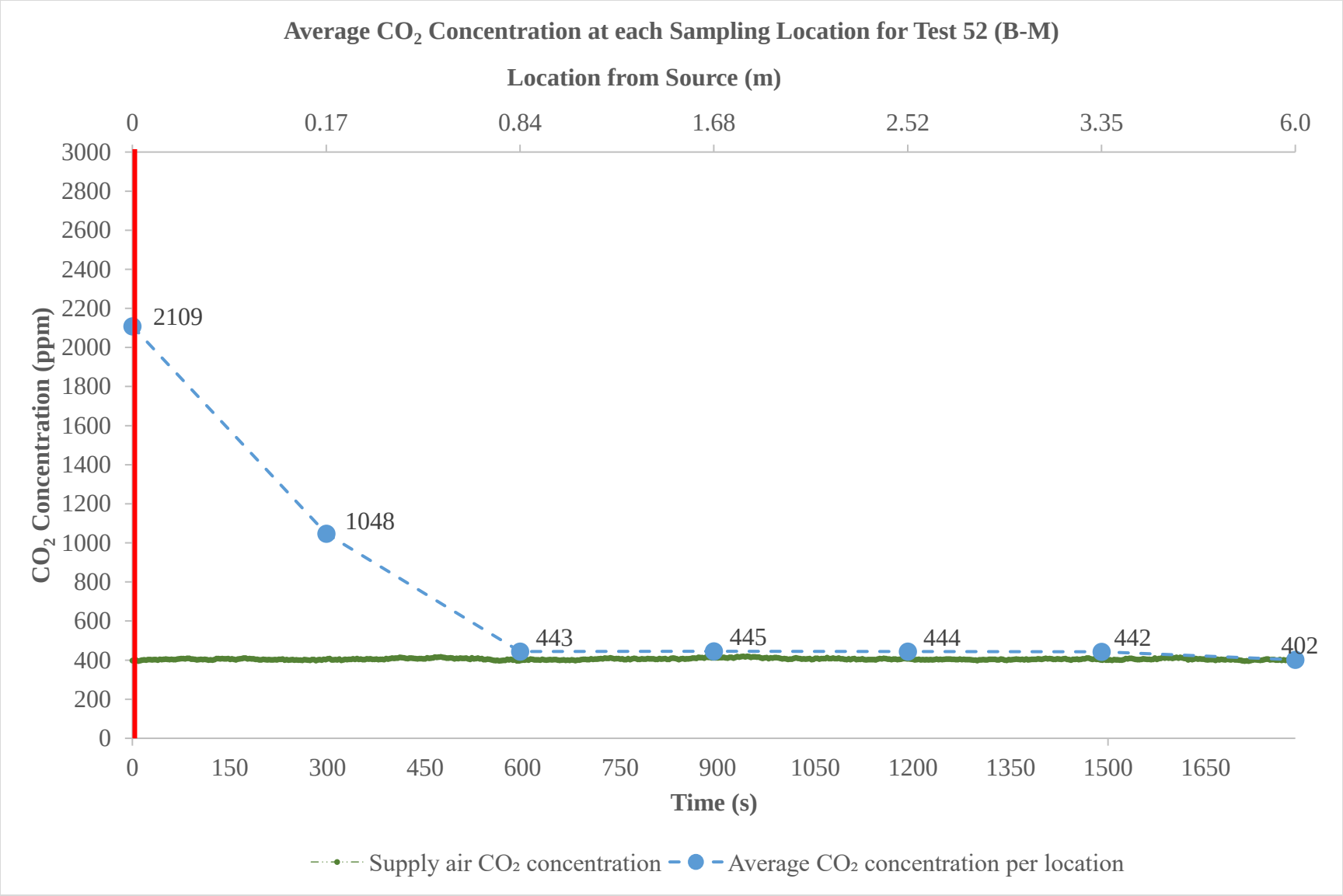

Figure I.70 Average CO_2 concentration at each sampling location for Test 52 (B-M) ISOPass deployed.

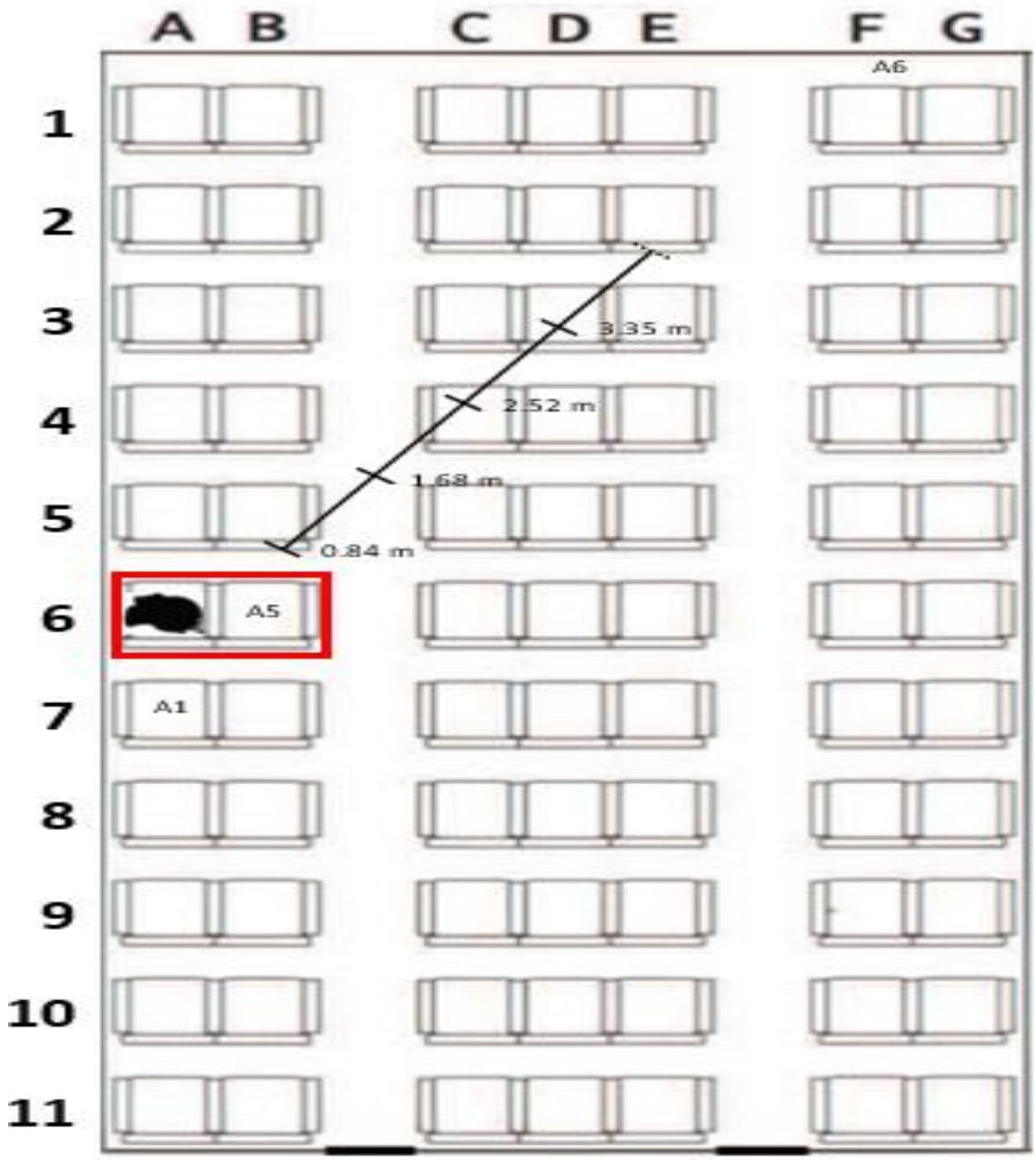

Figure I.71 Test 53 (B-M) ISOPass deployed source location and sampling tree orientation.

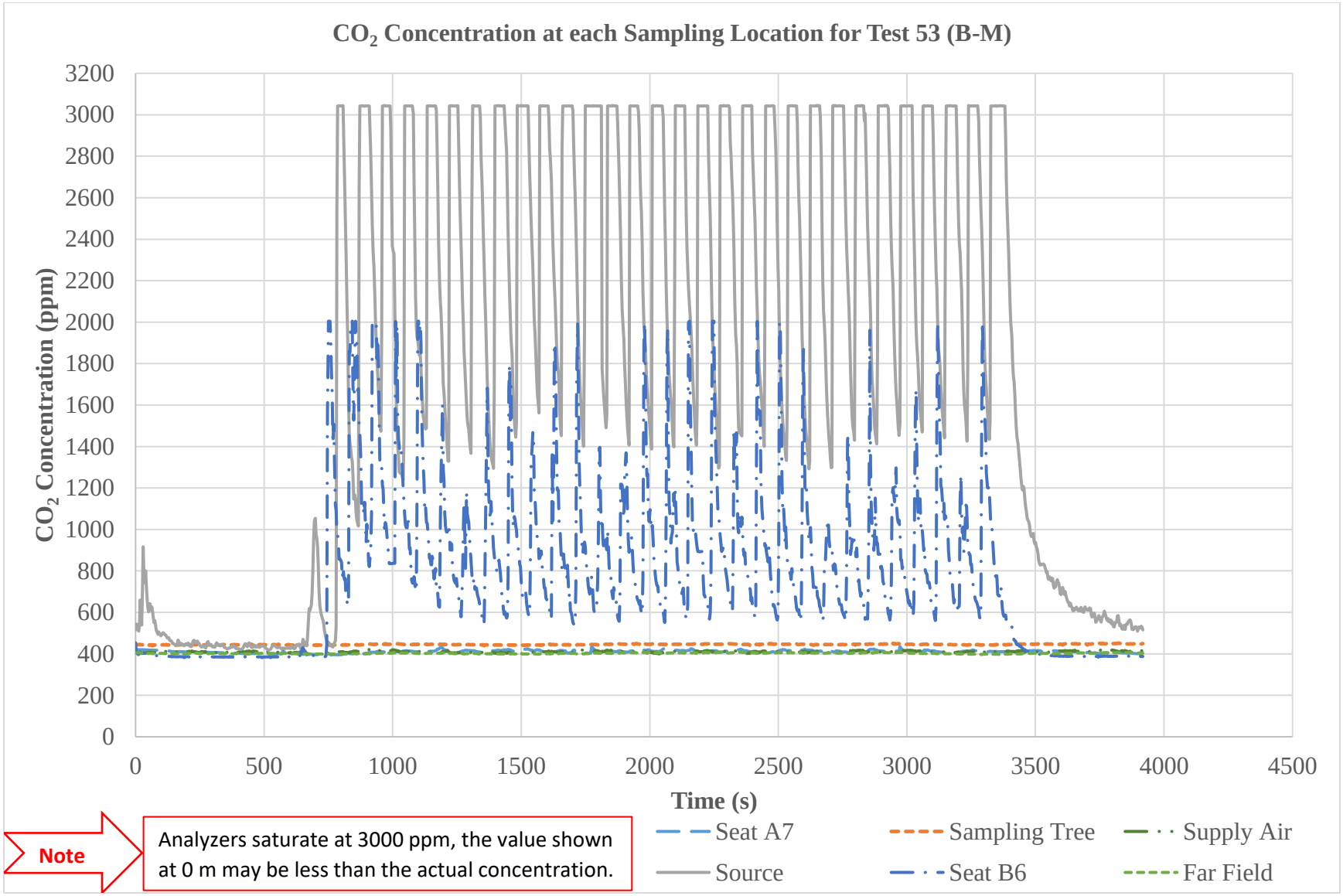

Figure I.72 Ininstantaneous CO_2 concentration at each sampling location for Test 53 (B-M) ISOPass deployed.

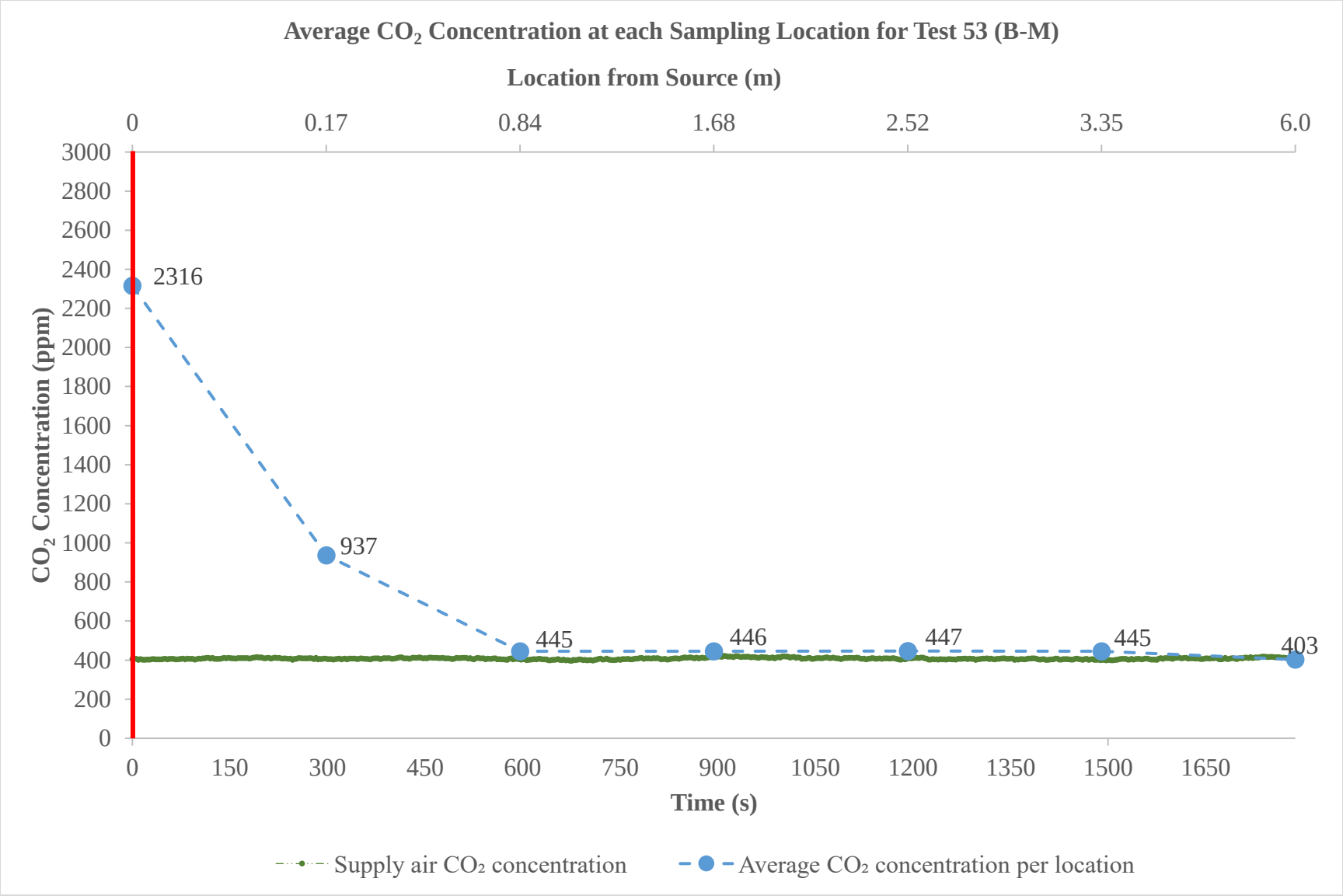

Figure I.73 Average CO_2 concentration at each sampling location for Test 53 (B-M) ISOPass deployed.

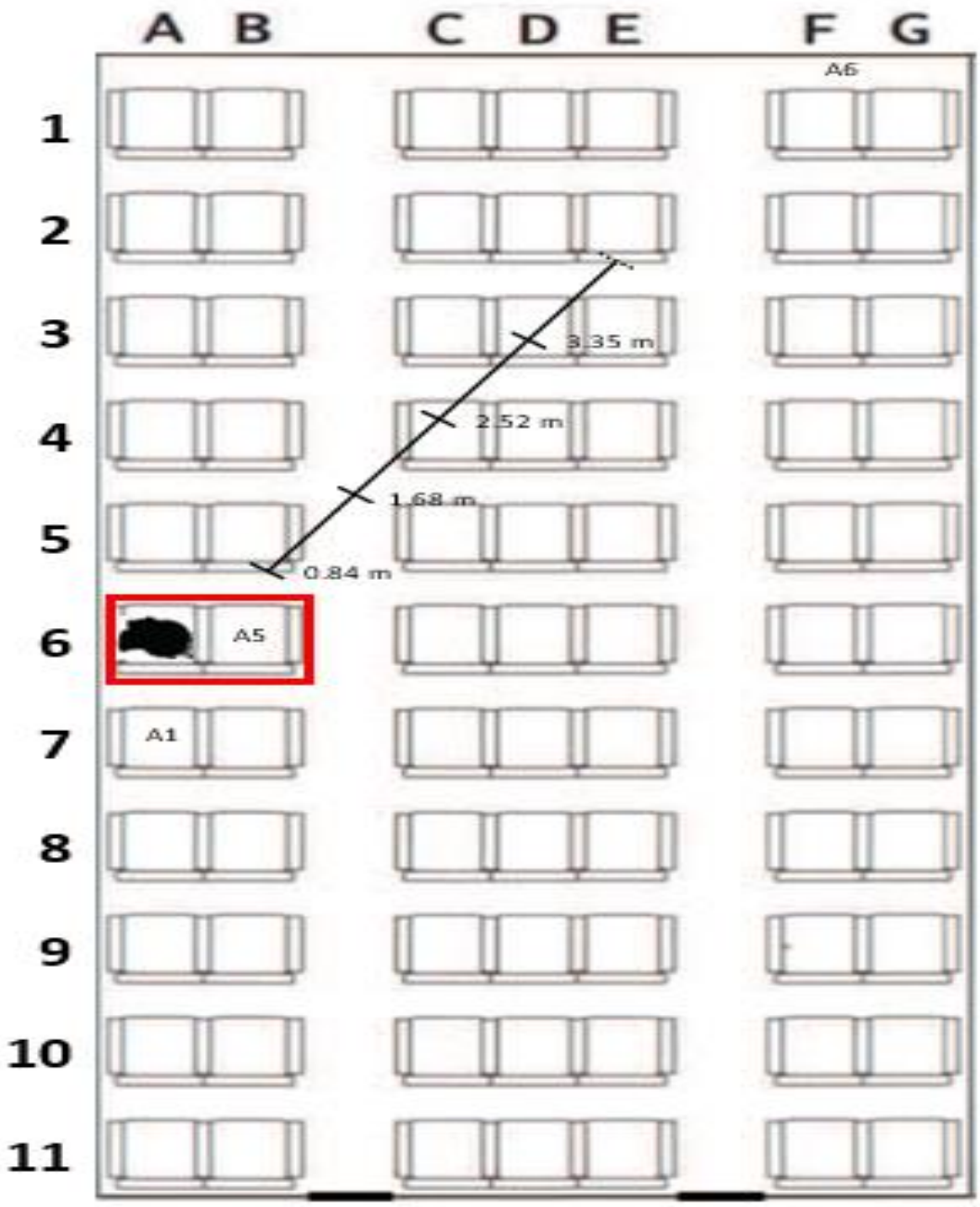

Figure I.74 Test 54 (B-M) ISOPass deployed source location and sampling tree orientation.

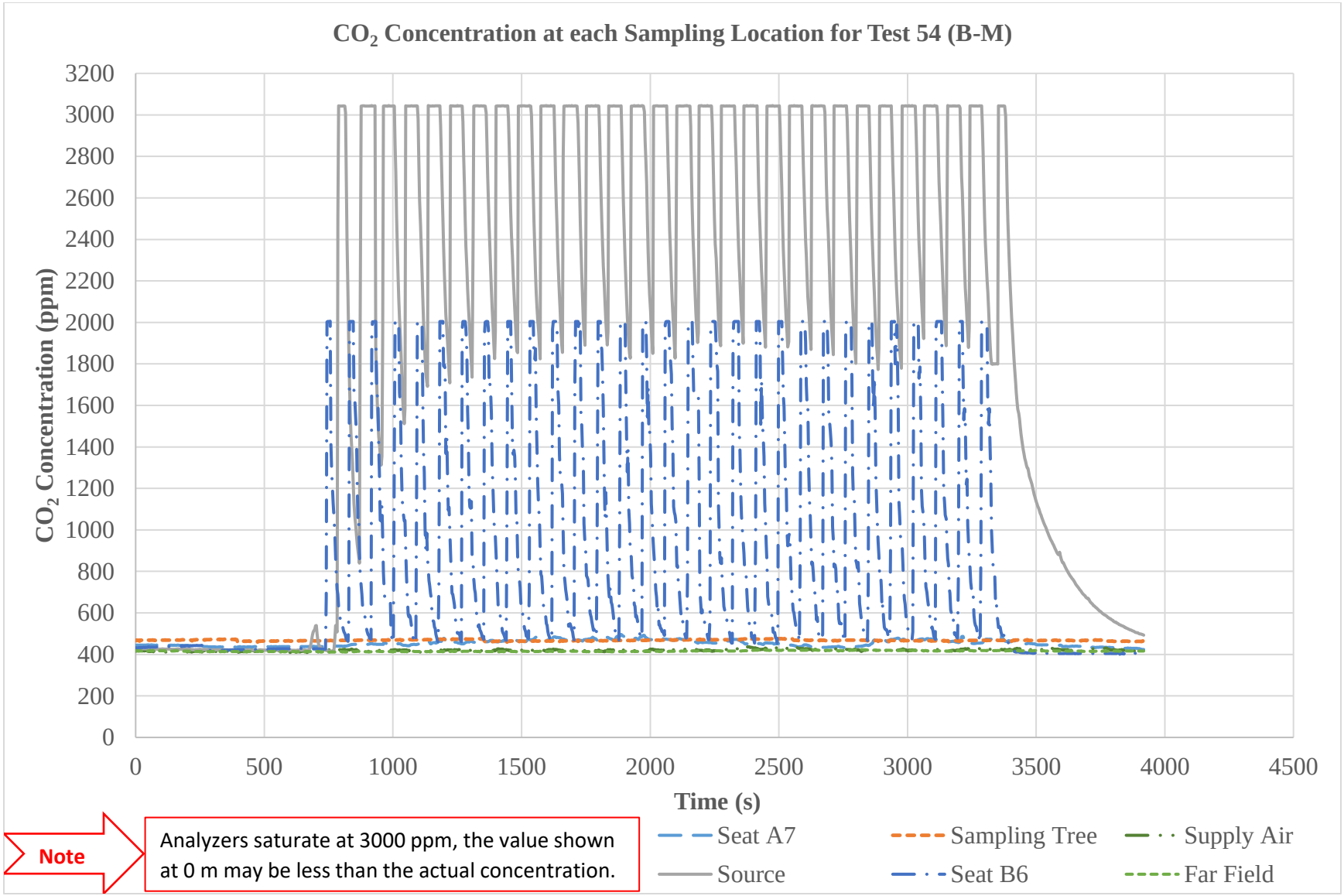

Figure I.75 Ininstantaneous CO_2 concentration at each sampling location for Test 54 (B-M) ISOPass deployed.

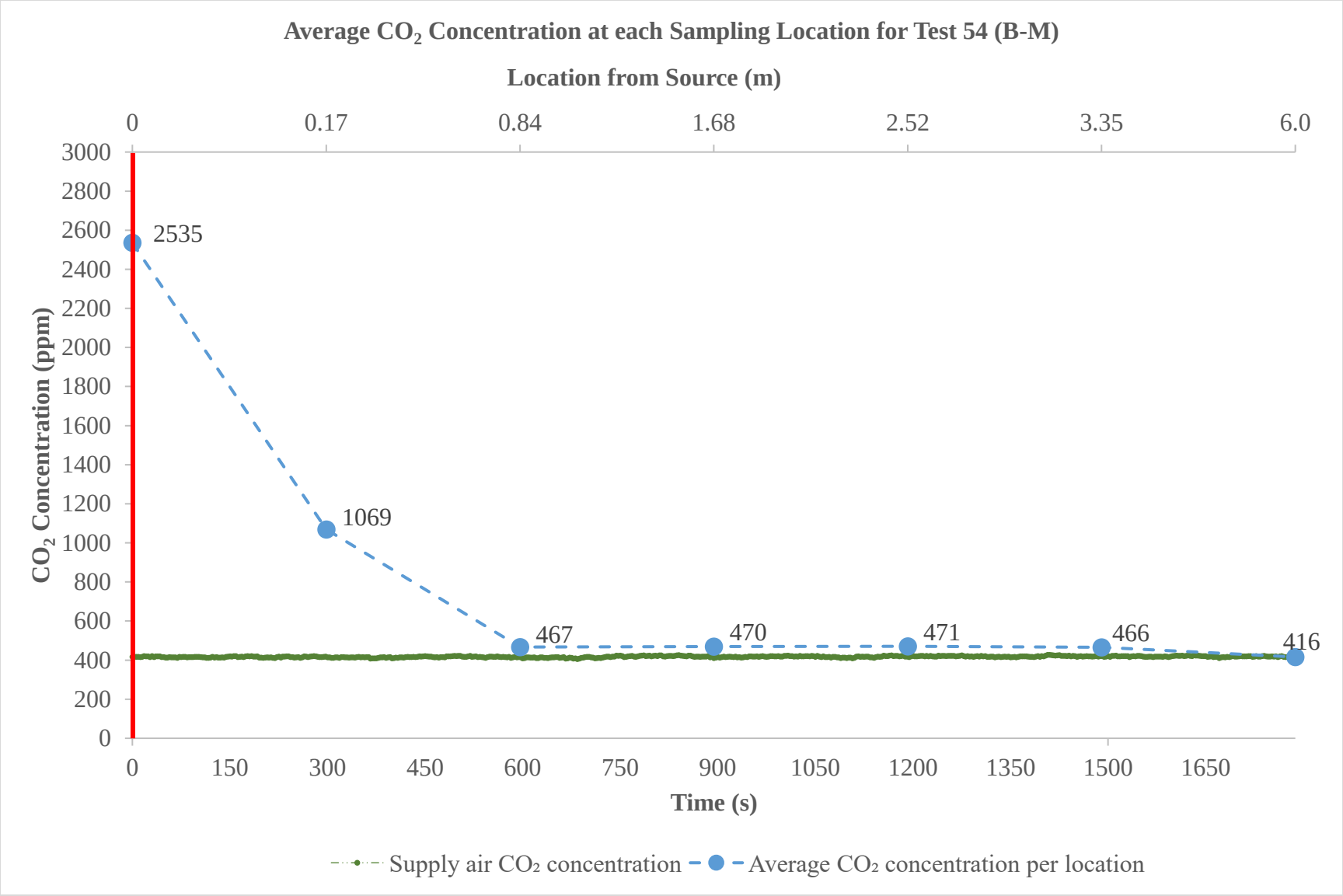

Figure I.76 Average CO_2 concentration at each sampling location for Test 54 (B-M) ISOPass deployed.

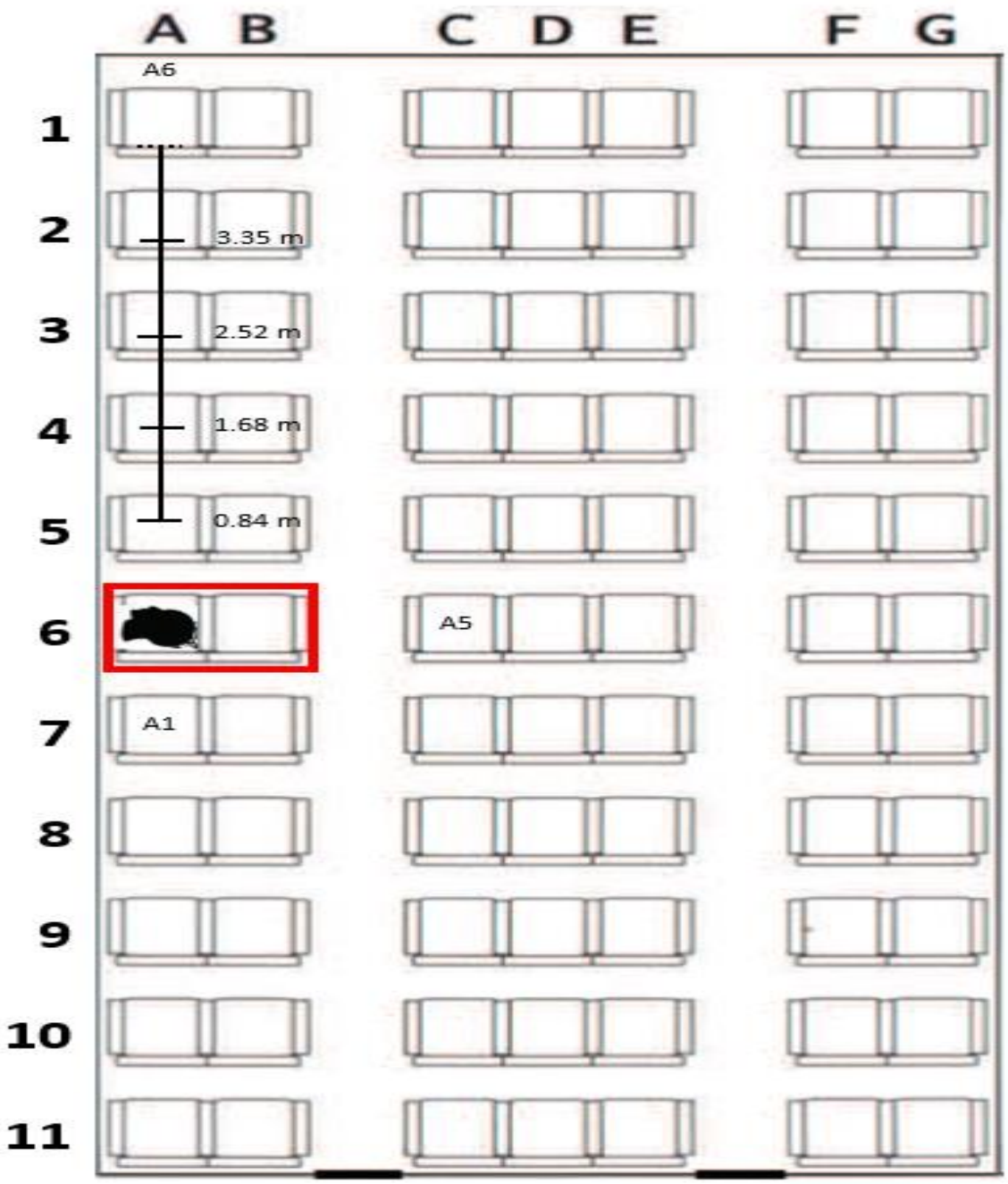

Figure I.77 Test 64 (B-M) ISOPass deployed source location and sampling tree orientation.

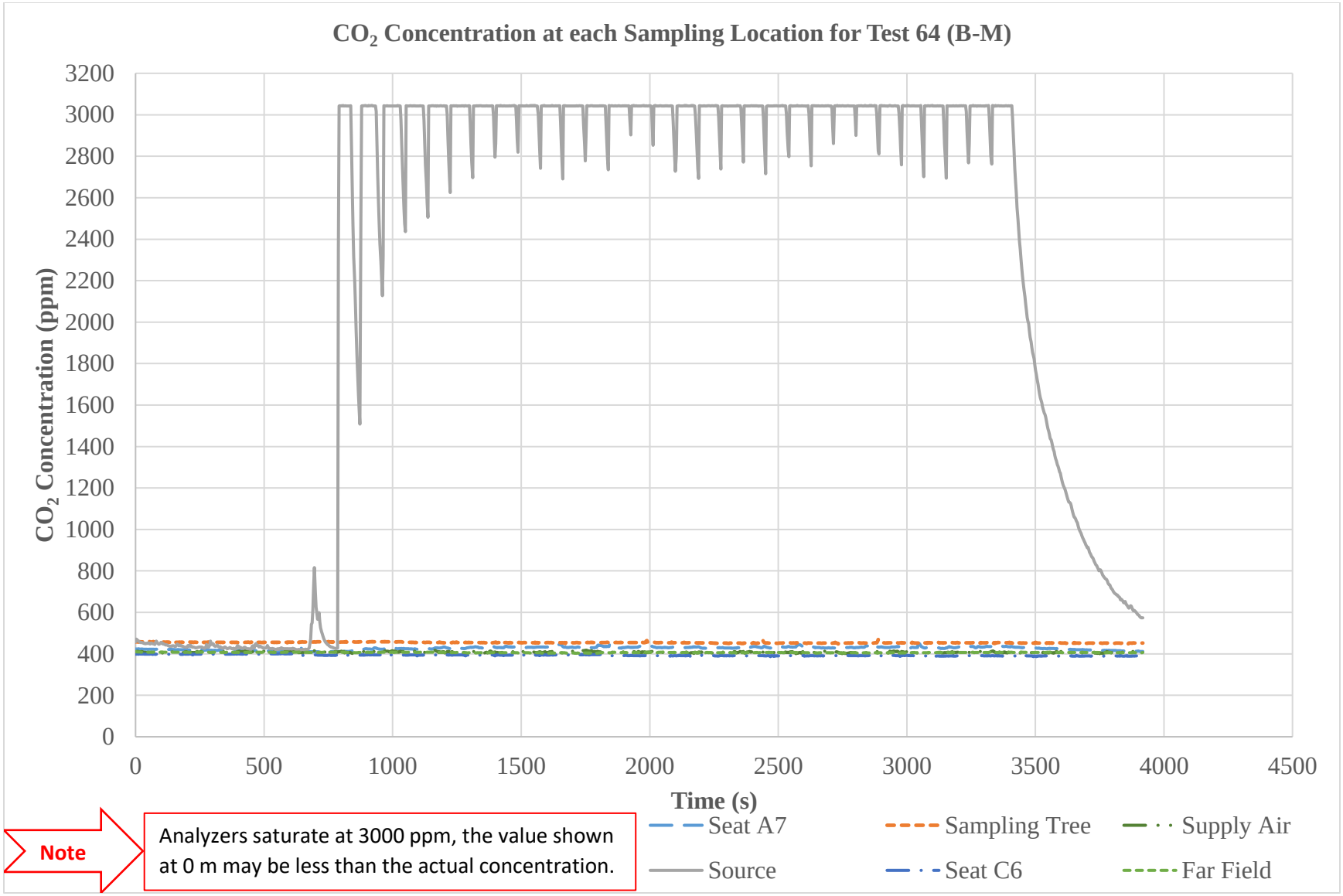

Figure I.78 Ininstantaneous CO_2 concentration at each sampling location for Test 64 (B-M) ISOPass deployed.

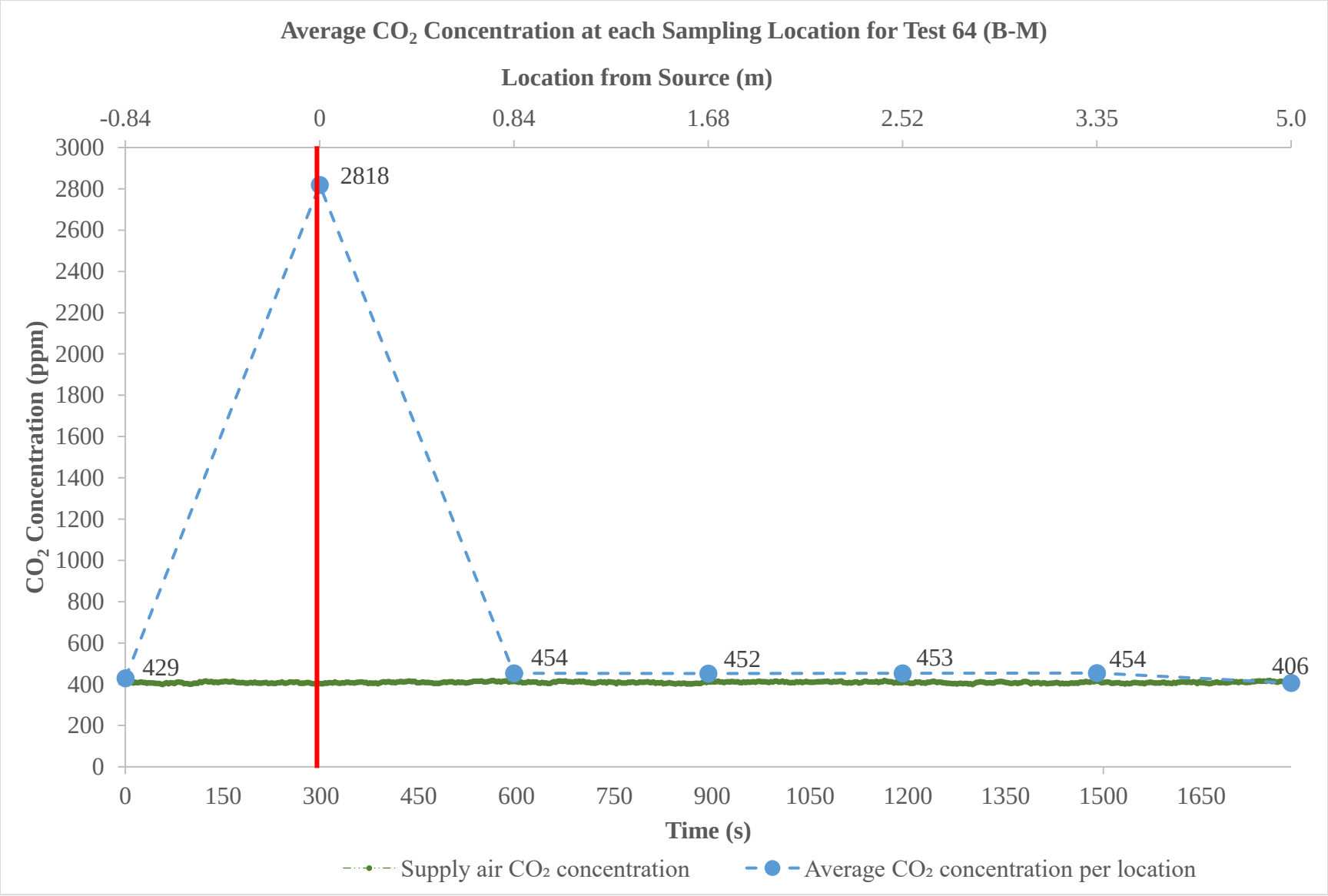

Figure I.79 Average CO_2 concentration at each sampling location for Test 64 (B-M) ISOPass deployed.

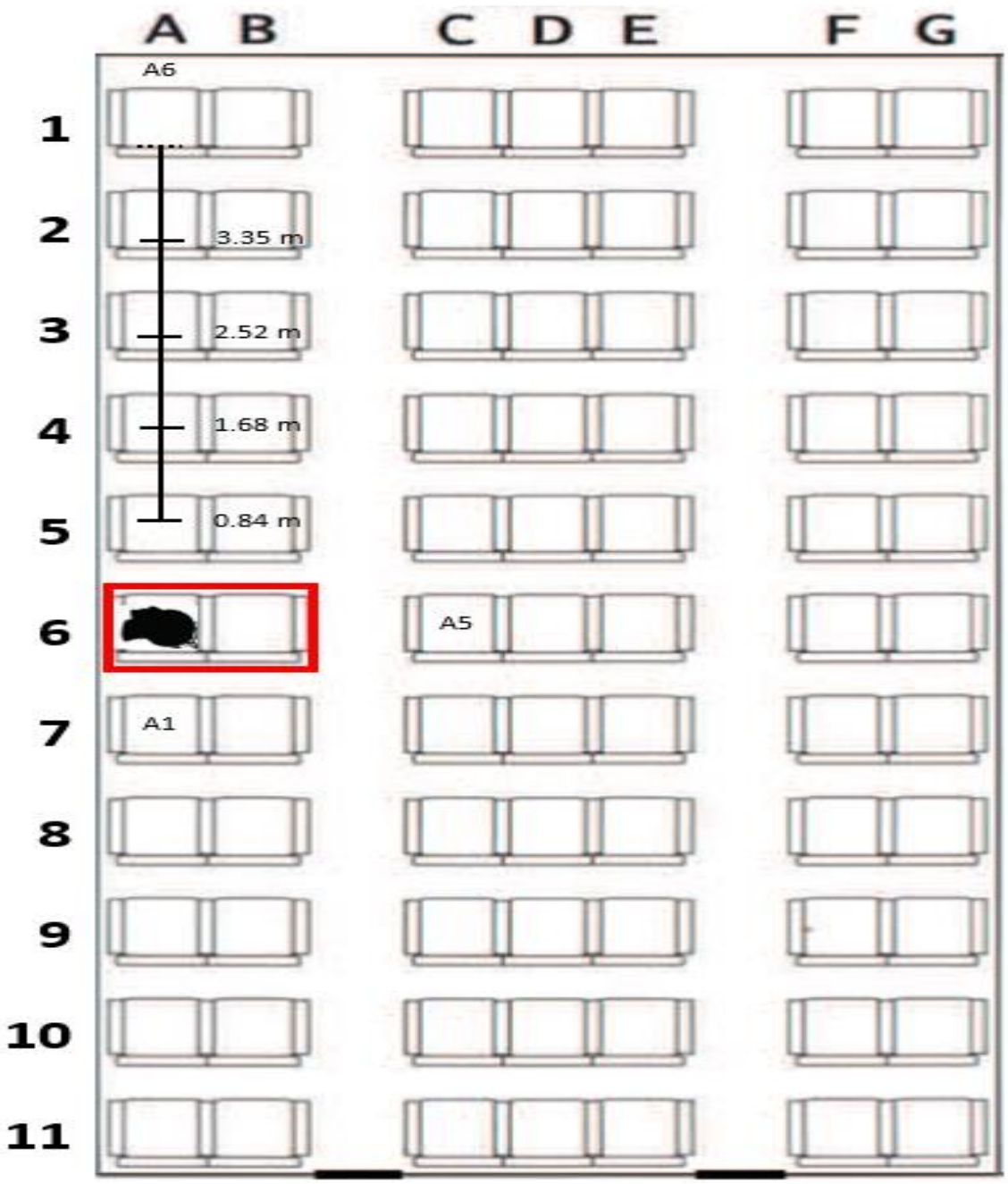

Figure I.80 Test 65 (B-M) ISOPass deployed source location and sampling tree orientation.

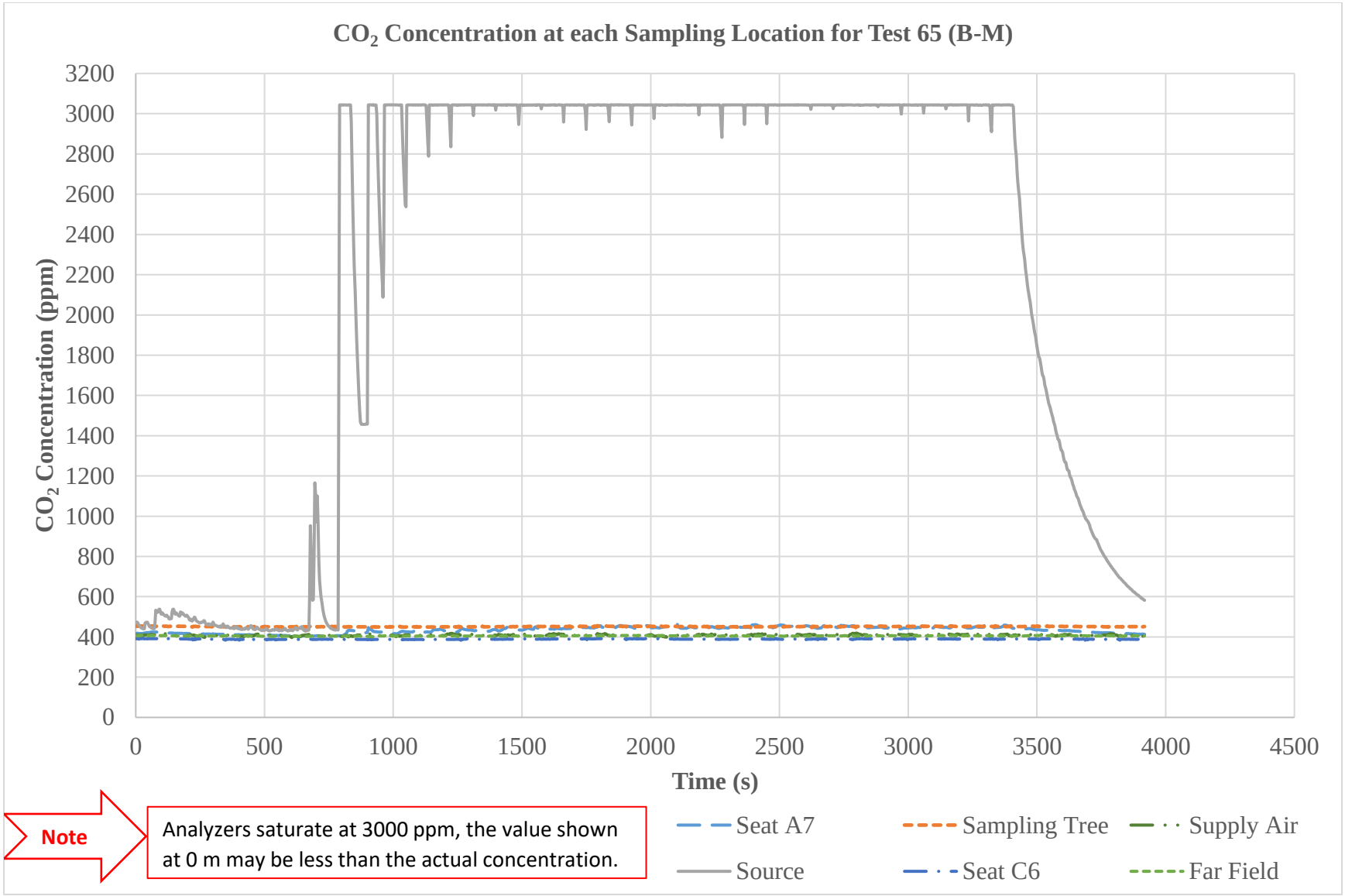

Figure I.81 Ininstantaneous CO_2 concentration at each sampling location for Test 65 (B-M) ISOPass deployed.

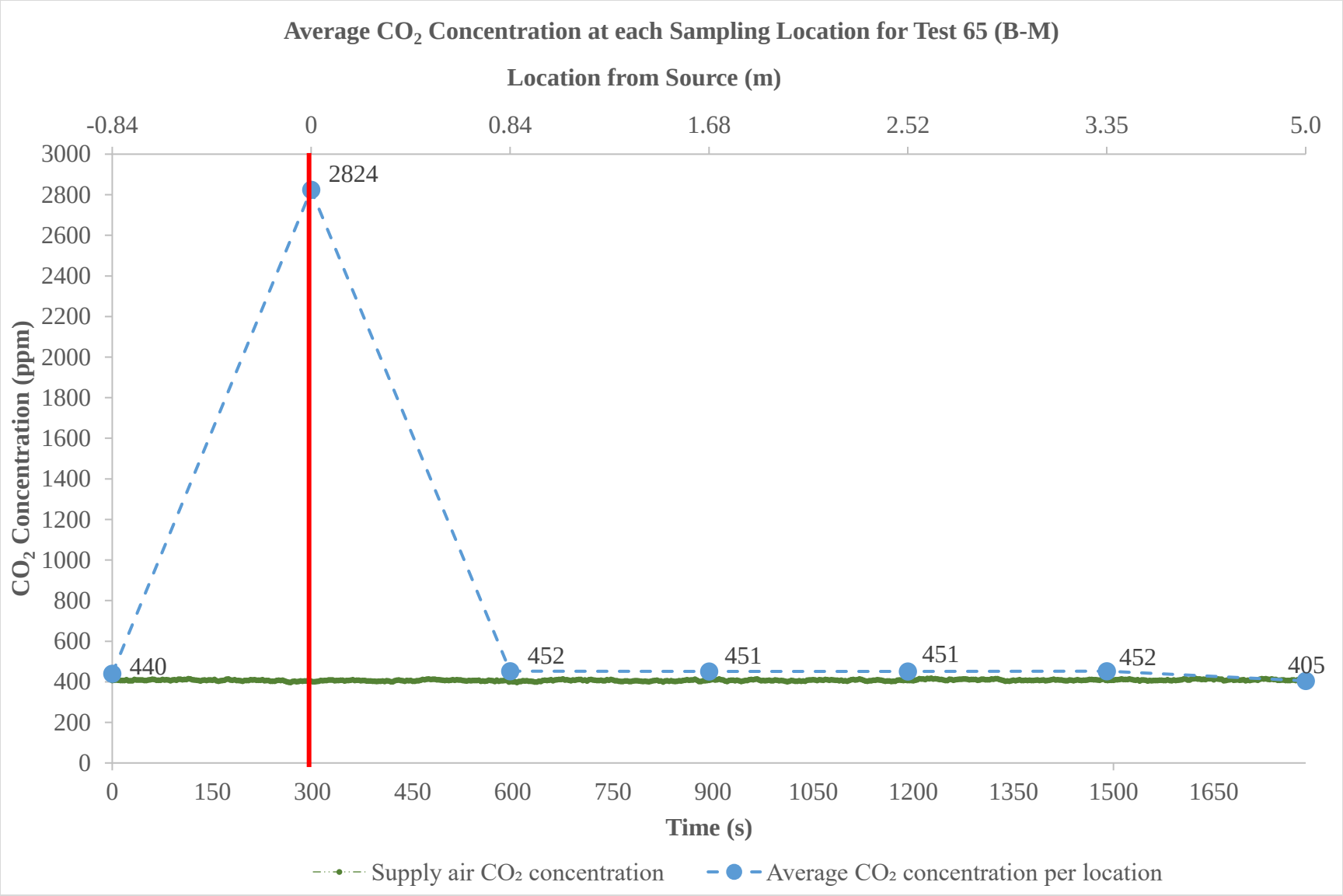

Figure I.82 Average CO_2 concentration at each sampling location for Test 65 (B-M) ISOPass deployed.

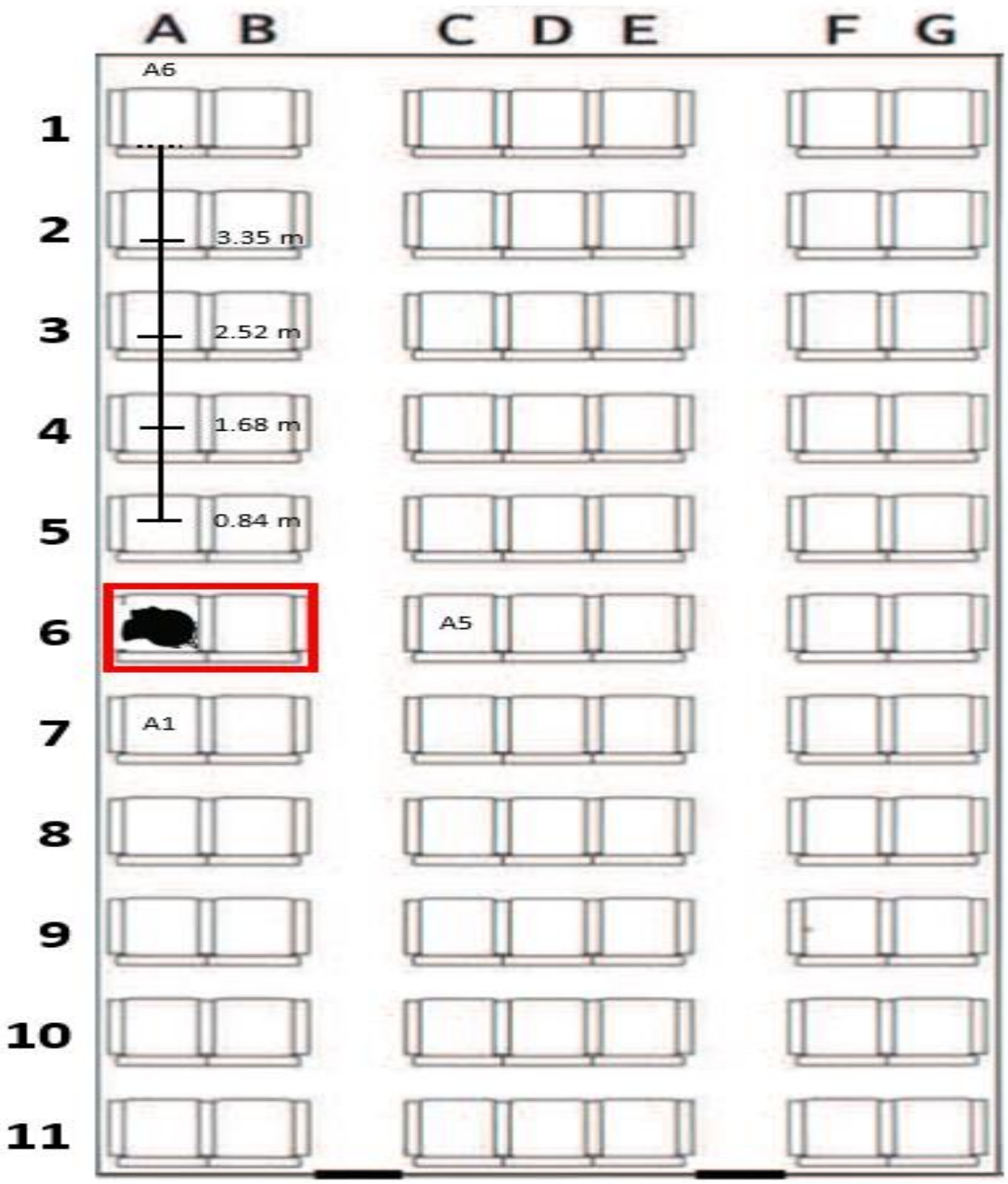

Figure I.83 Test 66 (B-M) ISOPass deployed source location and sampling tree orientation.

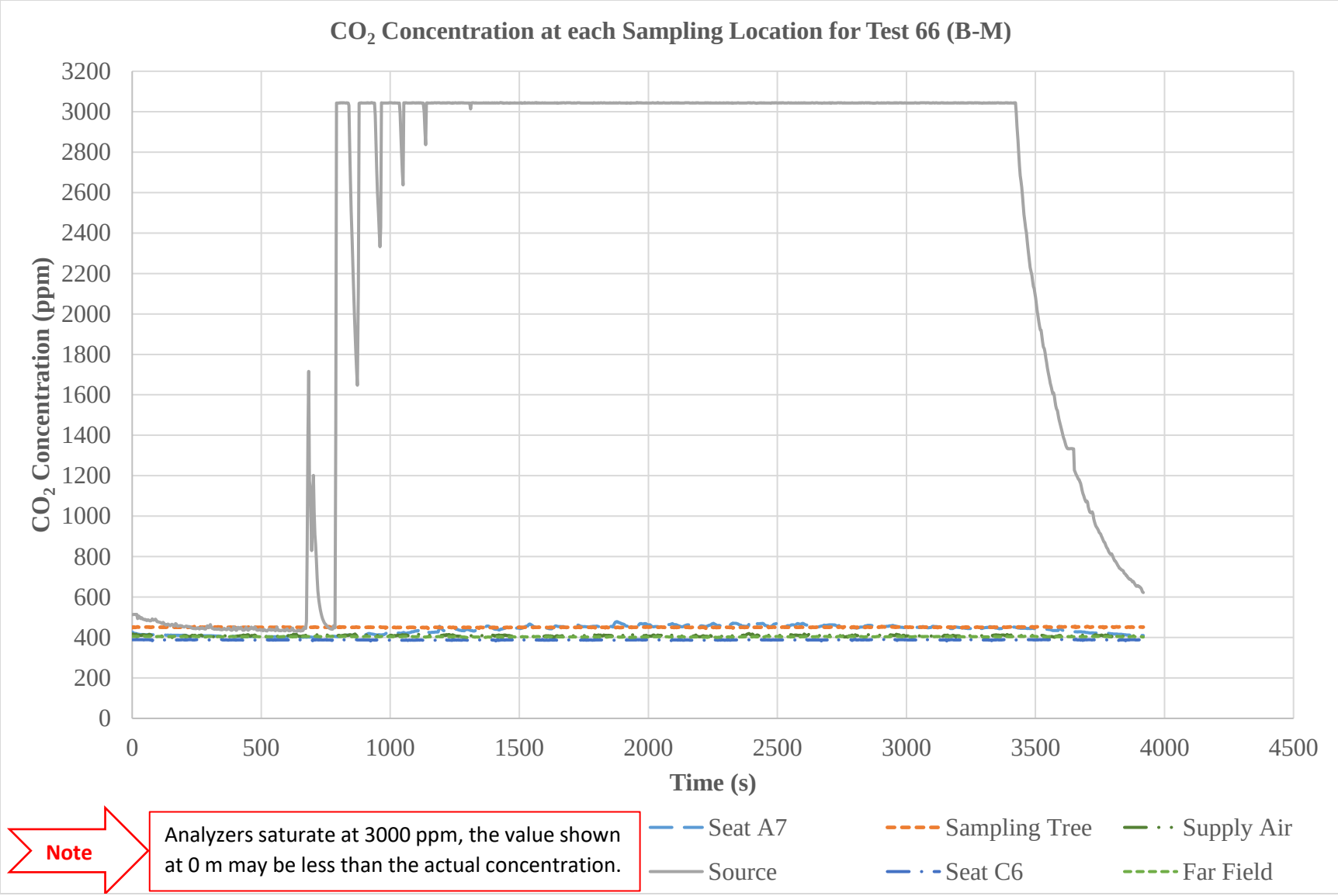

Figure I.84 Ininstantaneous CO_2 concentration at each sampling location for Test 66 (B-M) ISOPass deployed.

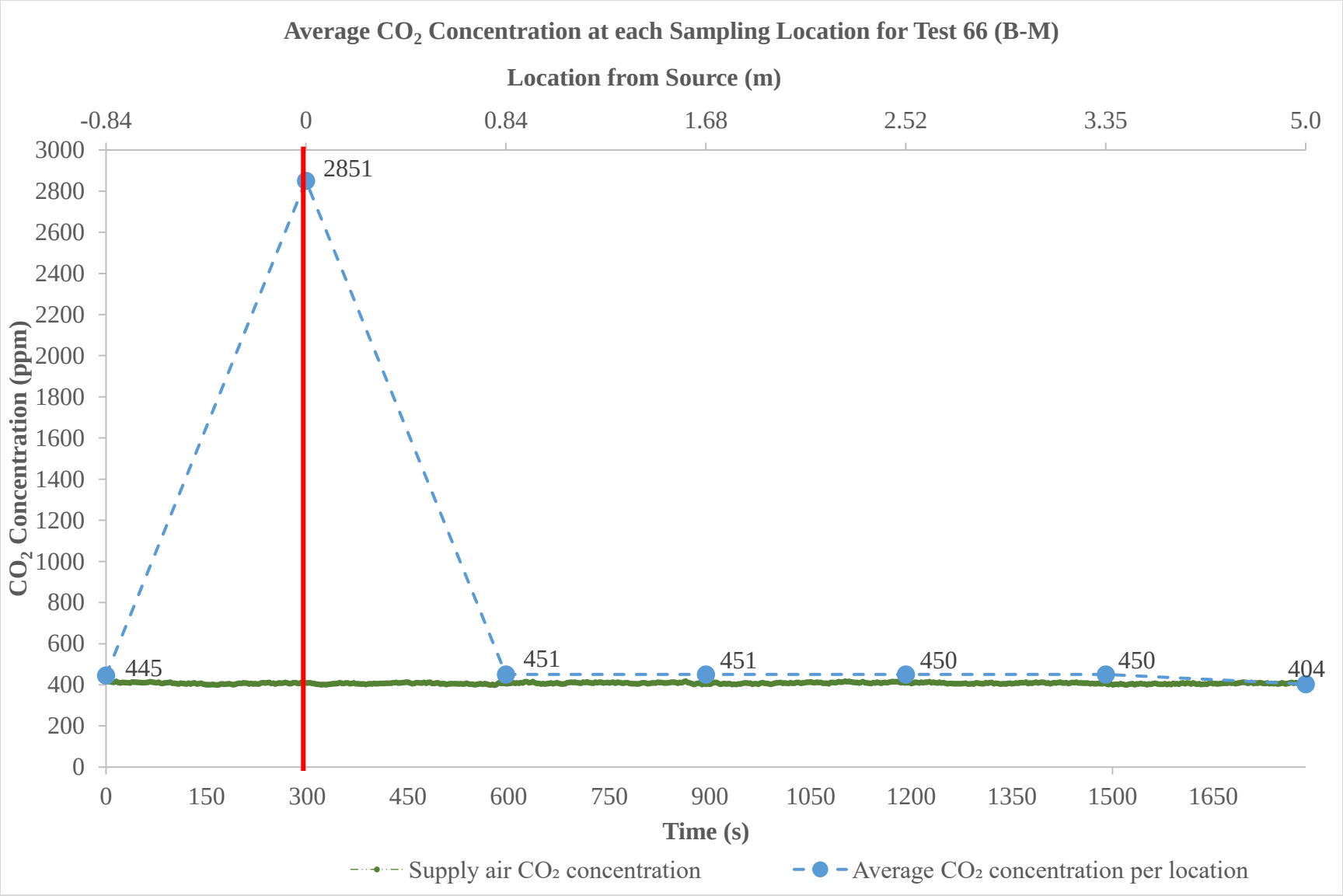

Figure I.85 Average CO_2 concentration at each sampling location for Test 66 (B-M) ISOPass deployed.

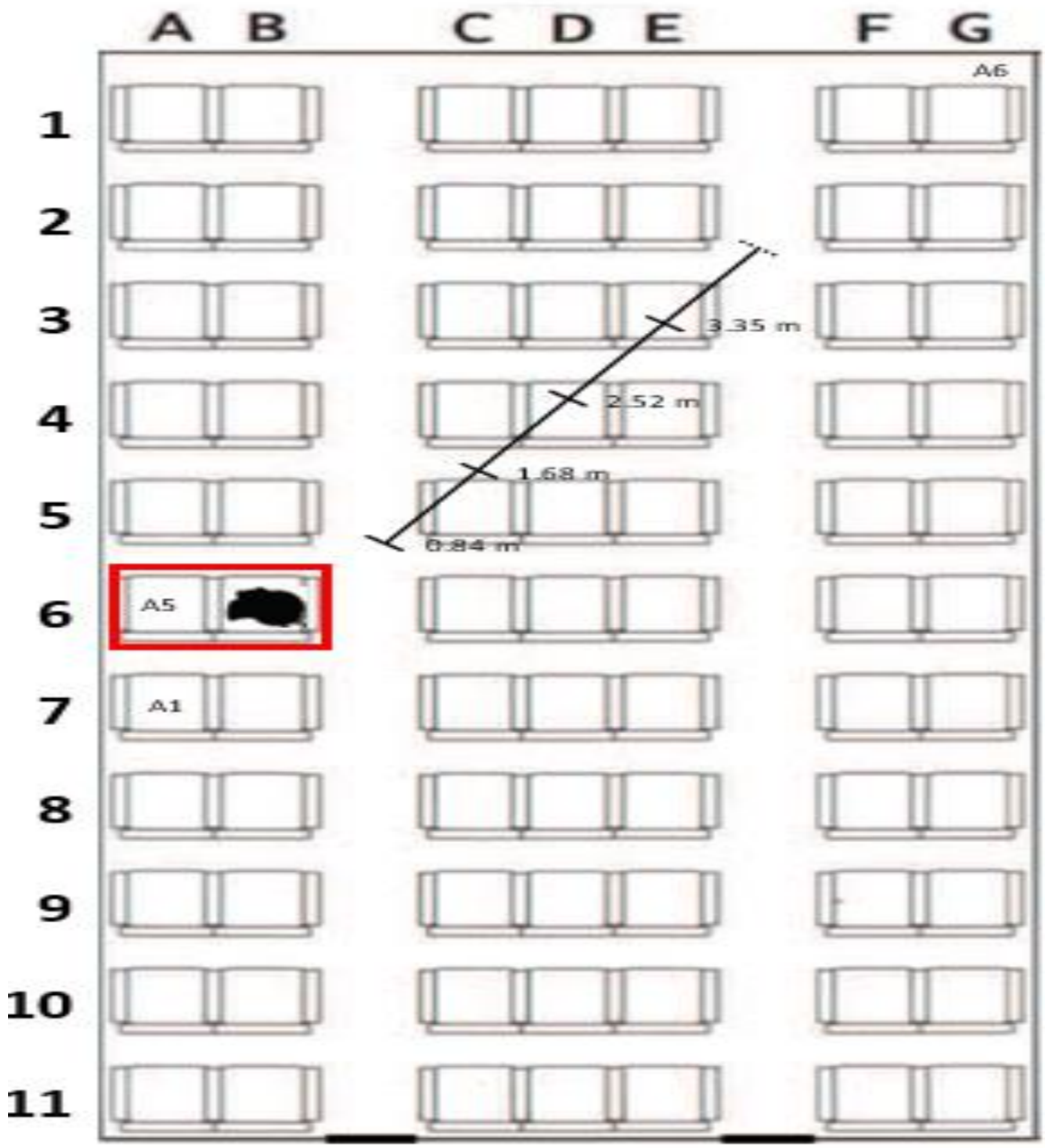

Figure I.86 Test 55 (B-M) ISOPass deployed source location and sampling tree orientation.

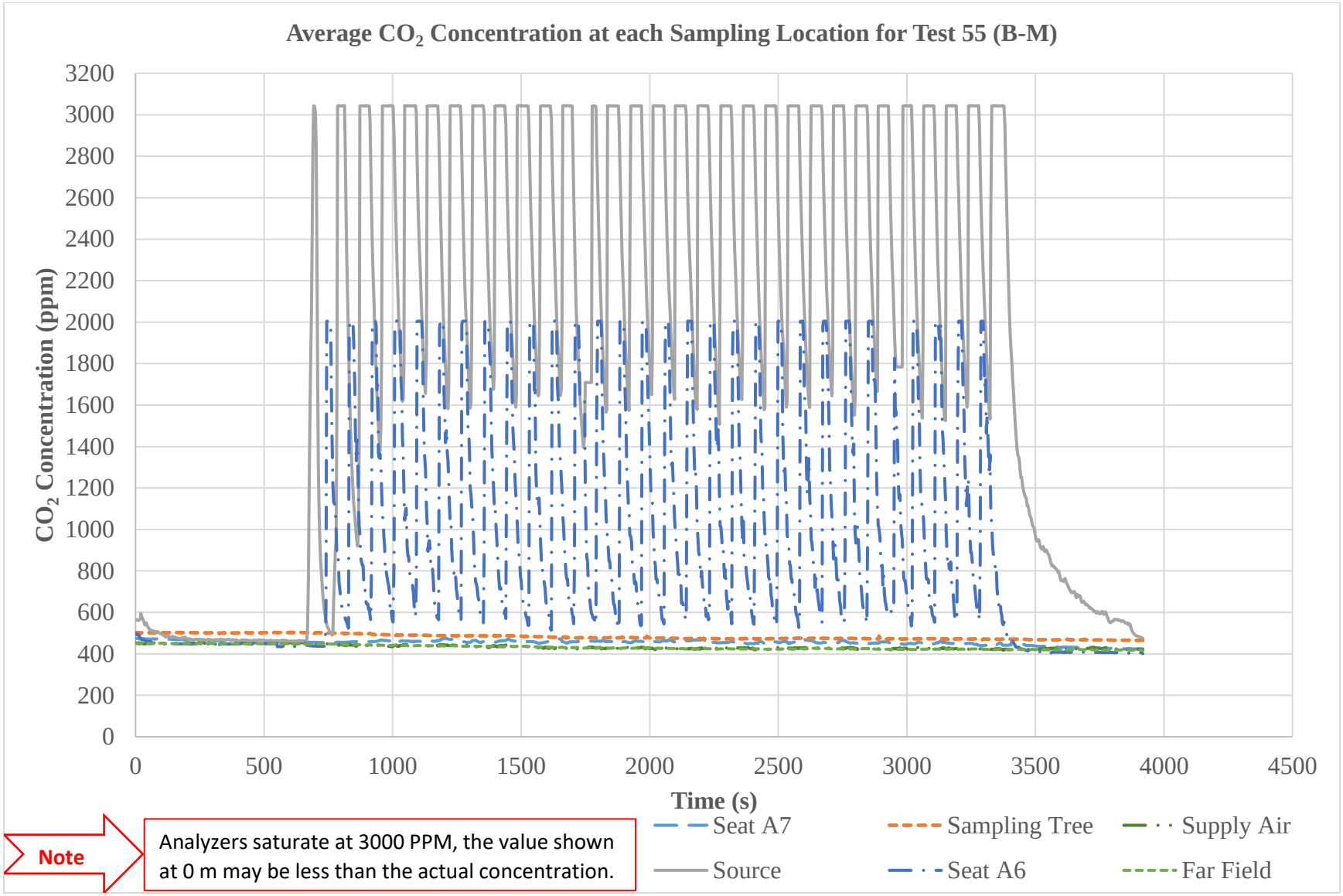

Figure I.87 Ininstantaneous CO_2 concentration at each sampling location for Test 55 (B-M) ISOPass deployed.

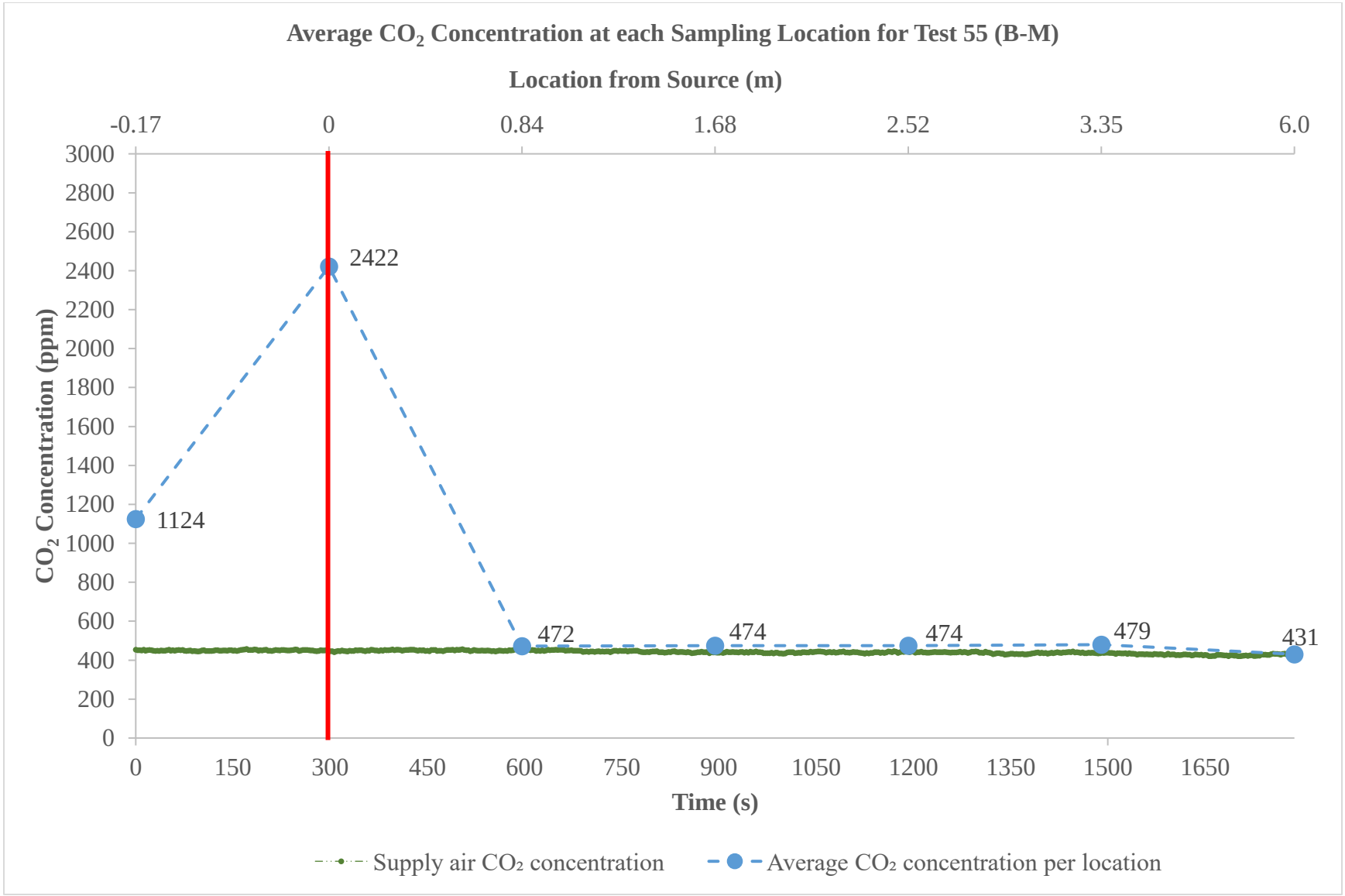

Figure I.88 Average CO_2 concentration at each sampling location for Test 55 (B-M) ISOPass deployed.

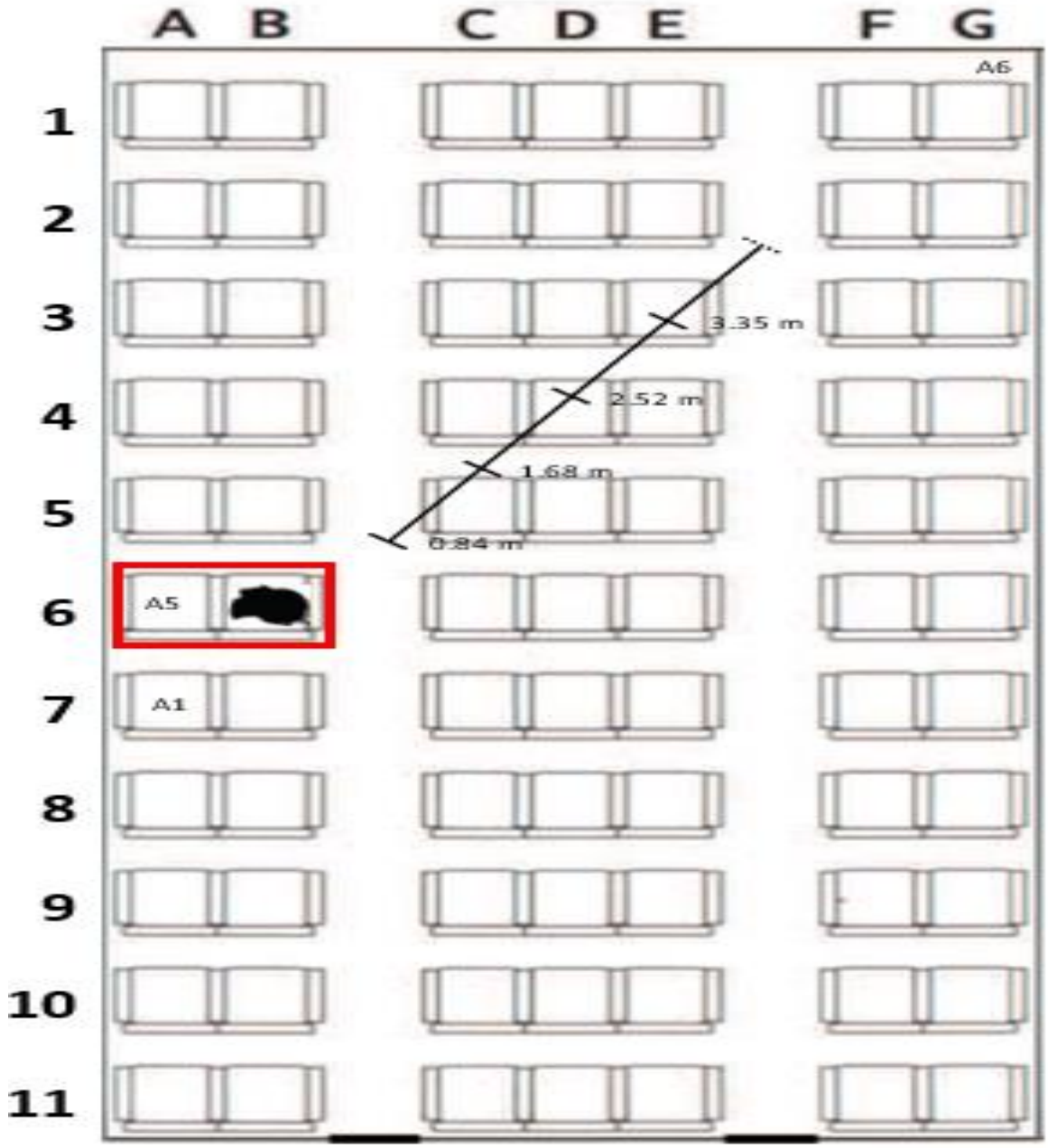

Figure I.89 Test 56 (B-M) ISOPass deployed source location and sampling tree orientation.

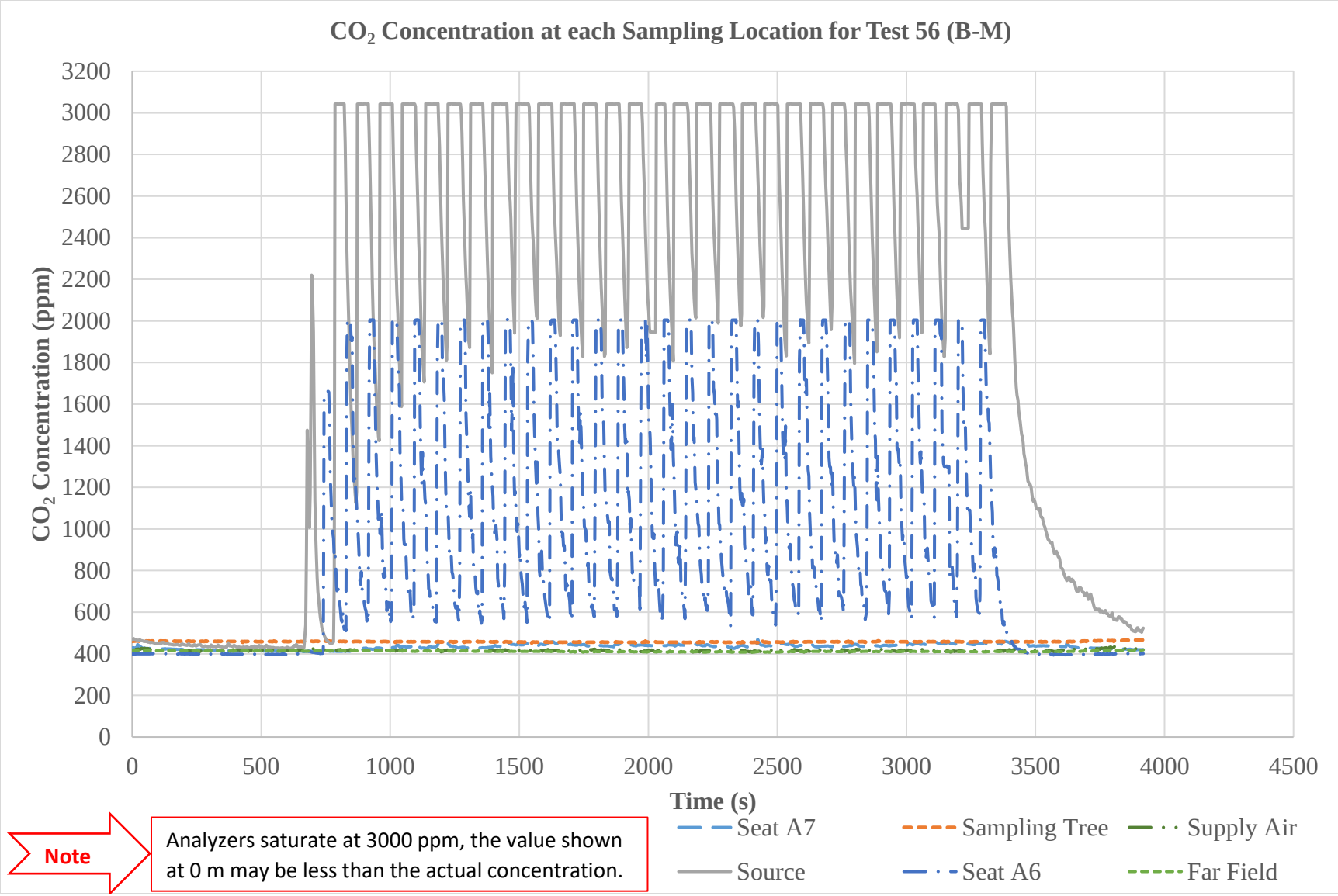

Figure I.90 Ininstantaneous CO_2 concentration at each sampling location for Test 56 (B-M) ISOPass deployed.

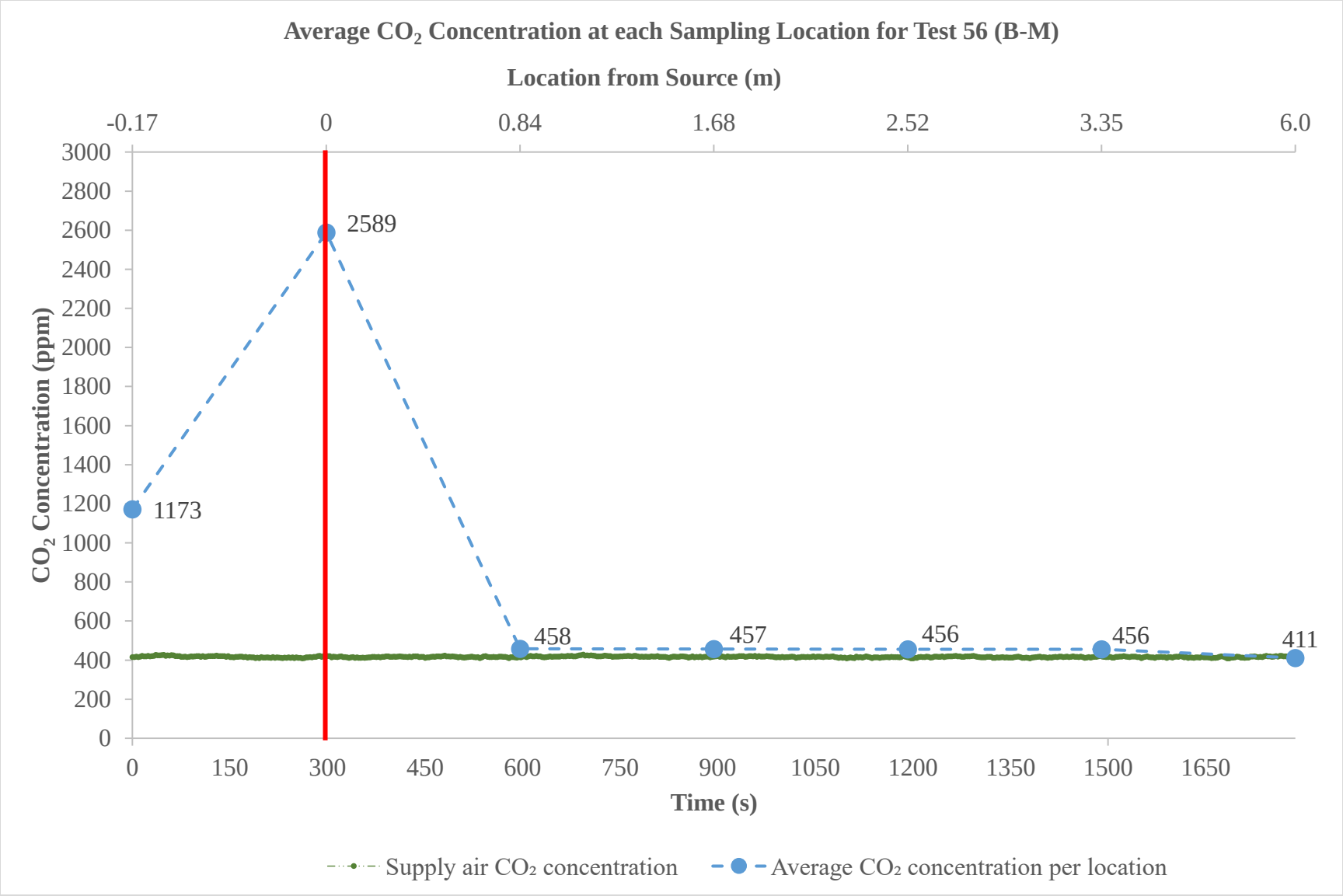

Figure I.91 Average CO_2 concentration at each sampling location for Test 56 (B-M) ISOPass deployed.

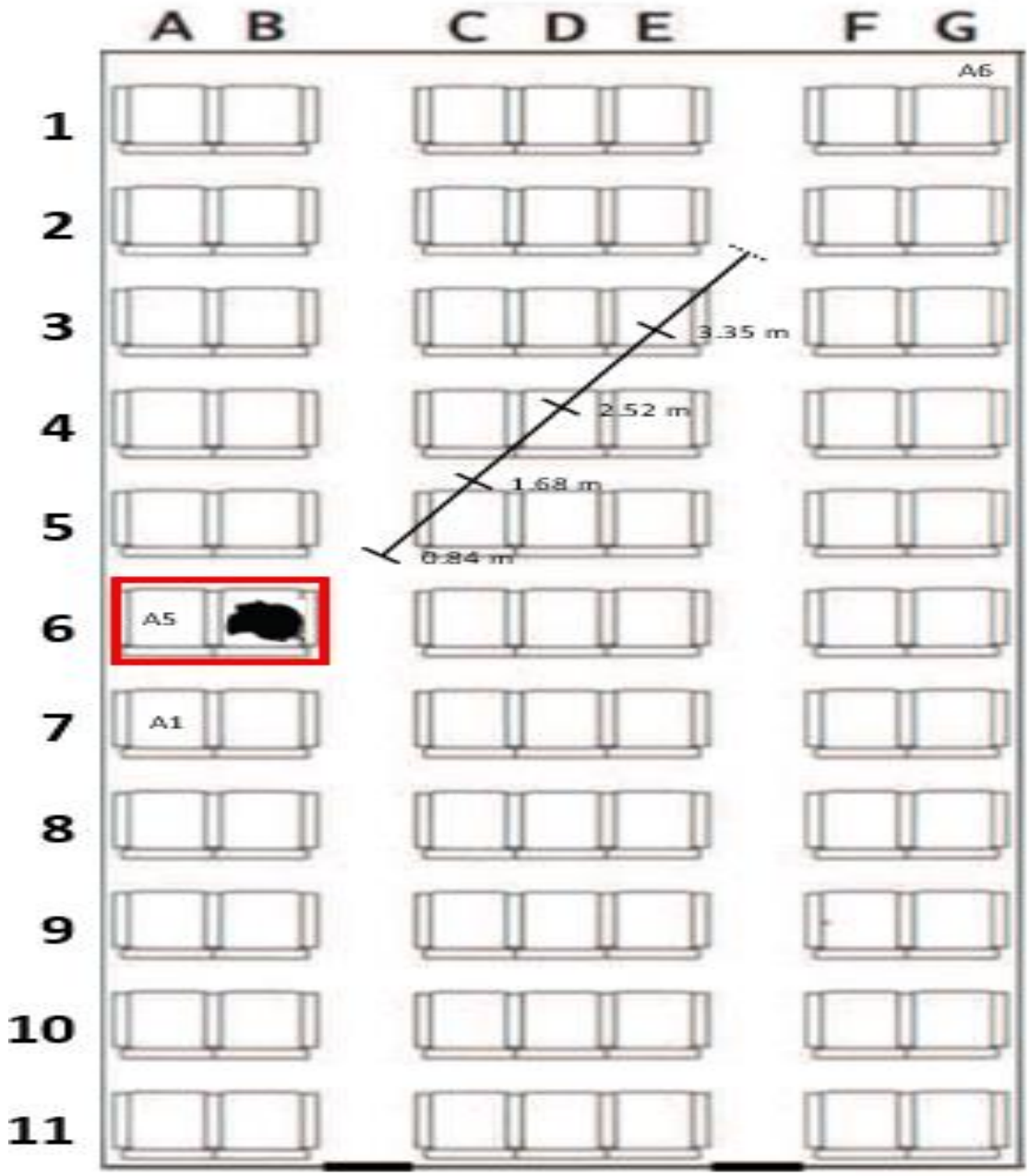

Figure I.92 Test 57 (B-M) ISOPass deployed source location and sampling tree orientation.

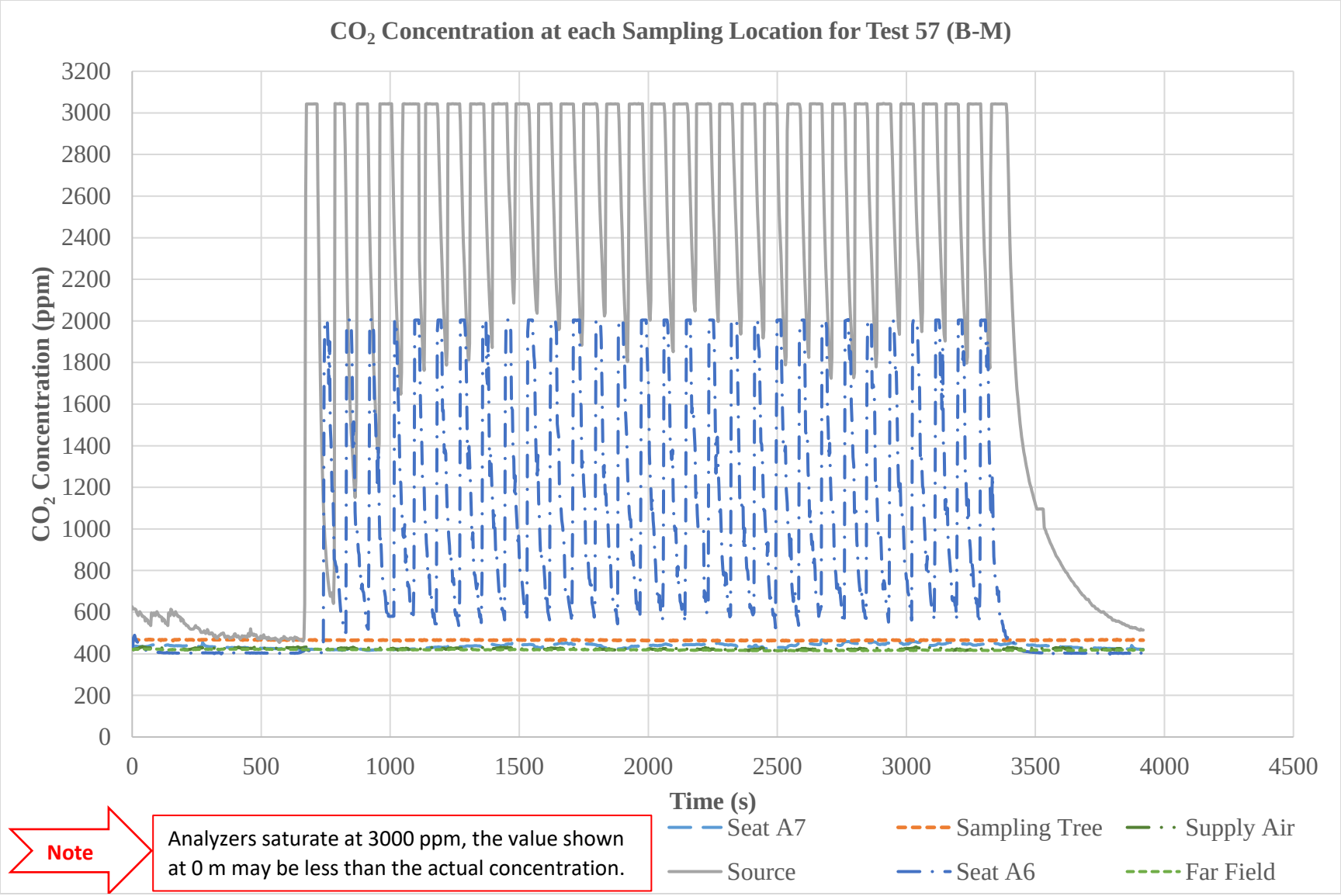

Figure I.93 Ininstantaneous CO_2 concentration at each sampling location for Test 57 (B-M) ISOPass deployed.

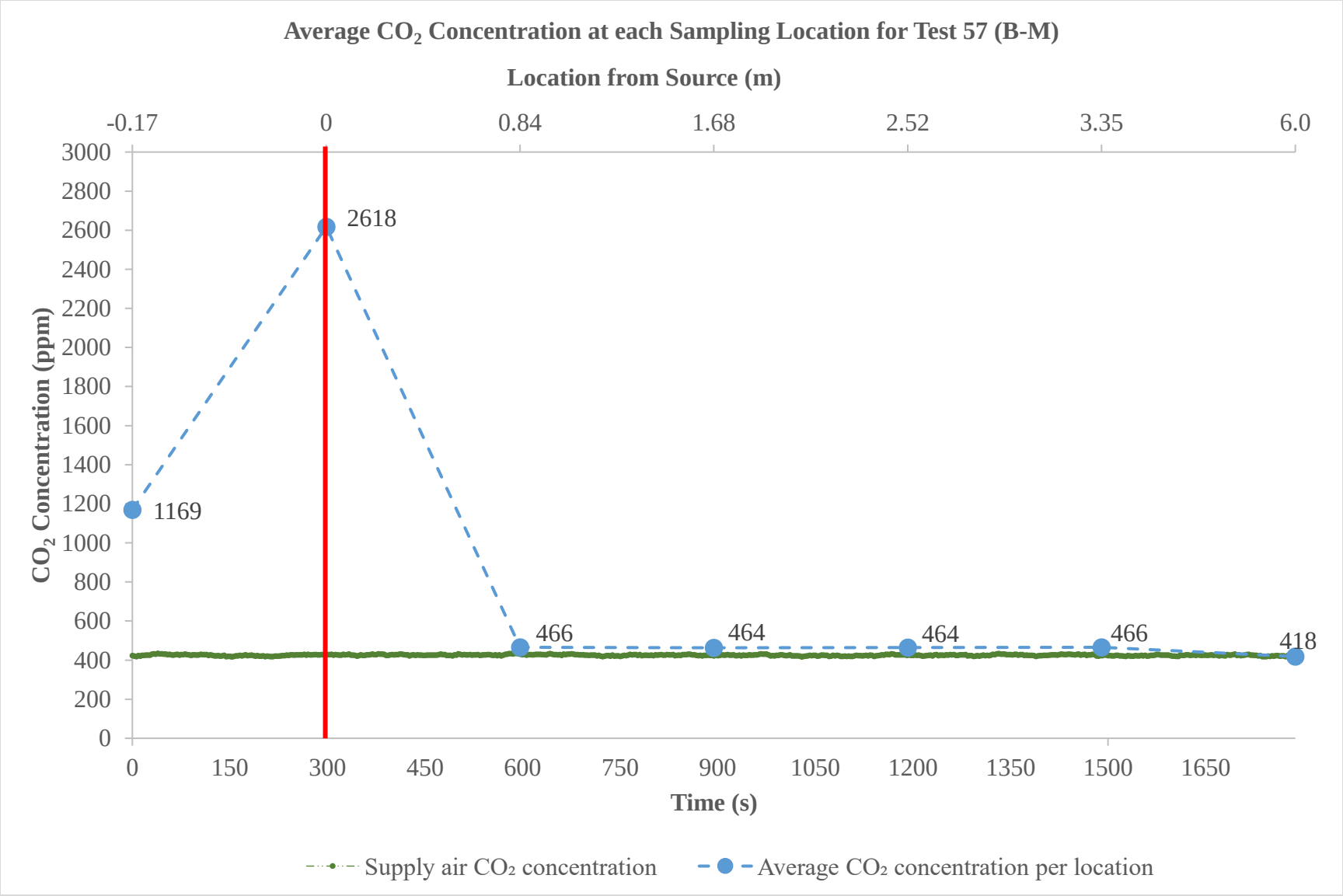

Figure I.94 Average CO_2 concentration at each sampling location for Test 57 (B-M) ISOPass deployed.

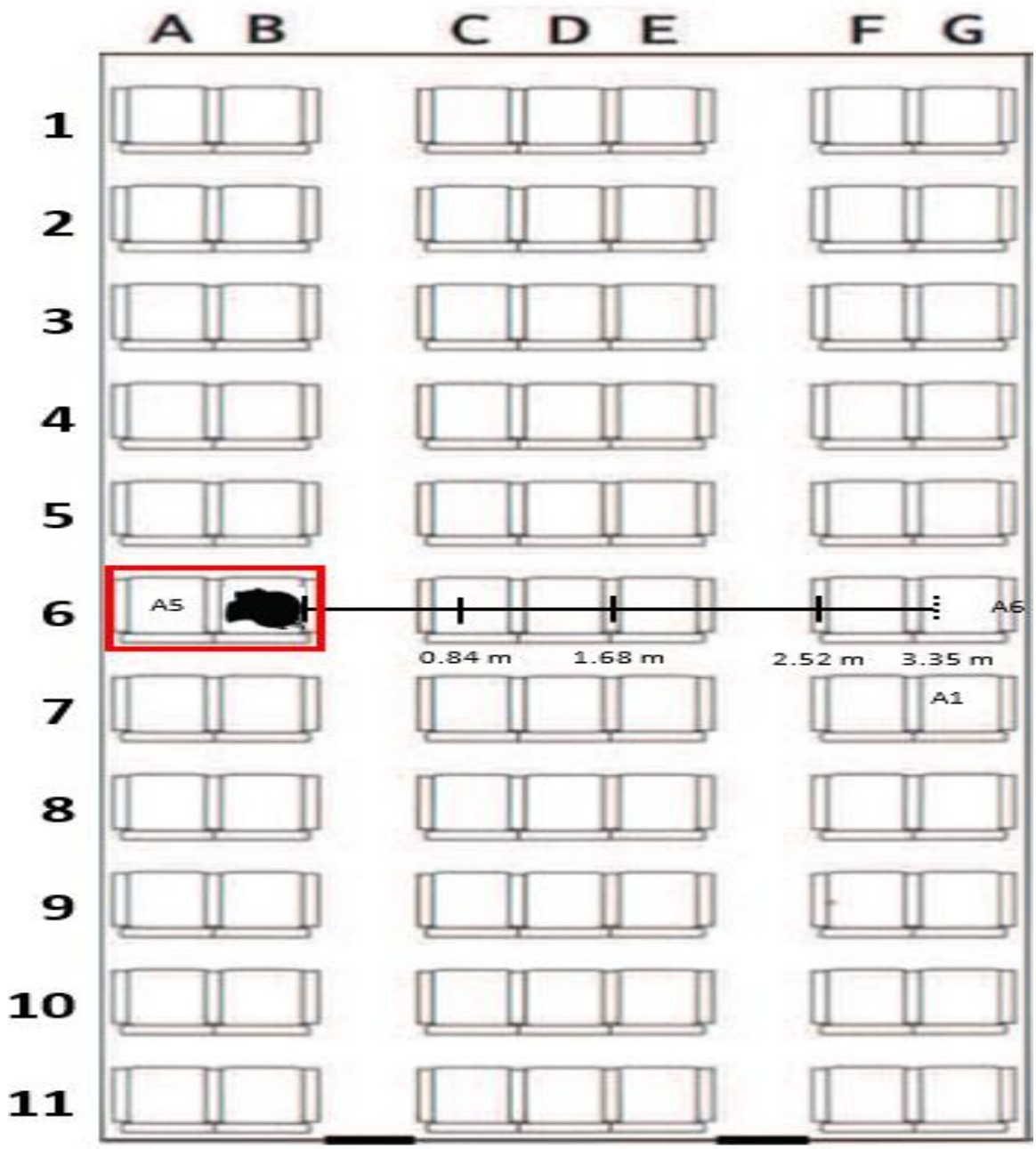

Figure I.95 Test 58 (B-M) ISOPass deployed source location and sampling tree orientation.

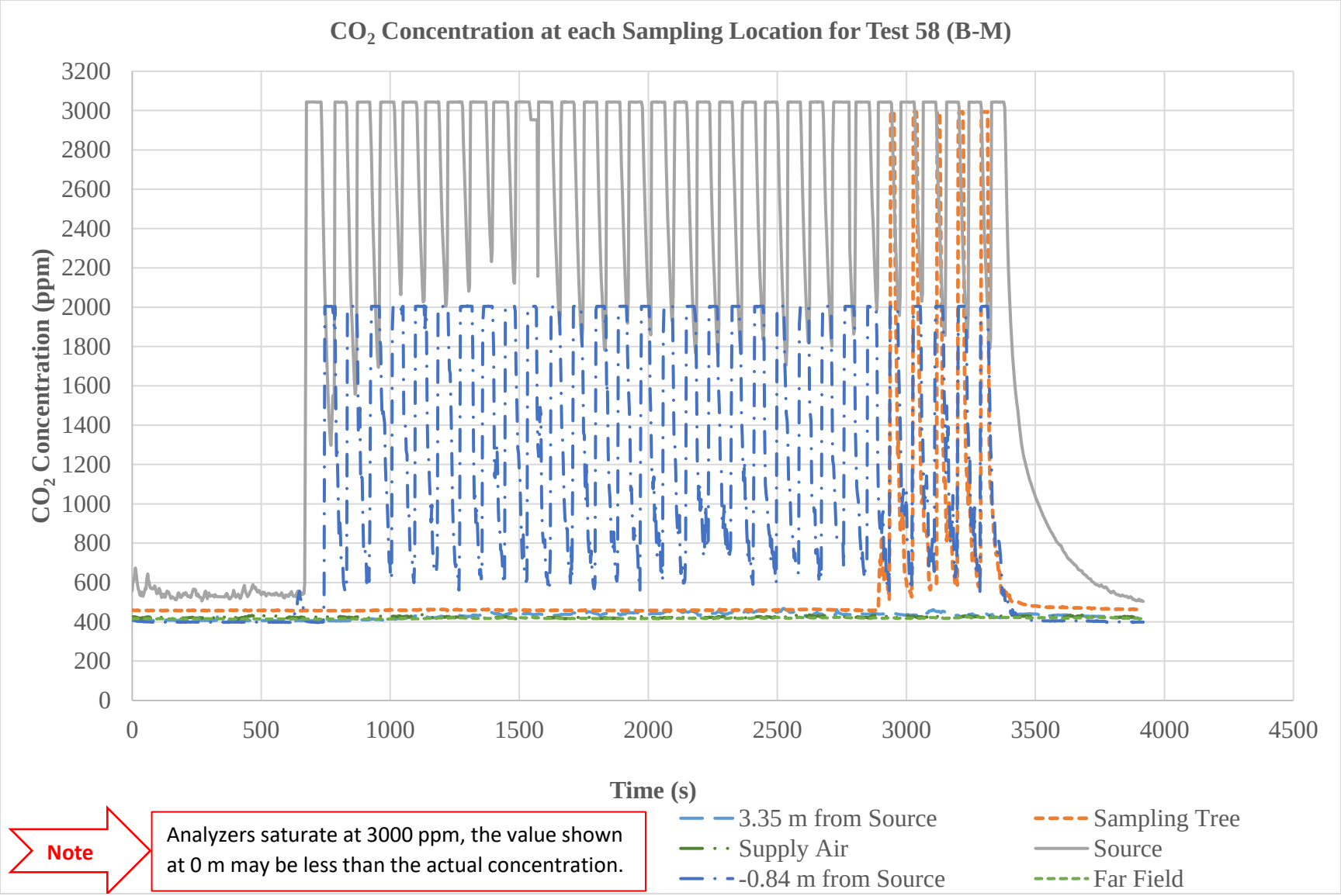

Figure I.96 Ininstantaneous CO_2 concentration at each sampling location for Test 58 (B-M) ISOPass deployed.

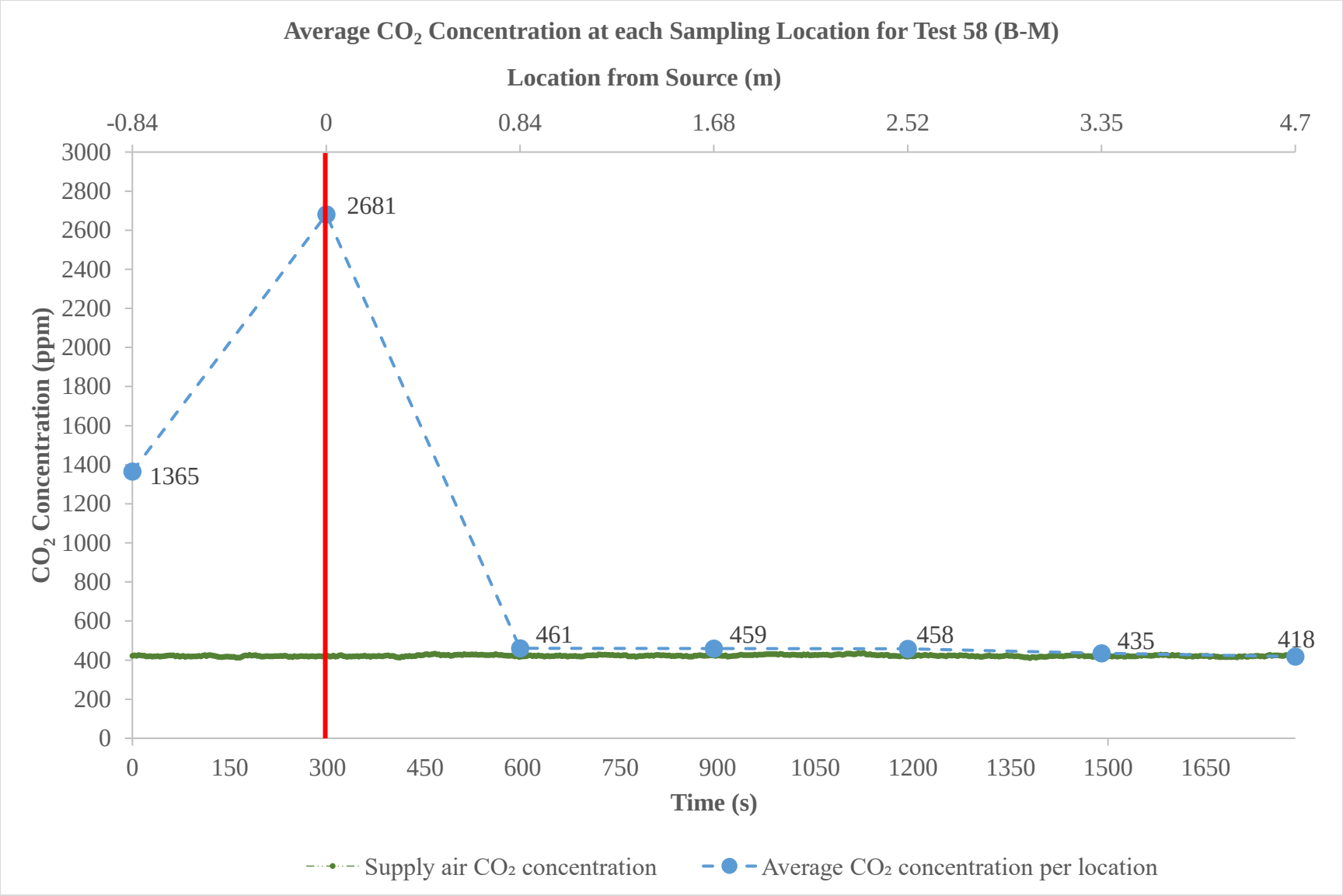

Figure I.97 Average CO_2 concentration at each sampling location for Test 58 (B-M) ISOPass deployed.

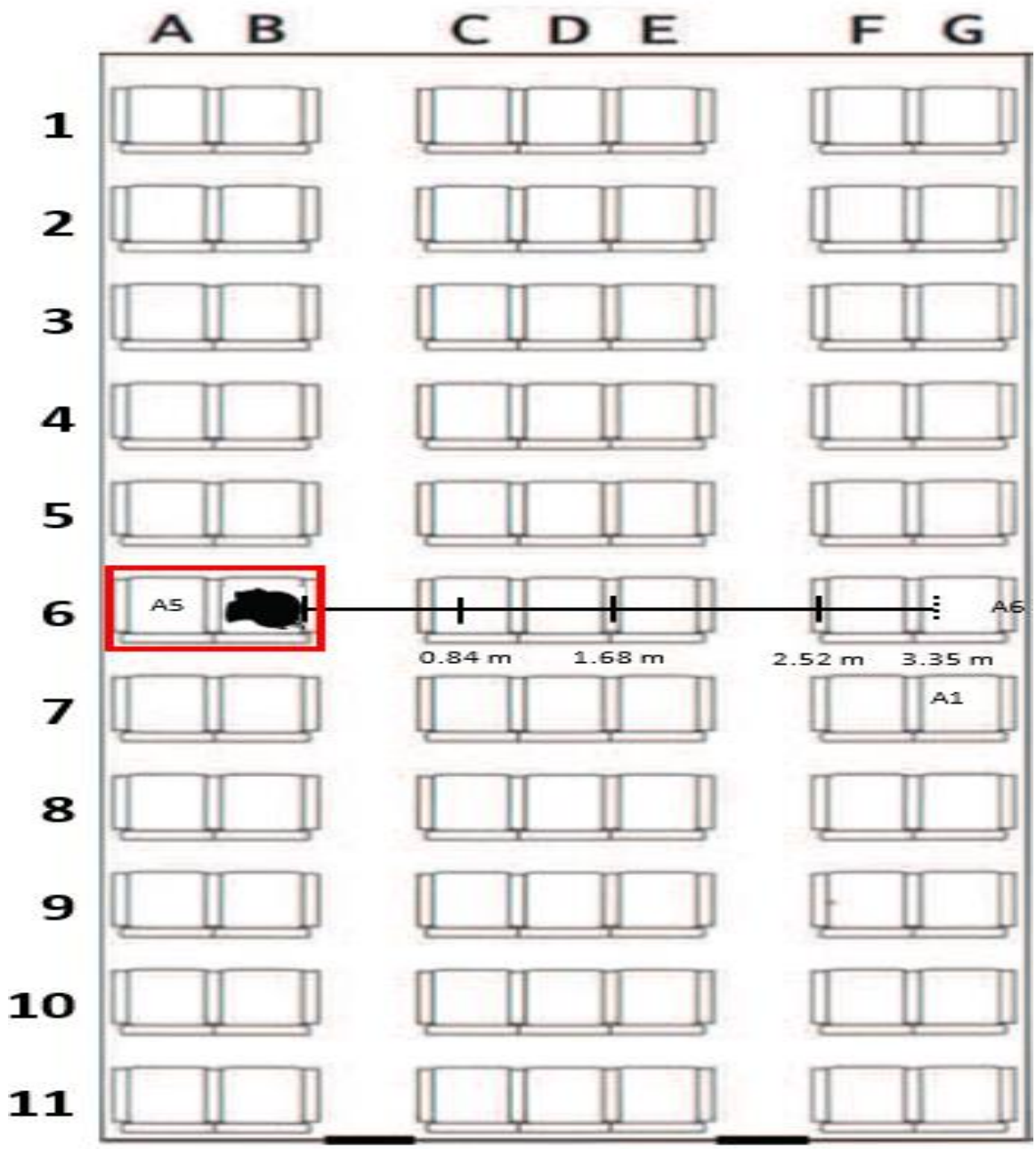

Figure I.98 Test 59 (B-M) ISOPass deployed source location and sampling tree orientation.

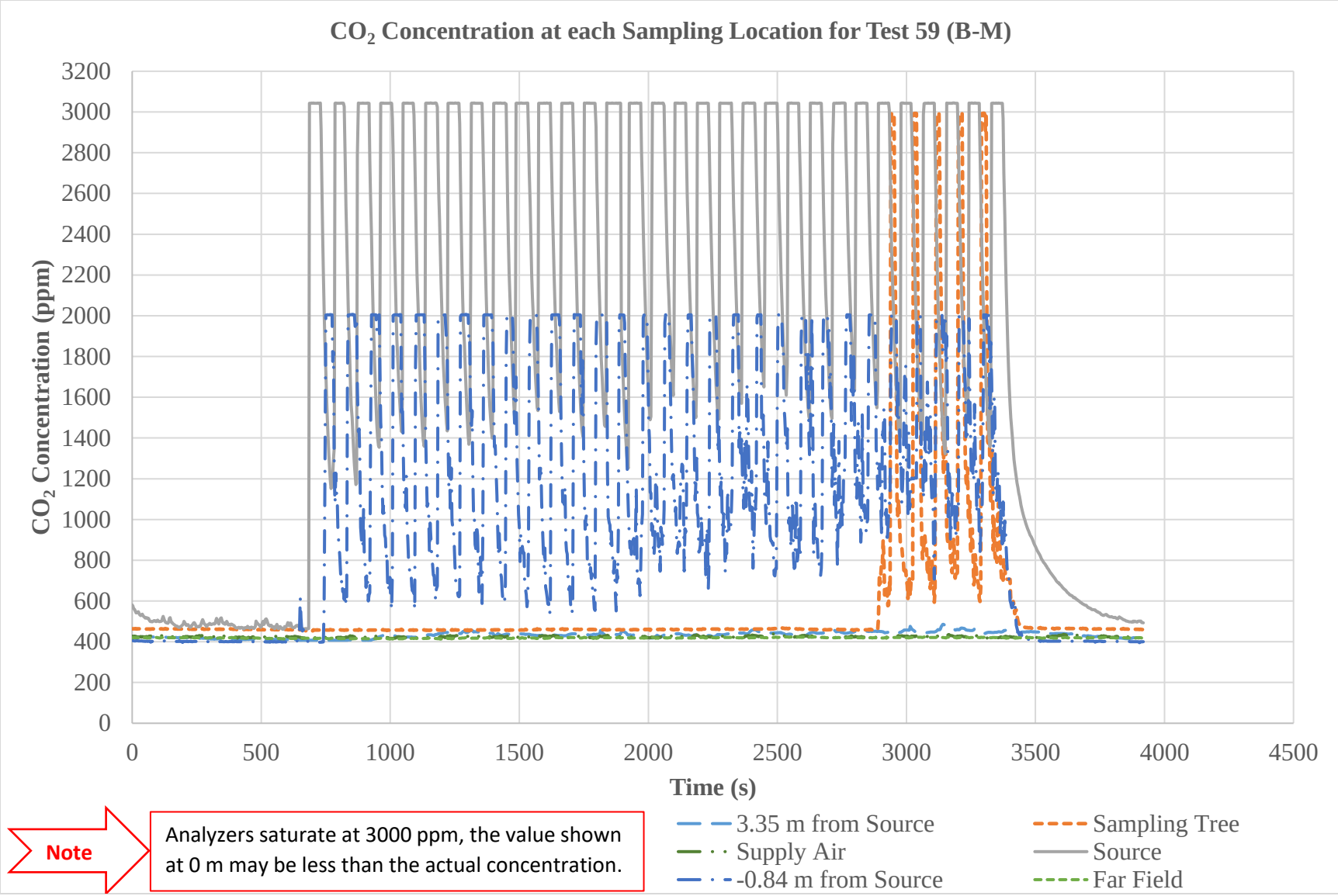

Figure I.99 Ininstantaneous CO_2 concentration at each sampling location for Test 59 (B-M) ISOPass deployed.

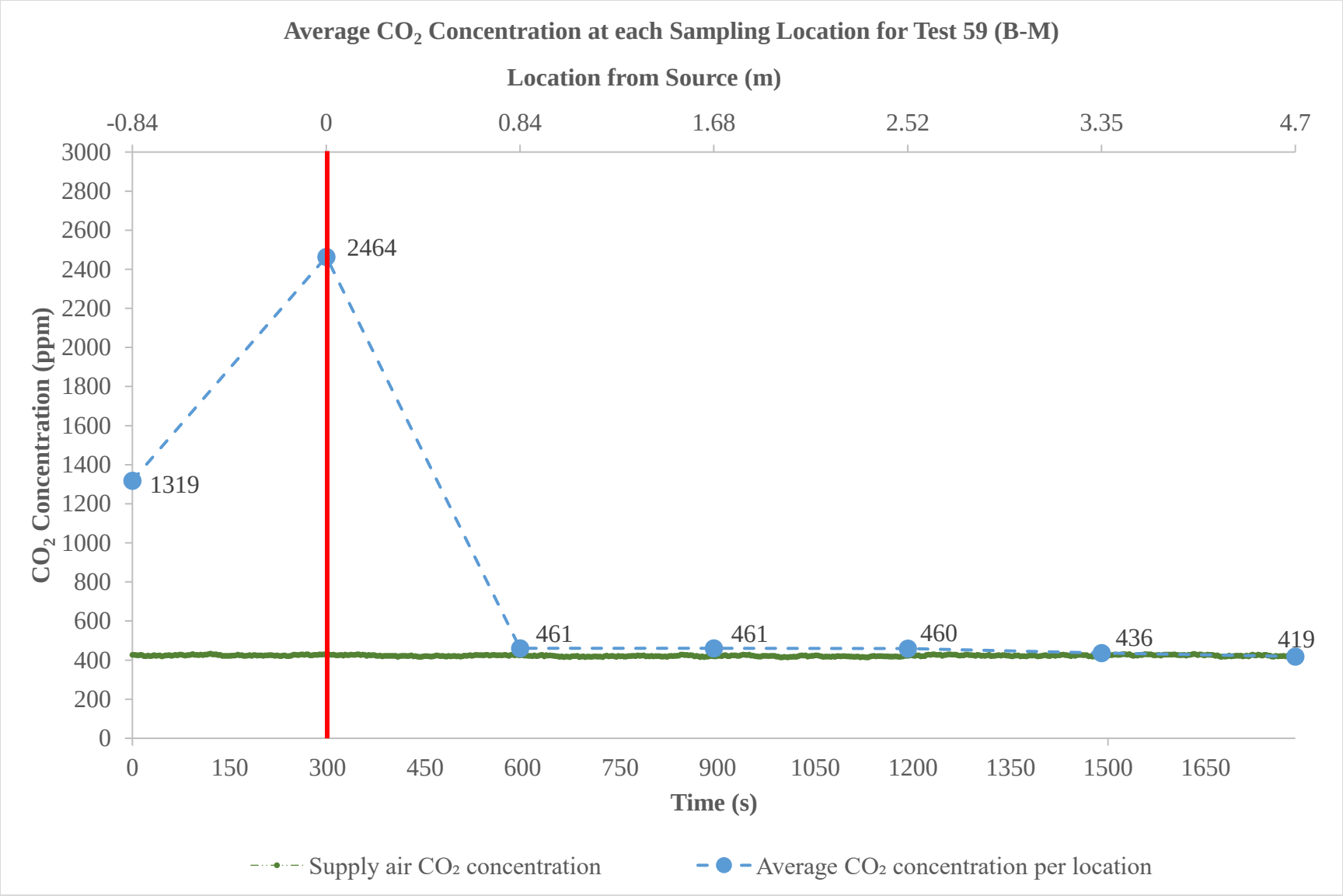

Figure I.100 Average CO_2 concentration at each sampling location for Test 59 (B-M) ISOPass deployed.

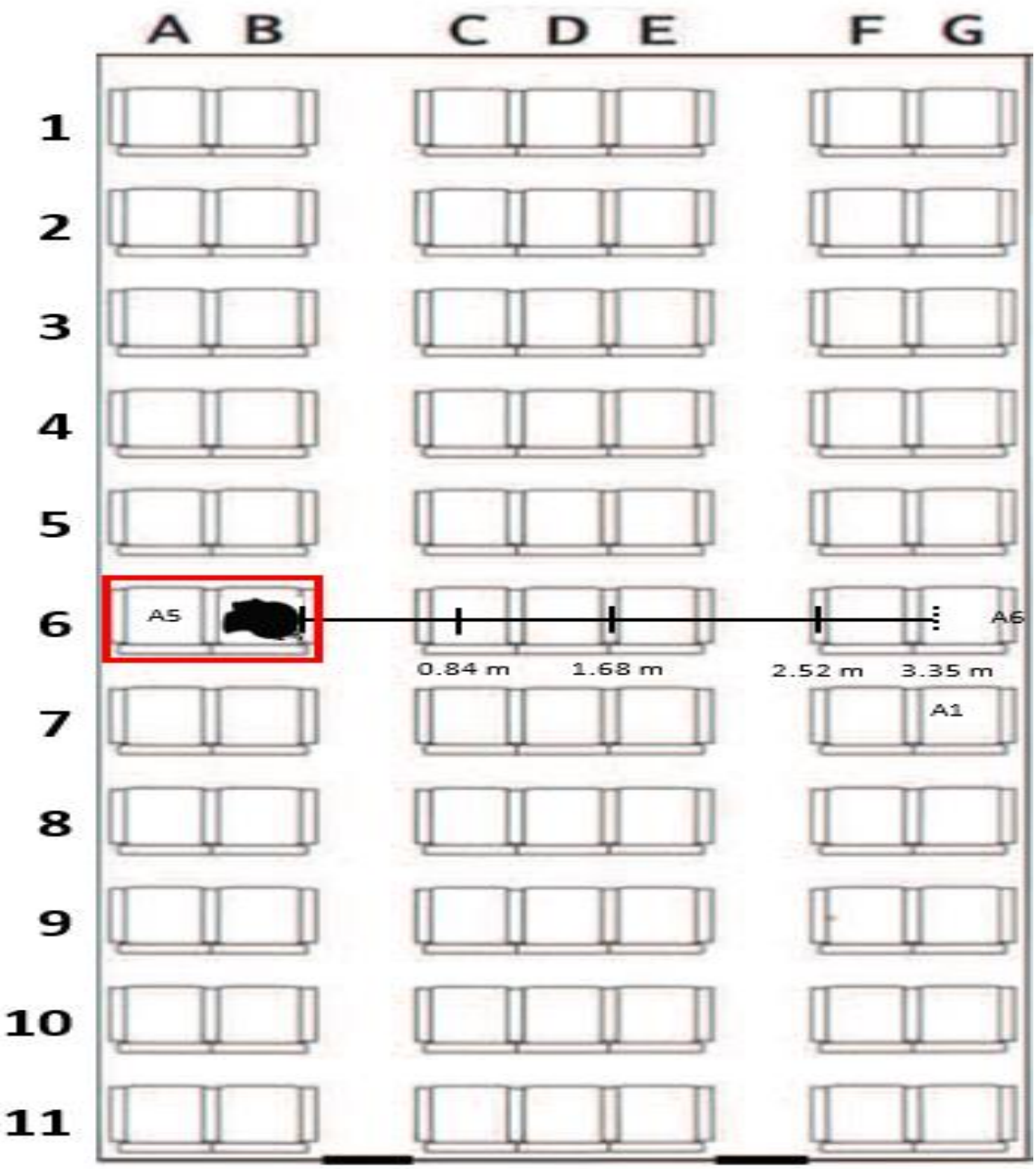

Figure I.101 Test 60 (B-M) ISOPass deployed source location and sampling tree orientation.

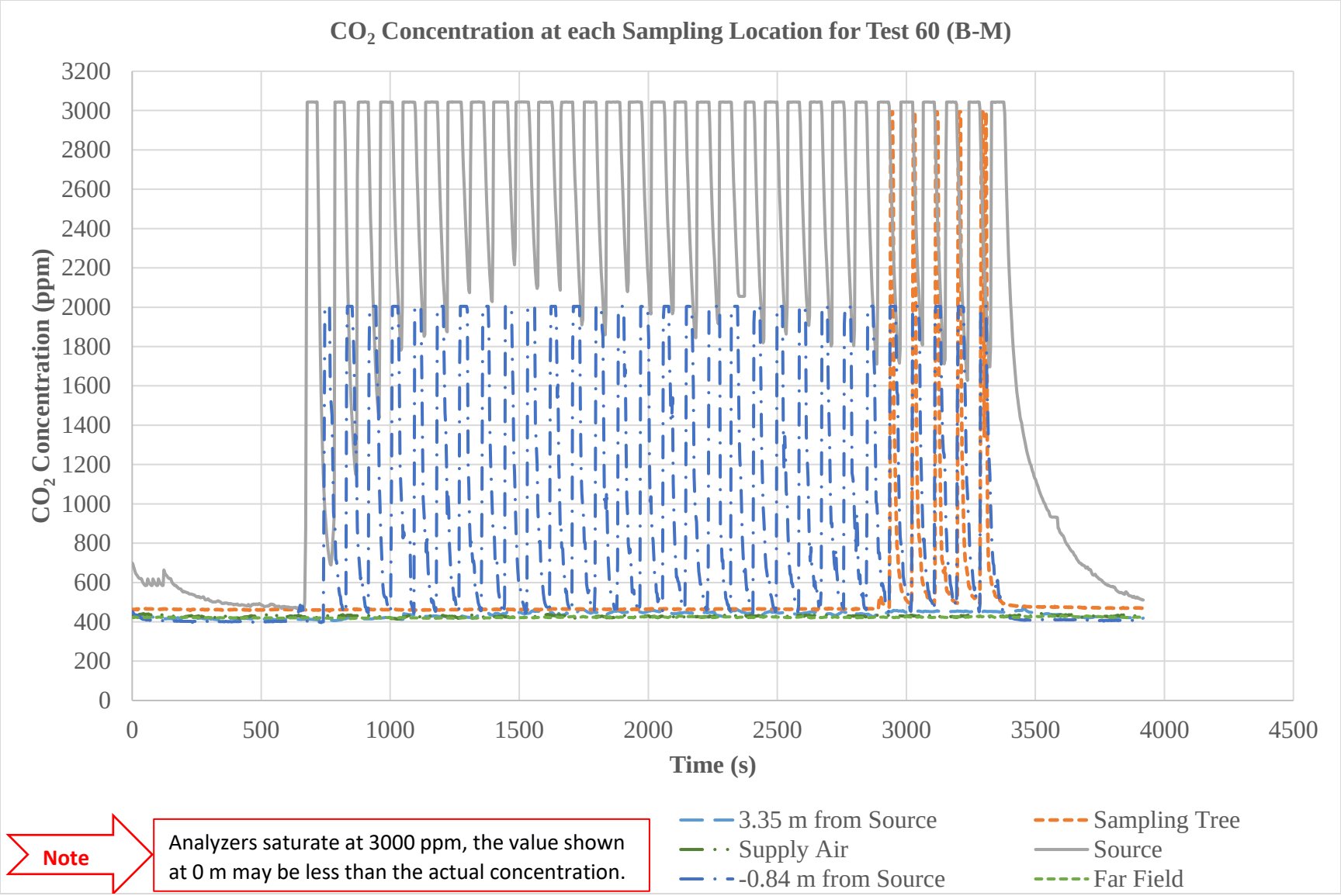

Figure I.102 Ininstantaneous CO_2 concentration at each sampling location for Test 60 (B-M) ISOPass deployed.

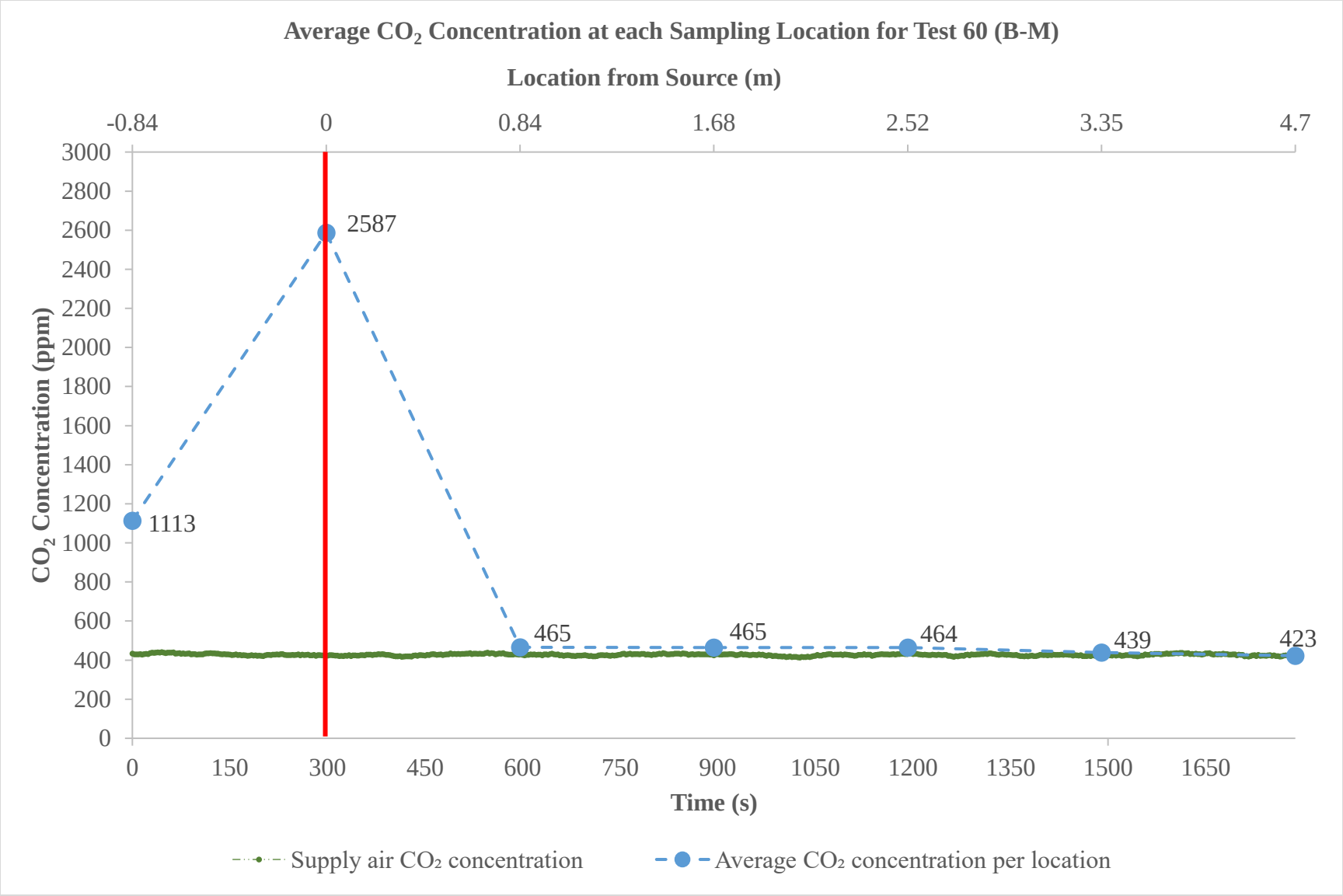

Figure I.103 Average CO_2 concentration at each sampling location for Test 60 (B-M) ISOPass deployed.

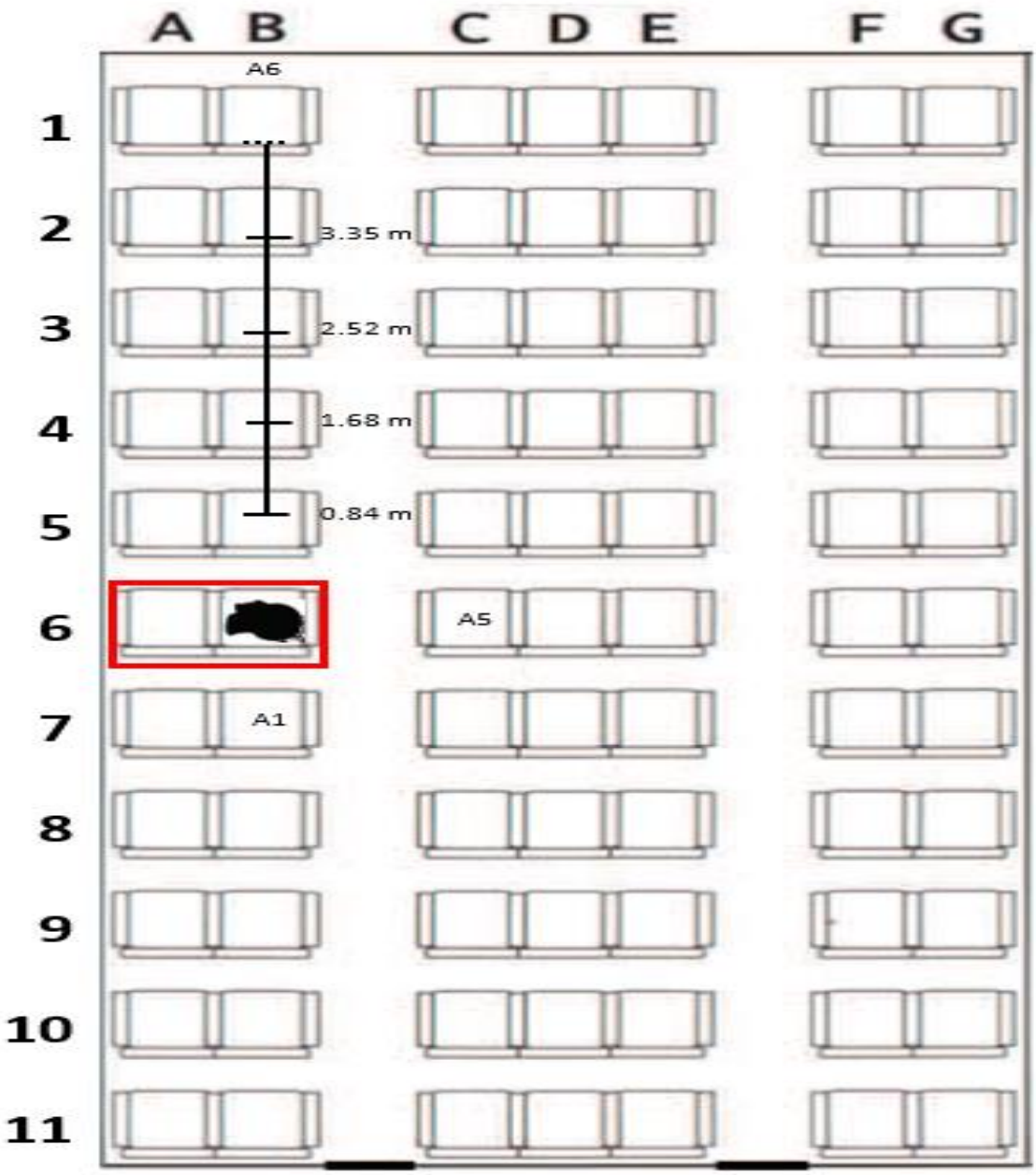

Figure I.104 Test 61 (B-M) ISOPass deployed source location and sampling tree orientation.

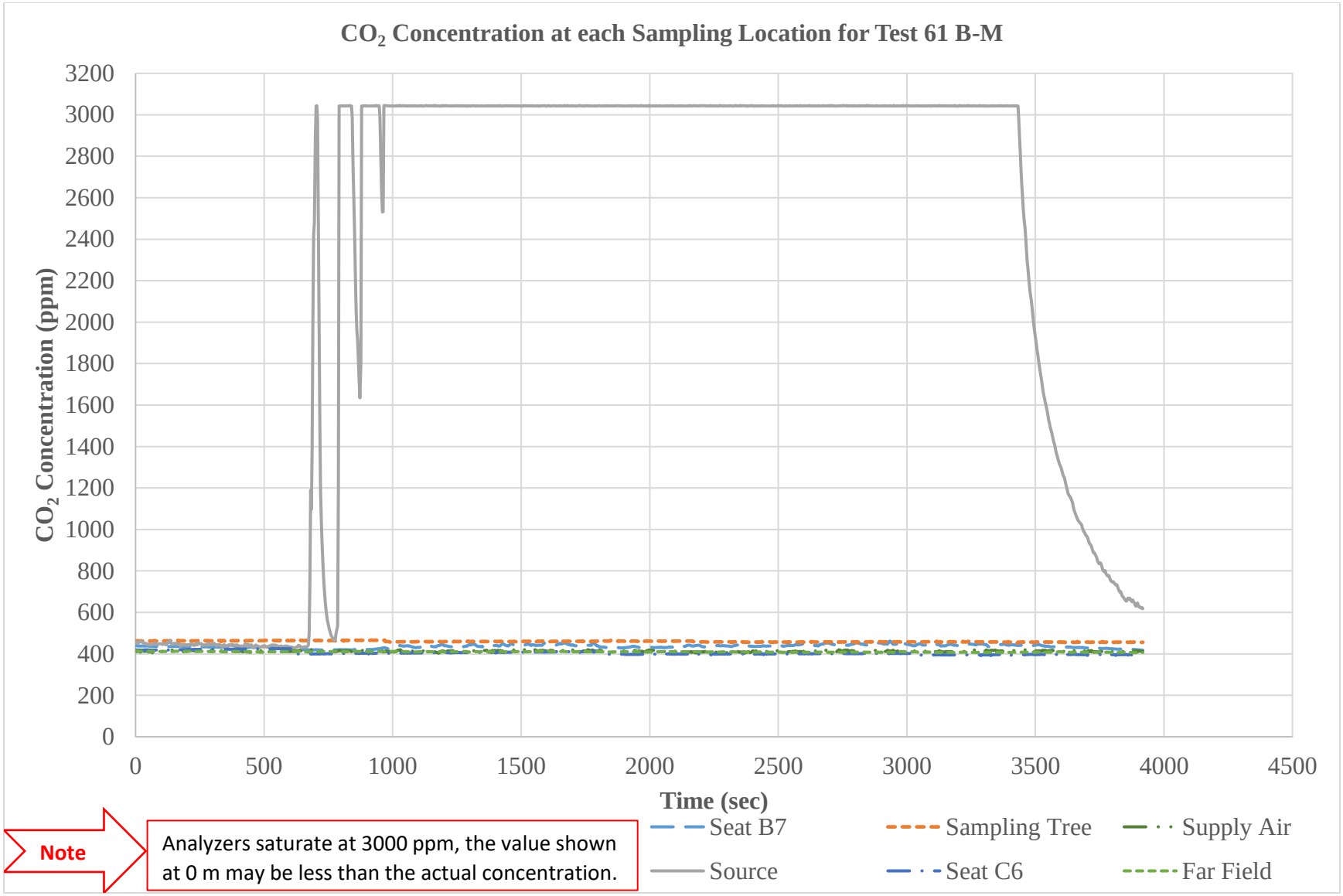

Figure I.105 Ininstantaneous CO_2 concentration at each sampling location for Test 61 (B-M) ISOPass deployed.

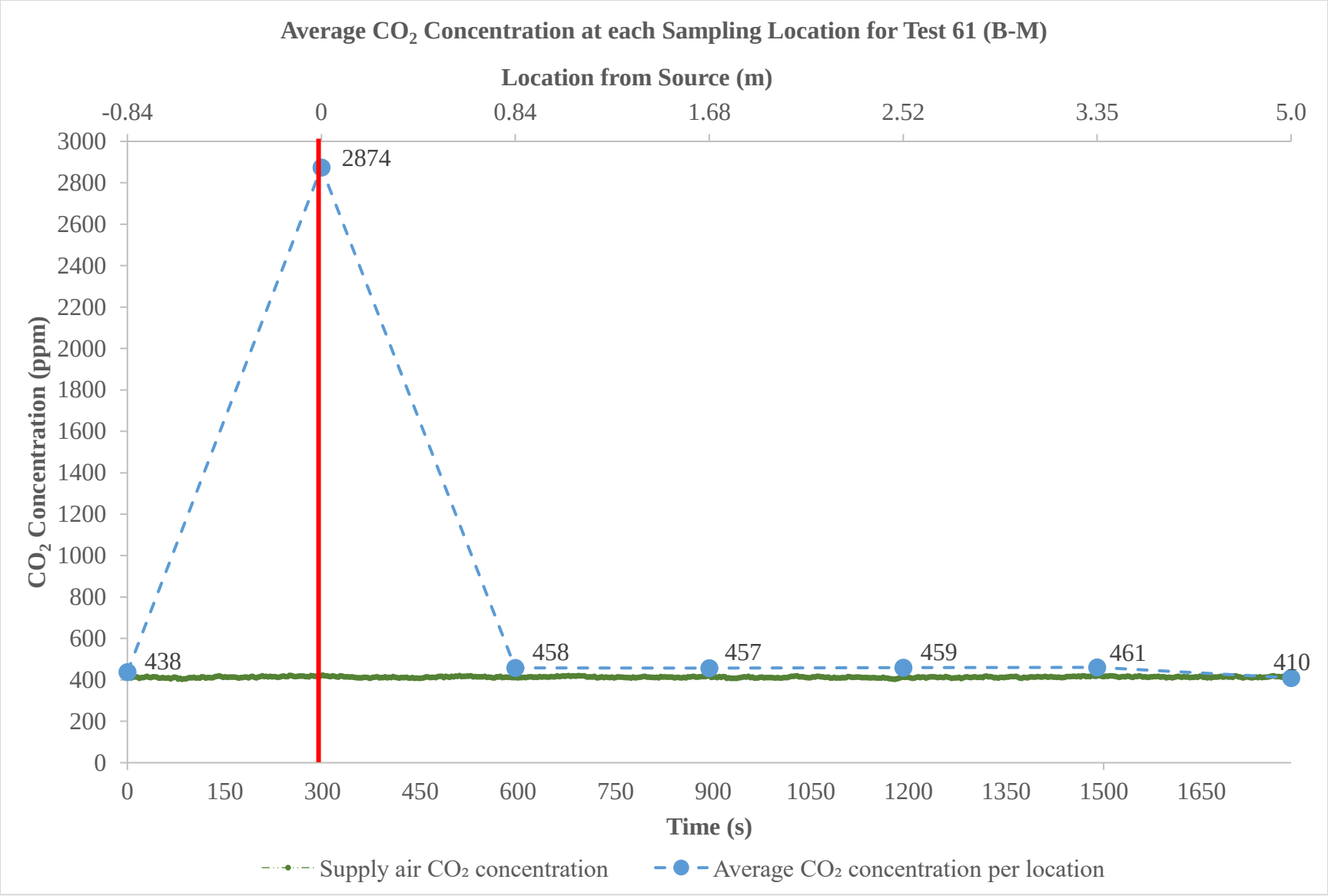

Figure I.106 Average CO_2 concentration at each sampling location for Test 61 (B-M) ISOPass deployed.

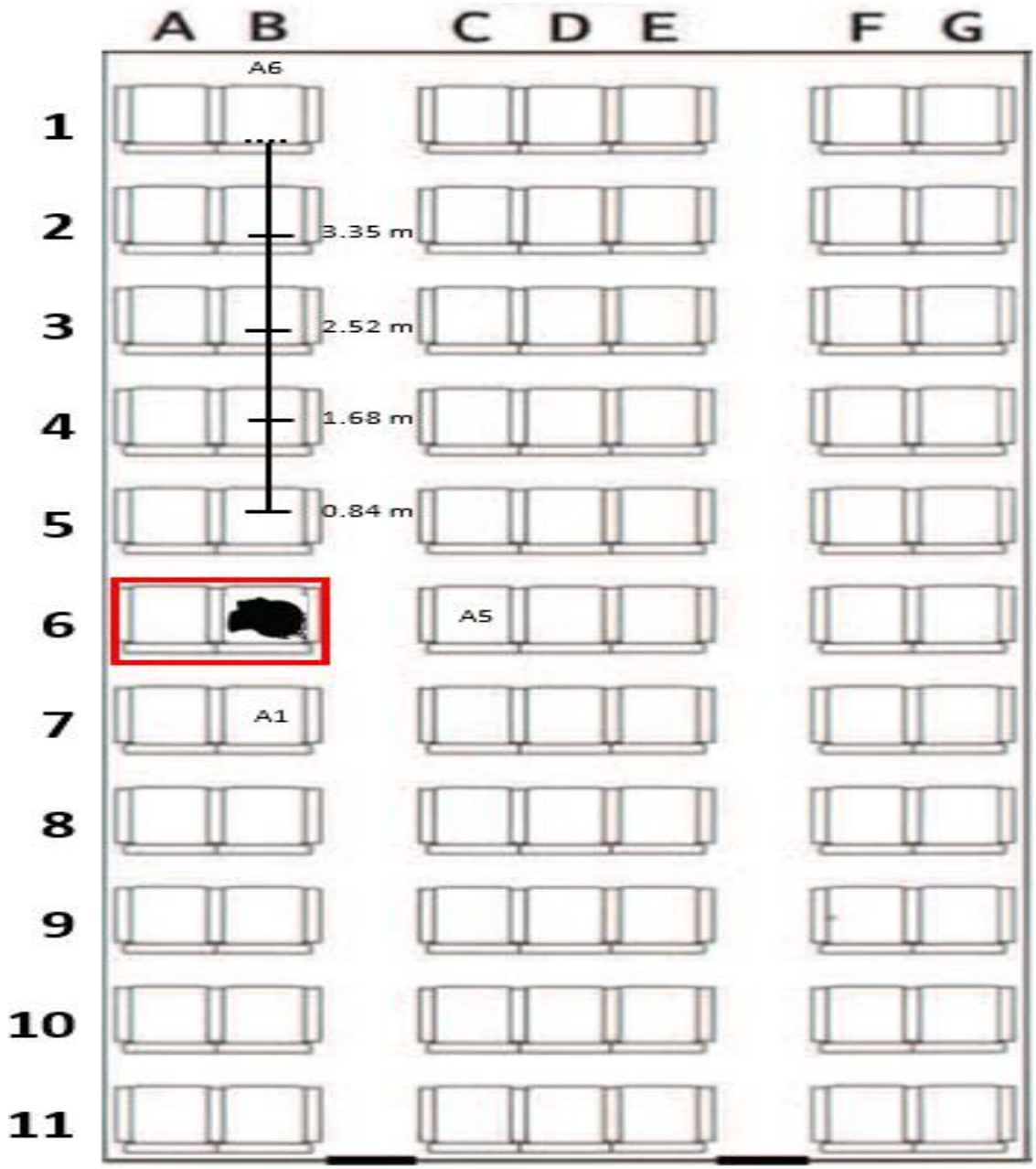

Figure I.107 Test 62 (B-M) ISOPass deployed source location and sampling tree orientation.

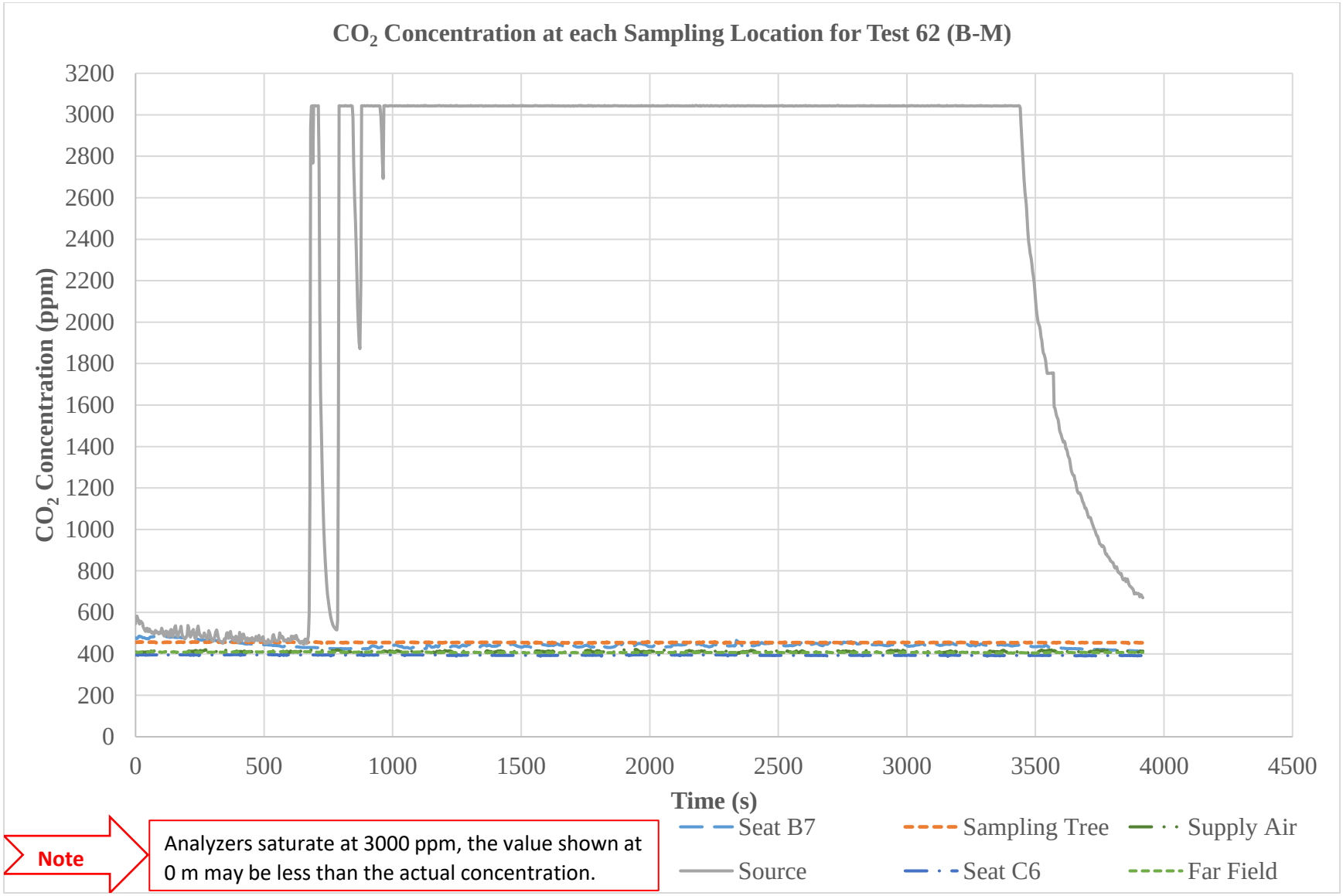

Figure I.108 Ininstantaneous CO_2 concentration at each sampling location for Test 62 (B-M) ISOPass deployed.

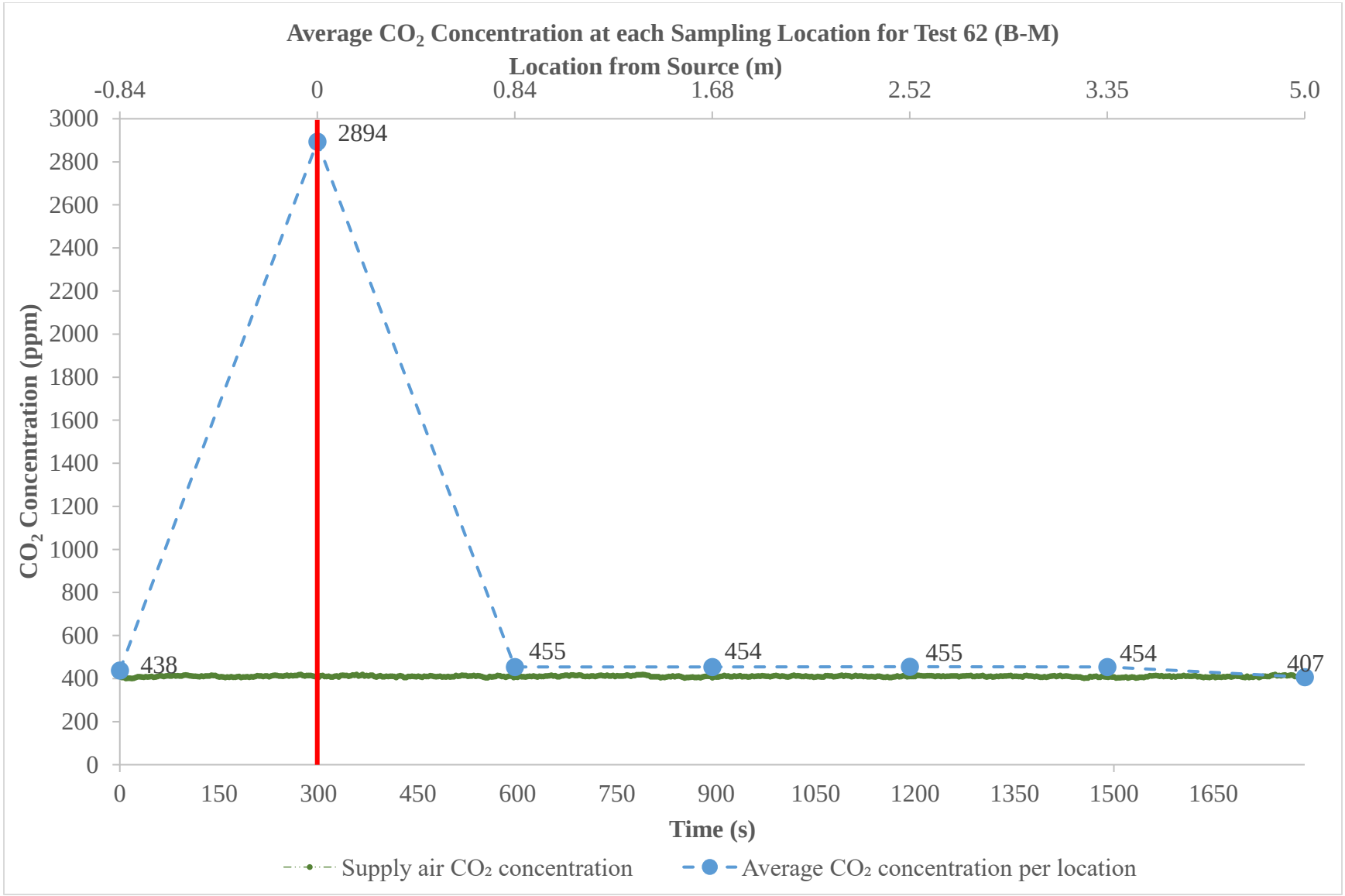

Figure I.109 Average CO_2 concentration at each sampling location for Test 62 (B-M) ISOPass deployed.

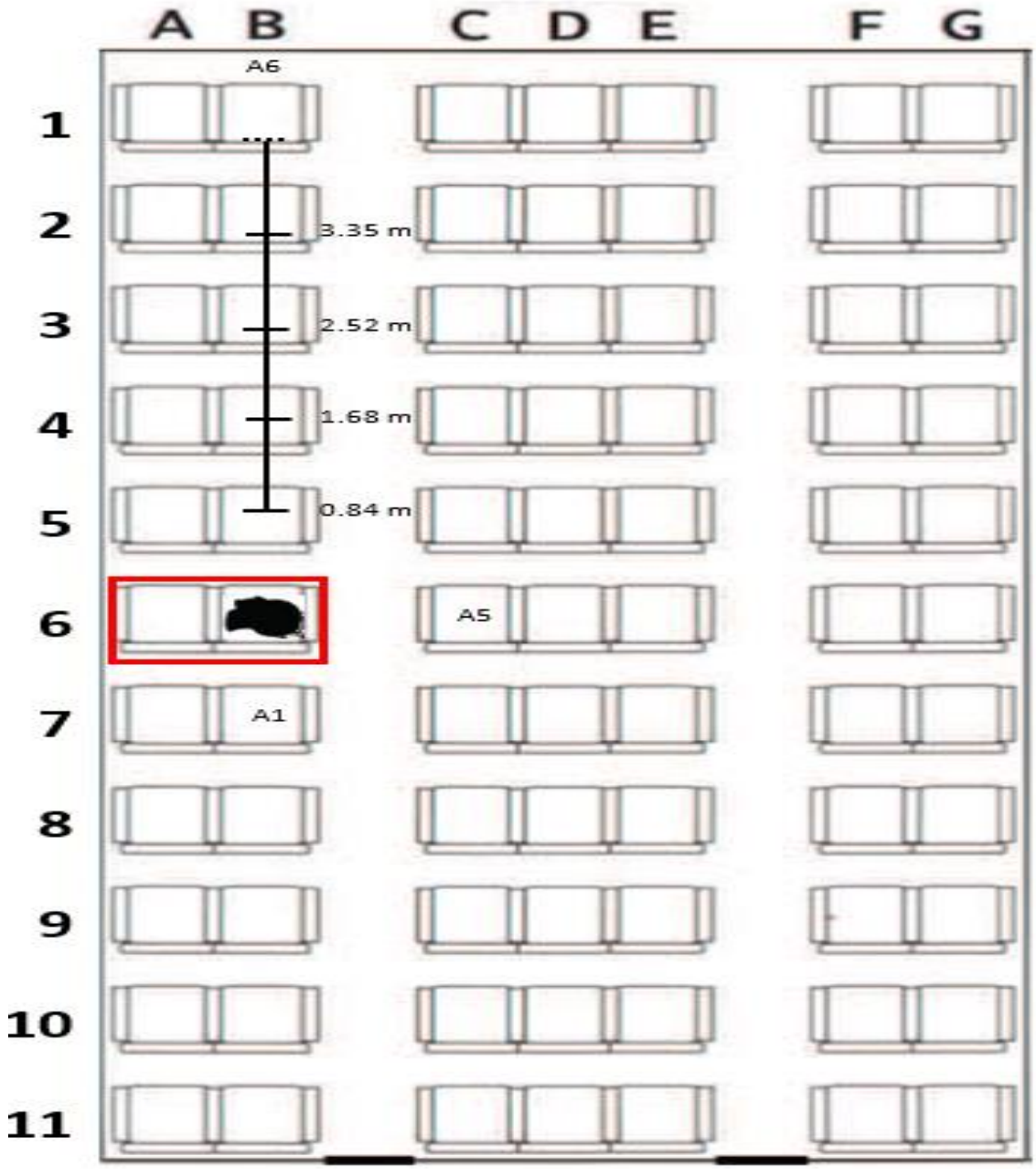

Figure I.110 Test 63 (B-M) ISOPass deployed source location and sampling tree orientation.

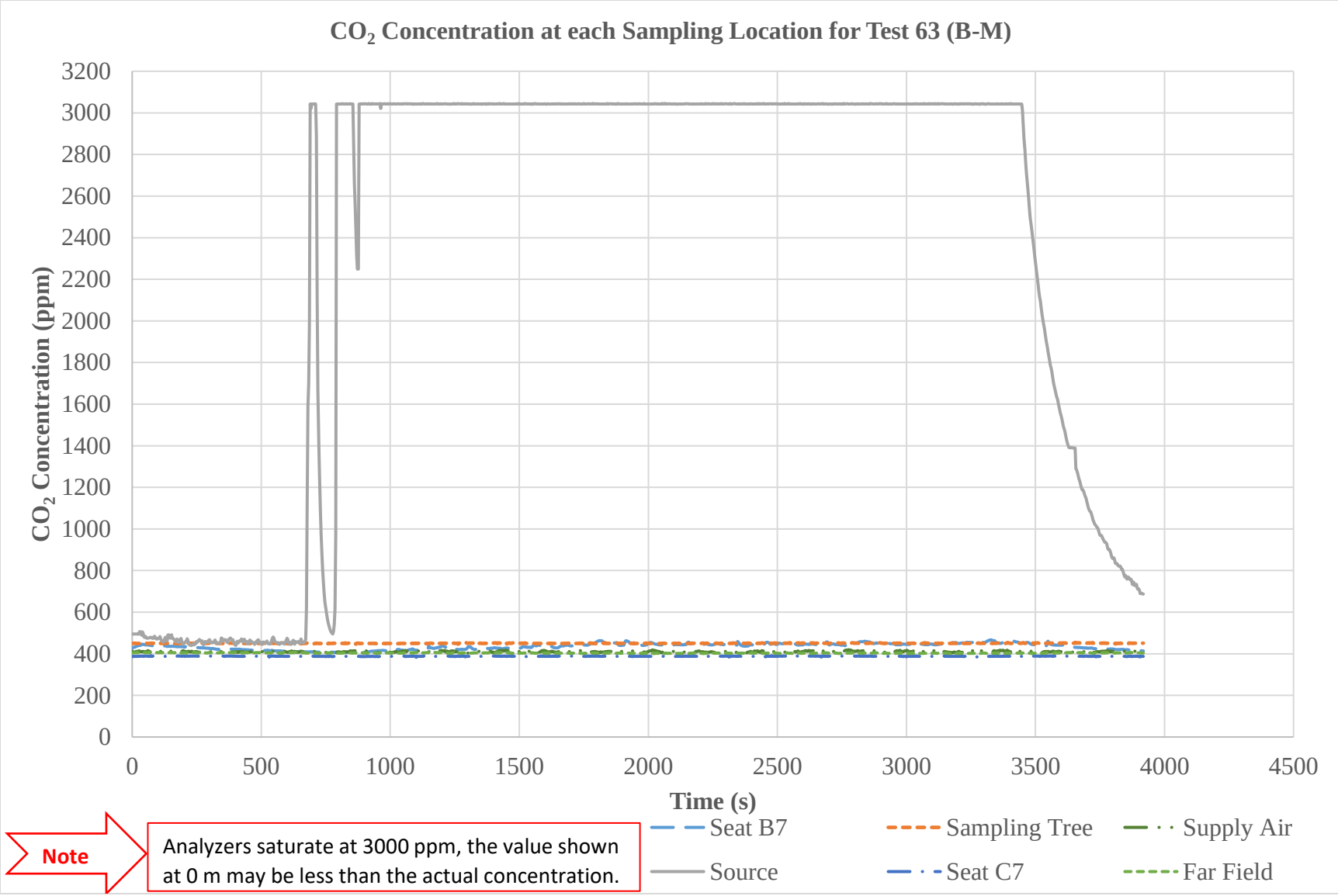

Figure I.111 Ininstantaneous CO_2 concentration at each sampling location for Test 63 (B-M) ISOPass deployed.

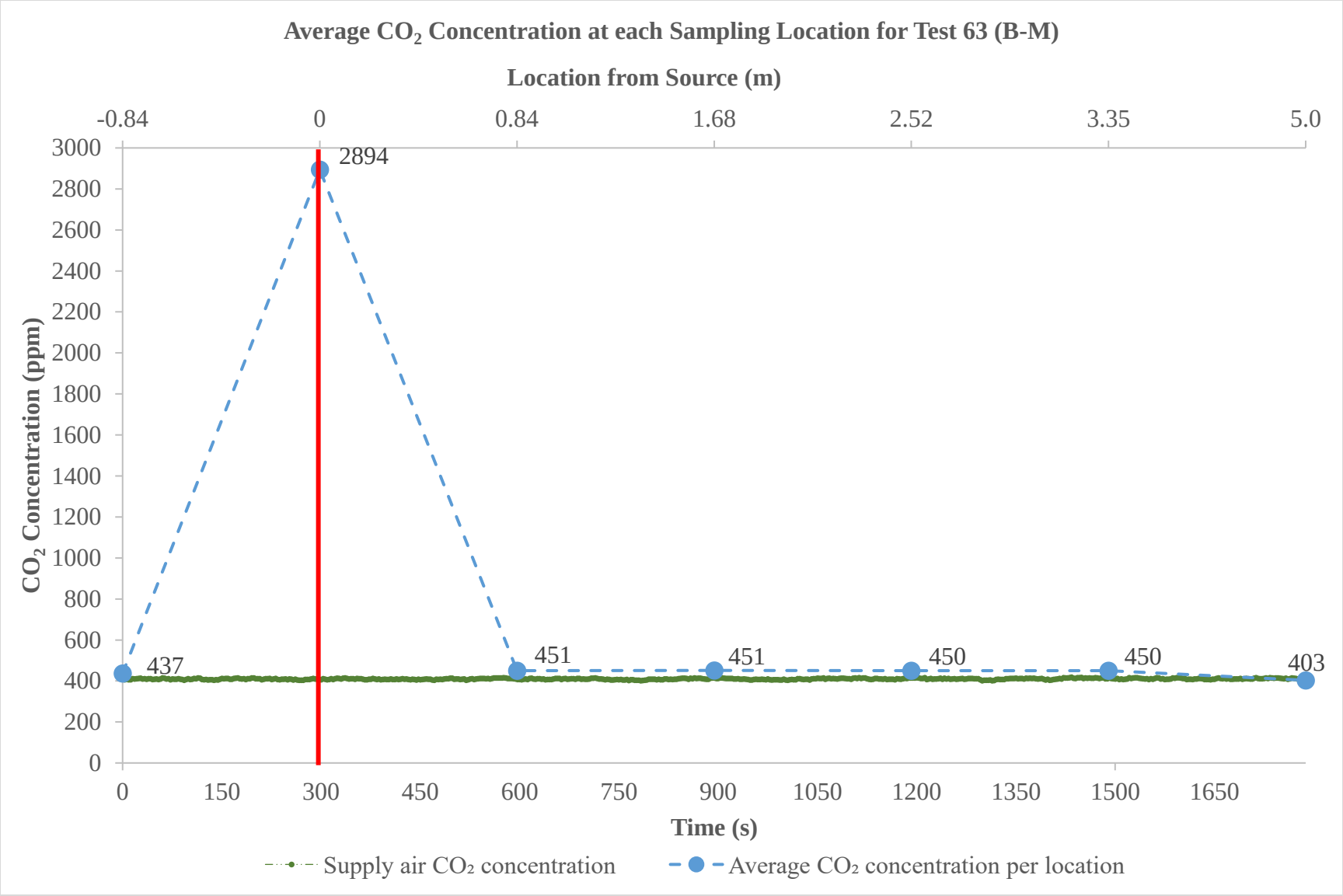

Figure I.112 Average CO_2 concentration at each sampling location for Test 63 (B-M) ISOPass deployed.

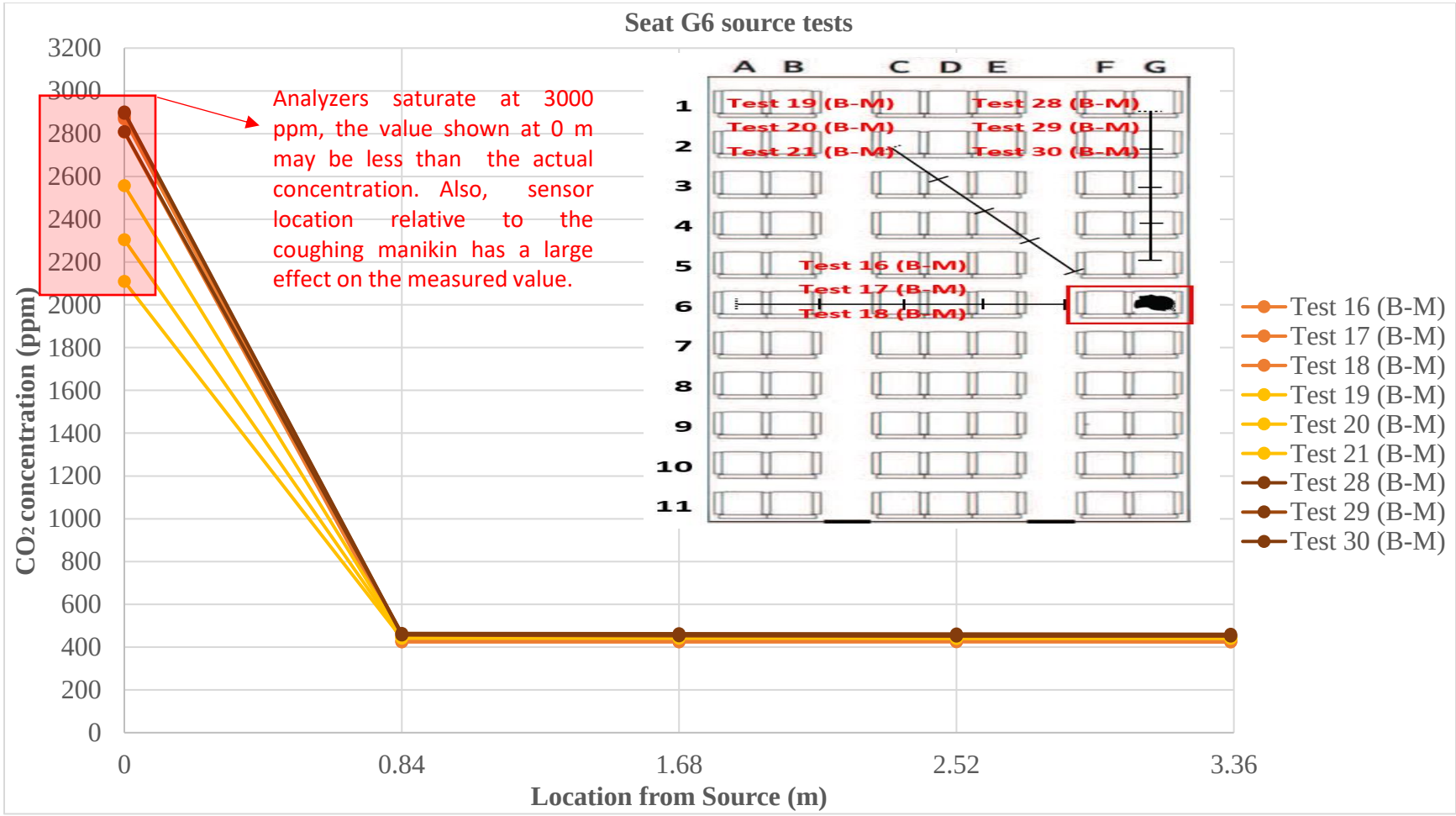

Figure I.113 Seat G6 coughing manikin source tests in the Boeing 767 cabin mockup with the ISOPass deployed.

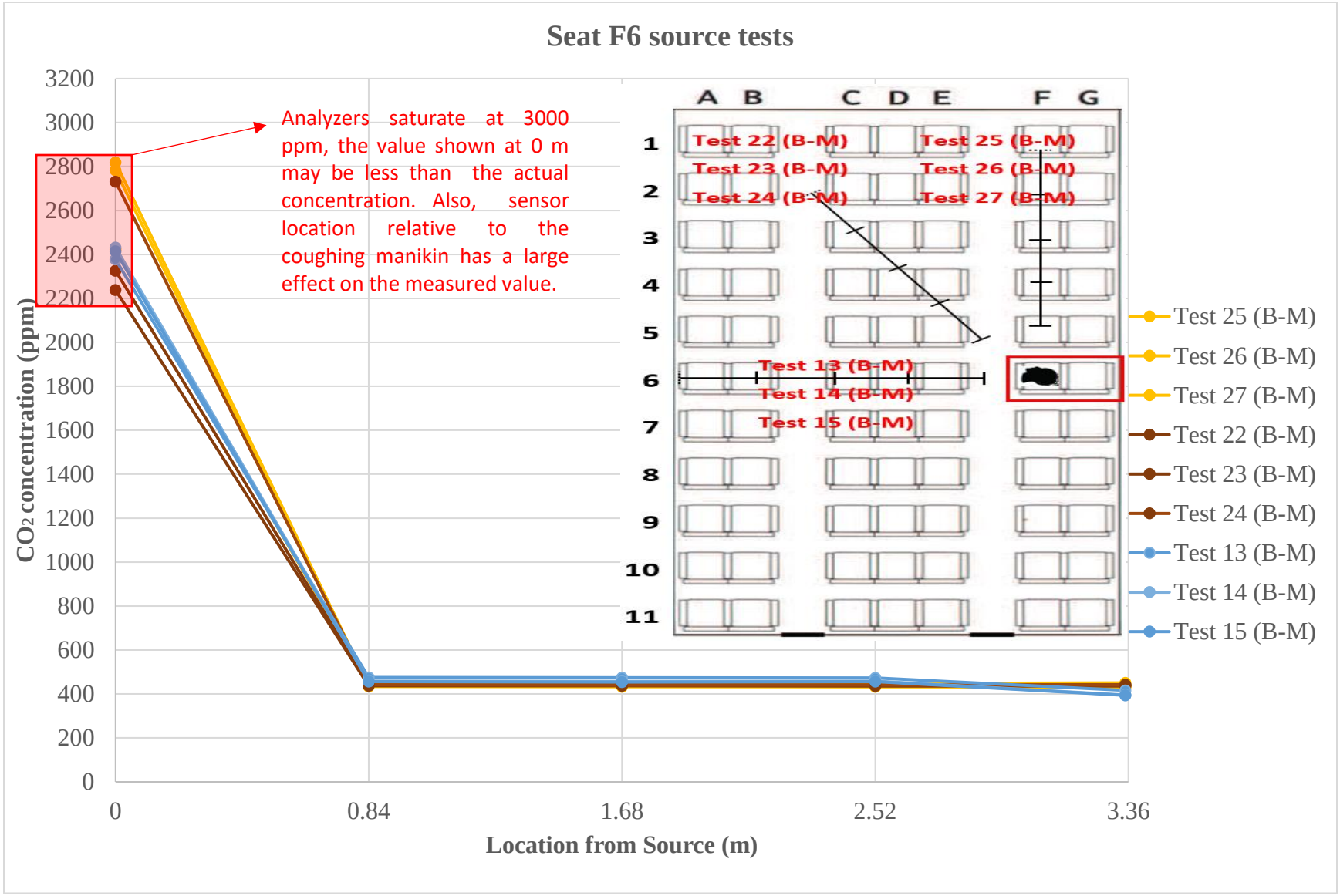

Figure I.114 Seat F6 coughing manikin source tests in the Boeing 767 cabin mockup with the ISOPass deployed.

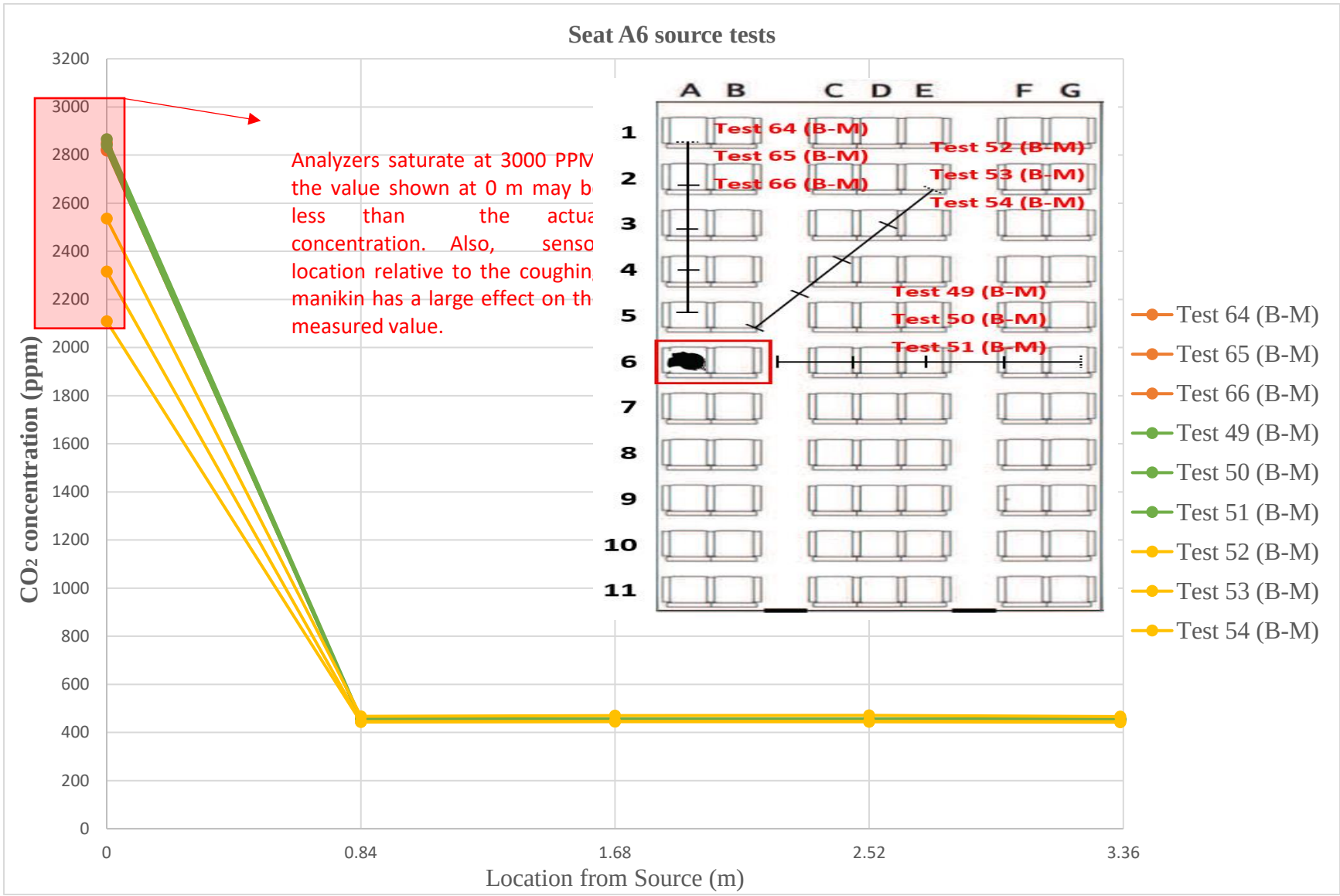

I. 115 Seat A6 coughing manikin source tests in the Boeing 767 cabin mockup with the ISOPass deployed.

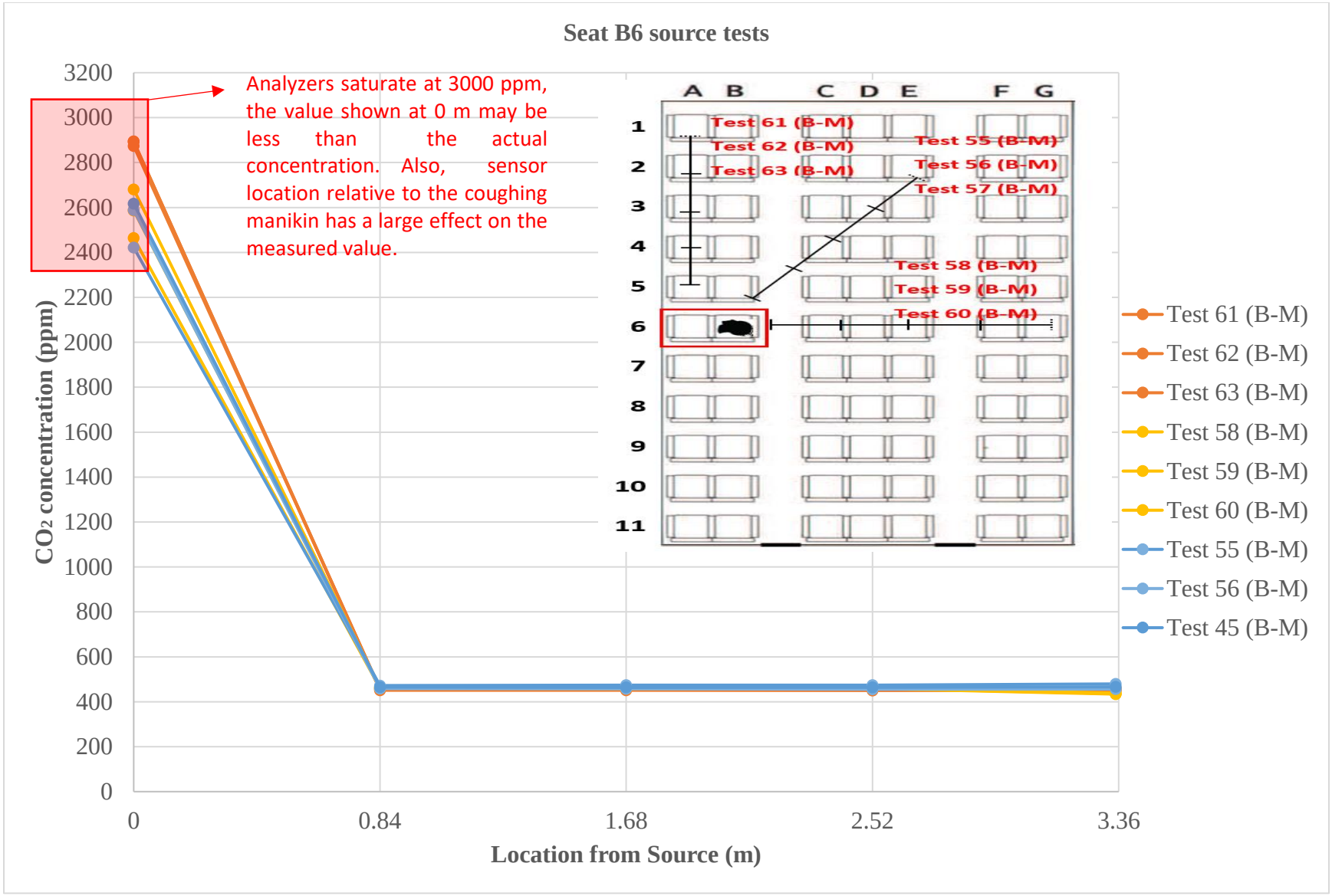

Figure I.116 Seat B6 coughing manikin source tests in the Boeing 767 cabin mockup with the ISOPass deployed.

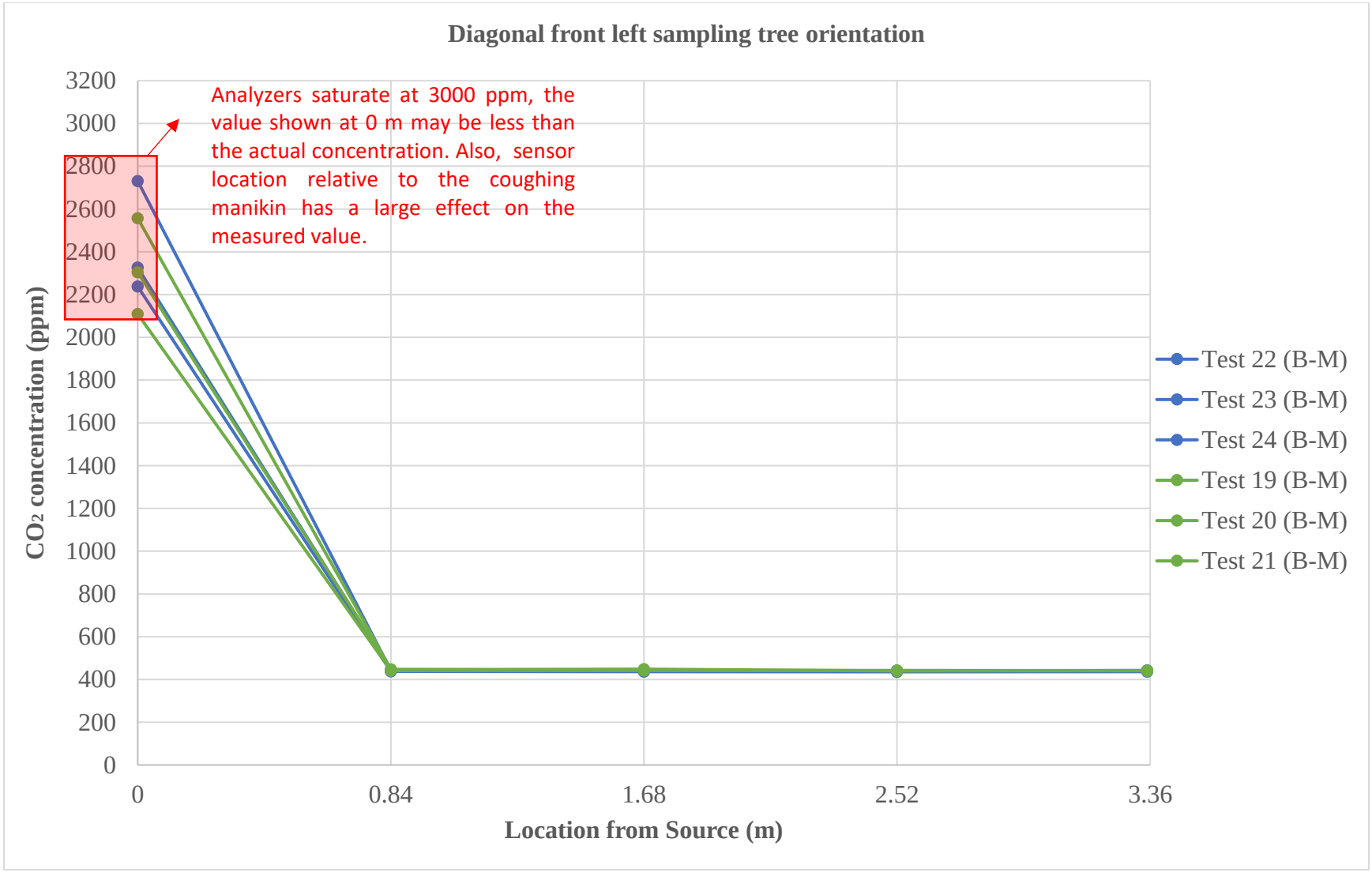

Figure I.117 Diagonal front left sampling tree orientation coughing manikin source tests in the Boeing 767 cabin mockup with the ISOPass deployed.

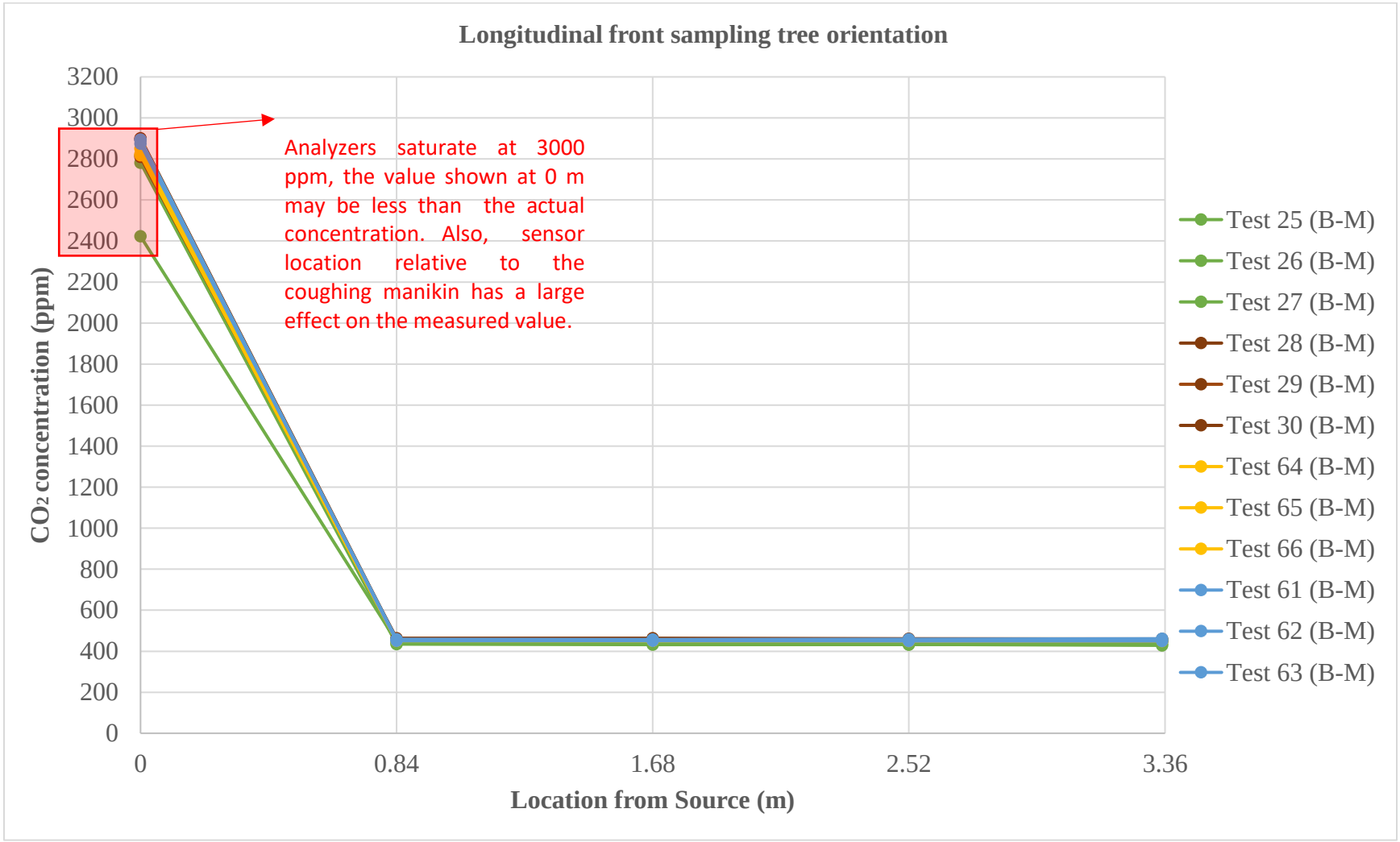

Figure I.118 Longitudinal front sampling tree orientation coughing manikin source tests in the Boeing 767 cabin mockup with the ISOPass deployed.

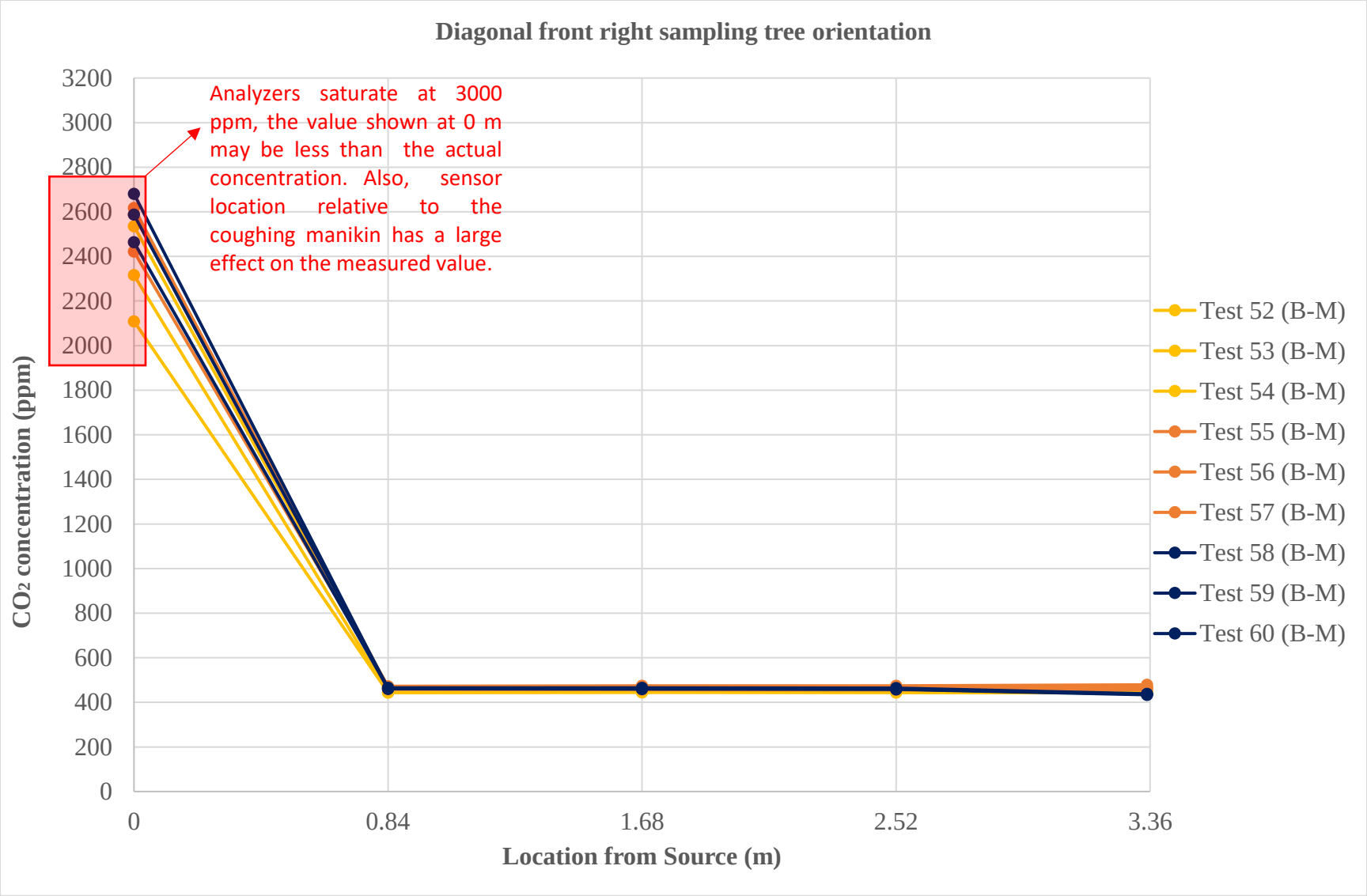

Figure I.119 Diagonal front right sampling tree orientation coughing manikin source tests in the Boeing 767 cabin mockup with the ISOPass deployed.

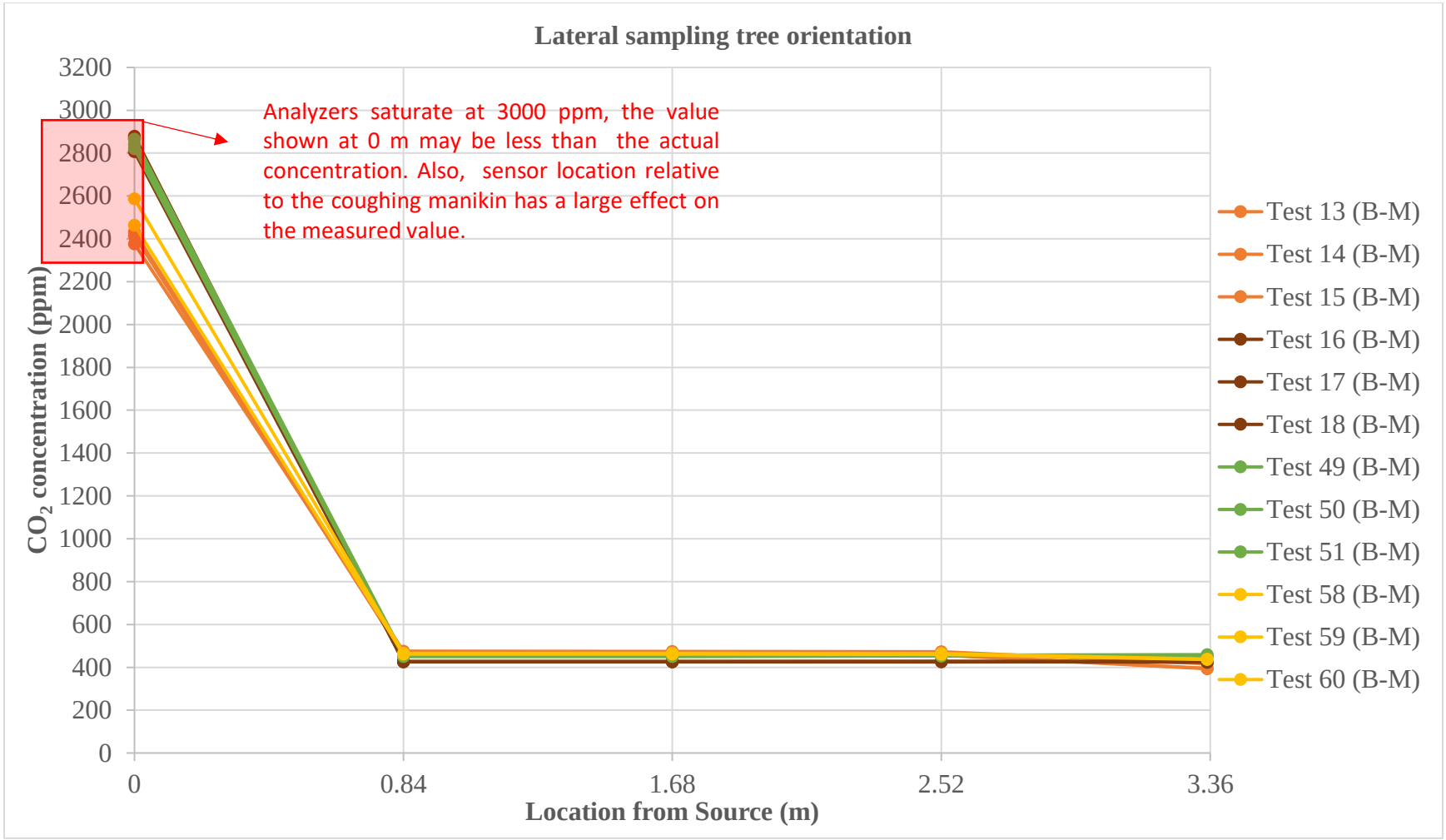

Figure I.120 Lateral sampling tree orientation coughing manikin source tests in the Boeing 767 cabin mockup with the ISOPass deployed.

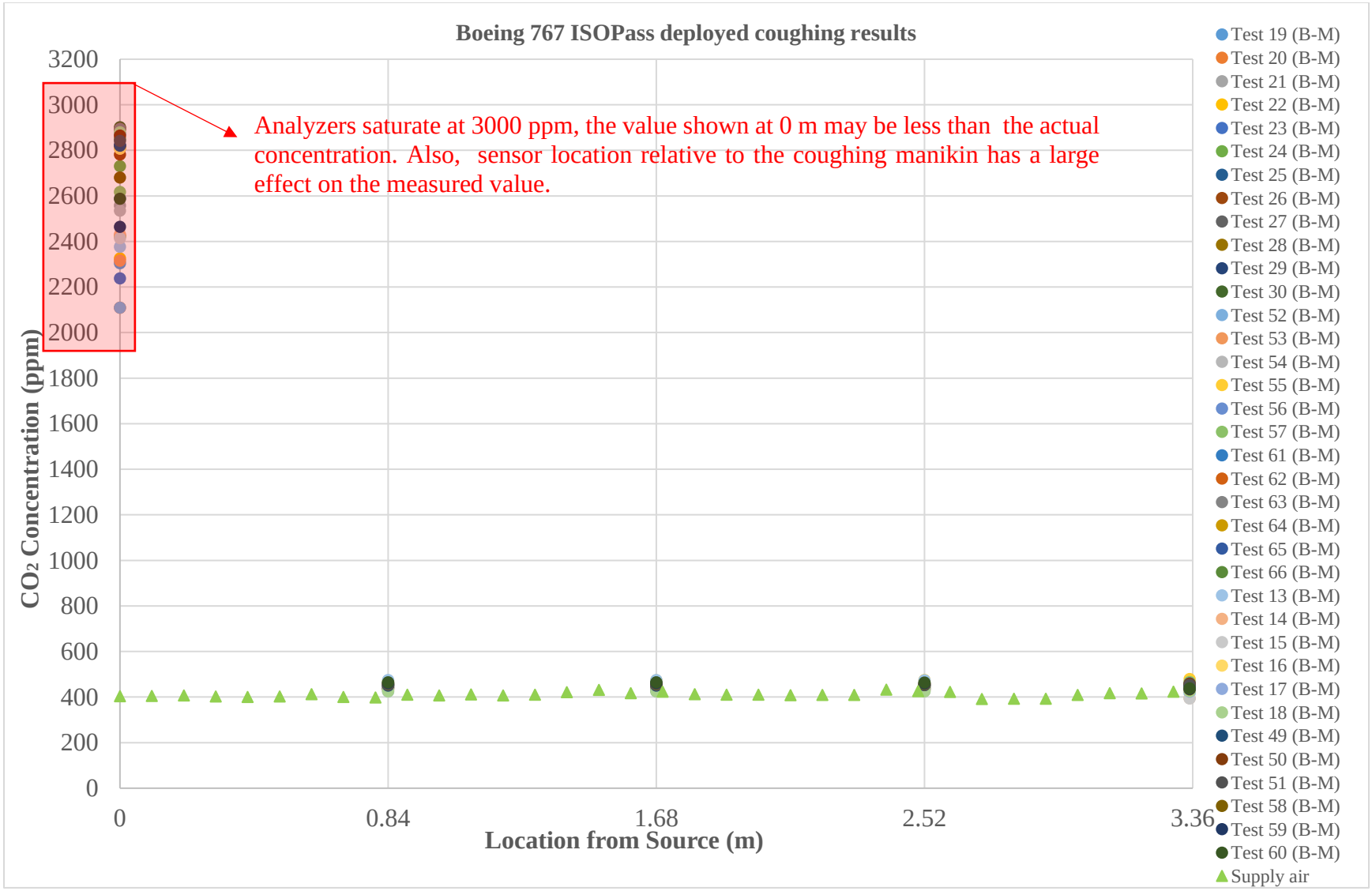

Figure I.121 Boeing 767 cabin mockup coughing manikin source tests with the ISOPass deployed.

Appendix J - Seat A6 Smoke Visualization Snapshots

J.1 Cross-sectional View

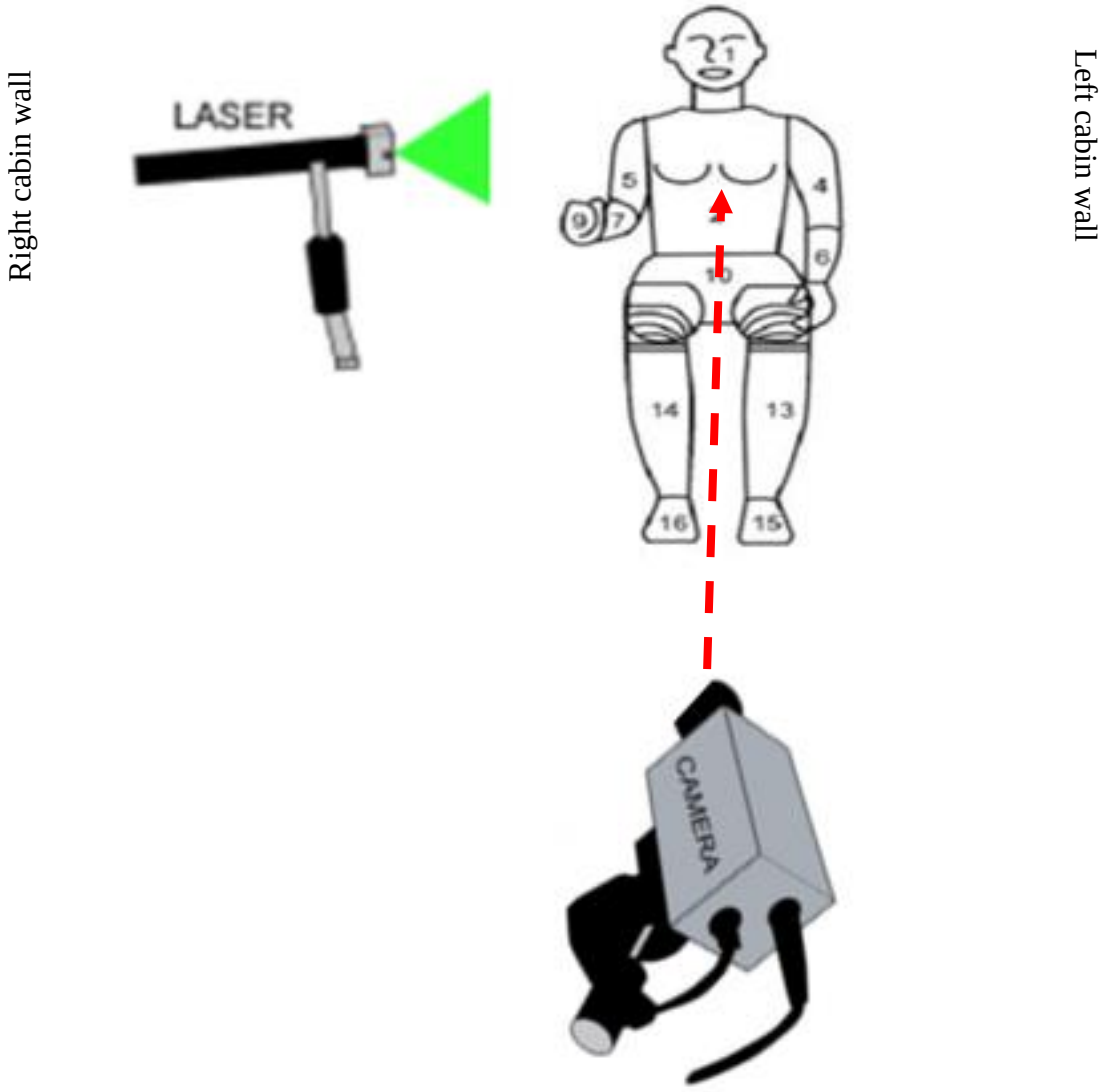

Figure J.1.1 A schematic showing the cross-sectional laser sheet direction and the camera location relative to the seat where the smoke generation source is located on seat A6.

Figure J.1.2 Seat A6 cross-sectional view snapshot 01

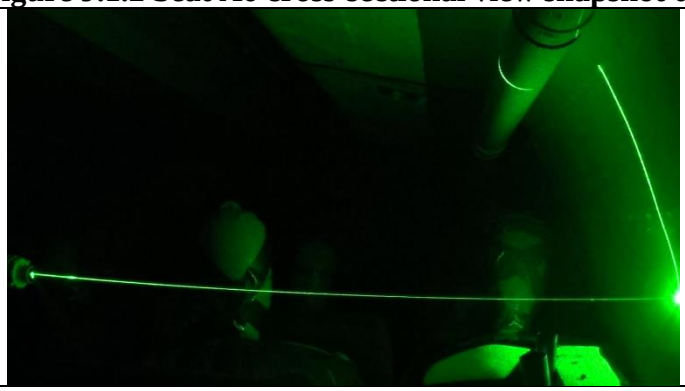

Figure J.1.3 Seat A6 cross-sectional view snapshot 02

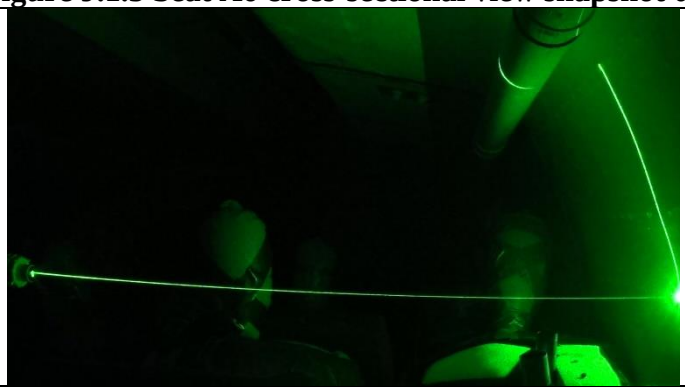

Figure J.1.4 Seat A6 cross-sectional view snapshot 03

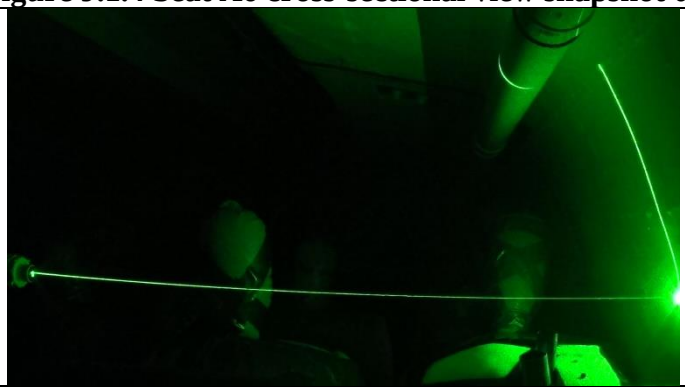

Figure J.1.5 Seat A6 cross-sectional view snapshot 04

Figure J.1.6 Seat A6 cross-sectional view snapshot 05.

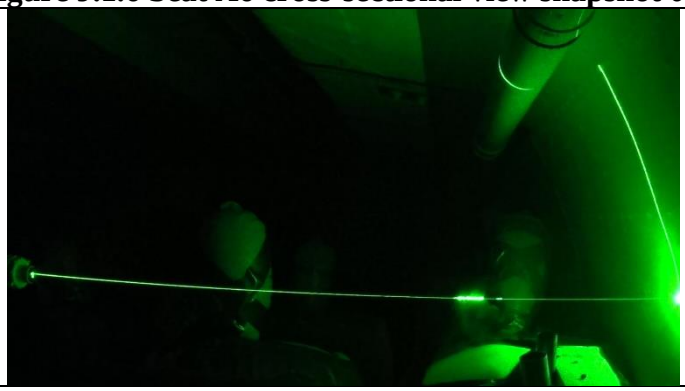

Figure J.1.7 Seat A6 cross-sectional view snapshot 06.

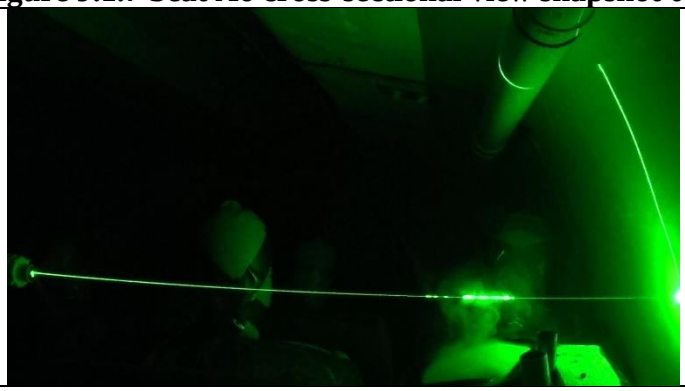

Figure J.1.8 Seat A6 cross-sectional view snapshot 07.

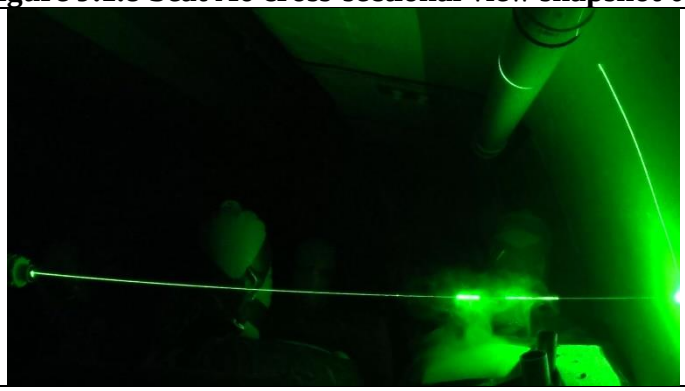

Figure J.1.9 Seat A6 cross-sectional view snapshot 08.

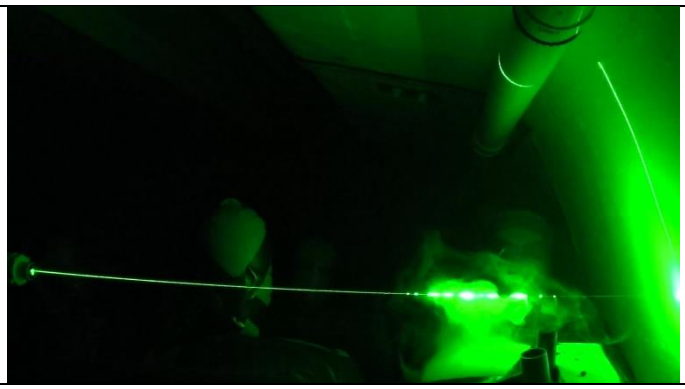

Figure J.1.10 Seat A6 cross-sectional view snapshot 09.

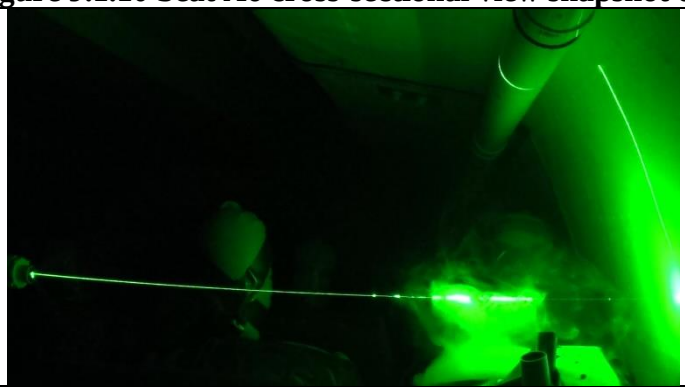

Figure J.1.11 Seat A6 cross-sectional view snapshot 10.

Figure J.1.12 Seat A6 cross-sectional view snapshot 11.

Figure J.1.13 Seat A6 cross-sectional view snapshot 12.

Figure J.1.14 Seat A6 cross-sectional view snapshot 13.

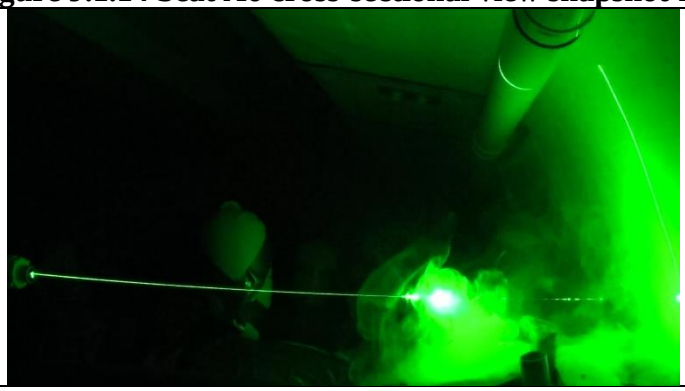

Figure J.1.15 Seat A6 cross-sectional view snapshot 14.

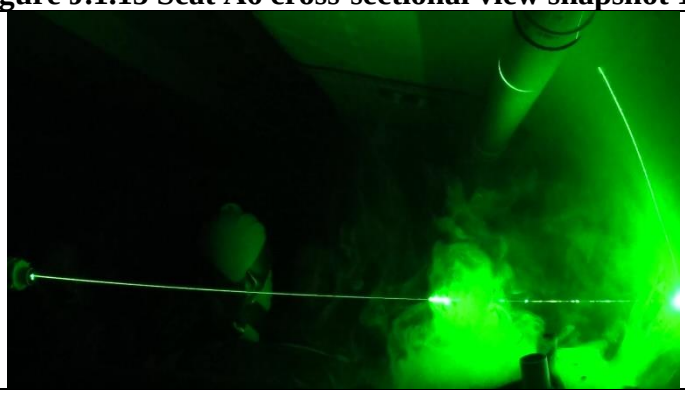

Figure J.1.16 Seat A6 cross-sectional view snapshot 15.

Figure J.1.17 Seat A6 cross-sectional view snapshot 16.

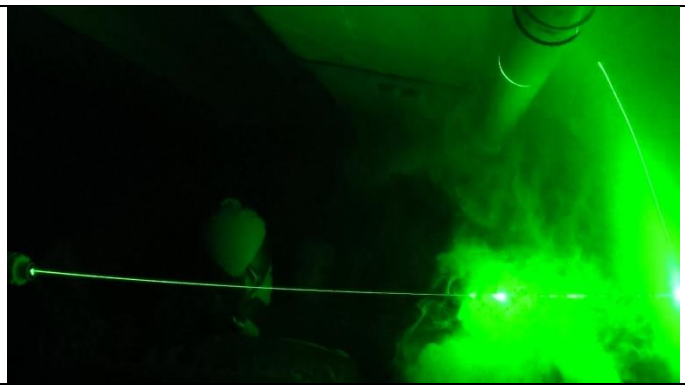

Figure J.1.18 Seat A6 cross-sectional view snapshot 17.

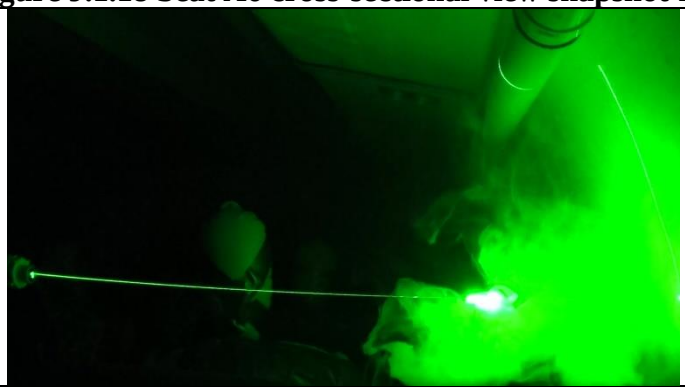

Figure J.1.19 Seat A6 cross-sectional view snapshot 18.

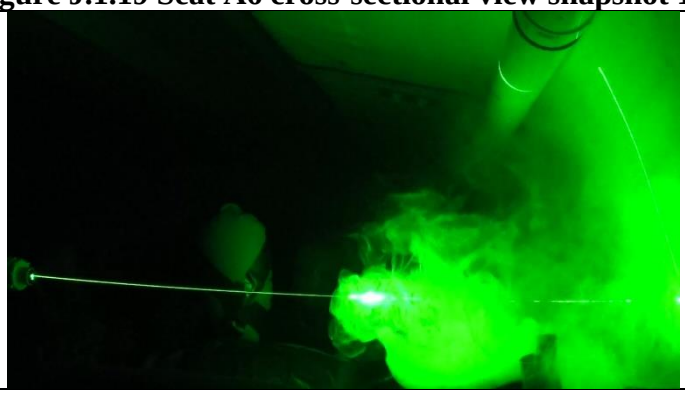

Figure J.1.20 Seat A6 cross-sectional view snapshot 19.

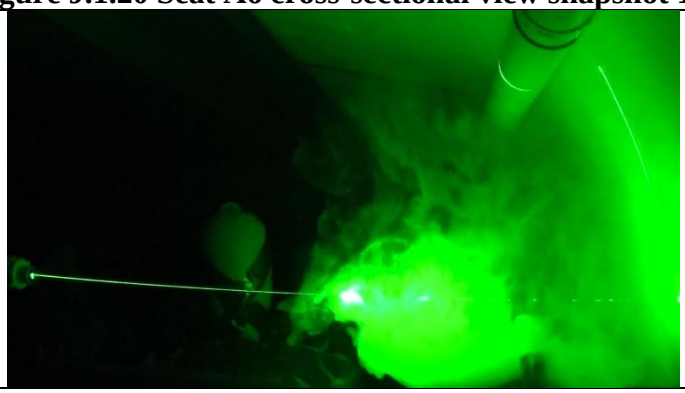

Figure J.1.21 Seat A6 cross-sectional view snapshot 20.

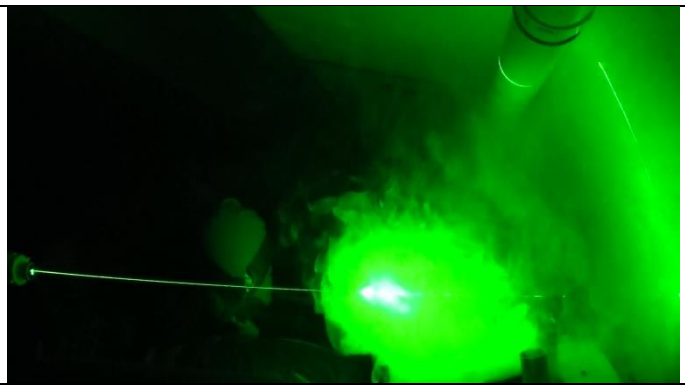

Figure J.1.22 Seat A6 cross-sectional view snapshot 21.

Figure J.1.23 Seat A6 cross-sectional view snapshot 22.

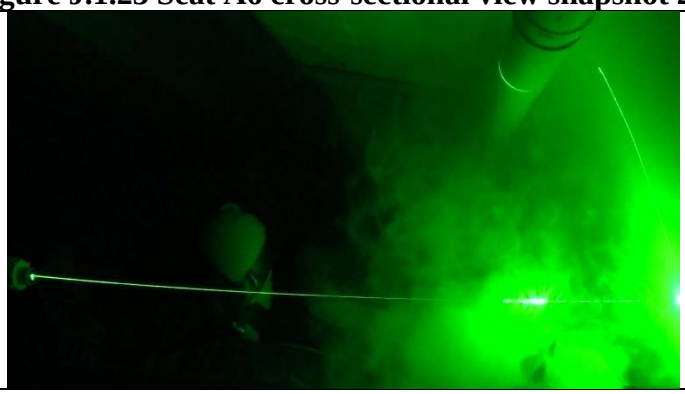

Figure J.1.24 Seat A6 cross-sectional view snapshot 23.

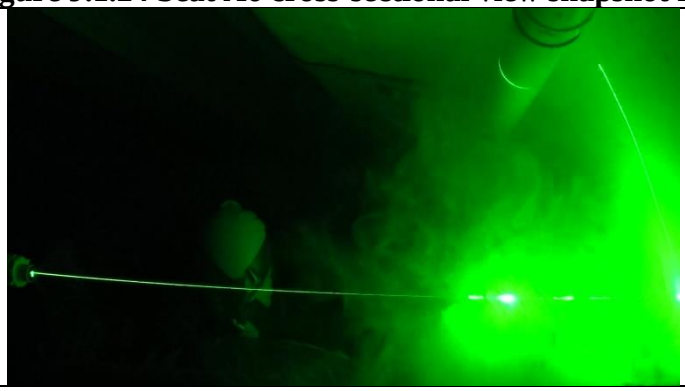

Figure J.1.25 Seat A6 cross-sectional view snapshot 24.

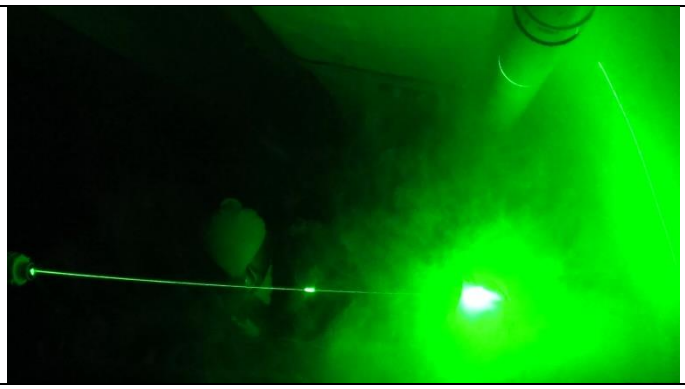

Figure J.1.26 Seat A6 cross-sectional view snapshot 25.

Figure J.1.27 Seat A6 cross-sectional view snapshot 26.

Figure J.1.28 Seat A6 cross-sectional view snapshot 27.

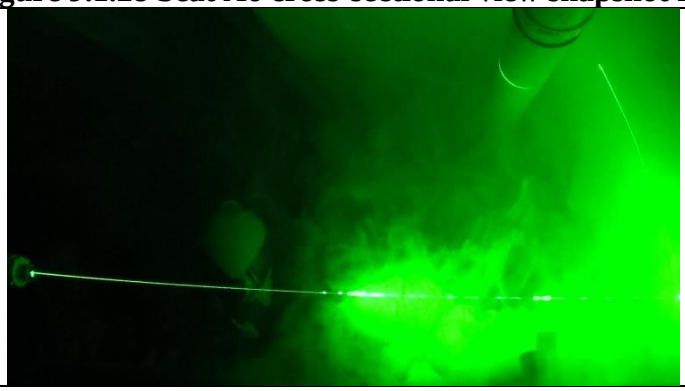

Figure J.1.29 Seat A6 cross-sectional view snapshot 28.

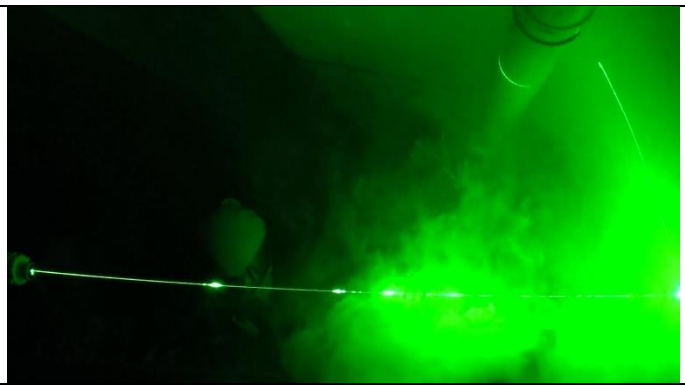

Figure J.1.30 Seat A6 cross-sectional view snapshot 29.

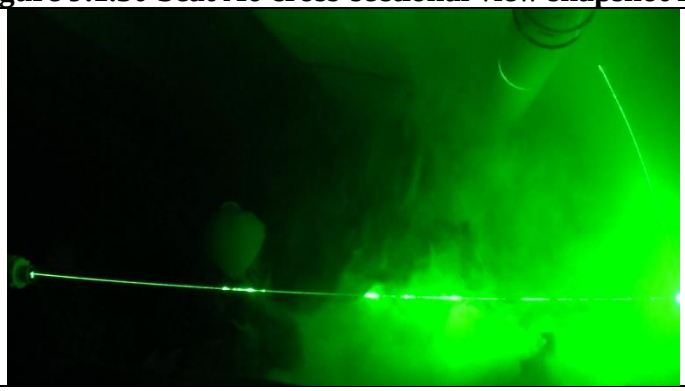

Figure J.1.31 Seat A6 cross-sectional view snapshot 30.

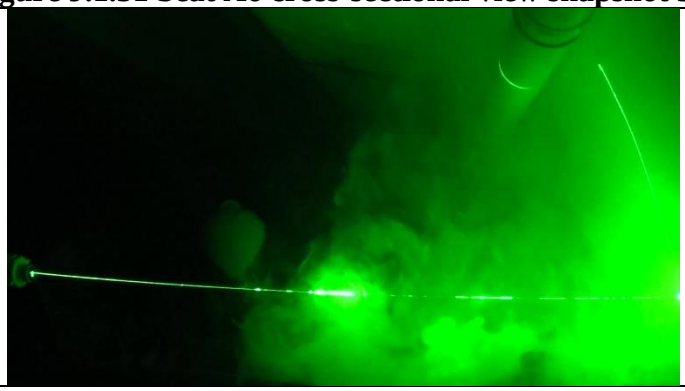

Figure J.1.32 Seat A6 cross-sectional view snapshot 31.

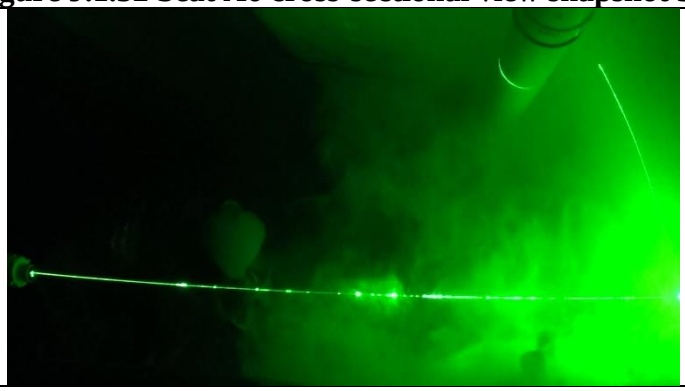

Figure J.1.33 Seat A6 cross-sectional view snapshot 32.

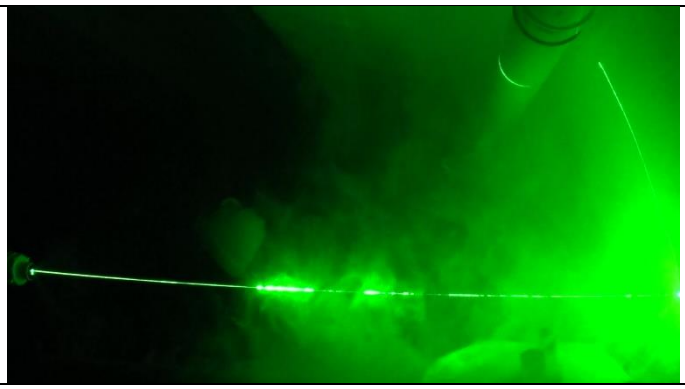

Figure J.1.34 Seat A6 cross-sectional view snapshot 33.

Figure J.1.35 Seat A6 cross-sectional view snapshot 34.

Figure J.1.36 Seat A6 cross-sectional view snapshot 35.

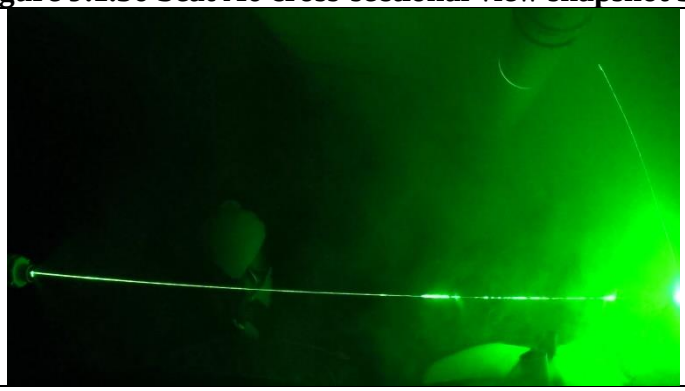

Figure J.1.37 Seat A6 cross-sectional view snapshot 36.

Figure J.1.38 Seat A6 cross-sectional view snapshot 37.

Figure J.1.39 Seat A6 cross-sectional view snapshot 38.

Figure J.1.40 Seat A6 cross-sectional view snapshot 39.

Figure J.1.41 Seat A6 cross-sectional view snapshot 40.

Figure J.1.42 Seat A6 cross-sectional view snapshot 41.

Figure J.1.43 Seat A6 cross-sectional view snapshot 42.

Figure J.1.44 Seat A6 cross-sectional view snapshot 43.

Figure J.1.45 Seat A6 cross-sectional view snapshot 44.

Figure J.1.46 Seat A6 cross-sectional view snapshot 45.

Figure J.1.47 Seat A6 cross-sectional view snapshot 46.

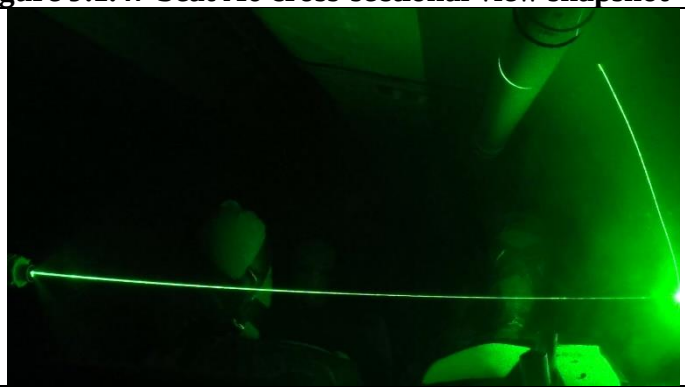

Figure J.1.48 Seat A6 cross-sectional view snapshot 47.

Figure J.1.49 Seat A6 cross-sectional view snapshot 48.

Figure J.1.50 Seat A6 cross-sectional view snapshot 49.

Figure J.1.51 Seat A6 cross-sectional view snapshot 50.

J.2 Frontal View

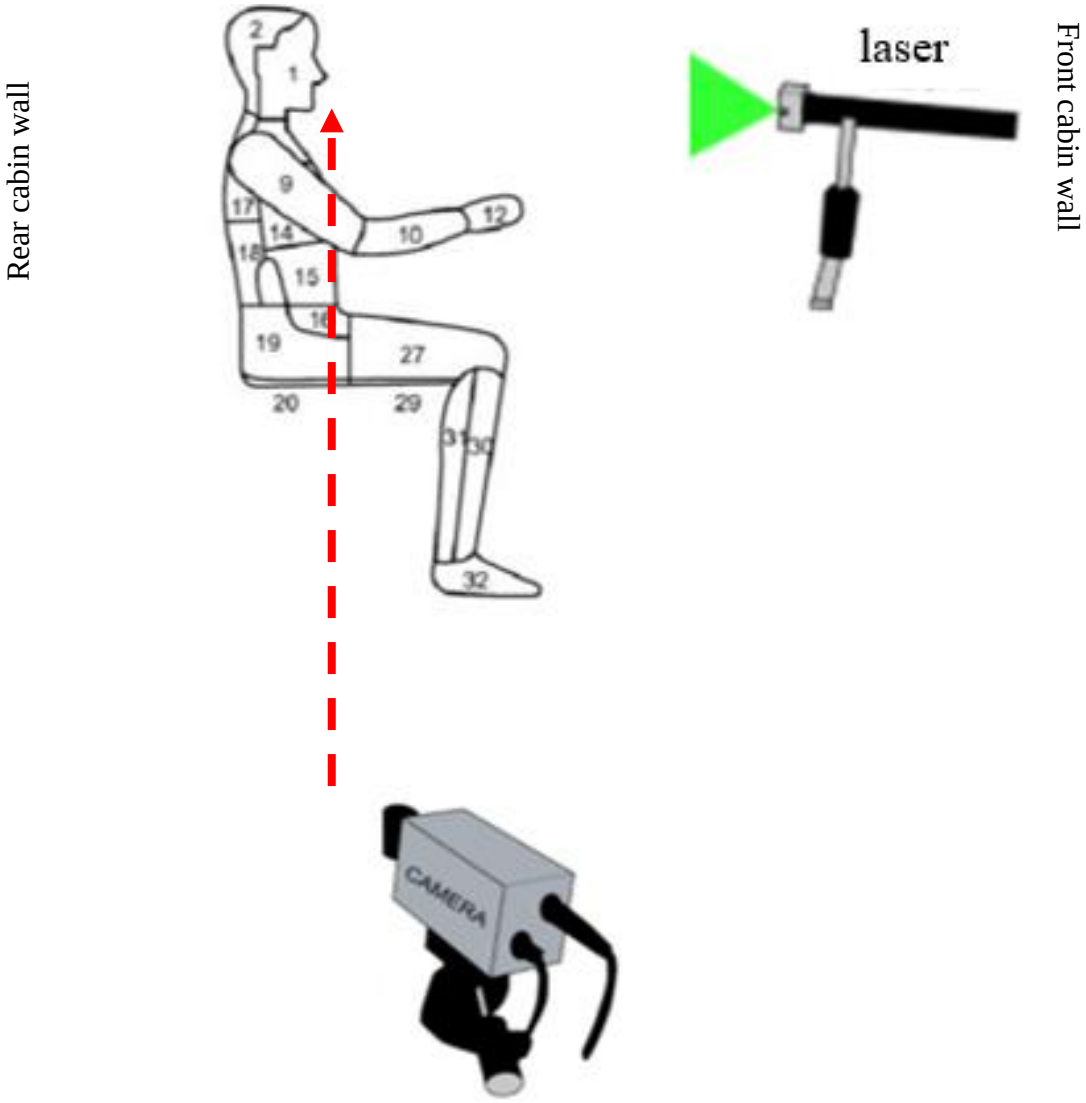

Figure J.2.1 A schematic showing the frontal laser sheet direction and the camera location relative to the seat where the smoke generation source is located on seat A6.

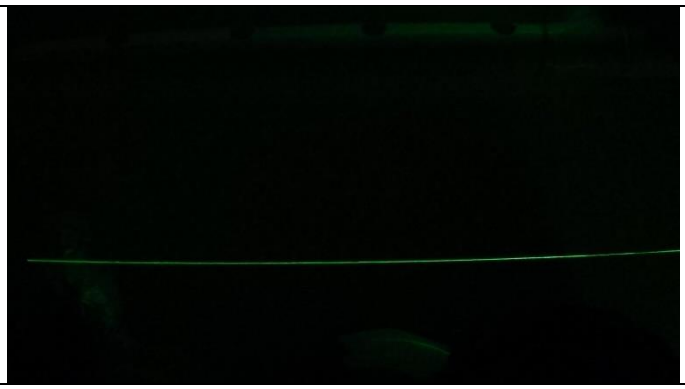

Figure J.2.2 Seat A6 frontal view snapshot 01.

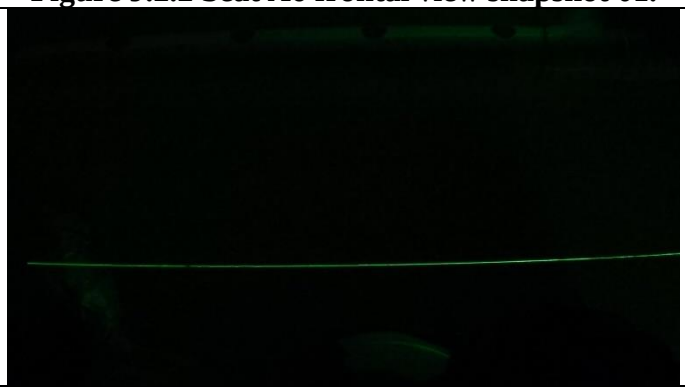

Figure J.2.3 Seat A6 frontal view snapshot 02.

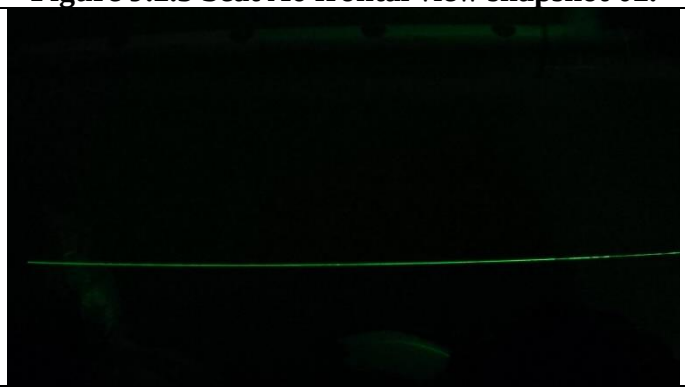

Figure J.2.4 Seat A6 frontal view snapshot 03.

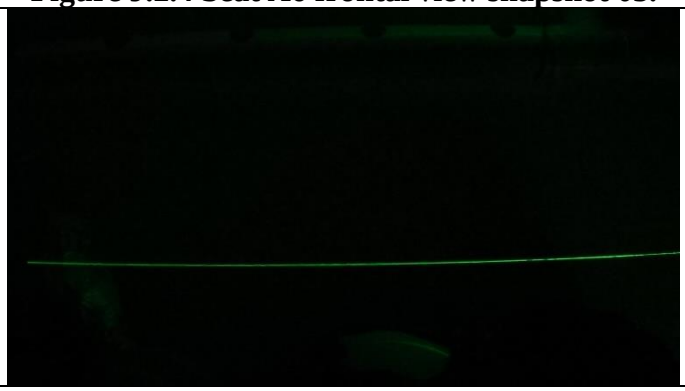

Figure J.2.5 Seat A6 frontal view snapshot 04.

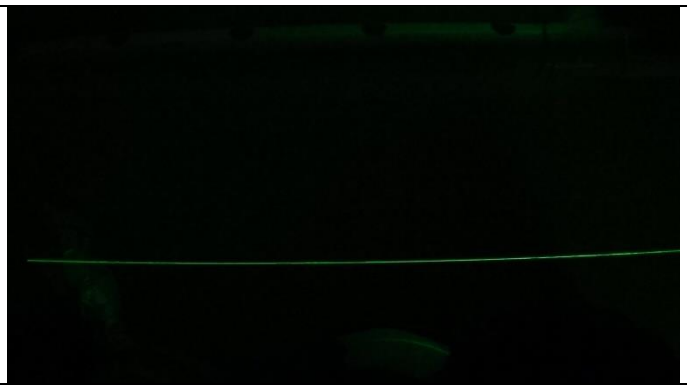

Figure J.2.6 Seat A6 frontal view snapshot 05.

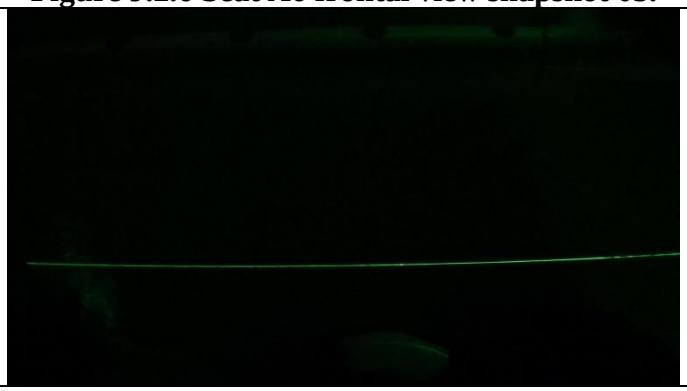

Figure J.2.7 Seat A6 frontal view snapshot 06.

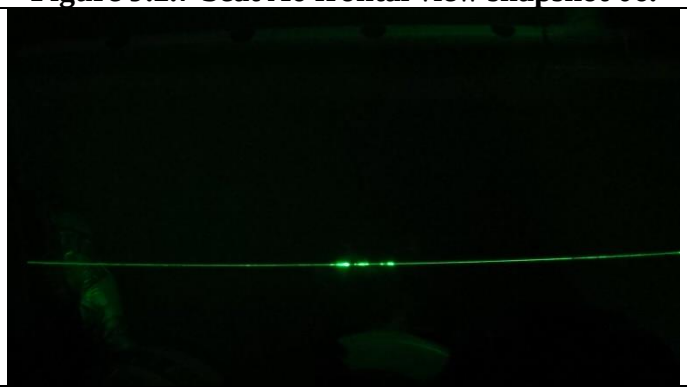

Figure J.2.8 Seat A6 frontal view snapshot 07.

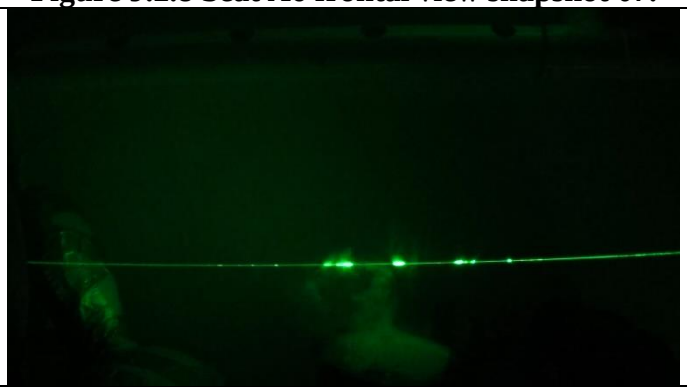

Figure J.2.9 Seat A6 frontal view snapshot 08.

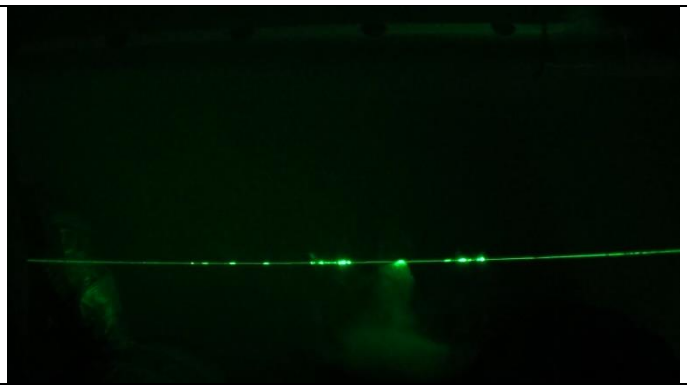

Figure J.2.10 Seat A6 frontal view snapshot 09.

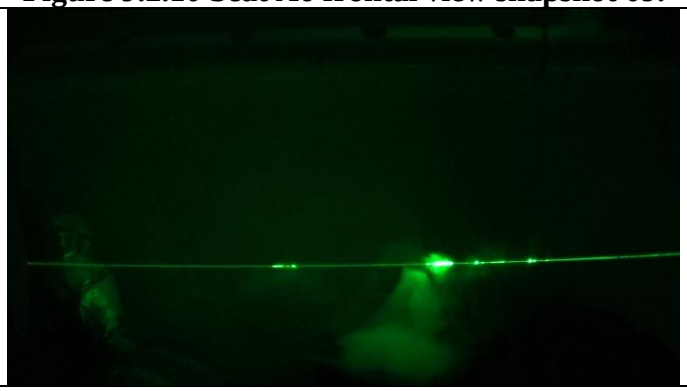

Figure J.2.11 Seat A6 frontal view snapshot 10.

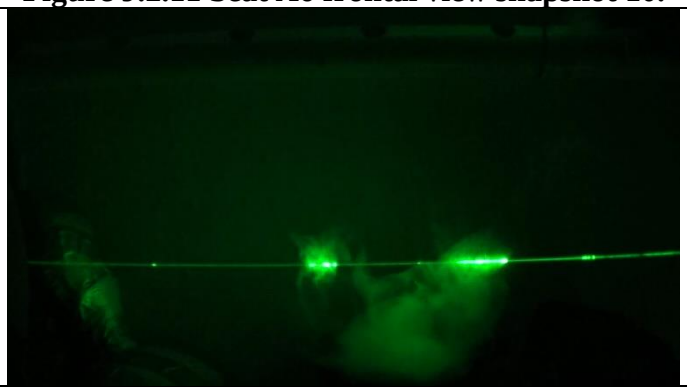

Figure J.2.12 Seat A6 frontal view snapshot 11.

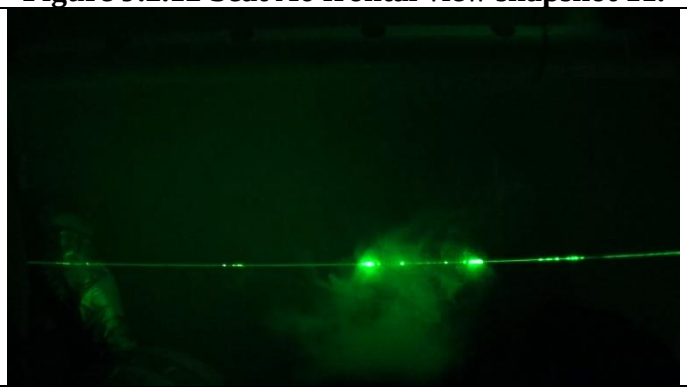

Figure J.2.13 Seat A6 frontal view snapshot 12.

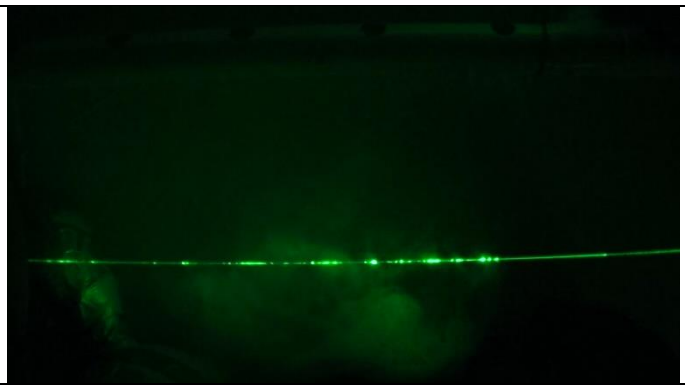

Figure J.2.14 Seat A6 frontal view snapshot 13.

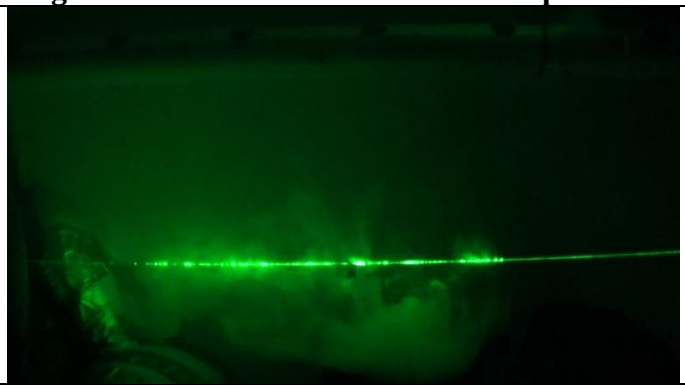

Figure J.2.15 Seat A6 frontal view snapshot 14.

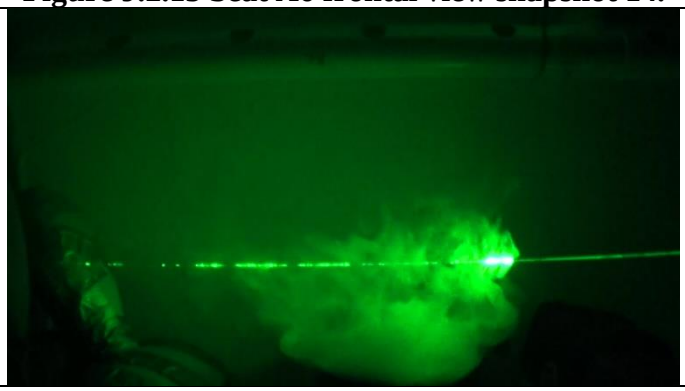

Figure J.2.16 Seat A6 frontal view snapshot 15.

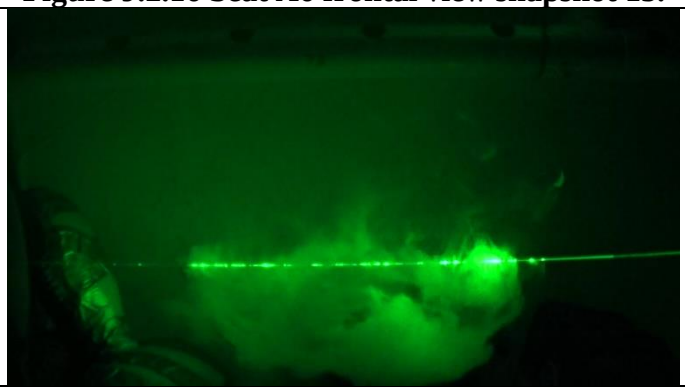

Figure J.2.17 Seat A6 frontal view snapshot 16.

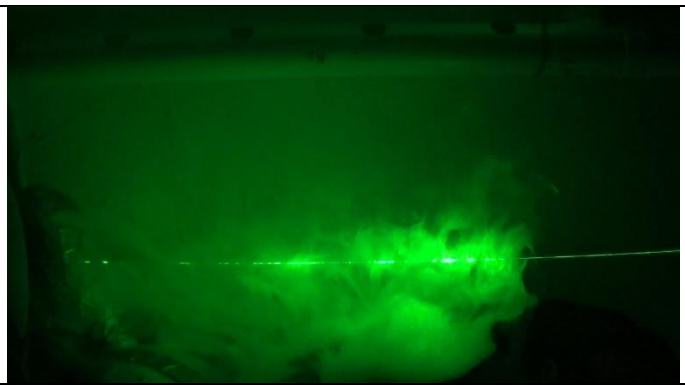

Figure J.2.18 Seat A6 frontal view snapshot 17.

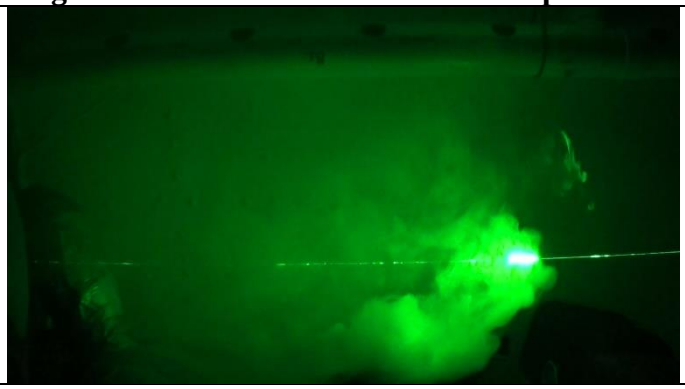

Figure J.2.19 Seat A6 frontal view snapshot 18.

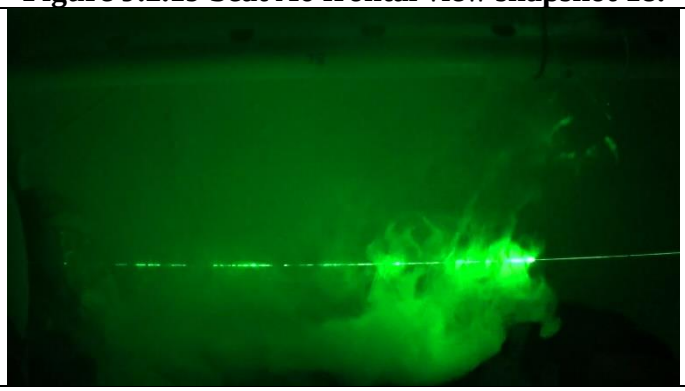

Figure J.2.20 Seat A6 frontal view snapshot 19.

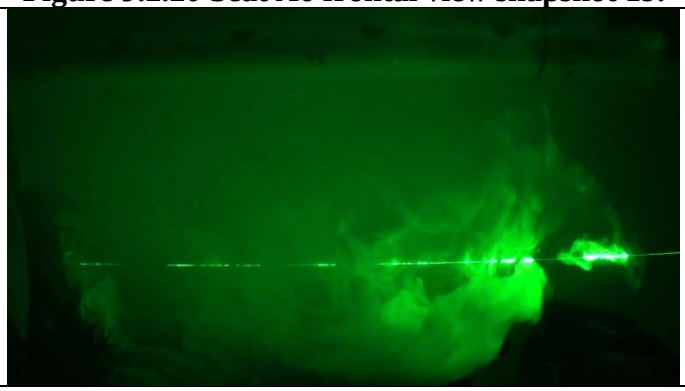

Figure J.2.21 Seat A6 frontal view snapshot 20.

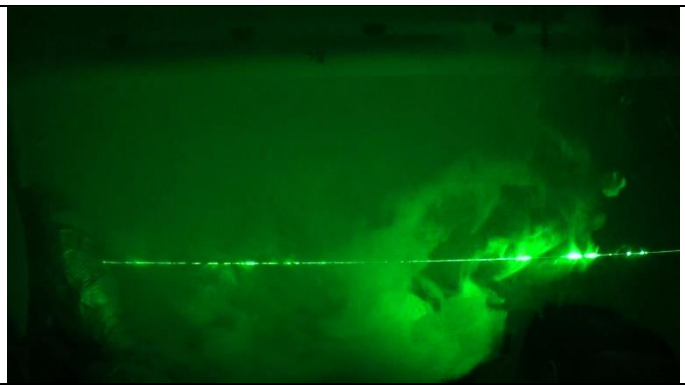

Figure J.2.22 Seat A6 frontal view snapshot 21.

Figure J.2.23 Seat A6 frontal view snapshot 22.

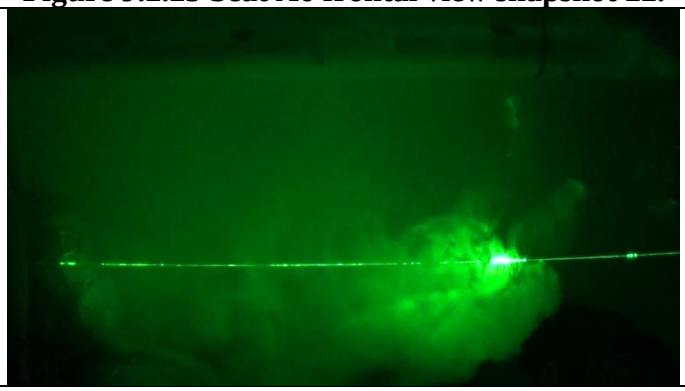

Figure J.2.24 Seat A6 frontal view snapshot 23.

Figure J.2.25 Seat A6 frontal view snapshot 24.

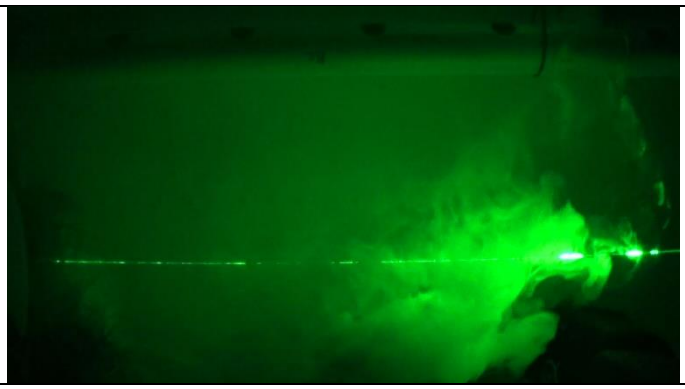

Figure J.2.26 Seat A6 frontal view snapshot 25.

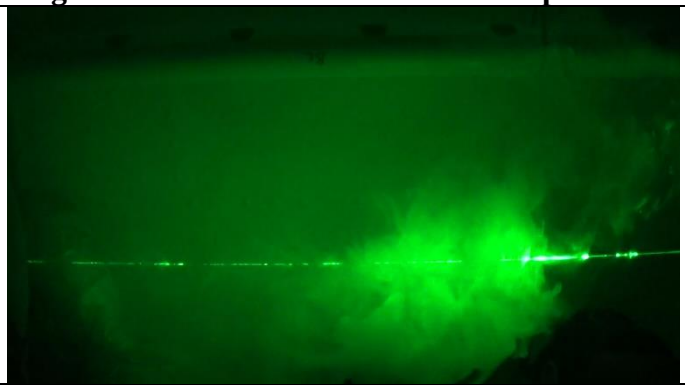

Figure J.2.27 Seat A6 frontal view snapshot 26.

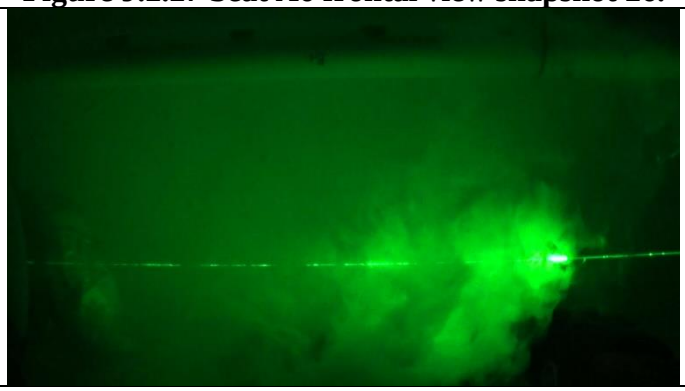

Figure J.2.28 Seat A6 frontal view snapshot 27.

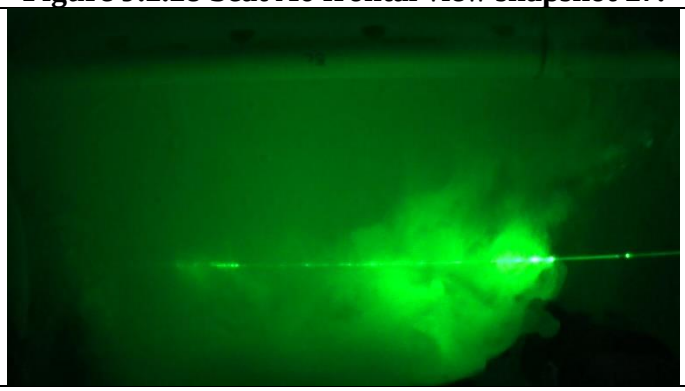

Figure J.2.29 Seat A6 frontal view snapshot 28.

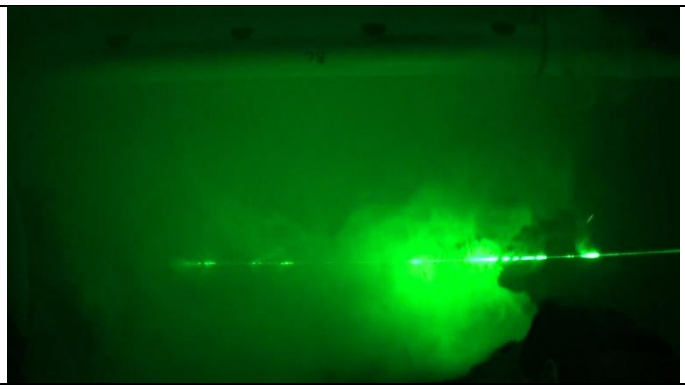

Figure J.2.30 Seat A6 frontal view snapshot 29.

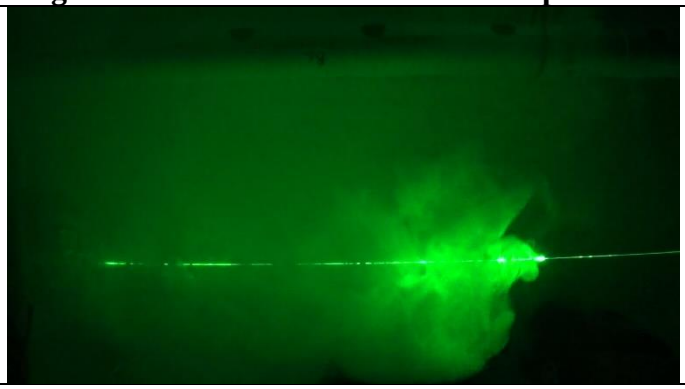

Figure J.2.31 Seat A6 frontal view snapshot 30.

Figure J.2.32 Seat A6 frontal view snapshot 31.

Figure J.2.33 Seat A6 frontal view snapshot 32.

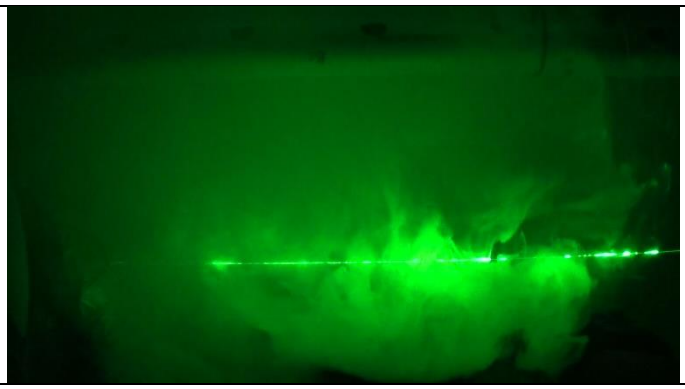

Figure J.2.34 Seat A6 frontal view snapshot 33.

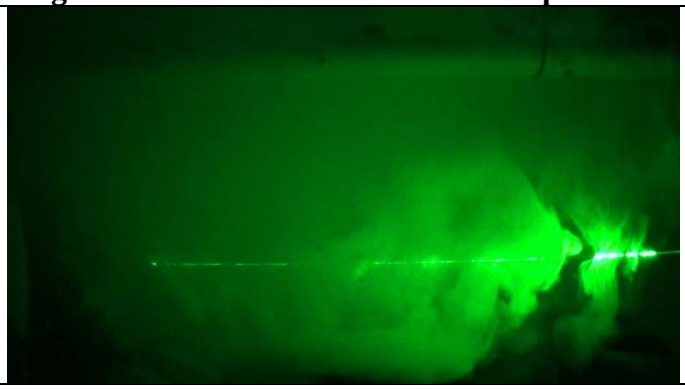

Figure J.2.35 Seat A6 frontal view snapshot 34.

Figure J.2.36 Seat A6 frontal view snapshot 35.

Figure J.2.37 Seat A6 frontal view snapshot 36.

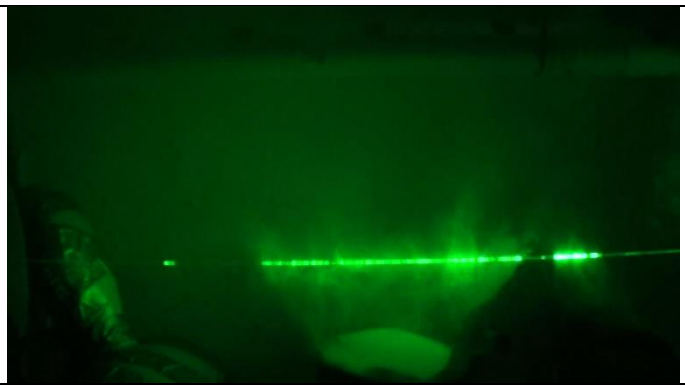

Figure J.2.38 Seat A6 frontal view snapshot 37.

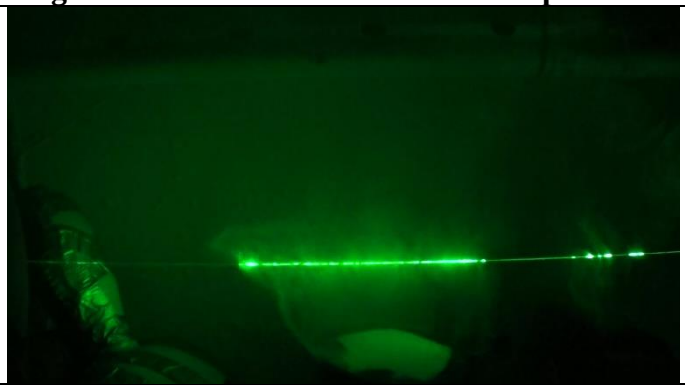

Figure J.2.39 Seat A6 frontal view snapshot 38.

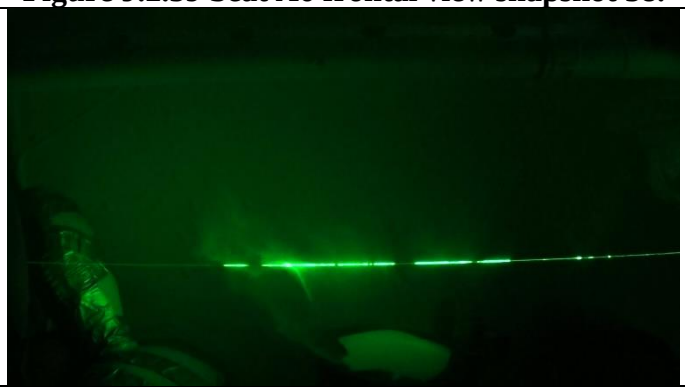

Figure J.2.40 Seat A6 frontal view snapshot 39.

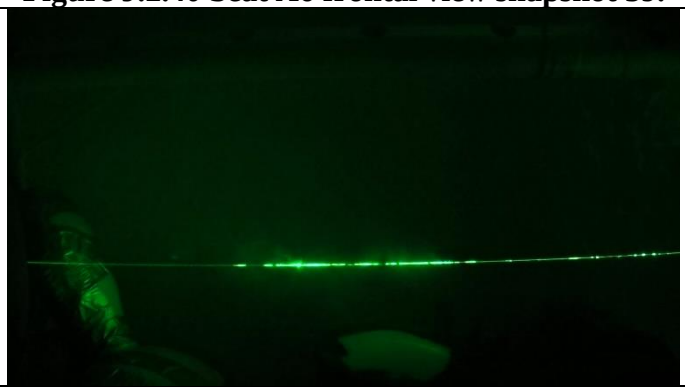

Figure J.2.41 Seat A6 frontal view snapshot 40.

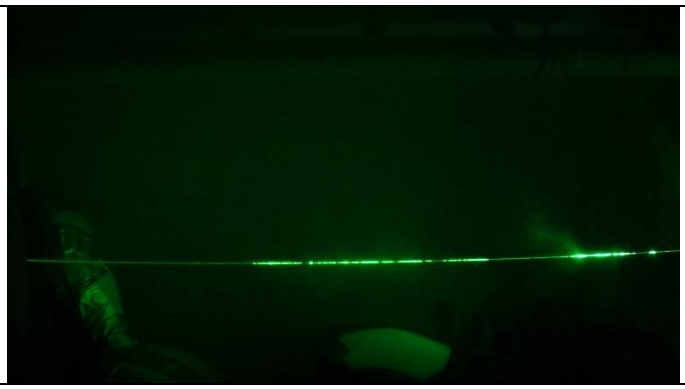

Figure J.2.42 Seat A6 frontal view snapshot 41.

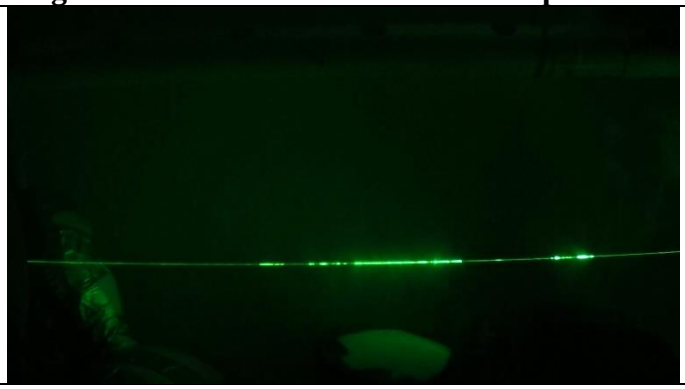

Figure J.2.43 Seat A6 frontal view snapshot 42.

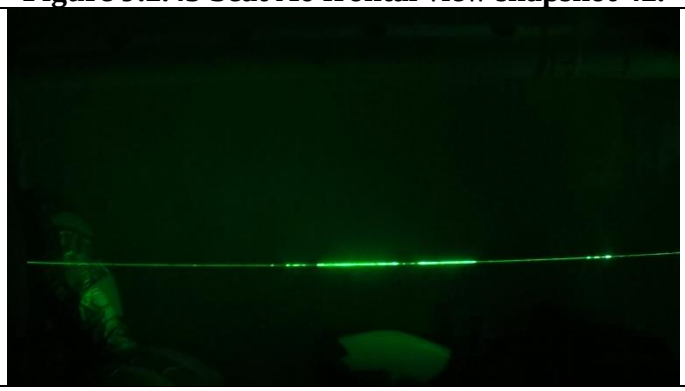

Figure J.2.44 Seat A6 frontal view snapshot 43.

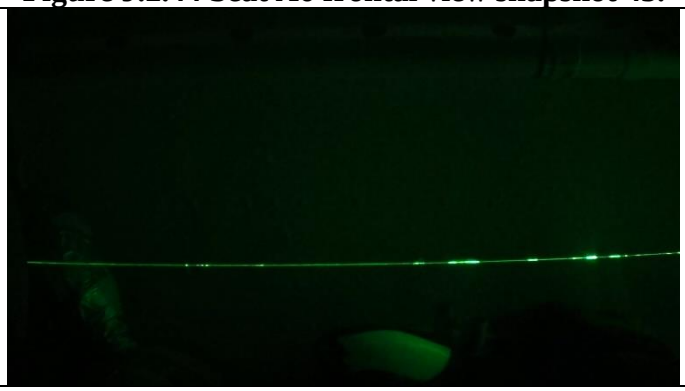

Figure J.2.45 Seat A6 frontal view snapshot 44.

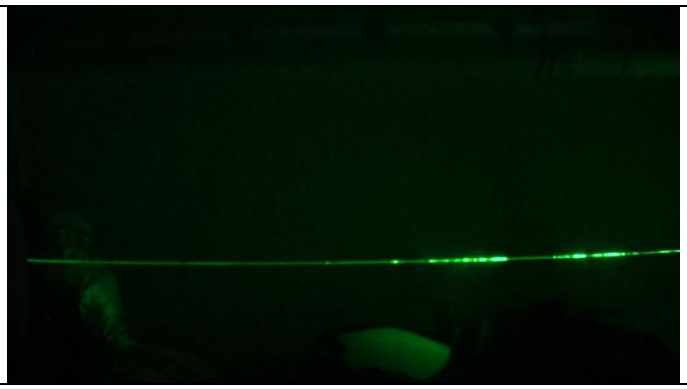

Figure J.2.46 Seat A6 frontal view snapshot 45.

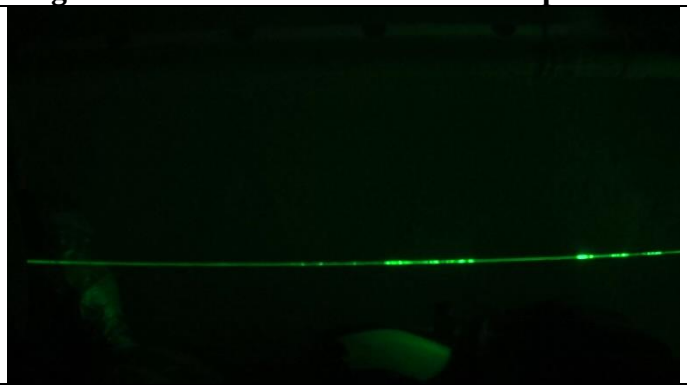

Figure J.2.47 Seat A6 frontal view snapshot 46.

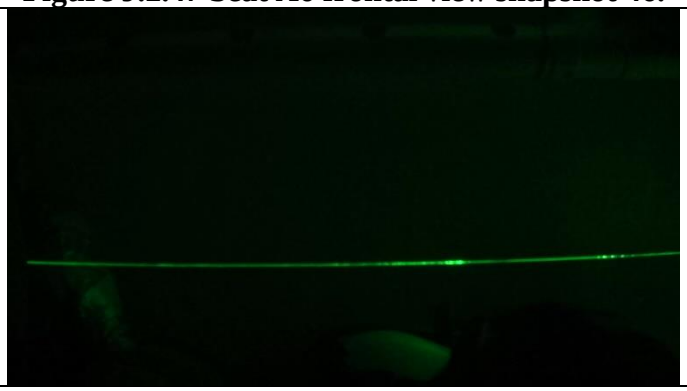

Figure J.2.48 Seat A6 frontal view snapshot 47.

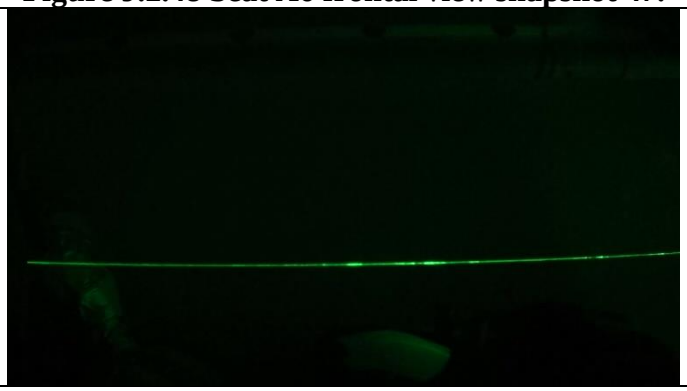

Figure J.2.49 Seat A6 frontal view snapshot 48.

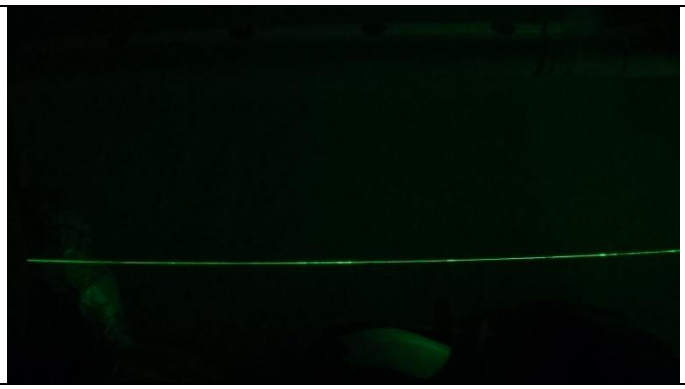

Figure J.2.50 Seat A6 frontal view snapshot 49.

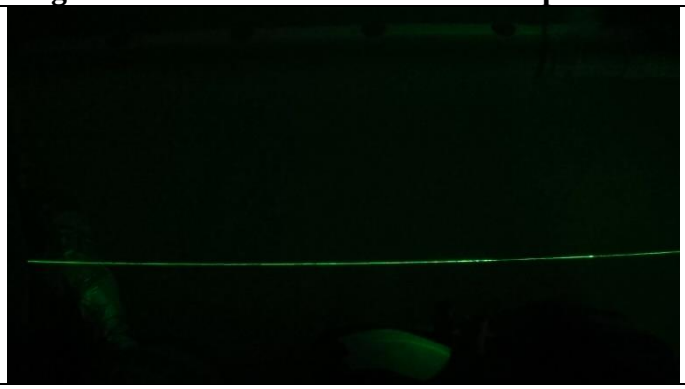

Figure J.2.51 Seat A6 frontal view snapshot 50.

Appendix K - Seat D1 Smoke Visualization Snapshots

K.1 Cross-sectional View

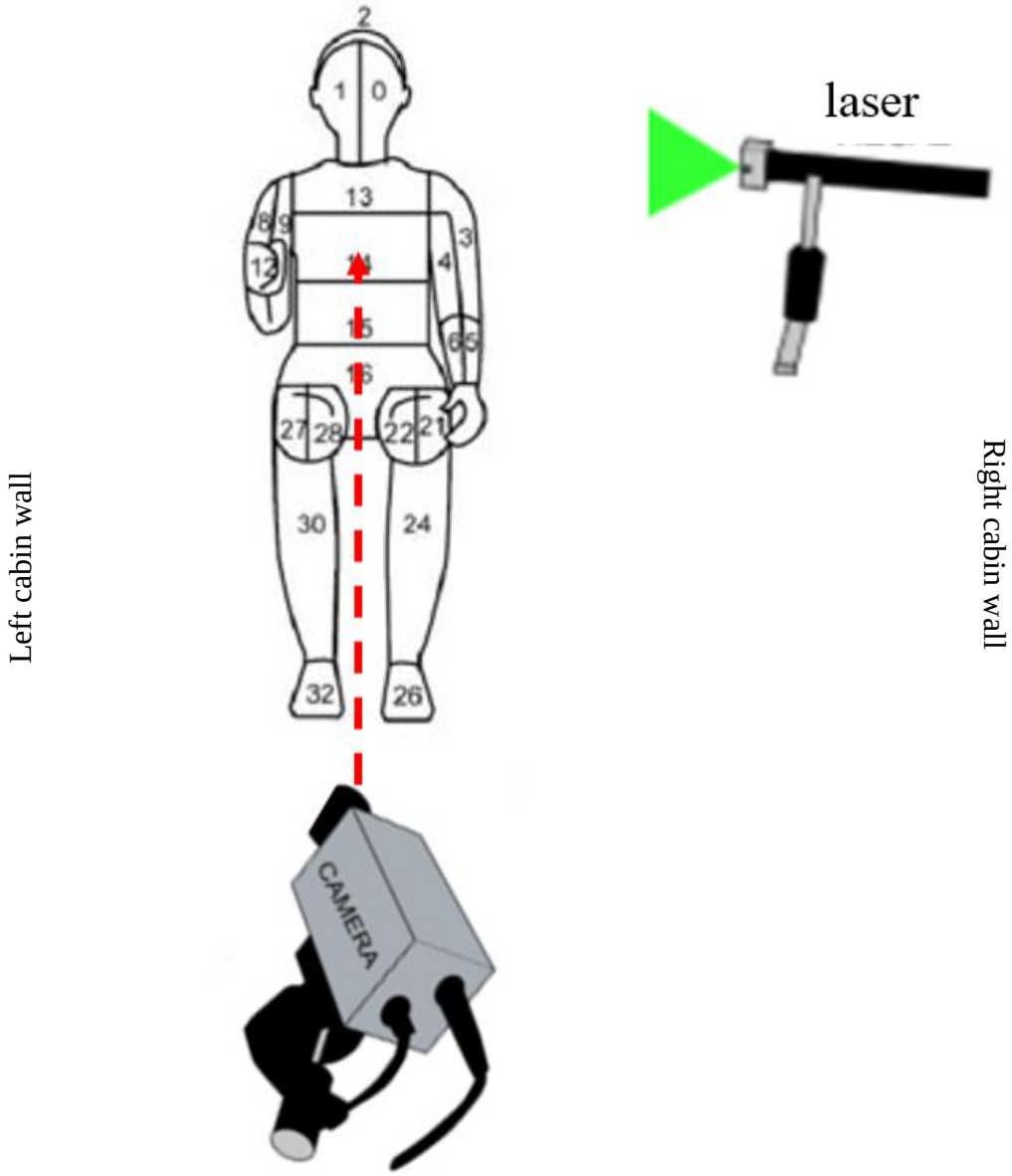

Figure K.1.1 A schematic showing the cross-sectional laser sheet direction and the camera location relative to the seat where the smoke generation source is located on seat D1.

Figure K.1.2 Seat D1 cross-sectional view snapshot 01.

Figure K.1.3 Seat D1 cross-sectional view snapshot 02.

Figure K.1.4 Seat D1 cross-sectional view snapshot 03.

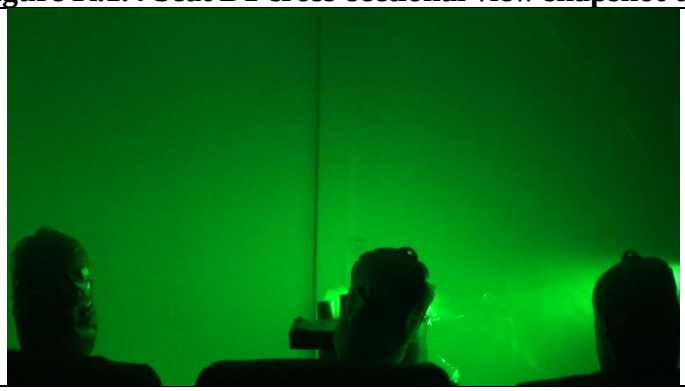

Figure K.1.5 Seat D1 cross-sectional view snapshot 04.

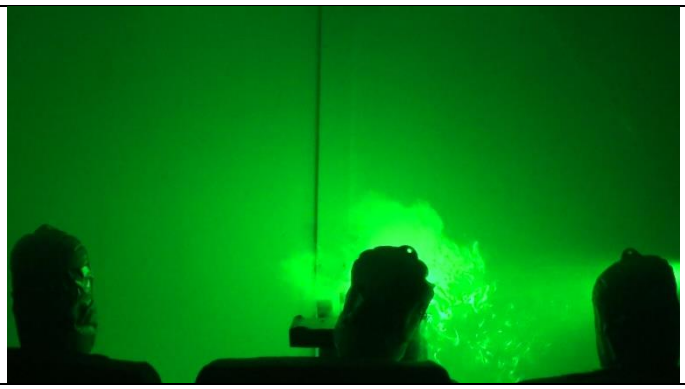

Figure K.1.6 Seat D1 cross-sectional view snapshot 05.

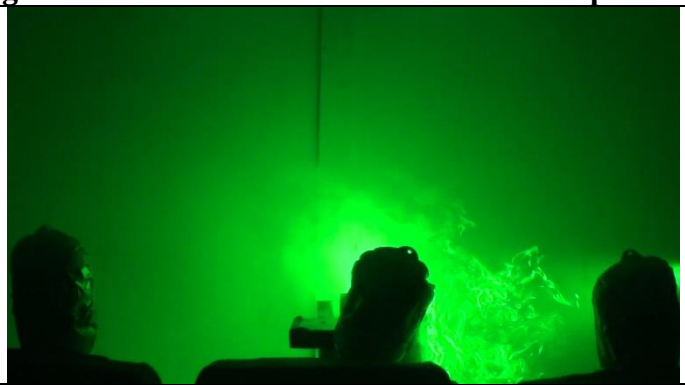

Figure K.1.7 Seat D1 cross-sectional view snapshot 06.

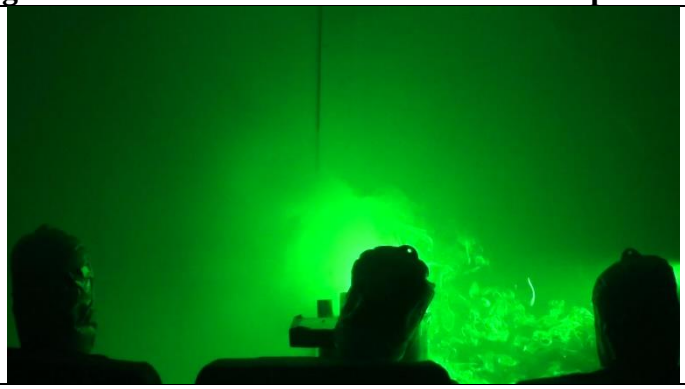

Figure K.1.8 Seat D1 cross-sectional view snapshot 07.

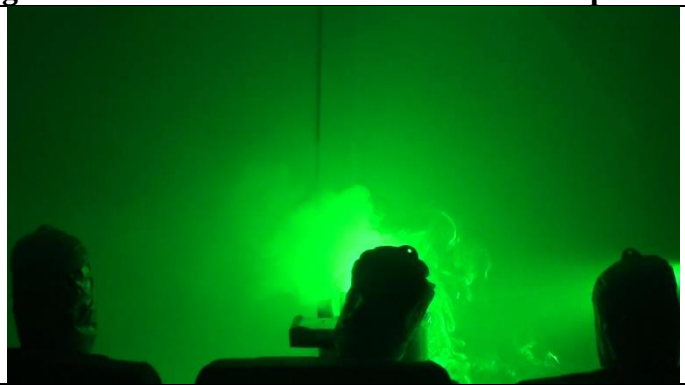

Figure K.1.9 Seat D1 cross-sectional view snapshot 08.

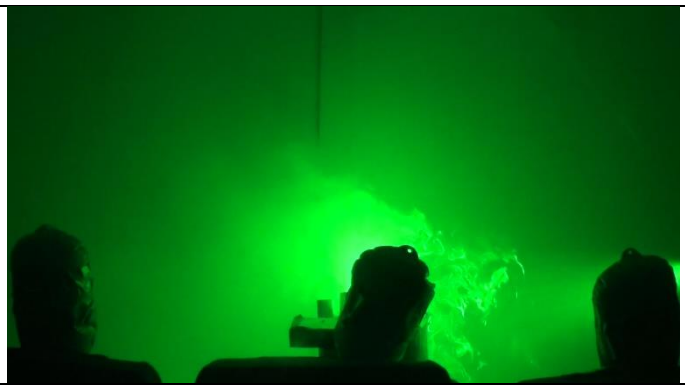

Figure K.1.10 Seat D1 cross-sectional view snapshot 09.

Figure K.1.11 Seat D1 cross-sectional view snapshot 10.

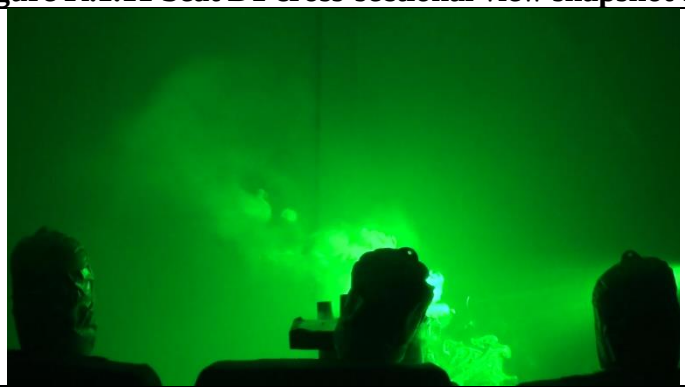

Figure K.1.12 Seat D1 cross-sectional view snapshot 11.

Figure K.1.13 Seat D1 cross-sectional view snapshot 12.

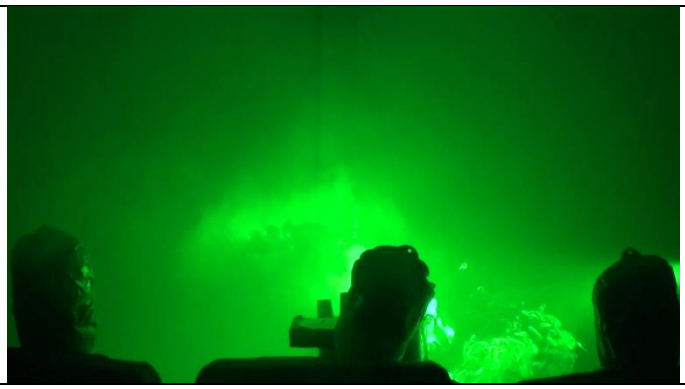

Figure K.1.14 Seat D1 cross-sectional view snapshot 13.

Figure K.1.15 Seat D1 cross-sectional view snapshot 14.

Figure K.1.16 Seat D1 cross-sectional view snapshot 15.

Figure K.1.17 Seat D1 cross-sectional view snapshot 16.

Figure K.1.18 Seat D1 cross-sectional view snapshot 17.

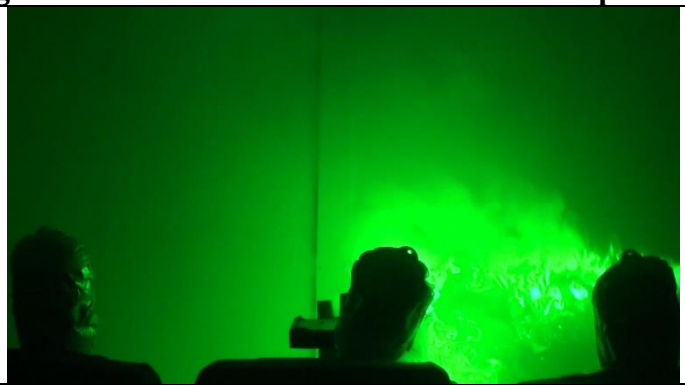

Figure K.1.19 Seat D1 cross-sectional view snapshot 18.

Figure K.1.20 Seat D1 cross-sectional view snapshot 19.

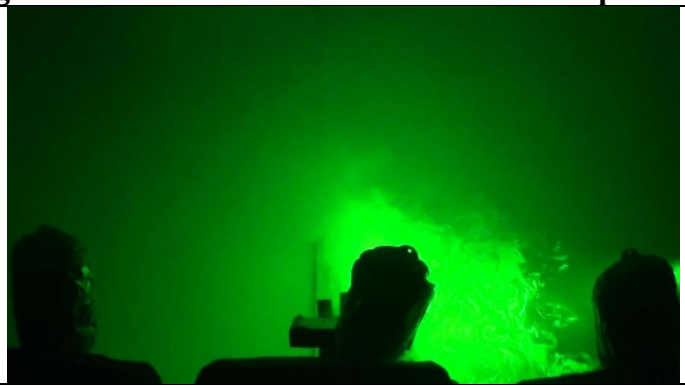

Figure K.1.21 Seat D1 cross-sectional view snapshot 20.

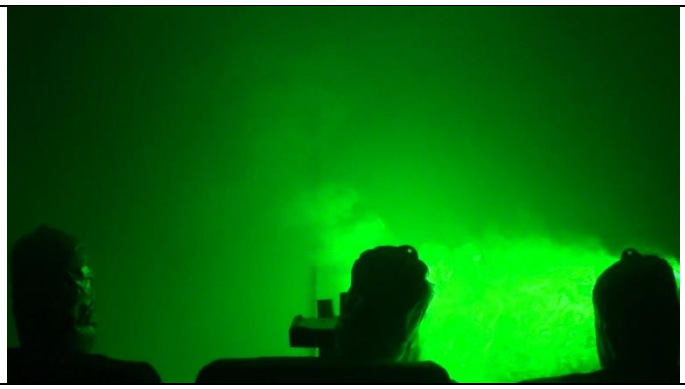

Figure K.1.22 Seat D1 cross-sectional view snapshot 21.

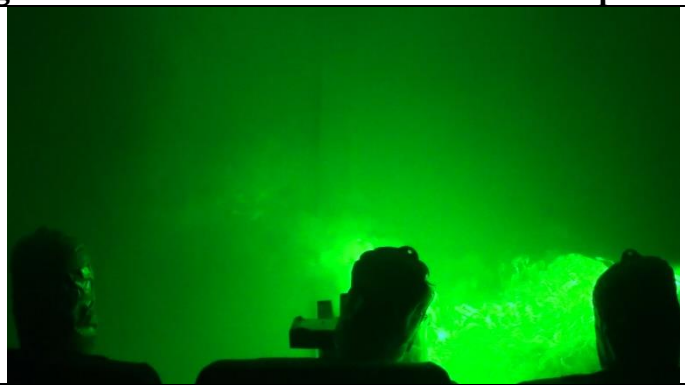

Figure K.1.23 Seat D1 cross-sectional view snapshot 22.

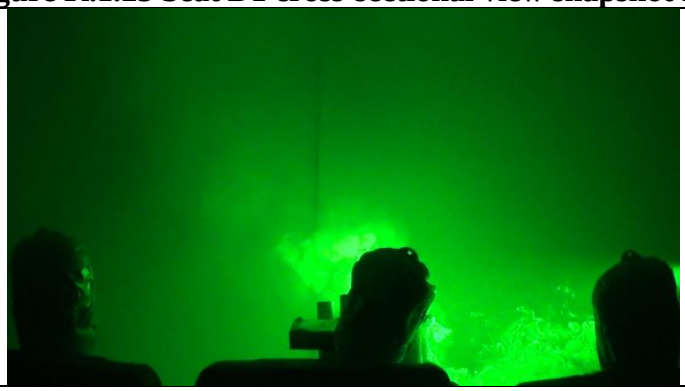

Figure K.1.24 Seat D1 cross-sectional view snapshot 23.

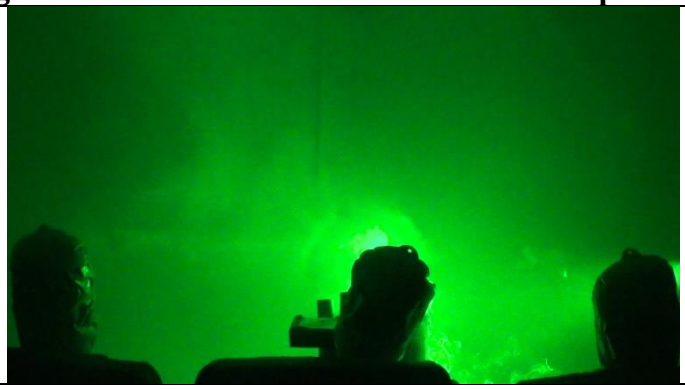

Figure K.1.25 Seat D1 cross-sectional view snapshot 24.

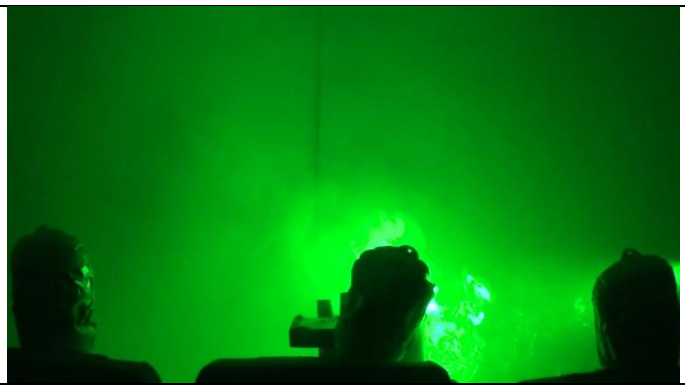

Figure K.1.26 Seat D1 cross-sectional view snapshot 25.

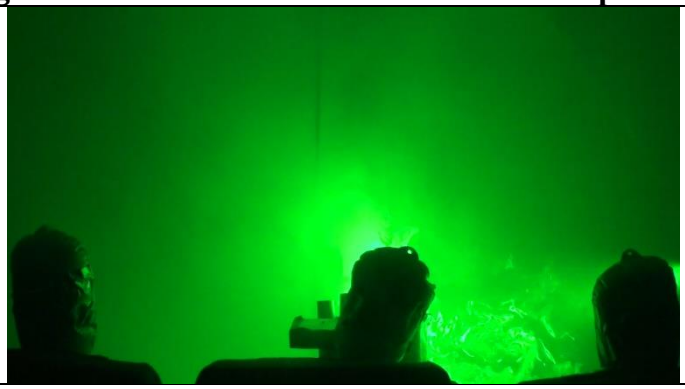

Figure K.1.27 Seat D1 cross-sectional view snapshot 26.

Figure K.1.28 Seat D1 cross-sectional view snapshot 27.

Figure K.1.29 Seat D1 cross-sectional view snapshot 28.

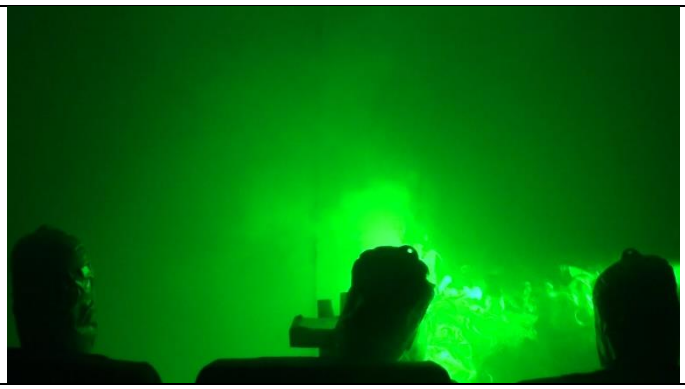

Figure K.1.30 Seat D1 cross-sectional view snapshot 29.

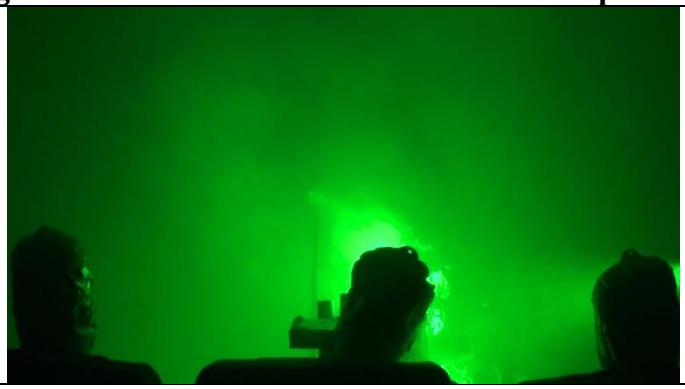

Figure K.1.31 Seat D1 cross-sectional view snapshot 30.

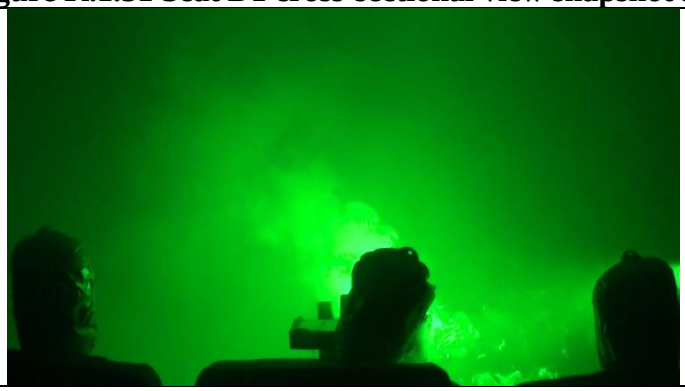

Figure K.1.32 Seat D1 cross-sectional view snapshot 31.

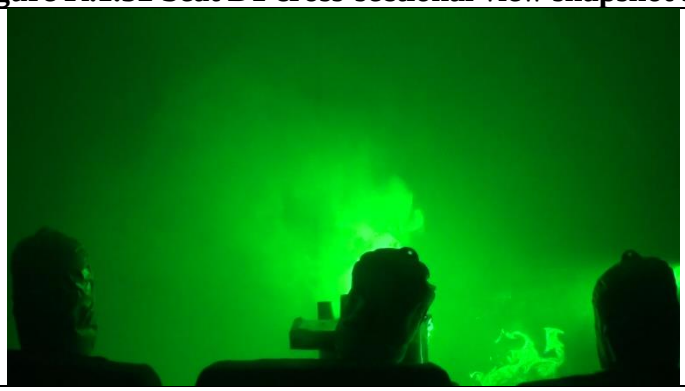

Figure K.1.33 Seat D1 cross-sectional view snapshot 32.

Figure K.1.34 Seat D1 cross-sectional view snapshot 33.

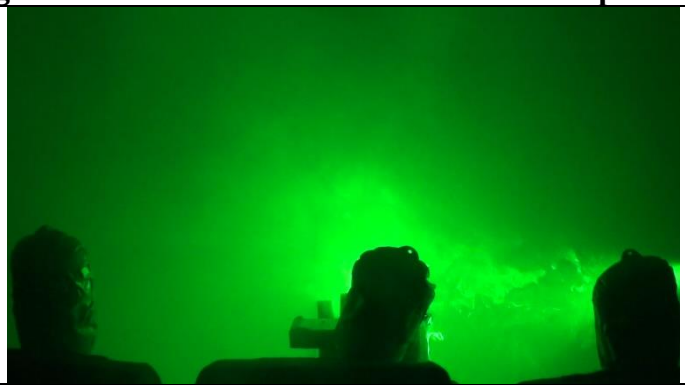

Figure K.1.35 Seat D1 cross-sectional view snapshot 34.

Figure K.1.36 Seat D1 cross-sectional view snapshot 35.

Figure K.1.37 Seat D1 cross-sectional view snapshot 36.

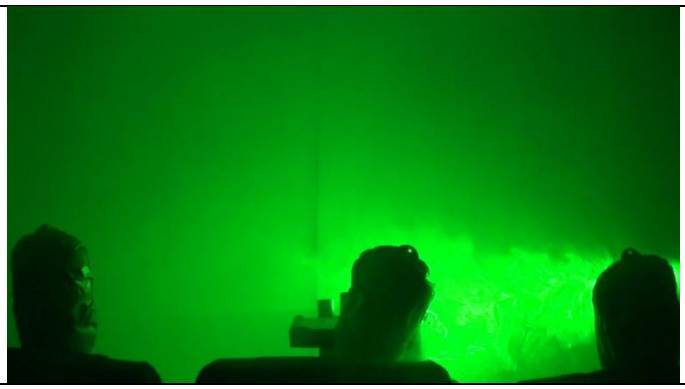

Figure K.1.38 Seat D1 cross-sectional view snapshot 37.

Figure K.1.39 Seat D1 cross-sectional view snapshot 38.

Figure K.1.40 Seat D1 cross-sectional view snapshot 39.

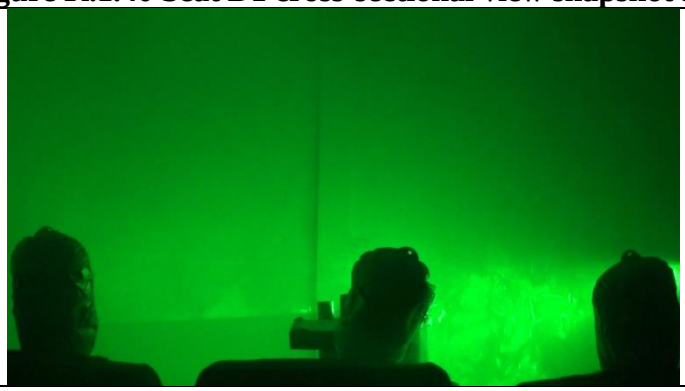

Figure K.1.41 Seat D1 cross-sectional view snapshot 40.

Figure K.1.42 Seat D1 cross-sectional view snapshot 41.

Figure K.1.43 Seat D1 cross-sectional view snapshot 42.

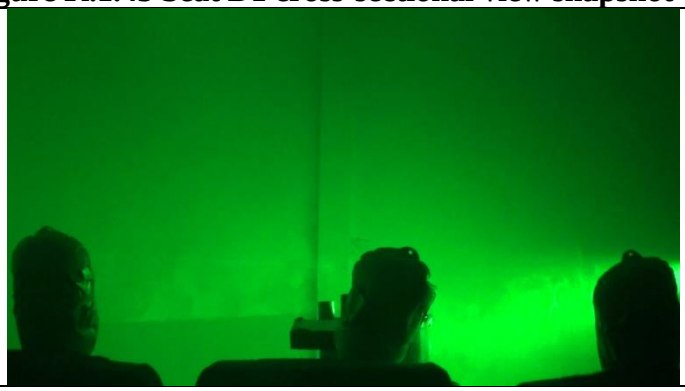

Figure K.1.44 Seat D1 cross-sectional view snapshot 43.

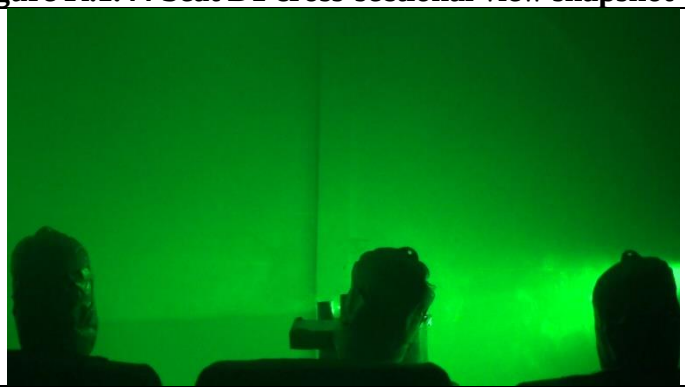

Figure K.1.45 Seat D1 cross-sectional view snapshot 44.

Figure K.1.46 Seat D1 cross-sectional view snapshot 45.

Figure K.1.47 Seat D1 cross-sectional view snapshot 46.

Figure K.1.48 Seat D1 cross-sectional view snapshot 47.

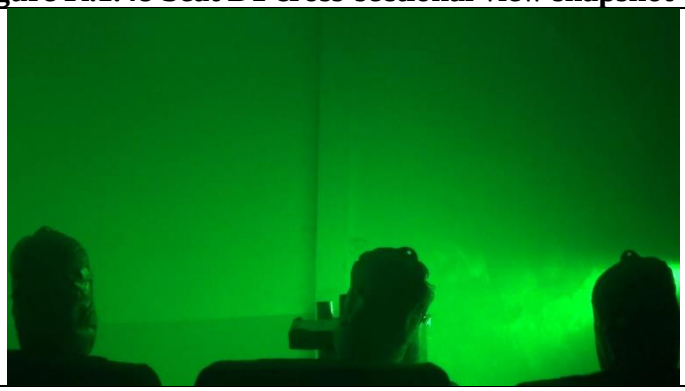

Figure K.1.49 Seat D1 cross-sectional view snapshot 48.

Figure K.1.50 Seat D1 cross-sectional view snapshot 49.

Figure K.1.51 Seat D1 cross-sectional view snapshot 50.

K.2 Frontal View

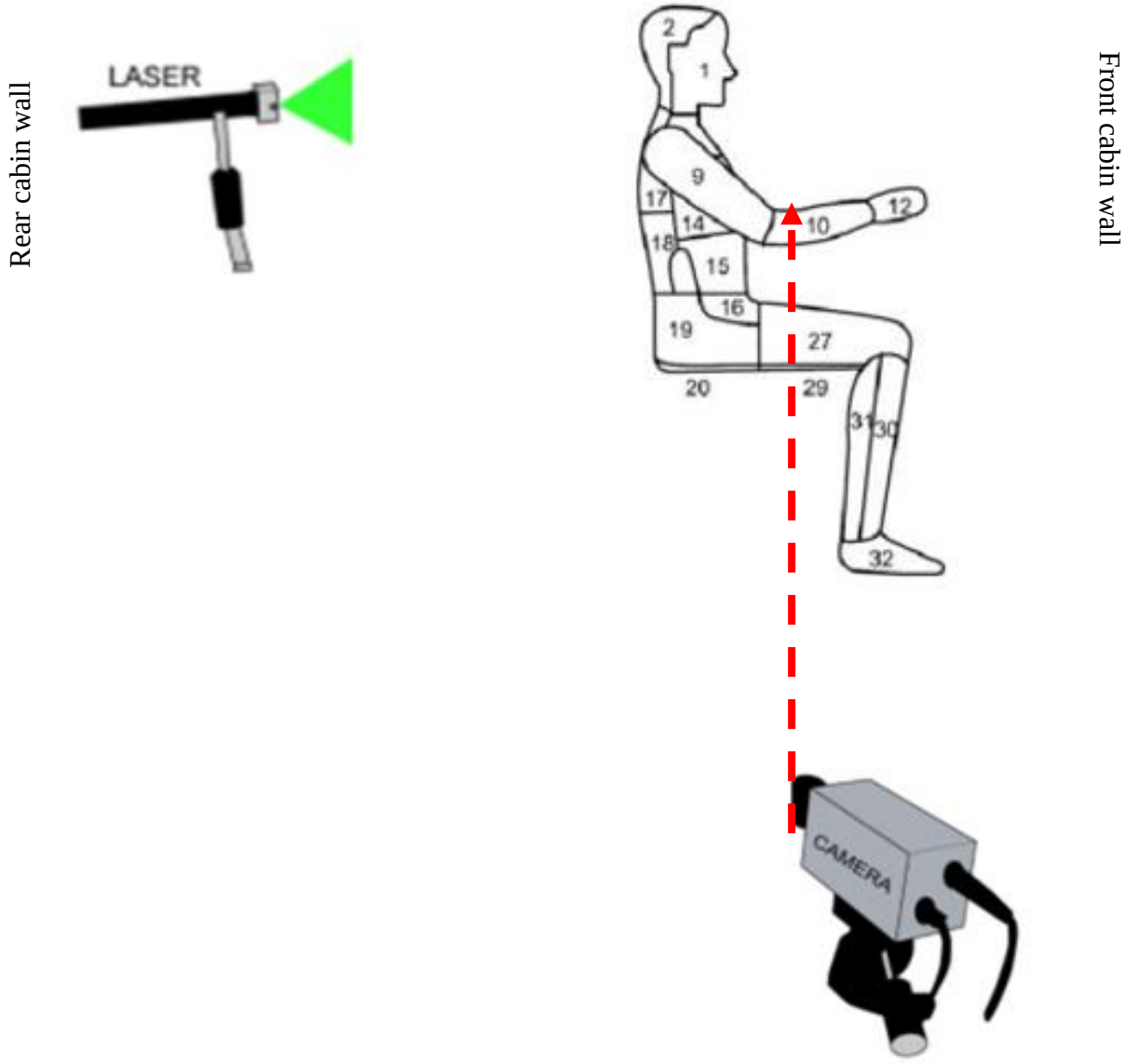

Figure K.2.1 A schematic showing the frontal laser sheet direction and the camera location relative to the seat where the smoke generation source is located on seat D1.

Figure K.2.2 Seat D1 frontal view snapshot 01.

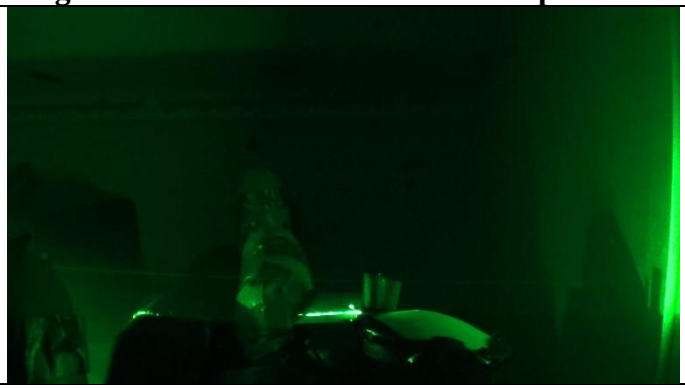

Figure K.2.3 Seat D1 frontal view snapshot 02.

Figure K.2.4 Seat D1 frontal view snapshot 03.

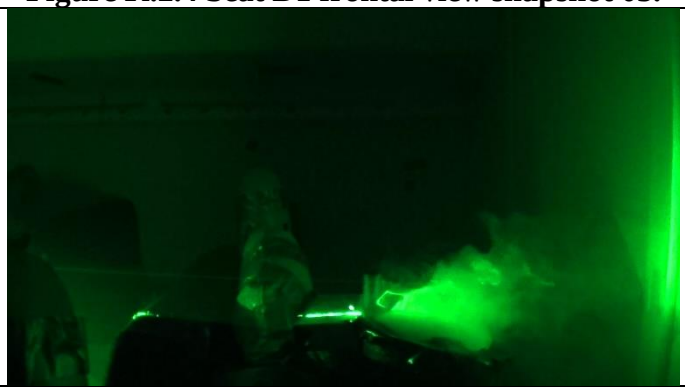

Figure K.2.5 Seat D1 frontal view snapshot 04.

Figure K.2.6 Seat D1 frontal view snapshot 05.

Figure K.2.7 Seat D1 frontal view snapshot 06.

Figure K.2.8 Seat D1 frontal view snapshot 07.

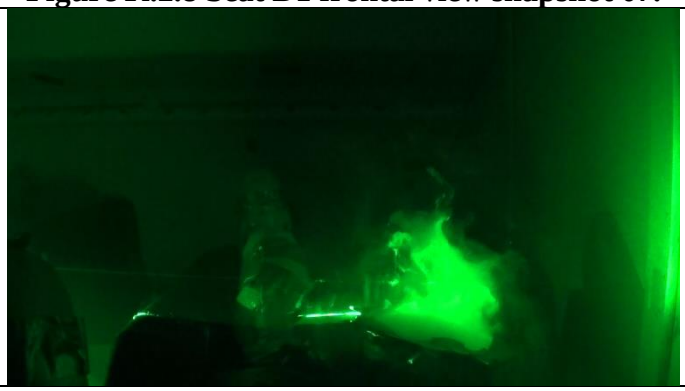

Figure K.2.9 Seat D1 frontal view snapshot 08.

Figure K.2.10 Seat D1 frontal view snapshot 09.

Figure K.2.11 Seat D1 frontal view snapshot 10.

Figure K.2.12 Seat D1 frontal view snapshot 11.

Figure K.2.13 Seat D1 frontal view snapshot 12.

Figure K.2.14 Seat D1 frontal view snapshot 13.

Figure K.2.15 Seat D1 frontal view snapshot 14.

Figure K.2.16 Seat D1 frontal view snapshot 15.

Figure K.2.17 Seat D1 frontal view snapshot 16.

Figure K.2.18 Seat D1 frontal view snapshot 17.

Figure K.2.19 Seat D1 frontal view snapshot 18.

Figure K.2.20 Seat D1 frontal view snapshot 19.

Figure K.2.21 Seat D1 frontal view snapshot 20.

Figure K.2.22 Seat D1 frontal view snapshot 21.

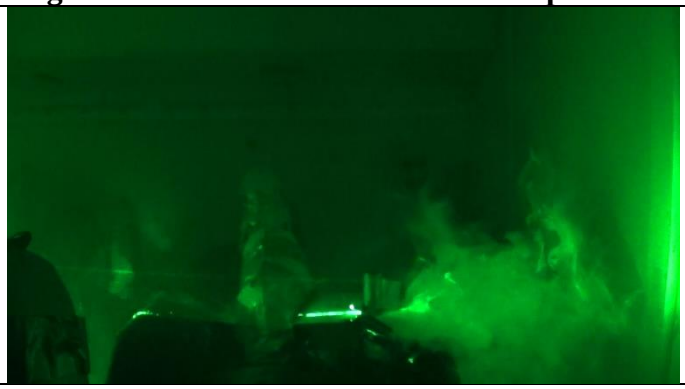

Figure K.2.23 Seat D1 frontal view snapshot 22.

Figure K.2.24 Seat D1 frontal view snapshot 23.

Figure K.2.25 Seat D1 frontal view snapshot 24.

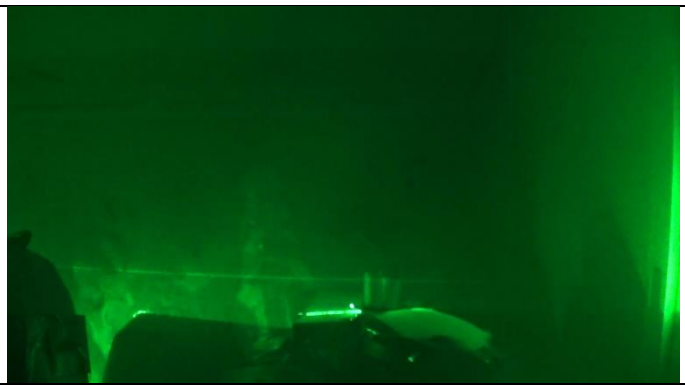

Figure K.2.26 Seat D1 frontal view snapshot 25.

Figure K.2.27 Seat D1 frontal view snapshot 26.

Figure K.2.28 Seat D1 frontal view snapshot 27.

Figure K.2.29 Seat D1 frontal view snapshot 28.

Figure K.2.30 Seat D1 frontal view snapshot 29.

Figure K.2.31 Seat D1 frontal view snapshot 30.

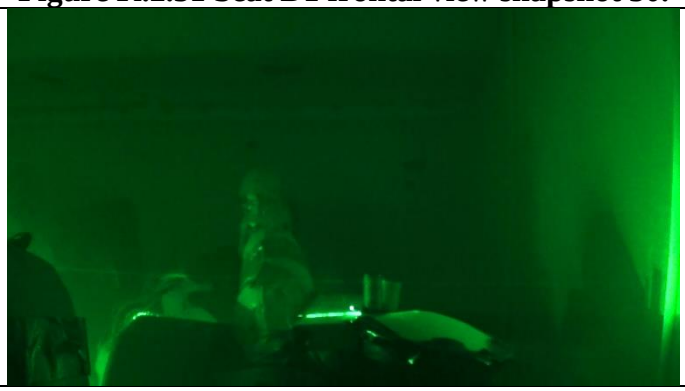

Figure K.2.32 Seat D1 frontal view snapshot 31.

Figure K.2.33 Seat D1 frontal view snapshot 32.

Figure K.2.34 Seat D1 frontal view snapshot 33.

Figure K.2.35 Seat D1 frontal view snapshot 34.

Figure K.2.36 Seat D1 frontal view snapshot 35.

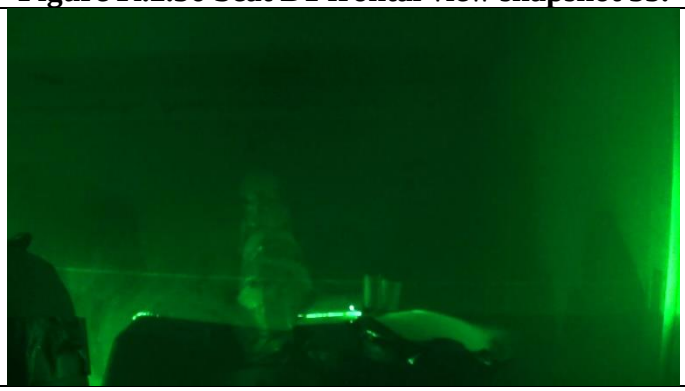

Figure K.2.37 Seat D1 frontal view snapshot 36.

Figure K.2.38 Seat D1 frontal view snapshot 37.

Figure K.2.39 Seat D1 frontal view snapshot 38.

Figure K.2.40 Seat D1 frontal view snapshot 39.

Figure K.2.41 Seat D1 frontal view snapshot 40.

Figure K.2.42 Seat D1 frontal view snapshot 41.

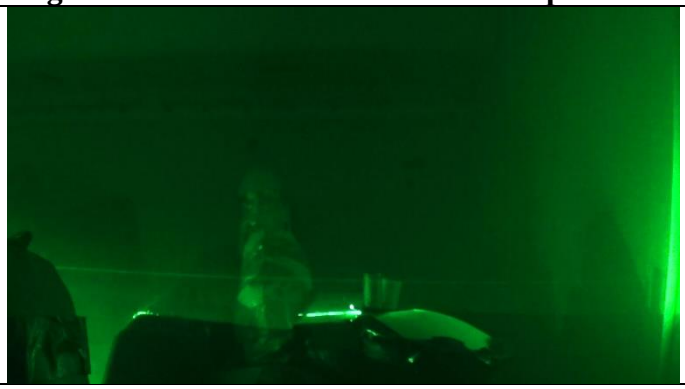

Figure K.2.43 Seat D1 frontal view snapshot 42.

Figure K.2.44 Seat D1 frontal view snapshot 43.

Figure K.2.45 Seat D1 frontal view snapshot 44.

Figure K.2.46 Seat D1 frontal view snapshot 45.

Figure K.2.47 Seat D1 frontal view snapshot 46.

Figure K.2.48 Seat D1 frontal view snapshot 47.

Figure K.2.49 Seat D1 frontal view snapshot 48.

Figure K.2.50 Seat D1 frontal view snapshot 49.

Figure K.2.51 Seat D1 frontal view snapshot 50.

Appendix L - Seat D6 Smoke Visualization Snapshots

L.1 Cross-sectional View

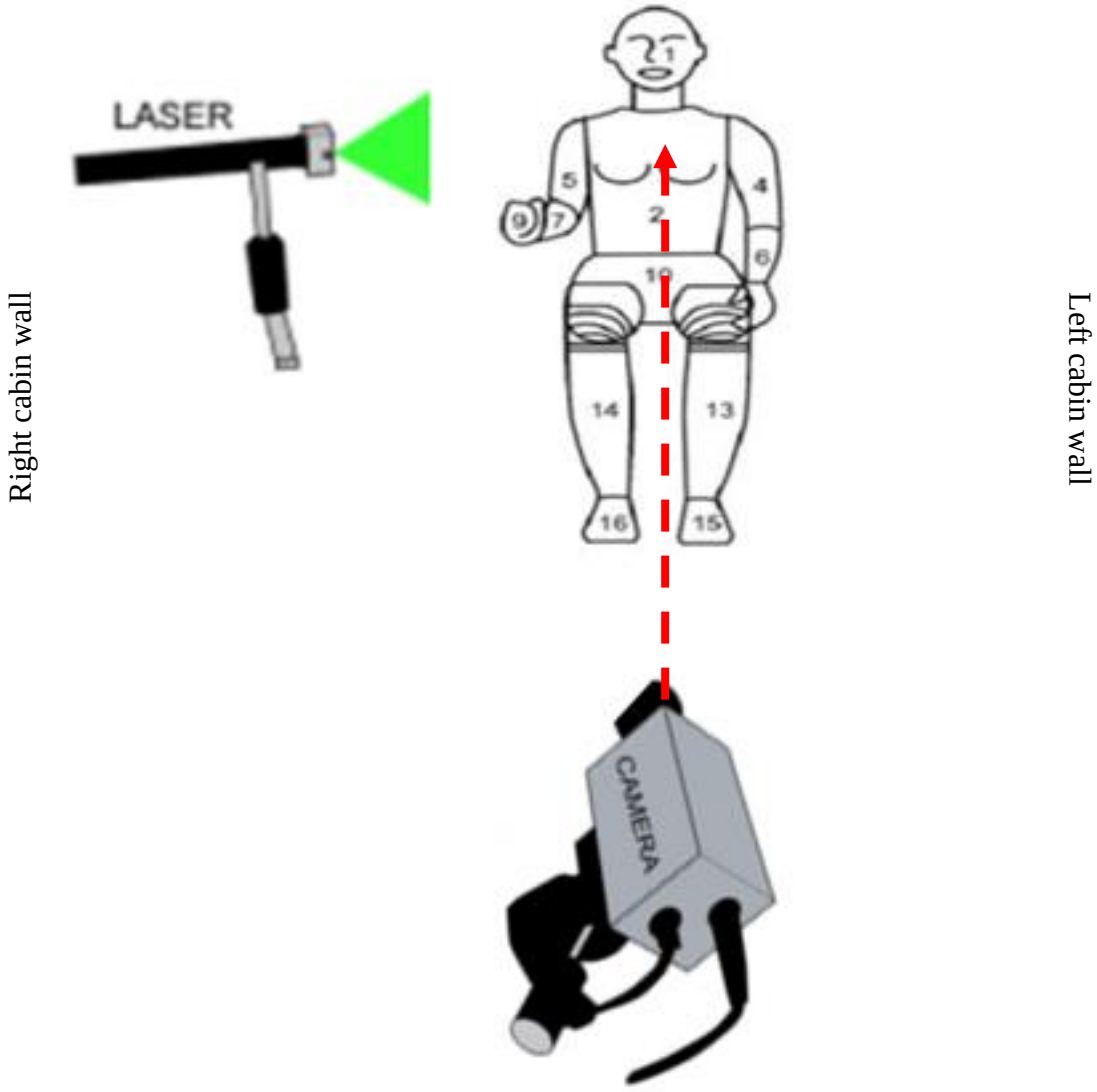

Figure L.1.1 A schematic showing the cross-sectional laser sheet direction and the camera location relative to the seat where the smoke generation source is located on seat D6.

Figure L.1.2 Seat D6 cross-sectional view snapshot 01.

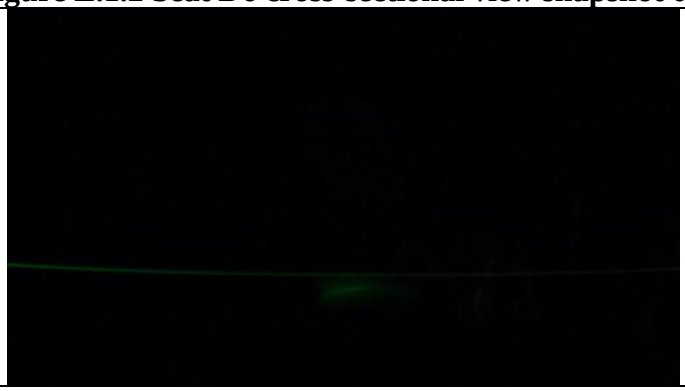

Figure L.1.3 Seat D6 cross-sectional view snapshot 02.

Figure L.1.4 Seat D6 cross-sectional view snapshot 03.

Figure L.1.5 Seat D6 cross-sectional view snapshot 04.

Figure L.1.6 Seat D6 cross-sectional view snapshot 05.

Figure L.1.7 Seat D6 cross-sectional view snapshot 06.

Figure L.1.8 Seat D6 cross-sectional view snapshot 07.

Figure L.1.9 Seat D6 cross-sectional view snapshot 08.

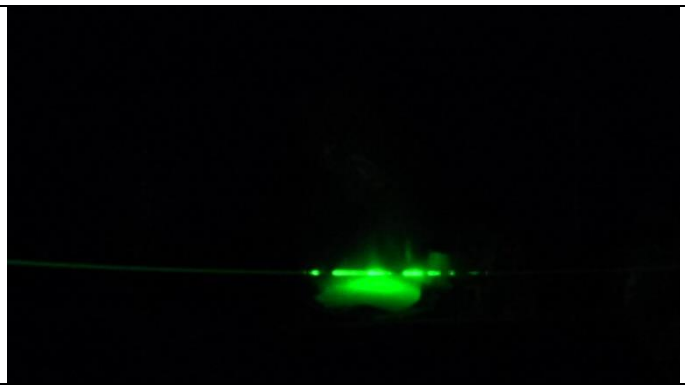

Figure L.1.10 Seat D6 cross-sectional view snapshot 09.

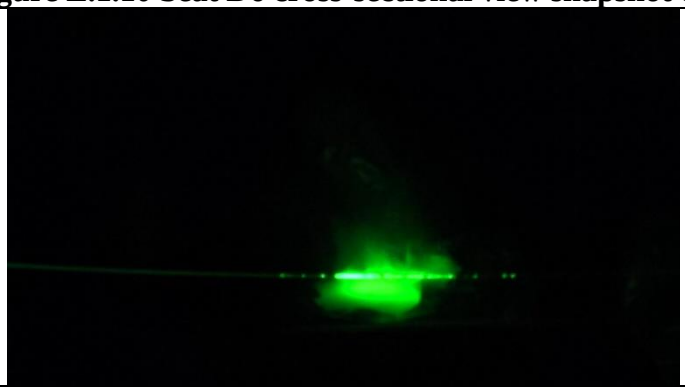

Figure L.1.11 Seat D6 cross-sectional view snapshot 10.

Figure L.1.12 Seat D6 cross-sectional view snapshot 11.

Figure L.1.13 Seat D6 cross-sectional view snapshot 12.

Figure L.1.14 Seat D6 cross-sectional view snapshot 13.

Figure L.1.15 Seat D6 cross-sectional view snapshot 14.

Figure L.1.16 Seat D6 cross-sectional view snapshot 15.

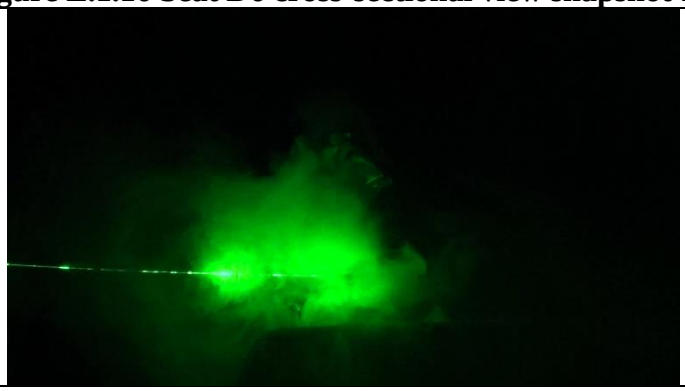

Figure L.1.17 Seat D6 cross-sectional view snapshot 16.

Figure L.1.18 Seat D6 cross-sectional view snapshot 17.

Figure L.1.19 Seat D6 cross-sectional view snapshot 18.

Figure L.1.20 Seat D6 cross-sectional view snapshot 19.

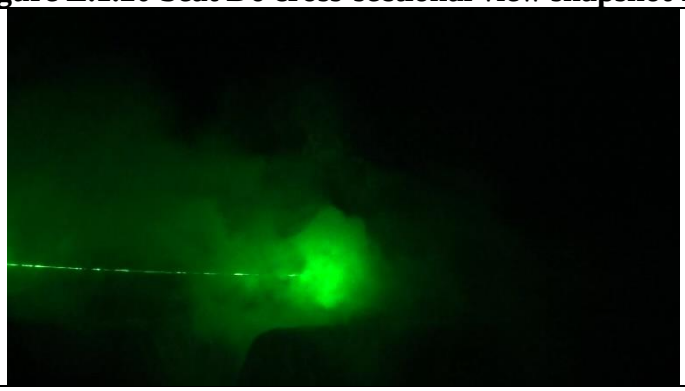

Figure L.1.21 Seat D6 cross-sectional view snapshot 20.

Figure L.1.22 Seat D6 cross-sectional view snapshot 21.

Figure L.1.23 Seat D6 cross-sectional view snapshot 22.

Figure L.1.24 Seat D6 cross-sectional view snapshot 23.

Figure L.1.25 Seat D6 cross-sectional view snapshot 24.

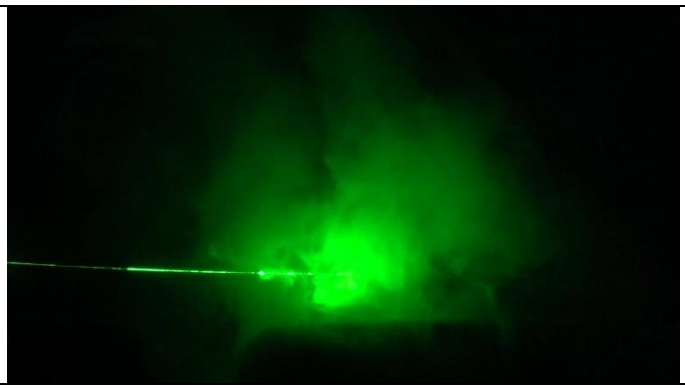

Figure L.1.26 Seat D6 cross-sectional view snapshot 25.

Figure L.1.27 Seat D6 cross-sectional view snapshot 26.

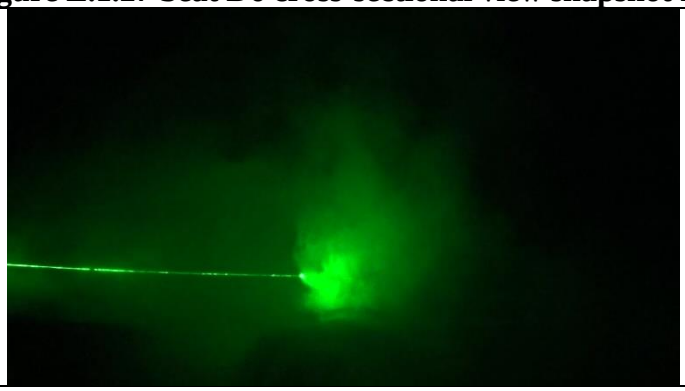

Figure L.1.28 Seat D6 cross-sectional view snapshot 27.

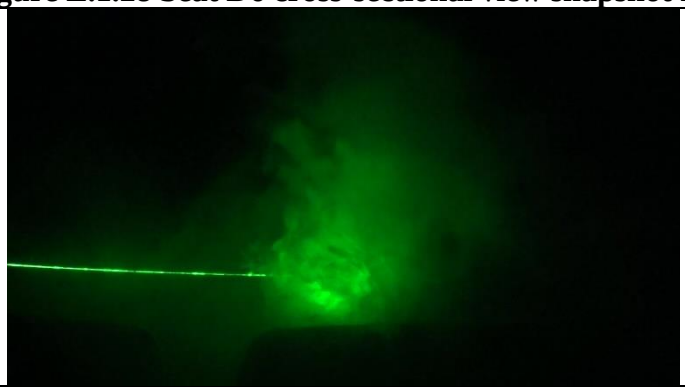

Figure L.1.29 Seat D6 cross-sectional view snapshot 28.

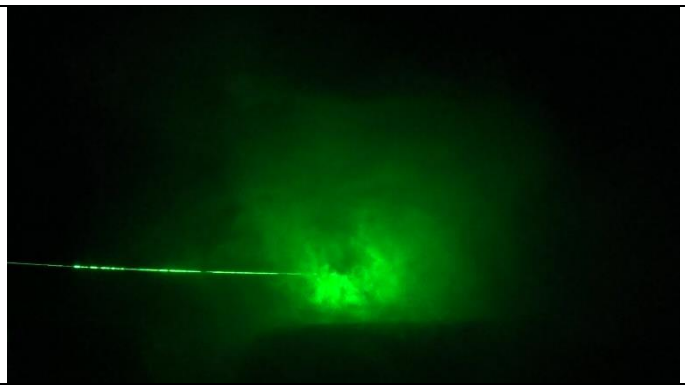

Figure L.1.30 Seat D6 cross-sectional view snapshot 29.

Figure L.1.31 Seat D6 cross-sectional view snapshot 30.

Figure L.1.32 Seat D6 cross-sectional view snapshot 31.

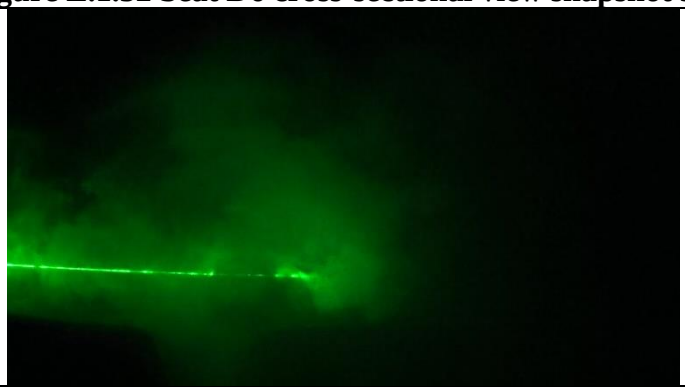

Figure L.1.33 Seat D6 cross-sectional view snapshot 32.

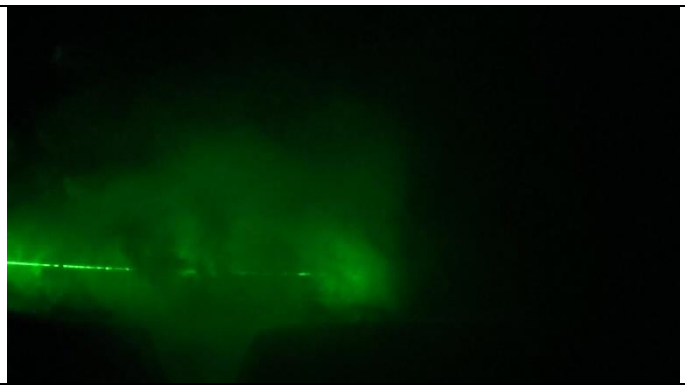

Figure L.1.34 Seat D6 cross-sectional view snapshot 33.

Figure L.1.35 Seat D6 cross-sectional view snapshot 34.

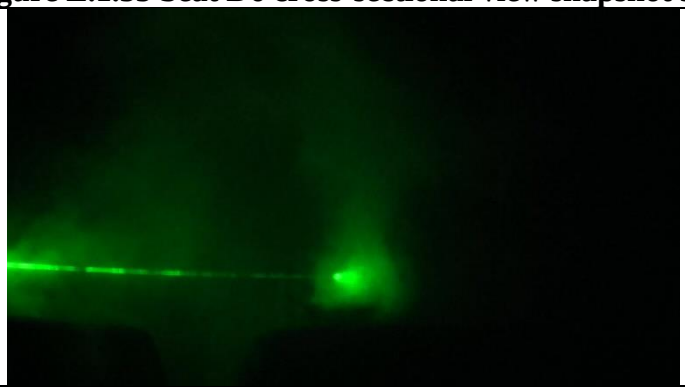

Figure L.1.36 Seat D6 cross-sectional view snapshot 35.

Figure L.1.37 Seat D6 cross-sectional view snapshot 36.

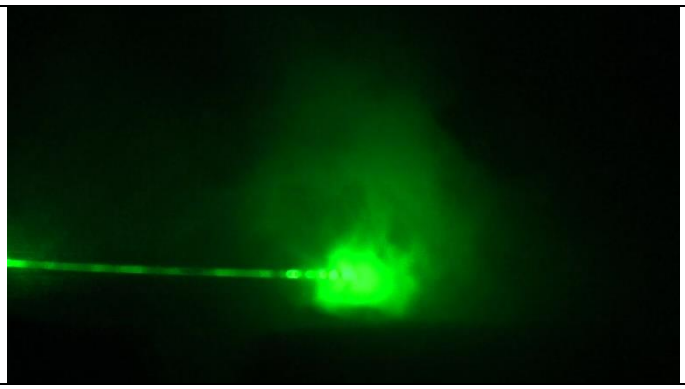

Figure L.1.38 Seat D6 cross-sectional view snapshot 37.

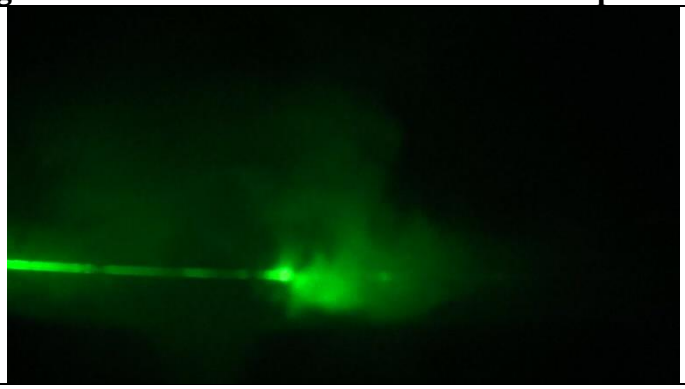

Figure L.1.39 Seat D6 cross-sectional view snapshot 38.

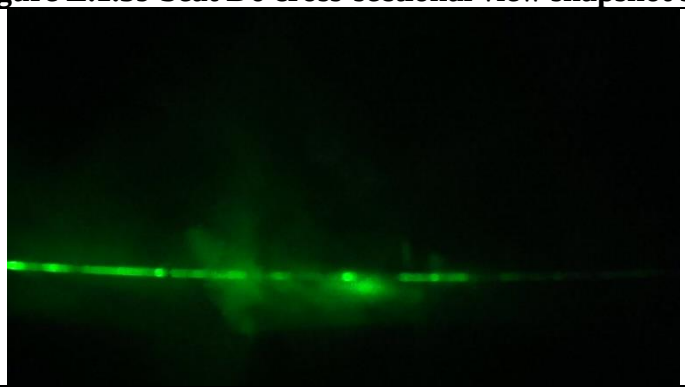

Figure L.1.40 Seat D6 cross-sectional view snapshot 39.

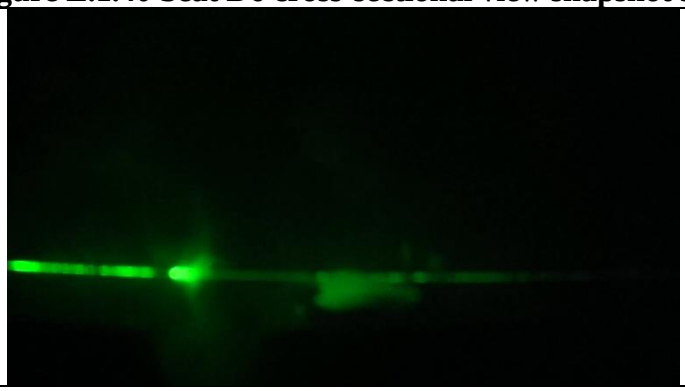

Figure L.1.41 Seat D6 cross-sectional view snapshot 40.

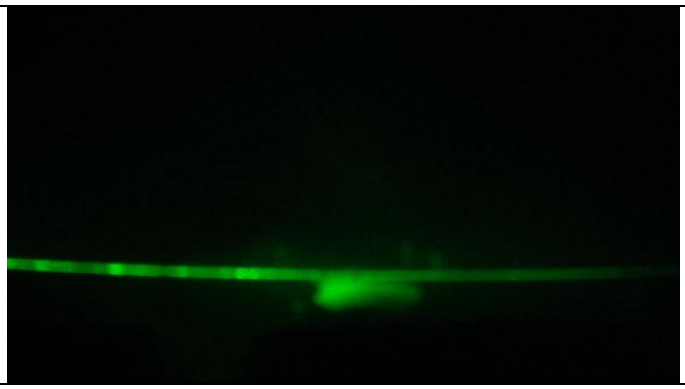

Figure L.1.42 Seat D6 cross-sectional view snapshot 41.

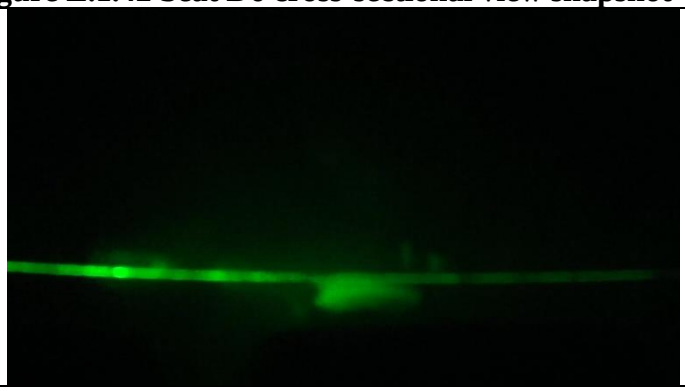

Figure L.1.43 Seat D6 cross-sectional view snapshot 42.

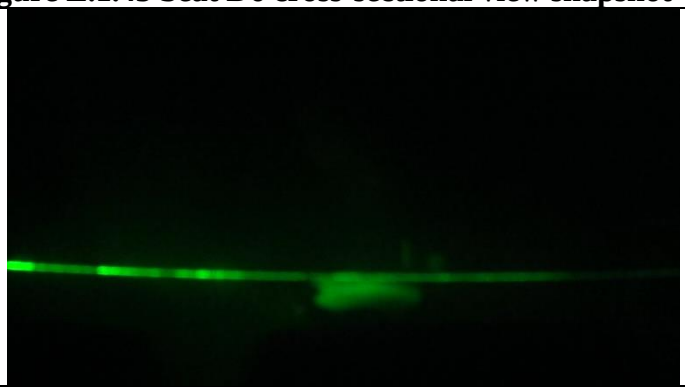

Figure L.1.44 Seat D6 cross-sectional view snapshot 43.

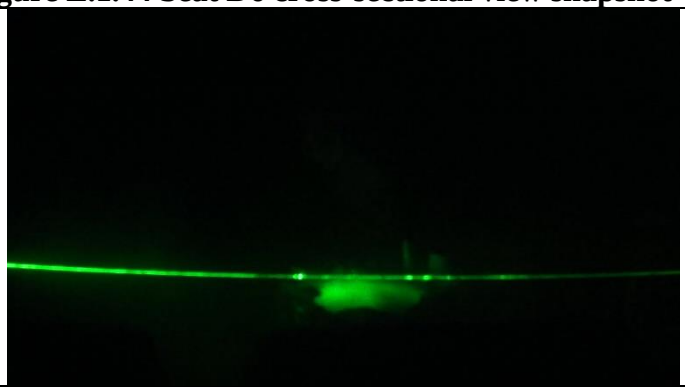

Figure L.1.45 Seat D6 cross-sectional view snapshot 44.

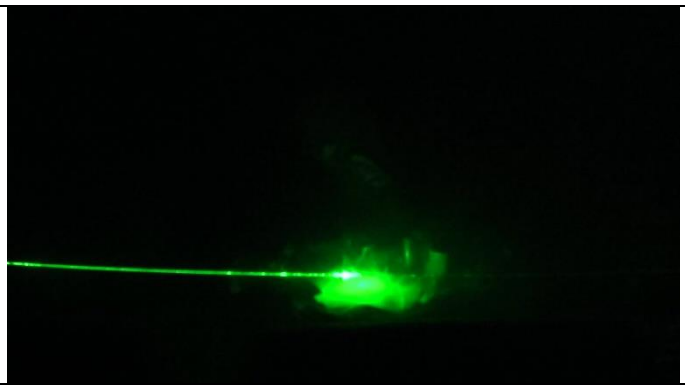

Figure L.1.46 Seat D6 cross-sectional view snapshot 45.

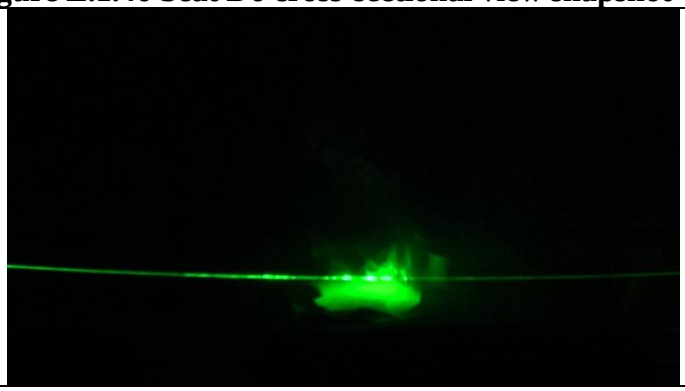

Figure L.1.47 Seat D6 cross-sectional view snapshot 46.

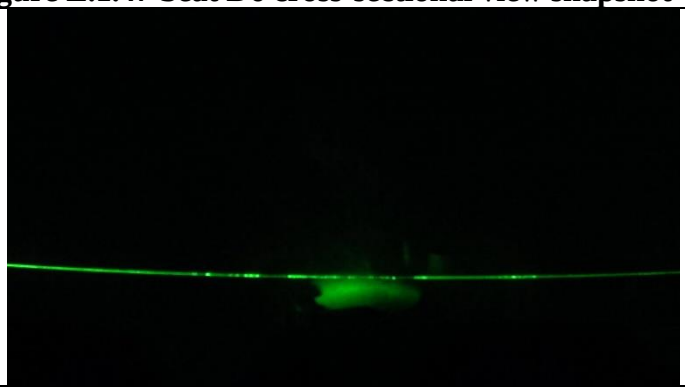

Figure L.1.48 Seat D6 cross-sectional view snapshot 47.

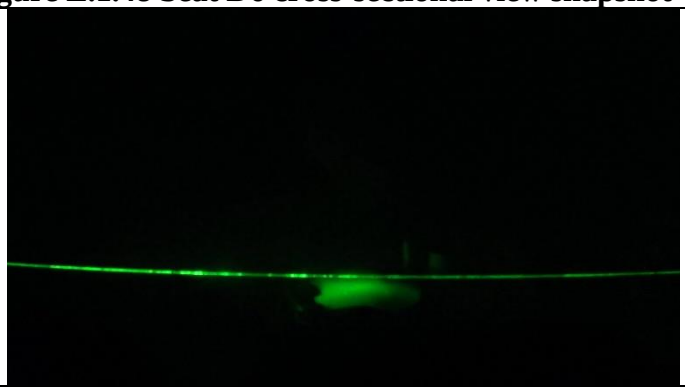

Figure L.1.49 Seat D6 cross-sectional view snapshot 48.

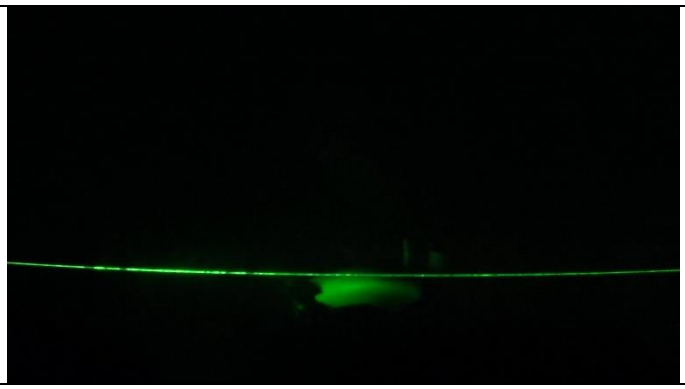

Figure L.1.50 Seat D6 cross-sectional view snapshot 49.

Figure L.1.51 Seat D6 cross-sectional view snapshot 50.

L.2 Frontal View

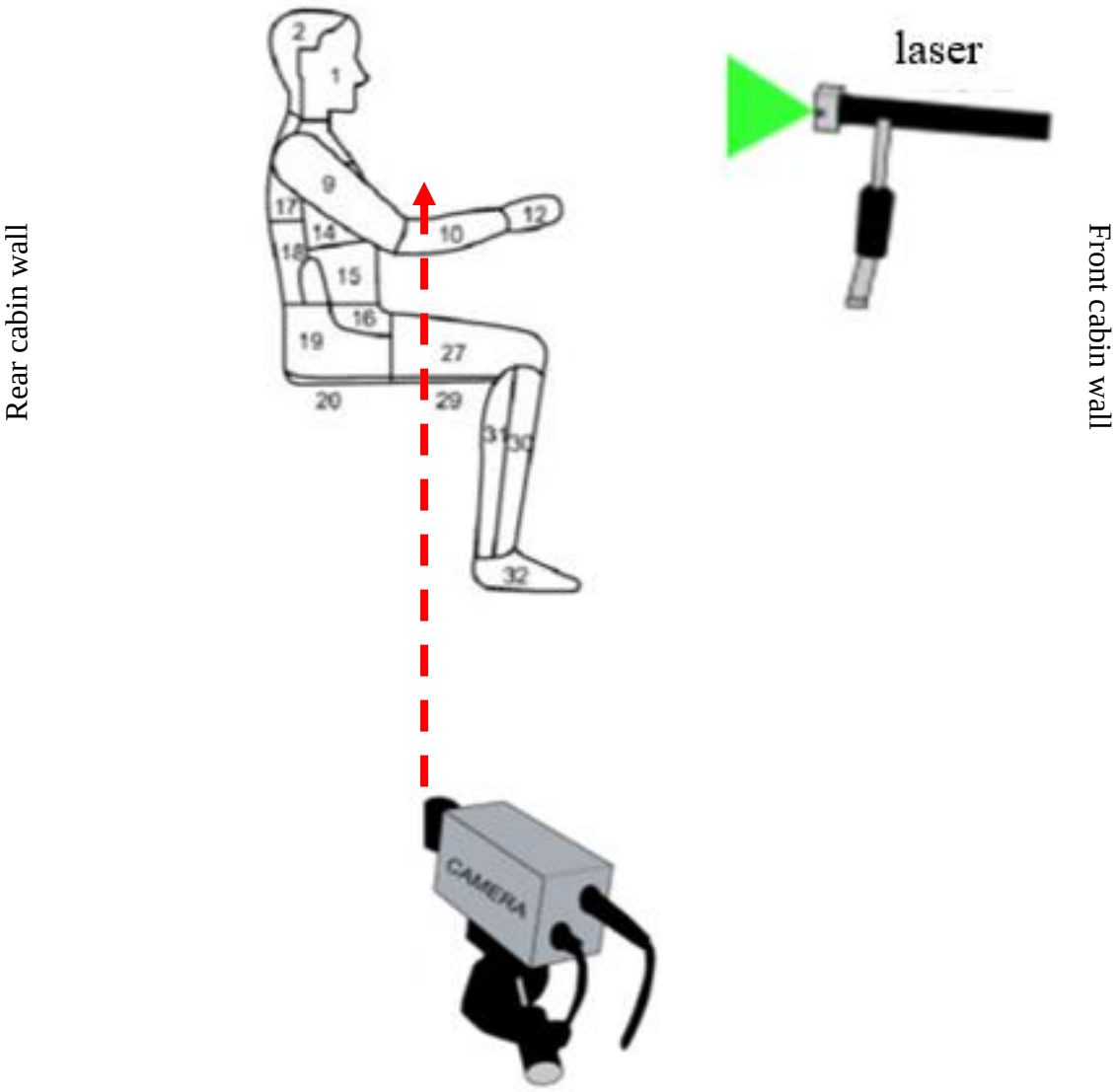

Figure L.2.1 A schematic showing the frontal laser sheet direction and the camera location relative to the seat where the smoke generation source is located on seat D6.

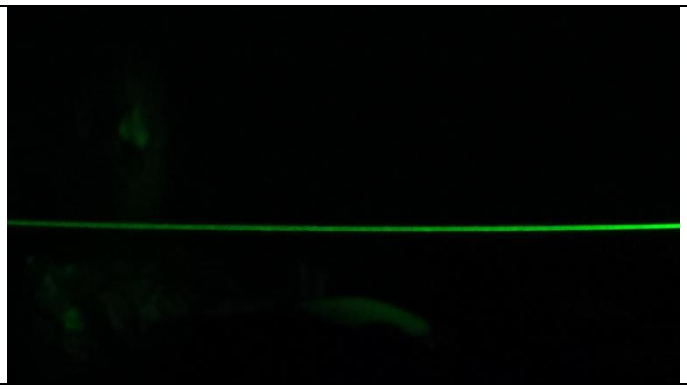

Figure L.2.2 Seat D6 frontal view snapshot 01.

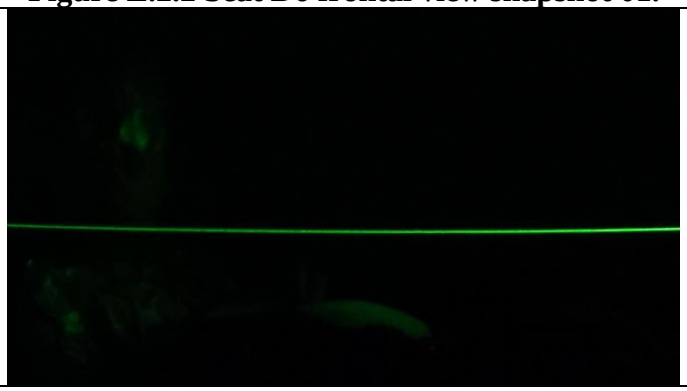

Figure L.2.3 Seat D6 frontal view snapshot 02.

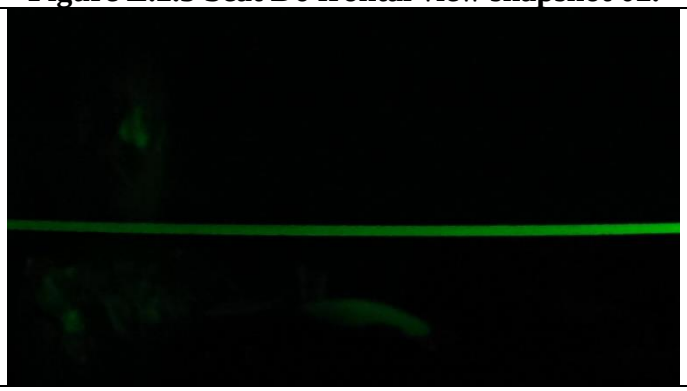

Figure L.2.4 Seat D6 frontal view snapshot 03.

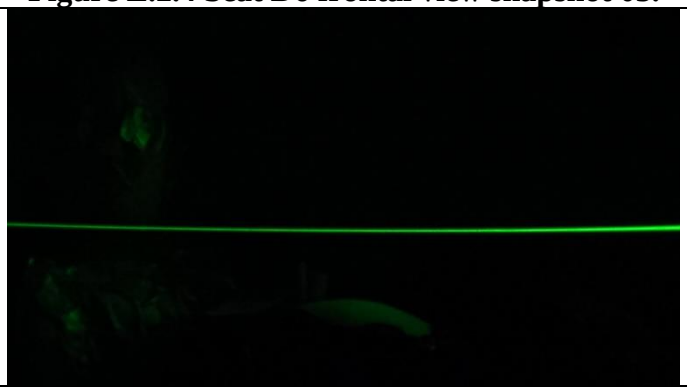

Figure L.2.5 Seat D6 frontal view snapshot 04.

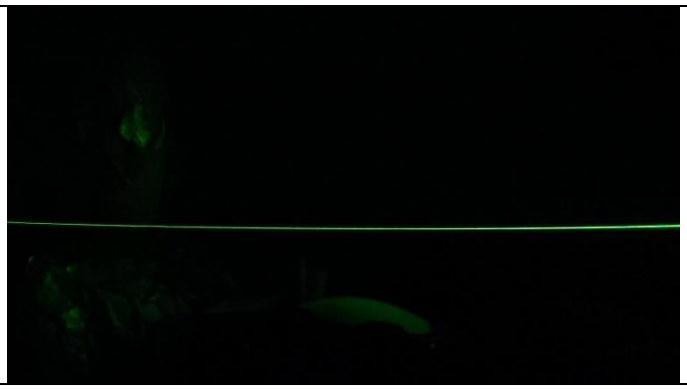

Figure L.2.6 Seat D6 frontal view snapshot 05.

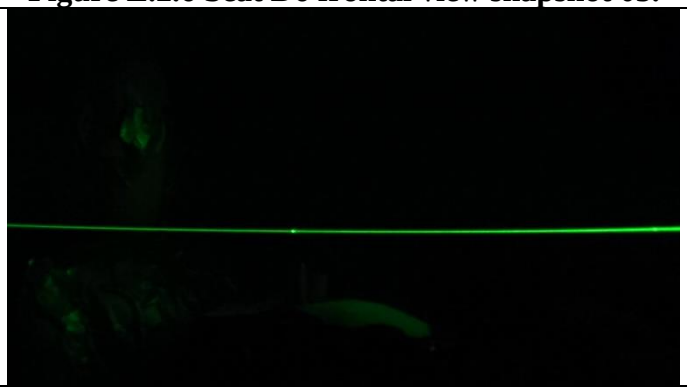

Figure L.2.7 Seat D6 frontal view snapshot 06.

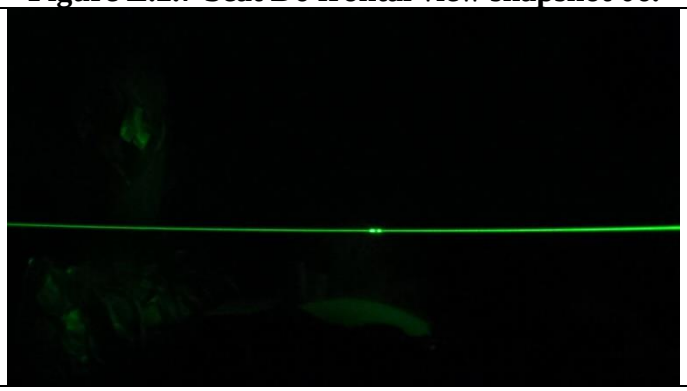

Figure L.2.8 Seat D6 frontal view snapshot 07.

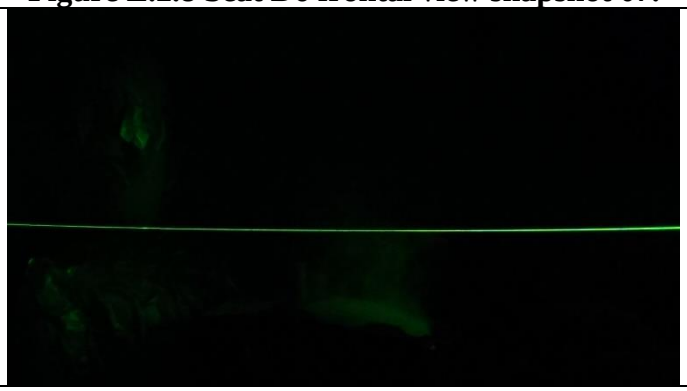

Figure L.2.9 Seat D6 frontal view snapshot 08.

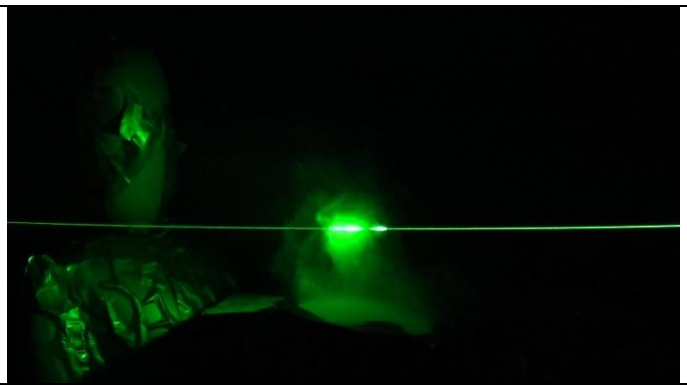

Figure L.2.10 Seat D6 frontal view snapshot 09.

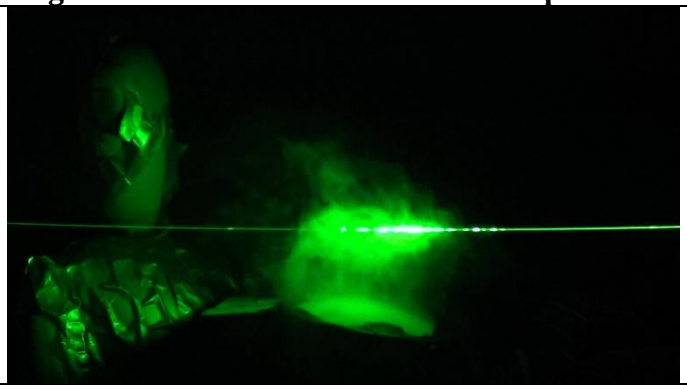

Figure L.2.11 Seat D6 frontal view snapshot 10.

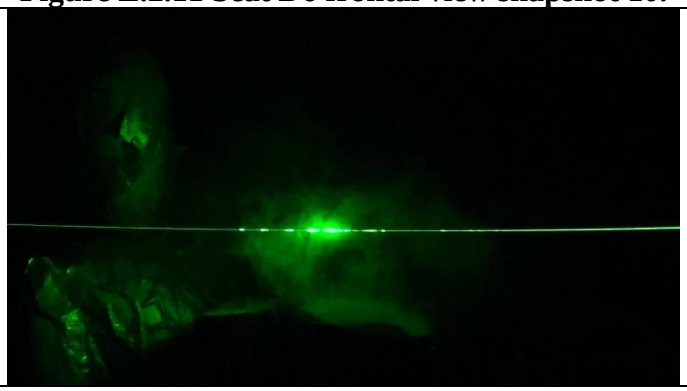

Figure L.2.12 Seat D6 frontal view snapshot 11.

Figure L.2.13 Seat D6 frontal view snapshot 12.

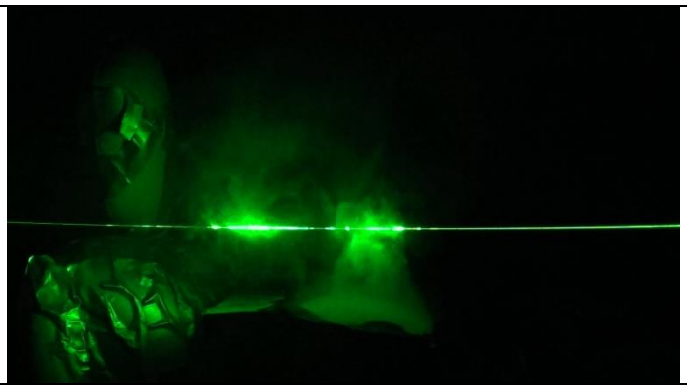

Figure L.2.14 Seat D6 frontal view snapshot 13.

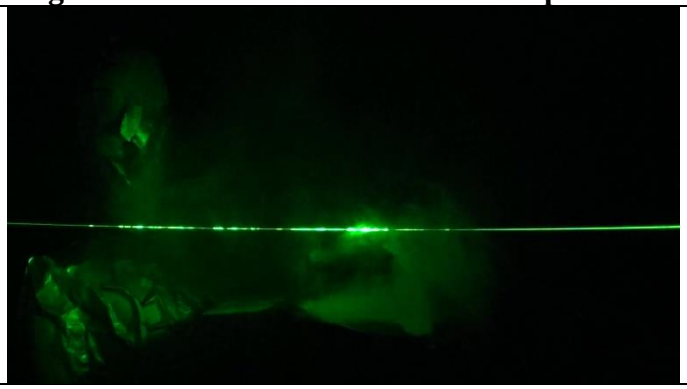

Figure L.2.15 Seat D6 frontal view snapshot 14.

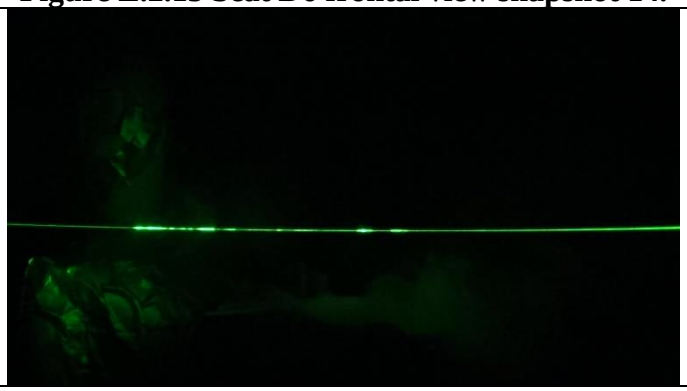

Figure L.2.16 Seat D6 frontal view snapshot 15.

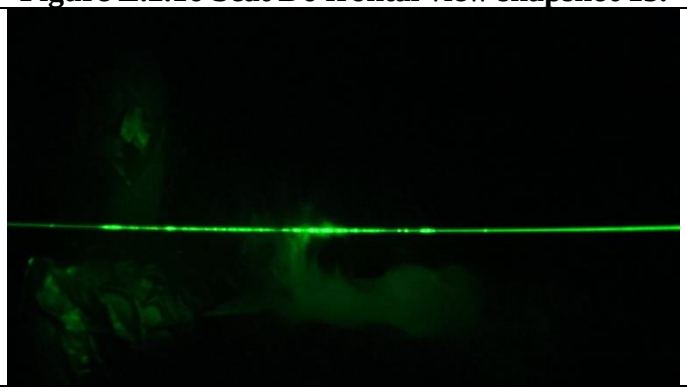

Figure L.2.17 Seat D6 frontal view snapshot 16.

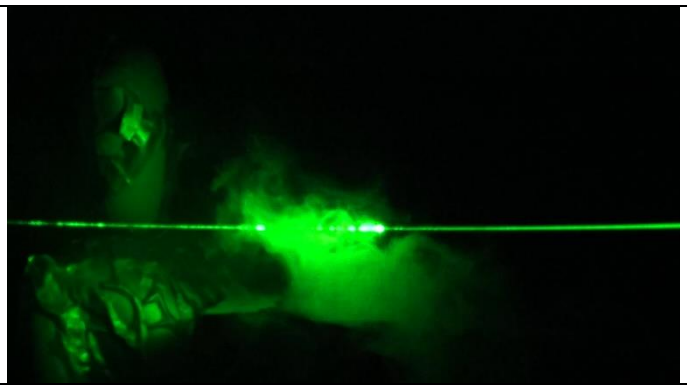

Figure L.2.18 Seat D6 frontal view snapshot 17.

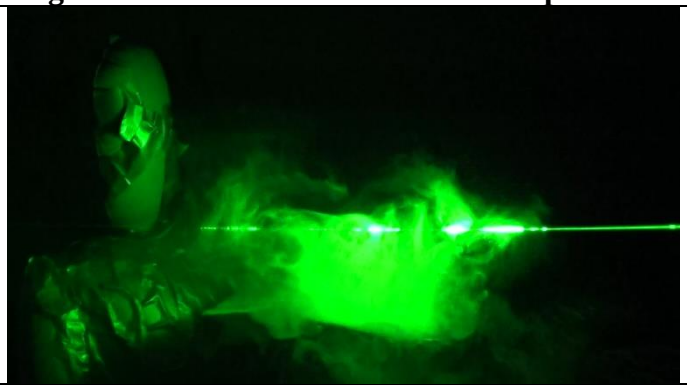

Figure L.2.19 Seat D6 frontal view snapshot 18.

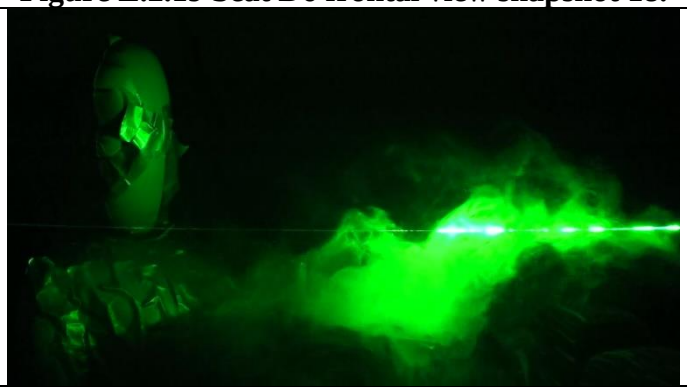

Figure L.2.20 Seat D6 frontal view snapshot 19.

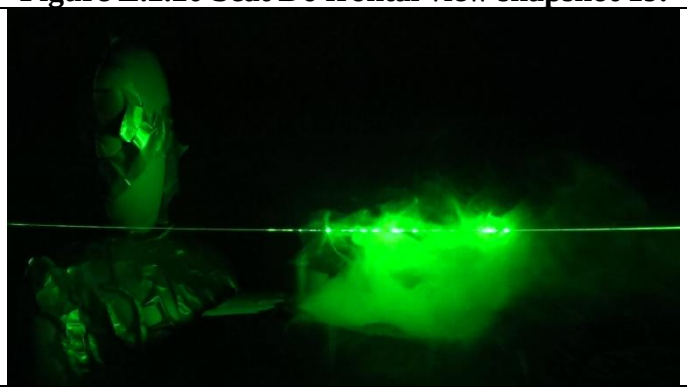

Figure L.2.21 Seat D6 frontal view snapshot 20.

Figure L.2.22 Seat D6 frontal view snapshot 21.

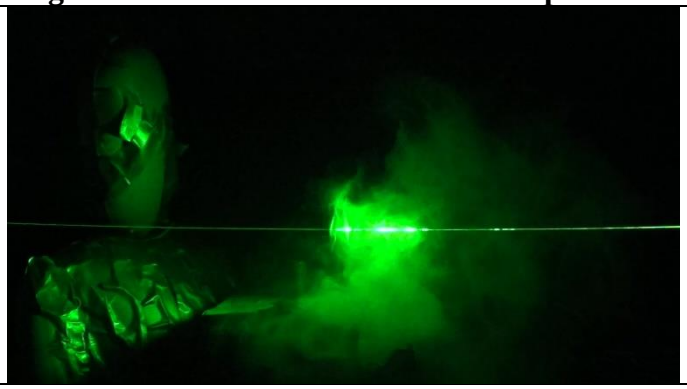

Figure L.2.23 Seat D6 frontal view snapshot 22.

Figure L.2.24 Seat D6 frontal view snapshot 23.

Figure L.2.25 Seat D6 frontal view snapshot 24.

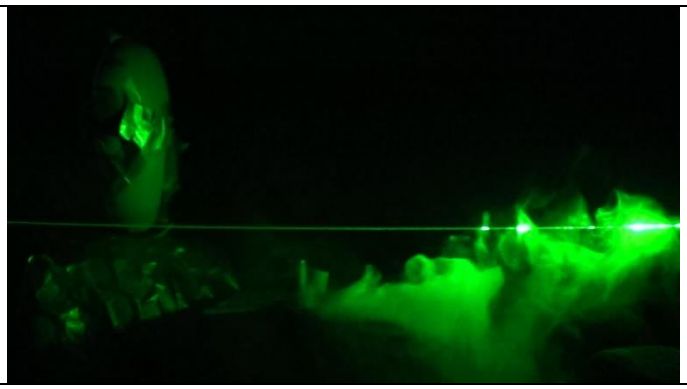

Figure L.2.26 Seat D6 frontal view snapshot 25.

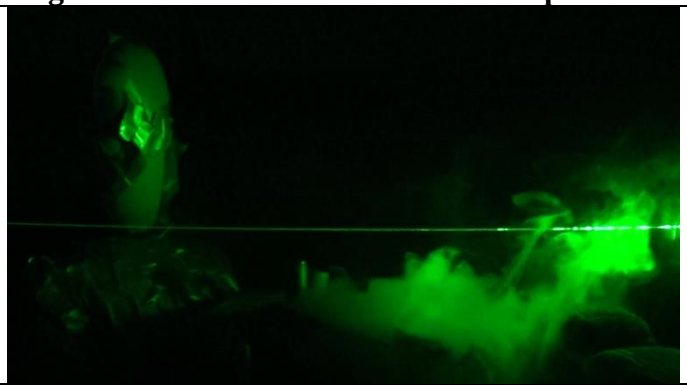

Figure L.2.27 Seat D6 frontal view snapshot 26.

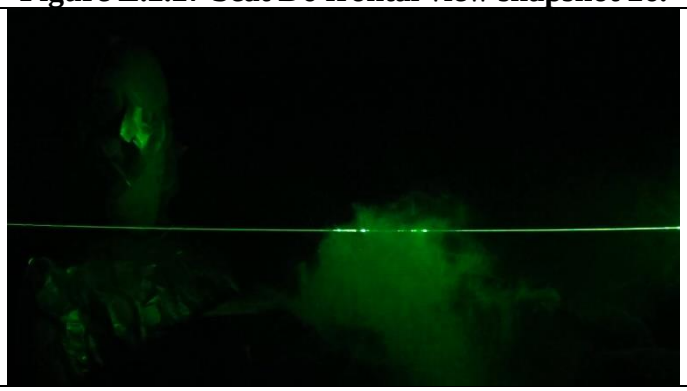

Figure L.2.28 Seat D6 frontal view snapshot 27.

Figure L.2.29 Seat D6 frontal view snapshot 28.

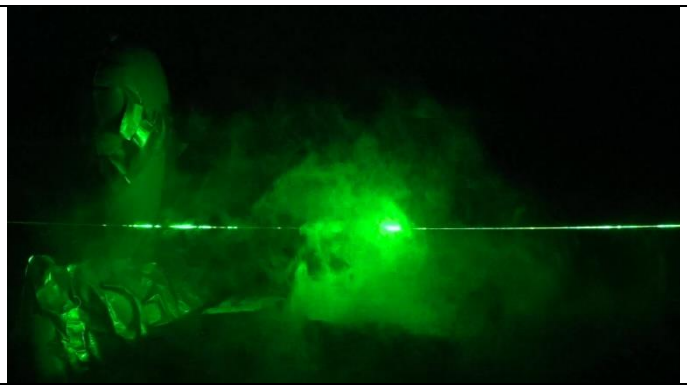

Figure L.2.30 Seat D6 frontal view snapshot 29.

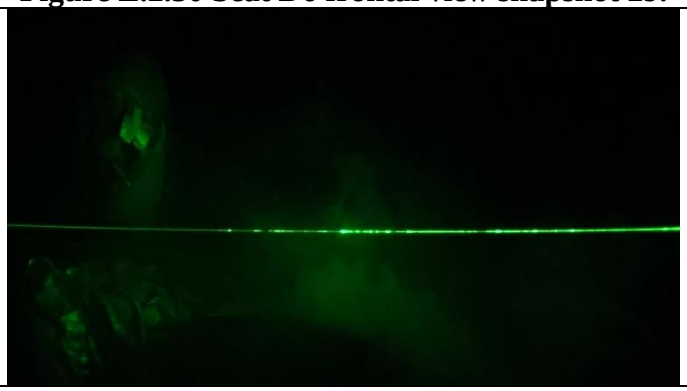

Figure L.2.31 Seat D6 frontal view snapshot 30.

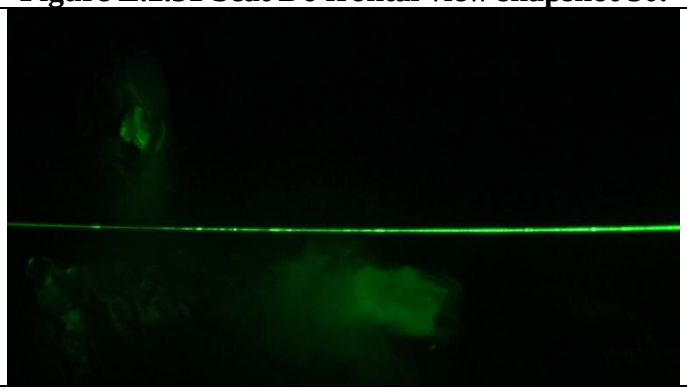

Figure L.2.32 Seat D6 frontal view snapshot 31.

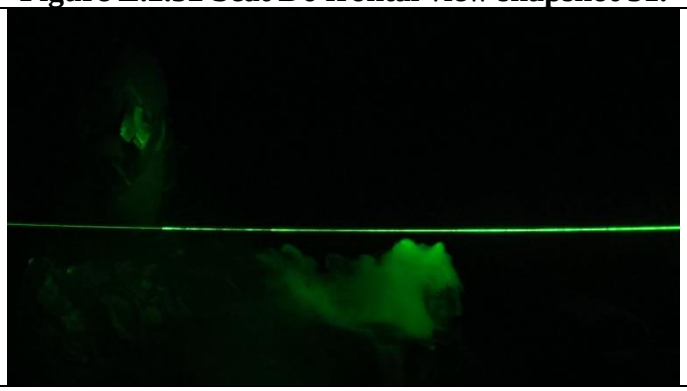

Figure L.2.33 Seat D6 frontal view snapshot 32.

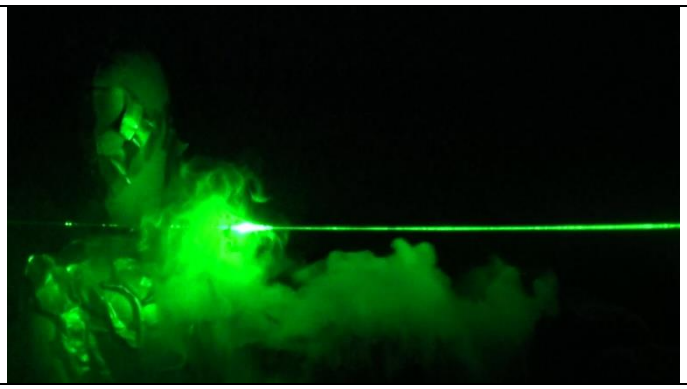

Figure L.2.34 Seat D6 frontal view snapshot 33.

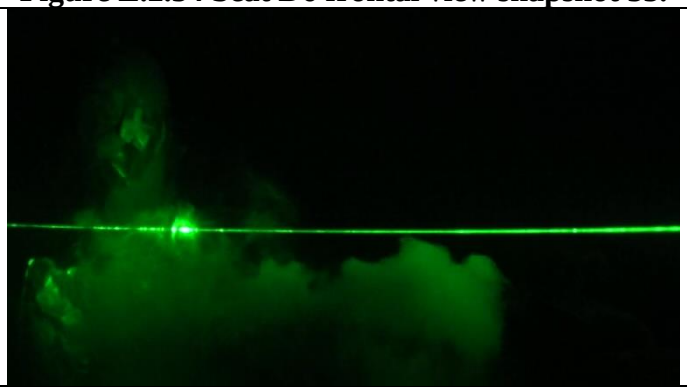

Figure L.2.35 Seat D6 frontal view snapshot 34.

Figure L.2.36 Seat D6 frontal view snapshot 35.

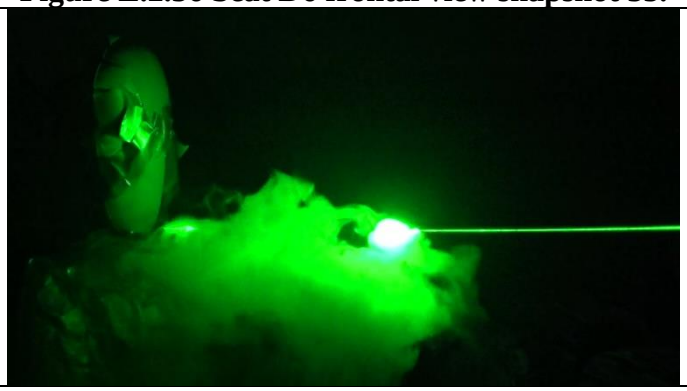

Figure L.2.37 Seat D6 frontal view snapshot 36.

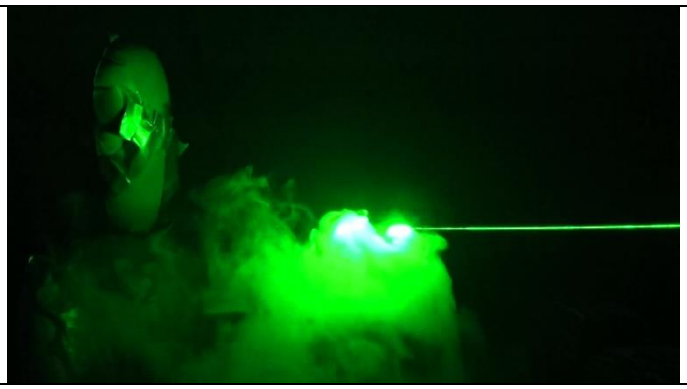

Figure L.2.38 Seat D6 frontal view snapshot 37.

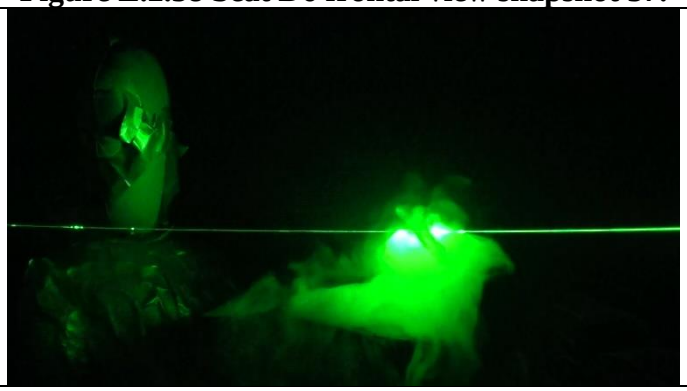

Figure L.2.39 Seat D6 frontal view snapshot 38.

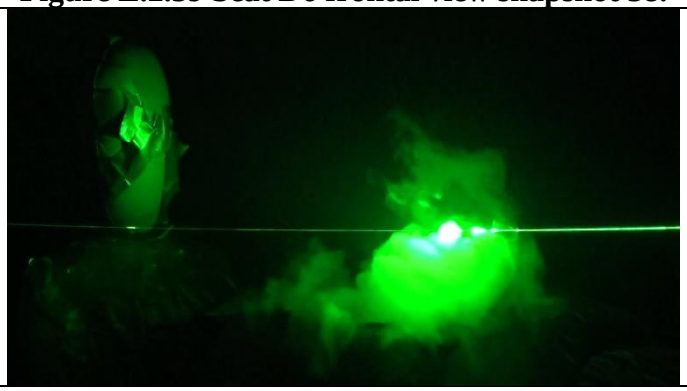

Figure L.2.40 Seat D6 frontal view snapshot 39.

Figure L.2.41 Seat D6 frontal view snapshot 40.

Figure L.2.42 Seat D6 frontal view snapshot 41.

Figure L.2.43 Seat D6 frontal view snapshot 42.

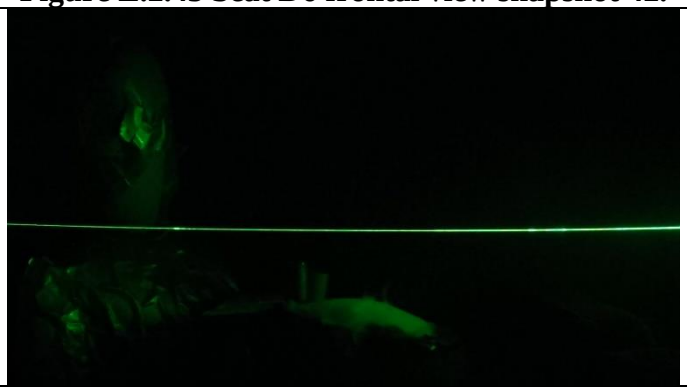

Figure L.2.44 Seat D6 frontal view snapshot 43.

Figure L.2.45 Seat D6 frontal view snapshot 44.

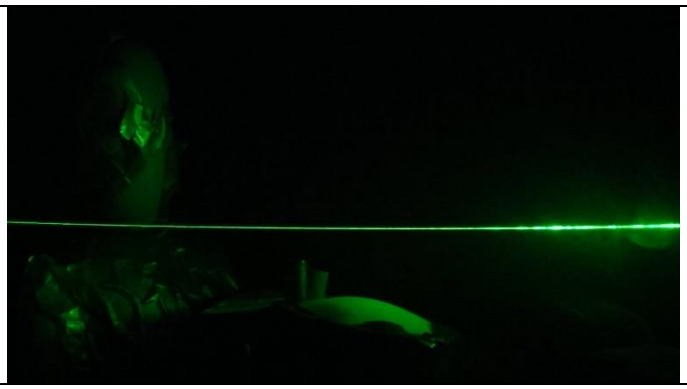

Figure L.2.46 Seat D6 frontal view snapshot 45.

Figure L.2.47 Seat D6 frontal view snapshot 46.

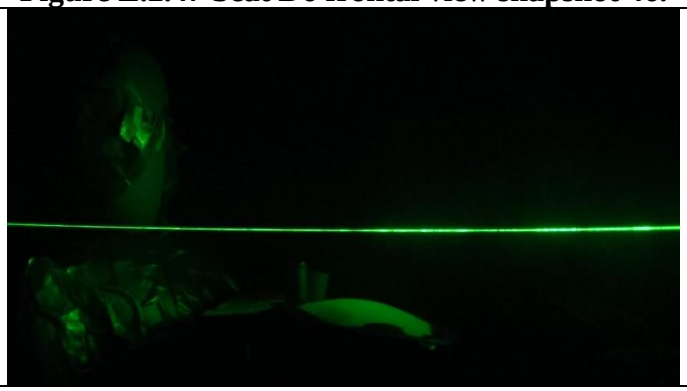

Figure L.2.48 Seat D6 frontal view snapshot 47.

Figure L.2.49 Seat D6 frontal view snapshot 48.

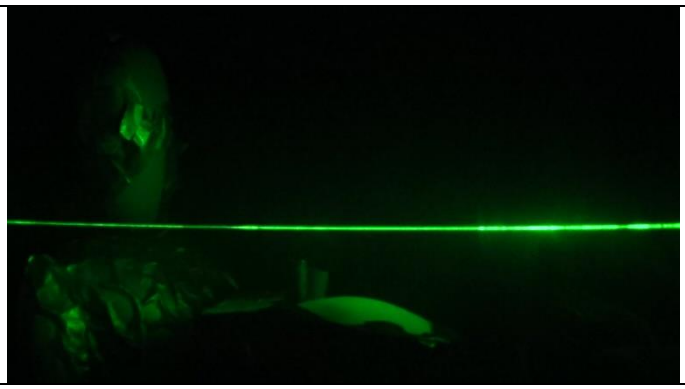

Figure L.2.50 Seat D6 frontal view snapshot 49.

Figure L.2.51 Seat D6 frontal view snapshot 50.

Appendix M - Seat D11 Smoke Visualization Snapshots

M.1 Cross-sectional View

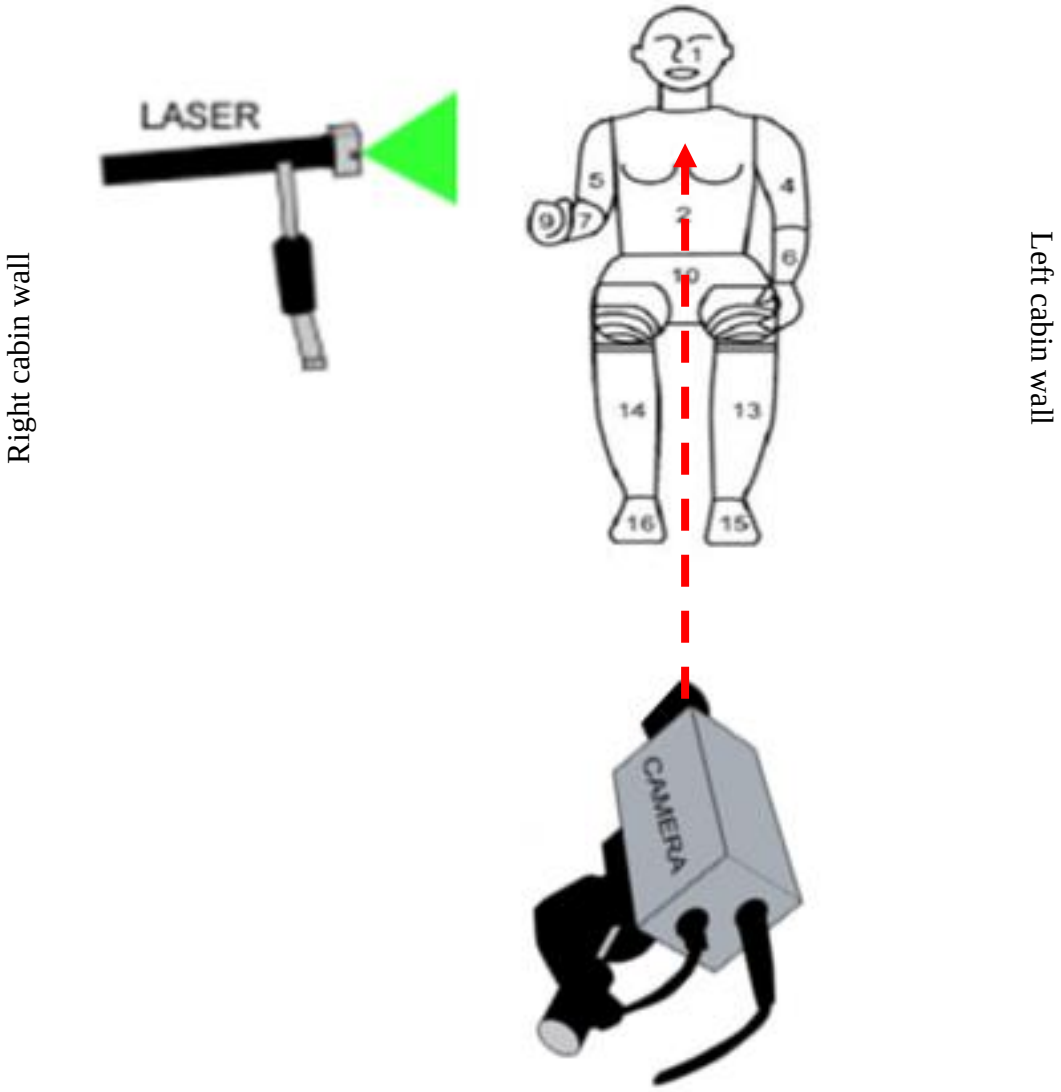

Figure M.1.1 A schematic showing the cross-sectional laser sheet direction and the camera location relative to the seat where the smoke generation source is located on seat D11.

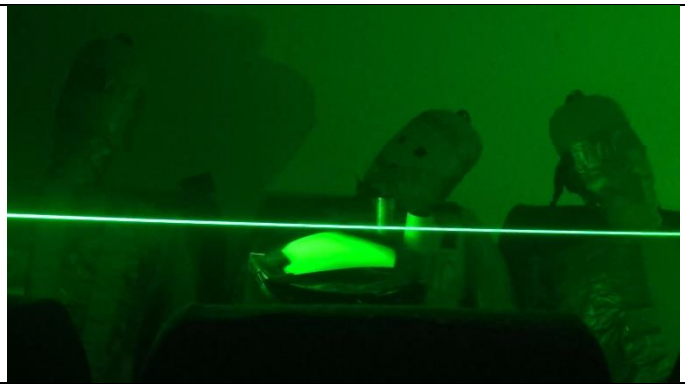

Figure M.1.2 Seat D11 cross-sectional view snapshot 01.

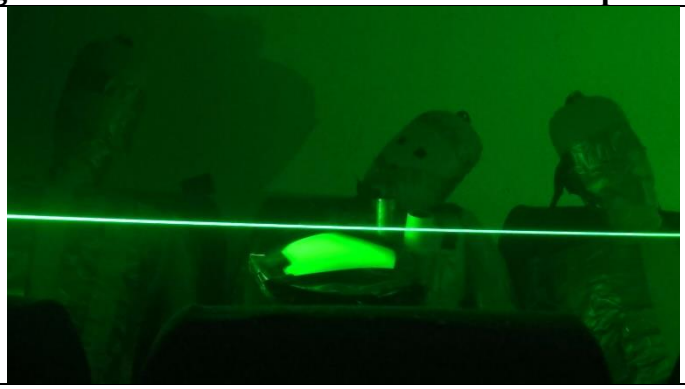

Figure M.1.3 Seat D11 cross-sectional view snapshot 02.

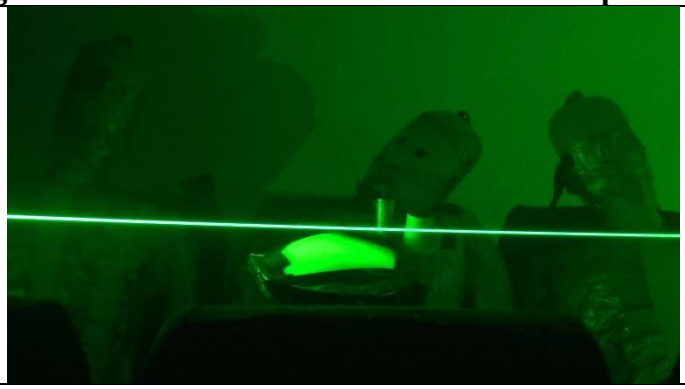

Figure M.1.4 Seat D11 cross-sectional view snapshot 03.

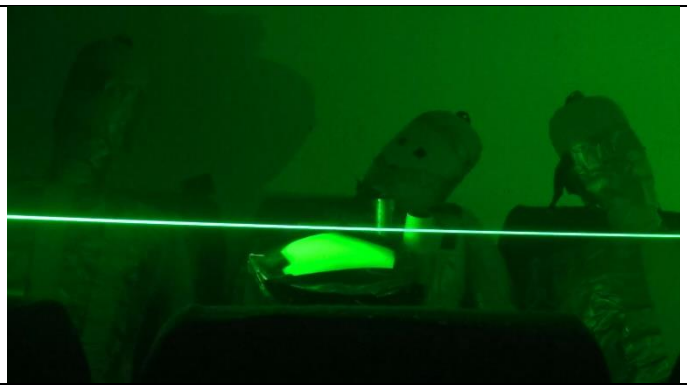

Figure M.1.5 Seat D11 cross-sectional view snapshot 04.

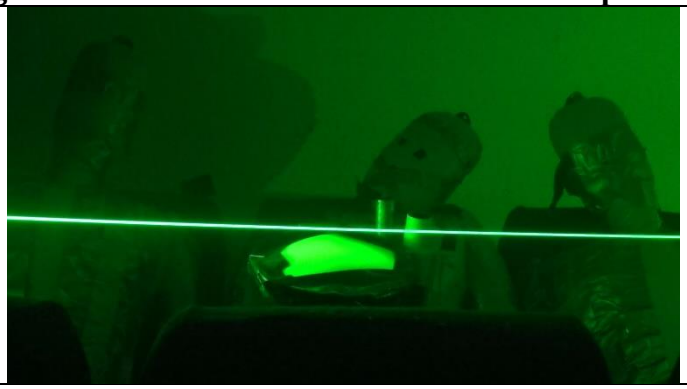

Figure M.1.6 Seat D11 cross-sectional view snapshot 05.

Figure M.1.7 Seat D11 cross-sectional view snapshot 06.

Figure M.1.8 Seat D11 cross-sectional view snapshot 07.

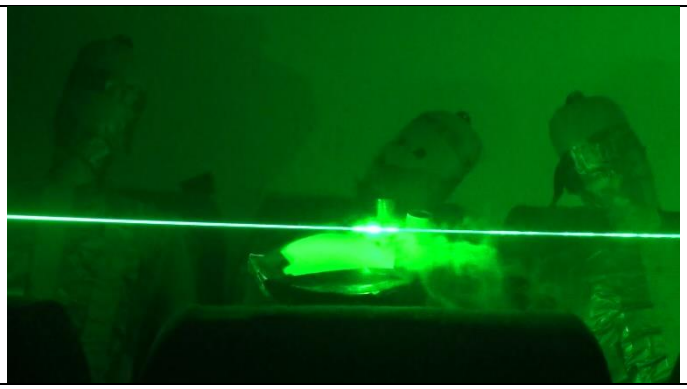

Figure M.1.9 Seat D11 cross-sectional view snapshot 08.

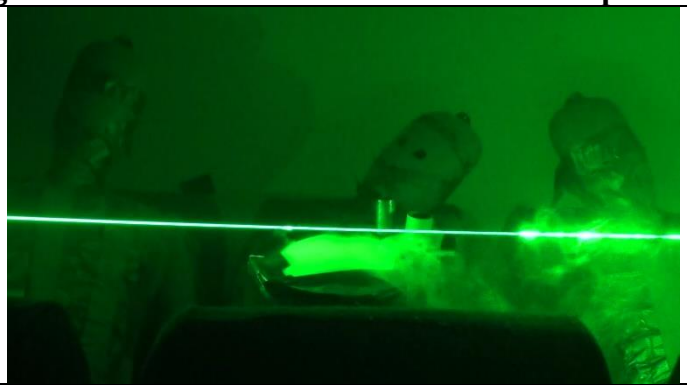

Figure M.1.10 Seat D11 cross-sectional view snapshot 09.

Figure M.1.11 Seat D11 cross-sectional view snapshot 10.

Figure M.1.12 Seat D11 cross-sectional view snapshot 11.

Figure M.1.13 Seat D11 cross-sectional view snapshot 12.

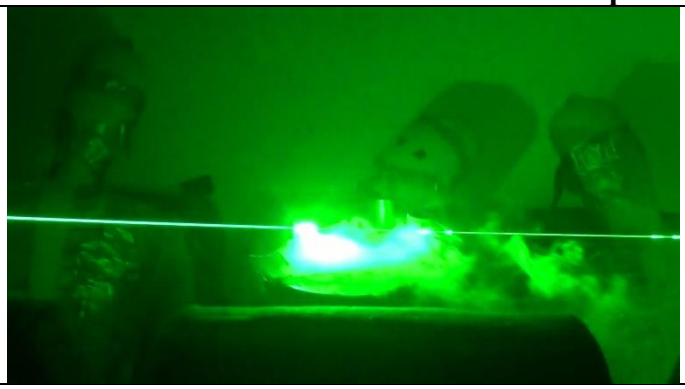

Figure M.1.14 Seat D11 cross-sectional view snapshot 13.

Figure M.1.15 Seat D11 cross-sectional view snapshot 14.

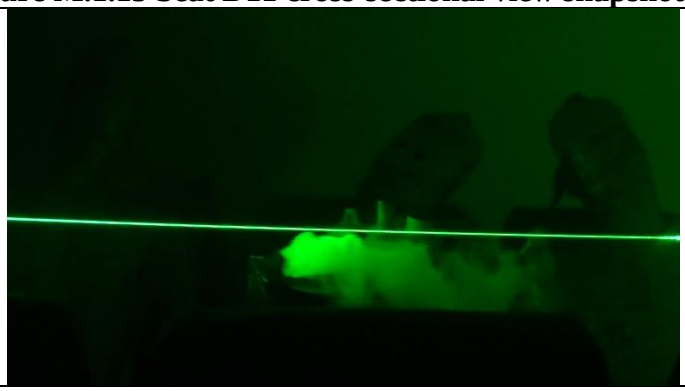

Figure M.1.16 Seat D11 cross-sectional view snapshot 15.

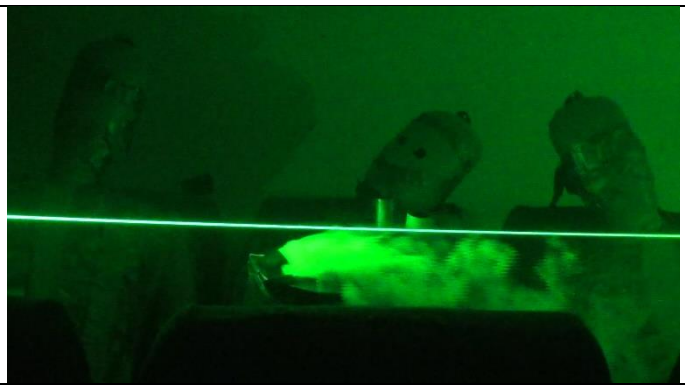

Figure M.1.17 Seat D11 cross-sectional view snapshot 16.

Figure M.1.18 Seat D11 cross-sectional view snapshot 17.

Figure M.1.19 Seat D11 cross-sectional view snapshot 18.

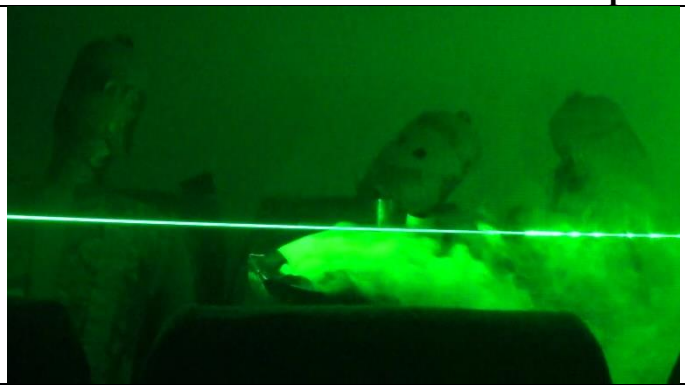

Figure M.1.20 Seat D11 cross-sectional view snapshot 19.

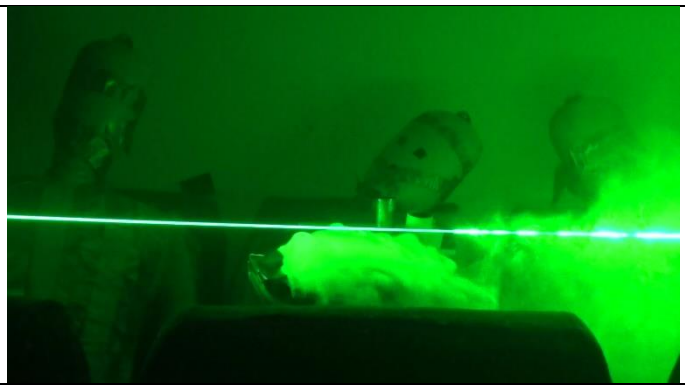

Figure M.1.21 Seat D11 cross-sectional view snapshot 20.

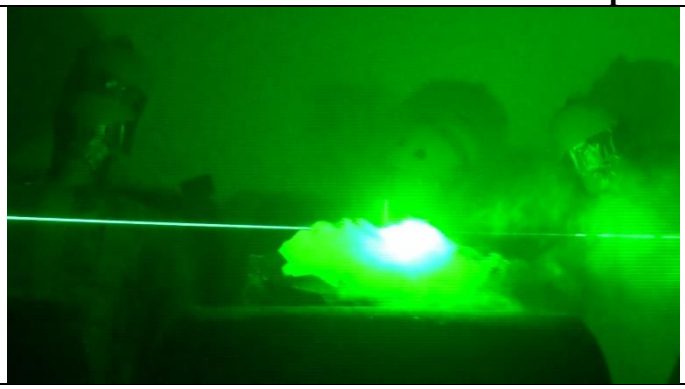

Figure M.1.22 Seat D11 cross-sectional view snapshot 21.

Figure M.1.23 Seat D11 cross-sectional view snapshot 22.

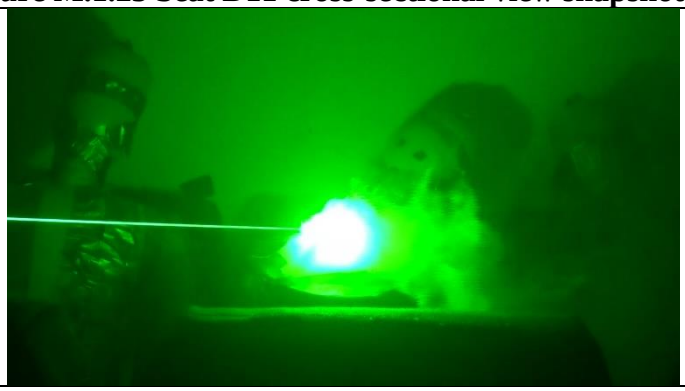

Figure M.1.24 Seat D11 cross-sectional view snapshot 23.

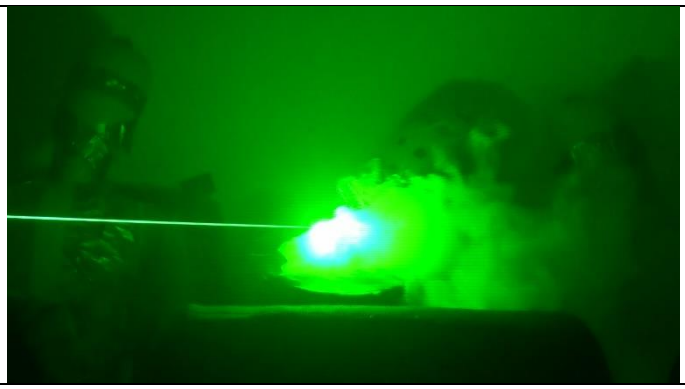

Figure M.1.25 Seat D11 cross-sectional view snapshot 24.

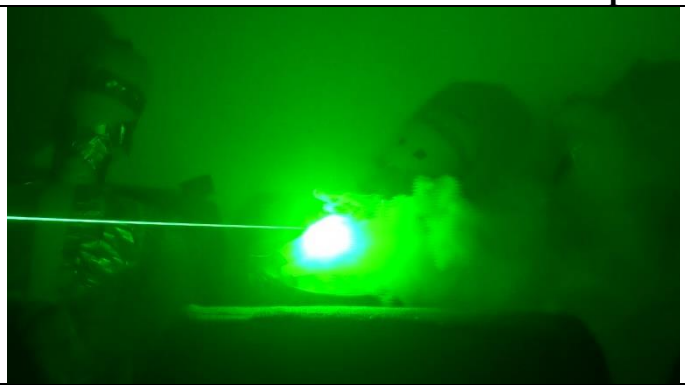

Figure M.1.26 Seat D11 cross-sectional view snapshot 25.

Figure M.1.27 Seat D11 cross-sectional view snapshot 26.

Figure M.1.28 Seat D11 cross-sectional view snapshot 27.

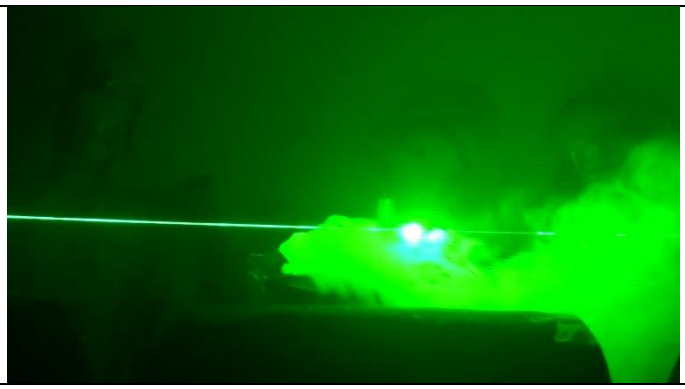

Figure M.1.29 Seat D11 cross-sectional view snapshot 28.

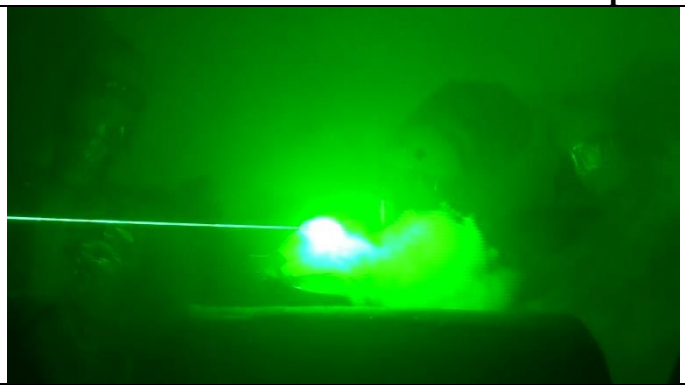

Figure M.1.30 Seat D11 cross-sectional view snapshot 29.

Figure M.1.31 Seat D11 cross-sectional view snapshot 30.

Figure M.1.32 Seat D11 cross-sectional view snapshot 31.

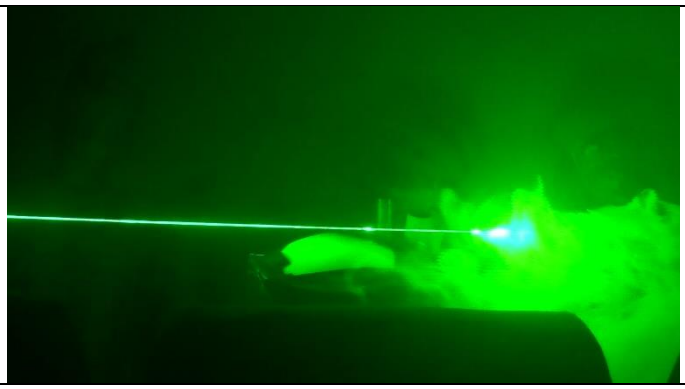

Figure M.1.33 Seat D11 cross-sectional view snapshot 32.

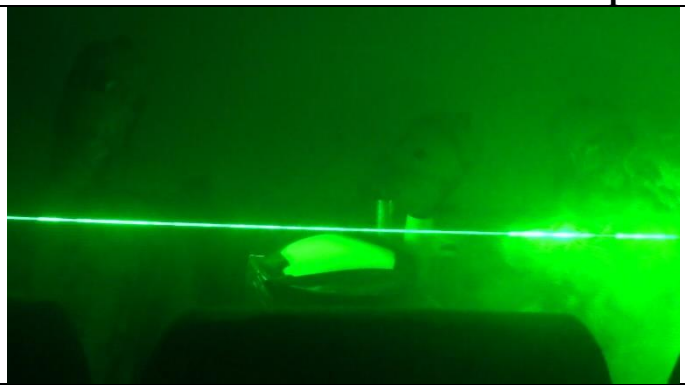

Figure M.1.34 Seat D11 cross-sectional view snapshot 33.

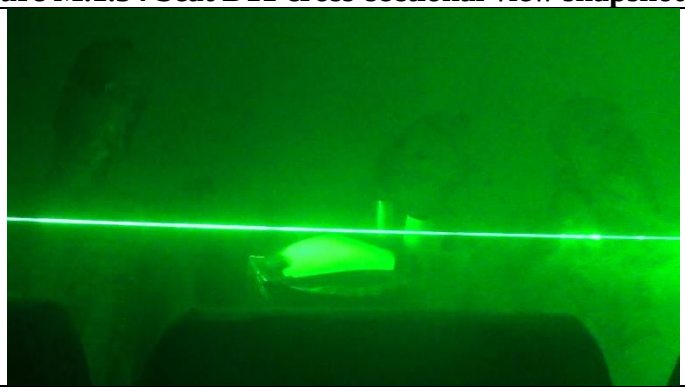

Figure M.1.35 Seat D11 cross-sectional view snapshot 34.

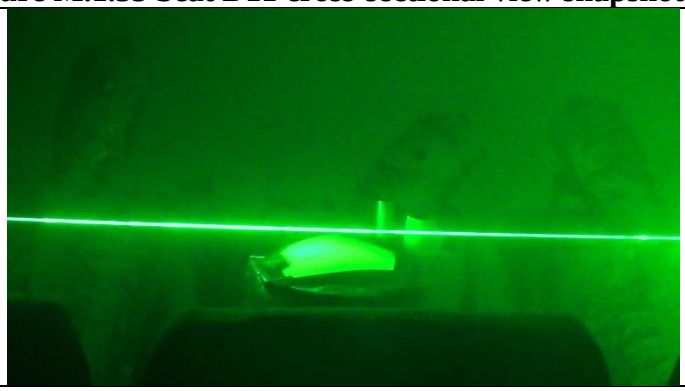

Figure M.1.36 Seat D11 cross-sectional view snapshot 35.

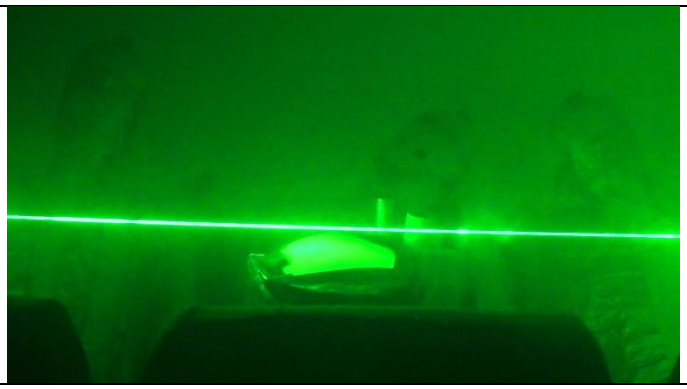

Figure M.1.37 Seat D11 cross-sectional view snapshot 36.

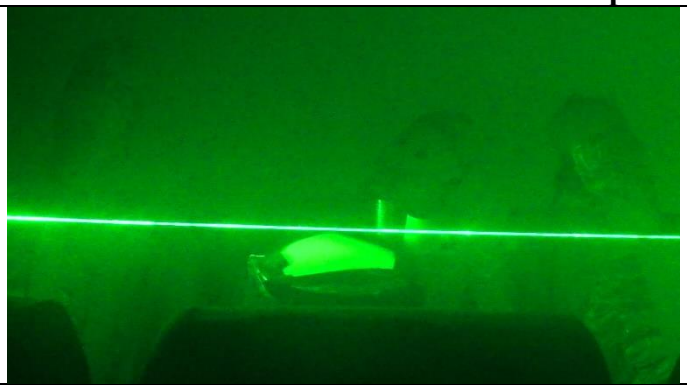

Figure M.1.38 Seat D11 cross-sectional view snapshot 37.

Figure M.1.39 Seat D11 cross-sectional view snapshot 38.

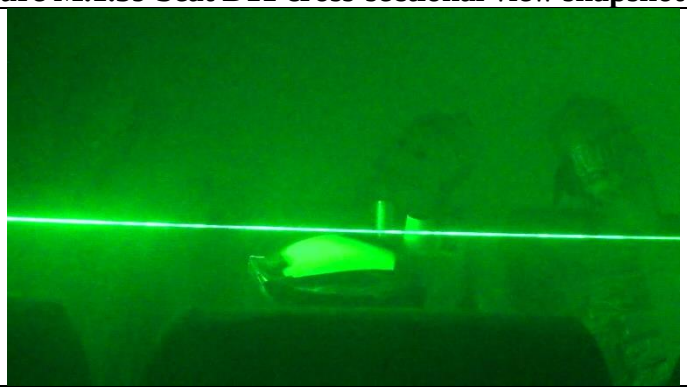

Figure M.1.40 Seat D11 cross-sectional view snapshot 39.

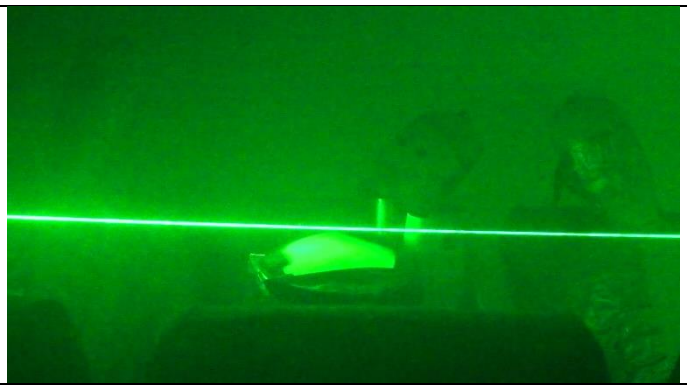

Figure M.1.41 Seat D11 cross-sectional view snapshot 40.

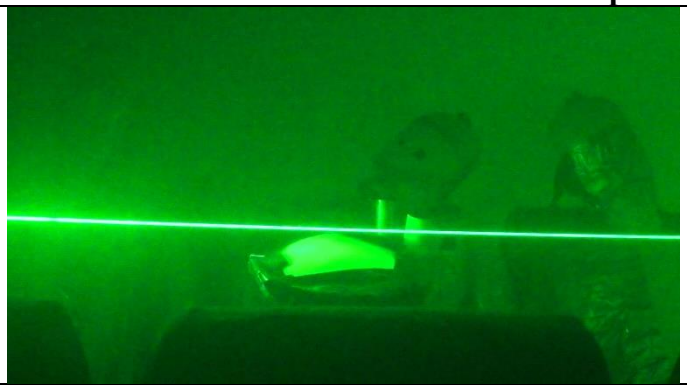

Figure M.1.42 Seat D11 cross-sectional view snapshot 41.

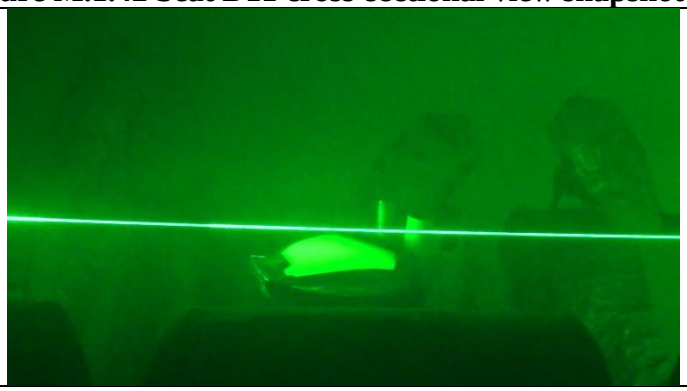

Figure M.1.43 Seat D11 cross-sectional view snapshot 42.

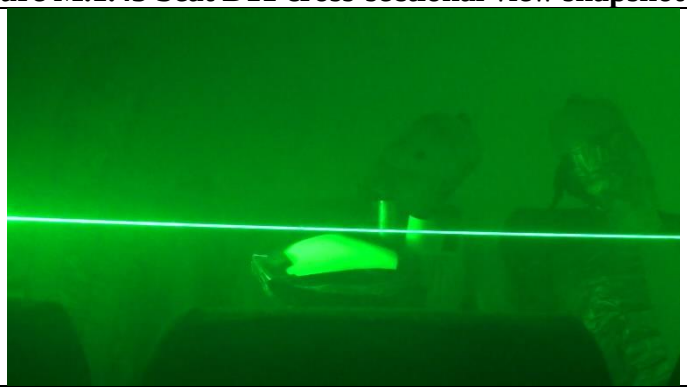

Figure M.1.44 Seat D11 cross-sectional view snapshot 43.

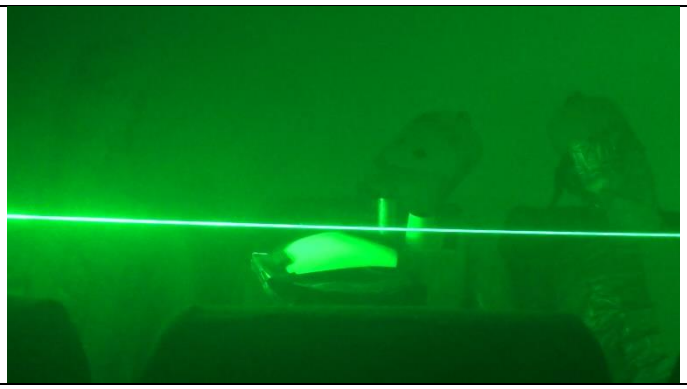

Figure M.1.45 Seat D11 cross-sectional view snapshot 44.

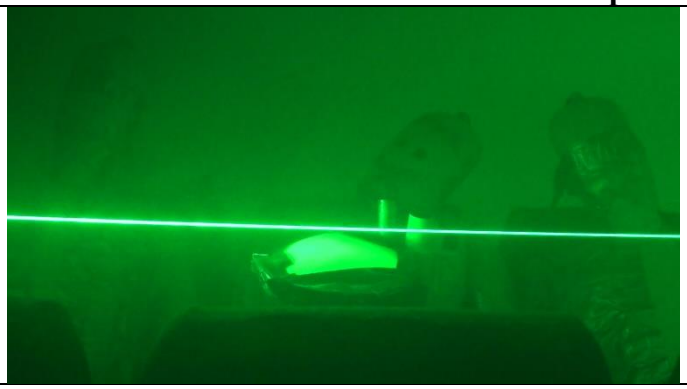

Figure M.1.46 Seat D11 cross-sectional view snapshot 45.

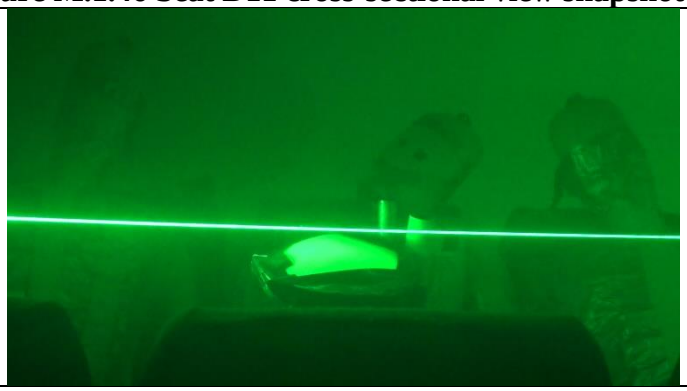

Figure M.1.47 Seat D11 cross-sectional view snapshot 46.

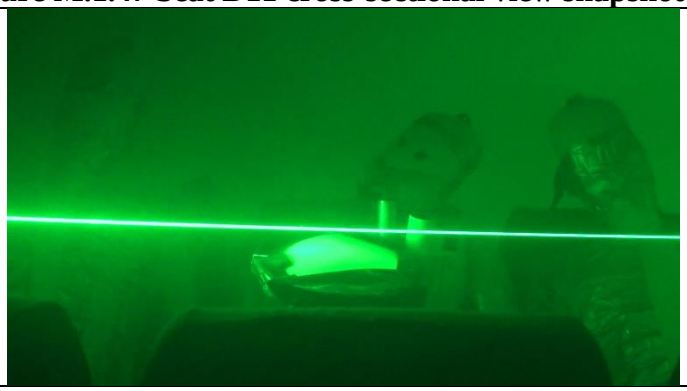

Figure M.1.48 Seat D11 cross-sectional view snapshot 47.

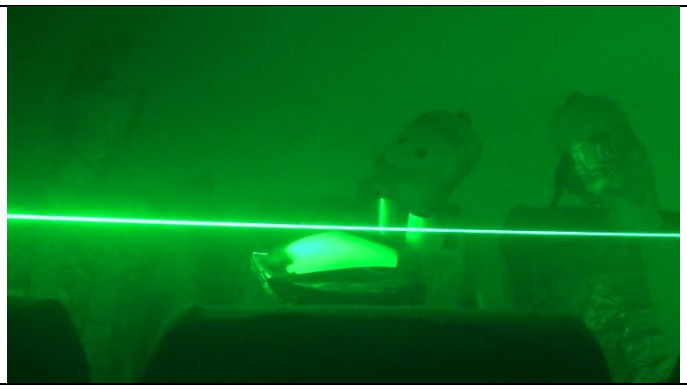

Figure M.1.49 Seat D11 cross-sectional view snapshot 48.

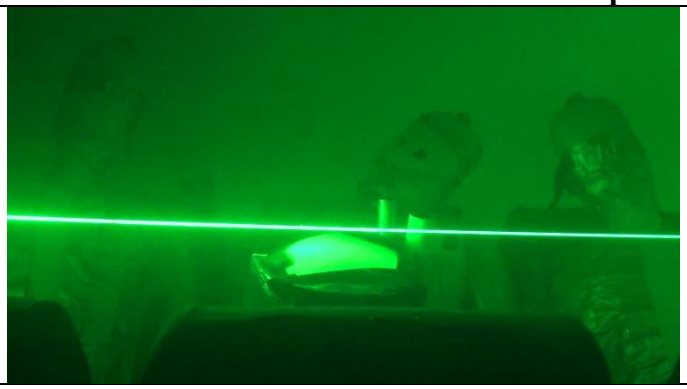

Figure M.1.50 Seat D11 cross-sectional view snapshot 49.

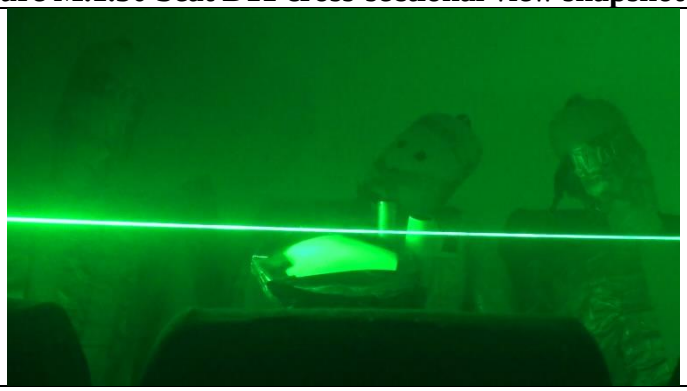

Figure M.1.51 Seat D11 cross-sectional view snapshot 50.

M.2 Frontal View

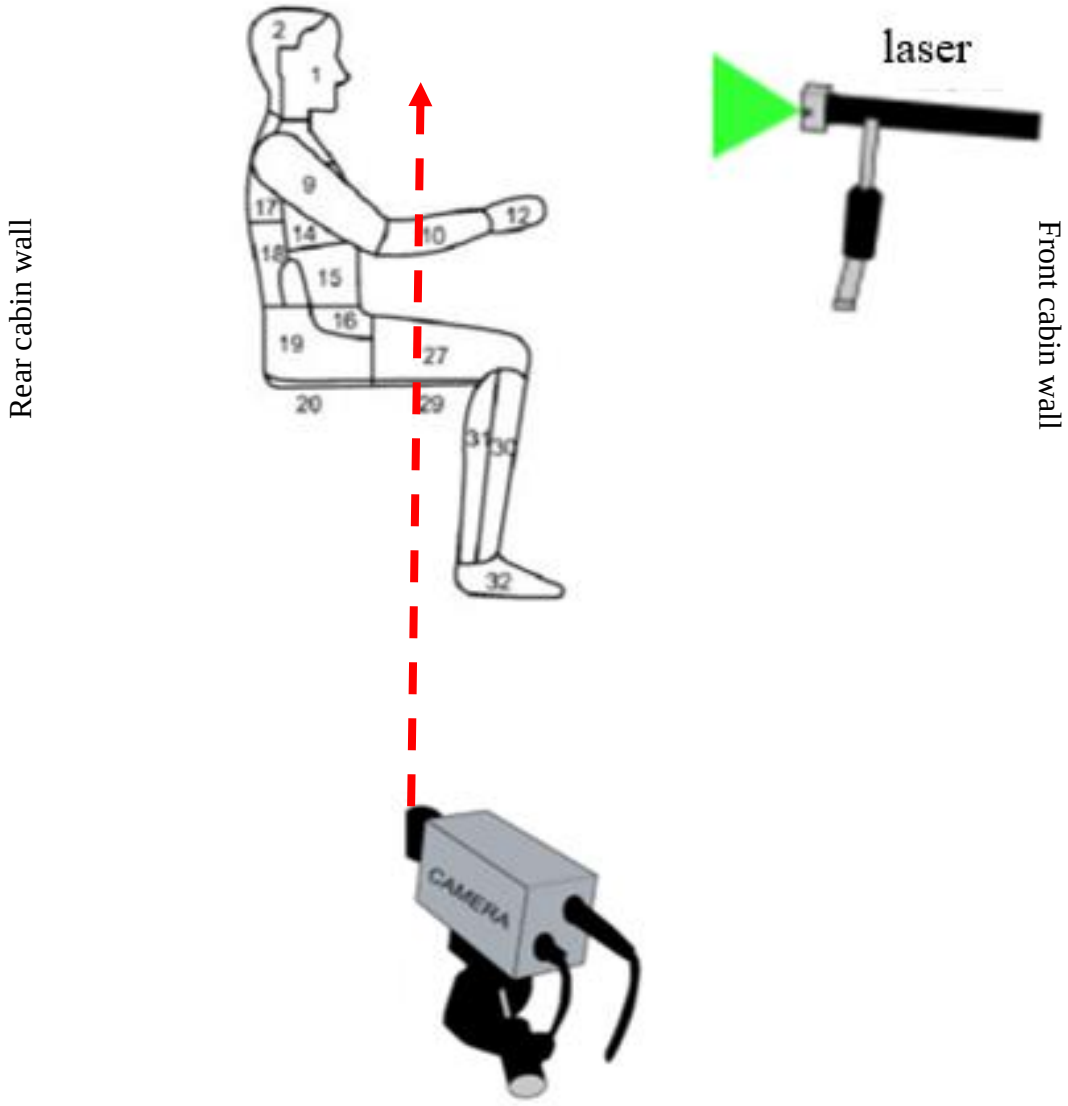

Figure M.2.1 A schematic showing the frontal laser sheet direction and the camera location relative to the seat where the smoke generation source is located on seat D11.

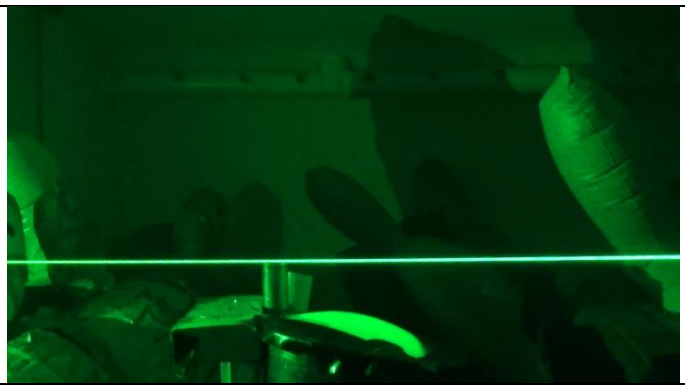

Figure M.2.2 Seat D11 frontal view snapshot 01.

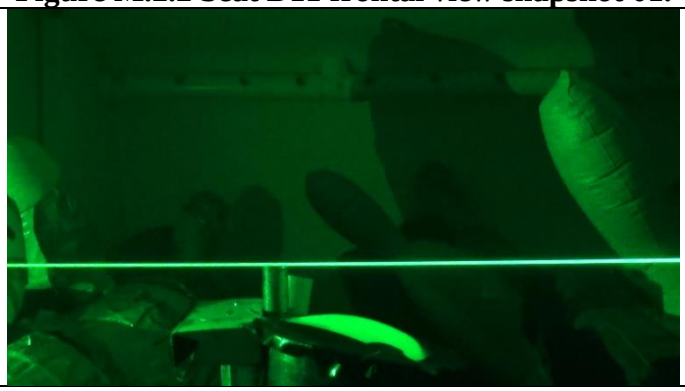

Figure M.2.3 Seat D11 frontal view snapshot 02.

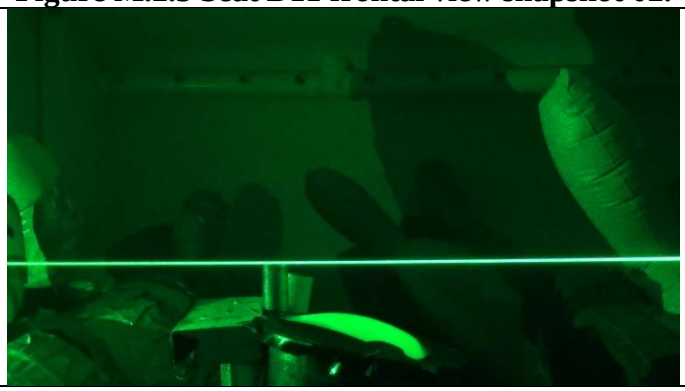

Figure M.2.4 Seat D11 frontal view snapshot 03.

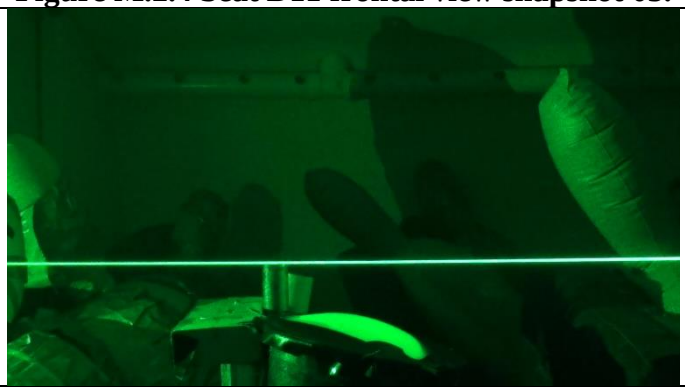

Figure M.2.5 Seat D11 frontal view snapshot 04.

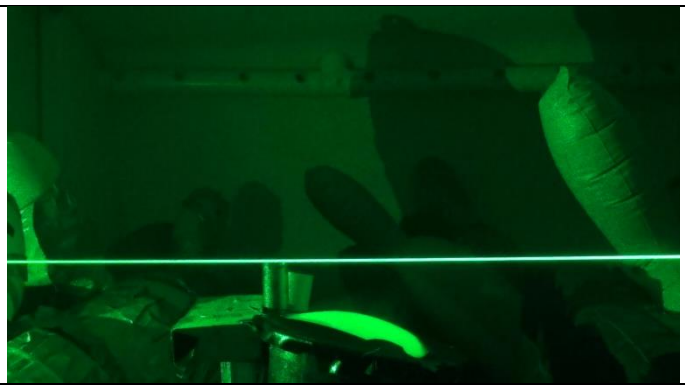

Figure M.2.6 Seat D11 frontal view snapshot 05.

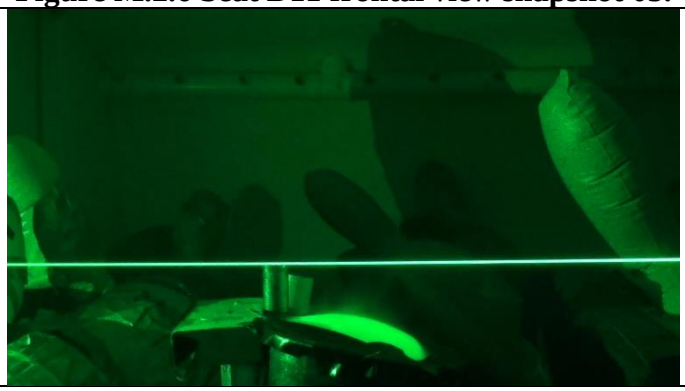

Figure M.2.7 Seat D11 frontal view snapshot 06.

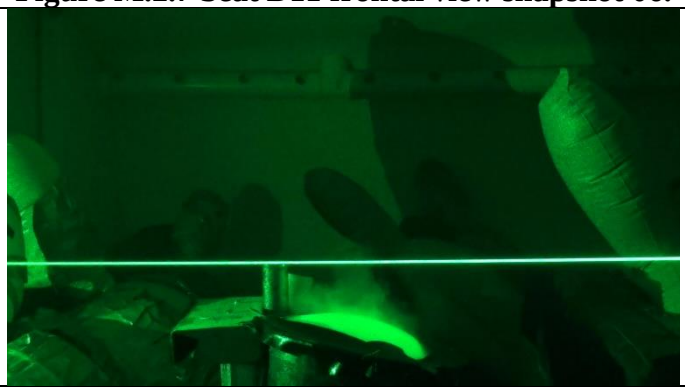

Figure M.2.8 Seat D11 frontal view snapshot 07.

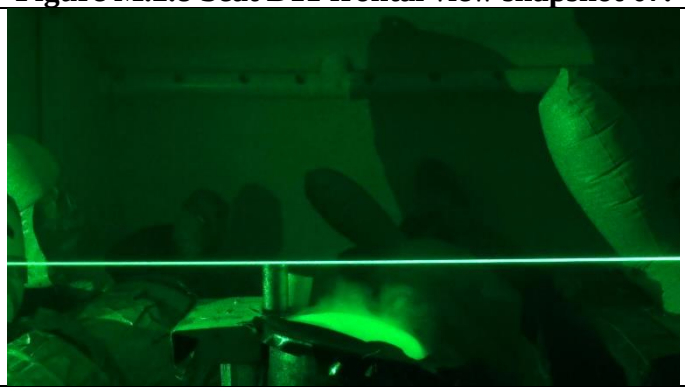

Figure M.2.9 Seat D11 frontal view snapshot 08.

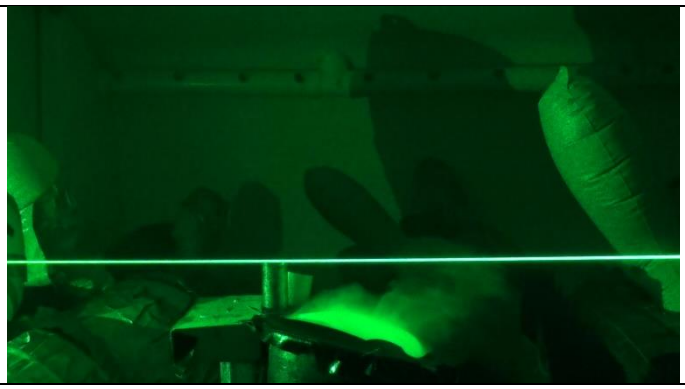

Figure M.2.10 Seat D11 frontal view snapshot 09.

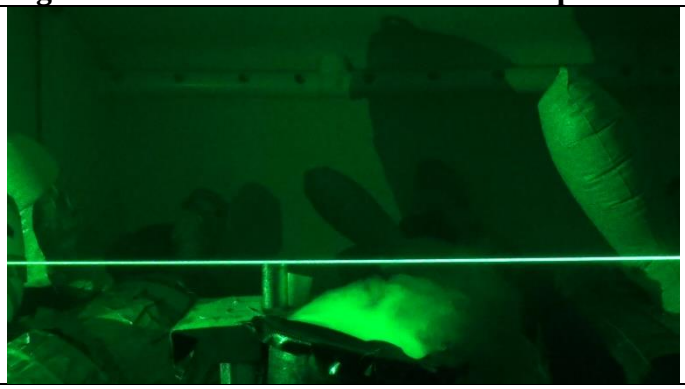

Figure M.2.11 Seat D11 frontal view snapshot 10.

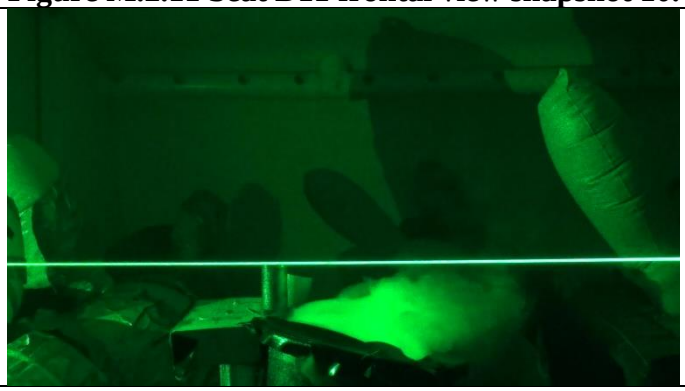

Figure M.2.12 Seat D11 frontal view snapshot 11.

Figure M.2.13 Seat D11 frontal view snapshot 12.

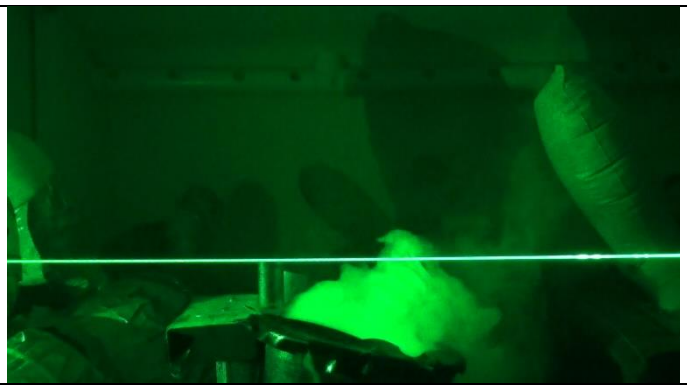

Figure M.2.14 Seat D11 frontal view snapshot 13.

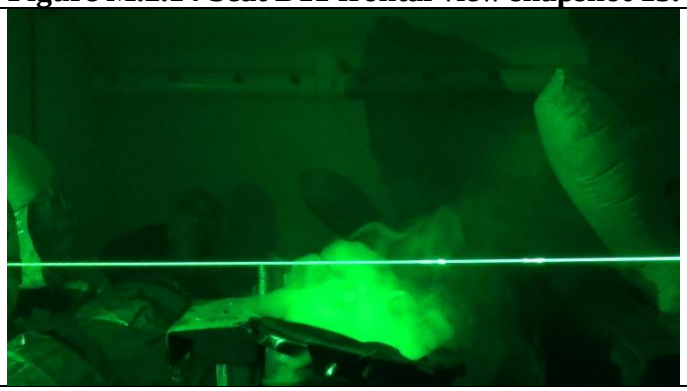

Figure M.2.15 Seat D11 frontal view snapshot 14.

Figure M.2.16 Seat D11 frontal view snapshot 15.

Figure M.2.17 Seat D11 frontal view snapshot 16.

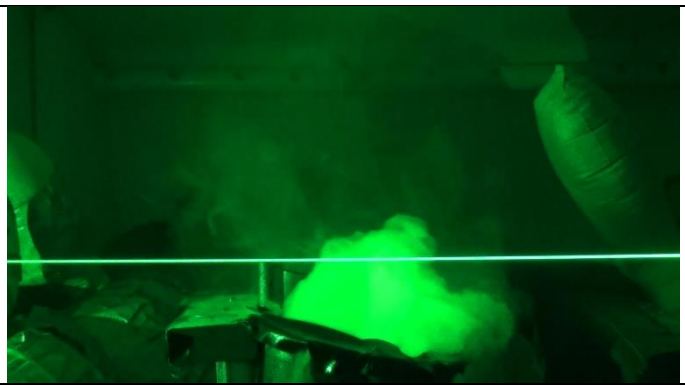

Figure M.2.18 Seat D11 frontal view snapshot 17.

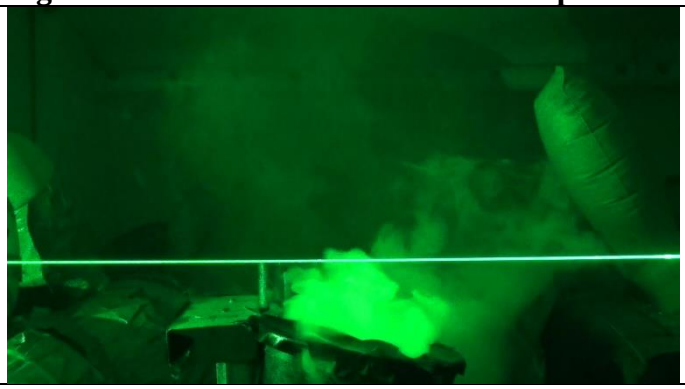

Figure M.2.19 Seat D11 frontal view snapshot 18.

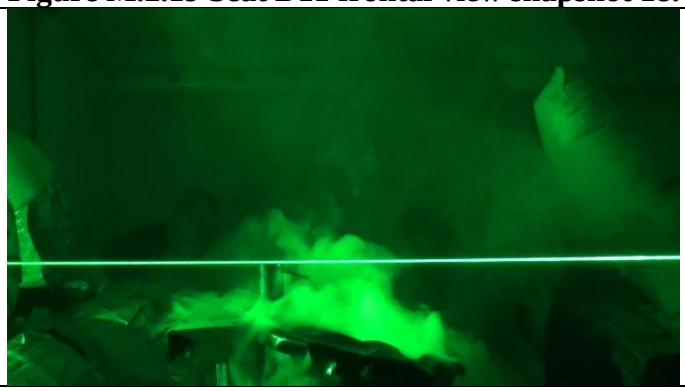

Figure M.2.20 Seat D11 frontal view snapshot 19.

Figure M.2.21 Seat D11 frontal view snapshot 20.

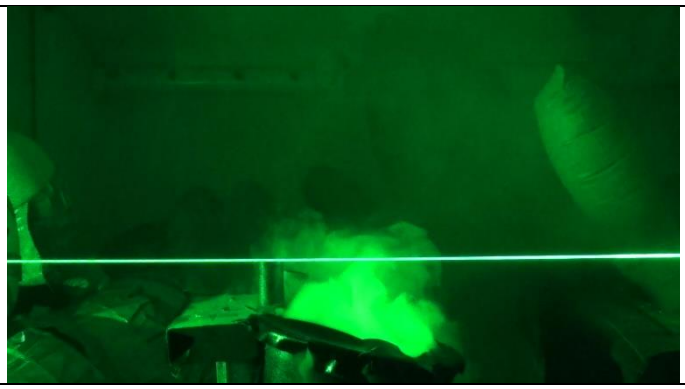

Figure M.2.22 Seat D11 frontal view snapshot 21.

Figure M.2.23 Seat D11 frontal view snapshot 22.

Figure M.2.24 Seat D11 frontal view snapshot 23.

Figure M.2.25 Seat D11 frontal view snapshot 24.

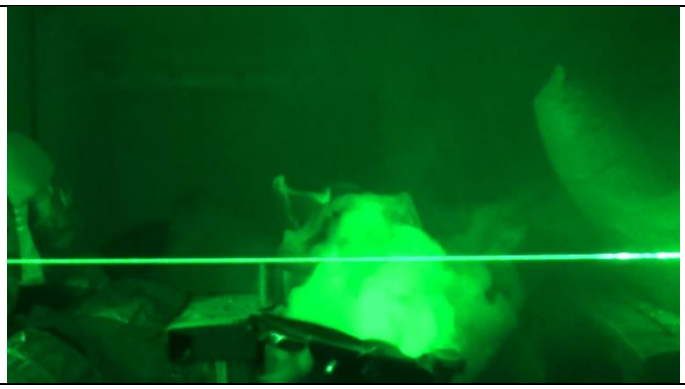

Figure M.2.26 Seat D11 frontal view snapshot 25.

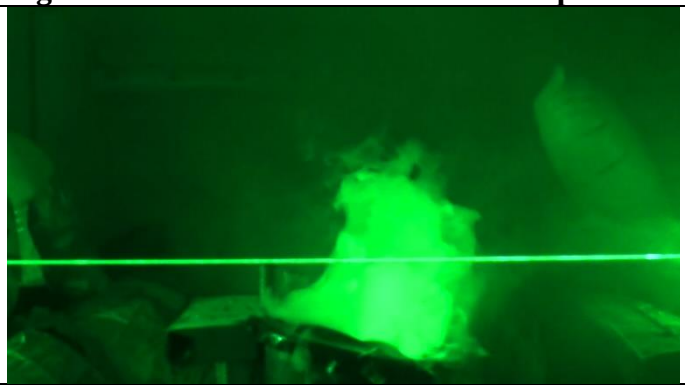

Figure M.2.27 Seat D11 frontal view snapshot 26.

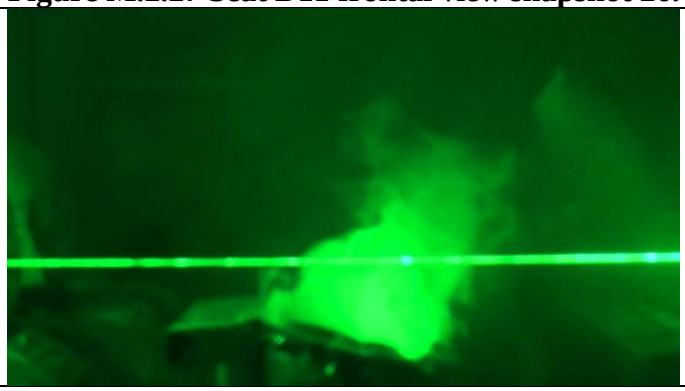

Figure M.2.28 Seat D11 frontal view snapshot 27.

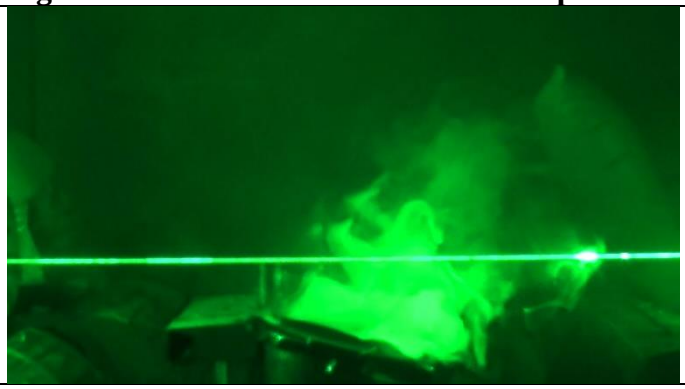

Figure M.2.29 Seat D11 frontal view snapshot 28.

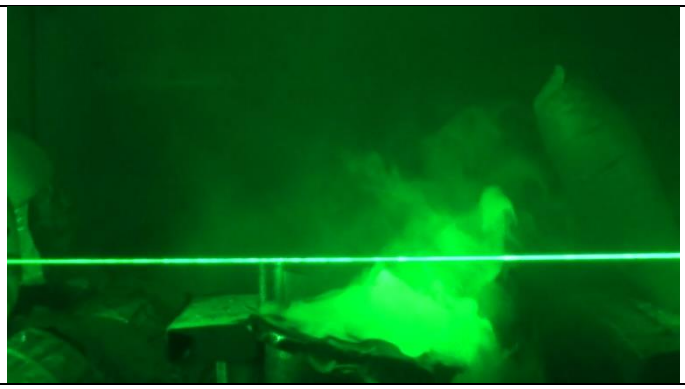

Figure M.2.30 Seat D11 frontal view snapshot 29.

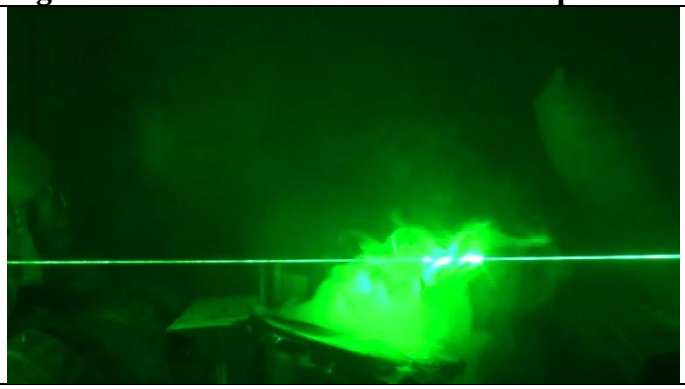

Figure M.2.31 Seat D11 frontal view snapshot 30.

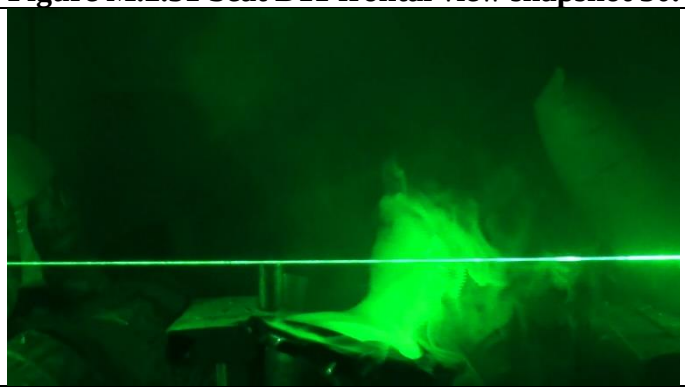

Figure M.2.32 Seat D11 frontal view snapshot 31.

Figure M.2.33 Seat D11 frontal view snapshot 32.

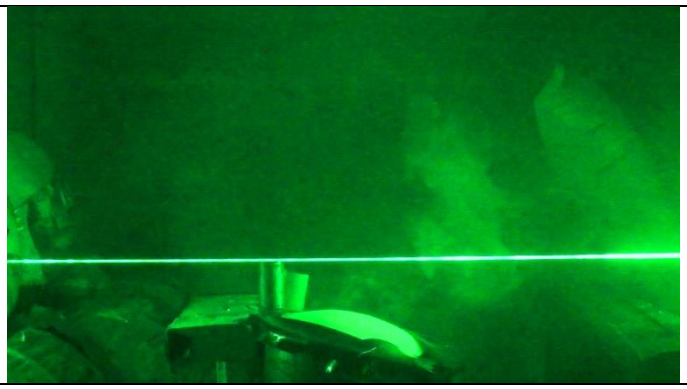

Figure M.2.34 Seat D11 frontal view snapshot 33.

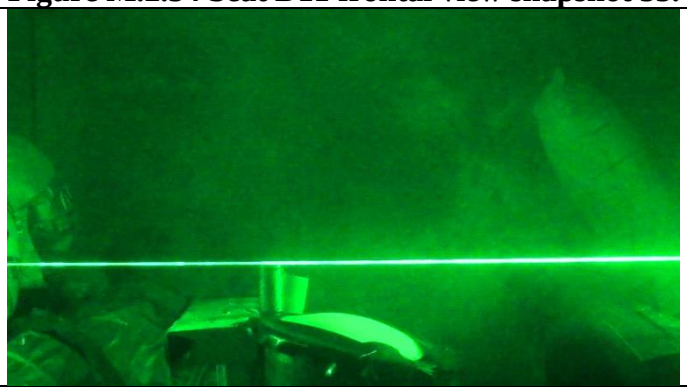

Figure M.2.35 Seat D11 frontal view snapshot 34.

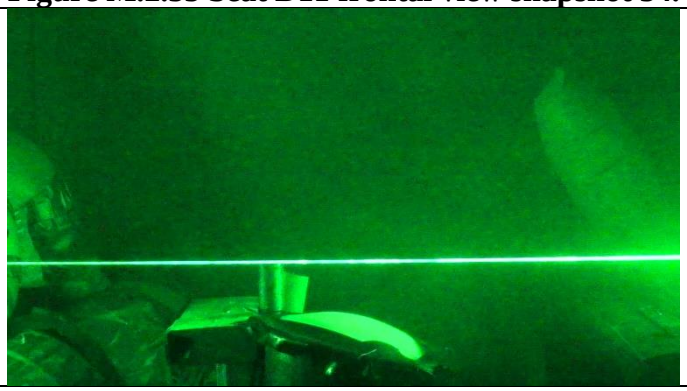

Figure M.2.36 Seat D11 frontal view snapshot 35.

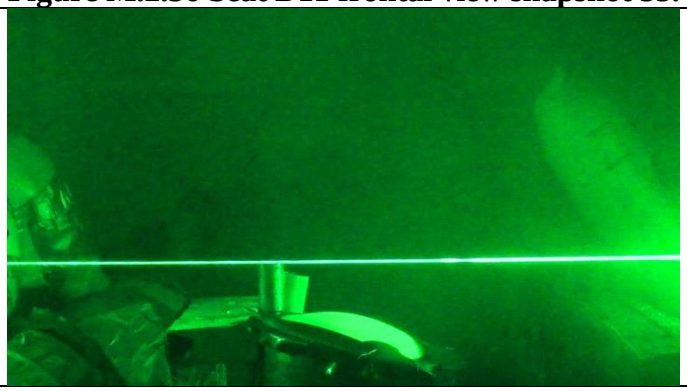

Figure M.2.37 Seat D11 frontal view snapshot 36.

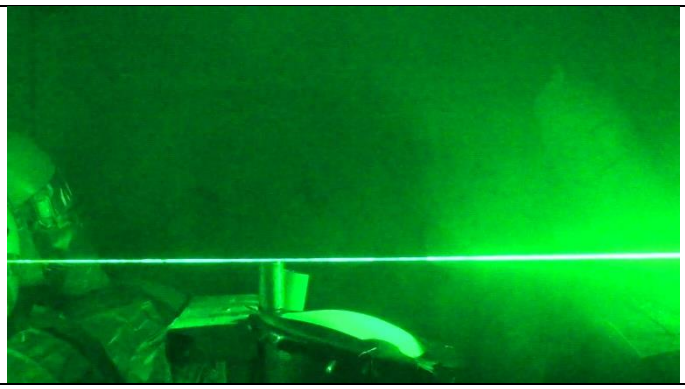

Figure M.2.38 Seat D11 frontal view snapshot 37.

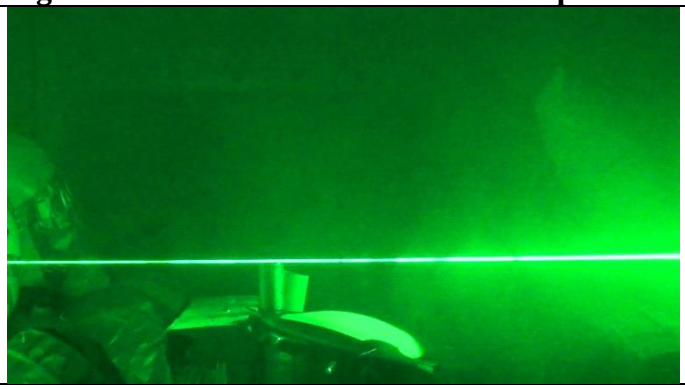

Figure M.2.39 Seat D11 frontal view snapshot 38.

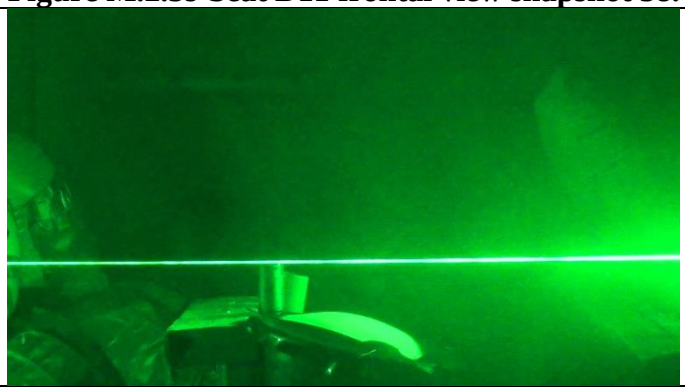

Figure M.2.40 Seat D11 frontal view snapshot 39.

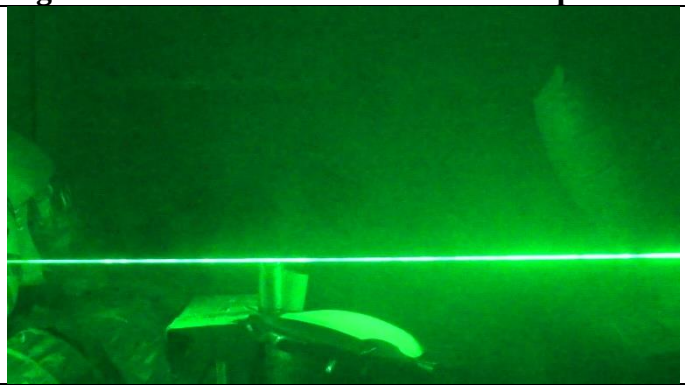

Figure M.2.41 Seat D11 frontal view snapshot 40.

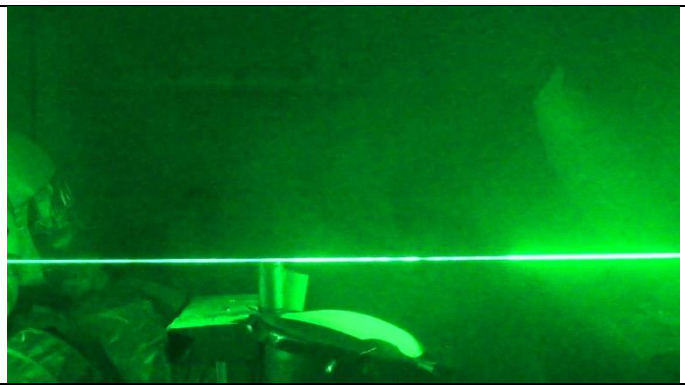

Figure M.2.42 Seat D11 frontal view snapshot 41.

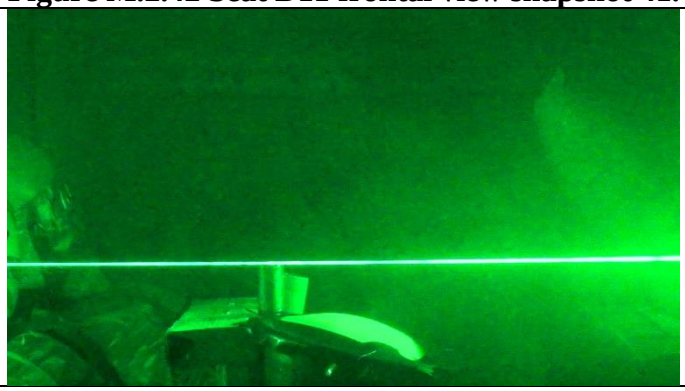

Figure M.2.43 Seat D11 frontal view snapshot 42.

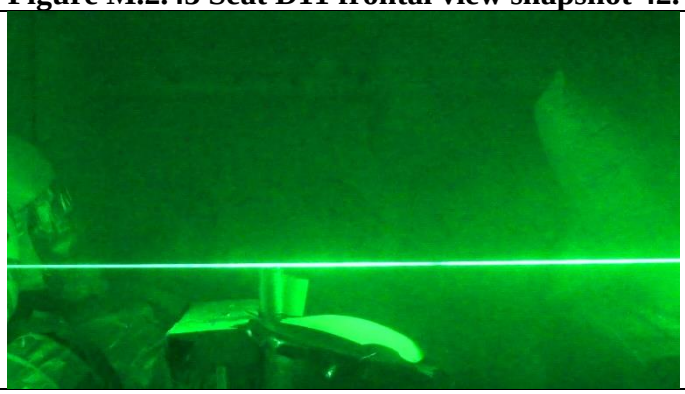

Figure M.2.44 Seat D11 frontal view snapshot 43.

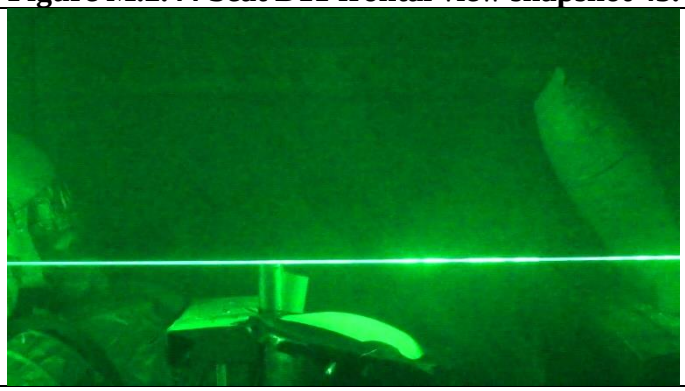

Figure M.2.45 Seat D11 frontal view snapshot 44.

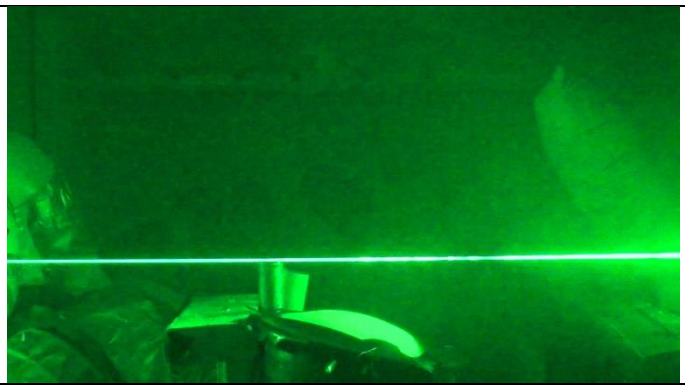

Figure M.2.46 Seat D11 frontal view snapshot 45.

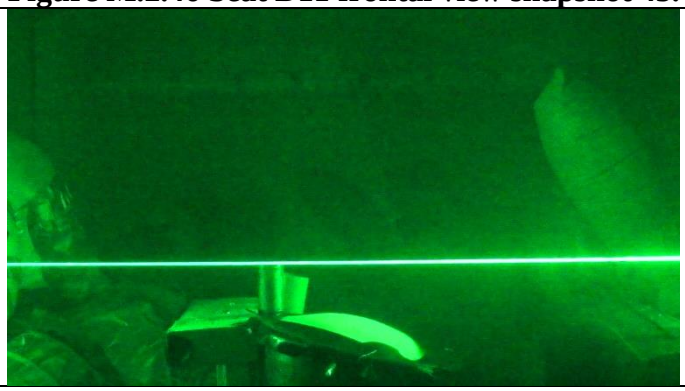

Figure M.2.47 Seat D11 frontal view snapshot 46.

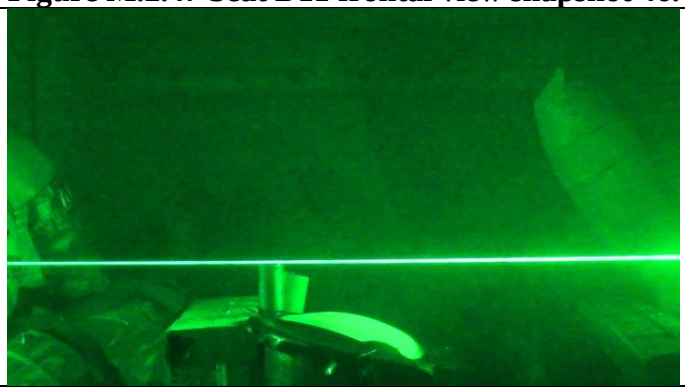

Figure M.2.48 Seat D11 frontal view snapshot 47.

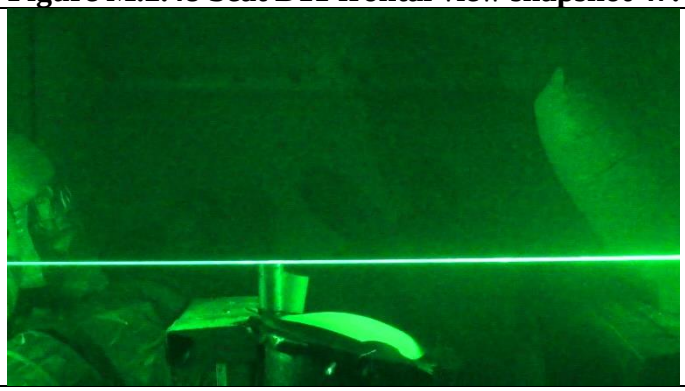

Figure M.2.49 Seat D11 frontal view snapshot 48.

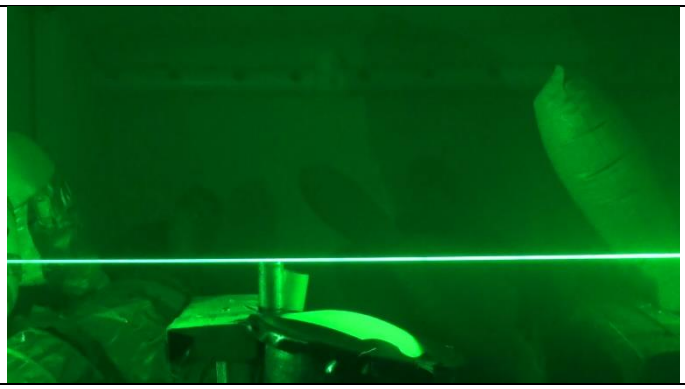

Figure M.2.50 Seat D11 frontal view snapshot 49.

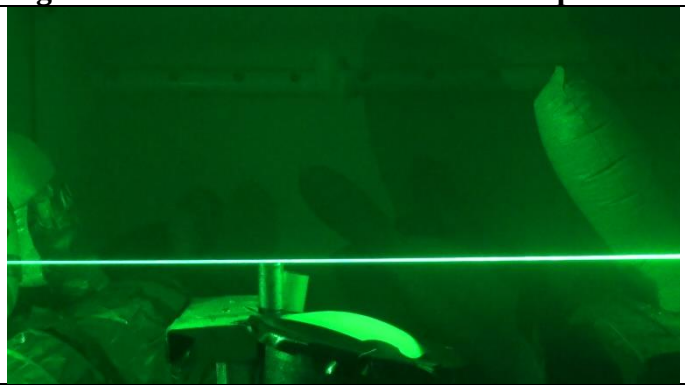

Figure M.2.51 Seat D11 frontal view snapshot 50.

Appendix N - Seat G6 Smoke Visualization Snapshots

N.1 Cross-sectional View

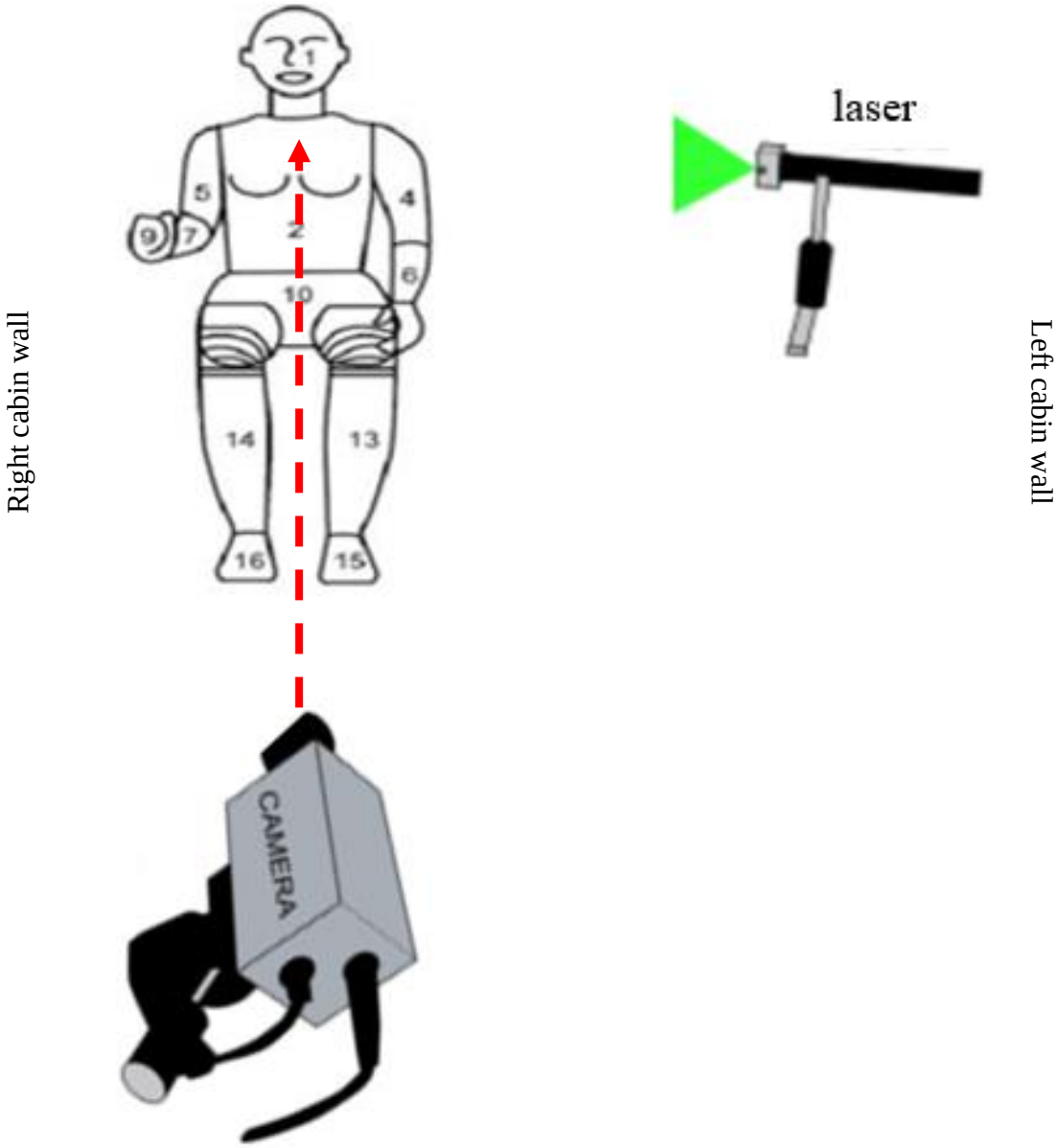

Figure N.1.1 A schematic showing the cross-sectional laser sheet direction and the camera location relative to the seat where the smoke generation source is located on seat G6.

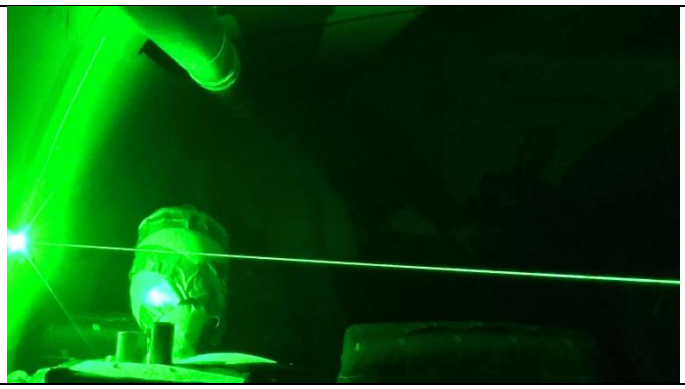

Figure N.1.2 Seat G6 cross-sectional view snapshot 01.

Figure N.1.3 Seat G6 cross-sectional view snapshot 02.

Figure N.1.4 Seat G6 cross-sectional view snapshot 03.

Figure N.1.5 Seat G6 cross-sectional view snapshot 04.

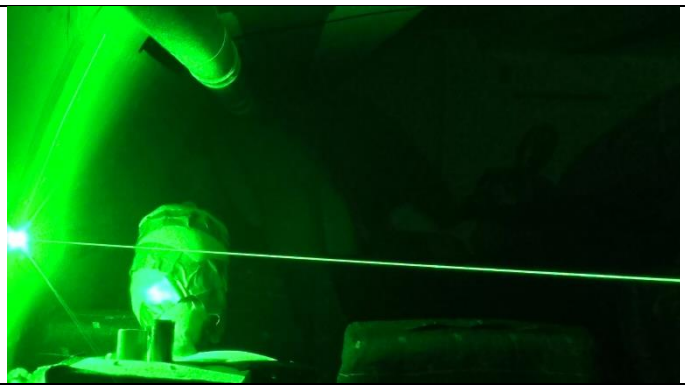

Figure N.1.6 Seat G6 cross-sectional view snapshot 05.

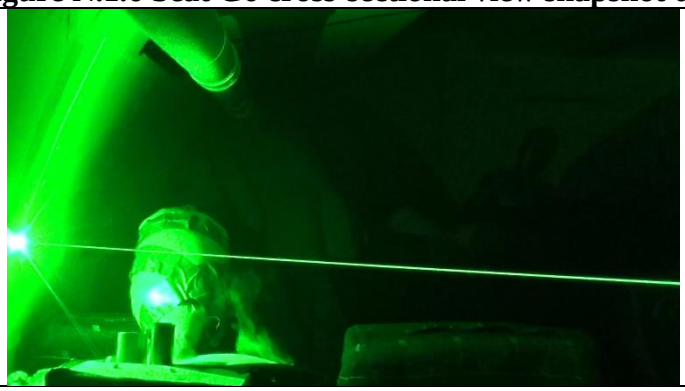

Figure N.1.7 Seat G6 cross-sectional view snapshot 06.

Figure N.1.8 Seat G6 cross-sectional view snapshot 07.

Figure N.1.9 Seat G6 cross-sectional view snapshot 08.

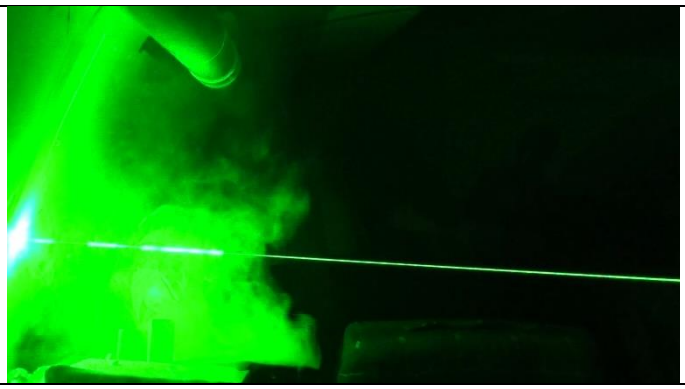

Figure N.1.10 Seat G6 cross-sectional view snapshot 09.

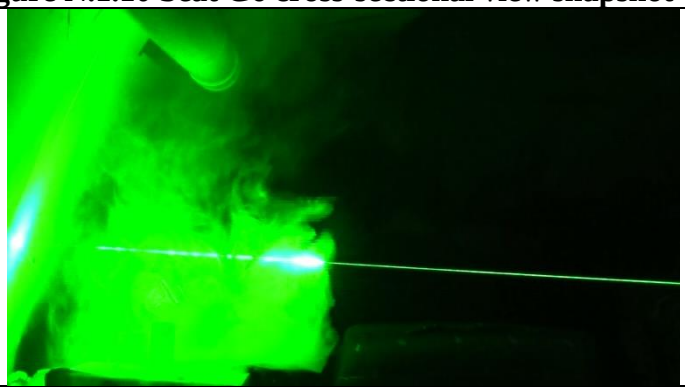

Figure N.1.11 Seat G6 cross-sectional view snapshot 10.

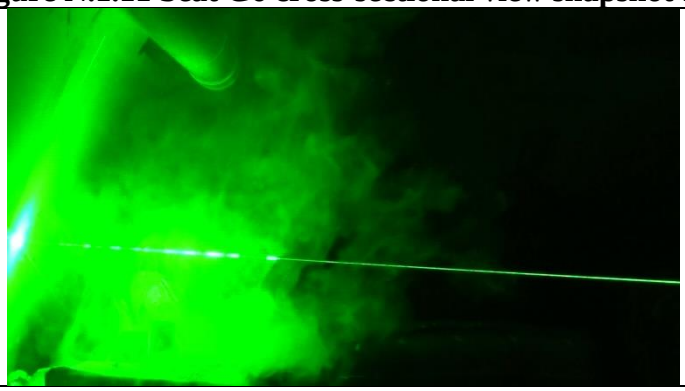

Figure N.1.12 Seat G6 cross-sectional view snapshot 11.

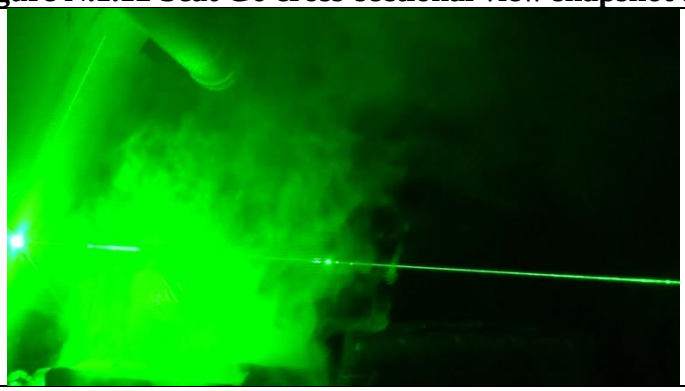

Figure N.1.13 Seat G6 cross-sectional view snapshot 12.

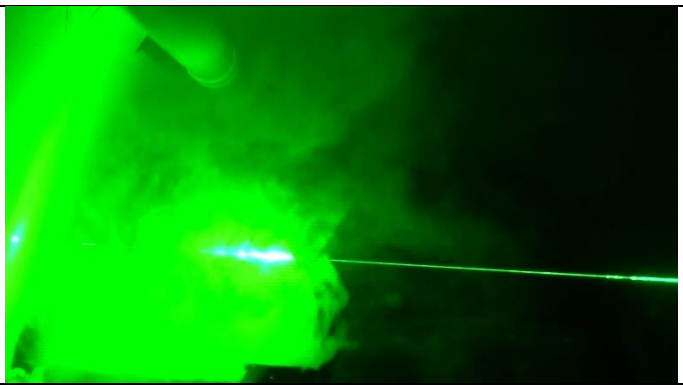

Figure N.1.14 Seat G6 cross-sectional view snapshot 13.

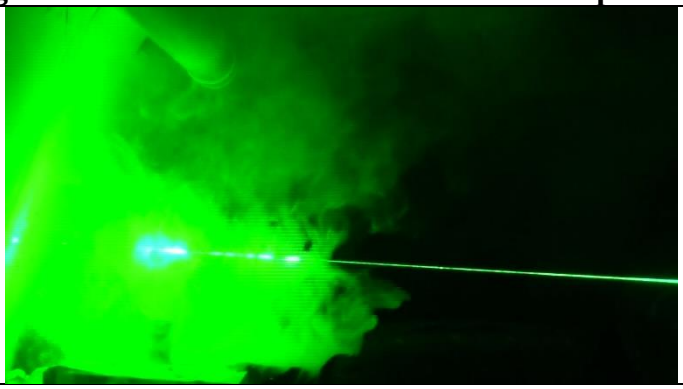

Figure N.1.15 Seat G6 cross-sectional view snapshot 14.

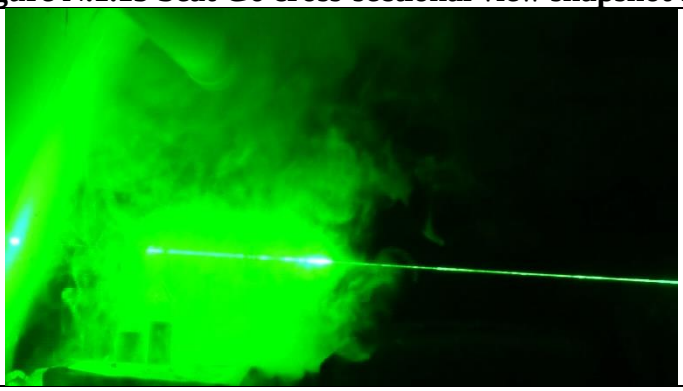

Figure N.1.16 Seat G6 cross-sectional view snapshot 15.

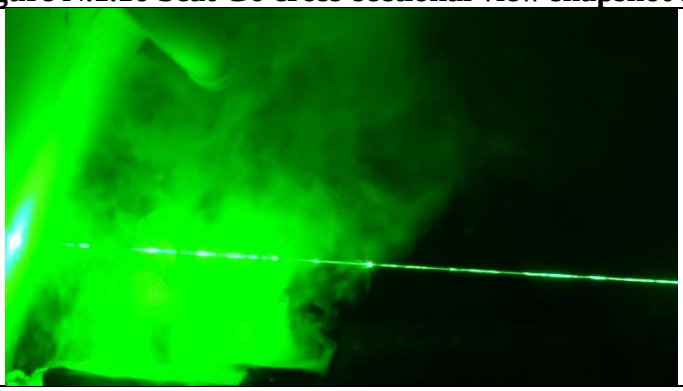

Figure N.1.17 Seat G6 cross-sectional view snapshot 16.

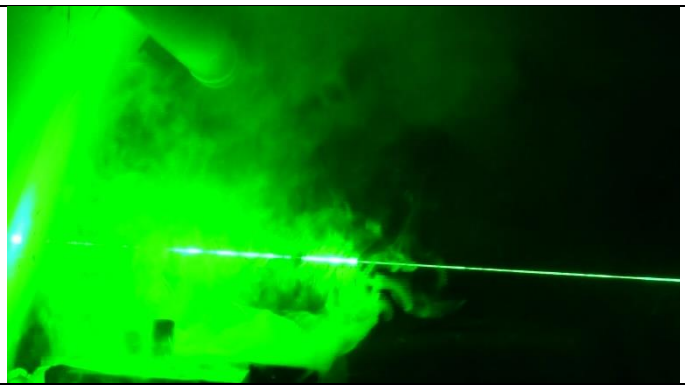

Figure N.1.18 Seat G6 cross-sectional view snapshot 17.

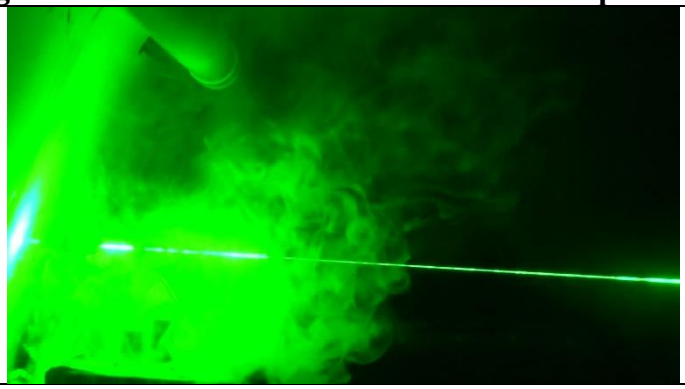

Figure N.1.19 Seat G6 cross-sectional view snapshot 18.

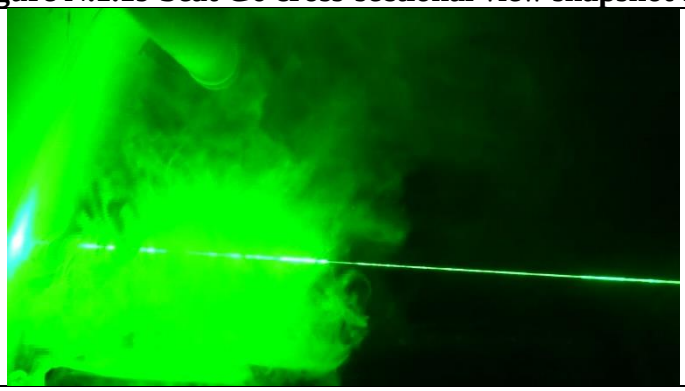

Figure N.1.20 Seat G6 cross-sectional view snapshot 19.

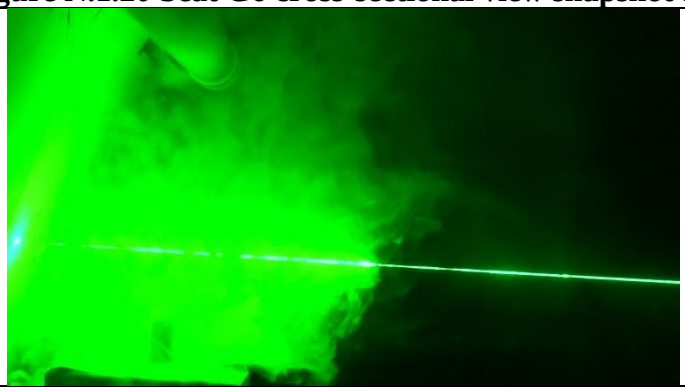

Figure N.1.21 Seat G6 cross-sectional view snapshot 20.

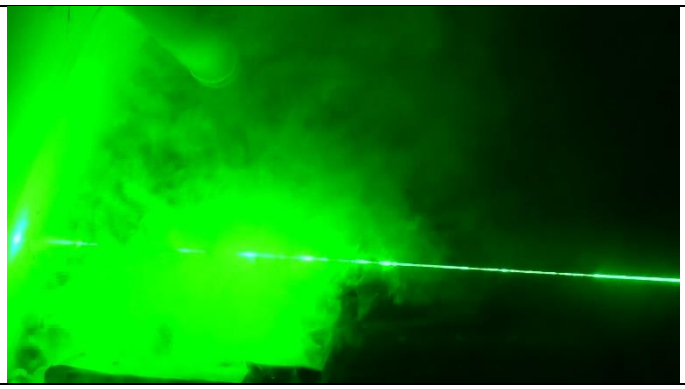

Figure N.1.22 Seat G6 cross-sectional view snapshot 21.

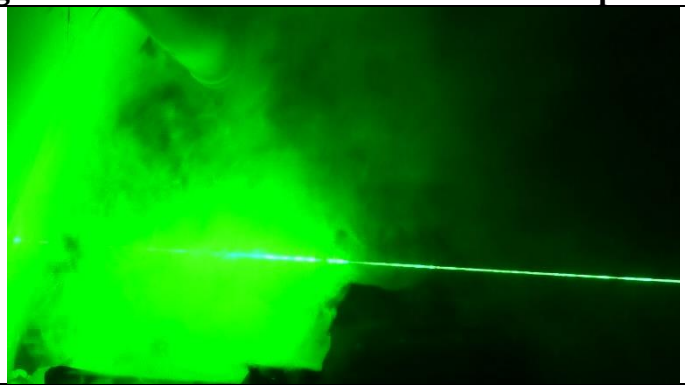

Figure N.1.23 Seat G6 cross-sectional view snapshot 22.

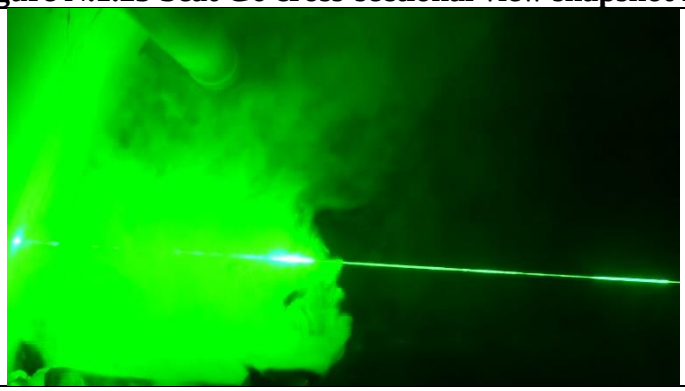

Figure N.1.24 Seat G6 cross-sectional view snapshot 23.

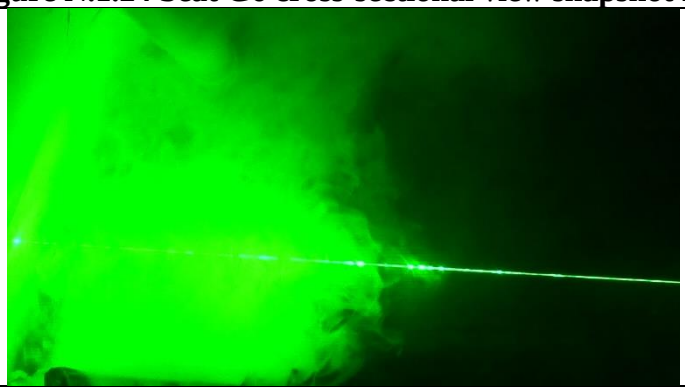

Figure N.1.25 Seat G6 cross-sectional view snapshot 24.

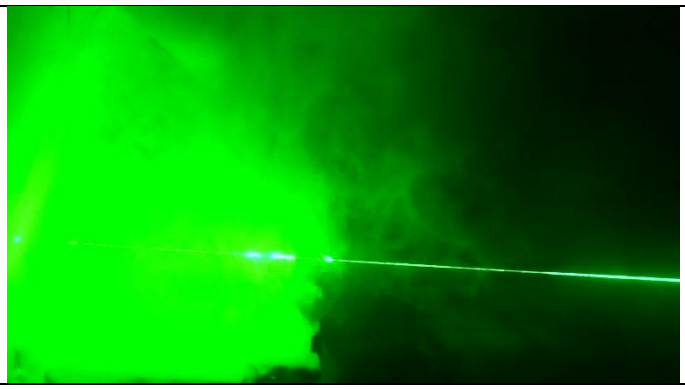

Figure N.1.26 Seat G6 cross-sectional view snapshot 25.

Figure N.1.27 Seat G6 cross-sectional view snapshot 26.

Figure N.1.28 Seat G6 cross-sectional view snapshot 27.

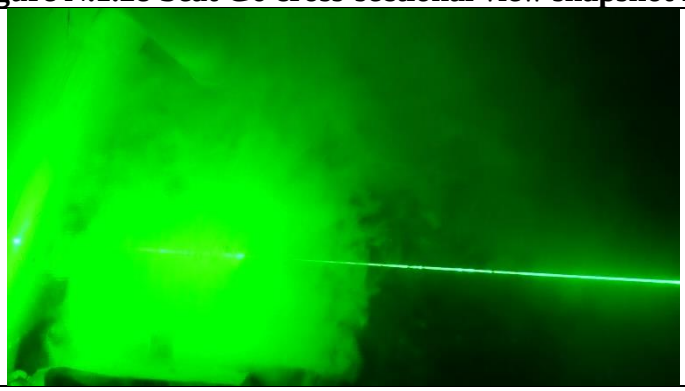

Figure N.1.29 Seat G6 cross-sectional view snapshot 28.

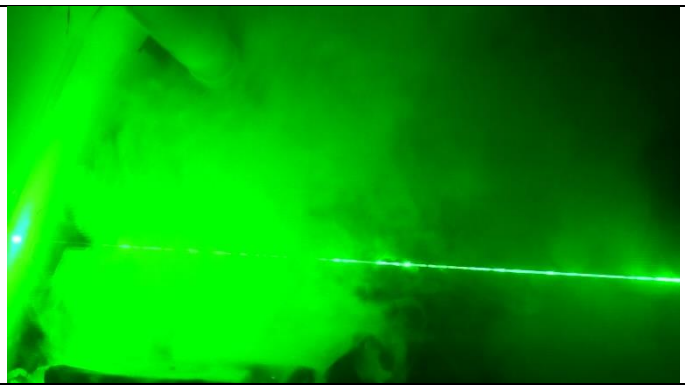

Figure N.1.30 Seat G6 cross-sectional view snapshot 29.

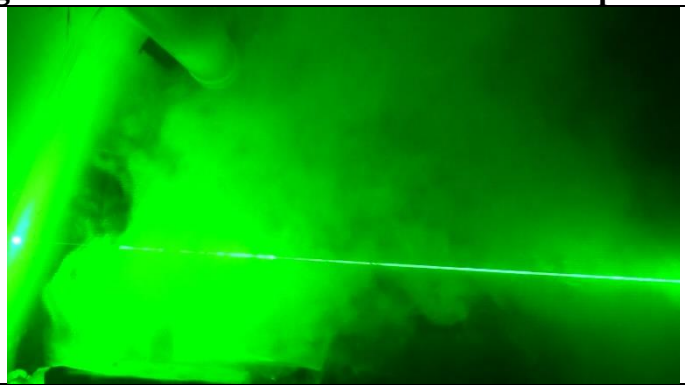

Figure N.1.31 Seat G6 cross-sectional view snapshot 30.

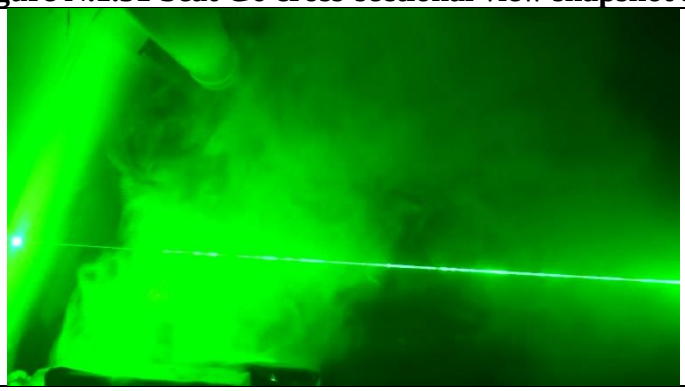

Figure N.1.32 Seat G6 cross-sectional view snapshot 31.

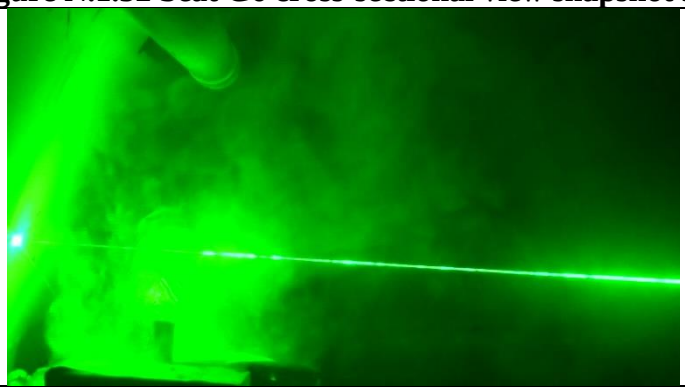

Figure N.1.33 Seat G6 cross-sectional view snapshot 32.

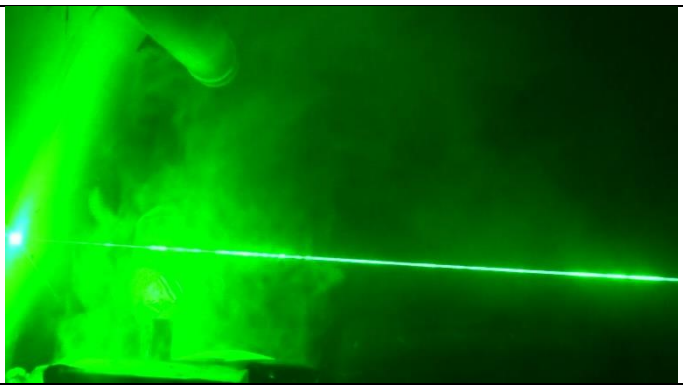

Figure N.1.34 Seat G6 cross-sectional view snapshot 33.

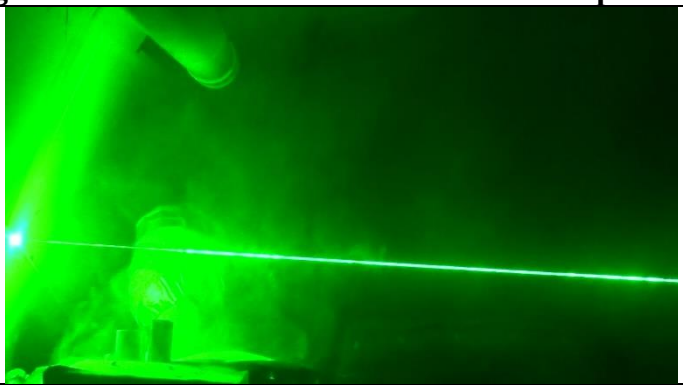

Figure N.1.35 Seat G6 cross-sectional view snapshot 34.

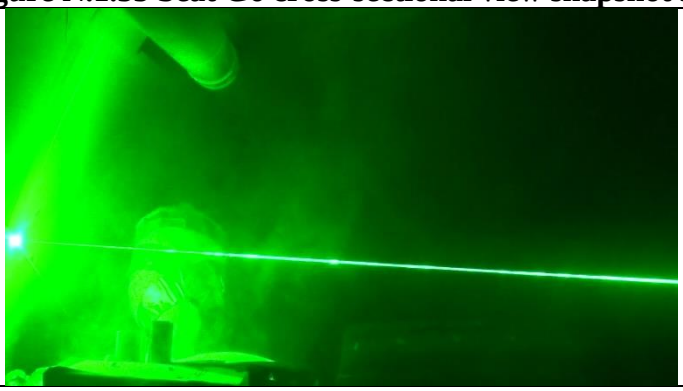

Figure N.1.36 Seat G6 cross-sectional view snapshot 35.

Figure N.1.37 Seat G6 cross-sectional view snapshot 36.

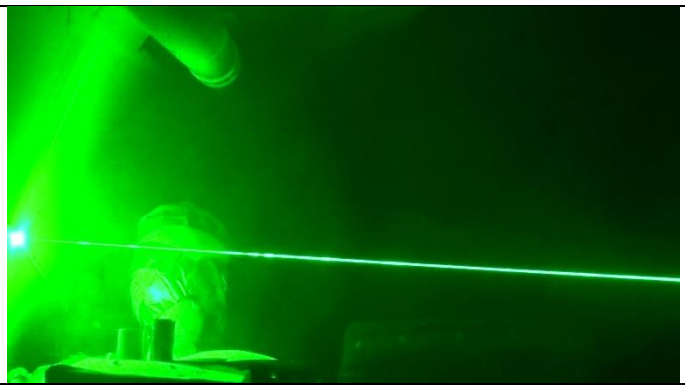

Figure N.1.38 Seat G6 cross-sectional view snapshot 37.

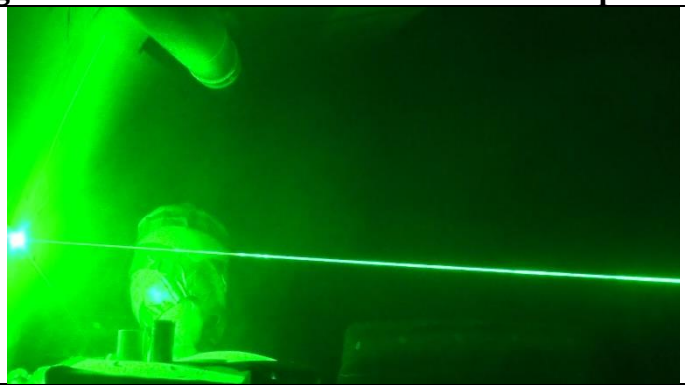

Figure N.1.39 Seat G6 cross-sectional view snapshot 38.

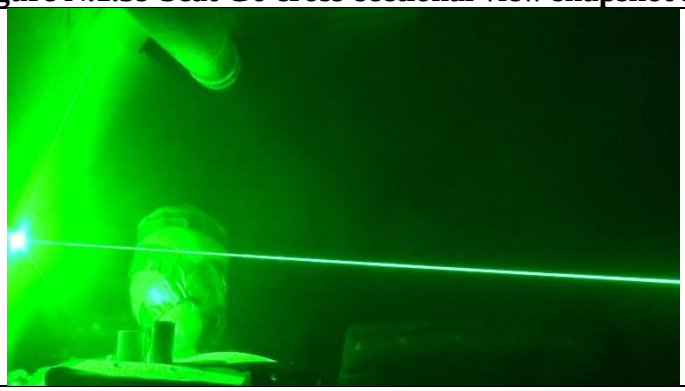

Figure N.1.40 Seat G6 cross-sectional view snapshot 39.

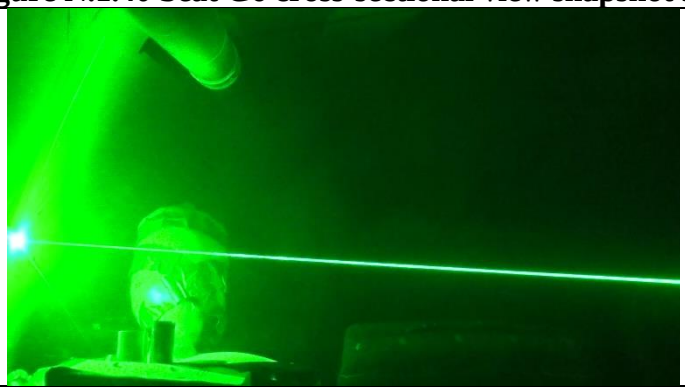

Figure N.1.41 Seat G6 cross-sectional view snapshot 40.

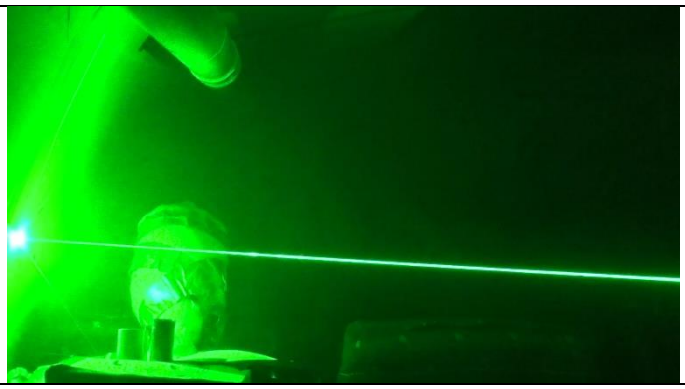

Figure N.1.42 Seat G6 cross-sectional view snapshot 41.

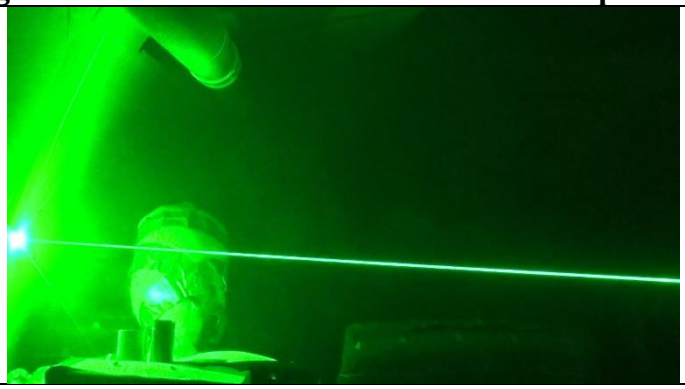

Figure N.1.43 Seat G6 cross-sectional view snapshot 42.

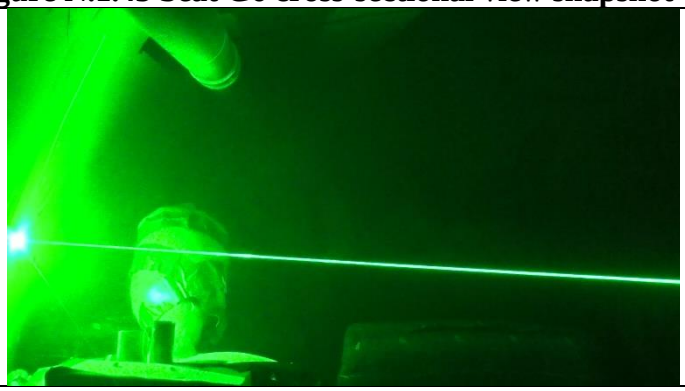

Figure N.1.44 Seat G6 cross-sectional view snapshot 43.

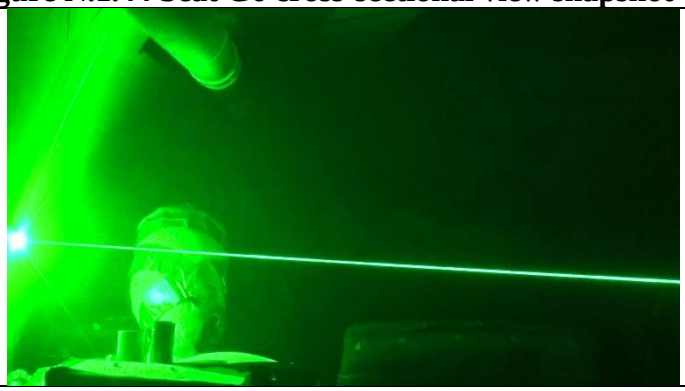

Figure N.1.45 Seat G6 cross-sectional view snapshot 44.

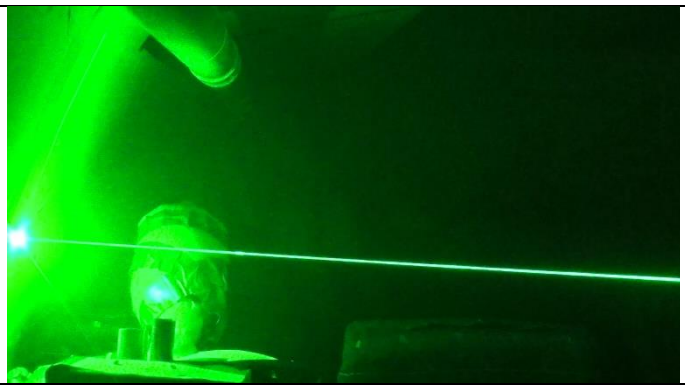

Figure N.1.46 Seat G6 cross-sectional view snapshot 45.

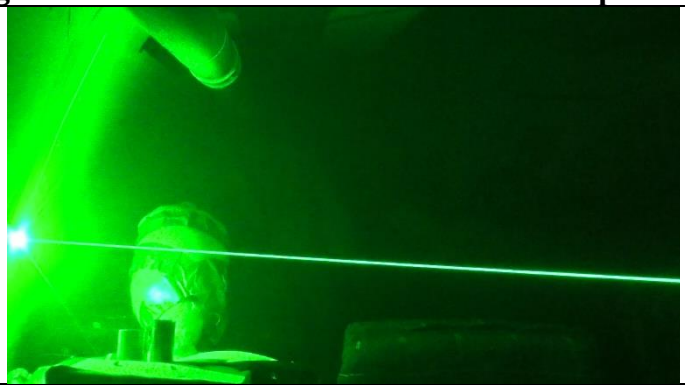

Figure N.1.47 Seat G6 cross-sectional view snapshot 46.

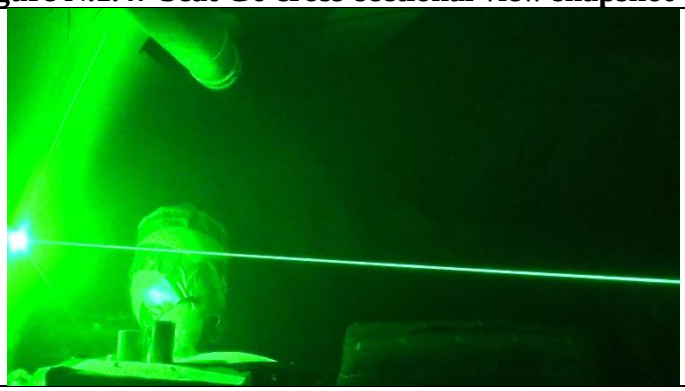

Figure N.1.48 Seat G6 cross-sectional view snapshot 47.

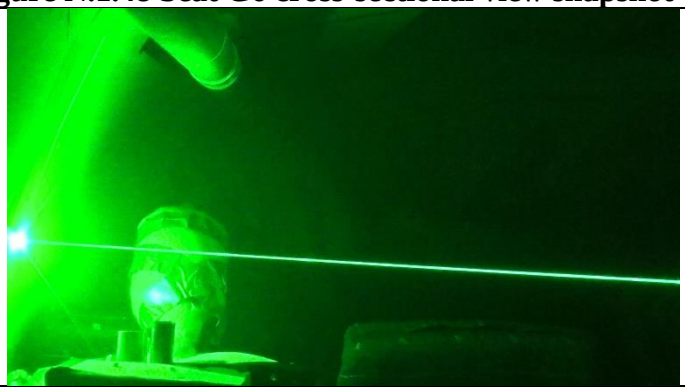

Figure N.1.49 Seat G6 cross-sectional view snapshot 48.

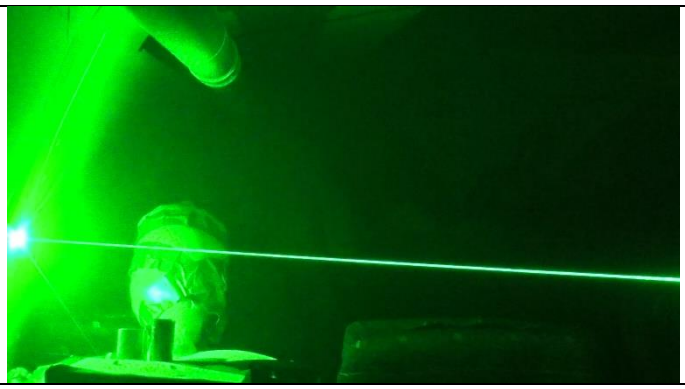

Figure N.1.50 Seat G6 cross-sectional view snapshot 49.

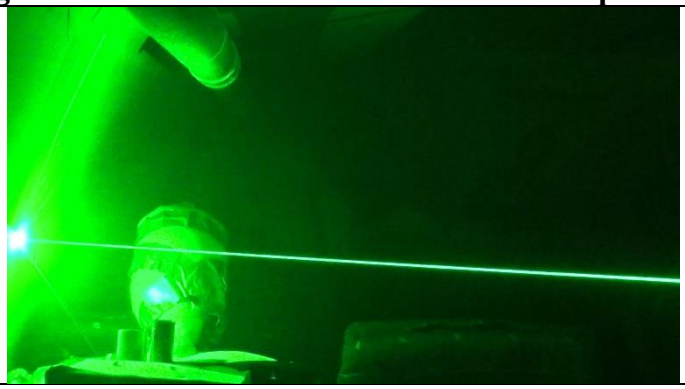

Figure N.1.51 Seat G6 cross-sectional view snapshot 50.

N.2 Frontal View

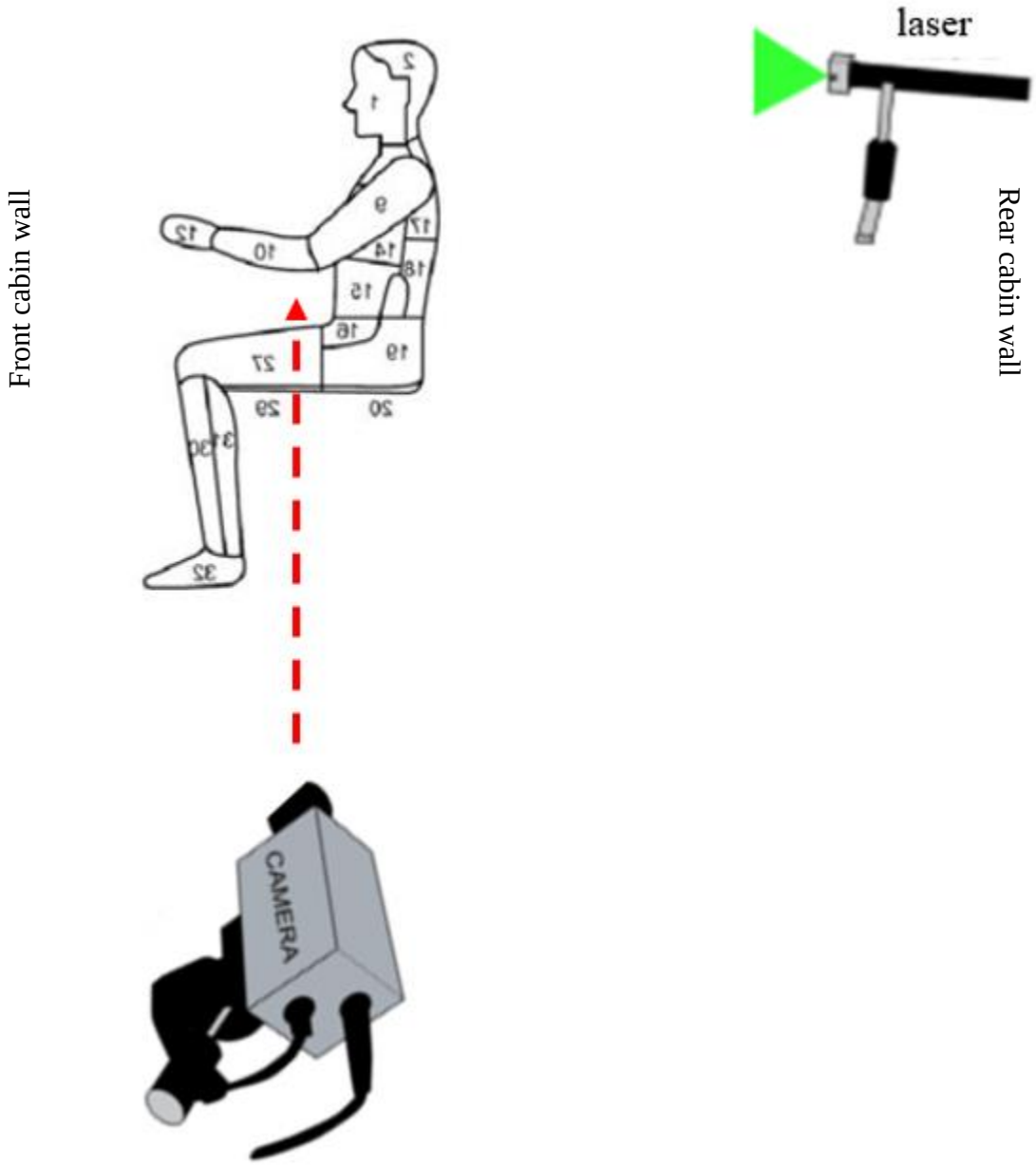

Figure N.2.1 A schematic showing the frontal laser sheet direction and the camera location relative to the seat where the smoke generation source is located on seat G6.

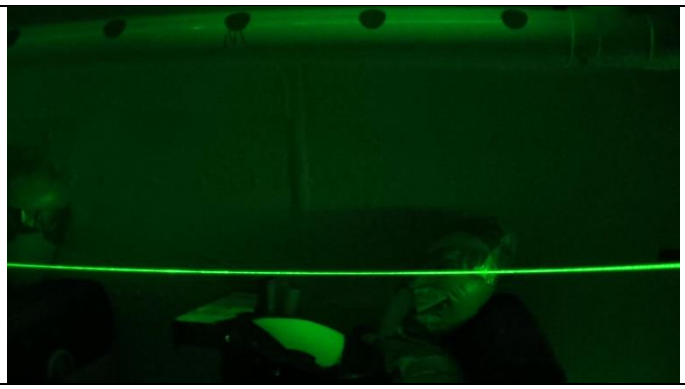

Figure N.2.2 Seat G6 frontal view snapshot 01.

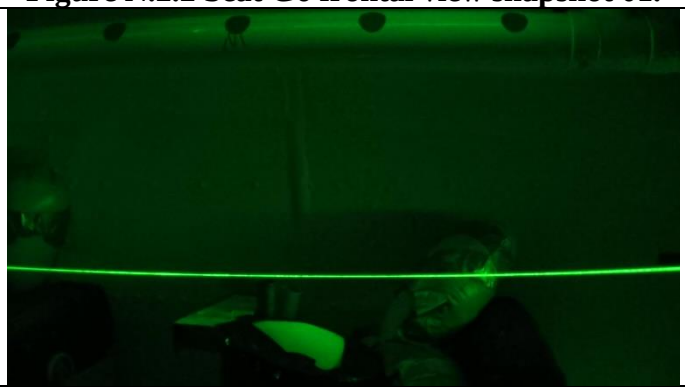

Figure N.2.3 Seat G6 frontal view snapshot 02.

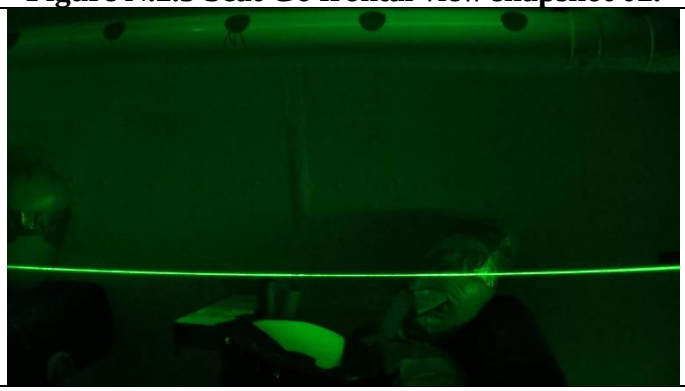

Figure N.2.4 Seat G6 frontal view snapshot 03.

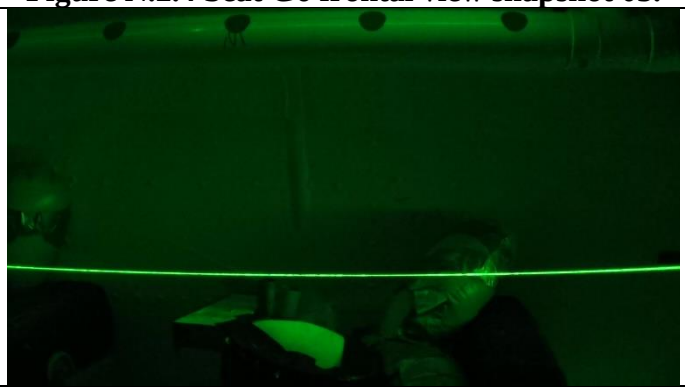

Figure N.2.5 Seat G6 frontal view snapshot 04.

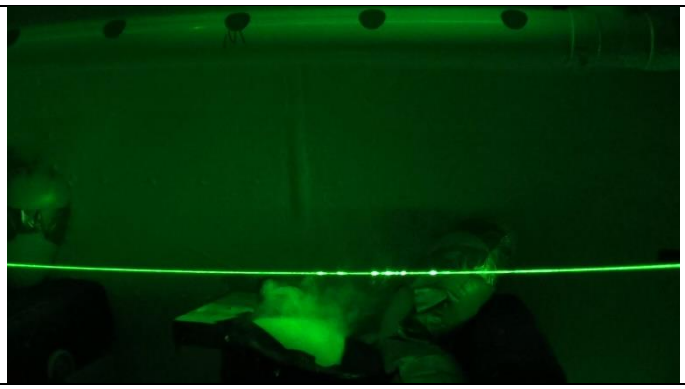

Figure N.2.6 Seat G6 frontal view snapshot 05.

Figure N.2.7 Seat G6 frontal view snapshot 06.

Figure N.2.8 Seat G6 frontal view snapshot 07.

Figure N.2.9 Seat G6 frontal view snapshot 08.

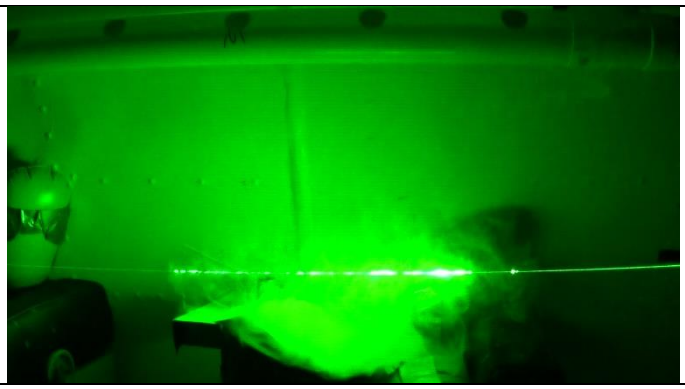

Figure N.2.10 Seat G6 frontal view snapshot 09.

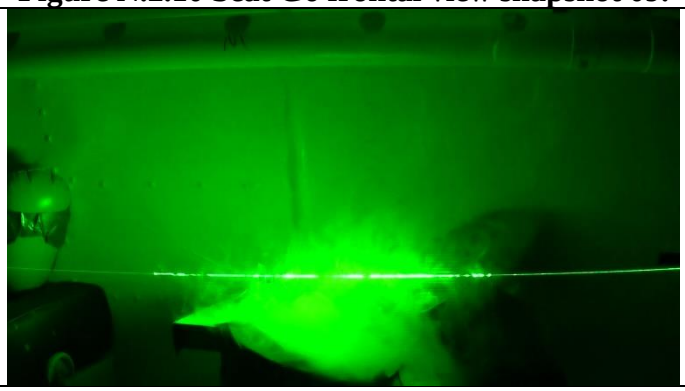

Figure N.2.11 Seat G6 frontal view snapshot 10.

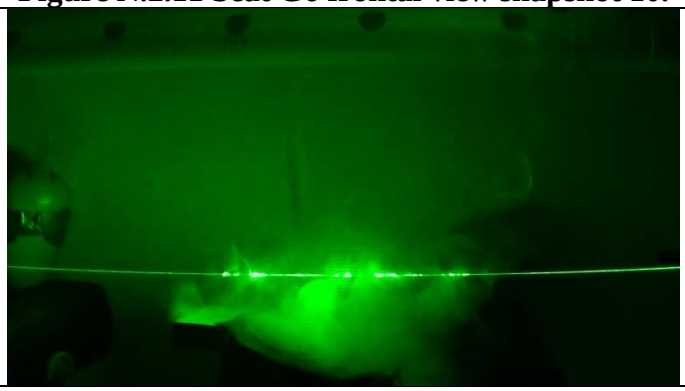

Figure N.2.12 Seat G6 frontal view snapshot 11.

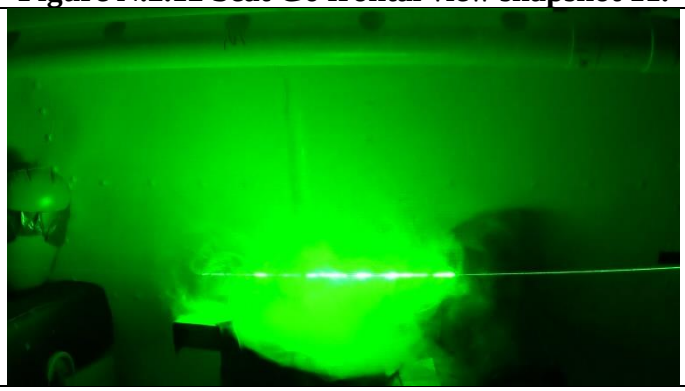

Figure N.2.13 Seat G6 frontal view snapshot 12.

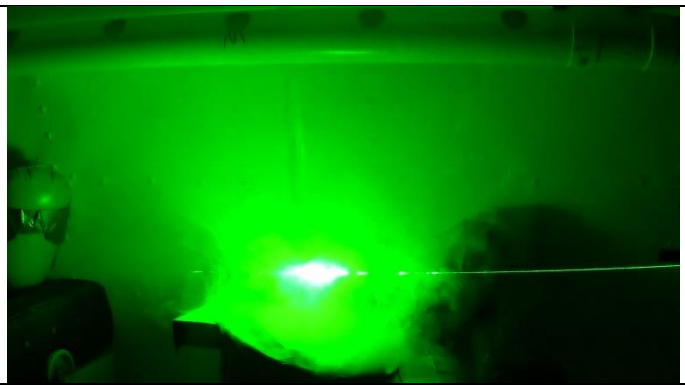

Figure N.2.14 Seat G6 frontal view snapshot 13.

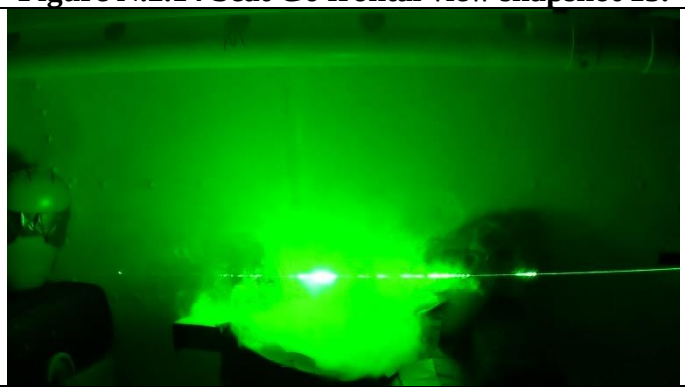

Figure N.2.15 Seat G6 frontal view snapshot 14.

Figure N.2.16 Seat G6 frontal view snapshot 15.

Figure N.2.17 Seat G6 frontal view snapshot 16.

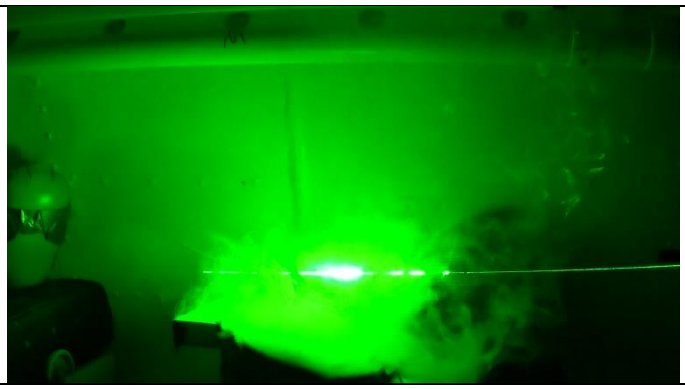

Figure N.2.18 Seat G6 frontal view snapshot 17.

Figure N.2.19 Seat G6 frontal view snapshot 18.

Figure N.2.20 Seat G6 frontal view snapshot 19.

Figure N.2.21 Seat G6 frontal view snapshot 20.

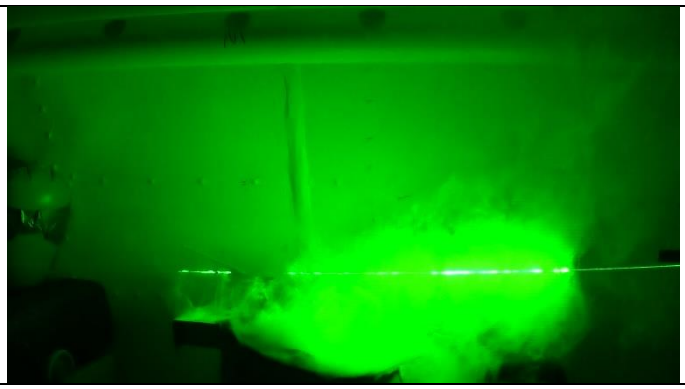

Figure N.2.22 Seat G6 frontal view snapshot 21.

Figure N.2.23 Seat G6 frontal view snapshot 22.

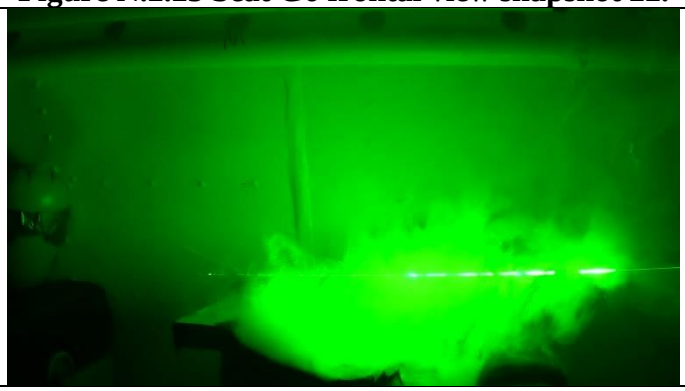

Figure N.2.24 Seat G6 frontal view snapshot 23.

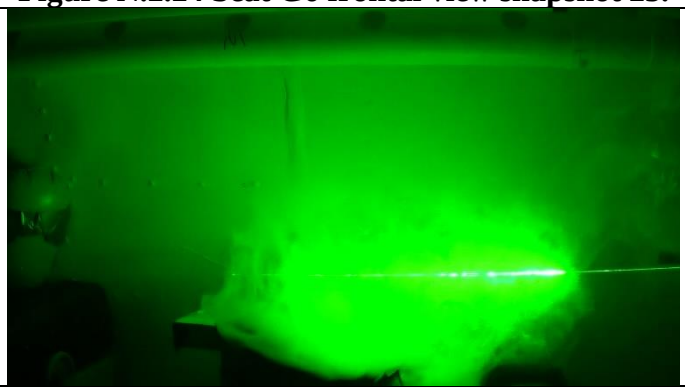

Figure N.2.25 Seat G6 frontal view snapshot 24.

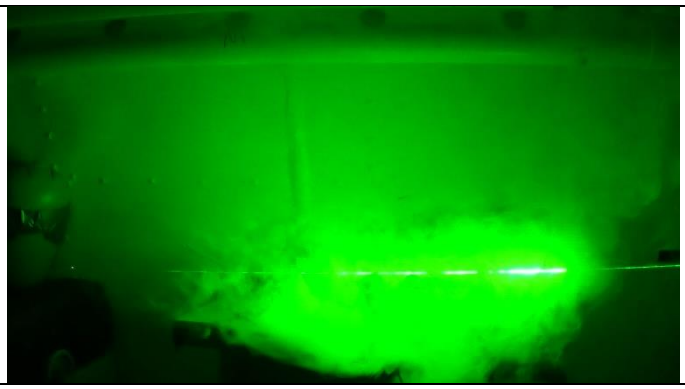

Figure N.2.26 Seat G6 frontal view snapshot 25.

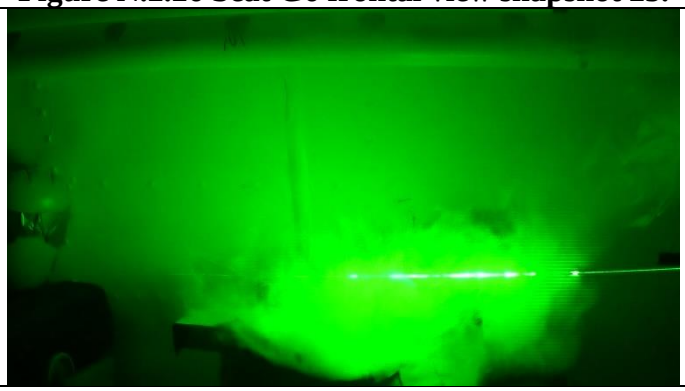

Figure N.2.27 Seat G6 frontal view snapshot 26.

Figure N.2.28 Seat G6 frontal view snapshot 27.

Figure N.2.29 Seat G6 frontal view snapshot 28.

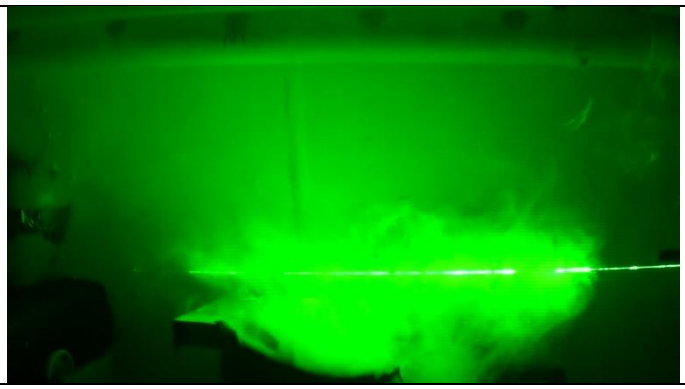

Figure N.2.30 Seat G6 frontal view snapshot 29.

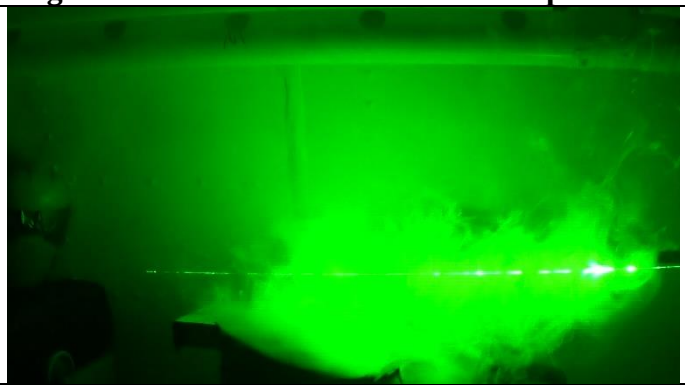

Figure N.2.31 Seat G6 frontal view snapshot 30.

Figure N.2.32 Seat G6 frontal view snapshot 31.

Figure N.2.33 Seat G6 frontal view snapshot 32.

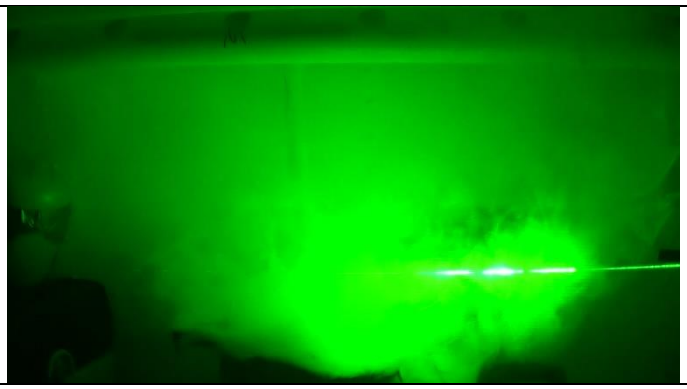

Figure N.2.34 Seat G6 frontal view snapshot 33.

Figure N.2.35 Seat G6 frontal view snapshot 34.

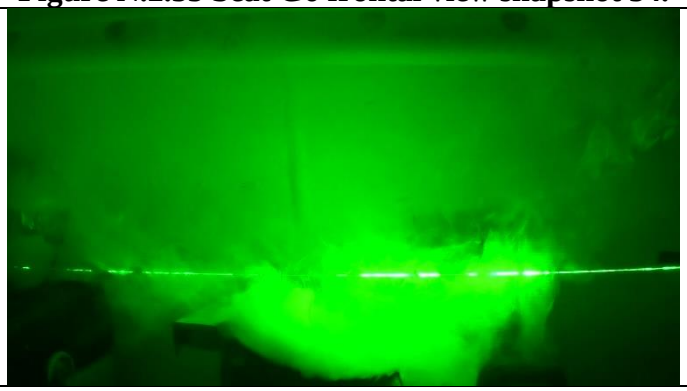

Figure N.2.36 Seat G6 frontal view snapshot 35.

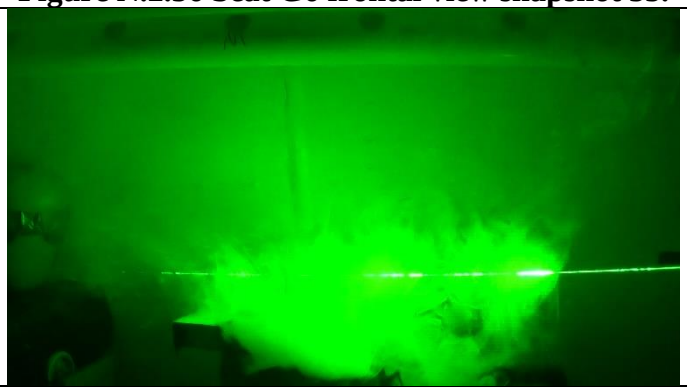

Figure N.2.37 Seat G6 frontal view snapshot 36.

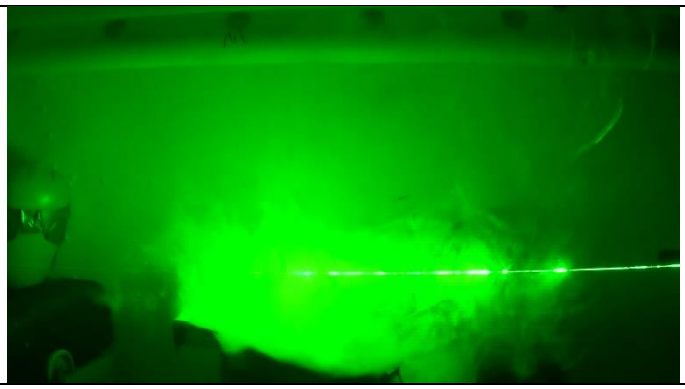

Figure N.2.38 Seat G6 frontal view snapshot 37.

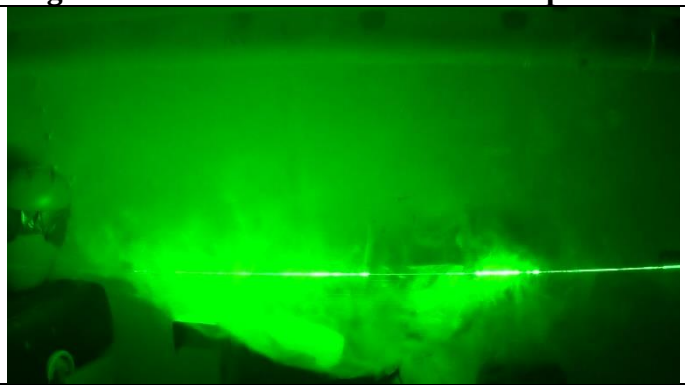

Figure N.2.39 Seat G6 frontal view snapshot 38.

Figure N.2.40 Seat G6 frontal view snapshot 39.

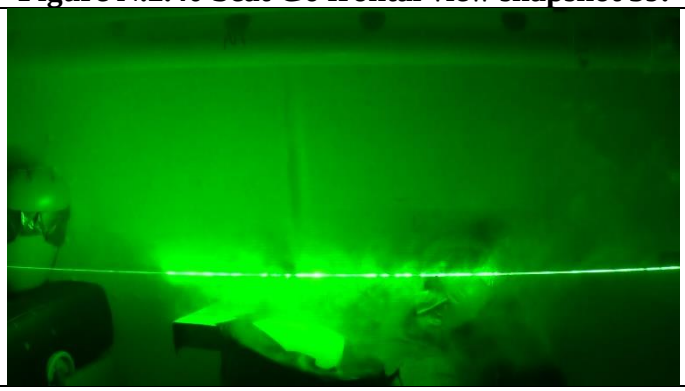

Figure N.2.41 Seat G6 frontal view snapshot 40.

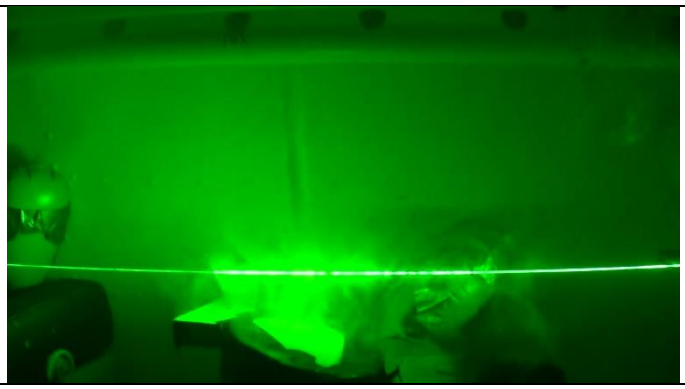

Figure N.2.42 Seat G6 frontal view snapshot 41.

Figure N.2.43 Seat G6 frontal view snapshot 42.

Figure N.2.44 Seat G6 frontal view snapshot 43.

Figure N.2.45 Seat G6 frontal view snapshot 44.

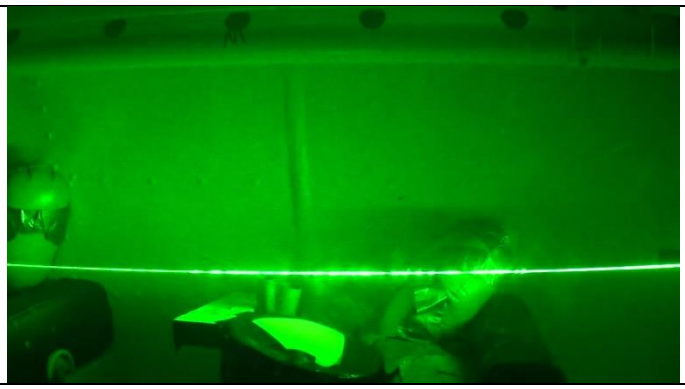

Figure N.2.46 Seat G6 frontal view snapshot 45.

Figure N.2.47 Seat G6 frontal view snapshot 46.

Figure N.2.48 Seat G6 frontal view snapshot 47.

Figure N.2.49 Seat G6 frontal view snapshot 48.

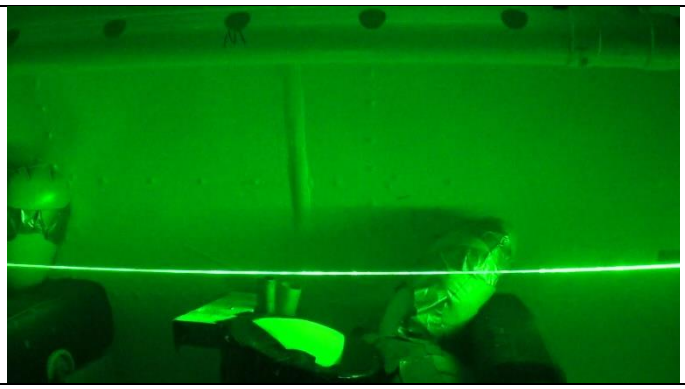

Figure N.2.50 Seat G6 frontal view snapshot 49.

Figure N.2.51 Seat G6 frontal view snapshot 50.

Appendix O - Analytical comparisons

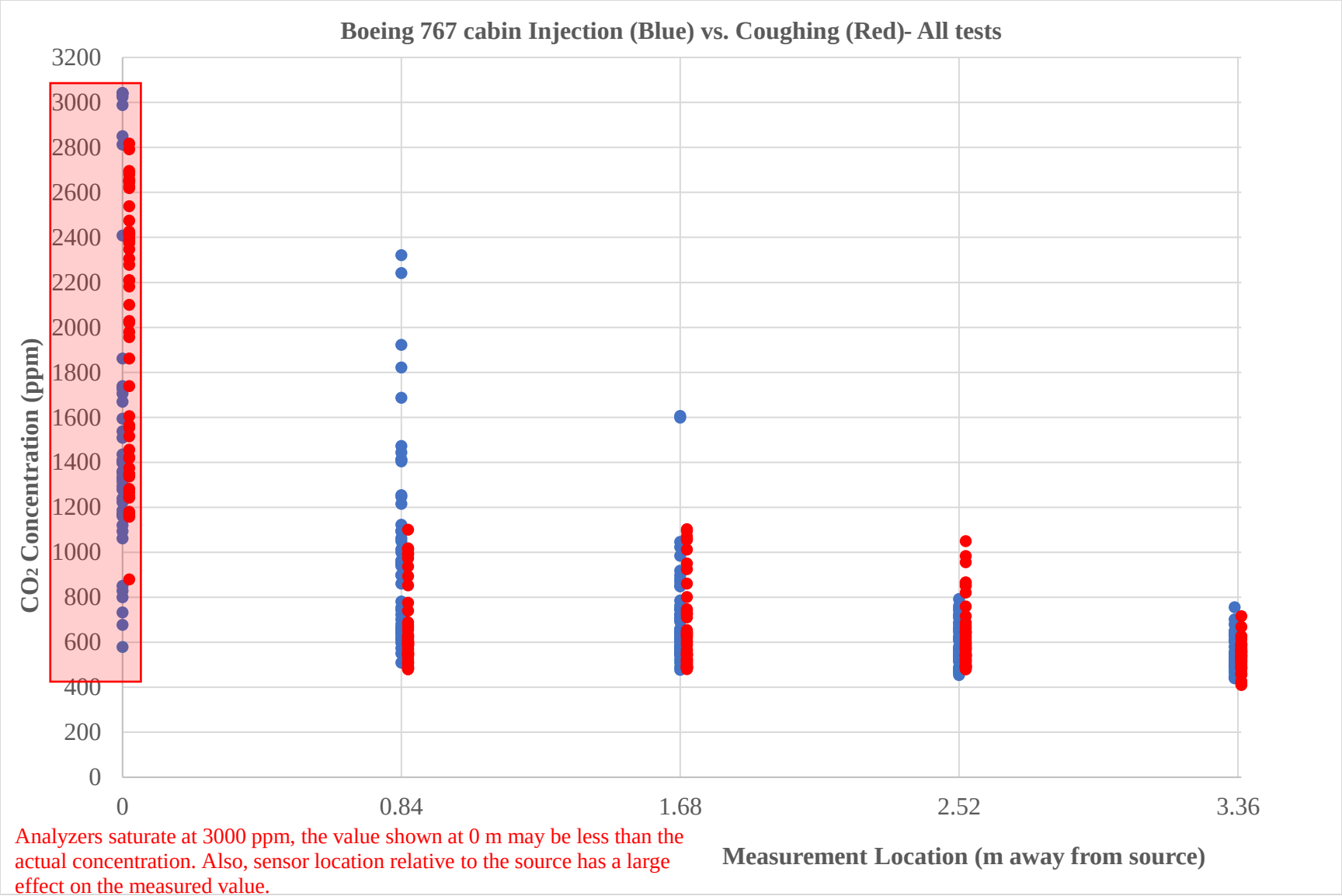

O.1 A comparison between all tests performed with a continuous injection source (Blue) vs. a coughing manikin (Red) in the Boeing 767 cabin mockup.

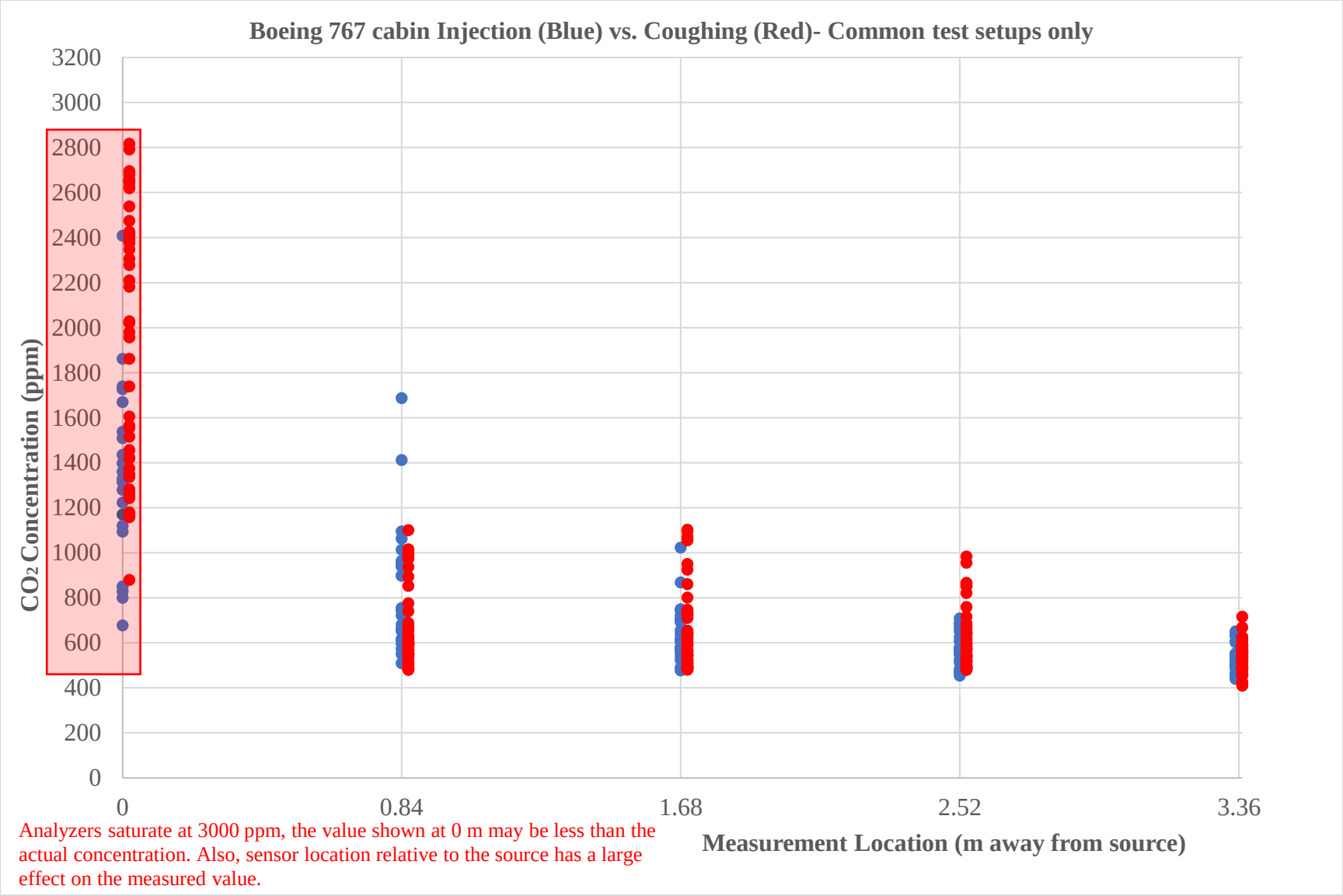

O.2 A comparison between common tests performed with continuous injection source (Blue) vs. coughing manikin (Red) in the Boeing 767 cabin mockup.

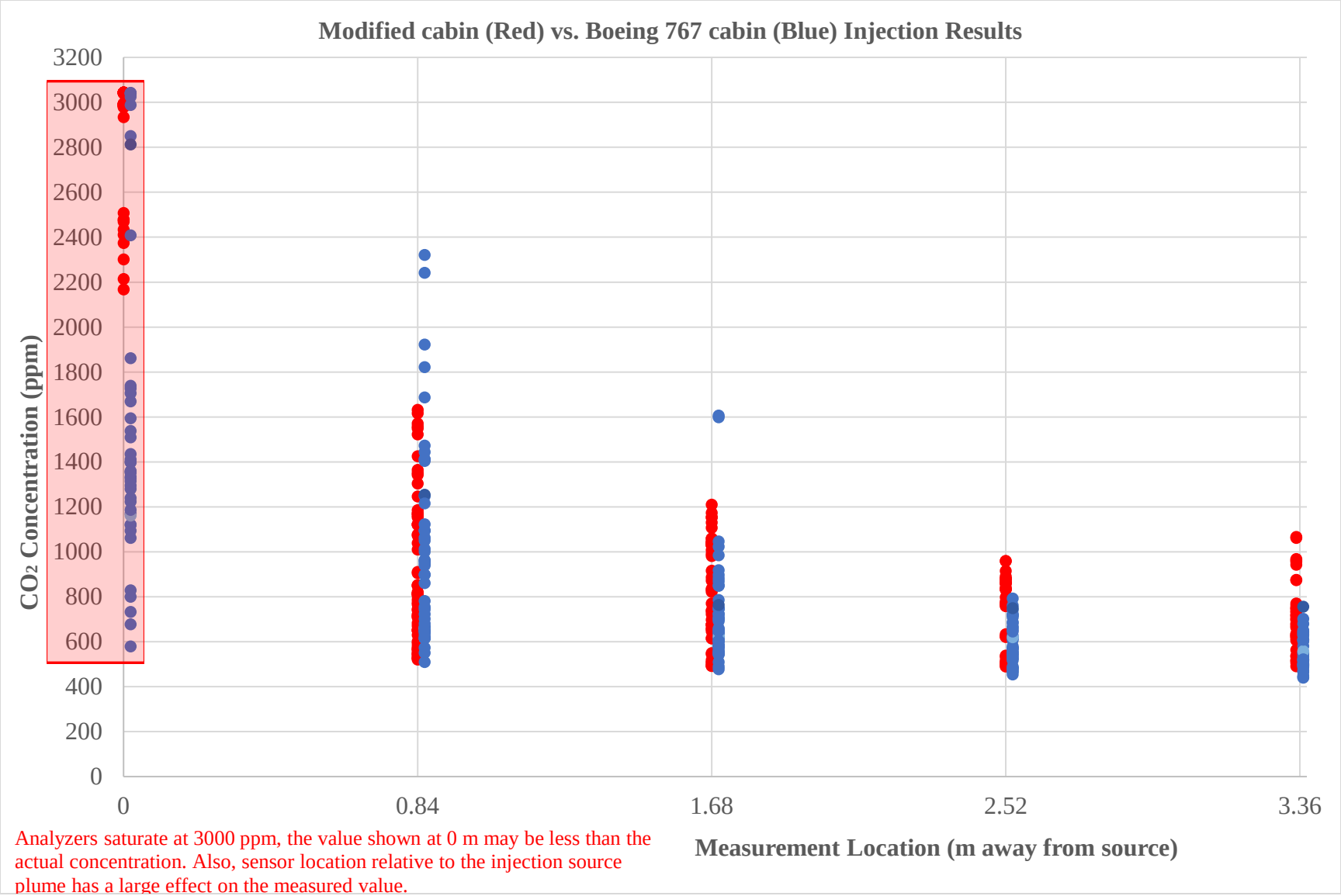

O.3 A comparison between all tests performed with a continuous injection source in the Boeing 767 cabin mockup (Blue) and the modified cabin (Red).

Appendix P - List of Publications

Conference Proceedings Publications:

[1] Mahmoud, S., Bennett, J.S., Hosni, M.H., and Jones, B.W, "Comparison of Pathogens Dispersion in an Aircraft Cabin Using Gas Injection Source Versus a Coughing Manikin", *ASME 2020 Fluids Engineering Division Summer Meeting FEDSM2020*, July 12-16, 2020, Orlando, Florida, USA.

[2] Mahmoud, S., Hosni, M.H., Jones, B.W. Bennett, J. et.al. , "Transport and Containment of Infectious Disease Expelled by Coughing in an Aircraft Cabin", *2020 ASHRAE Annual Conference*, June 27 – July 1, 2020.

[3] Mahmoud, S., Hosni, M. H., Jones, B., and Bennett, J., 2019, "Mapping The Potential For Infectious Disease Transmission In A Wide-Body Aircraft Cabin" *International Mechanical Engineering Congress and Exposition*, Salt Lake City, pp. 1–10.

Oral Presentations and Talks:

[1] Disease transmission and containment in aircraft cabins, International webinar series, Sankalchand Patel University, India, November 21st, 2020.

[2] Airborne Contaminant Transport and Disease Transmission in Aircraft, Kansas City Chapter Meeting - ASHRAE's Building Readiness Guide, September 14th, 2020.

[3] Aircraft Cabin Environment Research (ACER) Lab, Airbus, June 9th, 2020.

[4] Analyzing the Symmetry of Airborne Pathogens Dispersion in Airplane Cabins, ASHRAE, 2020 winter conference and expo, February 2nd, 2020.